Prestressed Concrete Analysis and Design

Fundamentals

Second Edition

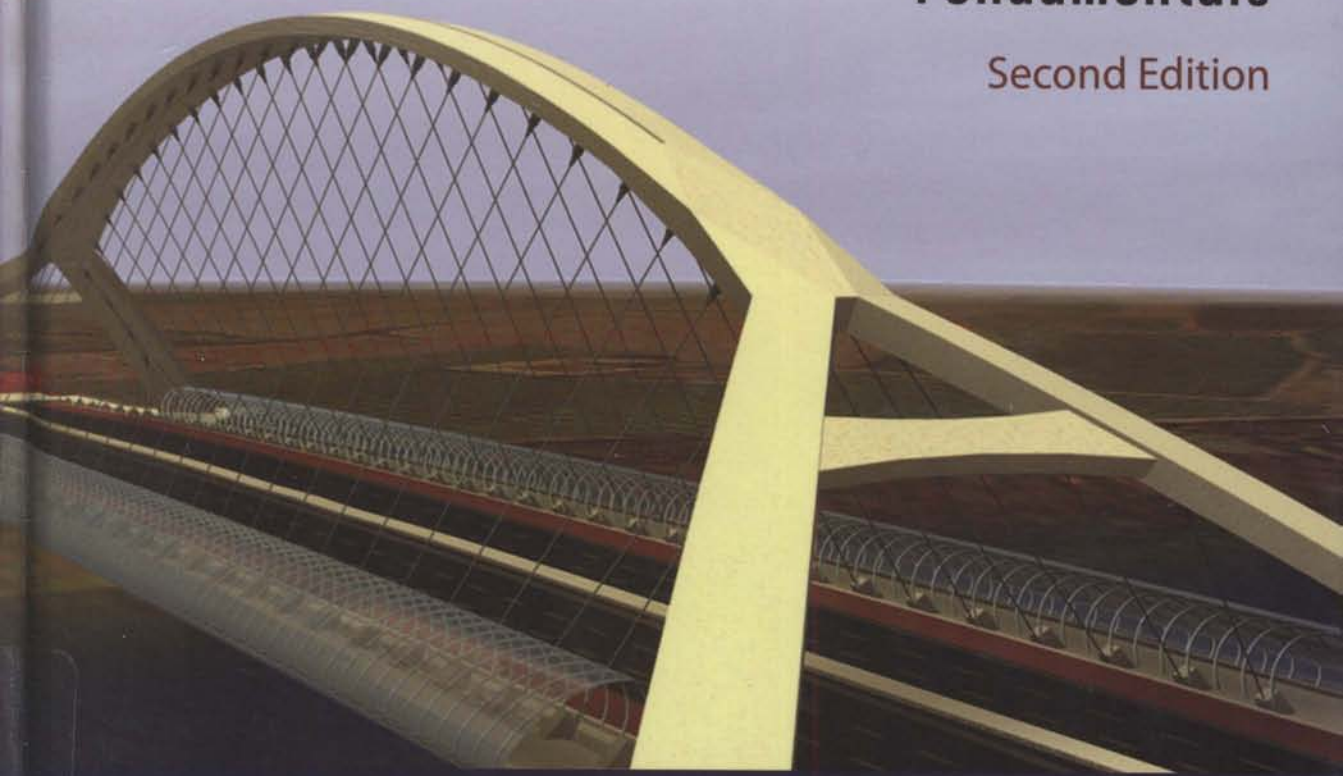

Antoine E. Naaman

PRESTRESSED CONCRETE ANALYSIS AND DESIGN

Fundamentals

2nd Edition

PRESTRESSED CONCRETE ANALYSIS AND DESIGN

Fundamentals

2nd Edition

Antoine E. Naaman
Professor of Civil Engineering
Department of Civil and Environmental Engineering
University of Michigan
Ann Arbor, Michigan 48109-2125, USA

Techno Press 3000
Ann Arbor, Michigan 48105
USA

Publisher's Cataloging-in-Publication
(Provided by Quality Books, Inc.)

Naaman, Antoine E.
Prestressed concrete analysis and design : fundamentals / Antoine E. Naaman. -- 2nd ed.
p. cm.
Includes bibliographical references and index.
ISBN 0-9674939-1-9

1. Prestressed concrete construction. I. Title

TA683.9.N3 2004 624.1'83412
QBI03-200942

Library of Congress Control Number
LCCN: 2004090275

Copy editor: *Ingrid Naaman*
Cover design: *Praveen Chompreda*

Prestressed Concrete Analysis and Design: Fundamentals – 2nd Edition
Copyright © 2004 by Antoine E. Naaman. All rights reserved. No part of this book may be reproduced in any form or by any means, translated into any language, stored in any data base or retrieval system, or transmitted in any form or by any means, without prior written permission from the author or the publisher.

Printed in the United States of America
10 9 8 7 6 5 4 3 2

Techno Press 3000
528 Green Road
Ann Arbor, Michigan 48105
USA
www.technopress3000.com

ISBN 0-9674939-1-9

Disclaimer: The author and publisher have used their best efforts in preparing this book. However, they make no warranty of any kind, expressed or implied, with regard to the material contained in the book, and shall not be liable in any event for the consequences of its use.

Trademark Notice: Product, corporate and/or professional association names may be registered trademarks and are used only for identification and/or explanation, without intent to infringe.

To my family,
the roots with earnest gratitude,
the branch with deepest love,
the buds with infinite wishes

In the true spirit of Engineering:
"Ask not what the world can do for you,
ask what you can do for the world."

CONTENTS

	Preface	xxiii
	Acknowledgments	xxix
Chapter 1	**Principle and Methods of Prestressing**	**1**
1.1	Introduction	1
1.2	Examples of Prestressing	2
1.3	History of Prestressed Concrete	4
1.4	Prestressing Methods	9
	1.4.1 Pretensioning	9
	1.4.2 Posttensioning	16
	1.4.3 Self-Stressing	18
1.5	Prestressing Systems	20
1.6	Particular Prestressing Techniques	21
	1.6.1 External Prestressing	21
	1.6.2 Circular Prestressing	23
	1.6.3 Stage Stressing	24
	1.6.4 Partial Prestressing	24
1.7	Prestressed Versus Reinforced Concrete	25
1.8	Example	28
1.9	Looking Ahead	32
	References	33
	Problems	37
Chapter 2	**Prestressing Materials: Steel and Concrete**	**41**
2.1	Reinforcing Steels	41
2.2	Prestressing Steel	45
	2.2.1 Types of Prestressing Tendons	46
	2.2.2 Production Process	49
	2.2.3 Mechanical and Stress-Strain Properties	51
	2.2.4 Relaxation	53
	2.2.5 Effects of Temperature	58
	2.2.6 Fatigue	59
	2.2.7 Corrosion	62
2.3	Concrete	64
	2.3.1 Composition	64
	2.3.2 Stress-Strain Curve	65
	2.3.3 Mechanical Properties	68
	2.3.4 Shrinkage	73
	2.3.5 Creep	75
	2.3.6 Fatigue	79
	2.3.7 Effects of Temperature	79

	2.3.8 Steam Curing	80
2.4	Constitutive Modeling	81
	2.4.1 Stress-Strain Curve of Concrete in Compression	81
	2.4.2 Stress-Strain Curve of Reinforcing Steel in Tension	84
	2.4.3 Stress-Strain Curve of Prestressing Steel in Tension	87
2.5	Concluding Remarks	90
	References	90
	Problems	93
Chapter 3	**The Philosophy of Design**	**95**
3.1	What is Design?	95
3.2	Analysis or Investigation Versus Design	96
3.3	Design Objectives	96
3.4	Limit State Design Philosophy	97
3.5	Common Design Approaches	99
	3.5.1 WSD (or ASD)	101
	3.5.2 USD, SD, or LRFD	102
	3.5.3 Plastic Design or Limit Design	105
	3.5.4 Nonlinear Design, Probabilistic Design	105
3.6	Design Codes	105
3.7	Loads	106
3.8	Allowable Stresses	109
	3.8.1 Concrete	109
	3.8.2 Prestressing Steel	111
	3.8.3 Reinforcing Steel	113
3.9	Load and Strength Reduction Factors	113
	3.9.1 Load Factors	113
	3.9.2 Strength Reduction Factors	115
3.10	Some Design Comparisons: Reinforced Versus Prestressed Concrete	116
	3.10.1 Practical Design Approach	116
	3.10.2 C-Force and C-Line	117
	3.10.3 Characteristic Response of RC, PC, and PPC in Bending in the Elastic Range of Behavior	118
	3.10.4 Curvature Computation	120
	3.10.5 Load Balancing Feature of Prestressing	121
3.11	ACI Code Viewpoint Related to Prestressed and Partially Prestressed Concrete	123
	3.11.1 Class Definition and Related Serviceability Design Requirements	123
	3.11.2 Tension Controlled and Compression Controlled Sections	125
3.12	Details of Reinforcement	126
3.13	Prestress Losses in Preliminary Design	129
3.14	Concluding Remarks	131
	References	131
Chapter 4	**Flexure: Working Stress Analysis and Design**	**135**
4.1	Analysis Versus Design	135
4.2	Concepts of Prestressing	140
4.3	Notations for Flexure	143

	4.3.1 Example: Computation of Sectional Properties	146
4.4	Sign Convention	146
	4.4.1 Examples	149
4.5	Loading Stages	151
4.6	Allowable Stresses	152
4.7	Mathematical Basis for Flexural Analysis	154
4.8	Geometric Interpretation of the Stress Inequality Conditions	158
4.9	Example: Analysis and Design of a Prestressed Beam	160
	4.9.1 Simply Supported T Beam	160
	4.9.2 Simply Supported T Beam with Single Cantilever on One Side	164
4.10	Use of the Stress Inequality Conditions for the Design of Section Properties	168
4.11	Examples of Use of Minimum Section Properties	174
	4.11.1 Minimum Weight Slab	174
	4.11.2 Minimum Weight Beam	176
	4.11.3 Selection of Optimum Beam from a Given Set of Beams	177
4.12	Limiting the Eccentricity along the Span	179
	4.12.1 Limit Kern Versus Central Kern	179
	4.12.2 Steel Envelopes and Limit Zone	183
	4.12.3 Example	186
	4.12.4 Limit Location of Draping Section	188
4.13	Some Preliminary Design Tips	190
4.14	Cracking Moment	191
4.15	Limiting the Amount of Prestressed Reinforcement	193
4.16	End Zone: Pretensioned Members	193
	4.16.1 Transfer Length and Development Length	193
	4.16.2 End Zone Reinforcement	195
4.17	End Zone: Posttensioned Members	196
	4.17.1 Analysis of Stresses	196
	4.17.2 Anchorage Zone Design	198
	4.17.3 Example: Design of End Zone Reinforcement	202
	References	204
	Problems	205
Chapter 5	**Flexure: Ultimate Strength Analysis and Design**	**211**
5.1	Load-Deflection Response	211
	5.1.1 RC Versus PC at Ultimate	214
5.2	Terminology	215
5.3	Flexural Types of Failures	216
5.4	Special Notation	217
5.5	General Criteria for Ultimate Strength Design of Bending Members	220
	5.5.1 Design Criteria	220
	5.5.2 Minimum Reinforcement or Minimum Moment Resistance: Code Recommendations	221
	5.5.3 ACI Code Provisions for Tension-Controlled, Transition, and Compression-Controlled Sections at Increasing Levels of Reinforcement	223

	5.5.4 AASHTO LRDF Recommendation on Maximum Reinforcement	230
5.6	Background for Analysis of Sections at Ultimate	231
	5.6.1 Objective – Assumptions	231
	5.6.2 Satisfying Equilibrium	233
5.7	Nominal Bending Resistance: Mathematical Formulation for Rectangular Section or Rectangular Section Behavior – Under-Reinforced and Tension-Controlled	233
	5.7.1 Force Equilibrium	234
	5.7.2 Moment Equilibrium	235
	5.7.3 Solution Procedure	236
5.8	Example: Nominal Bending Resistance of a Rectangular Section	237
	5.8.1 Partially Prestressed Section	237
	5.8.2 Fully Prestressed Section	239
	5.8.3 Unbonded Tendons	239
5.9	Nominal Bending Resistance: Mathematical Formulation for T-Section Behavior of Flanged Section	239
	5.9.1 Condition for T-Section Behavior	239
	5.9.2 Fully Prestressed Section	241
	5.9.3 Partially Prestressed Section	242
	5.9.4 Remark	244
5.10	Example: Nominal Bending Resistance of T Section	246
	5.10.1 Partially Prestressed Section	246
	5.10.2 Fully Prestressed Section	248
	5.10.3 Unbonded Tendons	248
	5.10.4 Odd Case	248
5.11	Stress in Prestressing Steel at Nominal Bending Resistance	249
	5.11.1 f_{ps} per ACI Code	249
	5.11.2 f_{ps} per AASHTO LRFD Specification for Bridge Design	251
	5.11.3 Author's Recommendation	253
5.12	Nominal Bending Resistance: Under-Reinforced Section, AASHTO LRFD Code	255
	5.12.1 Equilibrium Equations for Rectangular and Flanged Sections	255
	5.12.2 Solution for Members with Bonded Tendons	256
	5.12.3 Solution for Members with Unbonded Tendons	257
	5.12.4 Solution for Members with Both Bonded and Unbonded Tendons	258
	5.12.5 Example: PPC (Partially Prestressed Concrete) Rectangular Section with Bonded Tendons (AASHTO)	258
	5.12.6 Example: PPC (Partially Prestressed Concrete) T Section with Bonded Tendons (AASHTO)	259
5.13	Nominal Moment Resistance: Over-Reinforced and Non Tension-Controlled Sections	261
	5.13.1 ACI Code	261
	5.13.2 AASHTO LRFD	261
	5.13.3 Example of Over-Reinforced Section as per AASHTO LRFD	262
5.14	Concept of Reinforcing Index	267

	5.14.1 Definitions	267
	5.14.2 Meaning of ω_e	268
	5.14.3 Useful Relationships	269
	5.14.4 Relationship between Reinforcement Ratio, Reinforcing Index, and c/d_e	271
5.15	Justification for the Definition of ω_e and d_e and Their Relation to the Limitations on Levels of Reinforcement and Moment Redistribution	272
	5.15.1 Reinforced Concrete	272
	5.15.2 Prestressed Concrete	272
	5.15.3 Partially Prestressed Concrete	273
5.16	Derivation of Minimum Reinforcement Ratio, Minimum Reinforcing Index, or Minimum c/d_e	273
	5.16.1 Approximation: Minimum Reinforcement Ratio for Prestressed Concrete	273
	5.16.2 Minimum Reinforcing Index for RC, PC, and PPC	274
	5.16.3 Minimum c/d_e Ratio for RC, PC, and PPC Rectangular Sections	277
5.17	Satisfying Ultimate Strength Design Requirements	278
	5.17.1 Basis for Ultimate Strength Design (USD)	278
	5.17.2 Possible Remedies to Satisfy Inadequate Nominal Bending Resistance	279
5.18	Example: Analysis or Investigation Checking for All Ultimate Strength Design Criteria	280
5.19	Reinforcement Design for Ultimate Strength	282
	5.19.1 Example: Reinforcement Design for Nominal Resistance – Rectangular Section	283
	5.19.2 Example: Reinforcement Design for Nominal Resistance – T Section	288
5.20	Composite Beams	289
5.21	Continuous Beams and Moment Redistribution	290
5.22	Concluding Remarks	290
5.23	Additional Design Examples Based on USD	291
	5.23.1 Example 1: Analysis with Unbonded Tendons Illustrating Eq. (5.41)	291
	5.23.2 Example 2: Given A_{ps}, Design for A_s Based on USD – Unbonded Tendons	293
	5.23.3 Example 3: Given A_{ps}, Design for A_{ps} Based on USD – Unbonded Tendons	295
	5.23.4 Example 4: Given A_{ps}, Design for A_{ps} Based on USD – Bonded Tendons	295
	References	296
	Problems	297
Chapter 6	**Design for Shear and Torsion**	**303**
6.1	Introduction	303
6.2	Shear Design	304
6.3	Prestressed Versus Reinforced Concrete in Shear	304
6.4	Diagonal Tension in Uncracked Sections	306

6.5	Shear Stresses in Uncracked Sections	310
6.6	Shear Cracking Behavior	312
6.7	Shear Reinforcement after Cracking	314
6.8	ACI Code Design Criteria for Shear	318
	6.8.1 Basic Approach	318
	6.8.2 Shear Strength Provided by Concrete	320
	6.8.3 Required Area of Shear Reinforcement	323
	6.8.4 Limitations and Special Cases	324
	6.8.5 Critical Sections for Shear	325
6.9	Design Expedients	327
6.10	Example: Design of Shear Reinforcement	330
	6.10.1 Elaborate Approach to Determine v_c	331
	6.10.2 Alternate Conservative Approach to Determine v_c	334
	6.10.3 Design for Increased Live Load: Partially Prestressed Beam	334
6.11	Derivation of Concrete Nominal Shear Strength Equations (ACI Code)	336
6.12	AASHTO General Procedure for Shear Design	340
	6.12.1 General Sectional Procedure for Shear Design	341
	6.12.2 Special Considerations	349
	6.12.3 Example: Shear Design by AASHTO LRFD Code	351
6.13	Torsion and Torsion Design	354
6.14	Behavior under Pure Torsion	355
6.15	Background to Stress Analysis and Design for Torsion	358
	6.15.1 Torsional Stresses	358
	6.15.2 Torsional Cracking Strength	360
	6.15.3 Torsional Resistance after Cracking	361
	6.15.4 Combined Loading	364
	6.15.5 Design Theories for Torsion and Code Related Approaches	366
6.16	Design for Torsion by the 2002 ACI Code	368
	6.16.1 Definition of Section Parameters	368
	6.16.2 Basic Assumptions and Design Strategy	369
	6.16.3 Condition for Consideration of Torsion in Design	370
	6.16.4 Critical Section for Torsion	371
	6.16.5 Maximum Allowable Torsional Moment Strength	371
	6.16.6 Transverse Reinforcement Design	373
	6.16.7 Longitudinal Torsion Reinforcement	374
	6.16.8 Combining Shear and Torsion Reinforcement	374
	6.16.9 Minimum Torsion Reinforcement	375
	6.16.10 Spacing and Detailing	375
	6.16.11 Type of Torsion Reinforcement	376
	6.16.12 Design Steps for Combined Torsion and Shear	376
6.17	Example: Torsion Design of a Prestressed Beam	378
6.18	Shear and Torsion in Partially Prestressed Members	381
	References	382
	Problems	384
Chapter 7	**Deflection Computation and Control**	**389**
7.1	Serviceability	389
7.2	Deflection: Types and Characteristics	390

	7.2.1 Terminology / Notation	390
	7.2.2 Key Variables Affecting Deflections in a Given Beam	391
7.3	Theoretical Deflection Derivations	392
	7.3.1 Moment-Area Theorems	394
	7.3.2 Example	396
7.4	Short-Term Deflections in Prestressed Members	397
	7.4.1 Uncracked Members	397
	7.4.2 Cracked Members	400
7.5	Background to Understanding Long-Term Deflection	406
7.6	Additional Long-Term Deflection: Simplified Prediction Methods	408
	7.6.1 Additional Long-Term Deflection Using ACI Code Multiplier	410
	7.6.2 Additional Long-Term Deflection Using Branson's Multipliers	410
	7.6.3 Additional Long-Term Deflection Using Martin's Multiplier	411
	7.6.4 Additional Long-Term Deflection: Heuristic or "Rule of Thumb" Method	411
	7.6.5 Discussion	411
7.7	Deflection Limitations	412
7.8	Strategy for Checking Deflection Criteria	414
7.9	Example: Deflection of Uncracked or Cracked Prestressed Beam	416
	7.9.1 Fully Prestressed Beam – Uncracked under Full Service Load	416
	7.9.2 Partially Prestressed Beam	417
7.10	Integrating the Modulus of Concrete into Time-Dependent Deflection Calculations	420
	7.10.1 Age-Adjusted Effective Modulus	420
	7.10.2 Equivalent Modulus	422
	7.10.3 Equivalent Cyclic-Dependent Modulus	422
7.11	Long-Term Deflection by Incremental Time Steps	423
	7.11.1 Theoretical Approach	423
	7.11.2 Simplified C-Line Approach	423
7.12	Example: Time-Dependent Deflection Using the C-Line Approach	430
7.13	Example: Comparison of Long-Term Deflections Predicted from Different Methods	435
7.14	Deflection Control	437
7.15	Concluding Remarks	438
	References	439
	Problems	441
Chapter 8	**Computation of Prestress Losses**	**445**
8.1	Sources of Loss of Prestress	445
8.2	Total Losses in Pretensioned Members	448
8.3	Total Losses in Posttensioned Members	451
8.4	Methods for Estimating Prestress Losses	452
8.5	Lump Sum Estimate of Total Losses	453

	8.5.1 Background	453
	8.5.2 Lump Sum Estimate of Prestress Loss: AASHTO LRFD	455
8.6	Separate Lump Sum Estimate of Each Time-Dependent Loss – AASHTO LRFD	458
	8.6.1 Total Loss Due to Shrinkage	459
	8.6.2 Total Loss Due to Creep	460
	8.6.3 Total Loss Due to Relaxation	460
	8.6.4 Losses for Deflection Calculations	462
	8.6.5 Example: Losses Due to Relaxation	462
8.7	Loss Due to Elastic Shortening	463
	8.7.1 Pretensioned Construction: Approximate Method and AASHTO LRFD	464
	8.7.2 Pretensioned Construction: Accurate Method	465
	8.7.3 Posttensioned Construction: AASHTO LRFD	466
	8.7.4 Posttensioned Construction: Accurate Method	467
8.8	Example: Elastic Shortening Loss in Pretensioned Beam	468
8.9	Example: Computation of Prestress Losses for a Pretensioned Beam by Lump Sum Methods	470
	8.9.1 Lump Sum Estimate of Total Losses by AASHTO LRFD	470
	8.9.2 Lump Sum Estimates of Separate Losses by AASHTO LRFD	471
8.10	Example: Typical Stress History in Strands	471
8.11	Time-Dependent Loss Due to Steel Relaxation	473
8.12	Time-Dependent Loss Due to Shrinkage	475
	8.12.1 Example: Shrinkage Loss Assuming No Other Loss Occurs	477
8.13	Time-Dependent Loss Due to Creep	479
	8.13.1 Example: Creep Loss Assuming No Other Loss Occurs	482
8.14	Prestress Losses by the Time-Step Method	484
8.15	Example: Computation of Prestress Losses for a Pretensioned Beam by the Time-Step Method	486
8.16	Loss Due to Friction	491
	8.16.1 Analytical Formulation	491
	8.16.2 Graphical Representation	494
	8.16.3 Example: Computation of Losses Due to Friction	495
8.17	Loss Due to Anchorage Set	498
	8.17.1 Concept of Area Lost or Equivalent Energy Lost	501
	8.17.2 Example: Loss Due to Anchorage Set	502
8.18	Loss Due to Anchorage Set in Short Beams	504
	8.18.1 Example: Anchorage Set Loss in a Short Beam	506
8.19	Concluding Remarks	507
	References	507
	Problems	510
Chapter 9	**Analysis and Design of Composite Beams**	**515**
9.1	Types of Prestressed Concrete Composite Beams	515
9.2	Advantages of Composite Construction	516
9.3	Particular Design Aspects of Prestressed Composite Beams	518

9.4	Loading Stages, Shored Versus Unshored Beams	519
9.5	Effective and Transformed Flange Width and Section Properties	520
	9.5.1 Effective Flange Width	520
	9.5.2 Transformed Flange Width	522
	9.5.3 Cross Section Properties of Composite Section	524
9.6	Interface Shear or Horizontal Shear	525
	9.6.1 Evaluation of Horizontal Shear	525
	9.6.2 ACI Code Provisions for Horizontal Shear at Contact Surface	528
9.7	Flexure: Working Stress Analysis and Design	533
	9.7.1 Extreme Loadings	533
	9.7.2 Stress Inequality Conditions	534
	9.7.3 Feasible Domain, Limit Kern, Steel Envelopes	538
	9.7.4 Cracking Moment	539
	9.7.5 Minimum Section Moduli of Composite Sections	539
	9.7.6 Example: Selection of Optimum Beam from a Given Set of Beams	542
9.8	Flexure: Ultimate Strength Analysis and Design	545
9.9	Designing for Shear and Torsion	547
9.10	Deflections	548
9.11	Example: Prestressed Composite Floor Beam	550
9.12	AASHTO LRFD Provisions on Shear Tie Reinforcement at Contact Surface of Composite Beams	563
	9.12.1 Nominal Shear Transfer Resistance	563
	References	566
	Problems	567
Chapter 10	**Continuous Beams and Indeterminate Structures**	**571**
10.1	Advantages and Forms	571
10.2	Necessary Analytical Background	574
10.3	Sign Convention and Special Notation	575
10.4	Secondary Moments and Zero-Load-C (ZLC) Line	576
10.5	Example: Secondary Moments and Concordancy Property	579
10.6	Linear Transformation	582
10.7	Concordant Tendons	583
10.8	External Loads Equivalent to Prestressing	585
	10.8.1 Concept of Equivalent Load	586
	10.8.2 Application of Equivalent Load to a Continuous Tendon	588
	10.8.3 Example: Equivalent Load	589
	10.8.4 Example: Equivalent Load for a Circular and Parabolic Tendon Profile	592
10.9	Prestressing Moment and Elastic Stresses	596
	10.9.1 Moment Due to Prestressing, M_F	596
	10.9.2 Example: Prestressed Moments by the Equivalent Load Method	598
	10.9.3 Elastic Stresses in a Continuous Beam	603
10.10	Design Aids	604
10.11	Working Stress Analysis and Design	608

	10.11.1 Assumptions	608
	10.11.2 Analysis or Investigation	608
	10.11.3 Design	609
10.12	Limit Kern and Limit Zone	611
10.13	Load-Balancing Method	613
	10.13.1 General Approach	613
	10.13.2 Load Balancing of Edge-Supported Slabs	616
	10.13.3 Example: Load Balancing of an Edge-Supported Slab	618
	10.13.4 Load Balancing of Frames	620
	10.13.5 Limitations of Load Balancing	621
10.14	Ultimate Strength Analysis	621
	10.14.1 Treatment of Secondary Moments	622
	10.14.2 Limit Analysis	622
	10.14.3 Redistribution of Moments	625
	10.14.4 Secondary Moment and Moment Redistribution	627
	10.14.5 Prediction of Plastic Rotation in PPC Beams	627
10.15	Example: Design of a Prestressed Continuous Beam	629
10.16	Useful Design Aids for Continuous Beams	639
	References	643
	Problems	643
Chapter 11	**Prestressed Concrete Slabs**	**649**
11.1	Slab Systems	649
	11.1.1 General Design Approach	653
11.2	Unbonded Tendons in One and Two-Way Slab Systems	654
	11.2.1 Stress at Ultimate in Unbonded Tendons	655
11.3	Design of One-Way Slabs	657
	11.3.1 Design Procedure	658
	11.3.2 Minimum Bonded Reinforcement	659
	11.3.3 Temperature and Shrinkage Reinforcement	660
	11.3.4 Additional Design Notes	661
	11.3.5 Deflection	662
11.4	Example: Design of a Five-Span Continuous One-Way Slab Prestressed with Unbonded Tendons	662
11.5	Characteristics of Two-Way Flat Slabs	669
	11.5.1 Load Path	669
	11.5.2 Reinforcement Layout	670
	11.5.3 Theoretical Distribution of Moments	670
	11.5.4 Special Notations	673
11.6	Analysis and Design Methods	673
	11.6.1 Analysis	673
	11.6.2 Design	674
	11.6.3 Load Balancing	674
11.7	Analysis by the Equivalent-Frame Method	675
	11.7.1 General Approach	676
	11.7.2 Computation of Moments and Shear Forces	678
11.8	Design Distribution of Moments and Tendons	680
11.9	Preliminary Design Information and Design Tips	682
	11.9.1 Slab Thickness and Reinforcement Cover for Fire Safety	683

	11.9.2 Punching Shear	683
	11.9.3 Average Prestress	683
	11.9.4 Nonprestressed Reinforcement	684
	11.9.5 Deflection	684
11.10	Prestressed Flat Plates: Design for Flexure	684
	11.10.1 Working Stress Design	684
	11.10.2 Allowable Stresses	685
	11.10.3 Ultimate Strength Design	686
	11.10.4 Minimum Bonded Reinforcement	686
	11.10.5 Nominal to Cracking Moment Condition	688
11.11	Flat Plates: Design for Shear	688
	11.11.1 Concrete Shear Capacity	688
	11.11.2 Transfer Moment Between Columns and Slab	691
	11.11.3 Maximum Shear Stress in Critical Section	693
	11.11.4 Design Tips	698
	11.11.5 Shear Reinforcement	699
11.12	Deflection of Flat Plates	701
	11.12.1 Elastic Solution	702
	11.12.2 Equivalent Frame Approach	703
11.13	Summary of Design Steps for Two-Way Prestressed Flat Plates	706
11.14	Example: Design of a Two-Way Prestressed Flat Plate	707
	References	725
	Problems	727
Chapter 12	**Analysis and Design of Tensile Members**	**731**
12.1	Types of Tension Members	731
12.2	Advantages of Prestressed Concrete Tension Members	733
	12.2.1 Example: Relative Deformation of Tension Members	734
12.3	Behavior of Prestressed Concrete Tension Members	735
12.4	Analysis of Tension Members	739
	12.4.1 Service Stresses, Decompression, Cracking and Ultimate Load	739
	12.4.2 Short- and Long-Term Deformations	743
	12.4.3 Example: Analysis-Investigation of a Tension Member	745
12.5	Optimum Design of Tension Members	748
	12.5.1 Formulation of Design Criteria	748
	12.5.2 Design Approximations	753
	12.5.3 Minimum Cost Solution	754
	12.5.4 Example	756
12.6	Circular Structures: Tanks and Pressure Vessels	758
	12.6.1 Analysis of Stresses	761
	12.6.2 Design	765
	12.6.3 Example: Preliminary Design of Cylindrical Wall Thickness	767
	12.6.4 Practical Considerations for Design	768
12.7	Combined Tension and Bending	769
	References	770
	Problems	771

Chapter 13	**Analysis and Design of Compression Members**	**775**
13.1	Types and Their Advantages	775
13.2	Behavior of Columns	779
	13.2.1 Load-Deformation Response	779
	13.2.2 Classification	780
	13.2.3 Load-Moment Interaction Diagram	780
	13.2.4 ACI Code Design Interaction Diagram	783
13.3	Analysis of Short Columns	785
	13.3.1 Assumptions	785
	13.3.2 Basic Equations for Square and Rectangular Sections	787
	13.3.3 Partially Prestressed Square or Rectangular Sections	789
	13.3.4 Circular Hollow-Cored and I-Shaped Sections	790
13.4	Example: Column Load-Moment Interaction Diagram	793
13.5	ACI Code and Other Design Considerations	799
	13.5.1 Minimum Longitudinal Reinforcement	799
	13.5.2 Lateral or Transverse Reinforcement	799
	13.5.3 Minimum Size of Columns	801
	13.5.4 Minimum Eccentricity	802
	13.5.5 Transfer Zone	802
13.6	Slender Columns: Theoretical Background	802
	13.6.1 Definition of Braced, Unbraced, Sway and Non-Sway Columns or Frames	805
	13.6.2 Single and Double Curvature	807
	13.6.3 Terminology and Definitions	807
	13.6.4 Stiffness under Cracked Conditions for First-Order Frame Analysis	807
13.7	Slenderness Effects: ACI Code Philosophy	809
13.8	ACI Code Design Provisions for Slender Columns by the Moment Magnifier Method	811
	13.8.1 Sway and Non-Sway Condition	811
	13.8.2 Effective Length Factor k	812
	13.8.3 Effective Slenderness Ratio and Slenderness Condition	814
	13.8.4 Moment Magnification in Non-Sway Frames	816
	13.8.5 Magnified Moments in Sway Frames with $22 < kl_u / r < 100$	818
	13.8.6 Additional Design Checks	821
	13.8.7 Design According to the PCI Committee on Columns	822
13.9	Example: Slender Column Using the PCI Approach	824
	13.9.1 Non-Sway or Braced Column	824
	13.9.2 Sway or Unbraced Column	827
13.10	Design Expedients and Design Aids	830
	13.10.1 Preliminary Dimensioning	830
	13.10.2 Design Charts: Load-Moment Interaction Diagrams	831
13.11	Biaxial Bending	840
13.12	New Design Methodology for Slender Prestressed Columns	843

13.13	Concluding Remarks	846
	References	846
	Problems	849
Chapter 14	**Prestressed Concrete Bridges**	**851**
14.1	Scope	851
14.2	Types of Bridges	853
	14.2.1 Short-Span Bridges	854
	14.2.2 Medium- and Long-Span Bridges Using Precast Beams	854
	14.2.3 Long- and Very Long-Span Bridges	862
14.3	Rational Evolution of Bridge Form with Span Length	867
14.4	Special Construction Techniques for Bridges	869
	14.4.1 Segmental Construction	869
	14.4.2 Truss Bridges	872
	14.4.3 Stress Ribbon or Inverted Suspension Bridges	873
	14.4.4 Use of New Materials	875
14.5	Design Specifications and General Design Philosophy	878
	14.5.1 Limit States	878
	14.5.2 Load Combinations, Load Factors and Resistance Factors	881
	14.5.3 Allowable Stresses for Service Limit States	883
14.6	Bridge Live Loads	885
	14.6.1 Traffic Lane and Design (or Loading) Lane	885
	14.6.2 Basic Types of Live Loads	886
	14.6.3 Live Load Combinations for Design	887
	14.6.4 Conditions of Application of Live Loads	888
	14.6.5 Impact Factor	890
	14.6.6 Multiple Presence Factor	890
	14.6.7 Pedestrian Load and Sidewalk Load	890
	14.6.8 Deflection Limit	891
	14.6.9 Other Requirements	891
14.7	Distribution of Live Loads and Beam Distribution Factors	891
	14.7.1 Load Distribution Factors	892
	14.7.2 Remarks Related to a Particular Bridge Deck Type	899
	14.7.3 Simplified Distribution Factor by Heuristic Approach	900
14.8	Design Aids for Live Load Moments and Shears for One Loading Lane	901
	14.8.1 General Rule for Concentrated Loads in Simply Supported Spans	901
	14.8.2 Equations for Live Load Moments and Shears in Simply Supported Spans	902
	14.8.3 Design Chart for Simply Supported Spans	905
	14.8.4 Design Charts for Live Load Moments at Supports of Continuous Beams with Equal Spans	905
14.9	Moments and Shears in Typical Girders	909
14.10	Example: Composite Bridge with Cast-in-Place Reinforced Concrete Slab on Top of Prestressed I-Girders	910
	14.10.1 Live Load Moments and Shears at Critical Sections	910
	14.10.2 Detailed Design of Prestressed I Beams	913

14.11 Example: Bridge Deck with Adjacent Precast Pretensioned Box Beams 925
14.12 Example: Negative Live Load Moment in Two-Span Continuous Bridge Deck 930
14.13 Slabs for Bridge Decks and Solid Slab Bridges 932
14.13.1 Equivalent Strip Width for Slab Type Bridges and Distribution Factor for Slabs 933
14.13.2 Minimum Depth and Clear Concrete Cover 934
14.13.3 Cast-in-Place One-Way Prestressed Slabs 934
14.13.4 Traditional Design of Reinforced Concrete Deck Slabs 935
14.13.5 Empirical Design of Slabs 936
14.13.6 Temperature and Shrinkage Reinforcement 937
14.13.7 Moments for Slabs Supported on Four Sides 938
14.14 Example: Design of a Cast-in-Place Posttensioned Slab Bridge 938
14.15 Precast Bridge Beams Made Continuous by a Cast-in-Place RC Slab 942
14.15.1 Example: Prestressed Bridge Beams Made Continuous by Cast-in-Place RC Slab 944
14.16 Design Charts for Prestressed Bridge Beams 948
14.17 Preliminary Design Tips for Dimensioning 949
14.18 Other Design Considerations 951
14.19 Bridge Engineering: Looking Ahead 952
References 954
Problems 956

Chapter 15 Strut-and-Tie Modeling 961
15.1 Introduction 961
15.1.1 Background and Motivation 961
15.1.2 B- and D-Regions 962
15.1.3 Trusses and Strut-and-Tie Models 965
15.1.4 ACI Code Definition 966
15.2 Elements of Strut-and-Tie Models 967
15.2.1 Assumptions 968
15.2.2 Mechanical Requirements and Geometry Rules 969
15.2.3 Requirements for Nodal Zones 969
15.2.4 External and Unbonded Prestressing Tendons 970
15.2.5 Terminology / Notation 971
15.3 Design Steps to Build a Strut-and-Tie Model (STM) 971
15.3.1 Initial Checks 971
15.3.2 Design Steps 972
15.4 Design Philosophy 976
15.5 Design of Ties 976
15.5.1 Prestressing Tendons 977
15.6 Design of Struts 978
15.7 Design of Nodal Zones 981
15.7.1 Assumptions 981
15.7.2 Dimensioning 981
15.7.3 Anchorages 982
15.7.4 Nominal Strength 983

15.8	STM by AASHTO LRFD	984
15.9	Anchorage Zones of Prestressed Members	985
15.10	Example: Anchorage Zone Design by STM	987
	15.10.1 Two Spread-Out Anchorages	988
	15.10.2 Two Anchorages Placed Close to Each Other	997
15.11	Dapped-End Beams	998
15.12	Example: Dapped-End Beam Design by STM	1000
15.13	Examples of Applications of Strut-and-Tie Models to Various Structures	1007
15.14	Concluding Remarks	1013
	References	1013
	Problems	1015
Appendix A	**List of Symbols**	**1017**
Appendix B	**Unit Conversions**	**1030**
Appendix C	**Typical Post-Tensioning Systems**	**1033**
Appendix D	**Answers to Selected Problems**	**1053**
Appendix E	**Typical Precast / Prestressed Beams**	**1059**
Index		**1065**

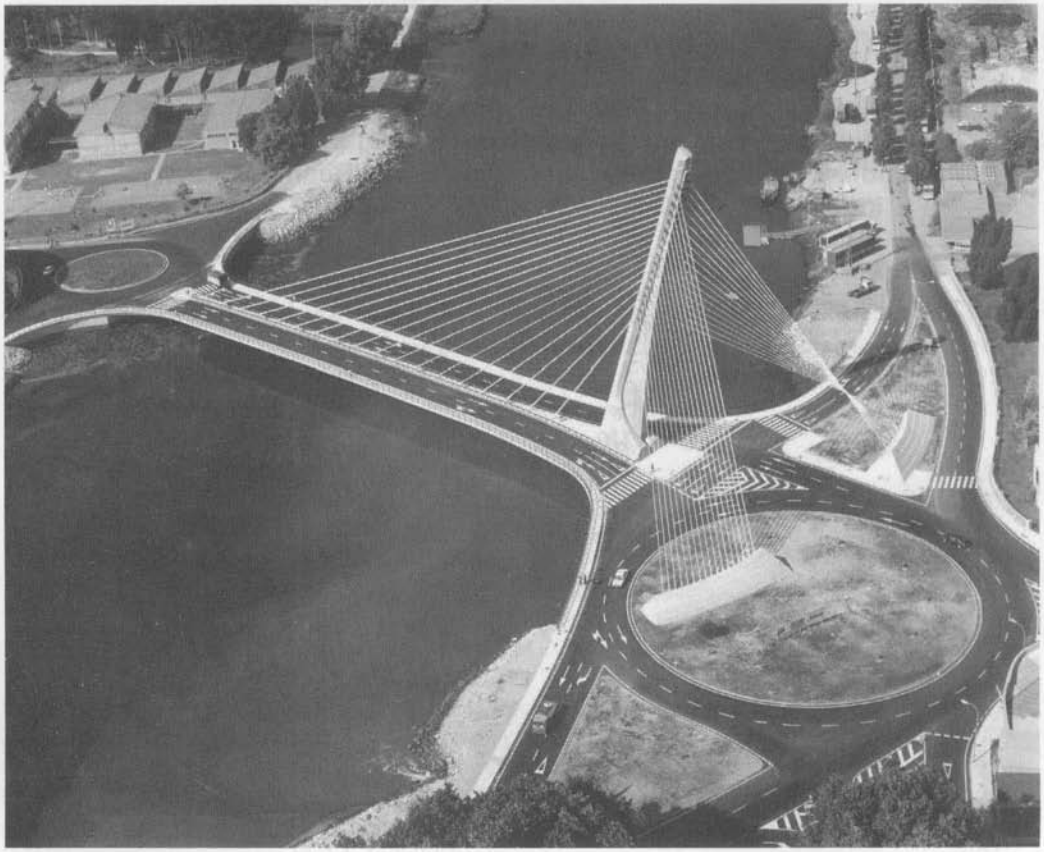

The Puente Sobre El Rio Bridge in Lerez, Spain, is a cable stayed bridge with a main span of 129 m (423 ft) and a prestressed concrete single box deck. (*Courtesy Carlos Fernandez Casado S.L.*).

PREFACE TO THE SECOND EDITION

Although historically prestressed concrete has experienced a slower start than reinforced concrete and its development has followed a different path, it has evolved into a reliable technology and has established itself as a major structural material. Prestressed concrete has made significant contributions to the precast manufacturing industry, the cement industry, and the construction industry as a whole. This has led to an enormous array of structural applications from bridges to nuclear power vessels, from buildings serving every use and occupancy to ships, and from lowly products, such as ties and piles, to monumental TV towers, and offshore drilling platforms. Seldom is a major construction project planned today without prestressed concrete being considered as one of the viable alternative solutions. A careful analysis of future trends indicates a substantial increase in the use of prestressed concrete. This is also supported by developments in partially prestressed concrete, which integrates both reinforced and prestressed concrete and treats them as the extreme boundaries of the same system. It has become almost inevitable to consider each material separately without considering their combination. The term structural concrete is increasingly used to allow both.

A similar trend is expected at the educational level. Design courses in prestressed concrete will be more widely offered at universities and may be moved from the list of technical electives to the list of required courses in structural engineering curricula. It is also likely that reinforced and prestressed concrete will be offered as part of the same general course or course sequence on structural concrete, hence essentially covering partially prestressed (or partially reinforced) concrete.

Audience and Educational Strategy. This book is written for advanced students and professionals. It is meant as a thorough teaching text, as well as a reference tool

for practicing engineers and researchers. It emphasizes the fundamental concepts of analysis and design of prestressed concrete structures and provides students a sufficiently strong basis for handling everyday design problems, and the tackling of the more complex problems with confidence. A particular effort is made throughout to synthesize and condense the essential information and to give an overview of the directions in which the design is proceeding. Self-sufficient logical design flow charts summarizing the step-by-step design procedure and containing all necessary design equations are often presented. They reduce the burden of guesswork and iterative tryout encountered in the design process, and are essential when programmable calculators and computers are used. Important formulas and equations are also condensed in tables for ready use. To provide a correlation with reinforced concrete design and to help engineers already familiar with reinforced concrete, the case of partially prestressed (or partially reinforced) concrete is often addressed. An extensive selection of references is given at the end of each chapter. An attempt was made to include not only necessary readings but also most recent research conducted in the United States for up-to-date information. Specifications of the 2002 ACI building code and relevant requirements of the AASHTO LRFD specifications (1998 to 2002 interims) are integrated in the text. When appropriate guidance is not available in the code, suggestions are made to accommodate at best the intent of the code.

Whenever possible, widely accepted symbols, such as those used in the ACI code are adopted and all symbols used in the text are defined and summarized for easy reference in Appendix A. A consistent notation and sign convention is followed throughout, allowing rigorous treatments when needed. This is essential, for instance, in the case of continuous beams where the sign of secondary moments cannot be visualized *a priori* and must be derived from the analysis.

Because of the inevitable future conversion from U.S. customary units to the International System of Units (SI), all important tables, figures, and design information, as well as dimensionally inconsistent equations, are given in dual units. However, because the prestressed concrete industry is not on the verge of change from U.S. customary units to SI units, all examples are treated in U.S. units to allow students and professionals to keep in touch with current practice. In addition, SI conversion factors and SI equivalents for some dimensionally inconsistent equations used in various flow charts are given in Appendix B.

Compared to the first edition released in 1982, this second edition is comprehensively expanded; it incorporates a countless number of minute improvements generated during more than twenty years of teaching and research since the printing of the first edition. These have added broader knowledge and technical wisdom to the material. Overall, more examples are given, numerous clarifications are provided, the number of figures and photographs is augmented, and, when relevant, remarks summarizing the author's opinion that may differ from codes are added. A chapter on strut-and-tie modeling has been added. The two main U.S. codes for prestressed concrete structures, that are, the ACI building code and

the AASHTO LRFD specifications for bridges, have seen enormous change and are significantly more voluminous than they were in the 1970's; moreover, while their articles and specifications were almost identical in the past, they are now very different in many cases; significantly more text is needed to explain these articles and apply them to practical examples.

Functional Organization. The text is organized into 15 chapters, which can be assembled according to their intended function:

- The first three chapters contain essential design information and reference data. They provide a general background on materials properties, design philosophy, and codes.
- Chapters 4 to 8 develop the fundamental basis and underlying principles for the analysis and design of prestressed concrete members. They include analysis and design for flexure by the working stress design method with an introduction to optimum design (Chapter 4), analysis and design for flexure by the ultimate strength design method with full coverage of partial prestressing (Chapter 5), design for shear and torsion and their combined effects with flexure (Chapter 6), design for deflection control with treatment of partically prestressed cracked sections and the incremental time-step method to predict long-term deflection (Chapter 7), and prediction of prestress losses either by lump sum estimates or by the accurate incremental time-step procedure (Chapter 8).
- Chapters 9 to 14 address the particular analysis and design aspects of structural elements or systems in various applications of prestressed concrete. They cover composite beams (Chapter 9), continuous beams (Chapter 10), one- and two-way slab systems (Chapter 11), prismatic tensile members and cylindrical tanks (Chapter 12), short and slender columns (Chapter 13), and bridges (Chapter 14).
- Chapter 15 on strut-and-tie modeling addresses a subject that is likely to be more extensively used in future codes and provides a research oriented path to Chapter 6.

Several appendixes are given at the end of the book, including a list of symbols (Appendix A), SI conversion factors (Appendix B), technical information on some post-tensioning systems (Appendix C), and answers to selected problems (Appendix D).

The general organization of this book remains essentially the same as in the first edition. Chapter 15, on strut-and-tie modeling, could be presented following Chapter 6 on shear and torsion. The material in the book is extensive and can cover up to two courses in prestressed concrete spanning from the senior undergraduate level to the advanced graduate level. Tentative course outlines are suggested next.

Course 1, Part 1: Fundamentals of Prestressed Concrete. In a first course on prestressed concrete the author recommends the following approach, assuming a semester-long course with 42 lectures of about one hour each:

- *Chapter 1,* introduction: Cover entirely in no more than two lectures.
- *Chapter 2* on materials for prestressing: Cover in less than two lectures; focus mainly on the properties of prestressing steels and their implication for design. Students can read the remaining material on their own as reading assignment and will refer back to these chapters when other topics are covered such as deflection, losses, columns, etc.
- *Chapter 3* on philosophy of design: Cover in about two lectures. Besides explaining the general philosophy of design as applied to prestressed concrete, explain curvature, the C-line or C force concept, load-balancing concept, and how prestress losses are bypassed in preliminary design by using the factor η.
- *Chapters 4 to 7* on working stress analysis and design, ultimate strength analysis and design, design for shear and torsion, and computation of deflections: These chapters should be covered in depth to insure a strong basis in the fundamentals of prestressed concrete and prepare students for detailed design. Depending on the time available, parts of certain chapters may be omitted. For instance, skip the design of anchorage zone in Chapter 4. In Chapters 5 and 6, depending on the time and audience, only the approach followed by ACI (or conversely by AASHTO) could be treated and the rest assigned as independent reading. In Chapter 6, omit the section on combined shear and torsion. In Chapter 7, the long-term deflection by incremental time steps could be left out to a more advanced treatment. Devote eighteen to twenty lecture hours for Chapters 4 to 7.
- *Chapter 8* on prestress losses: At a minimum, cover prestress losses by the total lump-sum estimate of total losses; lump sum estimates of individual losses could be covered next, and losses by the time-step procedure should be treated only if time allows. Students involved in research may benefit greatly from the treatment of losses by the time-step method, because it involves a deeper understanding of material behavior and its implication on structural response. However, generally, most students are less interested in probing prestress losses further than the minimum needed. For this reason it is suggested to leave the treatment of prestress losses to this later stage in the course. Also, it is recommended to leave the treatment of losses due to friction and anchorage set to a second course. Devote about two hours to this chapter.

Course 1, Part 2: Applications. In a second part of a first course, analysis and design related to specific applications are covered. The selection of topics should depend on the interest of the audience and the time available. The following sequence is recommended in priority:

- *Chapter 9* on composite beams: Cover entirely in about four lecture hours.

- *Chapter 14* on bridges: Cover almost entirely, at least including the example of Section 14.10 and Sections 14.16 to 14.19. Six lecture hours may be needed.
- *Chapter 13* on columns: Cover mostly non-slender columns, if time allows it. As an alternative, an introduction to secondary moments and Chapter 10 could be presented.

Based on years of teaching, it has been the author's experience that Parts 1 and 2 described above would amply cover a semester-long course on prestressed concrete, assuming time is allocated for two mid-term and a final exam.

Course 2: Advanced Topics in Pretressed Concrete. The following material is suggested for a second, more advanced course on prestressed concrete, as taught by the author at the University of Michigan:

- *Chapter 10* on continuous beams: Cover entirely.
- *Chapter 11* on prestressed one- and two-way slab systems: Cover entirely.
- *Volume 2* in progress (or from research papers): Analysis and design of partially prestressed beams with bonded tendons in the elastic uncracked, elastic cracked, and ultimate limit state.
- *Volume 2* in progress: Analysis of prestressed and partially prestressed beams with unbonded tendons in the elastic uncracked, elastic cracked, and ultimate limit state; particular application to external prestressing.
- *Volume 2* in progress (or from research papers): Design for serviceability limit states, including fatigue, cracking, and short- and long-term deflections.
- *Volume 2* in progress (or from research papers): Nonlinear analysis of prestressed and partially prestressed beams with both bonded and unbonded tendons; modeling material and sectional behavior (Section 2.4); pseudo-nonlinear analysis and compatibility analysis.
- *Volume 2* in progress (or from research papers): Optimum design concepts and applications to prestressed concrete.
- *Chapter 12* on tensile members: Cover entirely and illustrate the application of optimum design to tensile members.
- *Chapter 13* on columns: Assuming non-slender columns were covered in a first course, revisit this chapter with particular attention to slenderness effect in columns.
- *Chapter 15* on strut-and-tie modeling: After revisiting parts of Chapter 6 for shear, cover this chapter entirely.
- *Volume 2* in progress (or from research papers): Cover the potential use and implications for analysis and design, of fiber reinforced polymeric tendons in prestressed concrete.

- *Volume 2* in progress (or from research papers): Introduction to earthquake-resistant design and detailing of prestressed concrete structures; design for minimum ductility.

Parts of chapters that were omitted during the first course, such as anchorage zone design, prestress losses due to friction and anchorage set, and combined design for shear and torsion, could be covered during this second course as well. Also, it is strongly recommended to assign a term project with some research orientation as a necessary requirement for this second course.

In writing this text, I have attempted to synthesize and convey what I have learned and practically experienced in working with prestressed concrete to date. I believe that a current level of knowledge is only fully understood when a higher level has been attained and exploited. It is my sincere hope that those who will seek knowledge in this book will not be disappointed and will use it to further expand the knowledge base of prestressed concrete for the next generation.

Antoine E. Naaman

ACKNOWLEDGMENTS

ACKNOWLEDGMENTS TO THIS SECOND EDITION

The acknowledgments to the first edition remain applicable and are reproduced below.

Although the author is the main driving force in a textbook writing project, an infinite number of minute tasks contribute to its creation.

I am indebted to the many students who took my courses on prestressed concrete at the University of Michigan over the past twenty years, and who have influenced the approach followed in this second edition by asking pertinent questions and pointing out needed clarification or improvements to the first edition. For the past four years, since I have decided to work on this second edition, many students (some by now colleagues and friends) have helped me review the material in various chapters, check the numerical accuracy of the examples, redraw figures as needed, and add sections when relevant. They have helped make this second edition substantially more complete than the first one. In particular, I extend my sincere appreciation to Kulsiri Chandrangsu, Zuming Xia, Chuchai Sujirorakul, Thanasak Wongtanakitcharoen, Visit Likhitruangsilp, Shih-Ho Chao, and Praveen Chompreda.

Professor John Bolander (University of California, Davis) meticulously reviewed Chapters 1 to 10 and offered numerous constructive comments; Professors Akthem al Manaseer (San Jose State University) and Kiang Hwee Tan (National University of Singapore) kindly reviewed Chapters 1 to 8 and provided input for improvement. Dr. Fadi Al-khairi (Post-Tensioning Institute) provided detailed feedback to Chapter 11, and Professor Gustavo Parra-Montesinos (University of Michigan) expertly reviewed Chapters 6 and 15. I am grateful for their comments, suggestions, critique, and constructive evaluation.

Debbie Hemmeter professionally typed the first draft with constant dependability. Ingrid Naaman provided complete editorial touches with unquestionable reliability. To them, I extend my warmest gratitude.

Material taken and/or adapted from the American Concrete Institute (ACI) building code, other ACI Recommended Practices, and the AASHTO LRFD Bridge Design Specifications appears frequently throughout the text. The courteous cooperation of the ACI and AASHTO is gratefully acknowledged.

Many organizations graciously agreed to have materials or photographs reproduced in this second edition. They include:

Arenas and Asociados
Bouygues
Carl Walker, Inc.
Dywidag Systems International, Inc.
Figg Engineering
Freyssinet International
Precast/Prestressed Concrete Institute
Post-Tensioning Institute
T.Y. Lin International
VSL Corporation

Their help is kindly acknowledged.

I am particularly grateful to the University of Michigan for providing me an environment fostering excellence; I am grateful to my students who, by giving me the opportunity to teach, also gave me the opportunity to learn and develop.

Antoine E. Naaman

ACKNOWLEDGMENTS TO THE FIRST EDITION

Many people deserve my gratitude for their contribution to this volume and I would like to thank them for their help. I am particularly indebted to Daniel P. Jenny of the Prestressed Concrete Institute for his careful review of and constructive comments on the entire manuscript. Invaluable suggestions were also made by Professors E. J. Nawy, T. T. C. Hsu, M. K. Tadros, A. H. Mattock, and P. Balaguru, who all reviewed portions of the manuscript.

Special thanks are due to my former student, K. Visalvanitch, who reviewed the arithmetic of the entire manuscript with devotion and competence; to many students who, with or without their knowledge, have assisted throughout the years in checking examples and problems; to George D. Nasser of the Prestressed Concrete Institute for his generous, unconditional help in suggesting and providing photographs and figures from PCI publications; to Professor S. P. Shah, who was among the few to encourage me to undertake this project; and, finally, to my wife, Ingrid, for her careful typing and editing of the initial manuscript and for her support during this demanding endeavor.

Material taken and/or adapted from the American Concrete Institute (ACI) building code and other ACI Recommended Practices appears frequently throughout

the text. The courteous cooperation of the American Concrete Institute is gratefully acknowledged.

Many other individuals and organizations have given me their permission to adapt, use, or reproduce material from their publications in this book; I thank them for their courtesy. They are:

Abam Engineers, Inc.
American Associate of State Highway and Transportation Officials
Arvid Grand and Associates
Bureau BBR, Ltd. (Switzerland)
California Department of Transportation
Canadian Prestressed Concrete Institute
CCL Systems, Ltd. (U.K.)
CN Tower Limited (Canada)
Concrete Technology Corp.
C.V.G. – EDELCA (Venezuela)
Dywidag Systems International, Inc.
Engineering News-Record
Figg and Muller Engineers, Inc.
FIP, Fédération Internationale de la Précontrainte (U.K.)
Freyssinet International, Inc.
Ingenieurburo H. Rigendinger (Switzerland)
Inryco Inc., Post-Tensioning Division
Kurt Orban Company, Inc.
Mr. R. L'Hermite (France)
Material Service Corporation
Norwegian Constractors Group (Norway)
Portland Cement Association
Post-Tensioning Institute
Sika Chemical Corporation
Somerset Wire Company, Ltd. (U.K.)
Sumitomo Electric Industries, Ltd. (Japan)
Superior Concrete Accessories, Inc.
Supreme Products Division, The Measuregraph Company
TNO Metal Research Institute (The Netherlands)
U.S. Army Corps of Engineers (Sacramento District)
University of Illinois at Chicago Circle
VSL Corporation
Mr. R. J. Wheen

Antoine E. Naaman

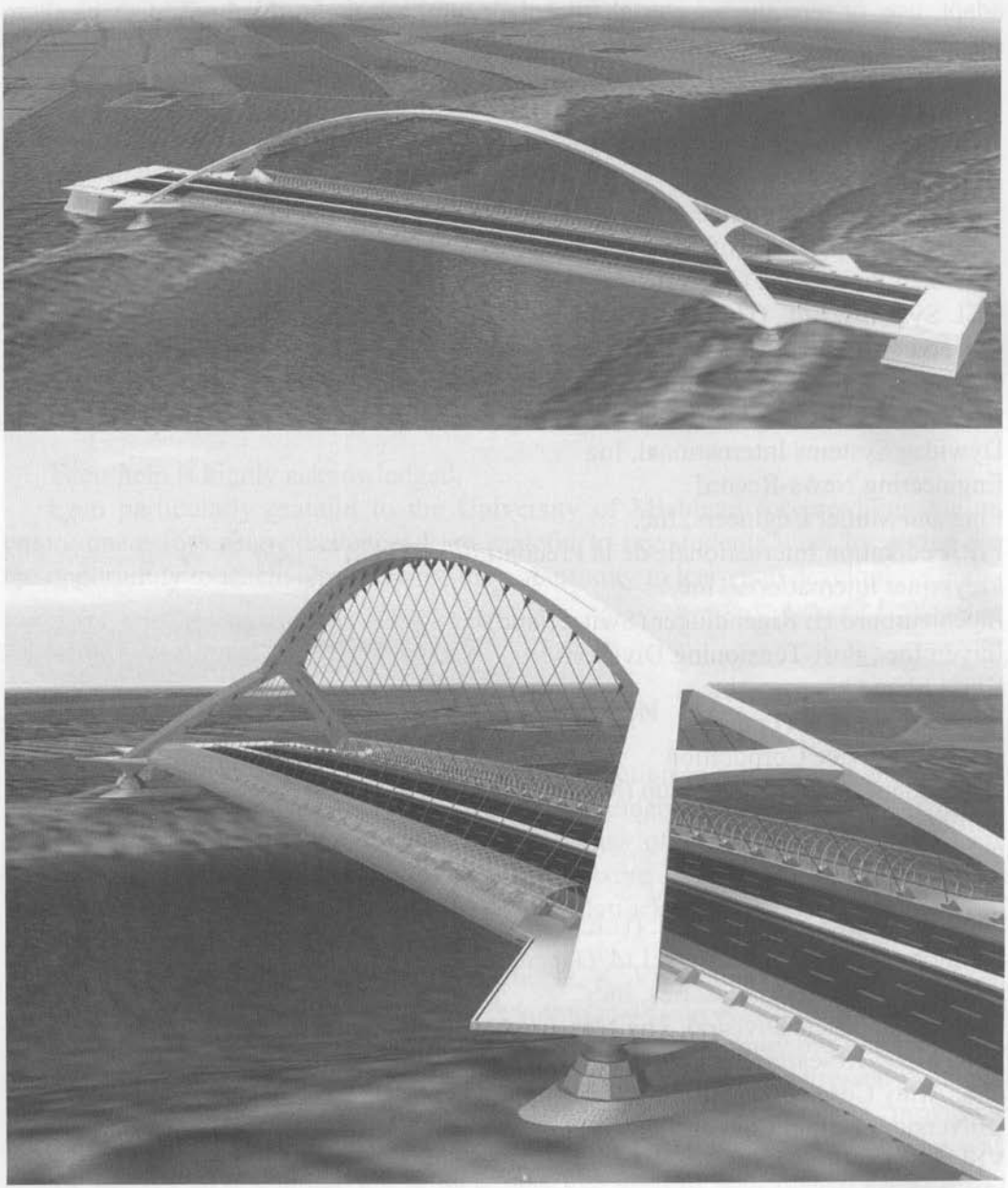

Model of the Third Millennium Bridge, Zaragoza, Spain. Designed by Arenas & Asociados, it spans 270 meters over the Ebro river. The deck is a prestressed concrete structure with internal bonded prestressing and external prestressing. The deck is designed primarily as a tensile member to resist the thrust from the arch. (*Courtesy Juan Arenas*).

PRINCIPLE AND METHODS OF PRESTRESSING

1.1 INTRODUCTION

Prestressing is the deliberate creation of permanent internal stresses in a structure or system in order to improve its performance. Such stresses are designed to counteract those induced by external loadings. Prestressing generally involves at least two materials, the stressor and the stressee which, when acting together, perform better than either one taken separately. Prestressing is a principle. The French mathematician Henri Poincaré once said, "A principle is neither true nor false, it is convenient." The principle of prestressing is indeed very convenient and has been widely applied. Its application to steel and concrete is relatively recent but has taken by far the biggest proportions.

The application of prestressing to concrete is in a way a natural result. Concrete is strong in compression and weak in tension. For design purposes its tensile resistance is discounted. Prestressing the concrete produces compressive stresses, either uniform or nonuniform, which will counteract tensile stresses induced by external loadings. The original concept, as promoted by Freyssinet [Refs. 1.5, 1.6], attempted to counteract tensile stresses entirely, thus producing a crack-free material during service. However, it has since evolved to counteract only in part externally-induced tensile stresses, thus allowing tension and controlled cracking in a way similar to reinforced concrete. This has led to what is called partial prestressing.

Partially prestressed concrete occupies the whole spectrum of the reinforcing range between fully reinforced and fully prestressed concrete. In a way it is a combination of both. Today it has become difficult to talk about either material separately, without talking about their combination. Since essentially they use the same basic components, steel, and concrete, their historical development will eventually be addressed simultaneously. Already, the term "structural concrete" is used by U.S. and European organizations to provide a unifying treatment of the subject. However, in this text we will mostly focus on the development of

prestressed concrete while pointing out similarities in treatment or approaches with reinforced concrete whenever possible.

1.2 EXAMPLES OF PRESTRESSING

Examples of prestressing are numerous among manufactured tools and products. Indeed, some are very old and illustrate the principle of prestressing. The hunter's bow is prestressed by the string to achieve a sharp recoil action during ejection of the arrow. The dried wooden staves forming a wooden barrel are prestressed by tightening metal bands around them. When the barrel is filled with liquid, the wooden staves expand, the prestress is increased and leakage is prevented. To prevent the relative movement between the iron tire and the wooden rim of a cartwheel, the tire is fitted around the rim while in a heated state. Upon cooling, contraction of the tire produces a permanent prestress in the form of a radial compression on the rim. The blade of a frame saw is prestressed (in tension) by twisting a rope at the opposite end of the frame (Fig. 1.1a). During the cutting operation the blade is pushed or pulled through the wood being cut. Part of the blade is subjected to external compression while the other is subjected to tension. The compression is counteracted by the internal pretension, thus no buckling occurs while tension adds up to the existing tension and the blade remains rigid. The spokes of the wheel of a bicycle are put in tension between the outer and inner rims (Fig. 1.1b). When load is applied to the axle, the lower spokes decompress but remain in tension while the upper spokes undergo increased tension. As all spokes remain in tension, the wheel keeps its rigidity. Tempered glass offers another example of prestressing where upon forming, the glass sheet is rapidly cooled. The skin, which cools first, gains rigidity and is slowly compressed by the core during its own hardening. Putting the skin in compression reduces the occurrence of surface cracks and decreases the risk of fracture under loading. The reader is encouraged to solve Problem 1.1 and develop figures similar to Figs. 1.1 and 1.2 for the system selected, with particular attentions to showing the corresponding forces acting on each material, and explaining how the system performs better because of their interaction.

Generally all concrete structures are reinforced with some type of reinforcement. Non-reinforced concrete members are assumed to carry only small gravity loads or perform non-critical, non-life-threatening load carrying function such as a slab on grade or a low height retaining wall. It would be unsafe to use a non-reinforced concrete beam to sustain any external load including its own weight. Figure 1.2a illustrates the response of such a beam under service load and how the reinforcement is placed to prevent its collapse. In reinforced concrete, reinforcing bars are placed where tension and cracking are expected, and become truly effective only when cracking occurs. In prestressed concrete, the tendons are stressed to apply a compressive force balancing the externally induced tensile stresses and preventing cracking. Here the reinforcement can be described as active as compared to being

passive for reinforced concrete. Figure 1.2b illustrates the effect of prestressing for a structural concrete member subjected to tension. The reinforced concrete member will crack under load. The prestressed concrete member will not crack because the uniform pre-compression stress induced by prestressing balances the tensile stresses induced by external loads; the resulting stress remains a compressive stress throughout the member.

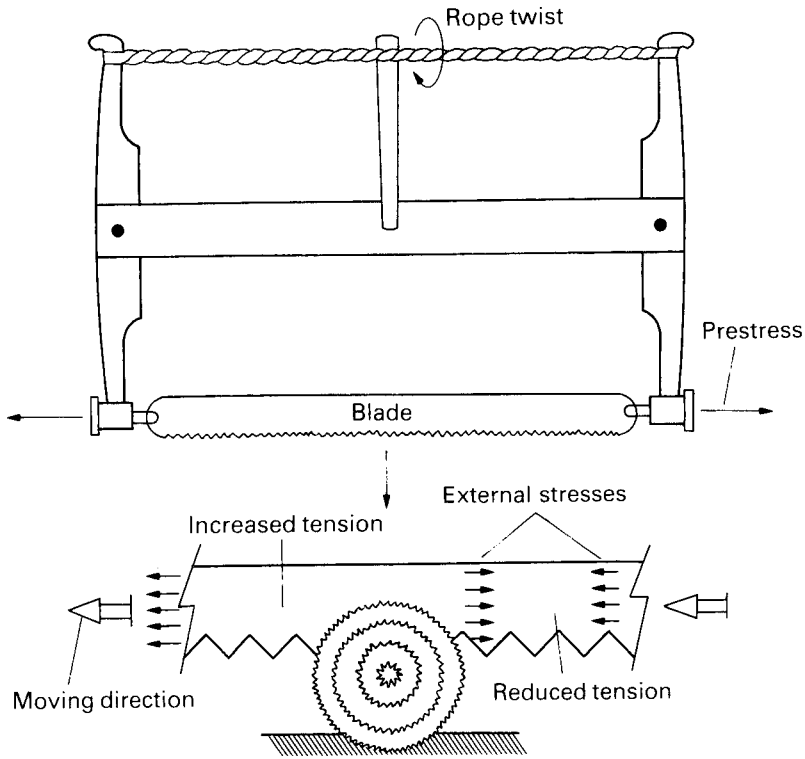

Figure 1.1a Prestressing in a frame saw.

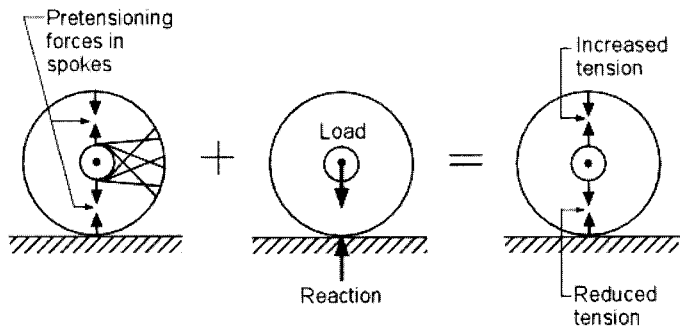

Figure 1.1b Prestressing in a bicycle wheel.

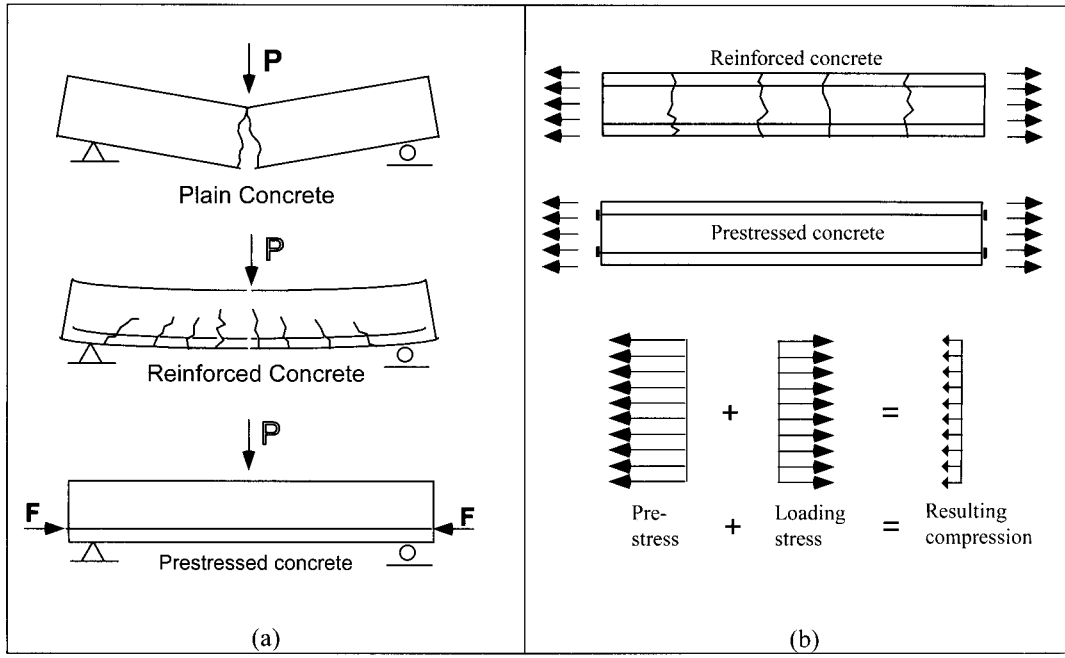

Figure 1.2 ***(a)*** **Response of plain, reinforced, and prestressed concrete to service loading.** ***(b)*** **Internal stresses designed to balance external stresses in prestressed tensile members.**

1.3 HISTORY OF PRESTRESSED CONCRETE

The first application of prestressing to concrete appears to be by P. H. Jackson, an engineer from California. In 1886 [Ref. 1.1] he obtained a U.S. patent for tightening steel tie rods in artificial stones (concrete blocks) and concrete arches used for slabs and roofs (Fig. 1.3). Shortly thereafter, in 1888, C. E. W. Doehring from Germany also obtained a patent [Ref. 1.2] for prestressing concrete slabs with metal wires. However, the performance of the first prestressed concrete structural elements was hindered by the low steel strengths available at the time. Because of the relatively low steel stresses used and the relatively high prestress losses due to creep and shrinkage of the concrete, the prestress would soon diminish dramatically, or vanish altogether. Retensioning was suggested by G. R. Steiner (United States,1908) to overcome this problem, while other researchers such as J. Mandl and M. Koenen [Ref. 1.3] of Germany attempted to identify and quantify prestress losses.

However, it was the French engineer Eugene Freyssinet [Refs. 1.5, 1.6] who first understood the importance of prestress losses and proposed ways to overcome them. Based on the experience in building arch bridges (at Vendre in 1907 and Plougastel in 1927) and prestressing them by external jacking at the crown to facilitate formwork removal, he suggested that very high strength steels and high elongations

must be used in prestressed concrete. High steel elongations would not be entirely counteracted by the shortening of the concrete due to creep and shrinkage. Later, in 1940, he introduced his first prestressing system, a wedge-anchored cable with 12 wires the principle of which is still in use today. Thereafter, he designed and built many bridges in prestressed concrete, starting with the bridge at Luzancy, France, in 1941. At that point the applications of prestressed concrete took off with much vigor in France and Europe and leaped into full competition with structural steel.

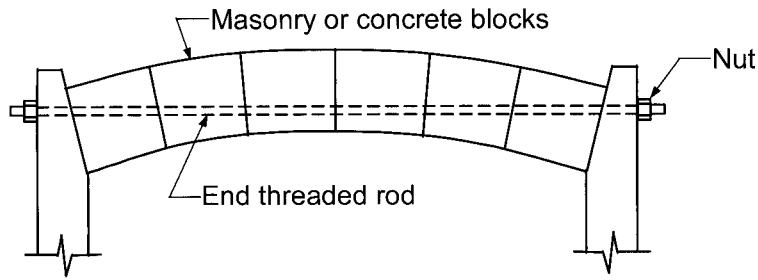

Figure 1.3 Jackson's first patent on prestressed concrete.

Although prestressed concrete planks and fence posts were produced by R. E. Dill in the United States since 1925 [Ref. 1.4], it was only in 1949/1950 that the first prestressed concrete bridge, the 155-foot-span (47-meter) Walnut Lane Bridge in Philadelphia, was built.

Simultaneously to and in continuation of the developments brought by E. Freyssinet many researchers contributed greatly to the full expansion of prestressed concrete. They include G. Magnel of Belgium [Ref. 1.10], Y. Guyon of France [Ref. 1.12], P. Abeles of England [Ref. 1.14] who developed the concept of partial prestressing, F. Leonhardt of Germany [Ref. 1.15], V. V. Mikhailov of Russia [Ref. 1.17], and T. Y. Lin of the United States [Ref. 1.26] to whom we owe the design method of load balancing which is so convenient for indeterminate structures (see Chapters 10 and 11).

Many prestressing systems and techniques were also developed and today prestressed concrete is widely accepted and used. Numerous books and textbooks on the design and construction of prestressed concrete structures were written and many associations and institutes contribute to the advancement of the state-of-the-art on prestressed concrete [Refs. 1.16 to 1.53].

Decades of experience have given prestressed concrete a proven record of reliable performance. At present, applications of prestressed concrete essentially occur in every structural element or building system: bridges, building components such as beams, slabs and columns, pipes and piles, pavements, ties, tanks, tunnels, stadia, nuclear power vessels, TV towers, floating storage, and offshore structures. Some examples are shown in Figs. 1.4 and 1.5.

(a) **The Pine Valley Creek Bridge was built by cast-in-place segmental cantilever construction with a main span of 450 ft (138 m).** *(Courtesy California Department of Transportation.)*

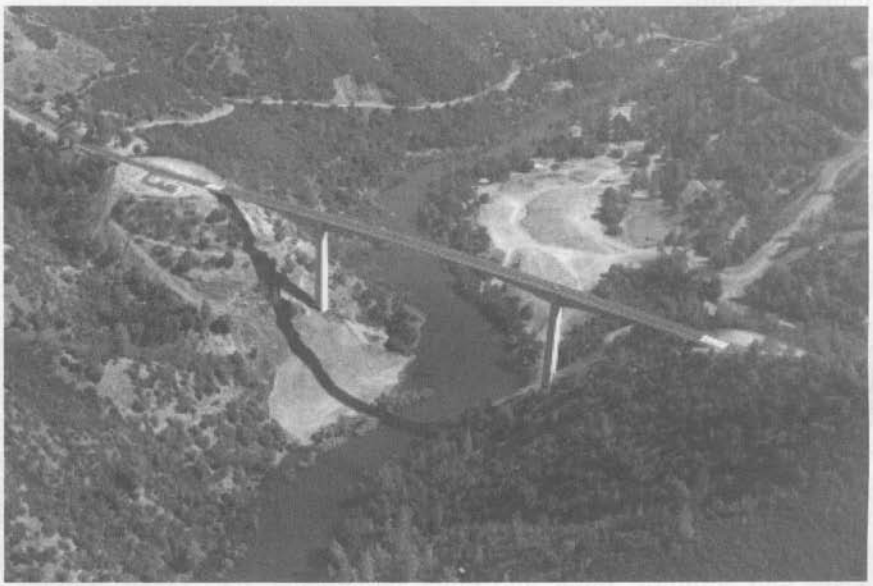

(b) **The Parrotts Ferry Bridge, California, has a main span of 640 ft (195 m), the longest lightweight concrete span in the world.** *(Courtesy U.S. Army Corps of Engineers.)*

Figure 1.4 Examples of prestressed concrete bridges.

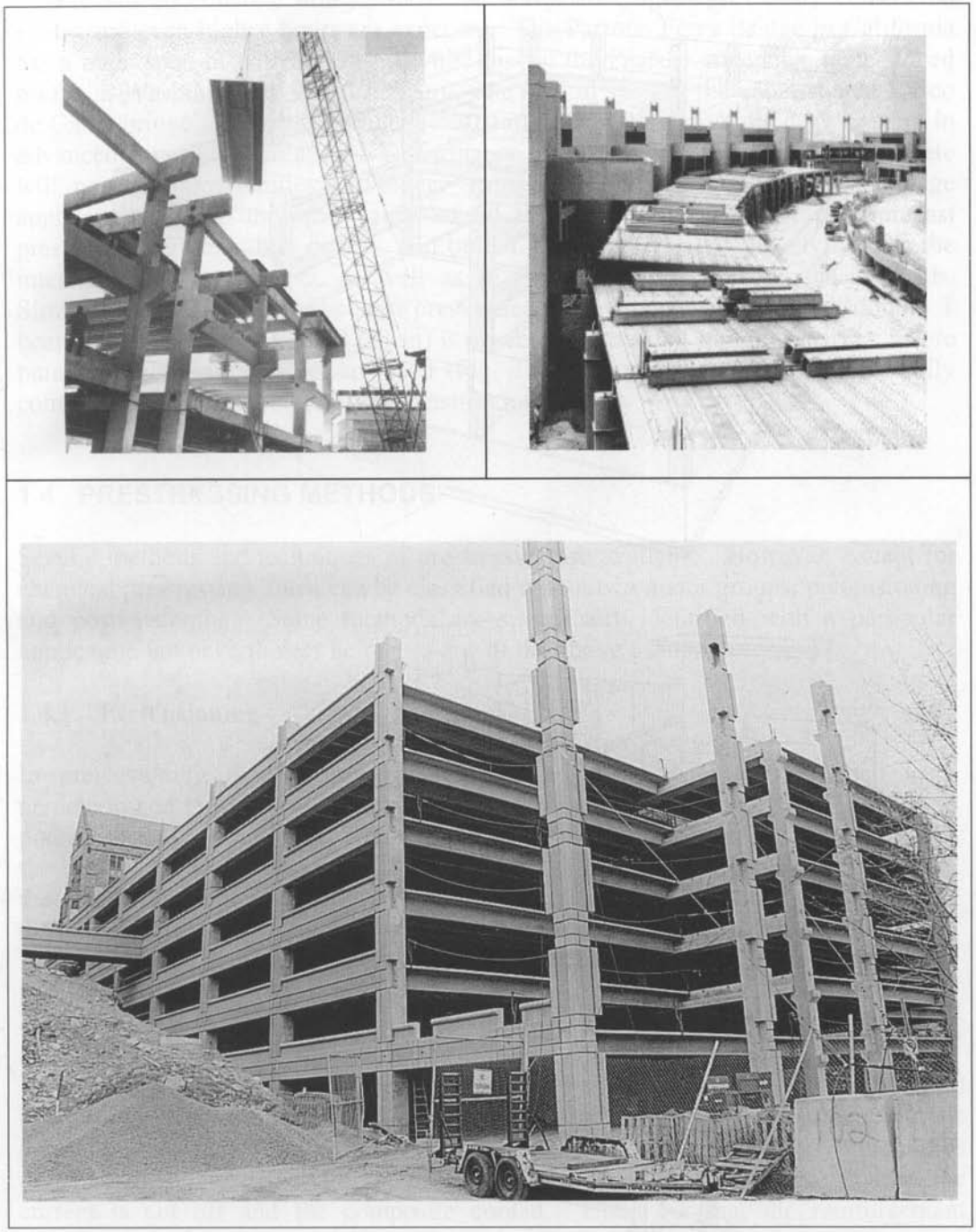

Figure 1.5 Examples of precast prestressed building structures.
(Courtesy Precast/Prestressed Concrete Institute.)

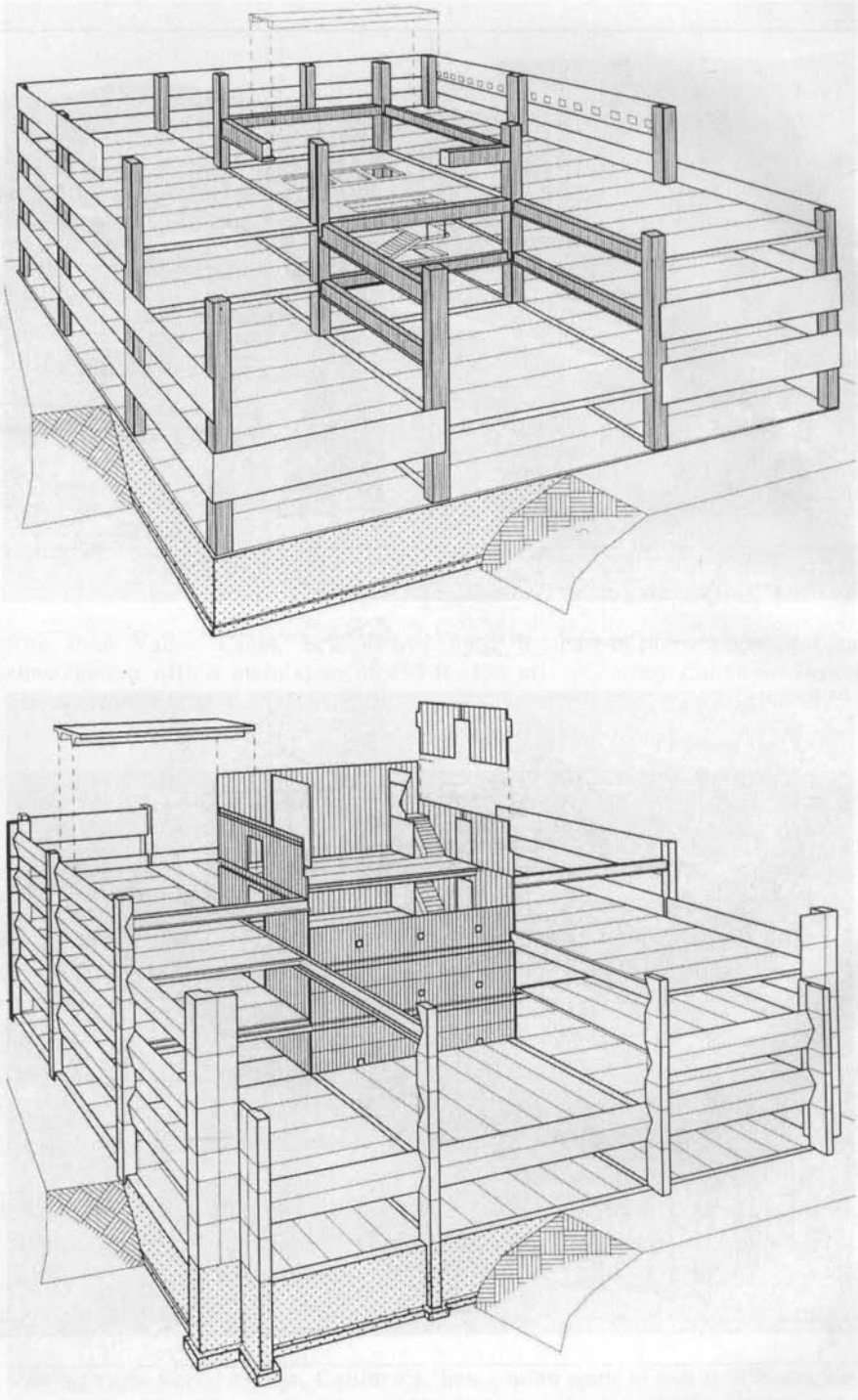

Figure 1.6 Typical building systems using precast prestressed concrete frames and shear walls. *(Courtesy Precast/Prestressed Concrete Institute.)*

Prestressed concrete bridges have reached span lengths previously considered exotic and even higher limits are expected. The Parrotts Ferry Bridge in California has a main span of 640 ft (195 m) while that of the Pasco-Kennewick cable-stayed bridge in Washington is 981 ft (299 m). The central span of the cable-stayed Vasco de Gama bridge in Lisbon, Portugal, is 420 m (1378 ft). Continued development in advanced materials such as high performance concrete and fiber reinforced concrete will provide opportunities for longer spans. In the United States bulk bridge applications are in the span range of 50 to 150 ft (15 to 46 m) with precast prestressed I girders, box girders, and bulb T girder bridges extensively used in the interstate highway system, as well as in most highways and secondary roads. Similar extensive usage of precast prestressed hollow-cored slabs, T and double T beams of spans of up to 100 ft (31 m) is observed in the U.S. building market, where numerous building systems are used (Fig. 1.6) making prestressed concrete fully competitive in many sectors of the construction industry.

1.4 PRESTRESSING METHODS

Several methods and techniques of prestressing are available. However, except for chemical prestressing, most can be classified within two major groups: pretensioning and posttensioning. Some methods are specifically identified with a particular application but nevertheless belong to one of the above groups.

1.4.1 Pretensioning

In pretensioning the prestressing tendons (wires, strands) are stretched to a predetermined tension and anchored to fixed bulkheads or molds. The concrete is poured around the tendons, cured, and upon hardening the tendons are released. As the bond between the tendons and the concrete resists the shortening of the tendons, the concrete is compressed. The prefix "pre" in pretensioning refers to the fact that the tendons are put in tension *prior* to hardening of the concrete.

In order to stretch the tendons, hydraulic jacks are generally used. Once the predetermined elongation is reached, the tendons are anchored to the bulkhead using anchors similar to those described for posttensioning. Anchors for individual strands are also called chucks. A typical chuck anchor is shown in Fig. 1.7.

Another technique for stretching the tendons is electrothermal or electrical prestressing, where high-strength deformed bars are heated by means of an electric current between 250° C and 450° C, then placed and anchored at the ends of the molds or a pretensioning bed. After pouring and hardening of the concrete matrix, the current is cut off and the composite cooled. Upon cooling, the reinforcement shortens, inducing compressive stresses in the matrix.

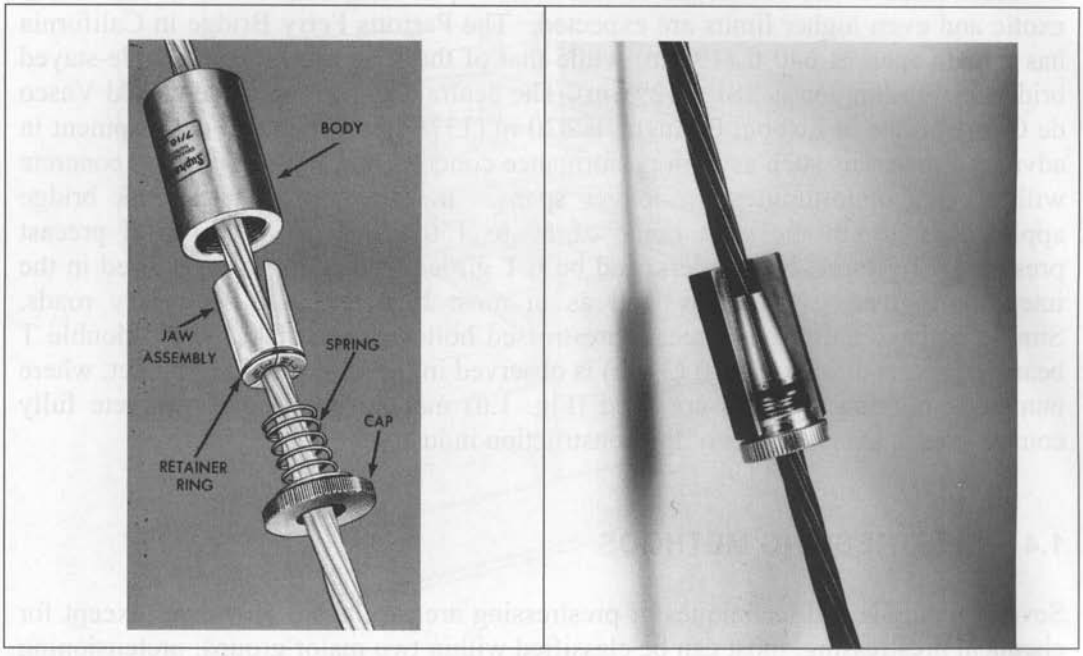

Figure 1.7 Typical chuck anchor for a single tendon. *(Courtesy Supreme Products Corporation.)*

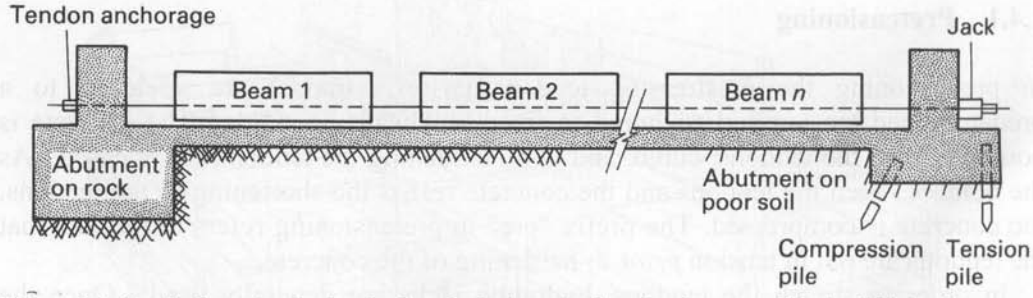

Figure 1.8 Typical pretensioning bed and abutments showing beams with straight tendons.

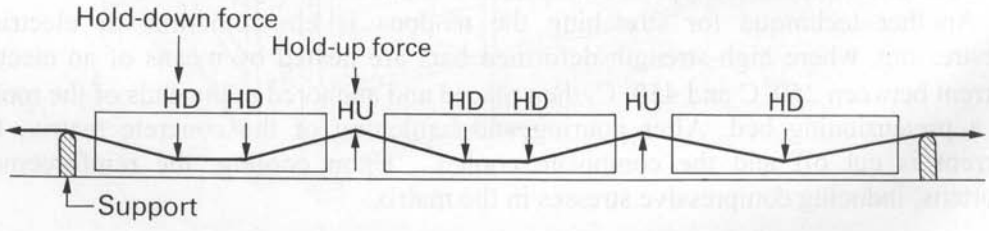

Figure 1.9 Typical pretensioning tendons profile with one or two draping points.

Electrochemical prestressing is not used in the United States but has been used in the Soviet Union and Eastern Europe. Its application was limited because it requires extra safety precautions and only leads to relatively low levels of prestress.

Depending on the pretensioned structural elements produced, the profile of the tendons is either straight (Fig. 1.8), such as in hollow-cored slabs, or allows for one or two deflection points (also called draping or hold-down points) such as in bridge girders (Fig. 1.9). Draping is generally achieved by pulling or pushing down part of the tendons to the desired position. A sketch of the "hold-down" procedure and typical draping devices is shown in Fig. 1.10. Whenever technically possible and for economy, contractors prefer single draping point to double-draping points.

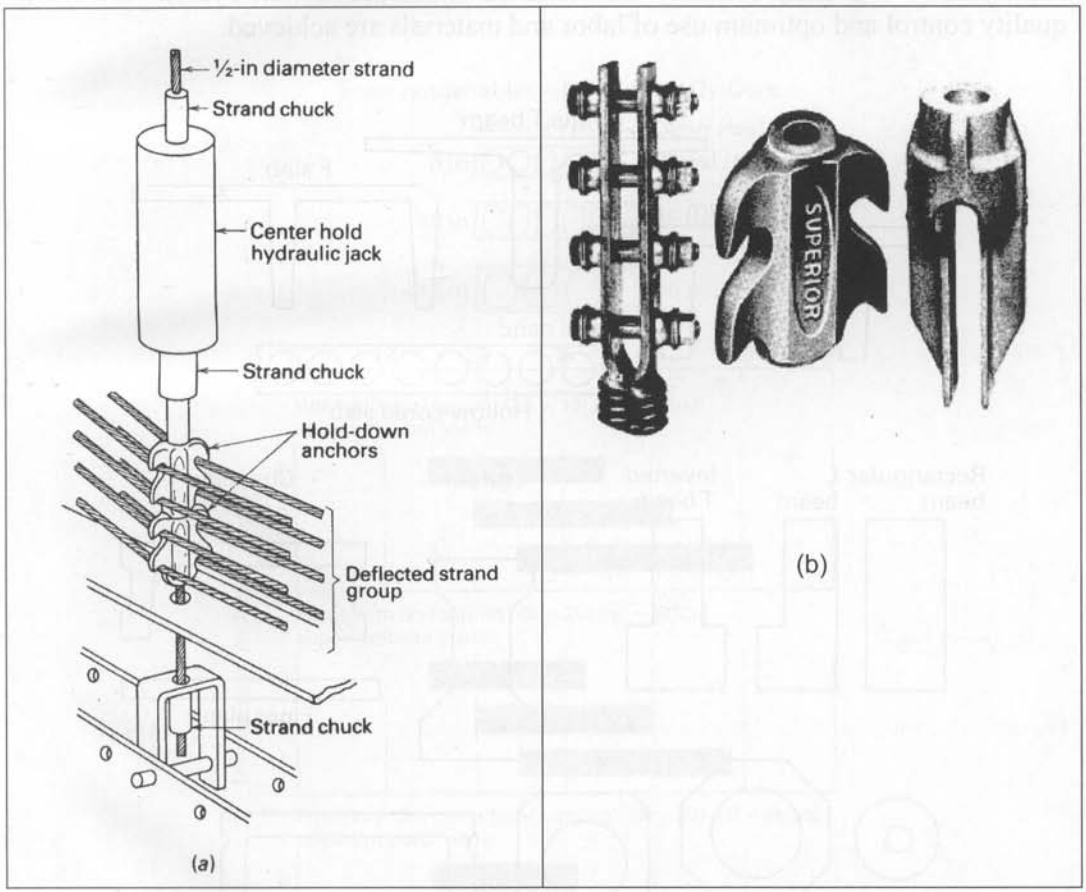

Figure 1.10 Typical hold-down procedure and typical hold-down anchors for draping prestressing strands. *(Courtesy Superior Concrete Accessories, Inc.)*

Small-diameter tendons are generally used in pretensioning to allow for the bond between steel and concrete to develop over a short distance. The most popular sizes

in the United States are the 3/8-in (9.5-mm-), the 1/2-in (12.5-mm-), and the 0.6-in (15.24 mm) diameter strands.

Pretensioning is the method most often used for the production of precast prestressed concrete elements in the United States, because it offers great potential for mechanization. Efficient long-line production techniques with casting bed lengths of up to 600 ft (182 m), where individual elements are cast end to end, are preferred, because they require a single tensioning operation. Elements of standardized cross sections are mass produced yet customized by varying the length of each element and by placing inserts, holes, or blockouts for the mechanical or electrical distribution systems. Accelerated curing often permits early removal of the elements and daily reuse of the forms (24-hour production cycle). Excellent quality control and optimum use of labor and materials are achieved.

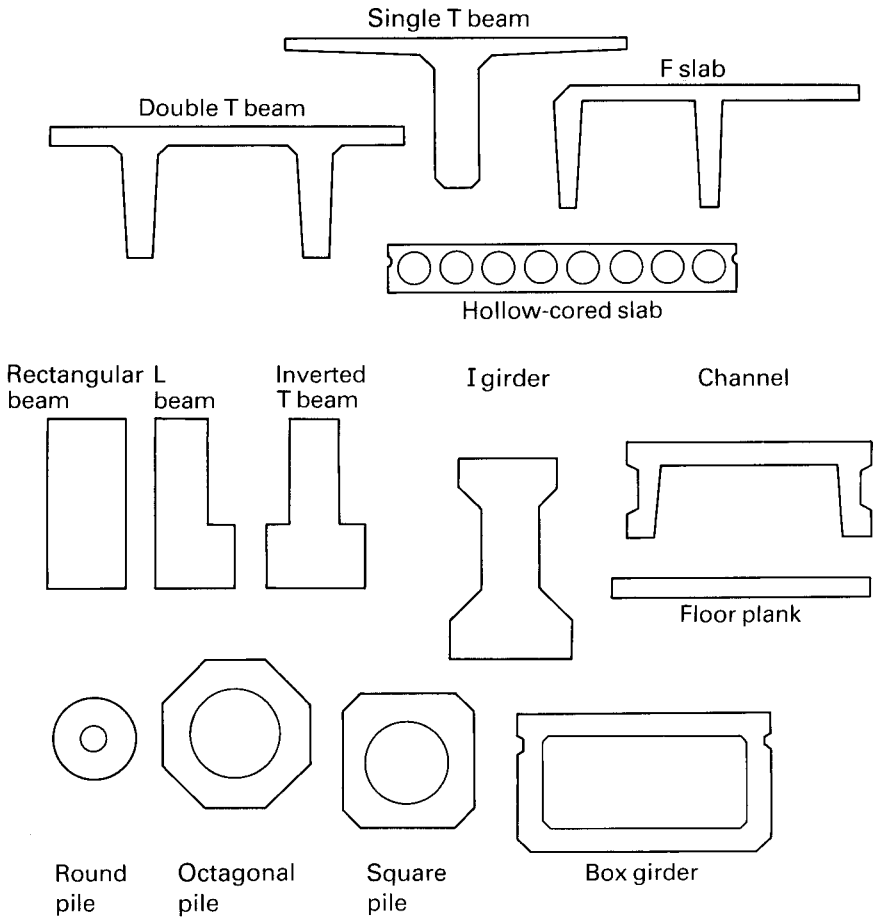

Figure 1.11 Typical standard sections of precast prestressed concrete products in the United States.

Typical elements and member cross sections aimed at particular applications were developed and standardized. The most common standard shapes in the United States are shown in Fig. 1.11. Spans of up to 150 ft (46 m) are not uncommon and are mostly limited by transportation and erection constraints. The longest single span precast prestressed bridge beams, known to the author, were used in the Bow Bridge near Calgary, Canada, where the span was 211 ft (64.5 m). Higher spans can be achieved by splicing, where two or three pretensioned elements are transported to site and assembled by posttensioning. Load tables and charts were developed by the industry so that for a given standard shape, external load, and span, the most appropriate section and tendon arrangement can be readily selected [Ref. 1.44]. A typical example is shown in Fig. 1.12 for hollow-cored slabs.

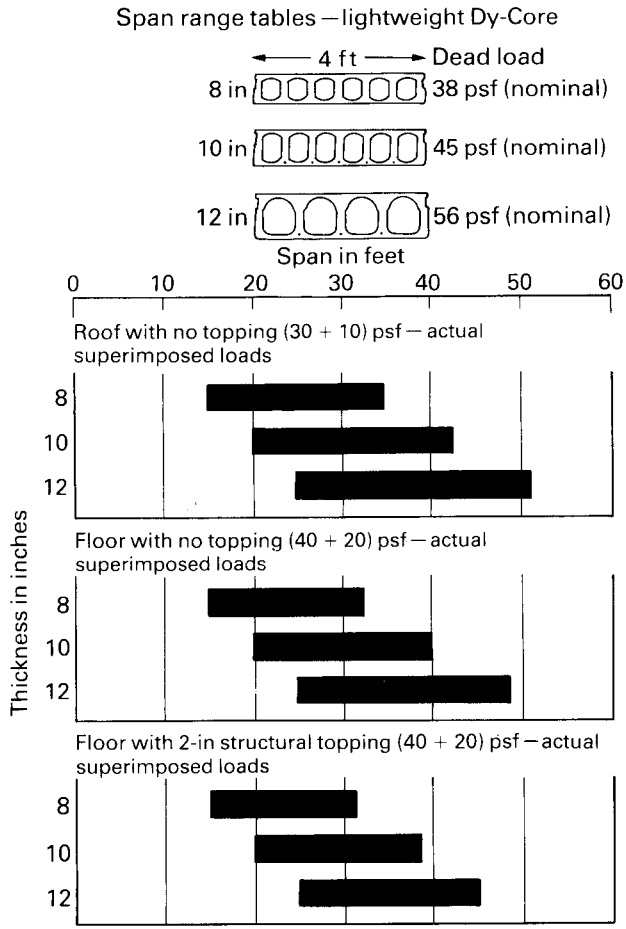

Figure 1.12 Example of load chart for prestressed hollow-cored slabs. *(Courtesy Material Service Corporation.)*

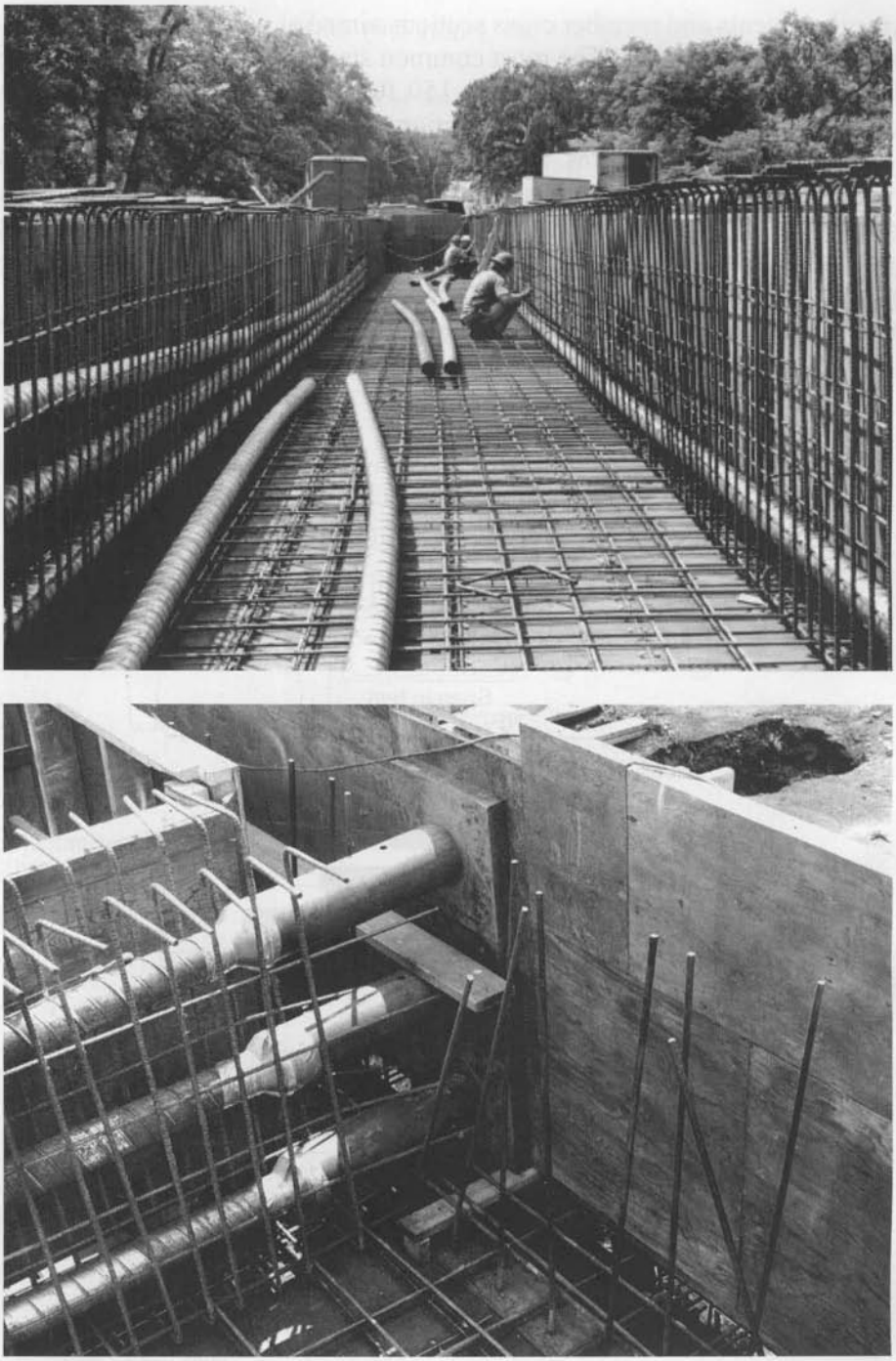

Figure 1.13 Sequential steps in posttensioning operations. *(Courtesy Inryco Inc., Post Tensioning Division.)*

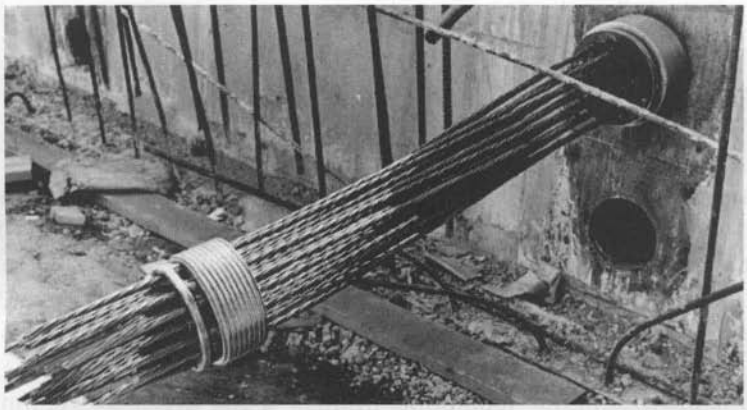

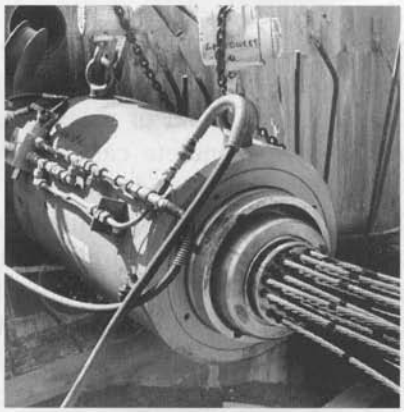

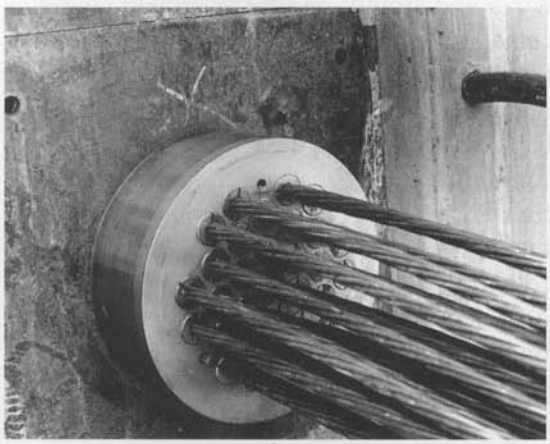

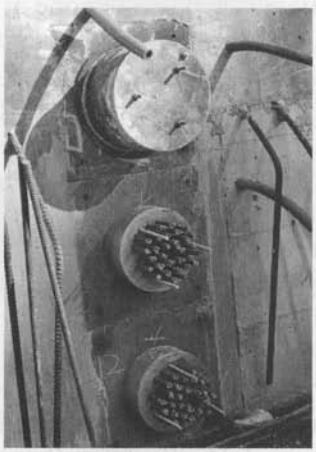

Figure 1.13 continued

1.4.2 Posttensioning

In posttensioning the tendons are stressed and anchored at the ends of the concrete member *after* the member has been cast and has attained sufficient strength.

Commonly, a mortar-tight metal pipe or duct (also called sheath) is placed along the member before concrete casting. The tendons could be preplaced loose inside the sheath prior to casting or could be placed after hardening of the concrete. After stressing and anchoring, the void between each tendon and its duct is filled with a mortar grout which subsequently hardens. Grouting ensures bonding of the tendon to the surrounding concrete, improves the resistance of the member to cracking and reduces the risks of corrosion for the steel tendons. Figure 1.13 gives a perspective of some typical posttensioning operations.

The above posttensioning technique implies using what are commonly called "bonded tendons." If the duct is filled with grease instead of grout, the bond would be destroyed throughout the length of the tendon, and the tendon force would apply to the concrete member only at the anchorages. This leads to "unbonded tendons." Unbonded tendons are generally coated with grease or bituminous material, wrapped with waterproof paper or placed inside a flexible plastic hose, and positioned in the forms prior to concrete casting. When the concrete gains sufficient strength, the tendons are stressed and anchored. They remain unbonded throughout their length and during service life of the structure. This technique is widely used in slab systems of residential and parking structures with several bays, because of its extreme efficiency and economy. The tendons are put in tension at the periphery of the slab and can span up to 10 consecutive bays. In external prestressing applications (see Section 1.6.1) the tendons are unbonded but placed outside (i.e., are not in contact with) the concrete section.

The tendons generally used in posttensioning are made out of wires, strands, or bars. Bars are tensioned one at a time, wires and strands can be tensioned singly or in groups. In one of the Freyssinet systems, 12 wires or strands forming a tendon can be pulled simultaneously. Up to 170 wires with 0.25 in (6.35-mm) diameter, can form a single tendon in the BBRV system and up to 31 strands with 0.6-in (15.2 mm) diameter can form a single tendon in the VSL system. These tendons carry very large forces. Tendons with a capacity of up to 1000 tons are commonly used in nuclear vessels. They often need specialized jacking and anchoring equipment. Typical anchorages based on different approaches are shown in Fig. 1.14 (see also Section 1.5). The proper construction, protection, and tensioning of a tendon with a large number of strands, such as in cable-stayed bridges is, by itself, a special technology. Hydraulic jacks are normally used and, along with tendons and anchorages, they are often an integral part of the posttensioning system selected. These systems are reviewed in Sec. 1.5.

Figure 1.15 illustates the components of post-tensioning applied to a typical bridge section. It can be observed that different technologies must be developed to effectively carry out a number of tasks (threading, tensioning, grouting, etc.).

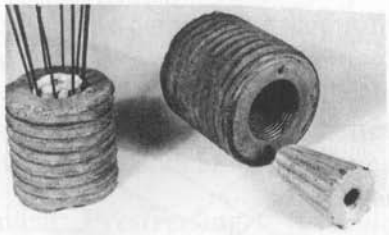

First Freyssinet wedge cone for 12 wires.

Freyssinet wedge cone for 12 strands.

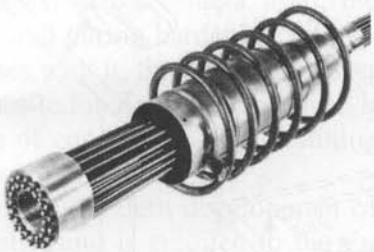

BBRV anchorage for buttonhead wedges.

Freyssinet multistrand K range anchorage.

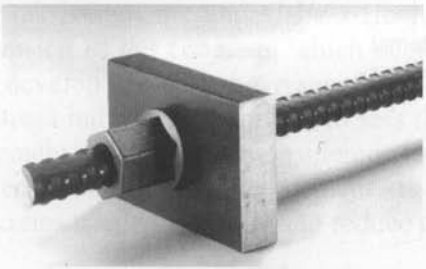

Dywidag threaded bar anchorage.

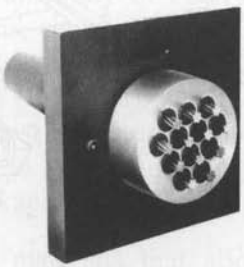

VSL multistrand type E anchorage.

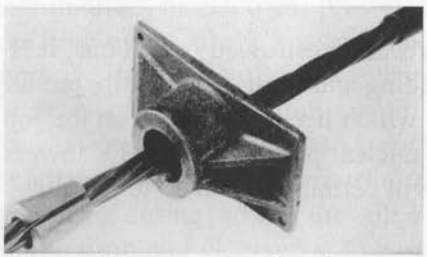

Inryco Cona monostrand anchorage.

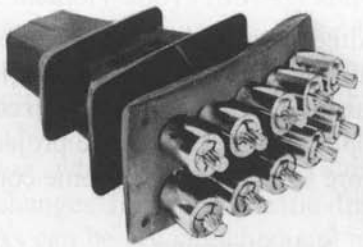

CCL systems multistrand anchorage.

Figure 1.14 Typical anchorages used in various prestressing systems.

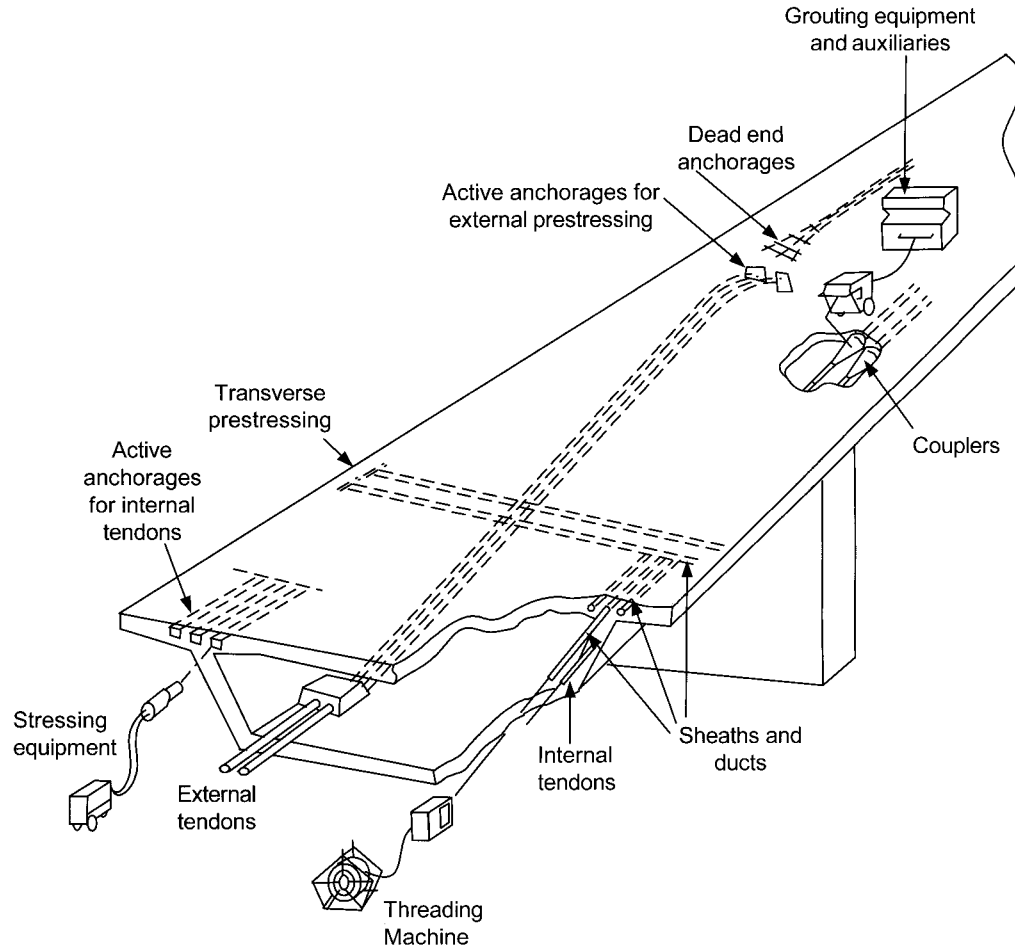

Figure 1.15 Essential components of post-tensioning operations. *(adapted from a brochure by Freyssinet.)*

Although posttensioning can be used in precast prestressed operations, it is most useful in cast-in-place construction where building and bridge girders are too large to be transported, and for customized structures which need tensioning on the job site. Its application in large scale projects, such as nuclear power vessels, TV towers, and offshore structures has become common and will certainly continue to expand.

1.4.3 Self-Stressing

Pretensioning and posttensioning represent two groups to which most prestressing techniques belong. Three other known methods of prestressing use the concept of self-stressing to minimize labor cost. They are: electrical or electrothermal

prestressing, expansive cement prestressing, and the use of special prestressing materials with deformation controlled recovery properties such as shape memory alloys (SMA). As mentioned above electrothermal prestressing could be considered a pretensioning method as well. In expansive cement prestressing, the matrix is responsible for activating self-stressing, while in the case of SMAs, it is the reinforcement. Both also could be used simultaneously.

Chemical Prestressing. Chemical prestressing, is not part of either the pretensioning or the posttensioning methods. In chemical prestressing the tendons are preplaced untensioned in the forms before the concrete is poured. Due to the special expansive cement used, the concrete, instead of shrinking, expands after curing and during hardening. As the steel is bonded or anchored to the concrete, it stretches with it, thus undergoing tension and inducing compression in the concrete. The tensile force must be balanced by the compression force in the matrix leading to a state of equilibrium. The resulting compressive stresses in the matrix creates the benefits of prestress.

The first modern development of expansive cement and its potential application to prestressing is credited to the French engineer, Henri Lossier [Ref. 1.7, 1946]. The idea was further developed in the Soviet Union [Ref. 1.11] and in the United States, mainly at the University of California, Berkeley [Ref. 1.13]. It was believed that chemical prestressing can be applied to elements with low levels of prestress, such as pavements and slabs. However, due to the difficulty of controlling the expansion of the concrete, which occurs in all directions, chemical prestressing did not develop beyond the research field in the United States. Also the effective prestress induced was limited to less than about 200 psi (1.4 MPa), which except in pavement systems is considered insufficient for most structural applications. Nevertheless, expansive cement is being applied to shrinkage-compensating concretes used in long slabs to reduce or eliminate shrinkage joints.

Shape Memory Materials. Today there are smart materials that allow us to envision self-stressing with effective prestress levels that can be controlled much more accurately, and can be of much larger magnitude than achieved with expansive cement matrices or electrical prestressing. Shape memory alloys (SMAs) and some special polymeric fibers possess the unique property of being able to be frozen temporarily in a particular state, then, with proper heat or radiation treatment, go back to a prior equilibrium state. The temperature dependent shape change (expansion-contraction) of SMAs, such as nitinol (Ni-Ti), is based on the crystalline phase change known as *martensitic transformation*, which occurs over a range of temperatures during which the alloy structure changes from martensitic form to austenitic form and vice-versa. In particular, SMAs can be pre-stretched and remain stable in this state at room temperature; then they can be used as reinforcement as in conventional reinforced concrete; however, after hardening of the concrete matrix, they can be heated to recover their deformation hence inducing prestressing. Compared to electrical prestressing, these materials do not need costly specialized

electric equipment and do not create safety problems in the field. The treatment (heat or radiation) can be applied any time after hardening of the matrix instead of during its curing and hardening. The special reinforcement needed, such as SMAs or special polymeric fibers, can be factory produced, stored, shelved, placed in the composite, and triggered to recover its deformation (inducing prestressing) at any appropriate time.

The idea of using advanced materials with properties that enable controlled deformation recovery is relatively new in prestressed concrete and, at time of this writing, only a few studies have been carried out [Ref. 1.43]. With the use of shape memory alloys, prestress levels can be controlled much more accurately, and can be of much larger magnitude. In laboratory experiments about 1200 psi (8.4 MPa) average prestress has been so far achieved.

Compared to pretensioning, the use of self-stressing by shape memory materials allows the reinforcement to be formed in any shape in two or three dimensional space without special devices. Compared to the use of expansive cement prestressing, the use of shape memory materials leads to better control of the prestress and higher levels of effective prestress. Compared to electrothermal prestressing, the use of shape memory materials provides higher levels of prestress and eliminates the need to be heated during the hardening stage of the concrete matrix. It is likely that their use in prestressed concrete will become widespread once their cost becomes competitive.

Finally, it is conceivable to combine the previous two self-stressing methods, that is, to have a matrix that expands and a reinforcement that contracts in order to produce the proper amount of prestressing.

Information on shape memory materials can be found in Refs. [1.35, 1.41 and 1.42].

1.5 PRESTRESSING SYSTEMS

As mentioned above tensioning the tendons can be achieved in several ways. The most common tensioning systems are mechanical. They are generally protected by patents. It is helpful to be familiar with the system used when detailing the steel reinforcement and positioning the end anchorages.

The basic principles used in these systems are few and essentially similar, but the details vary. Patents have been taken on the method of applying the prestress, the type of jack used, the method or device used to anchor the tendons, the number and diameter of wires or strands forming a tendon, tendon coating or protection, and so on.

Typical anchorage systems are shown in Fig. 1.14. Some are based on the principle of direct bearing. These include threaded bars anchored with nut and plate, such as for the Dywidag system, or wires with preformed end buttons bearing on a plate through an anchor head such as the BBRV system. In the buttoned wires system, sufficient accuracy is needed in estimating the exact length of the tendons

before and after tensioning. This is not critical if an anchor system based on wedge action or wedge and grip action is used. The wedge may accommodate, simultaneously, several wires or strands on its outer periphery, as in the Freyssinet system, or it may grip in sandwich a single bar or strand, as in the typical chuck of the Cona system. Several wedges holding one strand each can have the same anchor head, as in the VSL system. Dead anchors are also available. They are encased directly in the concrete and are generally used in short members, when tensioning from one end only is sufficient. Some of these prestressing systems are described in more detail in Appendix: C. Additional information, technical data, and even design aids are usually available from the various manufacturers of these systems.

1.6 PARTICULAR PRESTRESSING TECHNIQUES

Most prestressing methods have been classified in Sec. 1.5 as belonging to the pretensioning or the posttensioning group. Other classifications can be made according to particular attributes. Such an attribute may be, for instance, whether the tendons are bonded or unbonded, or whether they are internal or external to the concrete section. Some particular techniques are described below.

1.6.1 External Prestressing

Contrary to internal prestressing which implies that the tendons are in contact with the concrete, external prestressing refers to prestressing in which the force is externally applied. This can be achieved in two ways: by using jacks, primarily in temporary construction applications, or for permanent construction, by using external prestressing tendons placed outside the concrete member.

In the first case, the force is applied through hydraulic or flat jacks placed between the abutments and the ends of a concrete member (Fig. 1.16*a*). Flat jacks are thin steel or neoprene bags which, when inflated, exert a very high force over a very small distance (Fig. 1.16*b*). Several of these can be superimposed to obtain greater movement. Inflation of the jack is achieved using water or grout under pressure. When the desired movement is reached, the grout is allowed to harden. Flat jacks are very efficient and economical. However, over time, creep losses in the concrete and movements due to temperature differentials hinder their effectiveness. Thus, they cannot be reliably used as a permanent solution for prestressing.

In the second case, external unbonded prestressing tendons are placed outside the section of a structural member and anchored mostly at its ends. These tendons are primarily designed to represent only a portion of the total reinforcement of the structure (Fig. 1.17a). Typical applications of external prestressing include new structures, particularly bridges, and in strengthening, repair and rehabilitation of existing structures. Besides bridges, external prestressing has been used in building members, roofing structures, and circular structures such as silos, reservoirs, large

concrete pipes, and water tanks. Although the external prestressing of interest here applies to concrete members, the concept of external prestressing applies to steel, wood, masonry or other structures as well.

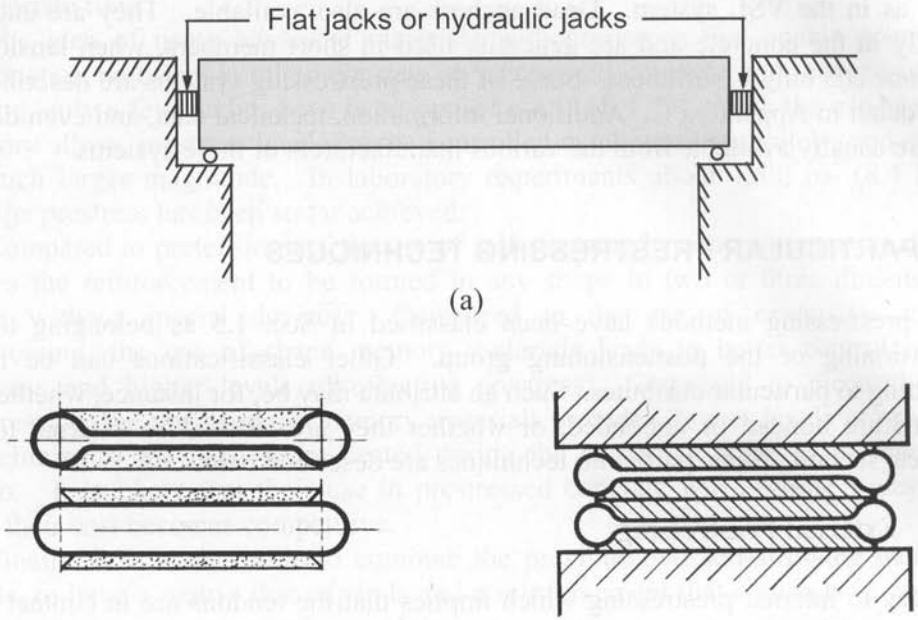

Figure 1.16 ***(a)*** **External prestressing: jacking against abutments.** ***(b)*** **Typical flat jacks.** *(Courtesy Freyssinet International.)*

External prestressing has been proven cost effective and technically attractive worldwide, because it leads to substantial cost savings and a dramatic decrease in construction time. Typically, to improve the load-carrying capacity of existing bridges, external tendons are placed outside the bridge girders, tensioned, and anchored at their ends (Fig. 1.17) Indeed, in a time where our infrastructure is in need of renewal, external prestressing provides one of the most efficient solutions to increase the rating capacity of existing bridges made from all structural materials (concrete, steel or timber). Note also that external prestressing tendons can be made out of steel or other reinforcing materials such as fiber reinforced polymeric (FRP) reinforcements.

Some information on analysis and design of beams prestressed with external tendons can be found in Ref. [1.48].

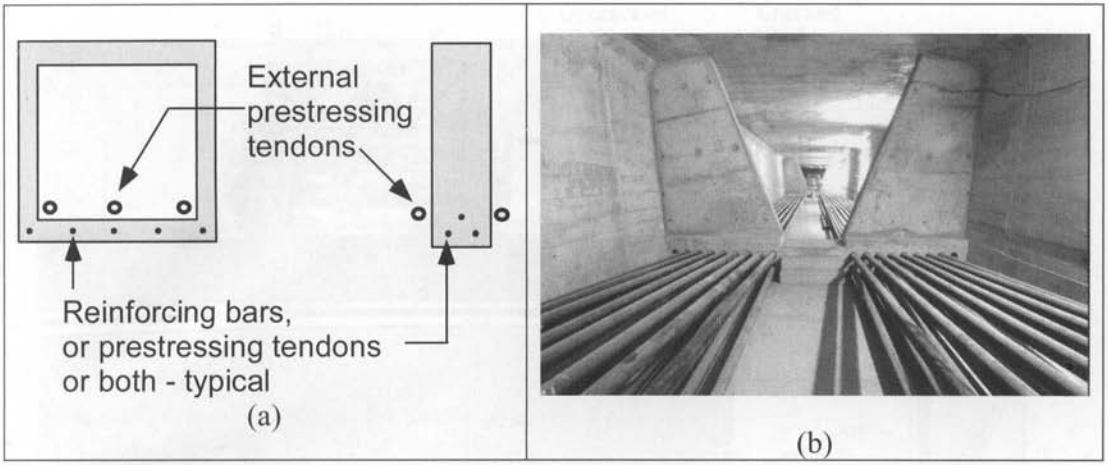

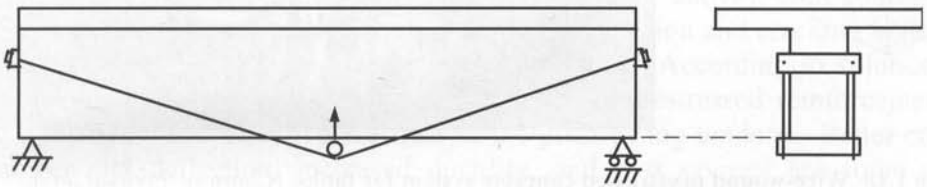

(c)

Figure 1.17 ***(a)*** **Typical external prestressing in beams.** ***(b)*** **External prestressing tendons inside the deck of Roquema bridge** *(Courtesy Freyssinet International).* ***(c)*** **Example of external prestressing to strengthen an old bridge.**

1.6.2 Circular Prestressing

Whereas the term linear prestressing generally refers to elongated elements such as beams, bridges, and piles, the term circular prestressing applies to pipes, pressure vessels, and tanks. Although no analytical difficulty exists in designing circular structures, some particular techniques were developed to prestress them efficiently. The most common one is the wire-wound technique in which the unreinforced concrete core of a pipe or tank is wrapped with a wire under tension, thus creating the uniform radial compression needed for prestressing the core. Upon completion the steel wire is protected with a layer of mortar usually applied by "shotcreting" or "guniting." To rapidly and economically place the wire under tension, it is drawn through a die (the preload method), or a special differential winding system is used.

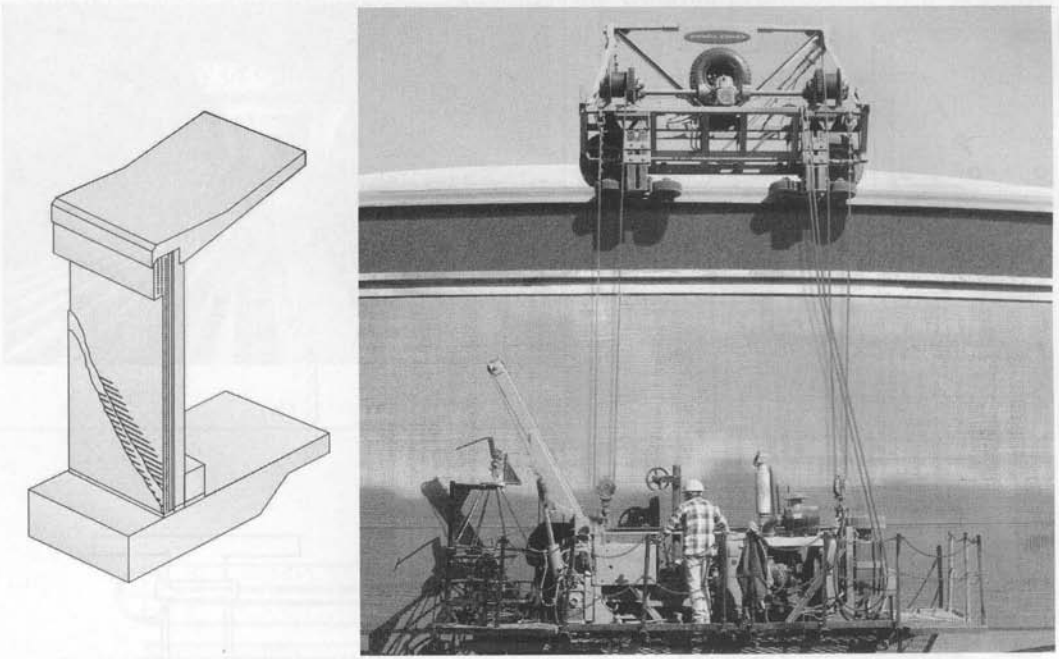

Figure 1.18 Wire-wound prestressed concrete system for tanks. (*Courtesy Preload Inc.*).

1.6.3 Stage Stressing

Stage stressing refers to the application of the prestressing force in stages. This is often done to avoid overstressing the concrete in its early age or when dead loads are applied in stages and their effect must be counteracted in steps. Stage stressing is generally achieved by fully stressing part of the tendons at each stage.

1.6.4 Partial Prestressing

Partial prestressing is a design concept that allows one or a combination of the following design solutions:

1. a concrete member reinforced with a combination of prestressed and nonprestressed reinforcement, the nonprestressed reinforcement being either ordinary reinforcing steel or non-stressed prestressing steel;
2. a prestressed concrete member designed to crack in tension-flexure under service load, and,
3. a prestressed concrete member in which the effective prestress in the steel is purposely kept lower than its maximum permissible value.

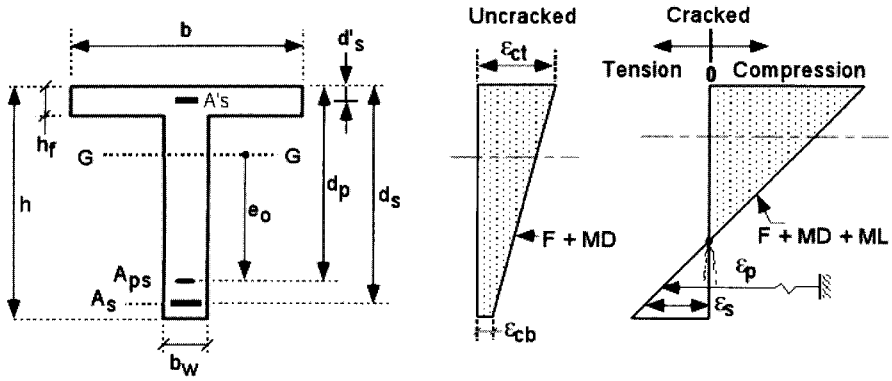

Figure 1.19 Typical conditions for partial prestressing.

Partial prestressing as used in this text, mostly implies a combination of prestressed and nonprestressed reinforcement (solution 1 above), both contributing to the resistance of the member. The aim is to allow tension and cracking under full service load while ensuring adequate ultimate strength. According to solution (3), partial prestressing can also be achieved without nonprestressed reinforcement by using a relatively low effective prestress in the prestressing tendons. Better control of camber and deflection, increased ductility, and cost savings are some of its advantages. Partial prestressing is covered in detail in Ref.[1.48].

Note that as far as reinforced concrete is concerned, partial prestressing could be termed partial reinforcing, especially when it comes to solution (1) above. This may explain why, in an attempt to provide a general terminology, the term "structural concrete" is also used to imply the whole spectrum of reinforcing and/or prestressing schemes.

1.7 PRESTRESSED VERSUS REINFORCED CONCRETE

In its earliest development prestressed concrete used to be mostly compared to reinforced concrete. The currently increasing awareness and use of partially prestressed concrete (or partially reinforced concrete, or structural concrete) renders such comparison somewhat inappropriate. Prestressed concrete and reinforced concrete are in effect the two extreme boundaries of the same system, and partially prestressed concrete can represent anything in between. Figure 1.20 provides a visual illustration of how these three structural materials are used in practical design.

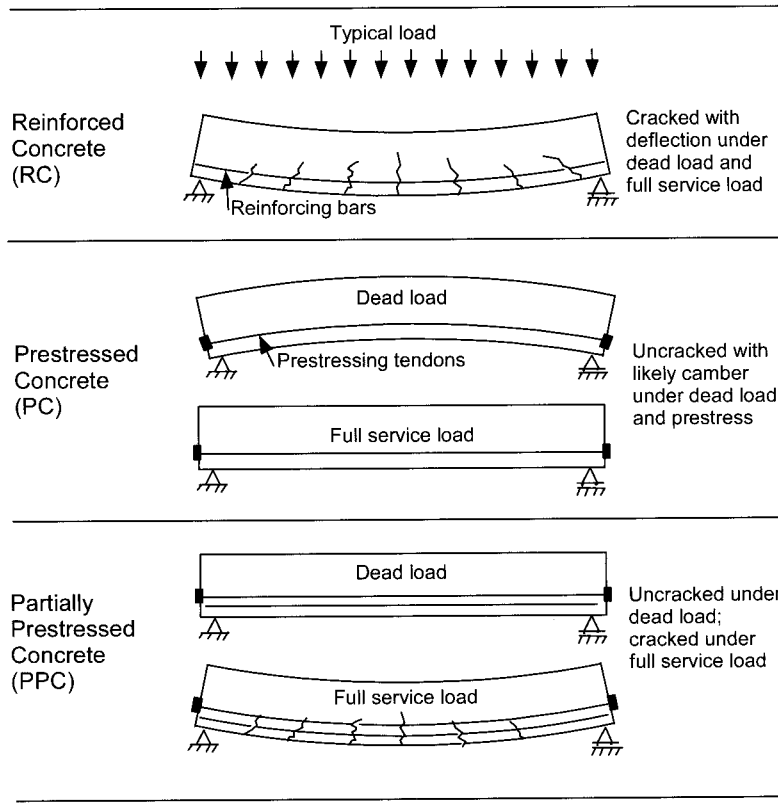

Figure 1.20 Typical comparison of the behavior of reinforced, prestressed and partially prestressed concrete beam under load.

Reinforced and prestressed concrete cannot be considered competitors because they complement each other in function and in application. Since prestressed concrete has become in part a manufactured product (by the precast prestressed industry) and since it permits increasingly longer spans, it is mostly competing with steel construction rather than with reinforced concrete. In all cases the use of concrete offers inherent advantages, such as fire resistance, high insulation qualities, low maintenance, low energy requirement, versatility, etc., which are common to both reinforced and prestressed concrete.

Following are some of the often cited advantages of prestressed concrete compared to reinforced concrete:

1. Prestressed concrete uses high-strength steel and concrete. Thus, it takes advantage of materials with superior qualities, and everything else being equal, needs smaller quantities of materials than reinforced concrete. At present, steel strengths of up to 300 ksi (2100 MPa) and concrete strengths of up to 15 ksi (105 MPa) are being used in the United States. Note that doubling the concrete strength, say from 5 to 10 ksi (35 to 70 MPa), will increase the cost of the

concrete matrix by only about 30 percent, but this represents only a small percentage of the cost of the structure.

2. In prestressed concrete, the entire concrete section is generally active in resisting the load, while in reinforced concrete only the uncracked part of the section is active (Figs. 1.19 and 1.20).
3. Because of 1 and 2 above, prestressed concrete members are lighter, more slender, and frequently aesthetically more appealing than their reinforced concrete counterparts. Their lighter weight is particularly important in long-span girders and bridges where the dead load is a dominant design factor.
4. Since prestressed concrete is crackless, it provides better protection than reinforced concrete against corrosion of the steel in aggressive environments, and it is more suitable for fluid-retaining structures such as tanks and nuclear vessels.
5. Prestressed concrete (fully or partially) provides the means for effective deflection control, especially under long-term sustained loading.
6. Prestressed concrete has better shear resistance than reinforced concrete, due to the slope of the tendons near the supports and to the precompression which reduces diagonal tension. Thus it will require fewer stirrups.
7. It is often claimed that prestressed concrete structures have an inherent safety since they undergo the most severe loading during initial tensioning of the steel. In effect they are pretested. If they pass this first test, they are likely to perform well under future service loads.

A priori, one cannot make a general statement on whether prestressed concrete is more or less economical than reinforced concrete. Prestressed concrete requires a higher level of technology, and often such technology is simply not available where the structure is to be built. Prestressed concrete uses less materials, but of a higher quality, than reinforced concrete and, at least in posttensioning, needs relatively expensive anchorages. Assuming the technology is available, its comparative cost depends very much on the type of structure and the design criteria. There are applications such as long-span bridges in which reinforced concrete cannot compete with prestressed concrete. But there are also areas where their range of applicability overlaps, and the choice for either one should be based not only on initial cost but also on other costs and performance criteria. The initial cost of the structure is no longer an all-important factor. It is the author's experience that for structural applications which fall within the capabilities of both reinforced and prestressed concrete, the initial cost difference using either material is often less than 10 percent. For instance, savings in total construction time may render a precast prestressed structure substantially more economical than its reinforced counterpart. Many tradeoffs must be considered before making a decision since some of the advantages of prestressed concrete may not always be needed.

1.8 EXAMPLE

The following example, in which reinforced and prestressed concrete solutions are compared, illustrates some of the features of prestressed concrete. Let us assume that a simply supported slab is to be built. Both reinforced and prestressed concrete are potential alternatives. Consider the following dimensional and materials properties (Fig. 1.21):

Slab depth h = 12 in (30.5 cm); unit slab width considered in the computations b = 12 in (30.5 cm); distance from extreme compressive fiber to centroid of tensile reinforcement $d_s = d_p$ = 10 in (25.4 cm); concrete compressive strength f'_c = 5000 psi (34.5 MPa); maximum allowable concrete compressive stress in service $\bar{\sigma}_{cs}$ = 2000 psi (13.8 MPa); yield strength of reinforcing steel f_y = 60 ksi (414 MPa); maximum allowable working stress of reinforcing steel $\bar{f}_s$ =24 ksi (165.6 MPa); effective stress in prestressing steel f_{pe} = 160 ksi (1104 MPa); span length L = 30 ft (9.14 m).

The concrete used is a lightweight concrete with a unit weight of 106.67 lb/ft^3 (16.76 kN/m^3) and the live load is assumed uniform with magnitude of 106.67 lb/ft^2 (5.11 kN/m^2). These values have been selected so as to lead to simple round numbers for the computed stresses.

The maximum moment at midspan due to the deadweight of the slab is given by:

$$M_D = \frac{106.67}{12} \times \frac{(30 \times 12)^2}{8} = 144,000 \text{ lb-in}$$

and the corresponding maximum stresses on the top and bottom fibers of the concrete section, assumed uncracked, are:

$$\sigma = \pm \frac{6M_D}{bh^2} = \pm \frac{6 \times 144,000}{12 \times 12^2} = \pm 500 \text{ psi } (3.45 \text{ MPa})$$

Because the live load moment M_L has the same magnitude as the dead load moment, it will also generate stresses of the same magnitude in the uncracked section. Several cases can be considered:

1. **Non-reinforced slab (plain concrete)**
   The magnitude of the extreme fiber stress due to the application of combined dead and live loads (Fig. 1.21*b*) is 1000 psi (6.9 MPa). This stress is acceptable in compression but is higher than the tensile strength of concrete in flexure (modulus of rupture). Hence cracking in the tensile zone and subsequent collapse of the slab will occur.

2. **Reinforced concrete slab: WSD approach**
   Let us determine the required amount of steel reinforcement using the Working Stress Design approach, assuming cracked section and linear elastic analysis. If we estimate the lever arm between the center of compression and the center of tension (Fig. 1.21*c*) at $0.875d_s$, the required area of steel reinforcement can be obtained from the moment equilibrium equation leading to:

$$A_s = \frac{M_D + M_L}{0.875 d_s \bar{f}_s} = \frac{288000}{0.875 \times 10 \times 24000} = 1.371 \text{ in}^2$$

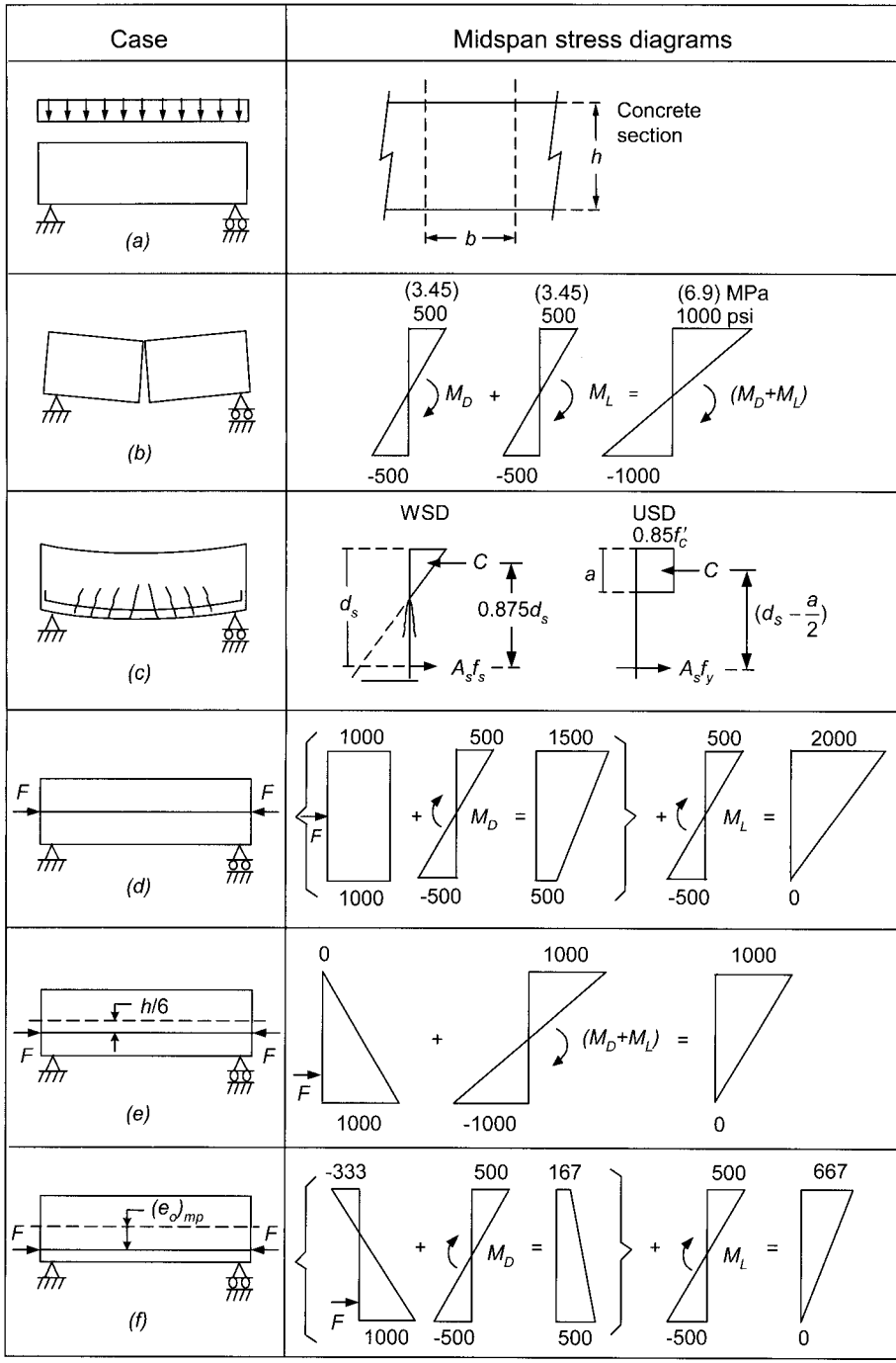

Figure 1.21 Typical schemes to increase the tensile resistance of a concrete element. ***(a)*** **Example slab.** ***(b)*** **Plain concrete.** ***(c)*** **Reinforced concrete.** ***(d)*** **Prestressed concrete: axial prestressing.** ***(e)*** **Eccentric prestressing.** ***(f)*** **Prestressing at maximum practical eccentricity.**

3. Reinforced concrete slab: USD approach

If the Ultimate Strength Design approach, according to the ACI code procedure, is used, the area of steel reinforcement can be obtained from solving the two equations of equilibrium of the section at ultimate capacity. The reinforcement is designed to generate an internal moment resistance (or nominal moment resistance) equal to the specified strength design moment (factored moment), with due consideration to a reduction factor ϕ (see Chapter 5); using the 2002 ACI code load and resistance factors (Tables 3.9 and 3.10):

$$M_u = 1.2M_D + 1.6M_L = 403,200 \text{ lb-in}$$

and

$$M_u = \phi M_n$$

where M_n is the nominal moment resistance of the section, and ϕ is a reduction factor (see Chapters 3 and 5).

The equations of force and moment equilibrium of the section at ultimate, assuming yielding of the steel, are given (Fig. 1.21*c*) by:

$$A_s f_y = 0.85 f'_c ba$$

and

$$\phi A_s f_y \left(d_s - \frac{a}{2} \right) = M_u = 403,200 \text{ lb-in}$$

The above two equations have two unknowns a and A_S. Assuming ϕ = 0.9 (Table 3.10) and solving for A_S leads to:

$$A_s = 0.784 \ in^2$$

Note that the steel area required using USD is substantially smaller than that using WSD.

4. Prestressed concrete slabs: uniform prestress

Let us assume that no tension is allowed in the slab. If the prestressing steel is directed along the centroid of the section, the stress induced by the prestressing force is uniform (Fig. 1.21*d*). Its magnitude should be at least equal to 1000 psi (6.9 MPa) to counteract the maximum tensile stress σ_b on the bottom fiber due to dead and live loads. Thus:

$$\sigma_g = -\sigma_b = (\sigma_b)_F = 1000 \text{ psi}$$

$$F = \sigma_g \times A_c = 1000 \times 144 = 144,000 \text{ lb}$$

$$A_{ps} = \frac{F}{f_{pe}} = \frac{144,000}{160,000} = 0.9 \text{ in}^2$$

where σ_g and $(\sigma_b)_F$ are the stresses at the centroid and at the bottom fiber of the concrete section, due to the prestressing force F, and A_{ps} is the area of prestressed reinforcement. Note, from Fig. 1.21*d*, that the effect of prestressing leads to an increase in compression on the top fiber of concrete. Such increase is not necessary since it adds to the compressive stresses induced by external loads. A more efficient distribution may be achieved by placing the prestressing force at an appropriate eccentricity as described next.

5. Prestressed concrete slab: eccentric prestress (central kern)

Let us assume that the prestressing force is placed at the lower limit of the middle third of the section (Fig. 1.21*e*). Its eccentricity e_o is equal to $h/6$. For a rectangular section, the middle third

of the section also bounds the central kern (see Chapter 4). In this case a triangular stress distribution with zero stress (no tension) on the top fiber is induced. If we want a stress of 1000 psi (6.9 MPa) at the bottom fiber, the average stress at the centroid of the section will be 500 psi (3.45 MPa) and the required prestressing force will be:

$$F = \sigma_g A_c = 500 \times 144 = 72{,}000 \text{ lb}$$

The corresponding area of prestressing steel is:

$$A_{ps} = \frac{F}{f_{pe}} = \frac{72{,}000}{160{,}000} = 0.45 \text{ in}^2$$

Its value is half that obtained for case 4. This result shows the importance of appropriately placing the prestressing force to achieve higher efficiency where needed.

6. Prestressed concrete slab: eccentric prestress (maximum eccentricity)

A prestressing force F placed at a constant eccentricity e_O from the centroid of the section is equivalent to the combined action of an axial force of magnitude F, directed along the centroid, and a moment of magnitude Fe_O (Fig. 1.22).

The corresponding stress on the bottom fiber of the section is given by:

$$(\sigma_b)_F = \frac{F}{A_c} + \frac{Fe_o}{(bh^2/6)}$$

which, since $bh = A_c$ can be written as:

$$(\sigma_b)_F = \frac{F}{A_c}\left(1 + \frac{6e_o}{h}\right)$$

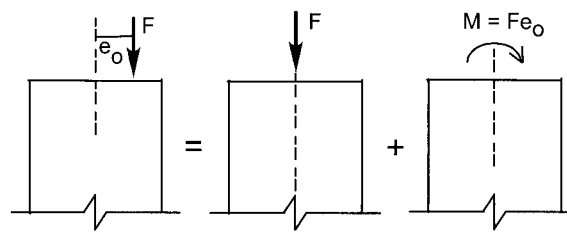

Figure 1.22

It is clear that for a given force F, the higher the eccentricity e_o, the higher the stress $(\sigma_b)_F$. Inversely given a required value of $(\sigma_b)_F$, the higher the eccentricity e_o, the smaller the prestressing force F and the higher the savings on the prestressing steel.

Let us assume that the maximum practical value of e_o to ensure a sufficient concrete cover of the steel is 4 in (10.16 cm) and that no tension is allowed in the section. The minimum prestressing force required to incur a stress of 1000 psi (6.9 MPa) on the bottom fiber is obtained by solving the following equation:

$$1000 = \frac{F}{144}\left(1 + \frac{6 \times 4}{12}\right)$$

for which $F = 48{,}000$ lb.

The corresponding area of prestressing steel is

$$A_{ps} = \frac{48,000}{160,000} = 0.30 \text{in}^2$$

Note that, although the prestressing force acting alone produces tension on the top fiber (Fig. 1.21*f*), because the dead load acts immediately upon application of the prestress, the resulting stress (at midspan) is still a compression. In order to avoid tension at the supports, the steel profile is generally draped upward instead of being left straight as assumed in this example.

7. **Prestressed concrete slab allowing tension**
If a tension of -212 psi (-1.46 MPa) is allowed on the bottom fiber under full service load, the equation given in the previous case would be written as:

$$(1000 - 212) = \frac{F}{144}\left(1 + \frac{6 \times 4}{12}\right)$$

for which F = 37,824 lb and

$$A_{ps} = \frac{37,824}{160,000} = 0.236 \text{ in}^2$$

Remarks: It is often said that one of the advantages of using prestressed concrete is that the dead load can be carried, entirely or in part, free. This can be illustrated by the above example, assuming no tension is allowed.

Let us compute the prestressing force which, if placed at the lower limit of the central kern (e_o = 2 in), would produce a compressive stress on the bottom fiber equal and opposite to that induced by the live load only. Thus:

$$500 = \frac{F}{144}\left(1 + \frac{6 \times 2}{12}\right)$$

for which F = 36,000 lb and A_{ps} = 36,000/160,000 = 0.225 in^2.

Using the above force, we can increase the eccentricity e_O to its maximum practical value of 4 in (10.16 cm). The corresponding stress on the bottom fiber due to F becomes equal to 750 psi instead of 500 psi. This increment of 250 psi will, in our case, balance 50 percent of the tensile stress produced by the dead load. We would have essentially carried 50 percent of the dead load at no charge. The other 50 percent will be carried by increasing the prestressing force to its value given in case 6. In some instances where the ratio of live load moment to dead load moment is large, the entire dead load can be carried free. This often happens for small span lengths, which are then described as "less than critical" spans [Ref. 1.8].

Using a similar approach, the reader may want to check that if the live load in the above example is doubled, the span becomes "less than critical," that is, the entire dead load may be carried free.

1.9 LOOKING AHEAD

Prestressed concrete has passed far beyond the developmental stage and has established itself as a major structural material. Similarly, prestressing techniques have evolved into a reliable technology. Prestressed concrete has made major

contributions to the construction and the cement industries. It has led to an incredible array of structural applications from bridges to nuclear power vessels and offshore structures. Seldom is a major project planned today without considering prestressing as one of the viable alternative solutions. Moreover, some innovative large scale structures could not be conceived without prestressed concrete (Fig. 1.23).

A careful analysis of prospects and opportunities indicates that the future of prestressed concrete is very bright. Constructed facilities and infrastructure systems will keep expanding not only in volume but also in reach. To achieve daring limits and efficiency, prestressed concrete will be needed. This is true for terrestrial structures as well as marine structures, under-water structures, under-ground structures and space structures.

Current market penetration for prestressed concrete in the United States is estimated at about 10 percent, and it is believed that a penetration of 30 percent will be achieved eventually [Ref. 1.29]. The same trend is expected in the future at the educational level. Design courses in prestressed concrete will very likely move from the list of elective courses to the list of required courses in civil engineering curricula.

Prestressed concrete structures contain all the beneficial attributes of concrete as a construction material plus those inherent to prestressing. The current widespread use of prestressed concrete in developed countries is astonishing. Because of its many advantages, particularly its durability, it is expected to remain one of the strongest construction systems on the market for the foreseeable future.

REFERENCES *(ordered chronologically)*

1.1 Jackson, P. H., U.S. Patent No. 357999, 1886/88.

1.2 Doehring, C. E. W., German Patent No. 53548, 1888/89.

1.3 Koenen, M., German Patent No. 249007, 1912.

1.4 Dill, R. E., U.S. Patent No. 1684663 (1925/28).

1.5 Freyssinet, E., and J. Seailles, French Patent No. 680 547, 1928.

1.6 Freyssinet, E., *Une Revolution dans les Techniques du Béton.* Paris: Librairie de l'Enseignement Technique, Leon Eyrolles, Editor, 1936.

1.7 Lossier, H., "Cements with Controlled Expansion and Their Application to Prestressed Concrete," *The Structural Engineer*, 24(10): 505-34, 1946.

1.8 Dobell, C., "Patents and Code Relating to Prestressed Concrete, *Journal of the American Concrete Institute*, 46: 713-24, 1950.

1.9 Freyssinet, E., The Birth of Prestressing, London: Public Translation, Cement and Concrete Association, 1954.

1.10 Magnel, G., *Prestressed Concrete*, 3rd ed. London: Concrete Publications Ltd., 1954.

1.11 Mikhailov, V. V., "New Developments in Self-Stressed Concrete," *Proceedings of the World Conference on Prestressed Concrete*, San Francisco, 1957.

1.12 Guyon, Y., *Prestressed Concrete*, Vols. 1 and 2. New York: John Wiley & Sons, 1953, 1960. Also, *Limit State Design of Prestressed Concrete*, translated from French, Halstead and Wiley, 1972.

1.13 Lin, T. Y., and A. Klein, "Chemical Prestressing of Concrete Elements Using Expanding Cements," *ACI Journal Proceedings*, 60(9): 1187-1218, 1963.

***(a)* ARCO floating terminal for liquid petroleum gas.** *(Courtesy Concrete Technology Corporation, Tacoma.)*

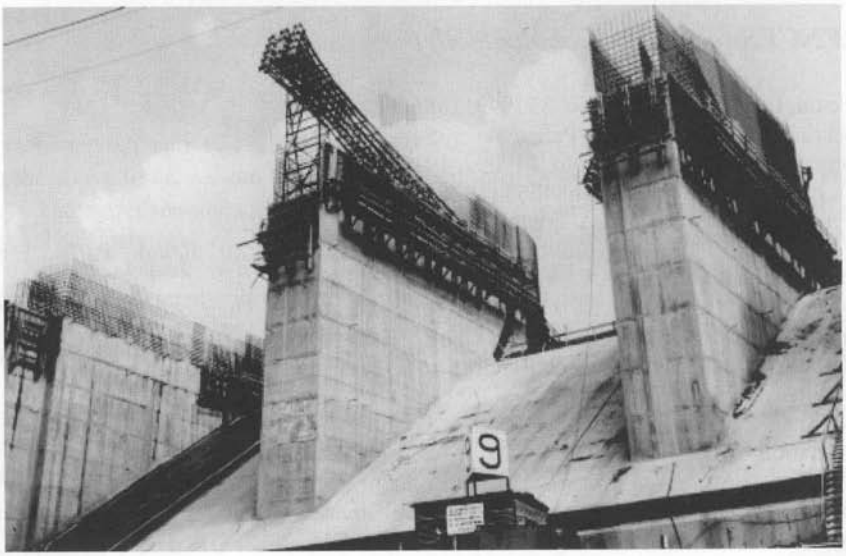

***(b)* Prestressing the spillway gate anchor at Guri Dam, first stage.** *(Courtesy C. V. G.-Edelca, Venezuela.)*

Figure 1.23 Unusual structures using prestressed concrete.

(c) **Condeep offshore oil platform – Statfjord Platform A.** *(Courtesy Norwegian Constractors, Oslo.)*

(d) **Canadian National Tower, Toronto.** *(Courtesy CN Tower Limited, Toronto.)*

Figure 1.23 (continued) Unusual structures using prestressed concrete.

1.14 Abeles, P., *An Introduction to Prestressed Concrete*, Vols. 1 and 2, Concrete Publications Ltd., London, 1964.
1.15 Leonhardt, F., *Prestressed Concrete Design and Construction*, English translation. Berlin: Wilhelm Ernst and Sohn, 1964, (1st ed., 1955, 2nd ed., 1962 in German).
1.16 Preston, K., and N. Sollenberger, *Modern Prestressed Concrete*. New York: McGraw-Hill Book Co., 1967.
1.17 Mikhailov, V. V., *Prestressed Concrete Structures: Theory and Design*, translated from Russian by J.H. Dixon. London: Cement and Concrete Association, 1969.
1.18 Khachaturian, N., and G. Gurfinkel, *Prestressed Concrete*. New York: McGraw-Hill Book Co., 1969.
1.19 Gerwick, Jr, Ben C., *Construction of Prestressed Concrete Structures*. New York: Wiley-Interscience, 1971. Also 2nd edition, Wiley Professional Paperback Series, 1993, 591 pp.
1.20 Ramaswamy, G. S., *Modern Prestressed Concrete*. London: Pitman Publishing, 1976.
1.21 Libby, J. R., *Modern Prestressed Concrete: Design Principles and Construction Methods*, 2nd ed. New York: Van Nostrand-Reinhold, 1977.
1.22 Warner, R. W., and K.A. Faulkes, *Prestressed Concrete*. Victoria, Australia: Pitman Publishing, 1979, 336 pp.
1.23 Bennet, Jr., W. B., "Prestressing: The Technique that Makes Concrete Fully Competitive," *Concrete Construction*, 25(2): 125-31, 1980.
1.24 Abeles, P. W., and B.K. Bardhan-Roy, *Prestressed Concrete Designer's Handbook*, 3rd ed. London: Viewpoint Publications, 1981.
1.25 Lacroix, R., and A. Fuentes, *Le Project de Béton Précontraint*, in French. Paris: Editions Eyrolles, 1981, 408 pp.
1.26 Lin, T. Y., *Design of Prestressed Concrete Structures*, 2nd ed. New York: John Wiley & Sons, 1963. Also, revised and enlarged 3rd ed. by T.Y. Lin and N. Burns, 1981.
1.27 Naaman, A. E., *Prestressed Concrete Analysis and Design: Fundamentals*. New York: McGraw Hill, 1982, 670 pp.
1.28 Mathivat, J., *The Cantilever Construction of Prestressed Concrete Bridges*. New York: John Wiley and Sons, 1983, 341 pp.
1.29 Cohn, M. Z. Editor, *Partial Prestressing: from Theory to Practice*, NATO-ASI Applied Science Series, Vol. 1, 405 pp, Vol. 2, 425 pp. Dordrecht, Netherlands: Martinus Nijhoff, 1984.
1.30 Naaman, A. E., "Partially Prestressed Concrete: Review and Recommendations," *Journal of the Prestressed Concrete Institute*, 30(6): 30-71, 1985.
1.31 Antonini, T., *Cemento Armado Precompresso*, 2nd ed., in Italian. Milan, Italy: Masso Italia Editori, 1986, 441 pp.
1.32 Nilson, A. H., *Design of Prestressed Concrete*. New York: John Wiley & Sons, 1978. Also, 2nd ed., 1987, 592 pp.
1.33 Naaman, A. E., and J. Breen, eds., *External Prestressing in Bridges*. Farmington Hills, MI: American Concrete Institute, ACI SP-120, 1990, 458 pp.
1.34 Walther, R., and M. Miehlbradt, *Dimensionnement des Structures en Béton*, in French. Lausanne, Switzerland: Presses Polytechniques Universitaires Romandes, 1990, 388 pp.
1.35 Duerig, T. W., K. N. Melton, D. Stockel, and C. M. Wayman, *Engineering Aspects of Shape Memory Alloys*. England: Butterworth-Heinemann, 1990.
1.36 IABSE Colloquium, *Structural Concrete*. Zurich, Switzerland: IABSE, 1991, 872 pp.
1.37 Collins, M. P., and D. Mitchell, *Prestressed Concrete Structures*. Upper Saddle River, NJ:: Prentice Hall, 1991, 766 pp.
1.38 Bruggeling, A. S. G., *Structural Concrete Theory and its Application*. Rotterdam, Netherlands: Balkema Publishers, 1991.
1.39 Chaussin, R., A. Fuentes, R. Lacroix and J. Perchat, *La Précontrainte*, in French. Paris: Presses de l'Ecole Nationale des Ponts et Chaussées, 1992, 525 pp.

1.40 Hsu, T. T. C. *Unified Theory of Reinforced Concrete*. Boca Raton, Florida: CRC Press, 1993, 313 pp.
1.41 Conti, E., and B. Foure, External Prestressing in Structures. Bagneux, France: AFPC – Association Francaise pour la Construction, 1993, 471 pp.
1.42 Hebda, D. A., and S. R. White, "Effect of Training Conditions and Extended Thermal Cycling on Nitinol Two-Way Shape Memory Behavior," *Smart Materials and Structures*, 4: 298-304, 1995, IOP Publishing, U.K..
1.43 Shaw, J. A., and S. Kyriakides, "On the Nucleation and Propagation of Phase Transformation Fronts in NiTi Alloy," *Acta Mater.* 45(2): 683-700, 1997, Elsevier Science Ltd., U.K.
1.44 Naaman, A. E., and N. Krstulovic-Opara, "Self-prestressed Fiber Reinforced Cement Composites." In *High Performance Fiber Reinforced Cement Composites - HPFRCC 3*, H.W. Reinhardt and A. E. Naaman, eds., RILEM Pro 6. Cachan, France: RILEM Publications S.A.R.L., 1999, pp. 75-90.
1.45 *PCI Design Handbook – Precast and Prestressed Concrete*, 5th ed. Chicago: Precast/Prestressed Concrete Institute, 1999.
1.46 Nawy, E. G., *Prestressed Concrete: a Fundamental Approach*, 3rd ed., New York: Prentice Hall, 2000.
1.47 *Post-Tensioning Manual*, 6th ed., Phoenix, Arizona: Post-Tensioning Institute, 2000.
1.48 Naaman, A. E., *Prestressed and Partially Prestressed Concrete: Advanced Topics*, textbook in preparation, 2003.
1.49 American Concrete Institute, Farmington Hills, Michigan 48219, U.S.
1.50 Portland Cement Association, Skokie, Illinois 60076, U.S.
1.51 Cement and Concrete Association, London, England.
1.52 Fédération Internationale de la Précontrainte (FIP), London, England. Also, Fédération Internationale du Béton (FIB).
1.53 Precast/Prestressed Concrete Institute, Chicago, Illinois 60606, U.S.
1.54 Post-Tensioning Institute, Phoenix, Arizona 85013, U.S.

PROBLEMS

1.1 Give an example of a system, device, instrument, or procedure in which the principle of prestressing is used. Describe it schematically. Explain how the prestress is applied and how it counteracts stresses induced during service. Draw schematically the corresponding forces and/or stresses.

1.2 Using the results obtained for the example described in Sec. 1.8, estimate the cost of the slab (say per unit area or unit strip) for cases 2 to 5 studied. For this, find out and use unit costs prevailing in the geographic area where you live. Draw conclusions from your findings. Two approaches could be considered:

1. Using global unit costs such as dollars per cubic yard of finished concrete in place, dollars per pound of reinforcing steel in place, and dollars per pound of prestressing steel in place.
2. Using unit costs broken down into two categories, such as material, labor and forms (precast versus cast in place).

1.3 A T beam (Fig. P1.3) is part of a slab system and supports in addition to its own weight a live load of 80 psf. The following information is provided:

- Concrete: f'_c = 7000 psi; $\bar{\sigma}_{cs}$ = 2700 psi (allowable stress in compression); normal weight concrete with unit weight = 150 pcf
- Reinforcing Steel: f_y = 60 ksi; $\bar{f}_s$ = 24 ksi (allowable tension)
- Prestressing Steel: f_{pu} = 270 ksi (failure stress); f_{pe} = 150 ksi (effective prestress); f_{py} = 240 ksi (yield stress).

1. Assuming reinforced concrete working stress design, that is, linear elastic cracked section behavior prevails, where transformed section properties apply. Determine the required area of tensile steel, A_S, and the curvature of the section at maximum service moment. Assume that the cover to the centroid of the steel is 3 inches from the bottom fiber. Then compute the nominal bending resistance at ultimate and the corresponding curvature of the section, using the ACI code rectangular stress block for the concrete and yielding of the steel. Assume that the strain at ultimate in the concrete extreme compression fiber is 0.003.
2. Assuming reinforced concrete ultimate strength design: determine the required area of tensile steel, A_S, and the curvature of the section at nominal bending resistance. Assume that the cover to the centroid of the steel is 3 inches from the bottom fiber, and the strain at ultimate in the concrete extreme compression fiber is 0.003. Then compute the curvature of the section at service load.
3. Assume prestressed concrete at service load: determine the minimum prestressing force (thus the area of prestressed reinforcement, A_{ps}) placed at an eccentricity e_o = 13.55 in, needed to achieve no tension in the section under maximum service moment. Determine the curvatures of the critical section: a) under prestress and dead load moment, and b) under prestress and maximum service moment.

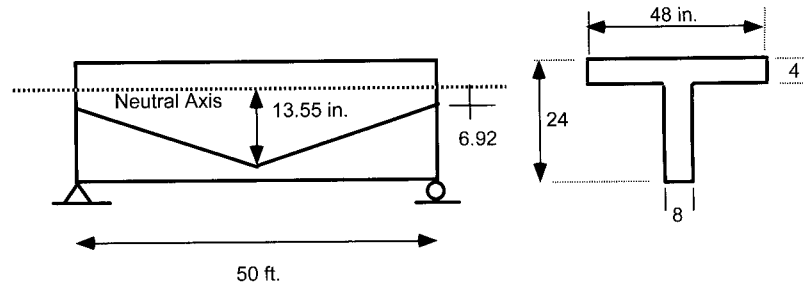

Figure P1.3

4. Assume the prestressing steel determined in (3) yields at ultimate similarly to reinforced steel, that is with a yield plateau. Using ACI's reinforced concrete approach for ultimate strength design, determine the nominal bending resistance of the section and its curvature at ultimate (similarly to Question 2).
5. Plot the relationship between applied external moment and curvature for the reinforced concrete section designed in (1) and (2) on the same graph as the prestressed concrete section designed in (3) and (4). Compare them and draw conclusions. Assume that the curve is made out of three points corresponding respectively to 0, service load (D+L), and ultimate load. For the prestressed case also show the point corresponding to combined effect of prestressing force and dead load. Refer to Sections 3.10.4 and 7.4 for the computation of curvature. Note that for a prestressed section subjected to zero external moment, the curvature is that which is due to prestressing.

Make any other reasonable assumptions you see fit.

Production of precast prestressed concrete hollow-cored slabs. Note the very small number of workers: one running the extruder (right), one cutting slab elements (left), and one operating the crane (center) . *(Courtesy Material Service Corporation.)*

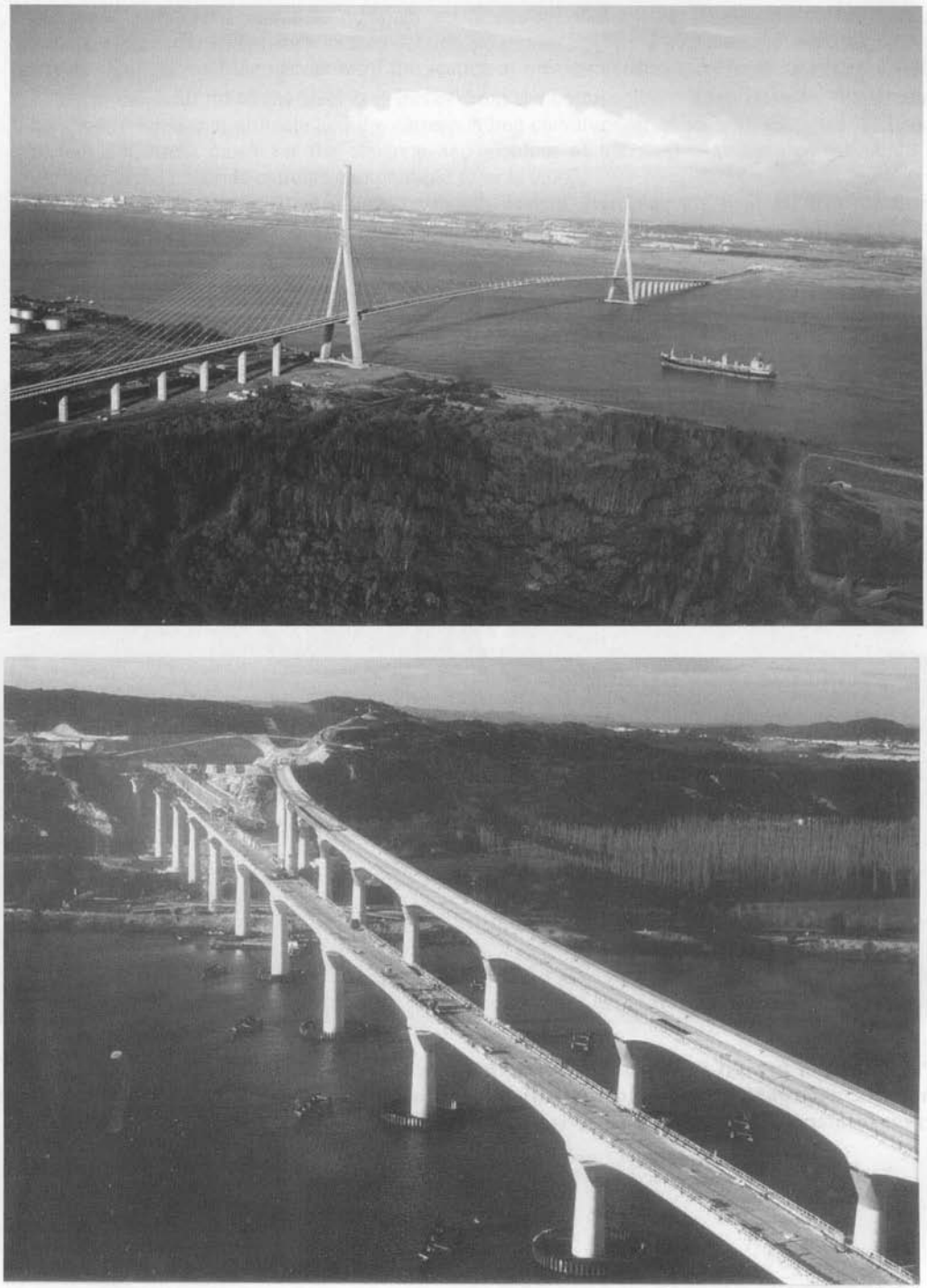

Top: Normandie bridge, France. Bottom: Avignon Viaduct, France. (*Courtesy Michel Virlogeux).*

PRESTRESSING MATERIALS: STEEL AND CONCRETE

Prestressed concrete utilizes high-quality materials, namely high-strength steel and concrete. In addition, ordinary reinforcing steel is extensively used in partially prestressed concrete and in applications in seismic zones. The full coverage of the characteristics of each component, steel or concrete, and their modeling is a treatise by itself. Their composition, properties, and manufacturing processes are extensively described in the technical literature. This chapter gives only a brief overview of their most important characteristics as needed in most common design situations. Information relevant to the understanding of prestressed concrete's structural behavior is provided. A direct approach is used to give the designer enough technical information to allow him/her to proceed in most common design problems. Additional information on the modeling of the materials and the structure can be found in Chapter 8 and Ref. [1.48]. Although other materials, such as fiber reinforced polymeric tendons, can be used for prestressing, only steel and concrete are considered next.

2.1 REINFORCING STEELS

Nonprestressed reinforcing steel is commonly used in prestressed concrete structures as shear reinforcement or supplementary reinforcement in regions of high local stresses and deformations. In partial prestressing it contributes to the main structural resistance to an extent equal to that of prestressing steel. In seismic applications, reinforcing steel is often used in both the tensile and compressive zones, as well as in confinement functions, in order to improve the ductility of the structure. Detailed information on reinforcing steels can be found in many books and textbooks on reinforced concrete, as well as in many standards and code specifications [Refs. 2.8, 2.9, 2.12, 2.19]. The Concrete Reinforcing Steel Institute keeps up-to-date information on the state of the art of reinforcing steels.

Some of the most important design characteristics of reinforcing steels are summarized in Tables 2.1 to 2.3. Table 2.1 provides information on the type and sizes of standard ASTM reinforcing bars used in the United States. Although smooth bars can be obtained, at present they are mostly deformed to improve their bonding properties. Welded wire fabrics and meshes are being increasingly used as main reinforcement in reinforced concrete slabs or supplemental reinforcement in prestressed slabs. They improve substantially the cracking performance of slabs prestressed with unbonded tendons. Typical sizes of wires, smooth or deformed, used separately or in welded meshes, are given in Table 2.2. Many sizes in between those shown are also available. In practice, welded meshes having any reasonable size opening of square or rectangular shape are manufactured as standard product or, on request, for a particular design. Common wire spacing in one of the two principal directions of the mesh are 2, 3, 4, 6, 8, 10, and 12 inches (50, 75, 100, 150, 200, 250, 300 mm). More details can be obtained from local suppliers or the Wire Reinforcement Institute.

Table 2.1 ASTM standard reinforcing bars.

Bar†	Nominal diameter		Nominal area		Nominal weight lb/ft	Nominal weight kg/m
	in	mm	in^2	mm^2		
3	3/8 = 0.375	9.52	0.11	71	0.376	0.56
4	1/2 = 0.500	12.70	0.20	129	0.668	0.994
5	5/8 = 0.625	15.88	0.31	200	1.043	1.552
6	3/4 = 0.750	19.05	0.44	284	1.502	2.235
7	7/8 = 0.875	22.22	0.60	387	2.044	3.042
8	1.0 = 1.000	25.40	0.79	510	2.670	3.973
9	1 1/8 = 1.128	28.65	1.00	645	3.400	5.060
10	1 1/4 = 1.270	32.26	1.27	819	4.303	6.404
11	1 3/8 = 1.410	35.81	1.56	1006	5.313	7.907
14	1 3/4 = 1.693	43.00	2.25	1452	7.650	11.38
18	2 1/4 = 2.257	57.33	4.00	2581	13.600	20.24

†Based on the number of eighths of an inch that add up to the nominal diameter.

The minimum tensile properties of reinforcing bars and wires are summarized in Table 2.3. Also shown is the corresponding ASTM standard designation. Although several grades are available, the most common grade in the United States is the A615 grade 60 deformed steel, which gives a minimum yield strength of 60 ksi (414 MPa). The A706 steel with the same minimum yield as the A615 has a higher strain to failure and is more ductile; it is most suitable in applications where ductility (seismic construction), weldability and bendability are important. Grade 75 steel, which has a minimum yield strength of 75 ksi (517 Mpa) and a minimum tensile strength of 100 ksi (690 MPa), is recommended mostly for use in large reinforced concrete columns.

Table 2.2 Characteristics of a selected set of reinforcing wires used in welded wire meshes.

Wire designation†	Nominal diameter		Nominal area‡	
	in	mm	in^2	mm^2
W2	0.159	4.039	0.020	12.9
W4, D4	0.225	5.715	0.040	25.8
W6, D6	0.276	7.010	0.060	38.7
W8, D8	0.319	8.103	0.080	51.6
W10, D10	0.356	9.042	0.100	64.5
W12, D12	0.390	9.906	0.120	77.4
W14, D14	0.422	10.719	0.140	90.3
W20, D20	0.504	12.801	0.200	129.0
W30, D30	0.618	15.697	0.300	193.6

†W for smooth, D for deformed.
‡Wire density = 490 lb/ft^3 or 7850 kg/m^3.

Table 2.3 ASTM standardized properties of reinforcing steels.

Reinforcing steel type	ASTM standard	Grade	Minimum yield strength		Minimum tensile strength	
			ksi	MPa	ksi	MPa
Reinforcing bars	A615 & A617	40	40	276	70	483
	A615 & A617	60	60	414	90	620
	A616	50	50	345	80	552
	A616	60	60	414	90	620
	A706*	60	60	414	80	552
	A615	75	75	517	100	690
Wire:						
Smooth	A82	...	70	483	80	552
Deformed	A496	...	75	517	85	586
Welded wire fabric:						
Smooth	A185	...	65	448	75	517
Deformed	A497	...	70	483	80	552

* A706 low alloy steel has a specified maximum yield strength of 78 ksi (538 MPa).

Typical stress-strain curves of reinforcing steels are shown in Fig. 2.1. Two different shapes can be identified: one, typical of most reinforcing bars, shows a well-defined yielding behavior, while the other, typical of wires, a smaller category of bars, and Grade 75, does not indicate a well-defined yielding. For this latter type the yield stress is defined as the stress corresponding to a total strain of 0.0035 (ACI)

or 0.005 (ASTM). In all cases the steel shows a significant strain-hardening behavior and sufficient ductility before failure.

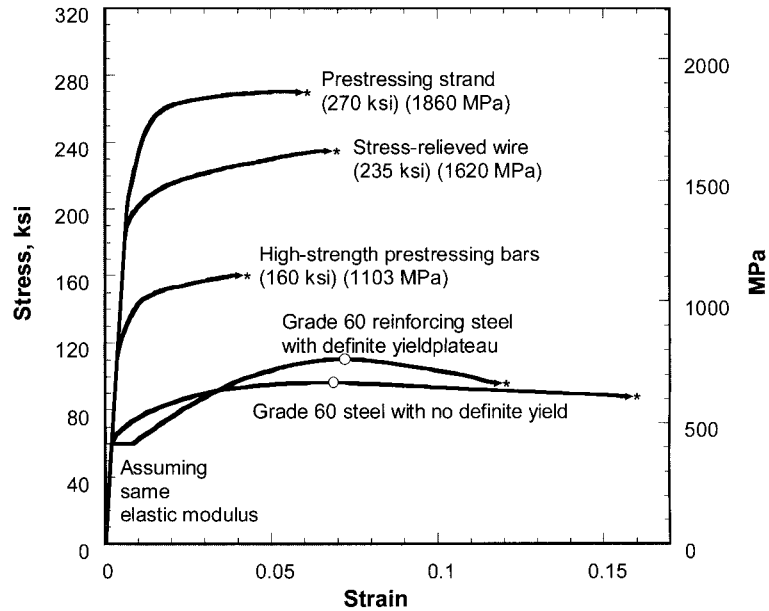

Figure 2.1 Typical stress-strain curves of reinforcing and prestressing steels.

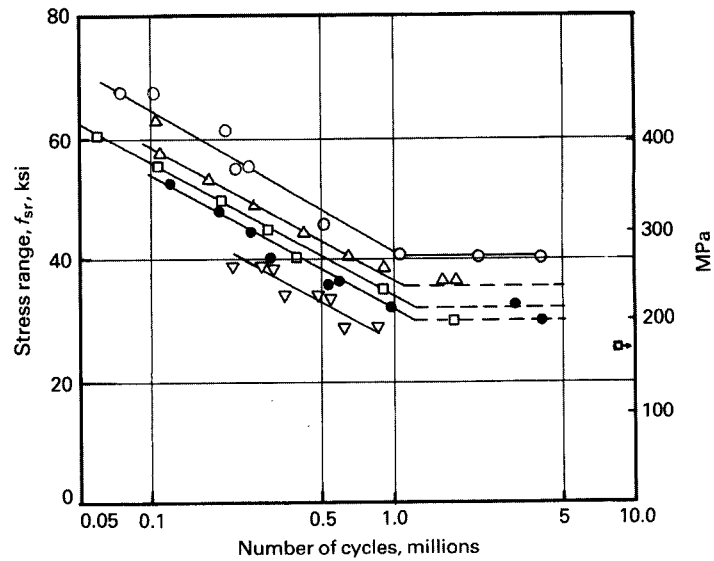

Figure 2.2 Representative fatigue test results for North American bars. *(Ref. 2.34, Courtesy Portland Cement Association.)*

Reinforcing steels exhibit good resistance to fatigue. Typical stress range versus number of cycles to failure curves are shown in Fig. 2.2. It can be generally observed that an endurance limit to fatigue seems to exist. On the basis of an extensive series of tests on North American bars [Ref. 2.34], the following conclusions were drawn: the fatigue strength that is the acceptable stress range for more than two million loading cycles is practically independent of the grade of steel but depends on the minimum applied stress and the degree of stress concentration induced in deformed bars during the deformation process. Other factors were also found to influence the fatigue strength, such as the nominal diameter and the yield strength, but to a lesser extent. The following relationship was proposed for use in design:

$$\Delta f_{sr} = 21 - \frac{f_{s\,min}}{3} + 8\frac{r}{h} \quad \text{in ksi}$$

or (2.1)

$$\Delta f_{sr} = 145 - \frac{f_{s\,min}}{3} + 55\frac{r}{h} \quad \text{in MPa}$$

where

Δf_{sr} = safe stress range for more than two million loading cycles
f_{smin} = minimum stress
r/h = ratio of base radius r to depth of rolled-on deformation (a value of 0.3 may be used in absence of specific information)

For values of acceptable stress ranges at a number of cycles smaller than two million, a number of best fit relationships of a semi-logarithmic form were also proposed in Ref. 2.34 and can be used for design.

2.2 PRESTRESSING STEELS

The importance of using, in prestressed concrete, high-strength steels that permit high elongations was mentioned in Chapter 1. Otherwise, the steel stress will decrease substantially or vanish with time due to prestress losses. As prestress losses in the steel (not including friction) can often approach 60 ksi (414 MPa), that is about equal to the typical yield strength of common reinforcing bars, it is clear that minimum tensile strengths substantially higher than this value are needed to achieve effective prestressing. Other desirable properties are also needed. Ideally a tendon material should not only have high strength but also (1) remain elastic up to relatively high stresses, (2) show sufficient ductility before failure, (3) have good bonding properties, low relaxation, good resistance to fatigue and corrosion, and (4) be economical and easy to handle. Clearly a tradeoff should be made, and high-strength steels offer a good compromise.

2.2.1 Types of Prestressing Tendons

Three types of steel tendons are used in prestressed concrete: wires, strands (or cables) made with several wires, and bars. Typical shapes and commonly available diameters are shown in Fig. 2.3; other particular shapes are given in Fig. 2.4.

Type	Size (Diameter)		Shape
	mm	in.	
Plain round wire	2.0 ~ 9.0	0.06 ~ 0.360	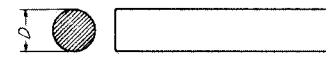
Indented wire	5.0 ~ 7.0	0.200 ~ 0.276	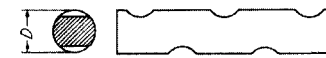
Sumi - Twist	7.3 ~ 13.0	0.276 ~ 0.512	
Two-wire strand	2.9 x 2	0.114 x 2	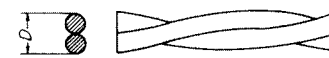
Seven-wire strand	6.2 ~ 15.2	0.250 ~ 0.600	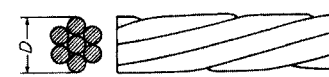
Nineteen-wire strand	17.8 ~ 21.8	0.700 ~ 0.860	
Round bar	9.2 ~ 32.0	0.362 ~ 1.260	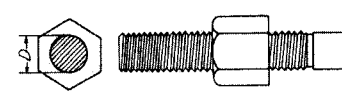
Threaded bar	23.0 ~ 32.0	0.906 ~ 1.260	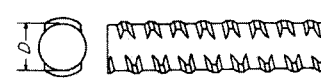

Figure 2.3 Common shapes and diameters of prestressing tendons. *(Courtesy Sumitomo's Tensioning Materials, Japan.)*

Prestressing tendons used in the United States are manufactured to meet minimum ASTM specifications described in the following standards: A421 for uncoated stress-relieved wires, A416 for uncoated seven-wire stress-relieved strands, and A722 for uncoated high-strength steel bars. Although these standards would guarantee minimum properties, actual properties depend greatly on the manufacturing process. Local manufacturers and suppliers should be consulted for particular details

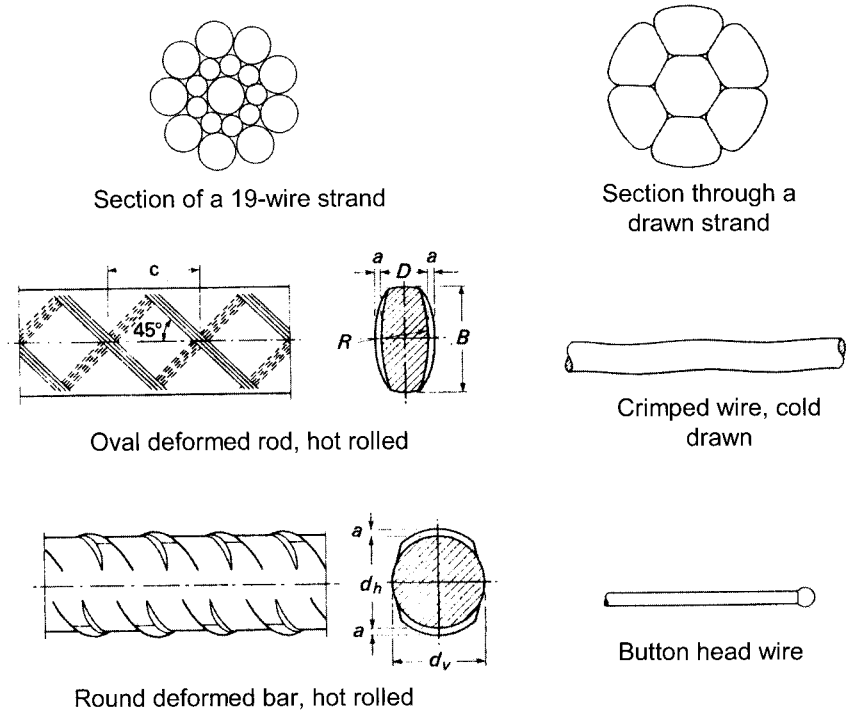

Figure 2.4 Shapes of some particular prestressing tendons. *(Adapted from Ref. 2.26.)*

The high tensile strength and adequate ductility of prestressing steels are generally obtained by using (1) high carbon hot rolled alloy steel, (2) cold drawn or deformed carbon steel, preferably tempered, and (3) hot rolled and heat treated carbon steel. Some of these treatments are clarified in the following section and in Fig. 2.5. When alloys are used, they comprise manganese, silicon, chromium, and, to a lesser extent, nickel.

Most prestressing wires are produced by the cold working (drawing or rolling) process. Wires are manufactured with different cross-sectional shapes and surface conditions: round or oval, smooth or indented, ribbed, twisted, or crimped. When cut to size, round wires used in some posttensioning systems can have button heads formed at their ends (Fig. 2.4). Typical characteristics of prestressing wires most frequently used in the United States are shown in Table 2.4.

Table 2.4 Typical characteristics of stress-relieved prestressing wires and strands

Prestressing steel	ASTM type or grade	Nominal diameter		Nominal area		Minimum tensile strength, f_{pu}	
		in.	mm	in^2	mm^2	ksi	Mpa
Stress-relieved wires (ASTM A421)	WA,†BA‡	0.192	4.88	0.0289	18.7	250	1725
	WA	0.196	4.98	0.0302	19.4	250	1725
	BA	0.196	4.98	0.0302	19.4	240	1655
	WA, BA	0.25	6.35	0.0491	31.6	240	1655
	WA	0.276	7.01	0.0598	38.7	235	1622
Stress-relieved 7-wire strands (ASTM A416)	Grade 250	0.25	6.35	0.036	23.22	250	1725
		0.313	7.94	0.058	37.42	250	1725
		0.375	9.53	0.080	51.61	250	1725
		0.438	11.11	0.108	69.68	250	1725
		0.500	12.54	0.144	92.90	250	1725
		0.600	15.24	0.216	139.35	250	1725
	Grade 270	0.375	9.53	0.085	54.84	270	1860
		0.438	11.11	0.115	74.19	270	1860
		0.500	12.54	0.153	98.71	270	1860
		0.563	14.29	0.192	123.87	270	1860
		0.600	15.24	0.216	139.35	270	1860

†Tendon density = 490 lb/ft^3 or 7850 kg/m^3.
‡Type WA wire for wedge or grip anchoring and type BA for button-head anchoring.

Prestressing strands are produced from several wires. In the seven-wire strand, six peripheral wires are wound helically over a central wire, which has a slightly higher diameter than the others. Because strands are made with relatively small diameter wires, they are much easier to handle (more flexible) than a single bar of the same nominal diameter and they achieve superior properties due to better quality control (Table 2.4). Most popular is the 1/2-inch diameter strand with a minimum tensile strength of 270 ksi (1860 MPa). One variety of seven-wire strand is the die-formed or drawn strand (Fig. 2.4). Drawing tightens the wires against each other and leads to a smoother outside surface. Mechanical properties such as strength and relaxation are enhanced. Common upper and lower tolerance limits on strand area and mass are +4 and -2 percent. The equivalent area is generally obtained from weighing, assuming a density of 490 lb/ft^3 (7850 kg/m^3).

Prestressing bars are manufactured with a smooth or ribbed surface. Smooth bars can be end-threaded mechanically to be used with anchoring systems based on nut and plate. The ribs in a ribbed bar are formed during the drawing process and act as a thread such as in the Dywidag system. Thus the bar can be anchored anywhere along its length. Prestressing bars are generally made with alloy steel heat treated to

achieve desirable properties. Common diameters and grades used in the United States are summarized in Table 2.5.

Table 2.5 Typical characteristics of prestressing bars.

Type	ASTM grade	Nominal diameter		Nominal area†		Minimum tensile strength f_{pu}	
		in	mm	in^2	mm^2	ksi	MPa
Smooth alloyed steel bars (ASTM A722)	145	0.750	19.05	0.442	283.9	145	1000
		0.875	22.22	0.601	387.1	145	1000
		1.0	25.40	0.785	503.2	145	1000
		1.125	28.57	0.994	638.7	145	1000
		1.250	31.75	1.227	793.5	145	1000
		1.375	34.92	1.485	954.8	145	1000
	160	0.750	19.05	0.442	283.9	160	1104
		0.875	22.22	0.601	387.1	160	1104
		1.0	25.40	0.785	503.2	160	1104
		1.125	28.57	0.994	638.7	160	1104
		1.250	31.75	1.227	793.5	160	1104
		1.375	34.92	1.485	954.8	160	1104
Deformed bars‡	...	0.625	15.87	0.280	180.6	157	1083
		1.0	25.4	0.852	548.4	150	1035
		1.0	25.4	0.852	548.4	160	1104
		1.25	31.75	1.295	835.5	150	1035
		1.25	31.75	1.295	835.5	160	1104
		1.50	34.92	1.630	1051.6	150	1035

†Bar density = 490 lb/ft^3 or 7850 kg/m^3.
‡Adapted from the *PCI Handbook*.

2.2.2 Production Process

A typical flow chart of the manufacturing process of prestressing steels is shown in Fig. 2.5. The process is self-explanatory. However, some particular procedures and terms need to be explained and will clarify some terms used in the preceding section:

1. *Patenting.* A heat treatment process which gives the hot rolled steel a suitable metallurgical structure leading to improved homogeneity, strength, and toughness.
2. *Pickling.* Chemical or mechanical removal of the hard scale of oxidized iron formed on the surface of the rod.

3. *Quenching and tempering.* A heat treatment process in which the steel is heated to about 800°C followed by rapid cooling (such as oil quenching) and subsequent tempering at about 450°C.
4. *Cold drawing.* A process in which the tendon is pulled through a die to reduce its cross-sectional area and improve its strength.

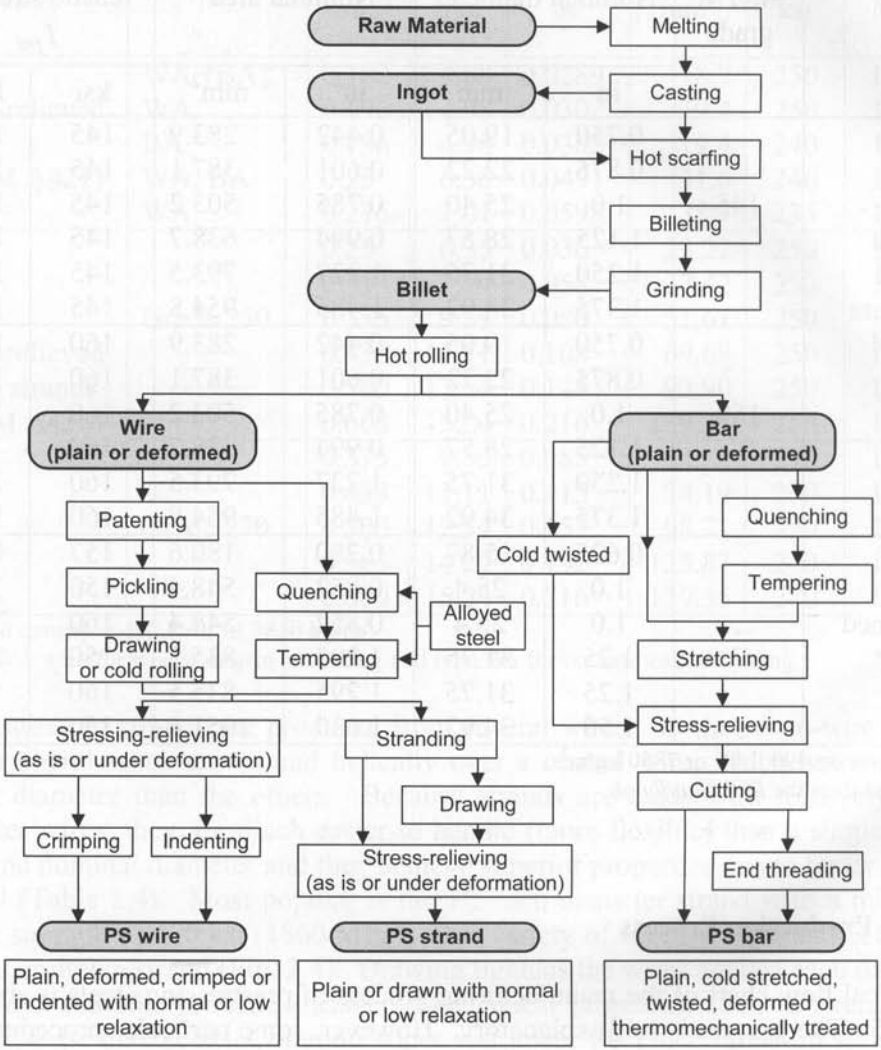

Figure 2.5 Flow chart illustrating typical production processes for prestressing steels.

5. *Stress-relieving.* Heating to an appropriate temperature, generally less than 500°C, to improve the mechanical properties, specifically ductility. Stress-relieving, under prescribed conditions of deformation, leads to improved relaxation characteristics (low relaxation tendons).

6. *Stabilizing.* Heating the tendon under high tension sufficient to produce a permanent elongation. It improves most mechanical properties and leads to low relaxation.
7. *Indenting.* Introduction of regular dents at the periphery of a wire to improve its bonding characteristics.
8. *Crimping.* Consists of a series of regular bends of the wire in one plane to improve its bonding characteristics.

Table 2.6 Minimum properties of prestressing tendons.

Prestressing steel	ASTM standard	ASTM minimum specified		Other expected properties		
				Elastic modulus		Prop. limit: f_{pp} at 0.01% offset strain
		Yield strength	Elongation at failure	ksi	MPa	
Wires	A421	$f_{py} = 0.85 f_{pu}$ at $\varepsilon_{py} = 0.010$	ε_{pu}=0.040 Gauge length: 10 in (254 mm)	29,000	200,000	75 to 85% of minimum specified strength
Strands: Stress-relieved	A416	$f_{py} = 0.85 f_{pu}$ at $\varepsilon_{py} = 0.010$	ε_{pu}=0.040 Gauge length: 24 in (610 mm)	27,000	186,000	70 to 75% of minimum specified strength
Low-lax	A416	$f_{py} = 0.90 f_{pu}$ at $\varepsilon_{py} = 0.010$				
Bars	A722	Smooth bars: $f_{py} = 0.85 f_{pu}$ at $\varepsilon_{py} = 0.0070$ Deformed bars: $f_{py} = 0.80 f_{pu}$ at $\varepsilon_{py} = 0.0070$	ε_{pu}=0.40 Gauge length: 20 bar diameter	28,000	193,000	60 to 65% of minimum specified strength

2.2.3 Mechanical and Stress-Strain Properties

The mechanical properties of prestressing steels of direct use in design must generally satisfy a number of minimum requirements. Such properties include the tensile strength and corresponding failure strain, the yield point, the proportional limit, and the modulus of elasticity. Steel tendons are manufactured to achieve actual properties generally superior to the minimum properties required by various standards. For instance, the minimum required (or specified) strength, f_{pu}, also called characteristic strength, corresponds to a value below which no more than five

percent of all test data will lie. It is associated with a standard deviation of 40 MPa (5.8 ksi)[Ref. 2.26].

A summary of ASTM minimum requirements related to the relevant mechanical properties of prestressing steels is given in Table 2.6. It can be seen that for a given characteristic strength f_{pu},the minimum yield strength should not be less than 0.85 f_{pu} for all tendons except deformed bars, and that their ultimate strain should not be less than four percent. More details on actual properties, their variability and modeling can be found in Ref. 1.48, where the nonlinear analysis of prestressed concrete members is addressed.

Typical stress-strain curves of prestressing steels in uniaxial tension are plotted in Fig. 2.1 and compared with those of reinforcing steels. It can be observed that prestressing steels (1) offer substantially higher strengths than reinforcing steels accompanied by lower failure strains, (2) do not show a well-defined yielding behavior, and (3) have a relatively high proportional limit. Their stress-strain curve can be represented by three successive portions: an initial linear elastic portion up to the proportional limit, a nonlinear portion with gradually decreasing slope, and a final almost linear strain-hardening portion with a small positive slope leading to failure.

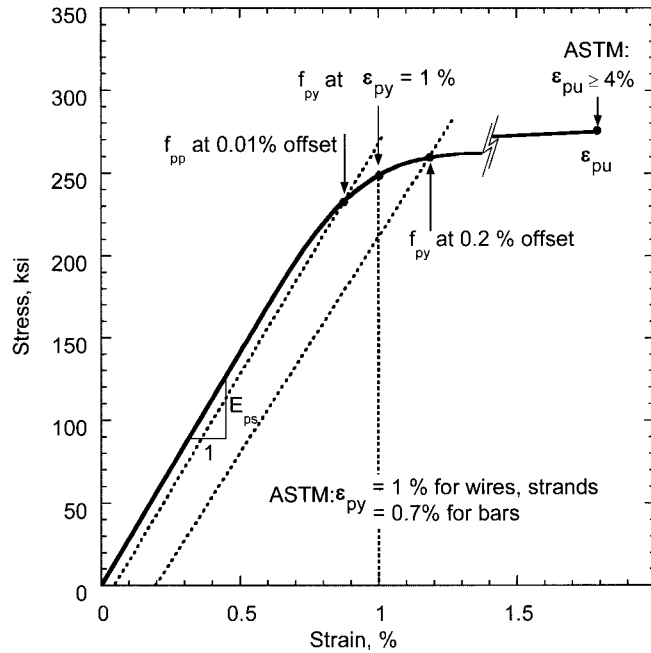

Figure 2.6 Typical determination of yield strength for a prestressing steel.

Because yielding of prestressing steels is not well defined, their yield strength is determined according to a strain criterion. Current ASTM standards specify that the yield stress of prestressing wires and strands should correspond to a total strain of

one percent, while a total strain of 0.7 percent is recommended for prestressing bars (Table 2.6). Another often used method to determine the yield stress is called the offset-strain method. In this method the yield stress corresponds to a permanent plastic strain of 0.2 percent (or 0.1 percent depending on the standard used). An example illustrating the determination of yield stress is shown in Fig. 2.6. Also shown is the determination of the proportional limit

Theoretically the proportional limit corresponds to the point at which the initial portion of the stress-strain curve deviates from linearity. In practice, however, the proportional limit is generally determined by the stress corresponding to a permanent (non-recoverable or off-set) strain of 0.01 percent (or 0.02 percent depending on some specifications).

The modulus of elasticity of steel is essentially a constant independent of strength. However, slight differences exist between the elastic moduli of prestressing steels. Straight wires (as reinforcing bars) generally show the highest modulus (Table 2.6). Because of alloying the modulus of prestressing bars is smaller. Since strands are manufactured by spiral winding, their equivalent modulus is smaller than that of the wire component. Typical values are given in Table 2.6, but the manufacturing process may influence the order shown and actual data should be preferably used when available.

2.2.4 Relaxation

Relaxation is the loss of tension over time in a stressed tendon maintained at constant length and temperature. Similarly to creep, which describes the change of strain with time at a constant stress, relaxation results from the adaptation of material to an externally applied constraint. The relaxation losses of prestressing steels are generally negligible for stresses smaller than 50 percent of ultimate strength. However, they increase rapidly with an increase in stress and temperature.

Typical variations of relaxation loss with time at various levels of initial stress and at various temperatures are shown in Figs. 2.7 and 2.8. It can be generally observed that relaxation continues over time but at a decreasing rate. However there is evidence [Ref. 2.53] that the relative influence of temperature within the ambient range diminishes over time while the influence of initial stress remains the same. In practice the long-term relaxation of prestressing steels is determined from short-term tests. Most commonly, the relaxation loss is experimentally determined at 1000 hours and a multiplier is used to estimate the relaxation at the end of life of the structure. Relaxation depends on the type and grade of steel. However, for the purpose of design, prestressing steels are divided into two groups, having either normal or low relaxation properties. A standard stress-relieved strand has normal relaxation. Low relaxation is about 25 percent of normal relaxation. Strands with low relaxation properties can be obtained by a process described as *stabilization*; in that process the strand is subjected to a temperature regime ranging from 20°C to 100°C for an extended period of time, while under a stress close to 70 percent of ultimate strength. In comparison to stress-relieved strand, this one is often identified

in practice as "low-lax." Typical relaxation losses at 1000 hours recommended by the FIP Commission of Prestressing Steels [Ref. 2.26] are given in Table 2.7 in percent of initial stress. Note that the higher the initial stress, the higher the relaxation loss. A multiplier of three is suggested to estimate normal life relaxation after 50 years. The corresponding relaxation loss can be very significant.

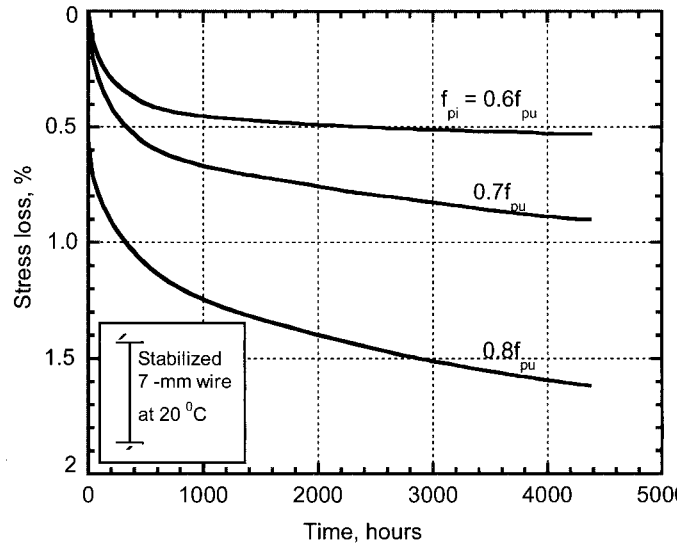

Figure 2.7 Typical effect of initial stress on relaxation of stabilized prestressing steel. *(Adapted from data by GKN, Somerset Wire and Strands, Cardiff, U.K.)*

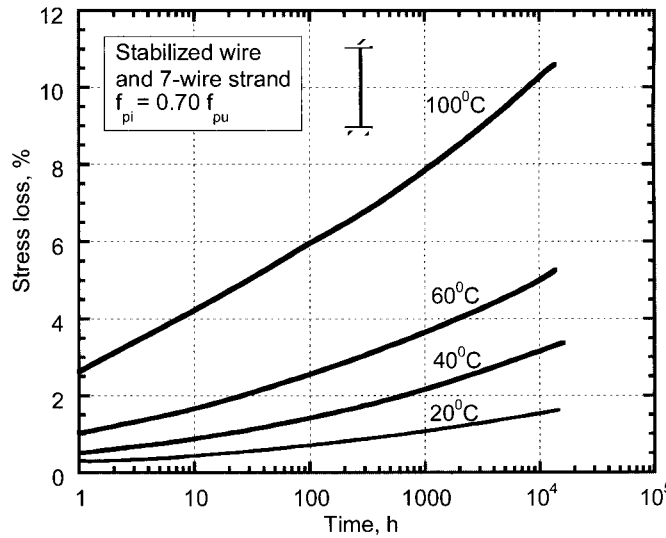

Figure 2.8 Typical effect of temperature on relaxation of stabilized prestressing steels. *(Adapted from data by GKN, Somerset Wire and Strands, Cardiff, U.K.)*

Table 2.7 Typical relaxation of prestressing steels at 1000 hours.

	f_{pi}/f_{pu}		
	0.6	0.7	0.8
FIP Commission:			
Normal relaxation (level 1) (stress-relieved strand)	4.5%	8%	12%
Low relaxation (level 2)	1%	2%	4.5%
ASTM A416 and A421 Low relaxation	.....	≤ 2.5%	≤ 3.5%

However, one must realize that in a prestressed concrete element the steel stress decreases over time not only because of relaxation but also because the concrete shortens due to creep and shrinkage. The tendon will shorten an equal amount and its initial stress level will decrease. As a result, the apparent relaxation loss is smaller than the pure relaxation otherwise obtained from a reference tendon maintained at constant length. The effect of creep and/or relaxation with time on the state of stress and strain in the material is illustrated in Fig. 2.9 and applies to steel, concrete, or their combination. A detailed treatment of this interaction can be found in Chapter 8 where prestress losses are covered.

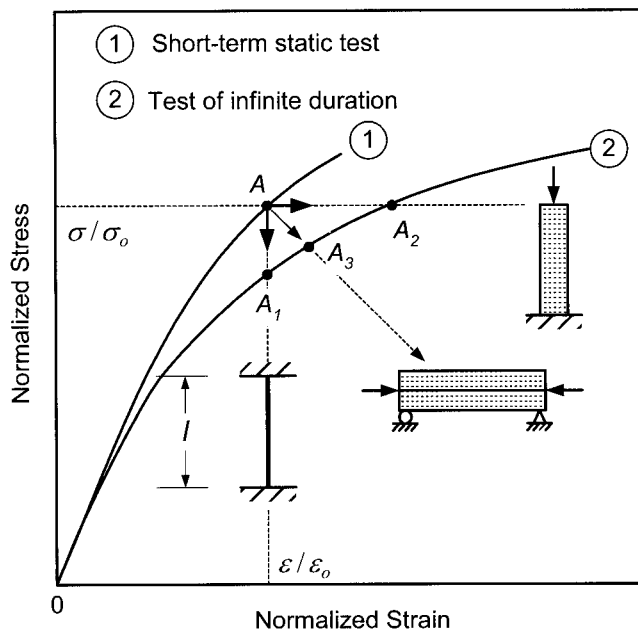

Figure 2.9 Effect of relaxation and creep on the state of stresses and strains.

An extensive investigation of the relaxation properties of stress-relieved wires was carried out by Magura et al. in the early 1960's [Ref. 2.37]. Based on their results, they proposed the following relationship to predict, in function of the initial stress, the stress in the prestressing steel at any time t:

$$f_{ps}(t) = f_{pi}\left[1 - \frac{\log t}{10}\left(\frac{f_{pi}}{f_{py}} - 0.55\right)\right] \tag{2.2}$$

where t is the duration of loading in hours and is not less than one hour, log t is to the base 10, and the ratio f_{pi}/f_{py} is not less than 0.55. For low relaxation steel a denominator of 45 is suggested instead of 10 under the log t term leading to:

$$f_{ps}(t) = f_{pi}\left[1 - \frac{\log t}{45}\left(\frac{f_{pi}}{f_{py}} - 0.55\right)\right] \tag{2.3}$$

As a first approximation Eqs. (2.2) and (2.3) can also be used for prestressing strands and bars. For a given time t, the stress in the prestressing steel, $f_{ps}(t)$, is a quadratic function of the initial stress, f_{pi}.

The stress loss due to pure relaxation can be computed from

$$\Delta f_{pR}(t) = f_{pi} - f_{ps}(t) = f_{pi}\frac{\log(t)}{K}\left(\frac{f_{pi}}{f_{py}} - 0.55\right) \tag{2.4}$$

in which $K = 10$ for stress relieved steel and 45 for low relaxation steel. Note that the loss in percent of the initial stress can be obtained by dividing the two sides of the equation by f_{pi}.

It was pointed out above that because of the effects of creep and shrinkage in a prestressed concrete member, the apparent relaxation of the steel will be smaller than the pure relaxation otherwise obtained from a reference strand and predicted by Eqs. (2.2) and (2.3). In lieu of a more exact analysis (see Chap. 8) the following relationship suggested by the FIP Commission on Prestressing Steels [Refs. 2.26] can also be used to estimate the apparent life relaxation:

$$(\Delta f_{pR})_{app} = (\Delta f_{pR})_{pure}\left[1 - 2\frac{\Delta f_{pS} + \Delta f_{pC}}{f_{pi}}\right] \tag{2.5}$$

where Δf_{pC} and Δf_{pS} are the life losses of stress in the prestressing steel due to creep and shrinkage of the concrete. Their values must be estimated and possibly revised

after a first iteration, because in effect creep losses depend on the stress in the steel which itself depends on relaxation.

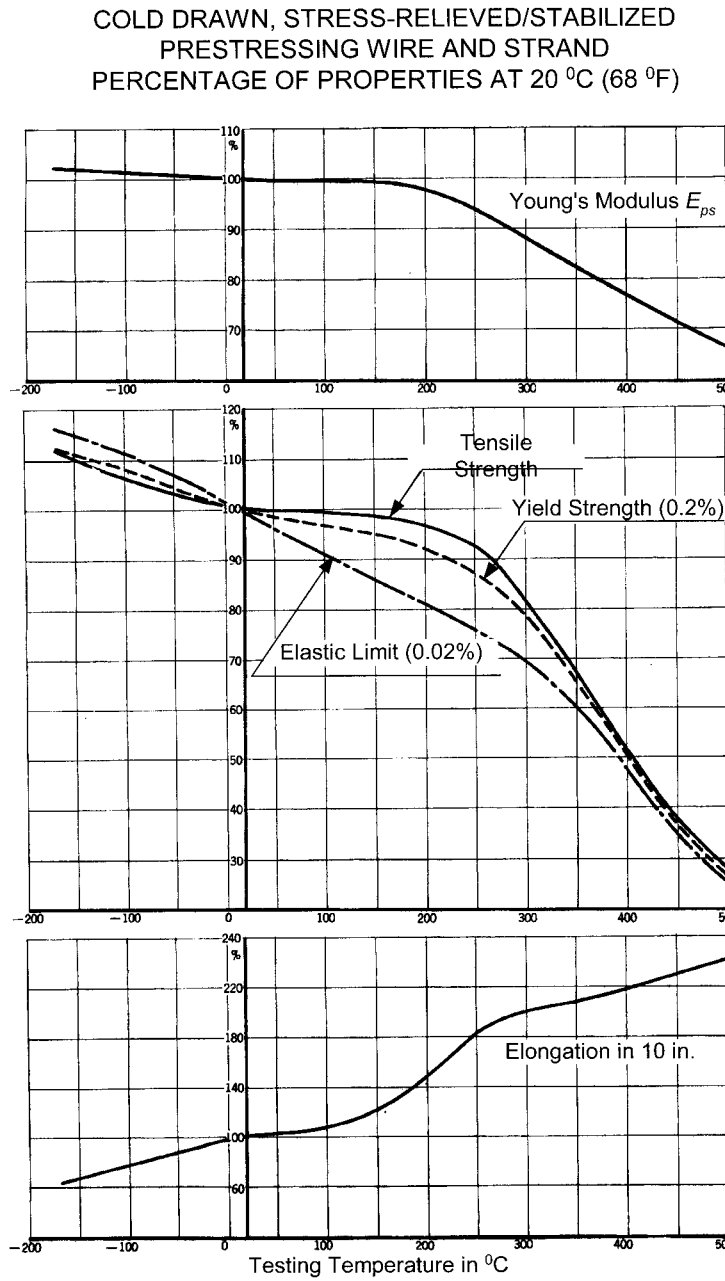

Figure 2.10 Effect of temperature on various properties of prestressing steels. *(Courtesy Shinko Wire Company Ltd., Japan.)*

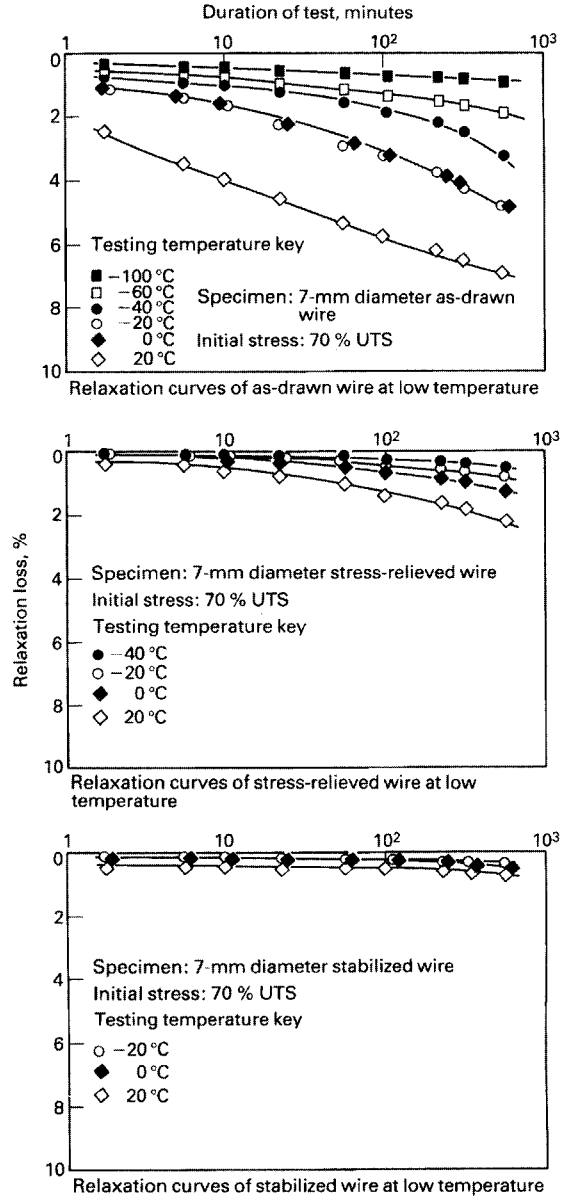

Figure 2.11 Effect of low temperature on relaxation of prestressing steels. *(From Ref. 2.27, Courtesy Federation Internationale de la Precontrainte.)*

2.2.5 Effects of Temperature

The mechanical properties of prestressing steels do not change appreciably when the ambient temperature varies over a reasonable range. This is generally the case for the strength, yield point, proportional limit, and elastic modulus. Even though a

change in temperature from 20 to 40°C (Fig. 2.8) seems to increase relaxation at 1000 hours by 50 percent, it may be assumed [Refs. 2.26, 2.37, 2.53], when extrapolating over a long period of time, that the relaxation loss at 40°C is about equal to that at 20°C. The only difference is that at higher temperature the relaxation loss will be reached at an earlier time.

Extreme temperature conditions can seriously affect the mechanical properties of prestressing steels [Ref. 2.23]. A sharp decrease in temperature will lead to an improvement in strength and modulus (Fig. 2.10), but a deterioration in ductility and impact resistance takes place. It is estimated that decreasing the temperature from 20 to -200°C will increase tensile and yield strengths by about 20 percent [Ref. 2.27]. Similarly, relaxation properties are substantially improved at low temperatures (Fig. 2.11). However, increasing the temperature produces opposite effects. Above 200°C a rapid deterioration can be expected (Fig. 2.10). This means that in the presence of fire a critical temperature may be reached at which external stresses will overcome the strength of the structure and collapse will follow. In designing for possible service at high temperature, it may be more appropriate to use alloy steel which undergoes a reduction in strength at temperatures above 350°C but, provided the heating period is not too long, regains its strength when cooled. Under similar conditions, cold worked and heat treated steels will suffer serious permanent reduction in strength. Note that if alloy steel is kept at temperatures between 350 and 550°C for sufficient periods of time (of the order of a few hours), it tends to become extremely brittle.

2.2.6 Fatigue

Fatigue is the process of deterioration of the mechanical properties of materials under fluctuating stresses. Such stresses are generally induced by the repetitive application of live loads on the structure. The resistance of a material to fatigue is often described by an *S-N* curve, where *S* represents the stress range in the material and *N* the number of cycles to failure, also called fatigue life. Below a certain stress range, termed endurance limit, some materials do not fail up to a quasi infinite number of cycles. Prestressing steels do not seem to have an endurance limit [Refs. 2.2, 2.24, 2.25, 2.26, 2.32, 2.34, 2.42, 2.55, 2.59, 2.65, 2.66]. At present, a fatigue life of two million cycles is considered a minimum and a life of up to ten million cycles is designed for in some particular applications. Typical *S-N* data for prestressing tendons are plotted in Fig. 2.12 [Ref. 2.42]. In prestressed concrete, the minimum stress in the steel is relatively high (50 to 60 percent of ultimate). As the *S-N* curve does not take into account the effect of minimum stress, a Goodman diagram can be used for the particular fatigue life considered in the design. A typical Goodman diagram for prestressing wires and strands proposed by Ekberg et al. [Ref. 2.25] is shown in Fig. 2.13, assuming a fatigue life of two million cycles. It can be seen that at a minimum stress of about 55 percent of ultimate, a fluctuating stress range of about 13 percent is acceptable. The FIP Commission on Prestressing

Steels suggests the use of a Smith diagram which is a modification of the Goodman diagram plotted with the mean stress instead of the minimum stress (Fig. 2.14).

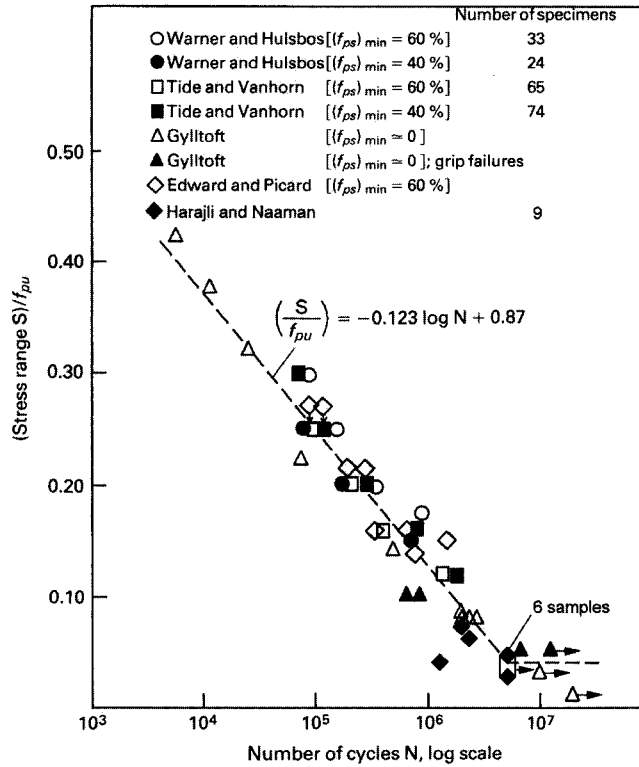

Figure 2.12 Typical S-N curve for prestressing tendons. *(From Ref. 2.42.)*

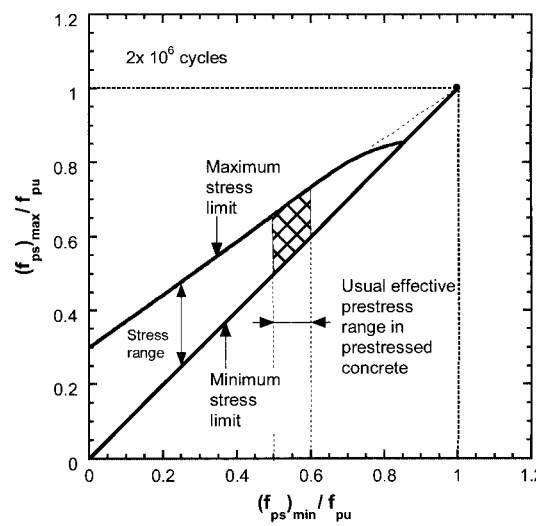

Figure 2.13 Typical Goodman diagram for prestressing wires and strands. *(From Ref. 2.25.)*

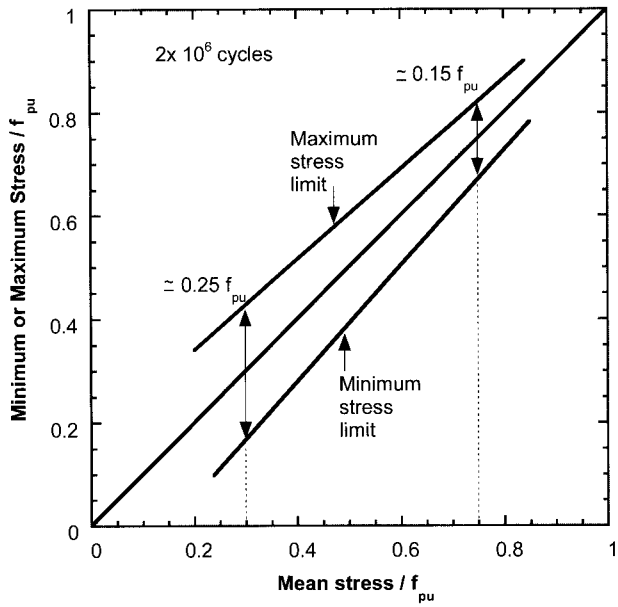

Figure 2.14 Typical Smith diagram for prestressing steels. *(From Ref. 2.26.)*

An endurance limit (that is the stress range for which the reinforcement will not fail for an infinite number of cycles) has not been found for prestressing steels; however, a fatigue life of 2 million cycles is considered to be sufficient for most applications. ACI Committee 215, charged to study fatigue in concrete structures [Ref. 2.6], recommends a maximum stress range of $0.10f_{pu}$ for prestressing strands and $0.12f_{pu}$ for wires, that is:

$$\begin{cases} \Delta f_{pr} = 0.10 f_{pu} & \text{for strands} \\ \Delta f_{pr} = 0.12 f_{pu} & \text{for wires} \end{cases} \tag{2.6a}$$

Such limits are substantially higher than stress range values observed in fully prestressed uncracked members. However, if cracking is allowed or if partial prestressing is used, the above limitations may become critical in the design. In European practice, a stress range of up to 200 MPa (29 ksi) is considered acceptable for prestressing tendons, while a safe design value below 150 MPa (22 ksi) is preferred. A stress range limit of 80 MPa (11.6 ksi) is recommended by the FIP Commission of Prestressing Steels [Ref. 2.26] for the anchorage-tendon system of bonded tendons.

In order to predict a maximum safe stress range at other than 2 million cycles, the following equation can be used, assuming a minimum stress not exceeding 60% f_{pu} [Ref. 2.42]:

$$\frac{\Delta f_{pr}}{f_{pu}} = -0.123 \log N_f + 0.87 \tag{2.6b}$$

where:

Δf_{pr} = maximum safe stress range for a fatigue life of N cycles
f_{pu} = specified tensile strength of the prestressing strand
N_f = number of cycles to failure

The above recommendations are derived from relatively high frequency cyclic tests. If cyclic loading is not continuously applied, the fatigue resistance tends to improve with the extent of the rest periods.

Extensive test data from partially prestressed concrete beams [Refs. 2.25, 2.28, 2.30, 2.32, 2.42, 2.44, 2.56] subjected to both constant and variable amplitude cyclic fatigue loading suggest that the stress range limits recommended above may be too optimistic. This is due to the possible effect of fretting friction, which develops between two adjacent wires or between the concrete and the steel at a cracked section during repetitive cyclic loading. Fretting [2.66] creates points of stress concentration, which may precipitate fatigue fracture of one wire leading to increased stresses on the other wires of a strand and subsequent premature failure. Overall, great variability is observed in the experimental results supporting the premise that fatigue behavior is probabilistic in nature and that each specimen tested is a random sample. Based on the above mentioned tests, the author offers the following recommendation. The design of cracked partially prestressed concrete beams should be based on limiting simultaneously the stress range in the reinforcement and the crack width range in the concrete. This last limitation attempts to control the effect of fretting or abrasion between wires of the same tendon or between the tendons and the concrete. On the basis of test results, realistic limits suggested could be set as: 112 MPa (16 ksi) for the stress range in the prestressing steel and 0.1 mm for the crack width range in the concrete under cyclic fatigue loading. The addition of ordinary reinforcing bars to a prestressed concrete member should enhance its fatigue properties even if such reinforcement is not needed for strength purposes.

The AASHTO LRFD code specifies that the stress range in prestressing tendons shall not exceed 18 ksi (126 Mpa) for radii of curvature in excess of 30 ft (9.14 m) and 10 ksi (70 Mpa) for radii of curvature in excess of 12 ft (3.65 m). A linear interpolation may be used for radii of curvature in between the above limits.

2.2.7 Corrosion

The magnitude and consequences of corrosion in prestressing steels are much more severe than in reinforcing steels. This is not only because high-grade steel is more susceptible to corrosion but also because the diameter of prestressing tendons is

relatively small. Thus, even a small uniform corrosive layer or a corroded spot can substantially reduce the cross-sectional area of the steel, induce stress concentrations, and eventually lead to premature failure. Exposure of unprotected prestressing steels to normal environments, even for short periods of time (a few months) can lead to an appreciable decrease in their tensile properties and a greater reduction in their fatigue resistance. Prestressing steels are generally susceptible to two major types of corrosion: electrochemical corrosion and stress corrosion. In the electrochemical corrosion an aqueous solution must be present, even in the form of a thin film, and air (oxygen) is needed. Stress corrosion causes brittleness in the steel under certain conditions of stresses and environments. Sensitivity to corrosion is different for different steels.

Everything else being equal, the reinforcement in a fully prestressed (uncracked) concrete beam is better protected against corrosion than the reinforcement in a partially prestressed (cracked) beam, because cracks may ease the passage of corrosive agents. Although corrosion also occurs along uncracked sections, it is generally agreed that cracking facilitates its initiation and progression.

It has been common practice in design to limit the size of crack widths in order to reduce the probability of corrosion. Several studies, however, seem to shy away from this approach by pointing out that corrosion may be due to many causes most of which do not need cracking to be activated. It appears that one of the best protections against corrosion of the reinforcement is still the use of a good sound concrete and not necessarily through crack width limitations. Concrete additives that lower the P.H. of the concrete are not recommended in prestressing applications.

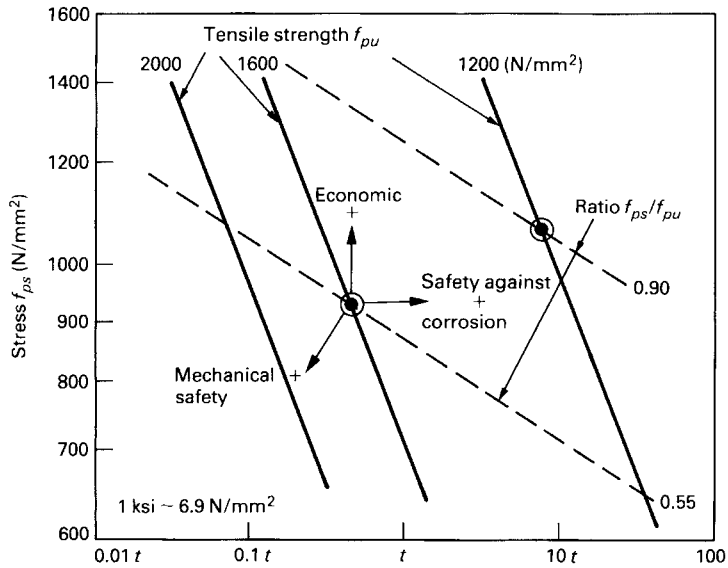

Figure 2.15 Relative lifetime of prestressing steels in a corrosive medium. *(Courtesy TNO Metal Research Institute, Netherlands.)*

Corrosion is very difficult to quantify, thus leaving the designer with his/her engineering judgment in taking appropriate protective measures against it [Refs. 2.26, 2.29, 2.55]. Qualitatively, however, the effect of important parameters on the rate of corrosion is best illustrated in a graph. Figure 2.15 shows the relative lifetime up to fracture of a cold-drawn stress-relieved wire placed in a particular medium causing corrosive cracking as a function of strength and stress-to-strength ratio. It can be seen that the higher the strength and the higher the applied stress, the smaller the lifetime of the wire. Figure 2.15 also illustrates the tradeoffs that must be made in prestressed concrete design between safety against corrosion, mechanical safety, and economy. The higher the strength and the higher the prestress, the more economical the structure, but also the higher its susceptibility to corrosion.

To guard against corrosion, prestressing steels must be transported and stored in closed waterproof containers and protected from damage and contamination during handling. When bonded tendons are used, as soon as the tensioning operation is completed, good quality grout should be injected in order to guard against water pockets and contaminants. A sufficient concrete cover will add to the protection of the tendons from corrosion. The concrete and admixtures used should contain the least amounts of calcium chloride. Unbonded tendons should be protected by an anticorrosive material such as asphalt, grease, oil, or a combination of grease and plastic tubing. The consequences of corrosion can be so serious that all appropriate precautions must be taken to prevent it or to reduce its effects.

2.3 CONCRETE

Extensive technical information on concrete and its use exists in the technical literature [Refs. 2.36, 2.39, 2.41, 2.46, 2.47, 2.61, 2.62]. Concrete is a versatile composite material of a very complex nature, yet it can be approached at any desired level of sophistication. The simplest is when only its compressive strength is specified for design. The technical level at which concrete must be approached is higher in prestressed concrete than in reinforced concrete. In designing a prestressed concrete structure, the designer does not only consider the strength of concrete but also its time-dependent properties such as creep and shrinkage. He/she has to assess their effects on the loss of prestress in the steel and the long-term deformation or deflection of the structure. In practice the corresponding procedure must be reduced to a manageable level.

2.3.1 Composition

The main components of concrete are Portland cement, aggregate (fine and coarse), and water. Five types of standard Portland cements are recognized in the United States. They are manufactured in accordance with ASTM Standard C150. Type I is a general purpose cement commonly used when the special properties of the other four types are not needed. Type II is for general concrete construction exposed to

moderate levels of sulfate attack or where moderate heat of hydration is required. Type III is for use where high early strength is required; it leads to a seven-day strength about equal to that achieved at 28 days by Type I cement. Type IV cement is for use when low heat of hydration is desired, and Type V when high sulfate resistance is needed. The first three types of cement are available with an A variety, such as Type IIIA, when air entrainment is desired.

To achieve higher strength properties, high cement contents, low water-to-cement ratios, and good quality aggregates are used. Normal weight coarse aggregates include granite, basalt, limestone, quartzite, and slate. They lead to a normal weight concrete with a density about 150 lb/ft^3 (23.6 kN/m^3). Structural lightweight aggregates include expanded shale clay and slate and lead to lightweight concretes of density between 100 lb/ft^3 and 120 lb/ft^3 (15.7 kN/m^3 to 18.9 kN/m^3). Sands, either normal weight or lightweight, are used as fine aggregates.

Admixtures are often added to fresh concrete to achieve a particular effect. Water-reducing admixtures and superplasticizers allow a substantial reduction in the water-cement ratio for the same workability of the mix, thus leading to increased strengths. They are also used to achieve a desired strength at lower cement content. Air entraining agents are commonly used in cold climates to improve the freeze-thaw resistance of concrete. In posttensioned construction expanding agents are added to the grout to ensure proper filling of the ducts. Viscosity agents are added to self-leveling and self-compacting concretes. Many other admixtures are available for use in concrete. Care should be taken to avoid admixtures that contain calcium chlorides since they cause corrosion of the reinforcement.

2.3.2 Stress-Strain Curve

Typical stress-strain curves of normal weight concretes in uniaxial compression adapted from Ref. [2.11] are shown in Fig. 2.16*a*. They comprise two main portions: an ascending portion up to the peak point (maximum stress) and a descending portion. The strength, f'_c, corresponds to the maximum stress. The ascending portion can itself be separated into two parts for the purpose of design: a quasi-linear portion up to about 40 percent of the strength followed by a nonlinear portion reaching to the peak point gradually. Note that the higher the strength of concrete, the higher the slope at the origin of the ascending portion. Thus, the higher the strength, the higher the elastic modulus. The tangent at the origin of the stress-strain curve gives the initial modulus (Fig. 2.16b). A line joining the origin to any point of the curve gives the secant modulus. The value of the secant modulus at 45 percent of the maximum stress is recommended by ACI for use in design. In the nonlinear portion of the stress-strain curve, the total strain is composed of an elastic strain and a permanent irrecoverable strain mostly attributed to microcracking. It is generally observed that unloading from any point of the curve, beyond the peak point, does not return to zero strain and is not parallel to the line giving the elastic modulus.

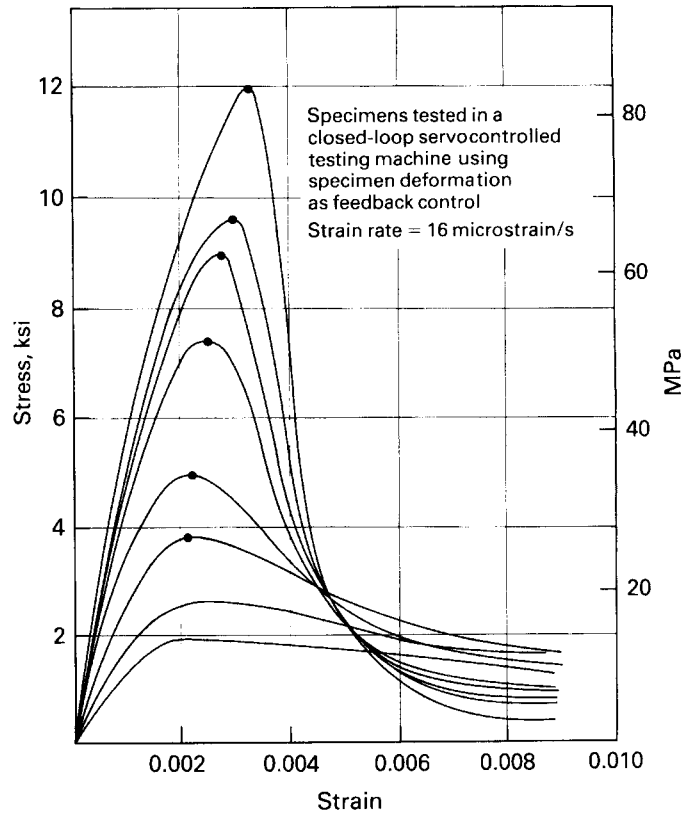

Figure 2.16a Typical stress-strain curves of normal weight concrete in compression. *(Adapted from Ref. 2.11.)*

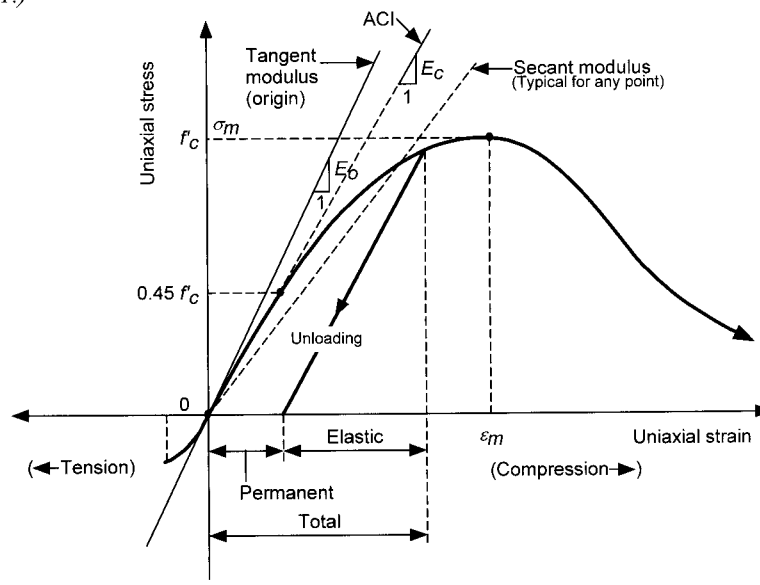

Figure 2.16b Determination of modulus from the stress-strain curve of concrete.

Concrete can be a very complex material in both its behavior and modeling. Figures 2.17a and 2.17b give an idea of the stress-strain response of concrete under imposed increments of strains in uniaxial compression, and an example of how such response can be modeled [Refs. 2.49, 2.50]. The reader is referred to specialized texts and studies for further information on the constitutive properties of concrete.

(a)

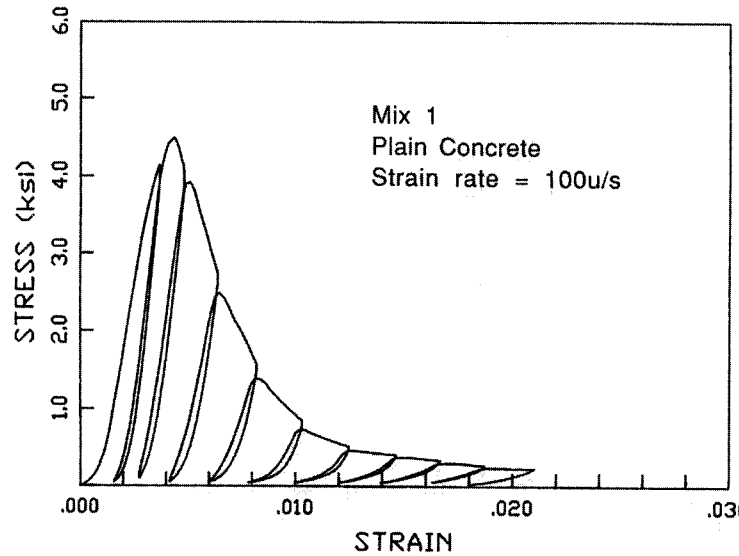

(b)

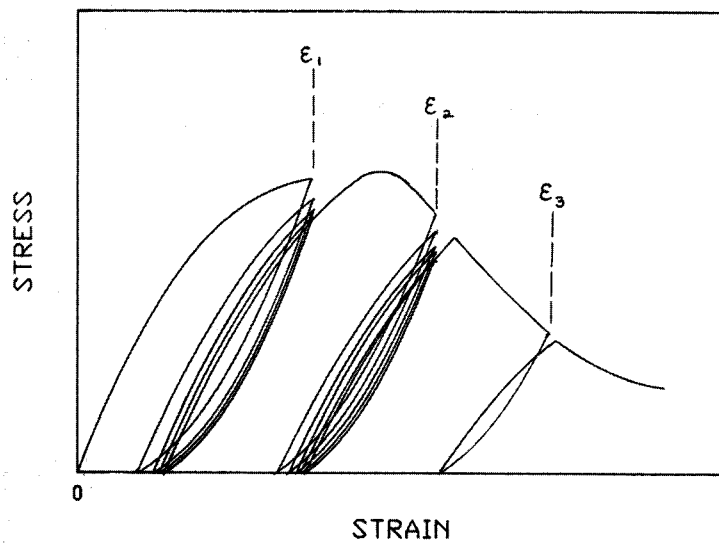

Figure 2.17 ***(a)*** **Experimental stress-strain response of concrete under repeated strain increments.** ***(b)*** **Example of modeling of such response [Refs. 2.49 and 2.50].**

Going back to Fig. 2.16a it can be observed that the higher the concrete strength, the steeper the descending portion of the stress-strain curve. A steep descending portion is often associated with brittleness or lack of ductility of the material. Concrete can be made much more ductile by proper addition of fibers or confinement. Moreover, structural ductility can be obtained even with brittle materials such as high-strength concretes as pointed out in Ref. 1.48 where the nonlinear analysis of prestressed concrete members is addressed. Another interesting characteristic of the descending portion is the presence of an inflection point. After the inflection point the curve tends asymptotically toward the strain axis, suggesting that very large plastic strains can be sustained by concrete. The inflection point is believed to represent the point at which the failure mode changes from split tension to sliding frictional shear mode.

Structural lightweight concretes have stress-strain curves similar in shape to those of normal weight concretes. However, for identical strengths their elastic modulus is smaller and the strain at the peak point is larger. It is important to realize that the shape of the stress-strain curve of concrete depends not only on the type of aggregate but also on many parameters, including the testing technique, the strain rate, and the amount of confinement.

Compressive strengths of up to 10 ksi (69 MPa) are not uncommon using structural lightweight concretes and up to 20 ksi (140 MPa) using normal weight concretes. Higher strengths, while possible, require special processes such as, for instance, heat and pressure in the case of reactive powder concrete (RPC) with compressive strengths exceeding 35 ksi (245 Mpa). Most common strength ranges for economical construction are considered next.

2.3.3 Mechanical Properties

Compressive strength is the most important design property of concrete. Many other properties can be related to it. For some applications only the desired compressive strength is specified in the design. In US practice the compressive strength is obtained from testing 6x12 in (150x300 mm) cylinders at the age of 28 days. When high-early-strength cement (Type III) is used, an age of seven days is commonly considered. The compressive strength corresponds to the maximum stress at the peak point of the stress-strain curve. The strength obtained from a cylinder test falls within a range of 70 to 90 percent of the strength obtained from a cube test. The higher the strength is, the higher the ratio. It is generally assumed in design that the actual compressive strength is equal to the design specified strength. In effect, the definition of design specified strength, f'_c, is such that a random compression test on the material should lead to a strength higher than or equal to f'_c with a probability of 90 percent.

Table 2.8 Common mechanical properties of structural concretes.

Property	Concrete type	Observed range†	Common design value	
			U.S. Units†	SI Units‡
Direct tensile strength, f'_{tc}	Normal weight	$-3\sqrt{f'_c}$ to $-5\sqrt{f'_c}$	$-3\sqrt{f'_c}$ or $-\frac{1}{3}\sqrt{\gamma_c f'_c}$	$-0.25\sqrt{f'_c}$ or $-0.0069\sqrt{\gamma_c f'_c}$
	Lightweight	$-2\sqrt{f'_c}$ to $-3.5\sqrt{f'_c}$	$-2\sqrt{f'_c}$ or $-\frac{1}{3}\sqrt{\gamma_c f'_c}$	$-0.17\sqrt{f'_c}$ or $-0.0069\sqrt{\gamma_c f'_c}$
Split cylinder tensile strength	Normal weight	$-6\sqrt{f'_c}$ to $-7\sqrt{f'_c}$	$-6\sqrt{f'_c}$ or $-0.6\sqrt{\gamma_c f'_c}$	$-0.50\sqrt{f'_c}$ or $-0.00138\sqrt{\gamma_c f'_c}$
	Lightweight	$-4\sqrt{f'_c}$ to $-5\sqrt{f'_c}$	$-4\sqrt{f'_c}$ or $-0.5\sqrt{\gamma_c f'_c}$	$-0.33\sqrt{f'_c}$ or $-0.00115\sqrt{\gamma_c f'_c}$
Modulus of rupture f_r	Normal weight	$-7.5\sqrt{f'_c}$ to $-12\sqrt{f'_c}$	$-7.5\sqrt{f'_c}$	$-0.62\sqrt{f'_c}$
	Lightweight	$-5\sqrt{f'_c}$ to $-9\sqrt{f'_c}$	$-0.75\left(7.5\sqrt{f'_c}\right)$, lightweight sand $-0.85\left(7.5\sqrt{f'_c}\right)$, normal sand	$-0.47\sqrt{f'_c}$, lightweight sand $-0.53\sqrt{f'_c}$, normal sand
Modulus of Elasticity E_c	Normal weight	$E_c = (27 \text{ to } 35)\gamma^{3/2}\sqrt{f'_c}$	$33\gamma_c^{3/2}\sqrt{f'_c}$ or $57{,}000\sqrt{f'_c}$	$0.043\gamma_c^{1.5}\sqrt{f'_c}$ or $4730\sqrt{f'_c}$
	Lightweight	$E_c = (25 \text{ to } 30)\gamma_c^{3/2}\sqrt{f'_c}$	$33\gamma_c^{3/2}\sqrt{f'_c}$	$0.043\gamma_c^{1.5}\sqrt{f'_c}$
Poisson's Ratio, ν	Normal and Lightweight	0.15 to 0.20	0.20	0.20

†Valid only for f'_c in pounds per square inch and γ_c in pounds per cubic foot. Tension negative, compression positive.

‡ f'_c in MPa and γ_c in kilograms per cubic meter.

In the United States most common values of f'_c for prestressed concrete structures are between 5 and 10 ksi (35 and 70 MPa) whether normal weight or lightweight concrete is used. Higher compressive strengths of 10 to 15 ksi (70 to 105 MPa) are used with normal weight concretes but to a much lesser extent. These strengths are on the average substantially higher than those specified for ordinary reinforced concrete construction.

Other useful mechanical properties of concrete can be related to its compressive strength. They include: its tensile strength determined from a uniaxial tensile test of a prism, its tensile strength determined from the split cylinder test, its modulus of rupture or tensile strength determined from a flexural test, and its elastic modulus determined from a compression test. The usual ranges of experimentally observed values of these properties in function of the compressive strength are summarized in Table 2.8 for normal weight and structural lightweight concrete. The lower limit is generally adopted in design. Note that the shear modulus of concrete ranges from about 40 to 60 percent of its elastic modulus, and the shear strength is of the same order as the direct tensile strength. The values of Table 2.8 are not applicable to high strength concretes, especially in the range exceeding 9 ksi (63 MPa), but can be used as a first approximation. In particular the expression predicting the modulus of elasticity of concrete becomes too optimistic at higher strength [Refs. 2.3, 2.18]. Thus for high strength concrete, the following expression derived in Refs. 2.18 and 2.48 is suggested:

$$\begin{cases} E_c = 40{,}000\sqrt{f'_c} + 1{,}000{,}000\left(\dfrac{\gamma_c}{145}\right)^{1.5} & \text{psi} \\ E_c = 3{,}320\sqrt{f'_c} + 6{,}900\left(\dfrac{\gamma_c}{2330}\right)^{1.5} & \text{MPa} \end{cases} \tag{2.7}$$

where γ_c is in pounds per cubic foot (or kg per cubic meter). Equation (2.7) is applicable for compressive strengths ranging from 3 to 12 ksi (21 to 83 MPa) for normal weight concrete and 3 to 9 ksi (21 to 62 Mpa) for structural lightweight concrete.

Although the compressive strength of concrete at 28 days is used as a reference, the actual compressive strength varies with time and depends on many other variables, including the type of cement and the curing history; the same is true of other mechanical properties which are related to the compressive strength. Typical variations over time of the compressive strengths of identical concretes made with different types of cements are shown in Fig. 2.18 [Ref. 2.61]. It is estimated that the strength at the end of a life span can be 20 to 30 percent higher than that at 28 days. The variation of early age strength is important in prestressed concrete structures because the prestress is often applied while the concrete is still young.

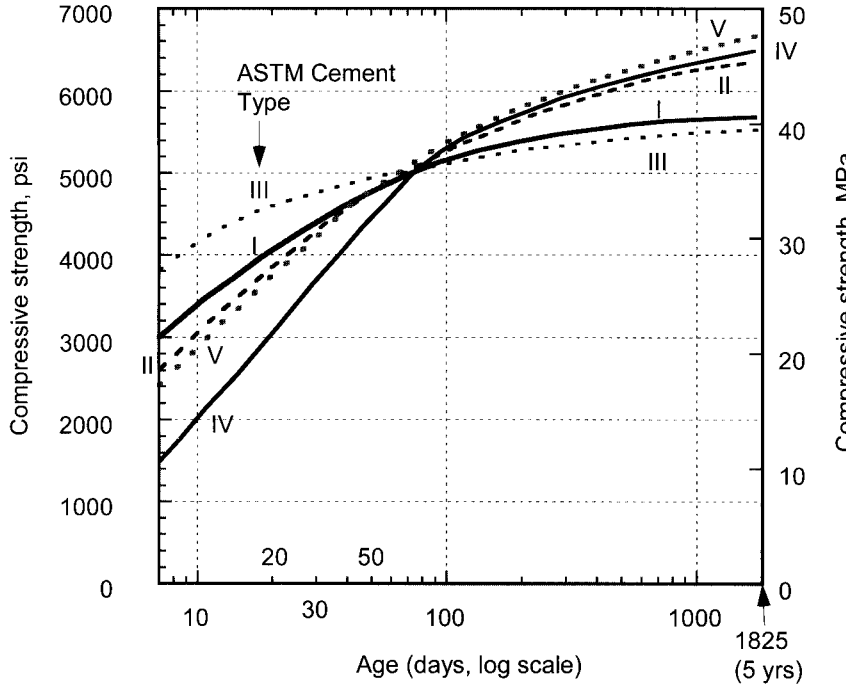

Figure 2.18 Typical variation of concrete strength with time [Ref. 2.61].

Several properties of concrete, other than the compressive strength, are also time dependent. They include shrinkage and creep. The knowledge of these properties will allow the prediction over time of prestress losses in the steel, stresses and strains in the section, and long-term deformations or deflections of the structure (see Chapters 7 and 8). Shrinkage and creep properties are covered in the next sections. Their variation with time is treated much in the same way as the compressive strength.

In general, the property of interest (strength, shrinkage, or creep) is related to a reference value by a time function. For instance, the strength of concrete at any time t can be put in the following form:

$$f'_c(t) = g(t) f'_c(28) \tag{2.8}$$

where $g(t)$ is a time function and f'_c (28) is the reference strength. Different types of time functions such as logarithmic or exponential functions have been used. Some are given in Chapter 8 in relation to prestress losses. Only one type of function, a fractional function initially proposed by Ross [Ref. 2.57] and recommended by ACI Committee 209 [Ref.2.4] will be described in this chapter. It was further extended by Branson and Kripanarayanan [Ref. 2.16] and lends itself to sufficient flexibility in modeling actual behavior. The general form of this time function as used in the prediction of strength, shrinkage, and creep is:

Table 2.9 Recommended relationships for some time-dependent properties of concrete.

Property	Relationship†	Values of constants of equations in second column	
		Moist-cured concrete	Steam-cured concrete
Compressive strength	For $t \geq 1$ day $f'_c(t) = \frac{t}{b+ct} f'_c(28)$ Same for normal weight and lightweight concrete	Type I cement: $b=4$ $c=0.85$ Type III cement: $b = 2.30$ $c = 0.92$	Type I cement: $b = 1$ $c = 0.95$ Type III cement: $b=0.70$ $c=0.98$
Shrinkage strain	$\varepsilon_S(t) = \frac{t}{b+t} \varepsilon_{SU} K_{SH} K_{SS}$ Same for normal weight and lightweight concretes using Type I or Type III cements. K_{SH} humidity correction factor K_{SS} shape and size factor	$40\% \leq H \leq 80\%$ $b = 35$ $t \geq 7$ *days* $K_{SH} = 1.40 - 0.01H$ K_{SS} = *see Table* 2.10 ‡ $80\% \leq H \leq 100\%$ $b = 35$ $t \geq 7$ *days* $K_{SH} = 3 - 0.03H$ K_{SS} = *see Table* 2.10 ‡	$40\% \leq H \leq 80\%$ $b = 55$ $t \geq 1$ *to* 3 *days* $K_{SH} = 1.40 - 0.01H$ K_{SS} = *see Table* 2.10 ‡ $80\% \leq H \leq 100\%$ $b = 55$ $t \geq 1$ *to* 3 *days* $K_{SH} = 3 - 0.03H$ K_{SS} = *see Table* 2.10 ‡
Creep coefficient	$C_C(t) = \frac{t^{0.60}}{10+t^{0.60}} C_{CU} K_{CH} K_{CA} K_{CS}$ K_{CH} humidity correction factor K_{CA} age at loading factor K_{CS} shape and size factor t_A age at loading	$t, t_A \geq 7$ *days* and $H \geq 40\%$ $K_{CA} = 1.25 t_A^{-0.118}$ $K_{CH} = 1.27 - 0.0067H$ K_{CS} = *see Table* 2.10 ‡	$t, t_A \geq 1$ *to* 3 *days* and $H \geq 40\%$ $K_{CA} = 1.13 t_A^{-0.095}$ $K_{CH} = 1.27 - 0.0067H$ K_{CS} = *see Table* 2.10 ‡

†Valid in all systems of units; H given in percent.

‡In lieu of Table 2.10, the author recommends the use of $K_{SS} = K_{CS} = 1.14 - 0.09(V/S) \geq 0.6$ for shrinkage and ≥ 0.68 for creep, where (V/S) is the volume-to-surface ratio of the member.

$$g(t) = \frac{t^a}{b + ct^a} \tag{2.9}$$

where t is the time in days and a, b, and c are constants; a and c can take on the value of one. Recommended numerical values of these constants for the strength of

concrete, shrinkage strain, and creep coefficient are given in Table 2.9 for moist-cured and steam-cured concrete. They can be used in absence of more specific data.

2.3.4 Shrinkage

Concrete contains more water than is strictly required by the chemical hydration reaction of the cement. The excess water is called free water. Its loss through evaporation leads to gradual shortening of the member with time, described as shrinkage. As the member shortens, the prestressing steel loses part of its prestress. This is called shrinkage loss. The evaluation of shrinkage loss as part of the total prestress losses is an important step in design.

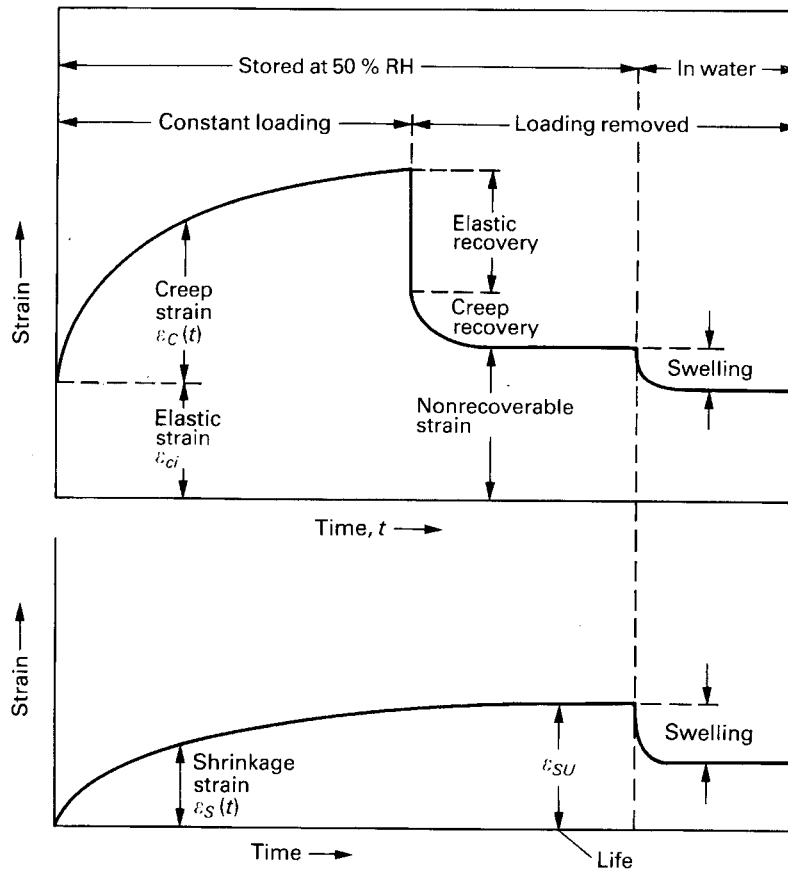

Figure 2.19 Schematic variation over time of shrinkage and creep strain of concrete.

Shrinkage depends on many variables. Most important are the amount of free water, the relative humidity of the environment, the ambient temperature, the type of aggregates used, and the size and shape of the structural member. Shrinkage is

assumed independent of loading and would not take place if the concrete is kept at 100 percent relative humidity. Shrinkage in concrete results primarily from the shrinkage of the cement paste; the aggregates shrink very little. Thus, differential internal stresses are created in the structure of concrete, leading to compression on the aggregates and tension in the paste accompanied by microcracking.

Mechanically, shrinkage is described by a shortening strain called shrinkage strain. The shrinkage strain of concrete $\varepsilon_S(t)$ under constant environmental conditions increases with time and tends asymptotically toward a final maximum value called ultimate shrinkage strain ε_{SU} (Fig. 2.19). For all practical purposes the ultimate shrinkage strain is assumed to occur at the estimated life of the structure. The rate of increase of $\varepsilon_S(t)$ is highest at early ages. Practically, for moist-cured concrete, about 50 percent of total shrinkage occurs within a month and about 90 percent within a year of exposure. Note that, once shrinkage has occurred, complete recovery will not take place, even if the member is placed again in water (Fig. 2.19).

Table 2.10 Size and shape factors for creep and shrinkage. *(Adapted from Ref. 2.51).*

Volume-to-surface ratio		Size and shape factor	
in	cm	Creep K_{CS}	Shrinkage K_{SS}
1	2.54	1.05	1.04
2	5.1	0.96	0.96
3	7.6	0.87	0.86
4	10.2	0.77	0.77
5	12.7	0.68	0.69
6	15.2	0.68	0.60

The shrinkage strain $\varepsilon_S(t)$ at any time t is generally related to the ultimate shrinkage strain ε_{SU} by a time function. The time function recommended by ACI Committee 209 [Ref. 2.4] is of the same form as that described earlier for predicting the strengths (Eq. 2.9). It is given in Table 2.9 where conditions of application are clarified and where other correction factors have been included in the overall relationship between $\varepsilon_S(t)$ and ε_{SU}. The factor K_{SH} is a correction factor that accounts for the influence of the relative humidity of the environment on shrinkage strain. K_{SS} is a correction factor that depends on the size and shape of the member, often described by the ratio of lateral surface to volume. K_{SS} can be omitted in the calculation if the least dimension of the member is less than 6 in (150 mm). However, the PCI committee charged to study prestress losses [Ref. 2.51] recommends the use of the shape and size factors and suggests the numerical values summarized in Table 2.10. Note that expressions for K_{SS} have also been

recommended in Ref. 2.4 for various sizes of members. It is felt, however, that the PCI committee approach is more direct and simpler to apply in all cases.

The author believes that further simplification can be achieved by using the same size and shape factor for creep and shrinkage. He suggests the expression given in the footnote of Table 2.9, that is:

$$\begin{aligned} K_{SS} &= K_{CS} = 1.14 - 0.09(V/S) \\ &\geq 0.60 \quad \text{for shrinkage} \\ &\geq 0.68 \quad \text{for creep} \end{aligned} \tag{2.10}$$

where V is the volume and S is the lateral surface of the member. Since great uncertainty is associated with the predictions of shrinkage and creep, such approximation is certainly acceptable.

The ultimate shrinkage strain of concretes used for prestressing varies generally between 0 and $10\text{x}10^{-4}$. Strain is nondimensional and is the same in all systems of units. It is zero for shrinkage compensating concrete and approaches 10×10^{-4} for lightweight concrete. Average values of 8×10^{-4} and 7.3×10^{-4} are suggested in Ref. 2.16 for moist-cured and steam-cured concretes, respectively, assuming standard conditions at 40 percent relative humidity. They are about twice those derived from the recommendation of the British code CP-110. It is the author's opinion that average values of ε_{SU} of $6\text{x}10^{-4}$ and $4\text{x}10^{-4}$, respectively, can be used under standard conditions for moist-cured and steam-cured normal weight concretes commonly used for prestressing. Alternatively, ε_{SU} can be evaluated from several prediction equations found in the technical literature. These equations are generally expressed as a simple function of one variable, such as relative humidity, total amount of mixing water, or modulus of elasticity (see Section 8.7).

2.3.5 Creep

Creep is the time-dependent strain in excess of elastic strain induced in a material subjected to a sustained stress. Unlike shrinkage, creep is caused by loading. Typical increase under constant load of creep strain $\varepsilon_C(t)$ with time is shown in Fig. 2.19. If the load is removed after a period of time, the initial elastic strain is recovered immediately. A part of the creep strain is gradually recovered over time and the remaining part is non-recoverable. If the load is maintained, the creep strain tends asymptotically toward a maximum value ε_{CU} called ultimate creep strain. It is considered attained at the end of the life of a structure. A simple rheological model to simulate creep behavior is shown in Fig. 2.20. A large body of information exists on the creep behavior of concrete and its modeling [Refs. 2.5, 2.14, 2.36, 2.39, 2.41, 2.46, 2.57, 2.60]. In practice, manageable procedures have been devised to account for creep. This is particularly relevant to prestressed concrete members, since they

"creep" under the effect of prestress, inducing significant stress losses in the steel and long-term deflections of the member.

The creep of concrete depends on many additional factors other than time. They include the relative humidity, the type of aggregate, the mix proportions, the age of the concrete at time of loading, and the size and shape of the member.

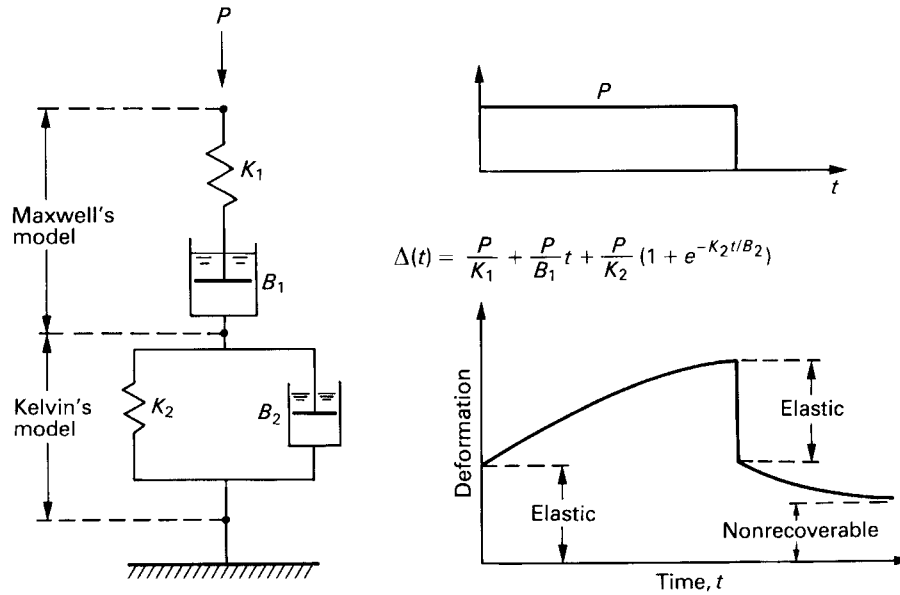

Figure 2.20 Burger's rheological model of concrete.

The creep strain of a given concrete is considered proportional to the initially applied stress. At any time t, the creep strain can be related to the initial elastic strain by a factor called creep coefficient, thus:

$$C_C(t) = \frac{\varepsilon_C(t)}{\varepsilon_{ci}} \tag{2.11}$$

With the life span of a structure, since $\varepsilon_C(t)$ tends toward ε_{CU} and, since ε_{ci} is a constant, $C_C(t)$ tends toward a maximum value C_{CU}, called ultimate creep coefficient and given by:

$$C_{CU} = \frac{\varepsilon_{CU}}{\varepsilon_{ci}} \tag{2.12}$$

Eliminating ε_{ci} from Eqs. (2.11) and (2.12) leads to:

$$\frac{C_C(t)}{C_{CU}} = \frac{\varepsilon_C(t)}{\varepsilon_{CU}} \tag{2.13}$$

Thus, the same time function can represent the variation of the creep strain or the creep coefficient. Similarly to the time function used for strength and shrinkage, the time function recommended for creep in Ref. 2.4 is reproduced in Table 2.9, where conditions of application are clarified. The relationship shown relates the creep coefficient at any time t to the ultimate creep coefficient. Several correction factors have been added to facilitate its direct use in design. The factor K_{CA}, called creep maturity coefficient, takes into account the age of concrete t_A at the time of loading. K_{CH} accounts for the relative humidity of the environment and K_{CS} for the shape and size of the member. The values of K_{CS} suggested in Ref. 2.51 are given in Table 2.10, while the effect of age at loading is illustrated in Fig. 2.21 [Ref. 2.36].

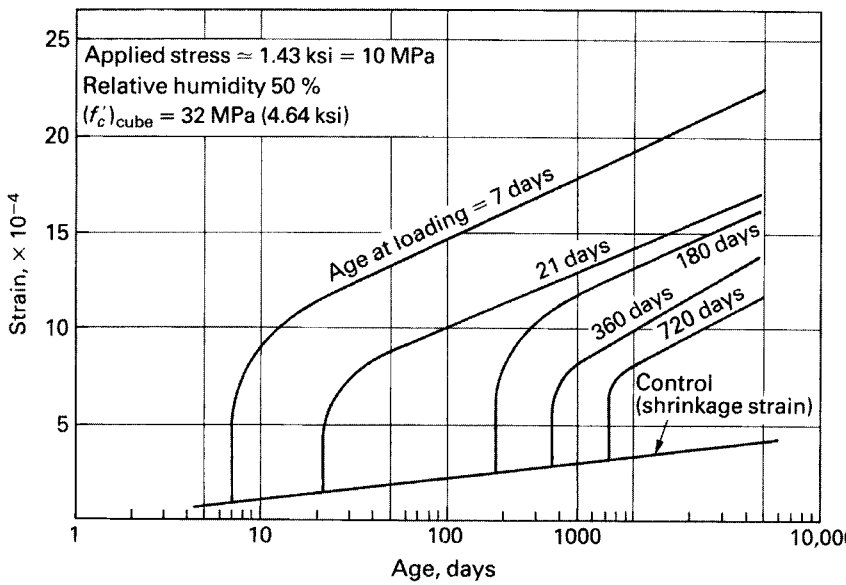

Figure 2.21 Effect of age at loading on creep of concrete. *(Adapted from Ref. 2.36.)*

Note that the equation initially proposed by Branson and Kripanarayanan was developed assuming concrete slump less than 4 in (100 mm) and a minimum member thickness of 6 in (150 mm) or less. An average value of the ultimate creep coefficient C_{CU} of 2.35 was also proposed for standard conditions and when specific data are not available. Other values of C_{CU} suggested in Ref. [2.48] are given in Table 2.11 for various concrete compressive strengths.

As pointed out earlier, the creep of concrete leads not only to losses of stress in the prestressing steel but also to long-term deformations or deflection of the structure. This is illustrated in Fig. 2.22 [Ref. 2.35], where the deflection of

prestressed and partially prestressed concrete beams is plotted versus time. Note that the deflection curve for a constant load is very similar in shape to the curve describing the variation of creep strain with time under constant conditions.

Table 2.11 Typical values of ultimate creep coefficients. *(Adapted from Ref. 2.48).*

Compressive strength		Ultimate creep coefficient†
psi	MPa	C_{CU}
3,000	20.7	3.1
4,000	27.6	2.9
5,000	34.5	2.65
6,000	41.4	2.4
7,000	48.3	2.2
8,000	55.2	2.0
10,000	69	1.6
12,000	83	1.4

† Interpolation acceptable for in between values.

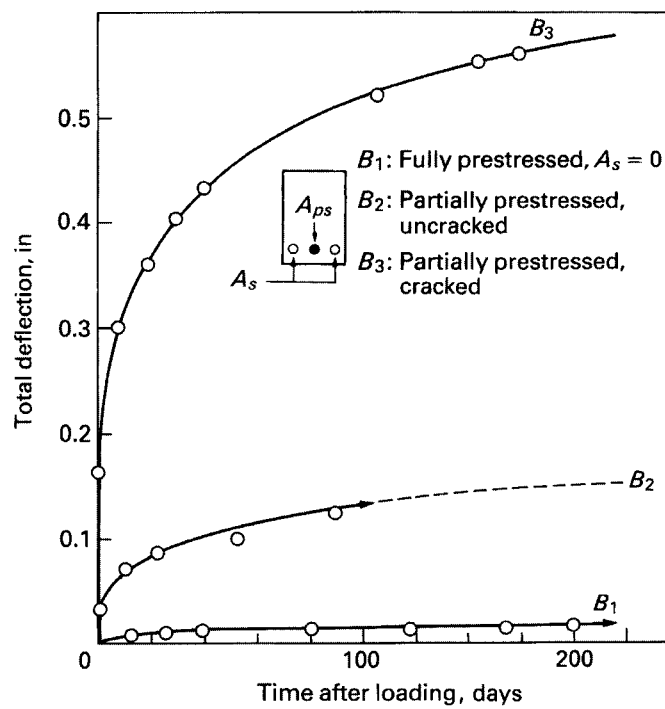

Figure 2.22 Typical variation of deflection with time under sustained loading. *(Adapted from Ref. 2.35.)*

In describing the concrete strain variations with time due to creep and shrinkage, it was essentially assumed above that constant environmental conditions, such as in a laboratory environment existed. However, actual conditions where continuous variations in temperature and humidity prevail, will lead to fluctuating curves with much less defined limiting values. This is particularly the case, for instance, for segmentally built bridges, where each segment has a different age, is loaded at different times and at different loadings, and undergoes its own strain history under the combined effects of creep, shrinkage, temperature, relative humidity, and external loads.

Finally, it is important to note that the proportionality of creep to the initial strain (Eq. 2.11) is only valid for stresses in the service loading range. At higher stresses the creep evolution is not proportional to initial strain.

2.3.6 Fatigue

It is generally observed that concrete in direct compression can sustain a fluctuating stress between 0 and 50 percent of its static compressive strength for at least ten million cycles. The fatigue strength of concrete for other types of stresses is estimated at 55 percent of the corresponding static strength. Such stress fluctuations are not often encountered in practice. Thus, failure of concrete by compression fatigue is rare. For the purpose of design, the stress range limit suggested by ACI Committee 215 on Fatigue [Ref. 2.6] and in Ref. [2.52] can be used:

$$\Delta f_{cr} = 0.4 f'_c - \frac{f_{c\,min}}{2} \tag{2.14}$$

where f'_c is the compressive strength and f_{cmin} the minimum stress.

2.3.7 Effects of Temperature

Concrete heated up to 200°C does not undergo significant physical or chemical changes. It generally loses all its free water at 100°C (212°F) and, except for some microcracking, maintains most of its mechanical characteristics. The strength properties of concrete generally increase with a substantial drop in temperature. However, this improvement depends on the water content of the concrete and is much higher for moist concrete than for dry concrete. Compressive strength increases of more than 200 percent have been observed for initially moist-cured concretes later tested at -150°C.

The coefficient of thermal expansion of concrete depends on many factors, including the mix proportions and the type of aggregate. An average range of 5.5 to 6.5×10^{-6} per degree Fahrenheit (10 to 12×10^{-6} per degree Celsius) can be used for normal weight concrete. For lightweight concrete a range of 4 to 6×10^{-6} per degree

Fahrenheit (7 to 11×10^{-6} per degree Celsius) is observed and depends on the amount of normal weight sand used.

2.3.8 Steam Curing

Curing involves the retention of sufficient free water in the concrete to facilitate the process of hydration. At ambient temperature a moist environment is generally maintained to ensure curing.

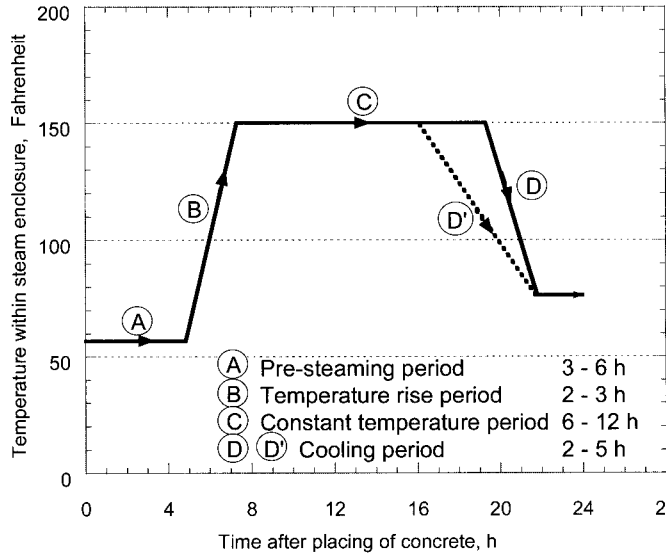

Figure 2.23 Typical low-pressure steam-curing cycle.

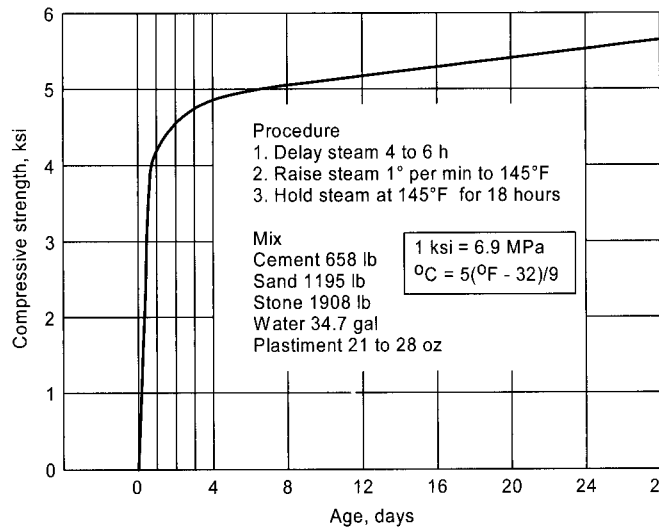

Figure 2.24 Typical time-strength curve for steam-cured concrete.

Mass produced precast prestressed concrete members must be removed from their molds as soon as possible to ensure an efficient production process. Their strength must be sufficient (0.65 to 0.8 f'_c) at that time to allow the transfer of prestress. This can be achieved by steam curing. Steam curing can be applied at low (atmospheric), high, or intermediate low-high pressures. It allows a production cycle of 24 hours. Low-pressure steam curing is most popular in the United States. A typical cycle of temperature within the steam enclosure versus time is shown in Fig. 2.23. The temperature of the concrete member follows a similar cycle with a time delay and smoother transitions. Curing generally starts with a slow temperature rise (40 to 60°F per hour) four to six hours after casting. The length of the maximum temperature period and the subsequent rates of temperature drops may be selected in many ways. Commonly, the total time between concrete casting and steam shutoff is about 18 hours. Typical variation of strength of steam-cured concrete versus concrete age is shown in Fig. 2.24 and illustrates the values achievable at one day. Steam curing leads not only to improved strength but also to better shrinkage and creep characteristics of the concrete as noted in Table 2.9.

2.4 CONSTITUTIVE MODELING

It is often useful to have a model of the stress-strain properties of the key structural materials used in a prestressed or partially prestressed concrete beam, especially when finite element analysis or non-linear analysis are used. This is generally referred to as constitutive modeling. In this chapter, constitutive modeling is limited to the prediction equations for the stress-strain response of concrete in uniaxial compression, and reinforcing and prestressing steel in uniaxial tension. No explanation is given on how these equations are obtained or how to fit or model a particular experimental curve with a prediction equation. Additional information can be found in Ref. [1.48].

2.4.1 Stress-Strain Curve of Concrete in Compression

The analytical expression for plain concrete under uniaxial loading should reflect the experimentally observed stress-strain curves (Fig. 2.16a). The stress should be a continuously increasing function of strain in the ascending portion. The function should have a zero slope at the peak or maximum stress and a prescribed slope at the origin. In the descending portion of the curve the stress should be a decreasing function of the strain and should remain positive even for large values of strains. If the descending portion must have zero slope at the peak and is assumed to have the strain axis as asymptote for large strains, then it should also have an inflection point. The above descriptive constraints are expressed analytically by boundary conditions to be satisfied by the analytic function selected.

Let us call σ and ε the stress and strain in the concrete in general where σ is assumed a function of ε. Often the relationship between σ and ε is also written in

the non-dimensionalized stress, non-dimensionalized strain system defined by:

$$Y = \frac{\sigma}{\sigma_m} \tag{2.15}$$

and

$$X = \frac{\varepsilon}{\varepsilon_m} \tag{2.16}$$

where the subscript "m" refers to the peak point or point of maximum stress (Fig. 2.17). Thus σ_m corresponds to f'_c used in the code.

Many expressions have been proposed to describe the stress-strain curve of concrete in compression. They can be grouped into several categories according to their form. They include exponential functions, polynomial functions, trigonometric functions, and fractional functions. Each of these expressions can be written in either the (σ,ε) system or the non-dimensionalized (X,Y) system, and contains one or more constants.

Hognestad and the European Concrete Committee (CEB) have proposed to use a parabola, that is, a second degree polynomial for the stress-strain curve of concrete. It is indeed one of the simplest forms. It is given by:

$$Y = X(2 - X) \tag{2.17}$$

or

$$\sigma = \sigma_m \left[2\frac{\varepsilon}{\varepsilon_m} - \left(\frac{\varepsilon}{\varepsilon_m} \right)^2 \right] \tag{2.18}$$

The first equation is non-dimensional. In order to get real stresses, the second equation needs the value of σ_m (that is, f'_c) and ε_m. Note that Eq. (2.18) has a fixed relative value of the initial modulus given by $E_O = 2E_m$, where E_m corresponds to the secant modulus at maximum stress, that is $E_m = \sigma_m / \varepsilon_m$. This is one of the main disadvantages of the parabolic expression, namely one cannot control simultaneously the elastic modulus and the strain at maximum stress. They are related.

While Eq. (2.18) has been often used to model the entire stress-strain curve of concrete, it is recommended here for the ascending branch only, because the symmetrical descending branch portion is not representative of real behavior. It has been common to use a descending branch for the stress-strain curve of concrete simulated by a sloping straight line, ending with an asymptote corresponding to $0.10\sigma_m$, that is, $0.10f'_c$. The straight line is given by:

$$\sigma = \sigma_m [1 - Z(\varepsilon - \varepsilon_m)] \qquad \text{valid for } \varepsilon \geq \varepsilon_m \text{ and } \sigma \geq 0.10\sigma_m \tag{2.19}$$

where Z is a factor that defines the slope of the line. Z can be taken equal to 100 for a concrete compressive strength of 25 MPa (3.6 ksi), 250 for a concrete compressive strength of 50 MPa (7.2 ksi), and 500 for a concrete compressive strength of 100 MPa (14.4 ksi), respectively. The Z slope can be modified to better fit a given experimental curve. Also, extrapolation could be used for other values of compressive strength. Both the values of Z and ε_m can be adjusted to different conditions, such as when confinement by closed stirrups or fiber reinforcement are used.

Generally σ_m (or f'_c) is a given design parameter. In order to numerically develop Eq. (2.18), the value of ε_m, the strain at maximum stress, is needed. As a first approximation the value of ε_m can be taken as:

$$\varepsilon_m = 0.00165 + 0.0000163\sigma_m \quad \text{where } \sigma_m \text{ is in MPa} \tag{2.20}$$

$$\varepsilon_m = 0.00165 + 0.000114\sigma_m \quad \text{where } \sigma_m \text{ is in ksi} \tag{2.21}$$

Typical examples of stress-strain curves according to the above equations are plotted in Fig. 2.25.

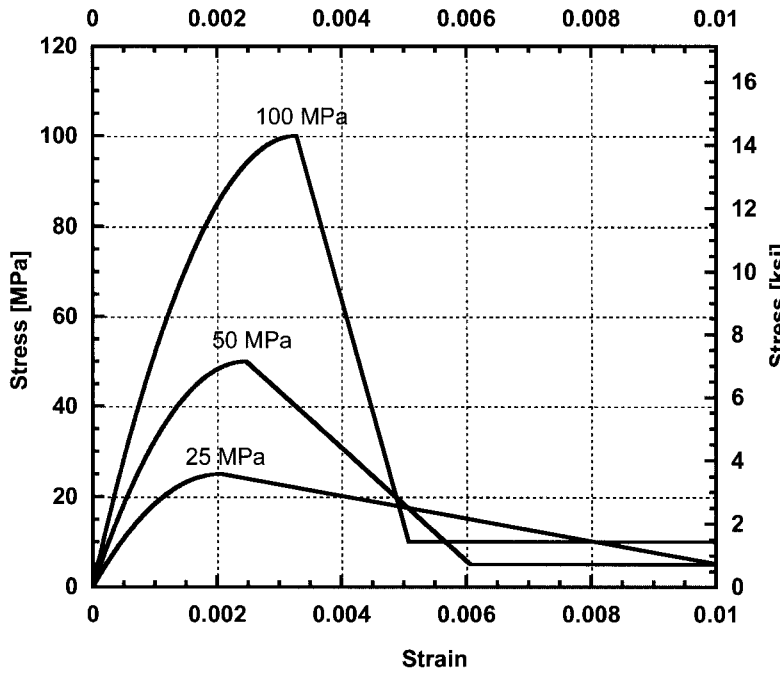

Figure 2.25 Stress-strain curves of concrete used for modeling purposes (Eqs. 2.18, 2.19).

2.4.2 Stress-Strain Curve of Reinforcing Steel in Tension

In comparison to modeling the behavior of concrete, modeling the behavior of reinforcing or prestressing steels offers a number of simplifications, namely: all steels have about the same modulus of elasticity, all steels have a sizeable initial linear elastic portion in their stress-strain response, all steels are manufactured products, that is, they are produced under strict quality control, their properties must satisfy a number of ASTM standards and consequently little variability generally exists between specified properties and actual properties. Low variability is also made possible by the nature of the material. Thus, if a representative analytic expression can achieve a good fit of actual behavior, there will be little uncertainty in the final results.

In the following sections engineering measures of stress are used, that is, the stress values are based on the original cross sectional area of a bar subjected to uniaxial tension.

The stress-strain curves of commonly used reinforcing bars can be classified according to two distinct types of behavior: one with a definite yield plateau and the other with no definite yield. For the first category, the shape of the stress-strain curve over its entire range comprises three portions (Fig. 2.26): 1) an initial elastic portion up to the yield point, 2) a yield plateau up to the onset of strain hardening, and 3) a strain hardening portion. For the second category only two portions are identified: a linear portion up to the proportional limit (in general yielding cannot be identified except when corresponding to a permanent strain such as by the 0.2% offset method), and 3) a strain hardening portion. Various analytic relationships were developed to represent the behavior of the two different categories of reinforcing steel; however, only the steel with a definite yield plateau is addressed here. More details are given in Ref. [1.48].

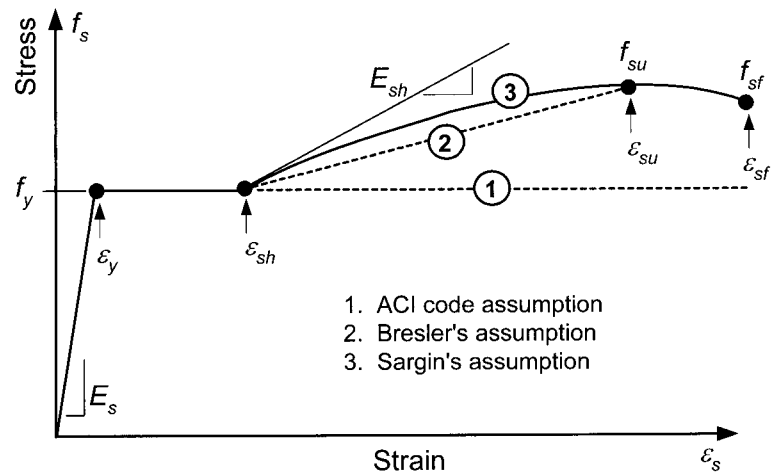

Figure 2.26 Typical models for the stress-strain curves of reinforcing steels with definite yield plateau.

The simplest representation of this type of steel is that adopted in the ACI code for routine design purposes; it consists of only two portions: an initial linear elastic portion up to yielding (the yield strength f_y is a specified design parameter) and a yield plateau with no strain hardening (curve No. 1 of Fig. 2.26). Ignoring the strain hardening effect in strength computations leads to a safer design. Bresler [Ref. 2.17] and Heimdahl and Biachini [Ref. 2.33] used the same initial representation but added a strain hardening portion represented by a straight line joining the point at onset of strain hardening to the point of maximum stress (curve No. 2 in Fig. 2.26).

Sargin [Ref. 2.59] proposed a curve consisting of three portions: an initial elastic portion, a yield plateau, and a strain hardening portion up to failure, which was represented by a parabola (curve 3 of Fig. 2.26). His expression is more representative of the real behavior of this category of steel. The three portions of the curve are given by the following equations:

$$f_s = E_s \varepsilon_s \quad \text{for} \quad 0 \le \varepsilon_s \le \varepsilon_y \tag{2.22}$$

$$f_s = f_y \quad \text{for} \quad \varepsilon_y \le \varepsilon_s \le \varepsilon_{sh} \tag{2.23}$$

$$f_s = f_y + E_{sh}(\varepsilon_s - \varepsilon_{sh})\left[1 - \frac{E_{sh}(\varepsilon_s - \varepsilon_{sh})}{4(f_{su} - f_y)}\right] \quad \text{for } \varepsilon_s > \varepsilon_{sh} \tag{2.24}$$

where f_s and ε_s represent stress and strain in the steel in general, the subscript y refers to yielding, the subscript sh refers to strain hardening, and the subscript u to ultimate or maximum stress. The parameters E_s, E_{sh}, ε_{sh}, f_y, f_{su} are supposed to be prescribed. Typically for reinforcing bars E_s = 200 GPa = 29,000 ksi.

Curve No. 3 of Fig. 2.26 illustrates Sargin's model for the strain hardening portion; the second term of the right side of Eq. (2.24) is a parabola. Its slope at the onset of strain hardening is equal to E_{sh} and its vertex corresponds to the maximum stress, f_{su}. However, such a parabola does not guarantee that the strain at maximum stress is equal to ε_{su}. To achieve that, one can specify the coordinates of the vertex to be (ε_{su}, f_{su}); however, in such a case, the tangent at the onset of strain-hardening will not be equal to E_{sh}. Note that after the maximum stress, the stress-strain curve of the steel undergoes strain softening until failure, that is, complete separation, which is represented by the subscript f on the curve. While the same parabola used for the strain hardening portion can also be used here, there are cases where the descending portion between points u and f is modeled separately.

Wang, Shah and Naaman [Refs. 2.62, 2.63] have shown that the above representation (Eqs. 2.22) to (2.24) provides an excellent fit up to maximum stress or failure of a reinforced concrete member. Because failure of the concrete section often occurs before maximum steel stress is reached, the need for an accurate

representation of the descending portion of the curve is generally minimal.

Each of the analytical expressions described above requires the knowledge of one or more characteristic parameters of the steel, depending on the level of accuracy desired, namely: E_s, E_{sh}, f_y, ε_{sh}, f_{su}, ε_{su}, f_{sf}, ε_{sf}. Wang et al. studied the experimental stress-strain curves of more than two hundred reinforcing bars obtained from different manufacturers and having various sizes from #3 to #11 (nominal diameters 3/8 in. to 11/8 in). Forty-two of these bars were of A615 grade 60 steel with definite yield plateau. From the observed data, linear regression equations were developed to give the value of each characteristic parameter of the curve as a function of the yield strength. Although, due to the various bar sizes and sources of supply, the correlation obtained between the best fit lines and the data was not always very good, these equations are summarized in Table 2.12 and could be used as a first approximation, because in real structural members bars of different sizes and from different sources are used simultaneously anyway. Very little information exists in the available technical literature on the characteristic parameters of reinforcing bars and thus Table 2.12 can be very useful for modeling these characteristics, short of direct experimental tests.

Examples of stress-strain curves generated using Eqs. (2.22 to 2.24) and Table 2.12 are shown in Fig. 2.27.

Table 2.12 Regression equations for typical properties of Grade 60 reinforcing bars with yield strength ranging from about 60 ksi (417 MPa) to 80 ksi (556 MPa).

Unit	ksi	MPa
Yield stress	f_y	f_y
Yield strain	$\varepsilon_y = f_y / E_s$	$\varepsilon_y = f_y / E_s$
Elastic modulus*	$E_s = -54.39 f_y + 33023$	$E_s = -54.39 f_y + 229500$
Strain at onset of strain hardening	$\varepsilon_{sh} = -9\text{x}10^{-5} f_y + 0.0145$	$\varepsilon_{sh} = -1.295\text{x}10^{-5} f_y + 0.0145$
Modulus at onset of strain hardening	$E_{sh} = -9.44 f_y + 1788$	$E_{sh} = -9.44 f_y + 12426$
Stress at ultimate (or maximum stress)	$f_{su} = 0.523 f_y + 73.2$	$f_{su} = 0.523 f_y + 508.7$
Strain at ultimate	$\varepsilon_{su} = -0.00023 f_y + 0.0867$	$\varepsilon_{su} = -3.309\text{x}10^{-5} f_y + 0.0867$
Stress at failure	$f_{sf} = 0.274 f_y + 77$	$f_{sf} = 0.274 f_y + 535.1$
Strain at failure	$\varepsilon_{sf} = -0.00221 f_y + 0.2868$	$\varepsilon_{sf} = -3.18\text{x}10^{-4} f_y + 0.2868$

* For all practical purposes a constant modulus of 29,000 ksi (200,000 MPa) should be used for all reinforcing bars.

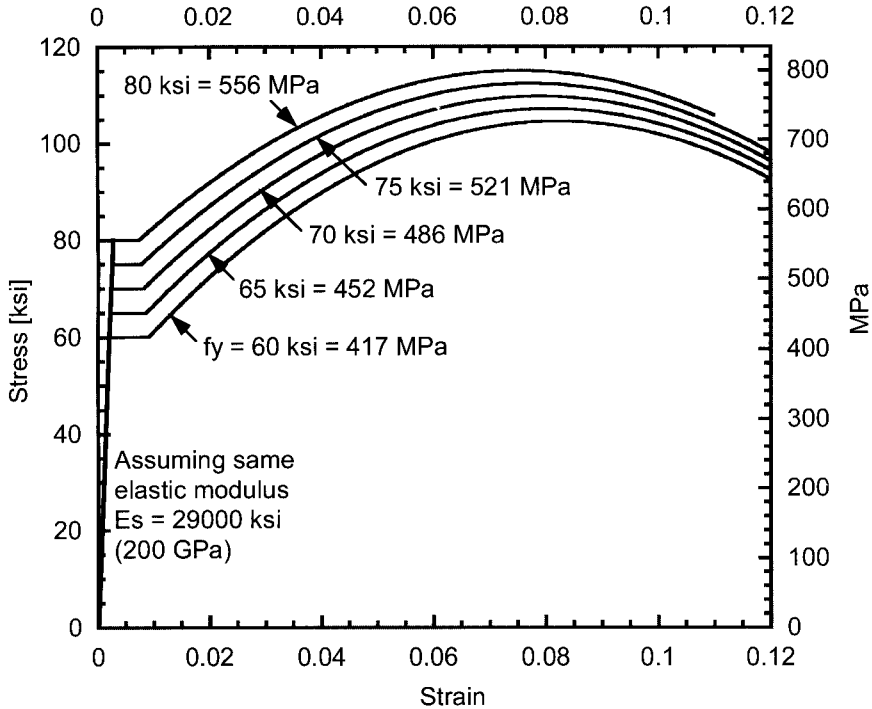

Figure 2.27 Predicted stress-strain curves of reinforcing steels with definite yield plateau.

2.4.3 Stress-Strain Curve of Prestressing Steels in Tension

Typical stress-strain curves of prestressing steels are shown in Fig. 2.1. They generally comprise three portions: a linear elastic portion up to the proportional limit, a nonlinear portion up to about 95 percent of ultimate strength, and an almost linear but slightly strain hardening (non-horizontal) portion up to failure.

Because of stringent quality control during production and ASTM specified minimum requirements on proportional limit, yield and ultimate strength, prestressing steels of the same category show generally little variability in their stress-strain behavior. Several prediction equations are discussed in Ref. 1.48 for the stress-strain curve of reinforcing and prestressing steels. One of the most accurate expressions is a power equation, first suggested by Menegotto and Pinto [Ref. 2.40]. Although the original intent of this equation was to represent the behavior of reinforcing steels (with no yield plateau), it ideally fits the behavior of prestressing steels and was first used by Mattock in a study on prestressed concrete using programmable calculators [Ref. 2.38]. An extensive evaluation by this author has indicated that the equation of Menogotto and Pinto, if applied to fit the behavior of prestressing steels, would give the least standard errors in comparison to the other relationships available in the technical literature [Ref. 2.42]. It also fits surprisingly

well the initial linear portion of the curve, almost to the same extent as a straight line. Similar observations were made by Devalapura and Tadros [Ref. 2.22]. The equation is given by:

$$f = E_{ps}\varepsilon\left[Q + \frac{1 - Q}{\left[1 + \left(\frac{E_{ps}\varepsilon}{Kf_{py}}\right)^{N}\right]^{1/N}}\right] \tag{2.25}$$

where f and ε represent respectively axial stress and strain in general, and E_{ps} is the elastic modulus. The coefficients Q, K, and N are determined from the characteristics of the experimental stress-strain curves as described in Ref. 1.48. Table 2.13 summarizes possible values of coefficients that can be used in the above equation to simulate the behavior of typical prestressing steels [Ref. 2.43].

Table 2. 13 Coefficients for the stress-strain relationship of typical prestressing steels.

Fitting Constraints	Stress-Strain Relationship Used	Type and Strength of Prestressing Steel		
		Bars 160 ksi (1104 MPa)	Wires 235 ksi (1620 MPa)	Strands 270 ksi (1863 MPa)
To Satisfy Minimum Specified ASTM Standards*	Menegotto and Pinto	$N = 4.24$ $K = 1.04728$ $Q = 0.01797$	$N = 2.91$ $K = 1.1470$ $Q = 0.00632$	Stress relieved: $N = 5.05$ $K = 1.1155$ $Q = 0.01699$ Low relaxation: $N = 7.39$ $K = 1.0852$ $Q = 0.00772$
Typical of Actual Behavior	Menegotto and Pinto (power equation)	$N = 7.1$ $K = 1.0041$ $Q = 0.0175$ for $E_{ps} = 28790$ $f_{py} = 141.8$ $f_{pu} = 160$ $\varepsilon_{pu} = 0.041$	$N = 6.06$ $K = 1.0325$ $Q = 0.00625$ for $E_{ps} = 29300$ $f_{py} = 222.4$ $f_{pu} = 244$ $\varepsilon_{pu} = 0.087$	$N = 7.344$ $K = 1.0618$ $Q = 0.01174$ for $E_{ps} = 27890$ $f_{py} = 243.5$ $f_{pu} = 278$ $\varepsilon_{pu} = 0.069$

* $f_{py} = 0.85 f_{pu}$; $\varepsilon_{py} = 0.010$ for wires and strands and 0.007 for bars, $\varepsilon_{pu} = 0.040$; E_{ps} = 27000 ksi for strands, 28000 ksi for prestressing bars and 29000 ksi for prestressing wires; 1 ksi = 6.9 MPa.

Two sets of values are given: one set corresponding to a curve passing by the minimum ASTM specified points, and the other set corresponding to actual representative experimental curves. They can be used for common design purposes.

(*a*)

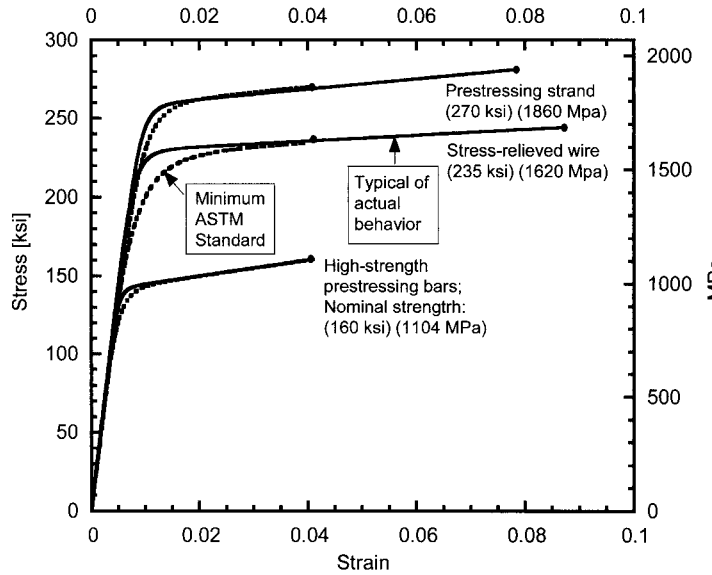

(*b*)

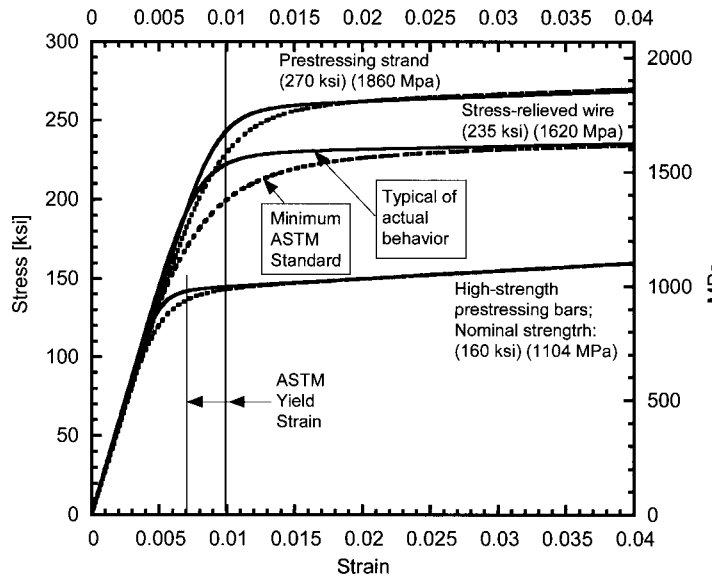

Figure 2.28 Typical stress-strain curves of prestressing steels plotted from Eq. (2.25). (a) Full scale. (b) Enlarged scale to show the yield point and the difference between actual curves and minimum ASTM curves.

Typical stress-strain curves using Eq. (2.25) and the coefficients given in Table 2.13 are plotted in Fig. 2.28. It can be observed that Eq. (2.25) provides realistic predictions for each of the steel types in comparison to the experimental curves of Fig. 2.1.

2.5 CONCLUDING REMARKS

The material properties summarized in this chapter are essential elements to the full understanding of prestressed concrete behavior. They help clarify the basis for many of the design procedures treated in later chapters. Not all of these properties are of immediate use in design. However, the more final the design and the more complex the structure, the greater is the need to account in design for the actual behavior of the materials and their interaction.

Two additional items could have been treated in this chapter: prestress losses and allowable stresses. Prestress losses depend not only on material properties but also on structural behavior and environmental conditions. At this point, their immediate and thorough treatment might confuse the reader newly acquainted with prestressed concrete, and therefore, it is left to Chapter 8. Allowable stresses are related to the strength properties of the materials. They are not properties by themselves; they are arbitrary design limits set in codes and guidelines and are given in the next chapter where different design philosophies and code recommendations are explained.

REFERENCES

2.1 American Concrete Institute - International, *ACI Manual of Concrete Practice*, Parts I, II, and III, Farmington Hills, Michigan: updated annually.

2.2 ACI Committee 215, "Considerations for Design of Concrete Structures Subjected to Fatigue Loading," *ACI Journal*, 71(3): 97-121, 1974. Revised in *ACI Manual of Concrete Practice*, 1992 and later editions.

2.3 ACI Committee 363, "State of the Art Report on High Strength Concrete," *ACI Manual of Concrete Practice*, Vol. 1. Farmington Hills, MI: American Concrete Institute, 1993 and later editions.

2.4 ACI Committee 209, "Prediction of Creep, Shrinkage, and Temperature Effects in Concrete Structures," *ACI Special Publication SP-27, Designing for Effects of Creep, Shrinkage, Temperature in Concrete Structures*, 1971, pp. 51-93.

2.5 ACI Committee 209, "Prediction of Creep, Shrinkage and Temperature Effects in Concrete Structures," *ACI Publication SP 76*, Farmington Hills, MI: American Concrete Institute, 1984, pp. 193-300.

2.6 ACI Committee 215, "Consideration for Design of Concrete Structures Subjected to Fatigue Loading," *ACI Journal*, 71(3): 97-121, 1974.

2.7 ACI Committee 216, "Guide for Determining the Fire Endurance of Concrete Elements," *Concrete International Design and Construction*, 3(2): 13-47, 1981.

2.8 ACI Committee 222, "Corrosion of Metals in Concrete," *ACI Journal*, 82(1): 3-32, 1985.

2.9 ACI Committee 439, "Steel Reinforcement Properties and Availability," *ACI Journal*, 74(10): 481, 1977.

2.10 ACI Committee 423, "State-of-the-Art Report on Partially Prestressed Concrete," *ACI Manual of Concrete Practice*, 423.5R-99, Farmington Hills, Michigan, 2000.

2.11 Ahmad, S., "Properties of Confined Concrete under Static and Dynamic Loads," Ph.D. thesis submitted to the University of Illinois at Chicago Circle, Department of Materials Engineering, Chicago, March 1981.

2.12 American Society of Testing and Materials, *Annual Book of ASTM Standards: Part 14*, Concrete and Mineral Aggregates, ASTM, Philadelphia.

2.13 American Society of Testing and Materials, "ASTM A82, A416, A421, A615, A616, A617, A706, A722," *Annual Book of ASTM Standards*, ASTM, Philadelphia.

2.14 Bazant, Z. P., and L. Panula, "Creep and Shrinkage Characterization for Analyzing Prestressed Concrete Structures," *PCI Journal*, 25(3): 86-122, 1980.

2.15 Beeby, A. W., "Cracking Cover, and Corrosion of Reinforcement," *Concrete International Design and Construction*,.5(2): 35-40, 1983.

2.16 Branson, D. E., and K. M. Kripanarayanan, "Loss of Prestress, Camber, and Deflection of Non-Composite and Composite Prestressed Concrete Structures," *PCI Journal*, 16(5): 22-52, 1971.

2.17 Bresler, B., *Reinforced Concrete Engineering*, Vol. 1. New York: John Wiley & Sons, Inc., 1974.

2.18 Carrasquillo, R. L., A. H. Nilson and F. O. Slate, "Properties of High Strength Concrete Subject to Short Term Loads," *ACI Journal*, 78(3): 171-78, 1981.

2.19 Concrete Reinforcing Steel Institute, *CRSI Manual of Standard Practice*, 26th ed., Chicago, Illinois, 1997, 97 pp.

2.20 Concrete Reinforcing Steel Institute, *Reinforced Concrete Fire Resistance*, CRSI, Chicago, Illinois, 1980, 256 pp.

2.21 Corley, W. G., J. M. Hanson, and T. Helgason, "Design of Reinforced Concrete for Fatigue," *Journal of the Structural Division*, ASCE, 104(ST6) June, 1978.

2.22 Devalapura, R., and M. K. Tadros, "Stress-Strain Modeling of 270 ksi Low-Relaxation Prestressing Strands," *PCI Journal*, Precast/Prestressed Concrete Institute, 37(2): 100-06, 1992.

2.23 Doi, Tomoika, Y. Tanaka, and M. Duraudi, "Physical Properties of Prestressing Steel at Low and Elevated Temperatures," Report No. DRG75-04, Shinko Wire Co. Ltd., Amagasaki, Japan.

2.24 Edwards, A. D., and A. Picard, "Fatigue Characteristics of Prestressing Strands," *Proceedings ICE*, Institute of Civil Engineers, London, Vol. 53, 1972, pp. 323-336.

2.25 Ekberg, C. G., R. E. Walther, and R. G. Slutter, "Fatigue Resistance of Prestressed Concrete Beams in Bending," *Journal of the Structural Division*, ASCE, July 1957, Paper No. 1304, pp. 1-17.

2.26 FIP Commission on Prestressing Steels and Systems, "Report on Prestressing Steels: Types and Properties," FIP, Wexham Spring, England, August 1976, 18 pp.

2.27 FIP Commission on Prestressing Steels and Systems, "A State of the Art Report on Materials of Prestressing and Reinforcement for Use Under Cryogenic Conditions", FIP Notes, May/June 1979, pp. 4-11.

2.28 Founas, M., "Deformations and Deflections of Partially Prestressed Concrete T-Beams under Static and Random Amplitude Fatigue Loading," Ph.D. Thesis, University of Michigan, Civil Engineering Department, 1989, 402 pp.

2.29 Gjorv, O. E., "Steel Corrosion of Reinforced and Prestressed Concrete Structures," Nordisk Betong, *Journal of the Nordic Concrete Federation*, No. 2-4: 147-51, 1982.

2.30 Harajli, M. H., "Deformation and Cracking of Partially Prestressed Concrete Beams under Static and Cyclic Fatigue Loading," Ph.D. Thesis, Civil Engineering Department, University of Michigan, Ann Arbor, March 1985.

2.31 Harajli, M. H., and A. E. Naaman, "Cracking in Partially Prestressed Concrete Beams under Static and Cyclic Loading." In *Cracking in Prestressed Concrete*, American Concrete Institute, SP-113, 1989, pp. 29-54.

2.32 Harajli, M. H., and A. E. Naaman, "Static and Fatigue Tests of Partially Prestressed Beams," *ASCE Journal of the Structural Division*, 111(7): 1602-18, 1985.
2.33 Heimdahl, P., and A. C. Bianchini, "Ultimate Strength of Beams Reinforced with Steel Having No Definite Yield Point," *ACI Journal*, Proceedings, 71(12): 600-03, 1974.
2.34 Helgason, T., J. M. Hanson, N. J. Somes, W. G. Corley, and E. Hognestad, "Fatigue Strength of High Yield Reinforcing Bars," *PCA Report to the Highway Research Board*, NCHRP, March 1975, 371 pp.
2.35 Jittawait, V., and M. K. Tadros, "Deflection of Partially Prestressed Concrete Members," Final Report, PCI Fellowship, Department of Civil Engineering, West Virginia University, 1979. (Also available as M.S. thesis of first author.).
2.36 L'Hermite, R., *Les Déformations du Béton* (in French), ed. Eyrolles Paris, 1961.
2.37 Magura, D. D., M. A. Sozen, and D. P. Siess, "A Study of Stress Relaxation in Prestressing Reinforcement," *PCI Journal*, 9(2): 13-57, 1964.
2.38 Mattock, A. H., "Flexural Strength of Prestressed Concrete Sections by Programmable Calculator," *PCI Journal*, 24(1): 32-54, 1979.
2.39 Mehta, P. K., *Concrete: Structure, Properties and Materials,* 2nd ed. Upper Saddle River, NJ: Prentice Hall Inc., 1993.
2.40 Menegotto, M., and P. E. Pinto, "Method of Analysis for Cyclically Loaded R.C. Plane Frames, Including Changes in Geometry and Non-Elastic Behavior of Elements under Combined Normal Force and Bending," *IASBE Preliminary Report for Symposium on Resistance and Ultimate Deformability of Structures under Well-Defined Repeated Loads*, Lisbon, 1973, pp. 15-22.
2.41 Mindess, S., and J. F. Young, *Concrete*. Upper Saddle River, NJ: Prentice Hall Inc., 1981.
2.42 Naaman, A. E., "Fatigue in Partially Prestressed Concrete Beams." In *Fatigue in Concrete Structures,* American Concrete Institute, SP-75-2, 1982, pp. 24-46.
2.43 Naaman, A. E., "Partially Prestressed Concrete: Review and Recommendations," *PCI Journal*, 30(5): 54-81, 1985.
2.44 Naaman, A. E., and M. Founas, "Partially Prestressed Beams under Random Amplitude Fatigue Loading," *ASCE Journal of Structural Engineering*, 117(12): 3742-61, 1991.
2.45 Nawy, E. G., *Fundamentals of High Performance Concrete*, 2nd ed. New York: John Wiley and Sons, 2000.
2.46 Neville, A. M., *Creep of Concrete: Plain, Reinforced, and Prestressed.* Amsterdam: North Holland Publishing Co., 1970.
2.47 Neville, A. M., *Properties of Concrete,* 4th ed. London: Pitman Books, 1996.
2.48 Nilson, A. H., and G. Winter, *Design of Concrete Structures*, 11th ed. New York: McGraw-Hill Book Co., 1991.
2.49 Otter, D., and A. E. Naaman, "Properties of Steel Fiber Reinforced Concrete under Cyclic Loading" *ACI Journal of Materials*, 85(4): 254-61, 1988.
2.50 Otter, D., and A. E. Naaman, "Model for Response of Concrete to Random Compressive Loads," *ASCE Journal of the Structural Division*, 115(11): 2794-2809, 1989.
2.51 PCI Committee on Prestress Loss, "Recommendations for Estimating Prestress Losses," *PCI Journal*, 20(4): 108-26, 1975.
2.52 PCI Committee on Design Handbook, "Volume Changes in Precast Prestressed Concrete Structures," *PCI Journal*, 22(5): 38-53, 1977.
2.53 Podolny, Jr., W., and T. Melville, "Understanding the Relaxation in Prestressing," *PCI Journal*, 14(4): 43-54, 1969.
2.54 Popovics, S., *Concrete Making Materials*. New York: McGraw-Hill Book Co., 1979.
2.55 Post-Tensioning Institute, *Guide Specifications for Post-Tensioning Materials*, in Post-Tensioning Institute Manual, 5th ed., Post-Tensioning Institute, Phoenix, Arizona, 2000.
2.56 Price, K. M., and A. D. Edwards, "Fatigue Strength of Prestressed Concrete Flexural Members," *Proceedings, Institute of Civil Engineers*, London, Vol. 47, October 1970, pp. 205-26.

2.57 Ross, A. D., "Creep and Shrinkage of Plain, Reinforced, and Prestressed Concrete: A General Method of Calculation," *Journal Institution of Civil Engineers*, London, November 1943, pp. 38-57.

2.58 Tide, R. H. R., and D. A.VanHorn, "A Statistical Study of the Static and Fatigue Properties of High Strength Prestressing Strand," *Fritz Engineering Laboratory Report* No. 309.2, Lehigh University, June 1966.

2.59 Sargin, M., "Stress-Strain Relationship for Concrete and the Analysis of Structural Concrete Sections," Study No. 4, Solid Mechanics Division, University of Waterloo, Waterloo, Ontario, Canada, 1971, 167 pp.

2.60 Troxell, G. E., H. E. Davis, and J. W. Kelly, *Composition and Properties of Concrete*, 2nd ed., New York: McGraw-Hill Book Co., 1968.

2.61 U.S. Bureau of Reclamation, *Concrete Manual*, 8th ed. Denver, CO: U.S. Government Printing Office, 1975.

2.62 Wang. P., S. P. Shah, and A. E. Naaman, "High Strength Concrete in Ultimate Strength Design," *ASCE Journal of the Structural Division*, 104(ST 11): 1761-73, 1978.

2.63 Wang, P.T., S. P. Shah, and A. E. Naaman, "Stress-Strain Curves of Normal and Lightweight Concrete in Compression," *Journal of the American Concrete Institute*, 75(11): 603-11, 1978.

2.64 Warner, R. F., and C. L. Hulsbos, "Fatigue Properties of Prestressing Strands," *PCI Journal*, 11(1): 32-52, 1966.

2.65 Waterhouse, R. B., *Fretting Fatigue*. Barking, Essex, UK: Applied Science Publishers Ltd., 1981.

PROBLEMS

2.1 (a) Using Eq. (2.3) plot on a semilogarithmic graph the percent loss due to relaxation (that is, $\Delta f_{pR}(t)/f_{pi}$) versus time in hours for values of f_{pi}/f_{py} = 0.6, 0.7, 0.8, and 0.9, respectively, assuming f_{pi} remains constant over time. (b) Compute the percent loss due to relaxation at the following times given in hours: 24, 10^2, 10^3, 10^4, 10^5, 10^6, assuming f_{pi}/f_{py} = 0.80.

2.2 Using the prediction relationship given in Table 2.9, plot two curves showing the strength of moist-cured and steam-cured concrete (in percent of their 28 days strength) versus time up to t = 90 days.

2.3 Using the information given in Table 2.9 and assuming K_{CS} = 1 and a standard value of the ultimate creep coefficient C_{CU} = 3, compute the ultimate creep coefficient for a moist-cured concrete member for the following conditions: H = 40, 60, and 80 percent and t_A = 7, 28, and 90 days, respectively.

2.4 Using the relationship given in Table 2.9, plot a curve showing the creep coefficient versus time up to t = 10,000 days for a precast rectangular concrete column with cross section of 15x15 in (380x380 mm). The following information is given: C_{CU} = 3, H = 60 percent, steam-cured concrete, t_A = 1 day.

2.5 Compute for the purpose of design the predicted direct tensile strength, modulus of rupture, and modulus of elasticity for normal weight and all lightweight concretes of compressive strength f'_c = 5000 psi, 7000 psi, and 9000 psi, respectively. Assume γ_c = 150 lb/ft^3 for normal weight concrete and 105 lb/ft^3 for lightweight concrete.

2.6 A precast pretensioned concrete column has a cross section of 12x12 in (300x300 mm). It is prestressed with 10 half-inch diameter stress-relieved strands of ultimate strength f_{pu} = 270 ksi. The concrete is normal weight, made with Type I cement, and the column is steam cured prior to release of prestress. Assume that the stress in the strands just after transfer (or release) of prestress is equal 185 ksi. Release of prestress is carried out 24 hours after casting, time at which shrinkage and creep of concrete and relaxation of the prestressing steel will start simultaneously. Assume that shrinkage, creep and relaxation are not related, occur independently, and do not influence each other. Also assume that the compressive strength of the concrete is 7000 psi at time of transfer and its modulus $E_c = 4770$ ksi ; both remain constant throughout. The relative humidity of the environment is $H = 60\%$.

Determine the average stress in the prestressing steel and in the concrete at 3, 7, 28, 90, 365, and 50x365 days after release of prestress. Use the relations given in Table 2.9 for creep and shrinkage, and Eq. (2.2) for relaxation. Use an ultimate shrinkage coefficient $\varepsilon_{SU} = 4\text{x}10^{-4}$ and an ultimate creep coefficient $C_{CU} = 2.2$ as taken from Table 2.11. Present your results in tabular form, showing, at any of the given times, the reduction in stress in the prestressing steel due to each effect, as well as the total reduction of stress due to the combined effects. Plot a graph on a semi-log scale showing the variation of the stress in the prestressing steel with time.

Main line of the Bang Na expressway in Bangkok, Thailand. Precast prestressed segmental span-by-span construction with a span of 44.4 m (146 ft). *(Courtesy Precast/Prestressed Concrete Institute.)*

THE PHILOSOPHY OF DESIGN

3.1 WHAT IS DESIGN?

In its most general definition "design is regarded as the process of selectively applying the total spectrum of science and technology to the attainment of an end result which serves a valuable purpose" [Hill, Ref. 3.19]. To design is to create, to put together something new, to re-arrange things in a new way and according to the latest state of the art. Design is an intersection of both art and science. It requires creativity combined with skill and knowledge.

Many professions have designers, including engineers of different specialties. The design process spans a wide range of responsibilities from a very global to a very detailed level. For instance, the term design applies to designing a mass transit system (transportation design engineer), designing a bridge (bridge design engineer), and designing the beam of a bridge or the reinforcement of a beam (structural designer).

Good design requires the ability of both analysis and synthesis. The designer should be capable of thinking in relationships and correlations. When working on a product the designer should be able to see the detail and the whole, the periphery and the core, the immediate and the ultimate; he/she should understand its internal interactions and external interfaces. Nature gives us the best examples of good designs. Many phenomena are a matter of design and infinite successions of design within design. In a way we are by design and design within design.

3.2 ANALYSIS OR INVESTIGATION VERSUS DESIGN

A fundamental difference exists between analysis and design. In dealing with civil engineering structures, design implies an unknown product, at least in part, while analysis implies investigating or reviewing a finished or proposed product. The analysis process, also called investigation or review process, is concerned with assessing the response of the structure to the application of loadings. It deals in part with the determination of stresses and stress or force resultants and in part with checking if the structure satisfies acceptable design criteria. This is often done by comparing actual findings with corresponding limits and ranges recommended in prevailing codes. To analyze is also to compare with what engineering judgment or the state of the art considers acceptable. Since it generally involves no unknown, the analysis process is easier than the design process.

In civil engineering structures, design involves the selection of many particulars among a large array of possibilities, such as the structural layout, the shape of a member, the structural material, and even the construction process. Within each step the design deals with the actual versus the ideal and at different levels of details. Although design does not necessarily imply finding the optimum solution, it certainly aims at being within an appropriate range of the optimum. Because of its inherent nature of dealing with unknowns and because infinite combinations of possibilities exist, design is mostly an iterative process. An efficient design process is one in which the number of iterations is reduced to a minimum. This often depends on the experience and skill of the designer. A distinction is made between preliminary design or designs in which many alternatives can be explored quickly (using engineering judgment, rule of thumb, etc.), and final design which is a more refined solution, ready for implementation.

More on some detailed steps of what "analysis versus design" implies in dealing with prestressed concrete beams can be found in Chapter 4. Similar comparisons could apply to other structural elements and systems.

3.3 DESIGN OBJECTIVES

In order to fulfill its purpose, a structure must satisfy a number of design objectives. Assuming that the need for a structure has been identified and justified, most basic design objectives are [Ref. 3.26]:

- feasibility
- constructability
- safety
- serviceability
- economy
- functionality
- aesthetics.

Although implied, the following criteria are also being increasingly considered in modern design:

- environmental impact,
- sustainability and maintainability
- ease of future demolition
- replacement.

Given available materials and technologies, a structure must be first of all feasible. At present, for instance, it is not possible to build a simply supported prestressed concrete bridge with a main span of more than about 500 meters. Feasibility and economy often go together. To be built, a proposed design must be reasonably economical in comparison to other potential alternatives. Assuming the above objectives are within range, a structure must be safe, that is, it should not collapse under loads foreseeable during its service life. It should also be serviceable, that is, it should perform properly under load and render the service for which it was built. A prestressed beam may be completely safe, yet unserviceable if it undergoes very large cambers. Similarly, a water tank may be safe but unserviceable if it cracks and leaks substantially.

The safety and serviceability of structures are generally achieved by satisfying a number of code limitations or criteria. To ensure safety, several design approaches are available and accepted by various codes. They are treated in more detail in the next sections. Serviceability generally includes aspects of cambers and deflections, fatigue, corrosion, cracking, and fire resistance. Serviceability criteria and how to satisfy them in the design of prestressed concrete structures are addressed in Chapter 7 and Ref. 1.48.

3.4 LIMIT STATE DESIGN PHILOSOPHY

The general design philosophy commonly adopted in structural engineering is based on satisfying a number of limit states [Refs. 3.17, 3.18, 3.20, 3.22].

> *A limit state is defined as the boundary between acceptable and unacceptable performance.*

Limit states are generally classified in two categories, namely, serviceability limit states, and ultimate strength limit states. However, a special category of limit states due to abnormal and rare conditions, such as a nuclear explosion or a 2000 years earthquake, can also be added. An allowable stress, or a maximum crack width, or a limit value of deflection belong to the category of serviceability limit states. Collapse of a structure due to excessive bending or shear belongs to the category of ultimate strength limit states. Fatigue falls somewhere in between. Since fatigue occurs generally under repeated service loads (elastic stresses), it can be

considered a serviceability limit state; however, it can be also argued that since fatigue leads to failure, it should be considered an ultimate limit state. Either way it is accommodated by the limit state design philosophy.

To accommodate a limit state, a design criterion is set. For instance, a crack width limit state implies that the crack width is less than or equal to a code specified value. It is then said in design that the structure must satisfy the maximum crack width limit state when subjected to service loads. Typically a design criterion takes on the following logical form:

$$\textit{Estimated value} \left\{ \begin{matrix} \geq \\ or \\ \leq \end{matrix} \right\} \textit{Prescribed value} \tag{3.1}$$

Whether the inequality is *more than or equal* or *less than or equal* depends on the particular case. Deflection should be less than or equal to a code defined limit, while resistance should be more than or equal to a code set limit.

1.	**Ultimate Strength Criteria**:	$M_u \leq \phi M_n$ $N_u \leq \phi N_n$ $V_u \leq \phi V_n$ $P_u \leq \phi P_n$	
2.	**Serviceability Criteria:** [Under specified service loads $(M_D + M_L)$ or $(M_D + \psi M_L)$ where $\psi \leq 1$]		
	(a) Allowable stress limit states: Actual stresses	$\leq$	Code limits
	(b) Fatigue: Stress ranges in steel and concrete	$\leq$	Code limits
	(c) Cracking: Predicted maximum crack width	$\leq$	Code limit
	(d) Camber and/or deflections: Predicted values	$\leq$	Code limits
	(e) Leakage under specified pressure	$\leq$	Code limit
	(f) Impact resistance or energy dissipation:	$\geq$	Code limit
	(g) Corrosion: Usually accounted for by more stringent limitations on crack width (h) Other limit states: Vibration, etc.		
3.	**Ductility Criterion:** Ductility index $\geq$ Specified index		
4.	**Reliability Criteria:** [where any of the above criteria represents a limit state, and a given probability of exceeding a limit state is the objective]		
5.	**Special Criteria:** Related to extreme earthquakes; nuclear explosions; accidental impact; volcanoes.		

Figure 3.1 Typical limit state criteria used in design.

Examples of design criteria corresponding to various ultimate strength limit states in bending, tension, shear and axial compression applicable to reinforced and prestressed concrete are shown in the top part of Fig. 3.1. The subscript u such as in M_u refers to ultimate. The subscript n such as in M_n refers to nominal. M_u is the applicable ultimate moment or the factored moment. M_n is the nominal moment resistance of the member, that is, its maximum bending resistance. The factor ϕ is the capacity reduction factor, which accounts for uncertainties in materials properties, analysis approximation, and the like (Section 3.8.2).

Figure 3.1 also shows a number of serviceability limit states relevant to concrete structures, such as allowable stresses, crack width, fatigue, deflection, and corrosion. Corresponding design criteria take on a common form, such as actual stress less than or equal to allowable stress (Eq. 3.2). Generally, in order to verify any serviceability criterion, it is necessary to: 1) estimate the variable of concern, and 2) find the corresponding limitation in the code. The variable of interest can be estimated from a prediction equation or through analysis of the structure. For instance, the deflection can be observed or predicted from an equation, while the deflection limit is taken from the prevailing code governing the construction of the structure. Similarly, an actual stress can be calculated using the principles of mechanics and the allowable stress is taken from the prevailing code. Among the serviceability criteria shown in Fig. 3.1, apart from stresses, only the camber and deflection criteria can be critical in fully prestressed concrete, while the other criteria are considered mostly when partially prestressed concrete is used.

To be rather complete, Fig. 3.1 also shows a number of other limit state criteria: a ductility criterion which may be important in seismic applications, reliability criteria if it is felt that a probabilistic analysis of the structure is more relevant than a deterministic analysis, and special criteria for abnormal conditions.

Limit state design (LSD) follows the above described philosophy; it combines some of the merits of ultimate strength design, working stress design, deterministic methods, and reliability theory. It implies [Ref. 3.21]:

1. Identification of all potential modes of failure, i.e., all significant limit states;
2. Determination of acceptable levels of safety to protect against occurrence of each limit state;
3. Consideration of the significant limit states.

Limit state design in relation to other commonly used design approaches is discussed further below.

3.5 COMMON DESIGN APPROACHES

In designing for safety, several design approaches can be followed. These approaches are generally based on theory and supported by experimental evidence. At the time of this writing, the limit state design (LSD) philosophy described above is most prevalent in structural engineering. Its general formulation evolved

following other design approaches, used at different times, and/or for different structural materials.

Currently encountered design approaches utilize the following terminology and are listed primarily in the order they were historically used by the design profession:

WSD, ASD:	Working Stress Design , or Allowable Stress Design
USD or SD:	Ultimate Strength Design, or Strength Design
LRFD:	Load and Resistance Factor Design
LSD:	Limit State Design

The working stress design (WSD) or allowable stress design (ASD), sometimes also called permissible stress design (PSD), are different terminologies for the same approach in which maximum stress criteria are specified; that is, some allowable stresses are not to be exceeded under service loads [Ref. 3.1, 3.7]. The ultimate strength design (USD), and the load and resistance factor design (LRFD) imply essentially the same philosophy wherein strength limit states and possible collapse are considered under factored loads [Refs. 3.2, 3.4, 3.8]. The limit state design (LSD), described in the previous section, is a general approach where all limit states such as stresses as well as collapse can be considered simultaneously. LSD is the general modern approach to follow (Fig. 3.1) and encompasses all the other approaches. The reasons for which a subset approach, such as WSD, is used, are: 1) either because WSD was used historically first, or 2) because, WSD was found from experience to be generally most critical (controlling) for a design with a typical material or structure.

Other terminology related to structural design approaches includes: plastic design, nonlinear design, and probabilistic design; these refer to a specific method of design but essentially should follow the same philosophy as the limit state design.

Note that WSD and USD may result in the same member design, but USD generally allows for a more rational distribution of safety reserve. Although a single approach may generally be sufficient, current practice in prestressed concrete (Section 3.10.1) involves the combination of working stress design (WSD) and ultimate strength design (USD or SD). LSD philosophy allows combining the two WSD and USD, while safety factors, load factors and resistance factors are obtained from a rational and complex calibration of data to achieve a consistent level of safety and reliability (or probability of survival) for every limit state considered.

Except for probabilistic design, design approaches begin with the choice of the specified loads to design for. The nature and magnitude of these loads depend on the type of structure. Some are described in Section 3.7.

3.5.1 WSD (or ASD)

In this approach the stresses under working loads are limited to permissible values or allowable stresses and the structure is analyzed assuming linear elastic materials and thus linear elastic behavior. Safety is ensured by selecting allowable stresses as relatively small fractions of the characteristic strengths of the component materials. Allowable stresses are specified in various codes and may vary from one code to another. Typical values for prestressed concrete are described in Section 3.7. For instance, the maximum permissible compressive stress on concrete flexural members may be taken as $0.45\, f'_c$. This implies a safety factor of (1/0.45) = 2.22 against concrete compressive failure under short term loading. Note that in the working stress design all types of loads are treated the same, no matter how different their variability is. This is less realistic than in the USD approach where each load is treated according to its degree of uncertainty. The design of prestressed concrete beams using the working stress design approach is covered in detail in Chapter 4.

When the WSD (or ASD) approach is used, the following general formulation (criterion) applies:

$$\boxed{|\textit{Actual Stress}| \leq |\textit{Allowable Stress}|} \tag{3.2}$$

where absolute values of stresses are considered. The allowable stress can be obtained from:

$$\textit{Allowable Stress} = \frac{\textit{Strength}}{\textit{Safety Factor}} \tag{3.3}$$

Assuming linear elastic behavior under bending, axial tensile load, or shear, the actual stress induced by loading in an uncracked section is directly proportional to the applied load:

$$\textit{Actual Stress} = \frac{N}{A_c} \qquad \text{for axial tensile load} \tag{3.4}$$

$$\textit{Actual Stress} = \frac{M}{Z} \qquad \text{for a bending moment} \tag{3.5}$$

$$\textit{Actual Stress} = \frac{VQ}{I\, b} \qquad \text{for a shear force} \tag{3.6}$$

where Z stands for elastic section modulus, Q for the moment of area above the shear plane, and b is the width of the shear plane. Other notation is standard. Tensile, bending and shear stresses in the linear elastic range of behavior can be computed as described in Chapters 4, 6, and 12.

Thus the allowable stress design criterion (Eq. 3.2) can be generally written as follows:

$$\sigma_i \leq \frac{1}{SF}\sigma_n \tag{3.7}$$

where σ_i is the stress due to loading i, σ_n is the equivalent elastic stress at nominal resistance, and SF is a safety factor larger than one. The summation of stresses is done over the applied load combination of interest. Assuming for instance a combination of dead load and live load (often termed service load, that is, $(D + L)$) leads to:

$$\sigma_D + \sigma_L \leq \frac{1}{SF}\sigma_n \tag{3.8}$$

where σ_D is the stress due to dead load and σ_L is the stress due to live load.

Since, under elastic bending, stresses and moments are directly proportional, Eq. (3.8) can be written:

$$M_D + M_L \leq \frac{1}{SF}M_n \tag{3.9}$$

where M_n is the nominal bending resistance. The safety factor is often taken between 2 and 2.5 in the WSD (or ASD) approach.

3.5.2 USD, SD, or LRFD

In this approach, the design working loads are multiplied by load factors and the structure is designed to resist the factored loads, at its ultimate capacity. The load factors are different for each type of load and are adjusted to reflect the degree of variability and uncertainty of that load. This is more realistic than in the WSD approach, where all loads are treated the same.

When either the USD, LSD, or LRFD approach is applied, the general format is given by the formula [Refs. 3.2, 3.8, 3.22]:

$$U = \Sigma\, \gamma_i Q_i \leq \phi R_n \tag{3.10}$$

where:

i = type of load, i.e., dead load, live load, wind, etc.
Q_i = nominal load effect
γ_i = load factor corresponding to Q_i

U = required or specified ultimate strength
$\Sigma\gamma_i Q_i$ = sum of factored loads = required or specified ultimate strength U
R_n = nominal strength or resistance
ϕ = resistance factor (or capacity reduction factor) corresponding to R_n
ϕR_n = design strength or design nominal resistance

The left side of Eq. (3.10) represents the required resistance, which is computed from structural analysis based on assumed loads, and the right side of Eq. (3.10) represents a limiting structural capacity provided by the selected members. In USD or LRFD, the designer compares the effect of factored loads to the strength actually provided. The term design strength refers to the resistance, ϕR_n, that must be provided by the selected member. The load factors, γ_i, and the resistance factor, ϕ, reflect the fact that loads, load effects (the computed forces and moments in the structural elements) and the resistances can be determined only to imperfect degrees of accuracy. The resistance factor, ϕ, is less than or equal to 1.0, because there is always a chance for the actual resistance to be less than the nominal value R_n predicted by analytical formulations. Similarly, the load factors, γ_i, reflect the fact that the actual load effects may deviate from the nominal values of Q_i, computed from the specified nominal loads. These factors account for unavoidable inaccuracies in the theory (i.e., seismic forces), variations in the material properties and dimensions (i.e., dead loads), and uncertainties in the determination of loads (i.e., wind load). They provide a margin of safety to account for unexpected loads; however, they do not account for gross error or negligence.

The required strength, $U = \Sigma\gamma_i Q_i$, is defined for design as the maximum (absolute value) of force obtained from the specified load combinations. The load factors and load combinations recognize that when several loads act in combination with the dead load, only one load takes on its maximum lifetime value at a time, while the other loads are at arbitrary point-in-time value. Each load combination models the design loading condition when a different load is at its maximum. Examples of load combinations specified by the ACI code are as follows (Table 3.9):

$1.2\,D + 1.6\,L$
$0.9\,D + 1.6\,W + 1.6\,H$

where D, L, and W represent either the loads themselves or the load effects (i.e., the forces or moments caused by the loads). The coefficients are the applicable load factors, γ_i.

Examples of resistance (or capacity reduction) factors given by ACI 318 [Ref. 3.4] for reinforced concrete are (Table 3.10):

ϕ = 0.9 for bending
ϕ = 0.75 for shear and torsion

When the USD approach is applied to bending, direct axial tension, or shear in reinforced or prestressed concrete, the following formulation is obtained:

$$\boxed{M_u = \gamma_D M_D + \gamma_L M_L \leq \phi M_n} \tag{3.11}$$

$$\boxed{N_u = \gamma_D N_D + \gamma_L N_L \leq \phi N_n} \tag{3.12}$$

$$\boxed{V_u = \gamma_D V_D + \gamma_L V_L \leq \phi V_n} \tag{3.13}$$

where M stands for bending moment, N for tensile axial load, V for shear force, and other notation is as above.

Note that the load and resistance factors are obtained from calibration using reliability analysis. Load factors are higher for loads with higher degree of uncertainty. This is why the live load factor for reinforced concrete is higher than the dead load factor. On the other hand, resistance factors are lower for types of members or materials with higher degree of uncertainty. This is why the capacity reduction factor, ϕ, for shear is smaller than that for bending.

In comparing Eq. (3.9) with Eq. (3.11), it can be observed that in the USD-LRFD approach, the effects of loads are multiplied by a factor (different for each load) and compared to the nominal resistance, while in the WSD-ASD approach, the load effects are used without modification and the resistance is divided by a factor. However, the difference lies in the fact that in USD-LRFD each load has a different load factor, while in WSD-ASD the same safety factor is applied to the effects of all loads. Figure 3.2 illustrates the two approaches assuming a tensile member of known nominal tensile resistance, N_n.

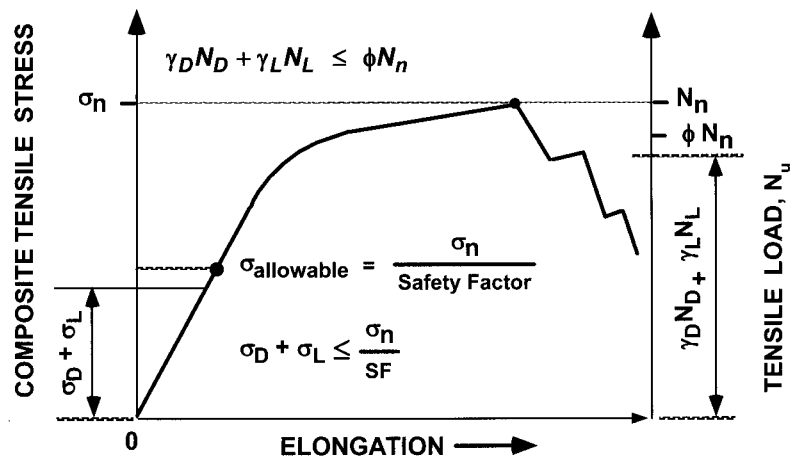

Figure 3.2 Illustration of the WSD (left axis) and USD (right axis) approach for a tensile member.

3.5.3 Plastic Design or Limit Design

This is a design based on the formation of plastic hinges, or yielding mechanisms, within a structure under loading. It has been mostly applied to statically indeterminate steel structures where it is observed that collapse cannot occur due to a single section undergoing yielding. A big reserve of strength generally exists between first yielding and general collapse. Limit design is recognized in the ACI code but to a very limited extent: Sections 8.4 and 18.10 of the code allow redistribution of negative moments in reinforced and prestressed concrete continuous members (see Sections 5.22 and 10.14 of this book). In effect, limit design for concrete structures is more often synonymous of nonlinear design than plastic design.

3.5.4 Nonlinear Design, Probabilistic Design

Nonlinear design typically makes use of accurate nonlinear stress-strain relationships of materials, equilibrium of forces, and compatibility of strains or deformations. For a prescribed loading history, the sequence of linear and nonlinear actions within a structure can be tracked and a more accurate picture of structural resistance and deformation is usually obtained.

The object of the probabilistic design is to ensure that there is an accepted probability for the structure not to reach any limit state. In probabilistic design, the applied load and the inherent resistance are assumed random variables. The margin of safety itself, which is defined as the difference between resistance and load, is a random variable. Its mean value is associated with the probability of failure, where failure means not only collapse but also unserviceability or violation of any other specified limit state. Probabilistic design is at the basis of limit state design (LSD), since the load and resistance factors are calibrated according to probability theory.

3.6 DESIGN CODES

Although basic engineering concepts and judgment can be used to design a structure, most of the guesswork can be reduced and better efficiency achieved if structural requirements set by design codes are satisfied. Design codes (such as Refs. 3.1 to 3.11) are written to protect the user and society as a whole. They provide information on methods of analysis and design, minimum design requirements and minimum expected performance. They represent a summary of the collective opinion or agreed upon state of knowledge of the profession.

In the United States most reinforced and prestressed concrete structures (except bridges) are designed in accordance with the Building Code Requirements for Reinforced Concrete (ACI 318) published by the American Concrete Institute [Refs. 3.3 and 3.4]. It is regarded as an authoritative statement of current good practice in the field of concrete structures. The ACI code is incorporated entirely or in part in

many municipal and regional codes in the United States and is used as a reference in many foreign countries.

Most prestressed concrete bridges for highways or railways in the United States are designed in accordance with three major codes: the AASHTO (American Association of State Highway and Transportation Officials) Standard Specifications for Highway Bridges [Ref. 3.1], the AASHTO LRFD Specification for Highway Bridge Design [Ref. 3.2] and the AREA (American Railway Engineering Association) Manual for Railway Engineering [Ref. 3.10, 3.11]. The AASHTO Standard specifications are essentially based on the working stress design, while the AASHTO LRFD specifications are essentially based on limit state design. Except for the LRFD specification and for some subtle differences, the sections of AASHTO Standard and the those of the AREA manual related to prestressed concrete are essentially identical in scope to the corresponding sections of the ACI code. However, the AASHTO LRFD specifications are significantly different. Some of these differences are discussed in Chapter 5 in relation to various limitations on reinforcement.

In this text, reference to the above documents (or simply codes) will frequently be made and preferably their latest editions should be used. These codes contain specific information on analysis and design methods, as well as service loads, load factors, and allowable stresses. These last three items will be discussed next.

3.7 LOADS

For the purpose of design, loads are classified into two main categories: dead loads (also identified as permanent loads) and live loads (also identified as transient loads).

Dead loads include primarily the self-weight of the structure and any permanent component such as tiles, false ceiling, and partitions. They are assumed to remain constant during the life of the structure. Self-weight is estimated from the dimensions of the element and the unit weight of the material. Dead loads due to partitions and the like are generally approximated by an equivalent uniform load applied to the surface area of the structure. Typical values of unit weights of some common materials are given in Table 3.1. In general, one can assume a unit weight of 150 lb/ft^3 (23.6 kN/m^3) for normal weight concrete (including the steel) and between 100 and 120 lb/ft^3 (15.7 to 18.9 kN/m^3) for structural lightweight concrete.
Unlike dead loads, live loads are variable in nature and fluctuate with time. They include (1) occupancy loads caused by people, furnishings, or movable objects, (2) vehicle loads such as trucks or trains, (3) snow, rain, water, ice, wind, earth pressure, temperature loads, effects of earthquakes, and the like. Occupancy loads are generally prescribed in various codes as uniformly distributed loads. The ACI code does not prescribe occupancy loads. However, the American National Standards Institute (ANSI) and the American Society of Civil Engineers (ASCE), as well as local and regional codes, prescribe such values. Typical selected values of occupancy loads recommended by the ASCE/ANSI code [Refs. 3.7 and 3.12] are

Table 3.1 Weights and specific gravity of various materials.
(Adapted from AISC Manual, Ref. 3.7)

Substance	Density† lb/ft³ (average)	Density† kg/m³ (average)	Specific gravity (range)
Building materials			
Asphaltum	81	1298	1.1-1.5
Brick (common)	120	1924	1.8-2.0
Cement, Portland, loose	90	1443	.....
Cement, Portland, set	183	2933	2.7-3.2
Earth, dry, loose	76	1218	.....
Earth, dry, packed	95	1523	.....
Earth, moist, loose	78	1250	.....
Earth, moist, packed	96	1539	.....
Glass (common)	156	2501	2.40-2.60
Lime, gypsum, loose	53-64	850-1026	.....
Lime, mortar, set	103	1651	1.4-1.9
Sand, gravel, dry, loose	90-105	1443 -1683	.....
Sand, gravel, dry, packed	100-120	1603 -1924	.....
Sand, gravel, wet	118-120	1892 -1924	.....
Timber, pine (various types, seasoned, 15 to 20% moisture by weight)	30-44	481-705	0.48-0.70
Timber, oak (various types, seasoned, 15 to 20% moisture by weight)	41-59	657 -946	0.65-0.95
Liquids			
Alcohol, 100%	49	785	0.79
Oils	58	930	0.90-0.94
Water, 4° C	62.43	1001	1.0
Water, ice	56	898	0.88-0.92
Water, snow, fresh fallen	8	128	0.125
Water, seawater	64	1026	1.02-1.03
Metals			
Aluminum, cast, hammered	165	2645	2.55-2.75
Copper, cast, rolled	556	8913	9.8-9.0
Iron, cast, pig	450	7213	7.2
Lead	710	11381	11.37
Steel, rolled	490	7855	7.85
Minerals			
Asbestos	153	2453	2.1-2.8
Granite, syenite	175	2805	2.5-3.1
Gypsum, alabaster	159	2549	2.3-2.8
Limestone, marble	165	2645	2.5-2.8
Pumice, natural	40	641	0.37-0.90
Quartz, flint	165	2645	2.5-2.8
Sandstone, bluestone	147	2356	2.2-2.5
Shale state	175	2805	2.7-2.9
Reinforced, prestressed concrete			
Normal weight	150	2404	2.3-2.5
Lightweight, structural	110-120	1763-1924	1.77-1.9

† 1 lb/ft³ = 16.03 kg/m³

Table 3.2 Typical values of uniformly distributed design live loads.
(Adapted from ANSI Code, Ref. 3.9)

Occupancy or use	Live load	
	lb/ft²	kPa or kN/m²
Assembly halls		
Fixed seats	60	2.9
Movable seats	100	4.8
Balcony (exterior)	100	4.8
Dining rooms, restaurants, dance halls	100	4.8
Garages (passenger cars) Floors shall be designed to carry 150% of the maximum wheel load anywhere on the floor	100	4.8
Hospitals		
Operating rooms	60	2.9
Private rooms	40	1.9
Hotels		
Guest rooms	40	1.9
Public rooms, lobbies, first floor corridors	100	4.8
Housing		
Private houses and apartments	40	1.9
Public rooms (in multifamily units)	100	4.8
Libraries		
Reading rooms	60	2.9
Stack rooms	150	7.2
Office buildings		
Offices	80	3.8
Lobbies	100	4.8
Schools		
Classrooms	40	1.9
Corridors	100	4.8
Sidewalks, driveways subject to trucking	250	12
Stairs and exitways	100	4.8
Storage warehouses		
Light	125	6
Heavy	250	12
Yards and terraces, pedestrians	100	4.8

reproduced in Table 3.2. A more extensive list can be found in Ref. [3.12] as well as particular details for other live loads. Wind loads of 15 to 30 lb/ft^2 ($\approx$0.7 to 1.4 kN/m^2) and snow loads of 10 to 40 lb/ft^2 ($\approx$0.5 to 2 kN/m^2) are common ranges for design in the US.

Vehicle loadings are prescribed by the AASHTO and AREA specifications for highway and railway bridges, respectively [Refs. 3.2, 3.10]. The live loads recommended by AASHTO comprise two groups: moving vehicle loads and equivalent lane loading in the form of a uniform load. Most critical load combinations and/or arrangement have to be considered in design. Many factors, such as impact, the number of lanes, the width of the lanes, and the stiffness of the structure are associated with bridge loadings; their description and treatment is discussed in Chapter 14.

3.8 ALLOWABLE STRESSES

In the working stress design approach a number of stress limits, called allowable stresses or permissible stresses, are needed. These allowable stresses are not to be exceeded by actual stresses under application of service loads. They are in general prescribed by the code adopted for the design. Typical values of allowable stresses imposed by the ACI code are summarized in Tables 3.3 to 3.8 for concrete, prestressing steel, and reinforcing steel, respectively.

3.8.1 Concrete

Allowable stresses for concrete (Table 3.3) are separated into two groups: the first one corresponds to initial stresses at time of transfer of prestress (before prestress losses), and the second one corresponds to final or service load stresses (after allowance for prestress losses). The subscript i such as in f'_{ci} is associated with the first group. Tension in concrete has been given a negative sign in accordance with the sign convention adopted in this text. Also given in Table 3.3 are the stresses in the equivalent SI system. Note that a tension of $-6\sqrt{f'_c}$ is generally allowed during service on the concrete precompressed fiber. A fictitious value of $-12\sqrt{f'_c}$ or more is allowed to accommodate partial prestressing.

Two allowable values of extreme fiber compressive stress in service due to prestress and total load are given to reflect the nature of the service load and its effect on long term properties, particularly creep, deflections, and fatigue. Thus, when the sustained dead load and live load are a substantial portion of total service load, the $0.45f'_c$ allowable stress limit may control. On the other hand when a large portion of the total service load consists of a transient temporary service load, the stress limit of $0.6f'_c$ may control. Most frequently the stress in compression under service load does not control the design of prestressed concrete flexural members.

Thus, the above distinction between the two values of allowable stress may not be of significance. In most of the examples given in this text, the lower limit of $0.45f'_c$ is considered to be on the safe side. Engineering judgment should be used to decide whether the higher allowable stress limit applies.

Numerical values of allowable stresses are given in Tables 3.4 and 3.5 for typical concrete strengths, in U.S. and SI units, respectively.

Table 3.3 Allowable stresses in concrete in prestressed flexural members. *(Adapted from ACI 318 Code, Ref. 3.3)*

	psi	MPa
1. Stresses immediately after prestress transfer (before prestress losses) shall not exceed the following:		
(a) Extreme fiber stress in compression	$0.60f'_{ci}$	$0.60f'_{ci}$
(b) Extreme fiber stress in tension except as permitted in *c*	$-3\sqrt{f'_{ci}}$	$-0.25\sqrt{f'_{ci}}$
(c) Extreme fiber stress in tension at ends of simply supported members	$-6\sqrt{f'_{ci}}$	$-0.50\sqrt{f'_{ci}}$
Where computed tensile stresses exceed these values, bonded auxiliary reinforcement (non- prestressed or prestressed) shall be provided in the tensile zone to resist the total tensile force in the concrete computed with the assumption of an uncracked section.		
2. Stresses at service loads (after allowance for all prestress losses) shall not exceed the following:		
(a) Extreme fiber stress in compression due to prestress plus sustained load	$0.45f'_c$	$0.45f'_c$
(b) Extreme fiber stress in compression due to prestress and total load	$0.60f'_c$	$0.60f'_c$
(c) Extreme fiber stress in tension in precompressed tensile zone	$-6\sqrt{f'_c}$	$-0.50\sqrt{f'_c}$
(d) Extreme fiber stress in tension in precompressed tensile zone of members (except two-way slab systems) where analysis based on transformed cracked sections and on bilinear moment-deflection relationships shows that immediate and long-time deflections comply with requirements stated elsewhere in the code	$-12\sqrt{f'_c}$	$-\sqrt{f'_c}$
3. The permissible stresses of sections 1 and 2 may be exceeded if shown by test or analysis that performance will not be impaired.		

The allowable stresses recommended by AASHTO for bridges [Refs. 3.1, 3.2] are different from the corresponding ACI code values. Mostly, the AASHTO LRFD code recommends allowable tensile stresses smaller than those given by ACI because of concerns about corrosion. Different stress limits are given for segmental and non-segmental construction. Allowable stresses by AASHTO should be used in bridge design and are given in Chapter 14.

Table 3.4 Typical values of allowable stresses in concrete (psi units).

	Specified compressive strength, f'_c, psi					
Allowable stress*	5000	6000	7000	8000	9000	10000
$0.60f'_{ci}$	2400	2880	3360	3840	4320	4800
$-3\sqrt{f'_{ci}}$	-190	-208	-224	-240	-255	-268
$-6\sqrt{f'_{ci}}$	-380	-416	-449	-480	-509	-536
$0.45f'_c$	2250	2700	3150	3600	4050	4500
$0.60f'_c$	3000	3600	4200	4800	5400	6000
$-6\sqrt{f'_c}$	-424	-465	-502	-537	-569	-600

*Assuming $f'_{ci} = 0.80f'_c$

Table 3.5 Typical values of allowable stresses in concrete (MPa units).

	Specified compressive strength, f'_c, MPa				
Allowable stress* ↓	30	40	50	60	70
$0.60f'_{ci}$	14.4	19.2	24	28.8	33.6
$-0.25\sqrt{f'_{ci}}$	-1.22	-1.41	-1.58	-1.73	-1.87
$-0.50\sqrt{f'_{ci}}$	-2.45	-2.83	-3.16	-3.46	-3.74
$0.45f'_c$	13.5	18	22.5	27	31.5
$0.60f'_c$	18	24	30	36	42
$-0.50\sqrt{f'_c}$	-2.74	-3.16	-3.54	-3.87	-4.18

*Assuming $f'_{ci} = 0.80f'_c$

3.8.2 Prestressing Steel

Allowable stresses in prestressing steels specified by the ACI code are summarized in Table 3.6. Different values are given depending on whether the stress applied occurs just before or after transfer of the force from the steel to the concrete. Previous editions of the code also used to specify a limiting final stress of $0.60f_{pu}$ after all losses. This does not seem to be necessary because, in practice, the actual final stress or effective prestress is seldom larger than $0.60f_{pu}$; it is commonly of the order of $0.5f_{pu}$ to $0.55f_{pu}$. The second column of Table 3.6 contains the code provisions in terms of the yield strength of the prestressing steel. The third and

fourth columns show the corresponding values in terms of the ultimate strength, f_{pu}, assuming either a stress relieved strand or a low relaxation strand, and keeping in mind the maximum limit of $0.8f_{pu}$ given in the code.

Table 3.6 Allowable stresses in prestressing steel. *(Adapted from ACI 318 Building Code, Ref. 3.3)*

	ACI code specs.	Stress relieved steel, $f_{py} = 0.85f_{pu}$	Low relaxation steel, $f_{py} = 0.90f_{pu}$
Tensile stress in prestressing steel shall not exceed the following:			
1. Due to prestressing steel jacking force, but not greater than the lesser of $0.80f_{pu}$ and the maximum value recommended by the manufacturer of the prestressing steel or anchorage devices	$0.94f_{py}$	$0.80f_{pu}$	$0.80f_{pu}$
2. Pretensioning tendons immediately after prestress transfer but not greater than $0.74f_{pu}$	$0.82f_{py}$	$0.70f_{pu}$	$0.74f_{pu}$
3. Post-tensioning tendons at anchorages and couplers immediately after tendon anchorage	$0.70f_{pu}$	$0.70f_{pu}$	$0.70f_{pu}$

Table 3.7 Typical values of allowable stresses in prestressing tendons.

	Specified ultimate strength, f_{pu}									
	Bar		Bar		Wire		Strand		Strand	
Allowable stress ↓	145 ksi	1000 MPa	160 ksi	1104 MPa	235 ksi	1622 MPa	250 ksi	1723 MPa	270 ksi	1860 MPa
At jacking $0.80f_{pu}$	116	800	128	882	188	1296	200	1378	216	1488
After transfer $0.74f_{pu}$	107	740	118	817	174	1200	185	1275	200	1376
After transfer $0.7f_{pu}$	101.5	700	112	773	164.5	1134	175	1206	189	1302

Note, from the third column of Table 3.6, that if f_{py} is taken equal to $0.85f_{pu}$ such as for a stress-relieved strand (see Section 2.3), then the limits of $0.82f_{py}$ and $0.94f_{py}$ become $0.7f_{pu}$ and $0.80f_{pu}$, respectively. On the other hand for a low relaxation strand for which $f_{py} = 0.90f_{pu}$, the above limits of $0.82f_{py}$ and $0.94f_{py}$ become $0.74f_{pu}$ and $0.85f_{pu}$, respectively. This last term is then limited by $0.80f_{pu}$. Often in this text, for simplicity, a limit of $0.7f_{pu}$ is used as the transfer stress.

Typical numerical values of allowable stresses as per the ACI code for various types of prestressing steels are given in Table 3.7 in both the US and the SI systems. Stress limits for prestressing tendons given by AASHTO LRFD specifications are very similar to those given by the ACI code.

3.8.3 Reinforcing Steel

Allowable stresses in the reinforcing steel are given in Table 3.8. As the current ACI code deals mostly with ultimate strength design, these stresses are not given directly in the body of the most current code but in Appendix B of the 1983 edition where working stress design (termed alternate design method) provisions are explained. In principle, they should apply to reinforcing steels used in prestressed concrete. Note that for cases where temporary tension in the concrete is to be resisted (such as in the note of case 1(*c*) of Table 3.3) a permissible stress of $0.60f_y$ or 30 ksi (207 MPa), whichever is smaller, can be used throughout.

Table 3.8 Allowable stresses in reinforcing steels. *(Adapted from ACI 318-83 Code, Ref. 3.3)*

	Allowable stress, $\overline{f_s}$	
Conditions of application	ksi	MPa
1. Grade 40 or grade 50 reinforcement	20	138
2. Grade 60 or greater and welded wire fabric (smooth or deformed)	24	165
3. For flexural reinforcement 3/8 in. (9.5 mm) or less in diameter, in one-way slabs of not more than 12 ft. (3.7 m) span	$0.50f_y \leq 30$	$0.50f_y \leq 207$

3.9 LOAD AND STRENGTH REDUCTION FACTORS

3.9.1 Load Factors

In ultimate strength design (USD) or strength design (SD), service loads are multiplied by load factors and the member is designed to resist the factored loads. Load factors adopted by the ACI code are summarized in Table 3.9 and are based on several studies dealing with reliability analysis and code calibration [Refs. 3.17, 3.18, 3.20, 3.22]. Different factors are given for different loadings. Their magnitude is in effect adjusted to reflect the degree of uncertainty associated with the type of loading. Thus, load factors for dead loads are smaller than those for live loads. Several load combinations are to be considered in design. Reduced load factors are used on some load combinations because of the low probability of their simultaneous occurrences.

Table 3.9 Load factors for determining required strength, *U*.
(Adapted from ACI 318-02, Ref. 3.3).

Conditions of application as per ACI Building Code [ACI 318-02]	Required strength U	ACI Eq. No.
The load factor on L in Eqs. (9-3) to (9-5) shall be permitted to be reduced to 0.5 except for garages, areas occupied as places of public assembly, and all areas where the live load L is greater than 100 psf. When wind load W has not been reduced by a directionality factor, it shall be permitted to use $1.3W$ in place of $1.6W$ in Eqs. (9-4) and (9-6). Where earthquake load E is based on service-level seismic forces, $1.4E$ shall be used in place of $1.0E$ in Eqs. (9-5) and (9-7). The load factor on H shall be set equal to zero in Eqs. (9-6) and (9-7) if the structural action due to H counteracts that due to W or E. Where lateral earth pressure provides resistance to structural actions from other forces, it shall not be included in H but shall be included in the design resistance.	Required strength U shall be at least equal to the effects of factored loads in Eqs. (9-1) through (9-7). The effect of one or more loads not acting simultaneously shall be investigated. • $U = 1.4(D + F)$ • $U = 1.2(D + F + T) + 1.6(L + H) + 0.5(L_r \text{ or } S \text{ or } R)$ • $U = 1.2D + 1.6(L_r \text{ or } S \text{ or } R) + (1.0L \text{ or } 0.8W)$ • $U = 1.2D + 1.6W + 1.0L + 0.5(L_r \text{ or } S \text{ or } R)$ • $U = 1.2D + 1.0E + 1.0L + 0.2S$ • $U = 0.9D + 1.6W + 1.6H$ • $U = 0.9D + 1.0E + 1.6H$ where: U = required strength to resist factored loads or related moments and forces D = dead loads E = load effects of earthquake F = loads due to fluids with well defined pressures and maximum heights H = loads due to weight and lateral pressure of soil and water in soil L = live loads L_r = roof live loads R = rain load S = snow load T = self-straining forces and effects arising from contraction or expansion resulting from temperature changes, shrinkage, moisture changes, creep in component materials, movements due to differential settlements, or combinations thereof W = wind loads	(9-1) (9-2) (9-3) (9-4) (9-5) (9-6) (9-7)

One of the combinations that often controls the design is the combination of dead and live loads ($1.2D + 1.6L$); it is often used in this text as typical in many examples.

It replaces the combination ($1.4D + 1.7L$) which was used in prior versions of the ACI code.

The reader is referred to the ACI code for further details about special conditions of applications and exceptions of the load combinations given in Table 3.9. In particular the ACI code leaves some leeway to engineering judgment as to when such load factors can be increased. Indeed it states: "*If special circumstances require greater reliance on the strength of particular members than encountered in usual practice, some reduction in the stipulated strength reduction factors ϕ or increase in the load factors γ may be appropriate for such members.*"

A large number of load types, load factors and their combinations is given in the AASHTO LRFD specifications for bridge design (Tables 14.1 and 14.2). These factors may be substantially different in magnitude from those recommended by the ACI building code. For flexural design, the simplest combination for strength is ($1.25D + 1.75(L + IM + PL)$), in which L stands for vehicular live load, IM for impact and PL for pedestrian load. An approach similar to that of AASHTO is taken by ACI Committee 343 in its report on the analysis and design of reinforced concrete bridge structures [Ref. 3.5].

3.9.2 Strength Reduction Factors

Table 3.10 Strength reduction factors ϕ. *(Adapted from ACI 318-02 Code, Ref. 3.3)*

	Resisting effect	ϕ
Reinforced and prestressed concrete	Flexure without axial load or tension controlled sections	0.90
	Compression-controlled sections:	
	(a) members with spiral reinforcement	0.70
	(b) other reinforced members	0.65
	Shear and torsion	0.75
	In earthquake resistant structures:	
	• Shear	0.60
	• Shear in joints and coupling beams	0.85
	Bearing on concrete (except for anchorages)	0.65
	Bearing in post-tensioned anchorage zone	0.85
	Bearing for strut-and-tie models and nodal zones	0.75
	Development length, bond	1.00
	Any effect using working stress design	1.00
Plain concrete	Bending, shear, compression and bearing in structural plain concrete	0.55

A concrete structural element is designed to achieve a nominal strength at least equal to the required strength obtained from factored loads. The nominal strength is

generally predicted using accepted analytic procedures. However, in order to account for the degree of accuracy or uncertainty with which the nominal strength can be predicted, a strength reduction factor ϕ is used. A safe design will be achieved when the required strength obtained from the factored loadings is less than or equal to the strength obtained as the product of the nominal strength by the reduction factor ϕ. Thus equations or criteria of the form of Eqs. (3.11) to (3.13) can be set.

Values of the strength reduction factor ϕ, given in the ACI code, are summarized in Table 3.10. Different numerical values apply to different types of load effects. Factors affecting the choice of these values include possible variability in materials properties, the nature, mode, and consequence of failure, should it occur, and dimensional inaccuracies [Refs. 3.22, 3.26].

The combined application of factored loads and strength reduction factors given by the ACI code is aimed at producing approximate probabilities of understrength of the order of 1/100 and overloads of 1/1000 [Ref. 3.25]. This results in a probability of structural failure of the order of 1/100,000.

Note that the resistance factors given by the AASHTO LRFD code are different from those given by ACI. In particular AASHTO allows a ϕ factor of 1 for flexure and tension of prestressed concrete (Section 14.5.2). Resistance factors by AASHTO are recommended for bridge design, but should be used simultaneously with the load factors from the same code (refer to Tables 14.1 and 14.2).

3.10 SOME DESIGN COMPARISONS: REINFORCED VERSUS PRESTRESSED CONCRETE

3.10.1 Practical Design Approach

The principles of limit state design (LSD) described in Section 3.4 apply to both reinforced and prestressed concrete. However, practical experience leads to selecting a sequence of steps in prestressed concrete design that is different from that used for reinforced concrete (Fig. 3.3). The design of prestressed concrete members is primarily controlled by allowable stresses (serviceability criteria), while the design of reinforced concrete members is controlled primarily by ultimate strength criteria. Typically the design of prestressed concrete starts by working stress design procedures (WSD) to help dimension the member; then ultimate strength design (USD) criteria are checked, and adjustments are made should a design criterion be violated. In comparison, the design of reinforced concrete members starts directly by USD procedures; generally allowable stresses are not of concern and serviceability criteria such as crack width and deflections can be accommodated by proper dimensioning and detailing. Thus, for all practical purposes, the design of reinforced concrete is primarily controlled by USD, while that of prestressed

concrete is primarily controlled by WSD; however, in addition, USD criteria must also be used in prestressed concrete.

Typical Sequence of Design Steps for Reinforced Concrete - RC				
Step	Approach	Example	Main unknowns	Reference
1	USD	$M_u \le \phi M_n$ $V_u \le \phi V_n$	A_s, a, b, d A_v	ACI, Textbooks on RC
2	Serviceability limit states	$\Delta_{LL} \le \frac{l}{360}$		
• Allowable stresses are not considered • Design is revised if any criterion is not satisfied				

Typical Sequence of Design Steps for Prestressed Concrete - PC				
Step	Approach	Example	Main unknowns	Reference in this text
1	WSD	$\lvert\sigma_{ts}\rvert_{actual} \le \lvert\bar{\sigma}_{ts}\rvert_{allowable}$	F *or* A_{ps}, e_o, b, h	Chapters 4, 9, 10, 12
2	USD	$M_u \le \phi M_n$ $V_u \le \phi V_n$	A_s, A_v	Chapter 5 Chapter 6
3	Serviceability limit states	$\Delta_{LL} \le \frac{l}{360}$		Chapter 7
• Design is revised if any criterion, including allowable stresses, is violated				

Figure 3.3 Typical design steps sequence comparing reinforced and prestressed concrete.

3.10.2 C-Force and C-Line

Integrating all the stresses over a prestressed concrete section leads to a compressive force resultant defined as the C force. In the absence of any external moment, the C force is equal and opposite to the prestressing force. Similarly to the prestressing

force F, which has an eccentricity e_o with respect to the neutral axis of bending, the location of the C force can be defined by an eccentricity, e_c (Fig. 3.4a).

The application of any external moment (Fig. 3.4b) adds stresses to the section; however, since a moment is a couple and the two forces of a couple balance each other (i.e., the sum of the forces of a couple is equal zero), the resulting compressive force in the concrete section remains equal to C. Adding a moment changes the stress diagram, but does not change the value of C. However, the line of action of C, that is its eccentricity, e_c, shifts from the line of action of F, which remains as placed at e_o. The difference between them is equal in magnitude to M/F as shown in Fig. 3.4c. This is exactly the same as to what happens in a column subjected to a concentric axial load, when a moment is added. The effect of the moment is to shift the action of the compression force to a line parallel and eccentric to the column's axis. In beams, the external moment varies along the span; thus the eccentricity of the C force also varies. The combined action of an external moment, such as the moment due to self-weight of the member, and the prestressing force, can be replaced by the action of the C force acting along its eccentricity, e_c. The use of the C force or the C-line (that is, the geometric location of the C force along the span) can be advantageous in some calculations such as for deflections, load balancing, and continuous members.

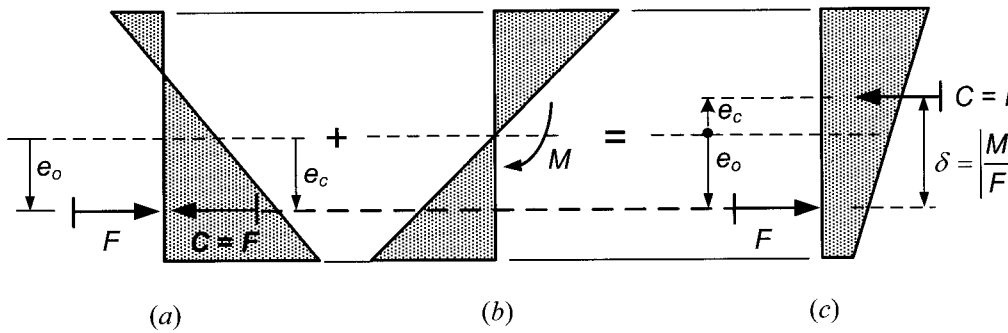

Figure 3.4 Effect of external moment on the eccentricity of the C force.

3.10.3 Characteristic Response of RC, PC, and PPC in Bending in the Elastic Range of Behavior

Typically a reinforced concrete beam is cracked under the effect of dead load, a fully prestressed concrete beam is uncracked under the effect of full service load (dead load plus live load), and a partially prestressed beam can have any behavior in between.

Usually a partially prestressed beam is designed to be uncracked under dead load and cracked under full service load. In all three cases linear elastic behavior is assumed up to at least full service load. Figure 3.5 provides a schematic

representation of typical stress or strain diagrams (assumed linear) along the section of either a reinforced, or a prestressed, or a partially prestressed concrete beam, under service loads. The behavior is significantly different in the three cases. It can be observed, for instance, that the neutral axis of bending of the cracked section in a reinforced concrete beam also corresponds to the zero stress point, and is independent of the applied moment. Thus an applied moment causes an increase in the resulting forces of the couple acting on the section ($C = T$) but the lever arm of the couple remains constant (Fig. 3.5*a*).

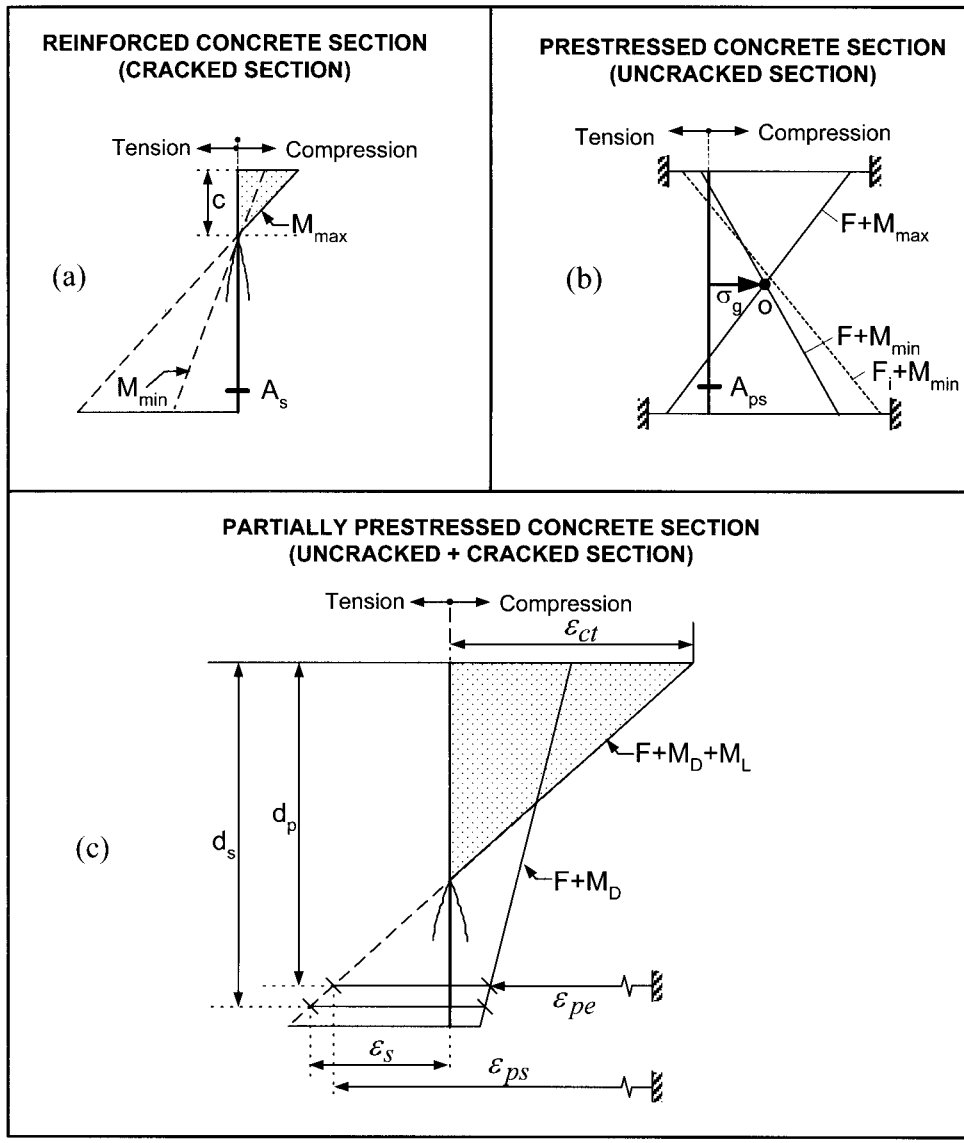

Figure 3.5 Comparison of bending response of RC, PC, and PPC sections in service.

In fully prestressed concrete (Fig. 3.5*b*), the section is uncracked and the neutral axis of bending is the centroidal axis of the uncracked section. The force resultant, C, of compressive stresses in the section is equal to F. An external moment causes no change in the force resultant in the concrete, that is, $C = F$; however, unlike in reinforced concrete, it causes a shift in the line of action of C, which deviates from the line of action of F, leading to an increase in the lever arm between them. In a partially prestressed beam (Fig. 3.5c), the zero stress point moves up or down depending on the magnitude of applied moment (below or above the cracking or decompression moment) and the neutral axis of bending is different for the cracked or uncracked section. Both the forces and the lever arm between them may vary simultaneously when an external moment is applied.

3.10.4 Curvature Computation

It is often necessary to determine the curvature of a concrete section under load. A key to curvature computation is the assumption that the strain distribution in a section under bending is linear even if the stress is not. Thus computing the curvature will be the same whether the section is cracked or uncracked, or whether the section is in the linear range of behavior or at ultimate. Figure 3.6 shows typical strain diagrams for an uncracked section, such as prestressed concrete, or a cracked section, such as reinforced concrete.

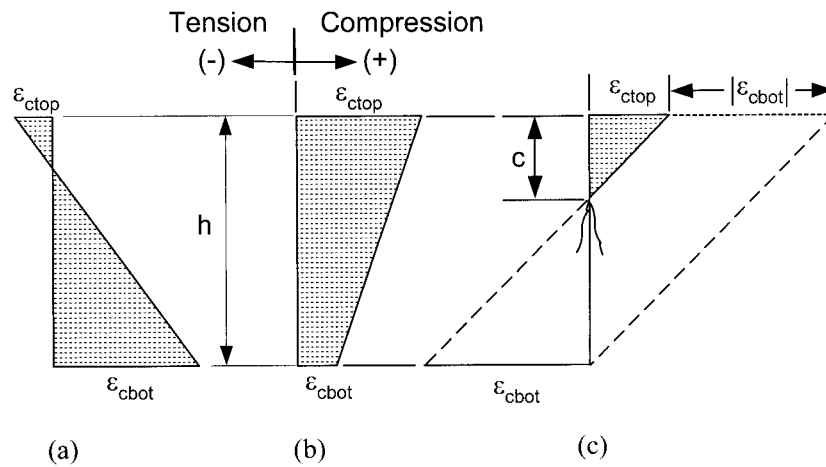

Figure 3.6 Definition of curvature. (a) Negative curvature of uncracked section. (b) Positive curvature of uncracked section. (c) Positive curvature of cracked section.

The curvature can be computed from either of the following expressions:

$$\varphi = \frac{\varepsilon_{ctop} - \varepsilon_{cbot}}{h} \tag{3.14}$$

or

$$\varphi = \frac{\varepsilon_{ctop}}{c} \tag{3.15}$$

where ε_{ctop} is the strain in the top fiber, ε_{cbot} is the strain in the bottom fiber, h is the depth of the section, and c is the depth of the neutral axis in a cracked section. Compressive strain is considered positive and tensile strain is considered negative. A positive value of curvature leads to a downward deflection in a beam while a negative value leads to an upward camber. Note that Eq.(3.14) may be more convenient for a prestressed concrete section, since stresses can be readily computed and strains are related to stresses by the Hooke's law, that is: $\sigma = E\varepsilon$. Equation (3.15) is more convenient for a cracked section such as reinforced concrete under either service or ultimate loads, or for prestressed concrete at ultimate. Note that the two expressions are essentially the same. Indeed if a line parallel to the strain diagram is plotted in Fig. 3.6*c* starting at the bottom fiber, it will lead to a strain on the top equal in magnitude to $\varepsilon_{ctop} + |\varepsilon_{cbot}|$. In such a diagram the value of h is the same as c in Fig. 3.6*b* and Eq. (3.15) applies.

The above expressions of curvatures are derived from the following fundamental relationship of mechanics:

$$\varphi = \frac{M}{EI} \tag{3.16}$$

However the flexural stress induced by a moment, M, is given by:

$$\sigma = \frac{Mc}{I} \tag{3.17}$$

Replacing M from Eq. (3.17) into Eq. (3.16) leads to:

$$\varphi = \frac{I\sigma}{EIc} = \frac{IE\varepsilon}{EIc} = \frac{\varepsilon}{c} \tag{3.18}$$

which is essentially the same equation as Eq. (3.15). Note that M should include the moment due to prestressing, if any.

3.10.5 Load Balancing Feature of Prestressing

The magnitude and profile of a prestressing tendon can be designed to balance external loading and lead to a member that is uniformly stressed. Load-balancing is intuitive and can be very convenient. Figure 3.7 shows three typical profiles of prestressing tendons designed to balance an external load. A uniform load, such as

dead load, generates an external moment with a parabolic moment diagram; the effect of such a moment can be balanced by a prestressing force with a parabolic tendon profile that generates a prestressing moment equal and opposite to the external moment.

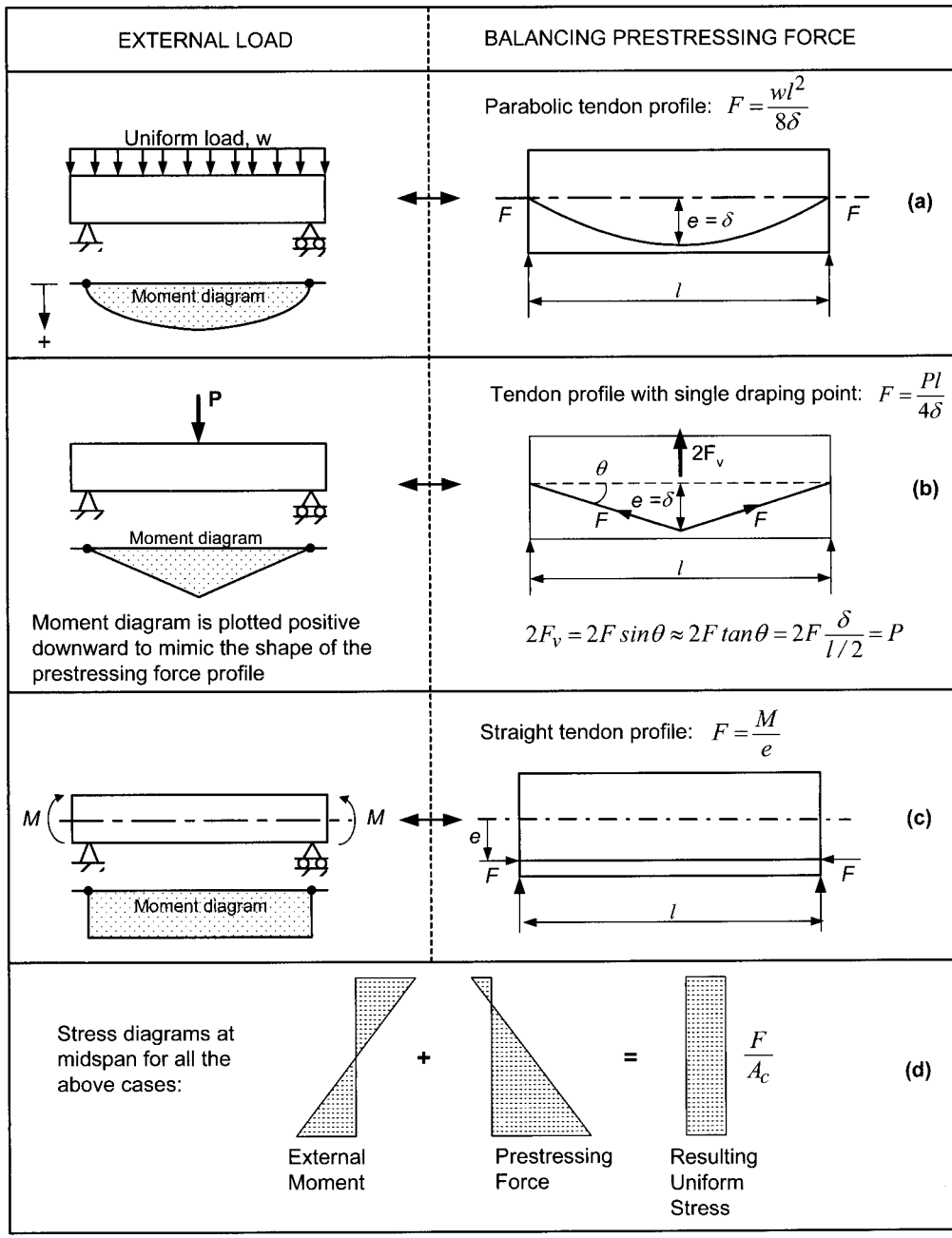

Figure 3.7 Typical examples of load balancing by prestressing.

Similarly, if the external load is a concentrated load at midspan, the prestressing tendon profile can be made of a broken line with a single draping point at midspan. If an external moment is applied at the support sections, it can be balanced by a straight tendon. In each example, the magnitude and eccentricity of the balancing prestressing force is as shown in Fig. 3.7.

Note that the eccentricity of the prestressing force at midspan is generally taken as large as practically feasible to reduce the magnitude of the prestressing force, and thus the cost. However, an infinite set of values of F and e can provide a solution, provided the resulting uniform compressive stress on the concrete section is acceptable. The combined effect of the external load and prestressing at any section leads to a uniform state of stress of magnitude F/A_c. This is illustrated in Fig. 3.7 (bottom figure) for the midspan section of the three examples considered. The designer can take advantage of load balancing by developing a composite with a uniform state of compressive stress throughout its length for a certain level of loading (such as dead load and prestressing). The effect of additional loads on a uniformly stressed member can be easily evaluated. Although very simple to understand and implement, load balancing can be advantageous in many complex design situations such as described in Chapter 10 for beams and frames, and Chapter 11 for slabs. Note finally that in each of the examples of Fig. 3.7, the profile of the prestressing tendon is similar in shape to that of the moment diagram plotted positive downward; should the diagram be plotted positive upward, the profile of the prestressing tendon will be opposite to that of the moment. This observation can be beneficially used to balance the external moment in design.

3.11 ACI CODE VIEWPOINT RELATED TO PRESTRESSED AND PARTIALLY PRESTRESSED CONCRETE

The 2002 edition of the ACI code attempts to provide a smooth transition from fully prestressed concrete to fully reinforced concrete, as well as a seamless transition from bending members to compression members. The two main items of concern in this text are discussed next.

3.11.1 Class Definition and Related Serviceability Design Requirements

Prestressed concrete flexural members are classified as Class U, Class T and Class C based on the computed extreme fiber stress, σ_{ts}, at service loads in the precompressed tensile zone, as follows:

- Class U: $|\sigma_{ts}| \le 7.5\sqrt{f'_c}$ in psi or $|\sigma_{ts}| \le 0.7\sqrt{f'_c}$ in MPa
- Class T: $7.5\sqrt{f'_c} \le |\sigma_{ts}| \le 12\sqrt{f'_c}$ in psi or $0.7\sqrt{f'_c} \le |\sigma_{ts}| \le \sqrt{f'_c}$ in MPa
- Class C: $|\sigma_{ts}| > 12\sqrt{f'_c}$ in psi or $|\sigma_{ts}| > \sqrt{f'_c}$ in MPa

in which U stands for uncracked, C for cracked, and T for transition between uncracked and cracked.

Table 3. 11 ACI 318-2002 serviceability design requirements and related code sections.

	Prestressed			Nonprestressed
	Class U	**Class T**	**Class C**	
Assumed behavior	Uncracked	Transition between uncracked and cracked	Cracked	Cracked
Section properties for stress calculation at service loads	Gross section 18.3.4	Gross section 18.3.4	Cracked section 18.3.4	No requirement
Allowable stress at transfer	18.4.1	18.4.1	18.4.1	No requirement
Allowable compressive stress based on uncracked section properties	18.4.1	18.4.2	No requirement	No requirement
Tensile stress at service load 18.3.3 (Absolute value)	$\le 7.5\sqrt{f'_c}$ psi $\le 0.7\sqrt{f'_c}$ MPa	$7.5\sqrt{f'_c} < f_t \le 12\sqrt{f'_c}$ $0.7\sqrt{f'_c} < f_t \le \sqrt{f'_c}$	No requirement	No requirement
Deflection calculation basis	9.5.4.1 Gross section	9.5.4.2 Cracked section, bilinear	9.5.4.2 Cracked section	9.5.2, 9.5.3 Effective moment of inertia
Crack control	No requirement	No requirement	10.6.4 Modified for strand	10.6.4
Computation of Δf_{ps} or f_s for crack control	Not applicable	Assumed uncracked	Cracked section analysis	$\frac{M}{A_s \times lever\ arm}$ or $0.6 f_y$
Side skin reinforcement	No requirement	No requirement	10.6.7	10.6.7

Table 3.11 summarizes the intent of the code. It can be observed that linear elastic behavior is assumed whether the section is cracked or not and that the main difference between Class U and Class T is that in Class T the stresses are computed as if the section is uncracked, while in reality the section is likely to be cracked. Indeed the tensile stress limit for Class T is higher than the modulus of rupture of concrete and thus is truly fictitious. In Class C a cracked section analysis is to be carried out. While the recommendation of the code implies that a cracked section

analysis may not be necessary for Class T sections, the author believes that a cracked section analysis may be necessary, depending on the conditions of the structure. For instance, an inverted T beam subjected to loads leading to a Class T member is likely to violate some serviceability limit states related to crack width and fatigue, and should therefore be analyzed as a cracked section.

In this book, mostly fully prestressed concrete (Class U) is considered for which uncracked sections are the norm. However, partially prestressed concrete beams are treated in Ref. [1.48] where details for a cracked section analysis are covered. Table 3.11 contains some other serviceability recommendations given in the code, such as whether to use the gross section or the cracked section to compute deflections; they are self-explanatory and will not be expanded upon here. The reader is referred to the code for additional details.

3.11.2 Tension Controlled and Compression Controlled Sections

The ACI code specifies a capacity reduction factor, ϕ = 0.9, for beams (in pure bending) larger than that for columns (ϕ = 0.70 or 0.65) in which primarily axial compression exists (see Section 3.9.2). However most columns are also subjected to some bending, and the code suggests a transition from compression to bending when the axial compression is smaller than ten percent of the nominal resistance of the column in compression, i.e., $0.10f'_cA_g$. This transition is achieved by evaluating the net tensile strain in the extreme layer of reinforcement closest to the tensile fiber.

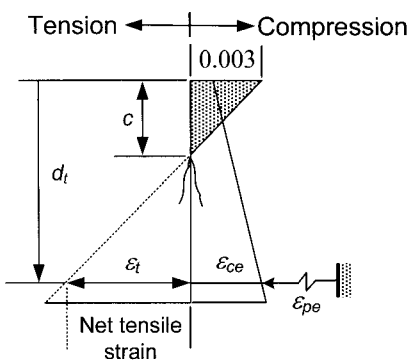

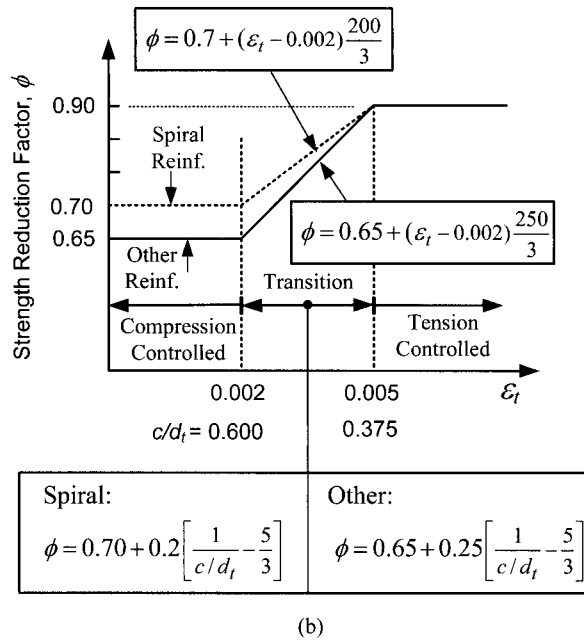

Figure 3.8 Definition of net tensile strain for a prestressed concrete beam and corresponding ϕ factor according to the 2002 ACI code.

The net tensile strain is defined as the tensile strain in the extreme tension steel at nominal strength, exclusive of strains due to prestress, creep, shrinkage and temperature (Fig. 3.8a). When the net tensile strain in the extreme tension steel is equal to or greater than 0.005, the section is defined as tension-controlled. In that case the ϕ factor is taken as 0.9, according to Table 3.10.

For Grade 60 reinforcement and for all prestressed concrete reinforcement, a section is assumed to be compression-controlled when the net tensile strain in the extreme tension steel is equal to or less than 0.002. In that case the ϕ factor is taken as 0.70 or 0.65 depending on whether the compression member is spirally reinforced or not. For sections in which the net tensile strain in the extreme tension steel at nominal strength is between the limits for compression-controlled and tension-controlled sections, ϕ shall be permitted to be linearly increased from that of compression controlled sections to 0.90, since the net tensile strain in the extreme tension steel at nominal strength increases from the compression-controlled strain limit to 0.005 (Fig. 3.8b). Equivalently, a similar approach is used in compression members when the axial compression decreases from $\phi P_n = 0.10 f'_c A_g$ to zero where pure bending occurs.

Assuming the ϕ factors defined by ACI in Table 3.10 are used, linear equations can be derived to determine the ϕ factors in the transition region. They are given in Fig. 3.7b in terms of the net tensile strain; however, they can also be expressed, as also shown, in terms of the ratio c/d_t (which is proportional to the net tensile strain) where c represents the depth of neutral axis at ultimate and d_t represents the distance from the extreme compression fiber of concrete to the extreme tension layer of reinforcement; so, if there are two layers of prestressing tendons, d_t is taken to the layer closest to the surface.

To allow moment redistribution of negative moment (see Sections 5.21 and 10.14.3) a net tensile strain limit of at least 0.0075 is recommended by the code.

A discussion on the interpretation of the above provisions and their use as amended in this text is given in Section 5.5.3.

3.12 DETAILS OF REINFORCEMENT

The designer should be able to see the whole and the detail. Although this text is not intended to cover detailing procedures, a minimum number of details is necessary in the early stages of design. Once the required amount of reinforcement is determined, it is the designer's responsibility to make certain that such reinforcement can be properly placed inside the concrete section. Information related to spacing of the tendons and the minimum protection or clear concrete cover of the reinforcement is needed.

Section 7.6 of the ACI code prescribes a clear distance between pretensioning tendons at each end of a member not less than four times the diameter for wires and three times the diameter for strands. Closer vertical spacing and bundling of strands

may be permitted in the middle portion of a span. Another requirement can be derived from Sec. 3.3.3 of the code where it is stated that the clear spacing between individual reinforcing bars, wires, bundles of bars, prestressing tendons, and ducts shall not be less than one-and-one-third times the maximum size of the coarse aggregate used in the concrete.

Table 3.12 Concrete protection of reinforcement in prestressed concrete.
(Adapted from ACI 318-02 Code, Ref. 3.4)

Conditions of application	Clear concrete cover (ACI Section 7.7.3)	
	in	mm*
The following minimum concrete cover shall be provided for prestressed and non-prestressed reinforcement, ducts, and end fittings except as provided in 7.7.5.1:		
(a) Concrete exposed to earth or weather:		
• Wall panels:		
No. 14 and No. 18 bars, prestressing tendons larger than 1 ½ in. (38 mm) diameter	1-1/2	38
No. 11 bar and smaller, prestressing tendons 1 ½ in (38 mm) diameter and smaller, W31 and D31 wire and smaller	3/4	19
• Other members:		
No. 14 and No. 18 bars, prestressing tendons larger than 1 ½ in (38 mm)diameter	2	50
No. 6 through No. 11 bars, prestressing tendons larger than 5/8 in diameter through 1 ½ in. (38 mm) diameter	1-1/2	38
No. 5 bar and smaller, prestressing tendons 5/8 in. (16 mm) diameter and smaller, W31 and D31 wire, and smaller	1-1/4	32
(b) Concrete not exposed to weather or in contact with ground:		
• Slabs, wall, joists:		
No. 14 and No. 18 bars, prestressing tendons larger than 1 ½ in (38 mm) diameter	1-1/4	32
Prestressing tendons 1 ½ in (38 mm) diameter and smaller	3/4	19
No. 11 bar and smaller, W31 or D31 wire and smaller	5/8	16
• Beams, columns:		
Primary reinforcement: d_b but not less than 5/8 (16 mm) and need not exceed 1 ½ in (38 mm)	d_b	d_b
Ties, stirrups, spirals	3/8	10
• Shells, folded plates members:		
Prestressing tendons	3/4	19
No. 6 bar and larger	5/8	16
No. 5 bar and smaller, W31 or D31 wire, and smaller	3/8	10

Posttensioning ducts may be bundled if it is shown that concrete can be satisfactorily placed and if provision is made to prevent the tendons from breaking through their ducts, when tensioned. Special precautions must be taken with

posttensioned tendons at the ends of a member where the anchors are placed. In general, additional stirrups are recommended near the ends of the member (with or without end blocks) and confining reinforcements in the form of spirals or grids are placed in the concrete directly behind the anchors.

A conservative rule of thumb (or heuristic rule) is to place the end anchors in such a way that the average stress in the concrete directly behind the anchor plate is less than $0.80f'_{ci}$ (up to f'_{ci} is often acceptable in confined concrete). A more representative approach can be found in Section 4.17.

Prestressing tendons must be placed inside a concrete section so as to have sufficient protection. A summary of the ACI (2002) code provisions for the minimum clear concrete cover of the reinforcement in prestressed concrete is given in Table 3.12. Note that the values are significantly smaller than those prescribed in previous editions of the code. Engineering judgment should always be exercised for any particular conditions.

It has been this author's experience that in dealing with prestressed pretensioned beams where tendons of not more than 0.6 in (15 mm) diameter are used, a cover of 2 inches (50 mm) to the centroid of the tendon and a center-to-center spacing of 2 inches (50 mm) between tendons commonly lead to a feasible and reasonable design (Fig. 3.9). Note that a center-to-center spacing of two inches (50 mm) leaves a clear spacing of about 1 ½ in (38 mm), often just sufficient to allow the internal vibration of the concrete during casting.

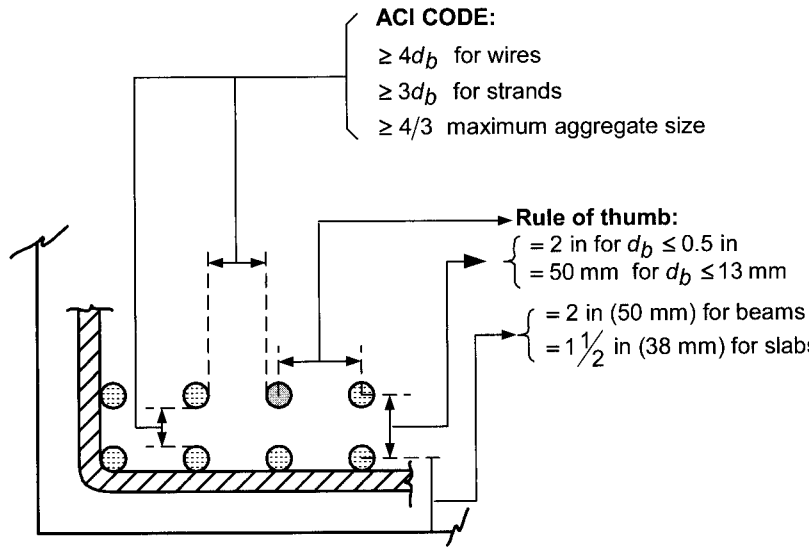

Figure 3.9 Practical detailing guidelines.

When posttensioning cables made of several tendons are used, it is desirable to leave a clear spacing larger than 2 in (50 mm). The prescribed amount should

depend on the capacity of the cable. Figure 3.9 summarizes information related to spacing that would satisfy the ACI code as well as a number of other codes, while very practical to remember; it forms a grid of 2 in (50 mm) spacing in each direction.

3.13 PRESTRESS LOSSES IN PRELIMINARY DESIGN

As pointed out in Chapter 2, substantial losses of stress occur in the prestressing steel due to relaxation of the steel and creep and shrinkage of the concrete. Other losses also take place, due to elastic shortening of the concrete at load transfer and due to friction between the tendons and the concrete. Several methods exist to estimate the total loss of prestress and may require different levels of difficulty. A basic and detailed treatment of prestress losses is given in Chapter 8. However, it is important to estimate some prestress losses, in advance, in routine situations, in order to proceed with the design. Their values may later be revised if necessary.

Lump sum estimates of individual losses are given in many technical documents (see References of Chap. 8). Lump sum values of total losses were suggested by the ACI-ASCE Joint Committee on Prestressed Concrete [Ref. 3.6]. They were recommended in previous editions of the ACI code and its commentary; however, they were later found to be unconservative.

The AASHTO Standard specifications [Ref. 3.1] suggest lump sum loss values for bridges where average standard conditions prevail, while the AASHTO LRFD specification provides more detailed estimates depending on the compressive strength of concrete, the partial prestressing ratio and the shape of the section.

In preliminary design, there is need to estimate some of the losses that occur after transfer of the stress from the prestressing steel to the concrete. Let us define by f_{pi} the initial stress in the prestressing steel at time of load transfer and by f_{pe} the effective stress remaining after all losses have taken place. The corresponding prestressing forces are defined as F_i and F. F_i is the force that the concrete experiences under initial loading. Thus f_{pi} may mean the stress just after transfer for a pretensioned member and just before transfer for a posttensioned member (see Eqs. 8.5 and 8.8). However, in preliminary design, f_{pi} is considered here to be the stress just after transfer for all cases. The difference between f_{pi} and f_{pe} essentially represents the time-dependent prestress losses after transfer. Thus, it does not include elastic shortening or initial relaxation for a pretensioned member, or frictional loss and anchorage set loss for a posttensioned member. In Table 3.13 the author provides for preliminary design a rough estimate of time-dependent losses after transfer, that is, the difference between f_{pi} and f_{pe}. Additional information can be obtained from reviewing Chapter 8. Note that in the preliminary design and dimensioning of the structure the above difference between f_{pi} and f_{pe} is not as useful as their ratio. Let us define:

$$\eta = \frac{f_{pe}}{f_{pi}} = \frac{F}{F_i} \tag{3.19}$$

$$f_{pe} = \eta f_{pi} = f_{pi} - (Prestress\ losses\ after\ transfer) \tag{3.20}$$

where F_i is the initial and $F = \eta F_i$ the final or effective prestressing force. Equation (3.19) can also be written as:

$$\eta = \frac{f_{pi} - (Prestress\ losses\ after\ tranfer)}{f_{pi}} \tag{3.21}$$

Since the stress in the steel generally varies along the length of the member, the coefficient η will also vary. However, η is needed mostly at the critical section of a simply supported beam or at a limited number of critical sections of a continuous beam. For all practical purposes it could be assumed to be the same for all critical sections. As a first approximation in design the value of η can be taken between 0.75 and 0.85. Indeed, assuming a 270 ksi (1860 MPa) stress-relieved strand with an initial stress $f_{pi} = 0.70f_{pu}$, and using the estimate given in Table 3.13 for normal weight concrete, leads to $\eta = 0.79$. For a low relaxation strand with $f_{pi} = 0.74f_{pu}$, η will be 0.825. Assuming a value of $f_{pi} = 0.70f_{pu}$, the corresponding value of the effective prestress, f_{pe}, will be somewhere between $0.55f_{pu}$ and $0.58f_{pu}$ for normal weight concrete. Such approximations will frequently be used in preliminary designs. However, a more exact assessment of prestress losses is recommended for final designs.

Table 3.13 Suggested lump sum estimates of time-dependent prestress losses after transfer of prestress for routine design (not including friction and anchorage set effects).

	$(f_{pi} - f_{pe})^*$			
	Stress relieved strand		Low relaxation strand	
	ksi	MPa	ksi	MPa
Pretensioned members:				
• Normal weight concrete	40	276	35	242
• Structural lightweight concrete	45	310	40	276
Posttensioned members:				
• Normal weight concrete	35	242	30	207
• Structural lightweight concrete	40	276	35	242

* Assuming $f_{pi} \leq 0.82 f_{py}$

Note that for a given section design, under-estimating prestress losses affects serviceability and allowable stress criteria, but has little effect on the ultimate resistance of the member.

3.14 CONCLUDING REMARKS

The limit state design philosophy covered in this chapter is not likely to change in the foreseeable future. Similarly, the key features of prestressed concrete and its characteristics in comparison to reinforced concrete will not change. However, additional research, experience, and knowledge will likely lead to changes in load and resistance factors, allowable stresses, code specifications, and construction details. In design, engineering judgment should always be exercised even in dealing with simple problems. Moreover, having a clear understanding of the fundamentals will help in handling any difficult situation, especially if not addressed by available codes of practice.

REFERENCES

3.1. American Association of State Highway and Transportation Officials, "*Standard Specifications for Highway Bridges*," 16th ed., AASHTO, Washington, DC, 1996.

3.2. American Association of State Highway and Transportation Officials, "*AASHTO LRFD Bridge Design Specifications*," AASHTO, Washington, DC, 1998.

3.3. ACI Committee 318, "*Building Code Requirements for Reinforced Concrete and Commentary*," ACI 318-95, American Concrete Institute, Farmington Hills, 1995.

3.4. ACI Committee 318, "*Building Code Requirements for Reinforced Concrete and Commentary*," ACI 318-02, American Concrete Institute, Farmington Hills, 2002.

3.5. ACI Committee 343, "Analysis and Design of Reinforced Concrete Bridge Structures," Report by ACI Committee 343, ACI 343R-77, American Concrete Institute, Detroit, 1977.

3.6. ACI- ASCE Joint Committee 423, "Tentative Recommendations for Prestressed Concrete," Reported by formerly ACI-323, *Journal of the American Concrete Institute*, 54(7), 1958, pp. 548-578.

3.7. American Institute of Steel Construction (AISC), *Manual of Steel Construction*, 9th ed., American Institute of Steel Construction, Chicago, 1989.

3.8. American Institute of Steel Construction (AISC), *Load and Resistance Factor Design, 3rd Ed,* American Institute of Steel Construction, Chicago, 2001.

3.9. American National Standard Institute, *Building Code Requirements for Minimum Design Loads in Buildings and Other Structures,* ANSI 58.1, New York, 1992.

3.10. American Railway Engineering Association (AREA), *Manual of Railway Engineering*, Washington, DC, 1973.

3.11. American Railway Engineering Association (AREA), *Specifications for Steel Railway Bridges*, Chicago, 1992.

3.12. American Society of Civil Engineers, *"Minimum Design Loads for Buildings and Other Structures – Code and Commentary*," ANSI/ASCE Standard 7-95, ASCE New York, 1996.

3.13. Ang, A. H. S., and W. H. Tang, "*Probability Concepts in Engineering Planning and Design: Volume 1. Basic Principles*." New York: Wiley, 1975.

3.14. Ang, A. H. S., and W. H. Tang, "*Probability Concepts in Engineering Planning and Design: Vol. 2. Decision, Risk and Reliability*." New York: Wiley, 1984.

3.15. British Standards Institution, *British Standard Code of Practice for the Use of Structural Concrete*, CP-110, London, 1972.
3.16. Comité Euro-International du Béton, *CEB-FIP Model Code for Concrete Structures*, 3rd ed., Paris, 1990.
3.17. Ellingwood, B., T. V. Galambos, J. G. MacGregor, and C. A. Cornell, " Probability Based Load Criteria: Load Factors and Load Combinations," *Journal of Structural Division*, ASCE, 108(ST5): 978-97, 1982.
3.18. Ellingwood, B., T. V. Galambos, J. G. MacGregor, and C. A. Cornell, "Development of a Probability Based Load Criterion for American National Standard A58," *NBS Special Publication* 577, Washington, DC: National Bureau of Standards, 1980.
3.19. Hill, P. H., *The Science of Engineering Design*. New York: Holt, Reinhart and Winston, Inc., 1975.
3.20. MacGregor, J. G., "Safety and Limit States Design for Reinforced Concrete," *Canadian Journal of Civil Engineering*, 3(4), 1976.
3.21. MacGregor, J. G., *Design, Reinforced Concrete: Mechanics and Design*, 3rd ed. Upper Saddle River, NJ: Prentice Hall, 1997, 939 pp.
3.22. Nowak, A. S., and K. R. Collins, "*Reliability of Structures*," Boston: McGraw Hill, 2000, 338 pp.
3.23. Naaman, A. E., and A. Siriaksorn, "Reliability of Partially Prestressed Beams at Serviceability Limit States," *Journal of the Prestressed Concrete Institute*, 27(6): 66-85. 1982. Also, Report No. 80-1, University of Illinois, Chicago, Department of Materials Engineering, June 1980, 126 pp.
3.24. Naaman, A. E., and A. M. Hamza, "Prestress Losses in Partially Prestressed High Strength Concrete Beams," *Journal of the Prestressed Concrete Institute* PCI Journal, 38(3): 98-114, 1993.
3.25. Winter, G., "Safety and Serviceability Provisions in the ACI Building Code," *ACI Special Publication*, SP-59, 1979.
3.26. White, R. N., P. Gergely, and R. G. Sexsmith, *Structural Engineering, Vol. 1: Introduction to Design Concepts and Analysis*. New York: John Wiley & Sons, 1972.

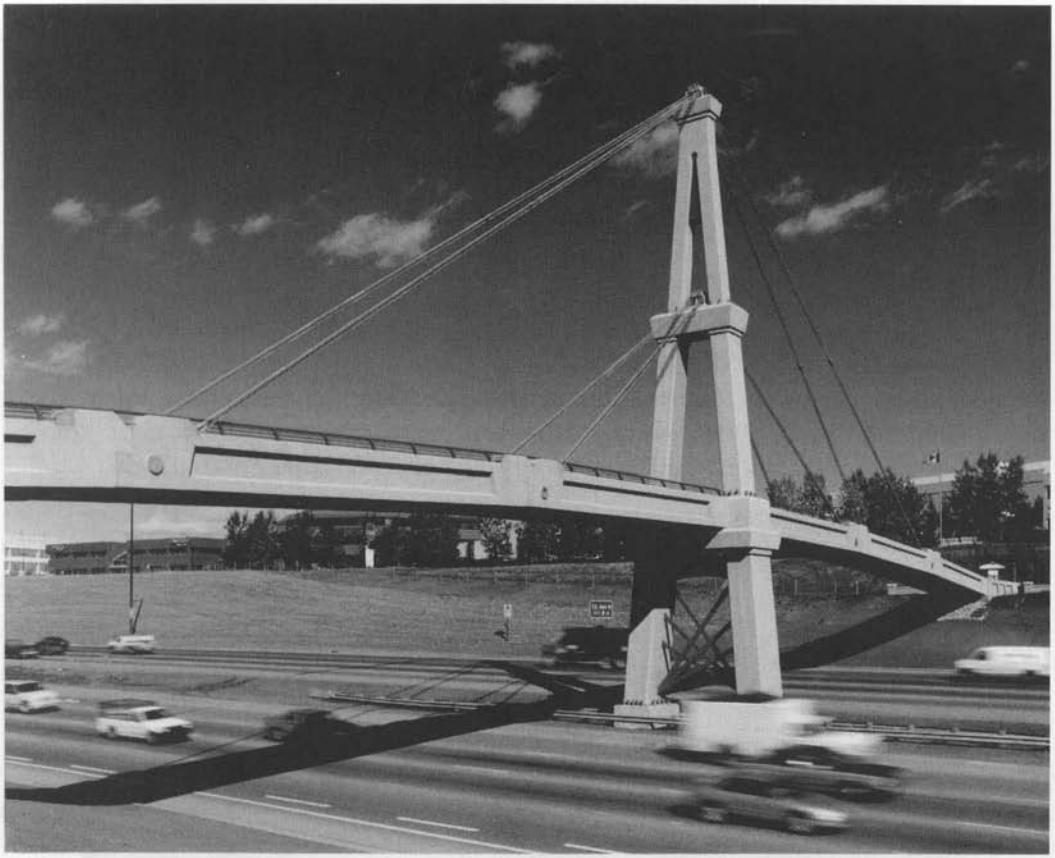

Fox Hollow Pedestrian Bridge, Calgary, Canada. This two-span, 90 m (295 ft), symmetrical cable stayed bridge used precast prestressed components for both the deck and the tower A-frame. *(Courtesy Precast/Prestressed Concrete Institute.)*

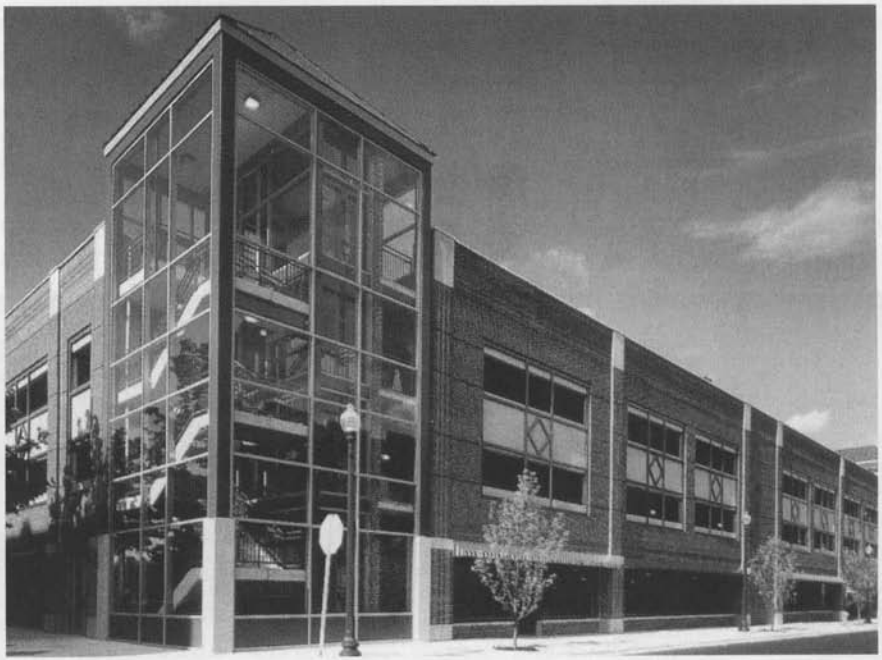

Arcadia parking structure illustrates the flexibility and aesthetics achievable using precast prestressed concrete elements. (*Courtesy Carl Walker Inc.).*

Erection of precast prestressed concrete elements for a parking structure. (*Courtesy Carl Walker Inc.).*

FLEXURE: WORKING STRESS ANALYSIS AND DESIGN

This chapter aims at providing answers to the following questions:

Q1: What is meant by analysis versus design?

Q2: In how many ways can the analysis of a prestressed concrete member be approached?

Q3: How to determine extreme stresses in a prestressed concrete section?

Q4: How to compute the necessary prestressing force, F, and its eccentricity, e_o, at the critical section of a given beam?

Q5: Can an optimum design, that is, a minimum prestressing force at a maximum eccentricity, be achieved? Is the maximum eccentricity practical and feasible?

Q6: If a concrete beam section is not given, how is a suitable section determined? How to select the most suitable section from a given set of beams?

Q7: Given the necessary prestressing force at the critical section of a beam, how to place the tendons along the span or at any other section? How to detail the reinforcement at the critical section in span, and at the support section? How to select the location of draping points?

Q8: How to determine the cracking moment of the section?

Q9: What precautions must be taken to design the end blocks of a beam?

4.1 ANALYSIS VERSUS DESIGN

Two categories of problems can generally be identified in dealing with prestressed beams: the first is called *analysis* or *investigation* and the second is described as *design*. While all unknowns are assumed given in analysis, a number of unknowns must be determined in design (Fig. 4.1).

The analysis or investigation process can be defined as follows: Given problem description and beam characteristics (such as loadings, span, cross-sectional dimensions, materials properties of steel and concrete, etc.) check if specified design criteria are satisfied at every section along the member.

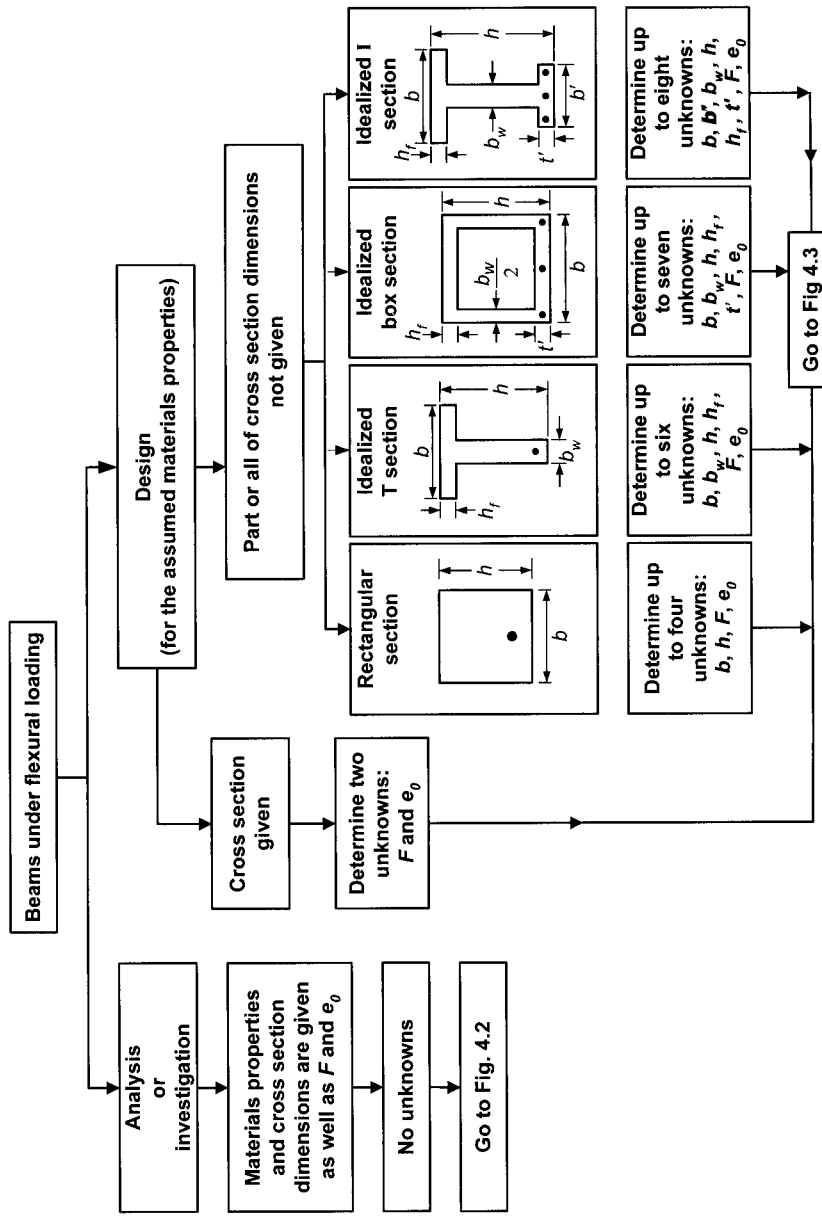

Figure 4.1 Levels of difficulty encountered in the flexural design of beams.

Design criteria involve many facets, such as flexure, shear, cracking, camber, and deflections (Fig. 4.2), but are limited in this chapter to flexural stresses under service conditions as specified by available codes of practice. It is important, however, to view the overall problem before getting into the details of every step.

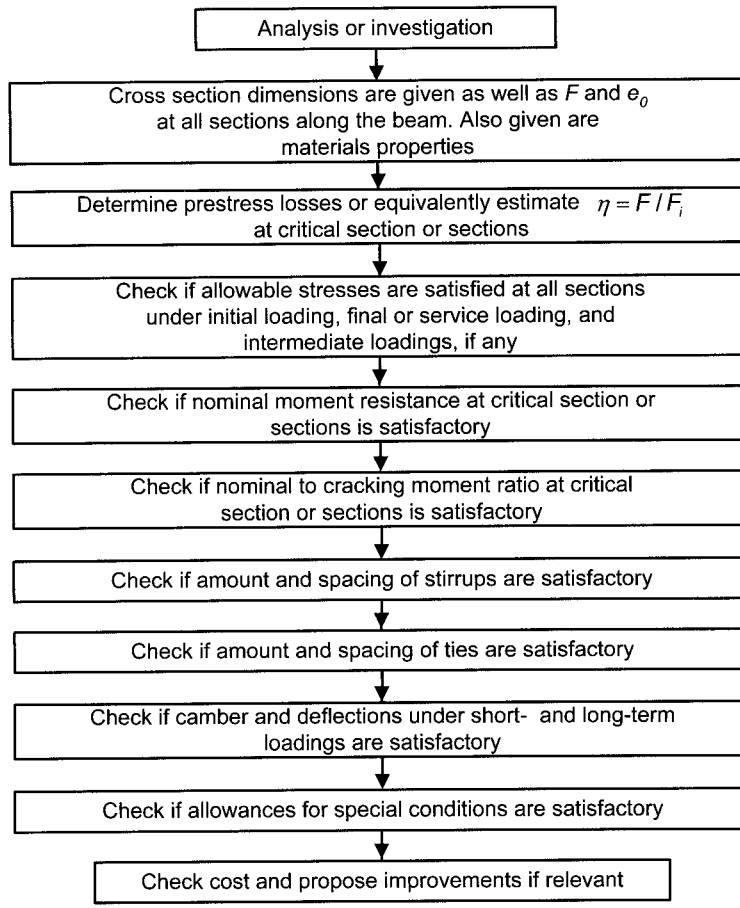

Figure 4.2 Major steps to be undertaken in the analysis or investigation of beams.

Similarly to the analysis process, the design process in its entirety requires also many steps (Fig. 4.3). In flexure, design usually implies the determination of some unknowns to satisfy specified allowable stresses under working load conditions. The complexity of the design increases with the number of unknowns involved, thus covering a whole range of specific problems (Fig. 4.1). For example, a design problem may imply the determination of the shape of the beam cross-section, its dimensions as well as the prestressing force and its eccentricity. If a rectangular shaped beam is desired, only four unknowns will have to be determined namely b, h, F, and e_O. The number of unknowns is reduced to three for a slab and can be equal to eight for an ideal I beam (Fig. 4.1). If a beam cross section is selected a priori, say

from a set of standard shapes, then only two unknowns are left, namely the prestressing force F and its eccentricity e_o. Note that knowing the value of F is equivalent to knowing the required area of prestressing steel.

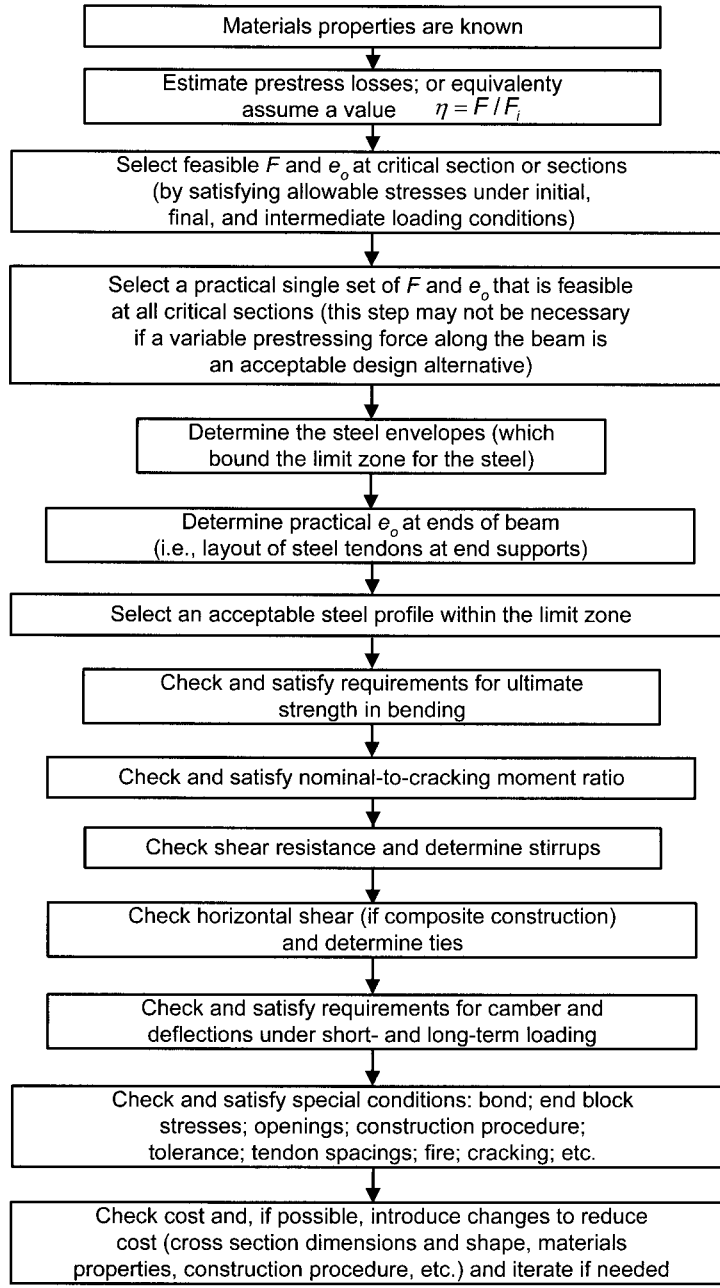

Figure 4.3 Major design steps after a beam cross section is selected.

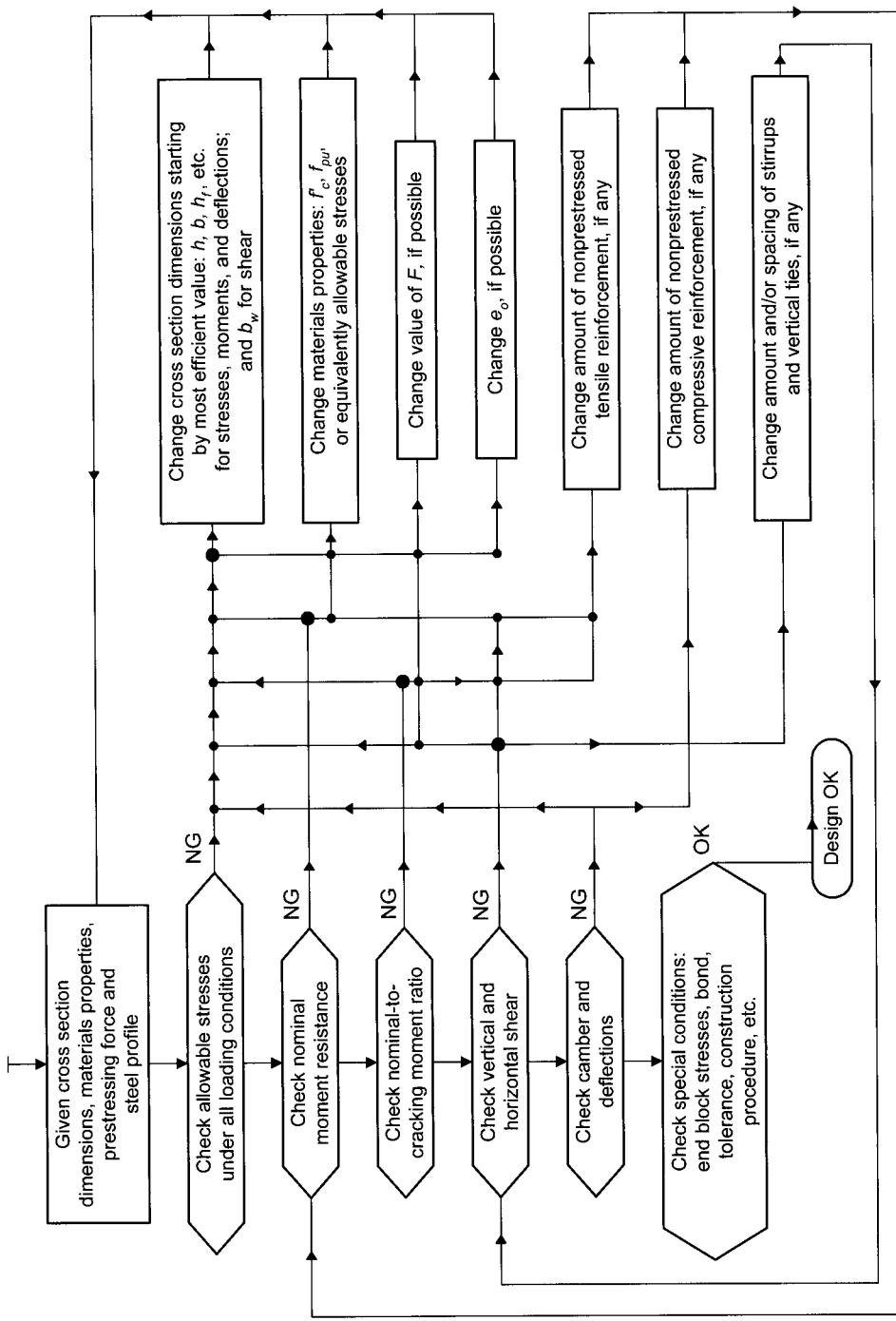

Figure 4.4 Iterative steps and possible remedies in the flexural design process.

It is important to realize that the design process described in Figs. 4.1 and 4.3 involves generally a repetitive procedure within each step and between steps in order to obtain a satisfactory and close-to-optimum solution. Often the designer has to assume a practical value for some of the unknowns in order to start the first cycle (see, for example, Sec. 14.17 on preliminary design of bridges). For instance, in selecting the size of a rectangular beam, the designer may assume a depth equal to four percent of the span and a width equal to half the depth. Once a satisfactory cross section has been arrived at, the problem is reduced to finding the values of F and e_o, and becomes substantially simpler.

Figure 4.4 is provided here in combination with Figs. 4.1 to 4.3 in order to allow the reader to view possible actions that might be taken in an iterative procedure not only for flexure but also for other aspects of the design, such as shear, and deflections. The above described first four figures also put in perspective the content of other chapters in relation to this one.

4.2 CONCEPTS OF PRESTRESSING

Three different concepts may be applied to analyze the behavior of prestressed concrete members (Fig. 4.5). The first concept treats prestressed concrete essentially as an elastic composite material with no specific consideration of the two major components, steel and concrete (Fig. 4.5*a*). For example, a prestressed concrete tie in which the uniform final prestress is 1000 psi (6.9 MPa) may be considered as an elastic material that can sustain tensile stresses of up to 1000 psi (6.9 MPa) without risk of cracking (whether these stresses are due to a tensile load or to a bending moment). It is the same as stating that a glass rod can sustain a tension of 10,000 psi (69 MPa) before failing or that a steel rod can sustain 60,000 psi (414 MPa) before yielding. This concept may be advantageous when tensile stresses in the concrete component are not allowed and for simple problems.

The second concept treats prestressed concrete in a way similar to reinforced concrete, where, in analyzing the section, the concrete component is seen to carry the compressive force while the steel component carries the tensile force (Fig. 4.5*b*). Thus the two components, steel and concrete, can be considered separately or in combination as free bodies in equilibrium under the effects of external forces and reactions. There is, however, a fundamental difference in behavior between a reinforced concrete section and a prestressed concrete section.

A reinforced concrete section is assumed to crack under flexural loading. The resulting compressive force in the uncracked portion of the concrete section and the tensile force in the steel are equal in magnitude and form an internal couple which resists the applied external moment. If, in the elastic range of behavior, the bending moment applied to the section increases, the forces of the couple increase while the distance between them remains constant (assuming the centroid of the steel remains the same).

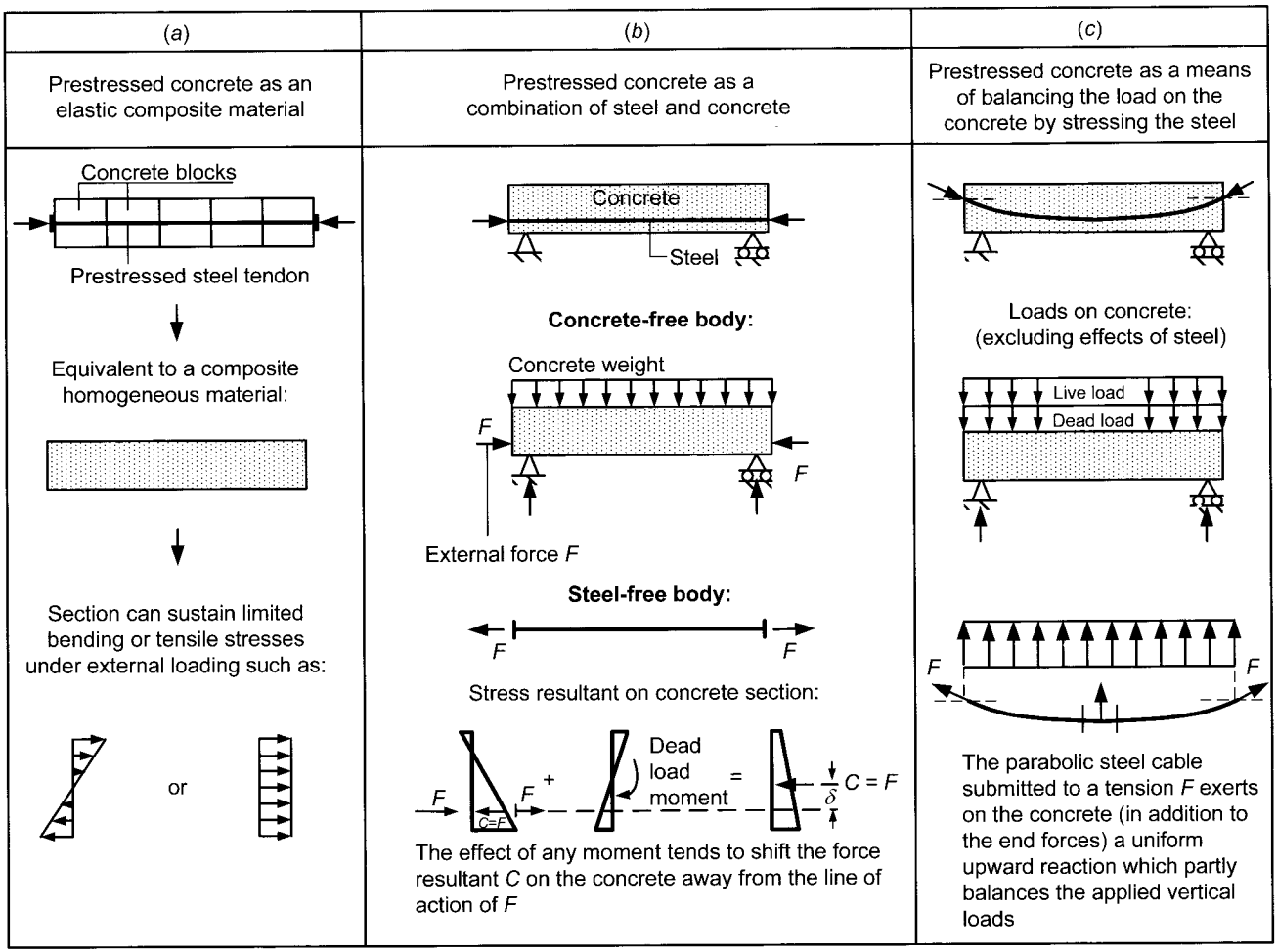

Figure 4.5 Three concepts used to analyze prestressed concrete elements.

A prestressed concrete section is assumed uncracked under service loads and, if the bending moment applied to the section increases, the forces of the couple remain essentially constant while the distance between them increases. This is illustrated next.

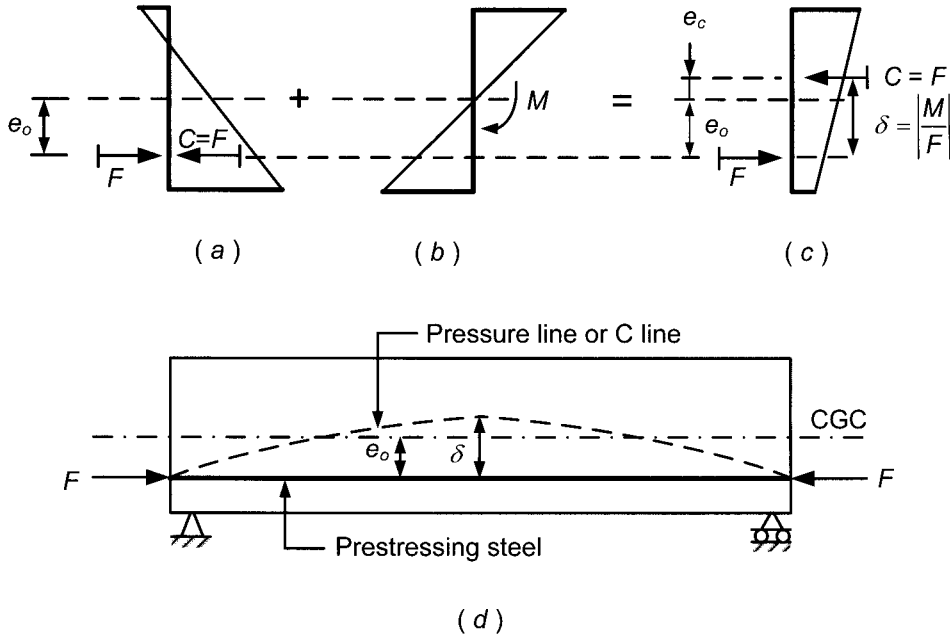

Figure 4.6 Effects of a moment on resulting stresses and C line in concrete.

Let us consider the stress diagram along a cross section of a simply supported beam (Fig. 4.6). If the beam is assumed weightless, the compressive force C on the concrete section considered as a free body is equal in magnitude to the prestressing force F and acts along the same line as F. The stress profile along the cross section due to C is shown in Fig. 4.6*a*. If a bending moment is applied to the section, it produces a stress diagram as shown in Fig. 4.6*b*. The resulting stress diagram due to the combined action of the prestressing force and the moment is shown in Fig. 4.6*c* (assuming no tension or cracking). The sum of the forces on the section is still equal to C since any external moment leads to an equal internal couple and the sum of the forces of a couple is zero. Therefore, the stress diagram shown in (*c*) can be seen as resulting from a compressive force C, same as in (*a*), but acting along a different line parallel to and located a distance δ from the line of action of F. This is the same as saying that the combined action of a bending moment and a force is equivalent to the action of the same force being displaced a certain distance δ parallel to its line of action. Note that δ is such that $\delta \times F = \delta \times C =$ external moment. It can be seen that an external moment acting on the section does not affect the value of $C = F$ but only changes the distance between them. (In fact because of the change in curvature due to loading, F changes slightly.) It is interesting to note that the location of C can be

characterized by an eccentricity e_c, similar to the eccentricity e_o of the prestressing force. The geometric lieu of C at every section along a given member is called pressure line or C-line. For the simply supported beam considered in this example and subjected to a prestressing force F and a bending moment due to its own weight and/or to a uniform load, the C line is schematically represented in Fig. 4.6*d*; it has a parabolic shape to reflect the bending moment diagram (see also C-line in Chapter 10).

The third concept used in analyzing prestressed beams is called the load-balancing concept. Here the entire concrete member is considered a free body subjected to externally applied loads including its own weight. The prestressing force and the steel profile are selected to directly balance *part* of these external loads (Fig. 4.5*c*). The beam is then in a state of uniform compression with zero deflection, and uncracked elastic beam theory is used to analyze the effects of the remaining part of the external loads. The load-balancing technique is an extremely simple and powerful technique for the design of continuous beams, two-way slabs, frames and shells. It has been first introduced by T.Y. Lin and is discussed in more detail in Chapter 10.

4.3 NOTATIONS FOR FLEXURE

In the most general case, the uncracked cross section of a prestressed concrete beam can be characterized, for design purposes, by a number of variables and geometric properties. Geometric properties can be determined directly from the dimensions of the cross section. Referring to Fig. 4.7, the following notations and definitions will be used:

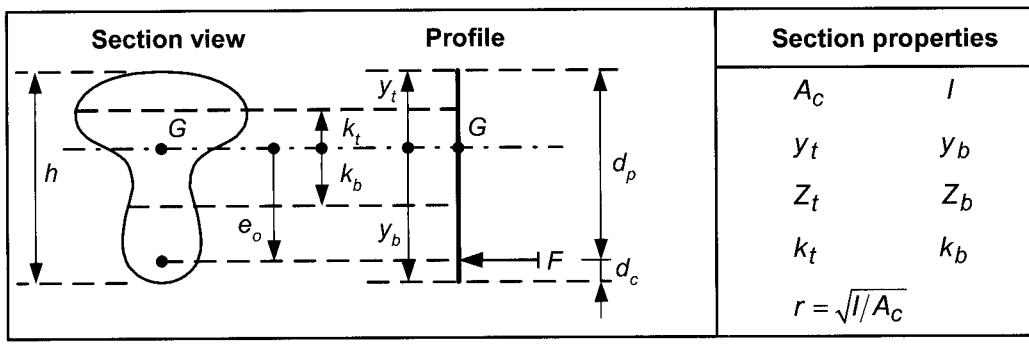

Figure 4.7 Typical characterization of beam cross section.

A_c = area of concrete cross section (it may indicate the net or gross area depending on the problem at hand and whether preliminary or final designs are considered; practically, in pretensioned members it is taken

as the gross area, while in posttensioned members it is often the net or the transformed area)

A_{ps} = area of prestressing steel

d_p = distance from extreme compression fiber to the centroid of prestressing steel (or force)

d_c = concrete cover from the precompressed tensile fiber to the centroid of prestressing steel (d_c can generally be estimated in a preliminary design and revised for the final design)

$(d_c)_{min}$ = minimum feasible value of d_c

e_o = eccentricity of the prestressing force (or centroid of prestressing steel) with respect to the centroid of the concrete section (e_o varies along the member, thus $e_o(x)$ is used when needed)

F = final prestressing force or effective prestressing force after all losses

h = total height of concrete section ($h = y_t + y_b = d_p + d_c$)

I = moment of inertia of the section with respect to an axis passing by its centroid (it generally implies gross sectional inertia; for a final design it may indicate the transformed inertia)

y_t = distance from the centroid of the concrete section to the extreme top fiber

y_b = distance from the centroid of the concrete section to the extreme bottom fiber

ρ_p = A_{ps}/bd_p prestressed reinforcement ratio (b is the width of a rectangular section or flange width of T section)

σ = stress in concrete in general (it will be used unless a widely standard notation such as f'_c applies)

Z_t = I/y_t = section modulus with respect to the top fiber

Z_b = I/y_b = section modulus with respect to the bottom fiber

r = $\sqrt{I/A_c}$ = radius of gyration of the section

k_t = $-I/A_c y_b = -Z_b/A_c = -r^2/y_b$ = distance from the centroid of the concrete section to the upper limit of the central kern

k_b = $I/A_c y_t = Z_t/A_c = r^2/y_t$ = distance from the centroid of the concrete section to the lower limit of the central kern

γ = $(-k_t + k_b)/h = I/(A_c y_t y_b) = r^2/(y_t y_b) = Z_t/(A_c y_b) = Z_b/(A_c y_t)$ = geometric efficiency of the cross section with respect to bending

Note that $y_b = e_o + d_c$ and $d_p = e_o + y_t$. The central kern defines an area within the concrete section where a compressive force will not lead to tensile stresses on any part of the section. The upper limit of the central kern, k_t, has been given a negative sign to be consistent with the sign convention given for e_o (Sec. 4.4) and because k_t can be seen as a particular value of e_o. The reinforcement ratio, ρ_p, of

prestressed concrete members is generally less than one percent and most values in beams and slabs practically fall between 0.1 and 0.5 percent.

The geometric efficiency of the section γ is equal to 1/3 for rectangular beams and 1 for a fictitious web-less I beam having two identical and infinitely thin flanges. Practically the value of γ ranges from about 0.45 to 0.50 for T beams and 0.55 to 0.65 for box beams.

It is important for the designer to rapidly determine the main cross-sectional properties for any given cross section of concrete. Some background information on the moment of inertia is given in Fig. 4.8 where the parallel axis theorem is explained. An example is given in the next section and can be essentially used as a model.

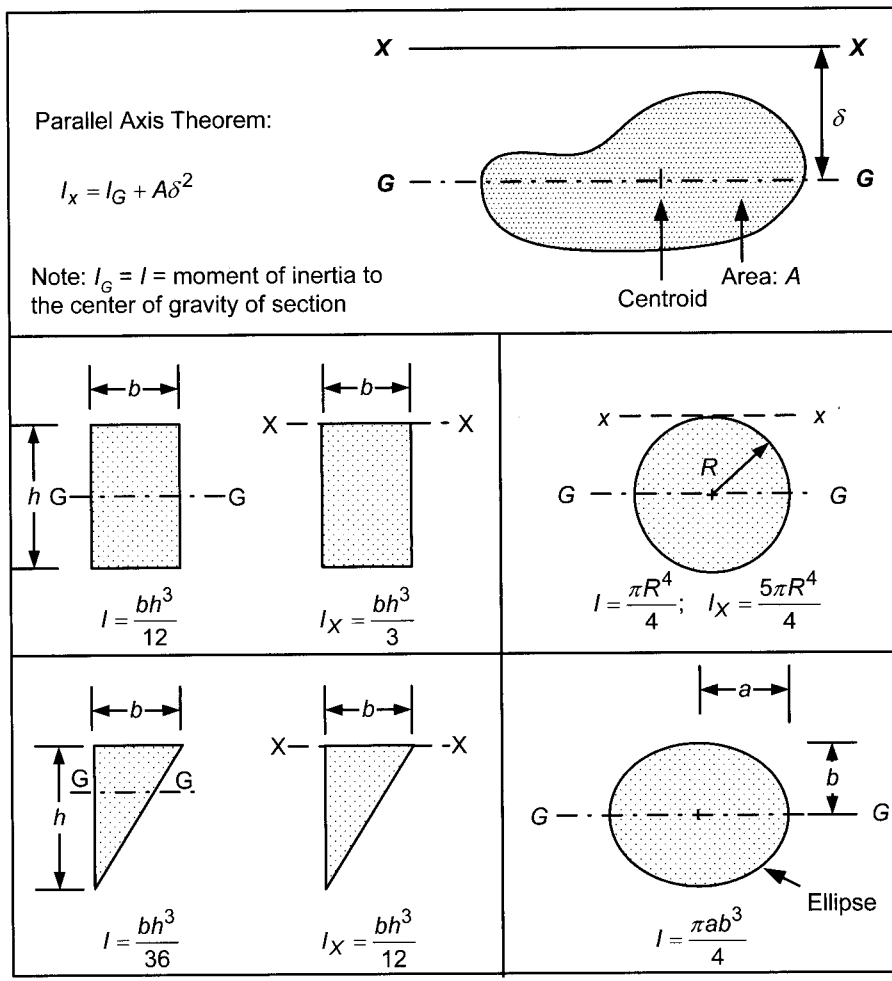

Figure 4.8 Parallel axis theorem and sectional moment of inertia.

4.3.1 Example: Computation of Sectional Properties

Determine the section properties of the beams shown in Fig. 4.9*a*. The cross section is divided into three parts, as shown in Fig. 4.9*b*. Typical calculations are set in a tabular form below; the method can be used for any section with any number of parts n. The centroid of each part A_i is assumed at a distance δ_i from the X-X axis.

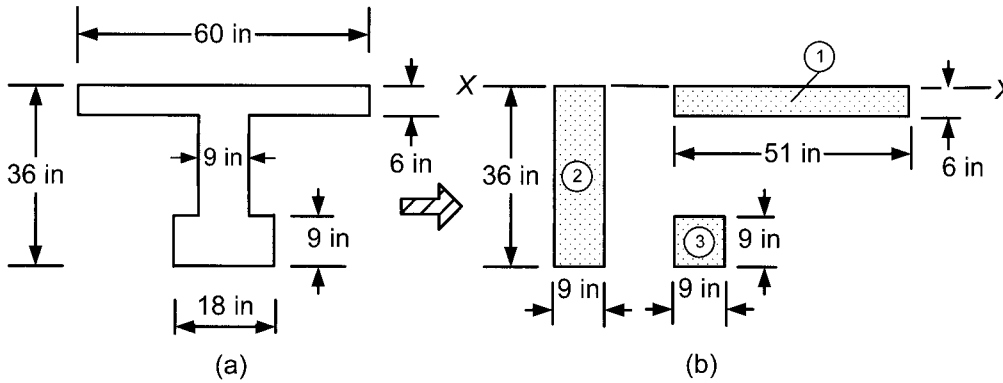

Figure 4.9

Part	Area A_i	δ_i	$A_i\delta_i$	$A_i\delta_i^2$	$(I)_i$	$(I_X)_i$
1	$51\times 6 = 306$	3	918.0	2,754	918	3,672
2	$9\times 36 = 324$	18	5832.0	104,976	34,992	139,968
3	$9\times 9 = 81$	31.5	2551.5	80,372.25	546.75	80,919
4						
.						
.	↓		↓			↓
.						
Total: $A_c = 711$		$Q = 9301.5 = \sum A_i\delta_i$				$I_X = 224{,}559$

Thus:

$$y_t = Q/A_c = 13.08 \text{ in}; \quad y_b = 36 - y_t = 22.92 \text{ in}$$

$$I = I_X - A_c y_t^2 = 102{,}916 \text{ in}^4$$

$$Z_t = 7868 \text{ in}^3; Z_b = 4490 \text{ in}^3$$

$$k_t = -Z_b/A_c = -6.32 \text{ in}; \quad k_b = Z_t/Ac = 11.07 \text{ in}$$

4.4 SIGN CONVENTION

Although in prestressed concrete many effects such as compression or tension can be found by inspection, it is very important to provide a consistent sign convention in order to reduce error in any complex and systematic analysis; of course, this is also

essential in any computerized design. The following rules of sign convention will be generally followed in this text:

1. Plus (+) for compressive stresses in concrete
2. Minus (-) for tensile stresses in concrete

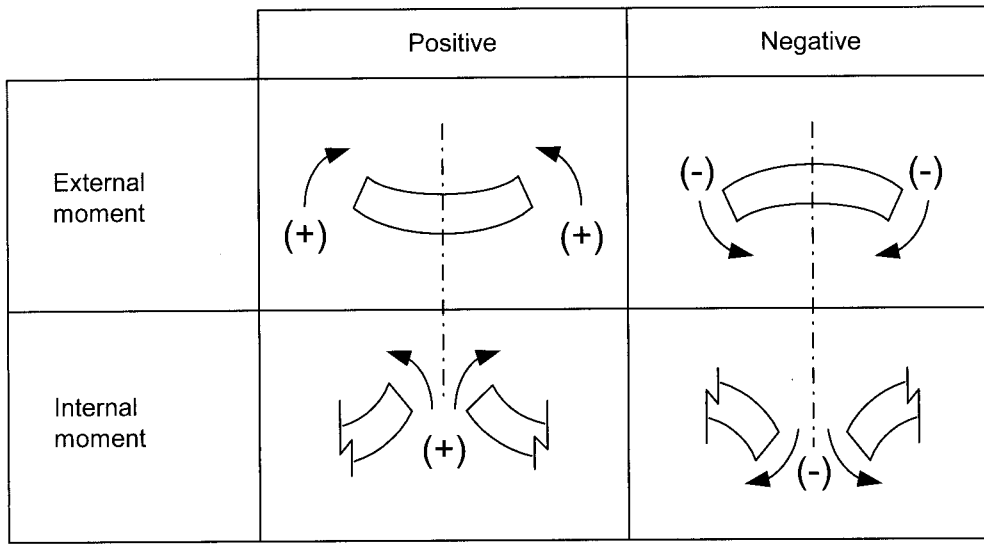

Figure 4.10 Sign convention for moments.

The two extreme fibers of a horizontal member (beam) will be referred to as top and bottom fiber. A vertical member is rendered horizontal by a clockwise rotation of $\pi/2 = 90^o$. Thus the left and right fiber of a vertical member are identical from a stress analysis viewpoint to the top and bottom fiber of a horizontal member, respectively. In order to evaluate the effect of a bending moment on stresses, the usual sign convention for moments, as described in Fig. 4.10, will be used. Thus a moment, which tends to bend a simply supported beam so that it will retain water (concave curvature), is considered positive. For instance, the moment due to the own weight of a simply supported beam is positive, while the moment at the intermediate support of a two-span continuous beam is negative (convex curvature). Therefore:

3. Use plus (+) the numerical value of the moment for positive moments and minus (-) for negative moments

An extreme fiber stress due to a bending moment of magnitude M can be calculated from the expression M/Z_t or M/Z_b where Z_t and Z_b represent the section moduli with respect to the top and bottom fibers, respectively. In order for flexural

stresses to show the correct sign corresponding to a tension or a compression, the following rule is set:

4. Multiply the above expression (M/Z_t or M/Z_b) by +1 if the stress to be calculated is on the top fiber and by -1 if it is on the bottom fiber. Give the moment its own sign, such as for example, 200 N-m or –150 N-m. Note that the same holds for stresses calculated at points "above" and "below" the neutral axis of bending of the section. For vertical members "left" replaces "top" or "above," and right replaces "bottom" or "below."

The prestressing force F acting on a concrete section with eccentricity e_o has the same effect as a concentric force F applied at the centroid of the section, thus inducing a uniform compressive stress (positive), and a moment of magnitude Fe_o. If e_o is positive downward such as in Fig. 4.6, the moment due to prestressing is negative (convex curvature) and its value is $(-Fe_o)$. The corresponding flexural stresses are given on the top fiber by:

$$+\left(\frac{-Fe_o}{Z_t}\right)=\frac{-Fe_o}{Z_t}$$

and on the bottom fiber by:

$$-\left(\frac{-Fe_o}{Z_b}\right)=\frac{Fe_o}{Z_b}$$

Another way to present these results is to follow the following rules:

5. Use the absolute value of the moment Fe_o (i.e., F and e_o are assumed positive)
6. Multiply the stress due to Fe_o by +1 when it is computed on a fiber on the same side as e_o with respect to the neutral axis, and by -1 when it is on the opposite side

Expressions for the stress on the top and bottom fibers due to a bending moment and to the prestressing force for a typical simply supported prestressed beam are summarized in Table 4.1. For each expression several equivalent forms can be used. However, some may be easier to handle in a particular problem.

The following sign convention will be used for the steel (prestressed or non-prestressed):

7. Plus (+) for tensile stresses
8. Minus (-) for compressive stresses

Table 4.1 Various expressions of stresses due to a moment or a prestressing force.

Effect of: ↓	Extreme fiber	Various expressions for stresses
Positive moment of magnitude M	Top	$\sigma_t = \frac{My_t}{I} = \frac{M}{Z_t} = \frac{M}{A_c k_b} = \frac{My_t}{A_c r^2}$
	Bottom	$\sigma_b = -\frac{My_b}{I} = -\frac{M}{Z_b} = +\frac{M}{A_c k_t} = -\frac{My_b}{A_c r^2}$
Prestressing force F at eccentricity e_o toward bottom fiber of beam	Top	$\sigma_t = \frac{F}{A_c} - \frac{Fe_o y_t}{I} = \frac{F}{A_c}\left(1 - \frac{e_o y_t}{r^2}\right) = \frac{F}{A_c}\left(1 - \frac{e_o A_c}{Z_t}\right) = \frac{F}{A_c}\left(1 - \frac{e_o}{k_b}\right) = \frac{F}{Z_t}(k_b - e_o)$
	Bottom	$\sigma_b = \frac{F}{A_c} + \frac{Fe_o y_b}{I} = \frac{F}{A_c}\left(1 + \frac{e_o y_b}{r^2}\right) = \frac{F}{A_c}\left(1 + \frac{e_o A_c}{Z_b}\right) = \frac{F}{A_c}\left(1 - \frac{e_o}{k_t}\right) = \frac{F}{Z_b}(e_o - k_t)$

It may seem awkward to have different sign conventions for stresses in the steel and concrete. However, the above recommended sign convention is natural for prestressed concrete because it generally leads to positive stresses in the concrete (compression) and in the steel (tension). If confusion may arise in some equations where compression steel is present, the absolute value sign will be used to warn the reader.

The following examples illustrate the use of the sign convention in computing the numerical values of stresses in a prestressed concrete section.

4.4.1 Examples

(a) Compute the stress on the bottom fiber at the midspan section of the simply supported prestressed beam shown in Fig. 4.11a for which F = 120 kips, e_o = 8 in, and the moment due the beam's own weight = 60 kips-ft.

The bending moment is positive and carries its own sign (rule 3), that is, +60 kips-ft. The stress on the bottom fiber, due to the moment is given by: $(-1)(M)/Z_b$ according to rules 4. and 3. of the sign conventions; i.e., (-1)(60x12,000)/1152 = -625 psi (tension). The stress due to the prestressing force is given by: $F/A_c + (+1)(Fe_o)/Z_b$ according to rules 1., 5., and 6. of the sign convention; i.e., (120,000/288) + (120,000x8)/1152 = 1250 psi (compression). Thus the resulting bottom fiber stress is given by: $(-M/Z_b) + (F/A_c + Fe_o/Z_b)$ = 625 psi (compression).

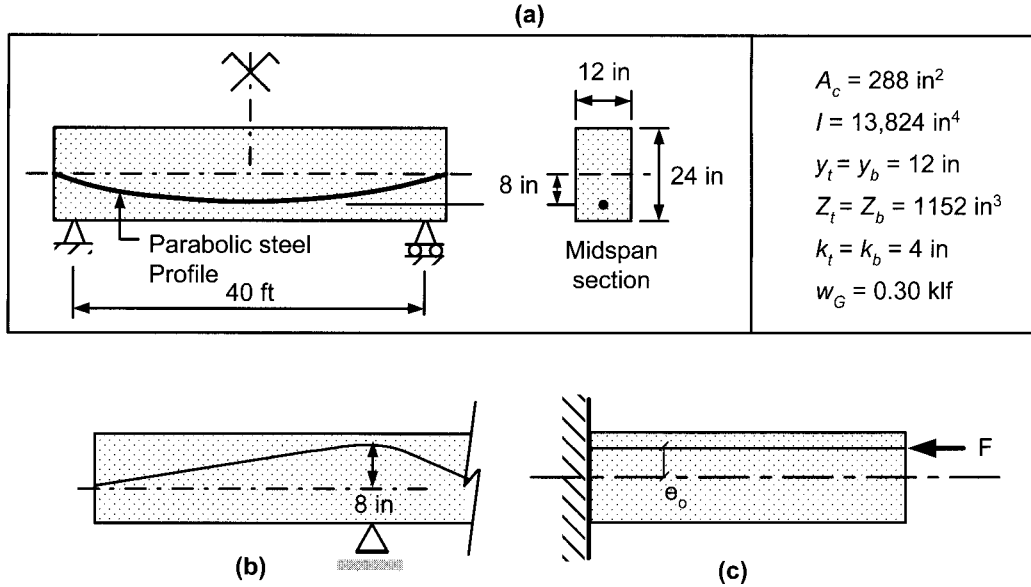

Figure 4.11

(b) Compute the stress on the bottom fiber at the support of a simply supported symmetrical beam with double cantilevers (Fig. 4.11b) assuming same section properties and same prestressing force as for Example **(a);** consider the eccentricity e_o = -8 in, and the external bending moment M = -15 kips-ft at the supports.

According to rules 3. and 4. of the sign convention, the stress due to the moment is given by: $(-1)(M/Z_b) = -1(-15)/Z_b$ = 15x12,000/1152 = 156.2 psi (compression); the stress due to the prestressing force according to rules 1, 5, and 6 is given by: $F/A_c + (-1)(Fe_o)/Z_b = F/A_c - Fe_o/Z_b$ = *120,000/288 - 120,000x8/1152* = - 416.6 psi (tension). Thus the resulting stress on the bottom fiber is equal to -260.4 psi (tension).

(c) Compute the stress on the top fiber of the fixed end section (Fig. 4.11c) of a cantilever beam assuming the following: M = -75 kips-ft; F = 120 kips; e_o = -8 in; the section is same as for Example (a). Using rules 3. and 4. of the sign convention, the stress due to the external moment is given by: $(+1)(M Z_t)$ = (+1)(- 75x12000/1152) = -781.25 psi (tension). Using rules 1., 5., and 6. the stress due to the prestressing force is given by: $F/A_c + (+1)(Fe_o)/Z_t$ = *120,000/288 + 120,000x8/1152* = 1250 psi (compression). The resulting stress on the top fiber is: -781.25 + 1250 = 468.75 psi (compression).

4.5 LOADING STAGES

In the design of prestressed concrete members, loading refers not only to externally applied loads such as dead and live loads but often also to a combination of these loads acting with the prestressing force on the concrete section. Several loading stages can be identified in the elastic range of behavior among which the *initial* and the *final* loadings are generally most critical.

The *initial loading* refers primarily to the stage where the prestressing force is transferred to the concrete and no external loads are present except the weight of the member. At this time the prestressing force is maximum since prestress losses have not yet taken place and the concrete strength is minimum since the concrete is still young; consequently, the stresses in the concrete can be critical. In pretensioned members, in order to speed production, the prestressing tendons are released simultaneously at a time when the strength of the concrete has reached 60 to 80 percent of its specified 28 days strength. By curing the concrete at higher temperatures, these strengths can be achieved in less than 24 hours after the concrete is poured. In posttensioned members, often the prestressing tendons are not tensioned all at the same time but rather in two or three steps to allow the concrete to reach its specified strength before the prestressing force is fully applied. For example, 20 percent of the tendons may be tensioned about three days after the concrete is poured to compensate shrinkage stresses, an additional 40 to 50 percent at about seven days in order to remove the molds, etc., and the rest at 28 days. This approach has also the advantage of distributing more uniformly the work of the posttensioning crew in the field. In most cases the initial loading leads to critical stresses and its effect must be carefully assessed.

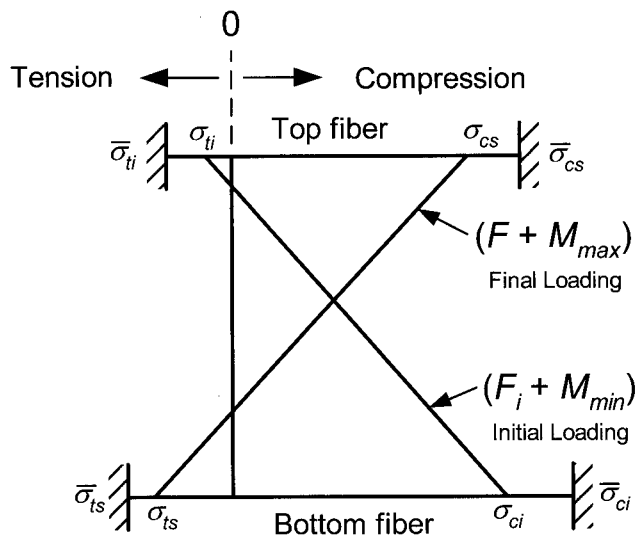

Figure 4.12 Typical stress diagrams under extreme loadings.

The *final loading* stage refers here to the most severe loading under service conditions; it is then assumed that all prestress losses have occurred, i.e., the prestressing force has its final and smallest value, and that the most critical combination of external loadings is applied; such a combination includes the weight of the member, superimposed dead load, live load, impact, and the like. Load combinations are generally specified in various codes and specifications (Chapter 3).

Although the initial and final loadings are often the two most critical loadings, some intermediate loadings may become critical in the design. For example, special conditions during handling, transportation, and erection of precast prestressed members may lead to stresses more critical than those induced by the initial and final loadings. Every particular case must be studied with care and if necessary integrated in the design.

Among all possible loadings applied to a prestressed section, two will bound the others in terms of flexural stresses, and will be identified as the *two extreme loading* conditions. In a majority of cases they are due to the effect of $(F_i + M_{min})$ and $(F + M_{max})$ where, under initial and final conditions, M_{min} and M_{max} are the minimum and maximum bending moments, respectively, and F_i and F are the initial and effective values of the prestressing force at the section considered. For example, M_{min} may be the same as the moment due to the weight of the member while M_{max} may be the moment due to weight plus the superimposed dead and live loads. The relation between the initial and the final prestressing force is described by their ratio $\eta = F/F_i$; η can be estimated in a preliminary design and then more carefully assessed in the final design (Section 3.13). It may happen that one or both extreme loadings do not necessarily correspond to what is generally described as the initial and/or final loadings. Although they must be clearly identified, their effect is treated similarly to the above approach. Typical stress diagrams on the concrete section of a pretensioned member are shown in Fig. 4.12. The two extreme loading conditions are shown to induce flexural stresses which are within allowable stress limits. Allowable stresses are represented by short vertical lines dashed on one side.

4.6 ALLOWABLE STRESSES

Allowable stresses on the concrete section as well as in the steel are generally provided by the codes of practice or specifications considered for a particular study. Typical values of allowable stresses are given in Section 3.8.

Since generally two extreme loading conditions (Fig. 4.12) provide bounds to all others, at least four allowable stresses on the concrete section must be considered in the design, namely two (tension and compression) for the initial loading and two (tension and compression) for the most severe final loading. Without specifically referring to any particular numerical value of allowable stresses, the following notation will be used in describing them:

$\bar{\sigma}_{ti}$ = allowable temporary tensile stress in the concrete (initial most severe loading); the subscript reads "top initial" or "tension initial" for a simply supported beam

$\bar{\sigma}_{ci}$ = allowable temporary compressive stress in the concrete (initial most severe loading); the subscript reads "compression initial" for a simply supported beam

$\bar{\sigma}_{ts}$ = allowable service tensile stress in the concrete (final most severe loading); the subscript reads "tension service"

$\bar{\sigma}_{cs}$ = allowable service compressive stress in the concrete (final most severe loading); the subscript reads "compression service"

$\bar{\sigma}_{csus}$ = allowable service compressive stress in the concrete under sustained load; the subscript reads "compression sustained"

In a composite construction one additional allowable stress must be considered, namely:

$\bar{\sigma}_{c\ slab}$ = allowable service compressive stress in composite slab

Note that in order to identify allowable stresses for concrete a bar is placed on top of the literal value. The same notation is used without the bar for actual stresses under same conditions. For the steel allowable stresses are given directly as a fraction of ultimate strength; thus no literal values are needed.

The 2002 ACI code specifies two values of allowable compression stress in service; one value, $\bar{\sigma}_{cs} = 0.60 f'_c$, is associated with the full service load, that is, M_{max}; the other value, $\bar{\sigma}_{cs} = 0.45 f'_c$, is associated with the sustained load, that is, generally the sum of dead load (weight), superimposed dead load, and possibly a portion of the live load considered permanent, M_{sus}. In most of the equations in this text, particularly Tables 4.2, 4.3, and 9.2, the combination M_{max} and $\bar{\sigma}_{cs}$ will be used to represent either one of the two conditions. However, numerical results will be checked for the most critical of the two combinations.

In a similar manner, the AASHTO LRFD Bridge Design Specifications (Table 14.5) specify three different values of allowable compression stress in service depending on the loading. Again, in order to minimize the number of equations, one literal equation will be generally written to represent the actual compressive stress for the appropriate combination of moment and allowable stress, then it will be used to check which of the three combinations is most critical.

4.7 MATHEMATICAL BASIS FOR FLEXURAL ANALYSIS

For the analysis, it is assumed that all materials behave elastically in the working range of stresses applied. The usual hypothesis of Hooke, Navier-Bresse, and Bernouilli are assumed valid, namely:

1. The materials (steel and concrete) are elastic and there is a proportional relationship between stresses and strains (Hooke's Law)
2. Plane sections remain plane after bending (Bernouilli), and
3. There is a perfect bond between steel and concrete

This is equivalent to saying that both the stress and strain diagrams along the section of concrete under bending are linear, and that the changes in strains in the steel and in the concrete at the level of the steel are identical. Also the load-deflection or moment-curvature curves are assumed linear for the loadings considered. Typical stress diagrams for the two extreme initial and final loadings have been described in Fig. 4.12. Note that the highest stresses in the section occur at the extreme top and bottom fibers.

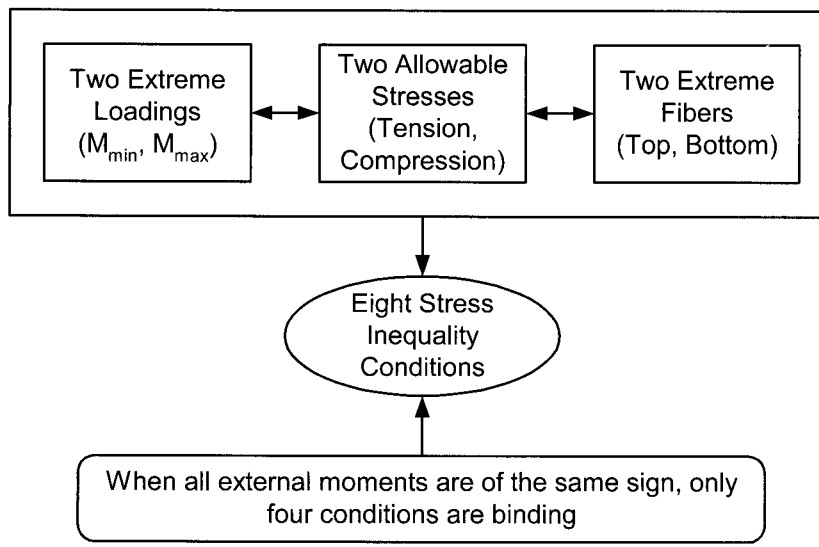

Figure 4.13 Basis for the stress inequality conditions.

Since two extreme loadings are generally critical and since for each, two allowable stresses must be specified, at least four allowable stresses must be considered in the analysis. Since under flexural loading maximum stresses occur on the two extreme fibers (top and bottom), eight inequality equations comparing actual stresses with allowable stresses can be derived (Fig. 4.13). They are of the form:

$$\text{(Actual stress)} \left\{ \begin{matrix} \geq \\ \text{or} \\ \leq \end{matrix} \right\} \text{(allowable stress)} \tag{4.1}$$

Let us develop one of these equations for a pretensioned simply supported member. The actual stress on the top fiber under initial conditions must be more than or equal to the allowable initial tensile stress (since tension is negative we use "more than or equal"). Therefore

$$\sigma_{ti} = \frac{F_i}{A_c} - \frac{F_i e_o}{Z_t} + \frac{M_{\min}}{Z_t} \geq \bar{\sigma}_{ti} \tag{4.2}$$

where $M_{\min}$ represents the dead load moment at the section considered. Equation (4.2) could also be rewritten in several different ways, one of which may be more suitable if a particular variable is to be emphasized, such as, for example:

$$\begin{cases} F_i \leq (M_{\min} - \bar{\sigma}_{ti} Z_t)/(e_o - k_b) \\ e_o \leq k_b + (1/F_i)(M_{\min} - \bar{\sigma}_{ti} Z_t) \\ 1/F_i \geq (e_o - k_b)/(M_{\min} - \bar{\sigma}_{ti} Z_t) \end{cases} \tag{4.3}$$

As mentioned above, eight inequality equations (which will also be described as "stress conditions", "stress constraints", or "stress limit states") can be derived and are similar in form to Eq. (4.2). However, in actual design problems, out of the eight conditions four are generally non-binding. For example, if for a simply supported member the tensile stress on the top fiber for the initial loading is of concern and is checked against allowable limit (as for Eq. (4.2)), there is certainly no need to check, against allowable limit, the compressive stress on the same fiber and for the same loading. If for the same loading we were checking the section at the intermediate support of a two-span continuous beam, we would check the stress on the top fiber against initial allowable compression and that eliminates the need to check against initial allowable tension. Thus the number of inequality equations that must be considered in the analysis at a given section is essentially reduced to four, i.e., four of them are binding, while the four others are not. The four that are binding in a particular design depend on the sign of the applied moments.

The eight stress inequality equations written in various ways are shown four at a time in Tables 4.2 and 4.3. They have been numbered in roman notation I to IV and I' to IV'. The coefficient η was defined in Section 3.13 and is the ratio of the final prestressing force after all losses to the initial prestressing force. For a cross section where all applied moments ($M_{\min}$ and $M_{\max}$) are positive, only stress inequalities I to IV need to be considered; similarly, if all applied moments are negative, stress inequalities I' to IV' become binding. When a particular section is subject to moments of different signs, it is possible, by inspection, to select out of the eight inequalities the four that would be binding; on the other hand, one can also check

systematically the eight inequalities against allowable stresses and select the four that are binding. This is typically what should be done if a computer program (or a spreadsheet) is written and the applied bending moment at any section can be of any sign.

Table 4.2 Useful ways of writing the four stress inequality conditions.

Way	Stress condition	Inequality equation
1	I	$(F_i / A_c)[1-(e_o / k_b)]+M_{\min} / Z_t \geq \bar{\sigma}_{ti}$
	II	$(F_i / A_c)[1-(e_o / k_t)]-M_{\min} / Z_b \leq \bar{\sigma}_{ci}$
	III	$[(F \text{ or } \eta F_i) / A_c][1-(e_o / k_b)]+M_{\max} / Z_t \leq \bar{\sigma}_{cs}$
	IV	$[(F \text{ or } \eta F_i) / A_c][1-(e_o / k_t)]-M_{\max} / Z_b \geq \bar{\sigma}_{ts}$
2	I	$e_o \leq k_b+(1/F_i)(M_{\min}-\bar{\sigma}_{ti}Z_t)$
	II	$e_o \leq k_t+(1/F_i)(M_{\min}+\bar{\sigma}_{ci}Z_b)$
	III	$e_o \geq k_b+[1/(F \text{ or } \eta F_i)](M_{\max}-\bar{\sigma}_{cs}Z_t)$
	IV	$e_o \geq k_t+[1/(F \text{ or } \eta F_i)](M_{\max}+\bar{\sigma}_{ts}Z_b)$
3	I	$F_i \leq (M_{\min}-\bar{\sigma}_{ti}Z_t)/(e_o-k_b)$
	II	$F_i \leq (M_{\min}+\bar{\sigma}_{ci}Z_b)/(e_o-k_t)$
	III	$F=\eta F_i \geq (M_{\max}-\bar{\sigma}_{cs}Z_t)/(e_o-k_b)$
	IV	$F=\eta F_i \geq (M_{\max}+\bar{\sigma}_{ts}Z_b)/(e_o-k_t)$
4	I	$1/F_i \geq (e_o-k_b)/(M_{\min}-\bar{\sigma}_{ti}Z_t)$
	II	$1/F_i \geq (e_o-k_t)/(M_{\min}+\bar{\sigma}_{ci}Z_b)$
	III	$1/F=1/\eta F_i \leq (e_o-k_b)/(M_{\max}-\bar{\sigma}_{cs}Z_t)$
	IV	$1/F=1/\eta F_i \leq (e_o-k_t)/(M_{\max}+\bar{\sigma}_{ts}Z_b)$
All	V	$e_o \leq (e_o)_{mp}=y_b-(d_c)_{\min}$ = maximum practical eccentricity towards bottom fiber

Note: for condition III, $M_{\max}$ and $\bar{\sigma}_{cs}$ may also be replaced by $M_{\text{sustained}}$ and $\bar{\sigma}_{csus}$ to satisfy the second provision on allowable compression given in the 2002 ACI Code.

Table 4.3 Useful ways of writing the four complementary stress inequality conditions.

Way	Stress condition	Inequality equation
1	I'	$(F_i / A_c)[1-(e_o / k_b)]+M_{\min} / Z_t \le \bar{\sigma}_{ci}$
	II'	$(F_i / A_c)[1-(e_o / k_t)]-M_{\min} / Z_b \ge \bar{\sigma}_{ti}$
	III'	$[(F \text{ or } \eta F_i)/ A_c][1-(e_o / k_b)]+M_{\max} / Z_t \ge \bar{\sigma}_{ts}$
	IV'	$[(F \text{ or } \eta F_i)/ A_c][1-(e_o / k_t)]-M_{\max} / Z_b \le \bar{\sigma}_{cs}$
2	I'	$e_o \ge k_b +(1/F_i)(M_{\min} -\bar{\sigma}_{ci}Z_t)$
	II'	$e_o \ge k_t +(1/F_i)(M_{\min} +\bar{\sigma}_{ti}Z_b)$
	III'	$e_o \le k_b +[1/(F \text{ or } \eta F_i)](M_{\max} -\bar{\sigma}_{ts}Z_t)$
	IV'	$e_o \le k_t +[1/(F \text{ or } \eta F_i)](M_{\max} +\bar{\sigma}_{cs}Z_b)$
3	I'	$F_i \ge (M_{\min} -\bar{\sigma}_{ci}Z_t)/(e_o -k_b)$
	II'	$F_i \ge (M_{\min} +\bar{\sigma}_{ti}Z_b)/(e_o -k_t)$
	III'	$F = \eta F_i \le (M_{\max} -\bar{\sigma}_{ts}Z_t)/(e_o -k_b)$
	IV'	$F = \eta F_i \le (M_{\max} +\bar{\sigma}_{cs}Z_b)/(e_o -k_t)$
4	I'	$1/F_i \le (e_o -k_b)/(M_{\min} -\bar{\sigma}_{ci}Z_t)$
	II'	$1/F_i \le (e_o -k_t)/(M_{\min} +\bar{\sigma}_{ti}Z_b)$
	III'	$1/(F \text{ or } \eta F_i) \ge (e_o -k_b)/(M_{\max} -\bar{\sigma}_{ts}Z_t)$
	IV'	$1/(F \text{ or } \eta F_i) \ge (e_o -k_t)/(M_{\max} +\bar{\sigma}_{cs}Z_b)$
All	V'	$\lvert e_o \rvert \le \lvert (e_o)_{mp} \rvert = y_t -(d_c)_{min}$ = maximum practical eccentricity towards top fiber

Note: for condition IV', $M_{\max}$ and $\bar{\sigma}_{cs}$ may also be replaced by M_{sutained} and $\bar{\sigma}_{csus}$ to satisfy the second provision on allowable compression given in the 2002 ACI Code.

Note that the stress inequalities I' to IV' given in Table 4.3 are described here as "complementary stress inequalities." This is because often one does not need to use them. It can be shown that if all applied moments are negative, stress conditions I to IV can still be used provided the concrete section is assumed in its inverted position (i.e., use properties of inverted section) and the sign of the moments is changed from negative to positive; the position of F within the cross section remains unchanged. It is because stress conditions I to IV can cover the majority of practical problems that

they are often encountered alone in the technical literature and with no reference to the four others.

In Tables 4.2 and 4.3, a fifth condition numbered V has been included and will be described as the "practicality condition." Essentially it states that the prestressing force must be inside the concrete section with an adequate cover $(d_c)_{\min}$. Thus the design eccentricity e_o must be less than or equal to a maximum practical value $(e_o)_{mp} = y_b - (d_c)_{\min}$. Although in an analysis or investigation problem, condition V is obviously satisfied, in a design problem condition V can be binding and can be used with advantage in optimizing or simplifying a solution. This is why it has been included in the tables. Note finally that in the case of external prestressing the maximum practical eccentricity is independent of the minimum concrete cover.

In an analysis or investigation problem, the above stress inequality equations can be directly checked as all quantities are known. Thus one can verify the allowable stress limit states. In a design problem, however, these inequalities can be used to either determine exactly, or put bounds on some of the unknown variables, such as prestressing force F, eccentricity e_o, and/or section properties. For example, if the concrete cross section is given, the stress conditions can be used to determine bounds on all the possible values of F and e_o that would be acceptable for the problem at hand. This is clarified in the next sections.

4.8 GEOMETRIC INTERPRETATION OF THE STRESS INEQUALITY CONDITIONS

The geometric interpretation of the stress inequality conditions has been first explored by Magnel [Ref. 1.10]. As emphasized throughout this text, the geometric representation can be a very useful and powerful technique for the solution of many problems where the working stress design approach is used.

Let us assume that the geometric properties of the concrete cross section are given including the depth of the section which can be estimated a priori; then only two unknown variables remain in equations I to IV, namely e_o and F_i (or $F = \eta F_i$). One can plot on a two-dimensional scale the curves corresponding to the four equations at equality. Each curve will separate the plane into two parts, one where the inequality is satisfied and the other where it is not. If e_o is plotted versus F_i, the curves will be hyperbola. However, if e_o is plotted versus $1/F_i$, then straight lines are obtained and the geometric representation is much simplified. For this reason, it is better to use the second way of writing the equations in Table 4.2 because they are written in the form: $e_o = a(1/F_i) + b$ where b is the intercept and a the slope of the line. When plotted as shown in Fig. 4.14, the inequality equations delineate a domain of feasibility limited by a quadragon A, B, C, D. Essentially any point inside this feasibility domain has coordinates F_i and e_o, which satisfy the four stress inequality conditions I to IV. The practicality condition V can also be represented at

equality on the same graph by a horizontal line parallel to the $1/F_i$ axis. If this line intersects the quadragon *A*, *B*, *C*, *D*, such as case (*b*) of Fig. 4.14, then a new reduced feasibility domain is defined such as *EBCDG*. Any point inside this new domain would have satisfactory (stress wise) and practically feasible values of F_i and e_o. If the line representing condition V does not intersect the domain *A*, *B*, *C*, *D*, such as in cases (*a*) or (*c*) of Fig. 4.14, then either there is no practical solution (case (*a*)) or any point inside *A*, *B*, *C*, *D* represents a practically feasible solution (case (*c*)). In case (*a*) a new concrete cross section must be used leading to higher section moduli. In case (*c*), since any point of the domain *A*, *B*, *C*, *D* is feasible, one must select the one leading to the smallest prestressing force, i.e., point *A*, intersection of lines representing conditions I and IV. The corresponding analytical solution is obtained by solving two equations, I and IV, to determine two unknowns, F_i and e_o. In case (*b*) the smallest value for the prestressing force is obtained by solving IV and V; the corresponding analytical solution is obtained by solving IV for F_i, after replacing e_o by $(e_o)_{mp} = y_b - (d_c)_{\min}$.

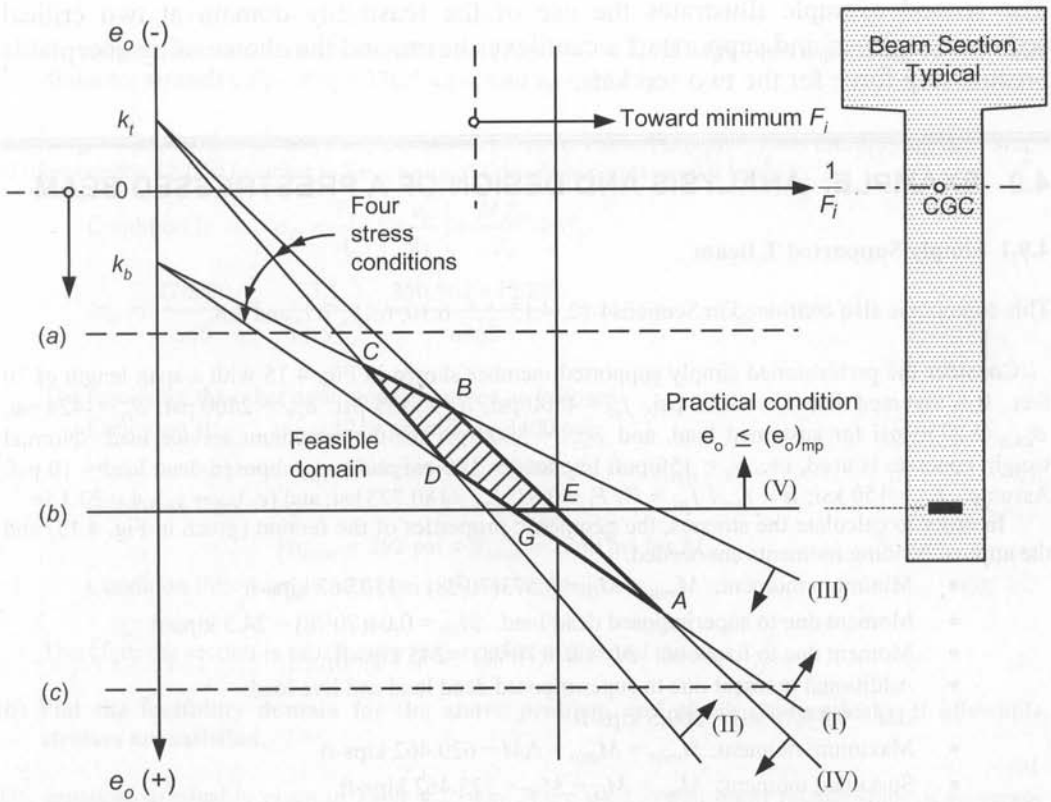

Figure 4.14 Feasibility domain defined by the stress inequality conditions.

Note that the geometric interpretation of the stress inequality conditions gives a very clear picture of the state of a given problem or what should be done about a particular problem. For example, in a given analysis or design problem, one can plot the feasibility domain and check if the proposed values of F and e_o are represented by a point that falls inside the domain; if it falls inside, there is no need to check the stresses; if it does not, one can spot right away the condition or conditions that are not satisfied and devise a corrective action. Other types of practical questions that can be best answered by using the above geometric representation are as follow:

1. Given an eccentricity e_o, what are the minimum and maximum feasible values of the prestressing force? The answer to this question could lead to finding a range of live loads which can be carried by a particular beam.
2. Given a prestressing force, what is the range of feasible eccentricities at a given section? This type of problem arises when, in a pretensioning bed, beams of different span lengths are prestressed simultaneously.

Two examples are treated next. In the first one, the geometric representation of the stress inequality conditions and the feasibility domain are used in both an investigation problem and a design problem where the concrete section is given. The second example illustrates the use of the feasibility domain at two critical sections (midspan and support) of a cantilever beam, and the choice of an acceptable prestressing force for the two sections.

4.9 EXAMPLE: ANALYSIS AND DESIGN OF A PRESTRESSED BEAM

4.9.1 Simply Supported T Beam

This example is also continued in Sections4.12, 4.15, 5.5, 6.10, 6.18, 7.7, and 7.8.

Consider the pretensioned simply supported member shown in Fig. 4.15 with a span length of 70 feet. It is assumed that f'_c = 5000 psi, f'_{ci} = 4000 psi, $\bar{\sigma}_{ti}$ = -189 psi, $\bar{\sigma}_{ci}$ = 2400 psi, $\bar{\sigma}_{ts}$ = -424 psi, $\bar{\sigma}_{csus}$ = 2250 psi for sustained load, and $\bar{\sigma}_{cs}$ = 3000 psi for the maximum service load. Normal weight concrete is used, i.e., γ_c = 150 pcf, live load = 100 psf and superimposed dead load = 10 psf. Assume: f_{pe} = 150 ksi; $\eta = f_{pe}/f_{pi} = F/F_i = 0.83$; f_{pi} = 180.723 ksi; and $(e_o)_{mp} = y_b - 4 = 23.1$ in.

In order to calculate the stresses, the geometric properties of the section (given in Fig. 4.15) and the applied bending moments are needed.

- Minimum moment: $M_{min} = M_G = 0.573(70^2/8) = 350.962$ kips-ft
- Moment due to superimposed dead load: $M_{SD} = 0.04(70^2/8) = 24.5$ kips-ft
- Moment due to live load: $M_L = 0.4(70^2/8) = 245$ kips-ft
- Additional moment due to superimposed dead load and live load: $\Delta M = 0.44(70^2/8) = 269.5$ kips-ft
- Maximum moment: $M_{max} = M_{min} + \Delta M = 620.462$ kips-ft
- Sustained moment: $M_{sus} = M_G + M_{SD} = 375.462$ kips-ft
- Prestressing steel: half-in diameter strands with a nominal tensile strength of 270 ksi

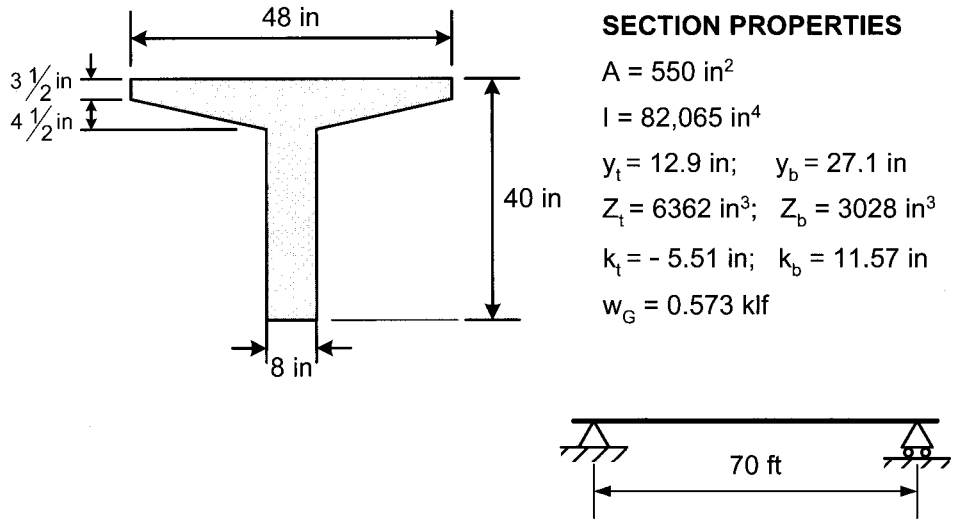

Figure 4.15

(a) Investigate flexural stresses at midspan given: F = 229.5 kips (corresponding to ten ½-in diameter strands), $F_i = F/\eta$ = 276.5 kips, and e_o = 23.1 in.

Referring to the four stress inequality equations given in Table 4.2 (way 1) and multiplying the values of moments by 12,000 in order to have units of pounds per square inch leads to:

$$\text{Condition I:} \qquad \sigma_{ti} = \frac{F_i}{A_c}\left(1 - \frac{e_o}{k_b}\right) + \frac{M_{min}}{Z_t} \geq \bar{\sigma}_{ti}$$

$$\sigma_{ti} = \frac{276500}{550}\left(1 - \frac{23.1}{11.57}\right) + \frac{350.962 \times 12000}{6362} \simeq 161 \text{ psi} > \bar{\sigma}_{ti} = -189 \text{ psi} \qquad \text{OK}$$

The results for the other conditions are given as follows:

Condition II: $\sigma_{ci} = 1219 \text{ psi} < \bar{\sigma}_{ci} = 2400 \text{ psi}$ OK

Condition III:
$$\begin{cases} \sigma_{cs} = 754 \text{ psi} < \bar{\sigma}_{cs} = 3000 \text{ psi for } M_{max} \\ \text{or} \\ \sigma_{csus} = 292 \text{ psi} < \bar{\sigma}_{csus} = 2250 \text{ psi for } M_{sus} \end{cases}$$ OK

Condition IV: $\sigma_{ts} = -292 \text{ psi} > \bar{\sigma}_{ts} = -424 \text{ psi}$ OK

Therefore the section is satisfactory with respect to flexural stresses.

(b) Plot the feasibility domain for the above problem and check geometrically if allowable stresses are satisfied.

The equations at equality given in Table 4.2 (way 2) are used to plot linear relationships of e_O versus $1/F_i$ on Fig. 4.16. They are reduced to the following convenient form, the first of which is detailed:

$$\text{Condition I:} \quad e_o \leq k_b + (1/F_i)(M_{\min} - \bar{\sigma}_{ti} Z_t) = 11.57 + (1/F_i)(350.962 \times 12000 + 189 \times 6362)$$

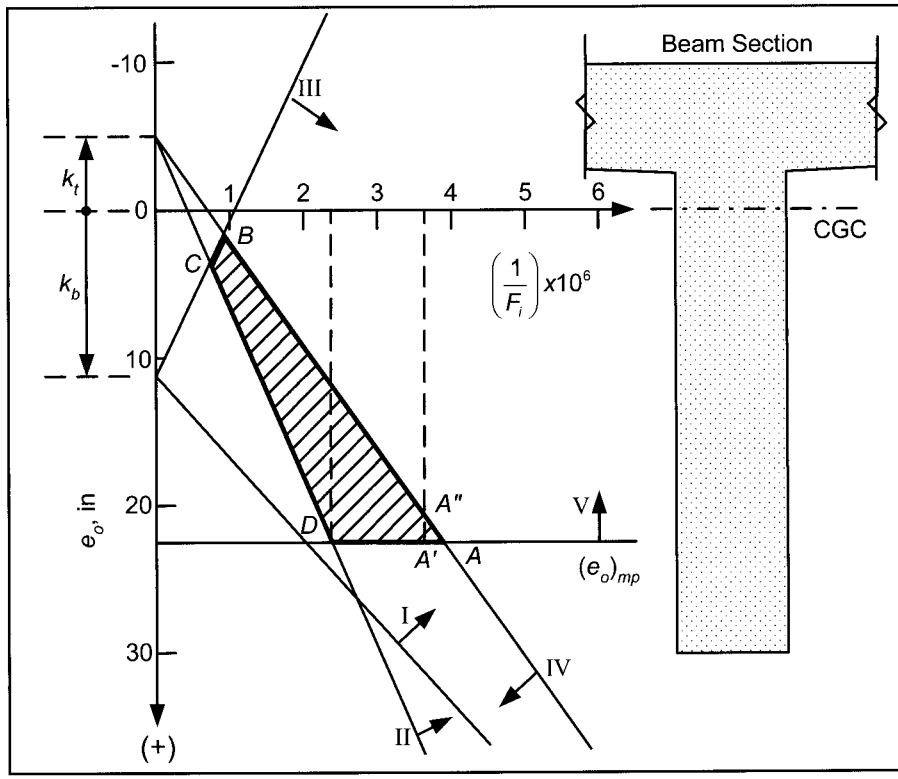

Figure 4.16 Feasibility domain for example 4.9.1.

which can be put in the following convenient form, for this as well as for the other conditions:

Condition I: $$e_o = 11.57 + 5.410\left(\frac{10^6}{F_i}\right)$$

Condition II: $$e_o = -5.51 + 11.4787\left(\frac{10^6}{F_i}\right)$$

Condition III:
$$\begin{cases} e_o = 11.57 - 14.024\left(\frac{10^6}{F_i}\right) & \text{for } M_{max} \\ e_o = 11.57 - 11.818\left(\frac{10^6}{F_i}\right) & \text{for } M_{sus} \Rightarrow \text{Controls} \end{cases}$$

Condition IV: $$e_o = -5.51 + 7.424\left(\frac{10^6}{F_i}\right)$$

where e_o is in inches and F_i is in pounds. Also equation V showing $(e_o)_{mp} = 23.1$ in is plotted in Fig. 4.16. The five lines delineate a feasibility domain *ABCD*.

Let us check if the given values of F_i and e_o are represented by a point which belongs to the feasible region:

$$\frac{1}{F_i} = \frac{1}{276,500} = 3.6 \times 10^{-6}$$

The representative point is shown in Fig. 4.16 as point *A'*. Since it is on line *AD*, it belongs to the feasible region and therefore all allowable stresses are satisfied. Note that all stresses would still be satisfied if the eccentricity is reduced to approximately 21 in for the same force. This is shown as point *A"* on line *AB* and allows the designer to accept a reasonable tolerance on the value of e_o actually achieved during the construction phase.

(c) Assuming the prestressing force is not given, determine its design value and corresponding eccentricity.

This is essentially a typical design problem where the concrete cross section is given. It can be solved directly analytically or from the graphical representation of the feasibility domain. In any case, the graphical representation helps in the analytical solution. It dictates the choice of point *A* of Fig. 4.16 as the solution that minimizes the prestressing force. Point *A* corresponds to the intersection of line V representing $(e_o)_{mp}$ with that representing stress condition IV. The corresponding value of F is obtained by replacing e_o by $(e_o)_{mp}$ in Eq. IV (way 3) of Table 4.2; that is:

$$F = \frac{M_{\max} + \bar{\sigma}_{ts} Z_b}{(e_o)_{mp} - k_t} = \frac{620.462 \times 12000 - 424 \times 3028}{23.1 + 5.51} = 215,368 \text{ lb}$$

and

$$F_i = \frac{F}{0.83} = 259,479 \text{ lb} \simeq 259.5 \text{ kips}$$

Graphically the coordinates of *A* can be read in Fig. 4.16 as $e_o = 23.1$ in and $1/F_i = 3.9 \times 10^{-6}$ which leads to $F_i \approx 257{,}000$ lb = 257 kips. It can be seen that the graphical solution gives essentially the same answer as the analytical one. Note that the practical value of the prestressing force to use in the design should correspond to an integer number of tendons. In this case, exactly 9.38 strands (1/2 in diameter, 270 ksi strength) each with a final force of 22.95 kips would be required. The number is rounded off to 10. The resulting higher prestressing force allows for an acceptable tolerance on the value of e_o, which can be varied now from 23.1 in to 21.33 in (see Table 4.5).

(d) If the beam is to be used with different values of live loads, what is the maximum value of live load it can sustain?

Referring to the stress inequality conditions, it can be observed that conditions I and II (which do not depend on the live load moment) do not change and therefore lines I and II of Fig. 4.16 are fixed. Increasing the value of the live load will increase the value of $M_{\max}$ and thus will change the slopes of lines III and IV so as to reduce the size of the feasible domain. Consequently, point *A* of the feasible domain will move in the direction of *AD* and line *BA* tends to rotate (about the intercept point k_t) toward *CD*. Similarly line III will rotate about the intercept, k_b, towards line I. The maximum value of live load correspond to the line that merges first with the other one. In this case, it is the live load that will make lines II and IV coincide or have same slopes. Therefore:

$$\frac{M_{max} + \bar{\sigma}_{ts} Z_b}{\eta} = 11.4787 \times 10^6$$

which leads to M_{max} = 10,811,193 lb-in = 900.93 kips-ft. Subtracting from M_{max} the values of moments due to dead load and superimposed dead load (375.462 kips-ft), leads to a live load moment of 525.468 kips-ft, from which the live load can be determined as 858 plf or 214.5 psf. The representative point in Fig. 4.16 is D which shows the following coordinates: e_o = 23.1 in and $10^6/F_i \simeq 2.5$, i.e., $F_i \simeq$ 400,000 lb = 400 kips. The reader is encouraged to check numerically in this case that the two allowable stresses $\bar{\sigma}_{ci}$ and $\bar{\sigma}_{ts}$ are attained exactly while the two others are satisfied, as indicated by the geometric representation. Note that such a design may have to be revised if the assumed value of e_o cannot be practically achieved. Note also that while the limit capacity of this prestressed beam in now attained from an allowable stress point of view, it can still be designed to carry a larger live load should partial prestressing be considered.

4.9.2 Simply Supported T Beam with Single Cantilever on One Side

Consider the same beam as in the previous example, that is, same section, same loading, same material properties, and same main span of 70 ft. However, assume that it has a cantilever on one side spanning 10 ft (Fig. 4.17a). Also assume that in addition to the dead and live loads already considered, a concentrated load of magnitude P = 30 kips is applied at the free end of the cantilever.

Plot the feasibility domain for the two critical sections (in span and at the right support) on the same graph and determine an acceptable prestressing force and its eccentricity at the two sections.

The dead and live loads have to be placed in such a way as to produce minimum and maximum moments at each critical section. In order to minimize the computations, only the condition for maximum service compression under maximum load will be considered; that is, the corresponding stress condition for allowable compression under sustained load will be ignored. In any case, these stresses generally do not control the design.

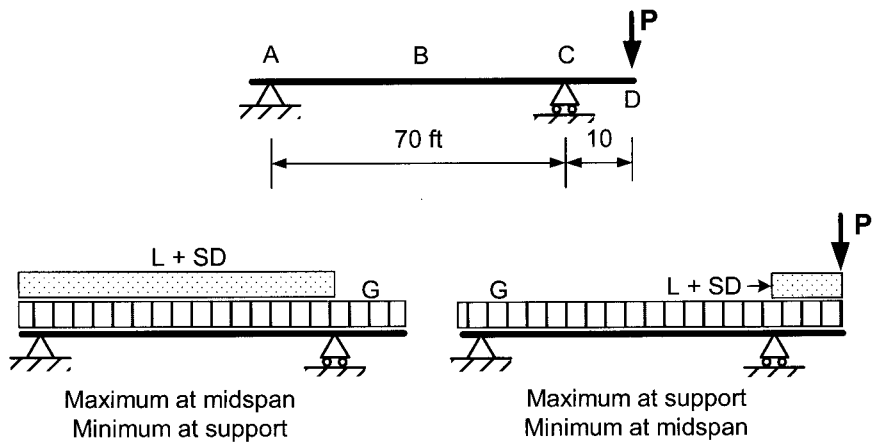

Figure 4.17a Loading arrangements leading to the maximum and minimum moments.

It can be shown that for the support section, C, the minimum moment is obtained when only the own weight of the beam is considered; the maximum moment is obtained when in addition to the own

weight of the beam, the concentrated load, P = 30 kips, the uniform live load and the additional uniform superimposed dead load are applied simultaneously. They lead to the following:

$M_{\min}$ = -28.65 kips-ft
$M_{\max}$ = -350.65 kips-ft

By placing the live load appropriately, it can be shown that the maximum moment in span occurs very near the midspan section, at 34.6 ft from the left support. The minimum moment occurs at 26.26 ft from the left support. However, for simplicity and in order to correlate with the previous example, the moments at the midspan section, B, are considered for the critical loading conditions. They are (Fig. 4.17a):

$M_{\min}$ = 336.65 kips-ft assuming initial loading, that is, while F_i is acting
$M_{\min}$ = 175.64 kips-ft assuming service loading, that is, while F is acting
$M_{\max}$ = 606.14 kips-ft

When F is present instead of F_i, the corresponding allowable stresses are the service stresses. To build the feasibility domain, the four inequality conditions, Way 2 of Table 4.2, are used. It can be shown that at the midspan section B:

I) $$e_o \le 11.57 + \frac{1}{F_i}(336.65\times10^3\times12 + 189\times6362)$$

$$e_o \le 11.57 + \frac{1}{F_i}(5,242,218)$$

II) $$e_o \le -5.51 + \frac{1}{F_i}(336.65\times10^3\times12 + 2400\times3028)$$

$$e_o \le -5.51 + \frac{1}{F_i}(11,307,000)$$

III) For the combination $M_{\max}$ and $\overline{\sigma}_{cs}$:

$$e_o \ge 11.57 + \frac{1}{0.83F_i}(606.14\times10^3\times12 - 3000\times6362)$$

$$e_o \ge 11.57 + \frac{1}{F_i}(-14,232,711)$$

IV) $$e_o \ge -5.51 + \frac{1}{0.83F_i}(606.14\times10^3\times12 - 424\times3028)$$

$$e_o \ge -5.51 + \frac{1}{F_i}(7,216,636)$$

V) $$e_o \le (e_o)_{mp} = 27.1 - 4 = 23.1 \text{ in}$$

Note that writing conditions I and II with $M_{\min}$ = 175.64 kips-ft, F instead of F_i, and the allowable service stresses instead of the allowable initial stresses, would lead in this example to two lines less critical than those obtained above.

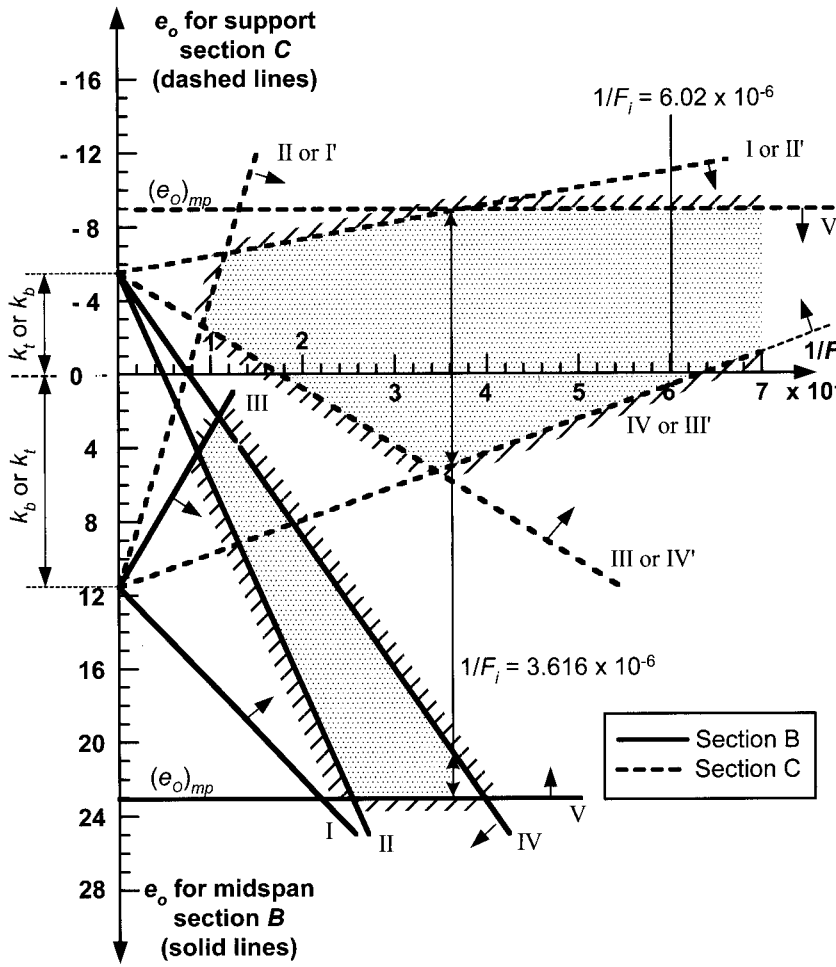

Figure 4.17b Feasible domains at the midspan and support sections for the cantilever beam of example 4.9.2 and Fig. 4.17a.

In order to obtain similar equations for the support section, C, we can invert the section, assume the moments are positive and use Table 4.2; or we can use Table 4.3 directly. The first approach is illustrated next. The properties of the inverted section are: $y_t = 27.1$ in; $y_b = 12.9$ in; $k_t = -11.57$; $k_b = 5.51$; $Z_t = 3028$; $Z_b = 6362$; $M_{\min} = 28.65$ kips-ft; $M_{\max} = 350.65$ kips-ft. Thus:

I) $$e_o \le 5.51 + \frac{1}{F_i}(28.65 \times 10^3 \times 12 + 189 \times 3028)$$

$$e_o \le 5.51 + \frac{1}{F_i}(916,092)$$

II) $e_o \le -11.57 + \frac{1}{F_i}(28.65\times10^3\times12 + 2400\times6362)$

$$e_o \le -11.57 + \frac{1}{F_i}(15,612,600)$$

III) $e_o \ge 5.51 + \frac{1}{0.83F_i}(350.65\times10^3\times12 - 3000\times3028)$

$$e_o \ge 5.51 + \frac{1}{F_i}(-5,874,940)$$

IV) $e_o \ge -11.57 + \frac{1}{0.83F_i}(350.65\times10^3\times12 - 424\times6362)$

$$e_o \ge -11.57 + \frac{1}{F_i}(1,819,653)$$

V) $e_o \le (e_o)_{mp} = 12.9 - 4 = 8.9$ in

The above equations taken at equality are plotted as straight lines (e_o versus $1/F_i$) in Fig. 4.17b. Note that for the support section (inverted), the positive direction for e_o is taken upward, and the corresponding k_t and k_b values (intercepts of the corresponding lines) are opposite to those of the midspan section.

It can be observed from the graph that the midspan section (B) governs the design. The intersection of lines IV and V at B leads to the minimum required prestressing force:

$$F = \frac{606.14\times12000 - 424\times3028}{23.1 + 5.51} = 209,360 \text{ lb} = 209.36 \text{ kips}$$

The corresponding number of strands is

$$N = \frac{209.36}{150\times0.153} = 9.12 \quad \text{thus select } N = 10 \text{ strands and } F = 229.5 \text{ kips}$$

The vertical line drawn in Fig. 4.17b for F = 229.5 kips, or $1/F_i = 3.616\text{x}10^{-6}$ shows that this force can be placed at an eccentricity at midspan (section B) ranging from 20.59 in to 23.1 in, and an eccentricity at the support (Section C) ranging from +4.99 in to –8.82 in. An example of strand layout for the midspan section is described in Section 4.12.3. For the support section, a solution can be achieved for instance by keeping 4 tendons straight throughout the beam even at the support C, and draping the remaining 6 tendons so that they have an eccentricity at the support equal –8.9 in. The resulting eccentricity of the 10 strands at the support would be e_o = 4.3 in, positive, but within the acceptable range (-8.82 to 4.99) at the support. To improve the eccentricity at the support, the four straight strands could be sheathed, thus unbonded along the cantilever portion. The remaining 6 strands would have an eccentricity e_o = -8.9 in at the support, and the corresponding vertical line for $1/F_i = 6.02\text{x}10^{-6}$ (Fig. 4.17b) shows that such a combination of force and eccentricity is acceptable at the support.

As mentioned earlier, the complementary inequality conditions given in Table 4.3 could have been used directly to obtain the feasibility domain of the support section. Indeed using Table 4.3 with the proper sign convention for the eccentricity and the moments leads to:

I′) $e_o \geq 11.57 + \frac{1}{F_i}(-28.65\times10^3\times12 - 2400\times6362)$

$$e_o \geq 11.57 - \frac{1}{F_i}(15{,}612{,}600)$$

II′) $e_o \geq -5.51 + \frac{1}{F_i}(-28.65\times10^3\times12 - 189\times3028)$

$$e_o \geq -5.51 - \frac{1}{F_i}(916{,}092)$$

III′) $e_o \leq 11.57 + \frac{1}{0.83F_i}(-350.65\times10^3\times12 + 424\times6362)$

$$e_o \leq 11.57 - \frac{1}{F_i}(1{,}819{,}653)$$

IV′) $e_o \leq -5.51 + \frac{1}{0.83F_i}(-350.65\times10^3\times12 + 3000\times3028)$

$$e_o \leq -5.51 + \frac{1}{F_i}(5{,}874{,}940)$$

V′) $|e_o| \leq |(e_o)_{mp}| = 12.9 - 4 = 8.9$ in $\Rightarrow e_o \geq -8.9$ in

If we assume that e_o is positive downward and negative upward, the above equations plotted at equality coincide exactly with the equations plotted in Fig. 4.17b for the support section.

4.10 USE OF THE STRESS INEQUALITY CONDITIONS FOR THE DESIGN OF SECTION PROPERTIES

It has been shown in the preceding two sections that in order to determine feasible values of F and e_o the stress inequality conditions can be used: (1) in an investigation problem to check if allowable stresses are satisfied, and (2) in a design problem where the concrete cross section is known. Since there are four stress inequality conditions, one can attempt to use them at equality to determine four unknowns, namely, F, e_o, and two others related to the dimensions or geometric properties of the section. Generally, the two section moduli Z_t and Z_b are sought because they do not necessarily relate to any particular shape of the section.

It is important to understand that here it is the main objective of the design to use the most efficient beam cross section, i.e., the smallest possible section moduli. Once a satisfactory section has been selected, the objective becomes to minimize the required prestressing force (or maximize the eccentricity).

To minimize the computational effort, only one equation will be considered for stress condition III, using the combination $\bar{\sigma}_{cs}$ and M_{max}. However, the approach can be similarly followed using $\bar{\sigma}_{csus}$ and M_{sus}. The final result could be checked for either case. Let us assume that we have a cross section such that at the critical

(say midspan) section of the beam the two allowable stresses $\bar{\sigma}_{ti}$ and $\bar{\sigma}_{ci}$ are attained exactly under initial loading. Referring to Fig. 4.18a, this means that under initial loading (F_i + $M_{\min}$) the flexural stress diagram along the section is represented by line *ab*.

Let us assume that prestress losses occur suddenly (or, equivalently, that time is allowed to pass so that prestress losses happen instantly) and that the loading becomes (F + $M_{\min}$), thus leading to a stress diagram represented by line *a'b'*. If an additional moment is applied, the stress diagram tends to rotate around point Ω, which represents the neutral axis of bending. Let us assume that such an additional moment is the moment increment $\Delta M = M_{\max} - M_{\min}$. If under the action of ΔM the two allowable stresses $\bar{\sigma}_{ts}$ and $\bar{\sigma}_{cs}$ are not attained, it indicates that the section moduli Z_t and/or Z_b of the section are larger than required (as $\Delta\sigma = \Delta M/Z$). Similarly, if the two allowable stresses are exceeded, it indicates that the section moduli are smaller than required. One can therefore attempt to determine the minimum required values of Z_t and Z_b for which the allowable stresses would be attained exactly.

Referring to Fig. 4.18b where the flexural stress diagrams of the steps assumed above are represented separately, let us, for example, determine the stresses on the top fiber.

For the initial loading (F_i + $M_{\min}$) we have:

$$\frac{F_i}{A_c}\left(1-\frac{e_o A_c}{Z_t}\right)+\frac{M_{\min}}{Z_t}=\bar{\sigma}_{ti} \tag{4.4}$$

Assuming that all prestress losses have occurred leads to a loading (F + $M_{\min}$) for which:

$$\frac{\eta F_i}{A_c}\left(1-\frac{e_o A_c}{Z_t}\right)+\frac{M_{\min}}{Z_t}=\sigma_1 \tag{4.5}$$

which can also be written as:

$$\eta\left[\frac{F_i}{A_c}\left(1-\frac{e_o A_c}{Z_t}\right)+\frac{M_{\min}}{Z_t}\right]-\frac{\eta M_{\min}}{Z_t}+\frac{M_{\min}}{Z_t}=\sigma_1 \tag{4.6}$$

Using Eq. (4.4) into Eq. (4.6) gives:

$$\eta\bar{\sigma}_{ti}+\frac{M_{\min}(1-\eta)}{Z_t}=\sigma_1 \tag{4.7}$$

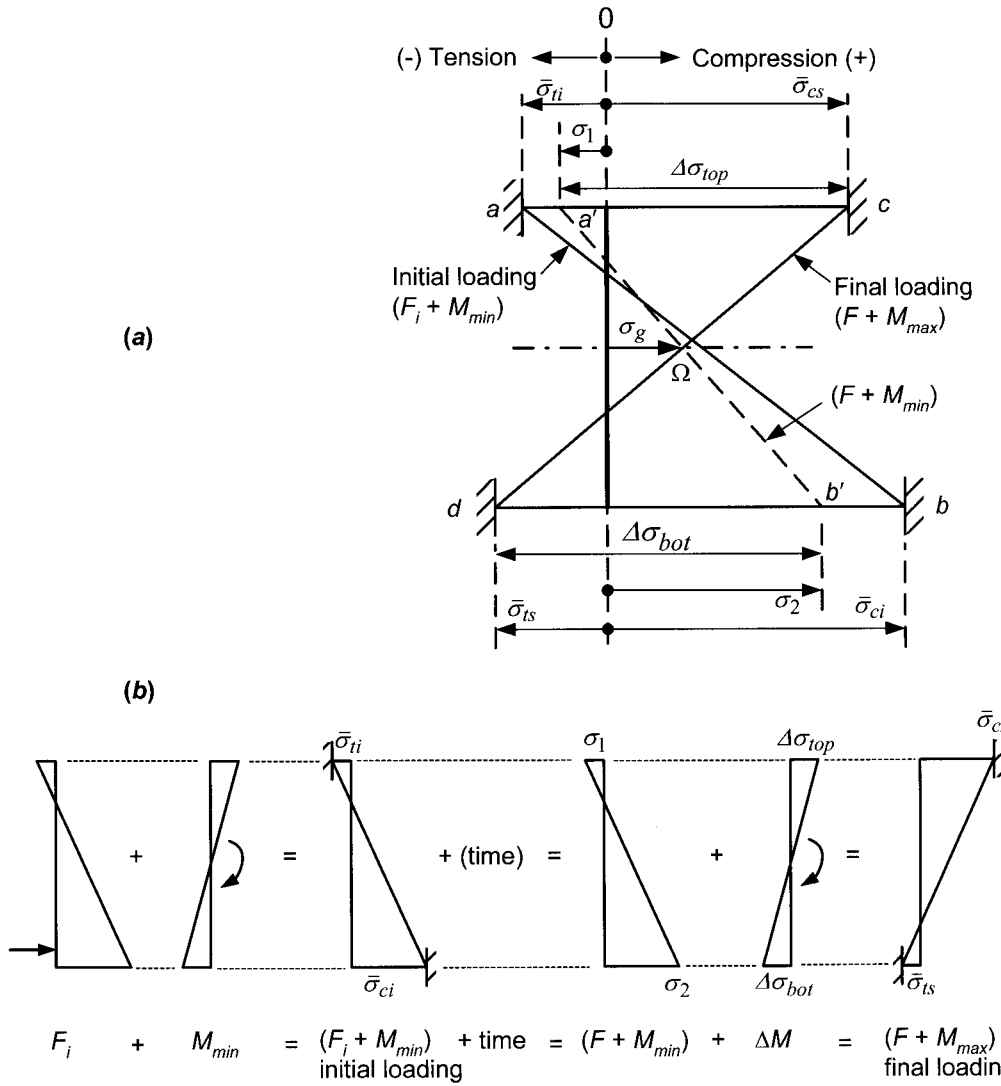

Figure 4.18 Conditions for most efficient use of beam section.

If we add a moment amplitude ΔM to the section, the corresponding additional stress on the top fiber will be:

$$\Delta\sigma_{top} = \frac{\Delta M}{Z_t} \tag{4.8}$$

The resulting stress due to the combined effect of ($F + M_{\min}$) and ΔM must be less than or equal to the allowable compressive stress $\bar{\sigma}_{cs}$, i.e.,

$$\sigma_1 + \Delta\sigma_{top} \le \bar{\sigma}_{cs} \tag{4.9}$$

Using Eqs. (4.7) and (4.8) in Eq. (4.9) gives:

$$\eta\bar{\sigma}_{ti} + \frac{M_{\min}(1-\eta)}{Z_t} + \frac{\Delta M}{Z_t} \le \bar{\sigma}_{cs} \tag{4.10}$$

Noting that $M_{\min} + \Delta M = M_{\max}$, Eq. (4.10) leads to:

$$\boxed{Z_t \ge \frac{M_{\max} - \eta M_{\min}}{\bar{\sigma}_{cs} - \eta\bar{\sigma}_{ti}}} \tag{4.11}$$

By similarly examining the state of stress on the bottom fiber, it can be shown that:

$$\boxed{Z_b \ge \frac{M_{\max} - \eta M_{\min}}{\eta\bar{\sigma}_{ci} - \bar{\sigma}_{ts}}} \tag{4.12}$$

Equations (4.11) and (4.12) have been first derived by Guyon [Refs. 4.6-4.7] and expanded thereafter by Nilson [Ref. 4.14] and the author [Ref. 4.15].

Equations (4.11) and (4.12) also can be rewritten in terms of ΔM and $M_{\min}$ as follows:

$$\boxed{Z_t \ge \frac{\Delta M + (1-\eta)M_{\min}}{\bar{\sigma}_{cs} - \eta\bar{\sigma}_{ti}}} \tag{4.13}$$

$$\boxed{Z_b \ge \frac{\Delta M + (1-\eta)M_{\min}}{\eta\bar{\sigma}_{ci} - \bar{\sigma}_{ts}}} \tag{4.14}$$

The advantage of this form is that it separates ΔM, which is independent of the beam cross section, from $M_{\min}$, which is generally equal to the dead-weight moment of the beam. Equations (4.11) and (4.12) or, equivalently, Eqs. (4.13) and (4.14) can be used in combination with up to two other stress inequality conditions to determine Z_t, Z_b, F, and e_o.

The above treatment leading to Eqs. (4.11) to (4.14) assumed only one set of values for the maximum moment and allowable compressive stress in service, namely $M_{\max}$ and $\bar{\sigma}_{cs}$. To satisfy the 2002 ACI Code, similar equations could be

developed for another set of values corresponding to M_{sus} and $\bar{\sigma}_{csus}$. The more critical set will control the design.

Note that the required values of Z_t and Z_b given by Eqs. (4.11) and (4.12) are functions of $M_{\min}$ (i.e., the dead load moment in this case), which itself depends on the weight of the section; knowing the weight of the section implies the knowledge of section dimensions, thus the values of Z_t and Z_b. In general, to start the design, a solution for the required values of Z_t and Z_b is obtained by assuming a cross section (and corresponding $M_{\min}$) and through a number of rapidly converging iterations. As observed earlier, the required values of Z_t and Z_b apply no matter what the shape of the cross section of concrete is. It can be shown, however, that the simpler the shape of the section, such as a slab, the easier it is to obtain a satisfactory solution [Ref. 4.15]. This is discussed in more details in the chapter on optimum design in Ref. 1.48.

The determination of a cross section of concrete having the minimum required values of Z_t and Z_b guarantees a feasibility domain for the prestressing force and its eccentricity (Fig. 4.14). This domain may be as small as a single point for which the four stress conditions are satisfied. However, the presence of a feasible domain satisfying the four allowable stress inequality conditions does not guarantee that the domain or part of it falls inside the cross section so as to allow the prestressing steel to be placed inside the beam. (Note: this may not be binding in the case of external prestressing.)

One additional requirement must therefore be satisfied, that is, that the eccentricity of the prestressing force is less than or equal to the maximum practical value set in design. Generally, once a beam cross section has been selected the practicality condition V (Table 4.2) is checked; if it is not satisfied, such as in case (*a*) of Fig. 4.14, the cross section dimensions must be changed accordingly. This will invariably lead to increases in section properties.

Once a satisfactory cross section of concrete has been selected either by direct solution or from a list of standard sections, the determination of F and e_o is achieved according to Sections 4.8 and 4.9.

Note that finding a concrete cross section with section moduli both exactly equal to those required may not be possible if a specific shape of cross section is desired. This happens, for example, if both required design values of Z_t and Z_b are equal and if a T section (unequal geometric properties) is desired, or if both values are unequal and a rectangular section is desired. Generally, it is possible to determine a section with one of the section moduli exactly equal to that required, while the other is larger than required.

The determination of section moduli Z_t and Z_b of a trial section, nonrectangular in shape, can be time consuming. Charts may be prepared to expedite the design at least during the trial-and-error phase. Such a chart (Fig. 4.19) has been developed for use with idealized I and box sections and applies (at the limit) to T and inverted T sections as well. It can be used (1) to estimate the section moduli of a concrete cross

section with given dimensions, or (2) to estimate the dimensions of a potential concrete section given required values of section moduli.

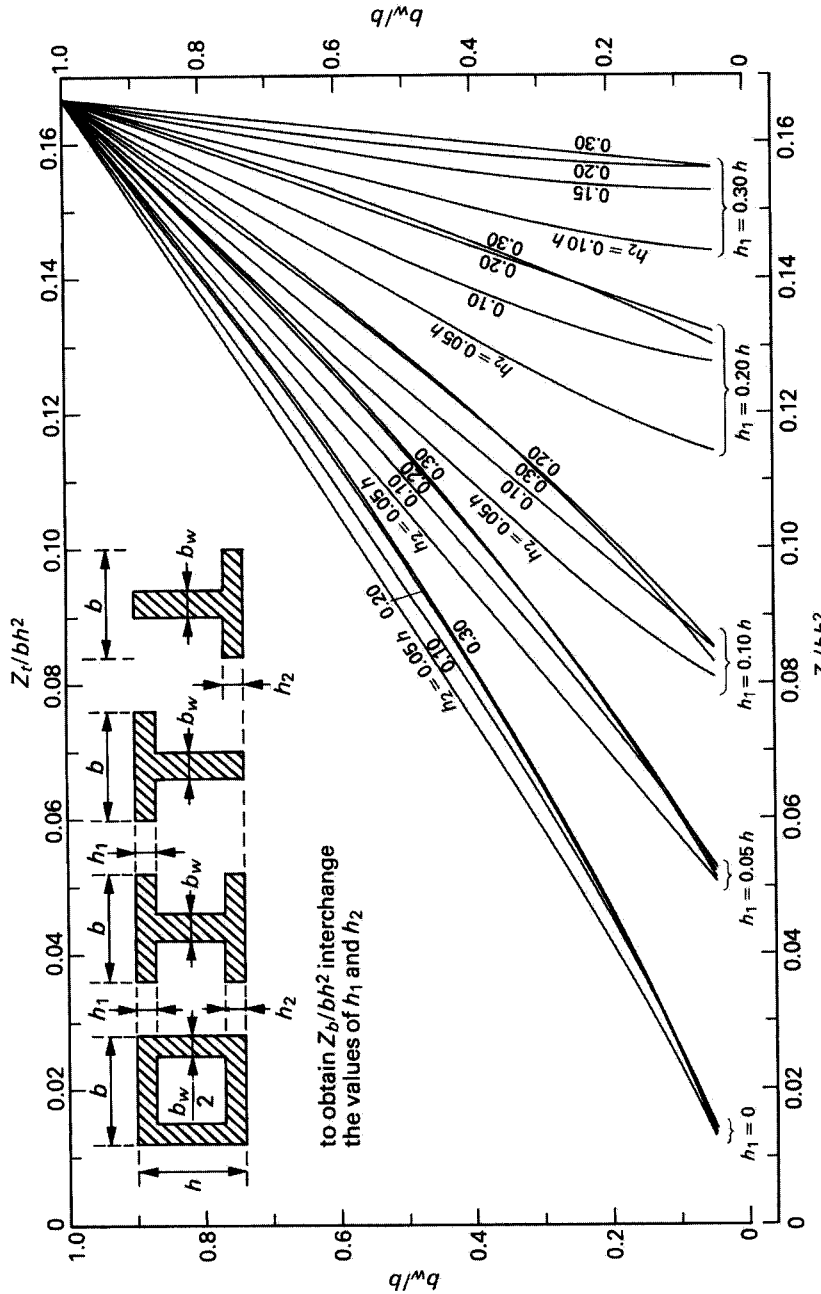

Figure 4.19 Chart to estimate section moduli of typical sections.

Although the methodology described in this chapter aims at using the most efficient cross section (or equivalently the least weight beam), it may not necessarily lead to a least cost design. However, for currently prevailing unit costs of conventional materials, steel and concrete, it seems to lead to a near minimum cost solution. More on minimum weight versus minimum cost designs can be found in Ref. 1.48.

4.11 EXAMPLES OF USE OF MINIMUM SECTION PROPERTIES

As mentioned in the previous section, the determination of a concrete cross section with section moduli equal to those required leads to a minimum weight beam. Three examples are treated next and illustrate the methodology used and the level of difficulties that may be encountered. The allowable stresses used do not necessarily correspond to a code value; only one combination for stress condition III is considered, the one corresponding to the allowable compression stress and the maximum service moment. The condition for sustained load could be considered instead, if controlling.

4.11.1 Minimum Weight Slab

Consider a simply supported prestressed slab with a span of $l = 40$ ft and:

$\bar{\sigma}_{ti} = -189$ psi $\quad \bar{\sigma}_{ci} = 2400$ psi

$\bar{\sigma}_{ts} = 0 \quad \bar{\sigma}_{cs} = 2250$ psi

$\eta = F / F_i = 0.80$

$(e_o)_{mp} = y_b - 3$

$\gamma_c = 150\ pcf$

$$I_g = \frac{bh^3}{12}$$

$$Z = Z_t = Z_b = \frac{bh^2}{6}$$

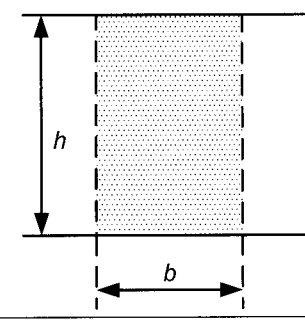

Figure 4.20*a* Slab section.

Design the least weight slab section assuming a live load of 500 psf (Fig. 4.20*a*).

Referring to the required section moduli given by Eqs. (4.11) and (4.12) it can be observed that both have the same numerator. As a slab, by symmetry, must have the same values of section moduli, the higher value obtained from Eqs. (4.11) and (4.12) will control; the controlling value corresponds to the equation with the smaller denominator. Let us call:

$$\left.\begin{array}{l}\Delta\bar{\sigma} = \text{the smaller of } \bar{\sigma}_{cs} - \eta\bar{\sigma}_{ti} = 2401\,\text{psi} \\ \qquad\qquad \text{and } \eta\bar{\sigma}_{ci} - \bar{\sigma}_{ts} = 1920\,\text{psi}\end{array}\right\} = 1920\ psi$$

thus the minimum required values of section moduli for the slab will be given by:

$$Z = \frac{M_{\max} - \eta M_{\min}}{\Delta\bar{\sigma}}$$

Let us assume that $M_{\min} = M_G$ at the midspan of the slab, and that $M_{\max} = M_G + \Delta M$ = moment due to dead load plus live load (and/or any additional load). The controlling value of Z can be written as:

$$Z = \frac{\Delta M}{\Delta\bar{\sigma}} + \frac{(1-\eta)M_G}{\Delta\bar{\sigma}}$$

But for a simply supported slab section of dimensions b and h, we have the following:

$$M_G = \gamma_c \frac{bhl^2}{96}$$

$$Z = \frac{bh^2}{6}$$

where γ_C is in pounds per cubic foot, b and h in inches, l in feet, and M in pound-inches. Replacing M_G and Z by their values in the above equation leads to:

$$\frac{bh^2}{6} = \frac{\Delta M}{\Delta\bar{\sigma}} + \frac{(1-\eta)}{\Delta\bar{\sigma}}\gamma_c \frac{bhl^2}{96}$$

which could be written as quadratic equation in h:

$$h^2\frac{b}{6} - h\frac{(1-\eta)\gamma_c bl^2}{96\Delta\bar{\sigma}} - \frac{\Delta M}{\Delta\bar{\sigma}} = 0$$

Note that this equation has two roots, one of them positive.
If we use a unit width for the slab, say b = 12 in, the positive root is given by:

$$h = \frac{1}{4}\left(\frac{(1-\eta)\gamma_c l^2}{8\Delta\bar{\sigma}} + \sqrt{\left[\frac{(1-\eta)\gamma_c l^2}{8\Delta\bar{\sigma}}\right]^2 + \frac{8\Delta M}{\Delta\bar{\sigma}}}\right)$$

which for our example with the values of l in feet and ΔM = live load moment = 1,200,000 lb-in, leads to:

$h = 18.47 \simeq 18.5$ in

The corresponding values of M_G, $M_{\max}$ and Z are:

M_G = 555,000 lb-in
$M_{\max}$ = 1,755,000 lb-in
Z = 684.5 in^3

One can check that the controlling required value of Z from Eq. (4.11) leads to about the same result as above.

It can be shown that the feasible domain for this slab section is similar to case (c) of Fig. 4.14; the corresponding minimum value of F is obtained from the coordinates of point A, intersection of lines I and IV for which $F = 195{,}797$ lb and $e_o = 5.88$ in.

Note that the determination of h as shown in this example does not guarantee that the feasible domain or part of it falls inside the concrete section so as to allow the prestressing steel to be placed inside the beam. Such a case may occur when the magnitude of the live load moment is small compared to that of the dead load moment. The general solution of this problem, for slabs and rectangular beams, is provided in Ref. 1.48.

4.11.2 Minimum Weight Beam

Consider a simply supported prestressed beam with a span $l = 40$ ft and:

$\bar{\sigma}_{ti} = -189$ psi $\quad \bar{\sigma}_{ci} = 2400$ psi

$\bar{\sigma}_{ts} = 0 \quad \bar{\sigma}_{cs} = 2250$ psi

$\eta = F / F_i = 0.80$

$(e_o)_{mp} = y_b - 3$

$\gamma_c = 150\ pcf$

Design a least weight beam section assuming the same live load moment as in the previous example, that is, $\Delta M = 1{,}200{,}000$ lb-in.

The required values of Z_b from Eq. (4.14) can be written as:

$$Z_b \geq \frac{\Delta M}{\eta\bar{\sigma}_{ci} - \bar{\sigma}_{ts}} + \frac{(1-\eta)M_G}{\eta\bar{\sigma}_{ci} - \bar{\sigma}_{ts}} = \frac{1{,}200{,}000}{1920} + \frac{0.2\,M_G}{1920}$$

or

$$Z_b \geq 625 + \frac{M_G}{9600}$$

and similarly from Eq. (4.13) we get:

$$Z_t \geq 500 + \frac{M_G}{12{,}005}$$

As the required value of Z_b is larger than that of Z_t, an inverted T section can be considered for the design.

The actual determination of Z_b and Z_t requires trial-and-error procedures and a few iterations, since the value of M_G is unknown.

In this case it is desirable to assume a depth h for the cross section and a web width b_w so as to achieve values of section moduli for a rectangular section ($h \times b_w$) slightly smaller than those required. A few iterations are necessary. Figure 4.19 can be used.

For the present example the following values were found adequate: $h = 22$ in, $b_w = 6$ in, to which a net bottom flange of 4×6 in was added; the cross section obtained has the geometric properties given in Fig. 4.20*b*. The corresponding dead load moment at midspan is:

$M_G = 390{,}000$ lb-in.

It can be checked that the required values of Z_b and Z_t, as derived from Eqs. (4.14) and (4.13), are equal to 665.6 in^3 and 532.5 in^3, respectively, and are slightly smaller than those provided; thus the proposed beam section seems adequate.

A_c = 156 in^2	I = 6693 in^4
y_b = 9.77 in	y_t = 12.23 in
Z_t = 547 in^3	Z_b = 685 in^3
k_t = -4.39 in	k_b = 3.51 in
w_G = 0.1625 klf	

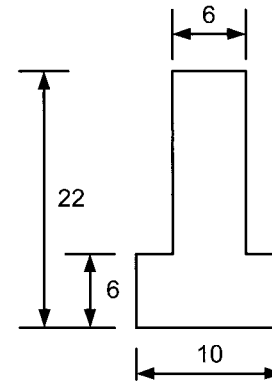

Figure 4.20*b* Optimum beam section.

It can be shown that the feasible domain for this section is similar to case (c) of Fig. 4.14; the corresponding minimum value of F is equal to 151,284 lb for an eccentricity $e_o \simeq 7$ in. Here, too, note that the determination of cross section dimensions as shown above does not always guarantee that the feasible domain or part of it falls inside the concrete section so as to place the prestressing reinforcement inside the beam.

4.11.3 Selection of Optimum Beam from a Given Set of Beams

A slab deck is composed of simply supported standard precast pretensioned double T concrete beams to be obtained from a local supplier (Fig. 4.20c). Typical cross section and available dimensions are given in Table 4.4 and Fig. 4.20c. These are made with lightweight concrete of unit weight 115 pcf. (See also Pb. 4.6 and Table P4.6 for a similar example with normal weight concrete.)

Other information is given as follows: f'_c = 5000 psi f'_{ci} = 3750 psi; span = 60 ft; $\bar{\sigma}_{ti} = -184$ psi; $\bar{\sigma}_{ci} = 2250$ psi; $\bar{\sigma}_{cs} = 2250$ psi; $\bar{\sigma}_{ts} = -424$ psi; η = 0.85; $(e_o)_{mp} = y_b$ - 3.5 in; superimposed dead load plus live load = 75 psf; f_{pe} = 155 ksi; area of one strand = 0.153 in^2. Select the least weight beam which satisfies the working stress design requirements in flexure and determine the corresponding values of F and e_o at midspan.

For any beam in the table:

$$M_{\min} = M_G = W_G \frac{l^2}{8} = W_G \frac{60^2}{8} = 450 W_G \text{ kips-ft where } W_G \text{ is in klf}$$

$$M_G = 5400 W_G \text{ where } W_G \text{ is in plf (as in the table) and } M_G \text{ is in lb-in}$$

$$M_{\max} = M_G + M_L = M_G + \Delta M$$

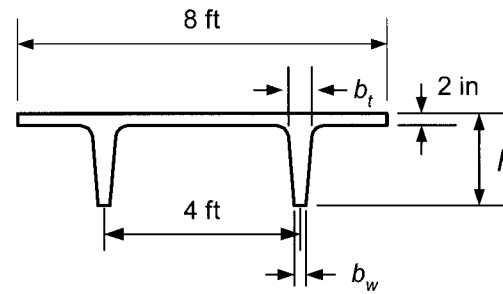

Figure 4.20c Standard precast section.

Table 4.4 Properties of standard sections considered (lightweight concrete).

h in	b_t in	b_w in	A in^2	I in^4	y_t in	y_b in	Z_t in^3	Z_b in^3	W_G plf
16	8.00	6.00	388	8,944	4.87	11.13	1,837	804	310
18	9.75	7.75	472	14,623	6.16	11.84	2,374	1,235	377
20	9.75	7.50	503	19,354	6.94	13.06	2,789	1,482	401
24	9.75	7.00	560	31,192	8.49	15.51	3,674	2,011	447
32	8.00	4.00	549	51,286	10.29	21.71	4,984	2,362	439

For a floor live load of 75 psf, the beam live load per linear foot is: 8x75 = 600 plf = 0.6 klf. Thus:

$$\Delta M = 0.6\frac{60^2}{8} = 270 \text{ kips-ft} = 3{,}240{,}000 \text{ lb-in}$$

From Eqs. (4.13) and (4.14) the required section moduli must be such that:

$$Z_b \geq \frac{\Delta M + (1-\eta)M_{\min}}{\eta\bar{\sigma}_{ci} - \bar{\sigma}_{ts}} = \frac{3240000 + (1-0.85)M_G}{0.85 \times 2250 + 424} = \frac{3240000 + 0.15M_G}{2336.5}$$

$$Z_b \geq \frac{3240000 + 0.15 \times 5400W_G}{2336.5} = 1386.7 + 0.3467W_G$$

$$Z_t \geq \frac{\Delta M + (1-\eta)M_{\min}}{\bar{\sigma}_{cs} - \eta\bar{\sigma}_{ti}} = \frac{3240000 + 0.15M_G}{2406.4}$$

$$Z_t \geq \frac{3240000 + 0.15 \times 5400W_G}{2406.4} = 1346.4 + 0.3366W_G$$

From Table 4.4, check if the given beams have section moduli that satisfy the above inequalities. The beams of depth 16 in and 18 in have a Z_b smaller than the above required value. They are not acceptable.

Try the next beam with h = 20 in, and W_G = 401 plf.
Actual Z_b = 1482 in^3
Minimum required $Z_b \geq$ 1386.7 + 0.3467xW_G
= 1386.7 + 0.3467x401 = 1525.72 in^3 Not good.

Try the next beam with h = 24 in, and W_G = 447 plf.
Actual Z_b = 2011 in^3
Minimum required $Z_b \geq$ 1386.7 + 0.3467xW_G
= 1386.7 + 0.3467x447 = 1541.67 in^3 O.K.
Actual Z_t = 3674 in^3
Minimum required $Z_t \geq$ 1346.4 + 0.3366xW_G
= 1346.4 + 0.3366x447 = 1496.86 in^3 O.K.

Hence the beam with h = 24 in is acceptable for the problem at hand. Note that since the next beam of depth h = 32 is slightly lighter (439 plf versus 447 plf) it is also acceptable. The choice of either beam may be dictated by architectural considerations such as minimum depth.

The above trial and error procedure would work also even if the first iteration were started with $W_G = 0$, that is not knowing where to start from a widely available set of beams. The procedure also allows to slowly build up a beam with geometric section moduli that satisfy the mechanical requirements.

The reader may want to check that for the above beam with $h = 24$ in, there is a feasible domain with a minimum prestressing force determined by stress condition IV and the maximum practical eccentricity. For the final design, a prestressing force of 332 kips (14 half-in diameter strands, 7 in each web) at an eccentricity of 11.01 in is used. The eccentricity is sufficient to allow the practical placement of the tendons.

4.12 LIMITING THE ECCENTRICITY ALONG THE SPAN

Once the required prestressing force and its eccentricity have been determined at the critical section, it is generally assumed that the same force will be used throughout the span. Thus there is a need to determine the limiting eccentricities of a known force at any section along the span so that none of the allowable stresses are violated. One way to do this is to build the feasibility domain (such as in Figs. 4.16 and 4.17) at several sections and select the upper and lower limits of eccentricities acceptable for a given prestressing force. However, this procedure is very tedious. A more elegant method is developed next. It requires first defining the limit kern.

4.12.1. Limit Kern Versus Central Kern

The central kern area of a section is a region within which an axial compressive force of any magnitude will not produce any tension in the section. The central kern of a rectangular section has a diamond shape and spans the middle third (one sixth on each side of the axis) of the section in either of the principal directions (Fig. 4.21a). The upper and lower limits of the central kern in the y direction have been defined in Sec. 4.4 as k_t and k_b, and can be determined for any type of cross section. For the same cross section throughout the span, they remain constant. It is observed that the central kern depends on the geometry of the section but is independent of the applied compressive force or the allowable stresses. The limit kern, however, accounts for these variables.

The limit kern is the area of the section within which an axial compressive force of a given magnitude can be placed without violating any of the allowable stresses (tension or compression). For the same cross section, force, allowable stresses, and moment sign (that is, either all moments are positive or all moments are negative), the limit kern remains the same throughout the span. The limit kern can be considered as bounding the geometric lieu of the resultant compression force (C line or pressure line) along the beam.

It was stated in Sec. 4.2 that the combined effect of an axial force $C = F$ and an externally applied moment M is equivalent to that of a force C displaced a distance $\delta = M/F$ from the line of action of F. The position of C with respect to the centroid of

the section can be characterized by an eccentricity e_c. It is easily shown (Fig. 4.6*c*) that:

$$e_c = e_o - \frac{M}{F} \tag{4.15}$$

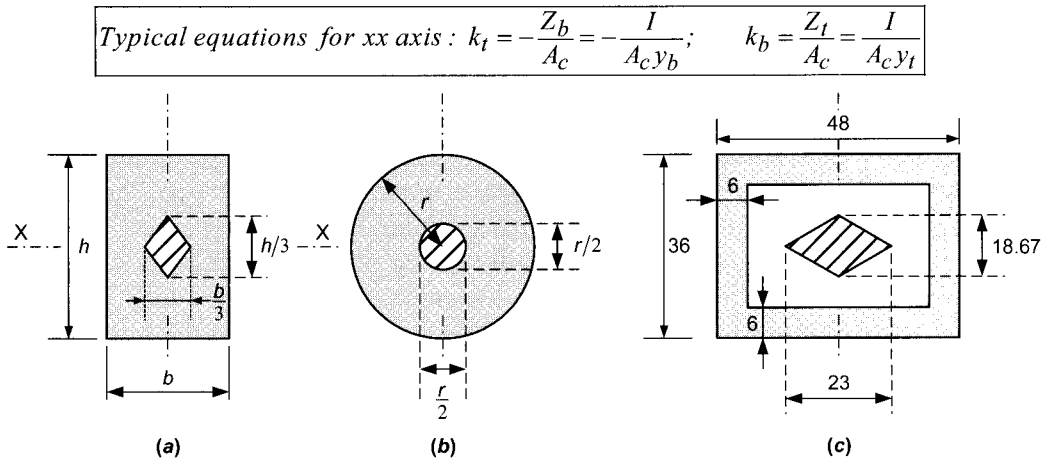

Figure 4.21 Central kern shape and size for: (*a*) Typical rectangular section; (*b*) Typical circular section; (*c*) Actual box section.

Note that, since e_o and M generally vary along the span, e_c also varies. In statically determinate structures e_c becomes equal to e_o when no external loading is applied. This is not the case for statically indeterminate structures (Chap. 10).

Similarly to the central kern, the limit kern is bound by an upper and a lower limit k'_t and k'_b, respectively. Their values can be determined as shown next from the four stress inequality conditions given in Table 4.2, assuming all applied moments are positive.

Let us first define the stresses at the centroid of the concrete section under the effect of initial force F_i and final or effective force F:

$$\begin{cases} \sigma_{gi} = \dfrac{F_i}{A_c} \\ \sigma_g = \dfrac{F}{A_c} = \dfrac{\eta F_i}{A_c} \end{cases} \tag{4.16}$$

The first stress inequality condition of Table 4.2 can be written as:

$$e_o - \frac{M_{\min}}{F_i} \le k_b - \frac{\bar{\sigma}_{ti} Z_t}{F_i} \tag{4.17}$$

Replacing Z_t by $k_b A_c$ and using the definition of σ_{gi} from Eq. (4.16) in Eq. (4.17) gives:

$$e_o - \frac{M_{\min}}{F_i} \le k_b \left(1 - \frac{\bar{\sigma}_{ti}}{\sigma_{gi}}\right) \tag{4.18}$$

Similarly, the three other stress inequality conditions lead to:

$$e_o - \frac{M_{\min}}{F_i} \le k_t \left(1 - \frac{\bar{\sigma}_{ci}}{\sigma_{gi}}\right) \tag{4.19}$$

$$e_o - \frac{M_{\max}}{\eta F_i} \ge k_b \left(1 - \frac{\bar{\sigma}_{cs}}{\sigma_g}\right) \tag{4.20}$$

$$e_o - \frac{M_{\max}}{\eta F_i} \ge k_t \left(1 - \frac{\bar{\sigma}_{ts}}{\sigma_g}\right) \tag{4.21}$$

The left-hand sides of Eqs. (4.18) to (4.21) represent the eccentricity (Eq. (4.15)) of the C force in the concrete for the two extreme loading conditions. At equality four limiting eccentricities are obtained, two of which will control (Fig. 4.22*a*). These last two represent the upper and lower limits of the limit kern, k'_t and k'_b. Thus:

$$k'_t = \text{the larger (algebraically) of} \begin{cases} k_b \left(1 - \dfrac{\bar{\sigma}_{cs}}{\sigma_g}\right) \\ \text{and} \\ k_t \left(1 - \dfrac{\bar{\sigma}_{ts}}{\sigma_g}\right) \end{cases} \tag{4.22}$$

$$k'_b = \text{the smaller (algebraically) of} \begin{cases} k_b \left(1 - \dfrac{\bar{\sigma}_{ti}}{\sigma_{gi}}\right) \\ \text{and} \\ k_t \left(1 - \dfrac{\bar{\sigma}_{ci}}{\sigma_{gi}}\right) \end{cases} \tag{4.23}$$

and the eccentricity of the C force shall satisfy the following condition:

$$k_t' \le e_c \le k_b' \tag{4.24}$$

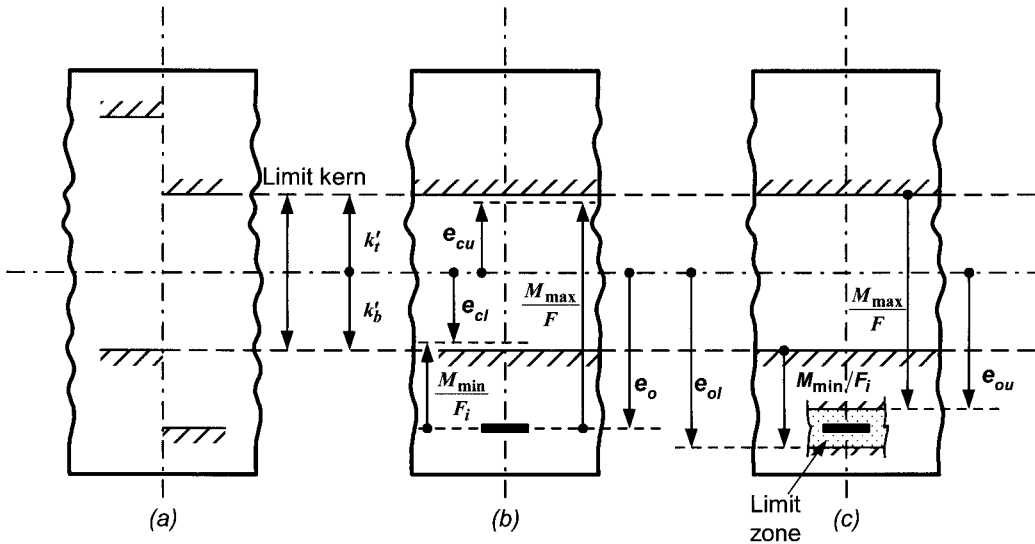

Figure 4.22 (a) Determination of limit kern. (b) Upper and lower limit of C line for given e_0. (c) Limit zone for the prestressing force.

Generally for a given force F and eccentricity e_o, the actual upper and lower limits of e_c, e_{cu} and e_{cl}, for the two extreme loadings will be within the limit kern (Fig. 4.22*b*).

The equations developed above imply the same concrete section, the same prestressing force, and the same allowable stresses throughout the span. If these vary, the equation remains the same but the numerical results will be different depending on the section considered.

The values of k_t' and k_b' given in Eqs. (4.22) and (4.23) were derived from the four stress inequality conditions of Table 4.2. These conditions were derived assuming both M_{min} and M_{max} are positive. If both moments were negative, the four complementary conditions given in Table 4.3 should be used and different expressions for k_t' and k_b' would be obtained. However, one can bypass this additional computation and still use the expression given in Eqs. (4.22) and (4.23) provided these steps are followed: (a) temporarily assume the section is inverted; (b) change the signs of the moments from negative to positive; (c) compute $(k_t')_{inv}$

and $(k'_b)_{inv}$ from Eqs. (4.22) and (4.23) for the inverted section and (d) compute, for the non-inverted section, $k'_b = (-k'_t)_{inv}$ and $k'_t = -(k'_b)_{inv}$.

If both positive and negative moments exist at a given section, the upper and lower limits of the limit kern should be determined from the stress inequality conditions that control the design. These conditions are taken from the eight conditions described in Tables 4.2 and 4.3. However, the advantages of using the limit kern vanish in such a case. Then, it is best to simply compute the upper and lower limit of eccentricity (steel envelopes) directly from the eight stress inequality conditions (way 2 of Tables 4.2 and 4.3).

4.12.2 Steel Envelopes and Limit Zone

The required prestressing force and its eccentricity are first determined at the critical section of the beam. Since F is assumed constant and since the applied external moment varies along the span, the eccentricity of the prestressing force should in general also vary. The task becomes: *Given a prestressing force and an external moment that varies along the span, find the limiting eccentricities of the force at each section so that none of the allowable stresses are violated.* The geometric lieu of the upper and lower limits of these eccentricities along the span are called the *steel envelopes* and the zone between them is called the *limit zone.*

It was shown in the preceding section that the C force in the concrete section is bound by the upper and lower limits of the limit kern k'_t and k'_b. As the eccentricity of the C force e_c is directly related to the eccentricity of the prestressing force e_o (Eq. (4.15)), the limiting eccentricities of the prestressing force can be directly derived from k'_t and k'_b. For the two extreme loadings applied we have (algebraically):

$$\begin{cases} e_c = e_o - \dfrac{M_{max}}{F} \geq k'_t & (4.25) \\ e_c = e_o - \dfrac{M_{min}}{F_i} \leq k'_b & (4.26) \end{cases}$$

from which the following condition on e_o is derived

$$k'_t + \frac{M_{max}}{F} \leq e_o \leq k'_b + \frac{M_{min}}{F_i} \qquad (4.27)$$

Thus the upper and lower limits of e_o, the eccentricity of the prestressing force, with respect to the centroid of the section, are:

$$\begin{cases} e_{ou} = k'_t + \dfrac{M_{\max}}{F} & (4.28) \\ e_{ol} = k'_b + \dfrac{M_{\min}}{F_i} & (4.29) \end{cases}$$

They vary along the span and define the limit zone for the prestressing steel. They can be easily calculated because, from structural analysis, the moments are already known throughout the beam. Note that the terms "upper" and "lower" describe respectively, how close or how far the steel is with respect to the centroid of the section.

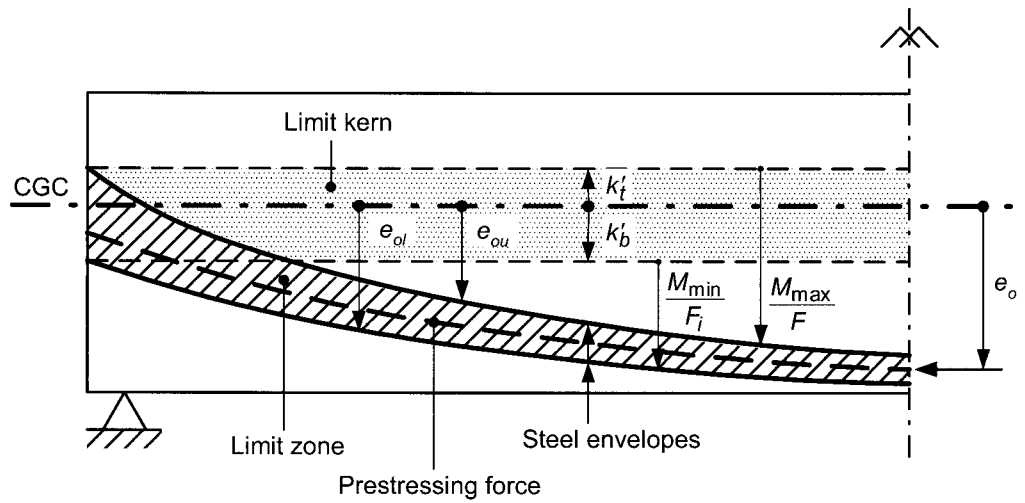

Fig. 4.23 Relationship between limit kern and limit zone.

In summary, in order to build the limit zone the following steps are recommended (Fig. 4.22*c*), assuming all moments are positive:

1. Determine from Eqs. (4.22) and (4.23) the values of k'_t and k'_b.
2. Determine from Eqs. (4.28) and (4.29) the values of e_{ou} and e_{ol}.

The above steps apply at any section along the span (Fig. 4.23). Once the limit zone is determined, the controlling prestressing force is placed inside this zone by adjusting the eccentricities of various tendons.

Note once more that finding the values of $e_{ou}(x)$ and $e_{ol}(x)$ at any section, x, can also be achieved in a most general way for any moment sign by applying systematically the eight stress inequality conditions (way 2 of Tables 4.2 and 4.3) at any section. Multiple equations for Condition III can be included. This is particularly useful if a computer program is used for the computation, if the prestressing force is variable, and/or if the section properties are variable along the span.

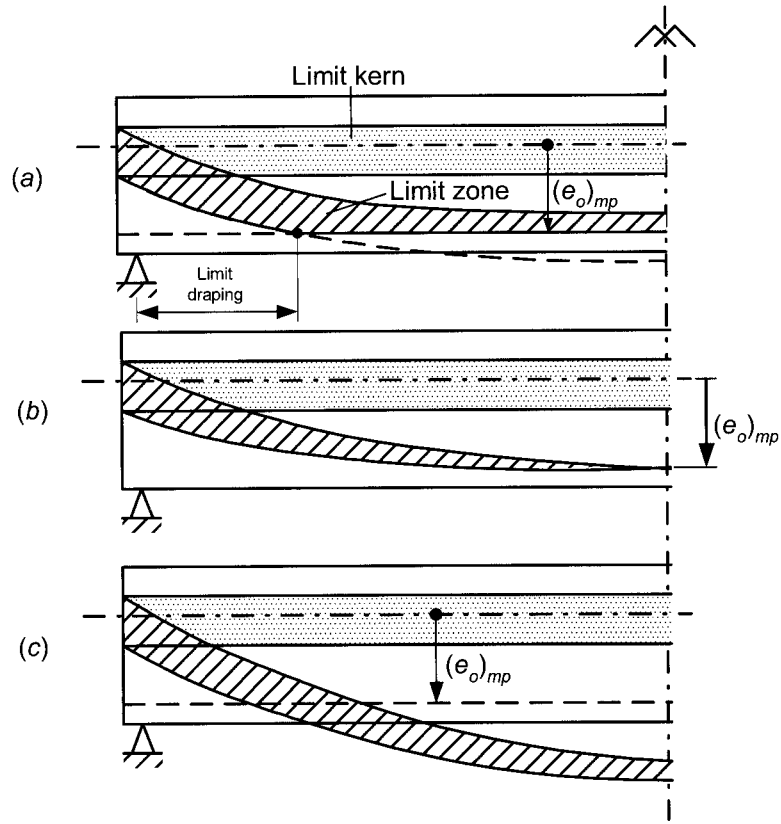

Fig. 4.24 Typical shapes of limit zone. (*a*) Most common design (lower limit controlled by maximum practical eccentricity). (*b*) Optimum design (only one set of F and e_o is feasible). (*c*) Inadequate concrete section (preliminary design).

Typical shapes of limit zones are shown in Fig. 4.24. Case (*a*) is most common and occurs when an adequate concrete section is selected; the lower steel envelope extends beyond the reach of the maximum practical eccentricity, but sufficient area remains to place the prestressing force. Case (*b*) of Fig. 4.24 applies to optimum design where a single set of values of F and e_o at midspan is feasible. Case (*c*) is typical of preliminary design in which an insufficient cross section of concrete is provided; the limit zone extends outside the beam, thus the prestressing force cannot be placed inside the section. To overcome such difficulty, larger concrete cross-section properties are needed.

Often in a preliminary design it is not necessary to determine the limit zone; the profile of the prestressing steel can be approximated by a parabola with a vertex ordinate equal to e_o at midspan and passing by the centroid of the concrete section at supports; another appropriate profile for pretensioned members is a profile with two draping points (Fig. 1.9) where the distance between the draping points is taken about equal to one-third the span length.

Note that the determination of the limit zone is often left to a later stage in the design after the requirements for ultimate and cracking moments are verified.

4.12.3 Example

The beam of example Sec. 4.9*a* is used to illustrate how the limit kern and the limit zone can be determined. First some detailing is needed. The beam is assumed to be pretensioned and to have two draping points for the steel profile. The location of the draping points will be determined from the limit zone. The configuration shown in Fig. 4.25*a* is selected for the midspan section and comprises six draped strands and four straight ones. Such detailing is in agreement with ACI code recommendations (Sec. 3.9). The resulting eccentricity of the centroid of the strands at midspan is within the feasible range (Fig. 4.16) and thus is acceptable. A detail of how the draped strands can be placed at the ends of the beam is shown in Fig. 4.25*b*. The centroid of the prestressing steel is brought close to that of the concrete section and within the central kern (also within the limit kern).

In order to determine the upper and lower limits of the limit kern, the stress at the centroid of the concrete is needed; thus:

$$\begin{cases} \sigma_g = \dfrac{F}{A_c} = \dfrac{229{,}500}{550} = 417.27 \text{ psi} \\ \sigma_{gi} = \dfrac{F_i}{A_c} = 502.74 \text{ psi} \end{cases}$$

The upper limit of the limit kern is given by Eq. (4.22):

$$k_t' = \text{the larger (algebraically) of} \begin{cases} k_b\left(1 - \dfrac{\overline{\sigma}_{csus}}{\sigma_g}\right) \\ \text{and} \\ k_t\left(1 - \dfrac{\overline{\sigma}_{ts}}{\sigma_g}\right) \end{cases} \rightarrow \begin{cases} 11.57\left(1 - \dfrac{2250}{417.27}\right) = -50.82 \\ \text{and} \\ -5.51\left(1 - \dfrac{-424}{417.27}\right) = -11.11 \end{cases}$$

Thus $k_t' = -11.11$ in.

Note that $\overline{\sigma}_{csus}$ was used in Eq. (4.22) above, since it is more critical here than $\overline{\sigma}_{cs}$

Similarly, the lower limit of the limit kern is given by Eq. (4.23):

$$k_b' = \text{the smaller (algebraically) of} \begin{cases} k_b\left(1 - \dfrac{\overline{\sigma}_{ti}}{\sigma_{gi}}\right) \\ \text{and} \\ k_t\left(1 - \dfrac{\overline{\sigma}_{ci}}{\sigma_{gi}}\right) \end{cases} \rightarrow \begin{cases} 11.57\left(1 + \dfrac{189}{502.74}\right) = 15.92 \\ \text{and} \\ -5.51\left(1 - \dfrac{2400}{502.74}\right) = 20.79 \end{cases}$$

Thus $k_b' = 15.92$ in.

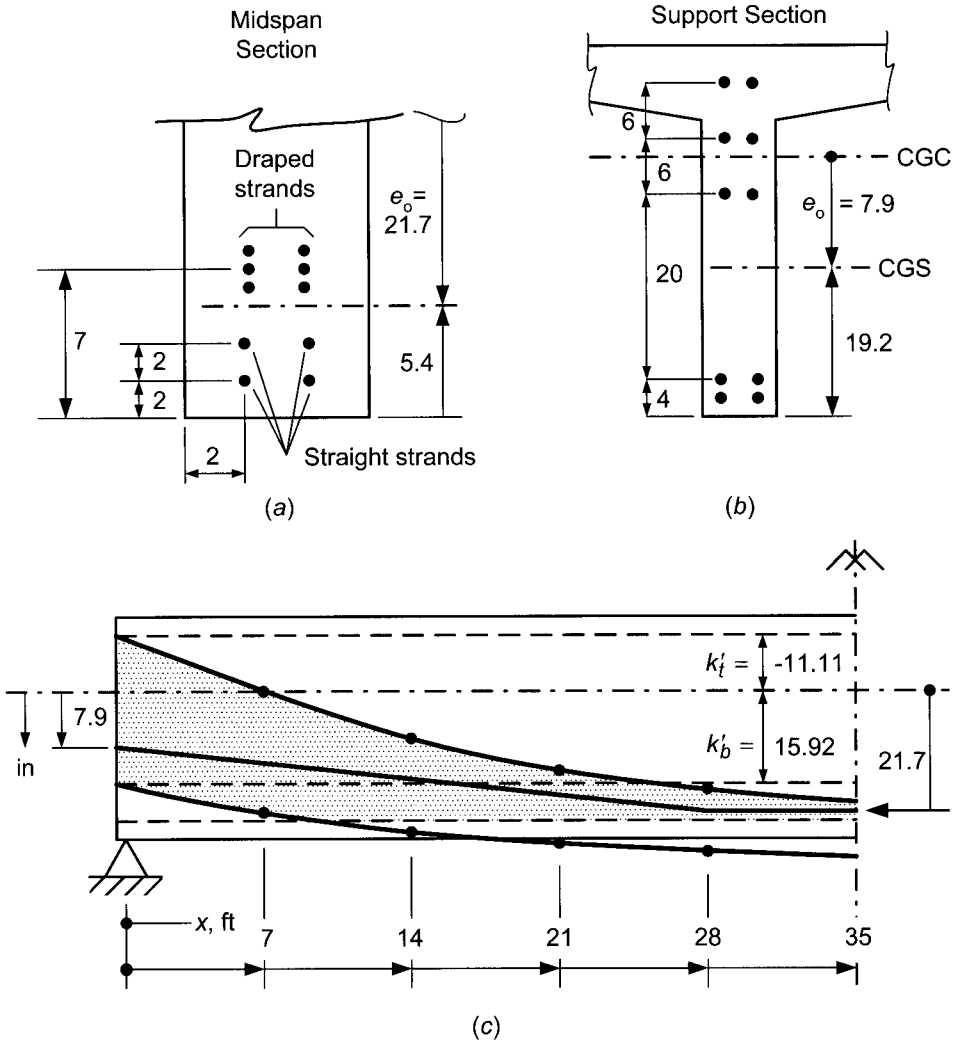

Fig. 4.25 Example beam. (*a*) Steel layout at midspan. (*b*) Steel layout at support. (*c*) Determination of the limit zone.

The upper and lower limits of the limit zone, or the steel envelopes, are determined from Eqs. (4.28) and (4.29). To proceed with the calculations, the minimum and maximum external moments are needed at each section considered. Their value at any section distant x from the support is given by:

$$(M_{\min}(x) \text{ or } M_{\max}(x)) = (w_{\min} \text{ or } w_{\max})\frac{x(\ell - x)}{2}$$

It is advisable to run the computations at every tenth of the span. The results are summarized in Table 4.5 for the half-span because of symmetry. The following values were used: $F = 229.5$ kips; $F_i = 276.5$ kips; $w_{\min} = w_G = 0.573$ klf; $w_{\max} = 1.013$ klf. Since the eccentricities are in inches and the prestressing force is in kips, the moments were calculated in kip-inch units.

Table 4.5 Results for example beam.

Distance x from left support, ft	0	7	14	21	28	35
$M_{\min}$, kips-in	0	1516	2695	3538	4043	4211
$M_{\max}$, kips-in	0	2680	4765	6254	7148	7445
$\frac{M_{\min}}{F_i}$, in	0	5.48	9.75	12.80	14.62	15.23
$\frac{M_{\max}}{F}$, in	0	11.68	20.76	27.25	31.14	32.44
$e_{ou} = k_t' + \frac{M_{\max}}{F}$	-11.11	0.57	9.65	16.14	20.03	21.33
$e_{ol} = k_b' + \frac{M_{\min}}{F_i}$	15.92	21.40	25.67	28.72	30.54	31.15
e_o, in	7.9	11.35	14.80	18.25	21.70	21.70

The upper and lower limits of the steel envelopes are plotted in Fig. 4.25*c*. Since the lower envelope extends below the concrete section, the limit zone (shaded area) is also limited by the maximum practical eccentricity, $(e_o)_{mp}$. A steel profile is selected to fit within the limit zone; it has a draping point at a distance from midspan equal to one-tenth of the span. It can be easily shown that the corresponding value of the eccentricity of the resultant prestressing force is given by:

$$\begin{cases} e_o(x) = 21.7 \text{ in} & \text{for } (28 \le x \le 35 \text{ ft}) \\ e_o(x) = 7.9 + 13.8\dfrac{x}{28} & \text{for } x < 28 \text{ ft} \end{cases}$$

where $e_o(x)$ is in inches and x in feet. The numerical values of $e_o(x)$ are summarized in the last line of Table 4.5.

4.12.4 Limit Location of Draping Section

Referring to Fig. 4.24a one can ask the question: for a tendon profile with two draping points, what is the minimum value of distance, x, from the left support at which draping can still be permitted without violating any of the allowable stresses at that section? In Fig. 4.25c, the draping section for the example beam was taken at a distance of 28 ft from the left support. However, it is clear from the limit zone that the draping point could have been selected closer to the support, as close as point D (Fig.4.25d). Point D can be obtained as the intersection of the curve representing the lower limit of the steel envelope (Eq. 4.29) with the line representing the actual eccentricity selected at midspan. As a first approximation, the maximum practical eccentricity can also be used instead of the midspan eccentricity; in that case another point D' close to D will be obtained.

Thus to obtain x for point D:

$$e_{ol}(x) = k'_b(x) + \frac{M_{min}(x)}{F_i} = k'_b(x) + \frac{M_G(x)}{F_i} = e_o(x = l/2) \tag{4.30}$$

Assuming a beam of uniform cross section, the dead load moment can be computed from:

$$M_G = W_G \frac{x(l-x)}{2} \tag{4.31}$$

Thus the value of x can be obtained from solving the following quadratic equation:

$$k'_b(x) + \frac{W_G x(l-x)}{2F_i} = e_o(x = l/2) \tag{4.32}$$

Applying Eq. (4.32) to the example beam of the previous section (Fig. 4.25*d*):

$$15.92 + \frac{0.573x(l-x)12}{2 \times 276.5} = 21.7 \text{ in}$$

where x is in ft, $l = 70$ ft, and W_G is in klf.

The above equation leads to the following quadratic equation:

$$x^2 - 70x + 464.85 = 0$$

for which there is one positive root: $x = 7.42$ ft, that is, the location of point D.

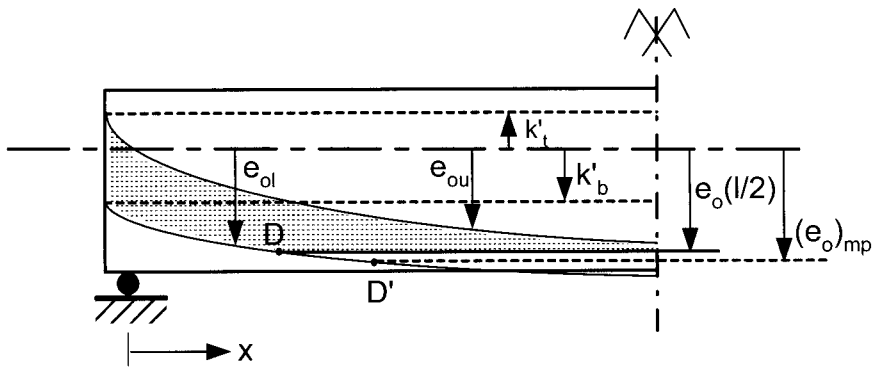

Figure 4.25 continued: (*d*) Limit location of draping point.

If instead of the actual eccentricity at midspan (21.7 in), the maximum practical eccentricity is used (23.1 in), the following quadratic equation would be obtained:

$$x^2 - 70x + 577.45 = 0$$

which leads to one positive root: $x = 9.55$ ft, that is, the location of point D'.

The above calculations can help determine more accurately the profile of the centroid of the prestressing tendons and can be especially useful when an optimum beam section is at hand.

4.13 SOME PRELIMINARY DESIGN TIPS

If the concrete cross section is properly selected for the problem at hand (such as from a handbook of standard beams), it is very likely that the maximum practical eccentricity (Fig. 4.14, case (*b*)) will control the design. It becomes clear that the prestressing force can then be determined from point *E*, which represents the intersection of stress condition IV with the line corresponding to $(e_o)_{mp}$. Referring to Table 4.2, the prestressing force can be determined from equation IV at equality in which e_o is replaced by $(e_o)_{mp}$, that is:

$$F = \eta F_i = \frac{M_{\max} + \bar{\sigma}_{ts} Z_b}{(e_o)_{mp} - k_t} \tag{4.33}$$

The designer can then check if the other three stress inequality conditions are satisfied for the values of F and e_o. A similar approach was used in the example Section 4.9.1.*c*. If the other three equations are not satisfied, it is then better to build the feasibility domain such as in Fig. 4.14 to see what needs to be done. Equation (4.33) necessitates the knowledge of a concrete cross-section since Z_b and $M_{\min}$ are needed. However, it is possible to get a very rough approximation of the prestressing force even in the absence of a concrete section.

Indeed, a very approximate method can often be used in cost estimate studies to estimate globally the value of the prestressing force, the prestressing steel content. It is derived from observing that, in order to have a feasible limit zone, the upper eccentricity limit of the prestressing force, e_{ou}, must be less than or equal to the lower eccentricity limit, e_{ol}, at the critical section. Thus using Eqs. (4.28) and (4.29):

$$k'_t + \frac{M_{\max}}{F} \leq k'_b + \frac{M_{\min}}{F_i} \tag{4.34}$$

Replacing F_i by F/η and solving for F leads to:

$$F \geq \frac{M_{\max} - \eta M_{\min}}{k'_b - k'_t} \tag{4.35}$$

which indicates that the minimum values of F is given by:

$$(F)_{\min} = \frac{M_{\max} - \eta M_{\min}}{k'_b - k'_t} = \frac{\Delta M + (1-\eta) M_{\min}}{k'_b - k'_t} \tag{4.36}$$

Because (1) η is generally around 0.80, (2) the dead load moment can be assumed to be of the same order as the live load moment, and (3) often no tension is allowed in the section, the following approximations can be made:

$$M_{\max} - \eta M_{\min} = M_{\min} + \Delta M - \eta M_{\min} \simeq 1.2\, \Delta M \tag{4.37}$$

$$k'_b - k'_t \simeq k_b - k_t = \gamma h \tag{4.38}$$

where γ is the geometric efficiency of the section (see Section 4.3). ΔM is independent of the beam cross section and γ, can be estimated within a reasonable range depending on the section shape as described in Sec. 4.3. The depth, h, can be estimated from the span such as $\ell/20$ for beams and $\ell/35$ for slabs. Thus Eq. (4.36) becomes:

$$\boxed{(F)_{\min} \simeq \frac{1.2\,\Delta M}{\gamma h}} \tag{4.39}$$

Note that a concrete cross section is not needed to apply Eq. 4.39. An estimate of the depth of the beam such as h = span/20 will lead to a very rapid approximation.

Applied to example Sec. 4.9.1*a*, Eq. (4.39) gives:

$$(F)_{\min} \simeq \frac{1.2 \times 269.5 \times 12}{0.427 \times 40} = 227.2 \text{ kips}$$

which is very close to the answer obtained in the exact analysis. If we did not know the value of γ, we could have estimated $\gamma = 0.45$ for a T section and obtained F = 215.6 kips.

4.14 CRACKING MOMENT

Although this chapter deals essentially with uncracked prestressed concrete beams, the load or moment at which cracking occurs is needed in the design (Chapter 5). The cracking moment is the moment for which the tensile stress on the extreme fiber of the concrete section reaches a value equal to the modulus of rupture of the concrete. For the bottom fiber of a prestressed concrete section subjected to a

positive moment (Fig. 4.26a), the cracking moment can be determined from satisfying the following equation:

$$\frac{F}{A_c}\left(1-\frac{e_o}{k_t}\right)-\frac{M_{cr}}{Z_b}=f_r \tag{4.40}$$

where the first term of the left-hand side of the equation is the stress due to the prestressing force and the second term is the stress due to the cracking moment just before cracking. Solving for M_{cr} gives:

$$M_{cr}=Z_b\left[\frac{F}{A_c}\left(1-\frac{e_o}{k_t}\right)-f_r\right]=F\left(e_o+\frac{Z_b}{A_c}\right)-f_rZ_b \tag{4.41}$$

$$\boxed{M_{cr}=F(e_o-k_t)-f_rZ_b}$$

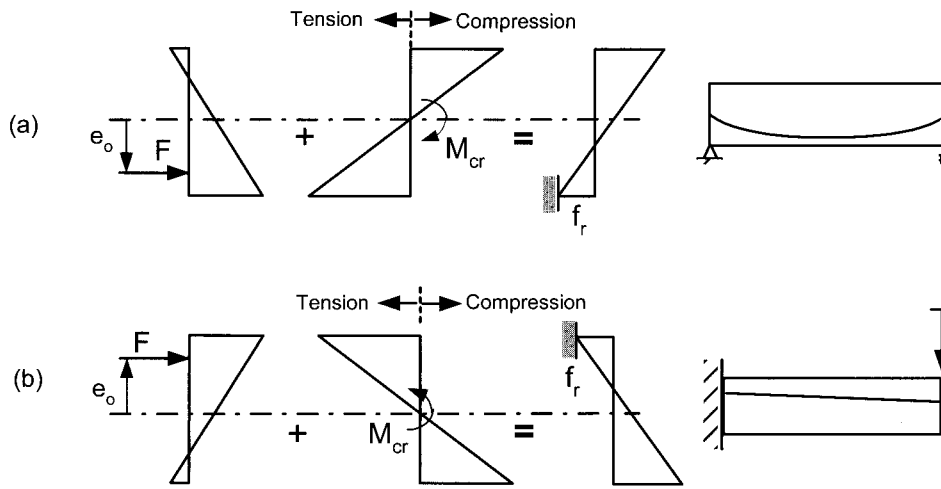

Figure 4.26 Cracking moment. (a) Positive for bottom fiber. (b) Negative for top fiber.

Note that the values of k_t and the modulus of rupture, f_r, are negative.

Let us assume $f_r = -7.5\sqrt{f'_c}$; the cracking moment of the beam treated in Example 4.9*a* is given by:

$$M_{cr} = 229{,}500\ (23.1 + 5.51) + 530 \text{ x } 3028 = 8{,}170{,}835 \text{ lb-in}$$

or

$$M_{cr} = 680.9 \text{ kips-ft}$$

It can be shown that the negative moment leading to cracking on the top fiber at the support of a prestressed concrete cantilever beam is given by (Fig.4.26*b*):

$$\boxed{M_{cr} = f_r Z_t - F(k_b - e_o)} \tag{4.42}$$

in which e_o and f_r are negative.

4.15 LIMITING THE AMOUNT OF PRESTRESSED REINFORCEMENT

The working stress design procedure followed in this chapter leads to the determination of the prestressing force or equivalently the area of prestressing steel, $A_{ps} = F/f_{pe}$, often described by its reinforcement ratio, $\rho_p = A_{ps}/(bd_p)$ (see also Chapter 5).

In order to ensure that the member is not reinforced to such an extent that it would lose its ductility, and not insufficiently reinforced so that it would collapse should cracking occur, the ACI and AASHTO codes contain some provisions that limit the amount of reinforcement (both upper and lower limits) used in design. Since these requirements have to do with the mode of failure of prestressed beams, they are covered in Chapter 5. In the majority of cases, the working stress design procedure followed in Chapter 4 leads to an amount of reinforcement that satisfies the code limitations, at least for minimum reinforcement; however, a final and complete design should satisfy the provisions described in Chapter 5.

4.16 END ZONE: PRETENSIONED MEMBERS

4.16.1 Transfer Length and Development Length

The prestressing force has to be transferred from the steel to the concrete. For pretensioned members, this is achieved gradually by bond between the two materials mainly at the end of the member, called end zone. The distance over which the effective prestressing force is transferred to the concrete is called transfer length l_t. After transfer, the tendons are assumed to have zero stress at the end of the member and an effective stress f_{pe} far away from the end. Hence, transfer length can be seen as the distance needed to develop the effective prestress f_{pe} in the tendons. Test results of transfer length of prestressing tendons commonly show large scatters.

It is generally agreed that the transfer length is influenced by many factors that depend on both the steel and the concrete. They include size and type of tendons (wires or strands), their surface conditions (smooth, deformed, rusted, and the like), tendon stress, method of transfer (sudden versus gentle release), concrete strength, concrete compaction, concrete confinement level (by stirrups or hoops), fiber reinforcement, if any, reinforcement index, and state of strain in the transfer region. Observed values of transfer length for most common conditions range from about 50

to 160 times the diameter of the tendon tested. The lower end range is more characteristic of prestressing strands, which, because of their twisted shape, have a good mechanical bond.

In order to develop the full design strength of the tendons, $f_{ps} > f_{pe}$, to resist flexural stresses at nominal moment resistance of the member (Chapter 5), additional bond length, beyond that needed to develop f_{pe}, is required. It is called the flexural bond length l_f. The flexural bond length l_f added to the transfer length l_t leads to a value called the development length l_d. The following minimum value of development length is prescribed by the ACI code for prestressing strands:

$$l_d = l_t + l_f = \left(\frac{f_{pe}}{3}\right) d_b + (f_{ps} - f_{pe}) d_b = \left(f_{ps} - \frac{2}{3} f_{pe}\right) d_b \tag{4.43}$$

where f_{pe} and f_{ps} are in kips per square inch and d_b is the diameter of the strand in inches. Equation (4.43) is graphically illustrated in Fig. 4.27. Using megapascals for stresses and millimeters for d_b and l_d leads to:

$$l_d = \frac{1}{7}\left(\frac{f_{pe}}{3}\right) d_b + \frac{1}{7}\left(f_{ps} - f_{pe}\right) d_b = \frac{1}{7}\left(f_{ps} - \frac{2}{3} f_{pe}\right) d_b \tag{4.44}$$

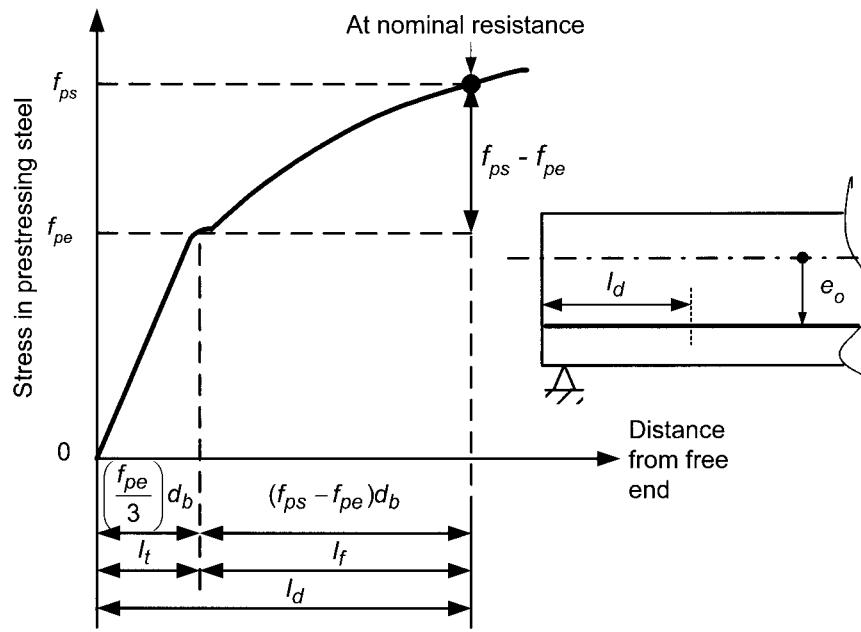

Figure 4.27 ACI assumed variation of steel stress with distance from free end for pretensioned strands.

Equation (4.43) is primarily based on tests of prestressing strands and, hence, does not apply to other types of tendons [Refs. 4.8 to 4.10]. An extensive survey of data related to transfer and development lengths can be found in Ref. [4.19] where regression equations are proposed to also predict l_t and l_d. These values are further discussed in Ref. [4.18] and adopted in the ACI code [Ref. 4.3].

The above prescribed minimum value of development length applies in the end zone of a member nearest each support. When partly sheathed (or blanketed) tendons are used, no bond will develop along the sheathed portion of the tendon. The bond will become effective only at the end of the sheathed portion, which generally falls outside the end zone. There, the stress transfer between steel and concrete is less effective since the compression, due to the vertical reaction, cannot be counted on and since tensile stresses, due to bending, may exist. The ACI code prescribes the doubling of the development length value given by Eq. (4.44) for cases where the bond does not extend to the end of a member, such as for blanketed strands. Note that sheathed or blanketed strands are sometimes used at the end of members to reduce the moment due to prestressing and related tensile stresses in the concrete; sheathing is used especially when straight tendons are used throughout the span. The ACI code also prescribes the doubling of development length given by Eq. (4.44) if the member is designed in such a way that tension will occur in the precompressed tensile zone under service loads.

4.16.2 End Zone Reinforcement

Because of high tensile splitting stresses that exist at the end of pretensioned members, their end zones must be additionally reinforced by vertical stirrups to limit the openings of cracks. The ACI code does not give on how to determine such reinforcement. However, the 16th edition of the AASHTO standard specifications prescribes the use of stirrups acting at a design stress of 20 ksi (138 MPa) to resist at least four percent of the total initial prestressing force F_i. They shall be placed within a distance $d_p/4$ of the end of the beam, the first stirrup being as close to the end as practicable. For at least a distance d_p from the end of the beam, nominal reinforcement shall be placed to enclose the prestressing steel in the bottom flange.

The necessary area of stirrup reinforcement in the end zone of a pretensioned member can also be estimated using a simple semi-rational approach proposed by Marshall and Mattock [Ref. 4.13], which leads to the following equation:

$$A_v = 0.021\frac{F_i h}{\bar{f}_s l_t} \tag{4.45}$$

where F_i is the prestressing force at transfer, l_t is the transfer length, A_v is the area of vertical stirrups to be uniformly distributed over a distance $h/5$ from the end of the beam and $\bar{f}_s$ is the design allowable stress in the stirrups. A value of $\bar{f}_s$ = 20 ksi

(138 MPa) is recommended by the AASHTO specifications, while a larger value of $\bar{f}_s$ = 30 ksi (207 MPa) is considered appropriate in the 5th edition of PCI Design Handbook. The transfer length l_t used in Eq. (4.45) can be taken either equal to 50 tendon diameters or it can be obtained from the first part of Eqs. (4.43) or (4.44).

Applying Eq. (4.45) to the beam of Example 4.9 leads to the following values:

$$h = 40 \text{ in}$$

$$l_t \simeq 50 \times \frac{1}{2} = 25 \text{ ft}$$

$$A_v = 0.021 \frac{276.5 \times 40}{20 \times 25} = 0.465 \text{ in}^2$$

Three #3 closed stirrups will be used within the first eight-inch distance from the end providing a total area of 0.66 in^2. The stirrups are provided in addition to other stirrups required to resist shear or torsional forces. If, instead of Eq. (4.45), we follow the simple AASHTO recommendations, the required area of stirrups will be given by:

$$A_v = 0.04 \frac{F_i}{\bar{f}_s} = 0.553 \text{ in}^2$$

which is also achieved practically using three #3 closed stirrups, as found earlier.

4.17 END ZONE: POSTTENSIONED MEMBERS

4.17.1 Analysis of Stresses

The prestressing force in a posttensioned member is transferred from the tendon to the concrete essentially by direct bearing through the anchorage. In the immediate vicinity of the bearing area very high compressive stresses exist and transverse tensile stresses develop in the nearby concrete. This is illustrated in Fig. 4.28*a* for a member of depth h assumed loaded uniformly at its center through a bearing plate of depth approximately equal to $h/4$. The high compressive stresses and high strains immediately behind the plate can cause bursting of the concrete, which generates high tensile stresses in the transverse direction away from the plate (Fig. 4.28*b*). The tensile stress field is such that splitting cracks tend to appear in the horizontal x-x plane accompanied by spalling cracks at the corners of the member (Fig. 4.28*c*). Such cracks must be contained by addition of proper reinforcement.

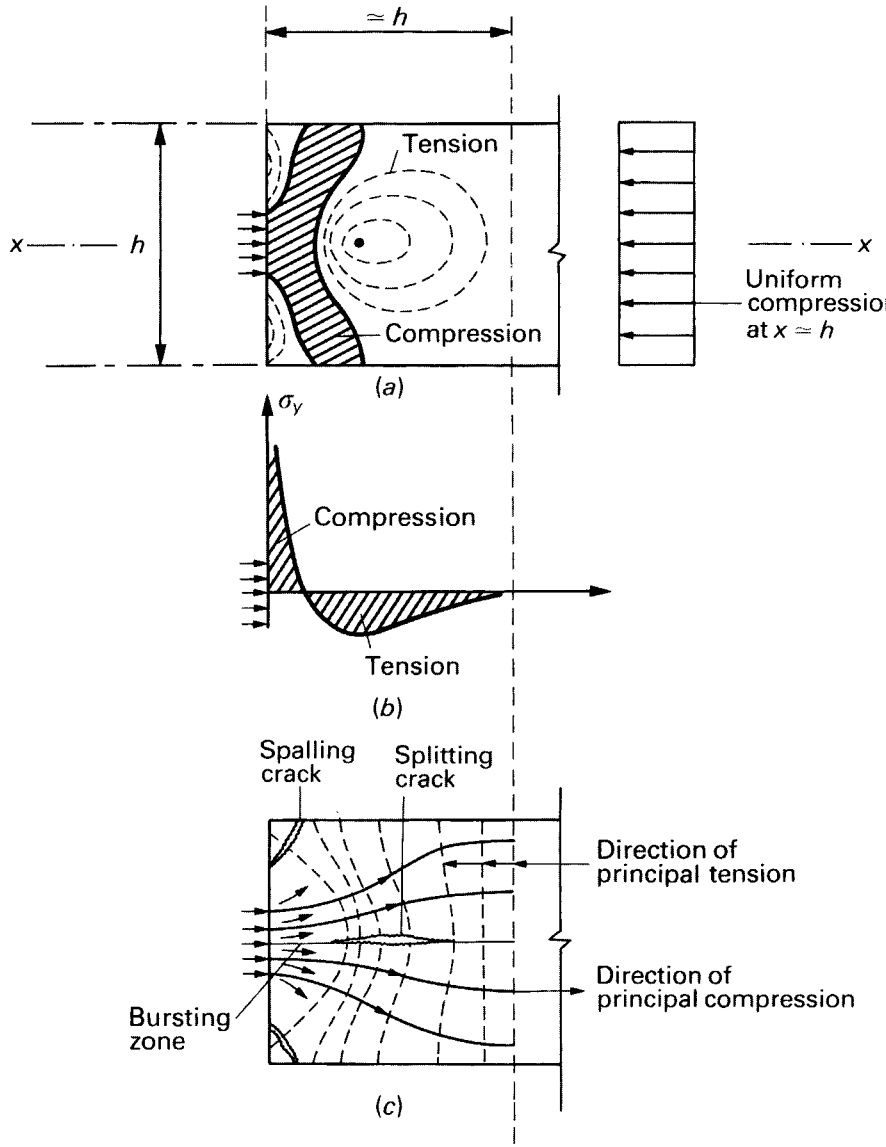

Fig. 4.28 End zone. (*a*) Compression stress transfer. (*b*) Lateral stress distribution. (*c*) Stress trajectories.

The effects described in Fig. 4.28 for a single tendon are cumulated and superimposed when many tendons are used. Hence, a zone with high stress concentrations and potentially dangerous cracking develops at the end of a posttensioned member. It is called lead-in zone, anchorage zone, or simply end zone as for pretensioned members. It extends for a distance about equal to the depth of the member, after which splitting tensile stresses become negligible. Elastic analysis indicates that, for a loading case such as shown in Fig. 4.28*a*, the transverse stress

(normal to the horizontal x plane) changes from compression to tension at about $0.1h$ and the maximum tensile stress occurs at about $0.3h$ from the end (Fig. 4.28*b*).

The accurate determination of stresses in the anchorage zones of posttensioned members is complex and may require extensive effort. Several methods, essentially based on elastic analysis, are available to estimate these stresses. They include in particular, the methods suggested by Guyon [Ref. 4.7], Magnel [Ref. 4.12], and Zielinski and Rowe [Ref. 4.20]. Most of these methods are also reviewed at length in traditional texts such as Refs. [4.1] and [4.11]. Although these methods lead to a sufficient understanding of the state of stress in the anchorage zone, they do not accurately represent actual conditions of the anchorage. This is because compressive stresses in the immediate vicinity of the anchorage can be of the same order as the strength of the concrete and, hence, are accompanied by high inelastic strains and deformations. Current computational methods, such as nonlinear finite elements, allow for a three-dimensional analysis that closely correlates with actual behavior. However, for economical reasons such techniques are used only for special applications. Increasingly, strut and tie models (Chapter 15), representing the path of local forces in the disturbed region of tendon anchorage zones, are being used as suggested in the ACI code [Ref. 4.3] and the PTI Post Tensioning Manual [Ref. 4.16]. Often design provisions are based on accumulation of past experience, semi-rational analysis, and engineering judgment. They are summarized next.

4.17.2 Anchorage Zone Design

At the ends of posttensioned members it has been customary to provide zones, called end blocks, of larger widths than the web widths of the members (Fig. 4.29). The end block is meant to allow for a practical distribution of the anchorages or bearing plates in the end zone and to reduce the magnitude of transverse tensile stresses. However, an investigation by Gergeley and Sozen has concluded that actual tensile stresses are not reduced, but rather increased [Ref. 4.5]. Nevertheless, as suggested by the ACI code, end blocks may still be necessary to accommodate the anchorages and for support bearing. Moreover, end blocks are specifically required by AASHTO for all posttensioned members.

According to the AASHTO specifications end blocks shall have a length at least equal to three-fourths the depth of the member, and in any case not less than 24 in (0.61 m). Preferably, they should be as wide as the narrower flange of the member. A closely spaced grid of both horizontal and vertical bars is required near the face of the end block to resist bursting stresses. When specific recommendations by the supplier of the end anchorages are not available, the grid shall consist of at least 3 bars on 3-in (75-mm) centers in each direction, placed not more than 1.5 in (38 mm) from the inside face of the anchor-bearing plate. In addition, closely spaced reinforcement shall be placed both vertically and horizontally throughout the length of the end block in accordance with accepted methods of end block stress analysis.

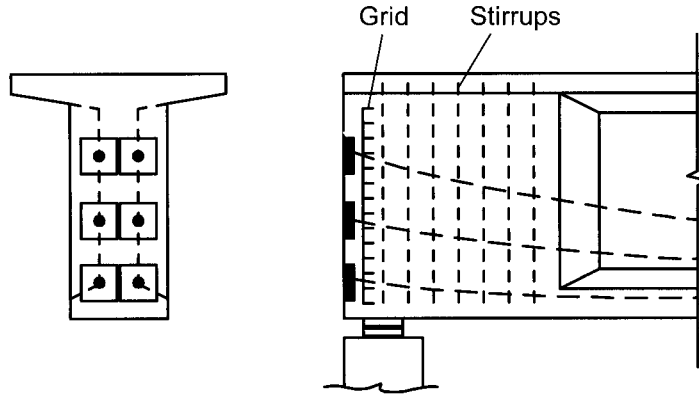

Figure 4.29 Typical end block and end block reinforcement.

The design of the anchorage zone (or end block) in posttensioned members is essentially reduced to: (1) sizing the anchorages to limit the stresses in the concrete, and (2) determining the transverse reinforcement to control splitting tensile cracking in the end zone.

The following procedure is taken from the 6th edition of the Post-Tensioning Manual published by the Post-Tensioning Institute. It is based on procedures recommended in earlier editions of the AASHTO specifications and the ACI commentary of the code, but somewhat modified to be less stringent. The reader is referred to the Post-Tensioning Manual for a detailed design of size of end anchorages, when either experimental data or a more refined analysis are not available. Next, only the limiting bearing stress is described, assuming that the bearing plate will have the appropriate thickness and stiffness.

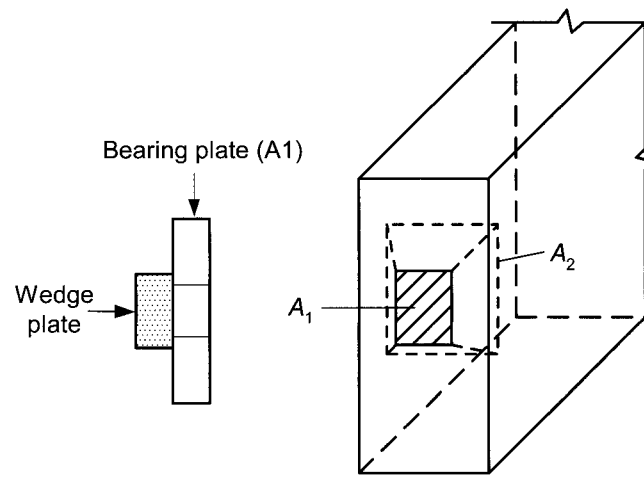

Figure 4.30 Assumed effective bearing area of anchorage.

The average bearing stress in the concrete just behind the anchorage (Fig. 4.30) should not exceed the following allowable values:

1. If no local zone confinement reinforcement is provided ($\rho_s = 0$), the allowable bearing stress under the maximum allowable tendon jacking force F_{jmax}:

$$\bar{\sigma}_{bi} = 0.5 f'_{ci} \sqrt{A_2 / A_1} \leq 1.0 f'_{ci} \tag{4.46}$$

where:

A_1 = gross bearing area of anchor plate of post-tensioning tendon

A_2 = maximum area of the portion of the anchorage surface that is geometrically similar to and concentric with the area of the anchor plate of the posttensioning tendon

$\bar{\sigma}_{bi}$ = allowable concrete bearing stress under the anchor plate of posttensioning tendons with the end anchorage zone adequately reinforced

f'_{ci} = compressive strength of concrete at time of prestress.

2. If a minimum local zone confinement reinforcement $\rho_s > 2\%$ is provided, the allowable bearing stress under F_{jmax} is limited to:

$$\bar{\sigma}_{bi} = 0.75 f'_{ci} \sqrt{A_2 / A_1} \leq 1.5 f'_{ci} \tag{4.47}$$

3. For ρ_s between 0 and 2%, the allowable bearing stress may be linearly interpolated between the values obtained from Eqs. (4.46) and (4.47).

4. If the maximum allowable jacking force, F_{jmax}, is not given, it can be taken equal to 80% of the tensile strength of the tendon.

The above allowable stresses assume normal weight concrete. For structural lightweight concrete the author recommends a reduction of at least 20%.

Consideration of the strength reduction factor ϕ (see Sec. 3.8) is already incorporated in Eqs. (4.46) and (4.47). The limiting values on $\bar{\sigma}_{bi}$ suggest that A_2/A_1 cannot be taken larger than about 4. The determination of A_2 is illustrated in Fig. 4.30. If the ACI code commentary (Sec. 10.16) is followed, A_2 can be determined by plotting from the periphery of A_1 planes sloping at a ratio of two to one (hence forming a truncated pyramid or, if A_1 is circular, a truncated cone). A ratio of three to one is recommended in the PTI Post-Tensioning Manual [Ref. 4.16] when the radius of the bearing plate is less than three times that of the wedge plate. Experience has shown that good control of end zone cracking can be achieved by keeping the bearing area of all anchorages to less than one-third the area of the end

section of concrete and, by providing grid or spiral reinforcement in the concrete immediately behind the anchorage or bearing plate.

Although, according to the ACI code, reinforcement shall be provided where required in anchorage zones to resist bursting, splitting, and spalling forces, no particular guidance is provided on how to determine such reinforcement. The PTI Post-Tensioning Manual recommends a procedure based on a strut-and-tie model. A simple method proposed by Gergeley and Sozen can also be used [Ref. 4.5]. It is based on considering the free body diagram of the end block in which a splitting horizontal crack has occurred, in any possible position, and the crack opening is resisted by vertical stirrups (Fig. 4.31). Moment equilibrium of the free body leads to the required area of stirrups. As a first approximation, the tensile force resisted by the stirrups can be placed at $h/4$ from the end and the counteracting compressive force in the plane of the crack can be placed at a distance h from the end.

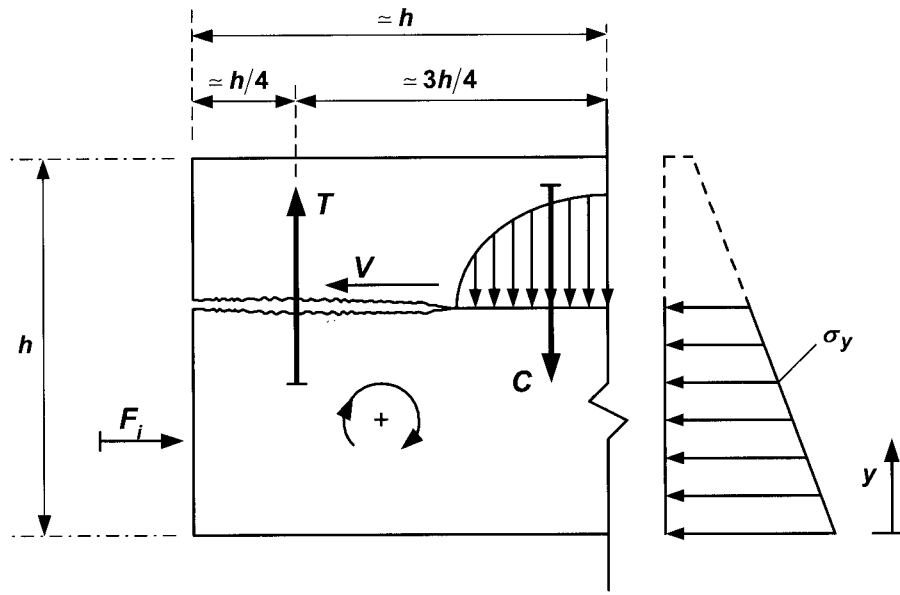

Figure 4.31 Free body model for end zone design (Ref. 4.5).

In analyzing the free body of the concrete end zone below the crack, the vertical component of the prestress at the support is neglected, and undisturbed bending stresses induced by the prestressing moment are assumed to act at the other end of the end block. Moments are then calculated in the transverse direction (along the horizontal plane) of the free body and reinforcement is provided to resist the maximum moment obtained. Note that the method assumes that there is a longitudinal crack in the end zone and the role of the reinforcement is to confine the crack. The likely position of such crack is at the level of the maximum moment obtained. When moments of different signs are obtained, they may indicate a

splitting crack away from the anchorage. Such cracks should also be confined by reinforcement. The procedure is best illustrated by an example. In Chapter 15 the same example is covered using a strut-and-tie model.

4.17.3 Example: Design of End Zone Reinforcement

Let us consider the beam of Examples 4.9 and 4.12.3 and assume that it will be posttensioned with the same initial prestressing force $F_i = 276.5$ kips at the same end eccentricity $e_o = 7.9$ in at the supports. According to ACI, no end block is needed since there will be very few anchorages in the end zone. For instance, two VSL-type cables (App. C), one with seven strands (and especially designed bearing plate) and one with three strands, can be used. The free body diagram of the end zone, assuming its length is equal to the depth of the beam, that is 40 in, and assuming a constant eccentricity for the prestressing force, is shown in Fig. 4.32*a*. The vertical component of the prestressing force is neglected. The prestressing force acts at the free end while elastic bending stresses, due to prestressing only, act at the other end. The moments on any horizontal plane of ordinate y can be computed from the contribution of both the prestressing force and the stresses. The moments due to the stresses can be computed by dividing the section vertically into several parts (say 10) and determining the equivalent force in each (that is, the equivalent stress block). Computations for this example are summarized in Table 4.6 and the net moment diagram is shown in Fig. 4.32*b*.

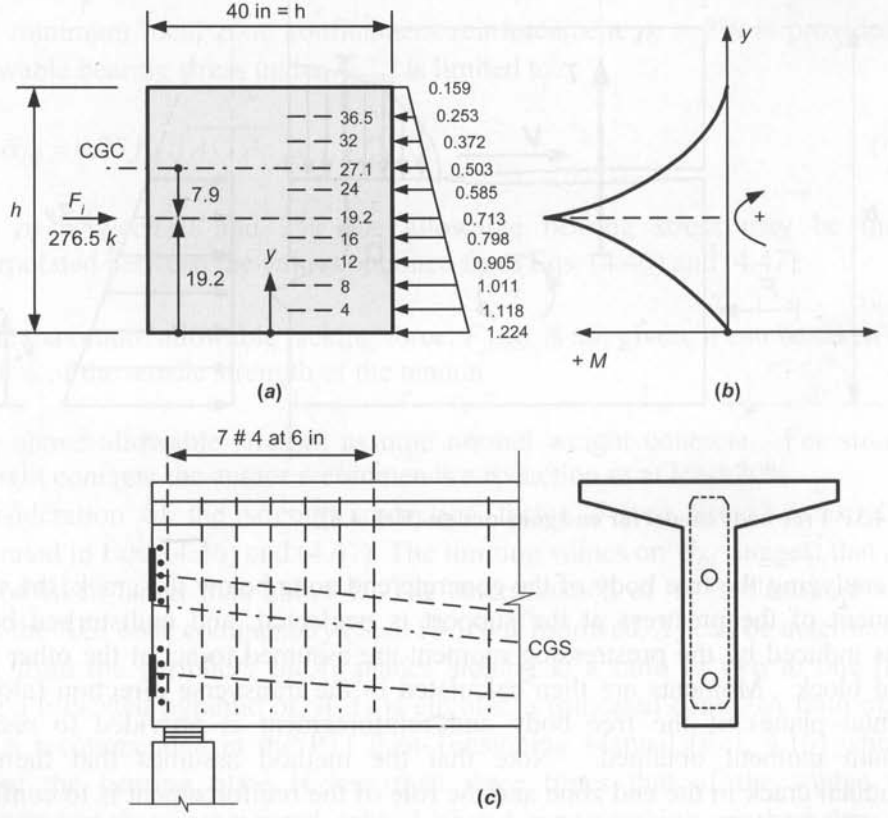

Figure 4.32 Design example. (*a*) End zone free body forces. (*b*) Moment diagram. (*c*) Reinforcement.

Table 4.6 Moments at horizontal sections of end zone.

Distance y from bottom fiber, in	Moment due to concrete stresses, kips-in	Moment due to F_i, kips-in	Net moment, kips-in
4	76.06	.....	76.07
8	295.17	.....	295.17
12	643.78	.....	643.78
16	1107.97	.....	1107.97
19.2	1553.69	.....	1553.69
24	2329.34	-1327.2	1002.14
27.1	2889.66	-2184.35	705.31
32	3850.24	-3539.20	311.04
36.5*	4831.62	-4783.45	48.17
40*	5714.5	-5751.2	-36.7 $\simeq$ 0

*The beam width at this level is larger than eight inches.

Referring to the stress diagram of Fig. 4.32*a*, the moment due to concrete stresses can be determined from:

$$(1.224 - \sigma_y)\frac{8y^2}{3} + 4\sigma_y y^2$$

where σ_y is the stress at level y. The above equation is obtained by dividing the trapezoidal stress diagram into a rectangle and a triangle. For instance, at $y = 27.1$ in, corresponding to the centroid of the concrete section, the moment due to concrete stresses is obtained from:

$$(1.224 - 0.503)\frac{8 \times 27.1^2}{3} + 4 \times 0.503 \times 27.1^2 = 2889.66 \text{ kips-in}$$

The moment due to the prestressing at the same level y is given by:

$$-F_i(y - 19.2) = -2184.35 \text{ kips-in}$$

and the net moment at level y is given by:

2889.66 - 2184.35 = 705.31 kips-in

Referring to Table 4.6, it can be observed that the maximum (net) moment occurs at $y = 19.2$ in. Hence, this will be the preferential level at which a splitting tensile crack may occur. The tensile force T contributed by the needed stirrups can be determined assuming that T acts at $h/4$ from the end of the beam, the corresponding compressive force C in the concrete acts at h from the end, and the couple produced by T and C is equal to the maximum moment, that is:

$$T\left(h - \frac{h}{4}\right) = 1553.69 \text{ kips-in}$$

from which:

$$T = \frac{1553.69}{30} \simeq 51.79 \text{ kips}$$

Using an allowable stress $\overline{f}_s = 20$ ksi leads to the following required area of stirrups

$$A_v = \frac{51.79}{20} = 2.59 \text{ in}^2$$

For this, seven #4 closed stirrups at approximately six-inch spacing can be used (Fig. 4.32*c*). These stirrups are in addition to those required in the design for shear (Chapter 6).

REFERENCES

4.1 Abeles, P. W., B. K. Bardhan-Roy, and F. H. Turner, *Prestressed Concrete Designer's Handbook*, 2nd ed. Wexham Springs, Slough, England: Viewpoint Publishers, Cement and Concrete Association, 1976, 548 pp.

4.2 American Association of State Highway and Transportation Officials (AASHTO), *Standard Specifications for Highway Bridges*, 16th Edition, 1996.

4.3 ACI Committee 318, "Building Code Requirements for Structural Concrete (ACI 318-99)," American Concrete Institute, Farmington Hills, Michigan, 1999.

4.4 Cement and Concrete Association, 1960, Publication 41.009, Wexham Springs, Slough, England, 32 pp.

4.5 Gergeley, P., and M. A. Sozen, "Design of Anchorage Zone Reinforcement in Prestressed Concrete Beams," *PCI Journal*, 12(2): 63-75, 1967.

4.6 Guyon, Y., *Prestressed Concrete, Vol. 1*. New York: John Wiley & Sons, 1960.

4.7 Guyon, Y., *Prestressed Concrete, Vol. 2*. New York: John Wiley and Sons, 1960, 741 pp.

4.8 Hanson, N. W., and P. H. Kaar, "Flexural Bond Tests of Pretensioned Prestressed Beams," *ACI Journal*, 30(7): 783-802, 1959.

4.9 Hanson, N. W., "Influence of Surface Roughness of Prestressing Strands on Bond Performance," *PCI Journal*, 14(1): 32-45, 1969.

4.10 Kaar, P. H., and D. D. Magura, "Effect of Strand Blanketing on Performance of Pretensioned Girders," *PCI Journal*, 10(6): 20-34, 1965.

4.11 Leonhardt, F., *Prestressed Concrete*. Berlin, Germany: Wilhelm Ernst and Sohn, 1964, 677 pp.

4.12 Magnel, M., *Prestressed Concrete*. New York: McGraw-Hill Book Co., 1954, 345 pp.

4.13 Marshall, W. T., and A. H. Mattock, "Control of Horizontal Cracking in the Ends of Pretensioned Prestressed Concrete Girders," *PCI Journal*, 7(5): 56-74, 1962.

4.14 Nilson, A. H., "Flexural Design Equations for Prestressed Concrete Members," *PCI Journal*, 14(1): 62-71, 1969.

4.15 Naaman, A. E., "Minimum Cost Versus Minimum Weight of Prestressed Slabs," *Journal of the Structural Division, ASCE*, 102(ST7): 1493-1505, 1976.

4.16 Post-Tensioning Institute, "Post-Tensioning Manual: 6th ed. Chapter 8, Anchorage Zone Design," Phoenix, AZ, 2000.

4.17 Precast/Prestressed Concrete Institute, "*PCI Design Handbook – Precast and Prestressed Concrete*," 5th ed., PCI, Chicago, IL, 1999.

4.18 Rose, D. R., and B. W. Russel, "Investigation of Standardized Tests to Measure the Bond Performance of Prestressing Stand," *PCI Journal*, 42(4): 56-60, 1997.

4.19 Zia, P., and T. Mostafa, "Development Length of Prestressing Strands," *PCI Journal*, 22(5): 54-65, 1977.

4.20 Zielinski, J., and R. E. Rowe, "An Investigation of the Stress Distribution in Anchorage Zones of Post-Tensioned Concrete Members," Research Report No. 9, September 1960, Publication 41.009, Cement and Concrete Association, Wexham Springs, Slough, England, 32 pp.

PROBLEMS

4.1 A plain concrete beam 12 x 18 inches in cross section supports, in addition to its own weight, a uniform live load of 100 plf on a simple span of 40 ft (Fig. P4.1). Assume γ_c = 150 pcf and $f'_c = 7000$ psi.

(*a*) Determine the bending stresses at midspan. Are such stresses allowable, if the modulus of rupture of the concrete is $-7.5\sqrt{f'_c}$?

(*b*) Find the magnitude of the smallest longitudinal force, which, if applied at the centroid of the cross section, would reduce the tensile stress at the bottom of the beam to zero under full load at midspan.

(*c*) Find the magnitude of the smallest longitudinal force, which, if applied at the bottom of the central kern at midspan, would also lead to zero stress at the bottom of the beam under full load.

(*d*) Find the magnitude of the smallest longitudinal force, which, if applied at 6 in from the center line, would also produce the same result.

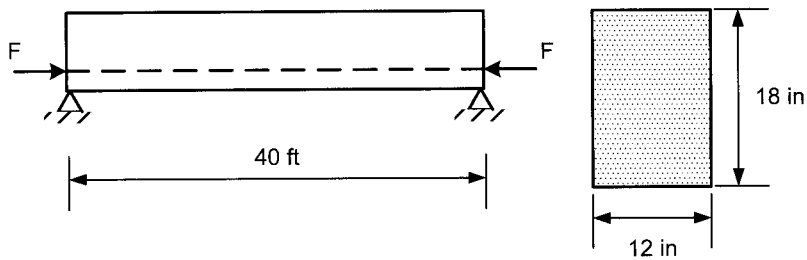

Figure P4.1

4.2 Consider the simply supported rectangular beam (Fig. P4.2) for which the following information is provided: $\bar{\sigma}_{ti} = 0$; $\bar{\sigma}_{ci} = 2400$ psi; $\bar{\sigma}_{ts} = 0$; $\bar{\sigma}_{cs} = 2400$ psi; span = 40 ft; M_G = 720,000 lb-in; $(e_o)_{mp} = 9$ in; $\eta = 0.80$. Determine the live load (w_L = plf) for which the point of intersection of the two lines representing stress conditions I and IV leads to a value of eccentricity equal $(e_o)_{mp}$.

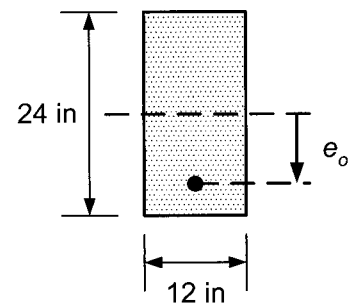

Figure P4.2

4.3 Consider the simply supported T beam shown in the figure below. The live load is assumed to be 600 plf. The following design information is given:
Concrete: normal weight with unit weight = 150 pcf; $f'_c = 8000$ psi; $f'_{ci} = 5600$ psi;
Allowable stresses: $\bar{\sigma}_{ti} = -224$ psi; $\bar{\sigma}_{ci} = 3360$ psi; $\bar{\sigma}_{ts} = -536$ psi; $\bar{\sigma}_{csus} = 3600$ psi; $\bar{\sigma}_{cs} = 4800$ psi;
Steel: $f_{pu} = 270$ ksi; $f_{pe} = 150$ ksi; $f_{py} = 240$ ksi (yield stress); $\eta = 0.8$; $d_{cmin} = 3$ in.
The prestressing steel consists of half-inch diameter strands.

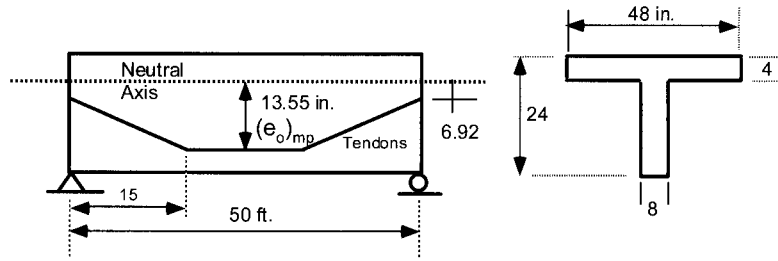

Figure P4.3

1. Build the feasible domain and determine the minimum value of prestressing force and corresponding eccentricity at midspan. Round off your answer to correspond to an integer number of strands, assuming the cross-sectional area of one strand is 0.153 in^2. (see Question 3).
2. Check if the prestressing force and eccentricity determined in 1 are acceptable at the section where the tendons are draped (15 ft from support). Suggest a solution if you see any problem.
3. Show an actual lay-out of strands at the midspan section to give you the eccentricity selected in 1. If possible use the maximum practical eccentricity. Also assume the eccentricity at the supports is as given in the figure; show an acceptable strand layout at the support section. Note this will determine the number of strands that are straight and the number that are draped. Some iteration may be needed here.
4. Determine the cracking moment at the midspan section.
5. Determine the curvature at midspan under initial and final loadings.
6. Using allowable stress design, determine the maximum value of live load that the beam is allowed to carry, and the corresponding value of prestressing force and eccentricity.

4.4 Given the rectangular simple span beam (Fig. P4.4) and the following information: span = 30 ft; live load = 0.64 klf; w_G = 0.225 klf; f'_c = 5000 psi; f'_{ci} = 4000 psi; $\bar{\sigma}_{ti}$ = -189 psi; $\bar{\sigma}_{ci}$ = 2400 psi; $\bar{\sigma}_{ts}$ = 0; $\bar{\sigma}_{csus}$ = 2250 psi; $\bar{\sigma}_{cs}$ = 3000 psi; η = 0.80; $(e_o)_{mp}$ = 7 in.

(*a*) Determine the magnitude and eccentricity of the minimum prestressing force at midspan. Build geometrically the feasible domain for F and e_o.

(*b*) Based on the answer found in (*a*) determine the limits of the limit kern.

(*c*) Using the information provided by (*a*) and (*b*) determine the envelopes of the prestressing force at every tenth of the span from support to midspan.

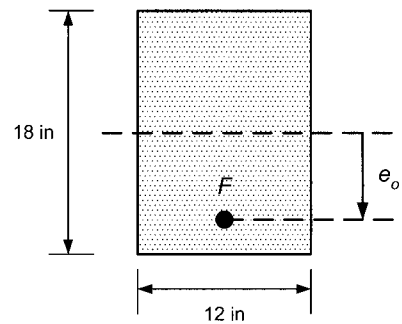

Figure P4.4

4.5 You are exploring the feasibility of posttensioning a double cantilever slab using straight prestressing bars (Fig. P4.5). Information on section properties, allowable stresses, loading and bending moments are given next:

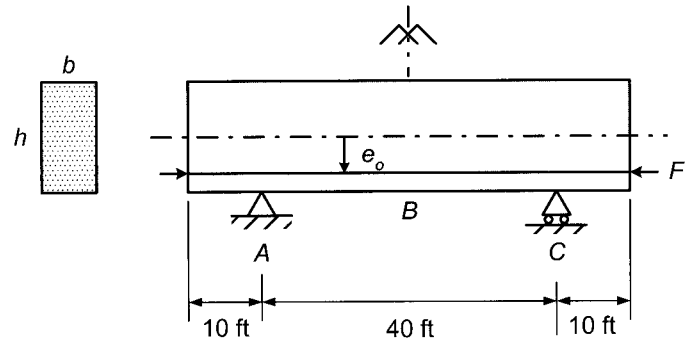

Figure P4.5

h = 15 in; b = 12 in; η = 0.8; $(e_o)_{mp}$ = 5 in; $\bar{\sigma}_{ti} = 0$; $\bar{\sigma}_{ci} = 2400$ psi; $\bar{\sigma}_{ts} = 0$; $\bar{\sigma}_{cs} = 2000$ psi; w_G = 187.5 plf; w_L = 100 psf; moments at support A: M_{max} = -172.5 kips-in and M_{min} = -112.5 kips-in; moments at midspan: M_{max} = 577.4 kips-in and M_{min} = 337.4 kips-in.

(*a*) Find graphically a prestressing force F and its eccentricity e_o suitable for the elastic solution of the problem (i.e., do not check ultimate moment, shear, etc.).

(b) If you were told that the minimum prestressing force for both sections A and B corresponds to satisfying stress condition IV, derive the analytical solution for question (*a*).

4.6 A foot bridge essentially uses a simply supported standard precast pretensioned double T concrete beam in its inverted position, to be obtained from a local supplier (Fig. P4.6). Typical cross section and available dimensions are given in Table P4.6 and Fig. P4.6. These are normal weight concrete beams.

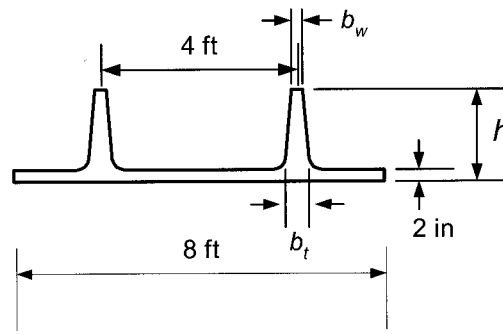

Figure P4.6

Table P4.6 Properties of beam sections (normal weight concrete).

h in	b_t in	b_w in	A in^2	I in^4	y_b in	y_t in	Z_b in^3	Z_t in^3	W_G plf
16	8.00	6.00	388	8,944	4.87	11.13	1837	804	404
18	9.75	7.75	472	14,623	6.16	11.84	2374	1235	492
20	9.75	7.50	503	19,354	6.94	13.06	2789	1482	524
24	9.75	7.00	560	31,192	8.49	15.51	3674	2011	583
32	8.00	4.00	549	51,286	10.29	21.71	4984	2362	572

Other information is given as follows: f'_c = 7000 psi; f'_{ci} = 5000 psi; $\bar{\sigma}_{ti} = -212$ psi; $\bar{\sigma}_{ci} = 3000$ psi; $\bar{\sigma}_{ts} = -502$ psi; $\bar{\sigma}_{csus} = 3000$ psi; $\bar{\sigma}_{cs} = 4200$ psi; $\eta = 0.80$; $(e_o)_{mp} = y_b - 2$ in; span length = 60 ft;

superimposed dead load plus live load = 500 plf; f_{pe} = 155 ksi; area of one strand = 0.153 in^2. Select the least weight beam which satisfies the working stress design requirements in flexure and determine the corresponding values of F and e_o at midspan. (Note that the solution by WSD may not satisfy USD criteria as described in Chapter 5, and the next beam in line may have to be selected).

4.7 A T beam (Fig. P4.7) supports in addition to its own weight a live load of 60 psf. The following information is provided: f'_c = 6000 psi; f'_{ci} = 4500 psi; $\bar{\sigma}_{ti}$ = –201 psi; $\bar{\sigma}_{ci}$ = 2700 psi; $\bar{\sigma}_{ts}$ = –465 psi; $\bar{\sigma}_{csus}$ = 2700 psi; $\bar{\sigma}_{cs}$ = 3600 psi; η = 0.80; $(d_c)_{\min}$ = 3 in; $(e_o)_{mp} = y_b - 3$ in; γ_c = 150 pcf; f_{pu} = 270 ksi; f_{pe} = 151 ksi; final effective force of 1 strand = 23.1 kips. Assume stress-relieved bonded strands.

(*a*) Assuming you are told there is a wide feasibility domain for F and e_o, determine the value of F necessary at midspan. Round off its value to the nearest integer number of strands. Check that all stresses are within allowable limits.

(*b*) Determine graphically the feasibility domain for the beam and find graphically the value of F (Use graph paper). This should lead to the same answer as in (a).

(*c*) Assuming the eccentricity is fixed at $e_o = y_b - (d_c)_{\min}$, what is the maximum value of F that the beam can be subjected to, without any of the allowable stresses being exceeded?

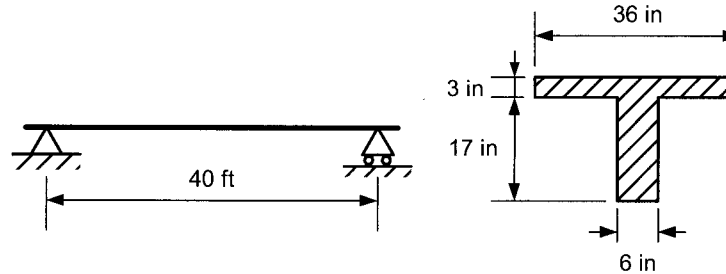

Figure P4.7

(*d*) Let us assume that the live load is not specified. Assuming the eccentricity is fixed at $e_o = y_b - (d_c)_{\min}$,, what is the maximum value of live load and corresponding F that can be applied to the beam (from a working stress design approach in flexure only).

Going back to question (a):

(*e*) Determine the two limits of the limit kern.

(*f*) Determine the upper and lower limits of the steel envelopes at every tenth of the span.

(*g*) Suggest a profile for the center of gravity of the prestressing steel along the beam. Show midspan as well as end cross section details.

4.8 A double cantilever simply supported beam (Fig. P4.8) supports in addition to its weight a live load of 80 psf and a concentrated load at its ends (as shown) of 750 lb. This concentrated load can be considered as a dead load due to the weight of a wall. The following information is given:

f'_c = 5000 psi; f'_{ci} = 4000 psi; $f_r = -7.5\sqrt{f'_c}$; γ_c = 150 pcf;

$\bar{\sigma}_{ti}$ = –189 *psi*; $\bar{\sigma}_{ci}$ = 2400 *psi*; $\bar{\sigma}_{ts}$ = –213 *psi*; $\bar{\sigma}_{csus}$ = 2250 psi; $\bar{\sigma}_{cs}$ = 3000 psi;

η = 0.80; $(d_c)_{\min}$ = 3 in; f_{pu} = 270 ksi; f_{pe} = 150 ksi; area of one strand = 0.153 in^2.

(*a*) Determine the required value of the prestressing force to be used throughout the length of the beam (i.e., check F at A, F at B, and select the largest value; then check that all stresses are satisfied). Think about using the feasibility domain for solution. Select F corresponding to an integer number of strands.

(*b*) Determine the upper and lower limits of the steel envelopes at support, midspan, quarter span, end *D*, and 5 ft from *D* (i.e., *E*).

(*c*) Plot graphically the limit zone and show an acceptable profile for the prestressing force.

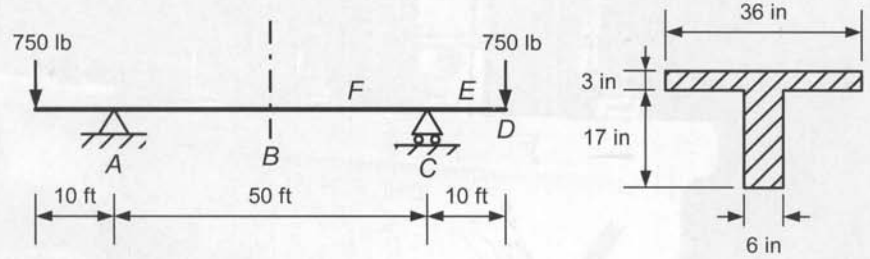

Figure P4.8

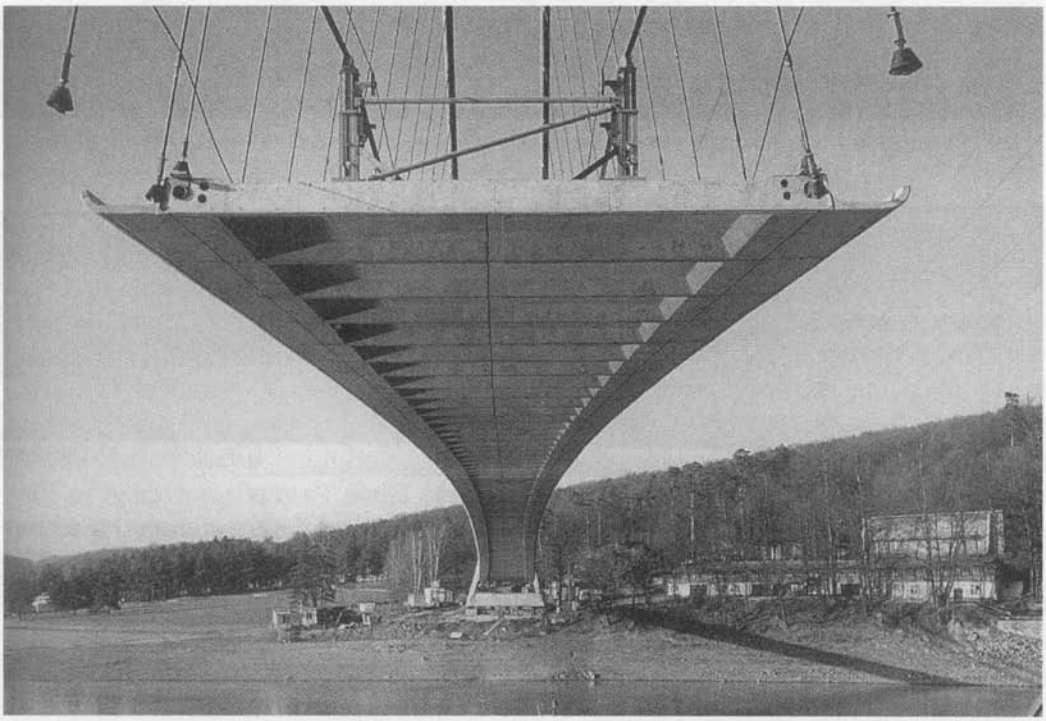

Deck of the 250 m (820 ft) main span Vranov Lake Pedestrian Bridge in the Czech Republic. It was built using fifteen precast segments placed progressively as for stress-ribbon bridges, then internally and externally post-tensioned for final construction. *(Courtesy Precast/Prestressed Concrete Institute.)*

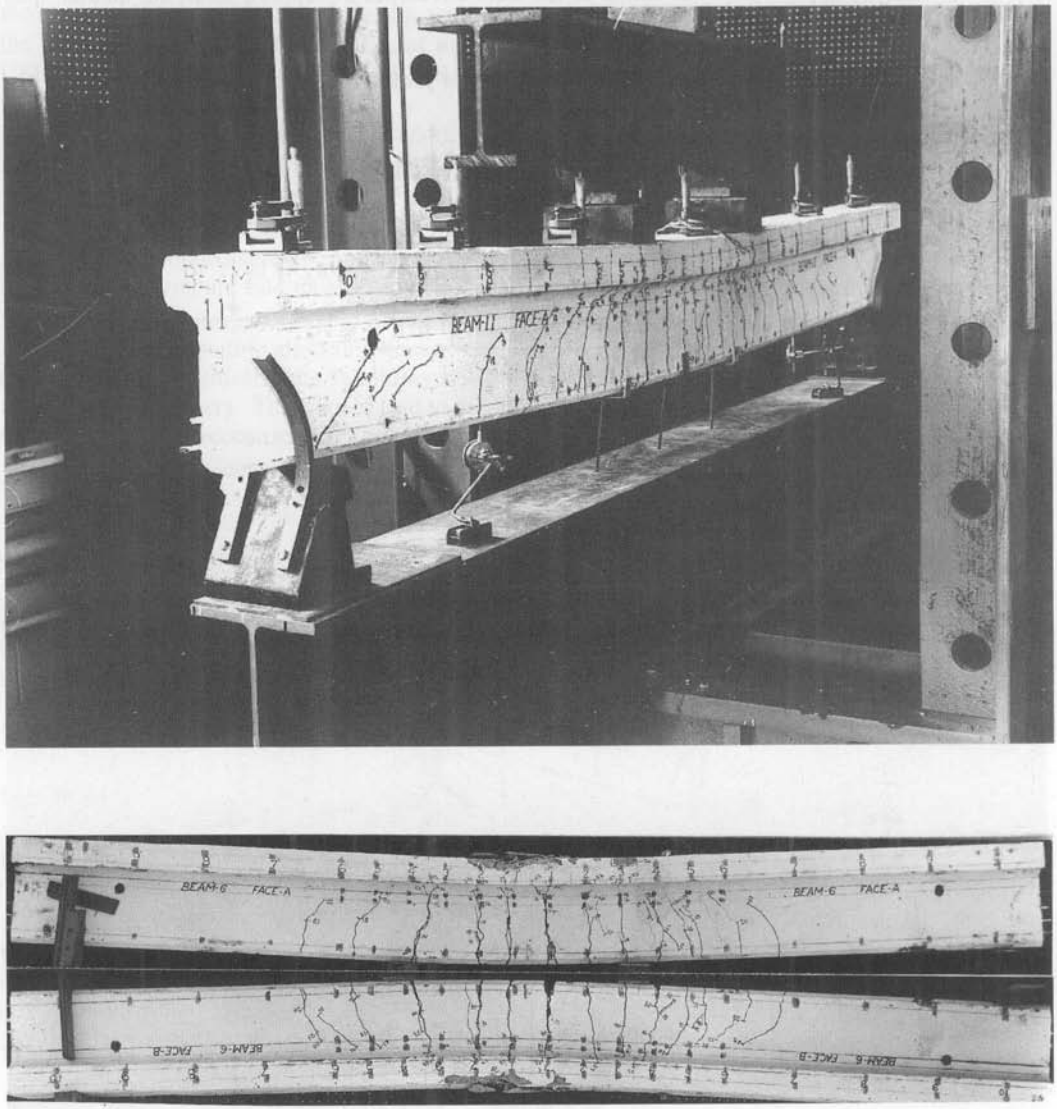

Cracking behavior at failure of test prestressed pretensioned beams. Lower photo shows the two faces of the tested beam. *(Courtesy Edward Nawy, Rutgers University.)*

FLEXURE: ULTIMATE STRENGTH ANALYSIS AND DESIGN

Similarly to reinforced concrete, prestressed concrete offers a great versatility in its flexural behavior. Depending on the values of the design variables and parameters, a prestressed concrete member can be made either to exhibit a great ductility after cracking and before failure, or to fail altogether in a sudden manner. It can be designed to carry a relatively small or large load before failure; thus, in order to achieve a good design, it is essential to understand first the causal effects of important variables on the behavior of prestressed concrete beams at ultimate.

5.1 LOAD-DEFLECTION RESPONSE

The overall behavior of a simply supported prestressed concrete beam subjected to a monotonically increasing load can be well described by its load-deflection curve. Such a typical curve is shown in Fig. 5.1 for an underreinforced beam with bonded tendons. The attributes "underreinforced" and "overreinforced" are explained in Section 5.3. Several points are marked on the curve and correspond to a particular state of behavior. Points 1 and 2 correspond to the theoretically predicted camber of the beam, assumed weightless, when either the initial or the effective prestress is applied. However, when the prestress is applied, self-weight acts automatically. Point 3 represents the camber due to the combined effects of self-weight and the effective prestressing force, assuming all prestress losses have taken place. Typical stress diagrams along the cross section of maximum moment corresponding to points 3 to 9 are also shown in Fig. 5.1. If additional load beyond self-weight is applied, several points of interest can be identified until failure. Point 4 represents the point

of zero deflection and corresponds to a uniform state of stress in the section (also called balanced stress state). Point 5 represents decompression or zero stress at the bottom fiber. If cracking has already occurred due to prior loading, or if the tensile strength of the concrete is assumed nil, point 5 would represent the boundary between cracked and uncracked section behavior and thus would take the place of point 6. Point 6 represents the onset of cracking in the concrete under first loading and, beyond point 6, the prestressed concrete section behaves similarly to a cracked reinforced concrete section subjected to combined bending and compression. If the applied load on the beam keeps increasing the stresses in the steel and the concrete extreme compressive fiber would continue to increase until either material reaches its nonelastic characteristics; this limit is represented by point 7 of Fig. 5.1.

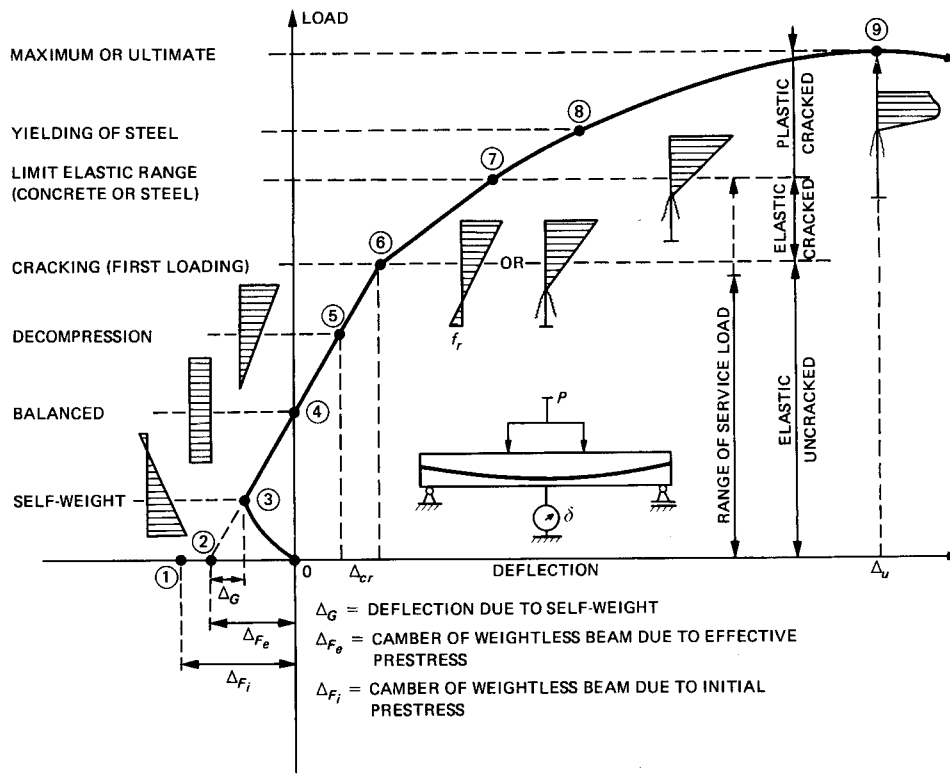

Figure 5.1 Typical load-deflection curve of a prestressed concrete beam (underreinforced, with bonded tendons, first loading).

At increasing loads, the steel would first reach its yielding strength (bonded tendons) represented by point 8, and finally, the maximum capacity of the beam is attained at point 9. Note that point 9 represents the point of maximum load, which is described both as the ultimate load and the load corresponding to the nominal

bending resistance (M_n). Generally beyond this point, the beam still provides some resistance to increasing deflections but at values of loads less than the ultimate load.

Figure 5.1 shows the load-deflection curve of a prestressed concrete beam using bonded tendons. Everything else being equal, if the prestressed tendons were unbonded, the load-deflection curve would, in comparison, fall under the first curve as shown in Fig. 5.2, and very likely failure at ultimate would occur before yielding of the steel. This is because under loading the increase in strain in the unbonded tendon is averaged (since no bond exists) over the length of the tendon between anchorages, and thus is much smaller than the strain increase in the bonded tendon taken at the section of maximum moment. More on the behavior of beams with unbonded tendons can be found in Refs. [5.4 and 1.48].

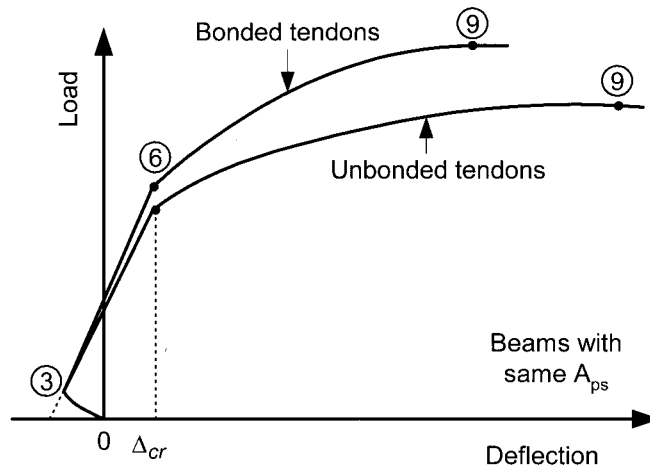

Figure 5.2 Effect of bonded versus unbonded tendons on load deflection curve.

It is informative to understand how the stresses in the prestressing steel and in the concrete's top fiber vary when the load applied on the beam increases to its maximum or ultimate value. This is illustrated in Fig. 5.3 where the stress values at the various stages described in Fig. 5.1 are qualitatively shown directly on the stress-strain curve of the steel and the concrete's top fiber (assuming an underreinforced beam with bonded tendons). Note that at the ultimate point 9, the stress in the prestressing steel, f_{ps}, is not equal to its ultimate tensile strength, f_{pu}. It is, in general, smaller because at maximum load, while the concrete reaches its maximum capacity, the stress in the steel increases to the level needed to maintain the force equilibrium in the section. Note that f_{ps} here is larger than the yield strength, f_{py}. This is mostly the case for underreinforced beams and leads us to explain the different types of failure that might be observed under flexural loading and their relation to the relative amount of reinforcement (Section 5.3).

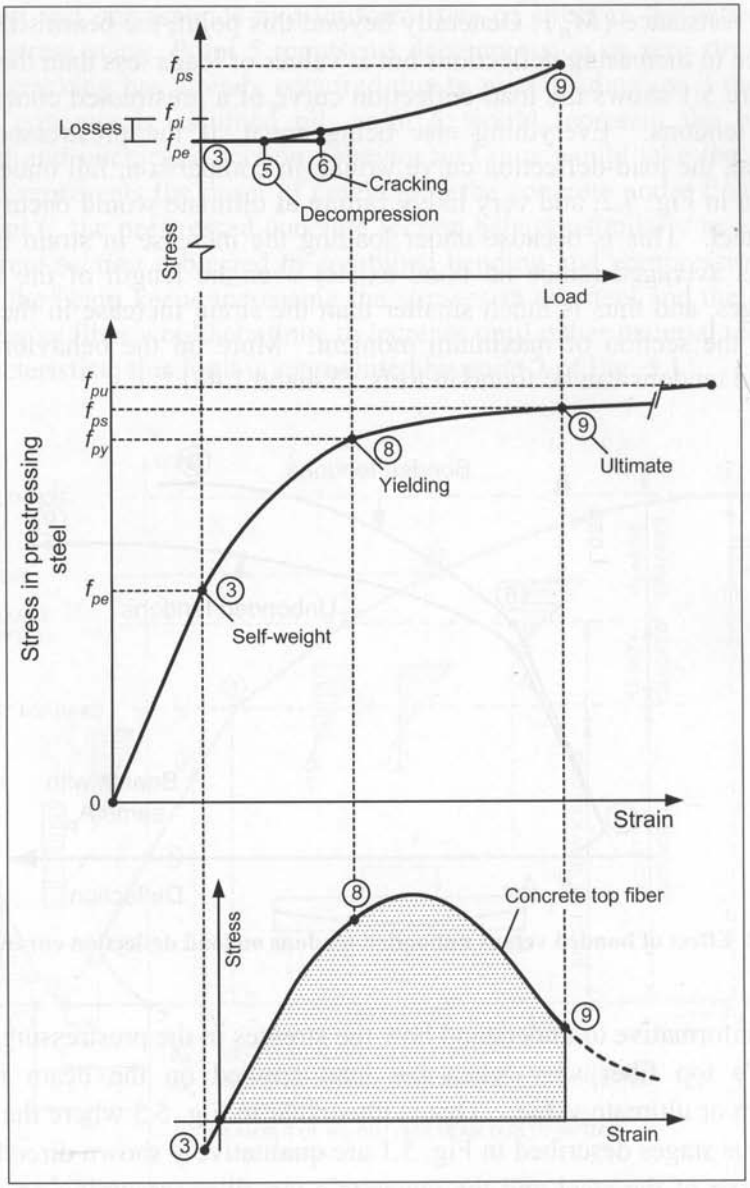

Figure 5.3 Variation of stresses in the concrete and the prestressing steel with applied load.

5.1.1 RC versus PC at Ultimate

Since the concrete in the compression zone fails in the same manner, whether the steel is prestressed or not, one question that comes to mind when comparing reinforced and prestressed concrete sections at ultimate (Point 9 of Fig. 5.1) in bending is: does the prestressing force make any difference at that point? If so, what

is the difference? Consider the stress in the prestressing steel when the load is increased from dead load up to ultimate (Fig. 5.4). Initially, the stress is at point A. Typically for bonded tendons, the stress moves to point B where yielding occurs, and then to point C where failure in the concrete compression zone occurs. It should be noted that once the prestressing steel goes into the nonlinear range of behavior, beyond yielding, the initial prestressing force vanishes gradually. Indeed, if the beam is unloaded along CD, which is about parallel to OA, the permanent non-recoverable strain (or deformation) is likely to become larger than the effective prestrain (ε_{pe}) thus nullifying the prestress. Should the beam be loaded again, along DC, it will behave like a reinforced concrete beam with the only difference that prestressing steel is used instead of reinforcing bars. Failure would occur at point C where the capacity of the concrete compression stress block is attained. Thus, for all practical purposes, the effect of the prestressing force vanishes at ultimate behavior at the section considered.

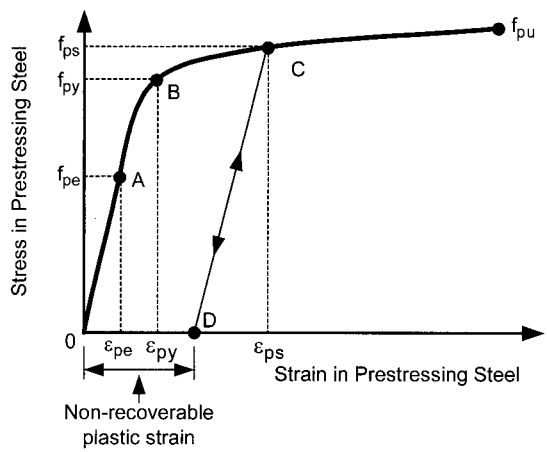

Figure 5.4. Illustration of how the effective prestress vanishes at the critical section at ultimate (mostly for bonded tendons).

5.2 TERMINOLOGY

The terms "fully reinforced concrete" or "fully prestressed concrete" used in this book imply the use, respectively, of either only reinforcing bars or only prestressing tendons to resist the same type of load in concrete structural members. For the purpose of this chapter, a partially prestressed concrete member is a concrete member reinforced with a combination of prestressed and nonprestressed reinforcement designed to resist simultaneously the same external bending load. The nonprestressed reinforcement may be either ordinary reinforcing steel or nontensioned prestressing steel; the prestressed reinforcement may be bonded, unbonded internal, or unbonded external to the concrete section (see Section 1.6).

Some abbreviations used include RC for reinforced concrete, PC for prestressed concrete, and PPC for partially prestressed concrete.

Partial prestressing permits the development of a unified theory of concrete structures in which conventional reinforced and prestressed concrete become special boundary cases. This is treated extensively in a second book in progress on prestressed and partially prestressed concrete [Ref. 1.48] and in Refs. [5.15, 5.18, 5.19, 5.23].

This chapter often refers to two documents, the American Concrete Institute (ACI) Building Code Requirements for Structural Concrete and Commentary (ACI-318), and the American Association of State Highway and Transportation Officials (AASHTO) Load and Resistance Factor (LRFD) Bridge Design Specifications [Refs. 5.1 to 5.3]. For brevity, they will simply be referred to as the ACI and AASHTO codes.

5.3 FLEXURAL TYPES OF FAILURES

The typical load-deflection response of a prestressed concrete beam as described in Fig. 5.1, is a desirable type of behavior; design limitations in various codes tend to ensure such behavior. However, other types of behavior can be observed. As the load is progressively increased on a simply supported prestressed concrete beam, the following types of flexural failures may occur depending on the amount of steel reinforcement provided:

1. Fracture of the steel immediately after concrete cracking, thus leading to sudden failure. This is generally due to an excessively small amount of reinforcement in the section; the beam is described as less than minimally reinforced.

2. Crushing of the concrete compressive zone, preceded by yielding and plastic extension of the steel (bonded tendons). This is generally the preferred mode of failure; the beam is described as underreinforced (Fig. 5.1). Referring to the terminology of the 2002 ACI code, the critical beam section can also be described as "tension-controlled."

3. Crushing of the concrete compressive zone before yielding of the steel. This is generally due to an excessively large amount of reinforcement in the section; the beam is described as overreinforced. Referring to the terminology of the 2002 ACI code, the critical beam section can also be described as "compression-controlled."

Figure 5.5 qualitatively illustrates the above types of failure, assuming an identical beam reinforced with increasing amounts of steel reinforcement. From a ductility and safety viewpoint, the second type of failure is most desirable. Thus,

codes and recommendations generally set limits to minimize the chances of failure due to either an excessively small or excessively large amount of reinforcement in the section. Note that, from the standpoint of behavior and failure modes at ultimate, there is no fundamental difference between reinforced, prestressed and partially prestressed concrete beams.

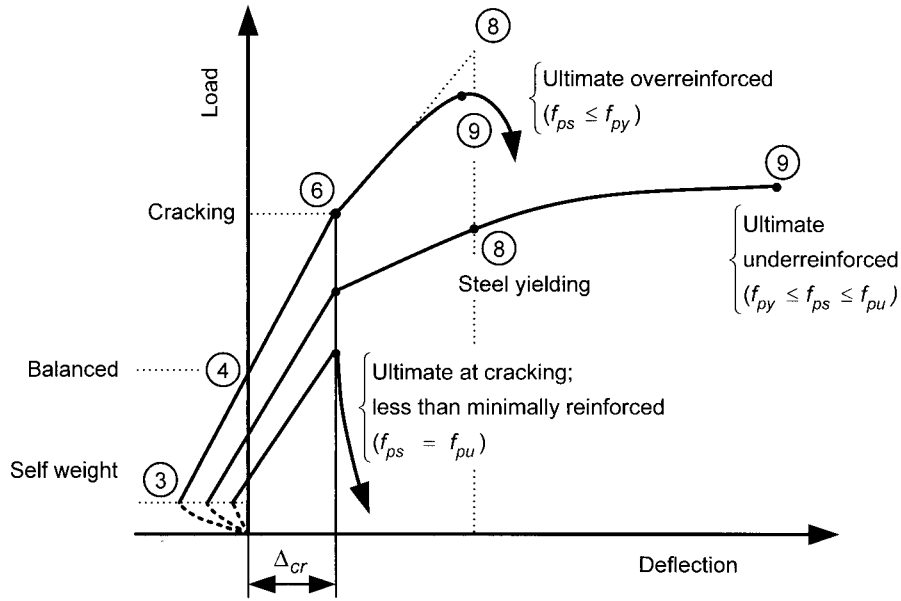

Figure 5.5 Typical change in load-deflection curve with an increase in the amount of reinforcement.

5.4 SPECIAL NOTATION

The computations and equations used in this chapter are often compared to some code provision, such as those of the ACI or AASHTO codes. To minimize confusion, key differences in the notation followed in this text and in the ACI Code are summarized in Fig. 5.6. Note, in particular, that the subscript s is used in this text as a subscript for the case of reinforcing steel, and the subscript p is used when dealing with prestressing steel. Moreover, the ACI Code defines d and d_p as the distance from the extreme compression fiber to the centroid of respectively the nonprestressed and prestressed steel reinforcement, which could be interpreted as the centroid of areas when both reinforcements are present. In this text, d_s and d_p are defined to the centroid of the tensile force in the reinforcing steel and the prestressing steel, respectively. Also, the variable d_e defines the distance from the extreme compression fiber to the centroid of the tensile force resultant in the tensile

reinforcement; the tensile force resultant includes reinforcing steel, prestressing steel, or any of their combinations. Such a definition offers numerous advantages as can be seen in many of the examples below.

ACI Code	**This Book (also AASHTO-LRFD)**
Notation: d to nonprestressed reinforcement d_p to prestressed reinforcement d' to compression steel d_t to extreme layer of tensile reinforcement	**Notation:** d_s to tensile force in nonprestressed reinforcement d_p to tensile force in prestressed reinforcement d_e to centroid of tensile force d' to force in compression steel
Definitions: • Reinforcement ratios: ρ_p, ρ, ρ' $\rho = \frac{A_s}{bd}; \rho_p = \frac{A_{ps}}{bd_p}; \rho' = \frac{A'_s}{bd}$ • Reinforcement indices: $\omega = \rho \frac{f_y}{f'_c} = \frac{A_s f_y}{bdf'_c}$ $\omega_p = \rho_p \frac{f_{ps}}{f'_c} = \frac{A_{ps} f_{ps}}{bd_p f'_c}$ $\omega' = \rho' \frac{f'_y}{f'_c}$ $\omega_p + \frac{d}{d_p}(\omega - \omega')$ $\omega_{pw}, \omega_w, \omega'_w$, reinforcement indices for flanged sections computed as for $\omega_p, \omega, \omega'$ except that b shall be the web width and reinforcement area shall be that required to develop compressive strength of web only.	**Definitions:** $d_e = \frac{A_{ps} f_{ps} d_p + A_s f_y d_s}{A_{ps} f_{ps} + A_s f_y}$ $\omega_e = \omega_p + \omega_s - \omega'$ $\omega_e = \frac{A_{ps} f_{ps} + A_s f_y - A'_s f'_y}{bd_e f'_c}$ 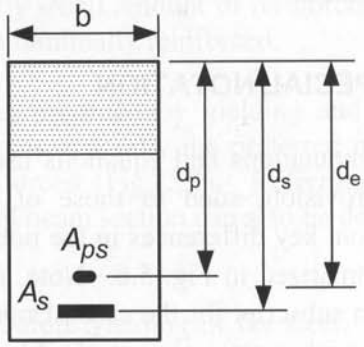

Figure 5.6 Special notation of this book compared to the ACI Code notation.

Fig. 5.6 also shows the definitions of reinforcement ratios and reinforcement indices as given in the ACI Code. For prestressed concrete, we have:

$$\rho_p = \frac{A_{ps}}{bd_p} \tag{5.1}$$

$$\omega_p = \rho_p \frac{f_{ps}}{f'_c} = \frac{A_{ps} f_{ps}}{bd_p f'_c} \tag{5.2}$$

In this chapter, the reinforcement ratios are seldom used except when applying ACI code provisions; instead an effective reinforcing index, ω_e, is utilized. Its definition reflects the state of equilibrium in the section when both prestressed and non-prestressed reinforcements are used and remains valid at the boundaries of fully reinforced and fully prestressed concrete. It is further explained in Sections 5.14.

The inset figure in the right column of Fig. 5.6 illustrates the definition of d_e for a partially prestressed concrete flexural member. When the tensile force due to the prestressing steel and that due to the reinforcing steel can be assumed lumped at the depths, d_p and d_s, respectively, the value of d_e can be computed from:

$$d_e = \frac{A_{ps} f_{ps} d_p + A_s f_y d_s}{A_{ps} f_{ps} + A_s f_y} \tag{5.3}$$

where:

A_{ps} = area of prestressing reinforcement in the tensile zone
f_{ps} = stress in the prestressing steel at nominal flexural resistance of the section (see related recommendations below)
d_p = distance from extreme compression fiber to centroid of tensile force in prestressed steel
A_s = area of nonprestressed tension reinforcement
f_y = specified yield strength of nonprestressed tensile reinforcement
d_s = distance from extreme compression fiber to centroid of tensile force in nonprestressed steel.

Generally, d_e is unknown a priori; d_p and d_s are used directly in the analysis and design of the section (force and moment equilibrium) leading to the nominal moment resistance; d_e is computed during that process. The definition of d_e could also be easily extended to multi-layered systems, such as columns, having different layers of prestressing reinforcement and/or conventional reinforcing bars.

While it is commonly assumed that the reinforcing steel yields at ultimate behavior of the member, the stress, f_{ps}, in the prestressing steel is unknown and should be determined as suggested farther below.

5.5 GENERAL CRITERIA FOR ULTIMATE STRENGTH DESIGN OF BENDING MEMBERS

5.5.1 Design Criteria

To satisfy strength design requirements in bending a number of criteria and related conditions must be satisfied. Figure 5.7 schematically illustrates how the nominal bending resistance M_n and its design value ϕM_n depend on the stress in the prestressing steel at ultimate, and are constrained by minimum and maximum reinforcement criteria and/or conditions related to various levels of reinforcement.

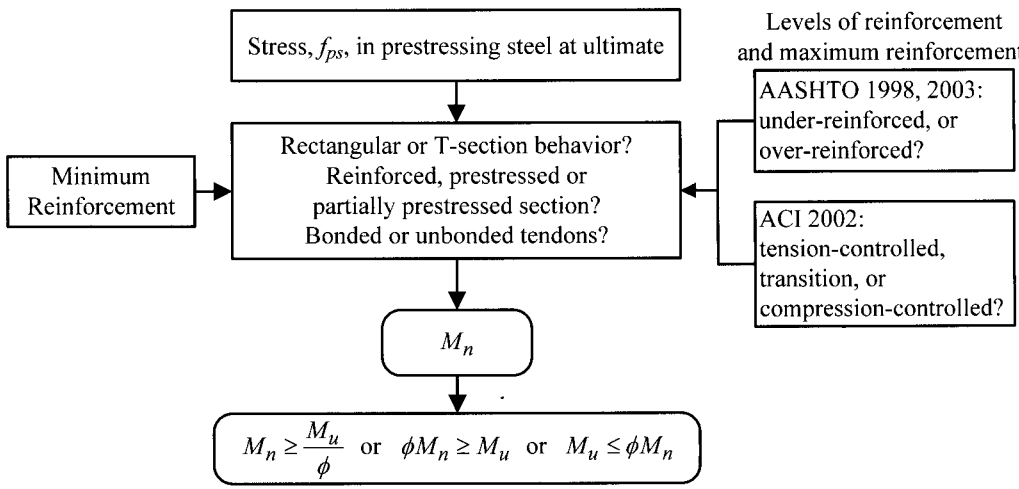

Figure 5.7 Overall constraints influencing the computation of nominal moment resistance, M_n.

1. *Criterion for minimum bending resistance*:

$$M_u \leq \phi M_n \tag{5.4}$$

where M_u is the factored moment due to external loads, M_n is the nominal moment resistance, and ϕ is the strength reduction factor in bending (see Table 3.10 and Section 5.17). In order to compute M_n, the stress in the prestressing steel at nominal bending resistance, f_{ps}, is needed.

2. *Criterion for minimum reinforcement* (Fig. 5.8). This criterion verifies if the amount of reinforcement is larger than or equal to a minimum value to insure that failure does not occur just after concrete cracking.

3. *Criterion for maximum reinforcement or increasing levels of reinforcement* (Figs. 5.11 and 5.14). This criterion evaluates the level of reinforcement in the section and dictates the way the nominal bending resistance is computed for design. The section is checked to evaluate if it is: 1) under-reinforced or over-reinforced according to the AASHTO LRFD code; or 2) tension-controlled, compression-controlled, or transition, according to the ACI 2002 code. Appropriate ϕ factors are used for each case.

4. *Criterion for moment redistribution* (Sections. 5.21 and 10.14.3). This criterion applies to continuous beams or statically indeterminate frames only. It allows for moment redistribution from one critical section to another, to account for the formation of plastic hinges.

Several provisions are given in various building and bridge codes to satisfy the above criteria. While the same underlying principles are used as a basis for such provisions, the actual provisions may be expressed differently, as done, for instance, in the ACI and AASHTO codes.

Note that for computing M_n, the treatment of flanged sections differs from that of rectangular sections and expressions for partially prestressed sections must remain valid at the boundaries of reinforced and prestressed concrete (Fig. 5.7). Also, the prediction equations for the value of f_{ps} at ultimate are different for bonded and unbonded tendons and will influence the sequence of design steps leading to M_n. This is true in spite of the fact that M_n values obtained following different codes such as ACI and AASHTO will generally be very close.

5.5.2 Minimum Reinforcement or Minimum Moment Resistance: Code Recommendations

When the amount of reinforcement is relatively small, it may not be sufficient to resist the increase in tensile force generated (or transferred to the reinforcement) immediately after concrete cracking to maintain moment equilibrium in the cracked section; thus, a brittle failure occurs by fracture of the reinforcement. To avoid such undesirable failure, codes of practice recommend minimum amounts of reinforcement by specifying a minimum value of the reinforcement ratio or a minimum nominal bending resistance.

Figure 5.8 summarizes the conditions set for minimum reinforcement in the ACI and AASHTO codes for reinforced and prestressed concrete. For reinforced concrete, ACI specifies a minimum area of reinforcement, while AASHTO specifies a minimum reinforcement ratio. For statically determinate members with a flange of width b in tension, ACI specifies that b_w in the equation giving $A_{s,min}$ shall be replaced by b or $2b_w$ whichever is smaller. When the flange is in compression, b_w is used.

2002 ACI Code	**2003 AASHTO – LRFD**
Reinforced Concrete [10.5]: • For units in psi and inch: $A_{s\,min} = \frac{3\sqrt{f'_c}}{f_y} b_w d_s \geq \frac{200}{f_y} b_w d_s$ • For units in MPa and mm: $A_{s\,min} = \frac{\sqrt{f'_c}}{4 f_y} b_w d_s \geq \frac{1.4}{f_y} b_w d_s$ **Prestressed and Partially Prestressed Concrete [18.8]:** $\phi M_n \geq 1.2 M_{cr}$	**All Cases (RC, PC, PPC) [5.7.3.3.2]:** $\phi M_n \geq 1.2 M_{cr}$ $\phi M_n \geq 1.33 M_u$ **Particular result for reinforced concrete [5.7.3.3.2-1]:** $\rho_s \geq \rho_{s\,min} = \frac{A_{s\,min}}{b_w d_s} = \frac{0.03 f'_c}{f_y}$ Note: for T sections, ρ_s is based on web only; $\rho_{s\,min}$ is unit independent.

Figure 5.8 Minimum reinforcement for flexural members.

For prestressed concrete, both the ACI and the AASHTO codes base their requirements on a minimum moment resistance. At any section of a flexural member, the amount of reinforcement shall be adequate to develop a design nominal moment resistance at least 1.2 times the cracking moment computed on the basis of the modulus of rupture, f_r, of the concrete material. Thus, the minimum reinforcement shall be such that:

$$\phi M_n \geq 1.2 M_{cr} \quad or \quad \frac{\phi M_n}{M_{cr}} \geq 1.2 \tag{5.5}$$

where M_n is the nominal bending resistance and M_{cr} is the cracking moment. The positive moment leading to cracking on the bottom fiber of a prestressed or partially prestressed concrete beam is given by Eq. (4.41):

$$M_{cr} = A_{ps} f_{pe} \left(e_o + \frac{Z_b}{A_c} \right) - f_r Z_b \tag{5.6}$$

For members reinforced with reinforcing bars only (i.e., reinforced concrete), Eq. (5.5) can be satisfied by providing a reinforcement ratio not less than the minimum reinforcement ratio given by:

$$\rho_{s\,min} = 0.03\frac{f'_c}{f_y} \tag{5.7}$$

where f_y is the yield strength of the reinforcing steel. Equation (5.7) is used in the AASHTO LRFD code. The proof of Eq. (5.7) is developed in Section 5.16.

In the negative moment region of T sections, such as at the supports of continuous beams, the cracking moment (top fiber cracking on flange side) may be relatively large because of a large Z_t. In that case, it may be difficult to satisfy Eq. (5.5), and AASHTO allows to bypass this condition provided $\phi M_n \geq 1.33 M_u$. ACI uses the same waiver as AASHTO for reinforced concrete; however, for prestressed concrete, ACI permits to waive the provision, provided the shear and flexural strength of the flexural member are at least twice that required.

5.5.3 ACI Code Provisions for Tension-Controlled, Transition, and Compression-Controlled Sections at Increasing Levels of Reinforcement

The 2002 ACI code states the following:

> *"Sections are tension-controlled when the net tensile strain in the extreme tension steel is equal to or greater than 0.005 just as the concrete in compression reaches its assumed strain limit of 0.003.... Sections are compression-controlled when the net tensile strain in the extreme tensile steel is equal to or less than the compression controlled strain limit at the time the concrete in compression reaches its assumed strain limit of 0.003.... For Grade 60 reinforcement and for all prestressed reinforcement, it shall be permitted to set the compression-controlled strain limit equal to 0.002."*

The net tensile strain, ε_t, is defined as the tensile strain in the extreme tension steel at nominal strength, exclusive of strains due to prestress, creep, shrinkage and temperature. Associated with this strain, the code introduced a new variable, d_t, defined as the depth from the extreme compression fiber to the extreme layer of tension steel.

Figure 5.9*a* illustrates the definition of net tensile strain for a prestressed member with bonded tendons, and Fig. 5.9*b* (see also Fig. 3.8) illustrates the provisions of the 2002 code for the ϕ factor. It gives the linear equations to compute the ϕ factor for the transition region in terms of either the net tensile strain or the ratio c/d_t (which is proportional to the net tensile strain). c represents the depth of neutral axis at ultimate and d_t represents the distance from the extreme compression fiber of concrete to the extreme tension layer of reinforcement. So if there are two or more layers of reinforcement, d_t is to the layer closest to the extreme tensile fiber of concrete.

Figure 5.10 shows different beam sections where the definition of d_t is illustrated versus the conventional depths, d_s and d_p, which are defined from the extreme

compression fiber to the centroid of the forces in the reinforcing steel and prestressing steel, respectively. Figure 5.10 also illustrates the definition of d_e as defined in the AASHTO LRFD Bridge Design Specifications [Ref. 5.1], that is the depth from the extreme compression fiber to the centroid of the tensile force resultant in the tensile reinforcement; it is described by Eq. 5.3. The depth d_e is adopted in this text for most requirements instead of d_t which is used only for detailing.

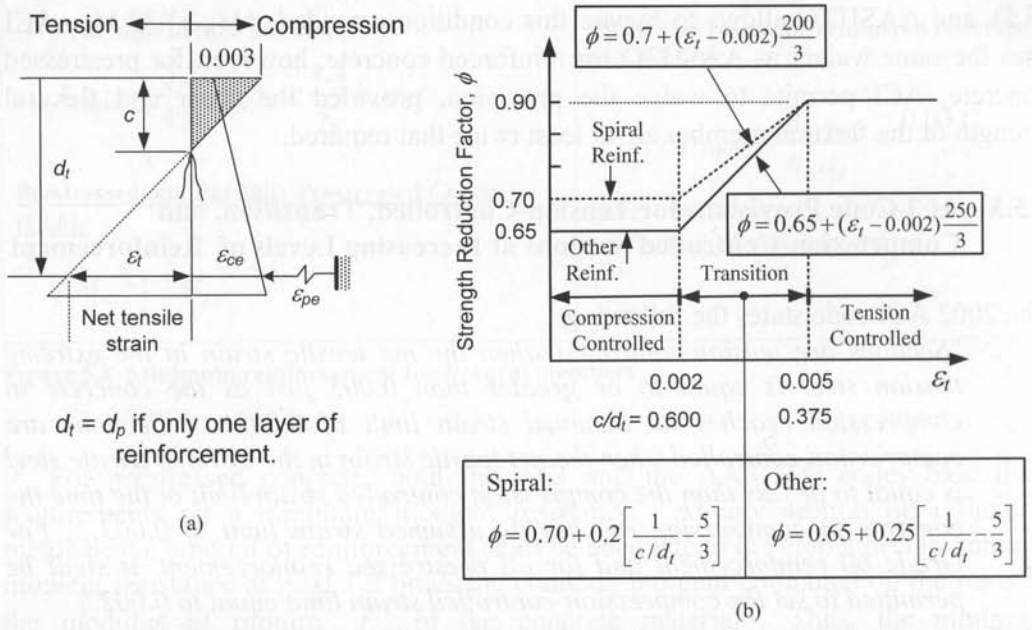

Figure 5.9 Definition of: (a) net tensile strain for a prestressed concrete beam with bonded tendons, and (b) corresponding strength reduction factor as per ACI code Fig. 9R3.2.

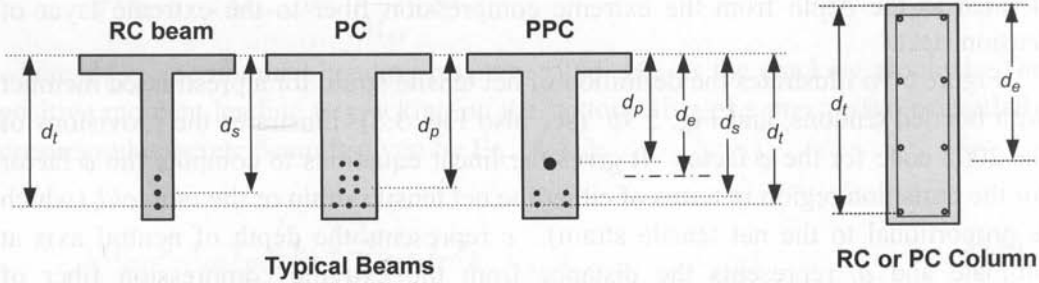

Figure 5.10 Definitions of various depths from extreme compression fiber to different layers of reinforcement.

For Grade 60 reinforcement and for all prestressed concrete reinforcement, a section is assumed to be compression-controlled when the net tensile strain in the extreme tension steel is equal to or less than 0.002. In that case the ϕ factor is taken

as 0.70 or 0.65 depending on whether the compression member is respectively spirally reinforced or reinforced (transversally) by other reinforcement.

Figure 5.11*a* and 5.11*b* summarize, respectively, the 1999 and 2002 ACI code approach regarding levels of reinforcement in a reinforced or prestressed concrete section. Several axes are drawn to illustrate the limits on various variables.

From Fig. 5.11*a* it can be observed that limiting the reinforcement ratio for reinforced concrete is the same as limiting the ratio c/d_s, or limiting the tensile strain at the centroid of the reinforcement, ε_s. For $0.75\rho_b$ the ratio $c/d_s = 0.44$ and $\varepsilon_s = 0.0038$. In Fig. 5.11*a*, the yield strength of conventional bars was taken as 60 ksi, and their modulus as 29,000 ksi, leading to a yield strain of 0.00207, which is rounded to 0.002. Another axis is drawn to show the limit for prestressed concrete in terms of the prestressing index, ω_p, which, according to Eq. (5.65), can be also put in terms of the c/d_p ratio. Figure 5.11*a* shows that there are different ways to provide a limit to the same level of reinforcement and that these limits are directly related. Depending on these limits, the code specifies a value of the capacity reduction factor, ϕ, used in design.

Figure 5.11*b* illustrates the approach in the 2002 ACI code where the strain axis summarizes the limits for sections that are tension-controlled, compression-controlled, or in the transition region. Corresponding values of the ϕ factor and the ratio c/d_t are shown on additional axes below the strain axis. Note that the value of net tensile strain of 0.002 in the 2002 code corresponds to the value of balanced reinforcement ratio, ρ_b, for reinforced concrete when only one layer of reinforcement is used. When the net tensile strain in the extreme tension steel is equal to or greater than 0.005, the section is defined as tension-controlled. In that case the ϕ factor is taken as 0.9. The value of a net tensile strain of 0.005 corresponds to a value of reinforcement ratio $\rho_s = 0.63\rho_b$ in reinforced concrete when only one layer of reinforcement is used. For sections in which the net tensile strain in the extreme tension steel at nominal strength is between the limits for compression-controlled and tension-controlled sections, ϕ is permitted to be linearly increased from its value for compression controlled sections to 0.90 as the net tensile strain in the extreme tension steel at nominal strength increases from 0.002 to 0.005 (Fig. 5.9*b*). In addition, for the purpose of achieving a minimum ductility in reinforced concrete flexural members, the code recommends to limit the net tensile strain to 0.004; thus, should the net tensile strain become smaller than 0.004 under pure bending, it is recommended to add compression reinforcement, hence reducing the c/d_t (or c/d_e) ratio and increasing the net tensile strain.

In comparing Figs. 5.11*a* and 5.11*b*, two observations can be made:

1. The net tensile strain limit corresponding to balanced conditions in the 1999 code is the same as the limit for compression-controlled section (i.e., 0.002) in the 2002 ACI code; however, the specified limits for tension-controlled and under-reinforced section do not match exactly; indeed the value of net

tensile strain of 0.005 in a singly reinforced concrete section would correspond to about $0.63\rho_b$.

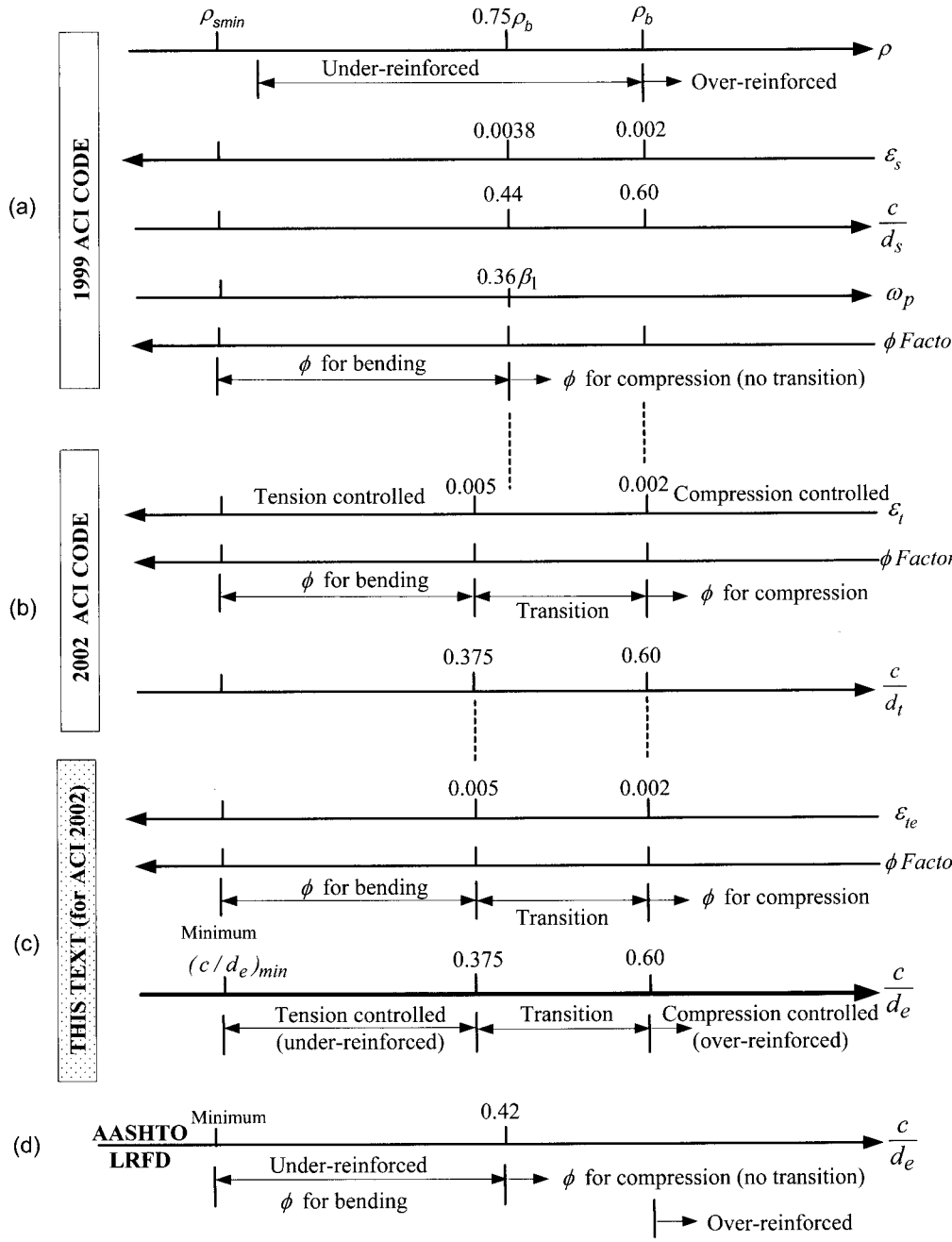

Figure 5.11 Comparison for limits of reinforcement in flexural members.

2. The use of d_t, as defined in Fig. 5.10, for any purpose other than detailing is not warranted since, to insure equilibrium of forces we need d_e as defined earlier in Eq. (5.3) especially if several layers of reinforcement or different combinations of it are present.

Figure 5.11*c* summarizes the approach followed in this text and justified below. It shows that all the bending reinforcement limits applicable to reinforced, prestressed, and partially prestressed concrete rectangular and flanged sections can be expressed in terms of a single ratio c/d_e, which can be easily calculated from the equations of equilibrium at nominal resistance. For comparison, Fig. 5.11*d* illustrates the current AASHTO LRFD limit of maximum reinforcement for under-reinforced sections for all structural concrete bending members.

Tensile Strain and c/d_e Ratio

Figure 5.12 illustrates the strain (and force) diagram at nominal bending resistance of a partially prestressed concrete section and, at the boundaries, applies to a reinforced or a prestressed concrete section as well. In all cases, the concrete stress block in compression (see Section 5.6) is assumed the same, while on the tensile side, the resisting tensile force, T, is provided by the reinforcement. This representation makes the composition of the reinforcement irrelevant since the tensile force T must equal the compression force C in all cases. The strain diagram allows us to use similar triangles leading to a direct relationship between strain ratios and depth ratios. The following relation can be derived:

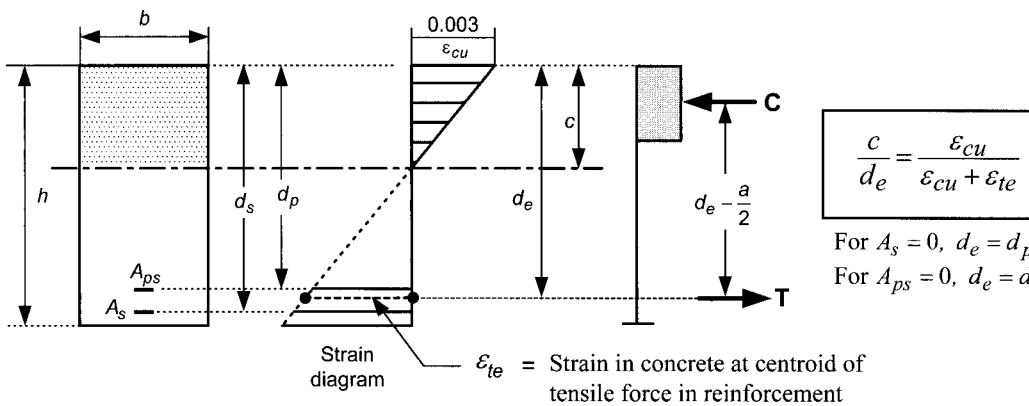

Figure 5.12 Relationship between c/d_e ratio and the strain in the concrete at the centroid of the tensile force in the reinforcement.

From the similar triangles in the strain diagram (Fig. 5.12):

$$\frac{\varepsilon_{cu}}{\varepsilon_{cu}+\varepsilon_{te}}=\frac{c}{d_e} \tag{5.8}$$

which leads to:

$$\varepsilon_{te} = \varepsilon_{cu}\frac{d_e - c}{c} = \varepsilon_{cu}\left(\frac{1}{c/d_e} - 1\right) \tag{5.9}$$

where:

c = depth of the compression stress block at nominal resistance

ε_{cu} = assumed failure strain of concrete in compression

ε_{te} = tensile strain in the concrete at the level of the centroid of the resultant tensile force in the tension reinforcement, that is at the level of d_e

d_e = depth from the extreme compression fiber to the centroid of the tensile force resultant in the tension reinforcement (prestressed and/or non-prestressed (Eq. 5.3)); note that $d_e = d_p$ for $A_s = 0$, and $d_e = d_s$ for $A_{ps} = 0$

Two remarks are relevant in relation to Eqs. (5.8 and 5.9):

1. Since ε_{cu} is taken as a constant, there is a unique relationship between the c/d_e ratio and the tensile strain in the concrete at the centroid of the tensile force, ε_{te}. This suggests that, while limiting the tensile strain is useful for background and understanding, using the c/d_e ratio is much simpler to implement in design.
2. Eqs. (5.8 and 5.9) use the *tensile strain in the concrete* at the level of the centroid of the tensile force. It is truly a fictitious tensile strain since the section is cracked. However, it follows the linear strain diagram assumed for compatibility. The tensile strain in the concrete is the same as the net tensile strain in the steel for reinforcing bars and bonded prestressing tendons. However, it is significantly different from the net tensile strain in unbonded prestressing tendons. Figure 5.13 illustrates the meaning of these strain cases. Thus using the tensile strain in the concrete, ε_{te}, is preferred because it applies to all cases and is much easier to compute from the stain diagram of Fig. 5.12.

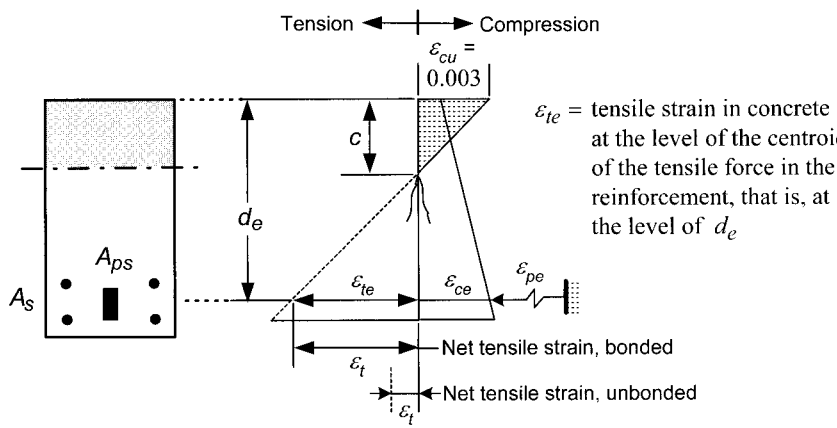

Figure 5.13 Definition of ε_{te} and d_e as adopted in this text.

Note finally that Eq. (5.8) is general in its form and is valid for any fiber in the tensile zone, such as the extreme layer of reinforcement, provided the strain and the depth are defined for the same fiber.

Amendments Adopted in this Text

The author strongly believes that the c/d_e ratio accommodates more easily and accurately than the net tensile strain the intent of the 2002 ACI code to provide a transition from tension-controlled to compression-controlled sections, and relates well with the previous recommendations (1999 ACI code) on maximum reinforcement and moment redistribution [Refs. 5.16, 5.19, 5.24, 5.28]. Moreover, as shown in Section 5.21 and 10.14, the moment redistribution requirement for structural concrete, and the minimum reinforcement requirement for reinforced concrete rectangular sections recommended in the 2002 ACI code can also be expressed in term of the ratio c/d_e.

The general approach by the 2002 ACI Code offers uniformity for all combinations of reinforcement and a smooth transition in reducing the ϕ factor between tension-controlled sections (such as beams) and compression-controlled sections (such as columns). However, in its original form, the code may lead to some inconsistent results essentially due to the use ε_t and d_t [Ref. 5.28]. For this reason the following amendments are adopted in this text:

- *Change the definition of d_t to d_e, that is: "depth to the centroid of the resultant tensile force in the tensile reinforcement."* This will imply a net tensile strain at the level of the centroid of the tensile force and will fix a major inconsistency where a section can be "tension-controlled" according to the 2002 code while over-reinforced, according to the 1999 code.

- *Change the definition of the net tensile strain in the extreme layer of reinforcement, ε_t, to mean ε_{te}, that is: "the tensile strain in the concrete at the level of the centroid of tensile force in the reinforcement, that is at the level of d_e."* This will take care of members prestressed with internal or external unbonded tendons, which otherwise will all be "compression-controlled" according to the 2002 code, and will be penalized with a reduced ϕ factor.

- *Define the limits for "tension-controlled", "compression-controlled" and "transition" in terms of the c/d_e ratio which is much easier to handle than the tensile strain, or net tensile strain.* The variables c and d_e are included in the equilibrium equations for nominal bending resistance and thus can be readily calculated. Figure 5.11*c* shows these limits which are consistent with the amendments adopted in this text. In particular the ϕ factor (Fig. 5.9*b*) expressed in terms of either the c/d_e ratio or ε_{te}, becomes:

$$
\begin{cases}
\bullet\ \text{For: } \dfrac{c}{d_e} \le 0.375 \ \text{ or } \ \varepsilon_{te} \ge 0.005 \ \Rightarrow \ \text{use } \phi = 0.9 \\
\bullet\ \text{For: } \dfrac{c}{d_e} > 0.60 \ \text{ or } \ \varepsilon_{te} < 0.002 \ \Rightarrow \text{use } \phi = 0.7 \text{ (spiral) or } 0.65 \text{ (other)} \\
\bullet\ \text{For: } \begin{cases} 0.375 < \dfrac{c}{d_e} < 0.60 \\ \text{or} \\ 0.005 < \varepsilon_{te} < 0.002 \end{cases} \Rightarrow \text{use } \begin{cases} \phi = 0.70 + 0.20\left(\dfrac{1}{c/d_e} - \dfrac{5}{3}\right) & \text{spiral} \\ \phi = 0.65 + 0.25\left(\dfrac{1}{c/d_e} - \dfrac{5}{3}\right) & \text{other} \end{cases}
\end{cases}
\tag{5.10}
$$

5.5.4 AASHTO LRFD Recommendation on Maximum Reinforcement

The AASHTO code has a single limitation on maximum reinforcement for reinforced, prestressed and partially prestressed rectangular or T sections, expressed as follows (Fig. 5.14):

$$\frac{c}{d_e} \le 0.42 \tag{5.11}$$

For $c/d_e \le 0.42$ the section is described as "under-reinforced" and a ϕ factor equal to 1 is used for prestressed concrete and 0.9 for reinforced concrete. For $c/d_e > 0.42$, the section is described as "over-reinforced" and a ϕ factor equal to 0.70 is used while the nominal bending moment is computed from the compression force of the couple assuming $c/d_e = 0.42$.

AASHTO – LRFD [5.7.3.3.1]

All Cases: RC, PC, PPC, Rectangular or T Sections:

$\dfrac{c}{d_e} \le 0.42 \rightarrow$ Underreinforced

$\dfrac{c}{d_e} > 0.42 \rightarrow$ Overreinforced

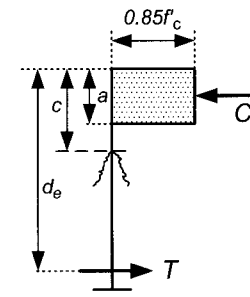

Figure 5.14 Limitation for maximum reinforcement according to the 2003 AASHTO LRFD.

5.6 BACKGROUND FOR ANALYSIS OF SECTIONS AT ULTIMATE

Before going into detailed analysis and design steps, it is necessary to provide first a basis for the analysis of the section at ultimate in order to compute its nominal bending resistance, M_n. Background information can be found in Refs. [5.7, 5.9, 5.10, 5.13, and 5.32 to 5.34].

5.6.1 Objective – Assumptions

The purpose of the analysis at ultimate or maximum load is generally to determine the nominal moment resistance, M_n, that is, the moment at ultimate behavior of the section, assuming that cross-sectional dimensions, material properties, and amounts of reinforcement are given. As pointed out earlier, the stress in the steel and in the concrete at ultimate are well outside their linear range of behavior. A more exact analysis (called strain compatibility analysis or non-linear analysis), which takes into account the actual stress and strain distributions in the section and the constitutive equations of the concrete and the reinforcement is presented in Refs. [5.15, 5.18, 5.23, and 1.48]. Such an accurate analysis, however, is not very efficient in everyday situations and codes of practice tend to propose simplifying assumptions, which allow for a quick but sufficiently accurate evaluation of nominal moment resistance. Widely accepted assumptions are (for most codes) as follows:

1. *Plane sections remain plane under loading* (that is, axial load and bending moment). Consequently, it is assumed that a linear strain distribution exists along the concrete section up to ultimate load.

2. *Perfect bond exists between steel and concrete.* A direct result of this assumption is that any strain change in the steel due to an applied load is equal to the strain change in the concrete at the level of the steel due to the same load. (The case of unbonded tendons, for which this assumption does not apply, must be treated separately and is discussed in Refs. [1.48, 5.20, 5.23]. However, for design, the approximations suggested in the codes and described below are sufficient.)

The ACI code proposes the following additional assumptions (Fig. 5.15):

3. *The limiting compressive strain of the concrete ε_{cu} is equal to 0.003.* This is regardless of the strength of the concrete, the shape of the section, and the amount of reinforcement. It is also considered the same for normal weight and structural lightweight concrete.

4. *The tensile strength of concrete is neglected.* Thus, the point of zero stress represents the boundary between the cracked and the uncracked part of the section.

5. *The total force in the concrete compressive zone can be well approximated* by considering a uniform stress of magnitude $0.85f'_c$ over a rectangular block of width b and depth $a = \beta_1 c$ (Eq. 5.19), where c represents the depth of the neutral axis and β_1 is a factor defined as follows for the US and SI system, respectively:

$$\begin{cases} \beta_1 = 0.85 \text{ for } f'_c \le 4000 \text{ psi} \\ \beta_1 = 0.65 \text{ for } f'_c \ge 8000 \text{ psi} \\ \beta_1 = 0.85 - 5\times10^{-5}(f'_c - 4000) \text{ psi for } 4000 \le f'_c \le 8000 \text{ psi} \end{cases} \quad (5.12)$$

$$\begin{cases} \beta_1 = 0.85 \text{ for } f'_c \le 28 \text{ MPa} \\ \beta_1 = 0.65 \text{ for } f'_c \ge 56 \text{ MPa} \\ \beta_1 = 0.85 - 5\times10^{-2}(f'_c - 28)/7 \text{ MPa for } 28 \le f'_c \le 56 \text{ MPa} \end{cases} \quad (5.13)$$

The concept of the rectangular stress block was first proposed by Whitney [Ref. 5.33, 5.34]. Other shapes of stress distribution such as the trapezoidal and parabolic shapes, or an exact shape (from tests), have been used and are accepted by the ACI code (Sec. 10.2.6). However, the rectangular distribution leads to the simplest prediction equations with little loss in accuracy. It is summarized in Fig. 5.15.

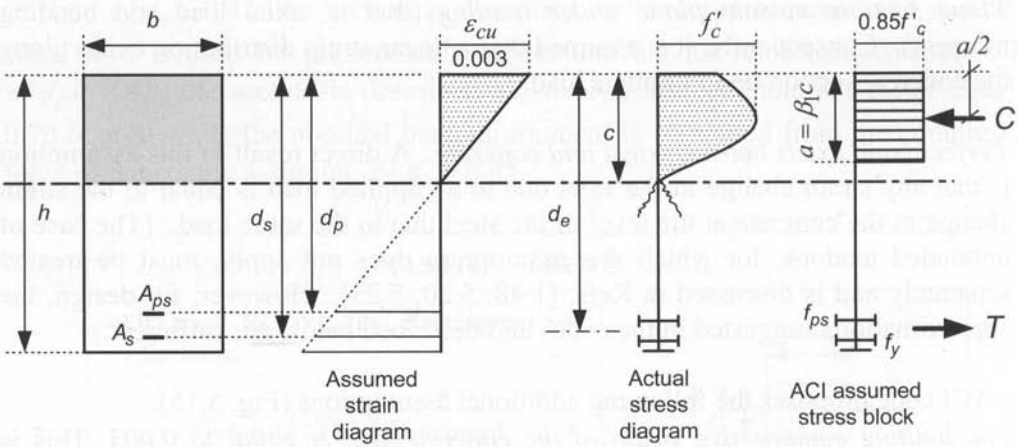

Figure 5.15 Stresses and strains at ultimate behavior, as assumed by the ACI code.

6. It is also assumed that when reinforcing steel is used, *its stress-strain curve is elastic perfectly plastic, and its stress at ultimate is its yield strength, f_y*. This is not the case for prestressing steel. Its stress at ultimate, f_{ps}, is unknown and generally given by a code prediction equation. Using a strain compatibility

analysis, it can be shown that this assumption is valid for the material properties currently used, namely the stress-strain curve of the reinforcing steel, the effective prestress, stress-strain curve of the prestressing steel, and the ultimate compressive strain of concrete. Figure 5.16 illustrates this assumption.

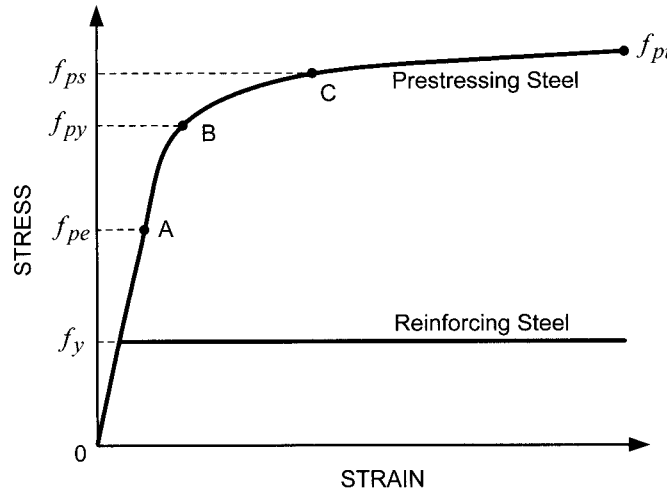

Figure 5.16 Typical stress-strain curves assumed for the reinforcement.

5.6.2 Satisfying Equilibrium

Whatever the assumptions and the particular approaches taken by different codes are, two equations of static's pertaining to the equilibrium of forces and moments of the section at ultimate can be written. They have a different form depending on the shape of the section and are developed below for rectangular and T or flanged sections with prestressed and nonprestressed conventional reinforcement. When only prestressing steel is used, set $A_s = 0$; when only reinforced concrete is used set $A_{ps} = 0$; the equations provided below remain valid.

5.7 NOMINAL BENDING RESISTANCE: MATHEMATICAL FORMULATION FOR RECTANGULAR SECTION OR RECTANGULAR SECTION BEHAVIOR – UNDER-REINFORCED AND TENSION-CONTROLLED

The approach described in Section 5.6 is applied here to a specific section. It is assumed that conditions relating to the minimum and maximum reinforcement provisions are satisfactory and that an under-reinforced and/or tension-controlled section is considered.

While the analysis method is based on the same principles of equilibrium, the step-by-step procedure and the sequence in which the steps are followed depend on the prediction equation for the stress in the prestressing steel at ultimate, f_{ps}. Two different representative cases are considered in this text, one related to the ACI code and the other to the AASHTO code. The first one is presented next while the second is described in Section 5.12.

5.7.1 Force Equilibrium

Referring to Figs. 5.15 and 5.17, the force equilibrium equation can be set by writing that the compressive force in the concrete compression block is equal to the total tensile force in the steel reinforcement, thus:

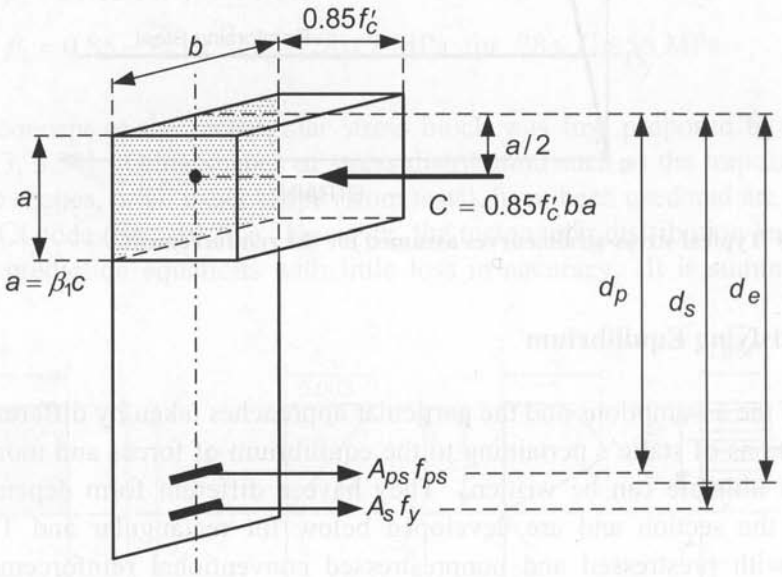

Fig 5.17 Rectangular section: forces at ultimate.

$$0.85f'_c b\beta_1 c = 0.85f'_c ba = A_{ps}f_{ps} + A_s f_y \tag{5.14}$$

where:

A_{ps} = area of prestressing reinforcement in the tensile zone

f_{ps} = stress in the prestressing steel at nominal flexural resistance of the section

A_s = area of nonprestressed tension reinforcement

f_y = specified yield strength of nonprestressed tensile reinforcement

c = depth of neutral axis at ultimate
a = depth of rectangular stress block = $\beta_1 c$ (Eq. 5.19)

If the equation predicting the value of f_{ps} is independent of a (or c), such as in the current ACI Code Eq. (5.32) or (5.33), then a can be calculated directly from Eq. (5.14) as:

$$a = \beta_1 c = \frac{A_{ps} f_{ps} + A_s f_y}{0.85 f'_c b} \tag{5.15}$$

However, if the prediction equation of f_{ps} is function of a or c, such as in the AASHTO code, then the solution can be obtained by solving simultaneously the two equations for two unknowns, a and f_{ps}. A solution procedure with the AASHTO equation is given in Section 5.12.

5.7.2 Moment Equilibrium

The moment equation states that the nominal moment resistance of the section is equal to the internal couple or moment of the above equal and opposite forces, thus:

$$\begin{cases} M_n = A_{ps} f_{ps} \left(d_p - \dfrac{a}{2} \right) + A_s f_y \left(d_s - \dfrac{a}{2} \right) \\ M_n = A_{ps} f_{ps} \left(d_p - \dfrac{\beta_1 c}{2} \right) + A_s f_y \left(d_s - \dfrac{\beta_1 c}{2} \right) \end{cases} \tag{5.16}$$

where

d_p = distance from extreme compression fiber to centroid of tensile force in prestressed reinforcement
d_s = distance from extreme compression fiber to centroid of tensile force in non-prestressed tensile reinforcement

It is worth mentioning that Eq. (5.16) is not unique in this form. It could be written in different ways; for instance, if the force in the concrete is used instead of using the force in the steel, Eq. (5.16) becomes:

$$M_n = 0.85 f'_c b a \left(d_e - \frac{a}{2} \right) \tag{5.17}$$

or

$$M_n = (A_{ps} f_{ps} + A_s f_y)\left(d_e - \frac{a}{2}\right) \tag{5.18}$$

in which d_e is the distance from the extreme compression fiber to the centroid of the tensile force resultant in the reinforcement; it can be computed from Eq. (5.3). Another way to write M_n is in function of the effective reinforcing index ω_e as defined later in Eq. (5.67).

5.7.3 Solution Procedure

Assuming sectional and material properties are given, Eqs. (5.14) and (5.16) contain three unknowns, a, f_{ps} and M_n. Thus, a third equation is needed to obtain a feasible solution. Generally, a prediction equation for f_{ps} is given in the code. In US practice, the expressions given in the ACI and AASHTO codes are different. They are explained in a separate section (Section 5.11), since their use leads to a different sequence in a number of design steps to be followed. In either case, a solution can be obtained from solving the three equations.

The depth of the equivalent rectangular stress block, a, is related to the depth of the neutral axis, c, at ultimate by the following relation (Figs. 5.15 and 5.17):

$$a = \beta_1 c \tag{5.19}$$

or inversely:

$$c = \frac{a}{\beta_1} \tag{5.20}$$

A flow chart illustrating the design steps leading to M_n assuming the prediction equations for f_{ps} are taken from the ACI code, is developed later in Fig. 5.24; examples of application are given next.

To satisfy certain provisions of the AASHTO code and to simplify some design problems, it is convenient to determine the depth, d_e, from the extreme compression fiber to the centroid of the tensile force resultant in the reinforcement. Its value can be estimated, at first, somewhere in between d_p and d_s assuming the reinforcement can be lumped into only two layers. Once the values of a, f_{ps} and M_n are obtained, Eq. (5.3) can then be solved to determine the exact values of d_e. Several provisions of the AASHTO code depend on the ratio c/d_e, and as shown in Fig. 5.11c, several provisions of the 2002 ACI code can be expressed in terms of c/d_e.

5.8 EXAMPLE: NOMINAL BENDING RESISTANCE OF A RECTANGULAR SECTION

5.8.1 Partially Prestressed Section

Determine the nominal moment resistance of a partially prestressed concrete rectangular section with dimensions given in Fig. 5.18, for which $f'_c = 5000$ psi, $\beta_1 = 0.80$, $f_r = -530.3$ psi, $f_{pu} = 270$ ksi, $f_{pe} = 0.55 f_{pu} = 148.5$ ksi, $f_{py} = 0.85 f_{pu}$, $f_y = 60$ ksi, $A_{ps} = 0.918$ in^2 or six 1/2-in diameter stress-relieved prestressing strands, $A_s = 1.2$ in^2 or two #7 reinforcing bars, $d_p = 20.75$ in, $d_s = 21.5$ in, $b = 12$ in. The prestressing tendons are assumed bonded. The steps followed next are according to the procedure described above and expanded in the flow chart (Fig. 5.24).

- From Eq. (5.1) and Fig. 5.6, compute

$$\rho_p = \frac{A_{ps}}{bd_p} = \frac{0.918}{12 \times 20.75} = 0.00369$$

$$\omega_s = \frac{A_s f_y}{bd_s f'_c} = \frac{1.2 \times 60}{12 \times 21.5 \times 5} = 0.05581$$

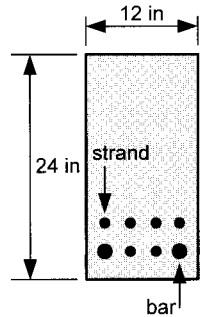

$A_{ps} = 0.918$ in^2 $f_{pe} = 148.5$ ksi
$d_p = 20.75$ in $f_{pu} = 270$ ksi
$A_s = 1.2$ in^2 $f_{py} = 229.5$ ksi
$d_s = 21.5$ in $f_y = 60$ ksi
$f'_c = 5$ ksi
$d_t = 22$ in (ACI)

Strands layout: 2 strands at 2 in, 2 strands at 4 in, and 2 strands draped at 4.375 in from bottom fiber

Figure 5.18

- $f_{pe} = 148.5 > 0.5 f_{pu} = 135$ ksi; thus use the ACI code equation to compute the stress in the prestressing steel at ultimate, f_{ps} (see Eq. 5.32 and review details in Section 5.11.1):

$$f_{ps} = f_{pu}\left[1 - \frac{\gamma_p}{\beta_1}\left\{\rho_p \frac{f_{pu}}{f'_c} + \frac{d_s}{d_p}(\omega_s - \omega')\right\}\right]$$

$$f_{ps} = 270\left(1 - \frac{0.4}{0.8}\left(0.00369 \frac{270}{5} + \frac{21.5}{20.75} 0.05581\right)\right) = 235.29 \text{ ksi}$$

- From Eqs. (5.15) and (5.20) compute

$$a = \beta_1 c = \frac{A_{ps} f_{ps} + A_s f_y}{0.85 f'_c b} = \frac{0.918 \times 235.29 + 1.2 \times 60}{0.85 \times 5 \times 12} = 5.647 \text{ in}$$

$$c = \frac{a}{\beta_1} = \frac{5.647}{0.80} = 7.06 \text{ in}$$

- From Eq. (5.16), compute the nominal moment resistance

$$M_n = 0.918 \times 235.29\left(20.75 - \frac{5.647}{2}\right) + 1.2 \times 60\left(21.5 - \frac{5.647}{2}\right)$$

$$= 5216.76 \text{ kips-in} = 434.73 \text{ kips-ft}$$

Note that the same result could have been obtained by using the compression force in the concrete in computing M_n. From Eqs. (5.3) and (5.17):

$$d_e = \frac{0.918 \times 235.29 \times 20.75 + 1.2 \times 60 \times 21.5}{0.918 \times 235.29 + 1.2 \times 60} = 20.937 \text{ in}$$

$$M_n = 0.85 \times 5 \times 12 \times 5.647\left(20.937 - \frac{5.647}{2}\right) = 5216.64 \text{ kips-in}$$

$$= 434.72 \text{ kips-ft (same as above)}$$

- Compute:

$$\frac{c}{d_e} = \frac{7.06}{20.937} = 0.337$$ (Note that the value of $\frac{c}{d_t} = \frac{7.06}{22} = 0.321$ per ACI is less stringent.)

- Compute design moment by ACI:

Referring to Fig. 5.11*c*, since $c/d_e = 0.337 \le 0.375$ the section is tension-controlled and the ϕ factor is 0.9. Thus $\phi M_n = 0.90 M_n = 391.26$ kips-ft .

Note: to illustrate the case of a section in the transition zone, assume $c/d_e = 0.397$ instead of 0.337. Since: $0.375 \le c/d_e = 0.397 \le 0.60$, the value of the ϕ factor (assuming non-spiral transverse reinforcement) is given by Eq. (5.10) (see also Fig. 5.9*b*):

$$\phi = 0.65 + 0.25\left(\frac{1}{c/d_e} - \frac{5}{3}\right) = 0.65 + 0.25\left(\frac{1}{0.397} - \frac{5}{3}\right) = 0.863$$

The design moment resistance acceptable by the ACI code (Section 5.17) is given by:

$$\phi M_n = 0.863 M_n = 0.863 \times 434.73 = 375.15 \text{ kips-ft}$$

- Compute design moment by AASHTO assuming f_{ps} is same as computed from ACI

Referring to Fig. 5.11*d*, since $c/d_e = 0.337 < 0.42$, the section is under-reinforced according to AASHTO and the value of the ϕ factor is 1 for prestressed concrete and 0.9 for reinforced concrete. Since the section has combined reinforcement, a value of 0.9 is taken here to be on the safe side. Thus the design moment resistance $\phi M_n = 0.9 M_n = 391.26$ kips-ft.

- The above computations were carried out assuming that the minimum reinforcement criterion is satisfied. Let us confirm this assumption. Compute the cracking moment from Eq. (5.6):

$$M_{cr} = 0.918 \times 148500\left(8.75 + \frac{1152}{288}\right) + 530.3 \times 1152 = 2349024 \text{ lbs-in}$$

$$= 195.75 \text{ kips-ft}$$

- Check minimum reinforcement criterion from Eq. (5.5)

$$\phi M_n = 391.26 \geq 1.2\, M_{cr} = 1.2 \times 195.75 = 234.9 \text{ kips-ft} \quad \text{O.K.}$$

5.8.2 Fully Prestressed Section

The reader may want to check that if $A_s = 0$ and $d_p = 21.33$ in (fully prestressed section), everything else being the same, the following results would have been obtained using the ACI code: $\rho_p = 0.00359$; $f_{ps} = 243.83$ ksi; $a = 4.389$ in; $M_n = 4283$ kips-in = 356.93 kips-ft; tension-controlled section; $\phi M_n = 321.24$ kips-ft.

5.8.3 Unbonded Tendons

If for the same partially prestressed section, unbonded tendons were used, everything else being the same, the following results would have been obtained using the ACI code: $f_{ps} = 172.050$ (assuming a span of 40 ft); $d_e = 20.984$ in; $a = 4.51$ in; $M_n = 4306.8$ kips-in = 358.9 kips-ft; tension controlled section; $\phi M_n = 323$ kips-ft. Note that the value of M_n for unbonded tendons is significantly smaller than that for bonded tendons (Section 5.8.1); this is primarily due to the value of f_{ps}.

The above example is treated using the AASHTO code in Section 5.12.5. Slight differences are observed in the results due to differences in the prediction equation of f_{ps} and the value of the ϕ factor.

5.9 NOMINAL BENDING RESISTANCE: MATHEMATICAL FORMULATION FOR T-SECTION BEHAVIOR OF FLANGED SECTION

It is assumed that conditions related to the minimum and maximum reinforcement provisions are satisfactory and that an underreinforced section (or tension-controlled section) is considered (Sections 5.3 and 5.5).

5.9.1 Condition for T-Section Behavior

According to the assumption that the tensile strength of concrete is neglected in the analysis, the portion of the concrete section that falls below the neutral axis is considered to offer no resistance and thus is, in effect, ignored in the computation of nominal moment. It could be of any shape, including the shape corresponding to that of a rectangular section. In approaching the analysis particular to T sections, it is important to realize that if the neutral axis falls in the flange (Fig. 5.19), the section is treated exactly the same as a rectangular section of same width b, and the corresponding equations developed above apply without any modifications. Thus, depending on the various variables and parameters, a T section, or generally a flanged section, does not necessarily imply T-section behavior at ultimate. In fact, since the depth of the neutral axis c at ultimate moment capacity of reinforced and prestressed concrete members is generally small in comparison to the depth of the

member, flanged sections behave often the same as rectangular sections. This is particularly true for small values of the reinforcement ratio or the reinforcing index. If, however, the neutral axis falls outside the flange (i.e., in the web), a special analysis must be undertaken.

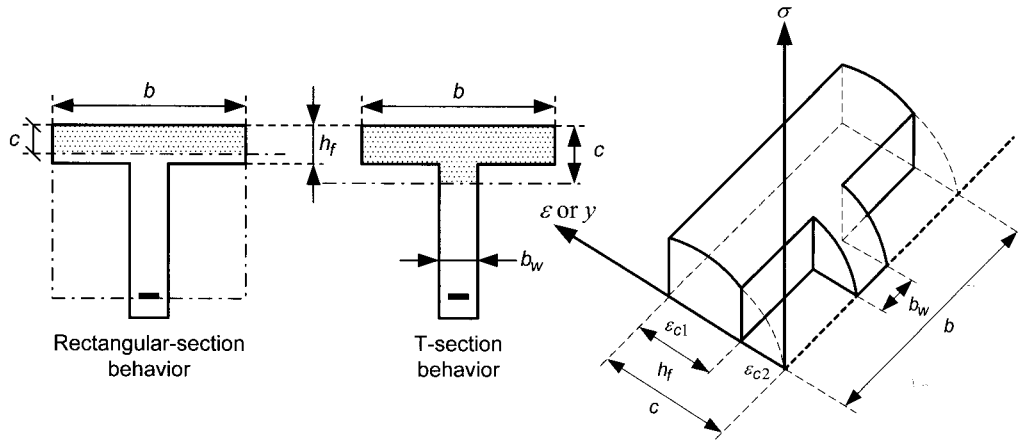

Figure 5.19 Rectangular or T-section behavior.

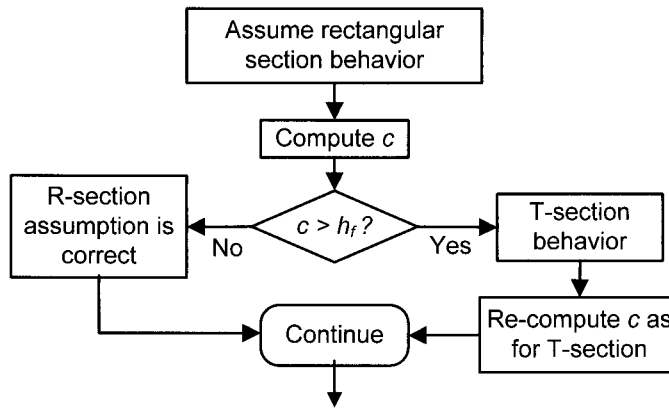

Figure 5.20 Steps to follow prior to considering T-section behavior.

It is clear that the first step would be to determine the depth of the neutral axis, c, assuming rectangular section behavior at ultimate capacity, as computed from Eqs. (5.15) and (5.20); c is then compared to the flange depth h_f of the T section and, if c is larger than h_f, the section is considered to behave as a T section. These steps are summarized in the flow chart Fig. 5.20. Of course, one can also assume T-section behavior at first and then go back to rectangular section behavior, if it is found that $c < h_f$.

The following approach is proposed in accordance to the ACI code: the T section is divided into two fictitious parts, one corresponding to the overhanging portion of the flange and the other to the web alone (Figs. 5.21 and 5.22); the analysis is then pursued where the two parts are treated separately as two rectangular sections and their nominal capacities are summed up to give the nominal capacity of the T section.

5.9.2 Fully Prestressed Section

When T section behavior exists, the usual ACI code approach is first to compute the areas of steel reinforcement needed to develop the ultimate strength of the overhanging portion of the flange and the web, respectively, and then to determine the corresponding forces and moments. This is illustrated in Fig. 5.21 for a fully prestressed section where most relevant equations are also given. The design steps to compute the steel areas and the depth of the stress block at ultimate, a, are given in the first row of equations derived from force equilibrium, while those to determine the nominal moment resistance are given in the last row. This procedure is exactly the same as that followed for reinforced concrete. However, in a partially prestressed section with both prestressed and non-prestressed reinforcement, it could be confusing to find in what proportion, if any, each type of reinforcement is associated with either the flange or the web. In such a case, the author suggests the use of forces instead of steel areas as shown next.

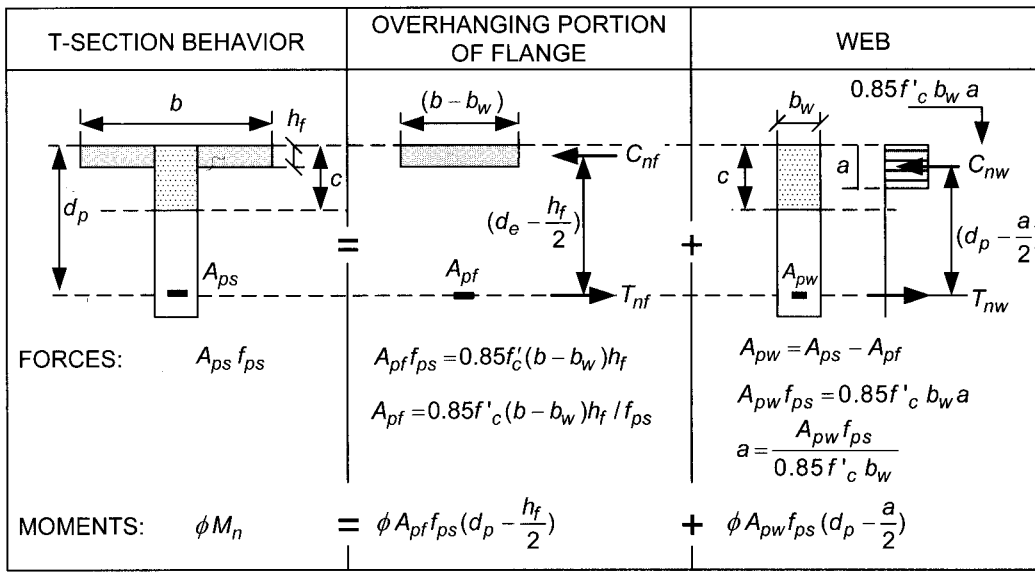

Figure 5.21 Fully prestressed T section: ACI code approach.

5.9.3 Partially Prestressed Section

In order to reduce the computational effort and clarify the approach used, it is essential to estimate first the value of d_e (Eq. (5.3)) when prestressed and nonprestressed reinforcement are used (i.e., partially prestressed section). The design may be revised if d_e is found inadequate at the end of the first iteration. As a first approximation, d_e can be taken somewhere in between d_p and d_s, or, to be on the safe side, d_e can be taken as the smaller of d_p or d_s.

Force Equilibrium

For $c \geq h_f$, the equation of force equilibrium in the section, which states that the total tensile force in the steel is equal to the sum of compressive forces in the concrete, can be written as (Fig. 5.21):

$$\begin{cases} A_{ps}f_{ps} + A_s f_y = 0.85f'_c(b-b_w)h_f + 0.85f'_c b_w \beta_1 c \\ A_{ps}f_{ps} + A_s f_y = 0.85f'_c(b-b_w)h_f + 0.85f'_c b_w a \end{cases} \tag{5.21}$$

If the equation predicting the value of f_{ps} is independent of a (or c), such as in the current ACI code Eqs. (5.32) or (5.33), then a can be calculated directly from Eq. (5.21) as:

$$a = \frac{A_{ps}f_{ps} + A_s f_y - 0.85f'_c(b-b_w)h_f}{0.85f'_c b_w} \tag{5.22}$$

However, if the prediction equation of f_{ps} is a function of a or c, such as in the AASHTO code (Eq. 5.35), then the solution can be obtained by solving simultaneously the two equations for two unknowns, a or c and f_{ps}. Examples with the AASHTO equation are given in Section 5.12.

Note that the total tensile force at ultimate can be separated into two parts, one, T_{nf}, balancing the compressive force, C_{nf}, in the overhanging portion of the flange, and the other, T_{nw}, balancing the compressive force, C_{nw}, in the web; thus:

$$T_n = A_{ps}f_{ps} + A_s f_y = T_{nf} + T_{nw} \tag{5.23}$$

$$T_{nf} = C_{nf} = 0.85f'_c(b-b_w)h_f \tag{5.24}$$

$$T_{nw} = C_{nw} = 0.85f'_c b_w a \tag{5.25}$$

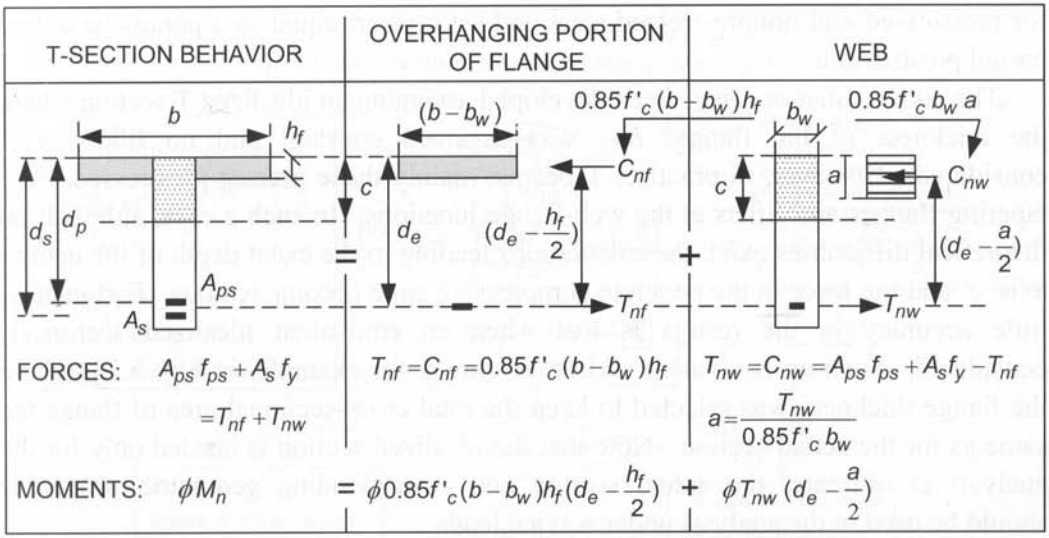

Figure 5.22 Partially prestressed T section: forces and moments at ultimate.

Moment Equilibrium

Referring to Fig. 5.22, the nominal moment resistance is given by:

$$M_n = T_{nf}\left(d_e - \frac{h_f}{2}\right) + T_{nw}\left(d_e - \frac{a}{2}\right) \tag{5.26}$$

or

$$M_n = C_{nf}\left(d_e - \frac{h_f}{2}\right) + C_{nw}\left(d_e - \frac{a}{2}\right) \tag{5.27}$$

The corresponding design moment resistance acceptable by the code is:

$$\phi M_n = \phi T_{nf}\left(d_e - \frac{h_f}{2}\right) + \phi T_{nw}\left(d_e - \frac{a}{2}\right) \tag{5.28}$$

Note that the approach followed above to analyze T-section behavior, although slightly different from that usually followed by the ACI code, leads to identical results. If the assumed value of d_e is found inadequate, a second iteration can be carried out using Eq. (5.3) and the value of f_{ps} obtained in this first iteration. On the other hand, Eq. (5.3) could be integrated directly in the solution: however, the problem will then contain four equations with four unknowns (a, M_n, f_{ps}, and d_e) and the solution becomes more tedious to obtain. A more general and rational procedure is proposed in Refs. [1.48 and 5.19] where the same proportion is taken

for prestressed and nonprestressed steel and set a priori equal to a parameter called partial prestressing ratio.

The above equations have been developed assuming an idealized T section where the thickness of the flange, h_f, was assumed constant and no fillets were considered. However, in practice, T beams, mainly those precast prestressed, have tapering flanges and fillets at the web-flange junctions. In such a case, although no theoretical difficulties exist, the calculations leading to the exact depth of the neutral axis c and the force in the concrete compressive zone become tedious. Fortunately, little accuracy in the results is lost when an equivalent idealized section is considered. Such an equivalent section is shown, for example, in Fig. 5.23, where the flange thickness was selected to keep the total cross-sectional area of flange the same as for the actual section. Note that the idealized section is needed only for the analysis at ultimate; the actual section and corresponding geometric properties should be used in the analysis under service loads.

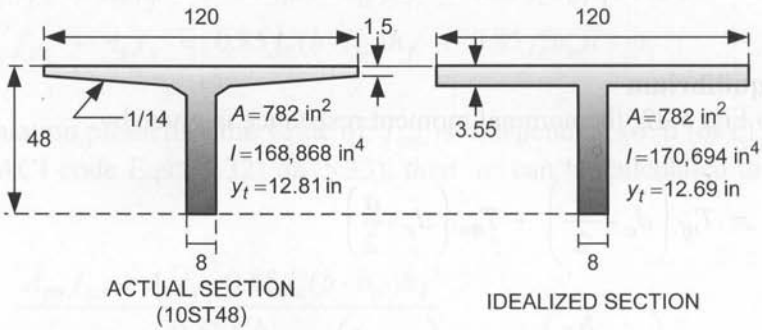

Figure 5.23 Typical example of actual and idealized T section.

5.9.4 Remark

A remark is in order here. In treating the overhanging portions of the flange according to the ACI code assumptions, an inconsistency may develop leading to some confusing results.

For instance, let us assume that in a particular problem the value of c is about equal to h_f; let us define c^+ as an infinitesimal amount higher than h_f and c^- as an infinitesimal amount smaller than h_f. If c^- is used, the T section is designed as a rectangular section, and in computing the compressive force in the concrete, the factor β_1 used in $a = \beta_1 c$, applies throughout; thus, Eq. (5.24) becomes:

$$T_{nf} = 0.85 f'_c (b - b_w) \beta_1 c^- = 0.85 f'_c (b - b_w) \beta_1 h_f \qquad (5.29)$$

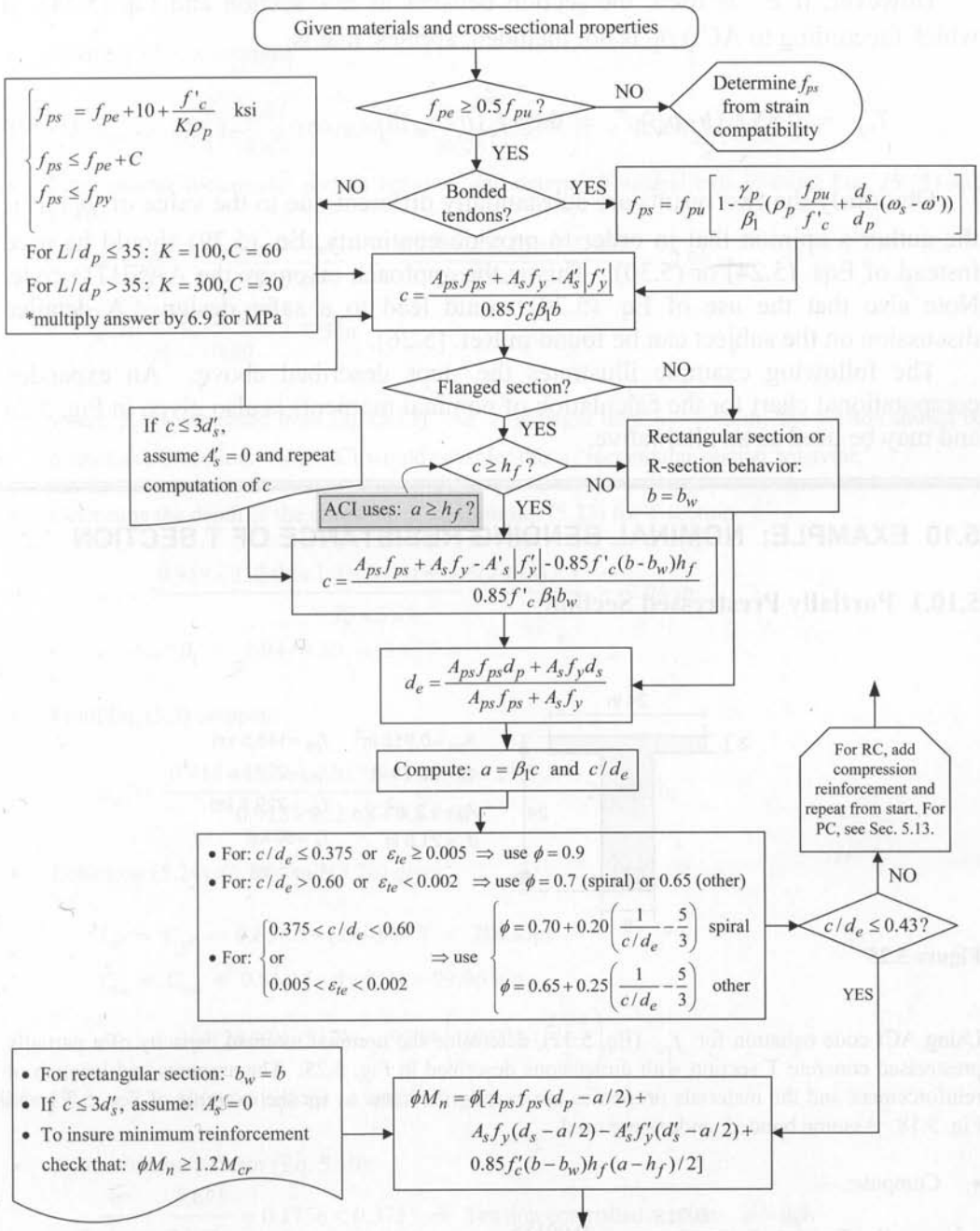

Figure 5.24 Flow chart to compute the nominal moment resistance of prestressed and partially prestressed concrete sections with bonded or unbonded tendons using provisions of the ACI Code.

However, if c^+ is used, the section behaves as a T section and Eq. (5.24), in which (according to ACI) β_1 is not included, applies, that is:

$$T_{nf} = 0.85 f'_c (b - b_w) c^+ = 0.85 f'_c (b - b_w) h_f \tag{5.30}$$

Obviously the two results are substantially different due to the value of β_1. It is the author's opinion that in order to provide continuity, Eq. (5.29) should be used instead of Eqs. (5.24) or (5.30). This is the approach taken by the AASHTO code. Note also that the use of Eq. (5.29) would lead to a safer design. A detailed discussion on the subject can be found in Ref. [5.26].

The following example illustrates the steps described above. An expanded computational chart for the calculation of nominal moments is also given in Fig. 5.24 and may be used as an alternative.

5.10 EXAMPLE: NOMINAL BENDING RESISTANCE OF T SECTION

5.10.1 Partially Prestressed Section

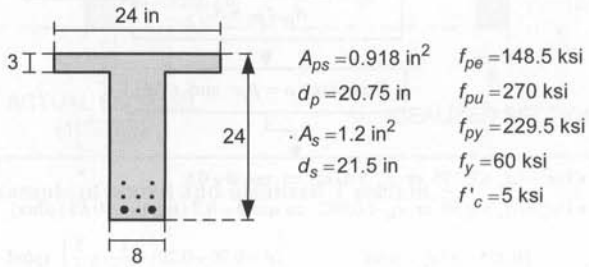

Figure 5.25

Using ACI code equation for f_{ps} (Eq. 5.32), determine the nominal moment capacity of a partially prestressed concrete T section with dimensions described in Fig. 5.25. The amounts and location of reinforcement and the materials properties are exactly the same as for the example of Sec. 5.8.1 and Fig. 5.18. Assume bonded tendons are used.

- Compute:

$$\rho_p = \frac{A_{ps}}{b d_p} = \frac{0.918}{24 \times 20.75} = 0.00185$$

$$\omega_s = \frac{A_s f_y}{b d_s f'_c} = \frac{1.2 \times 60}{24 \times 21.5 \times 5} = 0.02791$$

- Note: $f_{pe} = 148.5 > 0.5 f_{pu} = 135$ ksi, thus use code equation for f_{ps}.

- From Eq. (5.32), compute

$$f_{ps} = 270\left(1 - \frac{0.4}{0.8}\left(0.00185\frac{270}{5} + \frac{21.5}{20.75}0.02791\right)\right) = 252.61 \text{ ksi}$$

- First, assume rectangular section behavior and determine neutral axis c; using Eqs. (5.15) and (5.20):

$$a = \beta_1 c = \frac{A_{ps} f_{ps} + A_s f_y}{0.85 f'_c b} = \frac{0.918 \times 252.61 + 1.2 \times 60}{0.85 \times 5 \times 24} = 2.98 \text{ in}$$

$$c = \frac{a}{\beta_1} = \frac{2.98}{0.80} = 3.725 \text{ in}$$

where β_1 is computed from Eq. (5.12). As c is larger than $h_f = 3$ in, the section should be treated as a T section. Note ACI would consider this a "rectangular section behavior."

- Determine the depth of the stress block a from Eq. (5.22) for T section:

$$a = \frac{0.918 \times 252.61 + 1.2 \times 60 - 0.85 \times 5(24 - 8) \times 3}{0.85 \times 5 \times 8} = 2.94 \text{ in}$$

$$c = a / \beta_1 = 2.94 / 0.80 = 3.675 \text{ in}$$

- From Eq. (5.3) compute

$$d_e = \frac{0.918 \times 252.61 \times 20.75 + 1.2 \times 60 \times 21.5}{0.918 \times 252.68 + 1.2 \times 60} = 20.928 \text{ in}$$

- Equations (5.24), (5.25), and (5.26) give:

$$T_{nf} = C_{nf} = 0.85 \times 5 \times (24 - 8) \times 3 = 204 \text{ kips}$$

$$T_{nw} = C_{nw} = 0.85 \times 5 \times 8 \times 2.94 = 99.96 \text{ kips}$$

$$M_n = 204(20.928 - 3/2) + 99.96\left(20.928 - \frac{2.94}{2}\right)$$

$$= 5908.94 \text{ kips-in} = 492.36 \text{ kips-ft}$$

- Determine the ϕ factor (Eq. 5.10):

$$\frac{c}{d_e} = \frac{3.675}{20.928} = 0.1756 < 0.375 \rightarrow \text{Tension controlled section: } \phi = 0.9.$$

Note: c / d_t (ACI) $= 3.675 / 22 = 0.171 \leq 0.375 \rightarrow$ Tension controlled

The design moment resistance is given by:

$$\phi M_n = 0.9 \times M_n = 443.12 \text{ kips-ft}$$

The reader may want to check the results obtained for the following two particular cases.

5.10.2 Fully Prestressed Section

If $A_s = 0$ and everything else is kept the same, the following results would be obtained: $\rho_p = 0.00185$; $f_{ps} = 256.51$ ksi; $d_e = d_p = 20.75$ in; the section behaves as a rectangular section at ultimate with $a = 2.31$ in; $c = 2.89$ in, smaller than $h_f = 3$ in; $M_n = 384.6$ kips-ft; tension-controlled section; $\phi M_n = 346.15$ kips-ft.

5.10.3 Unbonded Tendons

If unbonded tendons are used instead of bonded tendons, everything else being the same as in Section 5.10.1 above, the following results would be observed: $\rho_p = 0.00185$; $f_{ps} = 185.53$ ksi using Eq. (5.33) with a span of 40 ft; $d_e = 20.97$ in; the section behaves as a rectangular section with $a = 2.38$ in; $c = 2.97$ in, smaller than $h_f = 3$ in; $M_n = 399.69$ kips-ft; tension-controlled section; $\phi M_n = 359.72$ kips-ft.

5.10.4 Odd Case

Examples (2) and (3) above did not present any difficulty or noticeable inconsistency; both had values of a and c smaller than h_f. However, for example (1), $a = 2.984$ was slightly smaller than $h_f = 3$ in, and $c = 3.725$ in was larger than h_f. When the computations were carried out again for T-section behavior, the values of a and c were 2.94 in and 3.675 in, respectively, smaller than previously calculated for rectangular section. Such an inconsistency will occur when, after assuming rectangular section behavior, one finds a smaller than h_f, and c larger than h_f. In such a case, the strict application of the ACI procedure may lead to a seemingly inconsistent result, as pointed out at the end of Section 5.9. To illustrate what may happen, let us assume that we have exactly the same problem as above (Fig. 5.25), except that h_f is 3.5 instead of 3 in. The computed values of a and c (assuming first rectangular section behavior) are: $a = 2.98$ in and $c = 3.725$ in. As c is larger than $h_f = 3.5$ in, the section behaves as a T section. If we attempt to determine again the depth of the stress block in the web using Eq. (5.22), we get:

$$a = \frac{0.918 \times 252.68 + 1.2 \times 60 - 0.85 \times 5(24 - 8)3.5}{0.85 \times 5 \times 8} = 1.94 \text{ in}$$

$$c = a/\beta_1 = 1.94/0.8 = 2.425 \text{ in}$$

Contrary to previous results, the above values would indicate that the neutral axis is now in the flange and a rectangular section behavior is at hand. This inconsistency can be avoided by using Eq. (5.29) instead of Eq. (5.30) in determining the contribution of the flange. If this is done, Eq. (5.22) would read:

$$a = \frac{A_{ps} f_{ps} + A_s f_y - 0.85 f_c (b - b_w) h_f \beta_1}{0.85 f_c' b_w} \tag{5.31}$$

which, for our example, with $\beta_1 = 0.80$, leads to $a = 3.34$ in and $c = 4.175$ in, both, as expected, larger than those assuming rectangular section behavior. This is the approach used in the AASHTO code. Since the value of β_1 can be as low as 0.65, it influences significantly the contribution of the overhanging portion of the flange [Ref. 5.26].

5.11 STRESS IN PRESTRESSING STEEL AT NOMINAL BENDING RESISTANCE

5.11.1 f_{ps} per ACI Code

In lieu of a more accurate analysis based on strain compatibility, the ACI code recommends the use of the following approximate values of f_{ps}, provided the effective prestress, f_{pe}, is not less than $0.5f_{pu}$.

Members with Bonded Prestressing Tendons

2002 ACI Code [18.7]	AASHTO LRFD 2003 [5.7.3.1.1-1]
Prestressed and partially prestressed sections with bonded tendons: $f_{ps} = f_{pu}\left[1-\frac{\gamma_p}{\beta_1}\left\{\rho_p\frac{f_{pu}}{f'_c}+\frac{d_s}{d_p}(\omega_s-\omega')\right\}\right]$ If compression steel is used, then: $\begin{cases}\rho_p\frac{f_{pu}}{f'_c}+\frac{d_s}{d_p}(\omega_s-\omega')\geq 0.17\\ d'\leq 0.15d_p\end{cases}$ and $\gamma_p = 0.28$ for $f_{py}\geq 0.9f_{pu}$ [low relaxation] $\gamma_p = 0.40$ for $f_{py}\geq 0.85f_{pu}$ [stress relieved] $\gamma_p = 0.55$ for $f_{py}\geq 0.80f_{pu}$ [bars] $\beta_1 = 0.85$ for $f'_c\leq 4$ ksi (28 MPa) $\beta_1 = 0.65$ for $f'_c\geq 8$ ksi (56 MPa) $\beta_1 = 0.85-0.05(f'_c-4)$ for $4\leq f'_c\leq 8$ ksi Note: 1 ksi = 6.9 MPa	Prestressed and partially prestressed sections with bonded tendons: $f_{ps} = f_{pu}\left(1-k\frac{c}{d_p}\right)$ where: $k = 2\left(1.04-\frac{f_{py}}{f_{pu}}\right)$ 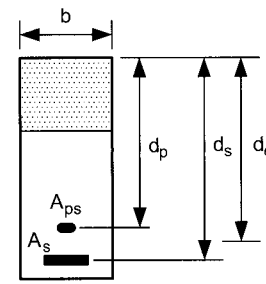 Note: the above provision is unit independent

Figure 5.26 Prediction equations for the stress in bonded prestressing tendons at ultimate bending resistance.

The stress in the bonded prestressing steel at nominal resistance can be estimated from (Fig. 5.26):

$$f_{ps} = f_{pu}\left[1-\frac{\gamma_p}{\beta_1}\left\{\rho_p\frac{f_{pu}}{f'_c}+\frac{d_s}{d_p}(\omega_s-\omega')\right\}\right] \tag{5.32}$$

where f_{pu} is the ultimate strength of the prestressed reinforcement, ρ_p is the reinforcement ratio of the prestressing steel given by Eq. (5.1), β_1 is as defined in Eq. (5.12), and ω_s and ω' are the reinforcing indices of the non-prestressed tensile and compressive reinforcement (Fig. 5.6). The factor γ_p depends on the yield strength of the prestressing tendons and is given by:

$\gamma_p = 0.28$ for f_{py}/f_{pu} not less than 0.90 (typical for low relaxation strands)
$\gamma_p = 0.40$ for f_{py}/f_{pu} not less than 0.85 (typical for stress-relieved strands)
$\gamma_p = 0.55$ for f_{py}/f_{pu} not less than 0.80 (typical for prestressing bars)

In order to include full contribution of the compressive reinforcement (i.e., stressed at f'_y), it is recommended that the value of c obtained from equilibrium be not less than $3d'_s$. Otherwise assume $A'_s = 0$. Note that Eq. (5.32) is valid in all systems of units. It is compared in Fig. 5.26 with the corresponding equation from the AASHTO code.

Code recommended values of f_{ps} generally apply to the tensile reinforcement assumed lumped near the tension face of the member.

Members with Unbonded Prestressing Tendons

The stress in the unbonded prestressing steel at nominal bending resistance can be estimated from Eq. (5.33) where L is the length of span for which nominal moment is being calculated.

Eq. (5.33) (ksi)	Eq. (5.33) (MPa)
$f_{ps} = f_{pe} + 10 + \dfrac{f'_c}{K\rho_p}$ ksi	$f_{ps} = f_{pe} + 69 + \dfrac{f'_c}{6.9K\rho_p}$ MPa
$f_{ps} \le f_{pe} + C$	$f_{ps} \le f_{pe} + C$
$f_{ps} \le f_{py}$	$f_{ps} \le f_{py}$
$K = 100$ and $C = 60$ for $L/d_p \le 35$	$K = 100$ and $C = 414$ for $L/d_p \le 35$
$K = 300$ and $C = 30$ for $L/d_p > 35$	$K = 300$ and $C = 207$ for $L/d_p > 35$

For slabs with unbonded tendons, an equation different from the above is suggested for simplification in Section 11.2.

The stress f_{ps} in unbonded tendons at ultimate is significantly smaller than if the same tendons were bonded. As a result, the area of steel required is higher for the same nominal moment resistance. This is a factor that should be considered in the total cost of the structure when specifying bonded versus unbonded tendons. Note

also that, unlike bonded tendons in which the stress at ultimate exceeds yielding, the stress in the unbonded tendons at ultimate is most likely to remain in the elastic range of behavior. The limitations on f_{ps} given in Eq. (5.33) account for this observation.

5.11.2 f_{ps} per AASHTO LRFD Specification for Bridge Design

Since ultimate strength design requirements often do not control the design (i.e. they are less critical than working stress and serviceability requirements), the AASHTO specification suggests two expressions for f_{ps} at ultimate, one fast and conservative to be used as a first approximation, and the other more accurate for final design. Should the conservative approach lead to $M_n \geq M_u / \phi$, there may be no need to go further.

Members with Bonded Prestressing Tendons

a. Approximate conservative method for preliminary design

$$f_{ps} = f_{py} \tag{5.34}$$

where f_{py} is the yield strength of the prestressing steel. This is similar to the case of reinforced concrete. An extensive evaluation of existing data and a comprehensive computerized nonlinear analysis by Harajli and Naaman [Ref. 5.8] have shown that the above equation is conservative for under-reinforced members.

b. Refined method

$$f_{ps} = f_{pu}\left(1 - k\frac{c}{d_p}\right) \tag{5.35}$$

where f_{pu} is the ultimate strength of the prestressing steel, and k is given by:

$$k = 2\left(1.04 - \frac{f_{py}}{f_{pu}}\right) \tag{5.36}$$

If any compression reinforcement is taken into account when calculating c or f_{ps}, the value of c should be larger than or equal to $3d'_s$ to insure yielding of the compression reinforcement, where d'_s is the depth from the extreme compression

fiber to the centroid of the compression reinforcement. If c is less than $3d'_s$, the contribution of the compressive reinforcement may be neglected. The equation for k was first calibrated by Loov [Ref. 5.11]. Equation (5.35) is compared to ACI code Eq. (5.32) in Fig. 5.26 and is integrated in the design flow chart Fig. 5.29.

Members with Unbonded Prestressing Tendons

a. Approximate conservative method for preliminary design

$$\begin{cases} f_{ps} = f_{pe} + 15 \quad \text{(ksi)} \\ f_{ps} = f_{pe} + 105 \quad \text{(MPa)} \end{cases} \tag{5.37}$$

The above equation was initially suggested in the 1963 version of the ACI Building Code. Naaman and Alkhairi [Refs. 5.21, 5.22] evaluated 143 test data from simply supported beams and found that the above equation was conservative in more than 90 percent of the cases. However, Eq. (5.37) may be optimistic for continuous slab systems with span-to-depth ratio larger than 35 [Refs. 5.6, 5.14]. In that case, the recommendation made in Ref. [5.27] and summarized in Sections 5.13 and 11.2 can be followed.

b. Refined method

$$f_{ps} = f_{pe} + 900\left(\frac{d_p - c}{L_e}\right) \le f_{py} \quad \text{ksi} \tag{5.38}$$

$$f_{ps} = f_{pe} + 6300\left(\frac{d_p - c}{L_e}\right) \le f_{py} \quad \text{MPa} \tag{5.39}$$

in which c is the depth of neutral axis at ultimate and L_e is an effective tendon length defined by:

$$L_e = \frac{2L_i}{2 + N_s} \tag{5.40}$$

where:

L_i = length of tendons between anchorages

N_s = number of support hinges crossed by the tendon between anchorages or discretely bonded points; for a continuous beam with anchorages at end supports, typially N_s is the number of intermediate supports

Equation (5.38 or 5.39) for f_{ps} and the force equilibrium equation (such as Eq. (5.14)) contain two unknowns, f_{ps} and c; an exact solution can be found by solving the two equations simultaneously for the two unknowns leading to a quadratic equation in c. On the other hand, AASHTO allows as a first approximation to compute c from the force equilibrium equation, assuming $f_{ps} = f_{py}$ in that equation; then iterate, that is, plug c in Eq. (5.38 or 5.39) and find a closer value of f_{ps}. Repeat if needed. A flow chart summarizing the computation of M_n for unbonded tendons using Eqs. (5.38) and (5.39) for f_{ps} is given in Fig. 5.30.

A note is in order here. A quick evaluation of Eq. (5.38) would indicate that the second term of the right side of the equation is very small. Indeed, if c is neglected, then L_e / d_p is of the order of 15 to 25 for beams and 35 to 45 for slabs. Thus the increase in stress beyond the effective prestress for a simply supported beam depends on the span-to-depth ratio, but is insensitive to a number of other important parameters.

5.11.3 Author's Recommendation

For members with bonded tendons and for partially prestressed concrete members, the AASHTO prediction equation (Eq. 5.35) is superior in its simplicity and generality to the ACI 2002 code equation (Eq. 5.32). It only requires that c be computed first by solving simultaneously the force equilibrium equation and the prediction equation of f_{ps}.

For members with unbonded tendons, the rationale recommended by the author is to provide the designer with a choice to use:

1. A very simple conservative equation for preliminary design when justified, such as Eq. (5.37) or Eqs. (11.1) and (11.2); for brevity, these equations are not repeated here.
2. A rational accurate equation for any design such as given in Eqs. (5.41) or (11.3), while keeping open the option of a true deflection compatibility analysis, if needed.

This approach was recommended by ACI 423 Sub-Committee on Unbonded Tendons and is documented in Refs. [5.27, 5.21, and 5.22]. For members prestressed with unbonded tendons, in lieu of a deflection compatibility analysis, the following prediction equation is recommended when accuracy is important and in order to capture the influence of several parameters:

$$f_{ps} = f_{pe} + \Omega_u E_p \varepsilon_{cu} \left(\frac{d_p}{c} - 1\right) \frac{L_1}{L_2} \leq 0.80 f_{pu} \tag{5.41}$$

where:

f_{pe} = effective prestress in the prestressed reinforcement
E_p = elastic modulus of prestressed reinforcement; it is applicable to steel and fiber reinforced polymeric reinforcements
ε_{cu} = failure strain of concrete in compression, assumed = 0.003
d_p = distance from extreme compression fiber to centroid of tensile force in the prestressed reinforcement
c = depth of neutral axis at nominal bending resistance
Ω_u = 3 / (L/d_p) for uniform or third point loading
Ω_u = 1.5 / (L/d_p) for one point midspan loading
L_1 = sum of lengths of spans loaded with live load and containing tendon(s) considered
L_2 = total length of tendon(s) between anchorages
L = length of span for which computation is carried out; at intermediate supports of continuous members, L can be taken as the average of the two spans on either side of the support.
f_{pu} = specified tensile strength of prestressed tendons

When not available from test results or from the manufacturer, the elastic modulus of prestressing steel can be taken as 28000 ksi or 196000 MPa. Eq. (5.41) holds for all systems of units. It was derived assuming the tendons are in the linear range of behavior. The limitation of $0.80f_{pu}$ corresponds to 94 percent of yield for stress relieved steel strand, and 89 percent of yield for low relaxation strand. It is also a safe limit for fiber reinforced polymeric tendons.

The value of depth of neutral axis, c, accounts for the presence of non-prestressed reinforcement and satisfies equilibrium at ultimate.

The coefficient Ω_u is called the strain reduction coefficient at ultimate and represents the ratio of average strain increase in the unbonded tendon to the strain increase in the equivalent bonded tendon at the section of maximum moment [Refs. 5.20 to 5.23, 5.4, 5.27]. It depends on the type of loading and the span-to-depth ratio. L_1 is equal to L if only one span is being loaded for maximum moment. If more than one span are being loaded, L_1 is equal to the sum of lengths of spans loaded by live loads. Equation (5.41) is based on a rational deflection compatibility analysis reduced to a strain compatibility analysis at the critical section through the strain reduction coefficient Ω_u. It assumes that the prestressing tendons remain in their linear elastic range of behavior. In order to obtain the value of f_{ps} from Eq. (5.41), the equation of force equilibrium in the section at ultimate (such as Eq. 5.14) and the prediction equation of f_{ps} (Eq. 5.41) must be solved simultaneously for c and f_{ps}. A typical design flow chart leading to the value of M_n assuming f_{ps} given by Eq. (5.41) is given in Fig. 5.31. Equation (5.41) was initially adopted in the 1995 draft of the AASHTO LRFD Specification for Bridge Design and later

recommended by ACI 423 Subcommittee on Members with Unbonded Tendons [Ref. 5.27].

Note that Eq. (5.41) was found safe for more than 92 percent of 159 tests observed with simply supported beams using steel tendons [Ref. 5.27, discussion]. It offers numerous advantages: it accommodates the case of continuous members where only one span is loaded; it takes into consideration the influence of tendon profile, span-to-depth ratio and loading conditions; it is more accurate and rational than current code equations; it accounts for the presence of non-prestressed reinforcing bars (partial prestressing) as well as bonded prestressed tendons; and, it accommodates other prestressing materials such as FRP tendons provided they remain in their linear elastic range of behavior.

Examples illustrating the use of this equation are given in Section 5.23.

5.12 NOMINAL BENDING RESISTANCE: UNDER-REINFORCED SECTION, AASHTO LRFD CODE

For all practical purposes, under-reinforced sections as defined by AASHTO fall mostly in the tension-controlled section region defined in the 2002 ACI code (Fig. 5.11). Since the AASHTO code specifies prediction equations for the stress in the prestressing steel (Eqs. 5.35 and 5.38) that are different from those given in the ACI code, the sequence of a number of computational steps leading to the nominal bending resistance is also different. The difference is mainly due to the prediction equation of f_{ps}, which depends on c, and whether the tendons are bonded or unbonded. The procedure to compute the nominal bending resistance of under-reinforced or over-reinforced flexural members is described next. The general case of a section containing prestressed and non-prestressed tensile steel and compression steel is considered.

5.12.1 Equilibrium Equations for Rectangular and Flanged Sections

Assuming a partially prestressed concrete section, the equations of force and moment equilibrium are given by:

- For a rectangular section or a rectangular section behavior of T section:

$$0.85 f'_c b \beta_1 c = A_{ps} f_{ps} + A_s f_y - A'_s \left| f'_y \right| \tag{5.42}$$

$$\phi M_n = \phi \left[A_{ps} f_{ps} \left(d_p - \frac{a}{2} \right) + A_s f_y \left(d_s - \frac{a}{2} \right) - A'_s \left| f'_y \right| \left(d'_s - \frac{a}{2} \right) \right] \tag{5.43}$$

- For T-section behavior of a flanged section:

$$0.85f'_c b_w \beta_1 c + 0.85f'_c(b - b_w)\beta_1 h_f = A_{ps}f_{ps} + A_s f_y - A'_s\left|f'_y\right| \tag{5.44}$$

$$\phi M_n = \phi\left\{A_{ps}f_{ps}\left(d_p - \frac{a}{2}\right) + A_s f_y\left(d_s - \frac{a}{2}\right) - A'_s\left|f'_y\right|\left(d'_s - \frac{a}{2}\right) + 0.85\,\beta_1 f'_c(b - b_w)h_f\left(\frac{a - h_f}{2}\right)\right\} \tag{5.45}$$

Note that Eqs. (5.44) and (5.45) revert to Eqs. (5.42) and (5.43), respectively, when b_w is taken equal to b, i.e., for rectangular section or rectangular section behavior of flanged section. The steps leading to a particular solution are described next.

5.12.2 Solution for Members with Bonded Tendons

Simplified Conservative Approach

- *Rectangular sections or rectangular section behavior of flanged sections*: Assuming $f_{ps} = f_{py}$, find c from the force equilibrium Eqs. (5.20 and 5.42):

$$c = \frac{A_{ps}f_{py} + A_s f_y - A'_s\left|f'_y\right|}{0.85f'_c\beta_1 b} \tag{5.46}$$

The above equation holds for c larger than or equal to $3d'_s$. Otherwise, either a strain compatibility analysis is recommended or the contribution of the compressive reinforcement is neglected.
Compute the depth of equivalent rectangular stress block, a, from:

$$a = \beta_1 c \tag{5.47}$$

Compute ϕM_n from Eq. (5.43).
Note that the above approach could be considered the first iteration of a more exact procedure, that is: given c from Eq. (5.46), compute f_{ps} from code equation, and repeat if needed.

- *T-section behavior of flanged sections*:

Assuming $f_{ps} = f_{py}$, find c from the force equilibrium Eq. (5.44):

$$c = \frac{A_{ps}f_{py} + A_s f_y - A'_s\left|f'_y\right| - 0.85f'_c(b - b_w)\beta_1 h_f}{0.85f'_c\beta_1 b_w} \tag{5.48}$$

Compute a from Eq. (5.47), then compute ϕM_n from Eq. (5.45).

Refined Approach

- *Rectangular sections or rectangular section behavior of flanged sections*:
  The value of c is first computed from solving simultaneously the force equilibrium equation at ultimate and the prediction equation for f_{ps}, that is, Eqs. (5.42) and (5.35) leading to:

$$c = \frac{A_{ps}f_{pu} + A_s f_y - A'_s\left|f'_y\right|}{0.85f'_c\beta_1 b + kA_{ps}f_{pu}/d_p} \tag{5.49}$$

  where k is from Eq. (5.36). Then a is calculated from Eq. (5.47), f_{ps} from Eqs. (5.35) and ϕM_n from Eq. (5.43).

- *T section behavior of flanged sections*:
  The solution for c is given by:

$$c = \frac{A_{ps}f_{pu} + A_s f_y - A'_s\left|f'_y\right| - 0.85f'_c\beta_1(b - b_w)h_f}{0.85f'_c\beta_1 b_w + kA_{ps}f_{pu}/d_p} \tag{5.50}$$

  Then a and f_{ps} are calculated from Eqs. (5.47) and (5.35), and the design nominal bending resistance ϕM_n is calculated from Eq. (5.45).

The steps integrating the above procedure are summarized in a logical flow chart Fig. 5.29.

5.12.3 Solution for Members with Unbonded Tendons

A similar approach is used for members prestressed with unbonded tendons. In a conservative design, f_{ps} is computed from Eqs. (5.37) or (11.1) and the remaining Eqs. (5.42) to (5.45) are applicable. For the case where f_{ps} is taken from AASHTO Eqs. (5.38) and (5.39) the solution is summarized in the flow chart of Fig. 5.30. For the more accurate case where f_{ps} is taken from Eq. (5.41), a detailed solution

initially given in Refs. [5.21, 5.22] leads to a quadratic equation in c. A flow chart summarizing the main steps and related equations is given in Fig. 5.31. It should be noted that the procedure is applicable to internal unbonded tendons as well as external unbonded tendons provided second order effects due to eccentricity variations are negligible [Ref. 5.4]. The procedure described in Fig. 5.31 seems lengthy because it involves solving a quadratic equation, but it provides a rational and reasonably accurate solution to a difficult problem [Ref. 5.27]. The solution can also be obtained by iteration as illustrated in the examples of Section 5.23.

5.12.4 Solution for Members with Both Bonded and Unbonded Tendons

When both bonded and unbonded tendons are present, a strain compatibility analysis of the section should lead to accurate prediction of nominal bending resistance. Strain compatibility, derived from member deformation, can be applied with unbonded tendons provided appropriate strain reduction coefficients are used as described in [Ref.5.23]. However, a conservative approach can be followed, based on the conservative prediction equations of f_{ps} suggested by AASHTO. The procedure is summarized in a flow chart, Fig. 5.32. The notation in these figures includes the standard terms augmented by the subscripts b and u to denote bonded or unbonded tendons, respectively.

5.12.5 Example: PPC (Partially Prestressed Concrete) Rectangular Section with Bonded Tendons (AASHTO)

Consider the same rectangular section of Fig. 5.18 repeated in Fig. 5.27 and in the example of Section 5.8.1. The following calculations follow the steps described in the flow chart Fig. 5.29 using the equations derived above in Sections 5.12.1 and 5.12.2.

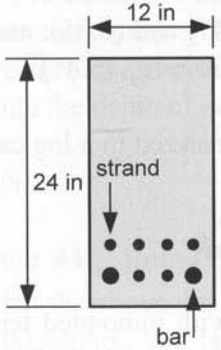

$A_{ps} = 0.918$ in^2 $\quad f_{pe} = 148.5$ ksi
$d_p = 20.75$ in $\quad f_{pu} = 270$ ksi
$A_s = 1.2$ in^2 $\quad f_{py} = 229.5$ ksi
$d_s = 21.5$ in $\quad f_y = 60$ ksi
$\quad f'_c = 5$ ksi

$d_t = 22$ in (ACI)

Strands layout: 2 strands at 2 in, 2 strands at 4 in, and 2 strands draped at 4.375 in from bottom fiber

Figure 5.27

Since $f_{pe} = 148.5 > 0.5 f_{pu} = 135$ ksi, use code equation to predict f_{ps}.

$$k = 2\left(1.04 - \frac{f_{py}}{f_{pu}}\right) = 2\left(1.04 - \frac{229.5}{270}\right) = 2(1.04 - 0.85) = 0.38$$

$$c = \frac{A_{ps}f_{pu} + A_s f_y - A'_s f'_y}{0.85 f'_c \beta_1 b + k A_{ps} f_{pu}/d_p} = \frac{0.918\times 270 + 1.2\times 60}{0.85\times 5\times 0.8\times 12 + 0.38\times 0.918\times 270/20.75}$$

$$c = 7.055 \text{ in}$$

$$f_{ps} = f_{pu}\left(1 - k\frac{c}{d_p}\right) = 270\left(1 - 0.38\frac{7.055}{20.75}\right) = 235.12 \text{ ksi}$$

$$d_e = \frac{A_{ps}f_{ps}d_p + A_s f_y d_s}{A_{ps}f_{ps} + A_s f_y} = \frac{0.918\times 235.12\times 20.75 + 1.2\times 60\times 21.5}{0.918\times 235.06 + 1.2\times 60} = 20.938 \text{ in}$$

$a = \beta_1 c = 0.8c = 5.644$ in; $a/2 = 2.822$ in

$$\frac{c}{d_e} = \frac{7.055}{20.938} = 0.337 < 0.42 \rightarrow \text{Underreinforced section}$$

In AASHTO the ϕ factor is equal 1 for prestressed concrete and 0.9 for reinforced concrete. Since this is a partially prestressed concrete section, a value of 0.9 is selected because it is on the safe side.

The design nominal bending moment is given by Eq. 5.43:

$$\phi M_n = \phi\left[A_{ps}f_{ps}\left(d_p - \frac{a}{2}\right) + A_s f_y\left(d_s - \frac{a}{2}\right)\right]$$

$$\phi M_n = 0.9\times[0.918\times 235.12(20.75 - 2.822) + 1.2\times 60(21.5 - 2.822)]$$

$$= 4692.96 \text{ kips-in} = 391.08 \text{ kips-ft}$$

It can be observed that the answer is not too different from that obtained in the example of Section 5.8.1 which was solved according to the ACI code. The section obtained was characterized as "tension-controlled" according to ACI and under-reinforced according to AASHTO. Note that the constraint for the minimum reinforcement criterion is similar here as described in Section 5.8.1.

5.12.6 Example: PPC (Partially Prestressed Concrete) T Section with Bonded Tendons (AASHTO)

Consider the same T section of Fig. 5.25 repeated in Fig. 5.28 and the example of Section 5.10. The following calculations follow the steps described in the flow chart Fig. 5.29 using the equations derived above in Sections 5.12.1 and 5.12.2.

Since $f_{pe} = 148.5 > 0.5f_{pu} = 135$ ksi, use code equation to predict f_{ps}.

$$k = 2\left(1.04 - \frac{f_{py}}{f_{pu}}\right) = 2\left(1.04 - \frac{229.5}{270}\right) = 2(1.04 - 0.85) = 0.38$$

$$c = \frac{A_{ps}f_{pu} + A_s f_y - A'_s f'_y}{0.85 f'_c \beta_1 b + k A_{ps} f_{pu}/d_p} = \frac{0.918\times 270 + 1.2\times 60}{0.85\times 5\times 0.8\times 24 + 0.38\times 0.918\times 270/20.75}$$

$c = 3.713$ in $> h_f = 3$ in $\rightarrow$ T-section behavior

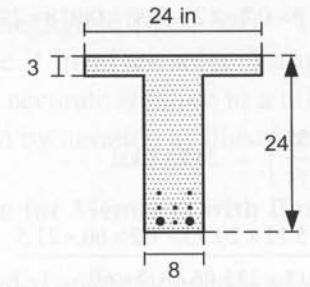

$A_{ps} = 0.918$ in^2 $f_{pe} = 148.5$ ksi
$d_p = 20.75$ in $f_{pu} = 270$ ksi
$A_s = 1.2$ in^2 $f_{py} = 229.5$ ksi
$d_s = 21.5$ in $f_y = 60$ ksi
$f'_c = 5$ ksi

Figure 5.28

Recompute c for T-section behavior:

$$c = \frac{A_{ps}f_{pu} + A_s f_y - A'_s f'_y - 0.85 f'_c \beta_1 (b - b_w) h_f}{0.85 f'_c \beta_1 b_w + k A_{ps} f_{pu}/d_p}$$

$$c = \frac{0.918\times 270 + 1.2\times 60 - 0.85\times 5\times 0.8(24-8)\times 3}{0.85\times 5\times 0.8\times 8 + 0.38\times 0.918\times 270/20.75} = 4.936 \text{ in}$$

$$f_{ps} = f_{pu}\left(1 - k\frac{c}{d_p}\right) = 270\left(1 - 0.38\frac{4.936}{20.75}\right) = 245.59 \text{ ksi}$$

$$d_e = \frac{A_{ps}f_{ps}d_p + A_s f_y d_s}{A_{ps}f_{ps} + A_s f_y} = \frac{0.918\times 245.59\times 20.75 + 1.2\times 60\times 21.5}{0.918\times 245.59 + 1.2\times 60} = 20.932 \text{ in}$$

$a = \beta_1 c = 0.8c = 3.95$ in; $a/2 = 1.97$ in

$$\frac{c}{d_e} = \frac{4.936}{20.931} = 0.236 < 0.42 \rightarrow \text{Underreinforced T section.}$$

In AASHTO the ϕ factor is equal 1 for prestressed concrete and 0.9 for reinforced concrete. Since this is a partially prestressed concrete section, a value of 0.9 is selected, because it is on the safe side. From Eq. (5.45):

$$\phi M_n = \phi\left[A_{ps}f_{ps}\left(d_p - \frac{a}{2}\right) + A_s f_y\left(d_s - \frac{a}{2}\right) + 0.85\beta_1 f'_c (b - b_w) h_f \left(\frac{a - h_f}{2}\right)\right]$$

$$\phi M_n = 0.9[0.918\times 245.59(20.75 - 1.97) + 1.2\times 60(21.5 - 1.97) + 0.85\times 0.8\times 5(24-8)3(3.95-3)/2]$$

$$= 5145.89 \text{ kips-in} = 428.82 \text{ kips-ft}$$

The value obtained is not too different from that using the ACI code approach in the example of Section 5.10 (tension-controlled section), and is primarily due to the difference in the numerical value of estimated f_{ps}.

5.13 NOMINAL MOMENT RESISTANCE: OVER-REINFORCED AND NON TENSION-CONTROLLED SECTIONS

5.13.1 ACI Code

The 1999 ACI code did not allow over-reinforced sections in conventional reinforced concrete, while it allowed prestressed concrete sections to be over-reinforced provided the moment resistance is computed from the compression zone assuming a prestressing index $\omega_p = 0.36\beta_1$ (equivalent to $c/d_p = 0.425$); also, in such a case the ϕ factor was reduced abruptly from 0.9 to 0.7. The 2002 ACI code does not refer to over-reinforced sections. It essentially states in Section 10.3.5 that "for nonprestressed flexural members and nonprestressed members with axial load less than $0.85f'_cA_g$, the net tensile strain at nominal strength shall not be less than 0.004." If we interpret the net tensile strain as being the strain in the concrete at the level the centroid of the tensile force (as discussed in Sec. 5.5.3), then the 0.004 strain limit would correspond to a limit of $c/d_e = 0.429$. This is also essentially the same as limiting the reinforcement ratio or index (Fig. 5.11). For reinforced concrete, the approach recommended by ACI is to add compression reinforcement to flexural members, which would otherwise have a net tensile strain smaller than 0.004, until the strain increases beyond 0.004. It is not clear in the 2002 ACI code if a similar approach is to be used for prestressed concrete. However, the approach recommended in the AASHTO LRFD code, which is essentially the same as that in the 1999 ACI code, could be followed.

5.13.2 AASHTO LRFD

Over-reinforced sections are defined by AASHTO as having a $c/d_e > 0.42$ (Fig. 5.14). In order to guarantee sufficient ductility at ultimate, the AASHTO code discourages the use of over-reinforced members (or sections) unless it is shown by test or analysis that performance will not be diminished. However, should the designer decide to use an over-reinforced section, the nominal bending resistance is then calculated using the compression force of the couple assuming $c/d_e = 0.42$ and a reduced ϕ factor = 0.7. The following equations can then be obtained:

- Rectangular section or rectangular section behavior of flanged section

$$\phi M_n = \phi f'_c b d_e^2 (0.36\beta_1 - 0.08\beta_1^2) \tag{5.51}$$

- T-section behavior

$$\phi M_n = \phi[f'_c b_w d_e^2 (0.36\beta_1 - 0.08\beta_1^2) + 0.85\beta_1 f'_c (b - b_w) h_f (d_e - 0.5h_f)] \tag{5.52}$$

Equation (5.51) is obtained from Eq. (5.67) in which the value of effective reinforcing index, ω_e, is replaced by the maximum allowed limit of $0.36\beta_1$. A similar result is obtained when replacing c/d_e by 0.42.

The above equations are integrated in the flow charts, Figs. 5.29 to 5.32.

5.13.3 Example of Over-reinforced Section as per AASHTO LRFD

Consider the rectangular section described in Figs. 5.18 and 5.27 and the same material properties. Assume that the section has 10 strands (instead of 6 strands) with $A_{ps} = 1.53$ in^2 at $d_p = 20$ in. Compute ϕM_n. Following the steps in the flow chart, Fig. 5.29, leads to:

Since $f_{pe} = 148.5 > 0.5 f_{pu} = 135$ ksi, use code equation to predict f_{ps}.

$$k = 2\left(1.04 - \frac{f_{py}}{f_{pu}}\right) = 2\left(1.04 - \frac{229.5}{270}\right) = 2(1.04 - 0.85) = 0.38$$

$$c = \frac{A_{ps} f_{pu} + A_s f_y - A'_s f'_y}{0.85 f_c \beta_1 b + k A_{ps} f_{pu} / d_p} = \frac{1.53 \times 270 + 1.2 \times 60}{0.85 \times 5 \times 0.8 \times 12 + 0.38 \times 1.53 \times 270/20}$$

$$c = 9.97 \text{ in}$$

$$f_{ps} = f_{pu}\left(1 - k\frac{c}{d_p}\right) = 270\left(1 - 0.38\frac{9.97}{20}\right) = 218.85 \text{ ksi}$$

$$d_e = \frac{A_{ps} f_{ps} d_p + A_s f_y d_s}{A_{ps} f_{ps} + A_s f_y} = \frac{1.53 \times 218.85 \times 20 + 1.2 \times 60 \times 21.5}{1.53 \times 218.85 + 1.2 \times 60} = 20.26 \text{ in}$$

$$\frac{c}{d_e} = \frac{9.97}{20.26} = 0.492 > 0.42 \rightarrow \text{Overreinforced section}$$

$$\phi M_n = \phi f'_c b d_e^2 (0.36\beta_1 - 0.08\beta_1^2) = 0.7 \times 5 \times 12 \times 20^2 (0.36 \times 0.8 - 0.08 \times 0.8^2)$$

$$\phi M_n = 3978.24 \text{ kips-in} = 331.52 \text{ kips-ft}$$

Although the value of d_e was calculated exactly above, the procedure could have been much faster if d_e was estimated a priori between d_p and d_s. Note that although this section has more reinforcement than that in the example of Section 5.8.1, its design nominal moment resistance is smaller because the code penalizes over-reinforced sections by imposing $\phi = 0.7$ instead of 0.9. Note also that when an over-reinforced section exists with bonded tendons, the stress in the tendons at ultimate tends to become smaller than f_{py}.

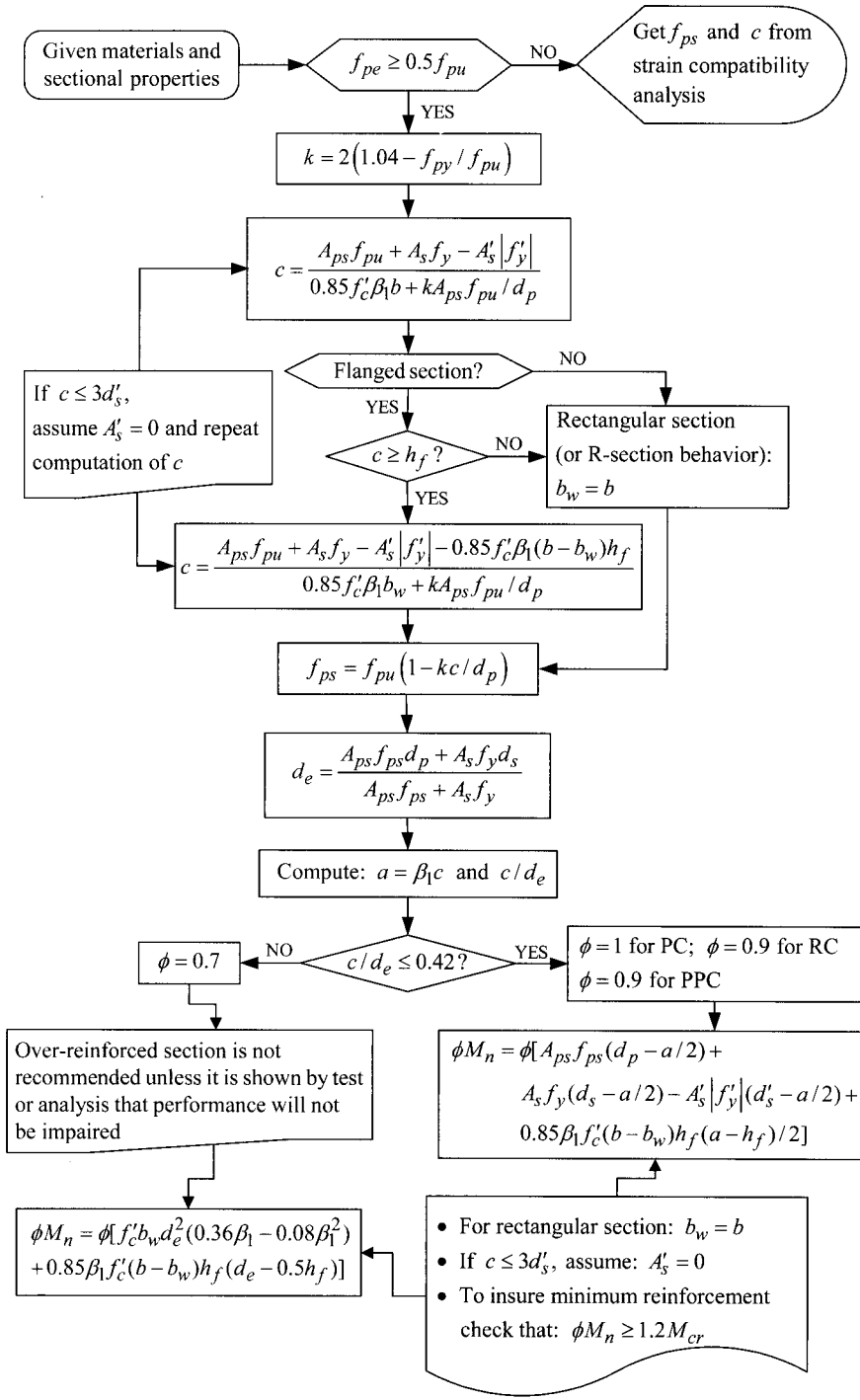

Figure 5.29 Flow chart to compute the nominal bending resistance of partially prestressed concrete sections with bonded tendons according to the provisions of the 2003 AASHTO LRFD code.

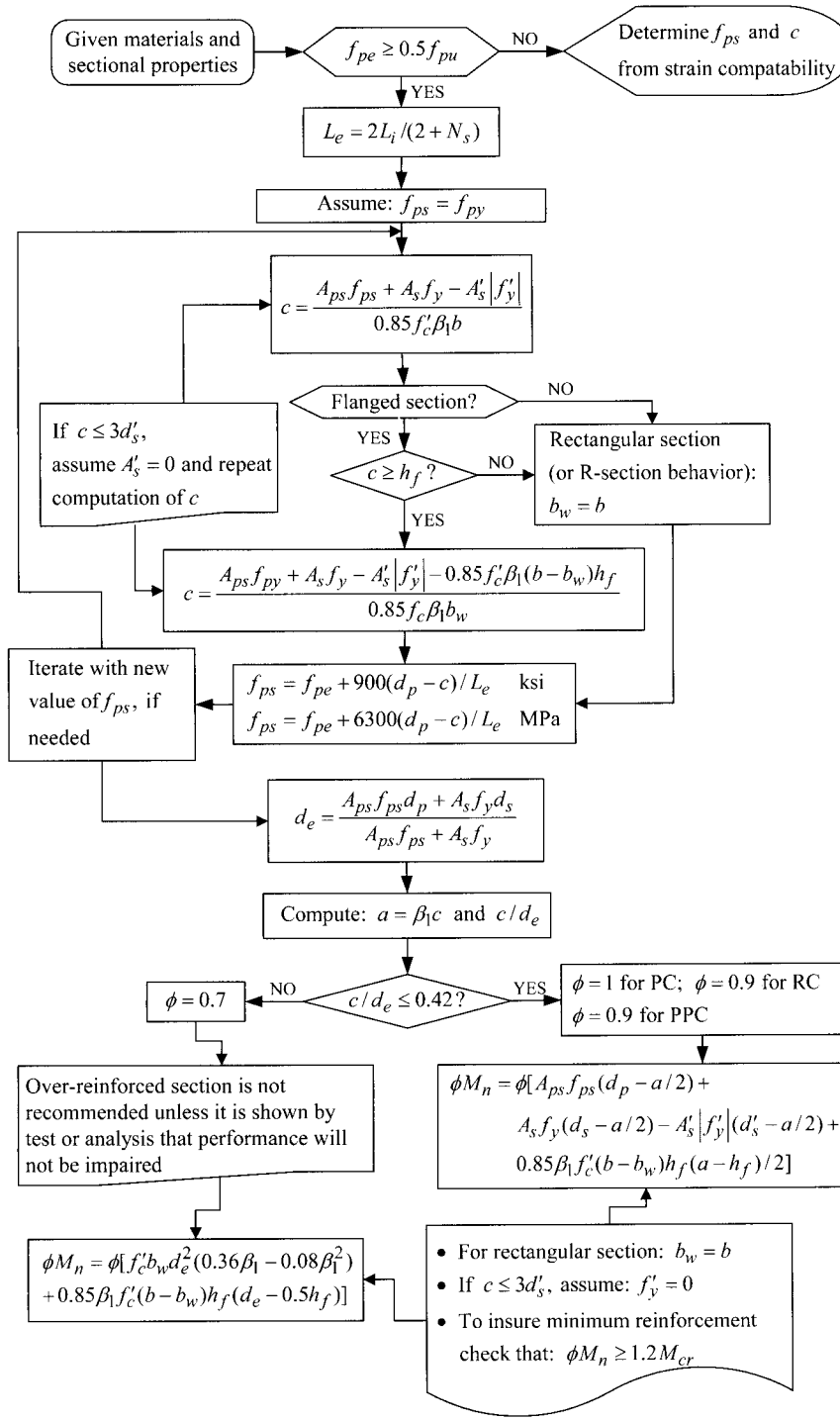

Figure 5.30 Flow chart to compute the nominal moment resistance of prestressed and partially prestressed concrete sections with unbonded tendons according to the provisions of the 2003 AASHTO LRFD code.

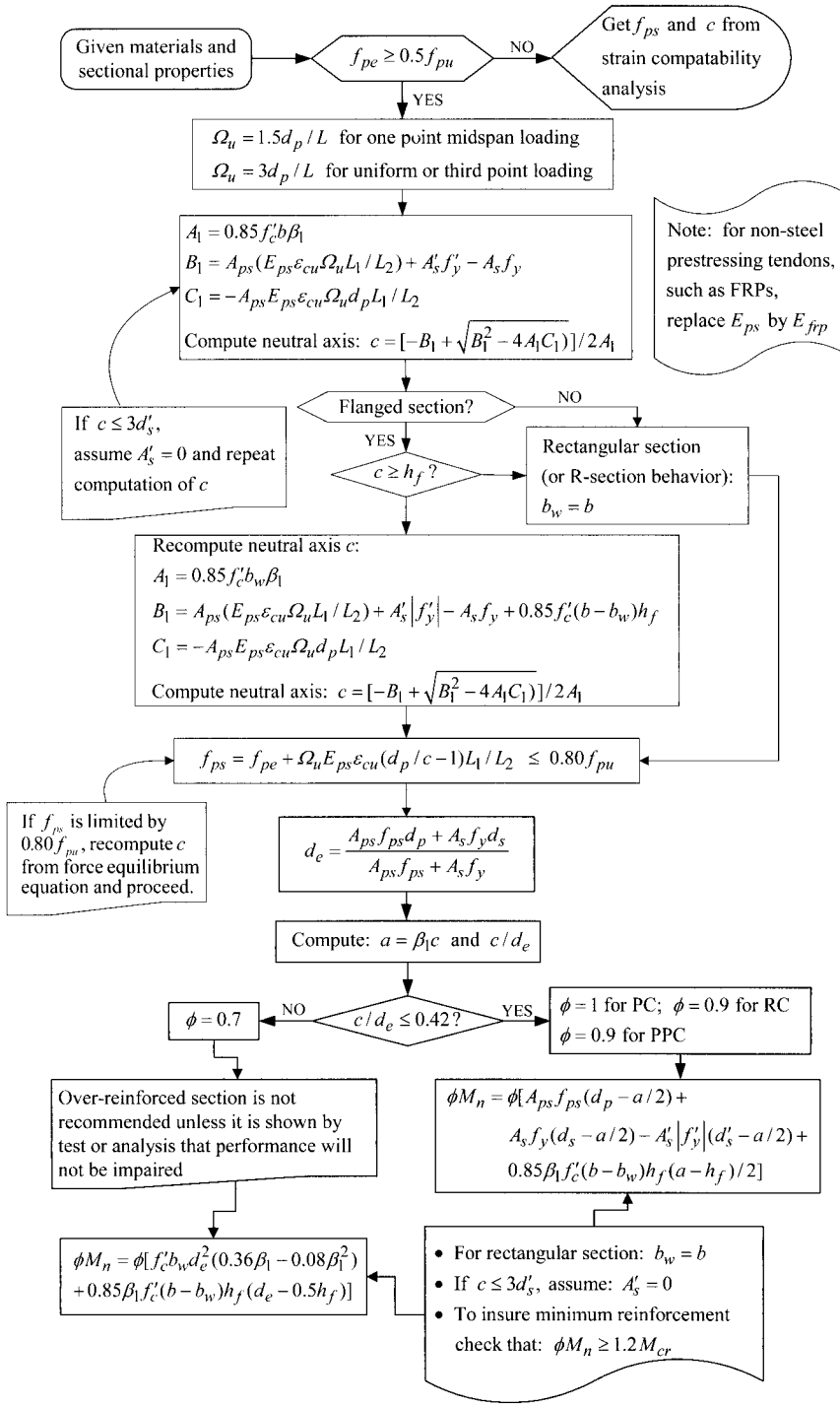

Figure 5.31 Flow chart for the nominal moment resistance of prestressed and partially prestressed concrete sections with unbonded tendons: refined approach recommended by author.

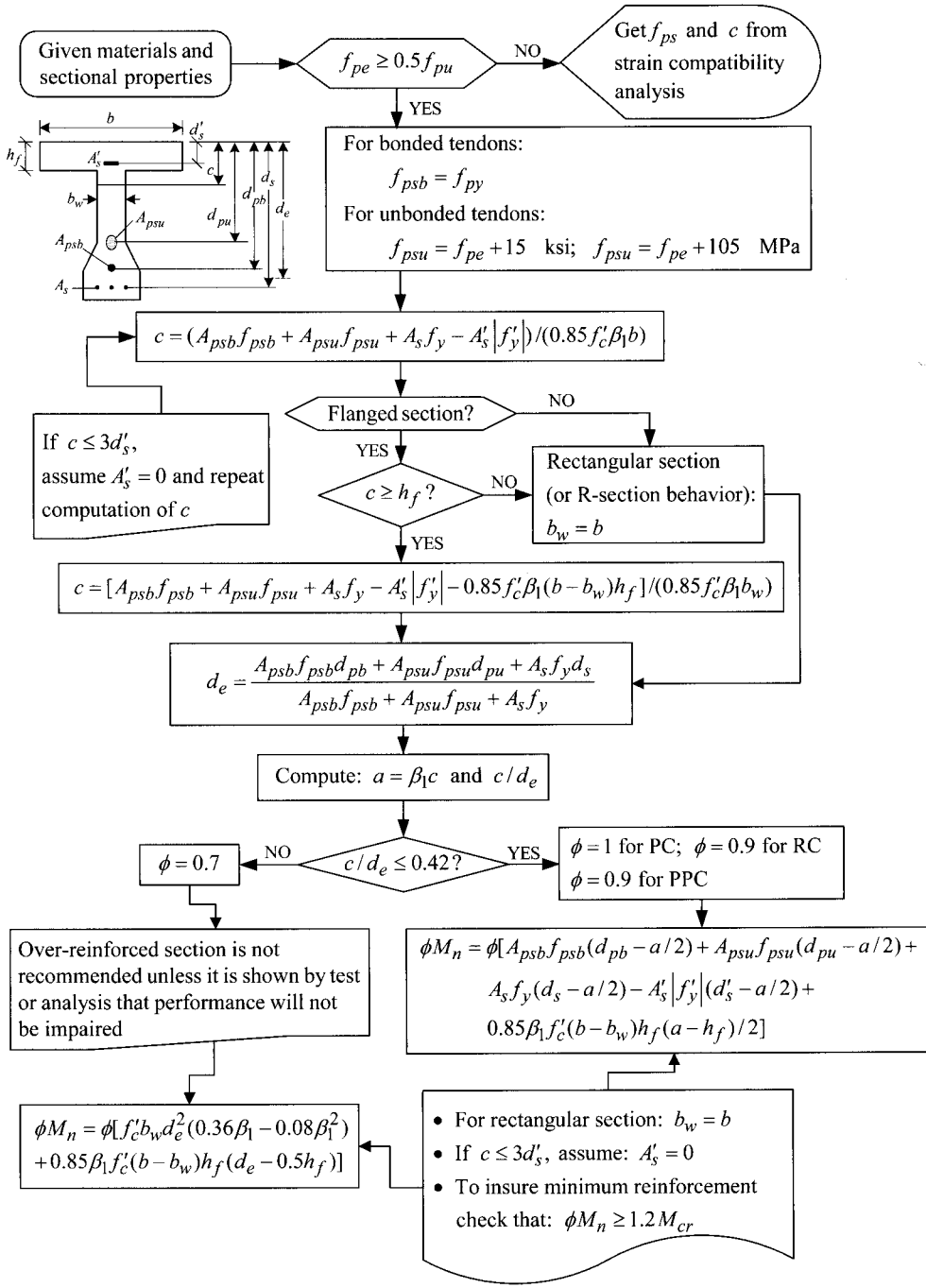

Figure 5.32 Flow chart to compute the nominal bending resistance of prestressed and partially prestressed concrete sections with a combination of bonded and unbonded tendons using the conservative approach.

5.14 CONCEPT OF REINFORCING INDEX

In this text, a particular effort is made to integrate the analysis and design of reinforced and prestressed concrete sections. This explains why some definitions below slightly differ from their ACI counterparts; however, they are rational and necessary to provide a unified design procedure. For this, it is important to understand the parallel that exists between the limiting values of the reinforcing index in prestressed concrete and the reinforcement ratio in reinforced concrete, as well as their relationship to the c/d_e ratio and the net tensile strain in the concrete as discussed in Section 5.5 and Fig. 5.11.

5.14.1 Definitions

Let us define the effective reinforcing index (or the global reinforcing index, or total reinforcing index), ω_e, as follows:

$$\omega_e = \omega_p + \omega_s - \omega' \tag{5.53}$$

where the partial reinforcing indices ω_p, ω_s and ω' are given by:

$$\omega_p = \frac{A_{ps} f_{ps}}{b d_e f'_c} = \rho_p \frac{f_{ps}}{f'_c} \tag{5.54}$$

$$\omega_s = \frac{A_s f_y}{b d_e f'_c} = \rho_s \frac{f_y}{f'_c} \tag{5.55}$$

$$\omega' = \left| \frac{A'_s f'_y}{b d_e f'_c} \right| = \rho' \frac{|f'_y|}{f'_c} \tag{5.56}$$

The absolute value of f'_y is used since it is a compressive stress in the steel and is negative. A_s and A'_s are the areas of the nonprestressed tensile and compressive reinforcement and d_e is the distance to the centroid of the tensile force in the reinforcement as defined in Eq. (5.3). Note that, for a purely prestressed section, $d_e = d_p$ and the above definitions of ω_p and ω_s become identical to those in the ACI code (Fig. 5.6). If we replace the partial reinforcing indices with their values in Eq. (5.53), the combined index, that is the effective reinforcing index, becomes:

$$\omega_e = \rho_p \frac{f_{ps}}{f'_c} + \rho_s \frac{f_y}{f'_c} - \rho' \frac{|f'_y|}{f'_c} = \frac{A_{ps} f_{ps} + A_s f_y - A'_s |f'_y|}{b d_e f'_c} \tag{5.57}$$

where ρ_p, ρ_s, and ρ' are the reinforcing ratios of the prestressing steel, the nonprestressed tensile steel, and the compressive steel, respectively.

In the ACI Code, for the web part of a flanged section, when T-section behavior occurs, the value of b in the above equations is replaced by b_w, and the reinforcement areas A_{ps}, A_s and A'_s are replaced by A_{pw}, A_{sw} and A'_{sw}, respectively. Note that A_{pw}, A_{sw} and A'_{sw} are the areas required to develop compressive resistance of the web only. In this book, we will try to avoid using such procedure, since several combinations of the values of A_{pw}, A_{sw} and A'_{sw} could lead to the same answer, that is, the same tensile force.

5.14.2 Meaning of ω_e

It is important to fully understand the meaning of the effective reinforcing index ω_e. It is a unifying parameter between reinforced, prestressed, and partially prestressed sections and can be very useful in design. As shown below, ω_e is directly proportional to the forces in the section at ultimate behavior, whether they come from the reinforcing steel, the prestressing steel, or their combination.

Let us assume that we have a rectangular section reinforced with prestressed and nonprestressed tensile and compressive reinforcement. Let us also assume that at ultimate capacity, the nonprestressed tensile and compressive steels yield. Equilibrium of the internal forces in the section leads to:

$$0.85 f'_c b a = A_{ps} f_{ps} + A_s f_y - \left| A'_s f'_y \right| \tag{5.58}$$

If we divide both sides by $b d_e f'_c$, the second term of the equation becomes:

$$\frac{0.85 f'_c b a}{b d_e f'_c} = \frac{A_{ps} f_{ps} + A_s f_y - A'_s f'_y}{b d_e f'_c} = \omega_e \tag{5.59}$$

and is reduced to:

$$0.85 \frac{a}{d_e} = \omega_e \tag{5.60}$$

Thus, ω_e can also be expressed as:

$$\omega_e = \frac{1}{b d_e f'_c} \times (\text{compressive force in concrete}) \tag{5.61a}$$

$$\omega_e = \frac{1}{bd_e f'_c} \times (\text{net tensile force in all the steel}) \tag{5.61b}$$

Generally, the assumption that the nonprestressed tensile steel yields at ultimate is valid. However, the compressive steel may not always yield at ultimate. When this is the case, a small difference will appear between the definition of ω_e (Eq. 5.57) and that derived from the force equilibrium Eq. (5.59) above. By assuming yielding of the compressive steel in the definition of ω', a small error is allowed in some cases, but the design procedure is greatly simplified. On the other hand, the compression reinforcement could be ignored, especially when it is present in a marginal amount.

5.14.3 Useful Relationships

Many of the equations derived in Sec. 5.7 can be put in function of ω_e. For instance, let us consider a partially prestressed concrete rectangular section. The force equilibrium can be written:

$$0.85 f'_c ba = A_{ps} f_{ps} + A_s f_y - \left| A'_s f'_y \right| = \omega_e b d_e f'_c \tag{5.62}$$

from which the depth of the stress block a can be obtained:

$$a = \frac{\omega_e d_e}{0.85} = 1.18\, \omega_e d_e \tag{5.63}$$

Thus, the depth of the neutral axis (Eq. 5.20) becomes:

$$c = \frac{1.18 \omega_e d_e}{\beta_1} \tag{5.64}$$

and:

$$\frac{c}{d_e} = \frac{1.18 \omega_e}{\beta_1} \tag{5.65}$$

It was shown in Fig. 5.12 that the ratio c/d_e is related on a one-to-one basis to the fictitious tensile strain in the concrete (or equivalently the net tensile strain in the bonded reinforcement) at nominal bending resistance. Assuming the failure strain of

concrete in compression to be $\varepsilon_{cu} = 0.003$ and using Eqs. (5.9) and (5.65) leads to the following relation:

$$\varepsilon_{te} = \varepsilon_{cu}\frac{d_e - c}{c} = \varepsilon_{cu}\left(\frac{1}{c/d_e} - 1\right) = \varepsilon_{cu}\left(\frac{0.85\beta_1}{\omega_e} - 1\right) \tag{5.66}$$

Thus there is also a one-to-one relation between the tensile strain in the concrete and the effective reinforcing index ω_e. For the tension-controlled strain limit of 0.005, the effective reinforcing index is equal to $0.319\beta_1$. For the compression-controlled strain limit of 0.002, the effective reinforcing index is equal to $0.51\beta_1$.

Replacing the value of a from Eq. (5.63) in Eq. (5.17) leads to the nominal moment resistance for rectangular section or rectangular section behavior of T section:

$$M_n = f'_c b d_e^2 \omega_e (1 - 0.59\omega_e) \tag{5.67}$$

The corresponding design nominal moment resistance is given by:

$$\phi M_n = \phi f'_c b d_e^2 \omega_e (1 - 0.59\omega_e) \tag{5.68}$$

Equation (5.67) combines the two equations of equilibrium of the section at ultimate leading to a quadratic equation in ω_e. It is sometimes convenient in design because it shows only one unknown, ω_e, instead of two, namely a and f_{ps}. However, it may be misleading because it suggests, at first look, a direct relation between M_n and f'_c while in reality M_n is generally only slightly sensitive to f'_c since f'_c is also in the denominator of ω_e.

When T-section instead of rectangular-section behavior exists, the nominal moment can be divided into two parts, one due to the resistance of the flange and one to that of the web; thus:

$$\phi M_n = \phi(M_{nf} + M_{nw}) \tag{5.69}$$

For T-section behavior, the author prefers the use of the forces in the concrete compression block, in order to avoid dealing with the reinforcing index associated with the web part of the section. This is particularly true for partially prestressed sections. In such a case:

$$\phi M_n = \phi\left[0.85 f'_c (b - b_w) h_f (d_e - h_f/2) + 0.85 f'_c b_w a (d_e - a/2)\right] \tag{5.70}$$

However, when only prestressing steel is present, the design nominal bending resistance for T-section behavior can also be written as follows:

$$\phi M_n = \phi\left[0.85 f'_c(b-b_w)h_f(d_p - h_f/2) + f'_c b_w d_p^2 \omega_{pw}(1-0.59\omega_{pw})\right] \quad (5.71)$$

A similar equation can be used for a fully reinforced concrete section by simply replacing ω_{pw} by ω_{sw}. The earlier comment that, in the expression of M_{nf}, the factor β_1 should preferably be used as a multiplier, applies here also, as done in the AASHTO code. However, to avoid confusion with the ACI code approach, β_1 is not included in the expression of M_{nf} in Eq. (5.71).

5.14.4 Relationship between Reinforcement Ratio, Reinforcing Index, and c/d_e

Given the definition of ω_e and its relationship to:

- the maximum compressive force in the concrete (Eq. 5.61)
- the net tensile force in the steel (Eq. 5.61)
- the reinforcement ratio (Eq. 5.57)
- the ratio c/d_e (Eq. 5.65)
- the tensile strain in the concrete at nominal bending resistance (Eq. 5.66), and
- the nominal bending moment M_n (Eq. 5.67)

it can be noted that limiting the value of ω_e is the same as limiting the reinforcement ratio (for reinforced concrete), or limiting the prestressing index (prestressed concrete), or limiting the ratio c/d_e (AASHTO provision for reinforced, prestressed, or partially prestressed concrete), or limiting the net tensile strain (2002 ACI provisions for structural concrete). Some of these relationships are graphically illustrated in Fig. 5.11. There are situations where it is advantageous to use one variable versus another. For mechanical computations the effective index ω_e may be necessary, especially when dealing with design problems, partially prestressed concrete, and T-section behavior. On the other hand, for evaluating limits of reinforcement in any section, the c/d_e ratio is particularly advantageous for all cases. Indeed, limiting the ratio c/d_e to a single value applies to reinforced, prestressed, and partially prestressed rectangular and T sections with and without compression reinforcement.

Limiting c/d_e or ω_e as defined in this text is like limiting the total tensile force in the reinforcement, thus limiting, through equilibrium, the compression force in the concrete stress block. Hence, one does not need to know how the compression force is balanced on the tensile side and what are the components of the tensile force. It suffices to say that the tensile force is equal to the compressive force. This will

bypass the use of partial reinforcing indices, whether for a rectangular section or the web part of a T section. When several types of reinforcement are used in the section, using c/d_e or the compressive force in the concrete, as adopted by AASHTO, offers numerous advantages in terms of clarity and reduction of computational effort.

In summary, in order to provide a consistent link between key parameters, it is essential to provide a rational and consistent definition of d_e and ω_e as done in this text, that is, values that guarantee consistency at the limits and amenable to satisfying the equations of equilibrium in the section in all cases.

5.15 JUSTIFICATION FOR THE DEFINITION OF ω_e AND d_e AND THEIR RELATION TO THE LIMITATIONS ON LEVELS OF REINFORCEMENT AND MOMENT REDISTRIBUTION

The choice of variable d_e (Eq. 5.3) is important since, in comparison to d_t as defined in Sect. 5.5.3, it guarantees similar relationship whether the section contains reinforcing steel, prestressing steel or a combination of both. Below is the proof, assuming a rectangular section.

5.15.1 Reinforced Concrete

Tensile force in steel = Compression force in concrete

$$A_s f_y = 0.85 f'_c b\, a = 0.85 f'_c b\, \beta_1 c \tag{5.72}$$

Dividing both sides by a constant $(bd_s f_y)$ leads to:

$$\rho = \frac{A_s}{bd_s} = \left[0.85\beta_1 \frac{f'_c}{f_y}\right]\left(\frac{c}{d_s}\right) \tag{5.73}$$

Multiplying Eq. (5.73) by f_y / f'_c leads to the definition of the reinforcing index, namely:

$$\omega_s = \frac{A_s f_y}{bd_s f'_c} = [0.85\beta_1]\left(\frac{c}{d_s}\right) = 0.85\left(\frac{a}{d_s}\right) \tag{5.74}$$

5.15.2 Prestressed Concrete

$$A_{ps} f_{ps} = 0.85 f'_c b\, \beta_1 c = 0.85 f'_c ba \tag{5.75}$$

Dividing both sides by a constant $(bd_p f'_c)$ leads to:

$$\omega_p = \frac{A_{ps} f_{ps}}{bd_p f'_c} = [0.85\beta_1]\left(\frac{c}{d_p}\right) = 0.85\left(\frac{a}{d_p}\right) \tag{5.76}$$

5.15.3 Partially Prestressed Concrete

$$A_{ps} f_{ps} + A_s f_y - A'_s f'_y = 0.85 f'_c b \beta_1 c = 0.85 f'_c b a \tag{5.77}$$

Dividing both sides by $(bd_e f'_c)$, leads to:

$$\omega_e = \frac{A_{ps} f_{ps} + A_s f_y - A'_s \left| f'_y \right|}{bd_e f'_c} = [0.85\beta_1]\left(\frac{c}{d_e}\right) = 0.85\left(\frac{a}{d_e}\right) \tag{5.78}$$

It can be observed that only the use of ω_e, and d_e as defined in Eqs. (5.57 and 5.3) will guarantee the same proportionality constant (here $0.85\beta_1$) in Eq. (5.78) as for the cases of reinforced concrete (Eq. 5.74), and prestressed concrete (Eq. 5.76). Moreover, only d_e as defined here (Eq. 5.3) reverts to d_s when A_{ps} is zero, or to d_p when A_s is zero, while maintaining equilibrium of forces in all cases.

Thus if a net tensile strain is to be used to provide some limit on the reinforcement, it should be defined at the centroid of the resulting tensile force in order for it to be useful for the equilibrium equations. The use of d_t (distance to the extreme layer of reinforcement) in the 2002 ACI code is perhaps useful for detailing, but is not rational for the equilibrium analysis of the section. The reader is referred to Ref. [5.28] for additional discussion on the subject.

5.16 DERIVATION OF MINIMUM REINFORCEMENT RATIO, MINIMUM REINFORCING INDEX, OR MINIMUM c/d_e

5.16.1 Approximation: Minimum Reinforcement Ratio for Prestressed Concrete

In a general case, it should be quite simple to determine the minimum amount of reinforcement, which corresponds to the fracture of the steel immediately after cracking of the concrete section, by writing that the ultimate moment is equal to the cracking moment as illustrated below. The positive moment leading to cracking on the bottom fiber of a simply supported beam is given by Eq. (5.6):

$$M_{cr} = A_{ps} f_{pe} \left(e_o + \frac{Z_b}{A_c} \right) - f_r Z_b \tag{5.79}$$

where f_r is the modulus of rupture of the concrete. For minimum reinforcement, the design moment resistance at ultimate, ϕM_n, can be determined as a first approximation assuming a lever arm equal to $0.95 d_p$ and a stress in the prestressing steel equal to its tensile strength; thus:

$$\phi M_n \approx \phi \times 0.95 A_{ps} f_{pu} d_p \tag{5.80}$$

where $\phi = 0.9$ for flexure. Equating M_{cr} to ϕM_n leads to:

$$A_{ps} = \frac{-f_r Z_b}{0.86 f_{pu} d_p - f_{pe}(e_o + Z_b / A_c)} \tag{5.81}$$

Dividing both sides by $b d_p$ leads to the minimum reinforcement ratio required:

$$\rho_{pmin} = \frac{A_{ps}}{b d_p} = \frac{-f_r Z_b}{b d_p [0.86 f_{pu} d_p - f_{pe}(e_o + Z_b / A_c)]} \tag{5.82}$$

To avoid brittle failure immediately after cracking, the ACI code recommends that the nominal moment be at least 20 percent higher than the cracking moment. The corresponding minimum reinforcement ratio, if determined as above, using the same approximation for the nominal moment as in Eq. (5.80), would be:

$$\rho_{pmin} = \frac{A_{ps}}{b d_p} = \frac{-1.2 f_r Z_b}{b d_p [0.86 f_{pu} d_p - 1.2 f_{pe}(e_o + Z_b / A_c)]} \tag{5.83}$$

Additional derivation for the particular case of reinforced concrete is given at the end of the next section.

5.16.2 Minimum Reinforcing Index for RC, PC, PPC

It was pointed out earlier (Fig. 5.8) that, in order to avoid sudden failure immediately after cracking, the ACI code recommends a minimum value of reinforcement area for reinforced concrete members while, for prestressed concrete, such a limit was indirectly set by requiring that the ultimate moment be 20 percent higher than the cracking moment. An attempt is made below to show that a particular value of the reinforcing index ω_e can be set as a common lower limit for reinforced concrete,

prestressed concrete and partially prestressed concrete. The design moment resistance of the above three classes of beams can be written as a function of ω_e (assuming rectangular section behavior) as (Eq. 5.67):

$$\phi M_n = \phi f'_c b d_e^2 \omega_e (1 - 0.59\omega_e) \qquad (5.67 \text{ and } 5.84)$$

Furthermore, their cracking moment (assuming positive external moment leading to cracking on the bottom fiber) can be most generally written as:

$$M_{cr} = A_{ps} f_{pe} \left(e_o + \frac{Z_b}{A_c} \right) - f_r Z_b \qquad (5.6 \text{ and } 5.85)$$

where, for a purely reinforced section, $A_{ps} = 0$. To avoid sudden collapse after cracking, we can write that:

$$\phi M_n \geq \alpha M_{cr} \qquad (5.86)$$

where α is a factor larger than or equal to 1. For prestressed concrete, the ACI and AASHTO codes recommend $\alpha = 1.2$.

Replacing Eqs. (5.80) and (5.85) in Eqs. (5.84) and (5.86) leads to a quadratic equation in ω_e with two positive roots; the smaller root gives the minimum required value of ω_e.

The solution is different if a fully reinforced or a fully prestressed concrete section is used, because the value of M_{cr} for a fully prestressed section is itself dependent on ω_e. The reader may want to check the following results, where f_r is assumed negative.

For reinforced concrete:

$$\omega_{smin} = 0.85 \left(1 - \sqrt{1 + \frac{2.3\alpha f_r Z_b}{\phi f'_c b d_s^2}} \right) \qquad (5.87)$$

For prestressed concrete:

$$\omega_{pmin} = 0.85 \left((1 - \lambda) - \sqrt{(1 - \lambda)^2 + \frac{2.36\alpha f_r Z_b}{\phi f'_c b d_p^2}} \right) \qquad (5.88)$$

where:

$$\lambda = \frac{\alpha}{\phi}\frac{f_{pe}}{f_{pu}}\left(e_o + \frac{Z_b}{A_c}\right)\frac{1}{d_p} \tag{5.89}$$

For partially prestressed concrete, the value of d_p in Eqs. (5.88) and (5.89) could be replaced by d_e, where d_e is the distance to the centroid of the tensile force. As a first approximation, an estimate between d_p and d_s can be used. Then the minimum effective reinforcing index becomes:

$$\omega_{emin} = 0.85\left((1-\lambda) - \sqrt{(1-\lambda)^2 + \frac{2.36\alpha f_r Z_b}{\phi f'_c b d_e^2}}\right) \tag{5.90}$$

In the above equations, the value of α can be taken = 1.2 as per the ACI and AASHTO codes. When the section has a minimum amount of bonded reinforcement, it can be shown that f_{ps} is very close to f_{pu}. In developing the above closed form solution of ω_{pmin} for prestressed concrete, it was assumed that $f_{ps} = f_{pu}$.

Note also that generally a T section, with a low reinforcement ratio or reinforcing index, behaves as a rectangular section at ultimate. The equation for its nominal resistance is similar to that of a rectangular section; however, its cracking moment will be substantially different. Thus, the above values of ω_{emin} cannot apply to T sections without some modification.

Particular Case of Reinforced Concrete

Equation (5.87) for the minimum reinforcing index in reinforced concrete can be used to derive a minimum reinforcement ratio. Using Eq. (5.87) in which $\alpha = 1.2$, $\phi = 0.9$, $f_r = -0.125f'_c = -f'_c/8$, and $Z_b = bd_s^2/6$, leads to the following numerical value:

$$\omega_{smin} = 0.85\left(1 - \sqrt{1 - \frac{2.36\times1.2\times0.125 f'_c b d_s^2}{6\times0.9 f'_c b d_s^2}}\right) \approx 0.028 = \rho_{smin}\frac{f_y}{f'_c} \tag{5.91}$$

from which:

$$\rho_{smin} = 0.028\frac{f'_c}{f_y} \tag{5.92}$$

In the 1998-2003 AASHTO LRFD code, the above value of ρ_{smin} has been rounded off, as shown in Fig. 5.8 to:

$$\rho_{smin} = 0.03\frac{f'_c}{f_y} \tag{5.93}$$

Note that in comparing Eq. (5.93) with the ACI code recommendation for reinforced concrete (Fig. 5.8), Eq. (5.93) offers the advantage of being non-dimensional (i.e. valid in any system of units).

5.16.3 Minimum c/d_e Ratio for RC, PC and PPC Rectangular Sections

Using Eq. (5.65) and the result of Eq. (5.91) leads, for reinforced concrete rectangular sections, to:

$$\left(\frac{c}{d_s}\right)_{min} = \frac{1.18\omega_{smin}}{\beta_1} = \frac{1.18\times 0.028}{\beta_1} = \frac{0.033}{\beta_1} \tag{5.94}$$

Equation (5.94) shows that the minimum reinforcement requirement for reinforced concrete rectangular sections can be put in terms of the c/d_s ratio. To achieve a similar result for prestressed or partially prestressed concrete, there is need to account for the increase in cracking moment due to prestressing. The author has developed a unified condition which, while not given in any code, reasonably simulates the requirements given by the ACI and AASHTO codes for the minimum reinforcement criterion. It applies to rectangular sections only, reinforced, prestressed, or partially prestressed. Using Eq. (5.94) and noting that the cracking moment depends on the effective prestress, f_{pe} (as also illustrated in Eq. 5.89) the following prediction equation was developed:

$$\frac{c}{d_e} \geq \frac{0.033}{\beta_1}\left(1+3PPR\left(\frac{f_{pe}}{f_{pu}}\right)^2\right) \tag{5.95}$$

where f_{pe} is between 0 and $0.65f_{pu}$. The partial prestressing ratio, PPR, is defined in Eq. (8.11). It is equal zero for fully reinforced concrete and 1 for fully prestressed concrete. Note that Eqs. (5.94) and (5.95) are non-dimensional, thus applicable in all systems of units.

It should be noted that the ACI code equation for minimum reinforcement in reinforced concrete (Fig. 5.8) can also be put in terms of the c/d_s ratio as follows:

$$\frac{c}{d_s} \geq \frac{3.53}{\beta_1 \sqrt{f'_c}} \geq \frac{200}{0.85\beta_1 f'_c} \tag{5.96}$$

5.17 SATISFYING ULTIMATE STRENGTH DESIGN REQUIREMENTS

5.17.1 Basis for Ultimate Strength Design (USD)

When the USD (also referred to as Strength Design) approach is applied, the general format is given by the formula (see also Chapter 3):

$$\text{Code Required Strength} \leq \phi \times \text{(Nominal Resistance)} \tag{5.97}$$

The left side of Eq. (5.97) represents the required strength, which is computed from structural analysis based upon assumed loads and load factors; the right side of Eq. (5.97) represents a limiting structural capacity provided by the selected members. Written in a general mathematical form, it leads to:

$$U = \Sigma \gamma_i Q_i \leq \phi R_n \tag{5.98}$$

where:

i = type of load, i.e., dead load, live load, wind, etc.
Q_i = nominal load effect
γ_i = load factor corresponding to Q_i
U = required or specified ultimate strength
R_n = nominal strength or resistance
ϕ = resistance factor (or capacity reduction factor) corresponding to R_n
ϕR_n = design strength or design nominal resistance

The required strength for design, $U = \Sigma \gamma_i Q_i$, is defined as the maximum (absolute value) of force obtained from the specified load combinations. Examples of load factors and related load combinations specified by the ACI code are given in Table 3.9. Values of the strength reduction factor, ϕ, as given in the ACI code are summarized in Table 3.10. Load and resistance factors recommended by the AASHTO code are given in Section 14.5.

When the USD approach is applied to bending, the following formulation is obtained for the most commonly encountered set of factors and simplest load combination:

$$M_u = \gamma_D M_D + \gamma_L M_L \leq \phi M_n \tag{5.99}$$

where M_u is the strength design moment (factored moment) required by the code, M_n is the nominal moment resistance, γ_D and γ_L are the dead and live load factors, respectively, and M_D and M_L are the dead load moment and the live load moment, respectively. In a typical design problem where some unknown is being calculated, Eq. (5.99) is often used in the following form

$$\frac{M_u}{\phi} \leq M_n \tag{5.100}$$

Using the numerical values given by ACI in Tables 3.9 and 3.10, Eq. (5.99) for a tension-controlled section becomes:

$$M_u = 1.2M_D + 1.6M_L \leq 0.9M_n \tag{5.101}$$

Generally, M_u represents the largest factored moment obtained from the various load combinations and factors described in Sec. 3.8.

Note that by the time M_n has been calculated, the condition related to maximum reinforcement or different levels of reinforcement (under- or over-reinforced, tension- or compression-controlled) would have been checked. However, the condition related to minimum reinforcement (Eq. 5.5) will still need to be checked since it depends on the value of M_n.

5.17.2 Possible Remedies to Satisfy Inadequate Nominal Bending Resistance

If it is found that the design nominal resistance is not sufficient, i.e., Eq. (5.99 or 5.100) is not satisfied, several corrective actions can be taken. They are listed below in order of their effectiveness and simplicity of implementation:

1. Add nonprestressed reinforcement
2. Increase the amount of prestressing steel; however, make sure that none of the allowable stresses are then violated under working stress conditions
3. Increase the eccentricity of the steel or equivalently d_p if possible without violating allowable stresses
4. Change materials properties and/or sectional dimensions

The above remedies can also be used in part when the nominal moment resistance is to be increased to satisfy the condition for minimum reinforcement, such as where the nominal moment resistance should be at least 20 percent higher than the cracking moment. In order of effectiveness, it is recommended to use first 1; then use 2 noting that the cracking moment will also increase; generally, option 3 is not available; and finally, use option 4.

5.18 EXAMPLE: ANALYSIS OR INVESTIGATION CHECKING FOR ALL ULTIMATE STRENGTH DESIGN CRITERIA

Consider the example beam of Sections4.9 and 4.12.3. Use the ACI code. The beam is reinforced with ten strands at a midspan eccentricity of e_o = 21.7 in (Fig. 5.33). Check all ultimate strength criteria for bending. Some calculations are arrived at using different approaches to illustrate the use of different formulae.

The following external moments were found:

M_G = 350.962 kips-ft; M_{SD} = 24.5 kips-ft

M_D = 375.462 kips-ft; M_L = 245 kips-ft

The design steps are similar to those given in the flow chart, Fig. 5.24.

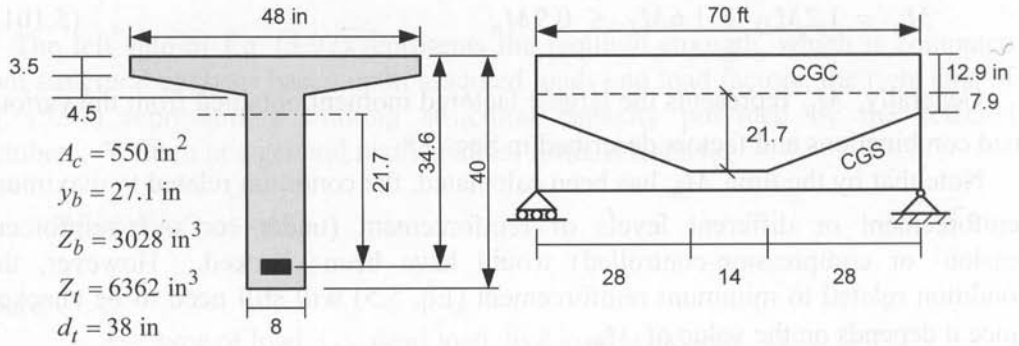

A_{ps} =1.53in^2; f'_c = 5000 psi; f_r = –530.3 psi; f_{pe} = 150 ksi; f_{pu} = 270 ksi; stress relieved strands.

Figure 5.33

$$A_{ps} = 10 \times 0.153 = 1.53 \text{ in}^2$$

$$d_p = e_o + y_t = 21.7 + 12.9 = 34.6 \text{ in}$$

$$\rho_p = \frac{A_{ps}}{bd_p} = \frac{1.53}{48 \times 34.6} = 0.00092$$

$$f_{ps} = 270\left(1 - \frac{0.4}{0.8}\rho_p \frac{270}{5}\right) = 263.28 \text{ ksi}$$

$$\omega_e = \omega_p = 0.00092 \frac{263.28}{5} = 0.0485$$

$$a = \frac{A_{ps} f_{ps}}{0.85 f'_c b} = \frac{1.53 \times 263.28}{0.85 \times 5 \times 48} = 1.98 \text{ in}$$

or $a = 1.18\omega_e d_p = 1.18 \times 0.0485 \times 34.6 = 1.98$ in

$$c = \frac{a}{\beta_1} = \frac{1.98}{0.8} = 2.475 \text{ in}$$

$$\text{or } c = \frac{1.18\omega_e d_p}{\beta_1} = \frac{1.18 \times 0.0485 \times 34.6}{0.80} = 2.475 \text{ in}$$

- Since we have a T section, check neutral axis location; as this beam has a tapering flange, an equivalent h_f value of 5.75 in can be taken:

  $c = 2.475 \text{ in} < h_f = 5.75 \text{ in}$

  Thus, design as a rectangular section.

- Check reinforcement limit criterion assuming rectangular section behavior:

  $$\frac{c}{d_e} = \frac{c}{d_p} = \frac{2.475}{34.6} = 0.071 < 0.375 \rightarrow \text{Tension-controlled section by ACI code}$$

  Thus $\phi = 0.9$ by ACI. Note that using $c/d_t = 2.475/38 = 0.065$ is less stringent.

  Similarly:

  $$\frac{c}{d_e} = \frac{c}{d_p} = \frac{2.475}{34.6} = 0.071 < 0.42 \rightarrow \text{Under-reinforced section by AASHTO}$$

  Thus $\phi = 1$ by AASHTO.

- Compute the design nominal moment resistance by ACI:

  $$\phi M_n = \phi A_{ps} f_{ps}\left(d_p - \frac{a}{2}\right) = 0.9 \times 1.53 \times 263.28\left(34.6 - \frac{1.98}{2}\right) = 12184.8 \text{ kips-in}$$

  $$= 1015.4 \text{ kips-ft}$$

  or

  $$\phi M_n = \phi f'_c b d_p^2 \omega_e (1 - 0.59\omega_e) = 12{,}184.8 \text{ kips-in} = 1015.4 \text{ kips-ft}$$

  or

  $$\phi M_n = \phi 0.85 f'_c b a\left(d_p - \frac{a}{2}\right) = 0.9 \times 0.85 \times 5 \times 48 \times 1.98\left(34.6 - \frac{1.98}{2}\right)$$

  $$= 12218.1 \text{ kips-in} = 1018.18 \text{ kips-ft}$$

  That is essentially the same answer.

- The cracking moment is given by Eqs. (4.38) or (5.6):

  $$M_{cr} = F\left(\frac{Z_b}{A_c} + e_o\right) - f_r Z_b = 229{,}500\left(\frac{3028}{550} + 21.7\right) + 530.3 \times 3028$$

  $$= 7{,}849{,}400 \text{ lb-in} = 654 \text{ kips-ft}$$

- Check minimum reinforcement criterion:

$$\frac{\phi M_n}{M_{cr}} = \frac{1015.4}{654} = 1.55 > 1.2 \quad \text{O.K. per ACI and AASHTO}$$

- Check ultimate strength criterion using ACI load and resistance factors:

$$M_u = 1.2M_D + 1.6M_L = 1.2 \times 375.462 + 1.6 \times 245 = 842.55 \text{ kips-ft}$$

$$\phi M_n = 1015.4 \text{ kips-ft} > M_u = 842.55 \text{ kips-ft} \quad \text{O.K.}$$

This beam design satisfies all USD criteria for flexural strength.

5.19 REINFORCEMENT DESIGN FOR ULTIMATE STRENGTH

The design of prestressed concrete beams in flexure starts generally by the working stress design procedure described in Chapter 4, where the prestressing force and the corresponding area of prestressing steel are determined. In order to satisfy ultimate strength requirements, the nominal moment resistance is then determined as shown in Sections 5.7 to 5.10, and its value is compared to the strength design moment specified by code. In this last step, it is assumed that materials properties and cross-sectional dimensions are known. In general, the working stress design approach (i.e., stress and serviceability limit states) controls the design in prestressed beams.

However, it is possible to design prestressed concrete sections strictly on the basis of ultimate strength, without prior reference to the working stress approach. This is similar to reinforced concrete design currently used in the ACI and AASHTO LRFD codes. It is illustrated below for a fully prestressed concrete section and in Refs. [5.17 and 1.48] for a partially prestressed section, where the use of the partial prestressing ratio (PPR) is described. Since only two equations of equilibrium are available at ultimate, two unknowns can be determined. They are the depth of the stress block, a, and the area of the prestressing steel, A_{ps}. A third equation provides the value of f_{ps} at ultimate. Thus, for such calculations one must assume all the other unknowns given, i.e., the cross-sectional dimensions, the material properties, and the loading conditions or, equivalently, the value of the strength design moment M_u (Eq. 5.99).

The purpose of the design is then to determine the area of prestressed reinforcement A_{ps}, which would lead to a design nominal moment resistance, ϕM_n, equal to the required strength design moment, M_u.

Going back to Eq. (5.99) it can be observed that, for a given M_u, the required value of ω_p can be determined from satisfying the quadratic relation (Eq. 5.67):

$$\omega_p(1-0.59\omega_p)=\frac{M_u}{\phi f'_c b d_p^2}=\frac{M_n}{f'_c b d_p^2} \tag{5.102}$$

Table 5.1 provides a numerical solution to the above equation. For any numerical value of $\frac{M_u}{\phi f'_c b d_p^2}$, entered in one of the cells of the matrix, the corresponding value of ω_e can be read from the first column and the first line, and vice versa. The table is general and applies to ω_s and ω_p as well.

For a fully prestressed section:

$$\omega_p = \frac{A_{ps} f_{ps}}{b d_p f'_c} \tag{5.2}$$

Given ω_p, since f_{ps} is a function of A_{ps} in Eqs. (5.32) or (5.33), the particular values of the two unknowns f_{ps} and A_{ps} can be determined by solving simultaneously Eq. (5.2) and, for the ACI code, Eq. (5.32) or (5.33).

The solution is given directly in the flow chart, Fig. 5.34, for fully prestressed rectangular and T sections with bonded and unbonded reinforcement using either the 2002 ACI or the 2003 AASHTO code prediction equation for f_{ps}.

The reader is encouraged to verify the equations given in Fig. 5.34. Note that once a value of A_{ps} is obtained, serviceability and other stress based criteria must be checked and the design revised if needed.

In the case of partially prestressed beams with both prestressed and nonprestressed reinforcements, the use of the prediction equation of f_{ps} as per ACI makes it significantly more complex to obtain a solution. A general solution is given in Ref. [1.48] for the case where the prediction equation of f_{ps} is as per Eq. (5.35).

Note that Eq. (5.102) is general and very useful; its numerical solution is provided in Table 5.1, where for a given value of $M_u / \phi f'_c b d_e^2$, one can get the corresponding value of ω_e and vice versa.

The following example illustrates the design procedure.

5.19.1 Example: Reinforcement Design for Nominal Resistance – Rectangular Section

Determine the area of prestressed reinforcement required to develop a design moment resistance $\phi M_n = M_u$ = 300 kips-ft in the rectangular section shown in Fig. 5.35 (same concrete section as Fig. 5.18) assuming the following properties: f'_c = 5 ksi; β_1 = 0.8; f_{pu} = 270 ksi; $f_{pe} = 0.55 f_{pu}$; d_p = 21 in; bonded tendons. Assume stress relieved strands, thus $\gamma_p = 0.4$ from Eq. (5.32).

Table 5.1 Numerical values of the reinforcing index ω_e versus $M_u/(\phi f_c' b d_e^2)$ and vice versa.

ω_e	0.000	0.001	0.002	0.003	0.004	0.005	0.006	0.007	0.008	0.009
0.0	0	0.0010	0.0020	0.0030	0.0040	0.0050	0.0060	0.0070	0.0080	0.0090
0.01	0.0099	0.0109	0.0119	0.0129	0.0139	0.0149	0.0159	0.0168	0.0178	0.0188
0.02	0.0197	0.0207	0.0217	0.0226	0.0236	0.0246	0.0256	0.0266	0.0275	0.0285
0.03	0.0295	0.0304	0.0314	0.0324	0.0333	0.0343	0.0352	0.0362	0.0372	0.0381
0.04	0.0391	0.0400	0.0410	0.0420	0.0429	0.0438	0.0448	0.0457	0.0467	0.0476
0.05	0.0485	0.0495	0.0504	0.0513	0.0523	0.0532	0.0541	0.0551	0.0560	0.0569
0.06	0.0579	0.0588	0.0597	0.0607	0.0616	0.0625	0.0634	0.0643	0.0653	0.0662
0.07	0.0671	0.0680	0.0689	0.0699	0.0708	0.0717	0.0726	0.0735	0.0744	0.0753
0.08	0.0762	0.0771	0.0780	0.0789	0.0798	0.0807	0.0816	0.0825	0.0834	0.0843
0.09	0.0852	0.0861	0.0870	0.0879	0.0888	0.0897	0.0906	0.0915	0.0923	0.0932
0.10	0.0941	0.0950	0.0959	0.0967	0.0976	0.0985	0.0994	0.1002	0.1011	0.1020
0.11	0.1029	0.1037	0.1046	0.1055	0.1063	0.1072	0.1081	0.1089	0.1098	0.1106
0.12	0.1115	0.1124	0.1133	0.1141	0.1149	0.1158	0.1166	0.1175	0.1183	0.1192
0.13	0.1200	0.1209	0.1217	0.1226	0.1234	0.1243	0.1251	0.1259	0.1268	0.1276
0.14	0.1284	0.1293	0.1301	0.1309	0.1318	0.1326	0.1334	0.1342	0.1351	0.1359
0.15	0.1367	0.1375	0.1384	0.1392	0.1400	0.1408	0.1416	0.1425	0.1433	0.1441
0.16	0.1449	0.1457	0.1465	0.1473	0.1481	0.1489	0.1497	0.1506	0.1514	0.1522
0.17	0.1529	0.1537	0.1545	0.1553	0.1561	0.1569	0.1577	0.1585	0.1593	0.1601
0.18	0.1609	0.1617	0.1624	0.1632	0.1640	0.1648	0.1656	0.1664	0.1671	0.1679
0.19	0.1687	0.1695	0.1703	0.1710	0.1718	0.1726	0.1733	0.1741	0.1749	0.1756
0.20	0.1764	0.1772	0.1779	0.1787	0.1794	0.1802	0.1810	0.1817	0.1825	0.1832
0.21	0.1840	0.1847	0.1855	0.1862	0.1870	0.1877	0.1885	0.1892	0.1900	0.1907
0.22	0.1914	0.1922	0.1929	0.1937	0.1944	0.1951	0.1959	0.1966	0.1973	0.1981
0.23	0.1988	0.1995	0.2002	0.2010	0.2017	0.2024	0.2031	0.2039	0.2046	0.2053
0.24	0.2060	0.2067	0.2075	0.2082	0.2089	0.2096	0.2103	0.2110	0.2117	0.2124
0.25	0.2131	0.2138	0.2145	0.2152	0.2159	0.2166	0.2173	0.2180	0.2187	0.2194
0.26	0.2201	0.2208	0.2215	0.2222	0.2229	0.2236	0.2243	0.2249	0.2256	0.2263
0.27	0.2270	0.2277	0.2284	0.2290	0.2297	0.2304	0.2311	0.2317	0.2324	0.2331
0.28	0.2337	0.2344	0.2351	0.2357	0.2364	0.2371	0.2377	0.2384	0.2391	0.2397
0.29	0.2404	0.2410	0.2417	0.2423	0.2430	0.2437	0.2443	0.2450	0.2456	0.2463
0.30	0.2469	0.2475	0.2482	0.2488	0.2495	0.2501	0.2508	0.2514	0.2520	0.2527
0.31	0.2533	0.2539	0.2546	0.2552	0.2558	0.2565	0.2571	0.2577	0.2583	0.2590
0.32	0.2596	0.2602	0.2608	0.2614	0.2621	0.2627	0.2633	0.2639	0.2645	0.2651
0.33	0.2657	0.2664	0.2670	0.2676	0.2682	0.2688	0.2694	0.2700	0.2706	0.2712
0.34	0.2718	0.2724	0.2730	0.2736	0.2742	0.2748	0.2754	0.2760	0.2766	0.2771
0.35	0.2777	0.2783	0.2789	0.2795	0.2801	0.2807	0.2812	0.2818	0.2824	0.2830
0.36	0.2835	0.2841	0.2847	0.2853	0.2858	0.2864	0.2870	0.2875	0.2881	0.2887
0.37	0.2892	0.2898	0.2904	0.2909	0.2915	0.2920	0.2926	0.2931	0.2937	0.2943
0.38	0.2948	0.2954	0.2959	0.2965	0.2970	0.2975	0.2981	0.2986	0.2992	0.2997
0.39	0.3003	0.3008	0.3013	0.3019	0.3024	0.3029	0.3035	0.3040	0.3045	0.3051

Notes: 1. Enter $\dfrac{M_u}{\phi f_c' b d_e^2}$ and get ω_e or vice versa; $\omega_e = \dfrac{A_{ps} f_{ps} + A_s f_y - A_s' \left| f_y' \right|}{b d_e f_c'}$

2. $\dfrac{M_u}{\phi f_c' b d_e^2} = \omega_e (1 - 0.59\omega_e)$ for rectangular section or rectangular section behavior

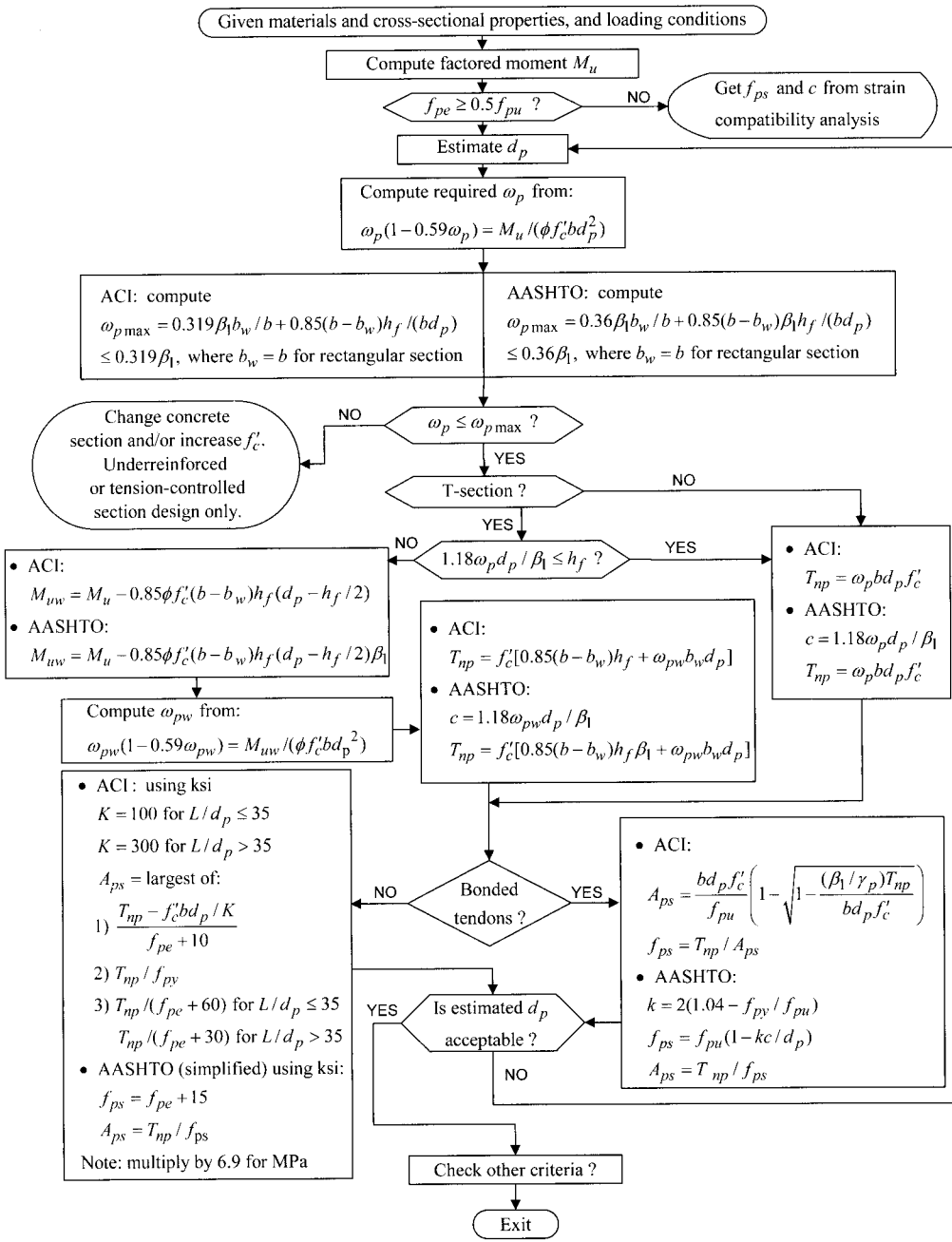

Figure 5.34 Flow chart to determine the reinforcement A_{ps} needed to develop a given nominal bending resistance.

Assume that the section will be tension-controlled according to ACI or under-reinforced according to AASHTO. Use $\phi = 0.9$. This value can be revised if needed after a first iteration.

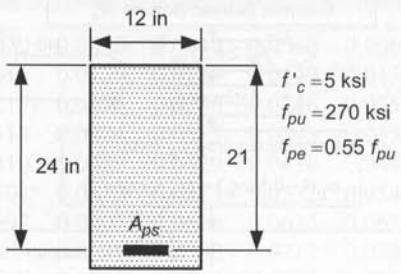

Figure 5.35

Referring to the flow chart Fig. 5.34 for the steps being followed, compute ω_p by solving the following quadratic equation:

$$\omega_p(1-0.59\omega_p) = \frac{M_u}{\phi f'_c b d_p^2} = \frac{300\times 12}{0.9\times 5\times 12\times 21^2} = 0.1512$$

for which $\omega_p = 0.168$ (also from Table 5.1). Note that ϕ was taken equal 0.9 per ACI and could be taken equal 1 per AASHTO. However, we will proceed with $\phi = 0.9$. From Eq. (5.65):

$$\frac{c}{d_e} = \frac{c}{d_p} = \frac{1.18\omega_e}{\beta_1} = \frac{1.18\times 0.168}{0.8} = 0.248 < 0.375 \rightarrow \text{Tension controlled section}$$

$$\frac{c}{d_e} = 0.248 < 0.42 \rightarrow \text{Under-reinforced section (AASHTO)}$$

ACI Equation for f_{ps}: Since we have a rectangular section, the total tensile force taken by the prestressing steel at nominal resistance is given by:

$$T_{np} = A_{ps} f_{ps} = \omega_p (b d_p f'_c) \qquad (5.103)$$

$$T_{np} = 0.168 \times 12 \times 5 \times 21 = 211.680 \text{ kips}$$

Solving for A_{ps} with f_{ps} from Eq. (5.32), assuming fully prestressed concrete only leads to:

$$A_{ps} = \frac{b d_p f'_c}{f_{pu}}\left(1-\sqrt{1-\frac{(\beta_1/\gamma_p)T_{np}}{b d_p f'_c}}\right) = \frac{12\times 21\times 5}{270}\left(1-\sqrt{1-\frac{2\times 211.68}{12\times 21\times 5}}\right) = 0.864 \text{ in}^2 \qquad (5.104)$$

and

$$f_{ps} = \frac{T_{np}}{A_{ps}} = 245 \text{ ksi}$$

AASHTO Equation for f_{ps}: If the AASHTO prediction equation for f_{ps} were used in the above problem, the solution would be:

$$c = \frac{1.18\omega_p d_p}{\beta_1} = \frac{1.18\times 0.168\times 21}{0.8} = 5.204 \text{ in}$$

$$k = 2\left(1.04 - \frac{f_{py}}{f_{pu}}\right) = 2(1.04 - 0.85) = 0.38$$

$$f_{ps} = f_{pu}\left(1 - k\frac{c}{d_p}\right) = 270\left(1 - 0.38\frac{5.204}{21}\right) = 244.57 \text{ ksi}$$

$$T_{np} = \omega_p\left(bd_p f_c'\right) = 0.168 \times 12 \times 21 \times 5 = 211.680 \text{ kips}$$

$$= A_{ps} f_{ps} = 244.57 \times A_{ps}$$

$$A_{ps} = 0.865 \text{ in}^2$$

which is almost the same answer as obtained above using the ACI code prediction equations for f_{ps}.

Unbonded Tendons Using ACI Equation for f_{ps}: If unbonded tendons were specified instead of bonded tendons, the computation steps up to T_{np} would be the same. Assuming a span L = 40 ft, leads to $L/d_p = 22.85 < 35$; thus: $K = 100$.

The solution for A_{ps} is:

$$A_{ps} = \frac{T_{np} - \dfrac{f_c' b d_p}{K}}{f_{pe} + 10} = \frac{211.68 - \dfrac{5 \times 12 \times 21}{100}}{148.5 + 10} = 1.256 \text{ in}^2 \qquad (5.105)$$

Equation 5.33 can be written as:

$$f_{ps} = f_{pe} + 10 + \frac{f_c' b d_p}{K A_{ps}} \qquad (5.106)$$

leading to:

$$f_{ps} = 148.5 + 10 + \frac{5 \times 12 \times 21}{100 \times 1.256} = 168.5 \text{ ksi}$$

$$\le f_{pe} + 60 = 208.5 \text{ ksi} \qquad \text{O.K.}$$

$$\le f_{py} = 229.5 \text{ ksi}$$

The conservative approach using AASHTO for unbonded tendons would have led to:

$$f_{ps} = 148.5 + 15 = 163.5 \text{ ksi}$$

$$A_{ps} = \frac{T_{np}}{f_{ps}} = \frac{211.68}{163.5} = 1.295 \text{ in}^2$$

It is clear that the use of unbonded tendons leads to a significantly smaller value of f_{ps} than for bonded tendons. As a result, the area of steel required is higher (here about 45% higher) for the same nominal moment resistance. This is a factor that should be considered in the total cost of the structure when specifying bonded or unbonded tendons. Note also that, unlike bonded tendons in which the stress at ultimate exceeds the yield stress, the stress in the unbonded tendons at ultimate will most likely remain in the elastic range of behavior.

Additional examples of design are given in Section 5.23.

5.19.2 Example: Reinforcement Design for Nominal Resistance – T Section

Determine the area of prestressed reinforcement required to develop a design moment resistance $\phi M_n = M_u = 450$ kips-ft in the T section shown in Fig. 5.36, assuming the same materials properties as for the preceding example and $d_p = 20$ in. Assume that the section will be tension-controlled according to ACI or under-reinforced according to AASHTO. Use $\phi = 0.9$. This value can be revised if needed after a first iteration.

Referring to the flow chart Fig. 5.34, the following steps are followed. Compute ω_p from Eq. (5.102):

$$\omega_p\left(1-0.59\omega_p\right) = \frac{M_u}{\phi f_c' b d_p^2} = \frac{450\times 12}{0.9\times 5\times 24\times 20^2} = 0.1250$$

which leads to a value of $\omega_p = 0.136$. Note that ϕ was taken equal 0.9 per ACI and could be taken equal 1 per AASHTO. However, we will proceed with $\phi = 0.9$.

To check if T-section behavior exists, compute c (Eq. 5.64):

$$c = \frac{1.18\omega_p d_p}{\beta_1} = \frac{1.18\times 0.136\times 20}{0.8} = 4.01 \text{ in} > h_f = 3 \text{ in} \rightarrow \text{T-section behavior}$$

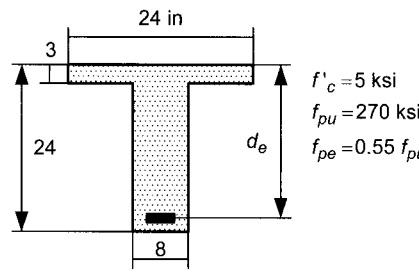

Figure 5.36

Thus, we have T-section behavior. The design strength required from the web is defined as M_{uw} and computed from (ACI approach is used):

$$M_{uw} = M_u - M_{uf} = M_u - 0.85\,\phi f_c'(b-b_w)\,h_f\left(d_p - \frac{h_f}{2}\right)$$

$$= 450 - \frac{3396600}{12000} = 450 - 283.05 = 166.95 \text{ kips-ft}$$

Compute ω_{pw} by solving the following equation:

$$\omega_{pw}(1-0.59\omega_{pw}) = \frac{M_{uw}}{\phi f_c' b_w d_p^2} = \frac{166.95\times 12}{0.9\times 5\times 8\times 20^2} = 0.139$$

for which ω_{pw} = 0.153 (also from Table 5.1). From Eq. (5.65):

$$\frac{c}{d_e} = \frac{c}{d_p} = \frac{1.18\omega_{pw}}{\beta_1} = \frac{1.18 \times 0.153}{0.8} = 0.226 < 0.375 \quad \rightarrow \text{Tension-controlled section (ACI)}$$

$$\frac{c}{d_e} = 0.226 < 0.42 \quad \rightarrow \text{Under-reinforced section (AASHTO)}$$

Compute the total tensile force taken by the prestressing steel at ultimate behavior and the required area of prestressing steel from:

$$T_{np} = f'_c[0.85(b - b_w)h_f + \omega_{pw}b_w d_p]$$

$$= 5[0.85 \times 16 \times 3 + 0.153 \times 8 \times 20] = 326.4 \text{ kips}$$

$$A_{ps} = \frac{bd_p f'_c}{f_{pu}}\left(1 - \sqrt{1 - \frac{(\beta_1/\gamma_p)T_{np}}{bd_p f'_c}}\right) = \frac{24 \times 20 \times 5}{270}\left(1 - \sqrt{1 - \frac{(0.8/0.4) \times 326.4}{24 \times 20 \times 5}}\right)$$

$$= 1.3046 \text{ in}^2$$

and

$$f_{ps} = \frac{T_{np}}{A_{ps}} = \frac{326.4}{1.3046} = 250.19 \text{ ksi}$$

The reader may want to: 1) go back to the analysis flow chart Fig. 5.24 and check backward if, indeed, for the reinforcement found here, the ultimate moment resistance designed for is achieved; 2) repeat this example assuming unbonded tendons; 3) repeat this example using the AASHTO code; and 4) using the same procedure and the ACI code, check the following results obtained for the example of Section 5.18: for $M_u = 842.55$ kips-ft, $\omega_p = 0.040$, $A_{ps} = 1.256$ in^2 and $f_{ps} = 264.5$ ksi. Note that the value of A_{ps} obtained from ultimate strength design is smaller than that using working stress design ($A_{ps} = 1.53$ in^2; see also Section 4.9). In most cases the value obtained from WSD is noticeably larger than that obtained from USD and that explains why the design of prestressed concrete beams generally starts by WSD.

5.20 COMPOSITE BEAMS

For a composite section made out of a cast-in-place concrete slab on top of a prestressed concrete girder or beam, the procedure leading to the ultimate or nominal moment resistance is similar to that of a T section, with one important modification. Because, in general, the cast-in-place slab has a compressive strength different from that of the prestressed girder, the effective width of the slab associated with the girder is to be multiplied by a factor equal to the ratio of their respective strengths, i.e., $(f'_c)_{\text{slab}}/(f'_c)_{\text{girder}}$. Then, the composite section is analyzed as a noncomposite T section assuming a uniform strength equal to that of the prestressed girder. Note that in Chapter 9 on composite beams, the transformed section was obtained by multiplying the effective width of the slab by the ratio of moduli of elasticity, i.e., $(E_c)_{\text{slab}}/(E_c)_{\text{girder}}$ instead of the ratio of strengths. As the moduli ratio is generally

higher than the strengths ratio, using the moduli ratio is optimistic. However, the difference between the two approaches is very small, since the resistance is primarily controlled by the reinforcement. In Chapter 9, Section 9.8, the author suggests the use of the transformed section (where the moduli ratio is used) throughout the analysis, including ultimate, because it is the speediest approach for all cases, and the error generated, if any, is minute. Note that the above remark on composite beams applies mostly if T-section behavior is observed. If a rectangular section behavior exists, the ultimate strength can be directly computed (similarly to a noncomposite section) using the effective width of the slab and $(f'_c)_{slab}$ since, below the neutral axis, the section is assumed cracked and the concrete part of the section does not contribute to the resistance (Fig. 5.19).

5.21 CONTINUOUS BEAMS AND MOMENT REDISTRIBUTION

The above computations have addressed specifically the ultimate strength of a prestressed or partially prestressed concrete section. If the section considered is the critical section, or section of maximum moment in a simply supported beam, then its ultimate bending resistance (nominal resistance) is also the ultimate bending resistance of that beam. The computation of the nominal bending moment at a given section of a continuous beam is similar to that of a simply supported beam. However, the value obtained at one critical section generally does not correspond to the failure moment of the beam itself, since many critical sections exist and plastic hinges may form at these sections. In such a case, the plastic hinge analysis approach may be applied to determine the maximum load at which collapse will occur (see Sec. 10.14).

Underreinforced and tension-controlled prestressed concrete sections generally undergo significant inelastic deformation (curvature or rotation) prior to failure. Such a property is qualified as ductility. In continuous beams and frames, ductility allows the formation of quasi plastic hinges at the sections of maximum moments. This permits redistribution of moments from the highly solicited sections to the less solicited ones. The ACI and AASHTO codes limit the percentage of moment that can be redistributed from one section to another. Details are given in Sec. 10.14.3.

5.22 CONCLUDING REMARKS

The problems and procedures addressed in this chapter cover the majority of design situations where flexure of prestressed and partially prestressed concrete beams at ultimate behavior are involved. Although an attempt was made to follow closely the recommendations and equations given by the ACI and AASHTO codes, diverging approaches and the author's opinion on some issues were pointed out where

necessary. The reader may want to supplement the present chapter by referring to Ref. [1.48], where design at ultimate is systematically explored for prestressed and partially prestressed concrete through nonlinear analysis and strain compatibility analysis.

5.23 ADDITIONAL DESIGN EXAMPLES BASED ON USD

The analysis and design examples described next are meant to illustrate the use of prediction equations of f_{ps} that depend on the depth of neutral axis c.

5.23.1 Example 1: Analysis with Unbonded Tendons Illustrating Eq. (5.41)

Consider the simply supported beam with the cross-sectional dimensions and material properties shown in Fig. 5.37. The section is reinforced with two No. 9 reinforcing bars and prestressed with four ½ in-diameter unbonded prestressing strands. The span length L is 40 ft.

Compute the stress in the unbonded tendons at nominal bending resistance using: 1) the 1999 ACI code Eq. (5.33), and 2) Eq. (5.41) recommended by the author.

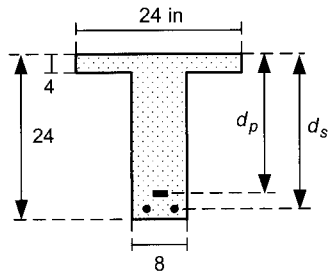

$f'_c = 7$ ksi
$\beta_1 = 0.70$
$\varepsilon_{cu} = 0.003$
$f_{pe} = 150$ ksi
$f_{pu} = 270$ ksi
$f_{py} = 229.5$ ksi
$f_y = 60$ ksi

$A_{ps} = 0.612$ in^2
$d_p = 18$ in
$E_p = 27000$ ksi
$A_s = 2$ in^2
$d_s = 21.5$ in
$E_s = 29000$ ksi

Figure 5.37 Beam section and properties considered.

Steel tendons: 2002 ACI code (Eq. 5.33)

Following the flow chart in Fig. 5.24:

$$\rho_p = \frac{A_{ps}}{bd_p} = \frac{0.612}{24 \times 18} = 0.001417$$

$$\frac{L}{d_p} = \frac{40 \times 12}{18} = 26.7 \le 35$$

$$f_{ps} = f_{pe} + 10 + \frac{f'_c}{100 \times \rho_p}$$

$$= 150 + 10 + \frac{7}{100 \times 0.00142} = 209.4 \text{ ksi}$$

$$f_{ps} = 209.4 \text{ ksi} \le f_{pe} + 60 = 210 \text{ ksi} \quad \text{O.K.}$$

$$\le f_{py} = 229.5 \text{ ksi} \quad \text{O.K.}$$

It should be noted that the ACI code Eq. (5.33) is not sensitive to the presence of A_s, be it zero or double the value given in the example.

Steel tendons: recommended Eq. (5.41)

The equation for force equilibrium of the section at nominal bending resistance assuming rectangular section behavior is written as

$$A_{ps}f_{ps} + A_s f_y = 0.85 f'_c b \beta_1 c \tag{5.14}$$

from which

$$c = \frac{A_{ps}f_{ps} + A_s f_y}{0.85 f'_c b \beta_1} = \frac{0.612 f_{ps} + 2\times 60}{0.85\times 7\times 24\times \beta_1} = \frac{0.612 f_{ps} + 120}{99.96} \tag{5.15}$$

$$c = 1.2005 + 0.00612 f_{ps} \tag{5.103}$$

For simply supported beams with uniform loading Eq. (5.41) leads to:

$$L_1 = L_2 \text{ and } \Omega_u = \frac{3}{L/d_p} = \frac{3}{40\times 12/18} = 0.1125$$

$$f_{ps} = f_{pe} + \Omega_u E_p \varepsilon_{cu}\left(\frac{d_p}{c} - 1\right)\frac{L_1}{L_2} = 150 + 0.1125\times 27{,}000\times 0.003\left(\frac{18}{c} - 1\right) \tag{5.41}$$

$$f_{ps} = 150 + 9.1125\left(\frac{18}{c} - 1\right) \tag{5.104}$$

Simultaneously solving Eqs. (5.103) and (5.104) leads to a quadratic equation in c:

$$c^2 - 2.0627c - 1.0038 = 0$$

Its solution leads to:

$c = 2.47$ in. and $f_{ps} = 207.3$ ksi $\le 0.8 f_{pu} = 216$ ksi O.K.

The solution of Eq. (5.103) and (5.104) could have also been obtained by iteration such as that in the following steps:

1. Starting with $f_{ps} = 0.80 f_{pu} = 216$ ksi, plug in Eq. (5.103) and compute $c = 2.52$ in;
2. Plug $c = 2.52$ in into Eq. (5.104) and compute $f_{ps} = 206$ ksi;
3. Plug $f_{ps} = 206$ ksi into Eq. (5.103) and compute $c = 2.46$ in;
4. Plug $c = 2.46$ in into Eq. (5.104) and compute $f_{ps} = 207.5$ ksi;
5. Plug $f_{ps} = 207.5$ ksi into Eq. (5.103) and compute c =2.47; and
6. Plug $c = 2.47$ into Eq. (5.104) and compute $f_{ps} = 207.3$ ksi.

For the iteration, the starting value of f_{ps} could also be that recommended in Eq. (5.37); that is, $f_{ps} = 150 + 15 = 165$ ksi. The iterations lead to the following successive results:

$c = 2.21$ in $\rightarrow f_{ps} = 215.1$ ksi $\rightarrow c = 2.517$ in $\rightarrow f_{ps} = 206.05$ ksi $\rightarrow c = 2.461$ in $\rightarrow$ $f_{ps} = 207.54$ ksi $\rightarrow c = 2.47$ in $\rightarrow f_{ps} = 207.3$ ksi; that is, same answer given in the previous steps.

It should be noted that, if the value of A_s is doubled, the recommended approach using Eq. (5.41) would lead to c = 3.5463 in and f_{ps} =187.14 ksi. This shows that when the section tends toward over-reinforcement, the stress in the prestressing tendons at ultimate decreases.

Glass FRP tendons

Assuming that instead of having steel tendons, glass FRP (Fiber Reinforced Polymer) tendons of same cross-sectional area $A_{ps} = 0.612$ in^2 are used. Their strength and elastic modulus are $f_{pu} = 300$ ksi and $E_p = 8000$ ksi, respectively.

The same equation of equilibrium (Eq. 5.14) as for steel tendons is obtained. Moreover, the 1999 ACI code Eq. (5.33) does not apply to FRP tendons. If used, it would lead to the same results as those for steel tendons.

However, using Eq. (5.41) leads to:

$$f_{ps} = f_{pe} + \Omega_u E_p \varepsilon_{cu} \left(\frac{d_p}{c} - 1 \right) \frac{L_1}{L_2}$$

$$= 150 + 0.1125 \times 8000 \times 0.003 \left(\frac{18}{c} - 1 \right)$$

$$f_{ps} = 150 + 2.7 \left(\frac{18}{c} - 1 \right) \tag{5.105}$$

The solution of Eq. (5.103) and (5.105) leads to: $c = 2.235$ in. and $f_{ps} = 169.04$ ksi.

Carbon FRP tendons

Assume that instead of having steel tendons, carbon FRP tendons of same cross-sectional area $A_{ps} = 0.612$ in^2 are used. Their strength and elastic modulus are, respectively, $f_{pu} = 315$ ksi and $E_p = 21{,}000$ ksi.

$$f_{ps} = f_{pe} + \Omega_u E_p \varepsilon_{cu} \left(\frac{d_p}{c} - 1 \right) \frac{L_1}{L_2}$$

$$= 150 + 0.1125 \times 21{,}000 \times 0.003 \left(\frac{18}{c} - 1 \right)$$

$$f_{ps} = 150 + 7.0875 \left(\frac{18}{c} - 1 \right) \tag{5.106}$$

The solution of Eqs. (5.103) and (5.106) leads to: $c = 2.40$ in and $f_{ps} = 196.07$ ksi.

5.23.2 Example 2: Given A_{ps}, Design for A_s Based on USD – Unbonded Tendons

In the previous example, the emphasis was on analysis or investigation where the areas of reinforcement were given. This and the following two examples illustrate design of the reinforcement.

This example simulates the case of slabs where the prestressing steel is determined from service analysis assuming a fictitious tensile stress larger than the modulus of rupture of concrete, and the amount of non-prestressed steel is determined from ultimate. Consider the section of Fig. 5.38 where the prestressing steel area is given, A_{ps} = 0.306 in^2, and corresponds to two 0.5-inch diameter prestressing strands. The area of reinforcing steel is to be determined based on USD. Assume that the factored design moment M_u = 340 k-ft.

The unknowns in this problem are: A_s, f_{ps} and c. They can be obtained from solving Eqs. (5.4), (5.14), (5.16), and (5.41) simultaneously, or with some excellent approximation as follows.

Equation (5.14): $0.306 f_{ps} + 60 A_s = 33.32c$

Equations (5.4) and (5.16): $\dfrac{M_u}{\phi} = \dfrac{340}{0.9} = M_n = 0.306 f_{ps}(20 - 0.35c) + 60 A_s (21 - 0.35c)$

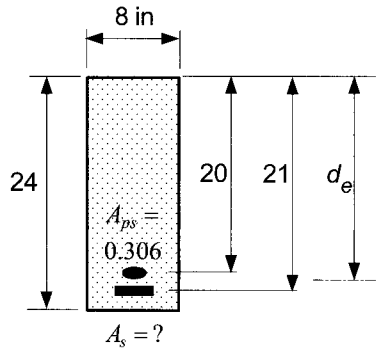

$f'_c = 7$ ksi $\quad f_{pu} = 270$ ksi
$\beta_1 = 0.70$ $\quad f_{pe} = 160$ ksi
$f_y = 60$ ksi $\quad L = 40$ ft
$M_u = 340$ k-ft
$d_p = 20$ in
$d_s = 21$ in

Figure 5.38 Section with area of reinforcing steel unknown.

Equation (5.41): $f_{ps} = 160 + \dfrac{3}{40\times 12/20} 27000\times 0.003\left(\dfrac{20}{c} - 1\right) = 160 + 10.125\left(\dfrac{20}{c} - 1\right)$

The combination of the two equations of equilibrium at nominal resistance of a rectangular section can be put in the following from (Eq. 5.102):

$$\frac{M_u}{\phi f'_c b d_e^2} = \omega_e(1 - 0.59\omega_e)$$

where d_e is to the centroid of the tensile force in the reinforcement and ω_e is the effective reinforcing index.

Estimate $d_e = 20.5$ that is somewhere between d_p and d_s.

Then Eq. (5.102) leads to:

$$\frac{340\times 12}{0.9\times 7\times 8\times 20.5^2} = 0.1926 = \omega_e(1 - 0.59\omega_e)$$

From Table 5.1 or from solving the above quadratic equation we get: $\omega_e = 0.2215$

Thus (Eq. 5.64):

$$c = \frac{1.18\omega_e d_e}{\beta_1} = \frac{1.18\times 0.2215\times 20.5}{0.7} = 7.65 \text{ in}$$

From Eq. (5.41):

$$f_{ps} = 160 + 10.125\left(\frac{20}{7.65} - 1\right) = 176.35 \text{ ksi}$$

From Eq. 5.14:

$$0.306\times 176.35 + 60A_s = 33.32\times 7.65$$

from which we get $A_s = 3.35$ in^2. O.K.

We could have also obtained A_s from the definition of the effective reinforcing index as follows:

$$\frac{0.306\times 176.35 + 60A_s}{7\times 8\times 20.5} = 0.2215 \rightarrow A_s = 3.34 \text{ in}^2 \quad \text{same as above. O.K.}$$

Clearly in the final design we will use integer number of bars and the real d_p and d_s, as is the case for all designs.

5.23.3 Example 3: Given A_s, Design for A_{ps} Based on USD – Unbonded Tendons

This example is typical for reinforced concrete beams needing to be strengthened such as by external prestressing. We will use the same beam as in Example 2 above and assume that the reinforcing steel area is given, that is (Fig. 5.39): $A_s = 3.35$ in^2. Also assume the factored moment: $M_u = 340$ k-ft.

For the same d_e, we get the same value of the effective reinforcing index, ω_e, the same value of c, and the same value of f_{ps} as in Example 2. Then from the first equation of equilibrium (Eq. 5.14) we get:

$$176.35A_{ps} + 3.35 \times 60 = 0.85 \times 7 \times 8 \times 0.7 \times 7.65 \rightarrow A_{ps} = 0.306 \text{ in}^2$$

which is about what we expected.

Note that if the ACI code Eq. (5.33) is used for the above two examples

$$f_{ps} = f_{pe} + 10 + \frac{f'_c}{300\rho_p} = 160 + 10 + \frac{7}{100 \times 0.001913} = 206.6 \text{ ksi}$$

the increment of stress would be: $\Delta f_{ps} = f_{ps} - f_{pe} = 206.6 - 160 = 46.6$ ksi, which is about 2.85 times the value of 16.35 obtained using Eq. (5.41). Because the beam is close to being compression-controlled ($c/d_e = 0.37$), it is likely that the ACI predicted value is too optimistic.

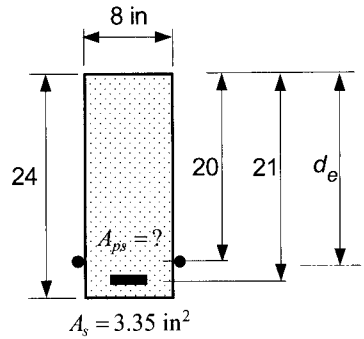

$f'_c = 7$ ksi $\quad f_{pu} = 270$ ksi
$\beta_1 = 0.70 \quad f_{pe} = 160$ ksi
$f_y = 60$ ksi $\quad L = 40$ ft
$M_u = 340$ k-ft
$d_p = 20$ in
$d_s = 21$ in

Figure 5.39 Section with area of prestressing steel unknown.

5.23.4 Example 4: Given A_s, Design for A_{ps} Based on USD – Bonded Tendons

Repeat the above Example 3 assuming bonded tendons. For the same d_e, we get the same value of the effective reinforcing index, ω_e, and the same value of c, as in Examples 2 and 3. Assuming low relaxation steel, the value of f_{ps} for bonded tendons is then given by Eqs. (5.35) and (5.36):

$$k = 2\left(1.04 - \frac{f_{py}}{f_{pu}}\right) = 2(1.04 - 0.9) = 0.28$$

$$f_{ps} = f_{pu}\left(1 - k\frac{c}{d_p}\right) = 270\left(1 - 0.28\frac{7.65}{20.5}\right) = 241.8 \text{ ksi}$$

From the first equation of equilibrium (Eq. 5.14) we get:

$$241.8A_{ps} + 3.35 \times 60 = 0.85 \times 7 \times 8 \times 0.7 \times 7.65 \rightarrow A_{ps} = 0.23 \text{ in}^2$$

REFERENCES

5.1 AASHTO, "*LRFD Bridge Design Specifications*," 2nd ed., American Association of State Highway and Transportation Officials, Washington, DC, 1998 and 2003.

5.2 ACI Committee 318, "*Building Code Requirements for Structural Concrete and Commentary (ACI) 318-1999*," American Concrete Institute, Farmington Hills, Michigan, 1999.

5.3 ACI Committee 318, "*Building Code Requirements for Structural Concrete (ACI 318-02) and Commentary (ACI 318R-02),*" American Concrete Institute, Farmington Hills, Michigan, 2002.

5.4 Alkhairi, F. M., and A. E. Naaman, "Analysis of Beams Prestressed with Internal or External Unbonded Tendons," *Journal of Structural Engineering*, ASCE, 119(9): 2680-2700, 1993.

5.5 British Standard Code of Practice for the Use of Structural Concrete, CP-110, British Standards Institution, London, 1972.

5.6 Burns, N. H., "Post-Tension Force Changes in Continuous Beams," ASCE Structures Congress Abstracts, 1990, ASCE New York, pp. 455-456.

5.7 Gurfinkel, G., and N. Khachaturian, "Ultimate Design of Prestressed Concrete Beams," University of Illinois, Urbana, Engineering Experiment Station, Bulletin 478, April 1965.

5.8 Harajli, M., and A. E. Naaman, "An Evaluation of the Ultimate Steel Stress in Partially Prestressed Flexural Members," *Journal of the Prestressed Concrete Institute*, 30(5): 54-81, 1985. See also closure to discussion in Vol. 31(4): 128-29, 1986.

5.9 Hognestad, E., N. W. Hanson, and D. McHenry, "Concrete Stress Distribution in Ultimate Strength Design," *ACI Journal*, Proceedings, 52(44): 455-79, 1955.

5.10 Janney, J. R., E. Hognestad, and D. McHenry, "Ultimate Flexural Strength of Prestressed and Conventionally Reinforced Concrete Beams," *ACI Journal,* Proceedings, 52(February): 601-17, 1956.

5.11 Loov, R. E., "General Equation for the Steel Stress for Bonded Prestressed Tendons," *PCI Journal,* 33(6): 108-37, 1988.

5.12 Mast, R. F., "Unified Design Provisions for Reinforced and Prestressed Concrete Flexural and Compression Members," *ACI Structural Journal*, 89(2): 185-99, 1992.

5.13 Mattock, H., L. B. Kriz, and E. Hognestad, "Rectangular Concrete Stress Distribution in Ultimate Strength Design," *ACI Journal*, Proceedings, 57(February): 877-928, 1961.

5.14 Mojtahedi, S., and W. L. Gamble, "Ultimate Steel Stresses in Unbonded Prestressed Concrete," *ASCE Structural Journal*, July: 1159-165, 1978.

5.15 Naaman, A. E., "Ultimate Analysis of Prestressed and Partially Prestressed Sections by Strain Compatibility," *PCI Journal*, 22(1): 32-51, 1977.

5.16 Naaman, A. E., "A Proposal to Extend Some Code Provisions on Reinforcement to Partial Prestressing," *PCI Journal*, 26(2): 74-91, 1981.

5.17 Naaman, A. E., "*Prestressed Concrete Analysis and Design-Fundamentals*," New York: McGraw-Hill Book Co., 1982, 670 pp.

5.18 Naaman, A. E., "An Approximate Nonlinear Design Procedure for Partially Prestressed Concrete Beams," *Computers and Structures*, 17(2): 287-93, 1983.

5.19 Naaman, A. E., "Partially Prestressed Concrete: Review and Recommendations," *Journal of the Prestressed Concrete Institute,* 30(6): 30-71, 1985.

5.20 Naaman, A. E., "A New Methodology for the Analysis of Beams Prestressed with Unbonded or External Tendons." In *External Prestressing in Bridges,* ACI SP-120, A. E. Naaman and J. Breen, eds., American Concrete Institute, Detroit, 1990, pp. 339-354.

5.21 Naaman, A. E., and F. M. Alkhairi, "Stress at Ultimate in Unbonded Prestressing Tendons – Part I: Evaluation of the State-of-the-Art," *ACI Structural Journal*, 89(5): 641-51, 1991.

5.22 Naaman, A. E., and F. M. Alkhairi, "Stress at Ultimate in Unbonded Prestressing Tendons – Part II: Proposed Methodology," *ACI Structural Journal*, American Concrete Institute, 89(6): 683-92, 1991.

5.23 Naaman, A. E., "Stress at Ultimate in Unbonded Tendons by Strain Compatibility." In *Progress in Structural Engineering*, D. E. Grierson, A. Franchi and P. Riva, eds., Amsterdam: Kluwer Academic Publishers, 1991, pp. 217-227.

5.24 Naaman, A. E., "Unified Design Recommendations for Reinforced, Prestressed, and Partially Prestressed Concrete Bending and Compression Members," *ACI Structural Journal,* 89(2): 200-10, 1992.

5.25 Naaman, A. E., "Unified Bending Strength Design of Concrete Members: AASHTO LRFD Code," *Journal of Structural Engineering,* ASCE, 121(6): 964-70, 1995.

5.26 Naaman, A. E., "Rectangular Stress Block and T-Section Behavior." In Open Forum, *PCI Journal*, 47(5): 106-12, 2002. Also, discussion and closure in *PCI Journal*, March-April 2003, pp. 117-119.

5.27 Naaman, A. E., N. Burns, K. French, W. Gamble, and A. Mattock, "Stresses in Unbonded Tendons at Ultimate: Recommendation," *ACI Structural Journal*, 99(2): 518-29, 2002. See also discussion and closure, *ACI Structural Journal*, 100(3): 394-99, 2003.

5.28 Naaman, A. E., "Limits of Reinforcement in the 2002 ACI Code: Transition, Flaws, Solution," *ACI Structural Journal,* 101(2), 2004.

5.29 Pannell, F. N., "The Ultimate Moment Resistance of Unbonded Prestressed Concrete Beams," *Magazine of Concrete Research*, 21(66): 43-54, 1969.

5.30 *PCI Design Handbook-Precast, Prestressed Concrete*, 5th ed., Precast/Prestressed Concrete Institute, Chicago, Illinois, 1999.

5.31 Tam A. and F. N. Pannell, "The Ultimate Moment of Resistance of Unbonded Partially Prestressed Reinforced Concrete Beams," *Magazine of Concrete Research*, 28(97): 203-08, 1976.

5.32 Warwaruk, J., M. Sozen, and C. P. Seiss, "Investigation of Prestressed Reinforced Concrete for Highway Bridges, Part 3: Strength and Behavior in Flexure of Prestressed Concrete Beams," University of Illinois, Urbana, Engineering Experiment Station, Bulletin 464, 1962, 105 pp.

5.33 Whitney, S., "Plastic Theory in Reinforced Concrete Design," *Transactions, ASCE*, 107: 251-326, 1942.

5.34 Whitney, S., and E. Cohen, "Guide for Ultimate Strength Design of Reinforced Concrete," *ACI Journal*, Proceedings, 53: 455-75, 1956.

PROBLEMS

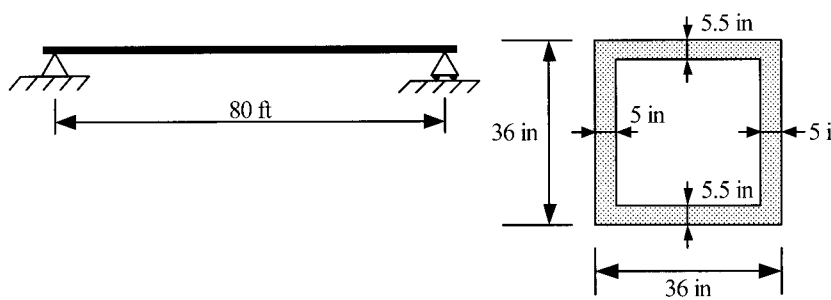

Figure P5.1

5.1 Investigate the prestressed concrete simply supported box beam (Fig. P5.1) according to the ACI and/or AASHTO codes given the following information: span 80 ft, $f'_c = 5000$ psi, $f'_{ci} = 4000$ psi,

live load = 100 psf, $A_{ps} = 2.45\ \text{in}^2$, $f_{pe} = 151$ ksi, F = 370 kips, $e_o = 15$ in at midspan, $\gamma_c = 150$ pcf, $\eta = 0.80$, $f_{pu} = 270$ ksi. Assume stress relieved strands and bonded tendons. Check stresses at initial and service loads, then check ultimate strength design criteria at midspan.

5.2 Consider the same cross section of the beam given in Prob. 5.1 (Fig. P5.1) and the same corresponding materials properties and e_o at midspan. Determine using the ACI and/or AASHTO codes: (a) the minimum area of prestressed reinforcement and corresponding value of the prestressing index that can be used without violating the code; (b) the maximum value of the prestressing index if an underreinforced section is desired, as per AASHTO; (c) the maximum value of the prestressing index if the tensile strain in the concrete at the level of the prestressed reinforcement $\varepsilon_{te} = 0.004$, as per ACI; and (d) in each of the above cases, the corresponding values of M_n and ϕM_n. Compare the results using the two codes. Note that the load and resistance factors for the AASHTO LRFD specifications are given in Chapter 14.

5.3 Determine the nominal moment resistance (M_n and ϕM_n) of the prestressed concrete beam section shown in Fig. P5.3 given the following information:

- bonded tendons, low relaxation strands
- $A_{ps} = 1.53\ \text{in}^2$, $f'_c = 7000$ psi, $e_o = 8.15$ in, $f_{pu} = 270$ ksi, $f_{pe} = 0.567 f_{pu}$, $A_c = 309\ \text{in}^2$
- $I = 25{,}500\ \text{in}^4$, $Z_b = 2170\ \text{in}^3$, $Z_t = 2080\ \text{in}^3$, $y_t = 12.25$ in, $y_b = 11.75$ in, $d_p = 20.4$ in

Check ultimate to cracking moment ratio. Repeat assuming nonprestressed reinforcement is added in the lower flange having: $A_s = 1.24\ \text{in}^2$, $f_y = 60$ ksi, $d_s = 22$ in. Use both the ACI and AASHTO codes and compare the results.

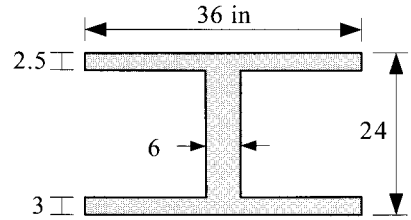

Fig. P5.3

5.4 Refer back to Prob. 4.7 after question (a) where it is assumed that the final prestressing force is achieved using three (stress relieved) strands at $d_c = 3$ in from bottom fiber. (a) Check ultimate moment requirements at midspan according to the ACI Code. Check also nominal to cracking moment requirements assuming a modulus of rupture $f_r = -7.5\sqrt{f'_c}$. (b) Repeat, assuming unbonded strands are used. If some requirements are then not satisfied, propose a solution to overcome them. (c) Repeat the problem using the AASHTO code.

5.5 Referring back to Prob. 4.8, check ultimate moment requirements and ratio of nominal to cracking moments at support and at midspan. Discuss the results observed at the support and provide a possible solution if a criterion is not satisfied.

5.6 The beam shown in Fig. P5.6 is to be used for an elevated structure designed for a transit system. The following information is given:

- $f'_c = 5000$ psi; $f'_{ci} = 4000$ psi
- $\bar{\sigma}_{ti} = -189$ psi; $\bar{\sigma}_{ci} = 2400$ psi; $\bar{\sigma}_{ts} = -213$ psi; $\bar{\sigma}_{csus} = 2250$ psi; $\bar{\sigma}_{cs} = 3000$ psi
- $f_{pu} = 270$ ksi; $f_{pe} = 150$ ksi; $\eta = f_{pe} / f_{pi} = 0.80$; stress relieved strands; bonded tendons

- $A_c = 576$ in^2; $I = 41{,}300$ in^4; $y_t = 10.33$ in; $y_b = 13.67$ in;
- $Z_t = 3990$ in^3; $Z_b = 3020$ in^3; $k_t = -5.24$ in; $k_b = 6.94$ in
- Live load = 1 klf; $w_G = 0.60$ klf
- $(e_o)_{mp} = 10.67$ in; $(d_c)_{\min} = 3$ in

This problem can be solved using either the ACI or the AASHTO code or both for comparison.

(a) Find the minimum value of F which satisfies all allowable stresses at midspan given the maximum and minimum moments: $M_{\max} = 8640$ kips-in; $M_{\min} = 3240$ kips-in. Round off the value of F to correspond to the nearest integer number of strands, assuming the final force per strand is 22.95 kips. Also, determine the eccentricity e_o at midspan.

(b) Check ultimate moment requirements and other criteria at midspan.

(c) Assume that the prestressing reinforcement is reduced to 16 strands, keeping the tendon profile unchanged. Determine the area of non-prestressed reinforcing bars, A_s, needed at midspan in addition to A_{ps}, to satisfy ultimate strength requirements according to the code. Assume $f_y = 60$ ksi and $d_s = 22.5$ in. Round off the values obtained to an integer number of #9 bars.

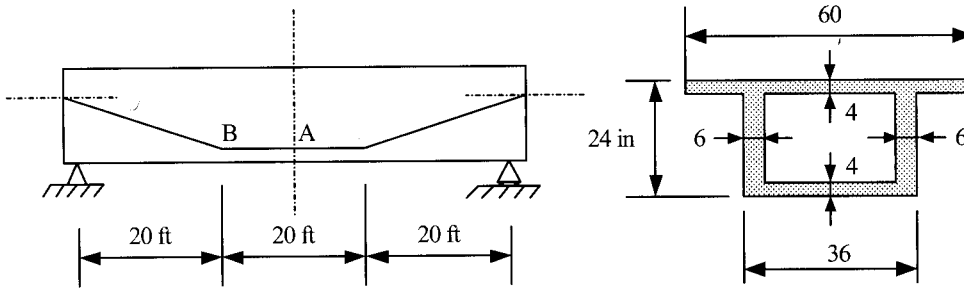

Figure P5.6

5.7 Determine the nominal moment resistance of a rectangular section given the following information: $b = 12$ in, $h = 24$ in, $f'_c = 8000$ psi, $f_{pu} = 270$ ksi, $f_{pe} = 148.5$ ksi, $f_y = f'_y = 60$ ksi, $A_{ps} = 1.07$ in^2, $A_s = 2$ in^2, $A'_s = 0.62$ in^2, $d_p = d_s = 21$ in, $d'_s = 2$ in. Check if, according to the assumptions used by the ACI code, the compression steel yields at ultimate.

5.8 Determine (strictly based on ultimate strength requirements) the area of prestressed reinforcement and its eccentricity needed to provide an ultimate moment resistance of 4000 kips-in to a rectangular section with the following properties: $b = 12$ in, $h = 24$ in, $f'_c = 6000$ psi, $f_{pu} = 270$ ksi. Make any assumption you deem reasonable. Select either the ACI or the AASHTO code or both for comparison.

5.9 Consider the simply supported T beam shown in Fig. P5.9. The beam is part of a slab spanning 70 ft. Normal weight concrete with a unit weight of 150 pcf is used. The live load is assumed to be 100 psf. The superimposed dead load is 10 psf. The following design information is given:

- $f'_c = 6000$ psi; $f'_c = 4500$ psi
- Allowable stresses: $\begin{cases} \bar{\sigma}_{ti} = -201 \text{ psi}; \ \bar{\sigma}_{ci} = 2700 \text{ psi}; \ \bar{\sigma}_{ts} = -465 \text{ psi}; \ \bar{\sigma}_{csus} = 2700 \text{ psi} \\ \bar{\sigma}_{cs} = 3600 \text{ psi} \end{cases}$
- $f_{pu} = 270$ ksi; $f_{pe} = 150$ ksi; $\eta = f_{pe} / f_{pi} = 0.80$; ½ in diameter stress relieved strands
- $(e_o)_{mp} = y_b - 4$ in, in all cases.

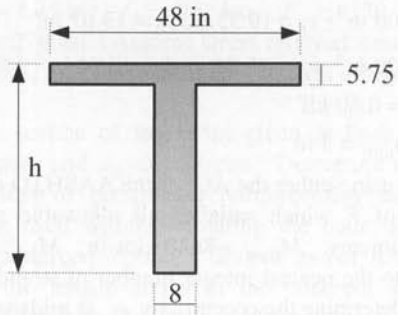

Figure P5.9

Use available computer programs, such as WSAD and USD, to undertake the basic computations. Round-off the number of strands to an integer number, N. The beam has a depth h, varying from 40 inches to the lowest value possible by design. Everything else being kept constant, design the beam for $h = 40 - 2n$, where $n = 1, 2, 3$, etc. until the problem has no feasible solution. Design implies here that both WSD and USD are satisfactory. The lowest value of h, should correspond to the minimum weight design for this problem. Prepare a table showing the following information: h, F, e_o, N, A_{ps}, A_c, controlling stress in WSD, M_u, M_n, ϕM_n.

5.10 The purpose of this problem is to evaluate and compare the nominal bending resistance, M_n, and other properties at ultimate of a prestressed concrete box section, using the ACI and AASHTO codes, for different amounts of reinforcement and different compressive strengths of concrete. Assume the strands properties are as follows: $A_{ps} = 0.153$ in^2 per strand; $f_{pe} = 150$ ksi; $f_{pu} = 270$ ksi; and $f_{py} = 0.85 f_{pu}$ for stress relieved strands, and $0.90 f_{pu}$ for low relaxation strands. A maximum of 46 strands is used. The first layer of 23 strands is at 2 in from the bottom. The next layer of up to 23 strands is at 3.75 in from the bottom. The corresponding d_p must be calculated for each number of strands used. The section is made from normal weight concrete with unit weight = 150 pcf.

The problem can be divided between a number of students with different parameters for each, as shown in Table P5.10. One additional parameter could be lightweight concrete versus normal weight concrete.

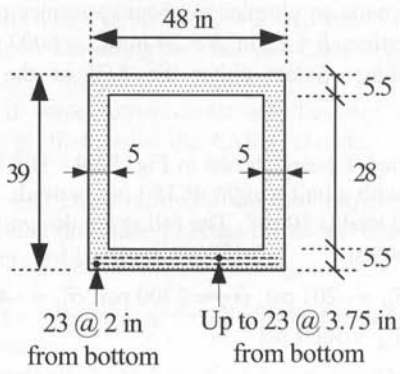

Figure P5.10

Table P5.10

Number of Strands	$f'_c = 5.8$ ksi	$f'_c = 8.5$ ksi	Stress-relieved Strand	Low Relaxation Strand	d_p, in
23					
35					
46					

For each of the cases assigned, prepare a table of results with the following information: N, A_{ps}, d_p, f_{ps}, c, M_n, ϕM_n, $1.2M_{cr}$, curvature at ultimate, rectangular or T-section behavior, tension-controlled or compression-controlled or transition by ACI (underreinforced or overreinforced by AASHTO). Discuss any difference you see between the ACI and AASHTO code results, and any other pertinent result.

Bridge over Happy Hollow Creek, Tennessee, USA. Nine spans precast prestressed concrete AASHTO bulb-tee girder made continuous for live load by a composite reinforced concrete deck. *(Courtesy Precast/Prestressed Concrete Institute.)*

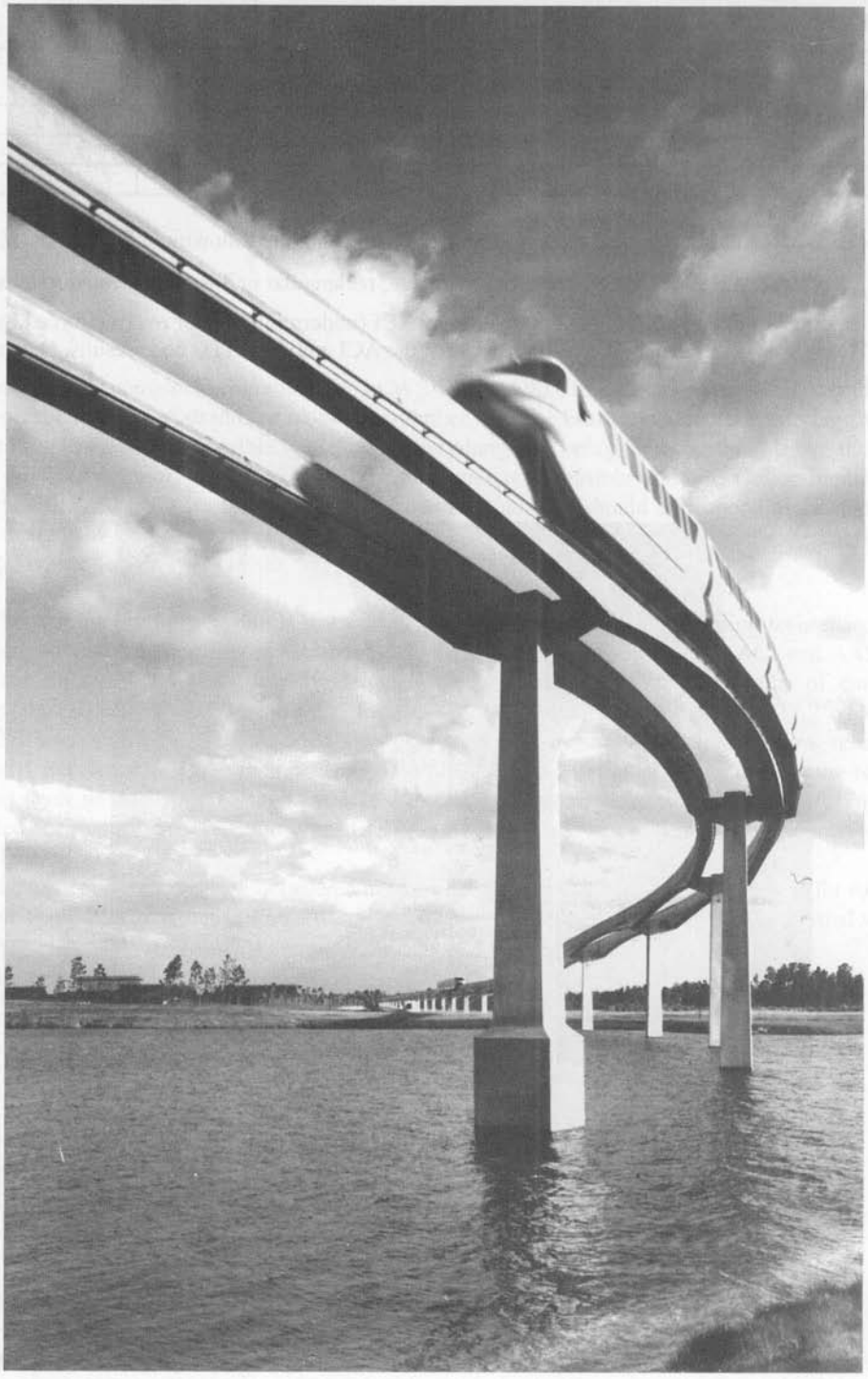

Prestressed concrete monorail structure at Disney World, Florida. *(Courtesy Precast/Prestressed Concrete Institute.)*

DESIGN FOR SHEAR AND TORSION

6.1 INTRODUCTION

The effects of external loadings on structures seldom lead to pure flexure alone. Other actions are simultaneously induced and include shear, torsion, and axial forces. Shear is most commonly encountered in combination with flexure. Its consideration in design logically follows that of flexure and represents a major step, as shown in Figs. 4.1 to 4.3. Torsion is dealt with only occasionally in everyday design.

Basically, shear and torsion are different in nature: shear is a force and torsion is a twisting moment. However, they both lead to similar shearing stresses in the structure. Such stresses can be resolved into a principal tensile stress, also called diagonal tension, and a principal compressive stress. The diagonal tension is of the greatest concern, because it induces cracking in the concrete. To ensure that such cracking does not lead to failure, transverse reinforcement resisting shear and/or torsion is generally provided in the form of stirrups or ties. Additional longitudinal reinforcement is also needed since both shear and torsion influence the demand on longitudinal reinforcement. However, the ACI code requires additional longitudinal reinforcement only in the design for torsion. Failure due to shear and/or torsion is brittle in nature and occurs with little warning; thus appropriate measures have to be taken to design for sufficient shear and torsion resistance.

There is considerable body of research and analysis of the behavior of reinforced concrete in shear has taken place [Refs. 6.5 to 6.10, 6.20, 6.21, 6.27 to 6.30, 6.44, 6.45], and general theories have been established to cover the whole range of

reinforcement, prestressed and non-prestressed. Examples include the truss model [Refs. 6.22 to 6.26, 6.33], the softened truss model developed by Hsu [Refs. 6.15 to 6.19], the compression field theory developed by Mitchell and Collins and the modified compression field theory developed by Vecchio and Collins [Refs. 6.7 to 6.9, 6.37 to 6.39, and 6.46, 6.47], and generally strut and tie models [Refs. 6.42, 6.43]. Some details are given in Section 6.15.5. Based on these theories, special provisions exist in the ACI code and the AASHTO LRFD specifications for the design of reinforced and prestressed concrete members subjected to shear and/or torsion, in combination with bending. Information is given in this chapter to cover most common design problems involving shear and torsion of prestressed concrete. No attempt is made to use a sign convention for shear or torsional stresses. They are assumed positive throughout as treated in the code and various publications. Also assumed positive are values of specified factored strength and nominal resistance.

6.2 SHEAR DESIGN

In the earliest codes for reinforced and prestressed concrete the design for shear was based on limiting the magnitude of diagonal tension under working loads, thus providing a safety factor against cracking. However, in prestressed concrete an overload may induce substantial changes in compressive stresses, thus leading to disproportionately high increases in diagonal tension at some points of the section and seriously jeopardizing the corresponding margin of safety. Moreover, the magnitude and direction of principal tensile stresses theoretically derived lose their applicability once cracking occurs. After cracking, considerable changes in stresses and stress distribution take place. A drastic increase in crack widths and decrease in stiffness is observed. This explains why, although principal tension stresses remain a good measure for evaluation, shear design is now considered at the ultimate limit state in both the ACI and AASHTO codes [Refs. 6.1, 6.2], and shear reinforcement is determined for factored loads. Because concrete retains a significant shear resistance after cracking (shear carried in compression zone, crack roughness and aggregate interlocking), the full contribution of transverse reinforcement takes place mostly after cracking.

6.3 PRESTRESSED VERSUS REINFORCED CONCRETE IN SHEAR

It is often said that, with respect to shear, prestressed concrete offers two major advantages over reinforced concrete, namely:

1. For the same external loading, everything else being equal, the shear force in prestressed concrete is often smaller (because of the slope of the prestressing force) than that in reinforced concrete. This is illustrated in Fig. 6.1 where the

sign convention for shear adopted in this text is also given. It is observed that at any section x, the difference in shear between a prestressed concrete beam and an otherwise identical reinforced concrete beam is essentially due to the vertical component of the prestressing force $V_p = F \sin\alpha$. V_p generally acts in a direction opposite to the external loads, thus reducing the shear force in prestressed concrete, which at any section x is given by:

$$V(x) = V_{\text{loads}}(x) - F\sin(\alpha_x) \tag{6.1}$$

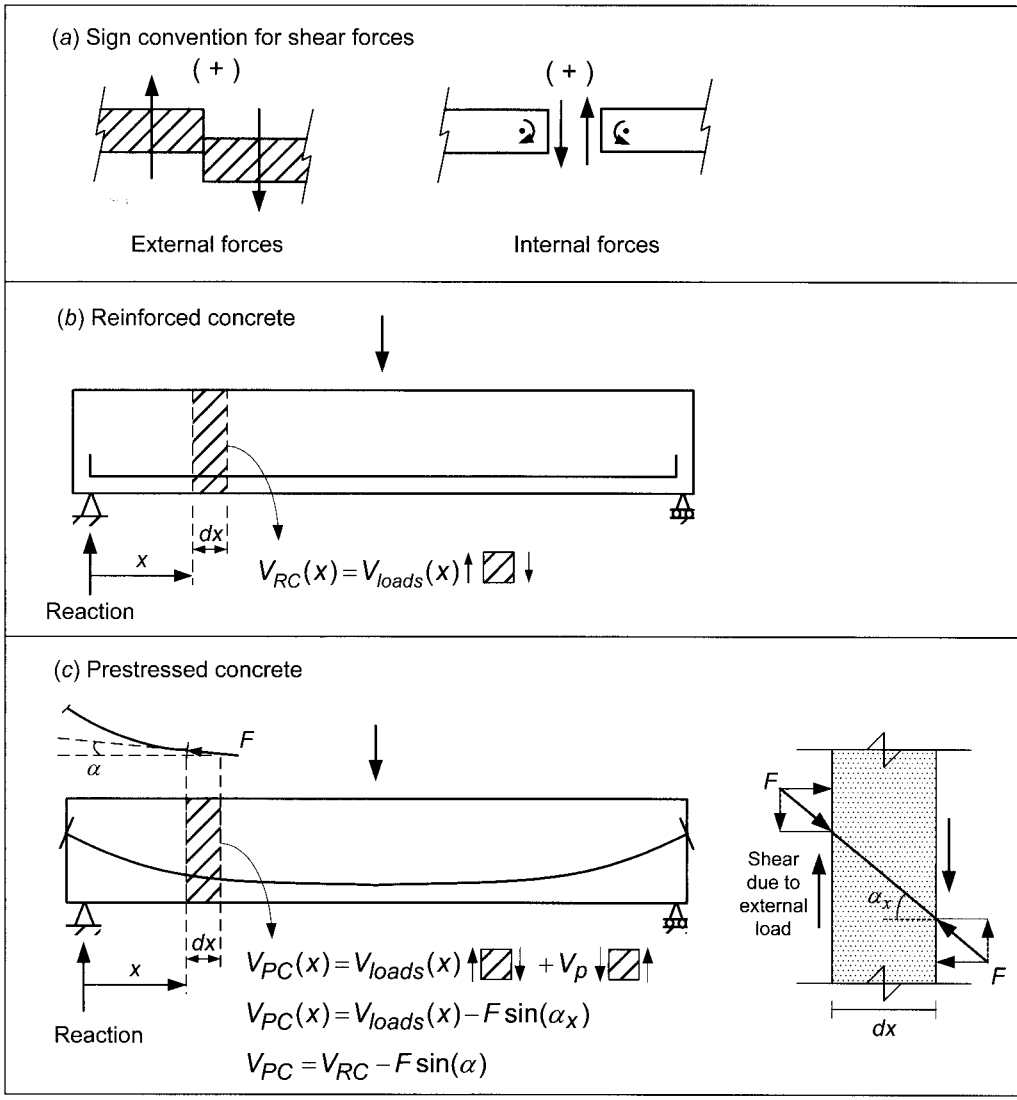

Figure 6.1 Shear in reinforced and prestressed concrete.

2. Due to the compression induced by prestressing, the diagonal tension is smaller in prestressed concrete than in reinforced concrete. Furthermore, its angle of inclination θ, with respect to the beam's axis, is reduced. This implies that if cracking occurs and if, for safe design, the inclined crack is assumed to cross at least one stirrup, the stirrups' spacing in prestressed concrete would be larger and their required area smaller than in reinforced concrete. Thus, a more economical solution (for shear) is obtained. The determination of principal tension is clarified in the next section.

6.4 DIAGONAL TENSION IN UNCRACKED SECTIONS

Let us analyze, assuming elastic behavior, the stresses on a square element of main axis *XX* and *YY* taken along a concrete beam subjected to transverse loading. If the beam is plain or reinforced, an element taken along the neutral axis, such as element *A* (Fig. 6.2), will not be subjected to any axial stresses, but only to shear stresses. If the beam is prestressed, an axial stress will be exerted on *A* in addition to the shear stress. The analysis, in this case, is similar to that of an element *B* taken above the neutral axis of a plain or reinforced concrete beam subjected to a positive moment.

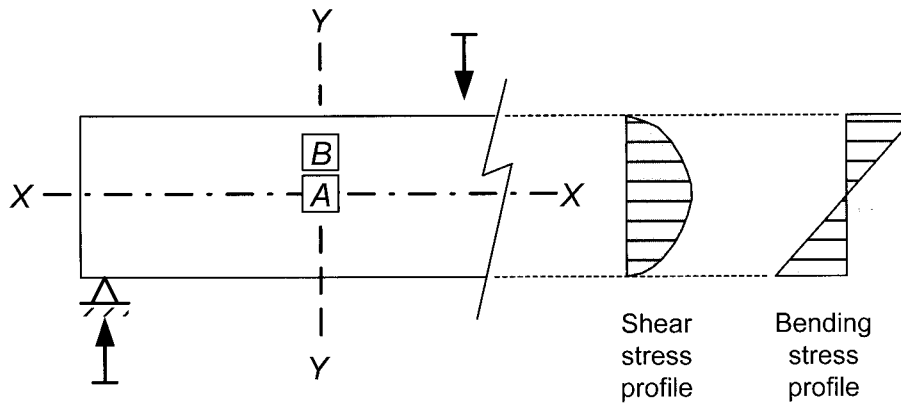

Figure 6.2 Typical shear and bending stress profiles along vertical plane *YY*.

To find the magnitude of principal stresses along an element of beam, it is convenient to construct the Mohr's circle of the element. The following general notation is adopted: σ for normal axial stress, υ (or v) for shear stress, σ_1 for principal tensile stress, σ_2 for principal compressive stress, *XX* for the horizontal plane, *YY* for the vertical plane, *CC* for the plane normal to the principal compression, and *TT* for the plane normal to the principal tension.

The Mohr's circle of an element, taken along the neutral axis of a nonprestressed beam, is shown in Fig. 6.3*a*. The point of the circle representing each plane of interest is indicated. Note that *XX* and *YY* are diametrically opposed, thus bounding an arc of angle 180° on the circle (that is, twice their actual angle of 90°). It can be observed that the magnitudes of principal stresses (points with zero shear ordinate) represented by points *CC* and *TT* on the circle are equal to the magnitude of the shear stress, and their angles of inclination are at 45° with respect to the horizontal and vertical axes. (The actual angle of a plane is half its angle on the Mohr's circle.) Also, the radius of the circle is equal in magnitude to the shear stress v.

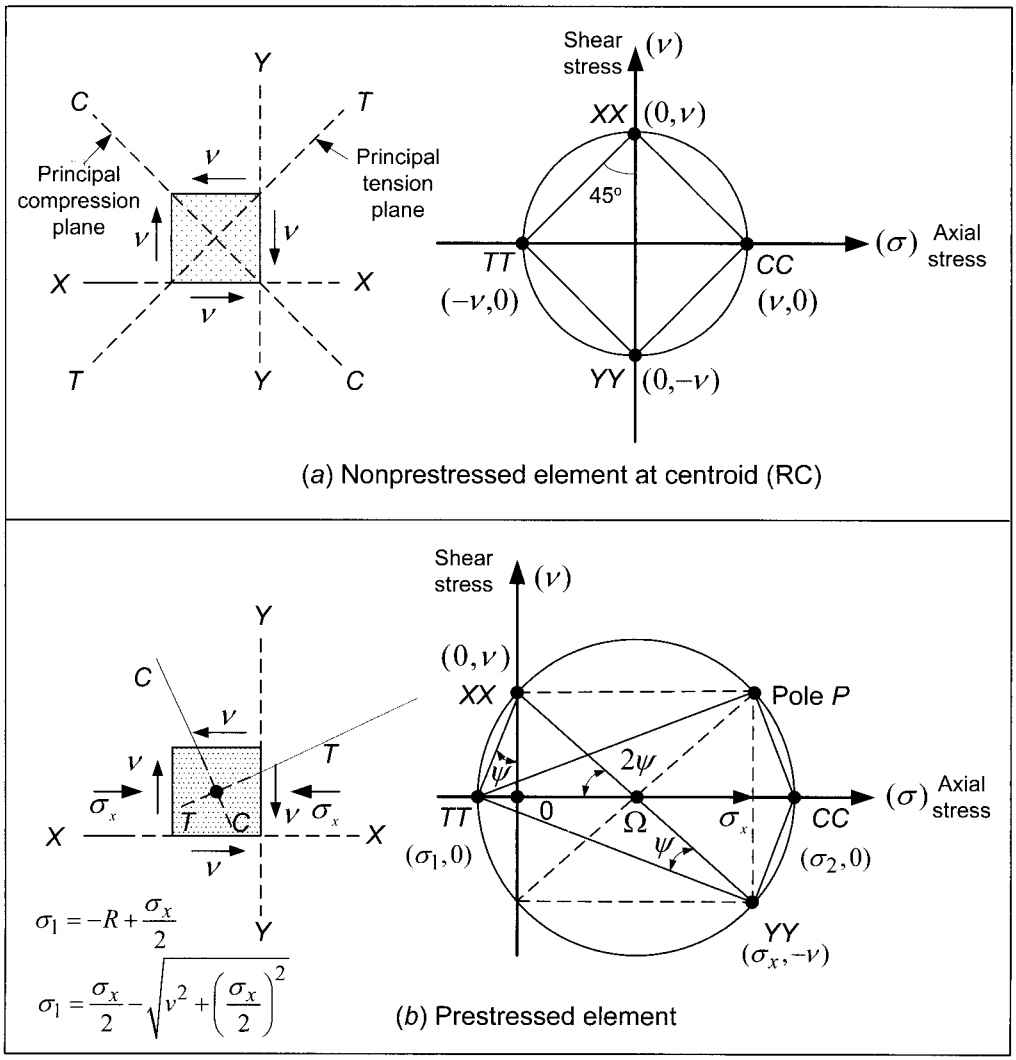

Figure 6.3 Mohr's circle for an element taken along the neutral axis.

Figure 6.3*b* gives the Mohr's circle for an element prestressed along its x axis. It can be observed that the magnitude of principal tension represented by the distance from the origin O to point TT is substantially smaller than in the previous case. Assuming υ and σ_x given, the radius of the circle can be determined from:

$$R = \sqrt{\upsilon^2 + \left(\frac{\sigma_x}{2}\right)^2} \tag{6.2}$$

The principal stresses are then computed from:

$$\sigma_1 = -R + \frac{\sigma_x}{2} = -\sqrt{\upsilon^2 + \frac{\sigma_x^2}{4}} + \frac{\sigma_x}{2} \tag{6.3}$$

$$\sigma_2 = R + \frac{\sigma_x}{2} = \sqrt{\upsilon^2 + \frac{\sigma_x^2}{4}} + \frac{\sigma_x}{2} \tag{6.4}$$

The angle of inclination ψ of the plane of principal tension with respect to the XX plane is obtained from (Fig. 6.3*b*):

$$\tan\psi = \frac{\sigma_1}{\upsilon} = \frac{\sigma_x}{2\upsilon} - \sqrt{1 + \left(\frac{\sigma_x}{2\upsilon}\right)^2} \tag{6.5}$$

It could also be obtained from:

$$\tan 2\psi = \frac{2\upsilon}{\sigma_x} \tag{6.6}$$

Note that, as $\tan\psi$ from Eq. (6.5) is smaller than 1, ψ is smaller than 45°.

There is one convenient method to determine the inclination of different planes from the Mohr's circle. First, a pole point is determined: the pole is a point of the circle representing the intersection of a line parallel to a known plane and passing by its representative point on the circle. For instance, a line parallel to the horizontal plane and passing by point XX intersects the circle at the pole. The pole has the following interesting property: any line passing by the pole and another point of the circle is parallel to the plane of the element represented by that point. For instance, the line joining P to point TT in Fig. 6.3*b* gives the actual direction of the TT plane.

In comparing the results obtained in Figs. 6.3*a* and *b*, it can be observed that both the principal tension and its inclination are smaller for a prestressed element than for a nonprestressed element. For the same shear stress υ, we have:

$$(\sigma_1)_{\text{prestressed}} = (\tan\psi)(\sigma_1)_{\text{nonprestressed}} \tag{6.7}$$

Mohr's circle representation can also be very useful when biaxial prestressing is applied. This occurs, for instance, when, in addition to horizontal prestressing, vertical prestressing is used near the supports of long bridges. Such technique can substantially reduce or eliminate diagonal tension. A typical representation is shown in Fig. 6.4 for an element subjected to shear stresses and compressive stresses σ_x and σ_y with $\sigma_x > \sigma_y$. The following expressions can easily be derived:

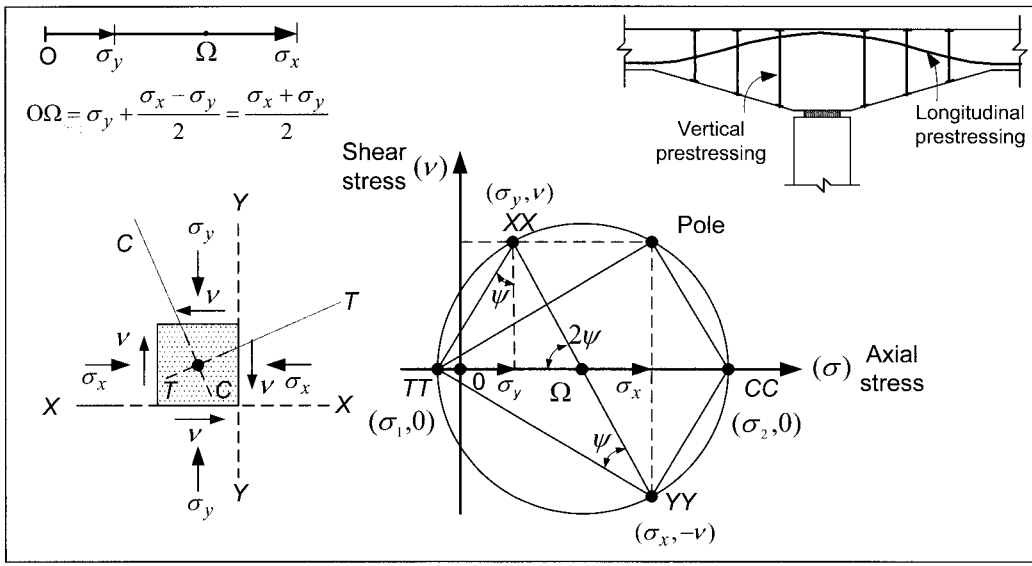

Figure 6.4 Mohr's circle for a biaxially prestressed element.

$$R = \sqrt{v^2 + \left(\frac{\sigma_x - \sigma_y}{2}\right)^2} \tag{6.8}$$

$$O\Omega = \frac{\sigma_x + \sigma_y}{2} \tag{6.9}$$

$$\sigma_1 = \frac{\sigma_x + \sigma_y}{2} - R \tag{6.10}$$

$$\sigma_2 = \frac{\sigma_x + \sigma_y}{2} + R \tag{6.11}$$

$$\tan 2\psi = \frac{2v}{\sigma_x - \sigma_y} \tag{6.12}$$

It is interesting to note that the principal tension can be eliminated by properly selecting the value of σ_y, the vertical prestress. Setting $\sigma_1 = 0$ in Eq. (6.10) and replacing R by its value from Eq. (6.8) leads to:

$$\sigma_y = \frac{\upsilon^2}{\sigma_x} \tag{6.13}$$

Note that, to compute the principal stresses, the values of υ and σ_x (shear and axial stress) are needed. The determination of σ_x under the combined effects of prestressing and external loads was covered in Chapter 4. The determination of shear stress υ is treated next.

6.5 SHEAR STRESSES IN UNCRACKED SECTIONS

The shear stress along any section of a flexural beam, assumed elastic uncracked, is given by (Fig. 6.5):

$$\upsilon_y = \left(\frac{Q}{b_y I}\right) V = \left(\frac{A_y \bar{y}}{b_y I}\right) V \tag{6.14}$$

where:

υ_y = shear stress at a distance y from the neutral axis (y within section)
Q = first static moment about the neutral axis of the portion of section outside the shear plane considered
A_y = area of the portion of section outside the shear plane
$\bar{y}$ = distance from neutral axis to the centroid of A_y
b_y = width of section at level y of shear plane considered
I = moment of inertia of the cross section.

Note that V is the shear force at the section of beam considered and, therefore, generally varies along the span. For a prestressed beam, V is the net shear (Eq. 6.1) due to the combination of applied load and prestressing.

For a given value of V and section dimensions, the shear stress υ_y at a given section varies along the section. Typical shear stress diagrams for common sections are shown in Fig. 6.5. It is observed that the maximum value of υ_y occurs when the shear plane considered is taken along the neutral axis of the beam. The magnitude of

maximum shear stress, also given in Fig. 6.5, can be put in the following form for rectangular and flanged sections:

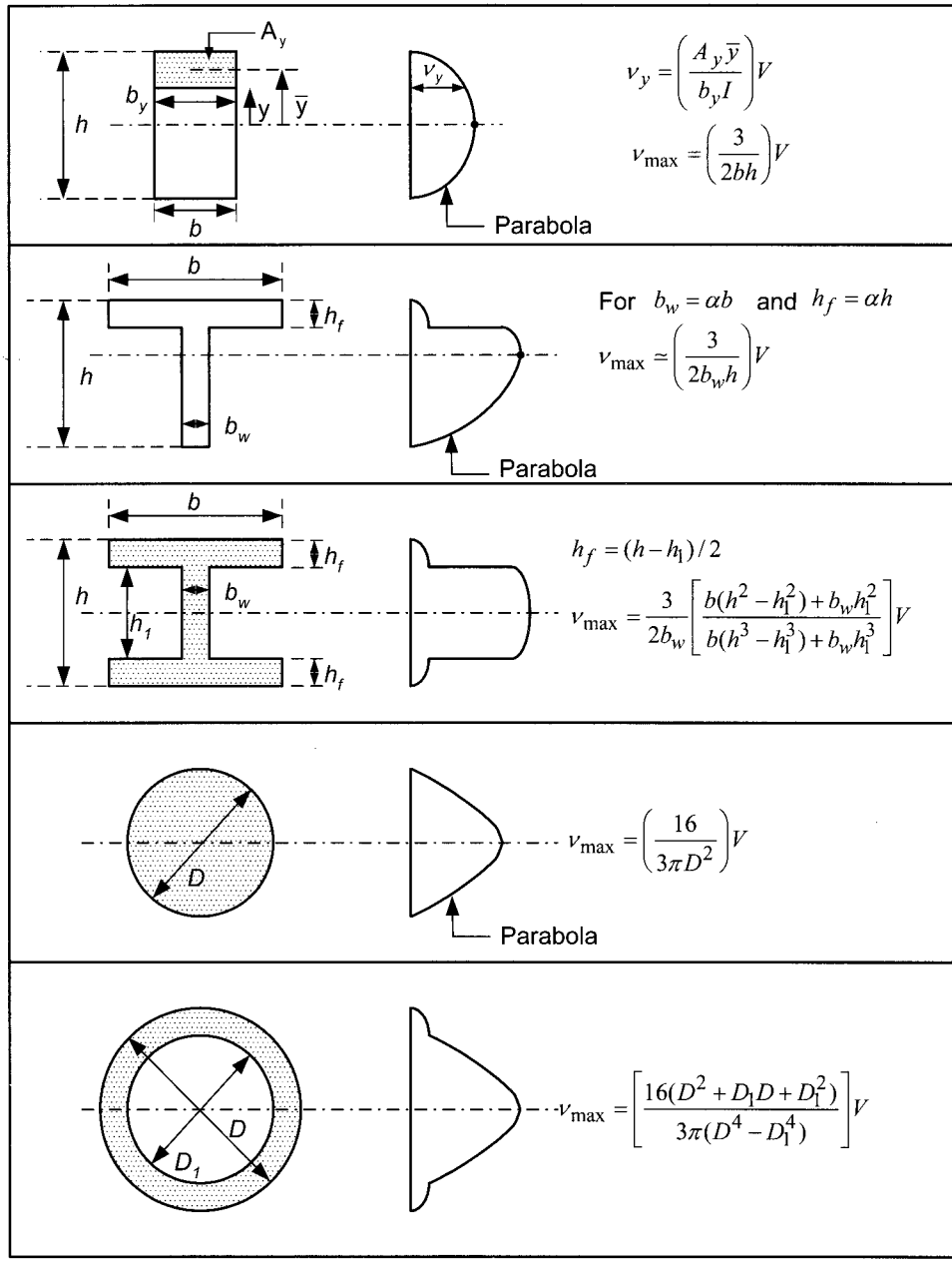

Figure 6.5 Typical shear stress diagrams and maximum shear stresses for various sections.

$$\upsilon_{\max} = \lambda \frac{V}{b_w h} \tag{6.15}$$

where λ is a factor larger than one. In computing an average shear stress from the shear force, the ACI code essentially adopts a value of λ equal to one and uses d (d_p or d_s) instead of h.

If cracking occurs, the shear stress distribution along the section will change. According to the analysis, it appears that the shear stress will be constant in the cracked region of the section.

6.6 SHEAR CRACKING BEHAVIOR

Structural cracking occurs in concrete when its tensile strength is exceeded. As any external loading generally leads to combined effects such as flexure and shear, it is likely that more than one type of cracking will be critical depending on the variables at hand.

An extensive number of investigations [Refs. 6.5, 6.20, 6.27 to 6.30, 6.44, 6.45] have shown or confirmed that two types of shear related cracks can develop in reinforced and prestressed concrete beams: *flexure-shear cracks* and *web-shear cracks* (Fig. 6.6*a*). The manner in which these cracks develop and grow strongly depends on the relative magnitude of shearing and flexural stresses.

Flexure-shear cracking is due to a combined effect of flexure and shear. The corresponding cracks start as flexural cracks (normal to the beam's axis). Then, due to the increased effect of diagonal tension at the tip of the crack, they deviate and propagate at an inclined direction corresponding essentially to the inclination of the diagonal tension plane. Typical flexure-shear cracks are shown in Fig. 6.6*a*. Flexure-shear cracking can lead to several types of failures [Refs. 6.4, 6.5, 6.12], schematically illustrated in Fig. 6.6*b*.

Very slender beams generally fail in flexure either by their tensile reinforcement or by the concrete compressive zone. However, in beams with smaller shear span-to-depth ratio, failure may occur by flexure-shear cracking before the flexural capacity is developed. In moderately slender beams, one of the cracks may continue to propagate until it becomes unstable, reaching throughout the depth of the beam and leading to what is described as diagonal tension failure. In relatively deep beams, a secondary crack, triggered by a flexure-shear crack, may propagate horizontally along the longitudinal reinforcement, leading to a loss of bond followed by a loss of anchorage near the support and subsequent failure described as shear tension failure. Alternatively, the concrete at the upper end of the crack may fail by crushing in what is described as shear compression failure.

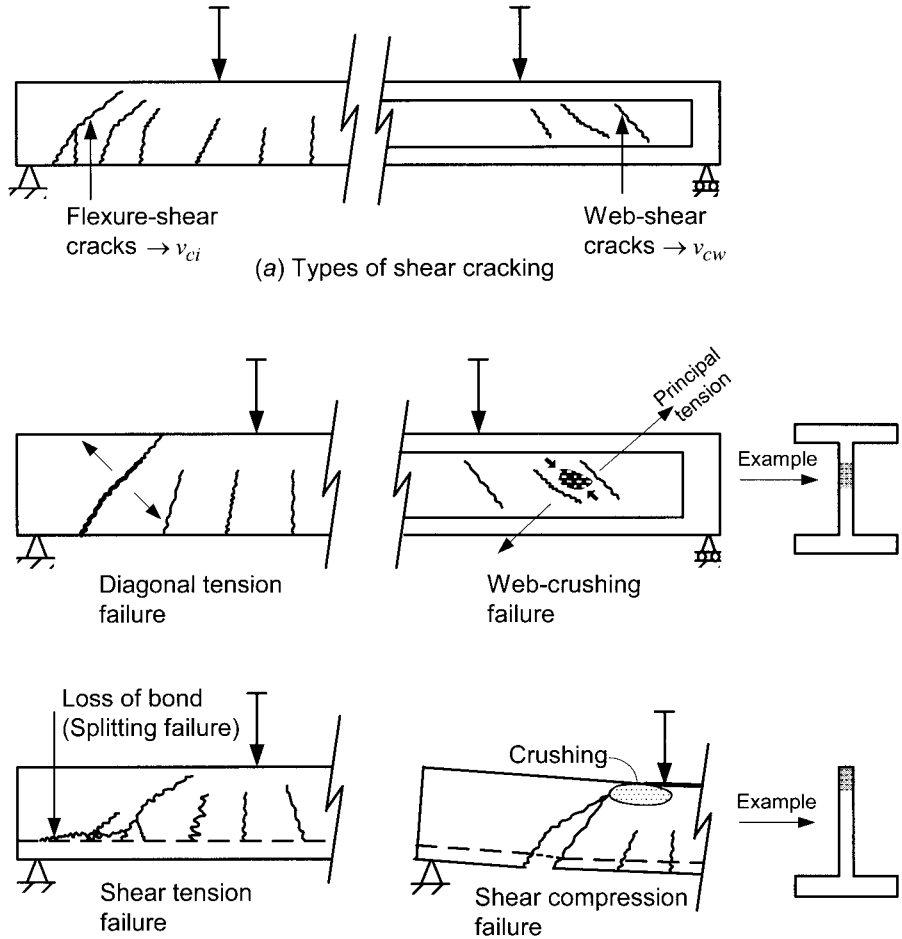

Figure 6.6 Shear cracking and shear failures.

Web-shear cracking (Fig. 6.6*a*) occurs when the magnitude of principal tension is relatively high in comparison to flexural stresses. It is characteristic of beams with narrow webs, such as I-beams, where cracking due to diagonal tension develops before flexural cracking. Web-shear cracking may lead to the same types of failures described for flexure-shear cracking, namely, diagonal tension, shear tension, and shear compression failures. In addition (Fig. 6.6*b*), crushing under diagonal compression may occur within the web, leading to web-crushing failure.

Figure 6.7 illustrates the above cracking classification and its schematic location within a typical beam. Understanding this figure is important, since the provisions of the ACI code for shear implicitly refer to this type of behavior.

Several models have been proposed to simulate shear cracking and failure mechanisms in reinforced concrete beams and include limit analysis mechanisms and analogies with arches, trusses or frames. The arch and truss analogies are illustrated in Fig. 6.8. The truss analogy is at the basis of the ACI code provisions to determine shear reinforcement. A more comprehensive treatment of each mechanism and their comparison can be found in Refs. [6.6, 6.10, 6.20, and 6.32].

It is much preferable to avoid shear failure, since it is substantially more brittle than flexural failure. To supplement the shear resistance of concrete members and to ensure flexural failure prior to shear failure, shear reinforcement (also called web or transverse reinforcement) in the form of stirrups is generally provided. The function of shear reinforcement is explained in more detail in Ref. [6.30 and 6.32].

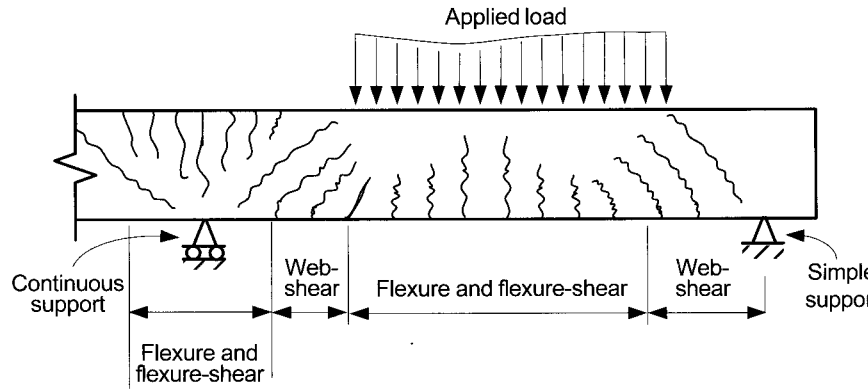

Figure 6.7 Typical cracking due to bending and shear in a reinforced concrete beam.

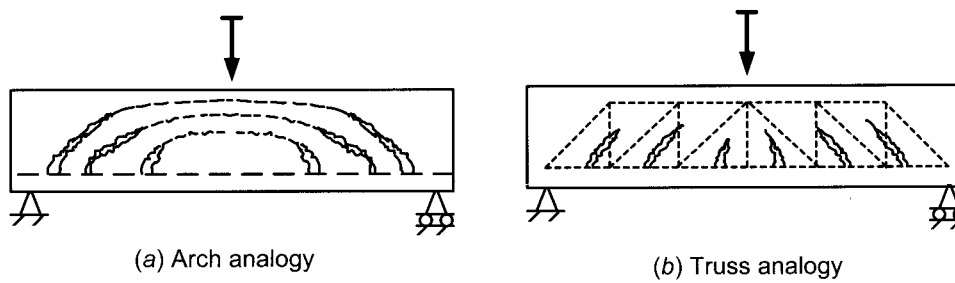

Figure 6.8 Typical analogies for shear failure mechanisms.

6.7 SHEAR REINFORCEMENT AFTER CRACKING

The approach used to determine shear reinforcement in prestressed concrete is identical to that used for reinforced concrete. It is assumed that a shear crack extends at 45° to the beam's axis, as shown in Fig. 6.9. The force carried by the web

reinforcement is assumed to balance a principal tension across the crack equal in magnitude to the shear stress υ. According to the ACI code, the portion of υ, balanced by the shear reinforcement, is the shear stress in excess of the shear strength contribution of the concrete. Let us call it υ_s. It is also assumed that, at the onset of shear failure, the shear reinforcement will be stressed to its yield strength f_y.

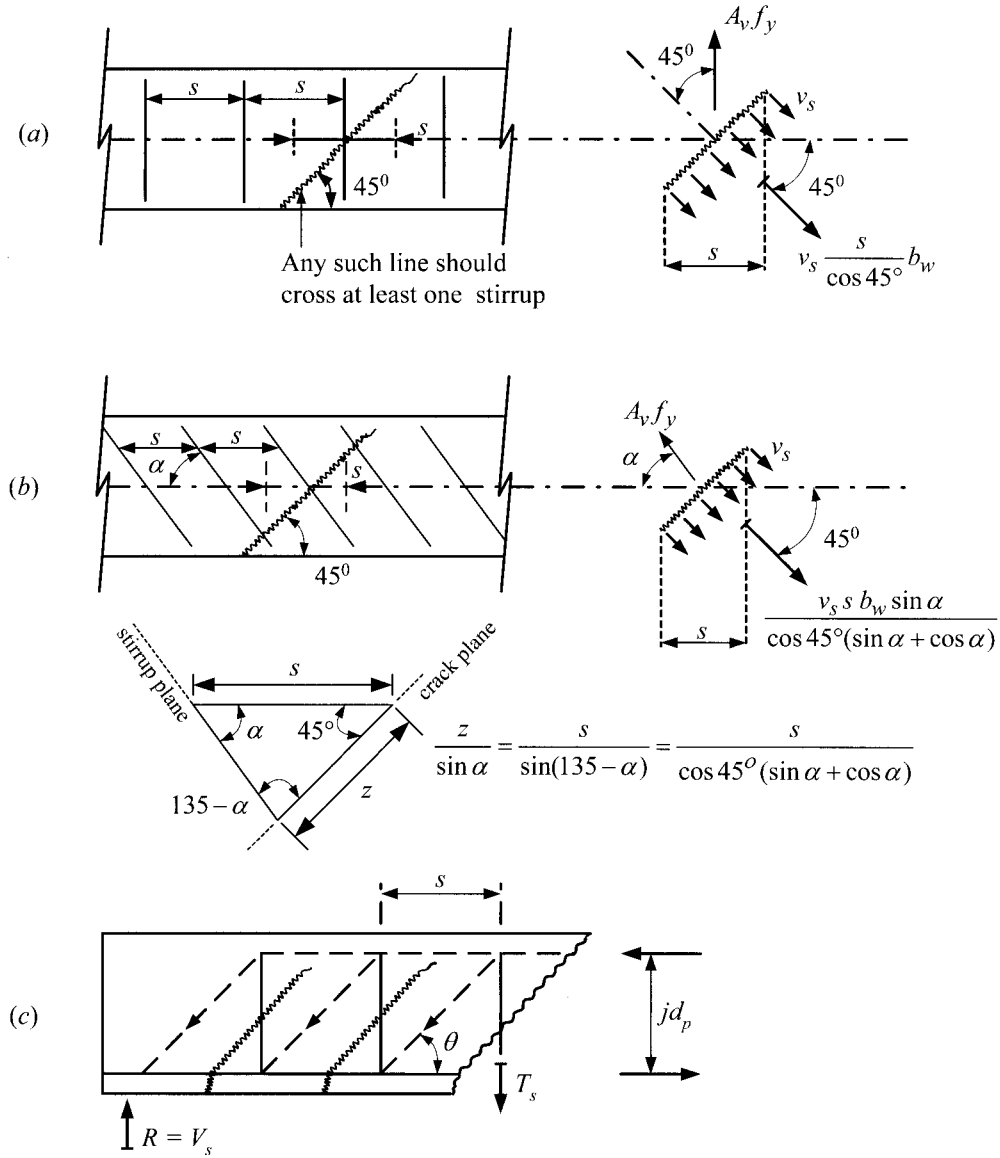

Figure 6.9 Shear resistance provided by *(a)* Vertical stirrups, *(b)* Inclined stirrups, *(c)* Truss analogy model (see also Chapter 15).

Let us first consider the case of shear reinforcement placed normally to the beam's axis (vertical stirrups) with spacing s (Fig. 6.9*a*). The crack can be divided in equal segments, each traversed by a single stirrup. A free body diagram of a typical segment is also shown in Fig. 6.9*a*. The length of the crack segment along its plane is given by $(s/\cos 45^\circ)$. Projecting the forces on the vertical axis leads to the following equilibrium equation:

$$A_v f_y = \left(\frac{b_w v_s s}{\cos 45^\circ} \right) \cos 45^\circ = b_w v_s s \tag{6.16}$$

from which the required area of vertical reinforcement (stirrups) is obtained:

$$A_v = \frac{b_w v_s s}{f_y} \tag{6.17}$$

If the stirrups were placed at an angle α to the beam's axis (inclined stirrups), an approach similar to the above would lead to the area of inclined reinforcement given by (Fig. 6.9*b*):

$$A_v = \frac{b_w v_s s}{f_y(\sin\alpha + \cos\alpha)} \tag{6.18}$$

Although inclined stirrups are more efficient than vertical stirrups, the increased labor cost associated with their placing seldom justifies their use.

Note that in designing the shear reinforcement according to the ACI code, the value of v_s in Eqs. (6.17) and (6.18) is replaced by the shear demand needed at ultimate $(v_u/\phi - v_c)$ as explained in Sec. 6.8.

Equations (6.17) and (6.18) were derived assuming a 45° shear crack. It is expected that a smaller angle will develop in prestressed beams, thus leading to a conservative design. ACI consider that an angle of 37.5 degrees is generally acceptable for prestressed concrete.

The above results can also be simply derived using the truss analogy model of the web reinforced cracked beam in which the stirrups act as tension members of the analogous truss, and the concrete struts running parallel to the diagonal cracks act as compression members (Fig. 6.9*c*). Assuming vertical stirrups, the shear at the section shown is given by:

$$V_s = T_s \tag{6.19}$$

where T_s is the tensile force in the stirrup (not to be confused with torsional moment). The web steel force per unit length is given by T_s / s in which $s = jd_p \cot\theta$. Hence,

$$\frac{T_s}{s} = \frac{V_s}{s} = \frac{V_s}{jd_p \cot\theta} \tag{6.20}$$

Assuming, as a first approximation, $jd_p \simeq d_p$ and $\theta = 45^\circ$ leads to:

$$\frac{T_s}{s} = \frac{V_s}{d_p} \tag{6.21}$$

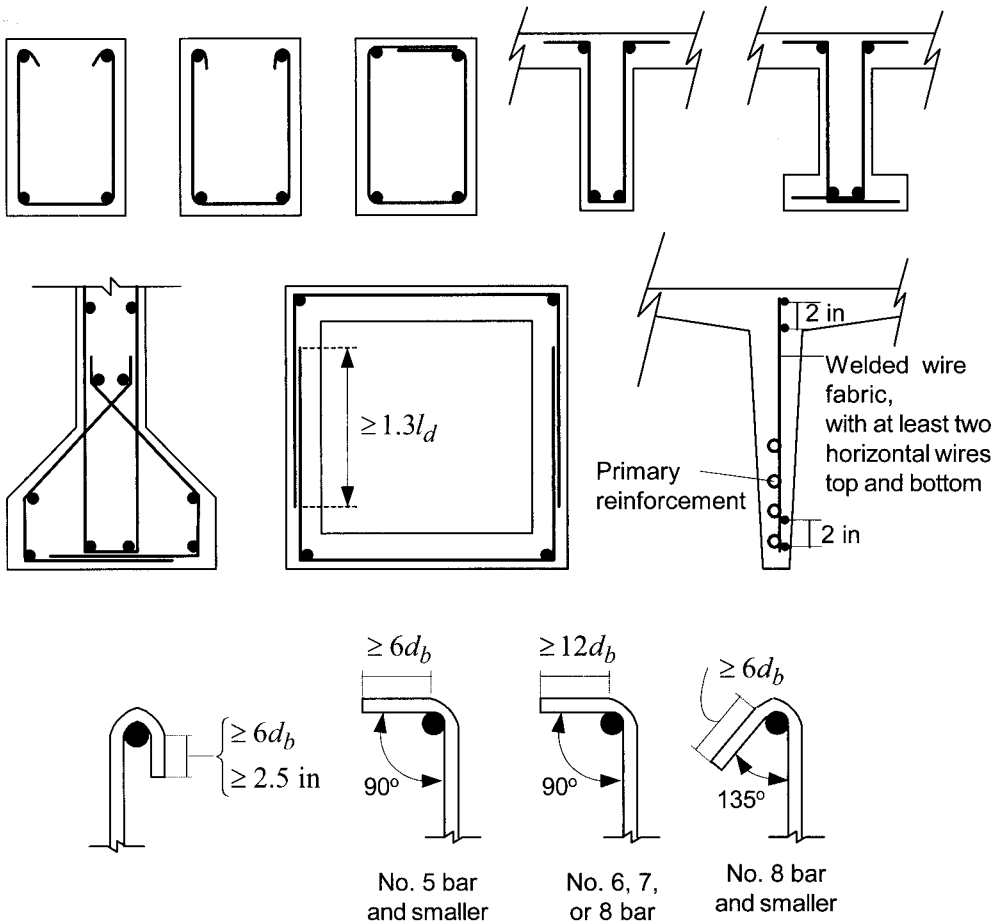

Figure 6.10 Typical shear reinforcement and standard hook dimensions for stirrups according to the ACI code.

Since stirrups are assumed to yield at ultimate, T_s is replaced by $A_v f_y$, thus:

$$A_v = \frac{V_s s}{f_y d_p} \tag{6.22}$$

in which:

$$V_s = v_s b_w d_p \tag{6.23}$$

Eq. (6.22) is identical to Eq. (6.17).

Shear reinforcement in prestressed beams consists mostly of stirrups. A stirrup has generally two legs, leading to an area of vertical reinforcement twice the cross-sectional area of the stirrup bar. Typical shapes of stirrups and standard hooks and ties, as recommended by the ACI code, are shown in Fig. 6.10. Stirrups used for shear can be "open" stirrups but must be appropriately anchored in the compressive zone of the member. Because of relatively high labor costs associated with the placing of stirrups, an alternative solution consisting of welded wire fabric is often used with precast prestressed concrete products (Fig. 6.10). Commercial welded wire fabrics used for shear reinforcement have few longitudinal wires and selected sets of transverse wire spacing covering a practical range. It is common practice to assume that the vertical wires are properly anchored in the tensile zone if at least two welded junctions are provided.

6.8 ACI CODE DESIGN CRITERIA FOR SHEAR

6.8.1 Basic Approach

As mentioned earlier, the ACI design approach is based on ultimate strength requirements (factored loads). A design shear strength at each section of a member is required. It is achieved by the combined contributions of concrete and shear reinforcement. The concrete is assumed to provide a prescribed shear resistance; the shear reinforcement (stirrups) provides the excess resistance, if any, needed to satisfy the required strength. In the 1971 edition of the code, shear related equations were given in stress units. From 1977 on, including the 2002 code, they are given in force units where the force is obtained by multiplying the shear stress by $b_w d_p$. Although the approaches used and the results obtained are identical, the author prefers the use of stresses, because they are independent of the size of the member and, thus, can be easily correlated when different solutions are compared. They also have the advantage of providing a warning or flag easily recognizable by the designer when a

limit is exceeded. However, each important equation is written in terms of both stresses and forces.

The required factored shear at each section of the member should be less than or equal to its shear resistance, that is:

$$\begin{cases} \upsilon_u \le \phi \upsilon_n \\ V_u \le \phi V_n \end{cases} \tag{6.24}$$

where:

υ_u, V_u = respectively design shear stress (psi) and force (lb) resulting from factor loads at section considered

υ_n, V_n = nominal shear strength of the section, stress (psi) and force (lb), respectively

ϕ = strength reduction factor (equal to 0.75 for shear as per 2002 ACI)

Equation (6.24) can be conveniently rewritten as:

$$\begin{cases} \dfrac{\upsilon_u}{\phi} \le \upsilon_n \\ \dfrac{V_u}{\phi} \le V_n \end{cases} \tag{6.25}$$

The design shear stress υ_u is obtained from

$$\upsilon_u = \frac{V_u}{b_w d_p} \tag{6.26}$$

where:

b_w = width of rectangular section or web width of flanged section

$d_p = d_p$ or $0.8h$ whichever is larger.

The provision to use $0.8h$ when the actual value of d_p is smaller than $0.8h$, is substantiated by test data. It is reasonable because the section is prestressed and the web area available to compute nominal shear stress is not a direct function of the location of the prestressing steel [Ref. 6.2].

The nominal shear strength υ_n is defined as the sum of the shear resistance of the concrete and the shear contribution of the web reinforcement at the section considered. That is:

$$\begin{cases} \upsilon_n = \upsilon_c + \upsilon_s \\ V_n = V_c + V_s \end{cases} \tag{6.27}$$

where:

υ_c, V_c = nominal shear strength (stress and force, respectively) provided by the concrete

υ_s, V_s = nominal shear strength (stress and force, respectively) provided by the shear reinforcement.

Note that in the ACI code, the contribution of the prestressing force to the shear resistance (V_p) is integrated in the value of V_c, while in the AASHTO LRFD code it is added to the right side of Eq. (6.27). The AASHTO code approach is covered in Section 6.12 (see also Eq. 6.53).

The relation between υ_c and V_c is similar to the relation between shear stresses and shear forces given in earlier equations, namely:

$$\upsilon_c = \frac{V_c}{b_w d_p} \text{ or } V_c = \upsilon_c b_w d_p \tag{6.28}$$

The values of $\upsilon_c, V_c, \upsilon_s$, and V_s are defined in the next sections.

6.8.2 Shear Strength Provided by Concrete

According to the ACI code, the value of υ_c is to be taken as the smaller of υ_{ci}, the resistance to flexure-shear cracking, and υ_{cw}, the resistance to web-shear cracking. The equations given by the code for υ_{ci} and υ_{cw} are simplified approximations of equations derived either theoretically from analyzing the section (υ_{cw}) or from a semi-rational analysis supported by experimental evidence (υ_{ci}). In order not to interrupt the flow of logical steps in the design process, the derivations of υ_{ci} and υ_{cw} are given below in Section 6.11.

Flexure-Shear Cracking Resistance. The flexure-shear cracking stress υ_{ci} is made out of three components (see Section 6.11): (1) the shear stress needed to transform a flexural crack into an inclined crack, estimated equal to $0.6\sqrt{f'_c}$, (2) the shear stress due to the self-weight of the member, V_G / bd_p, and (3) the additional factored shear stress that initially will cause a flexural crack to occur, $\Delta M_{cr} / (\Delta M_u / \Delta V_u) b_w d_p$. Hence, the shear resistance of the concrete, corresponding to flexure-shear cracking, is taken as (using the notation adopted in this text):

$$\begin{cases} \upsilon_{ci} = 0.6\lambda\sqrt{f_c'} + \dfrac{V_G}{b_w d_p} + \left(\dfrac{\Delta V_u \times \Delta M_{cr}}{\Delta M_u}\right)\dfrac{1}{b_w d_p} \geq 1.7\lambda\sqrt{f_c'} \\ V_{ci} = 0.6\lambda\sqrt{f_c'} b_w d_p + V_G + \left(\dfrac{\Delta V_u \times \Delta M_{cr}}{\Delta M_u}\right) \geq 1.7\lambda\sqrt{f_c'} b_w d_p \end{cases} \tag{6.29}$$

where:

λ = 1 for normal-weight concrete

λ = 0.85 for sand light-weight concrete

λ = 0.75 for all light-weight concrete

υ_{ci} = flexure-shear stress resistance, psi

V_{ci} = flexure-shear force resistance, lb

b_w = width of rectangular section or web width of flanged section

$d_p = d_p$ or $0.80h$ whichever is larger at section considered

V_G = shear force due to self-weight of member at section considered

ΔV_u = factored shear force due to superimposed dead load plus live load at section considered under same loading as ΔM_u

ΔM_u = factored bending moment due to superimposed dead load plus live load at section considered

ΔM_{cr} = moment in excess of self-weight moment, causing flexural cracking in the precompressed tensile fiber at section considered (equal $M_{cr} - M_G$)

The effect of self-weight shear V_G is considered separately for two reasons:

1. Self-weight is generally uniformly distributed, whereas live loads can have any distribution and can be concentrated loads. The ratio $\Delta M_u / \Delta V_u$, which appears in Eq. (6.28), remains constant at a given section when external loads increase proportionately, and is independent of load factors. Corresponding calculations are easier to handle.
2. By separating the effect of self-weight, Eq. (6.29) remains applicable to composite members. For such members, V_G should include not only the weight of the precast unit but also that of the cast-in-place slab. However, note that the construction sequence for composite members (i.e., shored versus unshored) influences the value of ΔM_{cr}, because part of the load is resisted by the precast section alone and part by the composite section. Appropriate section properties should be used to determine ΔM_{cr} (see Section 9.7.4).

Note that the cracking moment increment ΔM_{cr} used in Eq. (6.29) has to be computed assuming a modulus of rupture of $-6\sqrt{f'_c}$ instead of $-7.5\sqrt{f'_c}$. Using Eq. (4.41) and assuming the beam is statically determinate, leads to:

$$\Delta M_{cr} = Z_b\left[6\sqrt{f'_c} + \frac{F}{A_c}\left(1 + \frac{e_o A_c}{Z_b}\right)\right] - M_G \tag{6.30}$$

Web-Shear Cracking Resistance. The nominal resistance of the concrete, corresponding to web-shear cracking at the section considered, is to be taken as:

$$\begin{cases} \upsilon_{cw} = 3.5\lambda\sqrt{f'_c} + 0.3\sigma_g + \dfrac{V_p}{b_w d_p} \\ V_{cw} = (3.5\lambda\sqrt{f'_c} + 0.3\sigma_g) b_w d_p + V_p \end{cases} \tag{6.31}$$

where λ is defined in Eq. (6.29) and:

υ_{cw} = web-shear stress resistance, psi

V_{cw} = web-shear force resistance, lb

σ_g = compressive stress in the concrete at the centroid of the cross section or at the junction of web and flange if the centroid is in the flange, due to effective prestress

V_p = vertical component of prestressing force at section considered,

$= F \sin\alpha$

$d_p = d_p$ or $0.80h$ whichever is larger.

Alternatively, υ_{cw} may be theoretically computed as the shear stress corresponding to a combination of dead load and live load that results in a principal tensile stress of $-4\sqrt{f'_c}$ at the centroid of the section, or at the junction of web and flange when the centroid is in the flange. Its derivation is given in Sec. 6.11.

Alternate Conservative Estimate of υ_c or V_c. The computation of the values of υ_{ci} and υ_{cw}, given by the above expressions, is time-consuming, especially since several sections along the span must be considered. An alternative, more conservative method for beams with uniform loads is suggested in the code and can be used when the effective prestress f_{pe} is not less than $0.40 f_{pu}$ [Ref. 6.30]. The shear resistance of the concrete, in stress or force units, respectively, can then be taken as:

$$\begin{cases} \upsilon_c = 0.6\lambda\sqrt{f'_c} + 700\dfrac{V_u d_p}{M_u} & \begin{cases} \geq 2\lambda\sqrt{f'_c} \\ \leq 5\lambda\sqrt{f'_c} \end{cases} \\ V_c = (0.6\lambda\sqrt{f'_c} + 700\dfrac{V_u d_p}{M_u})b_w d_p & \begin{cases} \geq 2\lambda\sqrt{f'_c} b_w d_p \\ \leq 5\lambda\sqrt{f'_c} b_w d_p \end{cases} \end{cases} \tag{6.32}$$

where V_u and M_u are the factored shear and moment and d_p is the depth to the centroid of the prestressing force at the section considered. The ratio $V_u d_p / M_u$ is not to be taken greater than 1 and the lower bound value of $0.8h$ on d_p used elsewhere does not apply here. However, the lower bound value would apply to the multiplier $b_w d_p$ used to compute V_c.

6.8.3 Required Area of Shear Reinforcement

In order to determine the required area of shear reinforcement, the nominal shear strength provided by the reinforcement (υ_s) or (V_s) is needed. Its minimum design value is obtained from Eqs. (6.24) and (6.27) at equality. That is:

$$\begin{cases} \dfrac{\upsilon_u}{\phi} = \upsilon_n = \upsilon_c + \upsilon_s \\ \dfrac{V_u}{\phi} = V_n = V_c + V_s \end{cases} \tag{6.33}$$

from which:

$$\begin{cases} \upsilon_s = \left(\dfrac{\upsilon_u}{\phi} - \upsilon_c\right) \\ V_s = \left(\dfrac{V_u}{\phi} - V_c\right) \end{cases} \tag{6.34}$$

where υ_s is the required nominal shear resistance of the shear reinforcement in stress unit, and V_s is in force unit. The area of shear reinforcement can then be obtained from Eqs. (6.17) and (6.18) in which υ_s is replaced by its value from Eq. (6.34):

- For vertical stirrups:

$$A_\upsilon = \frac{(\upsilon_u/\phi - \upsilon_c)b_w s}{f_y} = \frac{(V_u/\phi - V_c)s}{f_y d_p} \tag{6.35}$$

- For stirrups inclined at an angle α to the beam's axis:

$$A_v = \frac{(v_u/\phi - v_c)b_w s}{f_y(\sin\alpha + \cos\alpha)} = \frac{(V_u/\phi - V_c)s}{f_y d_p(\sin\alpha + \cos\alpha)} \tag{6.36}$$

The above two equations can also be used to find the required spacing s for a given type of stirrup A_v :

- For vertical stirrups:

$$s = \frac{A_v f_y}{(v_u/\phi - v_c)b_w} = \frac{A_v f_y d_p}{V_u/\phi - V_c} \tag{6.37}$$

- For inclined stirrups:

$$s = \frac{A_v f_y(\sin\alpha + \cos\alpha)}{(v_u/\phi - v_c)b_w} = \frac{A_v f_y(\sin\alpha + \cos\alpha)d_p}{V_u/\phi - V_c} \tag{6.38}$$

6.8.4 Limitations and Special Cases

A number of design limitations relative to shear reinforcement are given in the ACI code:

1. *Maximum spacing.* The spacing s of shear reinforcement measured parallel to the axis of the member shall not exceed $3h/4$ or 24 in (61 cm). In common practice, the spacing is taken not less than 3 in (75 mm).
2. *Maximum shear.* The value of $(v_u/\phi - v_c)$ shall not exceed $8\lambda\sqrt{f'_c}$. If it does, the section is insufficient for shear resistance and its dimensions should be changed (namely, change b_w and/or d_p). Moreover, the code stipulates that if $(v_u/\phi - v_c)$ exceeds $4\lambda\sqrt{f'_c}$, the spacing obtained from Eqs. (6.35) to (6.38) should be halved and should not exceed $3h/8$ or 12 in (30 cm). Alternatively, if the spacing is kept the same, the area of stirrups should be doubled.
3. *Minimum shear reinforcement.* Shear reinforcement restrains the growth of inclined cracking and, hence, increases ductility and provides sufficient warning of failure. Otherwise, in an unreinforced web, the sudden formation of inclined cracking might lead directly to sudden failure. Accordingly, the code requires a minimum area of shear reinforcement to be provided in all reinforced and prestressed concrete structural members when the factored shear stress v_u

exceeds half the design shear strength of concrete ϕv_c, except in: (1) slabs and footings, (2) concrete joist construction for which the code allows a 10 percent increase in v_c, and (3) beams with total depth not greater than 10 in (25 cm), two and one-half times the thickness of the flange or one-half the web width, whichever is greatest.

When the effective prestress f_{pe} exceeds $0.40 f_{pu}$ (which is commonly the case in prestressed concrete), the minimum required area of shear reinforcement may be computed from:

$$(A_v)_{\min} = \frac{A_{ps}}{80}\frac{f_{pu}}{f_y}\frac{s}{d_p}\sqrt{\frac{d_p}{b_w}} \tag{6.39}$$

where d_p has a lower bound value of $0.80h$ and other notations are standard.

A more general equation for the minimum required area of shear reinforcement is given in the code and applies to reinforced as well as prestressed concrete (with no limitation on the effective prestress). It is given by:

$$(A_v)_{\min} \geq \begin{cases} 0.75\sqrt{f'_c}\,\dfrac{b_w s}{f_y} \\ 50\dfrac{b_w s}{f_y} \end{cases} \tag{6.40}$$

where b_w and s are in inches and f_y is in pounds per square inch. Equation (6.40) will generally require greater minimum shear reinforcement in typical building members than will Eq. (6.39).

4. *Lightweight concrete.* When prestressed lightweight concrete is used instead of normal weight concrete, the same procedure to determine the shear reinforcement is used with the following modifications recommended by the code: When the split cylinder strength f_{tc} is specified for lightweight concrete and when $f_{tc}/6.7$ is less than $\sqrt{f'_c}$, replace $\sqrt{f'_c}$, by $f_{tc}/6.7$ in the equations giving v_c. Also $\sqrt{f'_c}$, is not to be taken larger than 100.

6.8.5 Critical Sections for Shear

Contrary to reinforced concrete where commonly the most critical section is near the support, in prestressed concrete several sections along a typical beam, located between support and midspan, may be more critical than the near support section. This is why shear is to be investigated at several sections along the span. Indeed, near the support, the compression due to prestressing reduces the diagonal tension,

while the bending moment is very small. Further away from the support, the combination of bending, shear and prestressing, produces a larger diagonal tension more critical in design.

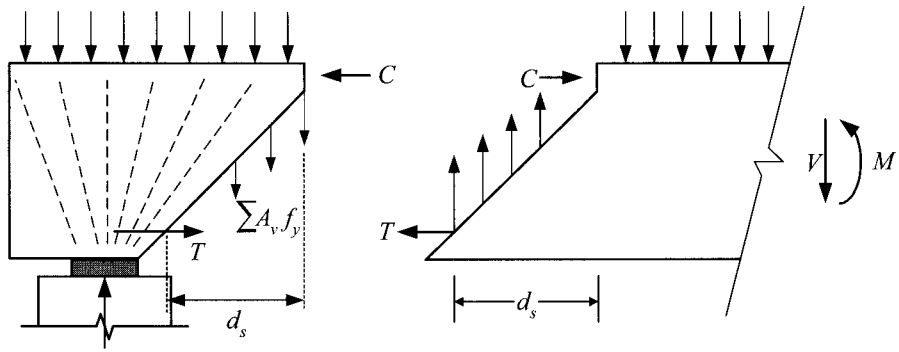

Figure 6.11 Illustration of direct load transfer to support within distance d_s, and contribution of shear reinforcement along a typical shear crack.

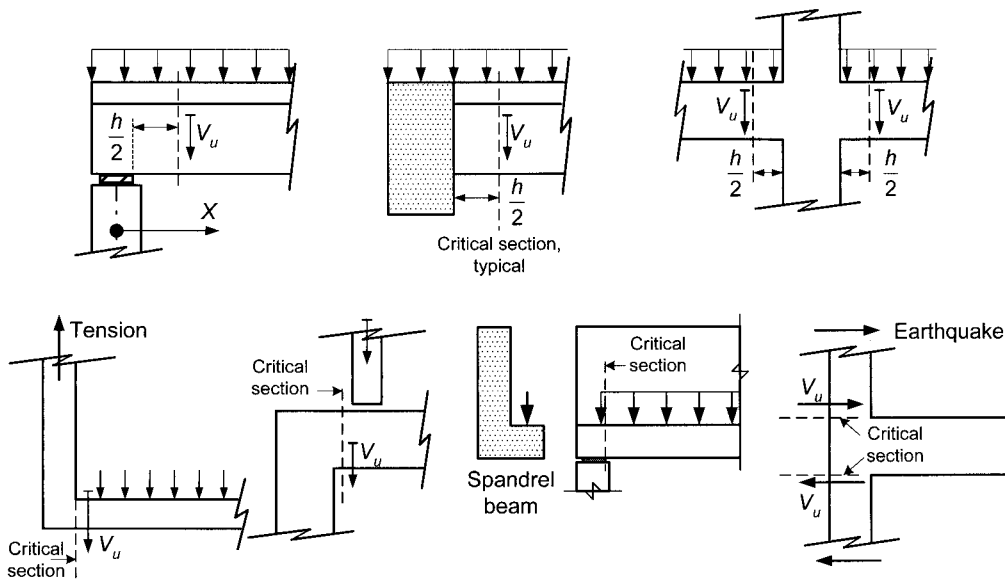

Figure 6.12 Typical support conditions for locating first critical section in shear design.

For nonprestressed members the first critical section for shear is taken at a distance d_s from the face of support, and the shear reinforcement required at that section is extended to the support. Figure 6.11 provides a justification for this assumption by showing that, for a typical shear crack inclined at 45 deg, loads placed

at a distance smaller than d_s transfer directly to the support. For prestressed members, the first critical section for shear is to be taken at $h/2$ from the face of the support and the same shear reinforcement required at $h/2$ is to be used at sections located at a distance less than $h/2$.

However, in some particular cases, the first critical section must be taken at less than $h/2$, as illustrated in the lower part of Fig. 6.12 [Ref. 6.2]. Indeed these are sections where the shear load must be considered at the face of the support.

In the design of slabs and footings, shear reinforcement is not required when $\upsilon_u < \phi\upsilon_c$. Similarly to what is done for beams, the first critical section in each direction is to be taken at $h/2$ from the face of the support (or column). Simultaneously, punching shear must be checked along a critical section perpendicular to the plane of the slab with perimeter b_o (Fig. 6.13) located a distance $d_p/2$ from the perimeter of the concentrated load or reaction area. The value of υ_c to be used for punching shear in prestressed and nonprestressed slabs is explained in Section 11.11.1.

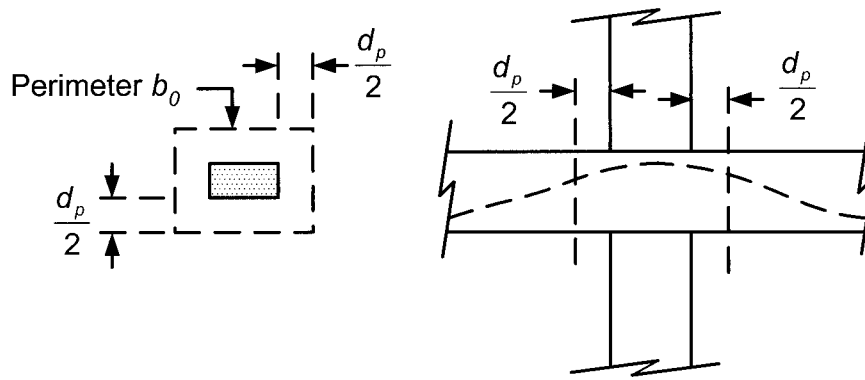

Figure 6.13 Critical section for punching shear in slabs.

6.9 DESIGN EXPEDIENTS

Design for shear can be very time consuming, since one does not know a priori the locations of the critical sections which require more than the minimum amount of reinforcement. It is not uncommon to find out (assuming uniform loading) that excess reinforcement is needed at two sections along the span and is not needed at a section in between.

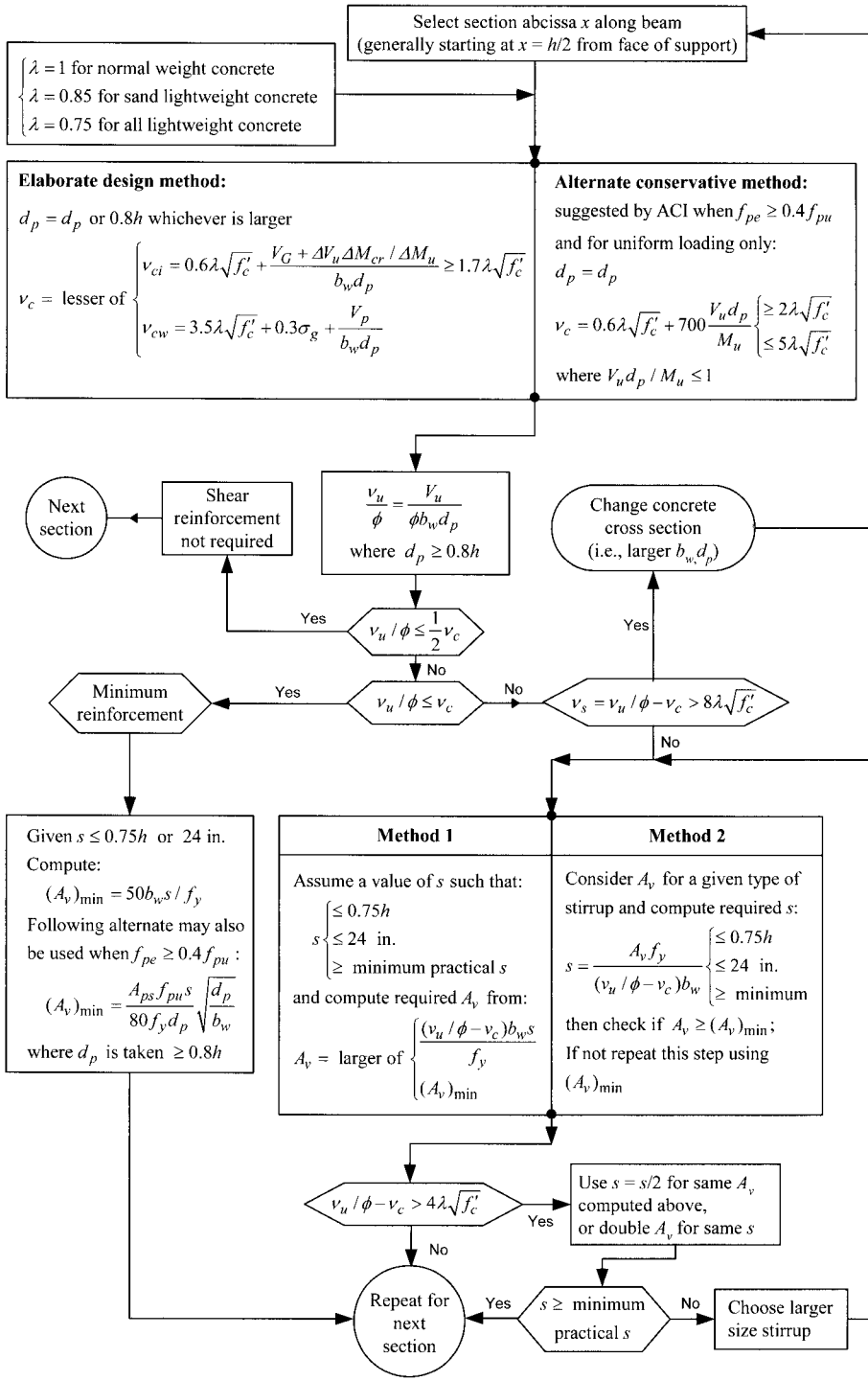

Figure 6.14 Flow chart for the design of shear reinforcement in prestressed beams.

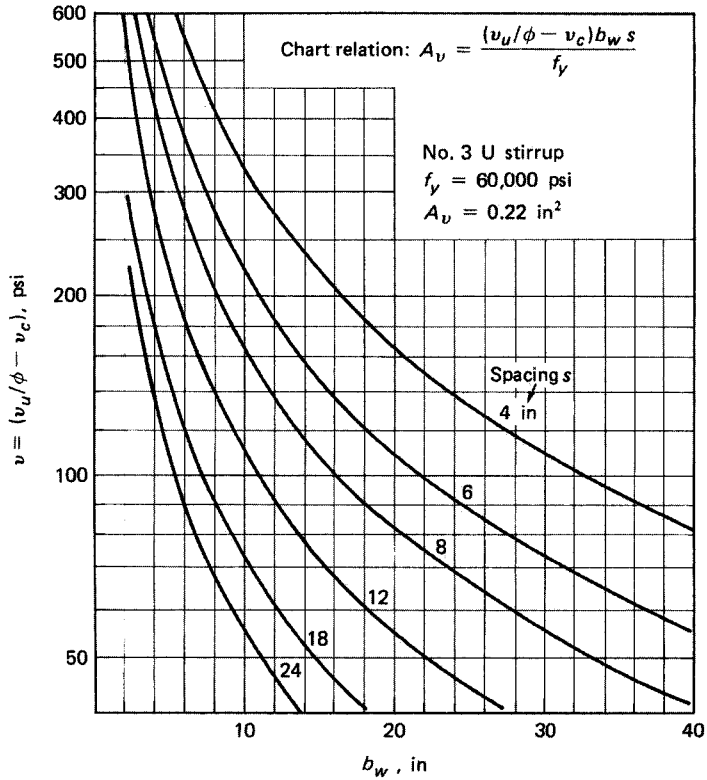

Figure 6.15 Design chart for stirrup spacing.

In most common design problems involving prestressed beams, it is very likely that the minimum amount of shear reinforcement $(A_v)_{\min}$ at the maximum allowable spacing of $0.75h$ or 24 in ($\simeq$ 60 cm) will prevail throughout the span. If the alternative method to determine v_c is considered, its lower bound value of $2\sqrt{f'_c}$ can be used as a first approximation in design and checked against the value of v_u/ϕ at several sections. Only if significant differences exist, the more accurate analysis will be pursued.

In order to ease the design procedure, a design flow chart for shear is proposed in Fig. 6.14. It applies to normal- and light-weight prestressed concrete beams and synthesizes most of the steps encountered if the ACI code approach is followed. As in each complete iteration only one section is considered, it is appropriate to organize the numerical results in a table, such as in Tables 6.1 and 6.2 of the example in Section 6.10.

Once the computations are completed, the results can be directly used to determine stirrups' areas and spacing. However, a graphical representation of the variation of shear stresses and strengths may give a better visual presentation of stirrup distribution along the span. Such a typical graph is shown in Fig. 6.17 for the

example of Section 6.10. As only a discrete number of sections is analyzed, the graph can help isolate graphically the segments of the span where same shear reinforcement and spacing prevail.

Often, in practice, a type of stirrup is selected for a given beam, say a #3 U stirrup, and the spacing is selected at each section according to the design requirements. However, only a discrete number of spacings is considered, such as 4, 6, 8, 12, 18 and 24 in (10, 15, 20, 30, 45 and 60 cm). Thus, one can go backward and, given A_v and a spacing, find graphically the value of $(v_u/\phi - v_c)$ resisted by the shear reinforcement and the corresponding segment of beam where such spacing applies. Charts can be developed to determine the value of $(v_u/\phi - v_c)$ that can be resisted by a certain stirrup at a certain spacing. Using Eq. (6.35) for vertical stirrups, we have:

$$\left(\frac{v_u}{\phi} - v_c\right) = \frac{A_v f_y}{b_w s} \tag{6.41}$$

which can be plotted versus b_w for different values of s, assuming A_v and f_y are given. Such a chart for a #3 U stirrup with f_y = 60 ksi (414 MPa) is given in Fig. 6.15.

6.10 EXAMPLE: DESIGN OF SHEAR REINFORCEMENT

The T beam described in Sections 4.9.1, 4.12.3, and 5.18 is considered (Fig. 6.16). The design characteristics of interest to this example are: h = 40 in, b_w = 8 in, A_c = 550 in^2, A_{ps} = 1.53 in^2, y_t = 12.9 in, Z_b = 3028 in^3, f'_c = 5000 psi (normal weight concrete), F = 229.5 kips, $f_{pe} > 0.4 f_{pu}$, l = 70 ft, live load = 0.4 klf, superimposed dead load = 0.04 klf, self-weight w_G = 0.573 klf. For normal weight concrete, $\lambda = 1$.

The final eccentricity of the prestressing force along the half span was arrived at in Sec. 4.12.3 and is given by:

$$\begin{cases} e_o = 21.7 \text{ in} & \text{for } x \geq 28 \text{ ft} \\ e_o = 7.9 + 13.8\dfrac{x}{28} & \text{for } 0 \leq x < 28 \text{ ft} \end{cases}$$

The corresponding actual values of d_p are given by:

$$\begin{cases} d_p = e_o + y_t = 21.7 + 12.9 = 34.6 \text{ in} & \text{for } x \geq 28 \text{ ft} \\ d_p(x) = e_o(x) + y_t = 20.8 + 13.8\dfrac{x}{28} \text{ in} & \text{for } 0 \leq x < 28 \text{ ft} \end{cases}$$

Let us define the following values of factored loads:

$$w_u = 1.2(0.573 + 0.04) + 1.6 \times 0.4 = 1.3756 \text{ klf}$$

$$\Delta w_u = 1.2(0.04) + 1.6 \times 0.4 = 0.688 \text{ klf}$$

The first critical section to be analyzed is taken at $h/2$ = 20 in from the face of the support. If a support pad eight inches wide is used, the location of the section from the center of the support becomes x = 20 + 8/2 = 24 in or 2 ft.

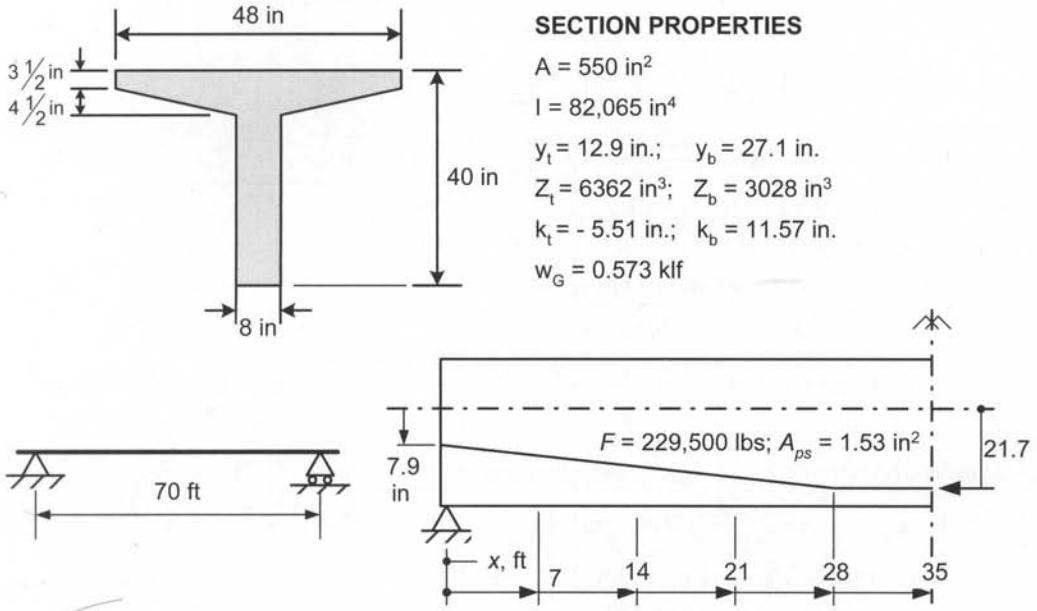

Figure 6.16

Two approaches will be followed, the more elaborate approach and the alternative conservative approach, according to the steps described in the flow chart Fig. 6.14. The computations for the first critical section are covered in detail next. Results obtained for this section and four others are summarized in Tables 6.1 and 6.2.

6.10.1 Elaborate Approach to Determine v_c

The eccentricity of the prestressing force at $x = 2$ ft is given by:

$$e_o = 7.9 + 13.8\frac{2}{28} = 8.9 \text{ in}$$

Thus

$$d_p = e_o + y_t = 8.9 + 12.9 = 21.8 \text{ in}$$

For the equations used in the elaborate approach, d_p is limited by $0.8h = 32$ in. Thus, use $d_p = 32$ in. Following the design flow chart Fig. 6.14, let us first compute v_{ci}. For this, we need the following values:

$$V_G = w_G\left(\frac{l}{2} - x\right) = 0.573 \times 33 = 18.91 \text{ kips}$$

$$\Delta V_u = \Delta w_u\left(\frac{l}{2} - x\right) = 0.688 \times 33 = 22.704 \text{ kips}$$

$$\Delta M_u = \Delta w_u \frac{x(l-x)}{2} = \frac{0.688 \times 2 \times 68}{2} = 46.784 \text{ kips-ft} = 561.41 \text{ kips-in}$$

$$M_G = w_G \frac{x(l-x)}{2} = \frac{0.573 \times 2 \times 68}{2} = 38.964 \text{ kips-ft} = 467.57 \text{ kips-in}$$

$$\Delta M_{cr} = Z_b \left[6\sqrt{f_c'} + \frac{F}{A_c}\left(1 + \frac{e_o A_c}{Z_b}\right)\right] - M_G$$

$$= 3028\left[6\sqrt{5000} + \frac{229{,}500}{550}\left(1 + \frac{8.9 \times 550}{3028}\right)\right] - 467{,}570$$

$$= 4{,}123{,}153 \text{ lb-in} = 4123 \text{ kips-in}$$

Thus, for $\lambda = 1$:

$$\upsilon_{ci} = 0.6\lambda\sqrt{f_c'} + \frac{V_G + (\Delta V_u \times \Delta M_{cr})/\Delta M_u}{b_w d_p}$$

$$= 0.6\sqrt{5000} + 1000\left(\frac{18.91 + (22.704 \times 4123)/561.41}{8 \times 32}\right) = 767.1 \text{ psi} > 1.7\lambda\sqrt{f_c'} = 120 \text{ psi}$$

In order to determine υ_{cw}, we need the following:

$$\sigma_g = \frac{F}{A_c} = \frac{229{,}500}{550} = 417.3 \text{ psi}$$

(*Note:* The centroid is in the web.)

$$\sin\alpha \simeq \tan\alpha = \frac{(e_o)_{28} - (e_o)_{\text{support}}}{28 \times 12} = \frac{21.7 - 7.9}{28 \times 12} = 0.04107$$

$$V_p = F \sin\alpha = 229{,}500 \times 0.04107 = 9426 \text{ lb}$$

Thus:

$$\upsilon_{cw} = 3.5\sqrt{f_c'} + 0.3\sigma_g + \frac{V_p}{b_w d_p}$$

$$= 3.5\sqrt{5000} + 0.3 \times 417.3 + \frac{9426}{8 \times 32} = 247.49 + 125.19 + 36.82 = 409.5 \text{ psi}$$

The shear resistance υ_c is the smaller of υ_{ci} and υ_{cw}. Thus at $x = 2$ ft:

$$\upsilon_c = 409.5 \text{ psi}$$

In order to determine υ_u, we need V_u:

$$V_u = w_u\left(\frac{l}{2} - x\right) = 1.3756(35 - 2) = 45.395 \text{ kips}$$

Thus:

$$\frac{\upsilon_u}{\phi} = \frac{V_u}{\phi b_w d_p} = \frac{45{,}395}{0.75 \times 8 \times 32} = 236.43 \text{ psi}$$

The value of υ_u/ϕ is to be compared to $\upsilon_c/2$ and υ_c. As $\upsilon_u/\phi = 236.43$ psi is more than $\upsilon_c/2$ but less than $\upsilon_c = 409.5$ psi, only minimum reinforcement is needed at this section.

Let us select a stirrup with $f_y = 60$ ksi, at a maximum spacing $s = 24$ in $< 0.75h$. As $f_{pe} > 0.4 f_{pu}$, the minimum area of shear reinforcement is obtained from:

Table 6.1 Summary of shear design computations for Example 6.10.1 using the elaborate method.

Section x, ft	V_G, kips	ΔV_u, kips	ΔM_u, kips-in	ΔM_{cr}, kips-in	d_p or $0.8h$ in	v_{ci}, psi	V_p, kips	v_{cw}, psi	v_c, psi	V_u, kips	v_u/ϕ, psi	$v_u/\phi - v_c$ psi	$\left(\frac{v_u}{\phi}-\frac{v_c}{2}\right)$ psi	A_v for s or s for A_v	$(A_v)_{min}$ at s_{max}
$0.5h = 2$	18.91	22.70	561.41	4123	32	767.1	9.426	409.5	409.5	45.395	236.4	negative	> 0		
$l/20 = 3.5$	18.05	21.672	960.79	3958	32	446.6	9.426	409.5	409.5	43.331	225.7	negative	> 0		(0.13 in^2
$2l/20 = 7$	16.044	19.260	1820.45	3638	32	255	9.426	409.5	255.3	38.517	200.6	negative	> 0		required)
$3l/20 = 10.5$	14.039	16.856	2578.97	3402	32	184	9.426	409.5	184	33.702	175.5	negative	> 0	use next	
$4l/20 = 14$	12.033	14.448	3236.35	3250	32	146	9.426	409.5	146	28.888	150.5	4.5	> 0	column	(0.22 in^2
.	.	.	.	.	.	121	9.426	409.5	146	.	.	.	(min.		provided
.	.	.	.	.	.	120	9.426	409.5	.	.	.	.	reinf.		at 24 in
$8l/20 = 28$	.	.	.	.	.	120	0	372.7	.	.	.	.	required)		spacing)
$l/2 = 35$						120	0	372.7	.	.	.	.			

Table 6.2 Summary of shear design computations for Example 6.10.2 using the conservative method.

Section	Distance x, ft	d_p, in	V_u, kips	M_u, kips-in	$\frac{V_u d_p}{M_u} \le 1$	$v_c \begin{cases} \le 5\sqrt{f'_c} \\ \ge 2\sqrt{f'_c} \end{cases}$ psi	$\frac{v_u}{\phi} = \frac{V_u^{\dagger}}{\phi b_w d_p}$ psi	$\left(\frac{v_u}{\phi}-v_c\right)$ psi	$\left(\frac{v_u}{\phi}-\frac{v_c}{2}\right)$ psi	A_v for s *or* s for A_v	$(A_v)_{min}$ at s_{max}
$0.5h$	2	21.8	45.395	1122.49	0.88	~~658~~, 353.5	236.4	Negative	> 0		
$l/20$	3.5	22.52	43.331	1921.02	0.51	~~399~~, 353.5	225.7	Negative	> 0		(0.13 in^2 required)
$2l/20$	7	24.25	38.517	3639.84	0.26	224.4	200.6	Negative	> 0	use next	
$3l/20$	10.5	25.8	33.702	5156.44	0.17	161.4	175.5	14.1	> 0	column	(0.22 in^2
$4l/20$	14	27.7	28.888	6470.82	0.12	~~126~~, 141.4	150.5	9.1	> 0		provided
.	.	.	.	.	.	.	.	.	(min.		at 24 in
.	.	.	.	.	.	.	.	.	reinf.		spacing
.	.	.	.	.	.	.	.	.	required)		throughout)
$l/2$											

† $d_p = d_p$ or $0.8h$ whichever is larger

$$(A_v)_{\min} = \frac{A_{ps} f_{pu} s}{80 f_y d_p}\sqrt{\frac{d_p}{b_w}} = \frac{1.53\times 270\times 24}{80\times 60\times 32}\sqrt{\frac{32}{8}} \simeq 0.13 \text{ in}^2$$

Note, a #3 U stirrup at a spacing of 24 in would provide 0.22 in^2 and thus would be adequate. The other sections covered in Table 6.1 lead to the same minimum reinforcement.

If, instead of selecting the spacing in the above equation, we would have selected the area of a #3 U stirrup, the required spacing would have been $s = 40.9$ in. Of course, then the maximum allowable spacing of 24 in would control, leading to the same result.

The alternate equation for minimum shear reinforcement would have given:

$$(A_v)_{\min} = \text{ larger of } \begin{cases} 50\dfrac{b_w s}{f_y} = 50\dfrac{8\times 24}{60{,}000} = 0.16 \text{ in}^2 \\ 0.75\sqrt{f'_c}\dfrac{b_w s}{f_y} = 53\dfrac{8\times 24}{60{,}000} = 0.17 \text{ in}^2 \end{cases}$$

It is also smaller than the reinforcement area of 0.22 in^2 provided.

Note that for a given area of reinforcement at a given spacing the maximum shear stress to be resisted by the reinforcement can be determined. In this case, we have:

$$\left(\frac{v_u}{\phi} - v_c\right) \le \frac{A_v f_y}{b_w s} = \frac{0.22\times 60{,}000}{8\times 24} \simeq 69 \text{ psi}$$

6.10.2 Alternate Conservative Approach to Determine v_c

In order to compute v_c, we need:

$V_u = 45.395$ kips (calculated above)

$$M_u = w_u \frac{x(l-x)}{2} = \frac{1.3756\times 2\times 68}{2} = 93.541 \text{ kips-ft} = 1122.5 \text{ kips-in}$$

$d_p = 21.8$ in

$$\frac{V_u d_p}{M_u} = 0.8816 < 1 \text{ OK}$$

Thus, for $\lambda = 1$:

$$v_c = 0.6\lambda\sqrt{f'_c} + 700\frac{V_u d_p}{M_u} = 42.43 + 700\times 0.8816 = 659.5 \text{ psi}$$

v_c is larger than $2\lambda\sqrt{f'_c} = 141.4$ psi but should be taken less than $5\lambda\sqrt{f'_c} = 353.5$ psi. Thus, use $v_c = 353.5$ psi. Results for the other sections are summarized in Table 6.2.

If we compare v_u/ϕ and v_c, we find out that, similarly to the previous case, a minimum reinforcement is sufficient.

6.10.3 Design for Increased Live Load: Partially Prestressed Beam

To illustrate a case where more than the minimum reinforcement is needed, let us assume that the specified live load for the previous example is increased from 0.4 klf to 1 klf. Let us also assume that the beam is designed as a partially prestressed beam, whereas the amount and profile of the prestressing steel are the same as described above but, in order to balance the increase in the required resistance, nonprestressed reinforcement is added. It amounts to four #9 bars with $A_s = 4$ in^2, $f_y = 60$ ksi, and $d_s = 36$ in at midspan. For simplicity, use d_p for the computation of v_c.

Table 6.3 Summary of shear design computations for Example 6.10.3.

Section, x (ft)	ΔV_u, kips	ΔM_u, kips-in	υ_{ci}, psi	υ_{cw}, psi	υ_c, psi	V_u, kips	υ_u/ϕ, psi	$\frac{\upsilon_u}{\phi}-\upsilon_c$, psi	Required s for A_υ = 0.22 in^2
$0.5h = 2$	54.384	1,344.8	767.1	409.5	409.5	77.075	401.4	.....	24 max.
$l/20$	51.912	2,301.4	446.6	409.5	409.5	73.571	383.2	.....	24 max.
$2l/20 = 7$	46.144	4,360.6	255	409.5	255	65.397	340.6	86	19.2
$3l/20$	40.376	6,177.5	184	409.5	183	57.222	298	115	14.3
$4l/20 = 14$	34.608	7,752.2	146	409.5	146	49.048	255.5	110	15
$5l/20$	28.840	9,084.6	121	409.5	121	40.873	212.9	92	18
$6l/20 = 21$	23.072	10,174.8	120	409.5	120	32.698	170.3	50	24 max.
$7l/20$	17.304	11,022.6	120	408.5	120	24.524	124.3	4	24 max.
$8l/20 = 28$	11.536	11,628.3	120	372.7	120	16.349	78.7	.....	24 max.
$9l/20$	5.768	11,992.7	120	372.7	120	8.175	39.4	.....	24 max.
$l/2 = 35$	0	12,112.8	120	372.7	120	0	0	.....	24 max.

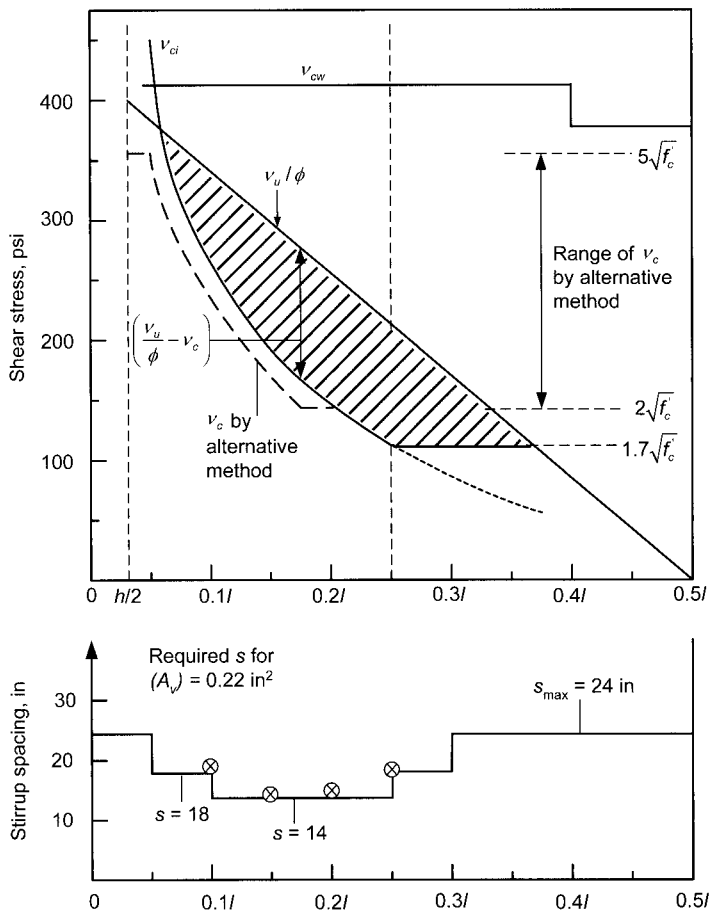

Figure 6.17 Shear stress distribution and stirrups spacing for example beam.

For this case, the values of V_G, d_p, M_{cr}, and V_p are the same as in the example of Section 6.10.1 and are given in Table 6.1. Due to the increase in live load, the following values of factored loads apply:

$$w_u = 1.2(0.573 + 0.04) + 1.6 \times 1 = 2.3356 \text{ klf}$$

$$\Delta w_u = 1.2 \times 0.04 + 1.6 \times 1 = 1.648 \text{ klf}$$

The corresponding computations ΔV_u, ΔM_u, υ_{ci}, υ_{cw}, υ_c, and the required spacing (Eq. (6.37)) of #3 U stirrups are summarized in Table 6.3. It can be observed that, although the live load has been substantially increased, the required amount of shear reinforcement is still relatively small. If the alternative conservative approach was used, the value of υ_c would have been the same as shown in Table 6.2. This is because the ratio V_u / M_u remains the same with an increase in uniform live load. The values of υ_{ci}, υ_{cw}, and υ_c, as well as the required stirrup spacing, are plotted versus x in Fig. 6.17. The shaded area corresponds to the part of the beam where stirrups are theoretically needed. It can be seen that the greatest need for stirrups is not near the support but instead in a region where flexure-shear cracking may control, here between $0.10l$ and $0.25l$.

To illustrate design of stirrups, consider the section at $x = 3l/20$ from the left support. Using Eq. (6.37) and No. 3 U-shaped stirrups leads to:

$$s = \frac{A_v f_y}{(\upsilon_u / \phi - \upsilon_c) b_w} = \frac{0.22 \times 60{,}000}{115 \times 8} = 14.35 \text{ in}$$

Table 6.3 gives the results for the other sections. Figure 6.17 provides a graphical illustration of shear resistance by the concrete, shear demand due to loading, and required stirrup spacing along the span.

Finally, note that, although shear may not be critical near the support, additional stirrups are needed to contain tensile splitting cracks in the end zone (see Section 4.17).

6.11 DERIVATION OF CONCRETE NOMINAL SHEAR STRENGTH EQUATIONS (ACI CODE)

The derivation of Eqs. (6.29) and (6.31), on which the ACI shear design provisions for prestressed concrete are based, is given in the commentary of the 1963 ACI code. It is essentially based on the work of MacGregor, Sozen, and Seiss [Refs. 6.28 and 6.29]. For flexure-shear cracking, their tests have indicated that, in order to reduce the capacity of a beam, a diagonal crack must have a projection on the longitudinal axis of the beam at least equal to the depth of the beam d. (d is used here instead of d_s to comply with the original notation; use d_p for fully prestressed beams.)

Flexure-Shear Cracking. Let us consider a section along the beam of abscissa x with respect to the support (Fig. 6.18). A flexural crack distant d from x in the direction of decreasing moments may lead to a diagonal crack which could be critical for section x. Tests have indicated that failure becomes imminent when a second flexural crack occurs at a distance $d/2$ from x and extends to the centroid of the section where the increase in the principal tensile stress triggers diagonal cracking. Collapse occurs for an additional load, the effects of which are described later. Let

us evaluate the load that led to the second flexural crack. The change in moment from section x to section $(x-d/2)$ is equal to the area under the shear diagram between these two sections. That is:

$$M - M_{cr} = \left(\frac{V + V_{cr}}{2}\right)\frac{d}{2} \tag{6.42}$$

where M and V are the moment and shear at section x and M_{cr} and V_{cr} are the cracking moment and corresponding shear at section $(x-d/2)$. The difference between V and V_{cr} over $d/2$ is generally small. Thus, as a first approximation:

$$M - M_{cr} = \frac{Vd}{2} \tag{6.43}$$

or

$$\frac{M}{V} - \frac{M_{cr}}{V} = \frac{d}{2} \tag{6.44}$$

from which:

$$V = \frac{M_{cr}}{M/V - d/2} \tag{6.45}$$

where V is the shear at section x. Note that V appears on the two sides of the equation. However, V can still be computed, because the ratio M/V remains constant at a given section when the applied load increases proportionately.

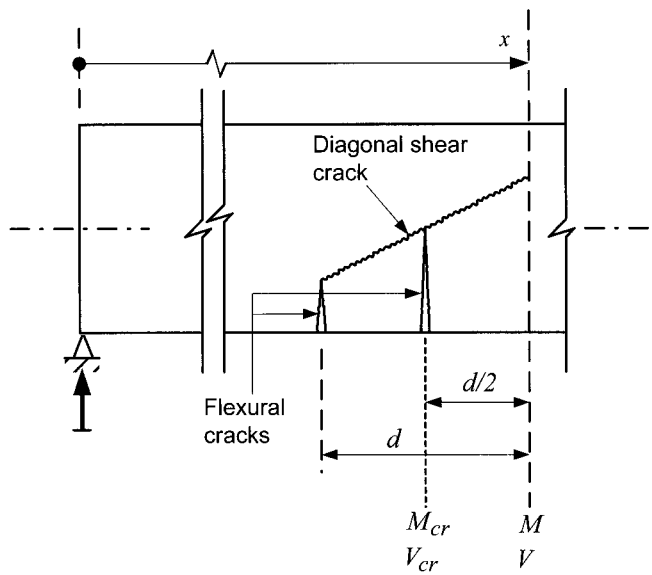

Figure 6.18 Flexure-shear cracking model.

It can be assumed that, in a beam test, the shear given by Eq. (6.45) is generated by external loads. In design, these loads are represented by superimposed dead loads and live loads. The corresponding shear acts in addition to the dead load shear V_G. Moreover, as mentioned earlier, tests have indicated that, in order for collapse to occur after development of the second flexural crack, a shear force increment estimated at $0.6\sqrt{f'_c}b_w d$ is needed. Hence, the total shear force V_{ci}, which will produce a flexure-shear failure, can be estimated from:

$$V_{ci} = 0.6\sqrt{f'_c}b_w d + \frac{M_{cr}}{M/V - d/2} + V_G \tag{6.46}$$

The above relationship is compared to actual data in Fig. 6.19 [taken from ACI SP10, 1965]. To simplify the above equation, the term $d/2$ is deleted, leading to a safer design limit. As M, V, and M_{cr} are due to additional external loads (superimposed dead load and live load), and as nominal shear resistance at ultimate is sought, they are replaced, using the notation of this text, by ΔM_u, ΔV_u, and ΔM_{cr}. Hence, Eq. (6.46) becomes:

$$V_{ci} = 0.6\sqrt{f'_c}b_w d + \frac{\Delta M_{cr}}{\Delta M_u / \Delta V_u} + V_G \tag{6.47}$$

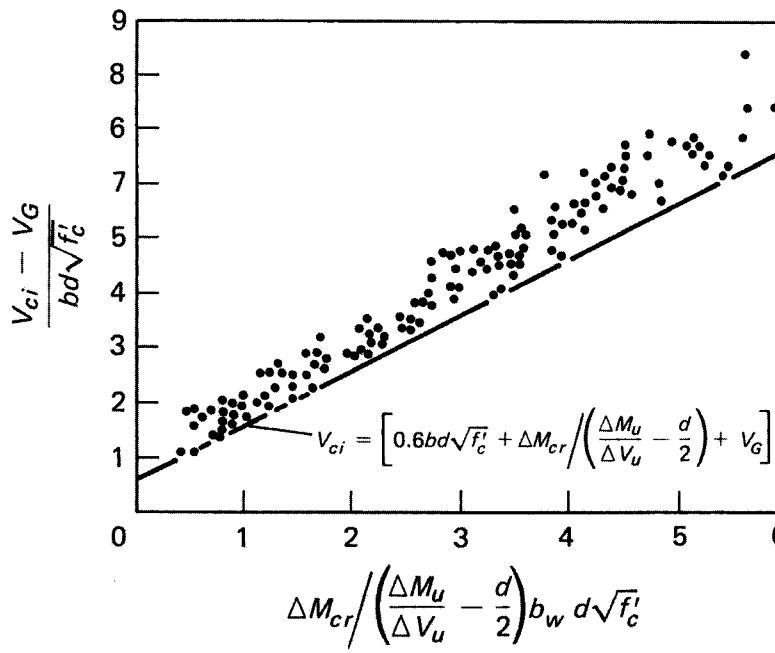

Figure 6.19 Comparison of Eq. (6.46) with experimental data [Ref. ACI SP10, 1965].

Dividing the two sides of Eq. (6.47) by $b_w d$ leads essentially to the flexure-shear strength (stress) υ_{ci}, given by Eq. (6.29).

Web-Shear Cracking. Web-shear cracking occurs when the maximum principal tensile stress becomes equal to the tensile strength of the concrete, f'_{tc}. The principal tensile stress is assumed maximum at the centroid of the section. Using Eq. (6.3) and assuming all stresses are positive (to keep up with the original derivation), the following relationship is derived to represent the onset of web-shear cracking:

$$f'_{tc} = \sqrt{\upsilon_{cw}^2 + \left(\frac{\sigma_g}{2}\right)^2} - \frac{\sigma_g}{2} \tag{6.48}$$

where σ_g is the compressive stress at the concrete centroid due to the effective prestressing force and υ_{cw} is the critical shear stress at web-shear cracking. Solving for υ_{cw} leads to:

$$\upsilon_{cw} = f'_{tc}\sqrt{1 + \frac{\sigma_g}{f'_{tc}}} \tag{6.49}$$

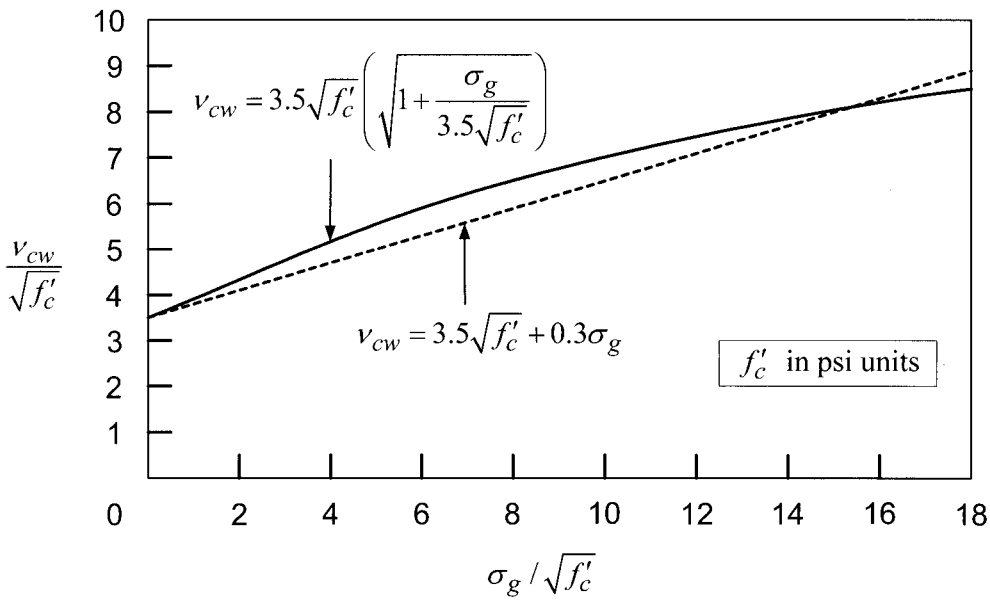

Figure 6.20 Nominal shear stress at web-shear cracking [Ref. ACI SP10, 1965].

The magnitude of f'_{tc} indicated by tests appears to be about $4\sqrt{f'_c}$. It is conservatively set equal to $3.5\sqrt{f'_c}$. Hence, Eq. (6.49) becomes:

$$\upsilon_{cw} = 3.5\sqrt{f'_c}\sqrt{1+\frac{\sigma_g}{3.5\sqrt{f'_c}}} \tag{6.50}$$

The curve representing Eq. (6.50) is plotted in Fig. 6.20 and compared to that representing a simplified form given by:

$$\upsilon_{cw} = 3.5\sqrt{f'_c} + 0.3\sigma_g \tag{6.51}$$

As the two curves are close, the simplified form is selected for design. In prestressed concrete, the shear stress value given by Eq. (6.51) is augmented by the shear stress generated by the vertical component of the prestressing force. It essentially leads to the nominal web-shear cracking resistance υ_{cw} given by Eq. (6.31).

6.12 AASHTO GENERAL PROCEDURE FOR SHEAR DESIGN

The AASHTO LRFD code recommends two possible approaches to design for shear:

1. Strut-and-tie model which applies at the level of the member and thus covers simultaneously many sections or regions along the member. A brief introduction to strut-and-tie modeling is given in Chapter 15.
2. Modified compression field theory which applies at the level of the section, that is, the design is carried out section by section in a manner similar to the procedure followed by the ACI code and explained in Section 6.8.

In the following treatment, only the sectional model is briefly summarized. It is based on the modified compression field theory which applies to shear as well as shear combined with torsion. The theory was initially developed by Mitchell and Collins [Refs. 6.7, 6.8, 6.9, 6.37, 6.38, 6.39], as the compression field theory, and later modified by Vecchio and Collins [6.46, 6.47]; it is an extension of the general truss model with the modified assumption that cracked concrete provides some resistance to shear. The main basis of the theory as reduced to code implementation is summarized in Fig. 6.21. The truss model, the struts at angle θ, equilibrium of forces in the longitudinal and transverse directions, and stresses in the Mohr's circle are all illustrated in the figure, which will help understand the equations used in the code. Note that the figure relates to a section with zero moment, and describes the tensile force N_v that develops in the longitudinal reinforcement due to shear only.

The modified compression field theory leads to a procedure and equations totally different from those used by the ACI code. Unlike the truss model for shear,

the modified compression field theory assumes that the concrete contributes some resistance in tension through concrete struts in between diagonal shear cracks. Since it was first adopted in the 1993 draft of the AASHTO LRFD code, the procedure has seen several refinements and adjustments which are simply reported here without explanation, and in accordance with the AASHTO LRFD code, Interim 2002, Article 5.8.3 [Ref. 6.1]. To minimize confusion, the notation and sign convention of AASHTO is adopted in this section.

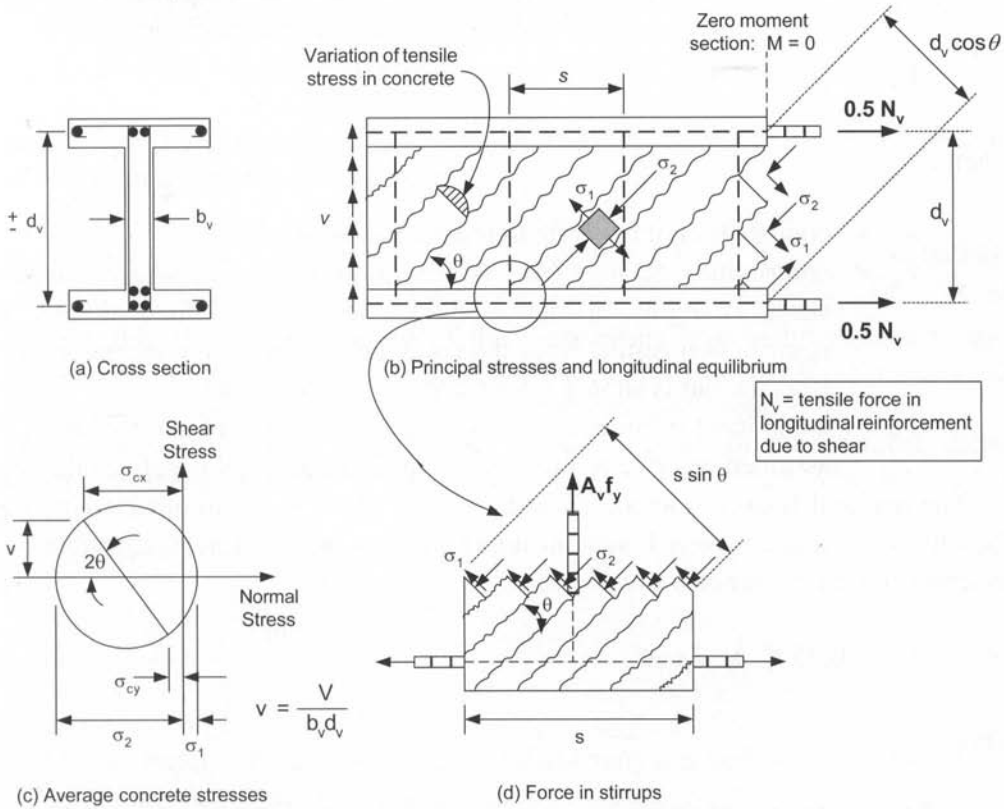

Figure 6.21 Equilibrium in concrete strut and steel tie according to the modified compression field theory. *(Adapted from Collins and Mitchell, 1997).*

6.12.1 General Sectional Procedure for Shear Design

In line with the general approach for LRFD or USD, the following equation must be satisfied at each section:

$$V_r = \phi V_n \geq V_u \tag{6.52}$$

where:

V_r = design shear resistance
V_n = nominal shear resistance

V_u = factored shear force
ϕ = capacity reduction factor = 0.9 for normal weight concrete, and 0.7 for structural lightweight concrete.

The nominal shear resistance at a given section is expressed as the sum of contributions from the concrete, the transverse reinforcement (i.e., shear reinforcement or strirrups), and the transverse component of the prestressing force, as follows:

$$V_n = V_c + V_s + V_p \tag{6.53}$$

where:

V_c = contribution of concrete to member shear strength
V_s = contribution of steel (that is stirrups or transverse steel) to member shear strength; in the modified compression field theory, this contribution results from the combined action of a concrete strut and steel tie, but is simply referred to as steel contribution
V_p = component of prestressing force in the direction of applied shear; it is assumed positive if it resists the applied shear and negative otherwise.

The nominal shear resistance V_n given by Eq. (6.53) is constrained according to the following equation which sets an upper limit on the combined contribution of concrete and transverse reinforcement:

$$V_n \leq 0.25 f'_c \, b_v \, d_v + V_p \tag{6.54}$$

where:

f'_c = design compressive strength of concrete at 28 days (ksi), taken less than 10 ksi
b_v = effective web width (in) taken as the minimum web width within the effective depth, d_v, modified for the presence of ducts, where applicable. For posttensioned members, b_v can be computed from the web width minus half the diameter of ungrouted ducts, or one quarter the diameter of grouted ducts.
d_v = effective shear depth (in); it is taken approximately equal ($d_e - a/2$) in which a is the depth of the stress block at nominal bending resistance of the midspan or critical section.

The effective depth d_v is also calculated from:

$$d_v = \text{larger of} \begin{cases} 0.9d_e \\ \text{or} \\ 0.72h \end{cases} \tag{6.55}$$

where:

d_e = effective depth for bending, that is, distance from extreme compression fiber to centroid of the tensile force in the tensile reinforcement at nominal bending resistance

h = overall member depth, (in)

Assuming vertical shear in a typical beam, the vertical or transverse component of the prestressing force is obtained from:

$$V_p = F \sin \alpha \tag{6.56}$$

where α is the angle of inclination of the prestressing force with respect to the longitudinal axis of the beam. A similar approach can be followed if the prestressed member is not horizontal such as in the case of a transversally loaded column.

The contribution of the concrete and transverse steel to the nominal shear resistance is estimated from:

$$V_c = 0.0316\, \beta \sqrt{f'_c}\, b_v d_v \tag{6.57}$$

$$V_s = \frac{A_v f_y d_v \cot \theta}{s} \tag{6.58}$$

where:

β = factor indicating the ability of diagonally cracked concrete to transmit tension between cracks

A_v = area of transverse reinforcing steel (in^2) within a distance s (in)

f_y = yield strength of the transverse steel reinforcement (ksi)

θ = angle of inclination of diagonal compressive struts (Fig. 6.21).

Equation 6.58 implies stirrups at 90 degrees to the member longitudinal axis. The angle θ is assumed to be a variable with a possible range from about 24 to 45 degrees. In comparison, typically ACI assumes a constant value of $\theta = 45$ degrees for reinforced concrete, and 37.5 degrees for prestressed concrete.

The factor 0.0316 is equal $1/\sqrt{1000}$ and converts the numerical results from psi to ksi. Thus, expressed in psi, the shear stress resistance provided by the concrete is $\beta\sqrt{f'_c}$. The coefficient β should be compared with the equivalent value used in the ACI code for reinforced concrete ($\beta = 2$) and for prestressed concrete. If we consider the limits set by the ACI code for the expressions of v_{ci}, and v_c (Eqs. 6.29

and 6.32) then we note that their equivalent β ranges from 1.7 (lower limit for v_{ci}) to 5 (upper limit for v_c by the conservative method). Comparatively in the AASHTO LRFD code, the value of β ranges from 1.29 to 6.32 (Table 6.4) for members with at least minimum transverse reinforcement.

In order to determine V_c and V_s, β and θ are needed. For nonprestressed concrete sections not subjected to axial tension and containing at least the minimum amount of transverse reinforcement, or having an overall depth of less than 16 in (400 mm), the values of β and θ can be conservatively taken as 2 and 45 degrees, respectively. Otherwise, and for prestressed members, β and θ are calculated from the following variables:

- v / f'_c, that is, the ratio between the shear stress at ultimate, v (Eq. 6.59), and the concrete compressive strength, f'_c
- ε_x, that is, the longitudinal strain in the web, assumed positive for tension
- s_x, that is, the crack spacing; this parameter is needed only for members without transverse reinforcement.

Physically, the longitudinal strain ε_x can be regarded as an average (smeared) strain in a reinforced concrete tensile tie (see also Remarks in Section 6.12.2).

The shear stress v is determined from:

$$v = \frac{V_u - \phi V_p}{\phi b_v d_v} \tag{6.59}$$

Assuming first an estimated value of the angle θ, the longitudinal strain ε_x is calculated from:

- For sections with at least minimum transverse reinforcement:

$$\varepsilon_x = \frac{\frac{M_u}{d_v} + 0.5N_u + 0.5\,(V_u - V_p)\cot\theta - A_{ps}f_{po}}{2\,(E_s A_s + E_p A_{ps})} \tag{6.60a}$$

- For sections with less than minimum transverse reinforcement:

$$\varepsilon_x = \frac{\frac{M_u}{d_v} + 0.5N_u + 0.5\,(V_u - V_p)\cot\theta - A_{ps}f_{po}}{E_s A_s + E_p A_{ps}} \tag{6.60b}$$

where:

M_u = factored moment at section considered (kip-in); it should be taken $\geq V_u d_v$

N_u = factored axial force taken positive if tensile (kips)

f_{po} = stress in the prestressing steel (ksi) which can be conservatively taken equal to the effective prestress f_{pe} . (See discussion in the remarks at the end of this section.)

E_s, E_{ps} = modulus of elasticity (ksi) of reinforcing steel and prestressing steel, respectively

A_s, A_{ps} = cross sectional area (in^2) of non prestressed reinforcement, and prestressing steel on the flexural tension side of a member, respectively.

If the calculated longitudinal strain ε_x from Eq. (6.60) is found negative, its value should then be determined from:

$$\varepsilon_x = \frac{\frac{M_u}{d_v} + 0.5N_u + 0.5\,(V_u - V_p)\cot\theta - A_{ps}f_{po}}{2\,(E_c\,A_{cf} + E_s\,A_s + E_p\,A_{ps})} \tag{6.60c}$$

where:

A_{cf} = area of concrete (in^2) on the flexural tension side of the member up to half its depth (Fig. 6.22)

E_c = modulus of elasticity of concrete (ksi)

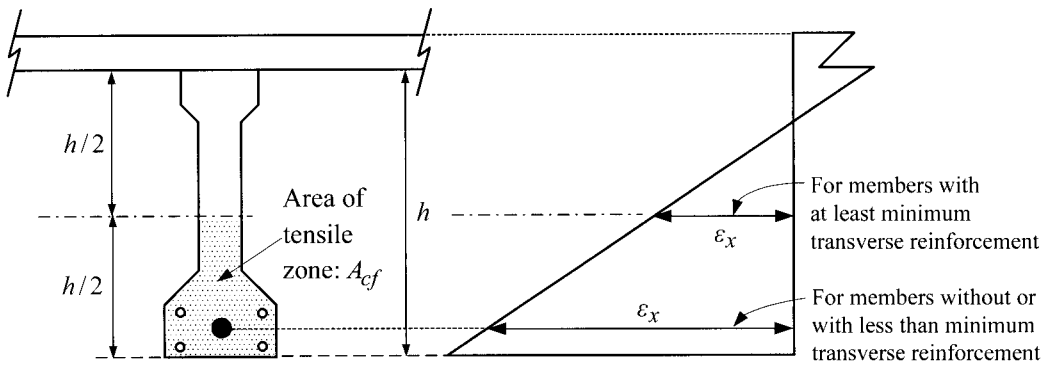

Figure 6.22 Definition of area of tensile zone.

Compared to Eq. (6.60a), Eq. (6.60c) introduces in the denominator the contribution of concrete area, A_{cf}. A_{cf} is defined as the area of concrete on the flexural tensile side of the section, below half the depth of the section, as shown in Fig. 6.22. Thus for a section symmetrical with respect to the x axis, $A_{cf} = 0.5A_c$. For a composite beam, the h is that of the precast section.

Table 6.4 Values of θ and β for concrete sections with at least minimum transverse steel reinforcement (from AASHTO LRFD, Interim 2002).

$\frac{v}{f'_c}$	$\varepsilon_x \times 1{,}000$										
	≤-0.20	≤-0.10	≤-0.05	≤0	≤0.125	≤0.25	≤0.50	≤0.75	≤1.0	≤1.5	≤2.0
≤ 0.075	22.3	20.4	21.0	21.8	24.3	26.6	30.5	33.7	36.4	40.8	43.9
	6.32	4.75	4.10	3.75	3.24	2.94	2.59	2.38	2.23	1.95	1.67
≤ 0.100	18.1	20.4	21.4	22.5	24.9	27.1	30.8	34.0	36.7	40.8	43.1
	3.79	3.38	3.24	3.14	2.91	2.75	2.50	2.32	2.18	1.93	1.69
≤ 0.125	19.9	21.9	22.8	23.7	25.9	27.9	31.4	34.4	37.0	41.0	43.2
	3.18	2.99	2.94	2.87	2.74	2.62	2.42	2.26	2.13	1.90	1.67
≤ 0.150	21.6	23.3	24.2	25.0	26.9	28.8	32.1	34.9	37.3	40.5	42.8
	2.88	2.79	2.78	2.72	2.60	2.52	2.36	2.21	2.08	1.82	1.61
≤ 0.175	23.2	24.7	25.5	26.2	28.0	29.7	32.7	35.2	36.8	39.7	42.2
	2.73	2.66	2.65	2.60	2.52	2.44	2.28	2.14	1.96	1.71	1.54
≤ 0.200	24.7	26.1	26.7	27.4	29.0	30.6	32.8	34.5	36.1	39.2	41.7
	2.63	2.59	2.52	2.51	2.43	2.37	2.14	1.94	1.79	1.61	1.47
≤ 0.225	26.1	27.3	27.9	28.5	30.0	30.8	32.3	34.0	35.7	38.8	41.4
	2.53	2.45	2.42	2.40	2.34	2.14	1.86	1.73	1.84	1.51	1.39
≤ 0.250	27.5	28.6	29.1	29.7	30.6	31.3	32.8	34.3	35.8	38.6	41.2
	2.39	2.39	2.33	2.33	2.12	1.93	1.70	1.58	1.50	1.38	1.29

Table 6.5 Values of θ and β for concrete sections without or with less than minimum transverse steel reinforcement (from AASHTO LRFD, Interim 2002).

s_{xe}	$\varepsilon_x \times 1{,}000$										
(in)	≤-0.20	≤-0.10	≤-0.05	≤0	≤0.125	≤0.25	≤0.50	≤0.75	≤1.00	≤1.50	≤2.00
≤ 5	25.4	25.5	25.9	26.4	27.7	28.9	30.9	32.4	33.7	35.6	37.2
	6.36	6.06	5.56	5.15	4.41	3.91	3.26	2.86	2.58	2.21	1.96
≤ 10	27.6	27.6	28.3	29.3	31.6	33.5	36.3	38.4	40.1	42.7	44.7
	5.78	5.78	5.38	4.89	4.05	3.52	2.88	2.50	2.23	1.88	1.65
≤ 15	29.5	29.5	29.7	31.1	34.1	36.5	39.9	42.4	44.4	47.4	49.7
	5.34	5.34	5.27	4.73	3.82	3.28	2.64	2.26	2.01	1.68	1.46
≤ 20	31.2	31.2	31.2	32.3	36.0	38.8	42.7	45.5	47.8	50.9	53.4
	4.99	4.99	4.99	4.61	3.65	3.09	2.46	2.09	1.85	1.52	1.31
≤ 30	34.1	34.1	34.1	34.2	38.9	42.3	46.9	50.1	52.6	56.3	59.0
	4.45	4.45	4.45	4.43	3.39	2.82	2.19	1.84	1.60	1.30	1.10
≤ 40	36.6	36.6	36.6	36.6	41.2	45.0	50.2	53.7	56.3	60.2	63.0
	4.06	4.06	4.06	4.06	3.20	2.62	2.00	1.66	1.43	1.14	0.95
≤ 60	40.8	40.8	40.8	40.8	44.5	49.2	55.1	58.9	61.8	65.8	68.6
	3.50	3.50	3.50	3.50	2.92	2.32	1.72	1.40	1.18	0.92	0.75
≤ 80	44.3	44.3	44.3	44.3	47.1	52.3	58.7	62.8	65.7	69.7	72.4
	3.10	3.10	3.10	3.10	2.71	2.11	1.52	1.21	1.01	0.78	0.62

Once ε_x is obtained for the assumed angle θ, the shear factor β and a new value for the angle θ can be read from Tables 6.4 and 6.5 (Tables 5.8.3.4.2-1 and 5.8.3.4.2-2 of the AASHTO LRFD). However, in order to verify the validity of the selected

angle θ and corresponding factor β, the new angle θ must be compared with the previously assumed value. If they differ, the procedure should then be repeated until the new and previously assumed angles θ are about equal.

Alternatively, the design procedure can be started by assuming a value of ε_x. Then, values of θ and β are read from Tables 6.4 or 6.5 and a new value of ε_x is determined using Eq. (6.60). If the calculated value of ε_x is equal to or smaller than the previously assumed value of ε_x, then the values of θ and β could be used for design. Otherwise, a new value of ε_x must be assumed. This process is illustrated in the flow chart Fig. 6.23 which is adapted from the AASHTO LRFD code. Typically, to start the iteration a value of $\varepsilon_x = 0.0005$ can be selected.

Note that Table 6.4 applies to concrete sections with at least minimum transverse steel reinforcement, while Table 6.5 applies to sections without transverse steel reinforcement or with transverse reinforcement less than the minimum required.

In order to determine θ and β in members with no transverse steel reinforcement or with web reinforcement less than the minimum required, the crack spacing parameter in Table 6.5, s_{xe}, is needed; it can be estimated from:

$$s_{xe} = s_x \frac{1.38}{a_g + 0.63} \leq 80 \text{ in} \tag{6.61}$$

where:

a_g = maximum aggregate size (in)

s_x = the lesser of either of the following two values, namely:

- d_v for members without stirrups and with conventional longitudinal reinforcement, or
- for members without stirrups but with well distributed longitudinal reinforcement, the maximum distance between layers of longitudinal reinforcement, provided the area of reinforcement in each layer is not less than $0.003 b_w s_x$ (see AASHTO Fig. C5.8.3.4.2-2).

With β and θ known, the concrete contribution to shear strength, V_c, is calculated from Eq. (6.57), and the required steel contribution to shear strength can then be determined from:

$$V_s = \frac{V_u}{\phi} - V_p - V_c = \frac{V_u}{\phi} - V_p - 0.0316\,\beta\,\sqrt{f'_c}\,b_v\,d_v \tag{6.62}$$

Finally, for a given area of transverse reinforcement, A_v, assumed normal to the longitudinal reinforcement, the required stirrup spacing can be determined from Eq. (6.58) as follows:

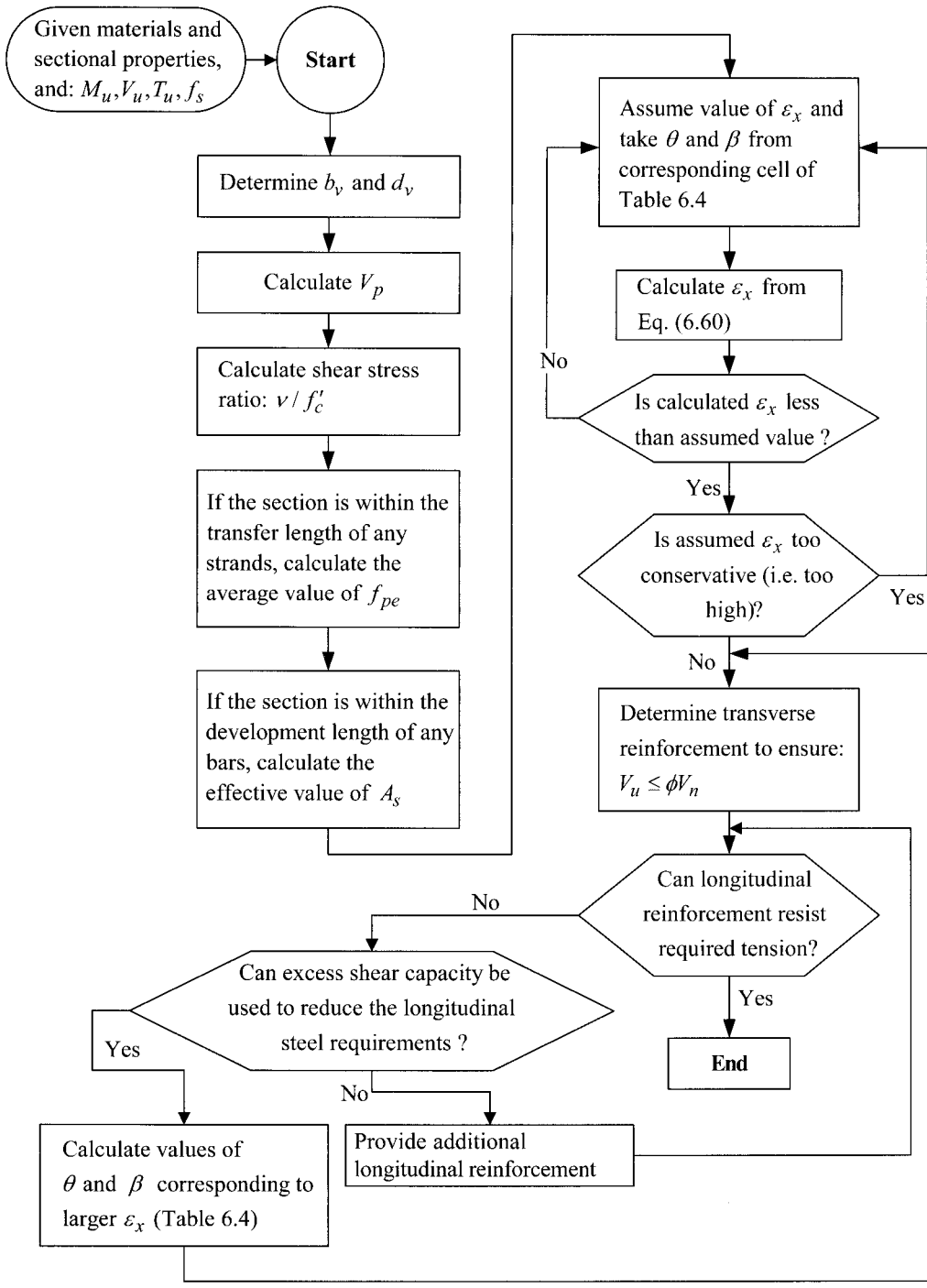

Figure 6.23 Flowchart for shear design (adapted from AASHTO 1998, Interim 2002)

$$s \leq \frac{A_v f_y d_v \cot\theta}{V_s} \tag{6.63}$$

A flowchart summarizing the general sectional procedure for shear design is given in Fig. 6.23; it is adapted from the 2003 AASHTO LRFD code. Two examples illustrating the procedure as applied to bridge beams are given in Sections 14.10 and 14.11.

6.12.2 Special Considerations

1. First Critical Section for Shear

If the reaction force in the direction of applied shear introduces compression into the end region of a member (that is generally the case), the distance between the critical shear section and the internal face of the support shall be taken as the larger of $0.5d_v \cot\theta$ or d_v.

2. Minimum Transverse Reinforcement

Except for slabs, footings and culverts, transverse reinforcement must be provided if:

$$V_u > 0.5\ \phi\ (V_c\ +\ V_p) \tag{6.64}$$

and the reinforcement should satisfy the following:

$$A_v \geq 0.0316\ \sqrt{f'_c}\ \frac{b_v\ s}{f_y} \tag{6.65}$$

Note that the minimum reinforcement specified in the right term of Eq. (6.65) leads to a value of $\beta = 1$. This should be compared to the factor 0.75 given by ACI in Eq. (6.40) where f'_c is in psi.

3. Maximum Spacing of Transverse Reinforcement

The spacing of transverse reinforcement shall satisfy the following conditions:

For $V_u < 0.1 f'_c b_v d_v$:

$$s \leq 0.8 d_v \leq 24 \text{ in}$$

For $V_u \geq 0.1 f'_c b_v d_v$:

$$s \leq 0.4 d_v \leq 12 \text{ in}$$

This approach is somewhat similar to the ACI approach where, for $(v_u/\phi - v_c) \geq 4\sqrt{f'_c}$ in psi, the stirrup spacing is halved (Section 6.8.4).

4. Minimum Longitudinal Reinforcement at Each Section

For sections not subjected to torsion, the longitudinal reinforcement shall be proportioned so that at each section the following equation is satisfied:

$$A_s f_y + A_{ps} f_{ps} \geq \left[\frac{M_u}{d_v \phi} + \frac{0.5N_u}{\phi} + \left(\frac{V_u}{\phi} - 0.5V_s - V_p\right)\cot\theta \right] \tag{6.67}$$

where ϕ values are the appropriate resistance factors corresponding to moment, shear, and axial resistance, as suitable. The reinforcement in Eq. (6.67) is assumed to be fully developed at the section considered.

If direct compression is introduced into the flexural compression zone of the member by the reaction force or applied load at the location of maximum moment, the area of longitudinal reinforcement on the flexural tension side of the member need not to be larger than that required to resist the maximum moment acting alone.

The longitudinal reinforcement on the flexural tension side of the member shall resist at least a tensile force T at the inside edge of the bearing area at simple end supports, given by:

$$T = \left(\frac{V_u}{\phi} - 0.5V_s - V_p\right)\cot\theta \tag{6.68}$$

in which V_u, V_s, V_p, and θ can be calculated at a distance taken as the larger of $0.5d_v \cot\theta$ or d_v from the face of the support.

5. Modifications for Lightweight Concrete

When lightweight aggregate concrete is used, AASHTO Article 5.8.2.2 recommends to replace the square root of the concrete compressive strength in Eq. (6.57) by:

$$4.7 f_{ct} \leq \sqrt{f'_c} \tag{6.69}$$

where f_{ct} is the splitting tensile strength of lightweight concrete (see Table 2.8). If f_{ct} is not known, $\sqrt{f'_c}$ shall be replaced by $0.75\sqrt{f'_c}$ for all-lightweight concrete or by $0.85\sqrt{f'_c}$ for sand-lightweight concrete. The unit stress is in ksi.

6. Remarks

Since the modified compression field theory was first introduced in the 1993 AASHTO LRFD code, the procedure has seen several adjustments. Among them are the values given in Table 6.4 and 6.5 and their limitations, the value of ε_x from Eqs. (6.60a) or (6.60c), the definition of A_{cf} and the definition of f_{po}. The last information available was reported above. However, at time of this writing,

conflicting information can be found in the code about f_{po} . In particular, it can be interpreted as the effective prestress, the stress at decompression at the level of the prestressing steel ($f_{po} = f_{pe} + f_{pc}E_p / E_c$), or the initial prestress just before transfer ($0.70f_{pu}$ to $0.75f_{pu}$). Using the effective prestress is on the safe side, since it leads to an increase in ε_x , thus a decrease in β (Table 6.4), a decrease in V_c and an increase in shear reinforcement; however, either value can be used until further clarification is released from AASHTO.

Physically, the longitudinal strain ε_x can be regarded as an average (smeared) strain in a reinforced concrete tensile tie with centroid assumed located at mid-depth of the member for members with at least minimum transverse reinforcement, and at d_v for members without or with less than minimum transverse reinforcement (Fig. 6.22 and Eqs. 6.60a and 6.60b). Note that it is not recommended to fictitiously increase the tensile reinforcement (which is present in the denominator of Eqs. (6.60a to 6.60c)), in order to reduce ε_x and thus reduce the required shear reinforcement.

Although the ACI and AASHTO methods for shear differ widely, it is observed that the limitations set on several equations in effect lead to similar design for most routine problems.

An example is treated next. Additional examples of bridge beam design for shear can be found in Sections 14.10.2 and 14.11.

6.12.3 Example: Shear Design by AASHTO LRFD Code

Consider the same example as in Section 6.10. The AASHTO LRFD specifications and notation will be used whenever possible. Articles of the code are identified by the letter A, followed by the code number in brackets. Let us check shear at *h/2* from the center of support and three other sections defined in Table 6.6. It can be shown that for the first section:

$x =$ distance from center of support $= h/2 = 1.67$ ft

= (on safe side since cot θ is not known yet)

$$e_o = 7.9 + \frac{21.7 - 7.9}{28} x = 8.72 \text{ in}$$

$b_v = 8$ in

$d_v =$ effective shear depth or lever arm of couple from Eq. (6.55) [A5.8.2.7]

$d_e = e_o + y_t = 8.72 + 12.9 = 21.62$ in

$d_v = 21.62 - 0.5 \times 1.98 = 20.63$ in $> 0.9\, d_e = 0.9 \times 21.62 = 19.46$ in O.K.

$> 0.72h = 0.72 \times 40 = 28.8$ in N.G.

Hence, $d_v = 28.8$ in at this section. Values of d_v for other sections are given in Table 6.7.

Shear forces at section $x = 0.5h = 1.67$ ft are given by (Table 6.6):

$V_{DC} = 19.1$ kips

$V_{DW} = 3.33$ kips

$V_{LL} = 11.33$ kips

Factored shear force assuming $\eta = 0.95$ [A3.4.1]:

$$V_u = 0.95 \times (1.25 \times 19.1 + 1.5 \times 3.33 + 1.75 \times 11.33) = 46.263 \text{ kips}$$

Note that the AASHTO load factors are also given in Tables 14.1 and 14.2.

Factored moments assuming the superimposed dead load due to asphalt is included [A3.4.1]:

$$M_u = 0.95 \times (1.25 \times 32.64 + 1.5 \times 5.70 + 1.75 \times 19.36) = 79.069 \text{ kips-ft} = 948.822 \text{ kips-in}$$

Assuming a draped tendon profile (see Fig. 6.16):

$$V_p = F \times \sin\alpha = 229.5 \times \sin(\alpha) = 229.5 \times 0.04107 = 9.426 \text{ kips}$$

From Eq. (6.59) [A5.8.3.4.2-1]:

$$v = \frac{V_u - \phi V_p}{\phi b_v d_v} = \frac{46.263 - 0.9 \times 9.426}{0.9 \times 8 \times 28.8} = 0.18 \text{ ksi}$$

$$\frac{v}{f'_c} = \frac{0.18}{5} = 0.04 < 0.1$$

Therefore, $s \le 0.8 d_v \le 24$ in (Section 6.12.2-3) [A5.8.2.7-1]

According to AASHTO [5.8.3.4.2], the shear resistance can be determined as follows:

First estimate: $f_{po} = f_{pe} + f_{pc}\frac{E_p}{E_c} = 0.70 f_{pu} = 189$ ksi [C5.8.3.4.2-1]

1st iteration. Assume $\theta = 21.8^o$; thus: $cot\,\theta = 2.5$

From Eq. (6.60a) [A5.8.3.4.2 interim 2000] and assuming at least minimum transverse reinforcement:

Check $M_u = 948.822$ kip-in $< V_u d_v = 1332.37$ kip-in, therefore use $M_u = V_u d_v$

Compute:

$$\varepsilon_x = \frac{(M_u / d_v) + 0.5 N_u + 0.5(V_u - V_p)\cot\theta - A_{ps} f_{po}}{2(E_s A_s + E_p A_{ps})}$$

Note: f_{po} may have to be reduced if first section falls within the transfer length. Assume here it is ok.

Table 6.6 Shear forces and moments at selected sections.

Distance from support	Beam Weight (DC)		SDL (DW)		LL	
Feet	Shear	Moment	Shear	Moment	Shear	Moment
	kips	kips-ft	kips	kips- ft	kips	kips- ft
0.00	20.06	0.00	3.50	0.00	11.90	0.00
1.67	19.10	32.64	3.33	5.70	11.33	19.36
17.50	10.03	263.22	1.75	45.94	5.95	156.19
23.33	6.69	311.97	1.17	54.44	3.97	185.11
35.00	0.00	350.96	0.00	61.25	0.00	208.25

$$\varepsilon_x = \frac{(1332.37/28.8)+0+0.5(46.263-9.426)2.5-1.53\times189}{2(0+27000\times1.53)} = -0.00238$$

Because ε_x is negative, it shall be calculated from Eq. (6.60c) [A5.8.3.4.2-3] which accounts for concrete in its denominator:

$$\varepsilon_x = \frac{(M_u/d_v)+0.5N_u+0.5(V_u-V_p)\cot\theta-A_{ps}f_{po}}{2(E_cA_c+E_sA_s+E_pA_{ps})}$$

$$\varepsilon_x = \frac{(1332.37/28.8)+0+0.5(46.263-8.83)2.5-1.53\times189}{2(4287\times160+0+27000\times1.53)} = -0.000135$$

where A_c is taken equal to the tensile area of concrete below the mid-depth of the section, that is, $20\times8=160$ in^2 (Fig. 6.22).

For a second iteration, we could go to a slightly lower value of $\theta = 20.4^o$, but the above assumed value is considered good enough. Thus assume that: $\theta = 21.8^o \Rightarrow$ Converged.

From Table 6.4: for $\frac{v}{f'_c} = \frac{0.18}{5} = 0.04$ and $\theta = 21.8^o$, $\cot\theta = 2.50$ and $\beta = 3.75$

Therefore:

$$V_c = 0.0316\times\beta\sqrt{f'_c}\,b_v d_v \quad \text{(Eq. 6.57) [A5.8.3.3-3]}$$

$$=0.0316\times3.75\times\sqrt{5}\times8\times28.8 = 61.05 \text{ kips}$$

$$V_s = \frac{V_u}{\phi}-V_p-V_c = \frac{46.263}{0.9}-9.426-61.05 = \text{ -19.07 (negative)} \quad \text{(Eq. 6.62)}$$

Check minimum required transverse reinforcement (Eq. 6.64) [A5.8.2.5]:

$$0.5\phi(V_c+V_p) = 0.5\times0.9\times(61.05+9.426) = 31.71 \text{ kips} < V_u = 46.26 \text{ kips}$$

Minimum reinforcement is needed.

Consider #3 U-shaped stirrups with $A_v = 0.22$ in^2

Check minimum reinforcement and spacing (Eq. 6.65) [A5.8.2.5-1]:

For $s \le \frac{A_v f_y}{0.0316\sqrt{f'_c}\,b_v} = \frac{0.22\times60}{0.0316\times\sqrt{5}\times8} = 23.35$ in

Select $s = 23$ in

Check maximum spacing (Section 6.12.2-3) [A5.8.2.7]

For: $V_u < 0.1f'_c b_v d_v$, $s \le$ smaller ($0.8d_v = 0.8\times28.8 = 23.04$ in or 24 in) = 23.04 in

$s < s_{max} = 23.04$ O.K.

So select a No. 3 U stirrups at 23 in spacing. Since this is the end section, it is likely that there will also be additional stirrups for confinement.

Computations for the other sections are summarized in Table 6.7. Note that the stirrup requirements are about same as obtained in Tables 6.1 and 6.2 using the ACI code.

Table 6.7 Summary of calculations at sections 0.5*h*, *L*/4, and *L*/3 from support.

Distance from support, ft		V_u kips	M_u kips-ft	d_v in	v ksi	v/f_c'	M_u kips-in	$V_v d_v$ kips-in
1.67	0.5h	46.26	79.07	28.80	0.18	0.04	948.82	1332.37
17.50	L/4	24.30	637.70	28.80	0.079	0.016	7652.45	699.84
23.33	L/3	16.21	755.79	31.31	0.037	0.0073	9096.44	507.54
35.00	L/2	0.00	850.26	37.06	0.00	0.00	10203.12	0

Distance from support, ft	ε_x	θ	β	V_c kips	V_s kips	s for min. reinf., in	Max spacing, in	s in
1.67	-0.000135	21.8	3.75	61.05	negative	23.35	23.04	23
17.50	-2.83×10^{-6}	21.8	3.75	61.05	negative	-	-	23*
23.33	0.0000977	24.3	3.24	57.34	negative	-	-	23*

* Assuming minimum reinforcement is used throughout.

6.13 TORSION AND TORSION DESIGN

Torsion in the form of moment or torque causes twisting of a member along its axis. Common structural concrete elements are often subjected to torsional moments due to unsymmetrical loading. However, the magnitude of these moments is generally small in comparison to other effects and, thus, torsion is not explicitly considered in their design. There are, however, structural members and/or loading conditions for which torsional effects may be significant and must be designed for. This is the case for spandrel beams, cantilevers, unsymmetrically loaded bridges, curved members, spiral stairways, and the like (Fig. 6.24).

Similarly to the behavior under shear, plain concrete can resist torsion up to cracking, but then essentially looses all resistance. Reinforced concrete behaves similarly to plain concrete up to cracking, but retains a significant torsional resistance after cracking.

In prior versions of the ACI code (1971-1989), the basic approach to designing for torsion was similar to that of designing for shear, that is, to consider the concrete contribution to the ultimate torsional strength of a member and then determine the torsional reinforcement, if needed, to balance the remaining portion of the required strength. This approach is explained in Section 6.14. In the 2002 ACI code, concrete torsional resistance after cracking is neglected to simplify the design procedure, as explained in Section 6.16.

Torsion reinforcement comprises both transverse reinforcement in the form of closed stirrups and longitudinal reinforcement (in excess of that needed for flexure) to be distributed along the periphery of the section. Limitations, similar to those

encountered for shear and bending on the minimum and maximum amounts of reinforcement, also exist for torsion.

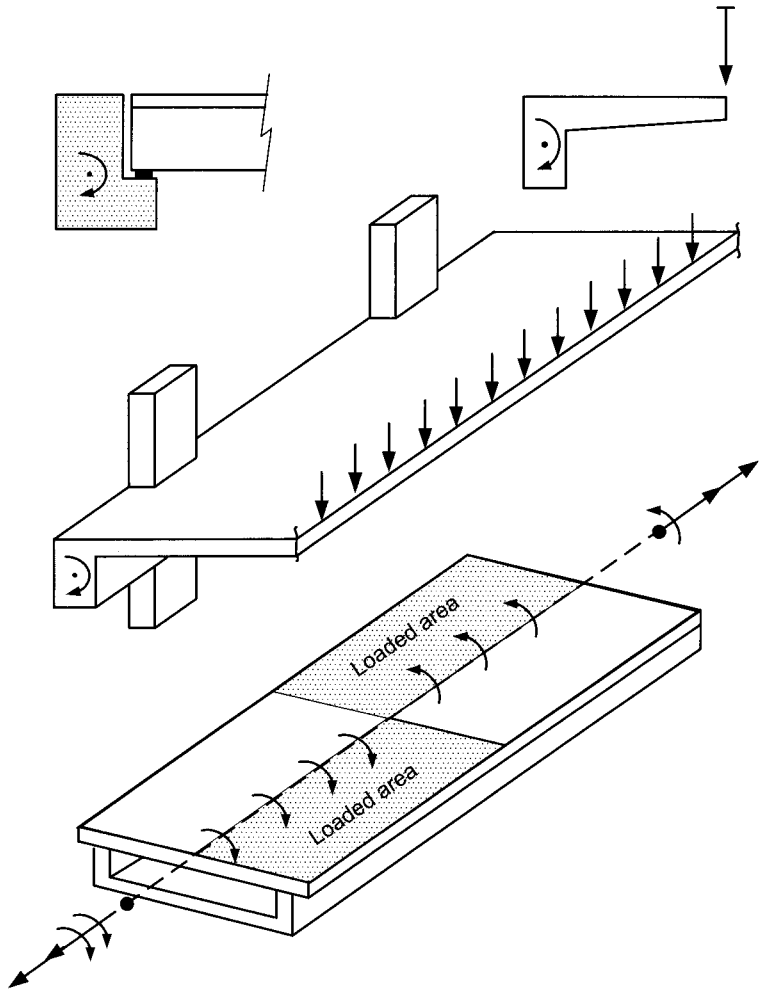

Figure 6.24 Typical structural members subjected to torsion.

6.14 BEHAVIOR UNDER PURE TORSION

According to St. Venant's torsion theory for elastic materials, plain concrete members subjected to an increasing torsional moment would eventually fail by developing a spiral type of cracking. However, the actual failure behavior of plain concrete is different. A tension crack generally develops in a plane inclined at about 45° to the axis of the twist and failure is sudden (brittle-like). There is evidence

[Ref. 6.16] that, with the exception of thin specimens, failure is mostly caused by bending induced by the bending component of the torsional moment (Fig. 6.25).

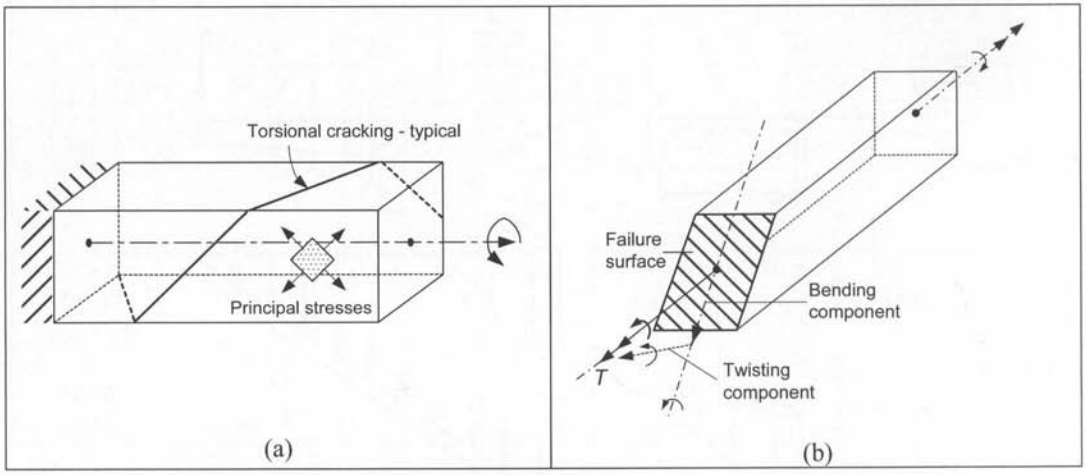

Figure 6.25 (a) Typical torsional cracking in concrete beams subjected to pure torsion. (b) Failure surface according to skew bending torsion model.

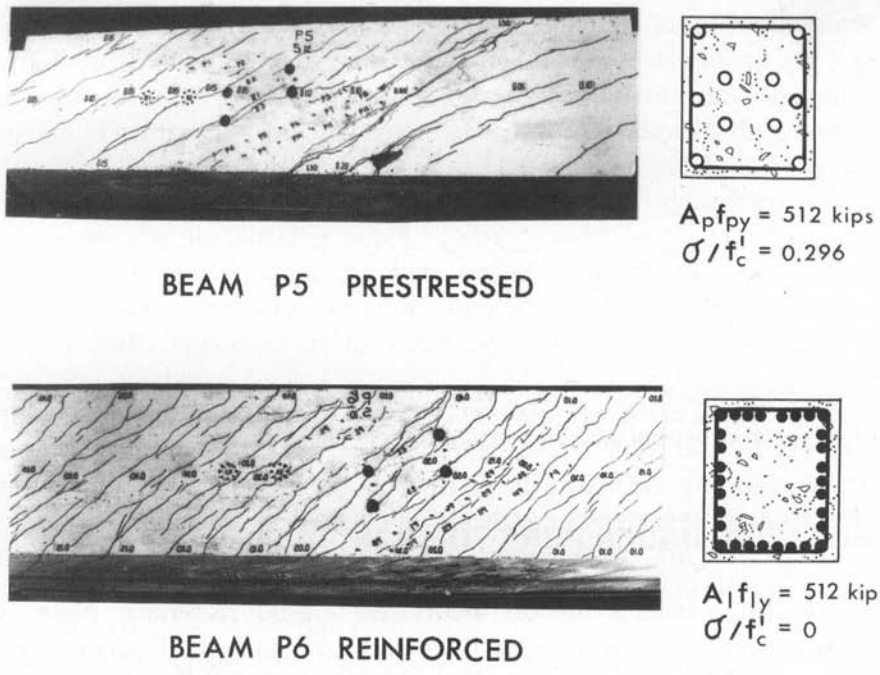

Figure 6.26 Typical torsion cracking of reinforced members.
(Ref. 6.8, courtesy Precast/Prestressed Concrete Institute.)

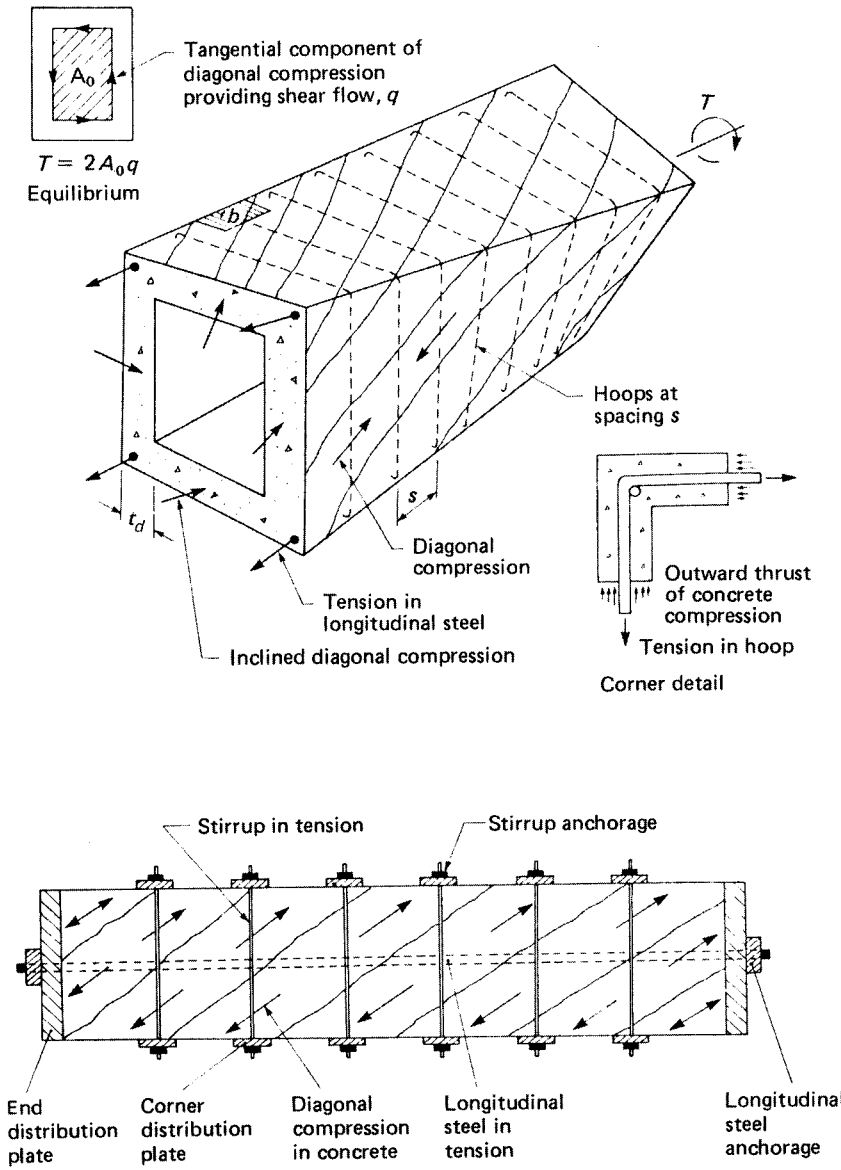

Figure 6.27 Idealized functions of concrete and reinforcement after torsional cracking. *(Ref. 6.7, courtesy American Concrete Institute.)*

If the concrete element is reinforced against torsion, its behavior before cracking is essentially identical to a plain concrete element. Cracking would occur at about the same torque as for the unreinforced element. Prior to cracking, the contribution of the torsional reinforcement is small, as evidenced by the low stresses recorded during testing. After cracking, the stiffness of the member drops suddenly to a

fraction of its precracking value and the stress in the reinforcement increases sharply to maintain equilibrium. With increasing torque, multiple inclined cracks develop at regular spacing and take the form of S shapes (Fig. 6.26). The principal compressive strain measured along elements of concrete bound by two cracks seems to increase at a rate faster than predicted by the theory. Similarly to the behavior in bending, redistribution of torsional stresses can occur in statically indeterminate structures.

In general, three types of failure by torsion can be observed [Ref. 6.17] depending on the amount of reinforcement, and they are comparable to the flexural types of failure. Beams underreinforced for torsion will fail by yielding of the steel, while overreinforced beams will fail by crushing of the concrete, mostly on the wider face of the member. A third mixed mode type of failure occurs in partially overreinforced members in which a combination of stirrup yielding or longitudinal steel yielding and concrete crushing occurs.

The functions after cracking of the different elements of a cracked concrete member reinforced for torsion can be visualized by referring to Fig. 6.27, taken from Ref. [6.7]. The figure is also useful in summarizing the information on the types of torsional reinforcement and the details that must be addressed in designing them.

6.15 BACKGROUND TO STRESS ANALYSIS AND DESIGN FOR TORSION

6.15.1 Torsional Stresses

This section provides background information. Its content was used in prior versions of the ACI code between 1971 to 1989. The reader is referred to the first edition of this book and the cited references for details of its application. While the following treatment is useful for understanding the shear and torsional behavior of structural concrete members, it is not necessary for applying the provisions of the 2002 ACI code covered in Section 6.16.

Using either the mathematical theory of elasticity, the plastic theory, or the skew bending theory, it can be shown that the magnitude of the maximum torsional shear stress in a rectangular section subjected to a torque T is given by:

$$t = \frac{T}{\eta x^2 y} \tag{6.70}$$

where:

x = shorter overall dimension of rectangular section
y = longer overall dimension of rectangular section
η = torsional coefficient

The value of η varies with y/x from 0.208 to 1/3 in the elastic theory, and from 1/3 to 1/2 in the plastic theory. For simplicity, an overall value of 1/3 can be adopted

for nonprestressed members. For prestressed members, a value of η is suggested in Eq. (6.73).

For a plain concrete section at the onset of cracking, Eq. (6.70) can be written as:

$$t_{cr} = \frac{T_{cr}}{\eta x^2 y} \tag{6.71}$$

where:

t_{cr} = torsional shear stress at cracking

T_{cr} = cracking torque

For flanged sections such as *T*, *I*, or *L* sections, the denominator of Eqs. (6.70) and (6.71) is replaced by $\Sigma \eta x^2 y$, in which Σ applies to the various rectangular parts of the section:

$$t_{cr} = \frac{T_{cr}}{\Sigma \eta x^2 y} \tag{6.72}$$

where:

x = shorter overall dimension of rectangular part of cross section

y = longer overall dimension of rectangular part of cross section

$\Sigma \eta x^2 y$ = the sum to be chosen as the largest value of several alternatives, if any (safer design)

The above equation is not exactly in accordance with the theory, but simplifies the results enormously.

For rectangular box sections, the code prescribed that an equivalent solid section may be used provided the wall thickness h' is at least $x/4$. If the wall thickness h' is less than $x/4$ but greater than $x/10$, an equivalent solid section may be taken, provided the term $x^2 y$ is multiplied $4h'/x$. When h' is less than $x/10$, the stiffness of the wall must be considered, since possible buckling and crushing may occur.

The denominator of Eqs. (6.70) to (6.72) is generally called the torsional constant, Θ. A summary of the torsional constants recommended for various sections in earlier versions of the ACI code (from 1971 to 1989), is given in Fig. 6.28.

It is generally accepted, that Eqs. (6.70 to 6.72) would remain the same for prestressed concrete, except for the value of η. Based on 218 test results, Zia and McGee [Ref. 6.49] have shown that the torsion coefficient η for prestressed members can be estimated as a first approximation from:

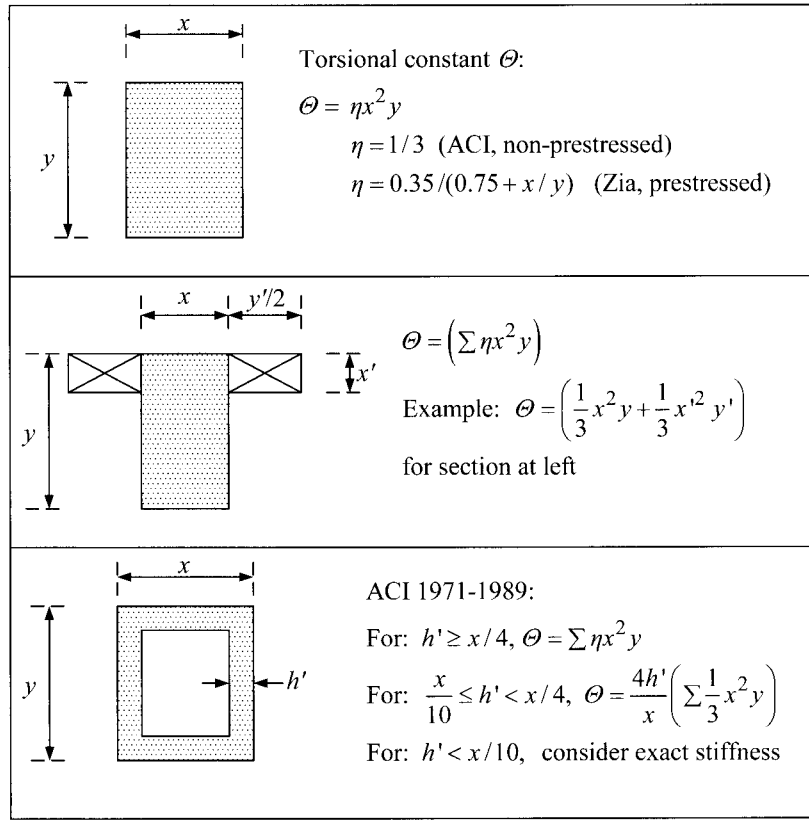

Figure 6.28 Summary of design torsional constants as per ACI code, 1971 to 1989, based on skew bending theory.

$$\eta = \frac{0.35}{0.75 + x/y} \tag{6.73}$$

One can generalize Eq. (6.72) for plain reinforced and prestressed concrete, using $\eta = 1/3$ for plain and reinforced concrete as per Fig. 6.28, and η from Eq. (6.73) for prestressed concrete. Note that, according to the discussion of Ref. [6.26], Eq. (6.73) is applicable to reinforced concrete as well as to prestressed concrete.

6.15.2 Torsional Cracking Strength

Theoretically and experimentally, it was shown in Refs. [6.15 and 6.16] that the cracking strength t_{cr} of a plain concrete beam subjected to pure torsion is approximately equal to $0.85 | f_r |$ where f_r is the modulus of rupture of the concrete. As a first approximation $0.85 | f_r |$ can be taken as $0.85(7.5\sqrt{f'_c}) \simeq 6\sqrt{f'_c}$. However, the torsional cracking strength of concrete, in presence of bending and shear, is

reduced. For instance, in his book [Ref. 6.15], Hsu uses a value of $5\sqrt{f'_c}$. On the other hand, a value of $4\sqrt{f'_c}$ is assumed in the 2002 ACI code for the torsional resistance under combined shear and torsion. Many reasons influence the choice of a variable for a code, including calibration and structural reliability considerations. The stress at cracking in a reinforced concrete beam is considered the same as for plain concrete. Therefore, the following general expression can be used to estimate the torque at cracking:

$$T_{cr} = t_{cr} \Sigma \eta x^2 y = \beta_t \sqrt{f'_c}\, \Sigma \eta x^2 y \tag{6.74}$$

where:

β_t = coefficient or multiplier of $\sqrt{f'_c}$ in psi, expressing the cracking resistance of concrete under shear stresses induced by the combination of shear forces and torsional moment.

As described above, β_t can be taken equal to 4, 5, or 6, depending on the situation (research or design, pure torsion or torsion combined with shear).

Hsu [Ref. 6.18] has shown that, if the beam is prestressed, its torsional cracking strength is increased with the average prestress and, for all practical purposes, can be estimated by:

$$(t_{cr})_{\text{prestressed}} = \left(\sqrt{1 + \frac{10\sigma_g}{f'_c}} \right) (t_{cr})_{\text{nonprestressed}} \tag{6.75}$$

or equivalently:

$$t_{cr} = \beta_t \sqrt{f'_c} \left(\sqrt{1 + \frac{10\sigma_g}{f'_c}} \right) \tag{6.76}$$

where σ_g = average prestress = F / A_c.

Note that Eq. (6.76) also applies to plain and reinforced concrete for which $\sigma_g = 0$. Knowing the cracking stress, the torque at cracking can be estimated from Eq. (6.74) in which η = 1/3 for nonprestressed members and η, given by Eq. (6.73), for prestressed members.

6.15.3 Torsional Resistance after Cracking

A plain concrete section subjected to torsion loses all its resistance after cracking. However, if it is reinforced with torsional reinforcement, the torsional strength contribution of concrete after cracking, t_c, is a significant portion of its precracking

strength t_{cr}. Hsu [Ref. 6.17] has shown experimentally that the after-cracking strength t_c is about 40 percent of the precracking strength t_{cr} in reinforced members. He also found that the magnitude of strength loss after cracking is the same for prestressed members as for nonprestressed (reinforced) members. Thus:

$$(t_{cr} - t_c)_{\text{prestressed}} \simeq (t_{cr} - t_c)_{\text{nonprestressed}} \tag{6.77}$$

where:

t_c = torsional strength of concrete after cracking (assuming torsional reinforcement is provided)

t_{cr} = torsional cracking strength

The same notation is used in Eq. (6.77) for prestressed and nonprestressed members to minimize confusion, yet each variable on each side of the equation may be numerically different.

\

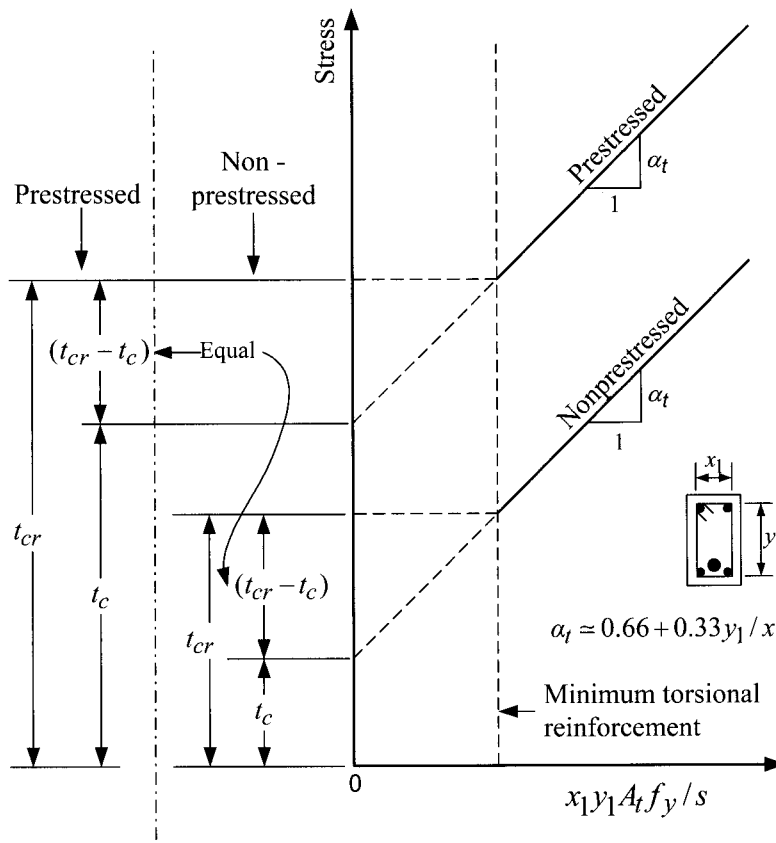

Figure 6.29 Graphical representation of the assumed torsion resistance after cracking.

The result of Eq. (6.77) is illustrated in Fig. 6.29, adapted from Ref. [6.49], where the concrete contribution to the torsional strength is plotted against the contribution of the torsional reinforcement. The two linear relations are approximate fits to actual data. Note that the two lines have the same slope, α_t, indicating that the contribution of torsional reinforcement after cracking is the same whether or not the member is prestressed. However, the concrete contribution, t_c, after cracking, is higher for a prestressed member than for a nonprestressed member. An estimated value for α_t was given in prior versions of the ACI code as: $\alpha_t = 0.66 + 0.33(y_1 / x_1)$, where x_1 and y_1 represented the shorter and longer center to center dimension of closed rectangular stirrup, respectively, and α_t was limited to 1.5.

For a nonprestressed member, the strength loss due to cracking can be expressed as:

$$t_{cr} - t_c = t_{cr} - \mu t_{cr} = (1-\mu)t_{cr} = kt_{cr} \tag{6.78}$$

where μ can be taken approximately equal to 0.4, as mentioned in Eq. (6.77). Thus, $k = 1 - t_c / t_{cr} = 0.60$.

If the member is prestressed, we will have:

$$(t_{cr} - t_c)_{\text{prestressed}} = k(t_{cr})_{\text{nonprestressed}} \tag{6.79}$$

and using Eqs. (6.76) and (6.79):

$$t_c = \left(\sqrt{1 + \frac{10\sigma_g}{f'_c}} - k \right) (t_{cr})_{\text{nonprestressed}} \tag{6.80}$$

The above equation can be generalized for prestressed and nonprestressed members with torsional reinforcement, assuming the cracking strength of the nonprestressed member is $\beta_t \sqrt{f'_c}$, thus:

$$t_c = \beta_t \sqrt{f'_c} \left(\sqrt{1 + \frac{10\sigma_g}{f'_c}} - k \right) \tag{6.81}$$

where:

t_c = torsional stress resistance contributed by concrete after cracking of a structural (prestressed or nonprestressed) concrete member

$k = 0.6$ for nonprestressed members, in which case $\sigma_g = 0$

$k = 1 - 0.133/\eta$ for prestressed members [Ref. 6.49] in which η is given by Eq. (6.73). Hence $k = (0.75 - 0.4x/7)/1.05$. The value of x/y is determined for the largest component rectangle where the web reinforcement is usually placed.

Therefore, for nonprestressed members, $t_c = 0.4\beta_t\sqrt{f'_c}$, $\eta = 1/3$, and the value of β_t is as discussed in Eq. (6.74). These values are useful to explain some equations found in various codes.

6.15.4 Combined Loading

Seldom do pure torsional loadings apply to structures. It is more likely that a combination of shear torsion and bending exists. Their interaction is generally represented by an interaction surface and, when taken two at a time, by an interaction curve. Circular, elliptic, parabolic, or linear interaction curves have been used to model the interaction of bending and torsion or torsion and shear [Refs. 6.13, 6.14, 6.22, 6.23, 6.25, 6.36, 6.49]. In the ACI code approach, design for bending is achieved separately (thus it does not need to be reconsidered), while that of torsion and shear is combined.

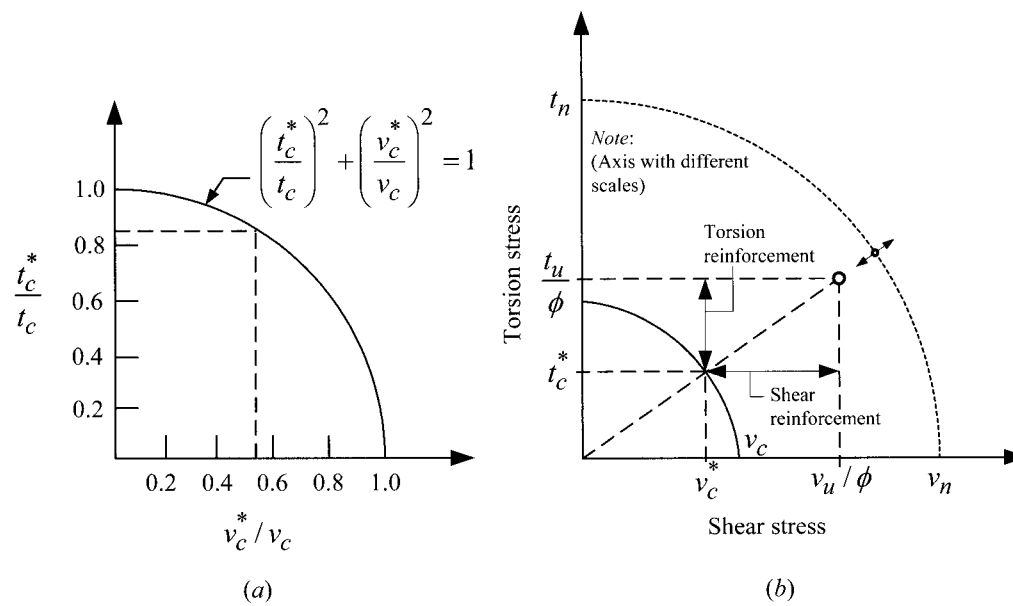

Figure 6.30 (*a*) Typical interaction curve for combined torsion and shear. (*b*) Typical representation of concrete and reinforcement contribution after cracking.

Tests have shown [Refs. 6.14 and 6.36] that the interaction between torsion and shear in prestressed and nonprestressed members can be adequately represented by a circular curve (Fig. 6.30*a*) of the form:

$$\left(\frac{t_c^*}{t_c}\right)^2 + \left(\frac{\upsilon_c^*}{\upsilon_c}\right)^2 = 1 \tag{6.82}$$

in which:

t_c^* = torsional strength in presence of flexural shear, $t_c^* \le t_c$

t_c = torsional strength when member is subjected to torsion alone

υ_c^* = shear strength in presence of torsion, $\upsilon_c^* \le \upsilon_c$

υ_c = shear strength when member is subjected to flexural shear alone (υ_c for prestressed members is lesser of υ_{ci} and υ_{cw} given by Eqs. (6.29) and (6.31))

Equation (6.82) also applies to plain concrete where the subscript *cr* (for cracking) replaces *c*. Note that, because of the circular shape of the curve, little reduction in strength is observed for one effect, unless the other effect is significant. For instance, about 90 percent of the shear resistance acting alone can be counted on if the torsion is less than 45 percent of the torsion resistance acting alone, and vice versa.

The design approach followed in the 1971 to 1989 versions of the ACI code for combined shear and torsional loading was the same as for shear loading, that is, the torsional strength of concrete in combined loading is considered first and then the web reinforcement, if needed, is proportioned to carry the excess torsion necessary to balance the ultimate required or factored torque (Fig. 6.30*b*). Thus, the following equations applies:

$$T_u \le \phi T_n \tag{6.83}$$

$$T_n = T_c^* + T_s \tag{6.84}$$

where T_s represents the contribution of torsional reinforcement. In the 2002 ACI code, the torsional resistance of concrete after cracking in presence of shear, that is T_c^*, is neglected to simplify the treatment of shear and torsion design; however, other factors are adjusted to make up for the shortfall.

6.15.5 Design Theories for Torsion and Code Related Approaches

Several theories and models have been proposed to explain the behavior of concrete and reinforced concrete in torsion [Ref. 6.15, 6.48].

Ritter, in 1899, and Morsch, in 1902, respectively proposed the "*truss analogy*" for the design of reinforced concrete beams for shear. This was a very simple model to help visualize the various forces in a member. The truss model assumed that concrete carries no tensile resistance and that all truss elements remain in the linear elastic range of behavior. The truss definition was later extended to the plastic truss model where it is assumed that vertical elements representing stirrups yield at nominal resistance. This assumption reduces the truss to a statically determinate truss for which equilibrium of forces can be easily resolved. It is essentially the basis of Fig. 6.9c.

In 1970-1972, Lampert et al. [Refs. 6.22 to 6.25] proposed a three-dimensional "*plastic space truss analogy*" in which the peripheral longitudinal reinforcement represents the booms of the truss, the closed stirrups form its vertical members, and the inclined concrete elements between cracks play the role of the diagonal compressive members. This model gave realistic predictions of actual behavior and gained acceptance with many researchers in the field. In particular, studies by two researchers and their co-workers led to two theories widely used in US and Canadian codes: the "*softened truss model*" developed by Hsu, and the "*compression field theory*" developed by Collins and Mitchell.

The ACI code provisions for shear and torsion in the 1971 to 1989 versions of the code were based on the "*skew bending theory*" initially proposed by Lessig [Ref. 6.26], and later developed for practical implementation by Hsu [Refs. 6.4, 6.16, and 6.19]. It assumes that concrete provides some resistance to shear and torsion and the reinforcement provides the rest.

The "*softened truss mode*" later developed by Hsu combines equilibrium of forces, constitutive material models (namely softened biaxial constitutive law for concrete), and compatibility of deformations (Mohr's circular compatibility) in a unified approach to predict the behavior of beams in shear and torsion. The softened truss model provides a nonlinear theory of membrane elements and is applicable throughout the loading history [Ref. 6.15].

The 2002 ACI code provisions for shear and torsion are based on the thin-walled tube analogy, where the area enclosed by the shear flow path is assumed to resist torsion, and on the plastic truss analogy. It is essentially a simplified interpretation of the softened truss model. In the previous versions of the code, the contribution of concrete to torsional resistance was included in the provisions. In the 2002 version of the ACI code, the concrete contribution to torsional resistance was dropped leading to a simpler set of equations allowing to consider torsion and shear simultaneously. This shortfall is made up for by calibrating the equations and reducing torsional reinforcement otherwise required.

An excellent review of the analytical background, derivation of equations and other details related to the code provisions can be found in MacGregor [Refs. 6.31, 632]. In addition, Hsu's book on "*Unified Theory of Reinforced Concrete*" [Ref. 6.15] is a necessary reading for any researcher seeking an in-depth understanding of the problem.

The "*compression field theory*" initially developed by Collins and Mitchell also uses the basic truss model, but allows the angle θ of the compression struts between diagonal cracks to be a variable instead of a constant at 45 degrees. The angle θ depends on the longitudinal strain in the equivalent tensile tie of the truss and the transverse reinforcement or stirrups (see Fig. 6.21). The compression field theory assumes that concrete carries no tension after cracking. The "*modified compression field theory*" is a modified version providing further refinement in which the concrete between cracks is assumed to carry some tension. The AASHTO LRFD provisions on shear and torsion and the Canadian code for reinforced concrete are based on the modified compression field theory. Detailed information describing the underlying assumptions and basic derivations can be found in Refs. [6.7 to 6.9, 6.37 to 6.39, and 6.46, 6.47]. Section 6.12 of this chapter covers the specific AASHTO LRFD provisions for shear. It should be noted that implementation of the theory to practice has seen numerous adjustments and refinements since it was first introduced in the 1993 code. It is advisable to review the latest version of the code for updates.

Another approach to designing for bending, shear and torsion simultaneously, is what is generally described as the "*strut-and-tie*" model. One of the earliest and most comprehensive treatment of "*strut-and-tie*" modeling and examples of applications are given by Schlaich et al. [Ref. 6.43]. A structural member can be modeled by a series of struts and ties interconnected at nodes to form a truss capable of carrying the applied load. The compression struts are made of concrete and the tensile ties are made of steel. The struts-and-ties configuration allows an easy visualization of the flow of forces in a member and thus the appropriate design for such forces. A great deal of research on the strut-and-tie modeling of concrete structures is ongoing at time of this writing. A summary of developments since the early work of Schlaich can be found in [Ref. 6.42]. However, because numerous strut-and-tie models can be developed for the same member, codifying such a procedure can be a real challenge. The 2002 ACI code introduced strut-and-tie modeling in its Appendix A. While a large number of researchers are working on strut-and-tie models for concrete structures, it is still too early, at time of this writing, to provide definite and simplified strut-and-tie procedures easily applicable in prestressed concrete design. Chapter 15 offers a brief introduction to strut-an-tie modeling and its current applications to prestressed concrete, with examples of anchorage zone design and dapped-end beams. It is observed that the rules recommended by various codes to estimate the strength of struts, ties, and nodal zones are likely to change over time. Therefore, the most recent version of the ACI code should be consulted prior to using the procedure.

6.16 DESIGN FOR TORSION BY THE 2002 ACI CODE

Since the first edition of this book [Ref. 1.27] the ACI code approach and specifications regarding torsion have changed significantly. They were initially based on the provisions explained in Section 6.14. Most importantly, the 2002 provisions allow a unified approach to shear and torsion in both reinforced and prestressed concrete, and overall they are simpler to implement. However, the reader may benefit from reviewing the summary treatment in the first edition for background information and additional understanding.

The design procedure described next is adapted directly from the ACI code [Ref. 6.2]. The code and its commentary should be consulted for additional details and to ascertain the conditions for final design. The provisions of the code are written in terms of forces. However, correlating forces with stresses, as described in the previous section, can be easily carried out.

To better understand the basis of each provision of the code, its derivation and justification the reader is referred to the texts by Hsu [Ref. 6.15] and MacGregor [Ref. 6.32] where extensive treatment is given.

6.16.1 Definition of Section Parameters

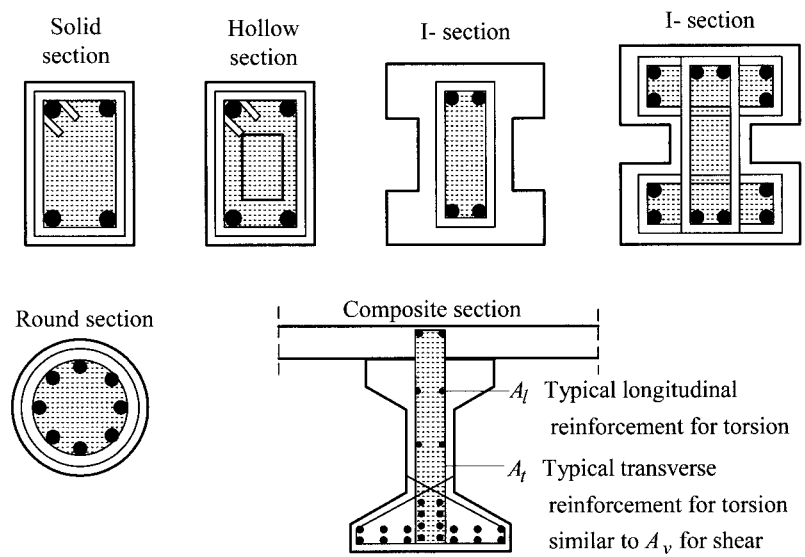

A_{cp} = area enclosed by outside perimeter of concrete cross section

p_{cp} = outside perimeter of the concrete cross section, in

A_{oh} = area enclosed by the centerline of the outermost closed torsional reinforcement

A_o = gross area enclosed by shear flow path; may be taken $\approx 0.85A_{oh}$

p_h = perimeter of centerline of outermost closed transverse torsional reinforcement, in.

Figure 6.31 Definition of A_{oh} and other terms used in torsion design.

The section parameters used in various torsion formulae are clarified first in Fig. 6.31. The darker portion in each section belongs to the area of concrete A_{oh} assumed to resist torsion and further defined below. Note this torsional area excludes the concrete cover which spalls off near nominal resistance.

6.16.2 Basic Assumptions and Design Strategy

The provisions of the 2002 ACI code on shear and torsion are the result of years of research and experience. In comparison to prior versions of the code, other codes, or other theories, the following information is useful to the designer. Not all details are included. The reader should consult the code for final design.

- Torsion does not need to be considered if the factored torsionsal moment, T_u, is smaller than a specified limit, here called $(T_u)_{\min}$, which is taken equal to about 25% of the torque leading to cracking, T_{cr}. The torsional cracking stress is taken equal to the cracking strength of concrete in biaxial tension-compression, assumed equal to $4\sqrt{f'_c}$ (see Eq. (6.74) for comparison).
- For compatibility torsion (see below) the code allows an upper design limit to the factored torsional moment.
- The section dimension and properties need to be increased if a condition based on combined factored torsional moment and shear force is not satisfied.
- When needed, torsional reinforcement consists of transverse reinforcement (mostly in the form of closed stirrups) and longitudinal reinforcement (mostly in the form reinforcing bars) distributed along the periphery of the member. Special spacing limitations are given in the code for both types of reinforcement.
- When torsional reinforcement is needed, it must also satisfy minimum transverse reinforcement requirements.
- Torsional reinforcement is calculated assuming that the torsional resistance of concrete after cracking, T_c, is zero, and thus the nominal torsional strength, T_n, comes from torsional reinforcement only. This is a simplifying assumption, but the code equations are calibrated to make up for the shortfall.
- The shear resisted by concrete after cracking, V_c, is assumed unchanged by the presence of torsion.
- For solid sections, the code assumes a circular interaction diagram between shear and torsional stresses, while for thin-walled hollow sections, it assumes a linear diagram.

The provisions of the code reflect two conditions under which torsion is considered in reinforced concrete members:

1. *Equilibrium torsion*: this condition prevails when the torsional moment cannot be reduced by redistribution of internal forces. For this condition torsional

reinforcement, when needed, must be provided to resist the full factored torsional moment.

2. *Compatibility torsion*: this condition prevails when redistribution of internal forces after cracking occurs to maintain compatibility of deformations leading to a reduction in the resulting torsional shearing stresses. Redistribution can happen in statically indeterminate structures. When redistribution can happen, the condition is described as compatibility torsion, and the code provides an upper design limit to the factored torsional moment taken equal to the cracking torque, T_{cr}. Thus if $T_u > \phi T_{cr}$ the code allows to design for only ϕT_{cr} provided redistribution of internal forces is accounted for in the design of other members of the structure.

6.16.3 Condition for Consideration of Torsion in Design

Torsion effects can be neglected when the factored torsional moment T_u at the section satisfies the following conditions:

(a) For non-prestressed members:

$$T_u \le (T_u)_{min} = \phi\sqrt{f'_c}\,\frac{A_{cp}^2}{p_{cp}} \tag{6.85}$$

(b) For prestressed members

$$T_u \le (T_u)_{min} = \phi\sqrt{f'_c}\,\frac{A_{cp}^2}{p_{cp}}\sqrt{1+\frac{f_{pc}}{4\sqrt{f'_c}}} \tag{6.86}$$

(c) For non-prestressed members subjected to axial tension or compression force:

$$T_u \le (T_u)_{min} = \phi\sqrt{f'_c}\,\frac{A_{cp}^2}{p_{cp}}\sqrt{1+\frac{N_u}{4A_g\sqrt{f'_c}}} \tag{6.87}$$

where:

T_u = factored torsional moment at section, lb-in
ϕ = strength reduction factor for torsion, equal 0.75 by 2002 ACI code
A_{cp} = area enclosed by outside perimeter of concrete cross section, in^2 (Fig. 6.31)
p_{cp} = outside perimeter of the concrete cross section, in (Fig. 6.31)

A_g = gross area of concrete section, in^2. For a hollow section, A_g is the area of concrete only and does not include the area of the void(s).

f_{pc} = compressive stress in concrete (after all losses) at centroid of cross section resisting externally applied loads or at junction of web and flange when the centroid lies within the flange, psi. In a composite member, f_{pc} is the resultant compressive stress at centroid of composite section or at junction of web and flange when the centroid lies within the flange, due to both prestressing and moments resisted by precast member acting alone.

N_u = factored axial load (lb) normal to cross section, occurring simultaneously with V_u and/or T_u; to be taken positive if compression.

If the section is hollow and is not statically indeterminate, A_g shall be used instead of A_{cp} in Eq. (6.87). Note that in the above equations $(T_u)_{min}$ is taken equal to 25% of the assumed cracking torque T_{cr} (Eq. 6.74).

6.16.4 Critical Section for Torsion

For non-prestressed members, the critical section for torsion can be taken at a distance d_s from the face of the support, unless a concentrated torque occurs within that distance; in such a case, the critical section is taken at the face of the support.

For prestressed members, the critical section for torsion can be taken at a distance $h/2$ from the face of the support, unless a concentrated torque occurs within that distance; in such a case, the critical section is taken at the face of the support.

The code does not address the case for partially prestressed members. The author recommends to follow the provisions for prestressed members with a value of d_e as suggested in Section 6.18.

6.16.5 Maximum Allowable Torsional Moment Strength

Even if torsional reinforcement is provided, the cross sectional dimensions and properties of the section shall be such that:

(a) For solid sections:

$$\sqrt{\left(\frac{V_u}{b_w d_e}\right)^2 + \left(\frac{T_u p_h}{1.7 A_{oh}^2}\right)^2} \le \phi\left(\frac{V_c}{b_w d_e} + 8\sqrt{f_c'}\right) \tag{6.88}$$

The above equation reflects a elliptical interaction diagram between shear and torsion.

(b) For hollow sections:

$$\left(\frac{V_u}{b_w d_e}\right)+\left(\frac{T_u p_h}{1.7A_{oh}^2}\right)\le\phi\left(\frac{V_c}{b_w d_e}+8\sqrt{f_c'}\right) \tag{6.89}$$

If the wall thickness varies around the perimeter of a hollow section, Eq. (6.89) shall be evaluated at the location where the left hand side of the equation is a maximum. If the wall thickness is less than A_{oh}/p_h, the second term on the left side of Eq. (6.89) shall be taken as:

$$\left(\frac{T_u}{1.7A_{oh}t}\right) \tag{6.90}$$

where t is the thickness of the wall of the hollow section at the location where the stresses are being checked. Equation (6.89) reflects a linear interaction diagram between shear and torsion.

The notation is as follows:

V_u = factored shear force at section, lb
V_c = nominal shear strength (force) provided by concrete, lb (Section 6.8.2)
A_{oh} = area enclosed by the centerline of the outermost closed torsional reinforcement
p_h = perimeter of centerline of outermost closed transverse torsional reinforcement, in
d_e = as defined in this text; it is equal d_s for reinforced concrete and d_p for prestressed concrete.

In Eqs. (6.88) and (6.89), the maximum design limit of T_u, that is, ϕT_{cr}, can be used when compatibility torsion conditions prevail. Also one should use $V_u/(b_w d_e)=v_u$ and $V_c/(b_w d_e)=v_c$ as calculated for shear (Fig. 6.14), that is, for prestressed concrete the value of $d_p=d_e$ is adjusted according to the code provisions.

Examining the right hand side of Eqs. (6.88) and (6.89) one can observe that a section shall not be allowed if the combined stress due to shear and torsion exceeds

$\phi\left(v_c + 8\sqrt{f_c'}\right)$, where v_c is the contribution of concrete to shear resistance as defined in Eqs. (6.29, 6.31 or 6.32) or Figure 6.14.

6.16.6 Transverse Reinforcement Design

The reinforcement required for torsion shall be determined to satisfy the general condition:

$$T_u \le \phi T_n \tag{6.91}$$

where:

$$T_n = T_c + T_{ts} = 0 + T_{ts} \tag{6.92}$$

and T_u is the factored torsional moment, T_n is the design torsional resistance, and T_{ts} is the torsional resistance provided by the torsional reinforcement. As mentioned above, it is assumed that concrete does not contribute any resistance to torsion (thus, T_c = 0) and that the torsional resistance is provided by the reinforcement alone, which includes stirrups and longitudinal steel. T_n can be estimated from:

$$T_n = T_{ts} = 2A_o f_{yv} \frac{A_t}{s_t} \cot\theta \tag{6.93}$$

where:

A_o = gross area of concrete enclosed by the shear flow path [Ref. 6.15]; it can be taken as a first approximation equal to $0.85A_{oh}$ (defined in Fig.6.31). The use of A_o reflects the fact that the cover of concrete may spall off under large deformations.

A_{oh} = area enclosed by centerline of the outermost closed transverse torsional reinforcement, in^2 (see Fig.6.31)

A_t = area of one leg of closed stirrup resisting torsion within a distance s_t, in^2

f_{yv} = yield strength of closed transverse torsional reinforcement, psi, not to exceed 60,000 psi (414 MPa)

s_t = spacing of torsion reinforcement measured in a direction parallel to the longitudinal reinforcement, in

θ = angle of compression diagonals in the truss analogy for torsion

Equation (6.93) is based on the space truss analogy with compression diagonals at an angle θ assuming the concrete carries no tension and the reinforcement yields; θ shall not be taken smaller than 30 degrees nor larger than 60 degrees. It shall be permitted to take θ equal to 45 degrees for nonprestressed members and 37.5

degrees for prestressed members with an effective prestress not less than $0.4f_{pu}$. If the effective prestress is less than $0.40f_{pu}$, θ can be taken equal to 45 degrees.

For a required nominal resistance, the transverse torsional reinforcement can be computed from Eq. (6.93):

$$\frac{A_t}{s_t} = \frac{T_u}{\phi 2 A_o f_{yv} \cot\theta} \tag{6.94}$$

For a given factored torsional force, T_u, the transverse reinforcement, A_t, can be calculated assuming a practical value of stirrup spacing, s_t, which can be estimated a priori from the limitations on spacing given in Sec. 6.16.10.

6.16.7 Longitudinal Torsion Reinforcement

In addition to the transverse reinforcement needed for torsion (Eq. 6.94), longitudinal reinforcement along the axis of the member is also required, and is a function of the transverse reinforcement. The additional longitudinal reinforcement required for torsion shall not be less than:

$$A_l = \frac{A_t}{s_t} p_h \frac{f_{yv}}{f_{yl}} (\cot\theta)^2 \tag{6.95}$$

where the ratio A_t / s_t shall be taken as the amount computed from Eq. (6.94), and f_{yl} is the yield strength of longitudinal torsional reinforcement, not to exceed 60,000 psi (414 MPa).

In prestressed members, the longitudinal reinforcement required for torsion may consist of unstressed tendons with a tensile yield force $A_{ps} f_{py} = A_l f_{yl}$.

6.16.8 Combining Shear and Torsion Reinforcement

Reinforcement required for torsion shall be added to that required for shear, moment, and axial force that act in combination with torsion. The most restrictive requirements for reinforcement spacing and placement shall be met.

Since the cross sectional area of stirrup for shear is defined in terms of all the legs of a given stirrup while the stirrup area for torsion is defined in terms of one leg only, the addition of stirrups to satisfy both shear and torsion is carried out as follows:

$$\text{Total stirrup requirement} = \frac{A_v}{s_v} + 2\frac{A_t}{s_t} \tag{6.96}$$

where s_v and s_t are the stirrup spacing for shear and torsion, respectively. In prestressed beams, the total longitudinal reinforcement including prestressing steel at each section shall resist the factored bending moment at that section plus an additional concentric longitudinal tensile force equal $A_l f_{yl}$ based on the factored torsion at that section (Eq. 6.95); the spacing of the longitudinal reinforcement shall satisfy the code requirements explained below.

6.16.9 Minimum Torsion Reinforcement

When the factored torsional moment exceeds the minimum value given by Eqs. (6.85) to (6.87), a minimum area of transverse and longitudinal torsional reinforcement is required by the ACI code.

- Minimum transverse closed stirrups shall be provided according to:

$$\frac{A_v}{s_v} + 2\frac{A_t}{s_t} \geq \left(\frac{A_v}{s_v} + 2\frac{A_t}{s_t}\right)_{min} = \text{larger of} \begin{cases} 0.75\sqrt{f'_c}\,\dfrac{b_w}{f_{yv}} \\ \dfrac{50 b_w}{f_{yv}} \end{cases} \tag{6.97}$$

- Minimum total area of longitudinal reinforcement shall be provided according to:

$$A_l \geq A_{l,min} = \left(\frac{5\sqrt{f'_c} A_{cp}}{f_{yl}}\right) - \left(\frac{A_t}{s_t}\right) p_h \frac{f_{yv}}{f_{yl}} \tag{6.98}$$

in which: A_t / s_t shall not be taken less than $25 b_w / f_{yv}$.

6.16.10 Spacing and Detailing

The spacing of transverse torsion reinforcement shall not exceed the smaller of $p_h / 8$ or 12 in. All stirrups must be closed stirrups. Typically a 135 deg standard hook around a longitudinal bar is required; additional details for minimum leg length and the case of welded wire fabric can be found in the code. Note that 90 deg hooks and lapped U-shaped stirrups are inadequate to resist torsion since they become ineffective when the cover of concrete spalls off.

The longitudinal reinforcement required for torsion shall be distributed around the inside perimeter of the closed stirrups, with a maximum spacing of 12 in (30 cm). There shall be at least one longitudinal bar or tendon at each corner of the stirrups.

To minimize buckling, bars shall have a diameter at least 0.042 (that is, 1/24) times the stirrup spacing, but not less than that of a No. 3 bar (9.5 mm).

6.16.11 Type of Torsion Reinforcement

As mentioned above, torsion reinforcement consists of both longitudinal and transverse reinforcement.

- Longitudinal reinforcement shall consist of longitudinal bars or tendons.
- Transverse reinforcement shall consist of:
  - → Closed stirrups or closed ties perpendicular to the axis of the member
  - → Closed cage of welded wire fabric with transverse wire perpendicular to the axis of the member
  - → In nonprestressed beams, spiral reinforcement.

The transverse reinforcement shall be anchored with standard hooks detailed according to code requirements.

Longitudinal torsion reinforcement shall be developed at both ends according to code recommendation for development length.

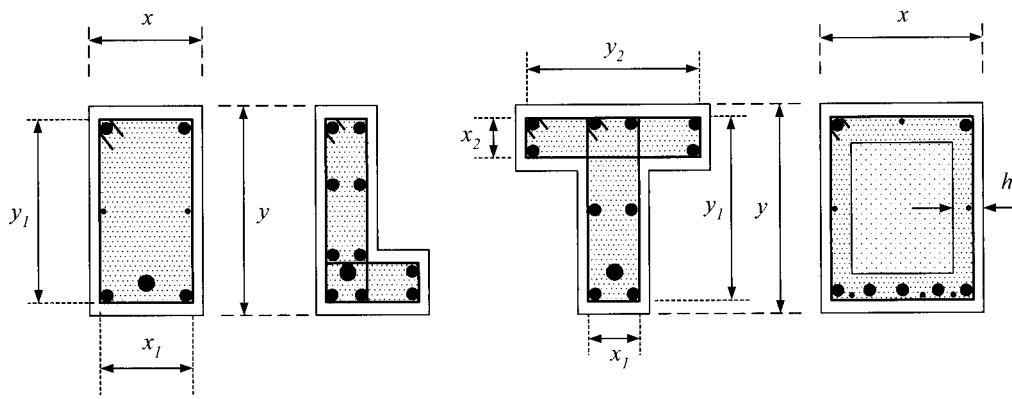

Figure 6.32 Typical layout of torsion reinforcement in different sections.

6.16.12 Design Steps for Combined Torsion and Shear

A flow chart summarizing the main design steps for torsion reinforcement is given in Fig. 6.33. While using the chart, care should be also taken to check details and exceptions given in the code prior to finalizing the design. Note that the flow chart accommodates the design for both torsion and shear. To carry out the computations, the contribution of concrete to shear resistance, V_c, is needed and can be obtained from Section 6.8.2 or the flow chart Fig. 6.14.

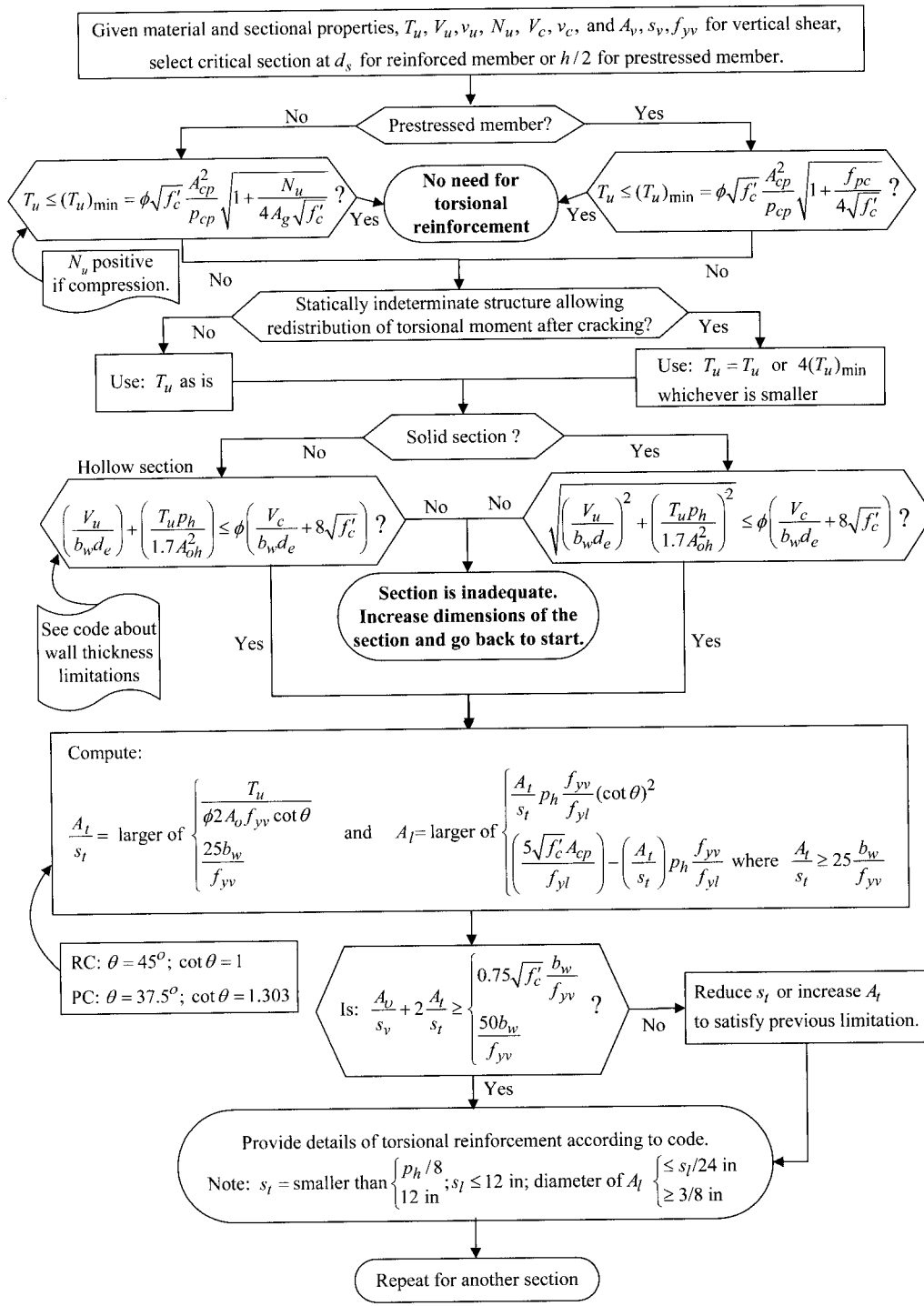

Figure 6.33 Proposed design flow chart for torsion (pure or combined) for prestressed and nonprestressed members.

Thus the d_p value used to compute V_c applies. This is also true for V_u. For uniform loading the approximation given in Eq. (6.32) for V_c can be used.

Compared to the ACI code, some notations are expanded such as for s_v and s_t to differentiate stirrup spacing, s, used for shear and torsion. Same spacing value s could be used for both. Also some equations are written in a slightly different form than given in the code to simplify the computations.

6.17 EXAMPLE: TORSION DESIGN OF A PRESTRESSED BEAM

Because a new example involving a combination of bending, shear, and torsion can be very lengthy, let us consider, for simplicity, the same beam (Fig. 6.34*a*) treated in the Examples of Sections4.9, and 6.10. Let us also assume that the beam is subjected to the same magnitude of dead and live loads. However, the design calls for a special loading condition in which a line load of magnitude equal to the live load of 0.40 klf can be applied at an eccentricity e = 1.5 ft from the axis of the beam. Restraint against rotation is provided at the ends of the beam by a transverse diaphragm. Thus, a torsional moment results at each section of the beam in addition to the bending moment and shear.

According to the ACI code procedure, the design for bending remains unchanged, while special design considerations must be taken for combined shear and torsion. The first critical section, at a distance x = 2 ft from the face of the support, will be covered in detail. A similar procedure can be followed for the other sections along the span.

The ultimate design torsional moment at the first critical section is given by:

$$T_u = (1.6w_L)\left(\frac{l}{2} - x\right)e = 1.6\times 0.4\times(35-2)\times 1.5 = 0.64\times 33\times 1.5$$

$$= 31.68 \text{ kips-ft} = 380160 \text{ lb-in}$$

The design ultimate shear force was determined in Example 6.10 (Tables 6.1 and 6.2). Its value is $V_u = 45.395$ kips. The corresponding value of v_u is given by:

$$v_u = \frac{V_u}{b_w d_p} = \frac{45395}{8\times 32} = 177.32 \text{ psi, where } d_p \geq 0.8h = 32 \text{ in}$$

The design flow chart for torsion (Fig. 6.33) will be followed for the main steps.

The beam cross section is first idealized to an equivalent T section with a constant depth flange of 5.75 in. Then it is separated into two rectangular parts, the web of dimensions 8 by 40 in, and the overhanging flange of dimensions 5.75 by 40 in (Fig. 6.34*b*). Sectional parameters are computed for the idealized section. In determining the dimensions x and y of the closed stirrups, the cover to the centroid of first layer of reinforcement (0.5-in diameter strands) was taken equal 2 in, from all sides.

Assuming No. 3 stirrups, leads to a cover to the centroid of stirrups equal:

$$2 - 0.5\times 0.5 - 0.5\times 3/8 = 1.5625 \text{ in}$$

The dimensions of closed loop stirrups are obtained as follows (Fig. 6.34*c*):

$$x_1 = 8 - 2\times 1.5625 = 4.875 \text{ in}$$

$$y_1 = 40 - 2\times 1.5625 = 36.875 \text{ in}$$

$$x_2 = 5.75 - 2\times 1.5625 = 2.625 \text{ in}$$

$$y_2 = 40 - 2\times 1.5625 = 36.875 \text{ in}$$

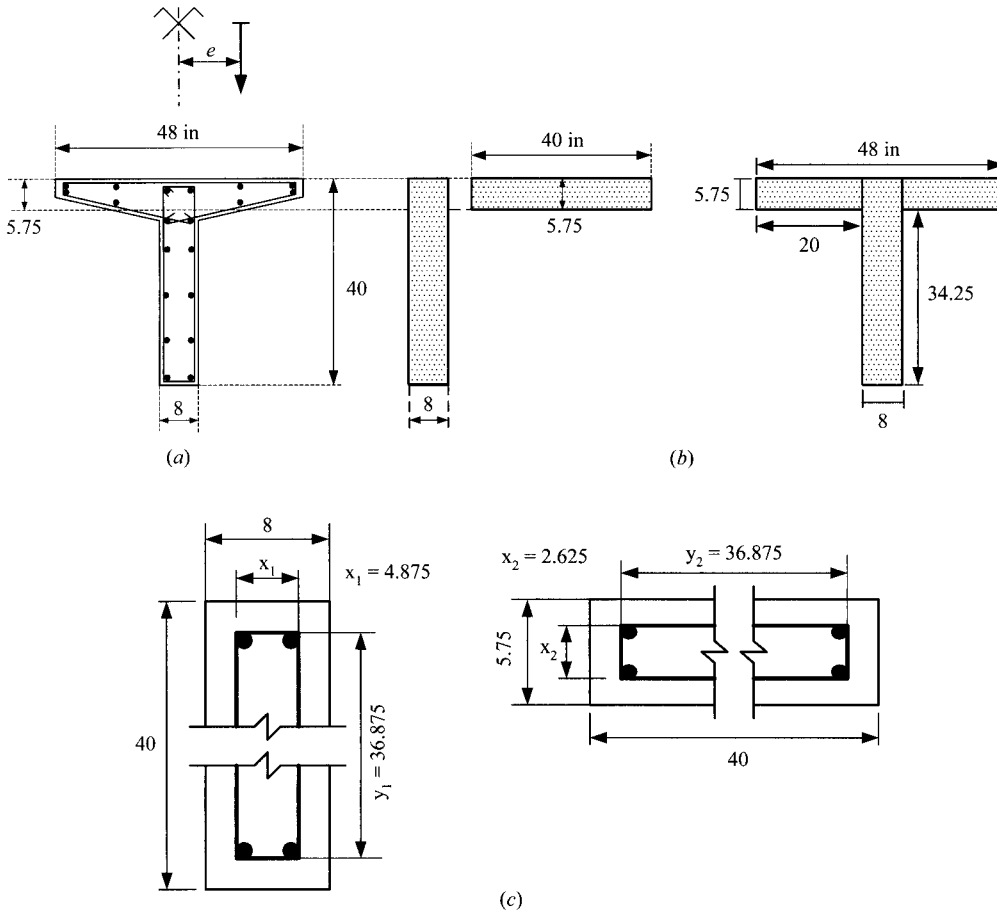

Figure 6.34

Let us compute first the torsional parameters of the section:

$$A_{cp} = A_g = 550 \text{ in}^2$$

$$p_{cp} = 48 + 2\times 5.75 + 2\times 20 + 2\times 34.5 + 8 = 176.5 \text{ in}$$

$$p_h = 2(y_1 + x_1) + 2(y_2 + x_2) = 2(36.875 + 4.875) + 2(36.875 + 2.625) = 162.5 \text{ in}$$

$$A_{oh} = y_1 x_1 + y_2 x_2 = 36.875\times 4.875 + 36.875\times 2.625 = 276.563 \text{ in}^2$$

$$A_o \approx 0.85 A_{oh} = 235.08 \text{ in}^2$$

The average prestress at the centroid of the section is given by:

$$f_{pc} = \sigma_g = \frac{F}{A_c} = \frac{229{,}500}{550} = 417.27 \text{ psi}$$

Following the steps in the flow chart of Fig. 6.33 (also Eq. 6.86):

$$(T_u)_{min} = \phi\sqrt{f_c'}\frac{A_{cp}^2}{p_{cp}}\sqrt{1+\frac{f_{pc}}{4\sqrt{f_c'}}} = 0.75\sqrt{5000}\frac{550^2}{176.5}\sqrt{1+\frac{417.27}{4\sqrt{5000}}}$$

$$= 143{,}000 \text{ lb-in} = 143 \text{ kip-in} = 11.92 \text{ kip-ft}$$

Check:

$T_u = 31.68$ kip-ft $> (T_u)_{min} = 11.92$ kip-ft $\rightarrow$ Torsional reinforcement is needed

Check if section dimensions are adequate. From shear design:

$d_e = d_p \geq 0.8h = 32$ in

$$v_c = \frac{Vc}{b_w d_p} = 409.5 \text{ psi}$$

$$v_u = \frac{V_u}{b_w d_p} = 177.32 \text{ psi}$$

For a solid section (Eq. 6.88):

$$\sqrt{\left(\frac{V_u}{b_w d_e}\right)^2 + \left(\frac{T_u p_h}{1.7A_{oh}^2}\right)^2} \leq \phi\left(\frac{V_c}{b_w d_e} + 8\sqrt{f_c'}\right) = 0.75(409.5 + 8\sqrt{5000}) = 731.39 \text{ psi}$$

$$\sqrt{(177.32)^2 + \left(\frac{380160 \times 162.5}{1.7 \times 276.563^2}\right)^2} = \sqrt{(177.32)^2 + (475.1)^2} = 507.11 < 731.39 \text{ psi} \quad \text{O.K.}$$

Thus the section dimensions and properties are adequate.

From Eqs. (6.94) and (6.98):

$$\frac{A_t}{s_t} = \text{larger of} \left\{ \begin{array}{l} \dfrac{T_u}{\phi 2A_o f_{yv}\cot\theta} = \dfrac{31.68 \times 12000}{0.75 \times 2 \times 235.08 \times 60000 \times 1.303} = 0.0138 \\ \dfrac{25b_w}{f_{yv}} = \dfrac{25 \times 8}{60{,}000} = 0.0033 \end{array} \right\} = 0.0138$$

$$A_l = \text{larger of} \left\{ \begin{array}{l} \dfrac{A_t}{s_t} p_h \dfrac{f_{yv}}{f_{yl}} (\cot\theta)^2 = 0.0138 \times 162.5(1.303)^2 = 3.807 \text{ in}^2 \rightarrow \text{controls} \\ \left(\dfrac{5\sqrt{f_c'}A_{cp}}{f_{yl}}\right) - \left(\dfrac{A_t}{s_t}\right) p_h \dfrac{f_{yv}}{f_{yl}} = \left(\dfrac{5\sqrt{5000} \times 550}{60000}\right) - 0.0138 \times 162.5 = 0.998 \text{ in}^2 \end{array} \right\}$$

Assuming a No. 3 stirrup size, of section 0.11 in^2, the following stirrup spacing is needed:

$$\frac{A_t}{s_t} = \frac{0.11}{s_t} = 0.0138 \rightarrow s_t = \frac{0.11}{0.0138} \approx 8 \text{ in}$$

Check stirrup spacing requirements:

$$s_t = 8 = \text{smaller than} \left\{ \begin{array}{l} \dfrac{p_h}{8} = \dfrac{162.5}{8} = 20.31 \text{ in} \\ 12 \text{ in} \end{array} \right. \rightarrow \text{O.K.}$$

The shear reinforcement provided at this section is No. 3 U-stirrup at 24 in (see Section 6.10). Thus:

$$\frac{A_v}{s_v} = \frac{0.22}{24} = 0.0092$$

Shear and torsion reinforcement must satisfy the following minimum reinforcement condition:

$$\frac{A_v}{s_v} + 2\frac{A_t}{s_t} = \frac{0.22}{24} + 2 \times 0.0138 = 0.0368 = \text{larger than} \begin{cases} 0.75\sqrt{f_c'}\,\dfrac{b_w}{f_{yv}} = 0.0071 \\ \dfrac{50 b_w}{f_{yv}} = 0.0067 \end{cases} \rightarrow \text{O.K.}$$

Following is a summary of the reinforcement needed for torsion and shear.

Since for shear one stirrup is needed at 24 in spacing, and for torsion one stirrup is needed at 8 in spacing, it is advisable to select one closed stirrup at 6 in spacing to cover both requirements in the web. Indeed we can verity that the transverse reinforcement provided is sufficient:

$$\frac{A_v}{s} = \frac{0.22}{6} = 0.367 \text{ (provided)} \approx 0.368 \text{ (required)}$$

In the flange, No. 3 closed stirrups are needed only for torsion.

The longitudinal reinforcement required for torsion can be satisfied using 19 No. 4 bars having each a cross section of 0.20 in^2, placed around the periphery of the section. Because of symmetry Fig. 6.34*a* shows 20 such bars. Their average spacing along the sides can be about 8 in and should satisfy the maximum spacing of 12 in allowed by the code. Longitudinal bars for torsion should also have a diameter larger than 0.042 times the stirrup spacing. Here the No. 4 bar has a diameter of 0.5 in > 0.042x6 = 0.25 in and is satisfactory. These longitudinal bars are in addition to the longitudinal reinforcement required for bending.

6.18 SHEAR AND TORSION IN PARTIALLY PRESTRESSED MEMBERS

A distinction was made throughout this chapter between a prestressed concrete member and a nonprestressed or reinforced concrete member. A review of the design approaches used for shear and torsion strongly suggests that partially prestressed members, which contain both prestressed and nonprestressed flexural reinforcement, can be designed essentially as prestressed members. The only difference between them is a lower value of the average prestress. In designing for shear and in order to be consistent with the procedures developed earlier for bending, the following value of d_e can be used:

$$d_e = \text{the larger of} \begin{cases} PPR d_p + (1 - PPR) d_s \\ \text{or} \\ PPR(0.8h) + (1 - PPR) d_s \end{cases} \tag{6.99}$$

where:

d_e = distance from extreme compressive fiber to centroid of tensile force in the reinforcement

d_p = distance from extreme compressive fiber to centroid of prestressing force

d_s = distance from extreme compressive fiber to centroid of tensile reinforcing steel

PPR = Partial Prestressing Ratio defined in Refs. [1.30 and 1.48]

As a first approximation, the value of PPR for Eq. (6.99) can be estimated from:

$$PPR \approx \frac{A_{ps} f_{py}}{A_{ps} f_{py} + A_s f_y} \tag{6.100}$$

REFERENCES

6.1 *AASHTO LRFD Bridge Design Specifications*, 2nd Edition. American Association of State and Highway and Transportation Officials, Washington, DC, 1998. Also Interim 2002.

6.2 ACI Committee 318, *Building Code and Commentary*. ACI 318-02/318R-02. American Concrete Institute, Farmington Hills, MI, 2002.

6.3 ACI Special Publication SP-18, *Torsion of Structural Concrete*. American Concrete Institute, Detroit, 1968.

6.4 ACI Special Publication SP-35, *Analysis of Structural Systems for Torsion*. American Concrete Institute, Detroit, 1973.

6.5 ASCE-ACI Joint Committee 426 Report, "The Shear Strength of Reinforced Concrete Members," *Journal of the Structural Division, ASCE*, 99(ST6): June, 1973, Chaps. 1-4, pp. 1091-1197. (Also reproduced in *ACI Manual of Concrete Practice*.)

6.6 Bresler, B., and J. G. MacGregor, "Review of Concrete Beams Failing in Shear," *Journal of the Structural Division, ASCE*, 93(55.2), 1967.

6.7 Collins, M. P., and D. Mitchell, "Shear and Torsion Design of Prestressed and Nonprestressed Concrete Beams," *PCI Journal*, 25(5): 32-100, 1980.

6.8 Collins, M. P., and D. Mitchell, "Design Proposals for Shear and Torsion," *PCI Journal*, 25(5), 1980, 70 pp.

6.9 Collins, M. P., and D. Mitchell, *Prestressed Concrete Structures*. Englewood Cliffs, NJ: Prentice Hall, 1991, 766 pp. Also 2nd Edition, Response Publications. Canada, 1997.

6.10 Cuevas, O. G., F. Robles, and R. Diaz de Cosio, "Strength and Deformation of Reinforced Concrete Elements," In *Reinforced Concrete Engineering*, Chap. 5, Vol. 1, Boris Bresler, ed. New York: John Wiley & Sons, 1974, pp. 194-301.

6.11 Fanella, D. A., and B. G. Rabbat, *Design of Concrete Beams for Torsion*. Engineering Bulletin EB106.02D, Portland Cement Association, Skokie, IL, 1997.

6.12 Fanella, D. A., B. G. and Rabbat, *Notes on ACI 318-02, Building Code Requirements for Structural Concrete with Design Applications*, Portland Cement Association, Skokie, IL, 2002.

6.13 Gangarao, H. V. S., and P. Zia, "Rectangular Prestressed Beams in Torsion and Bending," *Journal of the Structural Division, ASCE*, 99(St. 1): 183-98, 1973.

6.14 Henry, R. L., and P. Zia, "Prestressed Beams in Torsion, Bending, and Shear," *Journal of the Structural Division, ASCE*, (100(ST.5): 933-52, 1974.

6.15 Hsu, T. T. C., *Unified Theory of Reinforced Concrete*. Boca Raton: CRC Press, 1993, 313 pp.

6.16 Hsu, T. T. C., "Torsion of Structural Concrete – A Summary on Pure Torsion," in Ref. 6.3, pp. 165-78 and Hsu, T. T. C., "Torsion of Structural Concrete – Plain Concrete Rectangular Sections," in Ref. 6.3, pp. 203-38.

6.17 Hsu, T. T. C., "Torsion of Structural Concrete – Behavior of Reinforced Concrete Rectangular Members," in Ref. 6.3, pp. 261-306.

6.18 Hsu, T. T. C., "Torsion of Structural Concrete – Uniformly Prestressed Rectangular Sections without Web Reinforcement," *PCI Journal,* 13(2): 34-44, 1968.

6.19 Hsu, T. T. C., "Shear Flow Zone in Torsion of Reinforced Concrete," *Journal of Structural Engineering, ASCE*, 116(11): 3206-26, 1990.

6.20 Kani, G. N. J., "Basic Facts Concerning Shear Failure," *ACI Journal*, 63(6): 675-92, 1966.

6.21 Kani, G. N. J., "A Rational Theory for the Function of Web Reinforcement," *ACI Journal*, 66(3): 185-97, 1969.

6.22 Lampert, P., *Torsion und Biegung von Stahlbetonbalken (Torsion and Bending of Reinforced Concrete Beams)*, Bericht 27, Institute für Baustatik, Zurich, January 1970.

6.23 Lampert, P., "Torsion and Bending in Reinforced Concrete and Prestressed Concrete Members," *Proceedings of the Institution of Civil Engineers*, Vol. 50, December 1971, pp. 487-505.

6.24 Lampert, P., and B. Thürlimann, "Ultimate Strength and Design of Reinforced Concrete Beams in Torsion and Bending," *Publications*, International Association for Bridge and Structural Engineering, Zurich, Vol. 31-I, 1971, pp. 107-131.

6.25 Lampert, P., and M. P. Collins, "Torsion, Bending, and Confusion: An Attempt to Establish the Facts," *ACI Journal, Proceedings*, 69(8): 500-04, 1972.

6.26 Lessig, N. N., *Determination of the Load Carrying Capacity of Reinforced Concrete Elements with Rectangular Cross-Section Subjected to Flexure with Torsion*, Work 5, Institute Betona I Zhelezobetona, Moscow, 1959, pp. 4-28. Also available as Foreign Literature Study 371, PCA Research and Development Labs, Skokie, IL.

6.27 Lorentsen, M., "Theory of the Combined Action of Bending Moment and Shear in Reinforced and Prestressed Concrete Beams," *ACI Journal,* 62(4), 1965.

6.28 MacGregor, J. G., M. A. Sozen, and C. P. Siess, "Strength and Behavior of Prestressed Concrete Beams with Web Reinforcement," University of Illinois Civil Engineering Studies, Structural Research Series 210, Urbana, August, 1960.

6.29 MacGregor, J. G., M. A. Sozen, and C. P. Siess, "Strength of Concrete Beams with Web Reinforcement," *ACI Journal*, 62(12): 1503-19, 1965.

6.30 MacGregor, J. G., and J. M. Hanson, "Proposed Changes in Shear Provisions for Reinforced and Prestressed Concrete Beams," *ACI Journal*, (66(4): 276-88, 1969.

6.31 MacGregor, J. G., and M. G. Ghoneim, "Design for Torsion," *ACI Structural*, 92(2): 211-18, 1995.

6.32 MacGregor, J. G., *Reinforced Concrete Mechanics and Design*, 3rd Edition. Englewood Cliffs, NJ: Prentice Hall, 1997, 939 pp.

6.33 Marti, P., "Truss Models in Detailing," *Concrete International,* ACI, December 1985, pp. 66-73.

6.34 Mattock, A. H., and A. N. Wyss, "Full Scale Torsion, Shear and Bending Tests of Prestressed I-Girders," *PCI Journal*, 23(2): 22-40, 1978.

6.35 Mattock, M. A., and N. M. Hawkins, "Research on Shear Transfer in Reinforced Concrete," *PCI Journal,* 17(2): 55-75, 1972.

6.36 McGree, D., and P. Zia, "Prestressed Concrete under Torsion, Shear, and Bending," *ACI Journal*, 73(1): 26-32, 1976.

6.37 Mitchell, D., and M. P. Collins, "Diagonal Compression Field Theory – A Rational Model for Structural Concrete in Pure Torsion," *ACI Journal*, 71(8): 396-408, 1974.

6.38 Mitchell, D., and M. P. Collins "Detailing for Torsion," *ACI Journal*, 73(9): 506-11, 1976.

6.39 Mitchell, D., and M. P. Collins, "Influence of Prestressing on Torsional Response of Concrete Beams," *PCI Journal*, 23(3): 54-73, 1978.
6.40 Park, R., and T. Paulay, *Reinforced Concrete Structures*. New York: Wiley-Interscience, 1975, 769 pp.
6.41 Rangan, B. V., and A. S. Hall, "Strength of Prestressed Concrete I Beams in Combined Torsion and Bending," *ACI Journal*, 75(11): 612-18, 1978.
6.42 Reineck, K. H., "Editor, Examples for the Design of Structural Concrete with Strut-and-Tie Models," *Special Publication-208,* American Concrete Institute, Farmington Hills, MI, 2003.
6.43 Schlaich, J., K. Schafer, and M. Jennewein, "Toward a Consistent Design of Structural Concrete," *PCI Journal*, 32(3): 74-150, 1987.
6.44 Sozen, M. A., E. M. Swoyer, and C. P. Siess, "Strength in Shear of Beams without Web Reinforcement," Engineering Experiment Station Bulletin No. 452, University of Illinois, Urbana, April, 1959.
6.45 Taylor, H. P. J., "The Fundamental Behavior of Reinforced Concrete Beams in Bending and Shear," *Shear in Reinforced Concrete*, Special Publication SP-42, Vol. 1, American Concrete Institute, Detroit, 1972, pp. 43-77.
6.46 Vecchio, F. J., and M. P. Collins, "The Modified Compression Field Theory for Reinforced Concrete Elements Subjected to Shear," *ACI Journal, Proceedings*, 83(2): 219-31, 1986.
6.47 Vecchio, F. J., and Collins, M. P., "Compression Response of Cracked Reinforced Concrete," *ASCE Journal of Structural Engineering*, 119(12): 3590-3610, 1993.
6.48 Zia, P., "Torsion Theories for Concrete Members." In *Torsion of Structural Concrete*, SP-18, American Concrete Institute, Detroit, 1968, pp. 103-132.
6.49 Zia, P., and W. D. McGee, "Torsion Design of Prestressed Concrete," *PCI Journal,* 19(2): 46-65, 1974. Also Discussion in *PCI Journal*, November/December, 1974.
6.50 Zia, P., and T. T. C. Hsu, "Design for Torsion and Shear in Prestressed Concrete," ASCE Annual Convention, Chicago, 1978, Preprint No. 3423, 17 pp.

PROBLEMS

6.1 Because of high shear stresses (or principal tension) in the web of a beam near the supports, you propose to use vertical prestressing in combination with horizontal prestressing. Assuming $\sigma_x = \sigma_g = 700$ psi and υ = 400 psi, determine the magnitude of vertical prestress σ_y so that the principal tension is reduced at the centroid of the section to: (*a*) – 100 psi, or (*b*) zero,.

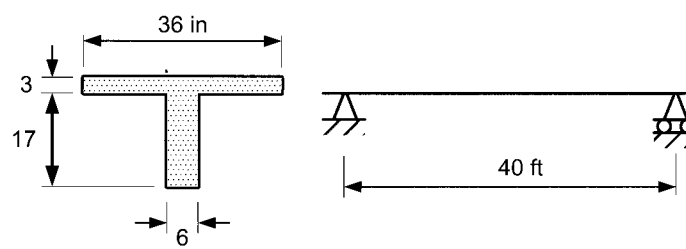

Figure P6.2

6.2 Go back to Prob. 4.7*g*, where a steel profile has been selected, and check shear requirements along the span (Fig. P6.2). What can you conclude if you are told that the beam is part of a joist slab system?

6.3 Go back to Prob. 4.8 and check shear requirements near the supports and at sections located 5 ft from the support on the cantilever side, and 5 and 10 ft on the span side.

6.4 The precast prestressed beam of Fig. P6.4 has been selected for the roof of a stadium. The beam is simply supported with, on one side, a cantilever of 20 ft. The following information is given:
Live load = 40 psf

Steel: 0.5 in diameter strands

$f_{pu} = 270$ ksi

$f_{py} = 245$ ksi

diameter = 1/2 in

area per strand = 0.153 in^2

f_{pi} at transfer = 175 ksi

$f_{pe} = 150$ ksi

Section properties:

$A_c = 615$ in^2

$I = 59{,}720$ in^4

$y_b = 21.98$ in

$y_t = 10.01$ in

$Z_b = 2717$ in^3

$Z_t = 5960$ in^3

$w_G = 0.641$ klf

Concrete

$f'_c = 5000$ psi $\quad f'_{ci} = 4000$ psi

$\bar{\sigma}_{ti} = -190$ psi $\quad \bar{\sigma}_{ci} = 2400$ psi $\quad \bar{\sigma}_{ts} = -424$ psi $\quad \bar{\sigma}_{csus} = 2250$ psi $\quad \bar{\sigma}_{cs} = 3000$ psi

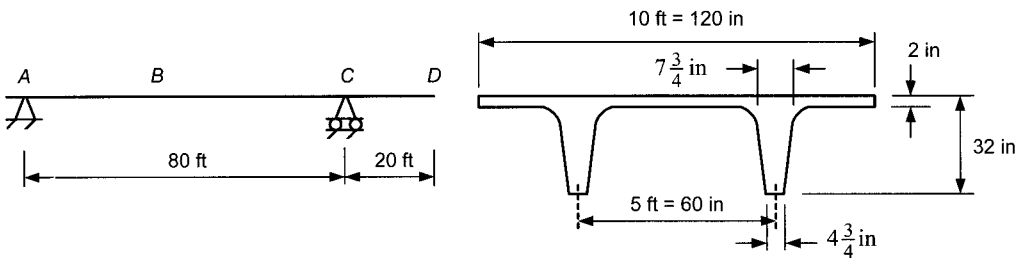

Figure P6.4

(*a*) Determine the position of point *B* at which maximum positive moment occurs. Build for sections *B* and *C* the two feasible domains of e_o versus $1/F_i$ and select a common satisfactory value of *F* corresponding to an even integer number of strands.

(*b*) Determine the strands' layout and their centroid at sections *B* and *C* and check the ultimate moment requirements according to ACI specifications at both sections. Is the ratio of ultimate to cracking moment at section *C* satisfactory?

(*c*) Assuming *F* constant along the beam, construct the limit zone and the steel envelopes. Suggest a satisfactory steel profile along the beam.

(*d*) Check shear requirements along the beam and determine the required stirrups. Plot graphically shear stresses versus abscissa and show the selected stirrup spacing.

6.5 An elevated guideway for a mobile lifting crane is made out of a series of consecutive simple span prestressed concrete beams. The maximum reaction from the wheel of the crane is $P = 30$ kips, and the span, center to center of supports, is 40 ft.

The beam cross-section is a symmetrical *I* section with: $b = 18$ in., $b_w = 6$ in., $h_f = 4$ in, and $h = 30$ in. The following information is provided:

$\bar{\sigma}_{ci} = 2400$ psi; $\bar{\sigma}_{ti} = -189$ psi; $\bar{\sigma}_{csus} = 2000$ psi; $\bar{\sigma}_{cs} = 3000$ psi; $\bar{\sigma}_{ts} = -422$ psi

$f'_c = 5000$ psi; $f'_{ci} = 4000$ psi; $f_{pu} = 270$ ksi; $f_{py} = 243$ ksi; $f_{pe} = 150$ ksi

$\eta = F / F_i = 0.85$; unit weight of concrete = 150 pcf; $E_c = 4286$ ksi; $E_{ci} = 3834$ ksi

$f_y = 60$ ksi; $d_s = 28$ in

Maximum practical eccentricity $(e_o)_{mp} = 13$ in

Stress relieved low relaxation strands with area per stand = 0.216 in^2

1. Design the beam as a fully prestressed beam for service load and check ultimate strength requirements for bending according to the ACI code. Use computer programs, if available, and summarize the results obtained.
2. Assume that the beam is designed as a partially prestressed beam with the following final prestressing force: F = 129.6 kips which corresponds to four strands with A_{ps} = 0.864 in^2; eccentricity at midspan = maximum practical eccentricity; eccentricity at support = 6 in; tendons profile = single draping at midspan. Use the ACI code.
   (*a*) Using ultimate strength design, determine the area of reinforcing steel A_s needed in addition to A_{ps} to satisfy nominal bending resistance criteria.
   (*b*) Determine the required shear reinforcement (i.e., spacing of No. 3 U stirrups) at the following sections along the span: 20 in, 5 ft, 10 ft, 15 ft, and 20 ft from the center of the left support. From the information obtained, plot a figure similar to Fig. 6.17 in this book. Use the elaborate method of analysis for shear.
3. Repeat question (2) using the AASHTO LRFD code.

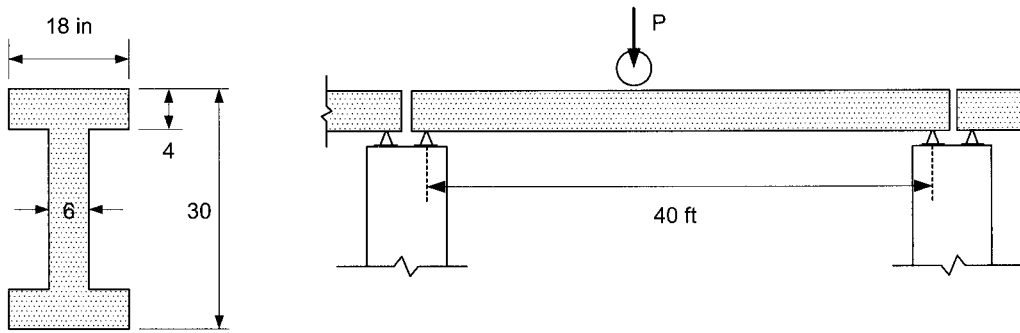

Figure P6.5

6.6 An L-shaped spandrel beam (also called ledger beam) is to be designed as part of a precast prestressed concrete parking structure. The spandrel beam supports, in addition to its own weight, the reactions from four double-T beams that are part of the floor system. The spandrel beam spans 29 feet between the columns, and the double-T beams span 44 feet. The floor surface is topped with a 2 in thick concrete topping leading to composite double-T beams. The topping adds 25 psf to the load, that is, 200 plf to each beam. The double-T beams are made of lightweight concrete. Each T-beam weighs 320 plf (8LDT24 from PCI Handbook). Figure P6.6 provides some details.

The purpose of this problem is to design the spandrel beam for bending, shear, and torsion according to the ACI code. The spandrel beam is subjected to concentrated loads (or reactions) imposed by each leg of the double-T beams. The following information is given:

Live load = 120 psf on floor, which is equivalent to 960 plf for the double-T beams.

$\bar{\sigma}_{ci} = 3000$ psi; $\bar{\sigma}_{ti} = -424$ psi; $\bar{\sigma}_{csus} = 3150$ psi; $\bar{\sigma}_c = 4200$ psi; $\bar{\sigma}_{ts} = -502$ psi

$f'_c = 7000$ psi; $f'_{ci} = 5000$ psi; $f_{pu} = 270$ ksi; $f_{py} = 243$ ksi; $f_{pe} = 150$ ksi

$\eta = F / F_i = 0.83$; unit weight of concrete = 150 pcf; $E_c = 5072$ ksi; $E_{ci} = 4286$ ksi

$f_y = 60$ ksi for stirrups; $d_{cmin} = 3$ in; $(e_o)_{\text{support}} = 6.5$ in.

The compressive strength of the concrete topping is 3500 psi.
The strands used are 0.6 inch in diameter.

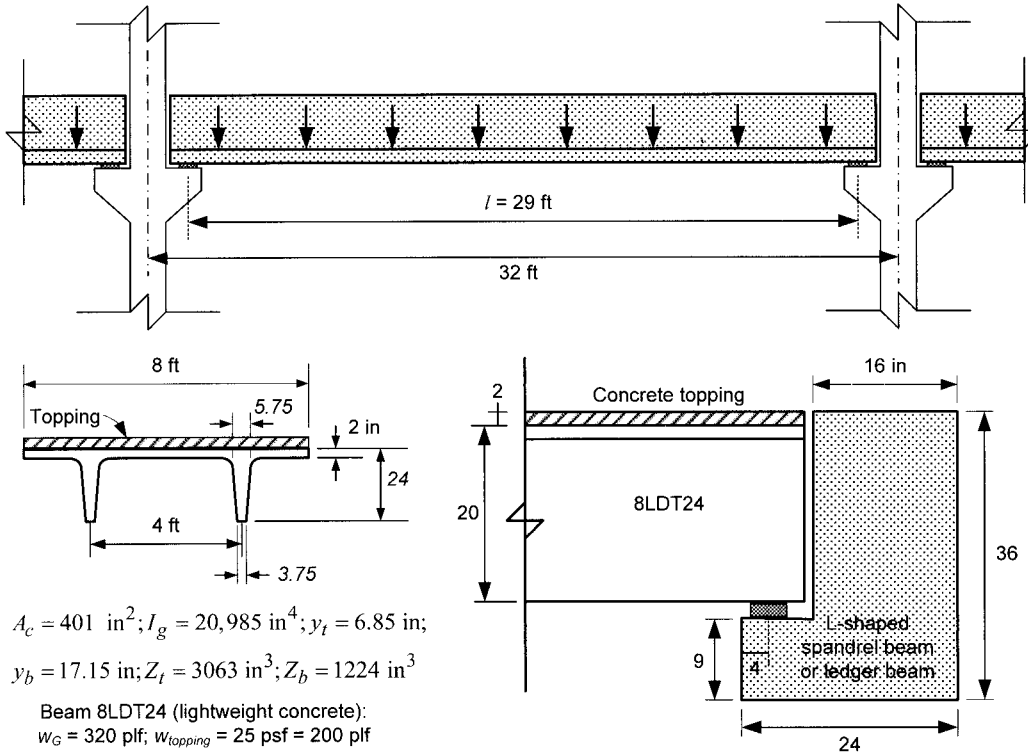

$A_c = 401$ in^2; $I_g = 20{,}985$ in^4; $y_t = 6.85$ in;

$y_b = 17.15$ in; $Z_t = 3063$ in^3; $Z_b = 1224$ in^3

Beam 8LDT24 (lightweight concrete):
w_G = 320 plf; $w_{topping}$ = 25 psf = 200 plf

Figure P6.6

1. Check that the prestressing force needed for the spandrel beam can be provided by seven bonded strands with a maximum practical eccentricity at midspan. Five strands are taken straight and 2 strands are draped with a single draping section at midspan. Nonprestressed reinforcement is placed near the top fiber to account for tension under initial loading.
2. Show a detailed cross section with the location of each prestressing strand at midspan and at support so as to achieve the design eccentricity at each section; $(e_o)_{\text{support}} = 6.5$ in.
3. Design the vertical shear reinforcement for the spandrel beam assuming no torsion is to be considered. Use the ACI code. It is suggested to check shear requirements at the location of each leg of the double-T beams, using the maximum shear force computed at that section (that is, prior to subtracting the reaction of the leg). This will reduce the number of sections analyzed to four for half the span. Use No. 3 closed stirrups (two legs).
4. Assuming the ends of the spandrel beam are restrained against torsional rotation, design the transverse and longitudinal torsion reinforcement. Draw a typical section showing the details of all reinforcements used.

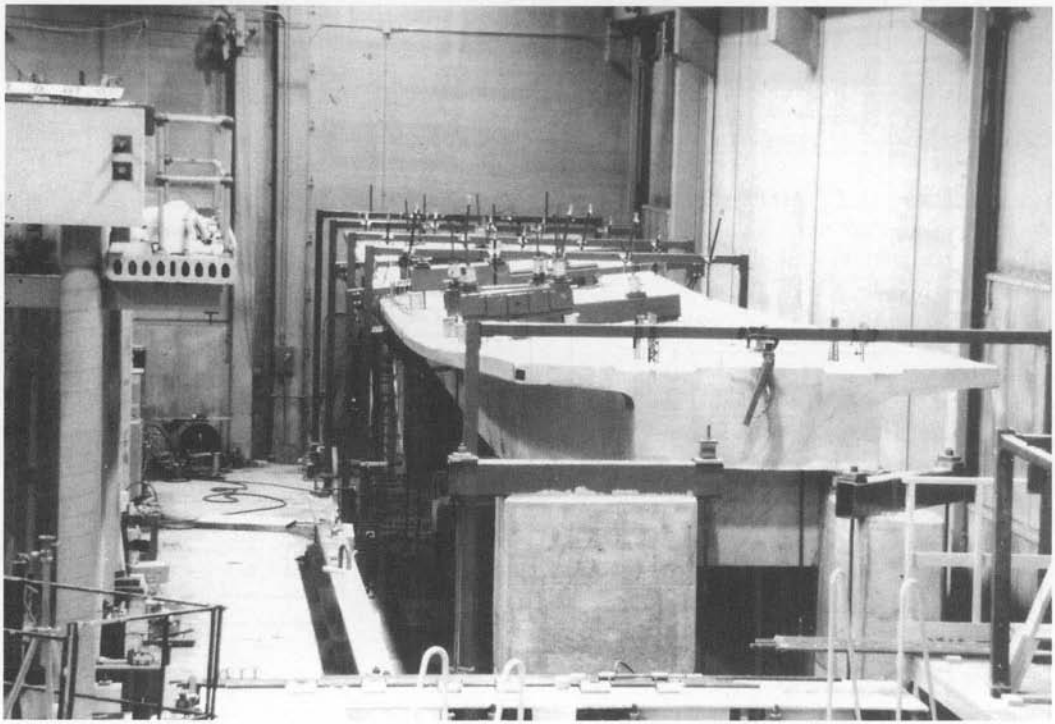

Full-scale test of prestressed concrete bridge beam under combined bending, shear and torsion. *(Courtesy Portland Cement Association.)*

DEFLECTION COMPUTATION AND CONTROL

7.1 SERVICEABILITY

Most prestressed concrete structures are first designed and dimensioned on the basis of allowable stresses and/or bending strength limit states (Section 3.4 and Fig. 3.3). If a sound design approach is followed and if code requirements with respect to permissible stresses, strength, shear and torsion are satisfied, it is very likely that the design can be finalized without any further modification. However, there are increasingly situations where it is essential to check if the serviceability of the structure is satisfactory. Serviceability refers to the performance of the structure in service. The most frequently considered serviceability limit states in prestressed concrete are related to short- and long-term camber or deflection, fatigue, cracking (primarily in partial prestressing), corrosion resistance, and durability (Fig. 3.1). Other limit states and related criteria, such as vibration characteristics, can also be set in the design. In designing for serviceability, loading does not necessarily imply full service load, but should be specified for each criterion. For instance, in evaluating fatigue, the repetitive load for building members may be taken as only 50 percent of the specified live load, while for railway bridges, the full live load should be considered. Similarly, in computing long-term deflection, the part of the live load that can be considered sustained must be carefully assessed and accounted for in addition to the permanent dead load.

Only the deflection limit state is addressed in this Chapter. Fatigue and cracking are more characteristic of partially prestressed members than of fully prestressed ones and are covered in Ref. [1.48] Some aspects of fatigue and corrosion of the component materials can be found in Chapter 2.

7.2 DEFLECTION: TYPES AND CHARACTERISTICS

Deflection is defined as the total movement induced at a point of a member from the position before application of the load to the position after application of the load. The maximum deflection, which in uniformly loaded simply supported beams occurs at midspan, is generally of main interest in design. A distinction is often made between "camber," which is the deflection caused by prestressing, and "deflection," which is that produced by external loads. They are identical in nature but generally opposite in sign. Typically, prestressing produces *upward* camber in a simply supported beam, while self-weight produces *downward* deflection. Their combination may produce an upward or a downward movement. In order to avoid confusion, the term "deflection" is used in its most general form, unless the separate effect of camber is addressed.

The following sign convention will be followed: plus (+) for downward deflection and minus (-) for upward deflection.

In reinforced concrete beams, deflection is due to external loads and is always downward. In prestressed concrete beams, deflection depends on the combined effect of prestressing and external loading. It can easily be controlled by changing the magnitude and profile of the prestressing force. It is not uncommon to achieve a zero deflection design in partial prestressing. In both reinforced and prestressed concrete members, deflection under sustained loading continues to increase with time, mainly due to the effects of creep and shrinkage of concrete and relaxation of prestressing steel. Excessive deflections, especially those developing over time, are common causes of trouble and must be limited.

At any time, t, the total deflection can be separated into two parts, an instantaneous short-term part and an additional, time-dependent part (Fig. 7.1). The time-dependent part at the end of service life is defined as the additional long term deflection and is of interest in ACI code design criteria. Furthermore, in computing deflection, a different approach is followed, whether the member is uncracked, such as in fully prestressed members, or cracked, such as in reinforced and partially prestressed members. Most of these differences and how to accommodate them are clarified in the following sections.

7.2.1 Terminology / Notation

t = time in general

t_A = age of member at time of loading

τ = $t - t_A$ = time lapse that occurs between age at loading and time considered

Δ_i = instantaneous deflection due to any load; it generally involves using the modulus of elasticity of the material and the prestressing force, if any, at time of loading

$\Delta_{add}(t)$ = additional deflection that takes place with time, t, after occurrence of the instantaneous deflection, assuming sustained load

Δ_{add} = additional long-term deflection used in the ACI code for the design service life of the structure

$\Delta(t)$ = total deflection at time, t, representing the sum of the instantaneous deflection and the additional time-dependent deflection at t, that is (Fig. 7.1): $\Delta(t) = \Delta_i + \Delta_{add}(t)$

$\Delta(life)$ = the sum of instantaneous deflection and additional long term deflection under sustained load at the service life of the structure

$\Delta_{add}(t, t_A)$ = additional deflection that takes place at time, t, for a member loaded at time t_A.

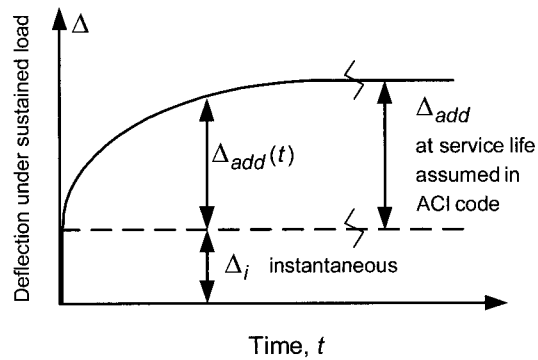

Figure 7.1 Definition of various deflection terms.

7.2.2 Key Variables Affecting Deflections in a Given Beam

In prestressed concrete beams, the deflection is due to the combined effect of prestressing and external load. Some background and typical deflection computations are covered in the following sections. However the following brief introductory overview will give an idea of the issues at hand. Assuming elastic behavior, the deflection of a given beam can be put in the following most general form that separates the effect of external load and prestressing:

$$\Delta = \frac{K_1}{EI} + \frac{K_2 F}{EI} \tag{7.1}$$

where K_1 is a parameter that depends on the applied load and the span, and K_2 is a parameter that depends on the tendon profile. Depending on the circumstances, the other three variables can have different values; they are: E, the elastic modulus, I, the moment of inertia, and F, the prestressing force. Figure 7.2 illustrates the

choices available for selecting each of these variables. The prestressing force varies with time and should be estimated from prestress losses at the time deflection is needed. The section may be uncracked or cracked, necessitating the use of the gross moment of inertia, the cracked moment of inertia, the effective moment of inertia, or other possible value. The elastic modulus of concrete may be used to estimate the effects of creep with time, and thus its value may be instantaneous for short-term loads, or equivalent for loads sustained up to a time t, or equivalent and cyclic for cyclic-fatigue loads (Section 7.10).

Equation (7.1) and Fig. 7.2 will become clearer to the reader following the treatment of this chapter.

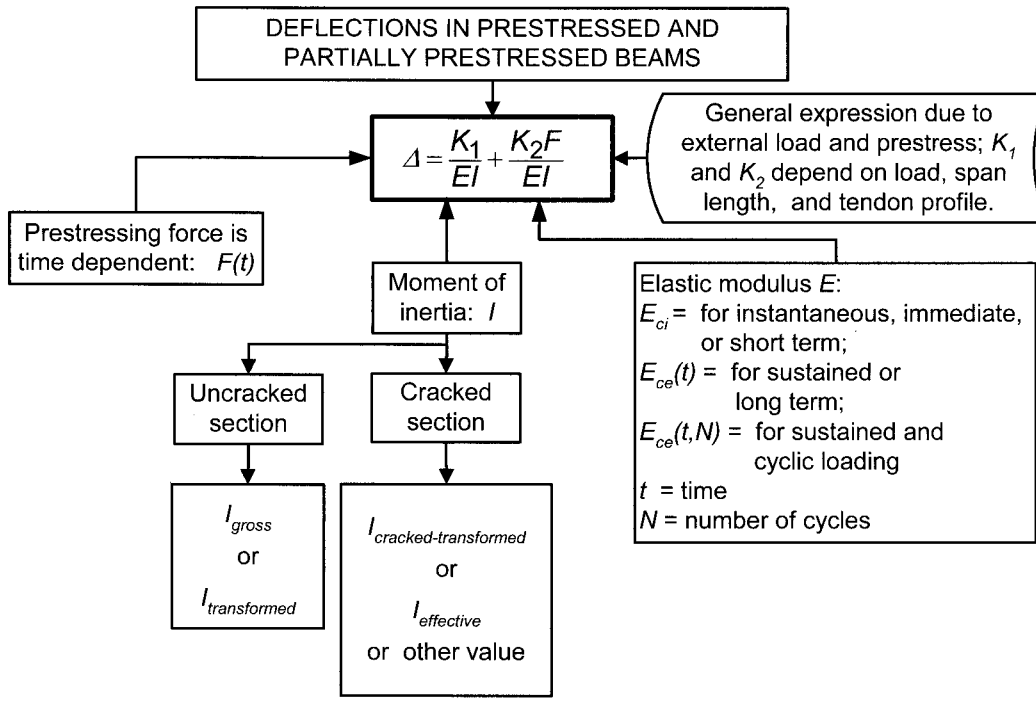

Figure 7.2 Key variables affecting deflection calculations.

7.3 THEORETICAL DEFLECTION DERIVATIONS

Based on general principles of mechanics and assuming linear elastic behavior, several methods can be used to compute the deflections or displacements of structures. One of the most convenient methods in structural design is the moment-area method, because it relies on the knowledge of the moments along the members, and these moments are generally known at this stage of the design. The moment-

area method was first developed by Mohr. It is based on the relationship between bending moment and curvature at any point of a flexural member, given by:

$$\phi = \frac{d\theta}{dx} = \frac{M}{EI} \tag{7.2}$$

where ϕ is the curvature or angle change per unit length of a deflected flexural member, θ is the angle between the tangents at two points of the deflected elastic curve, M is the applied bending moment, E *is* the elastic modulus of the beam material, and I is the moment of inertia in general. M is a function of x, and I can vary along the member. Two basic theorems are derived and are stated next without proof. The notation is reported in Fig. 7.3.

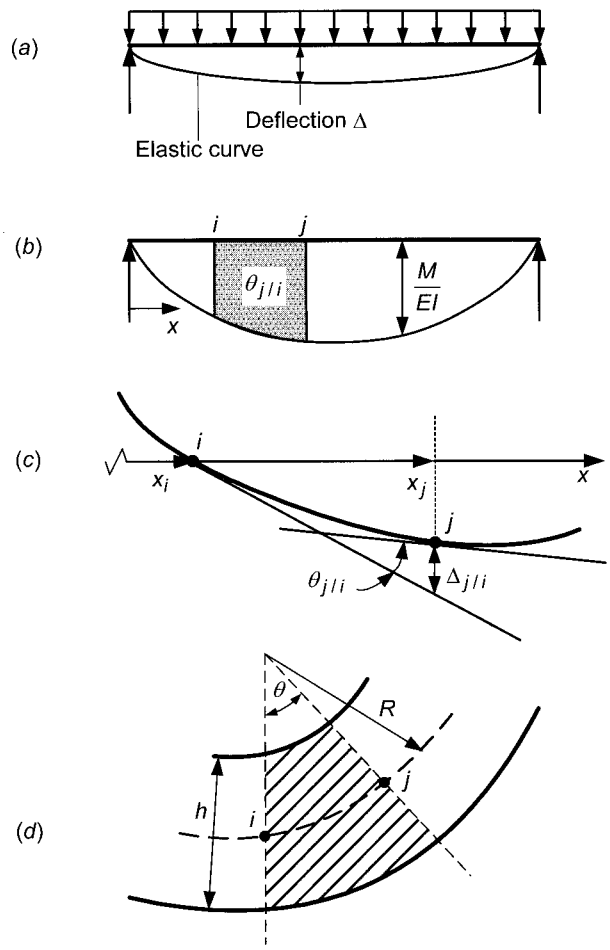

Figure 7.3 Illustration of deflection, rotation and curvature.

7.3.1 Moment-Area Theorems

1. **First moment-area theorem (or Rotation Theorem).** *The change in angle between points i and j on the deflected elastic curve of a flexural member, or the slope at point j relative to the slope at point i, is equal to the area under the M/EI diagram between points i and j, that is*

$$\theta_{j/i} = \int_{x_i}^{x_j} \left(\frac{M}{EI}\right) dx \tag{7.3}$$

The first moment-area theorem is essentially used to determine the rotation of one section j with respect to another section i.

2. **Second moment-area theorem (or Deflection Theorem).** *The deflection of point j of a flexural member, measured with respect to the tangent at another point i of the member, is equal to the first static moment taken about point j of the area under the M/EI diagram along the member between points i and j, that is:*

$$\Delta_{j/i} = \int_{x_i}^{x_j} x\left(\frac{M}{EI}\right) dx \tag{7.4}$$

Note that the change in slope or deflection is taken with respect to a tangent to the elastic curve. The appropriate choice of a base or reference tangent will substantially reduce the computations. For instance, although the midspan section deflects with respect to the support in a uniformly loaded beam, it is preferably selected as the reference section i because the elastic curve has zero slope or horizontal tangent at that section. The computations are run as if the supports are deflecting with respect to midspan. In most common design cases, the moment diagram is either parabolic or linear. Thus, the area under the moment diagram and its centroid with respect to a reference point can be easily determined from simple geometric shapes. Useful expressions for several common shapes of moment diagram or part of it are shown in Fig. 7.4.

Note that the moment-area theorems are essentially geometric relationships. They hold for any situation where the distribution of curvature can be determined. An example illustrating the use of the second moment-area theorem to compute deflection is given next.

M/EI Diagram	$\bar{x}_1$ *and* A_1	$\bar{x}_2$ *and* A_2
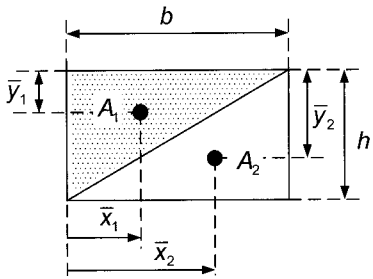	$\bar{x}_1 = \frac{b}{3}$ $\bar{y}_1 = \frac{h}{3}$ $A_1 = \frac{bh}{2}$	$\bar{x}_2 = \frac{2b}{3}$ $\bar{y}_2 = \frac{2h}{3}$ $A_2 = \frac{bh}{2}$
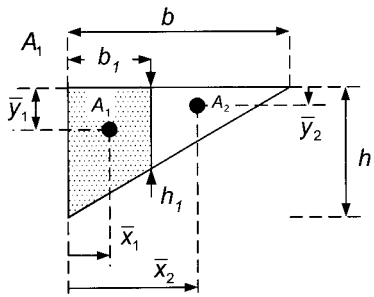	$\bar{x}_1 = \frac{b_1(2h+h_1)}{3(h+h_1)}$ $\bar{y}_1 = \frac{h_1^2+hh_1+h_2^2}{3(h+h_1)}$ $A_1 = \frac{b_1(h+h_1)}{2}$	$\bar{x}_2 = \frac{(2b_1+b)}{3}$ $\bar{y}_2 = \frac{h_1}{3}$ $A_2 = \frac{(b-b_1)h_1}{2}$
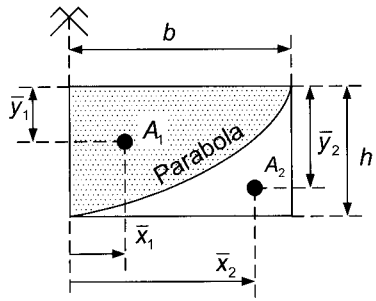	$\bar{x}_1 = \frac{3b}{8}$ $\bar{y}_1 = \frac{2h}{5}$ $A_1 = \frac{2bh}{3}$	$\bar{x}_2 = \frac{3b}{4}$ $\bar{y}_2 = \frac{7h}{10}$ $A_2 = \frac{bh}{3}$
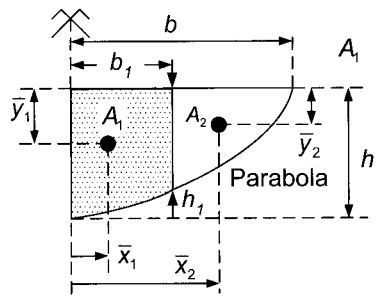	$\bar{x}_1 = \frac{3b_1}{4}\left(\frac{h_1+h}{2h+h_1}\right)$ $A_1 = \frac{b_1(2h+h_1)}{3}$	$\bar{x}_2 = \frac{3}{4}\left(\frac{b^2h-b_1^2h}{2bh-2b_1h-b_1h_1}\right)$ $A_2 = \frac{2bh}{3} - A_1$

Figure 7.4

7.3.2 Example

Determine the deflection (camber) for a simply supported beam with uniform cross section due to a prestressing force having a profile with two draping points, as shown in Fig. 7.5*a*. No external loading is considered.

The corresponding *M/EI* diagram is shown in Fig. 7.5*b*. The moment is negative and the corresponding deflection will be negative (i.e., camber). However, the sign will be shown only at the end of the computations in order not to carry negative signs with areas. The elastic curve is shown in Fig. 7.5*c*. The reference point i is taken at midspan, as it has a horizontal tangent to the elastic curve, and point j is taken at the support. The area under the *M/EI* diagram is divided into three parts: A_1, A_2, and A_3. According to the second moment-area theorem, the deflection is equal to the moment of these areas with respect to j.

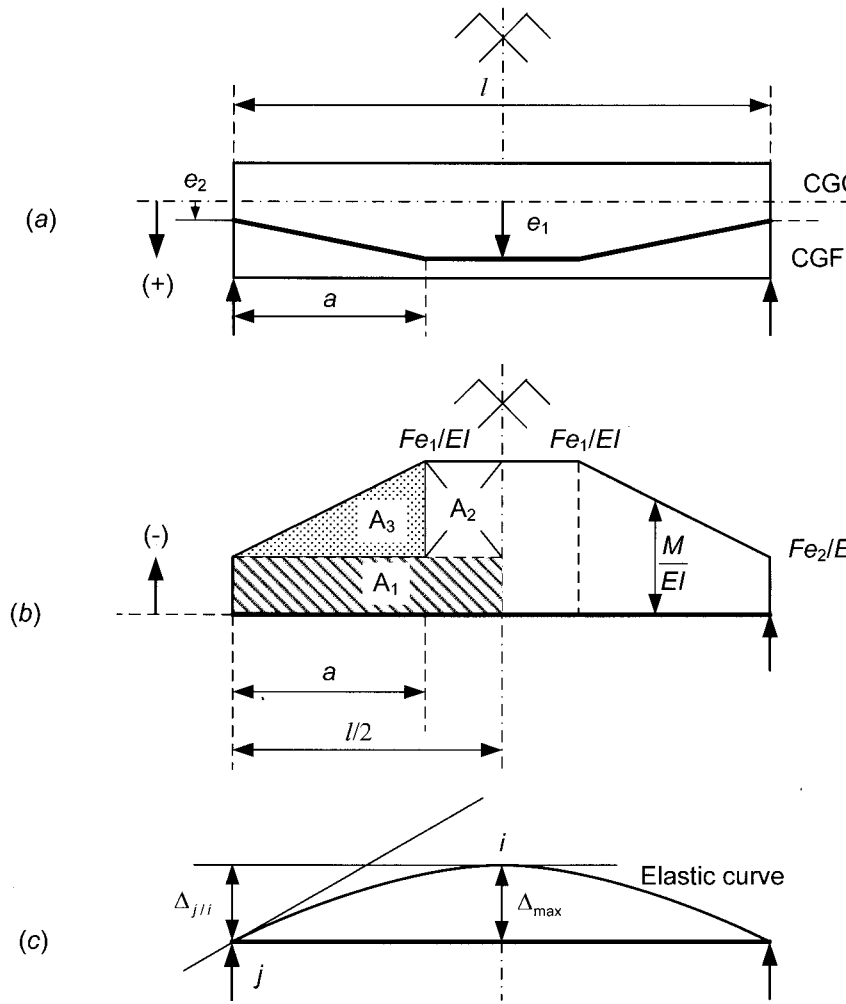

Figure 7.5 Deflection by the second moment area theorem.

Thus

$$\Delta_{j/i} = \frac{l}{4}A_1 + \frac{(l/2+a)}{2}A_2 + \frac{2a}{3}A_3$$
$$= \frac{l}{4}\frac{Fe_2}{EI}\frac{l}{2} + \left(\frac{l/2+a}{2}\right)\left(\frac{l}{2}-a\right)\left(\frac{Fe_1-Fe_2}{EI}\right) + \frac{2a}{3}a\left(\frac{Fe_1-Fe_2}{2EI}\right)$$

It can be reduced to:

$$\frac{Fl^2}{8EI}\left[e_1 + (e_2-e_1)\frac{4a^2}{3l^2}\right]$$

to which a minus sign should be applied. The result is the same as the expression shown in Fig. 7.6 for the same case.

7.4 SHORT-TERM DEFLECTIONS IN PRESTRESSED MEMBERS

The approaches treated next apply to the computation of instantaneous or short-term deflections. They also provide the basis for computing long-term deflections by the approximate methods described in Sec. 7.6.

7.4.1 Uncracked Members

Fully prestressed concrete members are uncracked under service loads and are assumed linear elastic. Their deflections can be determined using theoretical derivations identical to those described in the previous sections.

Typical formulas for deflections are given in Fig. 7.6 for several profiles of the prestressing force and several types of loading. Simply supported beams with constant prestressing force and constant sectional properties are assumed. Because superposition is valid in computing deflections for uncracked elastic members, many combinations are practically covered, such as a uniform load due to self-weight and a prestressing force following a single draping point profile. Note that two expressions are given for each case, one in function of the prestressing force and the other in function of the curvatures at the midspan section and at the support. The deflection expressed in function of the curvatures has the following most general form [Ref. 7.25]:

$$\Delta = \phi_1\frac{l^2}{8} + (\phi_2 - \phi_1)\frac{a^2}{6} \tag{7.5}$$

where ϕ_1 = curvature at midspan
ϕ_2 = curvature at the support
a = length parameter that is a function of the tendon profile used

Camber due to prestressing force	Deflection due to loading
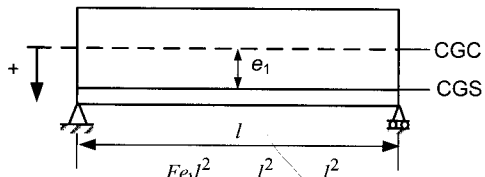 $\Delta = -\frac{Fe_1 l^2}{8EI} = \phi_1 \frac{l^2}{8} = \phi_2 \frac{l^2}{8}$ → (see footnote)	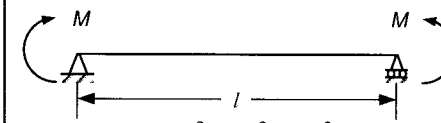 $\Delta = \frac{Ml^2}{8EI} = \phi_1 \frac{l^2}{8} = \phi_2 \frac{l^2}{8}$
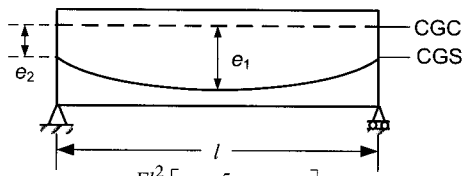 $\Delta = -\frac{Fl^2}{8EI}\left[e_2 + \frac{5}{6}(e_1 - e_2)\right]$ $= \phi_1 \frac{l^2}{8} + (\phi_2 - \phi_1)\frac{l^2}{48}$	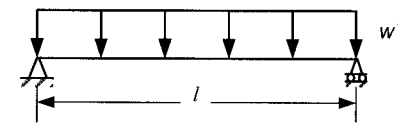 $\Delta = \frac{5wl^4}{384EI} = \phi_1 \frac{5l^2}{48}$ † Assumed uniform per unit length
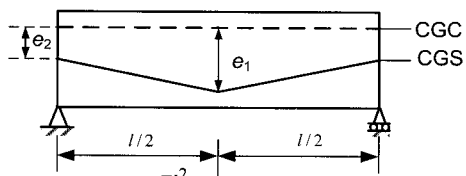 $\Delta = -\frac{Fl^2}{24EI}[2e_1 + e_2]$ $= \phi_1 \frac{l^2}{8} + (\phi_2 - \phi_1)\frac{l^2}{24} = \phi_1 \frac{l^2}{12} + \phi_2 \frac{l^2}{24}$	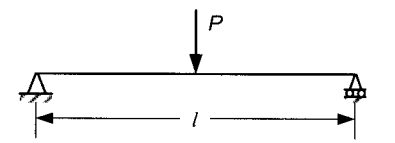 $\Delta = \frac{Pl^3}{48EI} = \phi_1 \frac{l^2}{12}$
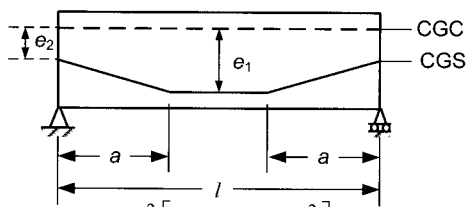 $\Delta = -\frac{Fl^2}{8EI}\left[e_1 + (e_2 - e_1)\frac{4a^2}{3l^2}\right]$ $= \phi_1 \frac{l^2}{8} + (\phi_2 - \phi_1)\frac{a^2}{6}$	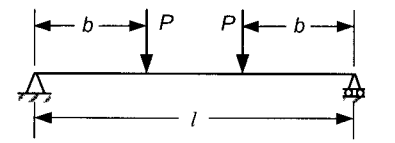 $\Delta = -\frac{Pb}{24EI}\left(3l^2 - 4b^2\right)$ $= \phi_1 \frac{3l^2 - 4b^2}{24}$
For the uncracked section, use I of transformed section or I_{gross} as first approximation. For the cracked section, use I_e = effective moment of inertia.	

Note: For a straight tendon profile with debonding over a distance a from each support, the camber due to prestressing is given by: $\Delta = -(Fe_1/EI)(l^2/8 - a^2/2) = \phi_1(l^2/8 - a^2/2)$

Figure 7.6 Typical midspan deflections for simply supported beams.

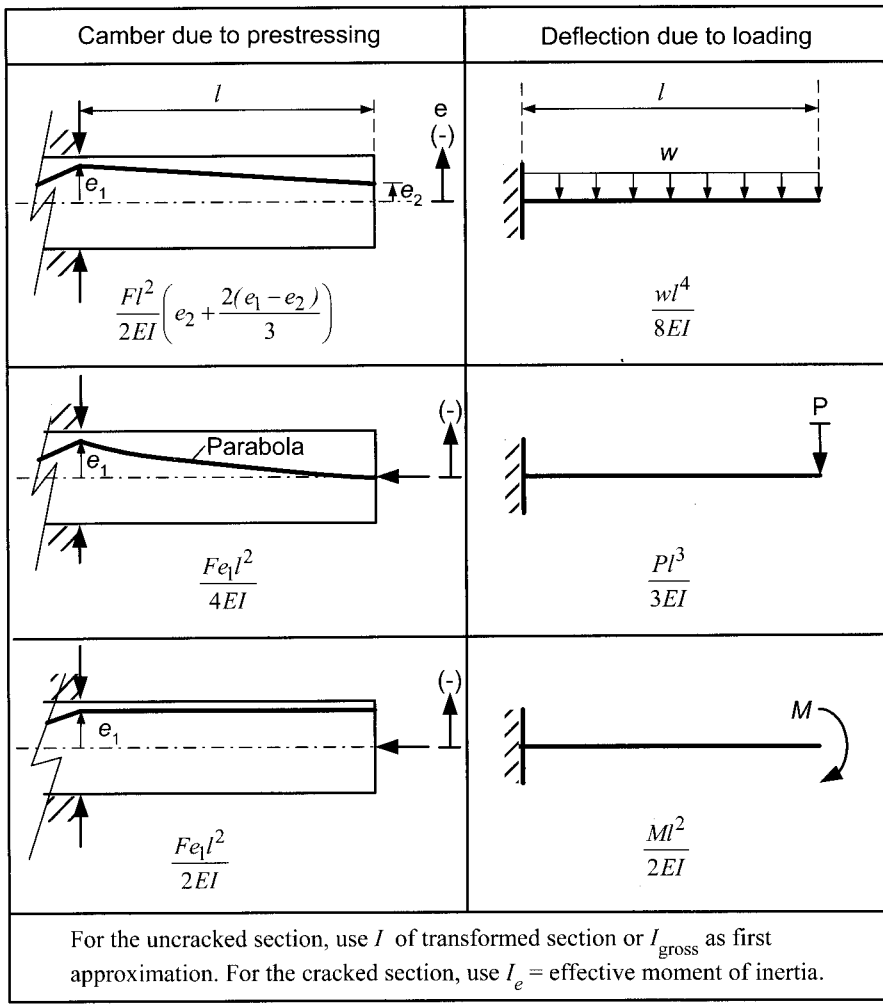

Figure 7.7 Typical end deflections for fixed end cantilever beams.

The values of a have been directly integrated in the expressions shown in Fig. 7.6. Typical formulas for deflections in cantilever beams are given in Fig. 7.7.

The curvature at any section can be computed from Eq. (7.2) or from the strain distribution along the section (Eq. 3.14) as:

$$\phi = \frac{M}{EI} = \frac{\varepsilon_{ct} - \varepsilon_{cb}}{h} \tag{7.6}$$

where ε_{ct} = strain on top fiber of section
ε_{cb} = strain on bottom fiber of section
h = depth of section

Equation (7.6) is illustrated in Fig. 7.8*a* for uncracked sections and in Fig. 7.8*b* for cracked sections where ε_{cb} vanishes and h is replaced by c. If M/EI is used, then the moment should include the moment due to prestressing.

In using all deflection expressions such as those given in Figs. 7.6 and 7.7, two important properties must be defined, namely, the modulus of elasticity of the concrete and the moment of inertia of the section (or of each section if variable depth is used).

The design modulus of elasticity of the concrete material (secant modulus at $0.45f'_c$ at 28 days) can be estimated from the expression recommended in the ACI code and given in Table 2.8.

However, the strength of concrete varies with age, and its modulus, too. In computing initial camber or deflection, it is common to use the initial modulus E_{ci} while E_c is considered for service load deflections.

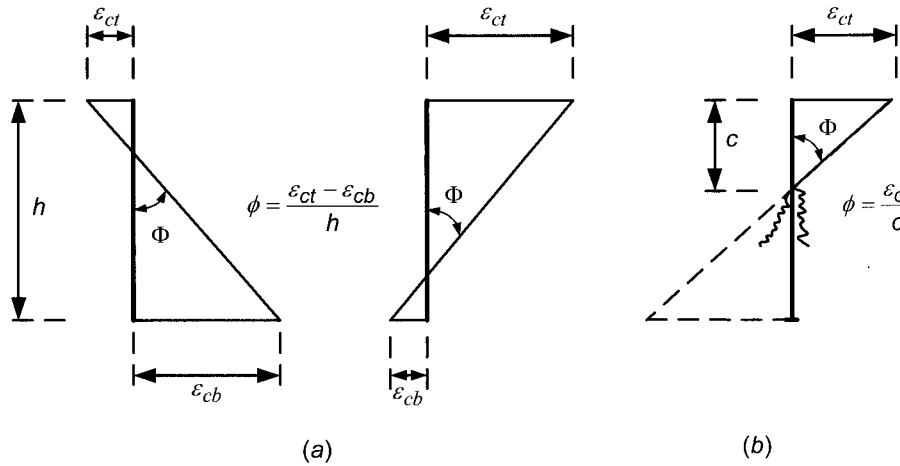

Figure 7.8 Representation of curvature. ***(a)*** **Uncracked section.** ***(b)*** **Cracked section.**

The moment of inertia of the section depends on whether the section is cracked or uncracked. When the section is uncracked, it is customary to use the gross moment of inertia I_g for pretensioned members and the net moment of inertia I_n for posttensioned members with unbonded tendons. In all cases with bonded tendons, the moment of inertia of the transformed section can be used. However, often the corresponding lengthier calculations do not result in a significant gain in accuracy.

7.4.2 Cracked Members

When cracking occurs in prestressed concrete members, cracks develop at several sections along the span similarly to reinforced concrete members. Theoretically, the cracked moment of inertia I_{cr} applies at cracked sections while the gross moment of

inertia applies in between cracks (Fig. 7.9*a*). It is generally accepted that methods used in reinforced concrete where cracking prevails, can be applied to cracked prestressed concrete as well, provided proper modification is made.

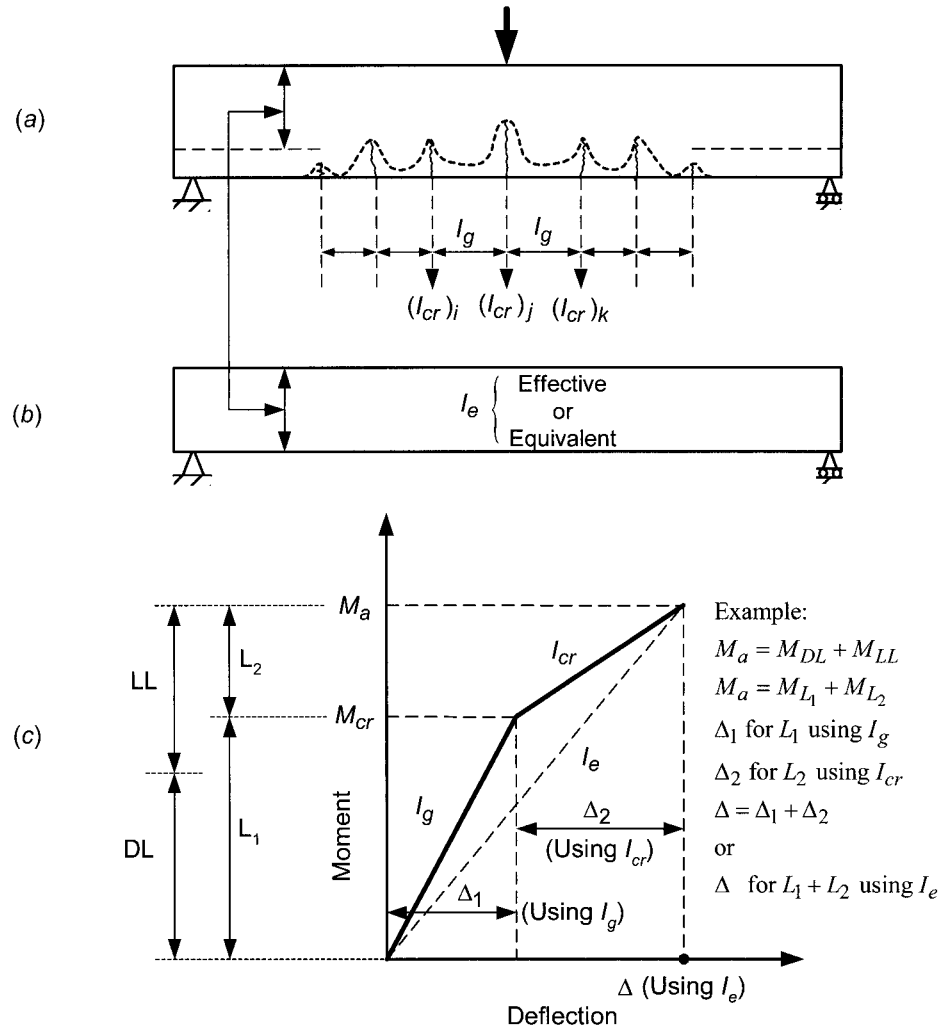

Figure 7.9 ***(a)*** **Moment of inertia of cracked member.** ***(b)*** **Effective moment of inertia.** ***(c)*** **Conceptual representation of bilinear moment deflection relation and effective moment of inertia.**

The ACI code requires that a bilinear moment deflection relationship (Fig. 7.9*c*) be used to calculate instantaneous deflections when the magnitude of tensile stress in service exceeds $|-7.5\lambda\sqrt{f'_c}|$ where $\lambda = 1$ for normal-weight concrete, 0.85 for sand-lightweight concrete, and 0.75 for all-lightweight concrete. This means that for

the portion of moment leading to $-7.5\lambda\sqrt{f'_c}$, I_g is used, while for the remaining portion of moment, I_{cr} is used. In Fig. 7.9c, the total load is divided into two parts: L_1 is the load leading to cracking, and L_2 is the increment of load from cracking to maximum. The total deflection, Δ, is the sum of deflections due to L_1 based on I_g and L_2 based on I_{cr}.

Effective Moment of Inertia. An alternative method is also allowed by the ACI code for cracked reinforced concrete members. An effective moment of inertia, I_e, is first determined and the deflection is then calculated for the total load by substituting I_e for I_g in the deflection calculations. The effective moment of inertia is an average value to be used throughout the span and is weighted depending on the extent of probable cracking under moment. It is an equivalent moment of inertia for a beam that is partly cracked (Figs. 7.9*a* and *b*). The difference between the bilinear moment-deflection approach and the I_e approach is illustrated in Fig. 7.9*c*.

The value of the effective moment of inertia of a partially cracked member, I_e, as originally suggested by Branson [Refs. 7.6 and 7.8] for reinforced concrete is given by:

$$I_e = I_{cr} + \left(\frac{M_{cr}}{M_a}\right)^3 (I_g - I_{cr}) \leq I_g \tag{7.7}$$

where I_{cr} = moment of inertia of the cracked section
I_g = gross moment of inertia of concrete section
M_{cr} = cracking moment for the beam at section of maximum moment M_a
M_a = maximum moment acting on the span at stage for which deflection is computed

Several studies have shown good agreement between measured deflections and deflections using I_e. Branson has also recommended the use of I_e for cracked prestressed and partially prestressed concrete members using bonded tendons [Ref. 7.9]. However, in such a case, the author recommends that both the cracking moment, M_{cr}, and the maximum moment, M_a, be decreased by an amount equal to the decompression moment M_{dec}. The decompression moment is the moment leading to zero stress on the precompressed concrete extreme fiber. For a simply supported prestressed or partially prestressed beam, the cracking moment can be obtained from Eq. (4.41), and the decompression moment from Eq. (4.41), in which f_r is set equal to zero. Hence, Eq. (7.7) becomes:

$$I_e = I_{cr} + \left(\frac{M_{cr} - M_{dec}}{M_a - M_{dec}} \right)^3 (I_g - I_{cr}) \leq I_g \tag{7.8}$$

where M_{dec} = decompression moment at section of maximum moment. Note that, for a simply supported beam where cracking occurs on the bottom fiber, the difference between M_{cr} and M_{dec} is equal to $f_r Z_b$.

The use of the decompression moment in Eq. (7.8) is meant to account for the effect of prestressing, which shifts the reference state of curvature prior to external loading from zero for reinforced concrete, to a non-zero state for prestressed concrete. A study by Watcharaumnuay and Naaman [Refs. 7.31, 7.32] has evaluated the use in Eq. (7.8) for a moment corresponding to zero curvature in the section, as well as a moment leading to decompression at the level of the prestressing steel; however, little difference was observed in the value of I_e.

Equations (7.7) and (7.8) apply to a simply supported beam or to a continuous beam assumed simply supported at its inflection points [Ref. 7.1]. For a cantilever beam, the value of I_e is taken at the face of the support.

Cracked Moment of Inertia. In order to compute I_e, the cracked moment of inertia is needed. The determination of I_{cr} for prestressed and partially prestressed concrete members is not as simple as for reinforced concrete because of the following reasons.

The neutral axis of bending in reinforced concrete is the same as the centroid of the cracked transformed section. Thus, the point of zero stress (neutral axis) along the section coincides with its centroid. This is not true for cracked prestressed concrete sections, as their point of zero stress can vary along the section depending on the magnitude of applied moment and/or the prestressing force. The moment of inertia of the section should be determined theoretically with respect to the centroid of the cracked section. For prestressed members, since the neutral axis varies with the applied moment, I_{cr} also varies with the location of neutral axis.. The value of I_{cr} should be in between the gross moment of inertia and the transformed moment of inertia of the cracked section, assuming the steel is not prestressed (equivalent to reinforced concrete). This is illustrated in Fig. 7.10, assuming that the applied external moment, M, is larger than the cracking moment and σ_{ct} is the stress in the extreme compression fiber of concrete (top fiber) under the combined effect of prestressing and external moment.

In order to obtain the values of depth of neutral axis, c, and stress at the top fiber, a cracked section analysis must be carried out where equilibrium, strain compatibility, and linear stress-strain relations are satisfied. This is usually done for partially prestressed beams and is covered in details in Ref. [1.48]. It is not within the scope of this text. Here we will simply assume that these values have been obtained from a prior analysis.

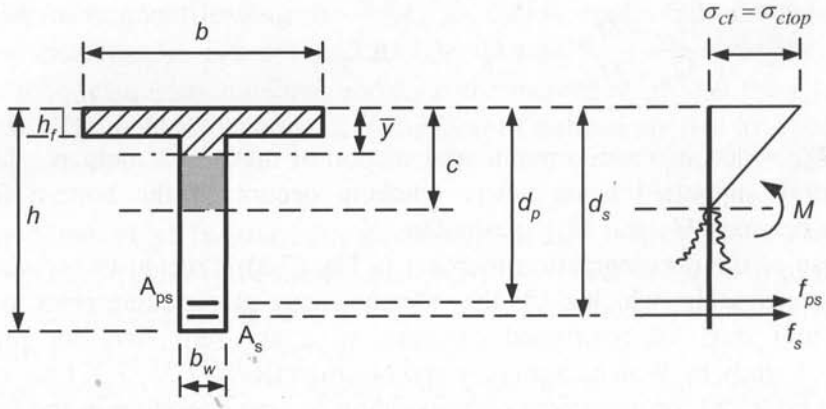

Figure 7.10 Typical stress diagram in a cracked prestressed or partially prestressed section under maximum service load.

To compute I_{cr} two methods are suggested next.

Assuming a prior cracked section analysis has led to the location of the neutral axis, c, the following expressions have been derived and apply to prestressed and partially prestressed rectangular and T sections (Fig. 7.10):

$$\bar{y} = \frac{(b-b_w)h_f^2/2 + b_w c^2/2 + n_p A_{ps} d_p + n_s A_s d_s}{(b-b_w)h_f + cb_w + n_p A_{ps} + n_s A_s} \tag{7.9}$$

and

$$I_{cr} = \frac{b_w \bar{y}^3}{3} + \frac{b_w (c-\bar{y})^3}{3} + (b-b_w)h_f(\bar{y}-h_f/2)^2 + \frac{(b-b_w)h_f^3}{12} + n_p A_{ps}(d_p-\bar{y})^2 + n_s A_s (d_s-\bar{y})^2 \tag{7.10}$$

where:

$\bar{y}$ = distance from extreme compressive fiber to the centroid of the cracked transformed section

c = distance from extreme compressive fiber to the neutral axis (zero stress) of the cracked section

b_w = b for rectangular sections

Equation (7.10) is valid for $\bar{y} \geq h_f$. Otherwise, recompute it using $b = b_w$. Generally, c is larger than $\bar{y}$, except if tensile loading is used. Nevertheless, the expression remains valid.

The simplest and more elegant method of calculating the cracked moment of inertia is from the moment versus curvature relationship, assuming the stress

distribution along the section has already been established in previous calculations. That is:

$$\phi_{cr} = \frac{\varepsilon_{ct}}{c} = \frac{M}{E_c I_{cr}} \tag{7.11}$$

where ε_{ct} is the strain on the extreme compressive fiber of concrete, that is, $\varepsilon_{ct} = \sigma_{ct} / E_c$, and the moment M includes the moment due to prestressing.

Equation (7.11) leads to:

$$I_{cr} = \frac{M \times c}{E_c \varepsilon_{ct}} = \frac{M \times c}{\sigma_{ct}} \tag{7.12}$$

For a statically determinate structure, the prestressing moment is equal to the primary moment, $-Fe_o$, for an uncracked section, and $-F(d_p - \bar{y})$ for a cracked section (Fig. 7.10). Thus, for a statically determinate member, Eq. (7.12) becomes:

- Uncracked section (for which the form of Eq. 7.12 remains valid):

$$I_{tr} = \frac{M \times c}{\sigma_{ct}} = \frac{[M_a - Fe_o]c}{\sigma_{ct}} \tag{7.13a}$$

- Cracked section:

$$I_{cr} = \frac{M \times c}{\sigma_{ct}} = \frac{[M_a - F(d_p - \bar{y})]c}{\sigma_{ct}} \tag{7.13b}$$

where M_a is the external moment due to applied loads and σ_{ct} is the stress on the extreme compressive fiber of concrete under the combined effect of external moment and prestressing. Generally, c and σ_{ct} are known at this stage of the design and M_a is the moment for which I_{cr} and the deflection are being determined.

It is important to realize that I_{cr} as well as I_e are not constants but depend on the particular loading for which deflection is being calculated. Thus, one cannot superimpose values of deflections in the cracked state for different loadings. Instead, the loads have to be superimposed first and the corresponding deflection calculated.

Note finally that if the value of c is not readily available, a lower bound estimate of I_{cr} can be obtained from Eq. (7.10) by simply assuming that the prestressing steel is not prestressed. In this case, $c = \bar{y}$ as in a cracked reinforced concrete section in the elastic range of behavior. The value c or $\bar{y}$ is then obtained from the first static moment of the cracked section, which leads to a quadratic equation in c.

Examples illustrating the above computations for a cracked and uncracked member are given in Section 7.9.

7.5 BACKGROUND TO UNDERSTANDING LONG-TERM DEFLECTION

Extensive research efforts have been undertaken to predict time-dependent deflections in reinforced and prestressed concrete structures more reliably [Refs. 7.7, 7.11, 7.12, 7.13, 7.14, 7.15, 7.16, 7.18, 7.25, 7.28, 7.29, 7.31, and 7.32]. It has been customary in everyday design to estimate the additional long-term deflection by multiplying the instantaneous deflection, Δ_i, by an appropriate factor. The basic reason behind this approach comes from analyzing the effect of creep and time on the stress-strain response of concrete. The variation of creep strain under initial loading is illustrated in Fig. 7.11*a*, assuming a prism of concrete subjected to a constant permanent load. At any time, t, the creep strain for a constant stress can be obtained by multiplying the instantaneous strain under that stress by the creep coefficient. Thus:

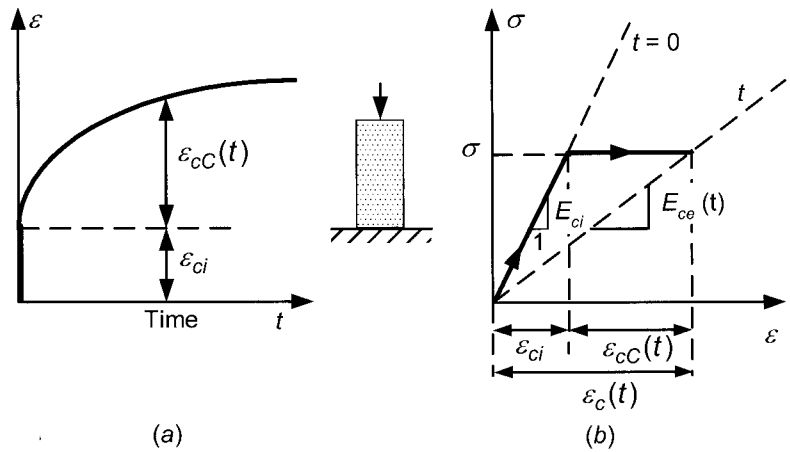

Figure 7.11 Relationship between (*a*) creep strain variation with time and (*b*) equivalent elastic modulus.

$$\varepsilon_{cC}(t) = \varepsilon_{ci} \times C_C(t) \tag{7.14}$$

Looking simultaneously at the stress-strain response of the material in its linear elastic range (Fig. 7.11b), one can separate the instantaneous elastic strain from the time-dependent creep strain. By definition, the ratio, σ/ε_{ci}, is equal to the initial elastic modulus, E_{ci}, that is the elastic modulus (or Young's modulus) at time of loading. With time, however, the ratio of stress to total strain decreases due to the creep strain. This effect can be simulated by using an equivalent or effective modulus (Fig. 7.11b). Its value is obtained from:

$$E_{ce}(t) = \frac{\sigma}{\varepsilon_c(t)} = \frac{\sigma}{\varepsilon_{ci} + \varepsilon_{cC}(t)} = \frac{\sigma}{\varepsilon_{ci} + \varepsilon_{ci}C_C(t)} = \frac{\sigma}{\varepsilon_{ci}(1 + C_C(t))} = \frac{E_{ci}}{1 + C_C(t)} \tag{7.15a}$$

$$E_{ce}(t) = \frac{E_c(t_A)}{1 + C_C(t, t_A)} \tag{7.15b}$$

Equation (7.15b) is the more general form of Eq. (7.15a) in which the age at loading is specified and the creep coefficient is for a concrete of age t loaded at age t_A. Equation (7.15) defines the effective modulus initially suggested by ACI Committee 435 to compute long-term deflection [Ref. 11] (Section 7.10).

Any deflection formula (Fig. 7.6) is an inverse function of the modulus. In general, one can write:

$$\Delta = \frac{K}{E} \tag{7.16}$$

where K depends on dimensional and loading properties. Applied to the initial instantaneous deflection, Eq. (7.16) gives:

$$\Delta_i = \frac{K}{E_{ci}} \tag{7.17}$$

If the loading is sustained for a time t, the time-dependent deflection becomes:

$$\Delta(t) = \frac{K}{E_{ce}(t)} \tag{7.18}$$

Replacing K in Eq. (7.18) by its value from Eq. (7.17) and $E_{ce}(t)$ by its value from Eq. (7.15a), leads to the total deflection at time t, assuming constant or sustained loading:

$$\Delta(t) = \Delta_i(1 + C_C(t)) \tag{7.19}$$

The above equation can be separated into two parts, a constant value, Δ_i, and a time-dependent value. Thus:

$$\Delta(t) = \Delta_i + C_C(t)\Delta_i \tag{7.20}$$

which can be written as (Fig. 7.11):

$$\Delta(t) = \Delta_i + \Delta_{add}(t) \tag{7.21}$$

At the end of the life of the member, it becomes:

$$\Delta(life) = \Delta_i + C_{CU}\Delta_i = \Delta_i(1 + C_{CU}) = \Delta_i + \Delta_{add} \tag{7.22}$$

in which:

$$\Delta_{add} = C_{CU}\Delta_i \tag{7.23}$$

and $\Delta(life)$ = life total deflection for the sustained loading considered

Δ_{add} = additional long-term deflection at end of service life as implied for instance in the ACI code.

The above formulation suggests that the additional long-term deflection, Δ_{add}, can be estimated by multiplying the instantaneous deflection by a factor. According to Eq. (7.23), the multiplier is equal to the ultimate creep coefficient. However, some other effects, such as those of shrinkage, relaxation, and the presence of non-prestressing steel, may be accounted for in the equation predicting Δ_{add}. Four such prediction equations are discussed in the next section.

Figures 2.22 and 7.12 illustrate the effect of time on the deflection of prestressed and partially prestressed beams. While Fig. 2.22 shows steady increase in camber and no cracking, it is interesting to note in Fig. 7.12 [Ref. 7.3] that the instantaneous deflection leads, for the beam and loading considered, to the development of one crack first. However, as the time-dependent deflection increases with time, the number of cracks increases to 16 and their width increases significantly.

7.6 ADDITIONAL LONG-TERM DEFLECTION: SIMPLIFIED PREDICTION METHODS

Deflections calculated from the various derived expressions (Figs. 7.6 and 7.7) are "instantaneous elastic" deflections. They are associated with short-term loading. If the load is sustained, such as in the case of dead loads and prestress, the deflection is then time-dependent. It will be termed total deflection at time t, that is, $\Delta(t)$. The total deflection is made out of two parts: an instantaneous elastic part and an additional time-dependent part (Fig. 7.1). The first part, Δ_i, is calculated as described earlier and is assumed to remain constant for a given load. The additional part increases with time and tends asymptotically toward Δ_{add} at the end of service life; Δ_{add} is the subject of a limit criterion in the ACI code. Four equations predicting Δ_{add} are described next.

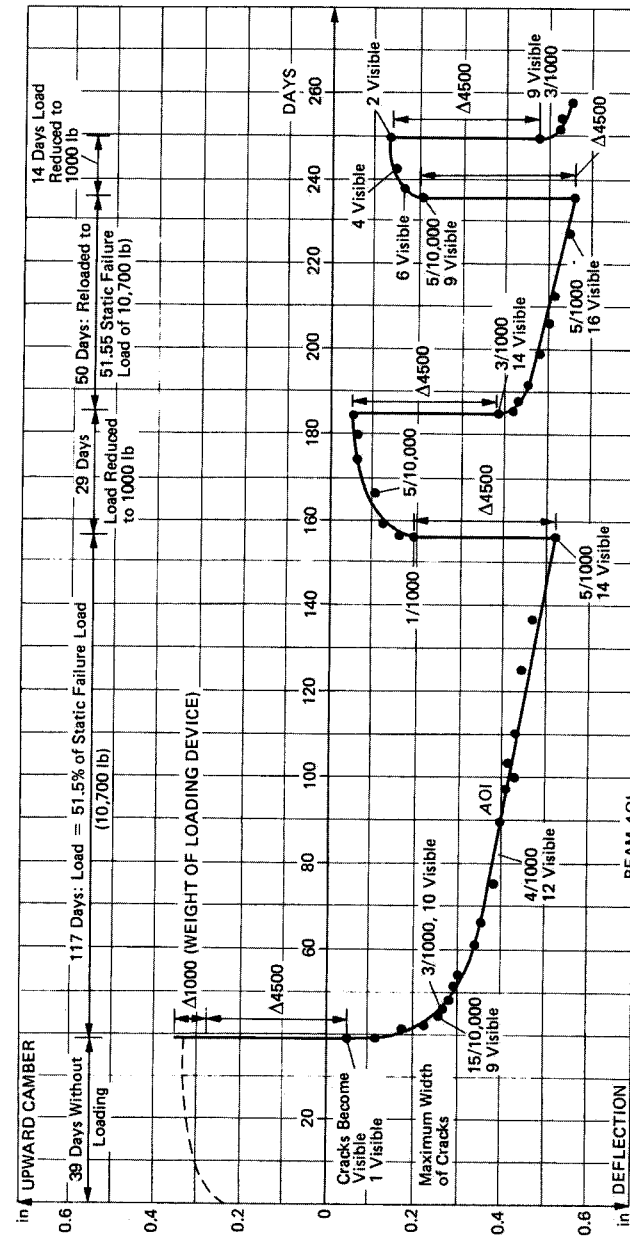

Figure 7.12 Deflection and cracking of a prestressed beam under sustained loadings versus time. *(Ref. 7.3, Courtesy Prestressed Concrete Institute.)*

7.6.1 Additional Long-Term Deflection Using ACI Code Multiplier

In Sec. 9.5.2.5, the ACI code suggests the following prediction equation for nonprestressed concrete (that is, reinforced concrete) members:

$$\Delta_{add}(t) = \lambda \Delta_i \tag{7.24}$$

where Δ_i is the instantaneous deflection and

$$\lambda = \frac{\xi(t)}{1+50\rho'} \tag{7.25}$$

in which $\xi(t) = 1$ for $t = 3$ months, $\xi(t) = 1.2$ for $t = 6$ months, $\xi(t) = 1.4$ for $t = 1$ year, and $\xi(t) = 2$ for $t = 5$ years. ρ' is the compression reinforcement ratio. It can be seen that, for all practical purposes, for a beam with no compression reinforcement, $\xi(t)$ is about equal to an average value of creep coefficient. Equation (7.25) is not implied for prestressed concrete but is given here for comparison.

7.6.2 Additional Long-Term Deflection Using Branson's Multipliers

Branson et al. [Refs. 7.7, 7.9, 7.25] suggested the following equation to predict the additional long-term deflection in prestressed noncomposite members:

$$\Delta_{add} = \left(\eta - 1 + \left(\frac{1+\eta}{2}\right) k_r C_{CU}\right)(\Delta_i)_{F_i} + k_r C_{CU}(\Delta_i)_G + K_{CA} k_r C_{CU}(\Delta_i)_{SD} \tag{7.26}$$

where: $\eta = F/F_i$ and F_i is the prestressing force immediately after transfer

$k_r = 1/(1 + A_s/A_{ps})$ where $A_s/A_{ps} \le 2$

C_{CU} = ultimate creep coefficient

E_{ci} = elastic modulus of concrete at time of transfer

E_c = design modulus of elasticity of concrete

K_{CA} = age at loading factor for creep (see Table 2.9)

The subscripts G and SD refer to self-weight and superimposed dead load, and A_s is the area of tensile reinforcing steel when present. The coefficient k_r shows that the presence of non-prestressed tensile reinforcement leads to a decrease in long term deflection. Note that Eq. 7.26 uses different multipliers for the prestressing force, self-weight and superimposed dead load, to account for the fact that the prestressing force decreases with time due to prestress losses, while the strength of concrete, thus its elastic modulus, increases with time. In computing Δ_i the appropriate values of

elastic modulus should be used. For instance, for a pretensioned beam, E_{ci} should be used for the prestressing force and self weight, and E_c should be used for the superimposed dead load, such as asphalt on a bridge or partitions in a building.

7.6.3 Additional Long-Term Deflection Using Martin's Multiplier

Based on an extensive evaluation of parameters influencing Δ_{add} at service life for typical precast prestressed members, Martin [Ref. 7.18] suggested the following equation:

$$\Delta_{add} = \lambda\Delta_i = \eta\frac{E_{ci}}{E_c}k_r C_{CU}\Delta_i \tag{7.27}$$

where the various terms are same as in Eq. 7.26.

Different design values of the multiplier λ were recommended for prestressed composite and noncomposite members depending on the separate effects of self-weight, prestressing, and superimposed dead load, if any. Values of (λ + 1), reflecting total deflection as in Eqs. (7.19) or (7.22), are given in Table 4.8.4.1 of the PCI handbook, sixth edition [Ref. 7.23] and generally vary between 1.80 and 3.

7.6.4 Additional Long-Term Deflection: Heuristic or "Rule of Thumb" Method

The heuristic or "rule of thumb" method is meant here as a gross approximation for routine design based on practical experience. In such a case the author recommends the following expression:

$$\Delta_{add} = 1.8(\Delta_i)_{F_i} + 2.2(\Delta_i)_G + 2(\Delta_i)_{SD} \tag{7.28}$$

where the notation is same as above. Note that the coefficients related to each term are average approximations of the coefficients in Branson's equation. So F_i and E_{ci} are used for the deflection due to F_i and G, and E_c is used for the deflection due to SD. These coefficients can be taken lower or higher, using engineering judgment. For instance, they can be decreased for high strength concrete, while, they should be increased for lightweight concrete. In many cases, such an approximation is sufficient to provide an idea whether the related deflection criterion is tight or satisfied by a large margin.

7.6.5 Discussion

Tadros et al. [Refs. 7.28 and 7.29] questioned the effectiveness of the k_r term in reducing downward deflection and pointed out that it can produce the opposite

effect. In another publication, Tadros et al. [Ref. 7.29] studied a typical beam example where, depending on the method used, the predicted deflection varied from +0.24 in to –1.59 in. Watcharaumnuay and Naaman [Refs.7.31, 7.32] developed a time-step model to evaluate deflections in partially prestressed beams; the model satisfies equilibrium, strain compatibility with time, and stress-strain relations. They observed that the higher the partial prestressing ratio, the higher the prestress losses; they also observed that in a cracked section the loss of prestressing force due to creep, shrinkage and relaxation is in great part balanced by the gain due to redistribution of stresses caused by cracking and creep; deflection is affected accordingly.

Additional models to predict time-dependent deflections in reinforced and prestressed concrete members, such as by Ghali and Favre [Ref. 7.15] and Dilger [Ref. 7.13] should also be consulted for in-depth investigations and/or for research studies.

Because of the uncertainty associated with the prediction of long-term deflections, engineers should apply common sense in selecting and using any of the simplified equations predicting Δ_{add}. In most common design problems involving prestressed concrete, simple multipliers such as in Eq. (7.28) should be satisfactory in detecting if deflection-related problems are likely to occur.

Section 7.11 describes two more exact methods to determine long-term and additional long-term deflections.

7.7 DEFLECTION LIMITATIONS

Although structural members can be properly designed for strength, they may develop excessive cambers or deflections over time. Hence, their behavior in service can be jeopardized. Fully prestressed bridge members, in which no tension or very little tension is allowed, often develop large cambers leading to an uneven road profile that seriously affects their riding properties. In building members, excessive camber or deflection can cause serious damage to window frames, partitions, and other nonstructural elements connected to them.

The ACI code provides two deflection limitations or acceptance criteria for building members. They essentially relate to deflections that occur after the structure has been built. Two categories of members are addressed: one where deflection is likely to damage attached nonstructural elements, and the other, where it is not. Limitations on the first category are more stringent. Two types of deflections are generally considered: the instantaneous (immediate) deflection due to live load alone, $(\Delta_i)_{LL}$, and that part of the deflection that occurs after elements are attached, Δ_{add}, that is, the additional long-term deflection due to dead or sustained

load. A summary of ACI limits on maximum permissible deflections is given in Table 7.1. When combining the statements in each of the three columns of the table, they can be formulated as follows:

- $|(\Delta_i)_{LL}| \le \ell/180$ for flat roofs not supporting elements that are likely to be damaged by excessive deflections
- $|(\Delta_i)_{LL}| \le \ell/360$ for floors not supporting elements that are likely to be damaged by excessive deflections
- $|(\Delta_i)_{LL} + \Delta_{add}| \le \ell/480$ for roofs or floors supporting elements that are likely to be damaged by excessive deflections
- $|(\Delta_i)_{LL} + \Delta_{add}| \le \ell/240$ for floors or roofs not supporting elements likely to be damaged by excessive deflections.

Table 7.1 Maximum permissible deflection limits of the ACI code. *(Courtesy American Concrete Institute.)*

Type of member	Deflection to be considered	Deflection limitation
Flat roofs not supporting or attached to nonstructural elements likely to be damaged by large deflections	Immediate deflection due to the live load, L	$\frac{\ell^{\dagger}}{180}$ ℓ = span
Floors not supporting or attached to nonstructural elements likely to be damaged by large deflections	Immediate deflection due to the live load, L	$\frac{\ell}{360}$
Roof or floor construction supporting or attached to nonstructural elements likely to be damaged by large deflections	That part of the total deflection which occurs after attachment of the nonstructural elements, the sum of the long-time deflection due to all sustained loads and the immediate deflection due to any additional live load‡	$\frac{\ell^{\Im}}{480}$
Roof or floor construction supporting or attached to nonstructural elements not likely to be damaged by large deflections		$\frac{\ell^{\dagger\dagger}}{240}$

†This limit is not intended to safeguard against ponding. Ponding should be checked by suitable calculations of deflection, including the added deflections due to ponded water, and considering long-time effects of all sustained loads, camber, construction tolerances, and reliability of provisions for drainage.

‡ The long-time deflection shall be determined in accordance with Section 9.5.2.3 or 9.5.4.2 but may be reduced by the amount of deflection which occurs before attachment of the nonstructural elements. This amount shall be determined on the basis of accepted engineering data relating to the time-deflection characteristics of members similar to those being considered.

ℑ This limit may be exceeded if adequate measures are taken to prevent damage to supported or attached elements.

†† But not greater than the tolerance provided for the nonstructural elements. This limit may be exceeded if camber is provided so that the total deflection minus the camber does not exceed the limitation.

The British code CP-110 essentially follows an approach similar to ACI but the numerical values of permissible deflections are slightly different.

For a typical beam, the two ACI code deflection criteria can be summarized in the following form:

$$|(\Delta_i)_{LL}| \le \left\{ \frac{\ell}{180} \text{ or } \frac{\ell}{360} \right\} \tag{7.29}$$

$$|(\Delta_i)_{LL} + \Delta_{add}| \le \left\{ \frac{\ell}{240} \text{ or } \frac{\ell}{480} \right\} \tag{7.30}$$

in which ℓ is the span length, and the word "*or*" reflects the type of member, or whether damage to attached elements is or is not acceptable.

Note that, for prestressed concrete, the second ACI code deflection criterion (Eq. 7.30) which involves the sum of additional long-term deflection and live load deflection should be used broadly, and utilizing engineering judgment as well. For instance, if the additional long-term deflection is negative (camber), and the live load deflection is positive (deflection), it is advisable to also check Δ_{add} taken alone against the code limit. The intent of the code is to minimize the absolute value of deflection increment over time. The absolute value of negative increment, say Δ_{add}, may be larger than that due to the sum of Δ_{add} and Δ_{LL}.

Permissible deflections prescribed in the AASHTO specifications for steel bridges are summarized in Table 7.2. No long-term effects are considered. Only the deflection due to live load plus impact is addressed. The permissible values are much more severe than those given in the ACI code for building members.

Examples of application of the two ACI code criteria on deflection to typical prestressed and partially prestressed beams are given in Section 7.9.

Table 7.2 Maximum permissible deflections of the AASHTO specifications for steel bridges.

Type of member	Deflection considered	Maximum permissible deflection	
		Vehicular traffic only	Vehicular and pedestrian traffic
Simple or continuous spans	Instantaneous due to service live load plus impact	$\frac{\ell}{800}$	$\frac{\ell}{1000}$
Cantilever arms		$\frac{\ell}{300}$	$\frac{\ell}{375}$

7.8 STRATEGY FOR CHECKING DEFLECTION CRITERIA

To compute deflections and check related code limitations involves a number of steps where different sectional and material properties can be used, such as either E_c

or E_{ci}, F or F_i, I_g or I_e. Figure 7.13 suggests a strategy to follow, as well as the appropriate variable to use for a given condition. Note that for a prestressed beam that is uncracked under full service load, the steps are straightforward. However, when the beam is cracked under full service load, the computation of live load deflection is obtained from the difference between a fictitious deflection before application of the live load, and the deflection after application of the live load assuming instantaneous short-term loading.

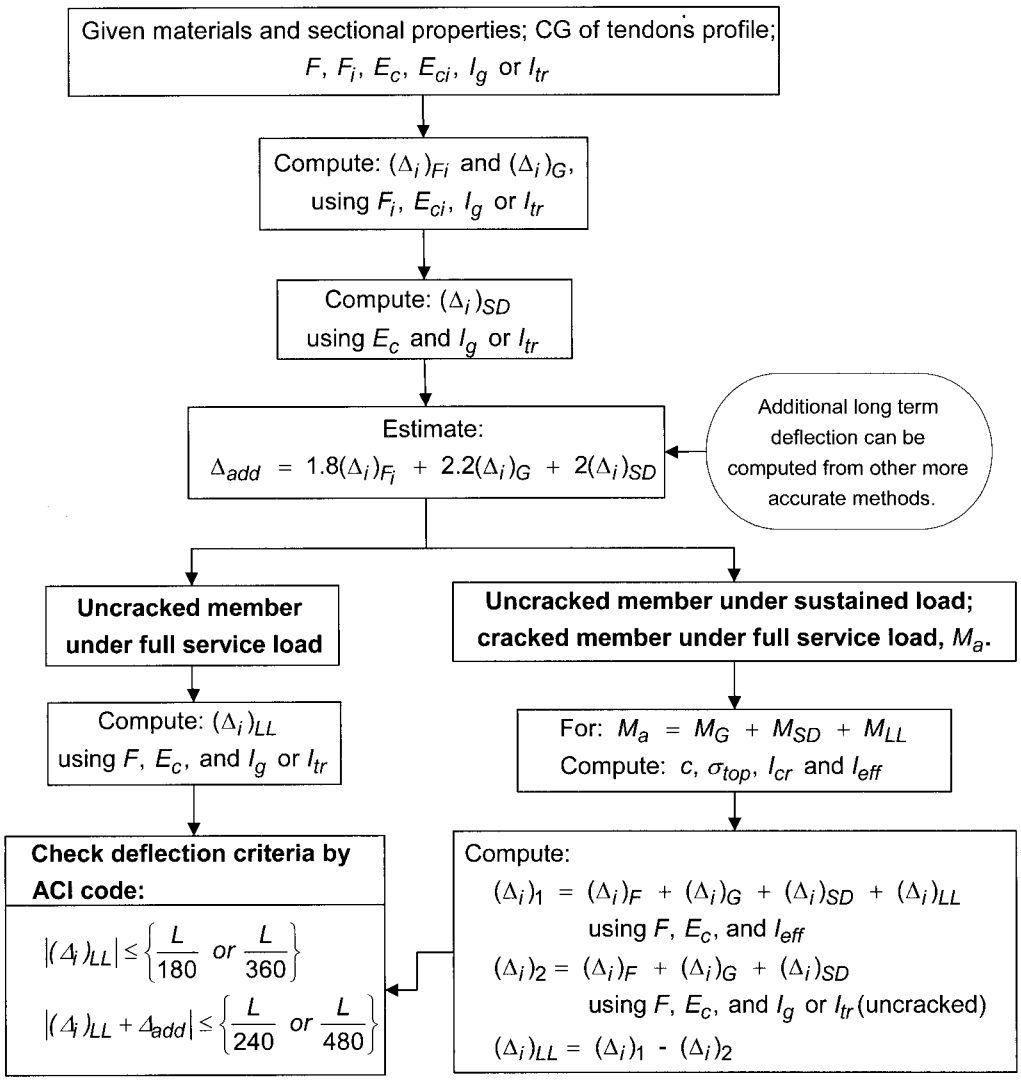

Figure 7.13 Flow chart illustrating the main steps for computing deflections and checking deflection criteria.

7.9 EXAMPLE: DEFLECTION OF UNCRACKED OR CRACKED PRESTRESSED BEAM

Let us consider the pretensioned beam described in Example 4.9*a*.

The following information is given and will be used when needed: span 70 ft, A_c = 550 in^2, I_g = 82,065 in^4, f'_c = 5000 psi, f_r = - 530.3 psi, E_c = 4.287 x 10^6 psi, E_{ci} =3.834 x 10^6 psi, E_{ps} = 27 x 10^6 psi, E_s = 29 x 10^6 psi, n_p = 6.298, n_s = 6.765, w_G = 0.573 klf, $w_D = w_G + w_{SD}$ = 0.613 klf, w_L = 0.4 klf; midspan moments: M_G = 350.96 kips-ft, M_D = 375.463 kips-ft, M_L = 245 kips-ft, $M_D + M_L$ = 620.463 kips-ft, e_o at midspan 21.7 in, e_o at support = 7.9 in, the prestressing steel profile has two draping points at 28 ft from the supports, C_{CU} = 2. Two cases are considered next, the first for a fully prestressed beam that remains uncracked under full service load, and the second for a partially prestressed beam that is uncracked under dead load and cracked under full service load.

7.9.1 Fully Prestressed Beam – Uncracked Under Full Service Load

The beam is exactly the same as in Example 4.9*a*. It is a fully prestressed beam designed to be uncracked under full service load; its cross section is shown in Fig. 7.14a. The following additional information is given:

A_{ps} = 1.53 in^2, F = 229.5 kips, f_{pe} = 150 ksi, η = 0.83, $F_i = F/0.83$ = 276.5 kips.

To compute the instantaneous deflection at transfer, the initial prestressing force, F_i, and the initial elastic modulus of concrete, E_{ci}, are considered, assuming the self-weight of the beam acts as soon as the prestressing force is transferred. Using the equations of Fig. 7.6, we have:

$$(\Delta_i)_{F_i} = -\frac{F_i l^2}{8E_{ci}I_g}\left[e_1 + (e_2 - e_1)\frac{4a^2}{3l^2}\right]$$

where e_1 and e_2 are the eccentricity of the prestressing force at midspan and at the supports, respectively, and a is the distance from the support to the draping point of the tendons. Thus:

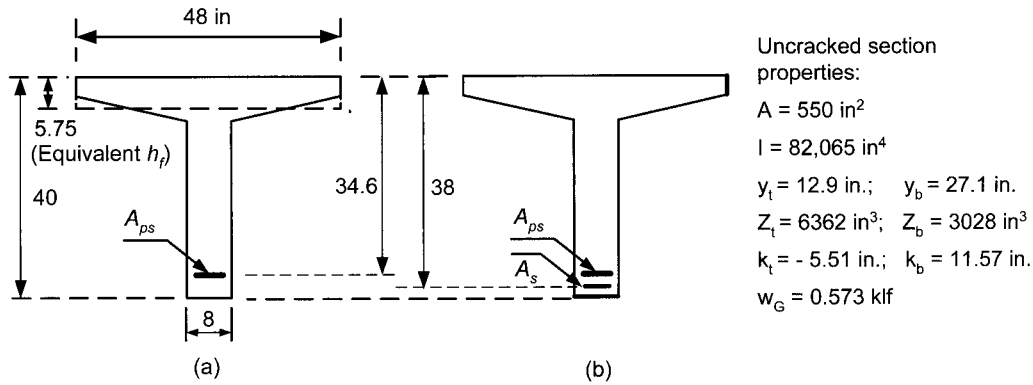

Figure 7.14 (a) Fully prestressed section. (b) Partially prestressed section.

$$(\Delta_i)_{F_i} = -\frac{276{,}500\times(70\times12)^2}{8\times3.834\times10^6\times82{,}065}\left[21.7+(7.9-21.7)\frac{4}{3}\left(\frac{28}{70}\right)^2\right]$$

$$(\Delta_i)_{F_i} = -1.454 \text{ in}$$

For the self-weight of the beam at time of transfer:

$$(\Delta_i)_G = \frac{5w_G l^4}{384E_{ci}I_g} = \frac{5\times(70\times12)^4\times573/12}{384\times3.834\times10^6\times82{,}065} = 0.984 \text{ in}$$

The resulting deflection at time of transfer is:

$$(\Delta_i)_{transfer} = (\Delta_i)_{F_i} + (\Delta_i)_G = -1.454 + 0.984 = -0.47 \text{ in}$$

The instantaneous deflection due to superimposed dead load is computed similarly, using F and E_c, that is:

$$(\Delta_i)_{SD} = \frac{5\times(70\times12)^4\times40/12}{384\times4.287\times10^6\times82{,}065} = 0.061 \text{ in}$$

The instantaneous deflection due to live load is given by:

$$(\Delta_i)_{LL} = \frac{5\times(70\times12)^4\times400/12}{384\times4.287\times10^6\times82{,}065} = 0.614 \text{ in}$$

The additional long term deflection using heuristic rule (Section 7.6.4) is estimated from:

$$\Delta_{add} = 1.8(\Delta_i)_{F_i} + 2.2(\Delta_i)_G + 2(\Delta_i)_{SD}$$

$$\Delta_{add} = 1.8(-1.454) + 2.2(0.984) + 2(0.061) = -0.33 \text{ in} \qquad \text{(camber)}$$

From the above values the ACI code limitations for deflections can be checked (Eqs. 7.29 and 7.30):

$$(\Delta_i)_{LL} = 0.61 \text{ in} < \frac{L}{360} = \frac{70\times12}{360} = 2.33 \text{ in} \qquad \text{O.K.}$$

$$(\Delta_i)_{LL} + \Delta_{add} = 0.614 - 0.33 = 0.28 \text{ in} \le \frac{L}{480} = \frac{70\times12}{480} = 1.75 \text{ in} \qquad \text{O.K.}$$

Since $(\Delta_i)_{LL}$ and Δ_{add} are of opposite sign, check also:

$$|\Delta_{add}| = 0.33 \le \frac{L}{480} = \frac{70\times12}{480} = 1.75 \text{ in} \quad \text{O.K.}$$

Note also that the long term deflection under sustained load, that is, the sum of the instantaneous and additional long-term deflection is estimated at:

$$\Delta(life) = -0.47 + 0.061 - 0.33 = -0.74 \text{ in (camber)}$$

7.9.2 Partially Prestressed Beam

Let us assume that the same beam is designed as a partially prestressed beam according to the method developed in Ref. [1.48]. This will allow us to study the case of a cracked or uncracked section, depending on the magnitude of the applied moment. The beam cross section is shown in Fig. 7.14b.

The following information is given: $A_{ps} = 1.071$ in^2, $A_s = 1.80$ in^2, $F = 160.650$ kips, $F_i = F/0.83 = 193.554$ kips. The beam is designed not to crack under the effect of dead load and to crack under the full effect of dead and live loads. Indeed the cracking moment $M_{cr} = 498$ k-ft $> M_{G+SD} = 375.463$ k-ft. Let us compute the instantaneous deflections in each case.

(a) Uncracked beam. The initial instantaneous deflection at time of transfer is calculated as above using the initial prestressing force and the initial elastic modulus of concrete. Using the equations of Fig. 7.6, we have:

$$\Delta_i = (\Delta_i)_{F_i} + (\Delta_i)_G = -\frac{F_i l^2}{8E_{ci}I_g}\left[e_1 + (e_2 - e_1)\frac{4a^2}{3l^2}\right] + \frac{5w_G l^4}{384E_{ci}I_g}$$

where e_1 and e_2 are the eccentricity of the prestressing force at midspan and at the supports, respectively, and a is the distance from the support to the draping point of the tendons. Thus:

$$\Delta_i = (\Delta_i)_{F_i} + (\Delta_i)_G = -\frac{193{,}554\times(70\times12)^2}{8\times3.834\times10^6\times82{,}065}\left[21.7 + (7.9-21.7)\frac{4}{3}\left(\frac{28}{70}\right)^2\right]$$

$$+\frac{5\times(70\times12)^4\times573/12}{384\times3.834\times10^6\times82{,}065}$$

$$\Delta_i = (\Delta_i)_{F_i} + (\Delta_i)_G = -1.0176 + 0.9838 = -0.0338 \text{ in}$$

Thus, an almost zero camber or deflection results at time of transfer. The instantaneous deflection due to superimposed dead load applied at a later date is given by:

$$(\Delta_i)_{SD} = \frac{5\times(70\times12)^4\times40/12}{384\times4.287\times10^6\times82{,}065} = 0.0614 \text{ in}$$

The additional long-term deflection due to the effect of prestressing and sustained dead load can be estimated from:

$$\Delta_{add} = 1.8(\Delta_i)_{F_i} + 2.2(\Delta_i)_G + 2(\Delta_i)_{SD}$$

$$\Delta_{add} = 1.8(-1.0176) + 2.2(0.9838) + 2(0.0614) = 0.455 \text{ in}$$

It is a downward deflection.

Note that the long-term deflection under sustained load, that is, the sum of the instantaneous and additional long-term deflection is estimated at:

$$\Delta(life) = -0.0338 + 0.061 + 0.455 = 0.48 \text{ in} \quad \text{(deflection)}$$

(b) Cracked beam. Following the strategy described in Fig. 7.13, let us compute the instantaneous deflection due to the effect of full external load (G, SD, LL), plus prestressing. It can be shown that the beam is cracked under such load. The corresponding depth of neutral axis (zero stress) at midspan is $c = 8.94$ in and the corresponding stress on the extreme compressive fiber of concrete is $\sigma_{ct} = 1186$ psi. We need to compute the cracked moment of inertia I_{cr} and the effective moment of inertia I_e. The cracked moment of inertia will be computed from Eq. (7.13), in which the moment M includes $M_a = (M_G + M_{SD} + M_L)$ and the moment of the prestressing force about the centroid of the cracked section. The location of the centroid of the cracked section $\bar{y}$ is given by Eq. (7.9). It can

be shown that $\bar{y} = 5.23$ in for the cross section considered. The moment due to the prestressing force is negative. Thus:

$$M_F = -F(d_p - \bar{y}) = -160.65(34.6 - 5.23)/12 = -393.191 \text{ kips-ft}$$

and

$$M_a = M_G + M_{SD} + M_L = 620.463 \text{ kips-ft}$$

$$M = 620.463 - 393.191 = 227.272 \text{ kips-ft}$$

The cracked moment of inertia is then given by (Eq. 7.13):

$$I_{cr} = \frac{M \times c}{\sigma_{ct}} = \frac{[M_a - F(d_p - \bar{y})]c}{\sigma_{ct}} = \frac{227.272 \times 12{,}000 \times 8.94}{1186} = 20{,}558 \text{ in}^4$$

In order to determine the effective moment of inertia, we need the cracking moment of the midspan section, M_{cr}. Using Eq. (4.41), it can be shown that $M_{cr} = 498.043$ kips-ft and $M_{dec} = 364.274$ kips-ft. Thus:

$$I_e = I_{cr} + \left(\frac{M_{cr} - M_{dec}}{M_a - M_{dec}}\right)^3 (I_g - I_{cr})$$

$$= 20{,}558 + \left(\frac{498.043 - 364.274}{620.463 - 364.274}\right)^3 (82{,}065 - 20{,}558) = 29{,}314 \text{ in}^4 < I_g \quad \text{O.K.}$$

Note that I_e is about 36% of I_g. Replacing I_g, F_i, E_{ci}, and w_G, respectively, by I_e, F, E_c, and $w = 1.013$ klf in the expression used earlier for Δ_i, the instantaneous deflection at midspan of the cracked beam, assuming all the above loads are instantaneous, is determined as (see also Fig. 7.13):

$$\Delta_i = (\Delta_i)_F + (\Delta_i)_{G+SD+L} = -\frac{Fl^2}{8E_cI_e}\left[e_1 + (e_2 - e_1)\frac{4a^2}{3l^2}\right] + \frac{5wl^4}{384E_cI_e}$$

$$= -\frac{160{,}650 \times (70 \times 12)^2}{8 \times 4.287 \times 10^6 \times 29{,}314}\left[21.7 + (7.9 - 21.7)\frac{4}{3}\left(\frac{28}{70}\right)^2\right] + \frac{5 \times (70 \times 12)^4 \times 1013/12}{384 \times 4.287 \times 10^6 \times 29{,}314}$$

$$= -2.115 + 4.355 = 2.24 \text{ in}$$

The deflection (fictitious) under sustained load and prestress, using F, E_c and I_g is given by:

$$\Delta_i = (\Delta_i)_F + (\Delta_i)_{G+SD} = -\frac{Fl^2}{8E_cI_g}\left[e_1 + (e_2 - e_1)\frac{4a^2}{3l^2}\right] + \frac{5wl^4}{384E_cI_g}$$

$$= -\frac{160{,}650 \times (70 \times 12)^2}{8 \times 4.287 \times 10^6 \times 82{,}065}\left[21.7 + (7.9 - 21.7)\frac{4}{3}\left(\frac{28}{70}\right)^2\right] + \frac{5 \times (70 \times 12)^4 \times 613/12}{384 \times 4.287 \times 10^6 \times 82{,}065}$$

$$= -0.756 + 0.941 = 0.186 \text{ in}$$

The instantaneous live load deflection is obtained from the difference between the deflection under full load in the cracked state, and the deflection under prestressing and dead load in the uncracked state, using F and E_c, and I_g (Fig. 7.13). Thus:

$(\Delta_i)_{LL} = 2.24 - 0.186 = 2.05$ in

The instantaneous deflection due to live load is significant because the beam is cracked.
From the above values the ACI code limitations for deflections can be checked (see Section 7.7):

$$(\Delta_i)_{LL} = 2.05 \text{ in} < \frac{L}{360} = \frac{70 \times 12}{360} = 2.33 \text{ in} \qquad \text{O.K.}$$

$$(\Delta_i)_{LL} + \Delta_{add} = 2.05 + 0.45 = 2.50 \text{ in} \begin{cases} \leq \dfrac{L}{240} = \dfrac{70 \times 12}{240} = 3.50 \text{ in} & \text{O.K.} \\ \geq \dfrac{L}{480} = \dfrac{70 \times 12}{480} = 1.75 \text{ in} & \text{N.G.} \end{cases}$$

It can be observed that should attached non-structural elements be sensitive to damage due to large deflections, the second deflection criterion will not be satisfactory. Some corrective measures may be taken according to Section 7.14.

7.10 INTEGRATING THE MODULUS OF CONCRETE INTO TIME-DEPENDENT DEFLECTION CALCULATIONS

In computing time-dependent deflections, the effect of creep can be integrated in the value of the elastic modulus of concrete. This is the case in Eqs. (7.15a) or Eq. (7.15b), which describe the effective modulus of concrete initially suggested by ACI Committee 435 to compute long term deflection. Equation (7.15b) uses a more general notation where age at loading is clearly defined versus the age of concrete. Other expressions for the modulus of elasticity of concrete, modified to account for the effect of creep have been used; some are summarized in Table 7.3.

7.10.1 Age-Adjusted Effective Modulus

The effective modulus approach described in Eq. (7.15) is the simplest and most widespread approximate method to analyze the effect of creep on the deflection of a concrete structural element. However, it can be shown that, for a given creep law, it may lead to a large error with respect to the theoretically exact solution, if aging of concrete is significant. The term "aging" refers to the change of the properties of concrete with the progress of its hydration. Hence, for a concrete member loaded at an early age, the effective modulus approach may be very inaccurate. Trost [Ref. 7.30] proposed a simple method to accommodate the effect of concrete aging by adding an aging coefficient to the effective modulus equation. The method was later expanded and refined by Bazant [Ref. 7.5], following a rigorous formulation. The proposed age-adjusted effective modulus takes on the following most general form [Ref. 7.5]:

$$E_{ce}(t,t_A) = \frac{E_c(t_A)}{1 + \chi(t,t_A) C_C(t,t_A)} \tag{7.31}$$

where:

$E_{ce}(t,t_A)$ = age-adjusted effective modulus at time t when loading occurs at time t_A

$E_c(t_A)$ = instantaneous elastic modulus at time t_A

$\chi(t,t_A)$ = aging coefficient at time t for a concrete member loaded at time t_A

$C_C(t,t_A)$ = creep coefficient at time t for a concrete member loaded at time t_A

Using a computerized analysis and a wide range of parameters, Bazant showed that the aging coefficient varies significantly with the age at loading t_A, the value of the creep coefficient, and whether a variable or a constant modulus is considered in the creep law. He also showed that, while other methods give exact solutions only when the applied stress is constant, the age-adjusted effective modulus applies in the case of constant stress, of constant strain (as in a stress relaxation test) and of straining a member by differential creep.

The observed range of the aging coefficient was 0.71 to 1 when a constant modulus was assumed in the creep law and 0.46 to 1 when a variable modulus was considered. The lower values correspond to early ages at loading. As a first approximation, when loading occurs at normal ages and deflections are estimated at a later date, a value of χ approximately equal to 0.85 is appropriate in common design applications. In such a case, the aging coefficient has essentially a delaying effect on the value of the effective modulus at a time t. A detailed discussion of the effect of the aging coefficient χ is given in Refs. [7.5, 7.22, and 7.30].

Table 7.3 Expressions for time adjusted modulus of concrete.

Source (Description)	Expression	Notation
ACI (Effective Modulus)	Eq. (7.15): $E_{ce}(t)=\dfrac{E_c(t_A)}{1+C_C(t,t_A)}$	$C_C(t,t_A)$ = creep coefficient at time t for a concrete loaded at time t_A $E_c(t_A)$ = elastic modulus at time t_A
Bazant (Age Adjusted Modulus)	Eq. (7.31): $E_{ce}(t,t_A)=\dfrac{E_c(t_A)}{1+\chi(t,t_A)C_C(t,t_A)}$	$\chi(t,t_A)$ = aging coefficient at time t for a concrete loaded at time t_A
Naaman (Equivalent Modulus)	Eq. (7.32): $E_{ce}(t,t_A)=\dfrac{E_c(t)}{1+C_C(\tau)}$	$E_c(t)$ = elastic modulus at time t $\tau=t-t_A$
Watcharaumnuay and Naaman (Apparent Cyclic Modulus)	Eq. (7.33): $E_{ce}(t,t_A)=\dfrac{f_{ct}(t,N)}{\dfrac{f_{ct}(t,N)}{E_c(t_A)}+\varepsilon_c(t,N)}$	$f_{ct}(t,N)$ = maximum compressive stress of concrete at time t and cycle N $\varepsilon_c(t,N)$ = strain due to $f_{ct}(t,N)$

7.10.2 Equivalent Modulus

In principle, the age adjusted effective modulus (Eq. 7.31) is the most correct modulus to use in deflection calculations. However, the age adjustment coefficient, χ, is not readily available, that is, it is not given by an explicit formula. A comparative study by Watcharaumnuay and Naaman [Ref. 7.31, 7.32] showed that changing the numerator of Eq. (7.31) from $E_c(t_A)$ to $E_c(t)$ while eliminating simultaneously the aging coefficient, leads to a negligible change in the numerical value of the modulus. Indeed, as both the numerator and the denominator of the fraction increase, their ratio remains about the same. This led to the use of the equivalent modulus of elasticity as follows:

$$E_{ce}(t,t_A) = \frac{E_c(t)}{1+C_C(\tau)} \tag{7.32}$$

in which $\tau = t - t_A$.

7.10.3 Equivalent Cyclic-Dependent Modulus

Structures subjected to cyclic fatigue loads are not only affected by time-dependent creep but also cyclic-dependent creep. It is rational to expect that a beam subjected to a number of load cycles, N, fluctuating around an average load over a period of time, t, will generally deflect more that a structure subjected to the same average but constant load over the same period of time. This is due to possible damage by fatigue in addition to the effect of time; it is not within the scope of this text. However, assuming no cyclic damage occurs, Watcharamnuay and Naaman [Refs. 7.31, 7.32] have used the following expression to tie the effects of cycles to time:

$$E_{ce}(t,t_A) = \frac{f_{ct}(t,N)}{\dfrac{f_{ct}(t,N)}{E_c(t_A)} + \varepsilon_c(t,N)} \tag{7.33}$$

where $f_{ct}(t,N)$ = maximum compressive stress of concrete at time t and cycle N, and $\varepsilon_c(t,N)$ = strain due to $f_{ct}(t,N)$. Note that N and t are related by the frequency of cycling.

7.11 LONG-TERM DEFLECTION BY INCREMENTAL TIME STEPS

7.11.1 Theoretical Approach

The additional long-term deflection is essentially caused by the simultaneous occurrence of creep and shrinkage of concrete and relaxation of the prestressing steel. As these effects are also associated with prestress losses, it is quite logical to combine the computations of deflections with those of prestress losses. A similar approach was suggested by Subcommittee 5 of ACI Committee 435 [Ref. 7.11]. Theoretically, the computation procedure for deflection at any time, t, due to a sustained load, may include the following steps:

1. Divide the span into several segments (about 20 is more than adequate), each to be represented by its average or midsection.
2. Divide the design life of the structure into several time intervals. These are not equal intervals but have increasing lengths. Typical sets are used in Chapter 8 on prestress losses, and in Table 7.5.
3. Select a time interval, starting in order by the first one. Determine the strain distributions, curvatures, and prestressing force at each section at the beginning of the time interval considered. For the first interval, these values correspond to the instantaneous effects and the initial prestressing force. Determine incremental creep and shrinkage strains and relaxation loss during the time interval. Compute new values of strains, curvatures, and prestressing force at each section at the end of the time interval. These will be used as reference values at the beginning of the next time interval. This procedure is then repeated for each time interval studied and at each section. Great care should be taken to ensure restoration of both equilibrium and strain compatibility at the end of each time interval.
4. By integrating or summing up along the beam the curvatures computed at the beginning of each time interval, the corresponding total time-dependent deflection can be determined. It will include the instantaneous deflection and the additional long-term deflection defined earlier.

The above procedure is time consuming for hand calculations, and the gain in accuracy over an approximate procedure is seldom justifiable in routine design. This is even more so, because the prediction equations that govern the variations of creep and shrinkage with time, as well as the values of ultimate creep and shrinkage, are by no means accurate.

7.11.2 Simplified C-Line Approach

The author has developed a technique to predict long-term deflections that combines theory with some simplified observations [Ref. 7.21]. It has the advantage of being

relatively simple and sufficiently accurate, yet manageable in terms of computational effort. Since the deflection is calculated at different time intervals, it allows for those special cases where values of deflections at intermediate times are needed. The procedure has the following characteristics and justifications:

1. A set of appropriate time intervals is selected; the total time-dependent loss of prestress and the percent prestress loss at the end of each time interval are estimated a priori. Note that, although an error may arise in estimating the total time-dependent prestress loss, little error will occur in the estimates of the percent loss at the end of each time interval. This is because the laws governing creep, shrinkage, and relaxation, and their prediction equations, lead to very similar percent values at identical times (see Chapter 8).

   By estimating a priori the percent of prestress loss with time, the secondary effects of shrinkage and relaxation are indirectly accounted for and the major effect of creep on long-term deflection can be isolated and expanded through the use of the effective or equivalent modulus.
2. Only one loading is considered during each time interval and comprises the combined effect of the prestressing force and the sustained external load. This is contrary to other methods where the loadings are separated into prestressing, self-weight, and superimposed dead load. Because of the combined loading, the beam is assumed equivalently prestressed by a force following the trajectory of the C-line instead of the trajectory of the prestressing steel (Fig. 7.15). The C-force is equal to $F(t)$ in magnitude. Its eccentricity at any section along the span is given by Eq. (4.15):

$$e_c = e_c(t) = e_o - \frac{M}{F(t)} \tag{7.34}$$

   where M is the externally applied moment and $F(t)$ varies with time, according to the assumed prestress loss. During any time interval, M and $F(t)$ are assumed constant, with the value of $F(t)$ taken at the beginning of the interval.

   Since in most common cases the variation of e_o along the span is either linear or parabolic and M is mostly parabolic (due to uniform self-weight), the profile of the trajectory of the C-line will be parabolic.
3. Only two sections are considered in the computations of time-dependent variables, the midspan section and the support section. This is because the deflection of the beam for the parabolic trajectory of the C-line can be calculated in function of the curvatures at the midspan and support sections. Such expressions are given in Fig. 7.6 for the prestressing steel. They can be used directly here, noting that e_1 and e_2 become the eccentricities of the C-force and are time dependent. In using these expressions, it is assumed that the C-force, as well as its eccentricity, remain constant during the time interval considered.

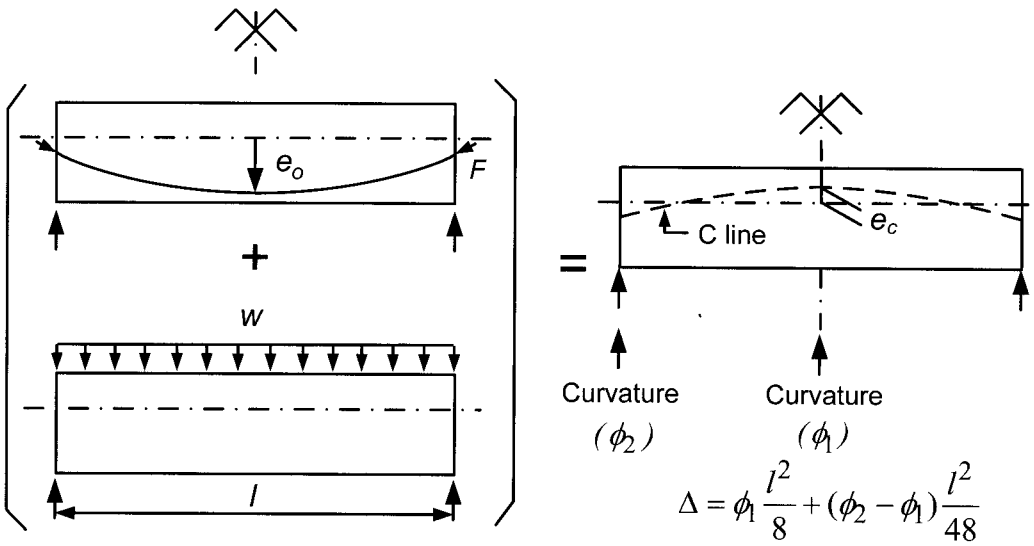

Figure 7.15 C-line approach for computing deflection under combined prestressing force and external load.

Thus, according to the above described procedure, the deflection of the beam during each time interval is given by (Fig. 7.15):

$$\Delta = \phi_1 \frac{l^2}{8} + (\phi_2 - \phi_1)\frac{l^2}{48} \tag{7.35}$$

or

$$\Delta = -\frac{F\ell^2}{8EI}\left[e_2 + \frac{5}{6}(e_1 - e_2)\right] \tag{7.36}$$

where e_1 and e_2 are the eccentricities of the C-force (Eq. 7.34) at midspan and at the supports, respectively, the C-line profile is assumed to be parabolic (Fig. 7.6), and E is the equivalent modulus described below. The curvature at any section can be obtained from Eqs. (7.2) or (7.6):

$$\phi = \frac{\varepsilon_{ct} - \varepsilon_{cb}}{h} \tag{7.6}$$

where ε_{ct} and ε_{cb} are the strain at the top and bottom fiber of the section, respectively. At the end of each time interval, assuming uncracked section, ε_{ct} and ε_{cb} can be determined from:

$$\varepsilon_{ct} = \frac{F}{E_{ce}(t)A_c}\left(1 - \frac{e_c}{k_b}\right) \tag{7.37}$$

$$\varepsilon_{cb} = \frac{F}{E_{ce}(t)A_c}\left(1 - \frac{e_c}{k_t}\right) \tag{7.38}$$

where $E_{ce}(t)$ is the equivalent modulus of elasticity of the concrete as influenced by creep, and e_c is the eccentricity of the C-force at the section considered (Eq. 7.34). Note that k_t is negative, and F and e_c are time dependent. In principle the age adjusted modulus of elasticity should be taken for better accuracy especially at early age loading; however, it was shown that the equivalent modulus gives comparable results and is easier to compute.

Note that instead of using Eq. (7.6), the curvature could have been calculated from *M/EI* for the uncracked or cracked section, as described in Eqs. (7.2) and (7.11).

Computation of Equivalent Modulus. Assuming that the short-term instantaneous modulus varies with time, the equivalent modulus of elasticity under sustained loading at any time, t, can be estimated, similarly to Eq. (7.32), from:

$$E_{ce}(t) = \frac{E_c(t)}{1 + C_C(\tau)} \tag{7.39}$$

where $E_c(t)$ = instantaneous elastic modulus of concrete at time t
t = age of concrete in days
t_A = age of concrete at loading
τ = time period after loading $= t - t_A \geq 0$
$C_C(\tau)$ = creep coefficient at $\tau = t - t_A \geq 0$

Figure 7.16 illustrates the meaning of t and τ.

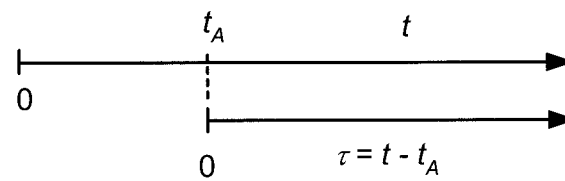

Figure 7.16

According to Tables 2.8 and 2.9, we have:

$$E_c(t) = 33\gamma_c^{1.5}\sqrt{f'_c(t)} \tag{7.40}$$

$$f'_c(t) = \frac{t}{b+ct} f'_c(28) \tag{7.41}$$

Thus:

$$E_c(t) = 33\gamma_c^{1.5}\sqrt{f'_c(28)}\sqrt{\frac{t}{b+ct}} = E_c\sqrt{\frac{t}{b+ct}} \tag{7.42}$$

where E_c is the design modulus of elasticity of concrete. Also, using Table 2.9, we have:

$$C_C(\tau) = \frac{\tau^{0.6}}{10+\tau^{0.6}} C_{CU} K_{CH} K_{CA} K_{CS} \tag{7.43}$$

in which $\tau = t - t_A$.

Replacing $C_C(\tau)$ and $E_c(t)$ by their values from Eqs. (7.42) and (7.43) into Eq. (7.39) leads to:

$$E_{ce}(t) = E_c \times \left(\sqrt{\frac{t}{b+ct}}\right) \times \left[\frac{10+(t-t_A)^{0.6}}{10+(t-t_A)^{0.6}(1+C_{CU}K_{CH}K_{CA}K_{CS})}\right] \tag{7.44}$$

in which the constants b and c and the factors K_{CH}, K_{CA}, and K_{CS} are given in Table 2.9.

For a given problem, Eq. (7.44) is reduced to a time function multiplied by the design modulus of elasticity of concrete E_c, generally taken at 28 days of age. The time function can be divided into two parts, one depending on t and the other on τ, that is:

$$E_{ce}(t) = E_c \times g_1(t) \times g_2(\tau) \tag{7.45}$$

where $\tau = t - t_A$. Figures 7.17 and 7.18 illustrate the variation of the two functions, $g_1(t)$ and $g_2(\tau)$, assuming a sustained load.

Note that the above procedure remains valid when a superimposed dead load is applied. In such a case, an interval is selected to start at the date of application of the superimposed dead load and an adjusted value of the age at loading factor for creep is used. If the beam cracks, the curvatures can then be obtained from the *M/EI* relation, Eqs. (7.2) and (7.11), in which I is replaced by I_e and M includes the moment due to prestressing as used in Eq. (7.13).

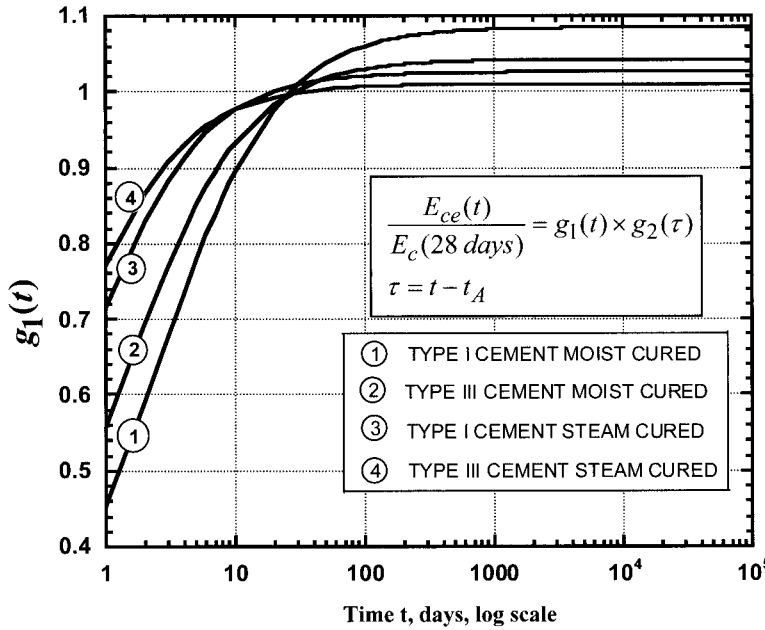

Figure 7.17 Variation of $g_1(t)$ versus time (Eq. 7.44).

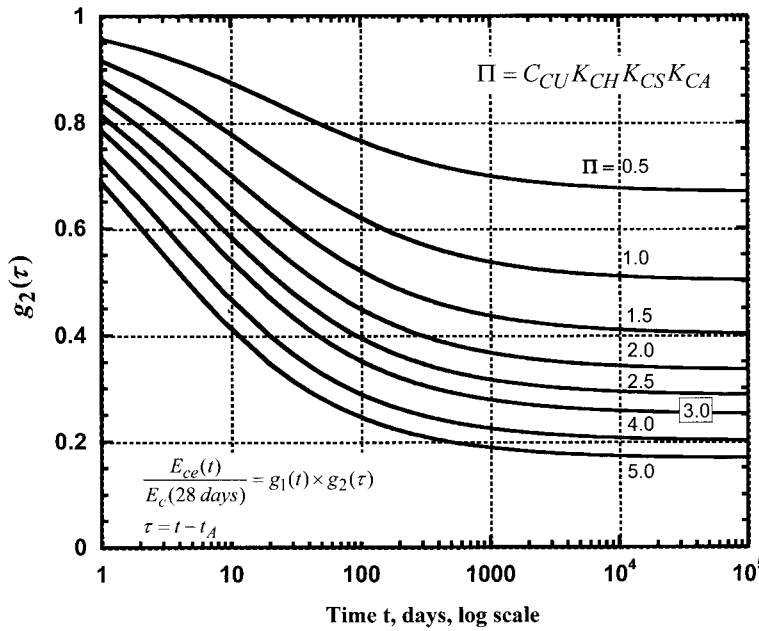

Figure 7.18 Variation of $g_2(\tau)$ versus time (Eq. 7.44).

The variation of concrete strain with time due to creep and age at loading is a dominant factor in any long-term deflection computation. Nondimensional graphs can be developed to predict such strains in common applications. A typical example [Ref. 7.19] is shown in Fig. 7.19. It is very convenient for use in preliminary estimates of long-term deflection, especially in segmental construction and composite structures, when excessive numerical computations are not favored.

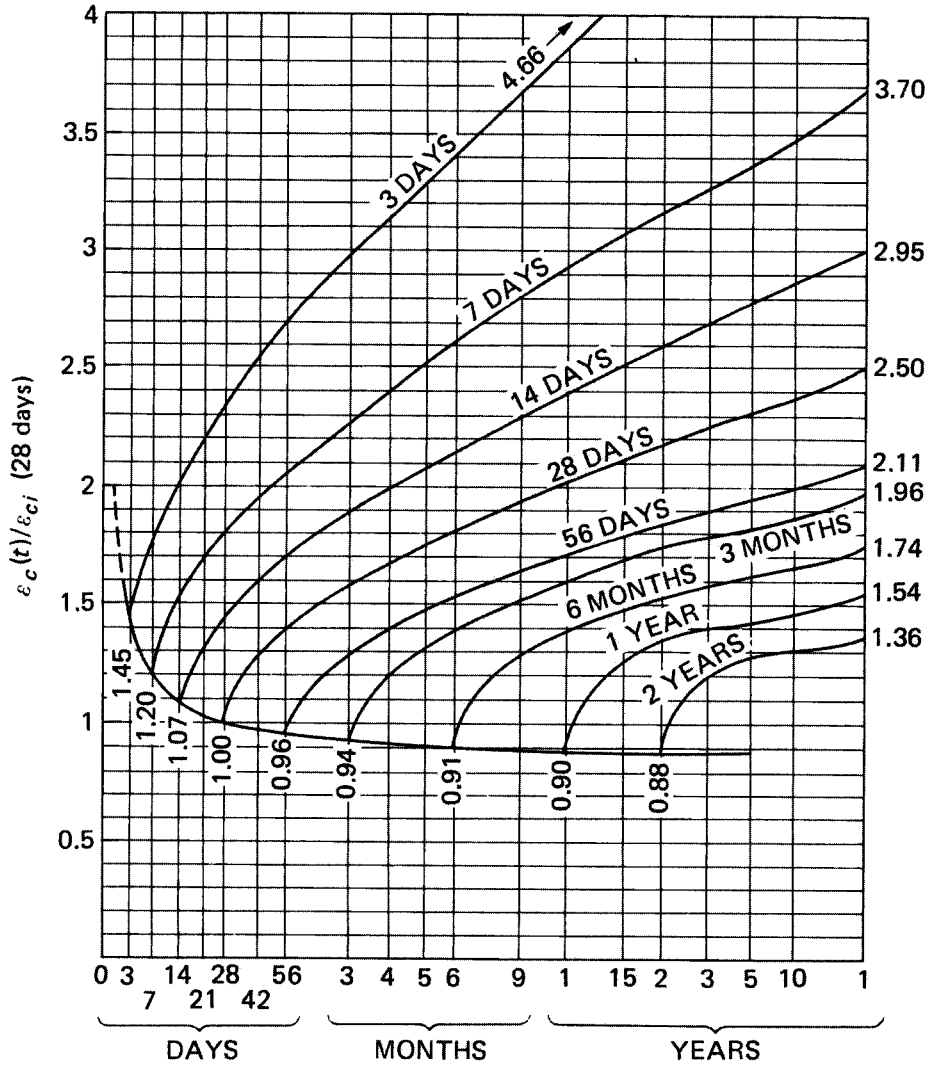

Figure 7.19 Typical design graph giving nondimensionalized concrete strains versus age and duration of loading. *(Ref. 7.19. Courtesy of the Prestressed Concrete Institute.) (Note: ε_{ci} (28 days) is the reference strain of a 28-day old concrete subjected to short-term load.)*

The C-line method, while practical, does not account for all possible effects or parameters and thus has its limitations. It was assumed that the prestressing force is the same at midspan and at the support. In pretensioned members, it is smaller at the supports due to the effect of bond development length. In posttensioned members, the loss of prestress due to anchor set may be significant.

Because of smaller eccentricity, the flexural stress distribution at the support section is different from that at midspan. Hence, different creep, relaxation, and prestress loss effects will be observed at these two sections. Correction factors may be introduced to refine the deflection computations. Also, in computing the deflection, a single parabolic profile was assumed for the C-line. In fact, the profile may be made of two half parabola, but with a vertex that does not coincide with the midspan. This is the case where uniform dead load is combined with a tendon with a single draping point profile. In such a case a slight error is introduced in comparison to the case of a single parabola with vertex at midspan.

7.12 EXAMPLE: TIME-DEPENDENT DEFLECTION USING THE C-LINE APPROACH

Consider the precast prestressed concrete double T beam shown in Fig. 7.20. Design parameters are summarized in Table 7.4. The beam is precast pretensioned and steam cured using Type III cement; release of prestress is done at one day of age after casting; thus $t_A = 1$. The sustained load is assumed to comprise the self weight and the prestress; it represents the load for which the long-term and additional long-term deflections are to be calculated.

Determine the equivalent modulus, $E_{ce}(t)$. The ultimate creep coefficient C_{CU} for the concrete material and the average relative humidity of the environment are given in Table 7.4. Referring to Eq. (7.44) and Table 2.9, the following values of the various constants for steam-cured concrete using Type III cement are obtained: $b = 0.70$, $c = 0.98$, and:

$$K_{CH} = 1.27 - 0.0067H = 0.935$$

$$K_{CA} = 1.13 t_A^{-0.095} = 1.13$$

$$K_{CS} = 1.14 - 0.09\, V/S = 0.979$$

$$\Pi = C_{CU} K_{CS} K_{CH} K_{CA} \doteq 2.59$$

The equivalent modulus of elasticity is thus given from Eq. (7.45):

$$E_{ce}(t) = E_c(28) \times g_1(t) \times g_2(\tau)$$

$$\tau = t - t_A = t - 1 \qquad \text{where } t_A \text{ is age at loading = 1 day}$$

$$E_{ce}(t) = E_c(28) \left\{ \sqrt{\frac{t}{0.7 + 0.98t}} \right\} \left\{ \frac{10 + (t-1)^{0.6}}{10 + (t-1)^{0.6}(\Pi + 1)} \right\}$$

where $E_c(28) = 4.287 \times 10^6$ psi $= E_c$, the design value of elastic modulus.

Several time intervals are selected, namely: t = 1, 7, 30, 90, 365, 50x365 days and the percent prestress loss at the end of each interval is estimated a priori as 0, 20, 45, 65, 85, and 100%. Note, the end of the first time interval is one day, the end of the second interval is seven days, and so on. The

computations for each time interval are summarized in Table 7.5. Let us follow them for the first interval, that is at one day or time of release.

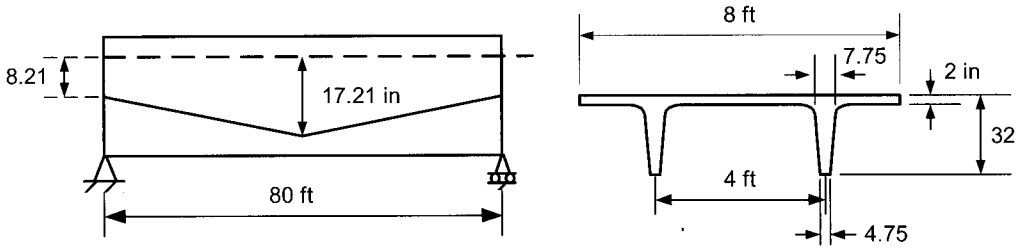

PCI Beam **8DT32**

$A = 567$ in^2; $I = 55{,}464$ in^4; $Y_b = 21.21$ in; $Y_t = 10.79$ in; $Z_t = 5140$ in^3; $Z_b = 2615$ in^3
$k_t = -4.61$ in; $k_b = 9.06$ in; $w_G = 0.32$ klf; $V/S = 1.79$ in

Figure 7.20

Table 7.4

Summary of Concrete Properties	Prestressing	Loading
$f'_c = 5000$ psi	$f_{pe} = 145$ ksi	$M_D = 472.8$ k-ft
$f'_{ci} = 4000$ psi	$f_{pu} = 270{,}000$ psi	$M_L = 256$ k-ft
$E_{ci} = 3.834 \times 10^6$ psi	$F = 354.96$ kips	$M_D + M_L = 728.8$ k-ft
$E_c = 4.287 \times 10^6$ psi	$F_i = 427.66$ kips	Dead weight: 0.591 klf
$(= E_c(28) =$ design value)	$\eta = 0.83$	Live load: 0.32 klf (40 psf)
$C_{CU} = 2.5$	$n_p = E_{ps}/E_c = 6.298$	Sustained load = dead load (self weight) plus prestress
$RH = 50\%$	$n_s = E_s/E_c = 6.765$	
$K_{CH} = 0.935$		
$K_{CA} = 1.13$		
$K_{CS} = 0.979$		
$\Pi = K_{CH} \times K_{CA} \times K_{CS} \times C_{CU} = 2.59$		

Determine the prestressing force with time. The prestressing force is equal to its initial value immediately after transfer, that is:

$$F_i = \frac{F}{\eta} = \frac{354.96}{0.83} = 427.66 \text{ kips}$$

Values of the prestressing force at the end of the other intervals are given in the fourth row of Table 7.5 and correspond to: $F_i - (F_i - F) \times$ (percent loss). The equivalent modulus at $t = 1$ day is obtained from:

$$E_{ce}(1) = E_c \sqrt{\frac{1}{0.7 + 0.98}} = 0.772 E_c = 3.307 \times 10^6 \text{ psi}$$

Moduli values for the other time intervals are given in Table 7.5 and can be computed directly, since the equation for $E_{ce}(t)$ depends only on E_c, t, and τ.

Three alternatives can be used to compute the deflection under sustained load at any time, t. They lead to the same result and are illustrated below. In one alternative the eccentricities of the C-line at the support and midspan sections are used to compute deflection. In the second and third alternatives, the deflection is computed from the curvatures at the midspan and support sections. The curvatures can be computed from the strains at the extreme fibers (as in alternative 2) or directly from the curvature equation, that is, M/EI (as in alternative 3). Uncracked section is assumed in all cases and the gross moment of inertia of the section is used. Again the first time interval is considered next for illustration.

Alternative 1

The deflection is computed from the eccentricities of the C-line (Eq. 7.36).

Midspan: the external moment $M = 472.8$ kips-ft

The eccentricity of the C-line is given by:

$$e_c(t) = e_o - \frac{M}{F(t)}$$

$$e_c(t) = 17.21 - \frac{472.8 \times 12}{427.66} = 3.943 \text{ in}$$

Support: $M = 0$

The eccentricity of the C-line is given by:

$$e_c(t) = e_o - \frac{M}{F(t)} = e_o = 8.21 \text{ in}$$

The trajectory of the prestressing steel is bilinear and the moment varies parabolically. Thus, the trajectory of the C line (Eq. 7.34) is biparabolic. In computing the deflection, we can assume as a first approximation that the expression, given in Eq. (7.36) for a single parabolic profile, applies. Thus:

$$\Delta = -\frac{F\ell^2}{8EI}\left[e_2 + \frac{5}{6}(e_1 - e_2)\right]$$

$E = E_{ce}(t)$; e = eccentricity of C-line

$$\Delta = \frac{427.66 \times 10^3 \times 80^2 \times 12^2}{8 \times 3.307 \times 10^6 \times 55464}\left[8.21 + \frac{5}{6}(3.943 - 8.21)\right]$$

$\Delta = -1.25$ in O.K.

The results are summarized in Table 7.5.

Alternative 2

The deflection can also be computed from the formula using curvatures (Fig. 7.6 or Eq. 7.35), that is:

$$\Delta = \phi_1 \frac{\ell^2}{8} + (\phi_2 - \phi_1)\frac{\ell^2}{48}$$

where the curvatures at the midspan and support sections can be computed from the strains at the extreme fibers of these sections due to the C-force (which combines self-weight and prestress). Eccentricities of the C-force at one day have been computed above.

Midspan:

$$\varepsilon_{ct}(t) = \frac{\sigma_{ct}(t)}{E_{ce}(t)} = \frac{427.66}{567 \times 3.307 \times 10^3}\left[1 - \frac{3.94}{9.06}\right] = 128.9 \times 10^{-6}$$

$$\varepsilon_{cb}(t)=\frac{\sigma_{cb}(t)}{E_{ce}(t)}=\frac{427.66}{567\times3.307\times10^{3}}\left[1+\frac{3.94}{4.61}\right]=423.0\times10^{-6}$$

$$\phi_1(t)=\frac{\varepsilon_{ct}-\varepsilon_{cb}}{h=32}=-9.191\times10^{-6}\ \text{in}^{-1}$$

Support:

$$\varepsilon_{ct}=\frac{427.66}{3.307\times10^{3}\times567}\left[1-\frac{8.21}{9.06}\right]=21.4\times10^{-6}$$

Table 7.5 Summary of Time-Dependent Deflection Computations for Example Beam.

		End time t_j of time interval (t_i,t_j), days					
		1	7	30	90	365	Life 50 × 365
Estimated % of time-dependent prestress loss		0	20	45	65	85	100
$F(t)$, kips		427.66	413.12	394.95	380.40	365.86	354.96
$E_{ce}(t)$, 10^6 psi		3.307	2.599	2.025	1.695	1.439	1.230
Alternative 1:							
$e_{c1}(t)$, midspan, in.		3.943	3.476	2.844	2.295	1.702	1.226
$e_{c2}(t)$, support, in.		8.21	8.21	8.21	8.21	8.21	8.21
$\Delta=-\frac{F\ell^2}{8E_{ce}I}\left[e_{c2}+\frac{5}{6}(e_{c1}-e_{c2})\right]$ in		-1.25	-1.408	-1.514	-1.529	-1.471	-1.432
Alternative 2:							
Midspan	ε_{ct}, 10^{-6}	128.9	172.8	236.1	295.6	364.2	440.1
	ε_{cb}, 10^{-6}	423.0	491.6	556.1	592.7	613.9	644.3
	ϕ_1, 10^{-6} in^{-1}	-9.19	-9.96	-10	-9.28	-7.80	-6.38
Support	ε_{ct}, 10^{-6}	21.4	26.4	32.5	37.3	42.3	48.0
	ε_{cb}, 10^{-6}	634.3	779.4	956.3	1100	1246	1415
	ϕ_2, 10^{-6} in^{-1}	-19.15	-23.53	-28.87	-33.2	-37.63	-42.72
$\Delta=\phi_1\frac{\ell^2}{8}+(\phi_2-\phi_1)\frac{\ell^2}{48}$, in		-1.25	-1.408	-1.514	-1.529	-1.471	-1.432
Alternative 3:							
$\phi_1=\frac{M}{E_{ce}(t)I}$, 10^{-6} in^{-1}		-9.19	-9.96	-10	-9.28	-7.80	-6.38
$\phi_2=\frac{M}{E_{ce}(t)I}$, 10^{-6} in^{-1}		-19.14	-23.53	-28.87	-33.2	-37.63	-42.72
$\Delta=\phi_1\frac{\ell^2}{8}+(\phi_2-\phi_1)\frac{\ell^2}{48}$, in		-1.25	-1.408	-1.514	-1.529	-1.471	-1.432

Note: 1 kip = 4448 N; 1000 psi = 6.895 MPa; 1 in^{-1} = 0.039 mm^{-1}; 1 in = 25.4 mm

$$\varepsilon_{cb} = \frac{427.66}{3.307\times10^3\times5.67}\left[1+\frac{8.21}{4.61}\right] = 634.3\times10^{-6}$$

$$\phi_2 = \frac{21.4-634.3}{32}10^{-6} = -19.15\times10^{-6} \text{ in}^{-1}$$

The resulting deflection is given by:

$$\Delta = \phi_1\frac{\ell^2}{8}+(\phi_2-\phi_1)\frac{\ell^2}{48} = -9.191\times10^{-6}\left(\frac{80^2\times12^2}{8}\right)+(-19.15+9.191)10^{-6}\frac{80^2\times12^2}{48}$$

$$\Delta = -1.25 \text{ in}$$

The results are summarized in Table 7.5.

Alternative 3

The deflection can also be computed using the direct expressions for curvatures given by Eq. (7.2), that is:

Midspan:

$$\phi = \frac{M}{EI}$$

$$\phi_1 = \frac{M}{E_{ce}(t)I} = \frac{M_D - F(t)e_o}{E_{ce}(t)I}$$

$$\phi_1 = \frac{472.8\times12000-427660\times17.21}{3.307\times10^6\times55464}$$

$$\phi_1 = -9.194\times10^{-6} \text{ in}^{-1}$$

Support:

$$\phi_2 = \frac{-427660\times8.21}{3.307\times10^6\times55464} = -19.14\times10^{-6} \text{ in}^{-1}$$

The resulting deflection is given by:

$$\Delta = \phi_1\frac{\ell^2}{8}+(\phi_2-\phi_1)\frac{\ell^2}{48} = -9.194\times10^{-6}\left(\frac{80^2\times12^2}{8}\right)+(-19.14+9.194)10^{-6}\frac{80^2\times12^2}{48}$$

$$\Delta = -1.25 \text{ in}$$

The above curvature values and corresponding deflection are exactly same as obtained earlier by alternatives 1 and 2. The numerical results for the various time intervals using the three alternatives are summarized in Table 7.5 .

Results from the C-line method can be used to determine the additional time-dependent deflection at any time, including the value at service life to be used in checking code limitations; indeed, referring to the last row of Table 7.5:

$$\Delta_{add} = \Delta(\text{life}) - \Delta(1 \text{ day}) = -1.432 + 1.25 = -0.18 \text{ in}$$

If we select to compute the initial deflection at release using E_{ci} instead of E_{ce}(1day), the additional long term deflection computed from the C-line approach would be equal -0.70 in.

In the C-line method, the use of a single parabola is advantageous for computational efficiency but may incur some error if the C-line is not made out of a single parabola (such as in the example

above). If the error is considered unacceptable, a similar procedure can be followed provided the deflection is calculated as the sum of separate deflections due to dead load and prestress. This will negate one of the advantages of the method, that is, only one loading is considered.

In this example the curvatures and corresponding deflection did not vary very widely with time. However, this is not always the case. Figure 7.21 illustrates the variation of curvatures at midspan and support sections with time for an example which was treated instead of this example in the first edition of this book (see Problem 7.6). It can be observed that the long-term effects are significant enough at midspan to change the stress and strain on the bottom fiber from compression to tension; for a higher sustained load, cracking would probably have developed, thus requiring the use of cracked section analysis.

Section 7.13 is a continuation of this example where additional long-term deflection values obtained using various methods are compared and deflection criteria checked.

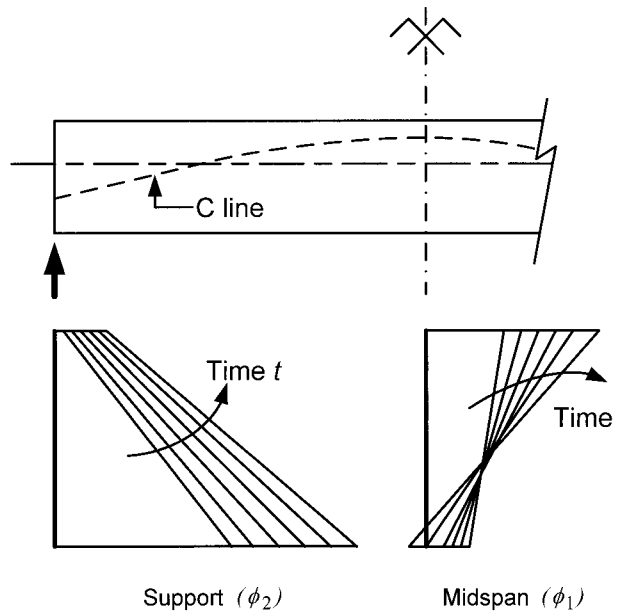

Figure 7.21 Typical variation of section curvature with time (as obtained from problem 7.6).

7.13 EXAMPLE: COMPARISON OF LONG-TERM DEFLECTIONS PREDICTED FROM DIFFERENT METHODS

This is the same example as in the previous section, except that the additional long-term deflection is calculated using various prediction equations and is compared to that obtained from the C-line approach. Also deflection criteria are checked.

1. Instantaneous Deflection

Determine the instantaneous deflection at release of prestress:

$$(\Delta_i)_{F_i} = -\frac{F_i \ell^2}{8E_{ci}I_g}\left(e_1 + \frac{e_2 - e_1}{3}\right)$$

$$= -\frac{427.663\times10^3\times80^2\times12^2}{8\times3.834\times10^6\times55464}\left(17.21 + \frac{8.21-17.21}{3}\right) = -0.232\times14.21 = -3.29 \text{ in}$$

$$(\Delta_i)_G = \frac{5W_G\ell^4}{384E_{ci}I_g} = \frac{5\times591/12\times80^4\times12^4}{384\times3.834\times10^6\times55464} = 2.56 \text{ in}$$

$$(\Delta_i)_{F_i} + (\Delta_i)_G = -0.73 \text{ in}$$

This is a real observable camber at release of prestress.

2. Δ_{add}: by the Heuristic Rule or Rule of Thumb (Eq. 7.28)

Δ_{add} = 1.8 x -3.29 + 2.2 x 2.56 = -0.29 camber

3. Δ_{add}: by Martin's Approach (Eq. 7.27)

$$\Delta_{add} = \lambda(\Delta_i)_{F_i+G}$$

$$(\Delta_i)_{F_i+G} = -0.73 \text{ in}$$

$$\lambda = \eta\frac{E_{ci}}{E_c}k_r C_{CU}; \quad k_r = 1$$

$$\lambda = 0.83\times\frac{3.834}{4.28}\times1\times2.5 = 1.86$$

$$\Delta_{add} = -1.86\times0.73 = -1.36 \text{ in}$$

4. Δ_{add}: by Branson's Approach (Eq. 7.26)

$$\Delta_{add} = \left[\eta - 1 + \frac{1+\eta}{2}k_r C_{CU}\right](\Delta_i)_{F_i} + k_r C_{CU}(\Delta_i)_G$$

$$k_r = 1; \quad C_{CU} = 2.5; \quad \eta = 0.83$$

$$\Delta_{add} = (-0.17 + 0.915\times1\times2.5)\times(-3.29) + 2.5\times2.56$$

$$= -6.92 + 6.4 = -0.57 \text{ in}$$

5. Δ_{add}: by ACI Code Multiplier (Eq. 7.24)

Although the ACI code multiplier is not meant for prestressed concrete, it is used next only to provide a comparison.

$$\Delta_{add} = \lambda(\Delta_i)_{F_i+G}$$

$$\lambda = \frac{\xi(t)}{1+50\rho'} = 2 \text{ for service life}$$

$$\Delta_{add} = 2\times(-0.73) = -1.46 \text{ in}$$

6. Comparison

Results from the above methods are summarized in Table 7.6. Note that the total long-term deflection at end of service life is equal to the instantaneous deflection plus the additional long-term deflection for the sustained loading considered. Note also that the difference between the instantaneous deflection obtained from the C-line approach and the other approaches is simply due to the different values of elastic modulus used, that is E_{ci} or E_{ce}(1day).

Table 7.6

Method of Computation	$(\Delta_i)_{Fi+G}$ in	Δ_{add} in	$\Delta_{(life)}$ in	Remark
Rule of Thumb	-0.73	-0.29	-1.02	smallest
Martin's	-0.73	-1.36	-2.09	
Branson's	-0.73	-0.57	-1.30	
C-Line	-1.25	-0.18	-1.43	
ACI multiplier	-0.73	-1.46	-2.19	highest

7. Check Deflection Limitations

The first ACI code criterion is expressed as:

$$(\Delta_i)_{LL} = \frac{5W_L\ell^4}{384EI} = \frac{5\times 320/12\times 80^4\times 12^4}{384\times 4.287\times 10^6\times 55464} = 1.24 \text{ in}$$

$$(\Delta_i)_{LL} = 1.24 \le \frac{\ell}{360} = \frac{80\times 12}{360} = 2.67 \text{ in} \quad \text{O.K}$$

The second ACI code criterion is expressed as:

$$\Delta_{add} + \Delta_{LL} \le \begin{cases} \ell/480 = 2 \text{ in} \\ \ell/240 = 4 \text{ in} \end{cases}$$

Applied to any of the cases in Table 7.6, it is satisfied; indeed, for the C-line results we have:

$$\Delta_{add} + \Delta_{LL} = -0.18 + 1.24 = 1.06 \le \begin{cases} \ell/480 = 2 \text{ in} \\ \ell/240 = 4 \text{ in} \end{cases}$$

The above criteria are largely satisfied using either one of the predicted values of Δ_{add}. If the margin is small and satisfying either criterion depends on the method of calculation, a more accurate computation procedure (such as the time-step procedure) may be warranted and/or other methods to control deflection explored.

7.14 DEFLECTION CONTROL

The deflection of prestressed and partially prestressed concrete members can be controlled to a great extent by properly selecting the magnitude and trajectory of the prestressing force. For commonly encountered reinforced concrete members, the ACI code waives deflection calculations, provided minimum thickness requirements are met. Minimum thicknesses for beams and slabs are given in Table 9.5*a* of the code in function of the span length. Similar limitations for prestressed concrete members may be developed by ACI Committee 435 in the future [Ref. 7.11].

Although it is difficult to establish rational limitations for prestressed members without referring to the prestressing force and its profile, two heuristic rules (rule of thumb) that were initially suggested by Lin [Ref. 1.11] may be of value:

1. Use a depth of prestressed member about 75 percent of the corresponding depth of a conventional reinforced concrete member.
2. Use $h \approx 1.5$ to $2\sqrt{M_{max}}$ where h = beam depth in inches and M_{max} = maximum moment in kips-feet. Note, as M_{max} includes the dead load moment, some iterations may be needed.

In practice, the depth of hollow core and solid slabs varies roughly between $l/45$ and $l/30$ and that of T or double T beams varies between $l/35$ and $l/25$. For simple span highway bridges, constant beam depths often vary between $l/25$ and $l/15$.

In addition to staying within practical depth limitations, the designer can take some appropriate actions to reduce camber or deflection. Some are easy to implement and include:

- Adding nonprestressed steel at appropriate locations (particularly in the compression zone) to restrain the deformation of concrete due to creep and shrinkage. The time-dependent part of the camber or deflection can be significantly reduced.
- Designing as a partially prestressed beam by replacing some prestressing tendons with reinforcing bars in tension, while providing sufficient nominal bending resistance. This will decrease the prestressing force and the corresponding camber.
- Changing the eccentricity of the prestressing force at the supports, thus influencing the value of camber due to prestressing.
- Changing the properties of the concrete such as increasing its compressive strength, as in high performance concrete. This will automatically increase the elastic modulus, and decrease the creep and shrinkage coefficients.

Other actions to control deflections include [Ref. 7.4]:

- Precambering at casting. This procedure attempts to balance the long-term deflection so as to achieve a final straight profile of the member.
- Delaying or staging the application of prestress. The effect is to decrease time-dependent deflections, since the concrete would have reached its full strength and maturity at time of prestressing. Stage stressing provides an in-between result.

In selecting any approach to control deflection, cost considerations must be weighted against better serviceability.

7.15 CONCLUDING REMARKS

In this chapter an attempt was made to separate deflection computations from other time-dependent properties, such as shrinkage and creep of concrete, relaxation of prestressing steel, and prestress losses. From a theoretical viewpoint, as well as accuracy, these could all be integrated in a time-step procedure such as described in Section 7.11. However, for most design situations, the material covered in this

chapter should provide sufficient information and basis of understanding to allow the designer to decide if a more comprehensive analysis is needed. For more in-depth coverage of deflections where time-dependent effects in prestressed and partially prestressed beams are considered, Refs. [7.10, 7.13, 7.14, 7.15 and 7.31] are especially recommended.

Note that the accurate prediction of deflections is hindered by many difficulties due to uncertain properties of materials (concrete and steel) and due to the behavior of the member itself, which may be cracked or uncracked. The level of difficulty increases in long-term deflection computations, since the properties of the constituent materials, the prestressing force, and environmental conditions are random variables and are time dependent. For instance, concrete aging leads to an increase in the short-term modulus of elasticity of concrete, while creep leads to a decrease in its effective modulus. Both concrete shrinkage and steel relaxation lead to a decrease in the prestressing force thus reducing the effect of creep and vice-versa. The time-dependent properties of constituent materials themselves are random variables, depend on many parameters, show large variability and are difficult to predict. This suggests that a reliability based model may be a more rational approach to follow for important structures where the deflection limit state is critical.

This final paragraph is devoted to a real deflection story. The Parrotts Ferry Bridge, a prestressed concrete box girder bridge with a main span of 640 ft (195 m), was built near Sonora, California, by the US Corps of Engineers. When completed in 1979, it had the longest prestressed lightweight concrete span in the world. Lightweight concrete was used because a reduced weight saved 10 percent of the structural cost and because a lighter structure would perform better in an earthquake. But soon after its completion, the main span started to sag with a first reported deflection of 20 in (500 mm). The main cause was attributed to the creep properties of the lightweight concrete, which were underestimated by the designer. Eventually, after a lengthy investigation involving both technical and legal issues, the bridge was strengthened several years later, using external prestressing tendons placed inside the box girders. Its sag was partly corrected and its deflection stabilized. The moral of the story is that long-term deflection is difficult to predict because it requires not only an accurate analytical model but also accurate knowledge of uncertain materials properties.

REFERENCES

7.1 ACI Committee 435, "Deflections of Continuous Concrete Beams," *ACI Journal*, 70(12): 781-87, 1973.

7.2 ACI Committee 435, Control of Deflections in Concrete Structures, ACI 435 R-95, Manual of Concrete Practice, American Concrete Institute, Farmington Hills, Michigan.

7.3 Abeles, P. W., E. I. Brown, II, and J. O. Woods, Jr., "Preliminary Report on Static and Sustain Loading Tests," *PCI Journal*, 13(4): 12-32, 1968.

7.4 Anderson, A. R., "Engineering for Camber," *PCI Journal*, 16(2): 7-9, 1971.
7.5 Bazant, Z. P., "Prediction of Creep Effects Using Age-Adjusted Effective Modulus Method," *ACI Journal,* 69(4): 212-17, 1972.
7.6 Branson, D. E., "Design Procedures for Computing Deflections," *ACI Journal*, 75(9): 730-42, 1968.
7.7 Branson, D. E., and K. M. Kripanarayanan, "Loss of Prestress, Camber, and Deflections of Non-Composite and Composite Prestressed Concrete Structures," *PCI Journal*, 16(5): 22-52, 1971.
7.8 Branson, D. E., *Deformation of Concrete Structures*. New York: McGraw-Hill Book Co., 1977.
7.9 Branson, D. E., "The Deformation of Non-Composite and Composite Prestressed Concrete Members," *Deflection of Concrete Structures*, ACI-SP-43, American Concrete Institute, Detroit, 1974.
7.10 Comité Euro-International du Béton, *CEB Manual – Cracking and Deformation*, Ecole Polytechnique Fédérale de Lauzanne, 1985, 232 pp.
7.11 "Deflections of Prestressed Concrete Members," Subcommittee 5 of ACI Committee 435, *ACI Journal*, 60(12): 1697-1727, 1963.
7.12 *Deflections of Concrete Structures*, ACI Special Publication SP-43, American Concrete Institute, Detroit, 1974.
7.13 Dilger, W. H., "Creep Analysis of Prestressed Concrete Structures Using Creep-Transformed Section Properties," *PCI Journal*, 27(1): 99-118, 1982.
7.14 Founas, M., "Deformations and Deflections of Partially Prestressed Concrete T-Beams under Static and Random Amplitude Fatigue Loading," Ph.D. Thesis, University of Michigan, Ann Arbor, 1989, 402 pp.
7.15 Ghali, A., and R. Favre, *Concrete Structures: Stresses and Deformations*. New York: Chapman & Hall, 1986, 348 pp.
7.16 Ghali, A., "Deflection of Reinforced Concrete Members: a Critical Review," *ACI Structural Journal*, 90(4): 364-73, 1993.
7.17 Harajli, M., "Deformation and Cracking of Partially Prestressed Concrete Beams under Static and Cyclic Fatigue Loading," University of Michigan, Ann Arbor, Department of Civil Engineering, Report No. UMCE 84-R1, 1984, 179 pp.
7.18 Martin, L. D., "A Rational Method for Estimating Camber and Deflections," *PCI Journal*, 22(1): 100-08, 1977.
7.19 Muller, J., "Ten Years of Experience in Precast Segmental Construction," *PCI Journal*, 22(1): 28-61, 1975.
7.20 Naaman, A. E., and A. Siriaksorn, "Serviceability-Based Design of Partially Prestressed Beams, Part I: Analytic Formulation," *PCI Journal*, 24(2): 64-89, 1979.
7.21 Naaman, A. E., "Time Dependent Deflection of Prestressed Beams by the Pressure-line Method," *PCI Journal*, 28(2): 98-119, 1983.
7.22 Neville, A. M., and W. H. Dilger, *Creep of Concrete: Plain, Reinforced and Prestressed*, Chapters 17-20. Amsterdam: North Holland Publishing Co., 1970.
7.23 *PCI Design Handbook - Precast and Prestressed Concrete,* 6th ed., Precast/Prestressed Concrete Institute, Chicago, Illinois, 2004.
7.24 "Proposed Revisions to ACI Building Code and Commentary Provisions on Deflections," ACI Committee 435, *ACI Journal*, 75(6): 229-38, 1978.
7.25 Shaikh, A. F., and D. E. Branson, "Non-Tensioned Steel in Prestressed Concrete Beams," *PCI Journal,* 15(1): 14-36, 1970.
7.26 Siriaksorn, A., and A. E. Naaman, "Serviceability-Based Design of Partially Prestressed Beams, Part 2: Computerized Design and Evaluation of Major Parameters," *PCI Journal*, 24(2): 40-60, 1979.

7.27 Tadros, M. K., "Designing for Deflection," Reprint of a paper presented at the PCI Seminar on Advanced Design Concepts in Precast Prestressed Concrete, PCI Convention, Dallas, October 1979.

7.28 Tadros, M. K., A. Ghali, and W. H. Dilger, "Effect of Non-Prestressed Steel on Prestress Loss and Deflection," *PCI Journal*, 22(2): 50-63, 1977.

7.29 Tadros, M. K., A. Ghali, and W. H. Dilger, "Time-Dependent Prestress Loss and Deflection in Prestressed Concrete Members," *PCI Journal*, 20(3): 1975.

7.30 Trost, E., "Implications of the Superposition Principle in Creep and Relaxation Problems for Concrete and Prestressed Concrete" (in German), *Beton- und Stahlbetonbau* (Berlin-Wilmersdorf), No. 10, 1967, pp. 230-238, 261-269.

7.31 Watcharaumnuay, S., "Deflection of Partially Prestressed Concrete Beams Subjected to Sustained and Cyclic Fatigue Loadings," Ph.D. Thesis, University of Illinois at Chicago, June 1984.

7.32 Watcharaumnuay, S., and A. E. Naaman, "Long Term Deflections in Partially Prestressed Concrete Beams," University of Michigan, Ann Arbor, Department of Civil Engineering, Report No. UMCE 85-10, 1985, 34 pp.

PROBLEMS

7.1 Go back to Prob. 4.7. Assume F = 69.3 kips with an eccentricity of 10.64 in at midspan and 3.64 in at supports. Compute the instantaneous and long-term deflections, assuming the beam is posttensioned seven days after casting and a parabolic tendon profile is used. Estimate the additional long-term deflection from the rule of thumb. Check if deflection criteria are satisfied according to the ACI code. Make any relevant assumption you deem necessary to complete your design.

7.2 Determine the short- and long-term deflection (or camber) of the beam described in Prob. 5.1, assuming the beam is precast prestressed, has an ultimate creep coefficient $C_{CU} = 3$, and will be in an average environment having 70 percent relative humidity. The centroid of the steel has a linear profile with a single draping point at midspan and an eccentricity of 4 in at the supports. Use Branson's method to estimate additional long-term deflection. Make any other relevant assumptions if needed.

7.3 Consider the simply supported T beam shown in Fig. P7.3. The live load is assumed to be 600 plf. The following design information is given: Normal weight concrete with unit weight = 150 pcf, $f'_c = 8000$ psi; $f'_{ci} = 5600$ psi; ultimate creep coefficient $C_{CU} = 2.2$. Allowable stresses: $\bar{\sigma}_{ti} = -224$ psi; $\bar{\sigma}_{ci} = 3360$ psi; $\bar{\sigma}_{ts} = -536$ psi; $\bar{\sigma}_{cs} = 3600$ psi. The prestressing steel consists of half-inch diameter strands: $f_{pu} = 270$ ksi; $f_{pe} = 150$ ksi; $f_{py} = 240$ ksi; $\eta = 0.80$; $d_{cmin} = 3$ in.

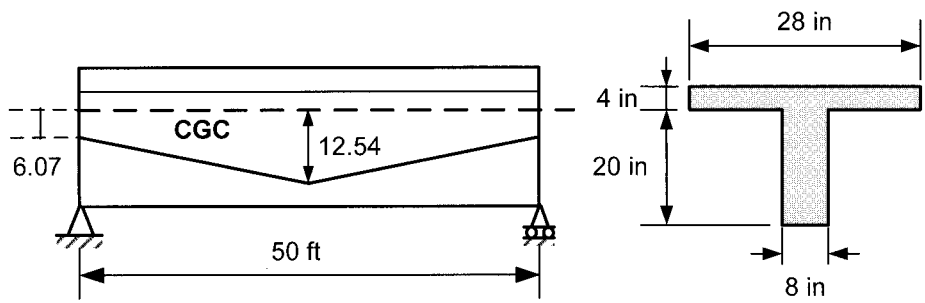

Figure P7.3

Section properties: $\begin{cases} A_c = 272 \text{ in}^2;\ I_g = 14970 \text{ in}^4;\ y_t = 9.06 \text{ in};\ y_b = 14.94 \text{ in}; \\ Z_t = 1652 \text{ in}^3;\ Z_b = 1002 \text{ in}^3;\ k_t = -3.68 \text{ in};\ k_b = 6.07 \text{ in}. \end{cases}$

Assume that, from working stress design, the required area of prestressing tendons was found to corresponds to 9 strands, i.e., A_{ps} = 1.377 in^2, at an eccentricity at midspan e_o = 12.54 in. The profile of the centroid of the prestressing force is draped at midspan with an eccentricity at support equal k_b.

1. Compute:
   a. The instantaneous deflection at transfer of prestress
   b. The additional long term deflection , under dead load and prestress using respectively:
      - The heuristic rule or rule of thumb
      - Martin's method
      - Branson's method.

   Summarize the results in a table showing the additional deflection and the total long-term deflection for each case (long-term deflection = instantaneous plus additional).
2. Check if deflection criteria are satisfied according to the ACI code. You can use any of the additional long-term deflection values obtained above. Discuss the results if you see fit.

7.4 Going back to Prob. 6.4, determine the short- and long-term deflections at the end *D* of the cantilever for the design you have achieved. Make any relevant assumptions you deem necessary to complete the calculations.

7.5 Consider the simple span precast prestressed concrete building member (Fig. P7.5) for which the following information is given: span center to center = 75 ft, live load = 40 psf, f'_c = 6000 psi, f'_{ci} = 4500 psi; allowable stresses: use ACI code; type of steel strands: ½-in diameter, 270 ksi ultimate strength; area = 0.153 in^2 per strand, f_{pJ} at jacking = 190 ksi, f_{pi} at transfer = 175 ksi, f_{pe} = 155 ksi; section properties: h = 32 in, A_c = 538 in^2, I = 49,329 in^4, y_b = 23.44 in, y_t = 8.56 in, Z_b = 2105 in^3, w_G = 0.560 klf.

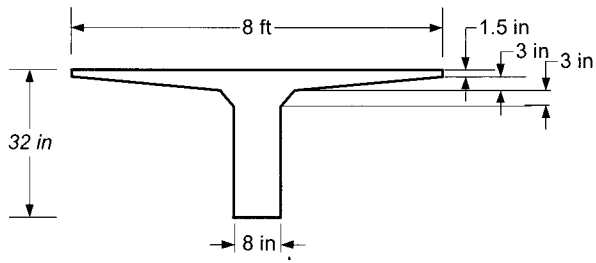

$A_c = 538 \text{ in}^2; I_g = 49{,}329 \text{ in}^4;$
$y_b = 23.44 \text{ in}; y_t = 8.56 \text{ in};$
$Z_b = 2105 \text{ in}^3; Z_t = 5763 \text{ in}^3;$
$k_t = -3.91 \text{ in}; k_b = 10.71 \text{ in};$
$w_G = 0.560 \text{ klf}$

Figure P7.5

(*a*) Determine the minimum required prestressing force at midspan and the corresponding number of strands. Use the closest higher integer number. Select an acceptable strand layout and determine the actual eccentricities of the prestressing force at midspan and support. Assume a steel profile with a single draping point.

(*b*) Calculate the ultimate resisting moment of the midspan section according to the ACI procedure.

(*c*) Check shear requirements at x = 1.75 ft, 8 ft, and 16 ft from the center of supports, and determine the amount and spacing of stirrups along the span.

(*d*) Compute deflections and check deflection limitations according to the ACI code. In estimating additional long-term deflection, use Branson's method and assume C_{CU} = 2 and RH = 40 percent.

Make any other assumptions needed to complete the design.

7.6 Solve problem 7.5. Assume that the beam is plant precast using Type III cement and steam-cured, with transfer of prestress at one day of age. Select a single draping tendon profile given by: $e_o(x) = 10.73 + \frac{6.28}{37.5}x$ where x is in feet and e_o in inches. Use the simplified C-line method to determine deflections with time and compare the additional long-term deflection obtained with that found in question (*d*). Select the following end of time intervals, tj, and corresponding loss of prestress;

t_j	1	7	30	90	365	50x365
% Loss	0	20	45	65	85	100

7.7 The inverted T beam shown in Fig. P7.7 is part of a simply supported roof structure. Its span, center to center of supports, is 50 ft. The following information is provided and should be used whenever needed.

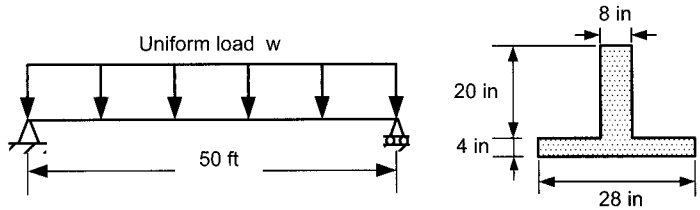

Figure P7.7

- $\begin{cases} f_c' = 6000 \text{ psi}, f_{ci}' = 3500 \text{ psi}, f_r = -530 \text{ psi}, \gamma_c = 150 \text{ pcf}; E_c = 4695 \text{ ksi}; \\ E_{ci} = 3834 \text{ ksi}; C_{CU} = 2.2 \end{cases}$
- Allowable stresses: $\bar{\sigma}_{ci} = 2100$, $\bar{\sigma}_{cs} = 2700$, $\bar{\sigma}_{ti} = -178$, $\bar{\sigma}_{ts} = -464$ psi
- $f_{pu} = 270$ ksi; $f_{pe} = 150$ ksi; $f_{py} = 243$ ksi; $E_{ps} = 27{,}000$ ksi; area of one strand = 0.153 in^2; low relaxation prestressing steel; $\eta = 0.83$.
- Span = 50 ft; $W_G = 283.34$ plf; Live load: 0.4 klf
- Minimum cover to c.g. of steel (d_c)min = 2 in. $f_y = 60$ ksi; $d_p = d_s = 22$ in.
- Section properties: $\begin{cases} A_c = 272 \text{ in}^2; \ I_g = 14970 \text{ in}^4; \ y_t = 14.94 \text{ in}; \ y_b = 9.06 \text{ in} \\ Z_t = 1002 \text{ in}^3; \ Z_b = 1652 \text{ in}^3; \ k_t = -6.07 \text{ in}; \ k_b = 3.68 \text{ in} \end{cases}$

Assume a live load of 0.4 klf and the minimum prestressing force, F, corresponding to 6 strands at maximum practical eccentricity at midspan. Assume the profile of the centroid of the prestressing force is draped at midspan with an eccentricity at support equal k_b.

1. Compute the following:
   a. The instantaneous deflection at transfer of prestress.
   b. The additional long term deflection using the heuristic rule (rule of thumb), Martin's method, and Branson's method, respectively. Summarize the results in a table showing the additional deflection and the total long-term deflection for each case (long-term deflection = instantaneous plus additional).
   For each case check if ACI code criteria for deflection limits are satisfied.
2. Assume $E_{ps} = 27{,}000$ ksi ; relative humidity = 40%; precast prestressed beam, steam cured with release at one day (age at loading); Type III cement. Make any other assumption you deem necessary. Determine the long-term deflection under dead load and prestress using the simplified C-line method. Select the following end of time intervals, t_j, and the corresponding loss of prestress. Organize your calculations in a table such as shown in the examples of Sections 7.12 and 7.13.

t_j	1	7	30	90	365	50x365
% Loss	0	20	45	65	85	100

7.8 An elevated guideway for a mobile lifting crane is made out of a series of consecutive simple span prestressed concrete beams. The maximum reaction from the wheel of the crane is equal to P = 30 kips, and the span, center to center of supports, is 40 ft. The beam cross section is rectangular with b = 12 in., and h = 30 inches. The following information is provided:
$\bar{\sigma}_{ci} = 2400$ psi; $\bar{\sigma}_{ti} = -189$ psi; $\bar{\sigma}_{cs} = 2000$ psi; $\bar{\sigma}_{ts} = -422$ psi; $\eta = F / F_i = 0.8$; unit weight of concrete = 150 pcf. Assume steam-cured concrete with an ultimate creep coefficient $C_{CU} = 2.4$.
$f'_c = 5000$ psi; $f'_{ci} = 4000$ psi; $f_{pu} = 250$ ksi; $f_{py} = 220$ ksi; $f_{pe} = 150$ ksi; area of one strand = 0.216 in^2; maximum practical eccentricity = 12.5 in; stress relieved normal relaxation strands; elastic modulus of concrete: $E_c = 4000$ ksi, $E_{ci} = 3500$ ksi; reinforcing steel: $f_y = 60$ ksi; $d_s = 27$ in. Assume that the prestressing steel profile is a single draping profile with eccentricity at midspan equal to 9.5 in, and eccentricity at support equal to zero.

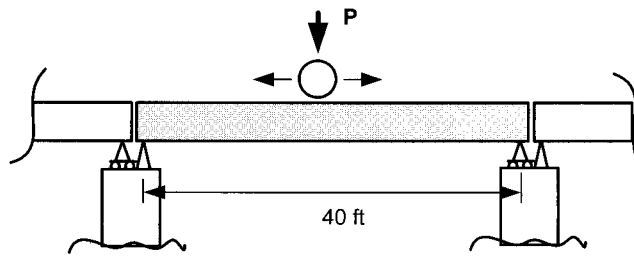

Figure P7.8

1. Compute for the following two cases:
   Case 1: Fully prestressed concrete beam: $A_{ps} = 1.728$ in^2
   Case 2: Partially prestressed concrete beam: $A_{ps} = 0.648$ in^2 and $A_s = 4$ in^2
   a. The deflection at transfer of prestress
   b. The additional long-term deflection using respectively, the rule of thumb, Martin's method, Branson's method, and the ACI 2002 method. Summarize the results in a Table showing the additional deflection and the total long-term deflection for each case (long-term deflection = instantaneous plus additional).
   For each case check if ACI code criteria for deflection limits are satisfied.
2. Consider the fully prestressed beam of Case 1. Assume $E_{ps} = 27{,}000$ ksi; $E_s = 30{,}000$ ksi; relative humidity = 60%; precast prestressed beam, steam cured with release at one day (age at loading); Type III cement. Make any other assumption you deem necessary. Determine the long-term deflection under dead load and prestress using the simplified C-line method. Select the following end of time intervals t_j, and the corresponding loss of prestress:

t_j	1	7	30	90	365	50x365
% Loss	0	20	45	65	85	100

3. Discuss if the C-line method to compute deflections can be applied to the beam of Case 2, and if so, what the main differences with Case 1 are.

COMPUTATION OF PRESTRESS LOSSES

8.1 SOURCES OF LOSS OF PRESTRESS

The stress in the tendons (hence, the prestressing force) of a prestressed concrete member continuously decreases with time, but at a decreasing rate, and asymptotically levels off after a long time. The total stress reduction during the lifespan of the member is called "total loss of prestress." As pointed out in Section 1.3, the total loss of prestress was the primary factor that hindered the early development of prestressed concrete. It is essential to estimate the magnitude of the total loss of prestress with reasonable accuracy, because it leads to the value of the effective prestressing force needed for design.

The total loss of prestress is generally attributed to the cumulative contribution of some or all of the following sources:

1. *Elastic shortening*. Because the concrete shortens when the prestressing force (in full or in part) is applied to it, the tendons already attached to the concrete also shorten, simultaneously losing part of their stress (Section 8.7 and Fig. 8.4).
2. *Relaxation* (or creep) of the stressed tendons. Relaxation is the loss of tension with time in a stressed tendon maintained at constant length and temperature. It is a property of the steel and is described in Sections 2.2.4, and 8.11.
3. *Shrinkage* of concrete. The gradual loss, with time, of free water from the concrete, called shrinkage, induces a shortening in the concrete, which leads to a loss of stress in the attached tendons (Section 8.12).
4. *Creep* of concrete. Creep is caused by the compressive stresses in the concrete. It induces a shortening strain in the concrete (in excess of the elastic strain), which increases with time and leads to a loss of stress in the attached tendons. Some background on creep of concrete and its effects on deflection is given in Sections 2.3.5, 7.5 and 8.12.

5. *Friction.* Loss due to friction occurs during tensioning of posttensioned tendons. It represents the difference in stress between the jacking end of the tendon and a section along the member.
6. *Anchorage set.* Many posttensioning anchorages of the wedge type require that the wedge "sets in" a certain distance in order to lock the tendon at end of jacking. This set (also called seating or slip) leads to a loss of stress in the tendon.
7. *Other factors.* These include restraining effects of adjoining elements and temperature effects, if any. As they depend on the type of structure, the corresponding stress loss cannot be covered here.

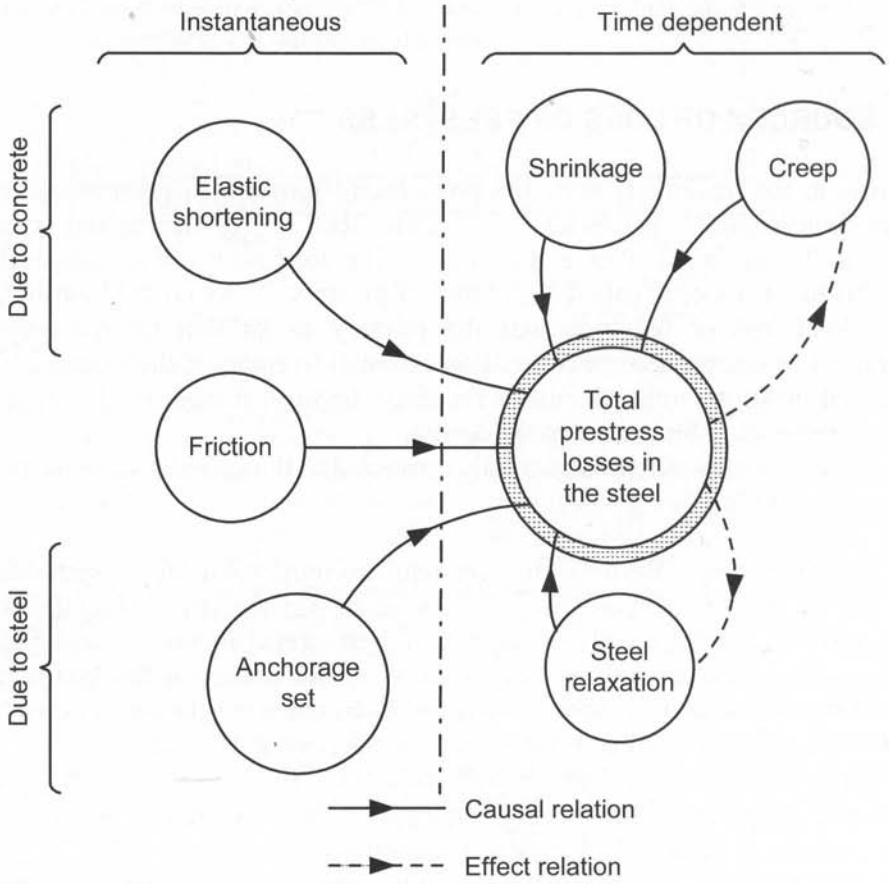

Figure 8.1 Interrelationships of causes and effects between prestress losses.

Each of the above sources leads to a separate prestress loss in the tendons. Prestress losses occur either instantaneously or with time. Instantaneous losses in pretensioned members are generally reduced to the effect of elastic shortening of the

members at transfer (or release) of prestress. In posttensioned members they include, in addition to the partial effect of elastic shortening, the effect of anchorage set and frictional losses between steel and concrete. Time-dependent losses include the effect of relaxation in the steel, as well as the effects of shrinkage and creep in the concrete. Some prestress losses are not only time-dependent but also inter-dependent. Figure 8.1 provides an overall diagram of how losses are cumulative and illustrates the interrelational causes and effects between the different sources of prestress losses. It can be observed, for instance, that relaxation reduces the stress in the steel, which in turn reduces the stress in the concrete; thus, creep loss, being dependent on the stress in the concrete adjacent to the steel, tends to diminish as well, leading to a reduced rate of loss in steel relaxation. Prestress losses affect all prestressed concrete elements.

The main sources of prestress losses, the stage at which they occur, and the corresponding designation of stress loss in the tendon are summarized in Table 8.1. Each loss is attributed a literal value with a subscript containing a capital letter representing the particular source. For instance, Δf_{pR} represents the total stress loss in the prestressing tendons due to *R*elaxation. Two literal values are associated with time-dependent losses, one is a function of time and the other is a particular value of that function. For example, the function $\Delta f_{pR}(t_i,t_j)$ represents the relaxation loss during a time interval (t_i, t_j), and the corresponding value Δf_{pR} represents the total or cumulative stress loss due to relaxation at the end of the life of the structure.

Table 8.1 Sources of prestress losses and time of their occurrence.

	Stage of Occurrence		Tendon stress loss	
Source of prestress loss	Pretensioned Members	Post-tensioned members	During time interval (t_i,t_j)	Total or during life
Elastic shortening of concrete (*ES*)	At transfer	At jacking	.....	Δf_{pES}
Relaxation of prestressed tendons (*R*)	Before and after transfer	After transfer	$\Delta f_{pR}(t_i,t_j)$	Δf_{pR}
Shrinkage of concrete (*S*)	After transfer	After transfer	$\Delta f_{pS}(t_i,t_j)$	Δf_{pS}
Creep of concrete (*C*)	After transfer	After transfer	$\Delta f_{pC}(t_i,t_j)$	Δf_{pC}
Friction (*F*)	.....	At jacking	.....	Δf_{pF}
Anchorage set (*A*)	Before transfer*	At transfer	.....	Δf_{pA}
Total	Life	Life	$\Delta f_{pT}(t_i,t_j)$	Δf_{pT}

* Very small and mostly neglected.

The object of this chapter is to provide a basic understanding of prestress losses and show how they can be numerically determined with different levels of accuracy. A very extensive list of references is given at the end of the chapter and should be consulted for additional information or in-depth analysis and modeling [Refs. 1 to 53].

It is generally assumed that the tendons of a member are tensioned to the same stress and have identical properties. The total loss of stress in the tendons Δf_{pT} is the sum of total losses due to each source. The magnitude of the total loss of prestress in a tendon varies along the member. In order not to add to an already congested notation, the variable x related to a particular section will not be introduced. It is thus assumed that prestress losses are being computed at a given section, most likely the critical section of interest. As a first approximation, concrete gross-sectional properties will be used when needed. Transformed section properties could be used for better accuracy.

8.2 TOTAL LOSSES IN PRETENSIONED MEMBERS

The total loss of prestress in pretensioned tendons comprises the following terms. Each describes the total loss due to a particular source:

$$\Delta f_{pT} = \left\{\Delta f_{pA} + \Delta f_{pR1}\right\} + \Delta f_{pES} + \left\{\Delta f_{pR2} + \Delta f_{pS} + \Delta f_{pC}\right\} \tag{8.1}$$

The notation is explained in Table 8.1. In Eq. (8.1) losses are grouped in brackets to indicate whether they occur prior, during, or after transfer of prestress. A loss due to anchorage set is shown in the first group. It is generally due to the set in the chuck (anchorage) of each prestressing strand at time of release of prestress (or seating) at the end abutment. In practical pretensioning operations, this loss is very small and depends not only on the anchorage set itself, but also on the length of the tendon. The longer the tendon the smaller the loss. For generality, it is considered in Eq. (8.1) but it can be taken equal to zero depending on the tensioning procedure. For instance, the loss can be eliminated by slightly overstressing or restressing and adding shims. Note that the 2002 ACI code limits the stress at jacking to $0.8f_{pu}$.

Because the tendons are tensioned and anchored some time before the prestressing force is transferred to the concrete, the total stress loss due to relaxation is divided into two parts, corresponding each to a time interval, one before transfer and one after transfer, namely:

$$\Delta f_{pR} = \Delta f_{pR1} + \Delta f_{pR2} = \Delta f_{pR}(t_o, t_t) + \Delta f_{pR}(t_t, t_l) \tag{8.2}$$

where:

t_o = time at jacking

t_t = time at transfer of prestress

t_l = design life time of the member

$\Delta f_{pR1} = \Delta f_{pR}(t_o, t_t)$ = stress loss due to relaxation between t_O and t_t

$\Delta f_{pR2} = \Delta f_{pR}(t_t, t_l)$ = stress loss due to relaxation between t_t and t_l

In pretensioned members elastic shortening (*ES*) occurs instantaneously at time of transfer t_t, that is, before shrinkage, creep, and the second relaxation loss (Δf_{pR2}) start occurring.

The total loss of prestress at a given section of a member can be related to the extreme stresses in the tendons, namely:

$$\Delta f_{pT} = f_{pJ} - f_{pe} \tag{8.3}$$

where:

f_{pJ} = stress in the prestressing tendons at end of jacking; this stress is assumed known as derived from the jacking force and should account for the effect of the deflecting device, if any, in pretensioned members; the subscript "capital *J*" is used to differentiate this stress from that at the end of any time interval (t_i, t_j)

f_{pe} = effective stress in the tendons after all losses, at section considered

The jacking force can be read from the pressure meter or other electronic transducer. Since the maximum stress in the tendons is limited by the code, f_{pJ} can be taken equal to $0.80 f_{pu}$. Some adjustment should be made if a deflecting device is used in pretensioned members.

In dealing with losses for pretensioned members f_{pJ} can be interpreted, for convenience, as:

f_{pJ1} = stress at jacking before seating of the chuck

or

f_{pJ2} = stress at jacking after seating of the chuck

The difference between them is the loss due to the set in the chuck. Since that loss is generally very small and can be compensated for by slightly overstressing or by adding shims under the chucks, the two values are often considered same and equal to the code recommended stress limit at jacking.

Thus, the effective stress in the tendons can be derived from Eq. (8.3) as follows:

$$f_{pe} = f_{pJ1} - \Delta f_{pT} \tag{8.4}$$

In pretensioned members the stress in the tendons immediately after transfer was defined in Sec. 3.10 and called f_{pi} for use in design. f_{pi} is the initial stress in the steel that the concrete experiences and is used to determine F_i, the initial value of the prestressing force. Although it is mostly used for the critical section (or sections) it can be defined at any section, because losses are different at each section. The value of f_{pi} can be determined from:

$$f_{pi} = f_{pJ1} - \Delta f_{pA} - \Delta f_{pR1} - \Delta f_{pES} = f_{pJ2} - \Delta f_{pR1} - \Delta f_{pES} \tag{8.5}$$

where Δf_{pR1} (or $\Delta f_{pR}(t_o, t_t)$) and Δf_{pES} can be obtained from Eqs. (8.17), (8.21), and (8.26). The loss due to anchorage set can be calculated exactly or taken based on prior experience. In the examples of Sections 8.6.5 and 8.10, a value of 3 ksi is used. Using Eqs. (8.1) to (8.5) leads to:

$$f_{pi} - f_{pe} = \Delta f_{pTD} = \Delta f_{pR2} + \Delta f_{pS} + \Delta f_{pC} \tag{8.6}$$

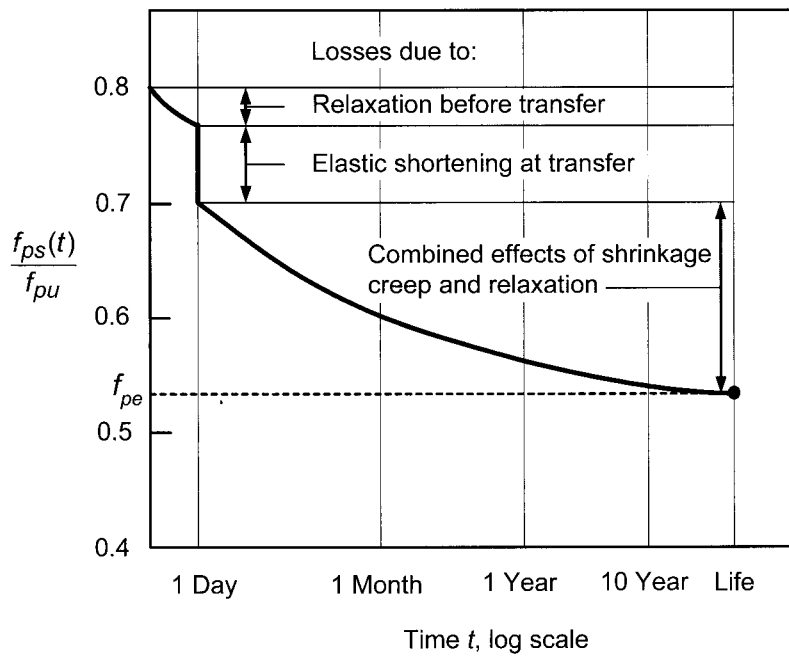

Figure 8.2 Typical variation of steel stress with time for pretensioned member (precast, steam-cured).

Thus the difference between f_{pi} and f_{pe} is equal to the sum of time-dependent losses, Δf_{pTD}, that occur after transfer of prestress. Also, the ratio $f_{pe} / f_{pi} f_{pe}/f_{pi}$ defines the value of the factor η used in design and described in Sec. 3.13. Note that in Eq. (8.6) the reference times for shrinkage and creep may be different from t_o, the reference time for relaxation. For plant precast elements, they are generally taken equal to the time at transfer.

A typical variation of stress in the prestressing tendons of a pretensioned member is schematically shown in Fig. 8.2. In estimating such stress variation a margin of error is generally accepted. Note that, because the sustained load on prestressed members may vary with time, losses can also be treated as ranges rather than absolute values, hence leading to a band instead of a single curve.

8.3 TOTAL LOSSES IN POSTTENSIONED MEMBERS

The total loss of prestress in posttensioned tendons is given by (see notation in Table 8.1):

$$\Delta f_{pT} = \left\{\Delta f_{pF} + \Delta f_{pES}\right\} + \Delta f_{pA} + \left\{\Delta f_{pR} + \Delta f_{pS} + \Delta f_{pC}\right\} \tag{8.7}$$

In Eq. (8.7) losses are grouped to differentiate instantaneous losses during tensioning, anchorage loss at release of prestress, and time-dependent losses after release. Equation (8.7) differs from Eq. (8.1) by only one term, related to friction. Moreover, if all tendons are tensioned simultaneously, no loss due to elastic shortening will occur, because the stressing jack bears on the concrete and offsets any shortening during tensioning. However, some elastic shortening loss takes place in an already anchored tendon when another tendon is being stressed. An overall value of Δf_{pES}, varying between zero and fifty percent of that obtained by pretensioning, is generally used throughout for all tendons; additional details are given in Section 8.7. The initial design stress f_{pi}, leading to the initial prestressing force F_i in a posttensioned member, is then given by:

$$f_{pi} = f_{pJ1} - \Delta f_{pES} - \Delta f_{pF} - \Delta f_{pA} \tag{8.8}$$

and the effective stress f_{pe} is obtained from Eq. (8.4). The stress, f_{pJ1}, is as defined above, that is, the stress at jacking just before anchorage set. Note that, unlike with pretensioned members, the loss due to anchorage set in posttensioned members is not uniform throughout the span and may be nil, depending on the location of the section. Additional information on the loss due to anchorage set can be found in Sections 8.17, and 8.18.

The effective prestress in posttensioned members can be obtained from:

$$f_{pi} - f_{pe} = \Delta f_{pTD} = \Delta f_{pR} + \Delta f_{pS} + \Delta f_{pC} \tag{8.9}$$

where Δf_{pTD} is the sum of time-dependent losses after transfer and, unlike Eq. (8.6) for pretensioned members, it includes the entire loss due to relaxation.

A typical variation of stress with time in a posttensioned tendon is schematically shown in Fig. 8.3. Here, too, one has to allow for some margin of error in predicting such variation and a stress band instead of a single curve may be more representative.

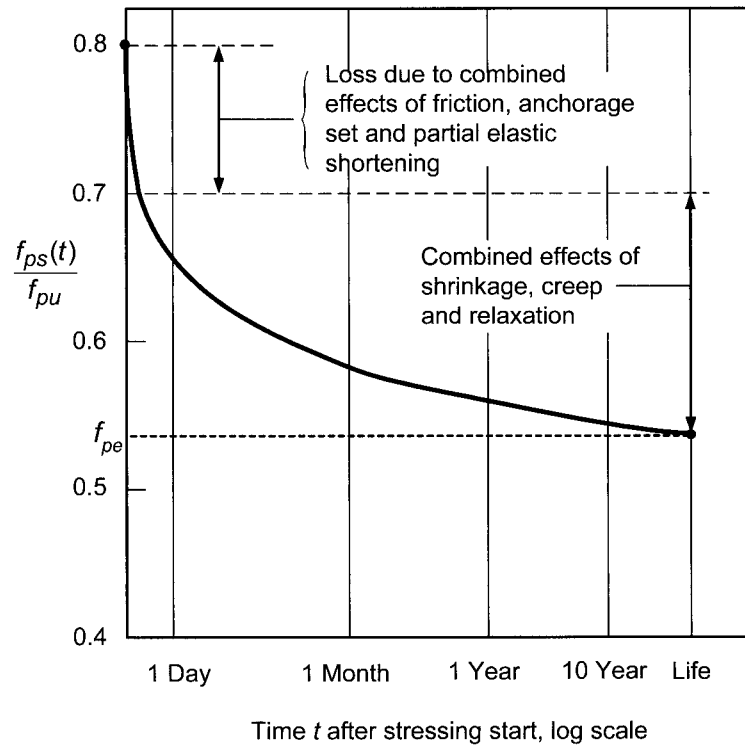

Figure 8.3 Typical variation of steel stress with time for posttensioned members.

8.4 METHODS FOR ESTIMATING PRESTRESS LOSSES

Many methods and design recommendations have been developed to predict prestress losses [Refs. 8.1 to 8.20, 8.24, 8.25, 8.32, 8.34 to 8.37, 8.45, 8.47, 8.48, 8.49, and 8.52]. For design purposes, they can be classified according to three levels of difficulty and related computational accuracy. The corresponding three approaches are identified as follows:

1. Lump sum estimate of the total time-dependent loss of prestress after transfer defined as:

$$\Delta f_{pTD} = \Delta f_{pR} + \Delta f_{pS} + \Delta f_{pC} \tag{8.10}$$

   In some studies the recommended lump sum includes elastic shortening loss; however, in this text it will be strictly interpreted as the total time-dependent loss after transfer. Note also that for pretensioned members, Δf_{pR2} (as in Eq. 8.6) is used instead of total Δf_{pR}.
2. Lump sum estimates of the separate total loss due to each time-dependent source, namely creep, shrinkage, and relaxation, Δf_{pC}, Δf_{pS}, Δf_{pR}.
3. Accurate determination of losses by the time-step method, including cause and effect relationships.

Computation of instantaneous losses (due to elastic shortening, friction, and anchorage set) is essentially the same for either one of the above approaches. However, the treatment of time-dependent losses is different. Each approach is described in more details in Sections 8.5, 8.6 and 8.14, respectively.

Note that the accurate determination of losses is more important for some structures than for others. Moreover, the more accurate and detailed the technique of predicting losses, the more extensive is the input information needed for material properties and environmental conditions. While in the lump sum estimate of total time-dependent loss, Δf_{pTD}, one may only need to know if the structure is pretensioned or posttensioned, in the time-step method, data on the basic materials properties, the shape of the structure, the age at loading, environmental conditions, and the like are necessary. A number of references are listed at the end of this chapter to provide a basic understanding of the various properties of concrete that are essential to the application of the time-step method in computing prestress losses [Refs. 8.12 to 8.31, 8.33, and 8.51]. Note that, although the ultimate strength of a prestressed member is insensitive to a misestimate in losses, an underestimate or an overestimate of losses can affect service behavior such as camber, deflection, and cracking.

8.5 LUMP SUM ESTIMATE OF TOTAL LOSSES

8.5.1 Background

Lump sum estimates of total prestress losses are used for convenience in design. For instance, Table 3.13 allowed us to proceed with the design of prestressed concrete members without having to fully explain prestress losses.

In 1958, ACI-ASCE Joint Committee on Prestressed Concrete [Ref. 8.1] recommended a total loss of 35 ksi (242 MPa) for pretensioned members and 25 ksi (173 MPa) for post-tensioned members. These were losses after transfer of prestress.

A study by Hernandez and Gamble [Ref. 8.24] of ten typical precast pretensioned bridge and building members, where prestress losses were accurately predicted using the time-step method, led to the following results: an average total loss of 45.48 ksi (313.6 MPa) with a standard deviation of 7.53 ksi (52 MPa) and a range of 33.91 to 59.98 ksi (234 to 413.6 MPa). The same beams were studied by *Zia* et al. [Ref. 8.52] in an attempt to provide a simplified procedure giving lump sum estimates of separate losses. In addition, 12 standard double T beams selected from the PCI Design Handbook [Ref. 8.36] were analyzed. The average total loss predicted was around 42.4 ksi (292.3 MPa) with a range of the same order as that observed by *Hernandez* and *Gamble*. Based on their evaluation, *Zia* et al. [Ref. 8.52] recommended maximum limit values of total prestress loss applicable when the tendon stress does not exceed $0.83 f_{py}$ immediately after anchoring. These limits are summarized in Table 8.2 and include creep, shrinkage, relaxation, and elastic shortening losses.

Table 8.2 Recommended maximum stress loss for pretensioned members [Zia et al., Ref. 8.52].

	Maximum loss† ksi (Mpa)	
Type of strand	Normal weight concrete	Lightweight concrete
Stress-relieved strand	50 (345)	55 (380)
Low-relaxation strand	40 (276)	45 (311)

† For $f_{pi} \leq 0.83 f_{py}$

Table 3.13 Suggested lump sum estimates of time-dependent prestress losses after transfer of prestress for routine design (not including friction and anchorage set effects).

	$(f_{pi} - f_{pe})^*$			
	Stress relieved stand		Low relaxation strand	
	ksi	MPa	ksi	MPa
Pretensioned members:				
• Normal weight concrete	40	276	35	242
• Structural lightweight concrete	45	310	40	276
Posttensioned members:				
• Normal weight concrete	35	242	30	207
• Structural lightweight concrete	40	276	35	242

* Assuming $f_{pi} \leq 0.82 f_{py}$

It is this author's approach to use as a first approximation for normal weight concrete a lump sum for total time-dependent loss, Δf_{pTD} after stress transfer, of 40 ksi (276 MPa) for pretensioned members and 35 ksi (242 MPa) for posttensioned members (excluding the effects of elastic shortening, friction and anchorage set). An increment of 5 ksi (35 MPa) is used for structural lightweight concrete and a reduction of 5 ksi (35 MPa) is used for low-relaxation strands. Table 3.13 summarizes the above and is recommended as a first approximation in design. It is reproduced in this chapter for convenience. Total loss values are reassessed and revised in the final design, if necessary.

8.5.2 Lump Sum Estimate of Prestress Loss: AASHTO LRFD

Losses due to anchorage set, friction, and elastic shortening are instantaneous losses whereas losses due to creep, shrinkage, and relaxation are time-dependent. Instantaneous losses should be estimated using the procedures suggested in Sections 8.7, 8.16, 8.17 and 8.18 and added to the time-dependent losses as appropriate. The AASHTO LRFD Bridge Design Specifications [Ref. 8.6] recommend a lump sum estimate of time-dependent losses based on an extensive evaluation using the time-step procedure and documented in Ref. [8.32]. It addresses losses in prestressed and partially prestressed concrete members with concrete compressive strength of up to 10 ksi (70 MPa), and is explained next.

AASHTO recommends that an approximate lump sum estimate of time-dependent prestress losses resulting from creep and shrinkage of concrete and relaxation of steel in prestressed and partially prestressed members may be taken as specified in Table 8.3 for:

- Posttensioned nonsegmental members with spans of up to 160 ft (50 m) and stressed at concrete age of 10 to 30 days, and
- Pretensioned members stressed after attaining a compressive strength $f'_{ci} = 3.5$ ksi (24 MPa)

provided that:

- Members are made from normal weight concrete or structural lightweight concrete
- The concrete is either steam- or moist-cured
- Prestressing is by bars, wires or strands with either normal or low relaxation properties, and
- Average exposure conditions and temperatures characterize the site.

With respect to "average exposure conditions," the values given in Table 8.3 should only be used when there has been previous satisfactory application to the general type of structure and construction method contemplated for use. For unusual

exposure conditions, more accurate estimates shall be obtained in accordance with methods supported by research or experience.

Table 8.3 Total lump sum estimate of time-dependent losses by AASHTO LRFD.

Type of Beam Section	Level	For Wires and Strands with: f_{pu} = 235, 250 or 270 ksi (1620, 1725 or 1860 MPa)	For Bars with f_{pu} = 145 or 160 ksi (1000 or 1104 MPa)
Rectangular beam, solid slab	Upper bound	29 + 4 PPR (ksi) 203 + 28 PPR (MPa)	19 + 6 PPR (ksi) 133 + 42 PPR (MPa)
	Average	26 + 4 PPR (ksi) 182 + 28 PPR (MPa)	
Box girder	Upper bound	21 + 4 PPR (ksi) 174 + 28 PPR (MPa)	15 (ksi) 105 (MPa)
	Average	19 + 4 PPR (ksi) 133 + 28 PPR (MPa)	
I-girder		$33\left[1-0.15\frac{f'_c-6}{6}\right]+6$ PPR (ksi) $231\left[1-0.15\frac{f'_c-42}{42}\right]+42$ PPR (MPa)	19 + 6 PPR (ksi) 133 + 42 PPR (MPa)
Single T, Double T, Hollow core and voided slab	Upper Bound	$39\left[1-0.15\frac{f'_c-6}{6}\right]+6$ PPR (ksi) $273\left[1-0.15\frac{f'_c-42}{42}\right]+42$ PPR (MPa)	$31\left[1-0.15\frac{f'_c-6}{6}\right]+6$ PPR (ksi) $217\left[1-0.15\frac{f'_c-42}{42}\right]+$ 42 PPR (MPa)
	Average	$33\left[1-0.15\frac{f'_c-6}{6}\right]+6$ PPR (ksi) $231\left[1-0.15\frac{f'_c-42}{42}\right]+42$ PPR (MPa)	

Notes: 1. For low-relaxation strands, the values specified in the table may be reduced by: 4.0 ksi (28 MPa) for box girders, 6.0 ksi (41 MPa) for rectangular beams, solid slabs, and I-girders, and 8.0 ksi (55 MPa) for single T's, double T's, hollow core, and voided slabs.

2. For members made from structural lightweight concrete the values specified in Table 8.3 shall be increased by 5.0 ksi (35 MPa).

3. The upper bound and the average are same for prestressing bars.

For segmental concrete bridges, lump sum losses may be used only for preliminary design purposes.

The PPR (Partial Prestressing Ratio) used in Table 8.3 is defined as follows:

$$PPR = \frac{\text{Nominal moment resistance contributed by prestressing steel}}{\text{Nominal moment resistance contributed by total steel}} \tag{8.11}$$

$$PPR = \frac{A_{ps} f_{ps} (d_p - a/2)}{A_{ps} f_{ps} (d_p - a/2) + A_s f_y (d_s - a/2)} \tag{8.12}$$

where f_{ps} is the stress in the prestressing steel at nominal bending resistance and other notation is standard. For sections where the depth to the reinforcing steel is of the same order as that to the prestressing steel, the ratio of moments can be replaced as a first approximation by the ratio of forces as follows:

$$PPR \approx \frac{A_{ps} f_{ps}}{A_{ps} f_{ps} + A_s f_y} \tag{8.13}$$

For prestress loss calculations, Eq. (8.13) can be further simplified by replacing f_{ps} by f_{py}; this is because, at time of computation of losses, the stress in the prestressing steel at ultimate may be unknown. Note that PPR is equal 1 for fully prestressed concrete, that is, for a beam containing prestressed reinforcement only.

The approximate lump sum estimates of time-dependent prestress losses given in Table 8.3 reflect values and trends obtained from a computerized time-step analysis of a large number of bridge and building members designed for a common range of variables, namely [Ref. 8.32]:

- Ultimate concrete creep coefficient ranging from 1.6 to 2.4
- Ultimate concrete shrinkage strain ranging from 0.0004 to 0.0006
- Relative humidity ranging from 40 to 100 percent
- Moist-curing or steam-curing of concrete, and
- A PPR ranging from 0.2 to 1.0.

Although in the reference study leading to Table 8.3, the concrete compressive strength was varied from 6 to 10 ksi (41 to 69 MPa), the author believes that Table 8.3 can apply to concrete compressive strengths ranging from 4 to 12 ksi (28 to 83 MPa). The losses given in Table 8.3 represent the sum of time-dependent losses after transfer of prestress. They are different for different types of sections. Should the section be unknown, the author recommends to use the values recommended for I-type girders.

For the case of high strength wires and strands, an upper bound estimate and an average estimate are provided in some cases in Table 8.3. The upper bound is

recommended when an adverse combination of parameters, such as low concrete compressive strength, low relative humidity, and moist-curing conditions exist. For members prestressed with bars, the difference between the average and the upper bound was found too insignificant to justify a different expression. Similarly, for box girders, I-girders, and solid rectangular beams, the effect of concrete compressive strength up to 10 ksi (70 MPa) was found to be negligible when prestressed bars are used. Note that differences between different types of sections may also be due to differences in the average level of prestress in the concrete.

Estimation of losses for partially prestressed concrete is analogous to that for fully prestressed concrete. The following remarks will help the reader understand possible differences:

- Instantaneous prestress losses, such as friction, anchorage set, and elastic shortening in partially prestressed members can be computed in exactly the same manner as for prestressed members. It is suggested, however, to use transformed section properties when a significant amount of non-prestressed reinforcement is present.
- The average stress in the concrete in a partially prestressed member is generally smaller than that in a fully prestressed member. Thus, for similar conditions, the loss of prestress due to creep will also be smaller.
- If the prestressing steel is tensioned to the same initial tensile stress as in the case of fully prestressed concrete, the intrinsic relaxation loss would be the same. However, because prestress loss due to creep is smaller in a partially prestressed member, and because the loss due to creep influences that due to relaxation, the relaxation loss in partially prestressed concrete members is slightly higher than in fully prestressed concrete members.
- The presence of a substantial amount of nonprestressed reinforcement, such as in partially prestressed concrete, influences stress redistribution along the section due to creep of concrete with time and generally leads to smaller prestress losses.
- Because a partially prestressed concrete member may be cracked under permanent load, the loss of prestress in the steel may be balanced in great part by the increase in stress in the steel at cracking. This increase in stress is needed to maintain equilibrium and account for the loss of tensile capacity contribution by the concrete section.

8.6 SEPARATE LUMP SUM ESTIMATE OF EACH TIME-DEPENDENT LOSS – AASHTO LRFD

Several methods can be found in the technical literature to estimate the separate contribution of each source of loss of prestress [Refs. 8.3, 8.6, 8.18, 8.19, 8.35, 8.36 and 8.52]. The total loss of prestress is then obtained by summing up the separate

contributions. Many of these methods have merit and can be used. However, because of the implied authority of the code, only the method described in the AASHTO LRFD Bridge Design Specifications [Ref. 8.6] and recommended by ACI Committee 343 on Bridge Structures [Ref. 8.3] is described next and illustrated by an example. It requires some basic information on materials properties and environmental conditions, but it is simple to implement.

Instantaneous losses are first calculated according to Sections 8.7, 8.16, 8.17 and 8.18, where appropriate.

Values of losses due to creep, shrinkage, and relaxation, more accurate than losses specified in the total lump-sum estimate of Table 8.3, may be determined as described in Sections 8.6.1 to 8.6.3 for prestressed members with:

- Spans not greater than 250 ft (75 m)
- Normal density concrete, and
- Concrete compressive strength in excess of 3.5 ksi (24 MPa) at time of prestress transfer.

For lightweight concrete, the loss of prestress shall be based on the representative properties of the concrete to be used.

For all considerations other than preliminary design, prestress losses for segmental construction, shall be determined by more refined procedures, including consideration of the time-dependent construction method and schedule shown in the contract documents.

8.6.1 Total Loss Due to Shrinkage

Loss of prestress due to shrinkage may be taken as:

- For pretensioned members:

$$\begin{cases} \Delta f_{pS} = (17 - 0.15H) \text{ (ksi)} \\ \Delta f_{pS} = (117 - 1.03H) \text{ (MPa)} \end{cases} \tag{8.14}$$

- For posttensioned members:

$$\begin{cases} \Delta f_{pS} = (13.5 - 0.123H) \text{ (ksi)} \\ \Delta f_{pS} = (93 - 0.85H) \text{ (MPa)} \end{cases} \tag{8.15}$$

where:

H = the average annual ambient relative humidity in percent.

8.6.2 Total Loss Due to Creep

Prestress loss due to creep may be taken as:

$$\Delta f_{pC} = 12 f_{cgp} - 7\Delta f_{cdp} \geq 0 \tag{8.16}$$

where:

f_{cgp} = concrete stress at center of gravity of prestressing steel at time of transfer of prestress (ksi or MPa)

Δf_{cdp} = change in concrete stress at center of gravity of prestressing steel, due to permanent loads, with the exception of the load acting at the time the prestressing force is applied. So essentially the self-weight of the member is not considered. Values of Δf_{cdp} should be calculated at the same section or sections for which f_{cgp} is calculated (ksi or MPa).

For a simply supported beam, f_{cgp} is generally due to the combined effect of prestress and dead weight. The larger than or equal sign in Eq. (8.16) is needed because a negative value could result in some cases of partial prestressing, but Δf_{pC} should not be taken as less than 0.

8.6.3 Total Loss Due to Relaxation

The total relaxation loss at any time after jacking shall be taken as the sum of losses that occur between jacking and transfer (Δf_{pR1}), and losses that occur after transfer (Δf_{pR2}). For posttensioned members, Δf_{pR1} is zero. For calculations of relaxation losses at any other time, refer to Section 8.11.

1. Between Jacking and Transfer

In pretensioned members, the relaxation loss in prestressing steel, initially stressed in excess of $0.50 f_{pu}$, may be taken as:

- For stress-relieved strand:

$$\Delta f_{pR1} = \frac{\log(24t)}{10}\left[\frac{f_{pJ2}}{f_{py}} - 0.55\right] f_{pJ2} \tag{8.17}$$

- For low-relaxation strand:

$$\Delta f_{pR1} = \frac{\log(24t)}{40}\left[\frac{f_{pJ2}}{f_{py}} - 0.55\right] f_{pJ2} \tag{8.18}$$

where:

t = time estimated in days from stressing to transfer (days)

f_{pJ2} = initial stress in the tendon at the end of stressing or jacking (ksi or MPa)

f_{py} = specified yield strength of prestressing steel (ksi or MPa)

The value of f_{pJ2} is estimated from the stress reading at the jack and the anchorage or chuck loss at seating, if any (see Eq. 8.3). If project-specific information is not available, the value of f_{pJ2} may be taken as $0.80 f_{pu}$ for the purpose of this calculation.

2. After Transfer

Losses due to relaxation of prestressing steel may be taken as:

- For pretensioning with stress-relieved strands:

$$\begin{cases} \Delta f_{pR2} = 20 - 0.4\,\Delta f_{pES} - 0.2(\Delta f_{pS} + \Delta f_{pC}) \text{ (ksi)} \\ \Delta f_{pR2} = 138 - 0.4\,\Delta f_{pES} - 0.2(\Delta f_{pS} + \Delta f_{pC}) \text{ (MPa)} \end{cases} \tag{8.19}$$

- For posttensioning with stress-relieved strands:

$$\begin{cases} \Delta f_{pR2} = 20 - 0.3\,\Delta f_{pF} - 0.4\,\Delta f_{pES} - 0.2(\Delta f_{pS} + \Delta f_{pC}) \text{ (ksi)} \\ \Delta f_{pR2} = 138 - 0.3\,\Delta f_{pF} - 0.4\,\Delta f_{pES} - 0.2(\Delta f_{pS} + \Delta f_{pC}) \text{ (MPa)} \end{cases} \tag{8.20}$$

where:

Δf_{pF} = the friction loss below the level of $0.70 f_{pu}$ at the point under consideration (see Section 8.16)

Δf_{pES} = loss due to elastic shortening

Δf_{pS} = loss due to shrinkage

Δf_{pC} = loss due to creep of concrete

- For prestressing steels with low relaxation properties conforming to AASHTO - M 203 or ASTM A 416 or E 328:

Use 30 percent of Δf_{pR2} given by Eqs. (8.19 or 8.20).

- For posttensioning with prestressing bars of 145 to 160 ksi (1000 to 1104 MPa) tensile strength:

  Loss due to relaxation should be based on approved test data. If test data are not available, the loss Δf_{pR2} may be assumed to be 3 ksi (21 MPa).

8.6.4 Losses for Deflection Calculations

For camber and deflection calculations of prestressed nonsegmental members with spans not exceeding 160 ft (48 m), made of normal weight concrete with a strength in excess of 3.5 ksi (24 MPa) at the time of prestress, f_{cgp} and Δf_{cdp} may be computed as the stress at the center of gravity of prestressing steel averaged along the length of the member.

8.6.5 Example: Losses Due to Relaxation

Generally the contractor or the manufacturer of prestressed concrete elements is responsible to determine the stress at time of transfer of prestress, based on equipment and anchorage devices. Let us consider the case of a pretensioned prestressed beam. The prestressing strands are tensioned and left anchored between abutments for about 24 hours prior to transfer of prestress.

Based on prior experience, length of prestressing bed, and chuck (anchorage) device used in tensioning, the contractor estimates that about 1.5% loss (or 3 ksi (21MPa)) of stress occurs at seating, that is, when the chucks are released by the jacks at the abutments.

The 2002 ACI building code (Table 3.6) limits the stress at jacking to $0.80 f_{pu} = 216$ ksi, and that is the value used by the contractor. Thus the stress in the tendons, just after seating of the chucks between abutments, becomes equal to $216 - 3 = 213$ ksi.

Next the concrete is cast and steam cured. The strands are cut twenty four hours after stressing, inducing transfer of stress between steel and concrete. During the first twenty four hours, the strands are subjected to relaxation. The relaxation loss depends on the type of strand. Assuming:

- Stress-relieved strands:

$$\Delta f_{pR1} = \frac{log(24t)}{10}\left[\frac{f_{pJ2}}{f_{py}} - 0.55\right] f_{pJ2}$$

$$\Delta f_{pR1} = \frac{log(24t)}{10}\left[\frac{213}{230} - 0.55\right] 213 = 11.05 \text{ ksi}$$

in which $t =$ 1 day; $f_{pJ2} =$ 213 ksi; $f_{py} =$ 230 ksi.

Thus the value of stress in the prestressing steel, just before transfer, is equal to:

$$(f_p)_{\text{just before transfer}} = 216 - 3 - 11.05 \approx 202 \text{ ksi}$$

- Low relaxation strands:

$$\Delta f_{pR1} = \frac{log(24t)}{40}\left[\frac{f_{pJ2}}{f_{py}} - 0.55\right] f_{pJ2}$$

$$\Delta f_{pR1} = \frac{log(24t)}{40}\left[\frac{213}{243} - 0.55\right] 213 = 2.40 \text{ ksi}$$

in which t = 1 day; f_{pJ2} = 213 ksi; f_{py} = 243 ksi.

Thus the value of stress in the prestressing steel, just before transfer, is equal to:

$$(f_p)_{\text{just before transfer}} = 216 - 3 - 2.40 = 210.60 \text{ ksi}$$

Once estimated for given conditions, the value of stress just before transfer can be used as typical in routine design. Tracking the stress history in the prestressing steel beyond this point is described in Example 8.10.

8.7 LOSS DUE TO ELASTIC SHORTENING

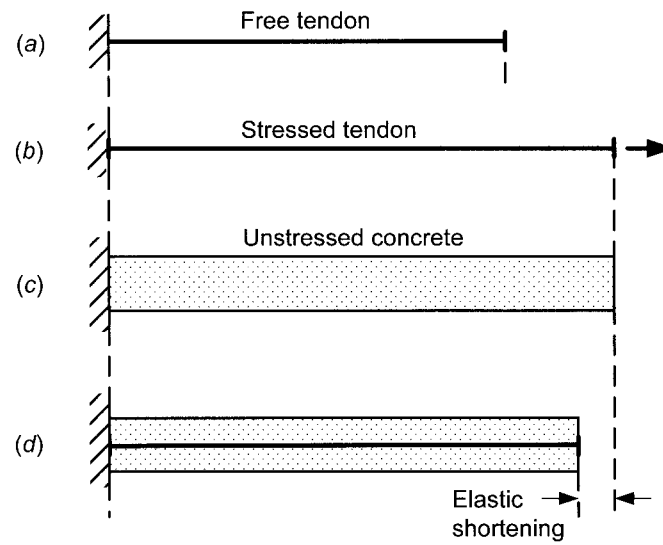

Figure 8.4 Schematic representation of elastic shortening. (a) Free tendon. (b) Stressed tendon. (c) Unstressed concrete. (d) Shortening at transfer.

Figure 8.4 illustrates elastic shortening. A tendon and a concrete prism are considered. At rest, the tendon is shorter than the prism. If the tendon is stretched (or stressed) to have the same length as the prism then attached to it and released,

both will shorten because the concrete undergoes compression and the tendon must follow. A state of equilibrium of forces is achieved for which the tendon and the prism have the same new length (Fig. 8.4*d*). The difference in length of the prism before and after release induces a stress change in the tendon, which is equal to its elastic shortening loss.

The loss of stress in the steel due to elastic shortening of the concrete should be determined using the modulus of elasticity of the concrete at the time of prestress transfer. Its calculated value must be treated differently, however, depending on whether pretensioning or posttensioning is used.

8.7.1 Pretensioned Construction: Approximate Method and AASHTO LRFD

It is assumed that the concrete at the time of transfer is instantaneously compressed and, therefore, experiences a sudden change in strain (Fig. 8.4). As the change in strain in the concrete is the same as that in the steel, the corresponding stress changes in each material are related. The following relation is generally used to estimate the stress loss due to elastic shortening:

$$\Delta f_{pES} = \left(\frac{E_{ps}}{E_{ci}}\right)(f_{cgp})_{F_i+G} = n_{pi}(f_{cgp})_{F_i+G} \tag{8.21}$$

where $(f_{cgp})_{Fi+G}$ represents the stress in the concrete at the centroid of the prestressing tendons due to the prestressing force and the dead load of the member, immediately after transfer. For a simply supported beam, its value is given by:

$$(f_{cgp})_{F_i+G} = (f_{cgp})_{F_i} + (f_{cgp})_G = \left(\frac{F_i}{A_c} + \frac{F_i e_o^2}{I}\right) - \left(\frac{M_G e_o}{I}\right) \tag{8.22}$$

where:

$(f_{cgp})_{F_i}$ = stress in the concrete at the centroid of the prestressing tendons due to the initial prestressing force F_i

$(f_{cgp})_G$ = stress in the concrete at the centroid of the prestressing tendons due to self-weight of member

Equation (8.21) is same as recommended by AASHTO LRFD with a slightly different notation.

Note that in order to use Eq. (8.21), $F_i = A_{ps} f_{pi}$ must be known, hence f_{pi} must be estimated and, according to Eq. (8.5), the loss due to elastic shortening must be known. Therefore, Eq. (8.21) must be considered a first approximation in which F_i is estimated a priori and revised thereafter, if needed.

The AASHTO LRFD suggest an approximate value of $f_{pi} = 0.65 f_{pu}$ for stress-relieved strands and high-strength bars, and $f_{pi} = 0.70 f_{pu}$ for low relaxation strand. However for components of unusual design, more accurate methods supported by research or experience should be used. A typical example of computation of elastic shortening loss is given in Section 8.8.

8.7.2 Pretensioned Construction: Accurate Method

The approximate design method described above is sufficient in practically all cases. However a more accurate method can be derived. · Since f_{pi} is theoretically unknown, another way to estimate elastic shortening is to exploit f_{pJ2}, the stress in the tendons immediately after jacking or seating. It is a known quantity. The following relation can then be easily derived:

$$\Delta f_{pES} = n_{pi}\left[\frac{f_{pi}}{f_{pJ2}}(f_{cgp})_{F_J} + (f_{cgp})_G\right] \tag{8.23}$$

in which:

$$F_J = A_{ps} f_{pJ2} \tag{8.24}$$

Replacing f_{pi} by its value from Eq. (8.5) in Eq. (8.23) gives:

$$\Delta f_{pES} = n_{pi}\left[\frac{f_{pJ2} - \Delta f_{pR}(t_o, t_t) - \Delta f_{pES}}{f_{pJ2}}(f_{cgp})_{F_J} + (f_{cgp})_G\right] \tag{8.25}$$

in which Δf_{pES} is on both sides of the equation. Solving Eq. (8.25) for Δf_{pES} leads to:

$$\Delta f_{pES} = \frac{(f_{cgp})_{F_J}[f_{pJ2} - \Delta f_{pR}(t_o, t_t)] + (f_{cgp})_G f_{pJ2}}{f_{pJ2}/n_{pi} + (f_{cgp})_{F_J}} \tag{8.26}$$

where f_{pJ2} and F_J (Eq. 8.24) are assumed to be known.

An example illustrating the use of Eqs. (8.21) and (8.26) is developed in Section 8.8. Note that, once Δf_{pES} is obtained, the value of f_{pi} can be calculated from Eqs. (8.5) or (8.8). Differences between the approximate method and the more accurate methods are generally small.

8.7.3 Posttensioned Construction: AASHTO LRFD

The AASHTO LRFD suggests that the loss due to elastic shortening in posttensioned members, other than slab systems, may be taken as:

$$\Delta f_{pES} = \left(\frac{N-1}{2N}\right)\frac{E_{ps}}{E_{ci}} f_{cgp} \tag{8.27}$$

where:

N = number of identical prestressing tendons
f_{cgp} = sum of concrete stresses at the center of gravity of prestressing tendons due to prestressing force after jacking and the self-weight of the member at the section of maximum moment

Note that the second part of the right hand side of the equation is same as the elastic shortening for pretensioned members (Eq. 8.21)

f_{cgp} values may be calculated using a steel stress reduced below its initial value to account for estimated elastic shortening, relaxation, and friction effects.

For posttensioned structures with bonded tendons, f_{cgp} may be taken at the center section of the span or, for continuous construction, at the section of the maximum moment.

For posttensioned structures with unbonded tendons, the value of f_{cgp} may be calculated as the stress at the center of gravity of the prestressing tendons averaged along the length of the member.

If tendons with two different numbers of strands per tendon are used, N may be calculated as:

$$N = N_1 + N_2 \frac{A_{ps2}}{A_{ps1}} \tag{8.28}$$

where:

N_1 = number of tendons in the larger group
N_2 = number of tendons in the smaller group
A_{ps1} = cross-sectional area of a tendon in the larger group
A_{ps2} = cross-sectional area of a tendon in the smaller group

In slabs where stretching of one tendon will have little effect on non-immediately neighboring tendons, an elastic shortening value equal to 25 percent of that of equivalent pretensioned construction (Eq. 8.21) is often used.

8.7.4 Posttensioned Construction: Accurate Method

The elastic shortening in posttensioned members varies from zero if all the tendons are tensioned simultaneously to half the value obtained for pretensioned members if an infinite number of tendons tensioned sequentially is used. Indeed the fraction $(N-1)/2N$ in Eq. (8.27) given by AASHTO tends toward 0.5 when N becomes infinitely large.

Theoretically, the loss due to elastic shortening in a given tendon and the corresponding average loss for many tendons can be determined exactly. If N is the number of tendons sequentially tensioned in a beam, the elastic shortening loss in the jth tendon due to the tensioning of tendons $j+1$ to $j+N$ is given by the following expression (Fig. 8.5):

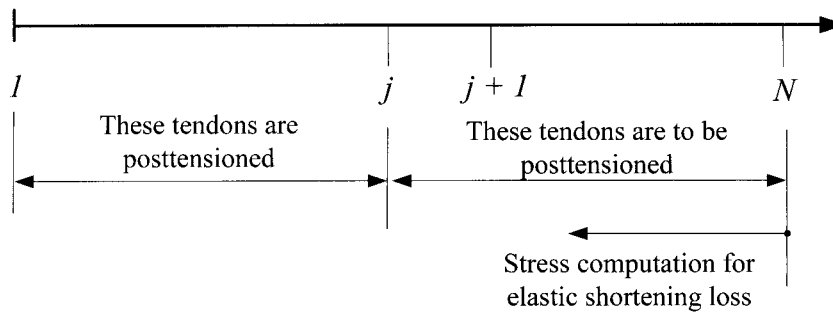

Figure 8.5 Tensioning sequence and loss of stress due to elastic shortening.

$$(\Delta f_{pES})_j = n_{pi} \sum_{k=j+1}^{N} \frac{f_{pk} A_{pk}}{A_c} \left(1 + \frac{e_j e_k}{r^2}\right) \tag{8.29}$$

where:

n_{pi} = moduli ratio at time of prestress = E_{ps}/E_{ci}

f_{pk} = stress in the kth tendon immediately after the last tendon has been tensioned

A_{pk} = area of kth tendon

e_j, e_k = eccentricities of jth and kth tendon with respect to the centroid of concrete section

A_c = area of concrete section (net area may also be used for better accuracy)

r = $\sqrt{I/a_c}$ radius of gyration of section (net section properties may also be used for better accuracy)

Note that the last tendon N does not experience any elastic shortening. Its stress f_{pN} is known and equal to f_{pJ}. So, it is recommended to start computation with the last tendon proceeding backward. Thus the stress in every other tendon is calculated. The average loss by elastic shortening to be applied throughout to the steel (ignoring the effects of friction) is then given by:

$$\Delta f_{pES} = \sum_{j=1}^{N} \frac{A_{pj}(\Delta f_{pES})_j}{\sum_{j=1}^{N} A_{pj}} \tag{8.30}$$

and if the tendons have all the same area:

$$\Delta f_{pES} = \frac{1}{N} \sum_{j=1}^{N} (\Delta f_{pES})_j \tag{8.31}$$

8.8 EXAMPLE: ELASTIC SHORTENING LOSS IN PRETENSIONED BEAM

Consider the simply supported pretensioned beam shown in Fig. 8.6, which will be used for this example as well as the examples covered in Sections 8.9 and 8.10. The following information is provided:

$A_{ps} = 2.142 \text{ in}^2; e_o = 14.56 \text{ in}; E_{ps} = 28000 \text{ ksi}; f_{pu} = 270 \text{ ksi};$

$f'_c = 5000 \text{ psi}; f'_{ci} = 4000 \text{ psi}; \gamma_c = 150 \text{ pcf}; E_c = 33\gamma_c^{1.5}\sqrt{f'_c}; E_{ps} = 28000 \text{ ksi}; n_{pi} = 7.3; n_p = 6.53;$

$\varepsilon_{SU} = 5\times10^{-4}; C_{CU} = 2; H = 70 \text{ percent}; \text{span } l = 70 \text{ ft}$

Assume that the beam is steam-cured, that transfer of the prestress occurs 24 hours (or 1 day) after tensioning, and that curing ends at time of transfer.

Compute the elastic shortening loss assuming stress-relieved strands are used.

$A_c = 474 \text{ in}^2; I = 21540 \text{ in}^4$
$y_t = 5.94 \text{ in}; y_b = 18.06 \text{ in}$
$Z_t = 3636 \text{ in}^3; Z_b = 1193 \text{ in}^3$
$k_t = -2.52 \text{ in}; k_b = 7.65 \text{ in}$
$r = 6.74 \text{ in}; w_G = 494 \text{ plf}$
LL=320 plf; span l = 70 ft

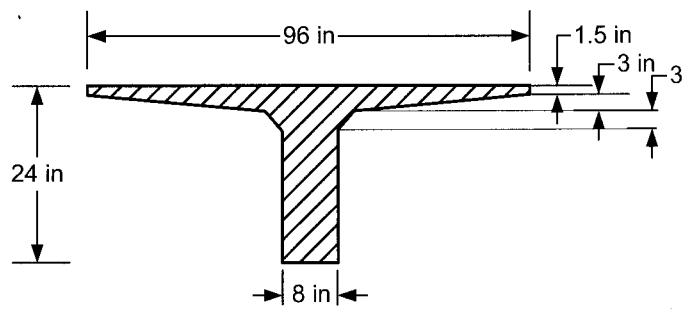

Figure 8.6 Properties of example beam.

Elastic shortening using AASHTO LRFD (Eq. 8.21):

$$\Delta f_{pES} = n_{pi}(f_{cgp})_{F_i+G}$$

where $(f_{cgs})_{F_i+G}$ is given by Eq. (8.22) in which F_i is replaced by $A_{ps}f_{pi}$; in this case f_{pi} is estimated equal to $0.65f_{pu}$ or 175.5 ksi, as per AAHSTO. Using Eq. (8.22):

$$(f_{cgp})_{F_i+G} = (f_{cgp})_{F_i} + (f_{cgp})_G = \left(\frac{F_i}{A_c} + \frac{F_i e_o^2}{I}\right) - \left(\frac{M_G e_o}{I}\right)$$

in which:

$$M_G = w_G \frac{l^2}{8} = 0.494\frac{70^2}{8} = 302.575 \text{ kips-ft} = 3630.9 \text{ kips-in}$$

$$(f_{cgp})_G = -\left(\frac{M_G e_o}{I}\right) = -\left(\frac{3630.9\times 14.56}{21540}\right) = -2.454 \text{ ksi}$$

$$(f_{cgp})_{F_i} = \left(\frac{F_i}{A_c} + \frac{F_i e_o^2}{I}\right) = \frac{175.5\times 2.142}{474} + \frac{175.5\times 2.142\times 14.56^2}{21540} = 4.493 \text{ ksi}$$

$$(f_{cgp})_{F_i+G} = 4.493 - 2.454 = 2.039 \text{ ksi}$$

and the loss due to elastic shortening is:

$$\Delta f_{pES} = 7.3\times 2.039 = 14.88 \text{ ksi}$$

If low relaxation strands were used, f_{pi} could have been estimated equal to $0.70f_{pu}$ or 189 ksi, as per AAHSTO LRFD. The calculated value of elastic shortening in that case would have been 17.4 ksi.

Note that the value of f_{pi} assumed for elastic shortening calculations is generally smaller than the real value that would be obtained from calculations, as shown in the example of Section 8.10.

Elastic shortening using exact method:

In this case the initial stress in the steel must be obtained directly from the stress at end of jacking. From the example of Section 8.6.5, the stress at end of jacking was estimated as $f_{pJ2} = 213$ ksi, and the relaxation loss prior to transfer was calculated as $\Delta f_{pR1} = 11.05$ ksi. Thus:

$$F_J = 213\times 2.142 = 456.246 \text{ kips}$$

$$(f_{cgp})_{F_J} = \frac{F_J}{A_c} + \frac{F_J e_o^2}{I} = \frac{456246}{474} + \frac{456246\times 14.56^2}{21540} = 5.453 \text{ ksi}$$

and from the example above: $(f_{cgp})_G = -2.454$ ksi

Using Eq. (8.26):

$$\Delta f_{pES} = \frac{(f_{cgp})_{F_J}[f_{pJ2} - \Delta f_{pR}(t_o, t_f)] + (f_{cgp})_G f_{pJ2}}{f_{pJ}/n_{pi} + (f_{cgp})_{F_J}}$$

$$\Delta f_{pES} = \frac{5.453(213 - 11.05) - 2.454 \times 213}{213/7.3 + 5.453} = 16.70 \text{ ksi}$$

This value is slightly larger than that obtained earlier. It is mostly due to the fact that the stress in the steel used in Eq. (8.26) is higher than that estimated from the AASHTO LRFD.

8.9 EXAMPLE: COMPUTATION OF PRESTRESS LOSSES FOR A PRETENSIONED BEAM BY LUMP SUM METHODS

Compute the time-dependent prestress losses at midspan for the simply supported pretensioned beam shown in Fig. 8.6. This is the same beam covered in Section 8.8. Stress-relieved strands are used.

Assume that the beam is steam-cured, that transfer of the prestress occurs 24 hours (or 1 day) after tensioning, and that curing ends at time of transfer. The value of stress immediately after transfer $f_{pi,}$ assumed here, corresponds to the maximum value allowed by the 2002 ACI building code, that is $f_{pi} = 0.82 f_{py} = 0.82 \times 0.85 f_{pu} = 0.70 f_{pu} = 189$ ksi . Example 8.10 illustrates how f_{pi} can be calculated from the stress known at the end of jacking and just before transfer.

8.9.1 Lump Sum Estimate of Total Losses by AASHTO LRFD

The beam has a T section and the environmental conditions are average. However, the concrete strength is rather on the low side and it is a fully prestressed beam, thus PPR = 1.

The total time-dependent loss of prestress after transfer can be estimated from (Table 8.3):

$$(\Delta f_{pTD})_{\text{after transfer}} = 33\left[1 - 0.15\frac{f'_c - 6}{6}\right] + 6 \text{ PPR (ksi)}$$

$$(\Delta f_{pTD})_{\text{after transfer}} = 33\left[1 - 0.15\frac{5 - 6}{6}\right] + 6 \times 1 = 39.8 \text{ (ksi)}$$

Note that using a concrete strength of 5 ksi (35 MPa) leads to an increase in loss when compared to the reference of 6 ksi (42 MPa) for which the base study was carried out.

If f_{pi} = 189 ksi, the effective prestress can be calculated from:

$$f_{pe} = f_{pi} - \Delta f_{pTD}$$

$$f_{pe} = 189 - 39.8 = 149.2 \text{ ksi}$$

The value of the ratio η used in preliminary design would be:

$$\eta = \frac{F}{F_i} = \frac{f_{pe}}{f_{pi}} = \frac{f_{pi} - 39.8}{f_{pi}} = \frac{189 - 39.8}{189} = 0.79$$

A closer evaluation of the stress history in the strands of this particular beam section is given in Section 8.10.

If low relaxation strands were used in this problem instead of stress relieved strands, the total loss of prestress after transfer would be (according to the footnote of Table 8.3): 39.8 – 8 = 31.8 ksi.

8.9.2 Lump Sum Estimates of Separate Losses by AASHTO LRFD

- *Shrinkage of concrete* (Eq. 8.14):

$$\Delta f_{pS} = 17 - 0.15H \quad \text{(ksi)} \quad = 17 - 0.15 \times 70 = 6.5 \text{ ksi}$$

- *Creep of concrete* (Eq. 8.16):

$$\Delta f_{pC} = 12(f_{cgp})_{F_i+G} - 7(\Delta f_{cgp})_{SD}$$

where $(f_{cgp})_{F_i+G}$ is calculated in Section 8.8 for the same beam and is equal to 2.039 ksi.

As no superimposed dead load exists in this problem, $(\Delta f_{cgp})_{SD}$ is nil and

$$\Delta f_{pC} = 12 \times 2.039 = 24.47 \text{ ksi}$$

- *Relaxation of prestressing steel after transfer* (Eq. 8.19):

$$\Delta f_{pR2} = 20 - 0.4\Delta f_{pES} - 0.2(\Delta f_{pS} + \Delta f_{pC})$$

$$\Delta f_{pR2} = 20 - 0.4 \times 14.88 - 0.2(6.5 + 24.47) = 7.85 \text{ ksi}$$

in which the elastic shortening loss is taken from the example of Section 8.8.

- *Total time-dependent loss after transfer* (Eq. 8.6):

$$(\Delta f_{pTD})_{after\ transfer} = 6.5 + 24.47 + 7.85 = 38.82 \text{ ksi}$$

It can be observed that, at least for this particular problem, the total loss of prestress after transfer, using the sum of separate losses, is not too different from that using the lump-sum estimate from Table 8.3, obtained in the previous example.

If low relaxation strands were used in this problem instead of stress-relieved strands, the lump sum loss estimate due to creep and shrinkage would be same. However, the loss due to relaxation is taken equal to 30% of the value obtained for stress-relieved strands, that is: 0.3x7.85 = 2.36 ksi. The total loss of prestress after transfer would then be: 6.5 + 24.47 + 2.36 = 33.33 ksi.

8.10 EXAMPLE: TYPICAL STRESS HISTORY IN STRANDS

To calculate prestress losses using the lump sum methods, we need to estimate the stress in the prestressing steel, f_{pi}, just after transfer. In the previous example, it was taken equal to $0.70f_{pu}$ = 189 ksi.

It is useful to trace the progression of stress in a strand from the time of stressing at the jacks to the effective prestress in service, and correlate it with some of the values obtained above. There are two limitations in the ACI building code that must be satisfied (see Table 3.6): the stress at jacking cannot exceed either $0.94f_{py}$ or $0.8f_{pu}$, and the stress after transfer to the concrete cannot exceed $0.82f_{py}$. Either limitation could control the design. Table 8.4 shows typical results for two cases for the beam of examples 8.8 and 8.9: one case where the strands are stress-relieved as in the above examples, and one case where they are low relaxation grade. For both the stress-relieved and low

relaxation strands, the stress limit at jacking of $0.80f_{pu}$ = 216 ksi controls. In Table 8.4, the elastic shortening loss was calculated by the exact method using Eq. (8.26).

The reader may want to repeat the example and check the numerical values obtained for the low relaxation strands reported in Table 8.4. Note that in this case, the elastic shortening loss is larger than that obtained earlier because the value of f_{pi} is larger than that assumed by AASHTO LRFD. Table 8.4 illustrates the values of some typical parameters used in preliminary design and supports the first hand approximations made, such as taking a value of η close to 0.8, an effective prestress f_{pe} of the order of 150 ksi, and prestress losses after transfer of the order of 20%.

Table 8.4 Typical stress history for an example beam using limits from the 2002 ACI building code.

	Stress relieved strand $f_{py} = 0.85f_{pu} \approx 230$ ksi	Low relaxation strand $f_{py} = 0.90f_{pu} = 243$ ksi
Stress at the jack, f_{pJ1} (limit by 2002 ACI code)	$0.94f_{py} = 216$ ksi $0.80f_{pu} = 216$ ksi	216 ksi $\le 0.94f_{py} = 228$ ksi 216 ksi = $0.80f_{pu}$ controls
Anchorage (chuck) loss, ksi	3	3
Stress at end of jacking, f_{pJ2}, ksi	213	213
Relaxation loss during 24 hours, ksi	11.05	2.40
Stress just before transfer, ksi	201.95	210.60
Elastic shortening loss (Eq. 8.26), ksi	16.7	18.07
Stress just after transfer, f_{pi}, ksi (limit by ACI 2002 code)	$185.25 < 0.82f_{py} \approx 189$ O.K.	$192.53 < 0.82f_{py} \approx 199.3$ O.K.
Lump sum of time dependent losses after transfer, ksi	39.8 ksi	31.8 ksi
Effective stress after losses, f_{pe}, ksi	185.25 - 39.8 = 145.45 ksi	192.53 – 31.8 = 160.73 ksi
Sum of total prestress losses, ksi	216 – 145.45 = 70.55 ksi	216 – 160.73 = 55.27 ksi
Percent loss in relation to f_{pJ1} = 216 ksi	32.7%	25.6%
Percent loss after transfer versus f_{pi}	39.8/185.25 = 21.5%	16.5%
Ratio $\eta = \frac{F}{F_i} = \frac{f_{pe}}{f_{pi}}$	0.785	0.835

8.11 TIME-DEPENDENT LOSS DUE TO STEEL RELAXATION

Relaxation of prestressing steels is discussed in Section 2.2.4. Also, computation of prestress loss due to relaxation before and after transfer of prestress, as per AASHTO LRFD, is described in Section 8.6.3. Next some background is given to allow computation of relaxation losses at any time, or during any time interval. The methodology can then be integrated in the time-step procedure to compute prestress losses more accurately.

At any time t and under normal temperature conditions, the stress in the prestressing steel tensioned initially to f_{pi}, can be estimated as described in Sec. 2.2.4 from the following relation [Ref. 8.29]:

$$f_p(t) = f_{pi}\left[1 - \frac{\log(t)}{K}\left(\frac{f_{pi}}{f_{py}} - 0.55\right)\right] \tag{8.32}$$

where t is in hours and is not less than one hour, $\log(t)$ is to the base 10, the ratio f_{pi}/f_{py} is not less than 0.55, and K is a constant taken equal 10 for stress-relieved strands; for low relaxation strands, K is taken equal 40 by AASHTO LRFD and 45 by the PCI Committee on Prestress Losses [Ref. 8.35]. Note that for $f_{pi} \le 0.55 f_{py}$ practically no relaxation losses take place. The definition of f_{pi} in Eq. (8.32) applies to the initial stress in the tendon for relaxation computation and is not necessarily same as the f_{pi} defined in Eqs. (8.5) and (8.8).

The PCI Committee on Prestress Losses [Ref. 8.35] suggests the use of the following equation to compute the relaxation loss of stress-relieved steel during an interval of time (t_i, t_j):

$$\begin{aligned}\Delta f_{pR}(t_i, t_j) &= f_p(t_i) - f_p(t_j) \\ &= \frac{f_p(t_i)}{K}\left(\frac{f_p(t_i)}{f_{py}} - 0.55\right)\log\left(\frac{t_j}{t_i}\right)\end{aligned} \tag{8.33}$$

where the time is in hours and is not less than one hour and f_{pi}/f_{py} is not less than 0.55. Note that Eq. (8.33) cannot be exactly derived from Eq. (8.32); the difference comes from the value of f_{pi} which is always updated to $f_p(t_i)$ at the beginning of any time interval. Equation (8.33) is valid under normal temperature conditions only.

As mentioned in Sec. 8.4, the stress in the steel is being continuously altered with time and a number of reasonable time intervals are selected to compute relaxation loss during each interval, as well as its cumulative value over preceding intervals.

An example of computation of relaxation loss is given in Table 8.5 for a free strand (not associated with a concrete element but fixed at constant length) at typical time intervals using Eq. (8.19) and assuming the following properties: stress-relieved strand; f_{pu} = 270 ksi; f_{py} = 230 ksi; K = 10; $f_{pi} = f_p(1\text{ hour}) = 213$ ksi; the starting time of an interval is taken the same as the end time of the immediately preceding interval. Some steps to explain the numbers in the table are given next:

- Start at one hour with $f_{pi} = f_p(t_i) = 213$ ksi (row (a) third column in Table 8.5). This is the stress at the beginning of the interval of 1 to 24 hours.
- Compute the stress loss during the first 24 hours from Eq. (8.33):

$$\Delta f_{pR}(1,24) = \frac{213}{10}\left(\frac{213}{230} - 0.55\right)\log\left(\frac{24}{1}\right) = 11.06 \text{ ksi}$$

  This value is shown in row (b), third column of Table 8.5.
- Also using Eq. (8.33) compute the stress in the prestressing steel at the end of the first time interval, that is at 24 hours:

$$f_p(t_j) = f_p(t_i) - \Delta f_{pR}(t_i, t_j) = 213 - 11.06 = 201.94$$

  This value is shown in row (c), third column in Table 8.5; this is the stress at the end of the first time interval between 1 hour to 1 day.
- The stress in the prestressing steel computed at the end of the first interval, $f_p(t_j) = 201.94$ ksi, is now taken as the stress at the beginning of the next interval, starting at 1 day and ending at 3 days (row (a), forth column of Table 8.5)
- The process is continued keeping track not only of the loss during an interval but also of the cumulative loss during all preceding intervals.

Table 8.5 Typical time-step computations of relaxation loss for a strand of constant length, fixed at its ends (not attached to a concrete member).

		Days						Years	
Time t_j at the end of interval (t_i, t_j)		1	3	7	30	90	365	5	50
(a)	$f_{ps}(t_i)$, ksi	213	201.9	198.8	196.5	192.7	190.1	186.9	183.4
(b)	$\Delta f_{pR}(t_i, t_j)$, ksi	11.06	3.16	2.30	3.78	2.65	3.19	3.43	4.54
(c)	$f_{ps}(t_j)$, ksi [(a) – (b)]	201.9	198.8	196.5	192.7	190.1	186.9	183.4	178.9
(d)	$\Sigma \Delta f_{pR}(t_i, t_j)$, ksi*	11.06	14.22	16.52	20.29	22.94	26.14	29.56	34.10
(e)	% Total relaxation	32.4	41.7	48.4	59.5	67.3	76.6	86.7	100.0
(f)	% Relaxation left	67.6	58.3	51.6	40.5	32.7	23.4	13.3	0

* Sum over preceding intervals.

The values shown in rows (e) and (f) of Table 8.5 are computed after completion of row (d) for 50 years.

A total relaxation loss of 34.1 ksi or about 16 percent of initial stress is observed at 50 years. Because of the effect of other losses, a much smaller relaxation loss would be observed when the tendon is attached to a prestressed concrete element as illustrated in the time step procedure example in Section 8.15. If, instead of using the time-step method over several time intervals, we use only a single interval (Eq. 8.33) between 1 hour and 50 years (438,000 hours), the total loss would be 45.2 ksi or 21.2 percent of initial stress.

8.12 TIME-DEPENDENT LOSS DUE TO SHRINKAGE

The shrinkage strain of a given concrete material increases with time up to an ultimate value generally associated with the service life of the member. The ultimate shrinkage strain depends on many parameters, including composition of the concrete mix, characteristics of the aggregates, relative humidity of the environment, curing history, and the like. Some relevant background information on the shrinkage strain of concrete is covered in Sec. 2.3 and Table 2.9, as well as in Refs. [8.4, 8.8, 8.21, 8.28, 8.30, 8.31, 8.33, 8.37, 8.50 and 8.51].

It is observed from Table 2.9 that the shrinkage strain at any time t for a concrete member can be predicted from the following general relation:

$$\varepsilon_S(t) = g(t)\varepsilon_{SU}K_{SH}K_{SS} \tag{8.34}$$

where:

$g(t)$ = time function
t = time in days after the end of curing
ε_{SU} = ultimate shrinkage strain of the concrete material
K_{SH} = correction factor which depends on the average relative humidity of the environment where the structure is built
K_{SS} = correction factor which depends on the shape and size of the member

The time function $g(t)$ tends toward unity when t tends toward t_l, the service life of the structure. Hence for all practical purposes, the shrinkage strain of a concrete member at the end of its service life is given by:

$$\varepsilon_S(t_l) = \varepsilon_{SU}K_{SH}K_{SS} \tag{8.35}$$

Because the shrinkage strain is assumed uniform throughout the concrete member and because the prestressing steel undergoes the same change in strain as the concrete, the total stress loss in the prestressing steel due to shrinkage is obtained from:

$$\Delta f_{pS} = E_{ps}\varepsilon_S(t_l) = E_{pS}\varepsilon_{SU}K_{SH}K_{SS} \tag{8.36}$$

Typical values of ε_{SU}, K_{SH}, and K_{SS} are given in Sec. 2.3 and Table 2.9. Other recommended values can be found in various references [Refs. 8.4, 8.33, 8.49]. In particular, a simple linear relation between water content in the concrete and ε_{SU} is sometimes used in practice as an estimate of ultimate shrinkage strain. It is given by:

$$\varepsilon_{SU} = \left[2 + \frac{11}{230}(w - 220)\right]10^{-4} \tag{8.37}$$

where w is the water content in pounds per cubic yard. Using the SI system, Eq. (8.37) becomes:

$$\varepsilon_{SU} = \left[2 + \frac{11}{1337}(w - 1279)\right]10^{-4} \tag{8.38}$$

where w is in Newtons per cubic meter.

When using the time-step method to compute losses, it is necessary to estimate the shrinkage strain at any time t and the incremental strain during a time interval (t_i / t_j). For this a time function is needed. Two such functions, which apply to tests where constant environmental conditions prevail, can be used when applicable. The time function suggested by ACI Committee 209 [Ref. 8.4] is described in Table 2.9 and given by:

$$g(t) = \frac{t}{b + t} \tag{8.39}$$

where t is in days and b is a parameter taken equal to 35 for moist-cured concrete and 55 for steam-cured concrete.

Another time function is sometimes used to predict the variation of shrinkage and creep strain of concrete with time. It is given by:

$$g(t) = 0.157 \ln (t) - 0.115 \tag{8.40}$$

where t is the time in days after curing. Equation (8.40) is valid for $t \geq 2.08$ days and $t \leq 1214$ days. For $t = 2.08$, $g(t) = 0$ and for $t = 1214$, $g(t) = 1$. Note that, unlike Eq. (8.39), this equation is not sensitive to the conditions of curing.

The magnitude of the stress loss in the prestressing steel due to shrinkage over a time interval (t_i,t_j) can be obtained from:

$$\begin{aligned}\Delta f_{pS}(t_i,t_j) &= \left|f_p(t_i) - f_p(t_j)\right| \\ &= E_{ps}\varepsilon_{SU}K_{SH}K_{SS}[g(t_j) - g(t_i)]\end{aligned} \tag{8.41}$$

where:

$f_p(t_i)$ = stress in the prestressing steel at time t_i
$f_p(t_j)$ = stress in the prestressing steel at time t_j

The starting time for the first time interval is assumed to represent the end of the curing period of the concrete.

Using the time function given by Eq. (8.39) in Eq. (8.41) leads to:

$$\Delta f_{pS}(t_i,t_j) = E_{ps}\varepsilon_{SU}K_{SH}K_{SS}\frac{b(t_j - t_i)}{(b+t_i)(b+t_j)} \tag{8.42}$$

where b is taken equal to 35 for moist-cured concrete and 55 for steam-cured concrete.

If the time function given by Eq. (8.40) is used in Eq. (8.41), the stress loss due to shrinkage over the time interval (t_i,t_j) takes the following form:

$$\Delta f_{pS}(t_i,t_j) = 0.157\, E_{ps}\varepsilon_{SU}K_{SH}K_{SS}\ln\left(\frac{t_j}{t_i}\right) \tag{8.43}$$

where the times are in days, are not more than 1214 days, and the starting time of the first interval must be set equal to 2.08 days. The stress loss at 1214 days is assumed the same as the loss at the end of service life.

An example is given next, assuming only shrinkage losses take place. In Sec. 8.15, an example where all prestress losses are simultaneously considered is covered. Note that Eqs. (8.42) and (8.43) apply only if constant environmental conditions are assumed.

8.12.1 Example: Shrinkage Loss Assuming No Other Loss Occurs

To illustrate the use of Eq. (8.42) and Eq. (8.43), let us compute the shrinkage loss in the tendons of a prestressed pretensioned concrete member, assuming no other loss is taking place. Transfer occurs at 24 hours after prestress, at which time shrinkage starts. The following input data are given: $\varepsilon_{SU} = 4\times10^{-4}$; $f_{pi} = 189$ksi; $E_{ps} = 28000$ ksi, relative humidity H = 60 percent, volume-to-surface ratio of member V/S = 1.5, moist-cured concrete. Using Tables 2.9 and 2.10 leads to:

- $K_{SH} = 0.80; K_{SS} = 1$. Hence, the ultimate shrinkage strain for the member is given by: $\varepsilon_{SU} K_{SH} K_{SS} = 4 \times 10^{-4}$. The computations for the first interval are as follows:
- Start at end of first day with f_{pi} = 189 ksi, immediately after transfer
- Compute prestress loss due to shrinkage between 1 and 3 days, that is (Eq. 8.42):

$$\Delta f_{pS}(1,3) = 28000 \times 5 \times 10^{-4} \times 0.80 \times 1 \frac{35(3-1)}{(35+1)(35+3)} = 0.573 \text{ ksi}$$

Table 8.6 Typical time-step computations of shrinkage losses, assuming only shrinkage is considered (Eq. 8.42).

		Days						Years	
Time t_j at the end of interval (t_i,t_j)		1	3	7	30	90	365	5	50
(a)	$f_p(t_i)$, ksi	---	189	188.43	187.45	184.15	181.26	179.10	178.33
(b)	$\Delta f_{pS}(t_i,t_j)$, ksi	0	0.57	0.98	3.30	2.89	2.16	0.77	0.18
(c)	$f_p(t_j)$, ksi	189	188.43	187.45	184.15	181.26	179.10	178.33	178.14
(d)	$\Sigma\Delta f_{pS}(t_i,t_j)$, ksi*	0	0.57	1.55	4.85	7.74	9.90	10.67	10.86
(e)	% Total shrinkage	0	5	14	45	71	91	98	100
(f)	% Shrinkage left	100	95	86	55	29	9	2	0

*Sum over preceding intervals.

Table 8.7 Typical time-step computations of shrinkage losses, assuming only shrinkage is considered (Eq. 8.43).

		Days				
Time t_j at the end of interval (t_i,t_j)		7†	30	90	365	1214 max
(a)	$f_p(t_i)$, ksi	189	186.87	184.31	182.38	179.92
(b)	$\Delta f_{pS}(t_i,t_j)$, ksi	2.13	2.56	1.93	2.46	2.11
(c)	$f_p(t_j)$, ksi	186.87	184.31	182.38	179.92	177.81
(d)	$\Sigma\Delta f_{pS}(t_i,t_j)$, ksi*	2.13	4.69	6.62	9.08	11.19
(e)	% Total shrinkage	19	42	59	81	100
(f)	% Shrinkage left	81	58	41	19	0

*Sum over preceding intervals. † Starting at 2.08 days.

The stress at the end of the interval, that is, 3 days, is computed as 189 – 0.57 = 188.43 ksi. It is used as the starting stress for the second interval and the process is continued.

Computed shrinkage losses during typical time intervals, using either Eq. (8.42) or Eq. (8.43) are summarized in Tables 8.6 and 8.7. The total stress loss due to shrinkage at the end of the service life is the sum of all losses over the various time intervals. It can also be computed from Eq. (8.36) and should be same as in Table 8.7, that is, 11.2 ksi; the corresponding value in Table 8.6 is smaller, because the time function reaches unity only for infinite time.

Rows (e) and (f) are completed only after total loss due to shrinkage at 50 years has been computed.

Note that the rate of loss, using Eq. (8.42), is smaller at early age, and higher thereafter, than that using Eq. (8.43). Note also that more than 50 percent of the stress loss due to shrinkage generally occurs within a month and more than 80 percent within a year of the end of curing.

8.13 TIME-DEPENDENT LOSS DUE TO CREEP

The creep strain of concrete depends on many factors, such as time, age at loading, relative humidity, type of aggregates, and the like. Some relevant background information is given in Sec. 2.3, Table 2.9 and Refs. [8.4, 8.8, 8.9, 8.12, 8.16, 8.30, 8.33, 8.42 and 8.51]. Equation (2.11) can be used to predict the creep strain of a concrete material at any time t, assuming a constant stress situation:

$$\varepsilon_C(t) = C_C(t)\varepsilon_{ci} \tag{8.44}$$

where:

ε_{ci} = instantaneous (initial elastic strain) due to loading

$C_C(t)$ = creep coefficient at time t

At the end of the service life of the structure assumed subjected to a constant stress, Eq. (8.44) takes the following form:

$$\varepsilon_{CU} = C_{CU}\varepsilon_{ci} \tag{8.45}$$

where:

ε_{CU} = ultimate creep strain of concrete material

C_{CU} = ultimate creep coefficient

The subscript i in ε_{ci} refers to "instantaneous" and should not be confused with that used for initial time. Typical values of ultimate creep coefficients are given in Table 2.11. An average value of 2.35 is suggested by ACI Committee 209 for routine design [Ref. 8.4].

The determination of the loss of prestress due to creep of concrete is very similar to the procedure followed for shrinkage. The ultimate creep strain ε_{CU} of a given material at the end of its service life is first estimated and correction factors are used

to account for member size and shape, age at loading, and relative humidity. Then a relation $g(t)$ is used to assess the creep strain $\varepsilon_C(t)$ at any given time t. Once the strain is known, the strain change over a time interval is determined and the corresponding stress loss is computed.

Using Eq. (8.44) and Table 2.9 leads to creep strain at any time t for a structural concrete member:

$$\varepsilon_C(t) = g(t) C_{CU} K_{CH} K_{CA} K_{CS} \varepsilon_{ci} \tag{8.46}$$

where:

$g(t)$ = time function
K_{CH} = correction factor depending on the average relative humidity of the environment where the structure is built
K_{CA} = age at loading factor
K_{CS} = shape and size factor

The time function suggested by ACI Committee 209 is given by:

$$g(t) = \frac{t^{0.60}}{10 + t^{0.60}} \tag{8.47}$$

where t is in days. Another time function, identical to that given by Eq. (8.40) for shrinkage, can also be used for creep.

The creep strain change in the concrete member, assuming constant stress or constant ε_{ci} over an interval of time (t_i,t_j), is given by:

$$\Delta\varepsilon_C(t_i,t_j) = \left[g(t_j) - g(t_i) \right] C_{CU} K_{CH} K_{CA} K_{CS} \varepsilon_{ci} \tag{8.48}$$

As steel and concrete are assumed bonded and, hence, undergo the same change in strain, the change in stress in the steel over a time interval (t_i,t_j) can be readily computed (assuming elastic response) from:

$$\begin{aligned} \Delta f_{pC}(t_i,t_j) &= E_{ps} \Delta\varepsilon_C(t_i,t_j) \\ &= E_{ps}[g(t_j) - g(t_i)] C_{CU} K_{CH} K_{CA} K_{CS} \varepsilon_{ci} \end{aligned} \tag{8.49}$$

For a prestressed concrete member, ε_{ci} is the elastic strain in the concrete at the centroid of the prestressing steel due to the applied sustained loading, that is, the combination of prestressing force and dead load. It can be easily computed from the corresponding stress. However, as the prestressing force varies with time due to

creep and other losses, the stress also varies and should be computed preferably at the beginning of any time interval considered. Hence, we have:

$$\varepsilon_{ci} = \frac{f_{cgp}(t_i)}{E_c} \tag{8.50}$$

where:

$f_{cgp}(t_i)$ = stress in the concrete at the centroid of the prestressing steel at time t_i due to the prestressing force and dead (or sustained) load

E_c = modulus of elasticity of concrete

Replacing ε_{ci} by its value from Eq. (8.50) in Eq. (8.49) leads to the stress loss in the prestressing steel due to creep over a time interval (t_i,t_j):

$$\Delta f_{pC}(t_i,t_j) = n_p C_{CU} K_{CH} K_{CA} K_{CS} f_{cgp}(t_i)[g(t_j) - g(t_i)] \tag{8.51}$$

in which $n_p = E_{ps}/E_c$, n_{pi} can replace n_p at early ages, and $f_{cgp}(t_i)$ can be computed from:

$$f_{cgp}(t_i) = \frac{f_p(t_i)A_{ps}}{A_c}\left(1+\frac{e_o^2}{r^2}\right) - \frac{M_D e_o}{I} \tag{8.52}$$

in which r is the radius of gyration of the section, that is, $r = \sqrt{I/A_c}$.

For the time function given by Eq. (8.47), Eq. (8.51) takes on the following form:

$$\Delta f_{pC}(t_i,t_j) = n_p C_{CU} K_{CH} K_{CA} K_{CS} f_{cgp}(t_i)\left[\frac{t_j^{0.60}}{10+t_j^{0.60}} - \frac{t_i^{0.60}}{10+t_i^{0.60}}\right] \tag{8.53}$$

For the time function given by Eq. (8.40), Eq. (8.51) takes on the following form:

$$\Delta f_{pC}(t_i,t_j) = n_p C_{CU} K_{CH} K_{CA} K_{CS} f_{cgp}(t_i) \times 0.157 \ln\left(\frac{t_j}{t_i}\right) \tag{8.54}$$

where the time is between 2.08 and 1214 days. Note that by using Eq. (8.51) in the time-step method to compute prestress losses, the value of the stress in the prestressing steel at time t_i, $f_p(t_i)$, depends on the total losses, including creep, over all time intervals preceding the interval considered. Hence, it can be computed from:

$$f_p(t_i) = f_{pi} - \sum_{\substack{\text{preceding} \\ \text{intervals}}} \Delta f_{pT}(t_i, t_j) \tag{8.55}$$

An example is given next, assuming only creep losses take place. Section 8.15 covers an example where all prestress losses are simultaneously considered.

8.13.1 Example: Creep Loss Assuming No Other Loss Occurs

In order to illustrate the stress loss computations due to creep, let us consider a pretensioned prestressed concrete tie (tensile member) of section 10 x 10 in, reinforced with four half-inch diameter stress-relieved strands placed symmetrically at each corner. The following information is provided: f_{pu} = 270 ksi, f_{pi} = 189 ksi, A_{ps} = 4 x 0.153 = 0.612 in^2, E_{ps} = 28,000 ksi, f'_c = 5000 psi, f'_{ci} = 4000 psi, E_c = 4.287 x 10^3 ksi, E_{ci} = 3.834 x 10^3 ksi, $n_{pi} = E_{ps}/E_{ci}$ = 7.3, $n_p = E_{ps}/E_c$ = 6.53, C_{CU} = 2, e_o = 0. The concrete is steam-cured, the age at loading t_A is one day, and the relative humidity of the environment is H = 57 percent. Referring to Tables 2.9 and 2.10, the following values of the various correction factors can be easily derived: K_{CA} = 1.13, K_{CH} = 0.885, and K_{CS} = 0.915 for a volume-to-lateral surface ratio of 2.5 in. The corresponding ultimate creep coefficient for the member is given by:

$$C_{CU} K_{CA} K_{CH} K_{CS} = 2 \times 1.13 \times 0.885 \times 0.915 \simeq 1.83$$

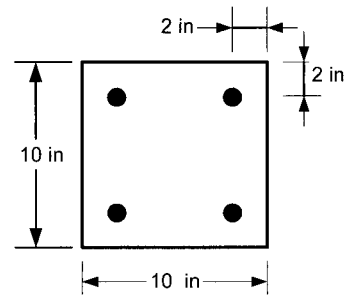

Figure 8.7

Let us assume the fictitious situation where only creep losses are considered, that is, no other effect but creep is taking place. It is also assumed that the prestressed tie is subjected to the effect of the prestressing force only, that is, no external force or moment are present.

Let us use the time function given by Eq. (8.40). The stress loss due to creep over a time interval (t_i,t_j) is obtained from Eq. (8.54). Hence:

$$\Delta f_{pC}(t_i, t_j) = n_p C_{CU} K_{CH} K_{CA} K_{CS} f_{cgp}(t_i) \times 0.157 \ln \left(\frac{t_j}{t_i} \right)$$

that is:

$$\Delta f_{pC}(t_i, t_j) = 1.83 \times 0.157 \times n_p \times f_{cgp}(t_i) \times \ln \left(\frac{t_j}{t_i} \right) = 0.2873 \times n_p \times f_{cgp}(t_i) \times \ln \left(\frac{t_j}{t_i} \right)$$

Table 8.8 Typical time-step computations of creep losses assuming only creep is considered (Eq. (8.54).

		Days				
	Time t_j at end of interval (t_i,t_j),	7*	30	90	365	1214 max
(a)	Moduli ratio n_{pi} or n_p	7.30	6.53	6.53	6.53	6.53
(b)	$f_p(t_i)$, ksi	189	186.06	182.95	180.64	177.73
(c)	$f_{cgp}(t_i)$, psi	1156.7	1138.6	1119.6	1105.5	1087.7
(d)	$\Delta f_{pC}(t_i,t_j)$, ksi	2.944	3.109	2.307	2.904	2.452
(e)	$f_p(t_j)$, ksi	186.06	182.95	180.64	177.73	175.28
(f)	$\Sigma\Delta f_{pC}(t_i,t_j)$, ksi †	2.944	6.053	8.360	11.264	13.72
(g)	% Total creep	21	44	61	83	100
(h)	% Creep left	79	56	39	17	0

† Sum over preceding intervals; * Starting at 2.08 days.

Table 8.9 Typical time-step computations of creep losses assuming only creep is considered (Eq. 8.53).

		Days						Years	
Time t_j at the end of interval (t_i,t_j)		1	3	7	30	90	365	5	50
(a)	Moduli ratio n_{pi} or n_p	---	7.30	6.53	6.53	6.53	6.53	6.53	6.53
(b)	$f_p(t_i)$, ksi	---	189.00	187.90	186.79	184.17	181.97	179.61	177.97
(c)	$f_{cgp}(t_i)$, psi	---	1156.7	1150.0	1143.1	1127.1	1113.7	1099.2	1089.1
(d)	$\Delta f_{pC}(t_i,t_j)$, ksi	0.00	1.10	1.12	2.62	2.20	2.36	1.65	0.94
(e)	$f_p(t_j)$, ksi	189	187.90	186.79	184.17	181.97	179.61	177.97	177.02
(f)	$\Sigma\Delta f_{pC}(t_i,t_j)$, ksi †	0.00	1.10	2.21	4.83	7.03	9.39	11.03	11.98
(g)	% Total creep	0	9	18	40	59	78	92	100
(h)	% Creep left	100	91	82	60	41	22	8	0

† Sum over preceding intervals.

A number of time intervals are selected and the corresponding computations of stress loss due to creep are shown in Table 8.8. For the correct use of the above equation, the starting time of the first time interval is set equal to 2.08 days, and the starting time of any other interval is set equal to the end time of the immediately preceding interval. The stress in the steel at the beginning of the first time

interval is taken equal to f_{pi}. It is assumed that the initial moduli ratio prevails during the first time interval while n_p prevails during the following intervals. Because there is no bending moment and the prestressing force is concentric, Eq. (8.52) leads to a uniform compressive stress given by:

$$f_{cgp}(t_i) = \frac{f_p(t_i)A_{ps}}{A_c}$$

For the first time interval, it leads to:

$$f_{cgp}(t_i) = \frac{189{,}000 \times 0.612}{100} = 1156.7 \text{ psi}$$

All other computations are summarized in Table 8.8. It can be observed that, similarly to shrinkage, more than 80 percent of creep losses occur within a year of age.

The reader may want to carry out similar computations of creep losses using Eq. (8.53). Corresponding numerical results are shown in Table 8.9. It can be observed that creep loss predictions are not too different from those obtained in Table 8.8 for which Eq. (8.54) was used.

8.14 PRESTRESS LOSSES BY THE TIME-STEP METHOD

The time-step method is an accurate technique to predict time-dependent losses due to relaxation of the steel and shrinkage and creep of concrete. Instantaneous losses are computed as for the other methods.

In order to fully understand the time-step method, it is essential to realize that time-dependent losses are also interdependent. Figure 8.1 provides an overall diagram of how total losses are cumulated and illustrates the interfering causes and effects between the different sources of loss of prestress.

It is also important to understand that the rate of stress loss due to one effect, such as relaxation, is being continuously altered by changes in the steel stress due to the other effects, such as creep and shrinkage. The rate of creep, in turn, is simultaneously altered by the changes in the steel stress due to relaxation and shrinkage. To account for these interdependent effects with time, a repetitive computation procedure, using successive time intervals, is used. Generally, the lengths of these time intervals are not equal and vary with the age of the concrete. Particular times corresponding to milestones in the life of the structure, such as addition of superimposed dead load, can be integrated in the selection. The stress in the steel at the beginning of any time interval is taken equal to that at the end of the preceding interval. It is assumed constant during a given time interval and used to compute incremental losses during that interval. The steel stress at the end of a time interval is obtained by subtracting the sum of incremental stress losses from the stress at the beginning of the interval. More accuracy can be obtained by increasing the number of intervals. The procedure is generally computerized for efficiency [Refs. 8.24, 8.32, 8.45, 8.46, 8.48, 8.49]; however, hand solution helped by a spreadsheet, can be as effective. A typical example of loss computations by the time-step method, with a reasonable number of time intervals, is covered in Section 8.15. A logical flow chart covering the main steps is given in Fig. 8.8.

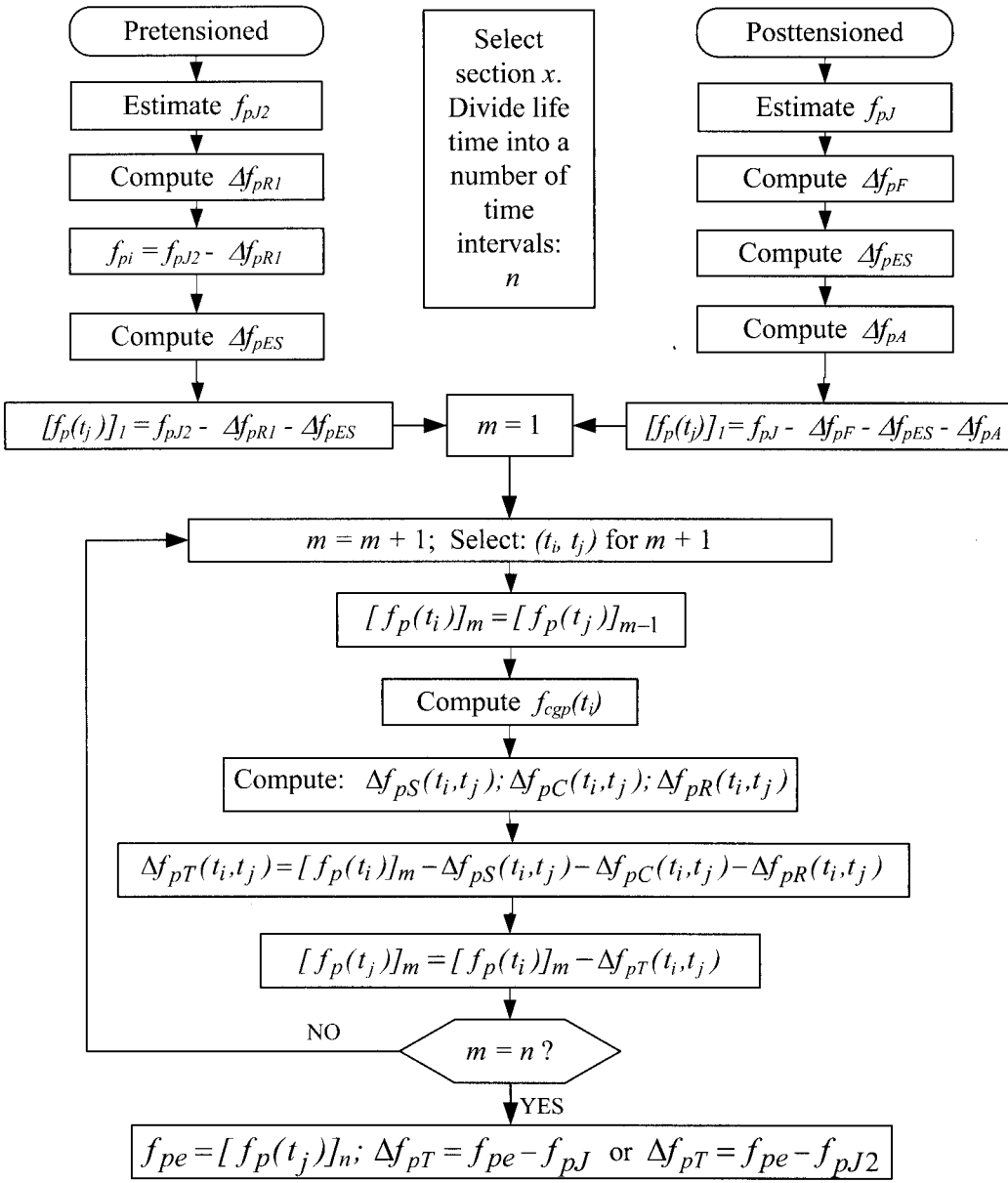

Figure 8.8 Logical flow chart to compute losses by the time-step procedure.

The use of the accurate time-step method to compute prestress losses provides a unique case study to understand the important aspects of the structural behavior of concrete, because it involves integrating simultaneously fundamental material properties, time, and stresses. The background information and the procedures

needed to determine the loss of stress due to each source, whether instantaneous or time-dependent, is covered in detail in the preceding sections. The following example shows how these are all integrated together to reflect real behavior.

8.15 EXAMPLE: COMPUTATION OF PRESTRESS LOSSES FOR A PRETENSIONED BEAM BY THE TIME-STEP METHOD

Compute the prestress losses at midspan for the simply supported pretensioned beam shown in Fig. 8.9 (same as Fig. 8.6) using the time-step method; this is the same beam covered in the examples of Sections 8.8, 8.9 and 8.10. The following information is given:

$A_{ps} = 2.142\ \text{in}^2; e_o = 14.56\ \text{in}; E_{ps} = 28000\ \text{ksi}; f_{pu} = 270\ \text{ksi}; f_{py} = 230\ \text{ksi}$ (stress relieved strand);

$f_{pJ1} = 216\ \text{ksi}; f_{pJ2} = 213\ \text{ksi}$

$f'_c = 5000\ \text{psi}; f'_{ci} = 4000\ \text{psi}; \gamma_c = 150\ \text{pcf}; E_c = 33\gamma_c^{1.5}\sqrt{f'_c}; n_{pi} = 7.3; n_p = 6.53;$

$\varepsilon_{SU} = 5\times10^{-4}; C_{CU} = 2; H = 70$ percent; span $l = 70\,ft$

Assume that the beam is steam-cured, that transfer of the prestress occurs 24 hours (or 1 day) after tensioning, and that curing ends at time of transfer. The value of stress immediately after seating at the abutments, f_{pJ2}, assumed here can be calculated from the stress known just after the jacking operation (see Table 8.4).

The ratio of volume to lateral surface per unit length of beam is approximately equal to 1.91 in. The corresponding values of shape and size correction factors for shrinkage and creep are obtained from Table 2.10: $K_{SS} \approx 0.97$ and $K_{CS} \approx 0.98$.

$A_c = 474\ \text{in}^2; I = 21540\ \text{in}^4$
$y_t = 5.94\ \text{in}; y_b = 18.06\ \text{in}$
$Z_t = 3636\ \text{in}^3; Z_b = 1193\ \text{in}^3$
$k_t = -2.52\ \text{in}; k_b = 7.65\ \text{in}$
$r = 6.74\ \text{in}; w_G = 494\ \text{plf}$
LL=320 plf; span l = 70 ft

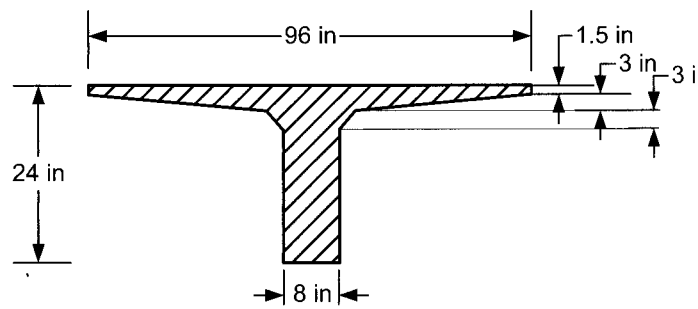

Figure 8.9 Properties of example beam.

Table 2.9 is used to determine the humidity correction factors for shrinkage and creep, and the age at loading factor for creep, assuming t_A = 1 day:

$$K_{SH} = 1.40 - 0.01H = 1.40 - 0.70 = 0.70$$

$$K_{CH} = 1.27 - 0.0067H = 1.27 - 0.0067 \times 70 \approx 0.80$$

$$K_{CA} = 1.13t_A^{-0.095} = 1.13$$

A number of appropriate time intervals are selected for the computations, as shown in Table 8.10. A typical example of computation is developed next for each type of prestress loss.

Losses before and during stress transfer:

Consider the first interval, that is between 1 hour and 1 day. The stress in the prestressing steel at 1 hour is 213 ksi (row (b), third column of Table 8.10). The relaxation loss at 24 hours, just before transfer can be determined from Eq. (8.17), using a value of $t_i = t_o = 1$ hour and a corresponding initial stress in the steel equal to $f_{pJ2} = 213$ ksi (see example 8.6.5). Thus:

$$\Delta f_{pR}(1,24) = \frac{213}{10}\left(\frac{213}{230} - 0.55\right)\log\left(\frac{24}{1}\right) = 11.06 \text{ ksi}$$

This result can be seen in row (f) third column of Table 8.10.

Elastic shortening is calculated as in the example of Section 8.8 using the exact approach, that is, Eq. (8.26). It leads to a loss $\Delta f_{pES} = 16.7$ ksi. It is shown in row (g), third column of Table 8.10.

The stress in the prestressing steel immediately after transfer of stress to the concrete, that is at the end of 1 day, is computed as: $f_{ps}(t_j) = 213 - 11.06 - 16.70 = 185.24$ ksi. This is the stress taken at the beginning of the second interval which starts at one day; it is shown in row (b), fourth column of Table 8.10. It essentially gives the value of f_{pi} used in preliminary design.

Time-dependent losses after stress transfer:

The force in the prestressing steel at the beginning of each time interval is equal to the force at the end of the preceding time interval and is given by:

$$F(t_i) = A_{ps} f_p(t_i) = 2.142 \times f_p(t_i)$$

where t_i represents the time at the beginning of the interval considered. The force in the prestressing steel is used to calculate the stress in the concrete at the centroid of the prestressing steel, $f_{cgp}(t_i)$; it is given by Eq. (8.52):

$$f_{cgp}(t_i) = \frac{f_p(t_i)A_{ps}}{A_c}\left(1 + \frac{e_o^2}{r^2}\right) - \frac{M_D e_o}{I}$$

and for the second time interval it leads to:

$$f_{cgp}(1) = \frac{185.25 \times 2.142}{474}\left(1 + \frac{14.56^2}{6.74^2}\right) - \frac{3630.9 \times 14.56}{21{,}540} = 2.2895 \text{ ksi}$$

Generally for any time interval:

$$f_{cgp}(t_i) = 0.02561 f_p(t_i) - 2.454 \text{ ksi}$$

During the first time interval, creep and shrinkage did not occur. However, creep and shrinkage start after transfer and thus induce losses during the following intervals, while relaxation continues.

Computation of losses due to creep, shrinkage, and relaxation for the second time interval from 1 to 7 days, are illustrated next.

In order to estimate the loss of stress due to creep over a time interval (t_i,t_j), Eq. (8.53) is used. That is:

$$\Delta f_{pC}(t_i,t_j) = n_p C_{CU} K_{CH} K_{CA} K_{CS} f_{cgp}(t_i)\left[\frac{t_j^{0.60}}{10 + t_j^{0.60}} - \frac{t_i^{0.60}}{10 + t_i^{0.60}}\right]$$

Table 8.10 Time-step computations of prestress losses for example beam.

		Time t_j at end of time interval (t_i,t_j), days					Years		Cumulative total loss over 50 years
		1	7	30	90	365	5	50 (life)	
(a)	Moduli ratio n_{pi} or n_p	7.3	7.3	6.53	6.53	6.53	6.53	6.53	.....
(b)	$f_{ps}(t_i)$, ksi	213	185.24	175.83	166.62	159.27	152.20	147.95	.....
(c)	$f_{cgs}(t_i)$, ksi	.....	2.289	2.048	1.812	1.624	1.443	1.334	.....
(d)	$\Delta f_{pC}(t_i,t_j)$, ksi	.....	4.511	4.543	3.421	3.328	2.094	1.119	19.02
(e)	$\Delta f_{pS}(t_i,t_j)$, ksi	.....	0.904	2.282	2.545	2.361	0.967	0.250	9.31
(f)	$\Delta f_{pR}(t_i,t_j)$, ksi	11.06	3.998	2.383	1.387	1.380	1.189	1.380	22.77
(g)	Δf_{pES}, ksi	16.70	.....	.....	.....	.....	.....	.....	16.70
(h)	$\Delta f_{pT}(t_i,t_j)$, ksi	27.76	9.412	9.208	7.353	7.068	4.250	2.748	67.80
(k)	$f_{ps}(t_j)$, ksi	185.24	175.83	166.62	159.27	152.20	147.95	145.20	
(m)	$\Sigma\Delta f_{pT}(t_i,t_j)$, ksi†	27.76	37.17	46.38	53.73	60.80	65.05	67.80	
(n)	$\frac{\Sigma\Delta f_{pT}(t_i,t_j)}{\Delta f_{pT}}\times 100\%$†	41%	55%	68%	79%	90%	96%	100%	
(p)	$\frac{f_{ps}(t_j)}{f_{pu}}$	0.69	0.65	0.62	0.59	0.56	0.55	0.54	

† Sum over preceding intervals.

$$\Delta f_{pC}(t_i,t_j) = n_p \times 2 \times 0.80 \times 1.13 \times 0.98 f_{cgp}(t_i)\left[\frac{t_j^{0.60}}{10+t_j^{0.60}} - \frac{t_i^{0.60}}{10+t_i^{0.60}}\right]$$

$$\Delta f_{pC}(t_i,t_j) = 1.772 n_p f_{cgp}(t_i)\left[\frac{t_j^{0.60}}{10+t_j^{0.60}} - \frac{t_i^{0.60}}{10+t_i^{0.60}}\right]$$

Applying the above equation to the second time interval between 1 and 7 days and using n_{pi} instead of n_p, leads to:

$$\Delta f_{pC}(1,7) = 1.772 \times 7.3 \times 2.2895\left[\frac{7^{0.60}}{10+7^{0.60}} - \frac{1^{0.60}}{10+1^{0.60}}\right]$$

$$= 1.971 \times 2.2895 = 4.511 \text{ ksi}$$

This value is shown in row (d), fourth column of Table 8.10.

In order to estimate the loss of stress due to shrinkage over a time interval (t_i,t_j), Eq. (8.42) is used, assuming $b = 55$. It gives:

$$\Delta f_{pS}(t_i,t_j) = E_{ps}\varepsilon_{SU}K_{SH}K_{SS}\frac{b(t_j-t_i)}{(b+t_i)(b+t_j)}$$

$$\Delta f_{pS}(t_i,t_j) = 28{,}000 \times 5 \times 10^{-4} \times 0.70 \times 0.97\frac{55(t_j-t_i)}{(55+t_i)(55+t_j)}$$

$$= 9.506\frac{55(t_j-t_i)}{(55+t_i)(55+t_j)}$$

Applying the above equation to the second time interval between 1 and 7 days leads to:

$$\Delta f_{pS}(1,7) = 9.506\frac{55(7-1)}{(55+1)(55+7)} \simeq 0.904 \text{ ksi}$$

This value is shown in row (e) of the fourth column of Table 8.10.

To compute the relaxation loss for the second time interval, Eq. (8.33) is used assuming stress relieved strands for which the constant $K = 10$:

$$\Delta f_{pR}(t_i,t_j) = \frac{f_p(t_i)}{K}\left(\frac{f_p(t_i)}{f_{py}} - 0.55\right)\log\left(\frac{t_j}{t_i}\right)$$

$$\Delta f_{pR}(1,7) = \frac{185.24}{10}\left(\frac{185.24}{230} - 0.55\right)\log\left(\frac{7}{1}\right) = 3.998 = 4 \text{ ksi}$$

The procedure is continued for all time intervals in which the stress in the steel at the beginning of an interval is taken equal to that at the end of the preceding interval. The results are summarized in Table 8.10. The last two rows of the table are completed only after the total loss at 50 years of service has been determined. The total loss obtained amounts to 67.80 ksi, that is, about 32 percent of the initial stress. Among these losses, the relaxation loss after transfer amounts to 22.77 – 11.06 = 11.71 ksi, the creep loss = 19.02 ksi, and the shrinkage loss = 9.31 ksi. The total time-dependent losses after transfer amount to 40.04 ksi. The above values should be compared with either the lump

sum estimate of total losses or the lump sum estimates of separate losses, such as described in Table 8.4.

Note that, if we did not use the time-step method, the relaxation loss over 50 years (438,000 hours) would have been $\Delta f_{pR}(1,438000) = 45.92$ ksi, which is more than twice the value obtained and illustrates the importance of using a time-step procedure. On the other hand if we calculated losses after transfer assuming one interval between one day and 50 years, the total loss would have been: $\Delta f_{pR}(24,438000) = 20.16$ ksi.

Figure 8.10 shows the variation of time-dependent losses with time; it also illustrates the cause and effect relationship between total losses and independent loss due to relaxation. Two curves are shown for relaxation and creep; for instance, one curve shows the relaxation loss computed as if only relaxation occurs (RE, ind), while no other loss occurs; "ind" stands for independent; the other curve is computed for relaxation loss (RE, total), while other losses due to shrinkage and creep occur simultaneously. The numerical values for relaxation are taken from Tables 8.5 and 8.10, respectively, and for creep they were computed for the case of (CR, ind.) and taken from Table 8.10 for (CR, total).

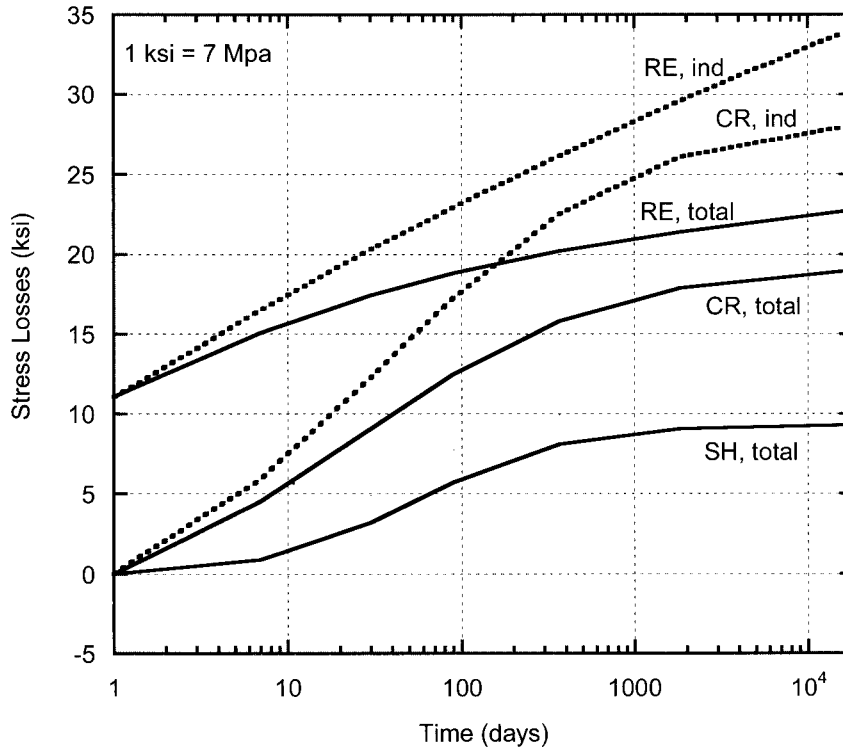

Figure 8.10 Comparison of time-dependent losses with time for example beam.

8.16 LOSS DUE TO FRICTION

If in a posttensioned member a tendon is tensioned to a certain stress at the anchorage, a section of this tendon located a distance x from the anchorage will experience a smaller stress. This is due to the stress losses generated by friction between the tendon and its duct over the segment between the two sections.

Because the loss due to friction is instantaneous and in order not to encumber the notation, the variable "time" will be dropped. Instead, the variable x, representing distance, will be used. Hence, $f_p(x)$ will represent the stress in the prestressing tendon at distance x from the jacking end at the particular time considered.

8.16.1 Analytical Formulation

Frictional losses are generally treated differently whether a linear effect or an angular effect is considered. The linear effect is explained by the law of dry friction, which leads to a frictional force between two surfaces in contact, directly proportional to the vertical force between them. The angular friction effect is illustrated by the analysis of a belt around a fixed drum (Fig. 8.11). It can be shown that, if a load T_2 is applied at one end of the belt, the load T_1, necessary at the other end to just initiate slippage in the direction of T_1, is given by:

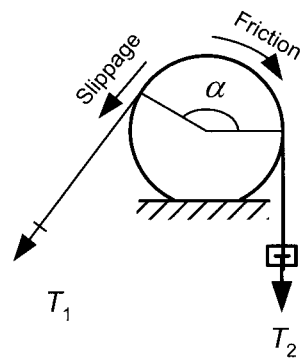

Figure 8.11 Belt friction.

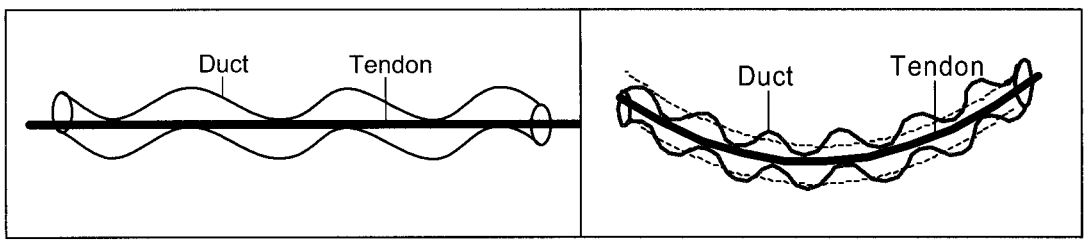

Figure 8.12 Wobbling effect.

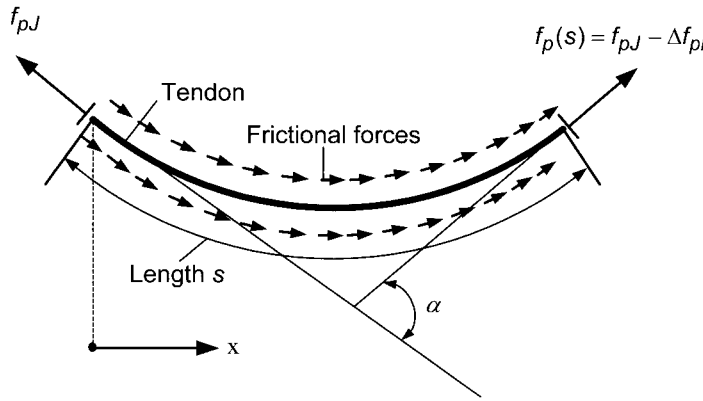

Figure 8.13 Representation of a curved prestressing tendon.

$$T_1 = T_2\, e^{\mu\alpha} \tag{8.56}$$

where μ is the coefficient of static angular friction and α is the angle between T_1 and T_2 in radians.

For posttensioned tendons, the linear effect is called the wobbling effect. It is due to the fact that, for a theoretically linear tendon, the tendon or its duct are never exactly linear (Fig. 8.12), thus leading to some form of friction. It is general practice to treat the wobbling effect of friction as an additional angular friction instead of as a linear one. This leads to the widely accepted formula giving the stress in the steel at a section s (Fig. 8.13) along the tendon as a function of the stress at the anchorage:

$$f_p(s) = f_{pJ} e^{-(\mu\alpha + Ks)} \tag{8.57}$$

where:

f_{pJ} = stress in the prestressing steel at the jacking end or at the anchorage
μ = coefficient of angular friction
K = wobble coefficient, per unit length
α = change in angle between the force at the anchorage and the force at s, in radians
s = curvilinear length of tendon from anchorage to section s

In general, the curvilinear abscissa s is well approximated for beams by its horizontal projection x, which leads to:

$$f_p(x) = f_{pJ} e^{-(\mu\alpha + Kx)} \tag{8.58}$$

The ACI building code accepts the approximation of Eq. (8.58) by the following equation:

$$f_p(x) = \frac{f_{pJ}}{1 + \mu\alpha + Kx} \tag{8.59}$$

provided $\mu\alpha + Kx \leq 0.30$. Note that Eq. (8.59) is derived from Eq. (8.58) by keeping the first term of the Taylor expansion of the exponential $e^{-(\mu\alpha + Kx)}$ and neglecting higher-order terms.

Table 8.11a Friction coefficients for posttensioned tendons *(Adapted from 2002 ACI building code.)*

	Wobble coefficient K		Curvature coefficient μ
Type of tendon	Per foot	Per meter	Per radian
Grouted tendons in flexible metal sheathing:			
Wire tendons	0.0010-0.0015	0.0033-0.0049	0.15-0.25
7-wire strand	0.0005-0.0020	0.0016-0.0066	0.15-0.25
High-strength bars	0.0001-0.0006	0.0003-0.0020	0.08-0.30
Grouted tendons in rigid metal duct*: 7-wire strand	0.0002	0.00066	0.15-0.25
Unbonded pre-greased tendons: Wire tendons and 7-wire strand	0.0003-0.0020	0.0010-0.00661	0.05-0.15
Unbonded mastic-coated tendons: Wire tendons and 7-wire strand	0.0010-0.0020	0.0033-0.0066	0.05-0.15

* From an earlier version of the code

Table 8.11b Friction coefficients for posttensioned tendons. *(Adapted from 1998 AASHTO LRFD.)*

		Wobble coefficient K		Curvature coefficient μ
Type of steel	Type of tendon	Per foot	Per meter	Per radian
Wire or strand	Rigid and semi-rigid galvanized metal sheathing	0.0002	0.00066	0.15–0.25
	Polyethylene	0.0002	0.00066	0.23
	Rigid steel pipe deviators for external tendons	0.0002	0.00066	0.25
High strength bars	Galvanized metal sheathing	0.0002	0.00066	0.30

ACI Committee 343 on Bridge Structures [Ref. 8.3] proposes an extension of Eq. (8.58) to account for the horizontal angular change α_h, if any, of the prestressing steel profile, in addition to the vertical angular change α. Although the presence of α_h is treated similarly to the presence of α, it will be assumed in the following analytical developments that only α is present.

The frictional coefficients α and K depend on many factors including the type of prestressing steel (wires, strands, or bars), the type of duct, and the surface conditions of both (rusted or galvanized).

A range of values recommended in the 2002 ACI building code [Ref. 8.2] and by AASHTO LRFD [Ref. 8.6] is given in Tables 8.11a and 8.11b, respectively. These can be used when experimental data for the materials are used, or when data recommended by the manufacturer are not available.

8.16.2 Graphical Representation

As the stress in the prestressing steel may be needed at several sections along the member, a graphical representation of Eq. (8.58) is often used. As this equation leads to an exponential curve on an arithmetic graph, a semi-log graph paper, in which a straight line is obtained, is generally preferred. This can be observed by taking the natural logarithm of Eq. (8.58), which leads to:

$$\ln (f_p(x)) = \ln (f_{pJ}) - (\mu\alpha + Kx) \tag{8.60}$$

Note that, if the value of α is zero, constant or directly proportional to x, Eq. (8.60) leads to a straight line on a semi-log graph, in which $f_p(x)$ is represented by the ordinate on the log scale and x is the abscissa on the arithmetic scale.

It can be shown that, as a first approximation, α is proportional to x, when the profile of the tendon is parabolic, which is generally the case for beams. Also, it can be shown that α is proportional to s in circular tendons. For the cases where α is proportional to x, Eq. (8.58) can be written in the following form [Ref. 8.32]:

$$f_p(x) = f_{pJ} e^{-\lambda x} \tag{8.61}$$

where:

$$\lambda x = \mu\alpha + Kx \tag{8.62}$$

Equation (8.61) leads to a straight line on a semi-log graph with a slope equal to minus λ. The value of λ can be obtained from Eq. (8.58) as:

$$\lambda = \mu\frac{\alpha}{x} + K \tag{8.63}$$

It is important to understand that the value of λ is constant only along a tendon segment the profile of which is represented by the same analytical equation. For a profile made out of different parabolas, several values of λ will be obtained for each parabolic segment.

Graphical representations of the variation of steel stress along the tendon are often used in combination with charts which lead to the value of $(\mu\alpha + Kx)$ or $e^{-(\mu\alpha+Kx)}$. However, the ready availability of electronic calculators, computers, and spread-sheets eliminates the need for such charts. The following example illustrates the graphical representation and the corresponding computations.

8.16.3 Example: Computation of Losses Due to Friction

A three-span continuous prestressed concrete beam has a tendon profile (Fig. 8.14) made out of a series of parabolic segments. Assuming $\mu = 0.15$, $K = 7.5 \times 10^{-4}$/ft, $f_{pJ} = 216$ ksi, $f_{pu} = 270$ ksi, and $E_{ps} = 28{,}000$ ksi, compute $f_{ps}(x)$ at several sections along the span and plot $f_{ps}(x)$ versus x on both an arithmetic and a semi-log scale, respectively. Because of symmetry, only half the structure is considered.

The value of α between the jacking end A and any point x can be obtained from the slopes of the parabolic profile at these points. The equation of a parabola can easily be derived if its vertex and one of its points are known. For instance, the first parabola of the end span (ABC) leads to the following equation:

$$e_o(x) = 1.5 - \frac{1.5}{24^2}(x-24)^2$$

where $e_o(x)$ and x are in feet and x is taken with respect to the jacking end. The slope at any point with respect to the horizontal axis (x axis) is given by:

$$\frac{\delta e_o(x)}{\delta x} = \frac{3}{24^2}(x-24)$$

As a first approximation, the slope at any point x is equal to the angle in radians between the tangent at x and the horizontal axis or the tangent at the vertex B. For instance, referring to Fig. 8.14, the angle between the jacking end A and the vertex B is given by the above equation for $x = 0$, that is:

$$\alpha_1 \approx \tan\alpha_1 = \frac{3\times 24}{24^2} = 0.125 \text{ radian}$$

Similarly, the angle between the vertex B and point C (Fig. 8.14) is given by:

$$\alpha_2 = \left|-\frac{3}{242}(52-24)\right| = 0.1458 \text{ radian}$$

Hence, the angle α between the tangents at two points, such as A and C, is the sum of angles of their tangents with respect to the horizontal axis. That is $\alpha = \alpha_1 + \alpha_2$.

Table 8.12 summarizes the values of α obtained at different sections, chosen to correspond to every end section and vertex of each parabola of the profile, as well as a section equally distant

between them. Corresponding stresses in the prestressing steel are determined from Eq. (8.58). For instance for the section at C we have:

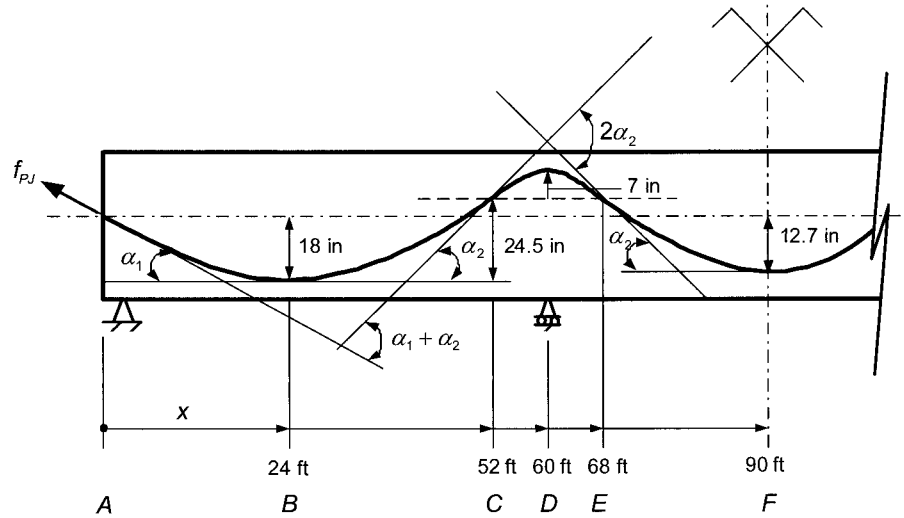

Figure 8.14 Tendon profile considered for computation of friction losses.

Table 8.12 Variation of steel stress due to friction for the tendon of the Example in Sec. 8.16.3.

Section	A	mid-sect.*	B	mid-sect.*	C	mid-sect.*
x, ft	0	12	24	38	52	56
α, radian	0	0.0625	0.125	0.1978	0.2706	0.3434
$\mu\alpha + Kx = \lambda x$	0	0.01838	0.03675	0.05817	0.07959	0.09351
$e^{-(\mu\alpha+Kx)}$	1	0.9818	0.9639	0.9435	0.9235	0.9107
$f_{ps}(x)$, ksi	216	212.07	208.20	203.80	199.48	196.71
$\Delta f_{ps}(x)$, ksi	0	3.93	7.80	12.20	16.52	19.29

Table 8.12 - continued.

Section	D	mid-sect.*	E	mid-sect.*	F
x, ft	60	64	68	79	90
α, radian	0.4162	0.4890	0.5618	0.6346	0.7074
$\mu\alpha + Kx = \lambda x$	0.1074	0.1213	0.1353	0.1544	0.1736
$e^{-(\mu\alpha+Kx)}$	0.8981	0.8857	0.8735	0.8569	0.8406
$f_{ps}(x)$, ksi	193.99	191.31	188.68	185.05	181.57
$\Delta f_{ps}(x)$, ksi	22.01	24.69	27.32	30.95	34.43

* Section equally distant from adjacent sections.

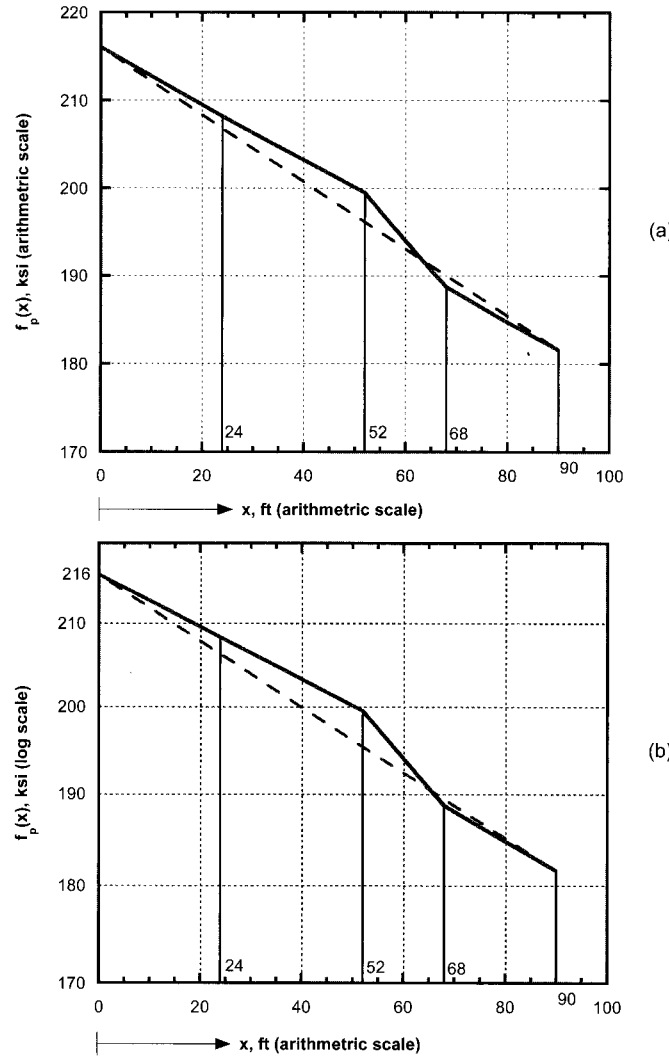

Figure 8.15 Typical stress reduction in the steel due to friction. (a) Arithmetic scale. (b) Semi-log scale.

$$f_p(x) = f_{pJ}e^{-(\mu\alpha+Kx)} = 216e^{-(0.15\times0.2706+7.5\times10^{-4}\times52)}$$

$$= 216e^{-0.0796} = 216\times0.9235 = 199.48 \text{ ksi}$$

This result also could have been obtained from Eqs. (8.63) and (8.61):

$$\lambda = \mu\frac{\alpha}{x} + K = 0.15\frac{0.2706}{52} + 7.5\times10^{-4} = 0.00153$$

$$f_p(x) = f_{pJ}e^{-\lambda x} = 216e^{-0.00153\times52} = 199.48 \text{ ksi}$$

The calculations are carried out similarly for all other sections. It can be seen that, at a section 90 feet from the support, the stress loss due to friction amounts to 34.43 ksi or about 16 percent of the stress at the jacking end. If only one end of the tendon is jacked, the stress loss at the other end would be about twice that at 90 ft. As such a loss is too excessive, both ends of the tendons should be jacked. This would lead to a stress profile symmetrical with respect to the midspan section of the interior span.

Figure 8.15*a* shows the variation of $f_p(x)$ versus x plotted on an arithmetic scale. It can be seen that the curve is made out of three slightly nonlinear segments. However, perfectly linear segments are obtained when $f_p(x)$ is plotted versus x on a semi-log graph, as seen in Fig. 8.15*b*.

If we compare Figs. 8.15*a* and 8.15*b*, we notice that they are almost identical. This is why an arithmetic scale is often used in practice and straight-line segments are shown for each parabolic portion of the tendon. They are assumed to approximate the exponential segments well. This result greatly simplifies the evaluation of loss due to the anchorage set, as explained next.

8.17 LOSS DUE TO ANCHORAGE SET

As defined earlier, the anchorage set in a wedge-type anchorage system is the distance the wedge "sets in" to lock the tendon at end of jacking. Thus the tendon length decreases by an equal amount. The set is defined here as δ. Typical values of anchorage set for wedge-type strand anchors vary between 1/8 in and 3/8 in (4 to 10 mm). A value of 0.25 in (6 mm) is often assumed in practice when specific information from the manufacturer is not available. Bar anchorage devices generally show smaller anchorage set than strand anchorage devices. Devices for large diameter strands or tendons show larger anchorage sets. Information for a specific system should be obtained from the manufacturer.

Let us assume that the stress in the tendon just before anchoring is represented by a straight line *ac* on a semi-log paper (Fig. 8.16), assuming stressing from one end only. Note that the stress at the jacking end is highest and the frictional force along the tendon is pointed toward the positive direction of x. If the anchorage sets a certain distance δ, there is a sudden drop in stress at the jacking end, from f_{pJ1} to f_{pJ2}, and the frictional force changes direction over a certain distance, X. The loss of stress at the jacking end is felt with gradually decreasing magnitude in the various sections of the tendons up to X. X is the abscissa of the section of tendon after which the loss due to the anchorage set is not felt and the stress in the steel is the same as just before the anchoring operation. Note also that, because the reversed frictional force depends on the same frictional coefficients as the initial frictional force, the slopes of the two lines *ab* and *a'b* (Fig. 8.16), representing the stress variations in the tendon just before and after anchorage set, are equal and opposite. The stress profile after anchoring is now represented by *a'bc*. In order to quantitatively define this profile, two unknowns must be determined, namely: the loss of stress at the jacking end $\Delta f_{ps}(0)$ and the distance X.

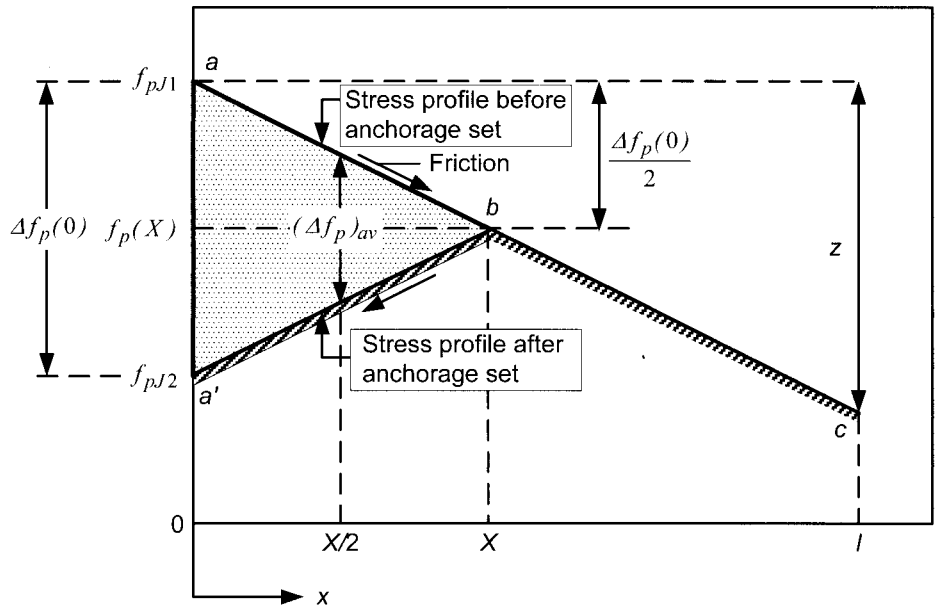

Figure 8.16 Schematic stress variation in the tendons from jacking end before and after anchorage set.

Due to the symmetry between *ab* and *a'b*, the loss of stress at the jacking end (Fig. 8.16) can be written as:

$$\Delta f_p(0) = f_{pJ1} - f_{pJ2} = 2\left[f_{pJ1} - f_p(X)\right] = 2(\Delta f_p)_{av} \tag{8.64}$$

where f_{pJ1} is the stress at jacking just before anchorage set, f_{pJ2} is the stress at the end section after anchorage set, and $f_p(X)$ is the stress in the tendon at section X. Note that the end section at $x = 0$ experiences a loss in stress equal to $\Delta f_p(0)$ after anchorage set, while the section at X does not experience any loss in stress. $(\Delta f_p)_{av}$ represents the average loss over the distance X; it can be obtained from the following equation:

$$(\Delta f_p)_{av} = f_{pJ1} - f_p(X) = f_p(X) - f_{pJ2} \tag{8.65}$$

which is due to the symmetry of the stress profile before and after anchorage set. Putting Eq. (8.61) in Eq. (8.65) and using Taylor's expansion (neglecting higher order terms) leads to:

$$(\Delta f_p)_{av} = f_{pJ1} - f_p(X) = f_{pJ1} - f_{pJ1}e^{-\lambda X}$$
$$\approx f_{pJ1} - f_{pJ1}(1-\lambda X) = f_{pJ1}\lambda X \tag{8.66}$$

Furthermore, the total shortening of the tendon over a distance X is equal to the anchorage set, δ. This corresponds to an average loss in strain $(\Delta\varepsilon_p)_{av} = \delta / X$. Using *Hooke*'s law for linear elastic materials, the average loss of stress in the tendon is related to the average loss of strain by:

$$(\Delta f_p)_{av} = E_{ps}\frac{\delta}{X} \tag{8.67}$$

From Eqs. (8.64), (8.66), and (8.67) we obtain:

$$\Delta f_p(0) = 2E_{ps}\frac{\delta}{X} = 2f_{pJ1}\lambda X \tag{8.68}$$

from which the value of X can be determined [Ref. 8.26]:

$$X = \sqrt{\frac{E_{ps}\delta}{f_{pJ1}\lambda}} \tag{8.69}$$

Table 8.13 Recommended values of λ and X for typical tendon profiles.

Tendon profile	Description	$\lambda = (\mu\alpha + Kx)/x$	For $X \le l$
Linear	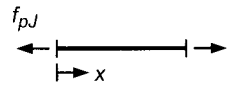	K	$X = \sqrt{\frac{E_{ps}\delta}{Kf_{pJ}}}$
Parabolic	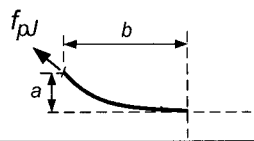	$(2\mu a/b^2 + K)$	$X = \sqrt{\frac{E_{ps}\delta}{(2\mu a/b^2 + K)f_{pJ}}}$
Circular	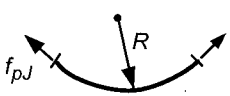	$\frac{\mu}{R} + K$	$X = \sqrt{\frac{E_{ps}\delta}{(\mu/R + K)f_{pJ}}}$
Any shape or combination of shapes (approximate approach over length l)	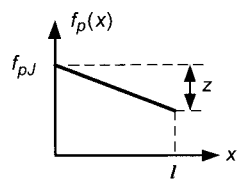	$\lambda = \left(\frac{z}{l}\right)\frac{1}{f_{pJ}}$	$X = \sqrt{\frac{E_{ps}\delta}{(z/l)}}$

These results could also be obtained analytically using integrals but are better understood geometrically from Fig. 8.16.

Note that the distance X depends both on f_{pJ1} and the frictional characteristics of the tendon represented by λ. Note also that Eq. (8.69) is valid, provided λ is constant over the tendon profile considered. Table 8.13 shows typical values of λ for different tendon profiles. Generally, different values of λ can be observed for different segments of the same tendon and X may not necessarily involve only one segment. It is with this is mind that, in design practice [Ref. 8.35], the following formula is used to determine X (Fig. 8.16 and Table 8.13, last row):

$$X = \sqrt{\frac{E_{ps}\delta}{(z/l)}} \tag{8.70}$$

where:

l = span or a known distance along the cable (assuming jacking from one end only)

z = loss in stress along l, equal to $(f_{pJ1} - f_p(l))$ where $f_p(l)$ can be computed from applying Eqs. (8.58 or 8.61) to the various segments of tendons along l

It can be shown that Eqs. (8.69) and (8.70) would give essentially identical results when the same parabola or circle exists along l. Note that (z/l) is the slope of line *abc* (Fig. 8.16) in the semi-log scale and is considered a first approximation of the average slope representing stress loss in the arithmetic scale.

In practice, one additional difficulty may be encountered. That is, the calculated value of X may be larger than the span length l or may include more than one curvilinear segment of the tendon profile. In order to solve for this type of problem, it is convenient to first define the area lost (or equivalent internal energy lost) under the stress versus abscissa diagram of the tendon, due to slippage generated by anchorage set.

8.17.1 Concept of Area Lost or Equivalent Energy Lost

Referring to Eq. (8.68), we can write:

$$\frac{\Delta f_p(0)}{2} X = E_{ps}\delta \tag{8.71}$$

The first term of Eq. (8.71) is equal to the area of the triangle *aba'* in Fig. 8.16 (shaded area) and is the area between the stress diagram prior to anchorage set and the stress diagram after anchorage set. It can be described as the area lost due to anchorage set. More generally, this result can be stated as:

The total area between the stress diagrams in the steel just before and just after anchorage set is equal to $E_{ps}\delta$.

It is important to note that the exponential curve representing $f_p(x)$ is generally flat in the portion of interest and is approximated by a straight line. This is why, in practice, the semi-log graph representation of $f_p(x)$ is assumed without much attention to the log values and the areas are calculated as if arithmetic scales are present. The following two examples illustrate the use of this result.

8.17.2 Example: Loss Due to Anchorage Set

Going back to the example in Section 8.16.3 and Fig. 8.14, answer the following questions.

Question 1: Using f_{pJ1} = 189 ksi, determine the values of X and $\Delta f_p(0)$, assuming δ = 0.2 in.

Compute first λ from Table 8.13 for a parabolic tendon profile:

$$\lambda = 2\mu\frac{a}{b^2} + K = 2\times 0.15\times\frac{18/12}{24^2} + 7.5\times 10^{-4} = 0.001531$$

From Eq. (8.69):

$$X = \sqrt{\frac{E_{ps}\delta}{\lambda f_{pJ1}}} = \sqrt{\frac{28{,}000\times 0.2/12}{0.001531\times 189}} = 40.16 \text{ ft}$$

Since X is smaller than 52 ft, distance at which a second parabolic segment starts, its numerical value is correct.

The stress at X is given by:

$$f_p(X) = f_{pJ1}e^{-\lambda X} = 189e^{-0.001531\times 40.16} = 177.73 \text{ ksi}$$

Note that Eq. (8.70) would lead to an almost equal value of X, that is:

For x = 52 ft (representing l in Table 8.13):

$$f_p(52) = f_{pJ1}e^{-\lambda X} = 189e^{-0.001531\times 52} = 174.54 \text{ ksi}$$

$$X = \sqrt{\frac{E_{ps}\delta}{z/l}} = \sqrt{\frac{28{,}000\times 0.2/12}{(189-174.54)/52}} = 40.97 \text{ ft}$$

The loss of stress at the jacking end is obtained from Eq. (8.68):

$$\Delta f_p(0) = 2\times 28{,}000\times\frac{0.2/12}{40.16} = 23.24 \text{ ksi}$$

The stress profile in the steel before release is represented in Fig. 8.17 by the segmented line *abcd*. After anchorage set, the new stress profile is given by *febcd*. Note that the highest stress is at point *e* and corresponds to a value of 177.73 ksi.

Question 2: In the previous question the stress at jacking, f_{pJ1} = 189 ksi, was purposely taken smaller than the maximum value allowed by the building code. If the code allows a temporary stress at the jacking end of up to $0.80f_{pu}$ (provided the stress is less than or equal to $0.70f_{pu}$ = 189 ksi after anchorage set), what value of jacking stress would you recommend to the jacking crew? Draw the stress profile before and after anchorage set.

Referring to Fig. 8.17, it is observed that the highest stress attained in the previous example is at point *e* and corresponds to a value of 177.73 ksi. As the code allows for a value of 189 ksi after anchorage set, and in order to achieve such a value, one can temporarily overstress at the jacking end. The difference between 189 and 177.73 is 11.3 ksi or about 12 ksi. Therefore it is proposed to recommend a stress at the jacking end of (189 + 12) = 201 ksi, which is less than $0.80f_{pu}$ = 216 ksi. The new stress profile (Fig. 8.17) follows the segmented line *a'b'c'd'* before release, and *a"e'b'c'd'* after anchorage set. Note that the lines *a'b'c'd'* and *abcd* are almost parallel. This observation prompted the use of $aa' \simeq ee' \simeq 12$ ksi in determining the overstress at the jacking end. Note that the highest stress occurs at point *e'* and is about 189 ksi. It can also be checked analytically from:

$$f_p(40.16) = f_{pJ1}e^{-\lambda X} = 201e^{-0.001531\times 40.16} = 189 \text{ ksi}$$

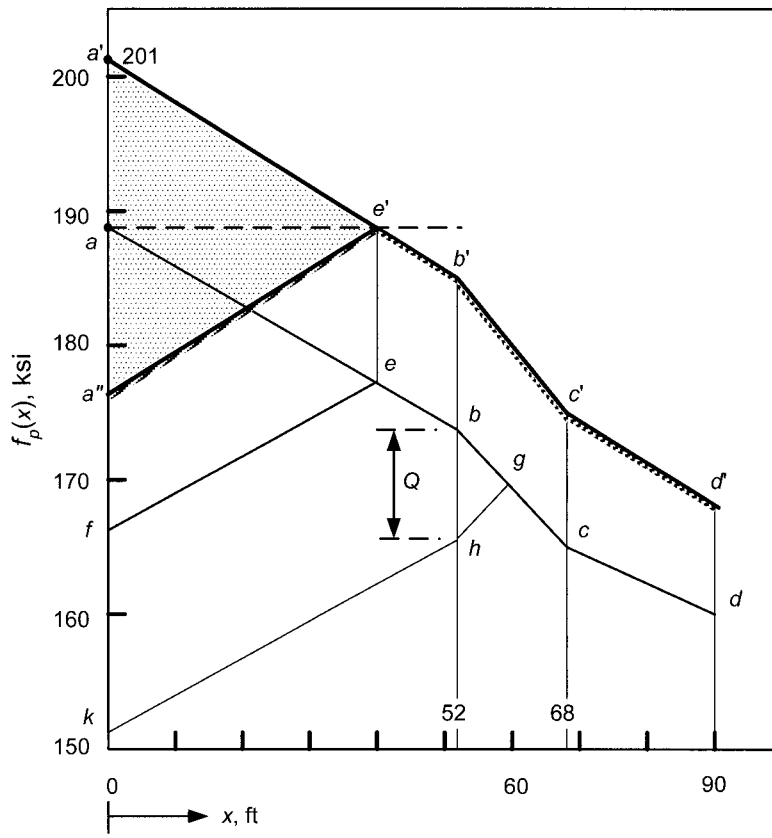

Figure 8.17 Stress profile before and after anchorage set for different stresses at jacking.

Question 3: Using $f_{pJ1} = 189$ ksi, determine the values of X and $\Delta f_p(0)$ for $\delta = 0.5$ in.

This question illustrates how the concept of area lost described in Section 8.17.1 is used. If we apply Eq. (8.69), using the same value of λ over the tendon profile, we would get $X = 63.49$ ft. This means that X is somewhere along the second parabolic segment, somewhere between b and c in Fig. 8.17, and Eq. (8.69) is not valid throughout as the value of λ changes from segment ab to bc. The solution can be achieved by using the concept area lost described in Section 8.17.1. Referring to Fig. 8.17, the steel stress profile before and after anchorage set is represented by the segmented lines *abgcd* and *khgcd*, respectively, where two quantities are unknowns, namely X, the abscissa of point g, and Q = vertical distance between points b and h, representing the stress difference between b and h. We can write the following equations (Fig. 8.17):

$$\text{Area lost} = \text{Area of trapezoid } abhg + \text{Area of triangle } bgh = E_{ps}\delta$$

$$\text{Area lost} = \frac{(\Delta f_p(0) + Q) \times 52}{2} + (X - 52)\frac{Q}{2} = E_{ps}\delta$$

$$\frac{Q}{2} = f_p(52) - f_p(X) = 174.54 - f_p(X)$$

$$f_p(X) = f_p(52) - [f_p(52) - f_p(68)]\frac{(X - 52)}{(68 - 52)} = 174.54 - (174.54 - 165.1)\frac{X - 52}{16}$$

$$\Delta f_p(0) = 2(f_{pJ} - f_p(52)) + Q = 2(189 - 174.54) + Q$$

Their solution leads to: $X = 58.4$ ft, $f_p(0) = 36.6$ ksi, and $Q = 7.68$ ksi. The above procedure is exact but cumbersome. If one accepts the practical code approximation of Eq. (8.69), where z is the loss over 90 ft length, the value of X would be:

$$X = \sqrt{\frac{28,000 \times 0.5/12}{(189 - 158.88)/90}} = 59.04 \text{ ft}$$

which is almost the same as the more exact value derived above. Note that the value of stress at 90 ft was obtained from (see Table 8.12 for x = 90 ft):

$$f_p(90) = f_{pJ1}e^{-\mu\alpha + kx} = 189e^{-0.1736} = 158.88 \text{ ksi}$$

8.18 LOSS DUE TO ANCHORAGE SET IN SHORT BEAMS

In the previous example it was assumed that the anchorage set δ and the span length l were such that X was less than l. It may happen that, in short beams, the value of X calculated from Eq. (8.69) is larger than l. Hence, Eq. (8.69) cannot be used, as it becomes obvious that X must equal l. In such a case, the area lost approach explained in Section 8.17.1 is used to determine the loss of stress $\Delta f_{ps}(0)$ at the jacking end. Equation (8.71) leads to:

$$\text{Area lost} = \left(\frac{\Delta f_p(0) + \Delta f_p(l)}{2}\right) l = E_{ps}\delta \tag{8.72}$$

and, referring to Fig. 8.18, we have:

$$\Delta f_p(0) = \Delta f_p(l) + 2[f_{pJ} - f_p^*(l)] \tag{8.73}$$

where $f_p^*(l)$ can be computed from Eq. (8.61) in terms of f_{pJ}. If a single parabola is involved in the profile such as for a simply supported beam, then:

$$f_p^*(l) = f_{pJ} e^{-\lambda l} \approx f_{pJ} - f_{pJ}\lambda l \tag{8.74}$$

The solution of the two above equations leads to:

$$\Delta f_p(0) = E_{ps}\frac{\delta}{l} + f_{pJ}\lambda l \tag{8.75}$$

$$\Delta f_p(l) = E_{ps}\frac{\delta}{l} - f_{pJ}\lambda l \tag{8.76}$$

From Fig. 8.18, we also have:

$$[f_{pJ} + f_p(0)]/2 = [f_p^*(l) + f_p(l)]/2 \tag{8.77}$$

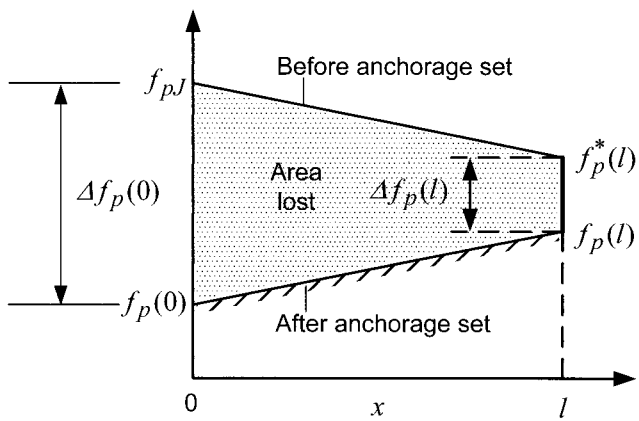

Figure 8.18 Typical tendon stress variation in short members before and after anchorage.

Referring to Fig. 8.18, it can be seen from the stress profile after anchorage set, that jacking must be applied only from one end because the final stress at the jacking end is smaller than that at the other end. There is no benefit in jacking at the other end. This may also be true in some other cases, even when X is less than l. In

general, a tradeoff must be made between the benefit of additional jacking and that of labor and material cost involved.

8.18.1 Example: Anchorage Set Loss in a Short Beam

A small beam is to be prestressed for testing in the laboratory. Its span length is 15 ft. Assume f_{pJ1} = 216 ksi, and the anchorage set δ = 0.2 in. Determine the stress in the tendon after anchorage set at the jacking end and the other end of the beam. Consider two cases, a pretensioned and a posttensioned beam.

- *Prestensioned beam*

If the beam is pretensioned, the stress and stress loss just before and just after anchorage set will be uniform throughout the length, as the steel is not yet in contact with the concrete. Thus the stress loss is:

$$\Delta f_p(0) = E_{ps}\frac{\delta}{l} = 28000\frac{0.20}{15\times 12} = 31.1 \text{ ksi}$$

The stress in the tendons after anchorage (or chuck) set is same throughout and equal:

216 – 31.1 = 184.89 ksi.

Note that in several examples (see Sections 8.8 to 8.10) we assumed that the loss due to chuck set in pretensioned members is very small; this is because we anticipated long prestressing beds. Indeed, if in the above example the length of the bed is 150 ft, the loss would only be 3.11 ksi. This justifies the use of f_{pJ2} = 216 – 3 = 213 ksi as a first approximation. On the other hand, the loss could be neglected in very long prestressing beds.

- *Posttensioned beam*

For the posttensioned beam, assume that the tendon profile is parabolic with a sag of 6 in, for the same span of 15 foot. Also assume the following: μ = 0.15, $K = 7.5\text{x}10^{-4}$, and δ = 0.2.

We know from the example of Sec. 8.17.2 that the anchorage loss will be felt over a distance beyond the span length. Thus from Table 8.13:

Compute:

$$\lambda = 2\mu\frac{a}{b^2} + K = 2\times 0.15\times\frac{6/12}{15^2} + 7.5\times 10^{-4} = 0.001417$$

$$f_p^*(l) = f_p^*(15) = f_{pJ1}e^{-\lambda x} = 216e^{-0.001417\times 15} = 211.46 \text{ ksi}$$

and from Eqs. (8.75) and (8.76):

$$\Delta f_p(0) = E_{ps}\frac{\delta}{l} + f_{pJ}\lambda l = 28000\frac{0.2}{15\times 12} + 216\times 0.001417\times 15 = 35.7 \text{ ksi}$$

$$\Delta f_p(l) = E_{ps}\frac{\delta}{l} - f_{pJ}\lambda l = 28000\frac{0.2}{15\times 12} - 216\times 0.001417\times 15 = 26.52 \text{ ksi}$$

Thus the stress at the jacking end after anchorage set is (Fig. 8.18):

$$f_p(0) = f_{pJ} - \Delta f_p(0) = 216 - 35.7 = 180.3 \text{ ksi}$$

The stress at the other end after anchorage set is given:

$$f_p(l) = f_p^*(l) - 26.52 = 211.46 - 26.52 = 184.94 \text{ ksi}$$

It can be observed that the stress at the nonjacking end is higher than that at the jacking end. Thus it would not make sense to try to jack from both ends.

8.19 CONCLUDING REMARKS

This chapter has presented a range of methods for calculating prestress losses and their variation with time; in doing so, it also provided a better understanding of the behavior of prestressed concrete members, and how various material properties are accommodated simultaneously as they change with time. If accuracy is not important and only the total losses are needed, the lump sum methods should be used as a first approximation. However, there are cases where the time-step method or similar approaches are necessary. Although a number of equations were given in this chapter to illustrate the variation with time of creep, shrinkage and relaxation properties, the use of a different set of equations should not change the approach adopted in the time-step procedure. Corresponding computations can be efficiently run using computers, programmable calculators, or spreadsheets. A large number of time intervals, as well as time intervals reflecting the real life of the member and related construction milestones, can be handled in the repetitive process to improve accuracy. Accuracy in estimating total losses, as well as losses at a certain point in time, may be important. It is generally not desirable to be conservative as service conditions such as camber, deflection, and cracking are directly affected. On the other hand, the nominal bending resistance will be effected very little by prestress losses.

REFERENCES

8.1 ACI-ASCE Committee 423 (formerly 323), "Tentative Recommendations for Prestressed Concrete," *ACI Journal*, 54(7): 545-78, 1958.

8.2 ACI Committee 318, *Building Code Requirements for Structural Concrete (ACI 318-02) and Commentary (ACI318R-02)*, American Concrete Institute, Farmington Hills, Michigan, 2002.

8.3 ACI Committee 343, "Analysis and Design of Reinforced Concrete Bridge Structures," ACI 343R-95, ACI Manual of Concrete Practice, American Concrete Institute, Farmington Hills, Michigan, 2002.

8.4 ACI Committee 209, "Prediction of Creep, Shrinkage, and Temperature Effects in Concrete Structures," ACI 209R-92 (Reapproved 1997), ACI Manual of Concrete Practice, American Concrete Institute, Farmington Hills, Michigan, 2002.

8.5 ACI Committee 435, "Control of Deflections in Concrete Structures," ACI 435R-95, ACI Manual of Concrete Practice, American Concrete Institute, Farmington Hills, Michigan, 2002.

8.6 American Association of State Highway and Transportation Officials (AASHTO), *LRFD Bridge Design Specifications*, 2nd ed., Washington, DC, 1998.

8.7 American Association of State Highway and Transportation Officials (AASHTO), *Standard Specifications for Highway Bridges*, 16th Edition, Washington, DC, 1996.

8.8 Bazant, Z. P., and L. Panula, "Creep and Shrinkage Characterization for Analyzing Prestressed Concrete Structures," *PCI Journal*, 25(3): 86-122, 1980.

8.9 Bazant, Z. P., and J-K. Kim, "Improved Prediction Model for Time-Dependent Deformations of Concrete: Part 2 – Basic Creep," *Materials and Structures / Matériaux et Construction*, 24(144): 409-21. Paris: RILEM, 1991.

8.10 Branson, D. E., and M. L. Christiason, "Time-Dependent Concrete Properties Related to Design Strength and Elastic Properties, Creep, and Shrinkage," ACI-SP 27, Designing for Effects of Creep, Shrinkage, and Temperature, American Concrete Institute, Detroit, 1971, pp. 257-277.

8.11 Branson, D. E., and K. M. Kripanarayanan, "Loss of Prestress, Camber, and Deflection of Non-Composite and Composite Prestressed Concrete Structures," *PCI Journal*, 16(5): 22-52, 1971.

8.12 Brooks, J. J., and A. M. Neville, "Estimating Long-Term Creep and Shrinkage from Short-Term Tests," *Magazine of Concrete Research,* 27(90), 1975.

8.13 Bandyopadhyay, T. K., "Determining Aging Coefficient and Time-Dependent Losses and Deformations of Prestressed Members with Due Consideration of Percentage of Steel," *Nuclear Engineering and Design Journal*, 156(1-2): 287-311, 1995.

8.14 Cole, H. A., "Direct Solution for Elastic Prestress Loss in Pretensioned Concrete Girders," *Practice Periodical on Structural Design and Construction Journal*, 5(1): 27-31, 2000.

8.15 FIP Recommendations, "Practical Design of Reinforced and Prestressed Concrete Structures," based on the CEB-FIP Model Code MC 78, Thomas Tedford Limited, London, 1984.

8.16 Ghali, A., and R. Favre, "*Concrete Structures: Stresses and Deformations.*" London-New York: Chapman and Hall, 1986, 352 pp.

8.17 Ghali, A., "Stress and Strain Analysis in Prestressed Concrete: A Critical Review," *PCI Journal*, 34(6): 80-97, 1989.

8.18 Glodowski, R. J., and J. J. Lorenzetti, "A Method for Predicting Prestress Losses in a Prestressed Concrete Structure," *PCI Journal*, 17(2): 17-31, 1972.

8.19 Grouni, H. N., "Prestressed Concrete: A Simplified Method for Loss Computation," *ACI Journal*, 70(2), 1973.

8.20 Grouni, H. N., "Loss of Prestress Due to Relaxation after Transfer," *ACI Journal*, 75(2): 64-66, 1978.

8.21 Hansen, T. C., and A. H. Mattock, "Influence of Size and Shape of Member on the Shrinkage and Creep of Concrete," *ACI Journal*, 63(2): 267-90, 1966.

8.22 Hanson, J. A., "Prestress Loss as Affected by Type of Curing," *PCI Journal*, 9(2): 69-93, 1967.

8.23 Halsey, T. J., and R. Miller, "Destructive Testing of Two Forty-Year-Old Prestressed Concrete Bridge Beams," *PCI Journal*, 41(5): 84-93, 1996.

8.24 Hernandez, H. D., and W. L. Gamble, "Time-Dependent Prestress Losses in Pretensioned Concrete Construction," Structural Research Series No. 417, Civil Engineering Studies, University of Illinois, Urbana, May 1975, 171 pp.

8.25 Huang, T., "Prestress Losses in Pretensioned Concrete Structural Members," Report No. 339.9, Fritz Engineering Laboratory, Lehigh University, Bethlehem, Pennsylvania, August 1973, 100 pp.

8.26 Huang, T., "Anchorage Take-up Loss in Post-Tensioned Members," *PCI Journal*, 14(4): 30-35, 1969.

8.27 Keydar, E., "Friction Losses in Prestressed Steel by Equivalent Load Method," *PCI Journal*, 35(2): 74-77, 1990.

8.28 Lyse, I., "Shrinkage and Creep of Concrete," *ACI Journal*, 31(8): 775-82, 1960.

8.29 Magura, D. D., M. A. Sozen, and C. P. Seiss, "A Study of Stress Relaxation in Prestressing Reinforcement," *PCI Journal*, 9(2): 13-57, 1964.

8.30 Mehta, P. K., and P. Monteiro, "Concrete: Structure, Properties, and Materials." Upper Saddle River, NJ: Prentice Hall, International Series, College Division, 1992, 548 pp.

8.31 Meyers, B. L., and D. E. Branson, "Design Aid for Predicting Creep and Shrinkage Properties of Concrete," *ACI Journal*, 69(9): 551-55, 1972.

8.32 Naaman, A. E., and A. A. Hamza, "Prestress Losses in Partially Prestressed High Strength Concrete Beams," *PCI Journal*, 38(3): 98-114, 1993.

8.33 Neville, A., "Properties of Concrete," 4th ed. New York: John Wiley and Sons, 1996, 844 pp.

8.34 Podolny, Jr., W., and T. Melville, "Understanding the Relaxation in Prestressing," *PCI Journal,* 14(4): 43-54, 1969.

8.35 PCI Committee on Prestress Losses, "Recommendations for Estimating Prestress Losses," *PCI Journal*, 20(4): 43-75, 1975. Also comments on vol. 21(2), 1976.

8.36 *PCI Design Handbook – Precast and Prestressed Concrete*, 5th ed., Prestressed Concrete Institute, Chicago, Illinois, 1999.

8.37 PCI Committee on Design Handbook, "Volume Changes in Precast Prestressed Concrete Structures," *PCI Journal*, 22(5): 38-53, 1977.

8.38 *"PCI Bridge Design Manual,"* Precast Prestressed Concrete Institute, Chicago, MNL-133-97, 1997.

8.39 Rao, C., and G. C. Frantz, "Fatigue Tests of 27-Year-Old Prestressed Concrete Bridge Box Beams," *PCI Journal*, 41(5): 74-83, 1996.

8.40 Pessiki, S., M. Kaczinski, and H. H. Wescott, "Evaluation of Effective Prestress Force in 28-Year-Old Prestressed Concrete Bridge Beams," *PCI Journal*, 41(6): 78-89, 1996.

8.41 Roberts-Wollmann, C. L., J. A. Arrellaga, J. E. Breen, and M. E. Kreger, "Field Measurements of Prestress Losses in External Tendons," *ACI Structural Journal*, 93(5): 595-601, 1996.

8.42 Ross, A. D., "Creep of Concrete under Variable Stress," *ACI Journal*, 29(9): 739-58, 1958.

8.43 Saiidi, M. S., J. Shields, D. O'Conner, and E. Hutchens, "Variation of Prestress Force in a Prestressed Concrete Bridge During the First 30 Months," *PCI Journal*, 41(5): 66-72, 1996.

8.44 Schultchen, E., and T. Huang, "Relaxation Losses in 7/16 in. Diameter Special Grade Prestressing Strands," Fritz Engineering Laboratory Report, No. 339.4, Lehigh University, Bethlehem, Pennsylvania, July, 1969.

8.45 Sinno, R., and H. L. Furr, "Hyperbolic Functions of Prestress Loss and Camber," *Journal of the Structural Division, ASCE*, 96(ST4): 803-21, 1970.

8.46 Sinno, R., and H. L. Furr, "Computer Program for Computing Prestress Loss and Camber," *PCI Journal*, 17(5): 27-38, 1972.

8.47 Steinberg, E. P., "Probabilistic Assessment of Prestress Loss in Pretensioned Prestressed Concrete," *PCI Journal*, 40(6): 76-85, 1995.

8.48 Tadros, M. K., A. Ghali, and W. H. Dilger, "Time-Dependent Prestress Loss and Deflection in Prestressed Concrete Members," *PCI Journal*, 20(3): 86-98, 1975.

8.49 Tadros, M. K., A. Ghali, and A. W. Meyer, "Prestress Loss and Deflection of Precast Concrete Members," *PCI Journal*, 30(1): 114-41, 1985.

8.50 Troxell, G. E., H. E. Davis, and J. W. Kelley, *Composition and Properties of Concrete*, 2nd ed. New York: McGraw-Hill Book Co., Inc., 1968.

8.51 Young, F., S. Mindess, and D. Darwin, "Concrete," 2nd ed. Upper Saddle River, NJ: Prentice Hall, 2002, 656 pp.

8.52 Zia, P., H. K. Preston, N. L. Scott, and E. B. Workman, "Estimating Prestress Losses," *Concrete International*, 1(6): 32-38, 1979.

8.53 Zarghamee, M. S., F. J. Heger, and W. R. Dana, "Concrete Creep and Shrinkage and Wire Relaxation in Buried Prestressed Concrete Pipe," *ACI Structural Journal*, 87(5): 512-22, 1990.

PROBLEMS

8.1 A pretensioned prestressed concrete tie (tensile member) of cross section shown in Fig. P8.1 is tensioned by four half-inch diameter stress-relieved prestressing strands. Stress transfer is achieved 24 hours after pouring. Steam-curing is used during this initial period. The following information is provided:

- $f'_c = 5000$ psi; $f'_{ci} = 4000$ psi at transfer; $f_{pJ2} = 204$ ksi; $f_{pu} = 270$ ksi; $f_{py} = 230$ ksi
- $A_{ps} = 4 \times 0.153 = 0.612$ in^2; $E_{ps} = 28000$ ksi; $\varepsilon_{SU} = 3.4 \times 10^{-4}$; $C_{CU} = 1.8$

Relative humidity H = 50 percent; normal weight concrete. It is assumed that the tie is not subjected to any bending moment.

Calculate the loss of prestress in the steel after 1, 3, 7, 30, 60, 365 days, 5 years, 50 years. It is assumed that time starts after seating at the jack, for which f_{pj2} is known. Order your calculations in a table.

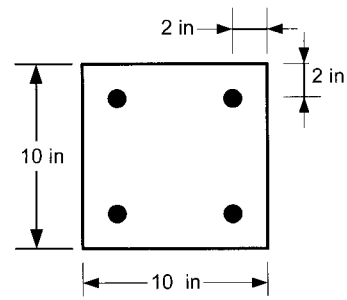

Figure P8.1

8.2 Calculate the total loss of stress in the steel at midspan of the pretensioned beam shown in Fig. P8.2 at different periods of time, given the following information. The beam is steam-cured and the steel is released after 24 hours of tensioning. Low relaxation strand is used.

- $f'_c = 6000$ psi; $f'_{ci} = 4500$ psi at transfer; $f_{pJ2} = 213$ ksi; $f_{pu} = 270$ ksi; $f_{py} = 243$ ksi
- $A_{ps} = 3 \times 0.153 = 0.459$ in^2; $e_o = 10.64$ in; $E_{ps} = 27000$ ksi; $\varepsilon_{SU} = 4 \times 10^{-4}$; $C_{CU} = 1.8$
- span l = 40 ft; normal weight concrete $\gamma_C = 150$ pcf; H = 80 percent.

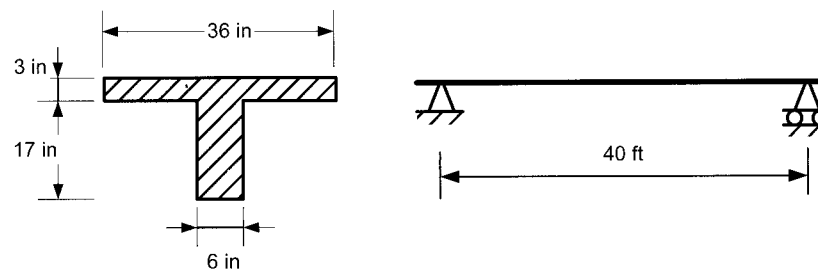

Figure P8.2

(*a*) Determine the loss due to relaxation and the elastic shortening loss at 24 hours

(*b*) Determine the total time-dependent prestress loss after transfer using the procedure recommended in AASHTO LRFD for lump sum estimate of total loss (Section 8.5)

(*c*) Determine the sum of separate time-dependent losses after transfer using the procedure recommended in AASHTO LRFD (Section 8.6)

(*d*) Calculate the loss of stress in the steel after 1, 7, 14, 30, 60, 365 days, and 50 years, using the time-step procedure (Section 8.14). To determine shrinkage and creep losses use Eqs. (8.42) and (8.54). Compare total losses with those obtained in (*a*), *(b)* and *(c)*.

8.3 A precast concrete column (Fig. P8.3) is pretensioned in plant with four strands (0.5-in diameter; 270-ksi strength). Three months later it is transported to site, erected, and fixed to its base footing by posttensioning with four unbonded rods (diameter 5/8 in; strength 160 ksi). It is assumed that just before tensioning the rods, the stress in the pretensioned strands is 165 ksi. Posttensioning the rods is achieved in two successive steps, two opposite rods at a time. Assume that the stress in the rods being tensioned is 112 ksi immediately after anchoring.

Determine the value of the prestressing force just after completion of the posttensioning operation. The following information is given:
$f'_c = 6000$ psi; $E_c = 4700$ ksi; $E_{ps} = 28000$ ksi; $n_p = 5.96$ ksi; $A_c = 180$ in^2; area of four strands = 4 x 0.153 = 0.612 in^2; area of one posttensioning rod = 0.307 in^2; force in one posttensioning rod = 34.38 kips at 112 ksi. Use gross area of concrete instead of net area whenever the area is used.

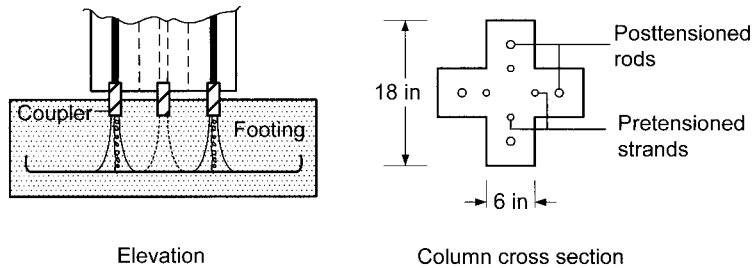

Figure P8.3

8.4 Show that for a parabolic cable profile, the angle α_x (Fig. P8.4) between the tangents at two points of abscissa 0 and x, respectively, is, as a first approximation, proportional to x. Derive the corresponding value of λ given in Table 8.13 for a parabolic profile.

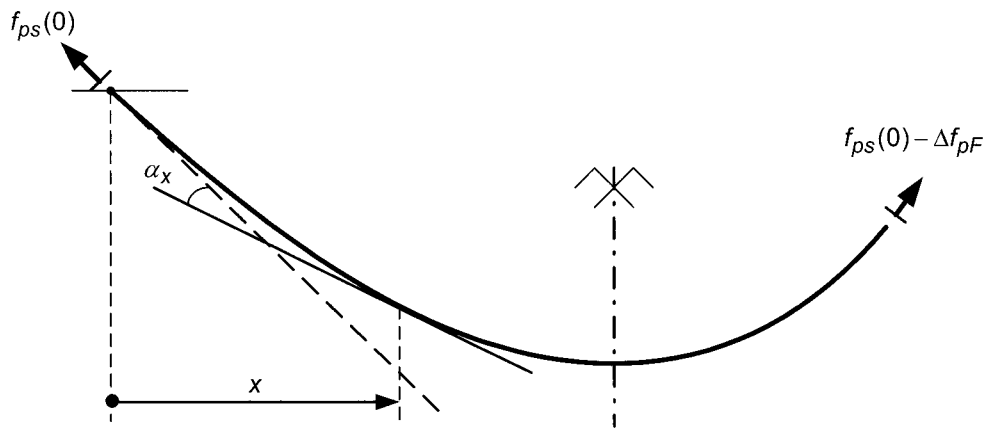

Figure P8.4

8.5 In a nuclear power vessel hoop tendons are posttensioned between buttresses which are 240^o apart, as shown in Fig. P8.5. The following information is given:
$\mu = 0.20$; $K = 5 \times 10^{-4}$ per foot; $E_{ps} = 27000$ ksi; anchor set $\delta = 0.5$ in; radian $= 57.29^o$
f_{pJ1} = stress in the prestressing steel at jacking end just prior to transfer = 216 ksi
(*a*) Calculate the stress in the steel at the anchorage immediately after transfer (i.e., after anchorage set), assuming circular tendons with a radius of 50 ft.
(*b*) If jacking is applied at only one end, what is the stress at the other end?
(*c*) Would you recommend stressing from both ends?

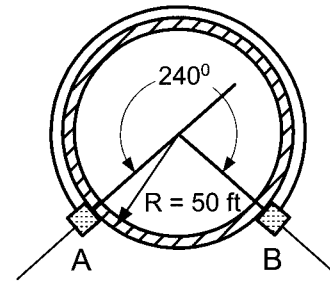

Figure P8.5

8.6 A simply supported posttensioned prestressed concrete rectangular beam (Fig. P8.6) requires a final prestressing force F at midspan (after all losses) equal to 265 kips. The following information is given:
$f'_c = 6000$ psi; $f'_{ci} = 4000$ psi;
$\bar{\sigma}_{ti} = -189$ psi; $\bar{\sigma}_{ci} = 2400$ psi; $\bar{\sigma}_{ts} = -213$ psi; $\bar{\sigma}_{cs} = 3600$ psi; $\bar{\sigma}_{csus} = 2700$ psi;
$E_{ps} = 27000$ ksi; $f_{pJ2} = 203$ ksi; $f_{pu} = 270$ ksi; $f_{py} = 243$ ksi; $\gamma_C = 150$ pcf; span $l = 60$ ft; live load = 200 plf; friction coefficient $\mu = 0.25$; wobble coefficient $K = 10 \times 10^{-4}$/ft; anchorage set $\delta = 0.2$ in. The steel profile follows a single parabola having its vertex at midspan.

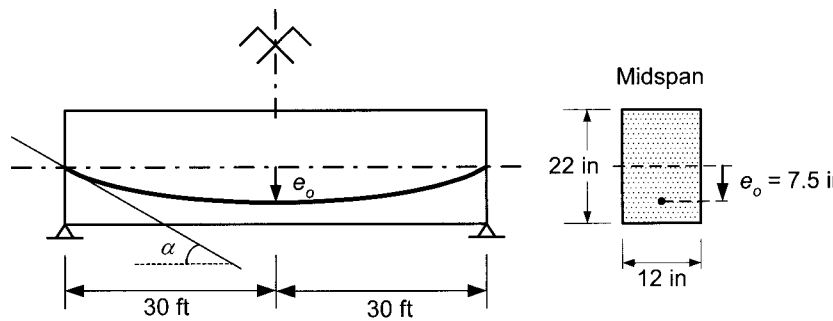

Figure P8.6

(*a*) Assuming a stress in the prestressing steel at the jack $f_{pJ1} = 190$ ksi, determine the stress profile in the steel along the beam before and after anchorage set (consider stressing from one end only). Should stressing be considered from both ends?
(*b*) In (*a*) the stress at jacking was taken purposely smaller than $0.8f_{pu} = 216$ ksi as allowed by the code. If the code also allows a maximum stress in the steel $= 0.74\, f_{pu} = 200$ ksi after transfer, what is the stress you would recommend at the jacking end?
(*c*) Based on the results derived in (*b*), determine total time-dependent losses using the lump-sum estimate of total loss recommended by AASHTO LRFD.

(*d*) Determine the effective stress in the steel at midspan after all losses and the required number of strands if the area of one strand is 0.153 in^2.

(*e*) Based on the results derived in (*b*), determine the sum of separate time-dependent losses at midspan using AASHTO LRFD and assuming the following: $\varepsilon_{SU} = 4 \times 10^{-4}$ in/in; $C_{CU} = 2$; $H =$ 70 percent; moist-cured concrete.

Montreal Olympic Stadium where C-shaped posttensioned rigid frames of segmentally precast elements were used. *(Courtesy Precast/Prestressed Concrete Institute.)*

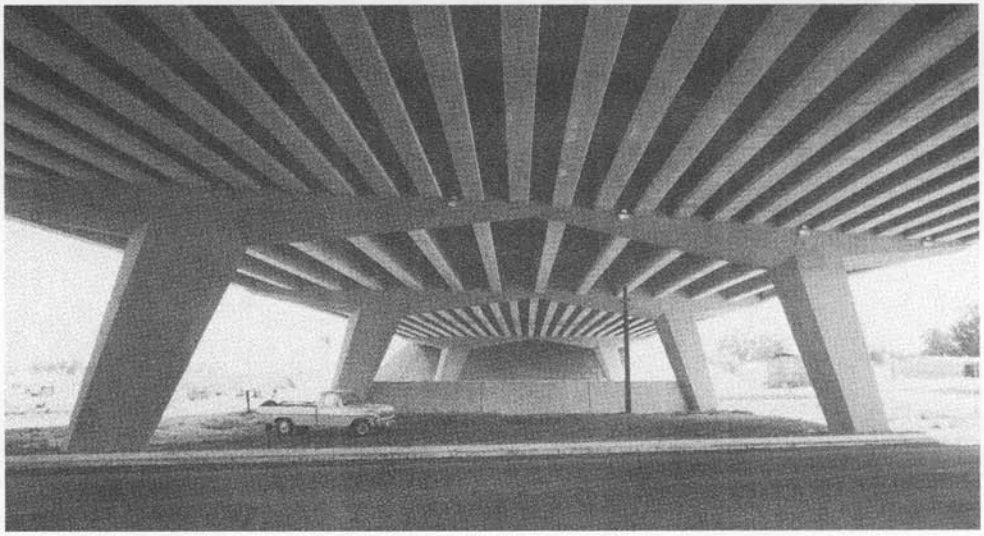

A composite bridge using precast prestressed concrete beams for a highway overcrossing in Walla Walla, Washington. *(Courtesy Precast/Prestressed Concrete Institute.)*

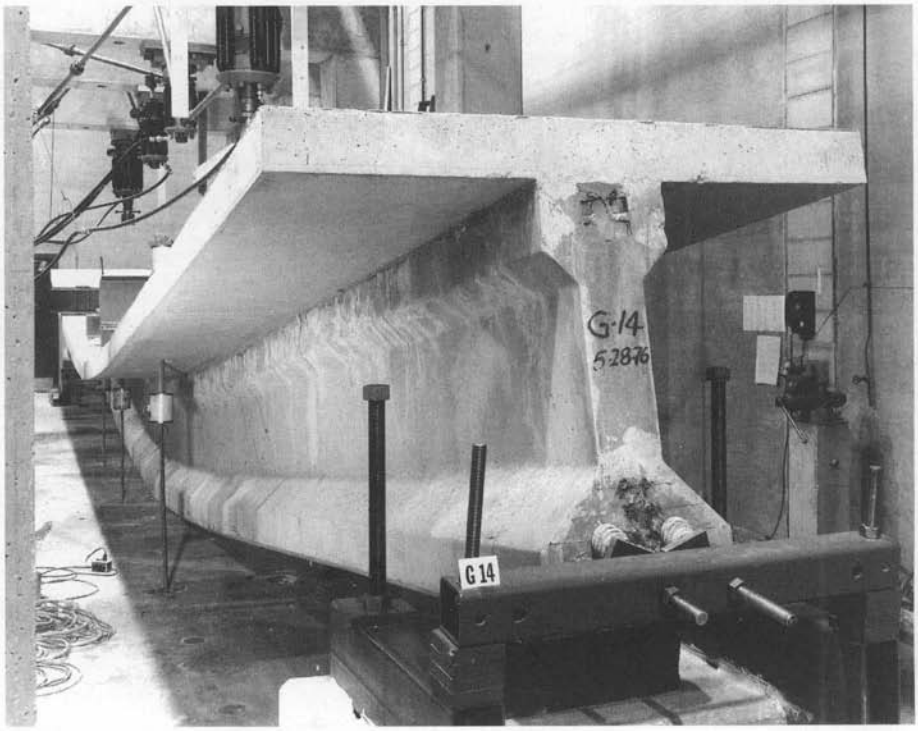

Full scale testing of composite prestressed concrete bridge beam. *(Courtesy Portland Cement Association.)*

CHAPTER 9

ANALYSIS AND DESIGN OF COMPOSITE BEAMS

9.1 TYPES OF PRESTRESSED CONCRETE COMPOSITE BEAMS

Composite construction implies the use, in a single structure acting as a unit, of different structural elements made with similar or different structural materials. Common examples include steel-concrete beams or columns, orthotropic steel decks, and sandwich panel construction. Generally two structural materials are utilized in the best possible manner: in a steel-concrete composite beam the steel is designed to carry tension and the concrete to carry compression.

In a composite member where only concrete is used as a material, the concrete is placed in at least two separate stages generally leading to two different unit weights and/or properties. This is the case for composites made with a precast reinforced or prestressed concrete element combined with a concrete element cast in place at a different time. When the precast element is also prestressed, it essentially simulates the function of the steel in a steel-concrete system; it will carry the tension without cracking.

In the United States the use of prestressed concrete composite beams seriously took off in the early fifties mostly in highway bridges where precast prestressed I beams of the AASHTO or BPR (Bureau of Public Roads) types were used in combination with cast-in-place reinforced concrete slabs [Ref. 9.3]. Prestressed composite construction in buildings materialized only a decade later [Ref. 9.4]. It has achieved significant growth since. The cause of this development is made clear in the next section where the advantages of composite construction are described.

Typical cross sections of prestressed concrete composite beams are shown in Fig. 9.1. Several alternatives can be identified where the cast-in-place concrete (CIPC) slab is poured either on top of the precast prestressed concrete (PPC) beams, or in between them, or both. The cast-in-place slab can act as a structural element allowing lateral transfer of loading as shown in Figs. 9.1 *a, b* and *c*, or as a topping

having a continuous interface with the precast element as shown in Figs. 9.1*d* and *e*. The former case is typical of bridge applications, while the latter is typical of building applications. Figure 9.1*f* also shows an interesting application where the cast-in-place element is itself a beam that may be subsequently reinforced or posttensioned.

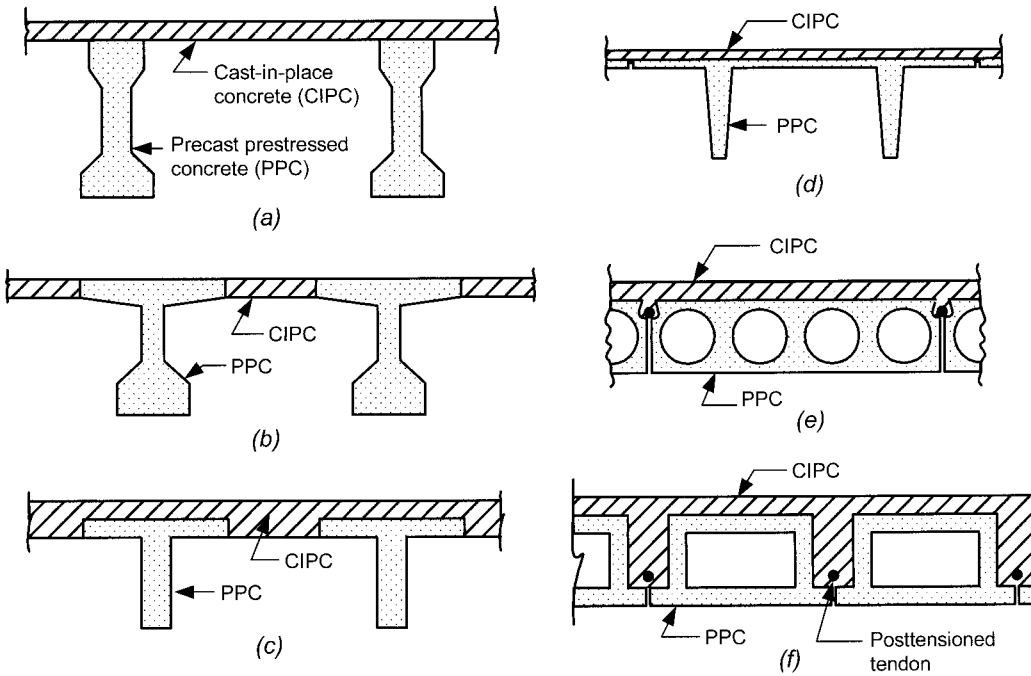

Figure 9.1 Typical cross sections of composite beams.

This chapter deals mostly with composite beams where a cast-in-place slab is poured on top (or on top and in between) of precast-prestressed beams or girders. The reader should find no conceptual difficulty in extending the approach to any other case and is referred to a number of basic references on composite construction listed at the end of this chapter [Refs. 9.2, 9.3, 9.14, 9.21, 9.25, 9.29].

9.2 ADVANTAGES OF COMPOSITE CONSTRUCTION

Composite construction can result in considerable savings in construction cost and is likely to remain a major alternative in many applications [Ref. 9.21]. Some of its often-cited advantages are clarified below:

1. Total construction time is substantially reduced when precast concrete elements are used.

2. Pretensioning in plant is more cost-effective than posttensioning on site. Because the precast-prestressed concrete element is factory-produced and contains the bulk of the reinforcement, rigorous quality control and higher mechanical properties can be achieved at relatively low cost. The cast-in-place concrete slab does not need to have high mechanical characteristics and thus is very suitable to field conditions. It is not uncommon to have a precast beam with a concrete compressive strength of 7 to 10 ksi (48 to 70 MPa) and a cast-in-place slab with a specified concrete compressive strength of 4 ksi (28 MPa) only.
3. The precast-prestressed concrete units are erected first and can be used to support the forms needed for the cast-in-place slab without additional scaffolding (or shoring) (Fig. 9.2a). In order to save removal time, the forms themselves can be replaced by stay-in-place precast (reinforced or prestressed) concrete panels as shown in Fig. 9.2b.

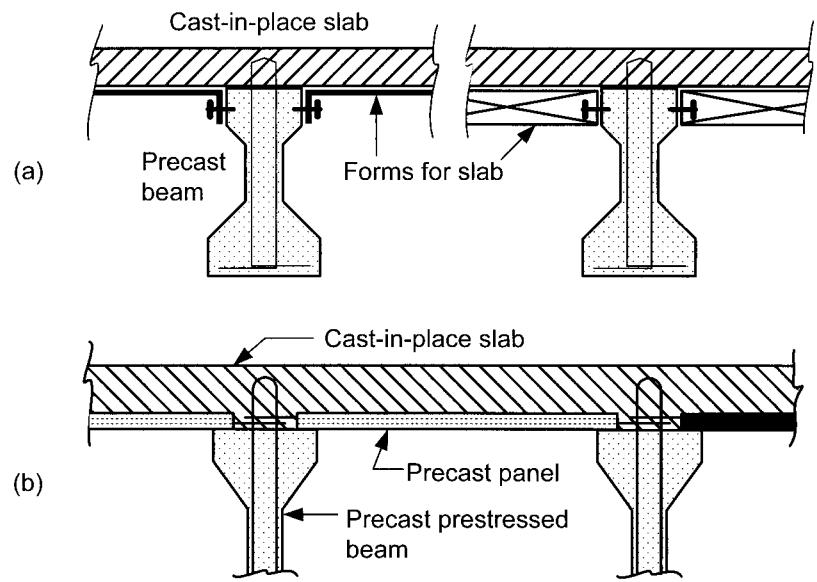

Figure 9.2

4. In addition to its contribution to the strength and stiffness of the composite member, the cast-in-place slab provides an effective means to distribute loads in the lateral direction. When the slab is used as a topping (Figs. 9.1*d* and *e*), and is essentially not reinforced, the need for costly longitudinal watertight joints between the precast units is eliminated. However, to improve water tightness, a light steel mesh may be added to the slab, particularly along the joints.
5. The cast-in-place slab can be poured continuously over the supports of precast units placed in series, thus providing continuity to a simple span system (Fig. 9.3). The continuity after slab hardening is assumed to act only for superimposed dead loads and live loads [Ref. 9.6].

6. In principle composite construction offers a very effective means of controlling deflections by properly sizing and designing the precast and cast-in-place elements. However, in practice it is difficult to accurately predict deflections. This is particularly true for composite construction where two different types of concrete of different properties and ages at loading are used, and where composite action is achieved only after a certain time has elapsed. In addition, the restraint provided by the cast-in-place slab can cause increases in prestress losses of the precast element and thus influence time-dependent deflections [Refs. 9.6 and 9.26].

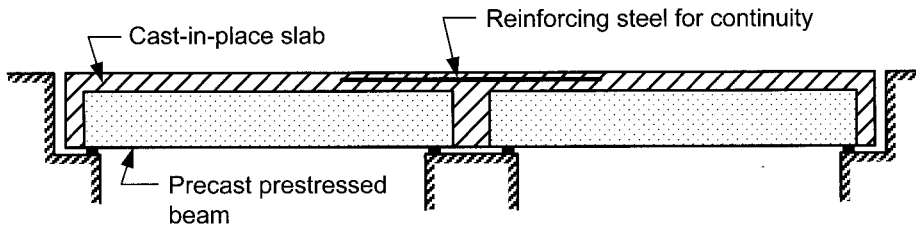

Figure 9.3 Precast prestressed beams made continuous for live loads by a cast-in-place slab.

Note that in any particular situation, the decision for a shored versus unshored construction should be carefully evaluated. Generally, unshored construction is favored; however, shored construction has the advantage of putting the concrete slab in compression immediately after the shores are removed, thus preventing cracking due to shrinkage or temperature effects.

One of the few limitations of composite construction is the size (overall dimensions and weight) of the precast prestressed units that can be transported and erected. In the United States precast beams spanning up to 50 m (160 ft) are not uncommon. Spliced girders or beams, assembled by post-tensioning on site, are considered for longer spans.

9.3 PARTICULAR DESIGN ASPECTS OF PRESTRESSED COMPOSITE BEAMS

The design of prestressed concrete composite beams can be essentially reduced to that of noncomposite beams, provided their differences are understood and accounted for. This is the main design strategy followed in this chapter which closely draws on the approach and line of thinking in Chapter 4. Particular design differences comprise:

1. The loading stages and their relation to whether the beam responds as a composite or noncomposite beam.

2. The transformed effective flange width and corresponding transformed section properties.
3. The horizontal shear at the interface between the precast beam and the cast-in-place slab to insure composite action.

Other design considerations, such as flexure by allowable stresses or ultimate strength, shear, torsion, and deflection are to a great extent very similar to those of noncomposite monolithic beams.

Each of the above-mentioned differences and similarities is addressed in one of the next sections, followed by the derivation of the main stress inequality equations for the working stress design procedure; then, a complete example is given to illustrate how to accommodate these characteristics in actual design.

9.4 LOADING STAGES, SHORED VERSUS UNSHORED BEAMS

The various loadings affecting composite beams can be separated into two groups, one involving the precast section alone, and the other involving the composite section (Table 9.1). Within each group two extreme loadings (a minimum and a maximum loading) can be identified for design. Loadings affecting the precast-prestressed beam are the prestressing force, the self-weight of the beam, and, if the beam is *unshored*, the weight of the cast-in-place slab, as well as other elements, such as diaphragms poured at the same time as the slab.

Table 9.1 Loading stages in prestressed composite beams during service.

		Loading combination		
Resisting section	Extreme loading stage	Unshored construction	Shored construction	Incremental maximum external moment
Precast section	1	$F_i + GP$	$F_i + GP$	.....
	2	$(F_i, F) + GP + S + A$	$(F_i, F) + GP$	M_p
Composite section	3	.....	$S + A$	.....
	4	$SD + L + I$	$S + A + SD + L + I$	M_c

Notation: (F_i, F) = initial prestressing force, effective prestressing force or any value in between; GP = precast girder self-weight; S = cast-in-place slab weight; A = additional weight acting with slab (diaphragms); SD = superimposed dead load; L = live load; I = impact load, if any.

Shoring (Fig. 9.4) implies the use, during slab pouring and curing, of temporary supports or shores under the precast beam and/or slab to relieve the beam from supporting the weight of the slab by itself. After hardening, the shores are removed,

the weight of the slab is released and the beam, acting now as a composite beam, sustains the additional weight of the slab. Further loadings by superimposed dead loads and live loads are resisted by the composite beam. Differences in loading between the shored and unshored cases are identified in Table 9.1, where the symbols used are explained. Since, depending on the loadings, either the precast or the composite section properties apply, the maximum external moment is given for each case. The maximum moment for the precast section is defined by M_p and the additional maximum moment on the composite section by M_c. Final stresses under combined loadings are obtained by superimposing the stresses induced by M_p on the precast section to those induced by M_c on the composite section. Their determination is covered in Sec. 9.7.

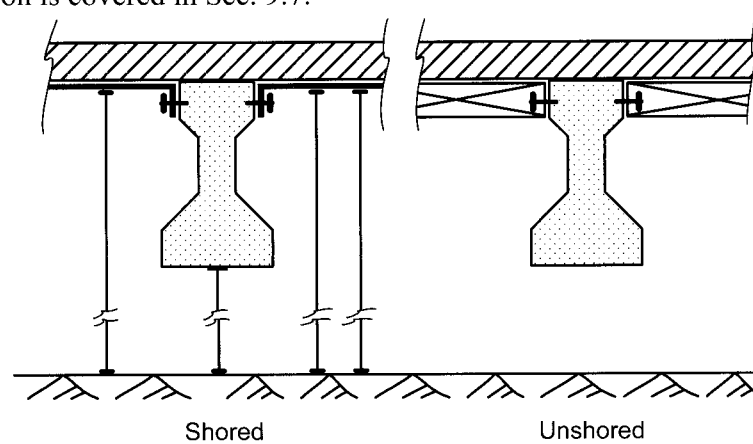

Figure 9.4 Typical shored versus unshored construction.

9.5 EFFECTIVE AND TRANSFORMED FLANGE WIDTH AND SECTION PROPERTIES

9.5.1 Effective Flange Width

Theoretically, when a monolithic beam with an infinitely wide flange is subjected to flexural loading, the compressive stress on the top fiber is not constant but varies transversely across the flange due to what is known as "shear lag" (Fig. 9.5*a*) [Refs. 9.21 and 9.28]. The stress is maximum at the level of the web and decreases away from it. It would be too complex to utilize the theoretical solution to calculate the compressive stresses in the flange. Instead, a simplified approach is adopted in design, where the flange is assumed to have an equivalent effective width b_e over which the flexural stress is assumed uniform transversely. In principle, the effective flange at a given section is determined to carry the same load as the real flange. From theory, the effective width itself is shown to vary along the span length (Fig. 9.5*b*) and depends on the type of loading (concentrated versus uniform loads), the dimensional properties of the section, and even the time-dependent parameters of the

concrete material such as creep and deflection. However, in practical design, the effective width is taken as a constant throughout the span.

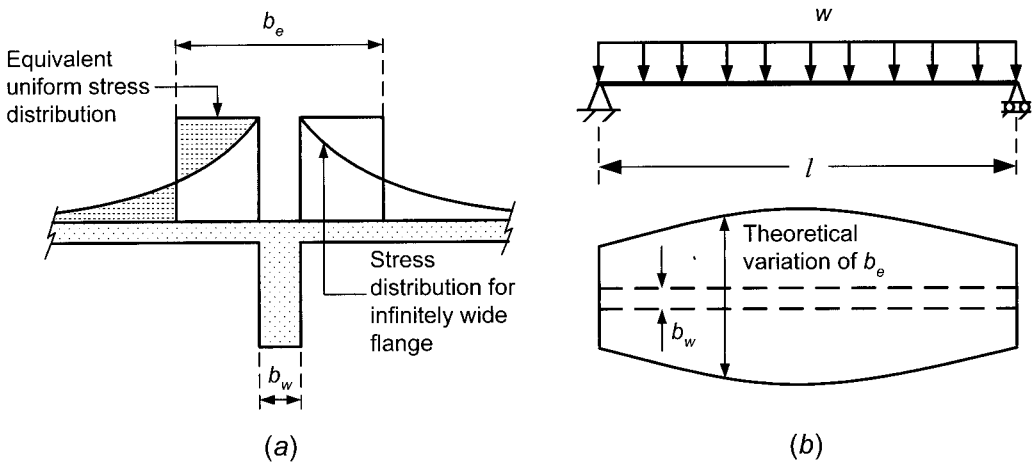

Figure 9.5 Distribution of compressive stresses in flanged beams and effective with, b_e.

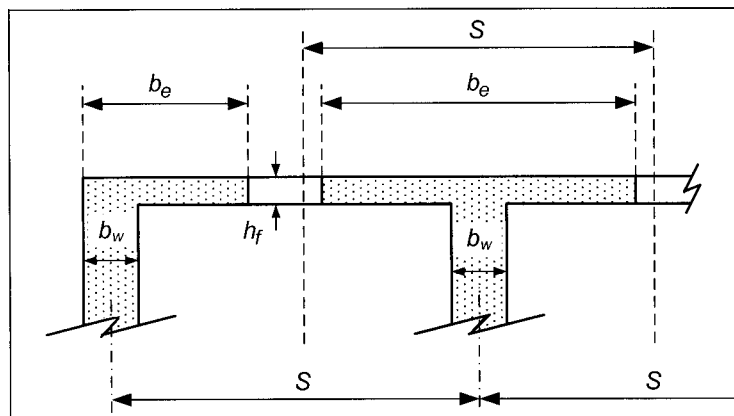

Source	Slab on one side	Slab on two sides
ACI	$b_e =$ lesser of $\begin{cases} b_w + 6h_f \\ (b_w + S)/2 \\ b_w + l/12 \end{cases}$	$b_e =$ lesser of $\begin{cases} b_w + 16h_f \\ S \\ l/4 \end{cases}$
AASHTO*	$b_e =$ lesser of $\begin{cases} b_w + 6h_f \\ (b_w + S)/2 \\ b_w + l/12 \end{cases}$	$b_e =$ lesser of $\begin{cases} b_w + 12h_f \\ S \\ l/4 \end{cases}$

* From AASHTO Standard specifications. The LRFD provisions are different and more complex.

Figure 9.6 Design values of effective flange width, b_e.

The ACI code and AASHTO specifications prescribe design values of the effective flange width b_e for reinforced and prestressed concrete noncomposite and composite flanged beams. They are summarized in Fig. 9.6 for beams with either a slab on one side only, such as end beams, or a slab on two sides, such as interior beams. They are to be used in determining the part of the section that resists the loads. Values given by AASHTO apply to nonisolated beams only (that are part of a slab system); if the beam is isolated, AASHTO imposes more stringent values of b_e.

In using I type precast sections, the value of b_w in Fig. 9.6 can be replaced by b_v, the width of the section at the interface with the slab. If a precast T section is used, it is safer to use b_w of the T, otherwise engineering judgment should be exercised in determining b_e. Note that some of the single T and double T standard precast-prestressed sections given in the PCI handbook have flange widths larger than the b_e values recommended in Fig. 9.6. However, as they are very efficiently designed and manufactured under plant conditions, such excess is considered acceptable.

The British code CP-110 recommends an effective flange width not to exceed the lesser of (1) the width of the web plus one-fifth the distance between points of zero moments, or (2) the actual width of the flange. For a continuous beam, the distance between points of zero moments can be taken as 70 percent of the clear span.

9.5.2 Transformed Flange Width

A prestressed composite beam is assumed to behave elastically under service load. The strain distribution along the entire section due to a bending moment is assumed linear and the stresses are calculated from the strains using Hooke's law. As two different materials are involved, the precast beam and the cast-in-place slab, and as each has a different modulus of elasticity, different stresses are generated in each material for the same strain. To account for this difference in design, one of the two materials or elements is transformed into a fictitious material or element having the same modulus of elasticity as the other one. This is done using the concept of transformed section, which is generally applied to the cast-in-place slab, transformed into a fictitious slab having same concrete as the precast beam. Figure 9.7a illustrates the assumptions and related computations, assuming the strength and elastic modulus of material A (precast beam) are larger than those of material B (cast-in-place slab). The two materials are assumed linear elastic. Linear strain distribution along the section suggests that the strain in material A would be same as that in material B, should material A replace material B. However, since the elastic modulus of A is larger than that of B, the stress σ_A will be larger than σ_B. To maintain the same compression force in the slab and the same centroid for that force, the slab depth is kept the same, but a new "transformed" width is needed.

Thus, typically the slab section of depth h_f and width b_e (Fig. 9.7b) is transformed into an equivalent section having same depth h_f and a transformed width b_{tr}. It can be easily shown (Fig. 9.7a) that b_{tr} is given by:

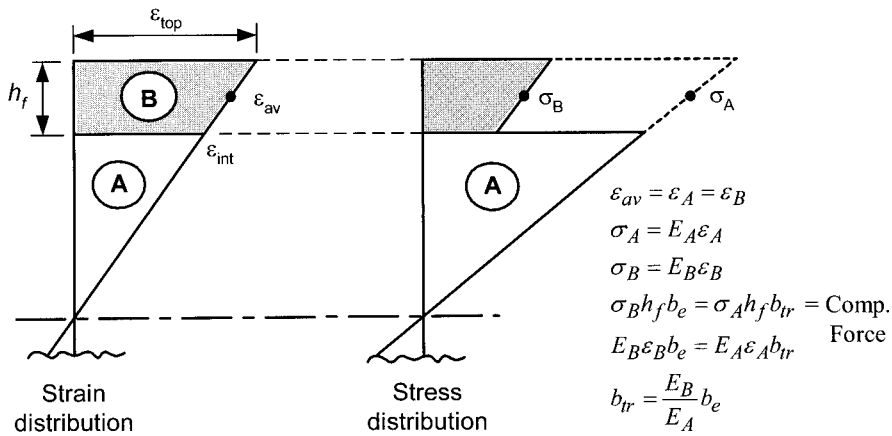

Figure 9.7*a* Effect of transforming material B into equivalent material A.

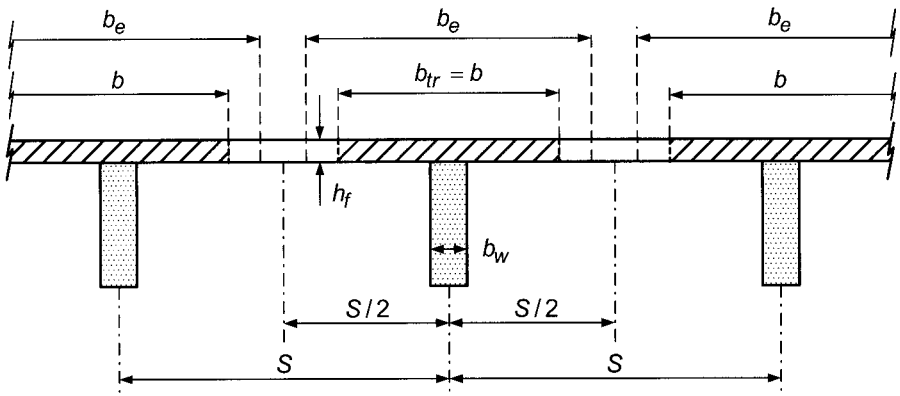

Figure 9.7*b* Transformed versus effective flange width.

$$b_{tr} = b_e \frac{(E_c)_{\text{CIPC}}}{(E_c)_{\text{PPC}}} = b_e n_c \tag{9.1}$$

where:

$(E_C)_{CIPC}$ = modulus of elasticity of the cast-in-place concrete slab

$(E_C)_{PPC}$ = modulus of elasticity of the precast-prestressed concrete beam

n_C = ratio of the above moduli = $\dfrac{(E_c)_{\text{CIPC}}}{(E_c)_{\text{PPC}}}$

Equation (9.1) ensures that, under bending (linear strain diagram), the total compressive force in the actual slab of width b_e is the same as the force in the transformed slab of width b_{tr} and having same modulus of elasticity as the precast beam.

9.5.3 Cross Section Properties of Composite Section

The use of a transformed width b_{tr} leads to a fictitious slab having the same strength and elastic modulus as the precast beam. Consequently, the composite section can also be considered transformed into an equivalent monolithic (non-composite) section having the same strength and modulus as the precast beam. Its geometric properties are determined and directly used in flexural design in the same manner as monolithic noncomposite sections (Fig. 9.8). In order to correlate with the notation used earlier to describe the flange width in general, let us call for the new transformed section:

$$b = b_{tr} \tag{9.2}$$

thus the area of the composite section is given by:

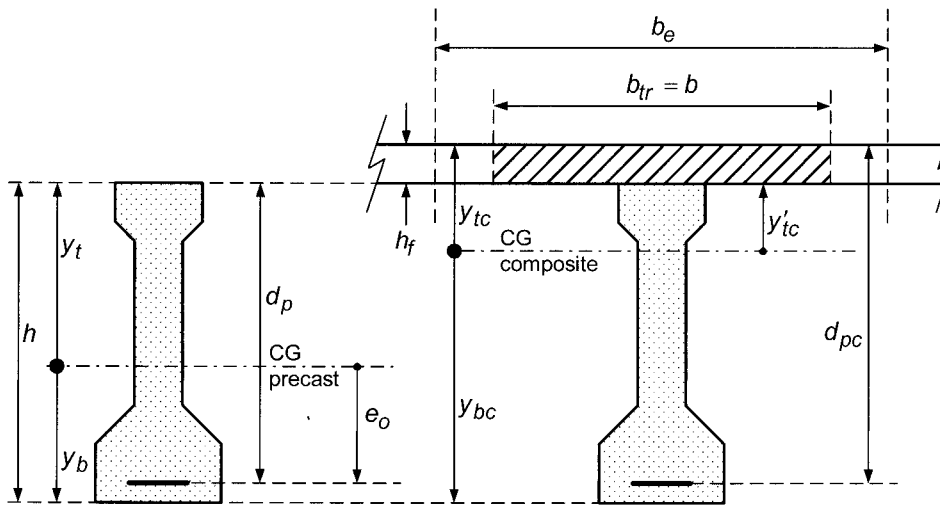

Figure 9.8 Geometric properties of precast and composite sections.

$$A_{cc} = A_c + h_f b_{tr} = A_c + h_f b = A_c + h_f b_e n_c \tag{9.3}$$

where A_c is the cross-sectional area of the precast concrete beam.

Other section properties listed in Fig. 9.8 are determined according to established procedures. The subscript c is used to differentiate them from those of the precast beam, such as Z_{bc} versus Z_b. An example is given in Section 9.11a.

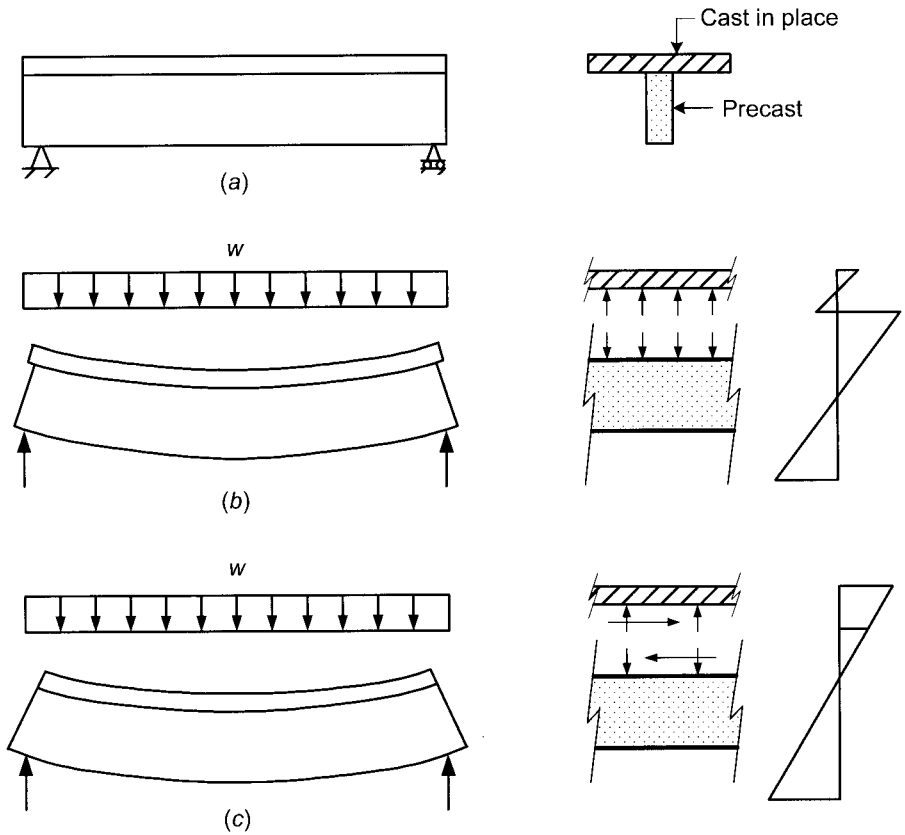

Figure 9.9 (*a*) Typical precast beam and cast-in-place slab. (*b*) Noncomposite action (zero interface shear). (*c*) Composite action (full interface shear).

9.6 INTERFACE SHEAR OR HORIZONTAL SHEAR

9.6.1 Evaluation of Horizontal Shear

The success of composite action depends on the shear resistance at the interface between the precast element and the cast-in-place element to allow full transfer of

stresses. If no shear resistance exists and a load is applied to the composite beam shown in Fig. 9.9*a*, the slab would slide with respect to the beam (Fig. 9.9*b*) and the system would act as if two separate elements were used. However, if sufficient shear resistance is provided, the slip between the two elements can be prevented and composite action can be counted on (Fig. 9.9*c*). Thus a good connection between the two components of the composite system is essential. This can be achieved by artificially roughening the interface surface, providing a bonding agent, and/or using shear connectors or ties, mostly in the form of extended stirrups. The problem of shear transfer in composite beams has been thoroughly researched and is relatively well documented [Refs. 9.4, 9.5, 9.7, 9.8, 9.11, 9.13, 9.15, 9.19, 9.20, 9.22, 9.27, 9.30].

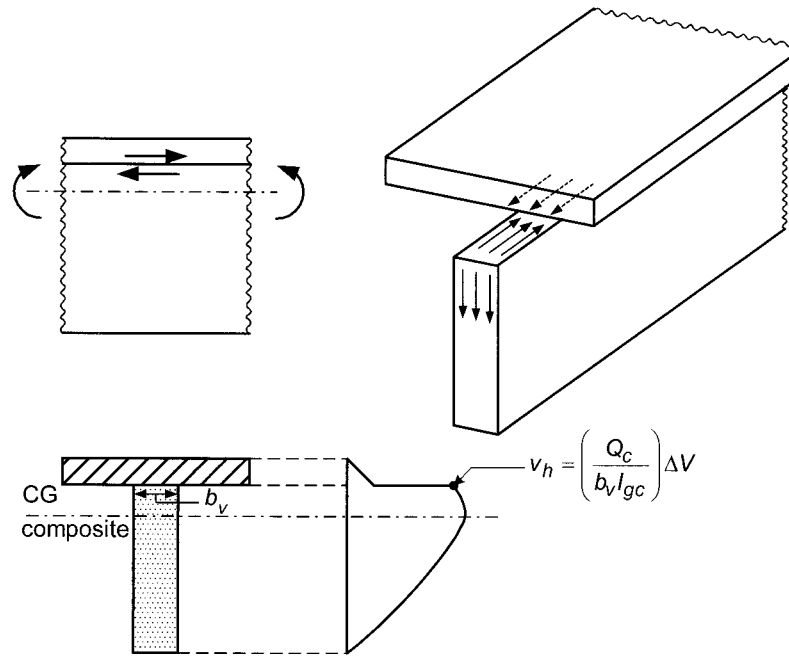

Figure 9.10 Interface horizontal shear stress.

The horizontal shear stress at the interface between the precast beam and the cast-in-place slab is generated by the loads acting on the composite section only. They are the additional dead load and live load, if the precast beam is unshored, to which the slab weight is added when the precast beam is shored. The horizontal shear stress due to bending is equal in magnitude to the vertical shear stress (Fig. 9.10) and can be derived for the interface surface as shown in Section 6.5, assuming an elastic uncracked section:

$$v_h = \frac{Q_c}{b_v I_{gc}} \Delta V \tag{9.4}$$

where:

Q_c = first static moment about the centroid of the composite section of the portion of section above the shear plane considered (that is essentially the flange)

b_v = width of shear plane considered (width of interface or contact surface)

I_{gc} = gross moment of inertia of composite section

ΔV = shear force acting on composite section only

For the same reasons as cited in Section 6.5 and for design purposes, the horizontal shear stress can be taken as:

$$v_h = \frac{\Delta V}{b_v d_{pc}} \tag{9.5}$$

where d_{pc} is the distance from the extreme compressive fiber of the composite section to the centroid of the prestressing steel (Fig. 9.11). It is also equal to the vertical shear stress generated by the same loading.

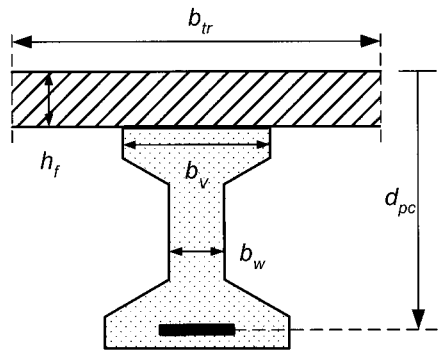

Figure 9.11

If ultimate strength design is considered, the use of ΔV in Eq. (9.5) becomes doubtful, since flexural cracking (or the neutral axis of bending) can cross the interface and the total shear force will be developed to maintain force equilibrium in the section. Thus, at ultimate, Eq. (9.5) is replaced by:

$$\boxed{v_{uh} = \frac{V_u}{b_v d_{pc}}} \tag{9.6}$$

where V_u is the factored total shear force and v_{uh} is the required design horizontal shear strength at the interface. Another way of analyzing the problem is through the

shear friction approach described in Section 9.6.2. In Eq. (9.6) the ACI code recommends the use of d_{pc} or $0.8h_c$, whichever is larger. If a partially prestressed precast beam is used, d_{pc} should be replaced by d_{ec}, the effective depth or distance to the centroid of the tensile force at ultimate (see Section 9.9).

9.6.2 ACI Code Provisions for Horizontal Shear at Contact Surface

An investigation of horizontal shear strength is required in all composite members and is treated similarly to other effects, such as vertical shear, bending, and the like.

Shear transfer resistance. As for vertical shear, torsion, and bending, the design for horizontal shear transfer is based on ultimate strength requirements. Shear forces are used by the ACI code, but equivalent shear stresses are preferably used in this text.

The design is based on satisfying the following relation:

$$\boxed{v_{uh} \le \phi v_{nh}} \tag{9.7}$$

where:

v_{uh} = factored design shear stress (Eq. 9.6)
v_{nh} = nominal horizontal shear strength
ϕ = strength reduction factor for shear = 0.75 (2002 ACI code)

The following limiting values of v_{nh} are recommended by the ACI code:

1. v_{nh} = 80 psi (0.55 MPa) when contact surfaces are clean, free of laitance, intentionally roughened to a full amplitude of 1/4 in (6.3 mm), and ties are not provided.
2. v_{nh} = 80 psi (0.55 MPa) when minimum ties (minimum area of stirrups extended through the contact surface) are provided in accordance with Eqs. (6.39) and (6.40) and the contact surfaces are not intentionally roughened but are clean and free of laitance. This means that the minimum shear reinforcement in the precast beam is extended to the cast-in-place slab and properly anchored. Minimum shear reinforcement is as specified in Chapter 6.
3. When both of the above conditions are simultaneously satisfied, that is, minimum ties are provided and the contact surfaces are intentionally roughened, clean, and free of laitance:

$$v_{nh} = \left(260 + \frac{0.6A_v f_y}{b_v s}\right)\lambda \le 500\ psi\ (3.45MPa) \tag{9.8}$$

where A_v is the area of minimum vertical tie or stirrups (extending through the contact surface), f_y is their yield strength, b_v is the width of the contact surface, s

is the tie spacing, and $\lambda = 1$ for normal weight concrete, $\lambda = 0.85$ for sand lightweight concrete, and $\lambda = 0.75$ all-lightweight (that is, sand and coarse aggregate) concrete. The value of f_y in the above equation should not be taken larger than 60 ksi (414 MPa).

Tie spacing, s, shall not exceed four times the least dimension of supported element (mostly slab thickness) or 24 in (600 mm). Ties for horizontal shear may consist of simple bars or wires, multiple leg stirrups, and vertical legs of smooth or deformed welded wire fabric. Ties must be fully anchored into all interconnected elements.

The minimum amount of vertical stirrups, designed according to Eq. (6.40), provides an equivalent shear stress resistance of 50 psi (0.345 MPa). Assuming these stirrups are extended as ties into the cast-in-place slab and assuming $b_v = b_w$, leads to a value of $v_{nh} = 290$ psi (2.03 MPa) from Eq. (9.8) for normal weight concrete. This value is significantly larger than the sum of resistances contributed from the limiting values in items (1) and (2) above, that is 160 psi (1.1 MPa).

Equation (9.8) can be used for v_{uh} up to 500ϕ psi (3.45ϕ MPa). If v_{uh} exceeds 500ϕ psi (3.45ϕ MPa) at the section considered, the design of tie reinforcement should proceed in accordance with shear friction theory, as described in Section 11.7 of the code, and summarized next; it is based on evaluating the shear friction at the contact surface between the precast beam and the cast-in-place slab. In any case, the value of v_{nh} shall not exceed $0.2f'_c$ or 800 psi (5.52 MPa), whichever is smaller; otherwise, section dimensions have to be changed.

Tie Reinforcement Using Shear Friction. According to the commentary of the ACI code, the design approach for shear friction assumes that a horizontal crack will form at the interface between the precast and the cast-in-place elements. Shear or tie reinforcement of area A_{vf} is provided to prevent this crack from causing failure. The slip of one crack face with respect to the other is accompanied by crack opening due to the roughness of the crack surfaces (Figs. 9.12*a* and 9.12*b*). Such opening is sufficient to cause yielding of the reinforcement crossing the crack, hence providing a clamping force $A_{vf}f_y$ across the crack faces. This interaction is illustrated by a friction model in Fig. 9.12c assuming a block subjected to a vertical force N equal to the yielding force of the reinforcement.

The applied shear is then resisted by a combination of (1) friction between the crack faces, (2) resistance of the protrusions on the crack faces to shearing, and (3) dowel action of the reinforcement (Fig. 9.12b). However, in the shear friction method it is assumed that all the shear resistance is due to friction between the crack faces. Hence, artificially high values of the friction coefficient μ are used in order to correlate predicted shear strengths with test results [Refs. 9.11, 9.19, 9.20, 9.22, 9.24].

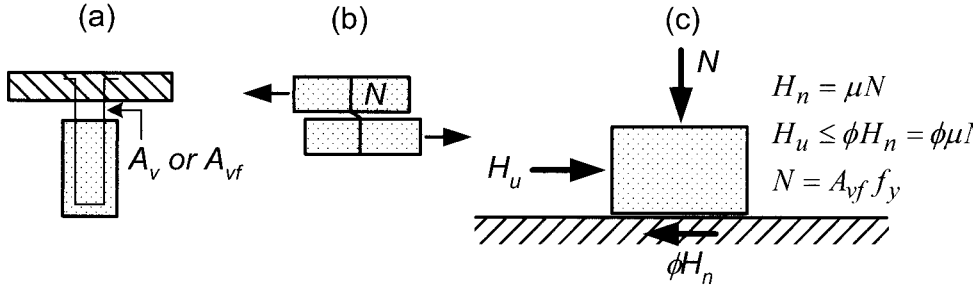

Figure 9.12 Illustration of shear friction resistance.

Referring to Fig. 9.12*c*, which describes how the frictional resistance is developed to balance the horizontal sliding force, the required area of shear-friction reinforcement can be calculated from:

$$A_{vf} = \frac{H_u}{\phi f_y \mu} \tag{9.9}$$

where:

H_u = total horizontal shear force at the interface (see explanation below)

f_y = design yield strength of shear reinforcement not to exceed 60 ksi (414 MPa)

ϕ = 0.75 according to the 2002 ACI code

μ = frictional coefficient to be taken equal to 1.4λ when concrete is placed monolithically, 1λ when concrete is placed against hardened concrete with intentionally roughened surface, and 0.7λ when concrete is placed against steel; a value of 0.4λ is recommended in the PCI handbook for concrete placed against smooth concrete.

λ = 1 for normal weight concrete, $\lambda = 0.85$ for sand-lightweight concrete, and $\lambda = 0.75$ for all-lightweight (that is, sand and coarse aggregate) concrete.

The value of H_u can be estimated by summing up the horizontal factored shear stresses over half the span for a simply supported beam and, as a first approximation, over ¼ the span for a continuous beam (assuming the points of zero moments are at the ¼ span). The corresponding value of A_{vf} is to be distributed over the distance considered, that is, ½ or ¼ the span length.

Alternatively, H_u may be determined as the horizontal force needed at the interface to allow the nominal moment resistance of the midspan section, or section of maximum moment, to develop (Fig. 9.13). Its value depends on whether the

neutral axis at ultimate is in the flange or in the web (precast beam). Using the ACI assumptions for the stress block at ultimate leads to:

$$H_u = \text{ the smaller of } \begin{cases} 0.85(f'_c)_{slab} b_e a \\ \text{and} \\ 0.85(f'_c)_{slab} b_e h_f \end{cases} \tag{9.10}$$

where h_f is the depth of the cast-in-place slab, and a is the depth of the stress block at ultimate. An insignificant error would result in the value of H_u should the properties of the transformed section be used in Eq. (9.10), that is, b_{tr} and $(f'_c)_{\text{precast}}$.

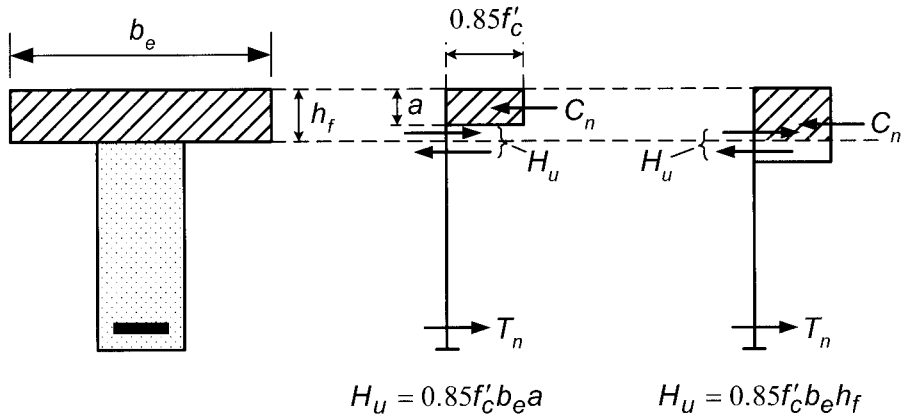

Figure 9.13 Interface shear at ultimate flexural capacity.

Tie Reinforcement at a Given Section. The author suggests another alternative to determining the area of tie reinforcement, which is slightly different from the above approach, but correlates well with the approach generally used for shear and torsion, in which the design requirements are checked at a given section, and repeated at other sections.

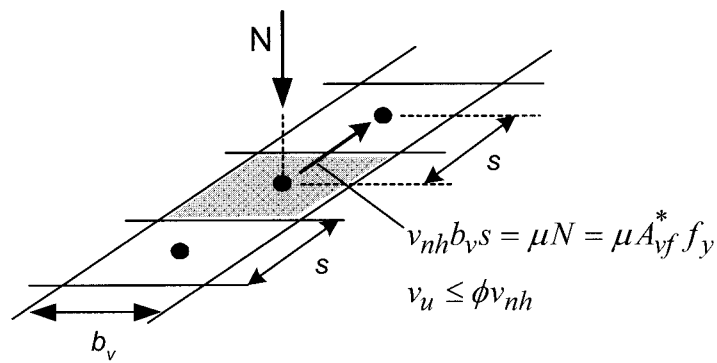

Figure 9.14

Referring to Fig. 9.14 and assuming the tie spacing is s, the tributary shear area of interface (or contact surface) covered by one tie is given by $b_v s$. Using the same principle of shear friction as above, the product of the nominal horizontal shear stress, v_{nh}, by the tributary area balances the frictional force μN provided by a vertical tie, leading to:

$$v_{nh} = \frac{A_{vf}^* f_y \mu}{b_v s} \tag{9.11}$$

where:

A_{vf}^* = area of shear-friction reinforcement extending across the interface over a distance s

s = spacing of shear-friction reinforcement, assumed vertical

and other notation is as defined earlier.

For the purpose of design we want at any section:

$$v_{uh} = \phi v_{nh} \tag{9.12}$$

Replacing v_{uh} by its value from Eq. (9.6) and v_{nh} by its value from Eq. (9.11) in Eq. (9.12) leads to:

$$A_{vf}^* = \frac{V_u}{\phi f_y \mu} \frac{s}{d_{pc}} \tag{9.13}$$

Similarly to the procedure for vertical shear reinforcement, the value of A_{vf}^* is to be determined at each section. This is unlike the value of A_{vf} from Eq. (9.9) which represents a total value of tie reinforcement to be distributed over the shear span. The possible advantage of Eq. (9.13) is that, in a computerized procedure, where every section is analyzed, tie reinforcement for a composite beam can be checked or designed at the same time as vertical shear reinforcement at every section.

A horizontal shear stress value, v_{uh}, of more than 500ϕ psi (3.45ϕ MPa) is seldom encountered in practice. Many composite members used in buildings, such as T's, double T's, and hollow-core slabs where a thin cast-in-place "topping" of about 50 mm in thickness is in full contact with the precast unit throughout its width, generally do not require any tie reinforcement (i.e., the shear stress is shown to be less than 80 psi (0.55 MPa)). Also, it is physically difficult to extend and bend the ties to properly anchor them in such thin elements. However, in most other cases of composite construction, it is good practice, whenever possible, to automatically extend the vertical stirrups into the cast-in-place slab, even if it is shown by design that this is not necessary.

An example, illustrating some of the computations for horizontal shear transfer, is given in Section 9.11*g*.

The AASHTO LRFD provisions on tie reinforcement in composite beams are summarized in Section 9.12 and illustrated in the example of Section 14.10.

9.7 FLEXURE: WORKING STRESS ANALYSIS AND DESIGN

Most of the concepts developed in Chapter 4 for the analysis and design of noncomposite beams apply to composite beams. The section properties of both the precast beam and the transformed composite beam (Fig. 9.8) are used when needed. The adopted notation and terminology are to be correlated with those of Chapter 4.

9.7.1 Extreme Loadings

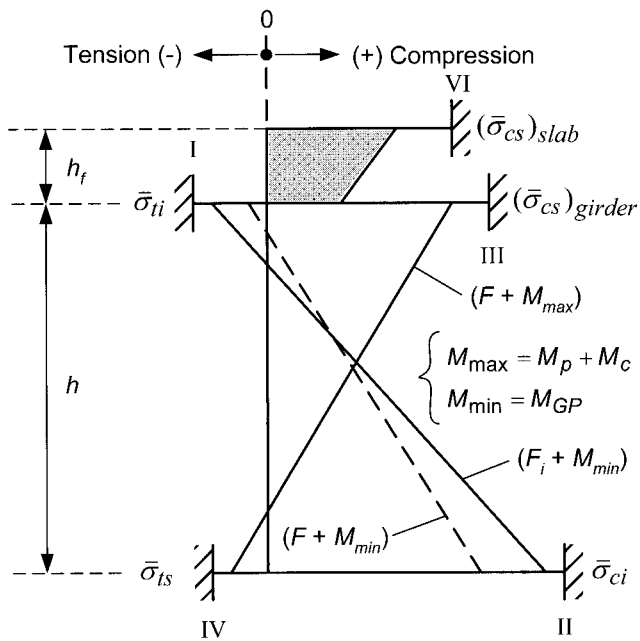

Figure 9.15 Extreme loading's stresses in composite section.

Whether the beam is shored or not, two extreme loading conditions for the composite system can be identified and essentially bound all others in terms of extreme fiber stresses on the precast beam (Fig. 9.15). The first extreme loading is the initial loading under initial prestressing force and self-weight of the precast beam, that is, (F_i + M_{GP} or M_{min}); the second extreme loading corresponds to the cumulative effects of the final prestressing force, self-weight of beam, weight of cast-in-place slab, additional dead load, and live load, that is, (F + M_{max}). In between these two

loadings the beam changes from noncomposite to composite and the corresponding bending moments generate different types of stresses. In order to follow the variations of stresses, the bending moment M_{max} is broken down into two parts, M_p and M_c, representing the maximum bending moments on the precast and composite sections, respectively (see also Table 9.1).

9.7.2 Stress Inequality Conditions

Assuming positive moments only, five stress inequality conditions can be written for the composite beam and are of the form:

$$\text{(Actual stress)} \left\{ \begin{matrix} \geq \\ \text{or} \\ \leq \end{matrix} \right\} \text{(Allowable stress)} \tag{9.14}$$

Four allowable stresses are binding for the precast beam and one for the cast-in-place slab. The two stress inequality conditions for the first extreme loading are identical to the noncomposite beam case (Table 4.2). They are given in Table 9.2 and are numbered I and II. Two other stress inequality conditions (numbered III and IV) can be written for the precast beam under the second extreme loading, and one condition can be written for the cast-in-place slab (numbered VI). In addition, the practicality condition, which states that the prestressing steel must be placed inside the section, also applies here and is given the same number (V) as in Tables 4.2 and 4.3.

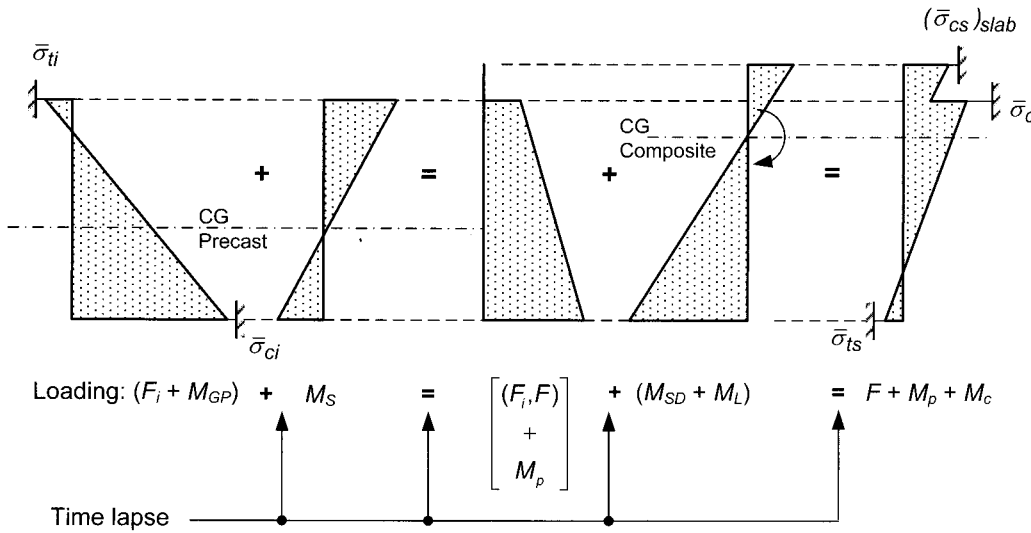

Figure 9.16 Loadings and corresponding stress diagrams: unshored composite beam.

Let us develop stress conditions III, IV, and VI for the composite beam, assuming unshored construction first. Referring to the stress-versus-loading diagrams of Fig. 9.16 and summing up the stresses on the top fiber of the precast beam we have:

$$\frac{\eta F_i}{A_c}\left(1-\frac{e_o}{k_b}\right)+(M_{GP}+M_S)/Z_t+(M_{SD}+M_L)\frac{y'_{tc}}{I_{gc}}\le \bar{\sigma}_{cs} \qquad (9.15)$$

where:

M_{GP} = bending moment due to self-weight of precast prestressed beam or girder
M_S = bending moment due to cast-in-place slab
M_{SD} = bending moment due to superimposed dead load
M_L = bending moment due to live load
y'_{tc} = distance from centroid of composite beam to top fiber of precast beam = $h - y_{bc}$

In the above equation, we have used the final value of the prestressing force. However, the effect of time, when needed, should not be ignored; it is described as "time lapse" in Fig. 9.16 and the notation (F_i, F) is used to remind the reader that any value between F_i and F may also apply, when relevant.

If the precast beam is shored during casting and curing of the cast-in-place slab, the slab weight will apply only when the section acts as a composite section. Referring to Fig. 9.17, the third stress inequality condition leads to:

$$\frac{\eta F_i}{A_c}\left(1-\frac{e_o}{k_b}\right)+M_{GP}/Z_t+(M_S+M_{SD}+M_L)\frac{y'_{tc}}{I_{gc}}\le \bar{\sigma}_{cs} \qquad (9.16)$$

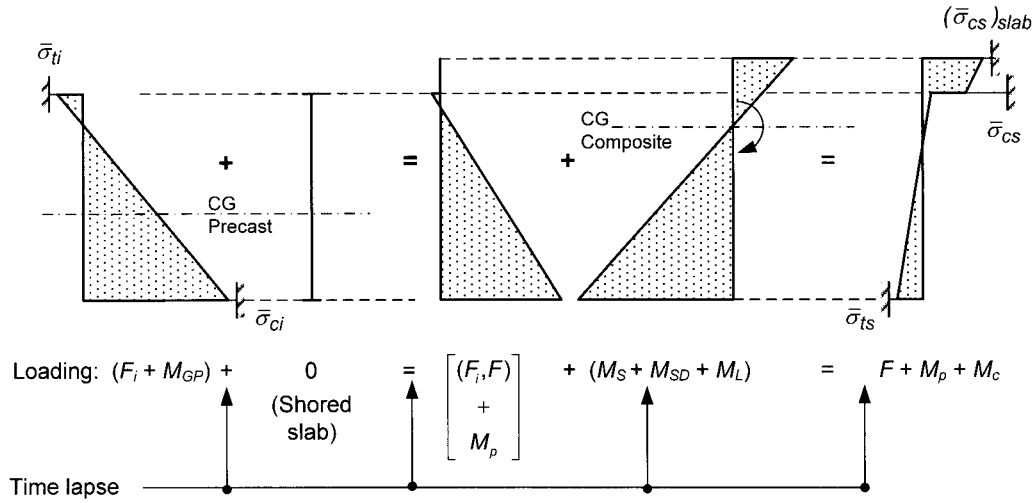

Figure 9.17 Loadings and corresponding stress diagrams: shored composite beam.

Equations (9.15) and (9.16) can be rewritten in a single form emphasizing the separate effects of the moments acting on the precast and composite beams, respectively, that is:

$$\frac{\eta F_i}{A_c}\left(1-\frac{e_o}{k_b}\right)+\frac{M_p}{Z_t}+\frac{M_c}{Z'_{tc}} \le \bar{\sigma}_{cs} \tag{9.17}$$

where:

M_p = sum of external bending moments acting on the precast beam
M_c = sum of external bending moments acting only on the composite beam
Z'_{tc} = I_{gc}/y'_{tc}

Table 9.2 Useful ways of writing the stress inequality conditions for composite sections.

Way	Stress condition	Inequality equation
1	I	$(F_i/A_c)[1-(e_o/k_b)]+M_{GP}/Z_t \ge \bar{\sigma}_{ti}$
	II	$(F_i/A_c)[1-(e_o/k_t)]-M_{GP}/Z_b \le \bar{\sigma}_{ci}$
	III	$(\eta F_i/A_c)[1-(e_o/k_b)]+M_p/Z_t+M_c/Z'_{tc} \le \bar{\sigma}_{cs}$
	IV	$(\eta F_i/A_c)[1-(e_o/k_t)]-M_p/Z_b-M_c/Z_{bc} \ge \bar{\sigma}_{ts}$
2	I	$e_o \le k_b+(1/F_i)(M_{GP}-\bar{\sigma}_{ti}Z_t)$
	II	$e_o \le k_t+(1/F_i)(M_{GP}+\bar{\sigma}_{ci}Z_b)$
	III	$e_o \ge k_b+(1/F_i)[(M_p+M_cZ_t/Z'_{tc}-\bar{\sigma}_{cs}Z_t)/\eta]$
	IV	$e_o \ge k_t+(1/F_i)[(M_p+M_cZ_b/Z_{bc}+\bar{\sigma}_{ts}Z_b)/\eta]$
3	I	$F_i \le (M_{GP}-\bar{\sigma}_{ti}Z_t)/(e_o-k_b)$
	II	$F_i \le (M_{GP}+\bar{\sigma}_{ci}Z_b)/(e_o-k_t)$
	III	$F=\eta F_i \ge (M_p+M_cZ_t/Z'_{tc}-\bar{\sigma}_{cs}Z_t)/(e_o-k_b)$
	IV	$F=\eta F_i \ge (M_p+M_cZ_b/Z_{bc}+\bar{\sigma}_{ts}Z_b)/(e_o-k_t)$
All	V	$e_o \le (e_o)_{mp}=y_b-(d_c)_{\min}=$ maximum practical eccentricity
	VI	$\frac{M_c}{Z_{tc}}\frac{(E_c)_{CIPC}}{(E_c)_{PPC}}=\frac{M_c}{Z_{tc}}n_c \le (\bar{\sigma}_{cs})_{\text{slab}}$

Note: to satisfy the second provision on allowable compression given in the 2002 ACI code for stress condition III, replace $\bar{\sigma}_{cs}$ by $\bar{\sigma}_{csus}$ and consider a live load moment equal zero.

The values of M_p and M_c are given for the unshored case by:

$$M_p = M_{GP} + M_S \tag{9.18}$$
$$M_c = M_{SD} + M_L \tag{9.19}$$

and for the shored case by:

$$M_p = M_{GP} \tag{9.20}$$
$$M_c = M_S + M_{SD} + M_L \tag{9.21}$$

Any additional load, such as weight of diaphragms or weight of attached elements, not accounted for in Eqs. (9.18) to (9.21) can be added to the values of M_p or M_c where appropriate (Table 9.1).

Following exactly the same approach, the fourth stress inequality condition related to the bottom fiber of the composite section at maximum load leads to:

$$\frac{\eta F_i}{A_c}\left(1-\frac{e_o}{k_t}\right)-\frac{M_p}{Z_b}-\frac{M_c}{Z_{bc}} \geq \bar{\sigma}_{ts} \tag{9.22}$$

with the notation as defined earlier.

The last stress inequality condition (VI) states that the maximum compressive stress in the cast-in-place slab top fiber at full service load is less than or equal to the allowable compressive stress in the slab, thus:

$$\frac{M_c}{Z_{tc}}\frac{(E_c)_{CIPC}}{(E_c)_{PPC}} = \frac{M_c}{Z_{tc}} n_c \leq (\bar{\sigma}_{cs})_{\text{slab}} \tag{9.23}$$

All the above stress inequality conditions are summarized in Table 9.2 and can be directly correlated with Tables 4.2 and 4.3 given for the noncomposite case. Three different ways of writing these equations are proposed, each emphasizing a particular variable, namely, the stress, the eccentricity e_o, and the prestressing force.

The sixth condition corresponding to Eq. (9.23) is largely satisfied in the great majority of cases. The five others can be treated in a manner exactly similar to that followed in Chapter 4. Thus the working stress analysis and design of composite beams are reduced to those of noncomposite beams and the concepts developed in Chapter 4 apply here with the equations given in Table 9.2. Hence a geometric feasibility domain can be built for composite beams from which a wide variety of solutions can be found. Some particular points are addressed next. An example is covered in Sec. 9.11*b*. Note that in Table 9.2, the eccentricity e_o is taken with respect to the centroid of the precast beam.

ACI and AASHTO Load-Stress Combinations. The 2002 ACI building code specifies two allowable stresses for the maximum compression in service: the first one, $\bar{\sigma}_{cs}$, is associated with the maximum service moment and is the one considered above in deriving stress condition III; a second allowable stress, $\bar{\sigma}_{csus}$, is associated with the moment due to the sustained load only. The corresponding stress condition formulation is essentially the same as above; for this, Eqs. (9.15) and (9.16) can be used with M_L taken equal to zero and $\bar{\sigma}_{cs}$ replaced by $\bar{\sigma}_{csus}$.

The AASHTO LRFD Bridge Design Specifications specify three allowable stresses for the maximum compression in service (see Table 14.3). They can also be easily formulated in a manner similar to the above.

However, in order not to delve into too many equations and possible load-stress combinations, the derivations in this chapter will focus mainly on the combination corresponding to the maximum service moment and $\bar{\sigma}_{cs}$ as shown in Eqs. (9.15) to (9.17) and in Table 9.2.

9.7.3 Feasible Domain, Limit Kern, Steel Envelopes

The following design similarities exist between a composite and a noncomposite beam:

1. The geometric feasibility domain can be built for the precast prestressed beam using the four stress inequality conditions (Table 9.2, way 2). Thus all the feasible combinations of F_i and e_o can be identified.

2. The second combination for stress condition III with the sustained load moment and $\bar{\sigma}_{csus}$ can be easily checked and used in the feasibility domain, should it control.

3. If a precast beam is properly selected a feasible domain will generally exist. It is then very likely that the prestressing force can be determined from stress condition IV (Table 9.2, way 3) in which e_o is replaced by $(e_o)_{mp}$.

4. Equations giving the upper and lower limits of the limit kern, k'_t and k'_b, for the precast beam, are the same as Eqs. (4.22) and (4.23) used for the noncomposite beam.

5. It can easily be shown (from Table 9.2, way 2, and Section 4.12.2) that the envelopes of the prestressing steel in the precast beam are given at any section along the span by:

Upper limit:

$$e_{ou} = \text{Larger algebraically of} \begin{cases} k_b\left(1-\dfrac{\bar{\sigma}_{cs}}{\sigma_g}\right)+\dfrac{M_p + M_c Z_t / Z'_{tc}}{F} & (9.24) \\ \text{and} \\ k_t\left(1-\dfrac{\bar{\sigma}_{ts}}{\sigma_g}\right)+\dfrac{M_p + M_c Z_b / Z_{bc}}{F} & (9.25) \end{cases}$$

Lower limit:

$$e_{ol} = \text{Smaller algebraically of} \begin{cases} k_b\left(1-\dfrac{\bar{\sigma}_{ti}}{\sigma_{gi}}\right)+\dfrac{M_{GP}}{F_i} & (9.26) \\ \text{and} \\ k_t\left(1-\dfrac{\bar{\sigma}_{ci}}{\sigma_{gi}}\right)+\dfrac{M_{GP}}{F_i} & (9.27) \end{cases}$$

9.7.4 Cracking Moment

Assuming the positive moment leading to cracking in a composite beam is larger than M_p, its value (in excess of M_p) for a simply supported beam may be obtained from:

$$\Delta M_{cr} = \frac{Z_{bc}}{Z_b}[\eta F_i(e_o - k_t) - M_p] - f_r Z_{bc} \qquad (9.28)$$

where f_r is the modulus of rupture of the concrete of the precast beam. Thus, the total moment leading to cracking in the composite beam is given by:

$$M_{cr} = \Delta M_{cr} + M_p \qquad (9.29)$$

9.7.5 Minimum Section Moduli of Composite Sections

As discussed in Section 4.10 for non-composite sections, it is also possible to use the stress inequality conditions to specify minimum values of section moduli for a composite section. That is, the four stress inequality conditions are used to determine four unknowns, namely, F, e_o, and the two section moduli of a beam. In the following derivations, it will be assumed that the compressive stress in the cast-in-place slab is not critical, and that the maximum moment is used in combination with $\bar{\sigma}_{cs}$ for the allowable compression in service.

Let us assume that we have a cross section, such that at the critical (say midspan) section of the beam the two allowable stresses $\bar{\sigma}_{ti}$ and $\bar{\sigma}_{ci}$ are exactly attained under initial loading. Referring to Fig. 9.18, the corresponding flexural stress diagram under $(F_i + M_{min})$ is represented by line *ab*.

Let us assume that prestress losses occur suddenly, and that the loading becomes $(F + M_{min})$, thus leading to the stress diagram *a'b'*. Let us also assume that an additional moment ΔM is applied and that the stresses on the top and bottom fiber reach exactly their allowable values, $\bar{\sigma}_{ts}$ and $\bar{\sigma}_{cs}$, respectively under ΔM. The above conditions, under which all four allowable stresses are exactly attained, define the minimum section moduli, that is, a beam with smaller section moduli will not be acceptable. The analytical derivation leads to slightly different equations depending on whether the beam is shored or not.

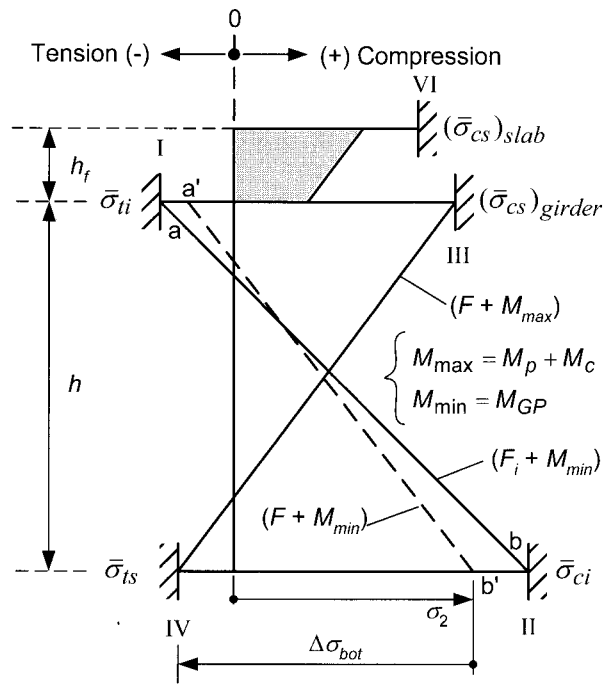

Figure 9.18

Unshored Beams. Consider the bottom fiber of the precast beam (Fig. 9.18). For the initial loading we have:

$$\sigma_{ci} = \bar{\sigma}_{ci} = \frac{F_i}{A_c}\left(1 - \frac{e_o}{k_t}\right) - \frac{M_{GP}}{Z_b} \tag{9.30}$$

from which:

$$\frac{F_i}{A_c}\left(1-\frac{e_o}{k_t}\right)=\bar{\sigma}_{ci}+\frac{M_{GP}}{Z_b} \tag{9.31}$$

Assuming all prestress losses occur immediately after release of prestress leads to a loading ($F + M_{min}$); using Eq. (9.31), the stress on the bottom fiber becomes:

$$\sigma_2 = \frac{\eta F_i}{A_c}\left(1-\frac{e_o}{k_t}\right)-\frac{M_{GP}}{Z_b}=\eta\left[\bar{\sigma}_{ci}+\frac{M_{GP}}{Z_b}\right]-\frac{M_{GP}}{Z_b}=\eta\bar{\sigma}_{ci}-(1-\eta)\frac{M_{GP}}{Z_b} \tag{9.32}$$

If we add a moment of amplitude ΔM to the section, the corresponding additional tensile stress on the bottom fiber of the precast beam will be:

$$\Delta\sigma_{bot}=-\frac{M_S}{Z_b}-\frac{M_c}{Z_{bc}} \tag{9.33}$$

The resulting stress due to the combined effect of ($F + M_{min} + \Delta M$) must be more than or equal to the allowable tensile stress in service, $\bar{\sigma}_{ts}$, that is:

$$\sigma_2+\Delta\sigma_{bot}\geq\bar{\sigma}_{ts} \tag{9.34}$$

Using Eqs. (9.32) and (9.33) in Eq. (9.34) gives:

$$\eta\bar{\sigma}_{ci}-(1-\eta)\frac{M_{GP}}{Z_b}-\frac{M_S}{Z_b}-\frac{M_c}{Z_{bc}}\geq\bar{\sigma}_{ts} \tag{9.35}$$

which leads to:

$$\boxed{Z_b\geq\frac{(1-\eta)M_{GP}+M_S}{(\eta\bar{\sigma}_{ci}-\bar{\sigma}_{ts})-M_c/Z_{bc}}} \tag{9.36}$$

Similarly, it can be shown that, for the top fiber, the section modulus must satisfy the following condition:

$$\boxed{Z_t\geq\frac{(1-\eta)M_{GP}+M_S}{(\bar{\sigma}_{cs}-\eta\bar{\sigma}_{ti})-M_c/Z'_{tc}}} \tag{9.37}$$

where: $Z'_{tc}=I_{gc}/y'_{tc}$ *and* $Z_{bc}=I_{gc}/y_{bc}$ as defined in Fig. 9.8.

In the above equations (Eqs. 9.36 and 9.37), it is essential for the denominator to be positive; this can be achieved by setting the following two conditions:

$$Z_{bc} \geq \frac{M_C}{(\eta\bar{\sigma}_{ci} - \bar{\sigma}_{ts})} \tag{9.38}$$

$$Z'_{tc} \geq \frac{M_C}{(\bar{\sigma}_{cs} - \eta\bar{\sigma}_{ti})} \tag{9.39}$$

The main remarks noted in Section 4.10 for noncomposites beams also apply here. Note that the above equations depend on the value of $M_{GP} = M_{min}$, which is unknown since Z_t and Z_b are unknowns. However a small number of iterations will lead to an acceptable beam section. This is illustrated in the example of Section 9.7.6.

Shored Beams. Using an approach similar to the one above, it can be shown that for a shored beam the following conditions are obtained:

$$\boxed{Z_b \geq \frac{(1-\eta)M_{GP}}{(\eta\bar{\sigma}_{ci} - \bar{\sigma}_{ts}) - M_c / Z_{bc}}} \tag{9.40}$$

$$\boxed{Z_t \geq \frac{(1-\eta)M_{GP}}{(\bar{\sigma}_{cs} - \eta\bar{\sigma}_{ti}) - M_c / Z'_{tc}}} \tag{9.41}$$

The main difference between the shored and the unshored beam (Eqs. 9.36 and 9.37) is in the moment M_S, due to the cast-in-place slab, which is now included in the value of M_c. The moments are assumed to be those at the midspan section, or critical section, of the beam.

9.7.6 Example: Selection of Optimum Beam from a Given Set of Beams

The floor of a low rise hotel/motel structure is made out of standard hollow-core concrete slab elements to be covered by a 2-in thick concrete topping (Fig. 9.19). The slab elements are assumed simply supported on walls with a span of 40 ft. They are available from the local precast-prestressed concrete manufacturer in sections that are four feet wide and of different depths. Dimensions and properties are given in Table 9.3 for the precast sections, and Table 9.4 for the composite sections. Note that $Z'_{tc} = I_{gc}/y'_{tc}$ as defined in Fig. 9.8. Normal-weight concrete of unit weight 150 pcf is used for the topping, thus making the topping weight equal to 25 psf or 100 plf. The weight of each section is given by the manufacturer in Table 9.3 and corresponds approximately to a unit weight of concrete of 142 pcf. Unshored construction is specified.

Other information is given as follows:

$f'_c = 5000$ psi; $f'_{ci} = 3500$ psi; $f'_{c-topping} = 4000$ psi;
$\bar{\sigma}_{ti} = -184$ psi; $\bar{\sigma}_{ci} = 2100$ psi; $\bar{\sigma}_{cs} = 3000$ psi; $\bar{\sigma}_{csus} = 2250$ psi; $\bar{\sigma}_{ts} = -424$ psi;
$E_c = 4287$ ksi; $E_{c-topping} = 3834$ ksi; $b_{tr} = 42.912$ in; span = 40 ft; $(e_o)_{mp} = y_b - 1.5$ in;
superimposed dead load plus live load = 80 psf; $f_{pe} = 155$ ksi; area of one strand = 0.153 in^2.

Select the least weight beam which satisfies the working stress design requirements in flexure and determine the corresponding values of F and e_o at midspan. Assume $f_{pe} = 155$ ksi, $\eta = 0.85$, and 1/2 in diameter strands with $A_{ps} = 0.153$ in^2 per strand.

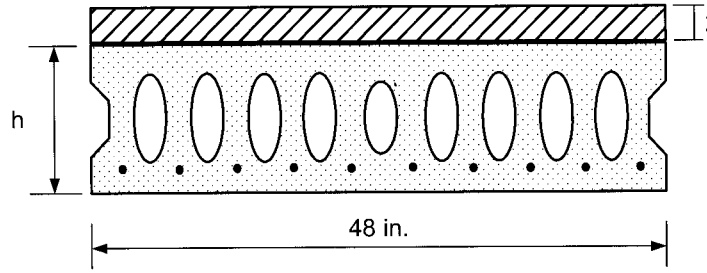

Figure 9.19
Standard hollow-core slab element with topping.

Table 9.3 Properties of standard normal weight concrete hollow-core slab sections.
(Licenced by Spancrete Machinery Corp.)

Section	Untopped - Noncomposite								
Width (in) × Depth (in)	A_c in^2	y_b in	y_t in	I_g in^4	Z_b in^3	Z_t in^3	k_b in	k_t in	w_G plf
48 × 4	138	2.00	2.00	238	119	119	0.86	-0.86	136
48 × 6	189	2.93	3.07	762	260.07	248.2	1.31	-1.37	184
48 × 8	258	3.98	4.02	1,806	453.77	449.25	1.74	-1.76	252
48 × 10	312	5.16	4.84	3,484	675.19	719.83	2.31	-2.16	304
48 × 12	355	6.28	5.72	5,784	921.02	1011.18	2.85	-2.59	344
48 × 15	370	7.87	7.13	9,765	1240.79	1369.56	3.70	-3.35	360

Table 9.4 Properties of composite hollow-core slab sections with 2 in topping.*

Section	Composite*, with 2 in topping					
Width (in) × Depth (in)	y_{bc} in	I_{gc} in^4	w_{Gc} plf	Z_{bc} in^3	Z'_{tc} in^3	y'_{tc} in
48 × 4	3.15	743	236	236	874	0.85
48 × 6	4.20	1,768	284	421	983	1.80
48 × 8	5.23	3,458	352	661	1249	2.77
48 × 10	6.42	5,808	404	905	1622	3.58
48 × 12	7.59	8,934	444	1177	2025	4.41
48 × 15	9.40	14,398	460	1532	2571	5.60

* $f'_c = 5000$ psi; $f'_{ci} = 3500$ psi; $f'_{c-topping} = 4000$ psi; $b_{tr} = 42.912$ in.

For any beam in the table:

$$M_{GP} = W_G \frac{l^2}{8} = W_G \frac{40^2}{8} = 200 W_G \text{ kips-ft} \quad \text{where } W_G \text{ is in klf}$$

$$M_G = 2400 W_G \quad \text{where } W_G \text{ is in plf (as in Table 9.3) and } M_G \text{ is in lb-in}$$

The cast-in-place topping, which here represents the composite slab, leads to a moment:

$$M_S = 0.1 \frac{40^2}{8} = 20 \text{ kips-ft} = 240{,}000 \text{ lb-in.}$$

For a floor live load of 80 psf, the beam live load per linear foot is: 80x4 = 320 plf = 0.32 klf. Thus:

$$M_c = M_L = 0.32 \frac{40^2}{8} = 64 \text{ kips-ft} = 768{,}000 \text{ lb-in.}$$

In order not to start with negative values of section moduli, the required section moduli must be such that (Eqs. 9.38 and 9.39):

$$Z_{bc} \geq \frac{M_c}{(\eta \bar{\sigma}_{ci} - \bar{\sigma}_{ts})} = \frac{768{,}000}{(0.85 \times 2100 + 424)} = \frac{768{,}000}{2209} = 347.67 \text{ in}^3$$

$$Z'_{tc} \geq \frac{M_c}{(\bar{\sigma}_{cs} - \eta \bar{\sigma}_{ti})} = \frac{768000}{(3000 + 0.85 \times 184)} = \frac{768000}{3156.4} = 243.32 \text{ in}^3$$

From Table 9.4, we cannot select the slab with depth = 4 in since its Z_{bc} value is less than 347.67 in^3. Hence, for the first iteration, we start by the element of depth 6 in. The properties of the selected slab element must satisfy the following two conditions (Eqs. 9.36 and 9.37):

$$Z_b \geq \frac{M_S + (1-\eta) M_{GP}}{(\eta \bar{\sigma}_{ci} - \bar{\sigma}_{ts}) - M_c / Z_{bc}}$$

$$Z_t \geq \frac{M_S + (1-\eta) M_{GP}}{(\bar{\sigma}_{cs} - \eta \bar{\sigma}_{ti}) - M_c / Z'_{tc}}$$

- First iteration: $h = 6$ in

$$Z_b = 260.07 \geq \frac{240000 + 360 w_G}{2209 - 768000 / Z_{bc}} = \frac{240000 + 360 \times 184}{2209 - 768000 / 421} = \frac{306240}{384.77} = 795.90 \text{ in}^3 \qquad \text{N.G.}$$

$$Z_t = 248.2 \geq \frac{306240}{(3000 + 0.85 \times 184) - 768000 / 983} = \frac{306240}{2375.12} = 128.94 \text{ in}^3$$

- Second iteration: $h = 8$ in

$$Z_b = 453.77 \geq \frac{240000 + 360 w_G}{2209 - 768000 / Z_{bc}} = \frac{240000 + 360 \times 252}{2209 - 768000 / 661} = \frac{330720}{1047.11} = 315.84 \text{ in}^3 \qquad \text{O.K.}$$

$$Z_t = 449.25 \geq \frac{330720}{(3000 + 0.85 \times 184) - 768000 / 1249} = \frac{330720}{2541.51} = 129.94 \text{ in}^3 \qquad \text{O.K.}$$

Note that if we considered the sustained loading condition as per the 2002 ACI code and assuming $M_L = 0$, we would also get:

$$Z_t = 449.25 \geq \frac{330720}{(2250 + 0.85 \times 184)} = \frac{330720}{2406.4} = 137.43 \text{ in}^3 \qquad \text{O.K.}$$

Hence the slab element of depth $h = 8$ in is acceptable for the problem at hand.

The reader may want to check that, for the above composite beam, there is a feasible domain with a minimum prestressing force determined by stress condition IV and the maximum practical eccentricity $(e_o)_{mp} = y_b - 1.5$ in, that is, Eq. IV, of Table 9.2:

$$F \geq \frac{M_p + M_c \dfrac{Z_b}{Z_{bc}} + \bar{\sigma}_{ts} Z_b}{(e_o - k_t)} = \frac{M_{GP} + M_S + M_L \dfrac{Z_b}{Z_{bc}} + \bar{\sigma}_{ts} Z_b}{(e_o - k_t)}$$

$$= \frac{604800 + 240000 + 768000 \dfrac{453.77}{661} - 424 \times 453.77}{(2.48 + 1.76)} = 278{,}214 \text{ lbs} = 278.214 \text{ kips}$$

It can be shown that the above prestressing force can be satisfied by using 12 strands, leading to 284.58 kips. However the hollow-core slab manufacturer suggests that a deeper slab be used for better deflection control, and to reduce the cost of prestressing. Using again Eq. IV of Table 9.2 and a slab element of depth $h = 10$ in leads to a prestressing force of 215.86 kips, which can be satisfied by using 10 strands leading to 237.15 kips. The reader may want to complete the example by checking other criteria such as ultimate moment, shear and deflection. It is also likely that cost considerations will lead to a deeper slab (see Problem 9.1).

9.8 FLEXURE: ULTIMATE STRENGTH ANALYSIS AND DESIGN

Failure in composite beams often occurs at the interface between the precast beam and the cast-in-place slab where excessive slip may develop under increased loading. However, if an adequate connection is provided to assure shear transfer, prestressed concrete composite beams at ultimate behave much in the same way as noncomposite beams.

The simplest and fastest approach to analyze a composite beam at ultimate is to assume a monolithic section with transformed slab width, b_{tr}, such as shown in Fig. 9.20a, and with the same concrete properties as the precast beam; this is also similar to the procedure used in the working stress design approach of the previous section. In such a case the analysis and design at ultimate are identical to those of noncomposite beams and the provisions developed in Chapter 5 as well as the design flowcharts (such as Figs. 5.19 and 5.22 to 5.25) apply, provided d_{pc} is used instead of d_p. The following remarks are in order:

1. Let us consider a composite beam made with a precast beam and a cast-in-place slab of effective width b_e larger than b_w or b_v (Fig. 9.20b). If at ultimate the neutral axis falls within the slab ($c < h_f$), the nominal bending moment, M_n, can

be computed using the compressive strength of the slab, $(f'_c)_{slab}$, and the effective width, b_e. If T-section behavior occurs (i.e., $c > h_f$) the properties of the precast beam must also be considered in addition to those of the slab. It is generally speedier to assume a section with b_{tr}, and the compressive strength of the precast beam, $(f'_c)_{precast}$, whether the neutral axis is smaller or larger than h_f. However, if the transformed width, b_{tr}, and the compressive strength of the precast beam $(f'_c)_{precast}$ are used instead of b_e and $(f'_c)_{slab}$, a slight error is introduced since b_{tr}/b_e is equal to the moduli ratio instead of the strength ratio. Since the elastic modulus of concrete is related to the square root of its compressive strength, the moduli ratio is equal to the square root of the strength ratio. The resulting error introduced in the value of nominal moment is generally insignificant, since ultimate resistance mostly depends on the nominal tensile force in the steel and the location of neutral axis, which would vary little.

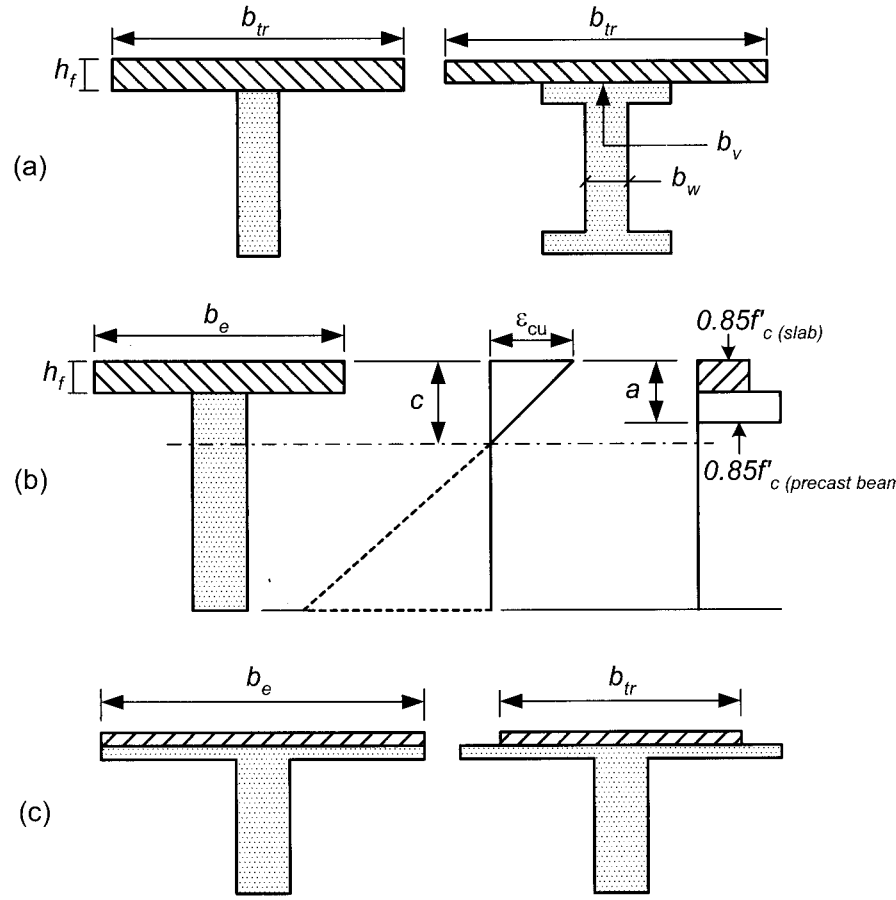

Figure 9.20

If the neutral axis falls in the precast beam and if a linear strain distribution is assumed at ultimate, a stress discontinuity occurs at the interface between the precast beam and the cast-in-place slab (assume that the concrete is of different properties than the precast beam). This discontinuity is also present when the ACI equivalent stress block at ultimate is used (Fig. 9.20b). Although it is not difficult to analyze the section with two different stress blocks, it is, however, much simpler (and with little loss in accuracy) to assume a monolithic section with transformed slab width b_{tr} and $(f'_c)_{precast}$, and proceed with the design.

2. When the composite beam is made of a precast T element with a topping such as in Fig. 9.20*c* in which the slab width is equal to the width of the top flange of the beam, it is recommended to use an equivalent monolithic T section having a flange width equal to the average between b_{tr} of the topping and b of the precast beam, and a flange depth equal to the sum of thicknesses of the topping and the flange of the precast T beam. Such approximation will speed up the design while the accuracy in predicting the nominal moment resistance is, for all practical purposes, not jeopardized.

The above remarks apply to most common design situations. A more exact analysis, using strain compatibility, could be applied for special cases. An example illustrating ultimate strength analysis of a composite beam is given in Sec. 9.11*e*.

9.9 DESIGNING FOR SHEAR AND TORSION

The analysis and design for shear and torsion of composite beams are similar to those of monolithic noncomposite beams, provided adequate shear transfer is ensured at the interface. The design is based on ultimate strength resistance to factored loads and the provisions given for noncomposite beams in Chapter 6, as well as the design flow charts (Figs. 6.13 and 6.25) apply here. Following are some design hints.

1. Use the geometric properties of the composite beam with the transformed cast-in-place slab, b_{tr}, and the mechanical properties of the precast beam. Thus the values of f'_c and b_w of the precast beam (b_w for T section or smallest width of I-section), and d_{pc} of the composite beam (instead of d_p) are used in the equations (Fig. 9.21a). If a tapered web is present, an average value of b_w can be taken.
2. Consider the total factored shear forces in the design, independently of whether they are applied to the precast or composite section.
3. Preferably, extend stirrups, even when not required, into the cast-in-place slab and anchor them with a 90° bend or equivalent (such as closed hooks). This will generally allow the design to satisfy minimum tie requirements for horizontal shear transfer at the interface and improve shear transfer resistance under

repeated loads [Ref. 9.22]. Note that, when the topping is thin, it is not always possible to extend the stirrups.

4. In the case of a partially prestressed beam (Fig. 9.21b), where prestressed and non-prestressed reinforcement is used, the value of d_{pc} should be replaced by d_{ec} defined as the depth from the extreme compression fiber of the composite section (such as top of cast-in-place slab) to the centroid of the tensile force in the reinforcement at nominal bending resistance.

An example of shear design in a composite beam is given in Sections 9.11f and 9.11g.

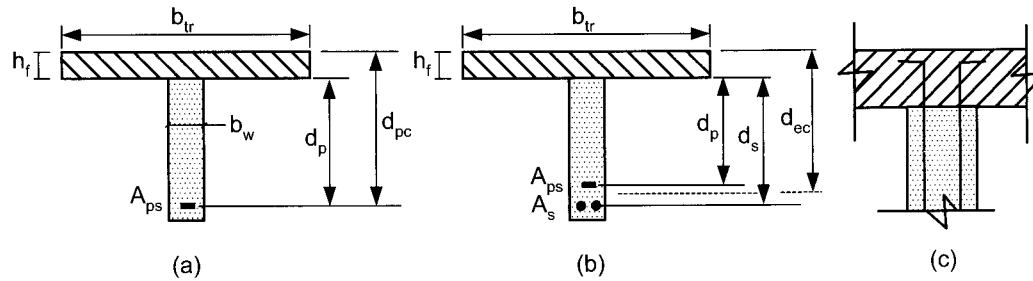

Figure 9.21

9.10 DEFLECTIONS

The determination of deflections in prestressed concrete composite beams presents a number of conceptual difficulties that are significantly more complex than those encountered in Chapter 7 for noncomposite beams. Following are the main reasons:

1. The beam acts as a noncomposite beam in its early life and as a composite beam after hardening of the slab.

2. Different time-dependent materials properties for the precast beam and the cast-in-place slab, and different ages at loading are present.

3. Because of 1 and 2 above, the time-dependent deflections are substantially influenced by the time and sequence of construction operations. At least two additional time-dependent deflections must be evaluated, one for the precast beam until addition of the cast-in-place slab, and one for the composite beam.

4. Once the slab is added, subsequent prestress losses in the precast beam lead to additional long-term deflection, the effect of which may be magnified by the restraint provided by the slab.

5. Differential shrinkage and creep between the precast beam and the cast-in-place slab influence long-term deflection [Ref. 9.18]. The shrinkage of the slab can have significant effects on the state of stress and stress redistribution in the precast section, and on deflection and cracking.

There is no simple answer to such a problem and although some solutions are proposed in the technical literature they still carry a number of simplifying assumptions and inherent uncertainties. References [9.16, 9.17 and 9.22] may be consulted for specific problems. In general, however, the simpler the approach the better it is, provided engineering judgment is used.

For common design problems the author recommends the following sequence:

1. Compute instantaneous elastic deflection due to prestressing force and self-weight of precast beam (that is under $(F_i + M_{GP})$). Call it $(\Delta_i)_1$. Sometimes, an average value of force between F and F_i and an average value of modulus between E_{ci} and E_c are used, such as in a post-tensioned beam, where the post-tensioning is applied over a period of time.

2. Estimate long-term additional deflection of precast beam up to the time at which the slab is added. Call it $(\Delta_{add})_2 = \lambda_1(\Delta_i)_1$ where λ_1 is a coefficient, similar to a creep coefficient, to be estimated for the age at which the slab is added (see note below and Chapter 7).

3. Determine instantaneous deflection in precast beam due to slab weight. Call it $(\Delta_i)_3$. Use properties of precast section, if beam is unshored, and composite section, if beam is shored. In the first case the time is that at which the slab is poured, while in the latter case, the time corresponds to that after the slab has hardened and the shores are removed.

4. Compute resulting deflection at time of addition to the slab, that is, $\Delta_4 = (\Delta_i)_1 + (\Delta_{\text{add}})_2 + (\Delta_i)_3$.

5. Determine instantaneous deflection due to additional dead load (such as diaphragms, piping, asphalt) acting on composite section, call it $(\Delta_i)_5$.

6. Compute resulting deflection in the composite beam, call it $\Delta_6 = \Delta_4 + (\Delta_i)_5$.

7. Estimate additional long-term deflection in the composite beam due to sustained load, call it $(\Delta_{\text{add}})_7 = \lambda_2 \Delta_6$ where λ_2 is a coefficient to be estimated, similarly to a creep coefficient, for the period spanning the remaining service life.

8. Compute the instantaneous deflection due to live load using composite section properties.

9. Check if deflection requirements (ACI or AASHTO codes) of Table 7.2 are satisfied.

Of course the coefficients λ_1 and λ_2 will depend on the material properties and the time-lapse between operations. For example: 1) using an ultimate creep coefficient $C_{CU} = 2.4$, 2) assuming that the cast-in-place slab is added at three months of age of the precast beam, and 3) assuming that about 50 percent of creep occurs at three months after loading; one can conclude that λ_1 is equal 1.2. The coefficient λ_2 can be estimated in a similar manner. Note that the creep coefficient decreases when the strength of concrete increases. Thus, engineering judgment must be exercised in selecting λ_1 and λ_2. Some common average values may be derived from Ref. [9.17] and the PCI handbook [Ref. 1.45]. Note that the additional long-term deflection in the composite beam, which can affect elements attached or connected to the beam, is given by $(\Delta_{add})_7$ only. A typical example of deflection computations for a composite beam is given in Section 9.11*h*.

9.11 EXAMPLE: PRESTRESSED COMPOSITE FLOOR BEAM

A composite floor system is made out of simply supported precast prestressed rectangular beams and a cast-in-place reinforced concrete slab (Fig. 9.22). Relevant dimensions and properties are given next.

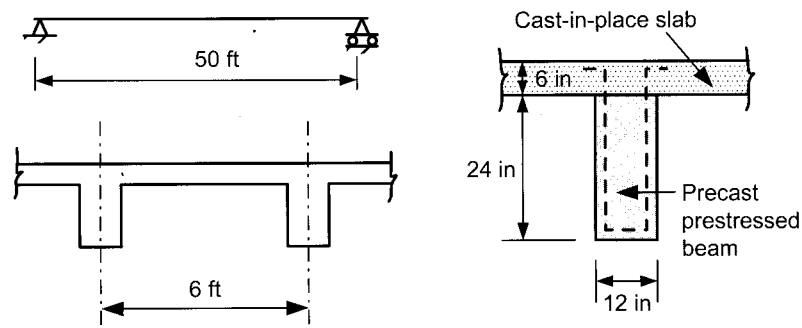

Figure 9.22

Precast beam:

$f'_c = 5000$ psi; $f'_{ci} = 4000$ psi; $\bar{\sigma}_{ti} = -190.0$ psi; $\bar{\sigma}_{ci} = 2400$ psi; $\bar{\sigma}_{ts} = -424$ psi;

$\bar{\sigma}_{cs} = 3000$ psi; $\bar{\sigma}_{csus} = 2250$ psi for sustained loading which corresponds here to $M_L = 0$

Cast-in-place slab: $f'_c = 4000$ psi; $(\bar{\sigma}_{cs})_{slab} = 1800$ psi (lightweight concrete)

Other information: Live load = 50 psf on slab; lightweight concrete slab with $\gamma_c = 110$ pcf; normal weight concrete beam with $\gamma_c = 150$ pcf; prestressing strands having ½- in diameter with area per strand equal to 0.153 in^2; cover to first layer of prestressing strands = 1.75 in; spacing between layers = 2 in; $f_{pu} = 270$ ksi; $f_{pe} = 150$ ksi; $f_{py} = 240$ ksi; $\eta = F / F_i = 0.85$.

Unshored construction is specified. The interface surface between the precast beam and the cast-in-place slab is intentionally roughened for proper shear transfer.

Provide a complete design for the prestressed beams, that is:

(a) Determine geometric properties of precast beam and composite section
(b) Determine F and e_o at midspan
(c) Determine feasibility domain
(d) Determine limit zone and select steel profile
(e) Check ultimate moment at midspan
(f) Find stirrups for vertical shear
(g) Check horizontal shear
(h) Check deflections

The weight of the precast beam is 0.3 klf and the weight of the slab is 0.33 klf. A summary of corresponding bending moments at midspan, and shear forces and moments at $h_c/2$ from the face of the support (that is, x = 30/2 + 6 = 21 in from center of support), is given in Table 9.5. Note that a 12 in wide bearing pad is assumed.

Table 9.5 Bending moments and shear forces for example beam.

Loading	Moments at midspan, (kips-ft)	Shear forces at first critical section (x =21 in), (kips)	Moments at first critical shear section, kips-ft	Resisting section
Precast beam	93.75	6.98	12.67	
Cast-on-place slab	103.125	7.67	13.93	Precast section
	---	---	---	
	$M_p = 196.875$	14.65	26.60	
Live load	$M_c = 93.75$	6.98	12.67	Composite section

a. Composite section properties. The effective width has to be determined first, that is:

$$b_e \le \begin{cases} b_v + 16h_f = 108 \text{ in} \rightarrow \text{(by ACI)} \\ S = 72 \text{ in} \\ l/4 = 150 \text{ in} \end{cases}$$

Thus:

$$b_e = 72 \text{ in}$$

and

$$b_{tr} = b_e \frac{(E_c)_{slab}}{(E_c)_{girder}} = 72 \times \frac{110^{1.5}\sqrt{4000}}{150^{1.5}\sqrt{5000}} = 40.44 \text{ in}; \quad n_c = 0.5617$$

The area of the composite section with transformed slab is given by:

$$A_{cc} = A_c + b_{tr}h_f = 288 + 40.44 \times 6 = 530.64 \text{ in}^2$$

The other geometric properties of the precast beam and the composite beam with transformed slab are summarized in Table 9.6.

Table 9.6 Properties of precast and composite sections for example beam.

Precast beam	Composite beam (with transformed slab)
$A_c = 288 \text{ in}^2$	$A_{cc} = 530.64 \text{ in}^2$
$y_t = 12 \text{ in}$	$y_{tc} = 11.14 \text{ in}$
$y_b = 12 \text{ in}$	$y_{bc} = 18.86 \text{ in}$
$h = 24 \text{ in}$	$h_c = 30 \text{ in}$
$I_g = 13{,}824 \text{ in}^4$	$I_{gc} = 44{,}182.3 \text{ in}^4$
$Z_t = 1152 \text{ in}^3$	$Z_{tc} = 3966.1 \text{ in}^3$
$Z_b = 1152 \text{ in}^3$	$Z_{bc} = 2342.6 \text{ in}^3$
$k_t = -4 \text{ in}$	$Z'_{tc} = 8595.8 \text{ in}^3$
$k_b = 4 \text{ in}$	$h_f = 6 \text{ in}$
$b_v = 12 \text{ in}$	$b_e = 72 \text{ in}$
$b_w = 12 \text{ in}$	$b = b_{tr} = 40.44 \text{ in}$

b. Prestressing force. Let us determine the required prestressing force and check stresses at midspan. As it is very likely that a feasible domain exists (see next section), stress condition IV at equality will be used to determine the minimum value of F assuming an eccentricity e_o equal to the maximum practical eccentricity $(e_o)_{mp} = 9.25$ in. Using Table 9.2, way 3, we have:

$$F = \eta F_i = \frac{(M_p + M_c Z_b / Z_{bc} + \bar{\sigma}_{ts} Z_b)}{e_o - k_t}$$

$$= \frac{196.875 \times 12{,}000 + 93.75 \times 12{,}000 \times 1152 / 2342.6 - 424 \times 1152}{9.25 + 4}$$

$$F = 183{,}191 \text{ lb} = 183.191 \text{ kips}$$

Each strand can carry a final force of 0.153 × 150 = 22.95 kips. The minimum required number of strands is:

$$N = \frac{183.191}{22.95} = 7.98$$

It is rounded off to 8 strands thus leading to:

$$\begin{cases} F = 22.95 \times 8 = 183.6 \text{ kips} \\ N = 8 \text{ strands} \\ F_i = F / \eta = F / 0.85 = 216 \text{ kips} \\ e_o = 9.25 \text{ in at midspan} \end{cases}$$

Details of strand layout for the midspan and support sections are suggested in Fig. 9.23. The steel profile is selected to have two draping points each at 15 ft from the center of support (see Section 9.11d and Fig. 9.25). Four strands are draped bringing the eccentricity of the prestressing force at the supports to 0.25 in.

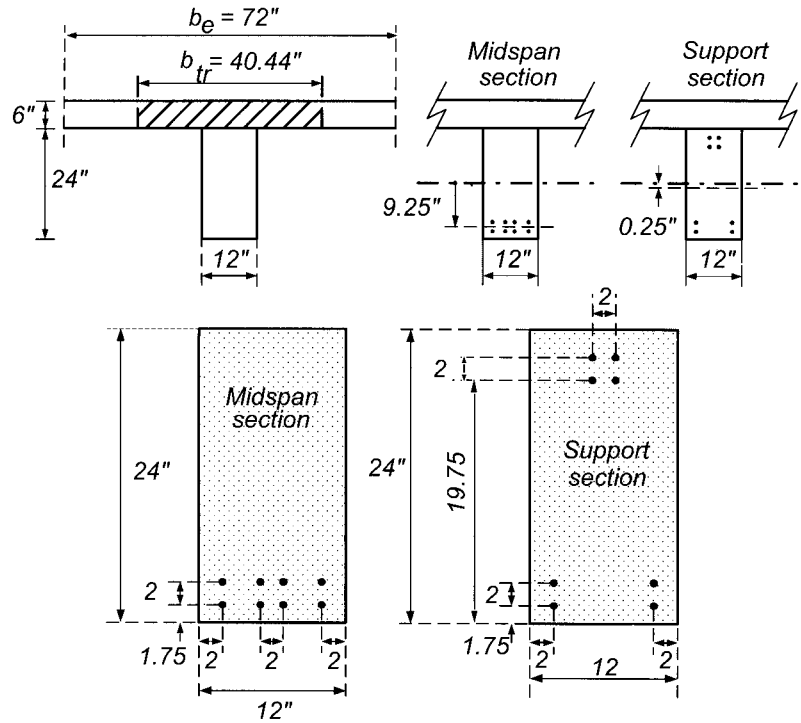

Figure 9.23

The reader may want to check that the extreme fiber stresses at midspan for the above values of prestressing force and eccentricity are as follows (use Table 9.2, way 1):

For the precast beam:

$$\sigma_{ti} = -7.8 \text{ psi} \quad > \bar{\sigma}_{ti} = -190 \text{ psi}$$

$$\sigma_{ci} = 1508 \text{ psi} < \bar{\sigma}_{ci} = 2400 \text{ psi}$$

$$\begin{cases} \sigma_{cs} = 1345 \text{ psi} < \bar{\sigma}_{cs} = 3000 \text{ psi} \\ \sigma_{csus} = 1214 \text{ psi} < \bar{\sigma}_{csus} = 2250 \text{ psi} \end{cases}$$

$$\sigma_{ts} = -419.30 \text{ psi} > \bar{\sigma}_{ts} = -424 \text{ psi}$$

For the cast-in-place slab:

$$\sigma_{cs} = n_c \frac{93.75 \times 12000}{3966.1} = 0.5617 \times 283.6 = 159.38 \text{ psi} < (\bar{\sigma}_{cs})_{\text{slab}} = 1800 \text{ psi} \qquad \text{O.K.}$$

It can be seen from the stresses other than σ_{ts} that the beam has still some capacity and could be used for longer spans or heavier live loads.

c. Feasibility domain. Although the approach followed above is sufficient, let us build the feasibility domain to illustrate its use for composite beams and also show that it leads to the same results (Fig. 9.24).

Condition I: $e_o \le k_b + (1/F_i)(M_{GP} - \bar{\sigma}_{ti} Z_t)$

$$e_o \le 4 + \frac{(93.75 \times 12000 + 190 \times 1152)}{F_i}$$

$$e_o \le 4 + \frac{1.34 \times 10^6}{F_i}$$

Condition II: $e_o \le k_t + (1/F_i)(M_{GP} + \bar{\sigma}_{ci} Z_b)$

$$e_o \le -4 + \frac{(93.75 \times 12000 + 2400 \times 1152)}{F_i}$$

$$e_o \le -4 + \frac{3.89 \times 10^6}{F_i}$$

Condition III: $e_o \ge k_b + (\frac{1}{\eta F_i})(M_P + M_c Z_t / Z'_{tc} - \bar{\sigma}_{cs} Z_t)$

$$e_o \ge 4 + \frac{\left(196.875 \times 12000 + 93.75 \times 12000 \times \frac{1152}{8595.8} - 3000 \times 1152\right)}{0.85 F_i}$$

$$e_o \ge 4 - \frac{1.11 \times 10^6}{F_i}$$ Less critical than that for sustained loading.

Indeed, for sustained loading, assuming $M_L = 0$:

$$e_o \ge 4 + \frac{(196.875 \times 12000 - 2250 \times 1152)}{0.85 F_i}$$

$$e_o \ge 4 - \frac{0.27 \times 10^6}{F_i}$$ → controls for stress condition III.

Condition IV: $e_o \ge k_t + (\frac{1}{\eta F_i})(M_P + M_c Z_b / Z_{bc} + \bar{\sigma}_{ts} Z_b)$

$$e_o \ge -4 + \frac{\left(196.875 \times 12000 + 93.75 \times 12000 \times \frac{1152}{2342.6} - 424 \times 1152\right)}{0.85 F_i}$$

$$e_o \ge -4 + \frac{2.86 \times 10^6}{F_i}$$

Condition V: $e_o \le (e_o)_{mp} = y_b - (d_c)_{\min} = 12 - 2.75 = 9.25$ in

The above five equations are plotted at equality in Fig. 9.24 and illustrate the feasibility domain.

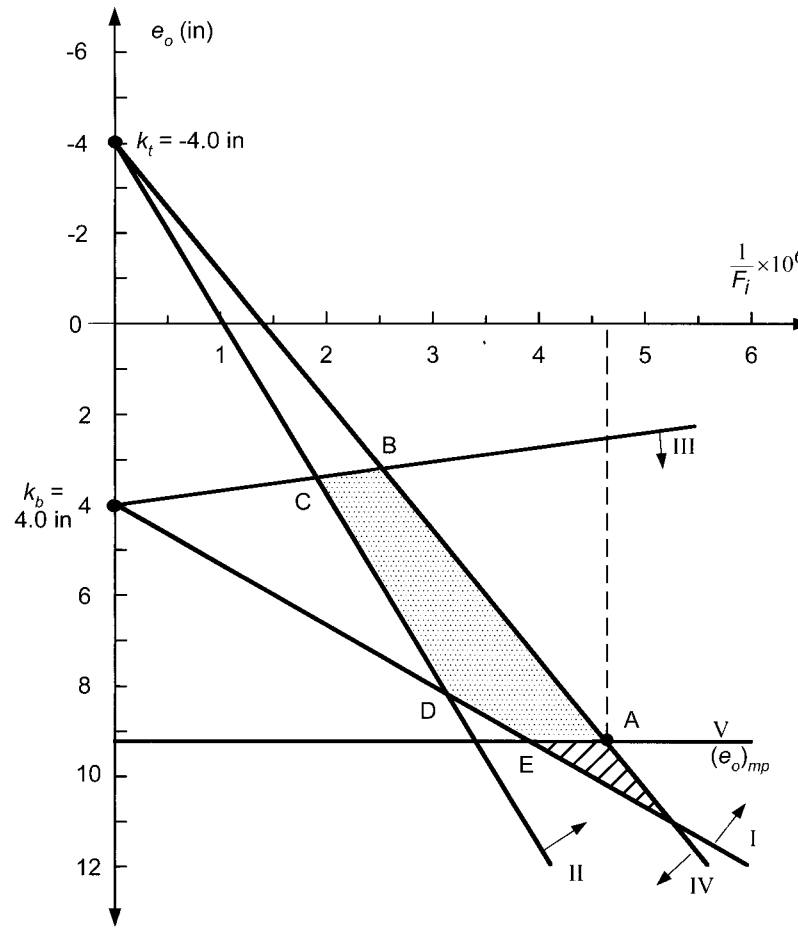

Figure 9.24

From the graph:

$$\frac{10^6}{F_i} \simeq 4.6 \rightarrow F_i \simeq 217{,}391 \text{ lbs} = 217.39 \text{ kips}$$

$$F = 0.85F_i = 184.78 \text{ kips}$$

$$N = 184.78 / 22.95 \simeq 8.05$$

use $N = 8$ strands

This is essentially the same result as the solution obtained in the previous section.

Hence use: $N = 8$; $F = 183.6$ kips; $F_i = 216$ kips; $e_o = 9.25$ in.

d. Determine limit zone and steel envelopes. Let us determine the steel envelopes. Using Eqs. (9.24) to (9.27):

$$e_{ou} \geq \begin{cases} k_b\left(1-\dfrac{\bar{\sigma}_{cs}}{\sigma_g}\right)+\dfrac{M_p+M_cZ_t/Z'_{tc}}{F} \\ k_t\left(1-\dfrac{\bar{\sigma}_{ts}}{\sigma_g}\right)+\dfrac{M_p+M_cZ_b/Z_{bc}}{F} \end{cases} = \begin{cases} 4\left(1-\dfrac{3000}{637.5}\right)+\dfrac{M_p+M_c\times 1152/8595.8}{183600} \\ -4\left(1-\dfrac{(-424)}{637.5}\right)+\dfrac{M_p+M_c\times 1152/2342.6}{183600} \end{cases}$$

$$e_{ou} \geq \begin{cases} -14.82+\dfrac{M_p}{183600}+\dfrac{0.134\times M_c}{183600} \\ -6.66+\dfrac{M_p}{183600}+\dfrac{0.4918\times M_c}{183600} \end{cases} \text{ that is, } e_{ou} = -6.66+\frac{M_p}{183600}+\frac{0.4918\times M_c}{183600}$$

$$e_{ol} \leq \begin{cases} k_b\left(1-\dfrac{\bar{\sigma}_{ti}}{\sigma_{gi}}\right)+\dfrac{M_{GP}}{F_i} \\ k_t\left(1-\dfrac{\bar{\sigma}_{ci}}{\sigma_{gi}}\right)+\dfrac{M_{GP}}{F_i} \end{cases} = \begin{cases} 4\left(1-\dfrac{(-190)}{750}\right)+\dfrac{M_{GP}}{216000} \\ -4\left(1-\dfrac{2400}{750}\right)+\dfrac{M_{GP}}{216000} \end{cases}$$

$$e_{ol} \leq \begin{cases} 5.01+\dfrac{M_{GP}}{216000} \\ 8.80+\dfrac{M_{GP}}{216000} \end{cases} \text{ that is, } e_{ol} = 5.01+\frac{M_{GP}}{216000}$$

Table 9.7

Section, ft →	0	5	10	15	20	25
M_{GP}, lb-in	0	405000	720000	945000	1080000	1125000
M_p, lb-in	0	850500	1512000	1984500	2268000	2362500
M_c, lb-in	0	405000	720000	945000	1080000	1125000
e_{ou}, in	-6.66	-0.95	3.51	6.68	8.58	9.22
e_{ol}, in	5.01	6.89	8.34	9.39	10.01	10.22
e_o, in	0.25	3.25	6.25	9.25	9.25	9.25

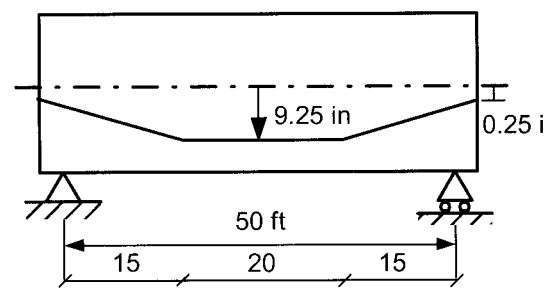

Figure 9.25

A tendon profile with double draping points located at 15 ft from the supports is selected as shown in the last row of Table 9.7 and Fig. 9.25. It is assumed that sustained loading with allowable

stress $\bar{\sigma}_{csus}$ does not change the values of the steel envelopes. However, the corresponding condition could be easily accommodated, if needed.

e. Ultimate moment requirements. Let us determine the ultimate moment resistance ϕM_n. It applies to the composite section. Following the flow chart (Fig. 5.24), which applies to composite sections, provided d_p is replaced by d_{pc}, we have:

$$A_{ps} = 8 \times 0.153 = 1.224 \text{ in}^2$$

$$\rho_p = \frac{A_{ps}}{bd_{pc}} = \frac{1.224}{40.44 \times (6+12+9.25)} = 0.00111$$

$$f_{ps} = f_{pu}\left[1 - \frac{\gamma_p}{\beta_1}\left\{\rho_p \frac{f_{pu}}{f'_c} + \frac{d_s}{d_p}\left(\omega_s - \omega'_s\right)\right\}\right]$$

$$= 270\left(1 - \frac{0.40}{0.80}(0.00111)\frac{270}{5}\right) = 261.90 \text{ ksi}$$

$$\omega_p = \rho_p \frac{f_{ps}}{f'_c} = 0.00111 \times \frac{261.90}{5} = 0.058142$$

Check depth of neutral axis at ultimate:

$$c = \frac{1.18\omega d_{pc}}{\beta_1} = \frac{1.18 \times 0.058142 \times 27.25}{0.80} = 2.34 \text{ in} < h_f = 6 \text{ in} \rightarrow \text{R-section behavior}$$

$$a = \beta_1 c = 0.8 \times 2.34 = 1.87 \text{ in}$$

Since $c < h_f$ we could have also calculated a based on the strength of the cast-in-place slab and b_e.

The neutral axis is in the flange. Analyze as a rectangular section with;

$$\frac{c}{d_e} = \frac{c}{d_{pc}} = \frac{2.34}{27.25} = 0.086 < 0.375 \rightarrow \text{Tension-controlled section (ACI 2002)}$$

Thus: $\phi = 0.9$ for bending, and

$$\phi M_n = \phi\left[A_{ps} f_{ps}\left(d_{pc} - \frac{a}{2}\right)\right]$$

$$= 0.9 \times 1.224 \times 261.90\left(27.25 - \frac{1.87}{2}\right)$$

$$= 7592.12 \text{ kips-in} = 632.68 \text{ kips-ft}$$

The moment resistance is to be compared with the required strength design moment obtained from factored loads. Referring to Table 9.5 and using the 2002 ACI code for load factors, we have:

$$M_u = 1.2M_D + 1.6M_L$$

$$= 1.2 \times 196.875 + 1.6 \times 93.75$$

$$M_u = 386.25 \text{ kips-ft}$$

$$M_u < \phi M_n \qquad \text{O.K.}$$

The cracking moment can be computed from Eqs. (9.28) and (9.29) and leads to:

$$\Delta M_{cr} = \frac{Z_{bc}}{Z_b}\left[\eta F_i (e_o - k_t) - M_p\right] - f_r Z_{bc}$$

$$f_r = -7.5\sqrt{f_c'} = -7.5\sqrt{5000} = -530.33 \text{ psi}$$

$$\Delta M_{cr} = \left[\frac{2342.6}{1152}\left[183600(9.25+4) - 196.875\times 12000\right] + 530.33\times 2342.6\right]$$

$$\Delta M_{cr} = 1385.10 \text{ kips-in} = 115.43 \text{ kips-ft}$$

$$M_{cr} = M_p + \Delta M_{cr} = 196.875 + 115.43 = 312.31 \text{ kips-ft}$$

Hence:

$$1.2M_{cr} = 374.772 \text{ kips-ft}$$

and

$$\phi M_n = 632.68 \geq 1.2M_{cr} = 374.772 \text{ kips-ft} \qquad \text{O.K.}$$

that is, the design nominal bending moment also satisfies the requirement of being at least 20 percent larger than M_{cr}.

f. Vertical shear. Let us check vertical shear at $h/2$ =15 in from the face of support, or 15 + 6 = 21 in from the center of support. Referring to Figs. 9.23 and 9.25 and the assumed steel profile, it can be shown that at the section under investigation

$$e_o \approx 1.30 \text{ in}$$

$$d_{pc} = \text{larger of} \begin{cases} 12+6+1.3=19.3 \text{ in} \\ 0.8h_c = 24 \text{ in} \end{cases}$$

Hence, d_{pc} = 24 in

Using the 2002 ACI provisions for shear design, we have:

$$V_u = 1.2V_D + 1.6V_L$$
$$= 1.2\times 14.65 + 1.6\times 6.98$$
$$= 28.75 \text{ kips}$$

Thus:

$$v_u = \frac{V_u}{b_w d_{pc}} = \frac{28750}{12\times 24} = 99.83 \text{ psi}$$

$$\frac{v_u}{\phi} = \frac{99.83}{0.75} = 133.1 \text{ psi}$$

The properties of the transformed composite section will be used in computing v_c, the shear resistance of concrete. Referring to the flow chart (Fig. 6.13), v_c is to be taken as the smaller of v_{ci} or v_{cw}. v_{ci} is given by Eq. (6.28):

$$v_{ci} = 0.6\sqrt{f_c'} + \frac{V_G}{b_w d_{pc}} + \frac{1}{b_w d_{pc}}\left(\frac{\Delta V_u \times \Delta M_{cr}}{\Delta M_u}\right) \geq 1.7\sqrt{f_c'} = 120.2 \text{ psi}$$

The value of V_G applies to the own weight of the composite section as if it was monolithic, hence (Table 9.5):

$$V_G = V_{GP} + V_S = 6.98 + 7.67 = 14.65 \text{ kips}$$

The values of ΔV_u and ΔM_u apply to the factored superimposed dead load and live load. Hence (Table 9.5):

$$\Delta V_u = 1.6 \times 6.98 = 11.168 \text{ kips}$$
$$\Delta M_u = 1.6 \times 12.67 = 20.272 \text{ kips-ft}$$

The value of ΔM_{cr} is obtained from Eq. (9.29) in which, assuming unshored construction, $M_p = M_{GP} + M_S$. Hence:

$$\Delta M_{cr} = \frac{Z_{bc}}{Z_b}[F(e_o - k_t) - M_p] - f_r Z_{bc}$$
$$= \left[\frac{2342.6}{1152}\left[183600(1.3+4) - 26.60 \times 12000\right] + 424.26 \times 2342.6\right]$$
$$= 2323.54 \text{ kips-in}$$
$$\Delta M_{cr} = 193.63 \text{ kips-ft}$$

Note that the value of modulus of rupture used in the above formula is: $f_r = -6\sqrt{f'_c} = -424.26$ psi. Thus, the shear-flexure cracking resistance v_{ci} is given by:

$$v_{ci} = 0.6\sqrt{5000} + \frac{14,650}{12 \times 24} + \frac{\dfrac{11,168 \times 193.63}{20.272}}{12 \times 24}$$
$$= 42.43 + 50.87 + 370.39 \simeq 463.69 \text{ psi}$$

The web-shear cracking resistance is given by Eq. (6.30):

$$v_{cw} = 3.5\sqrt{f'_c} + 0.3\sigma_g + \frac{V_p}{b_w d_{pc}}$$

Referring to Figs. 9.25 and noting that the draping point of the strands is taken at 15 ft from the support, it can be shown that:

$$V_p = F \sin\alpha = 183.60\left(\frac{9.25 - 0.25}{15 \times 12}\right) = 9.18 \text{ kips}$$

If the average prestress σ_g is computed for the composite section (safer design), the value of v_{cw} becomes:

$$v_{cw} = 3.5\sqrt{5000} + 0.3\frac{183,600}{530.64} + \frac{9180}{12 \times 24}$$
$$= 247.49 + 103.80 + 31.88 \simeq 383.17 \text{ psi}$$

The shear resistance of concrete is taken as the lesser of v_{ci} or v_{cw}. Hence,

$$v_c = 383.17 \text{ psi} \quad \text{and} \quad \phi v_c = 0.75 \times 383.17 = 287.37 > v_u = 99.82 \text{ psi}$$

As $\frac{v_u}{\phi} = 133.1 \text{ psi} < \frac{v_c}{2} = 191.6 \text{ psi} \rightarrow$ no shear reinforcement is needed.

However it may be on the safe side to provide #3 U stirrups at the following spacing:

$$s = \begin{cases} \leq 0.75h = 22.5 \text{ in} \\ \leq 24 \text{ in} \\ \geq 3 \text{ in} \end{cases}$$

Hence, #3 U stirrups at s = 22 in is used as a minimum reinforcement to be extended into the cast-in-place slab. It can also be shown that A_v is equal to:

$$(A_v)_{\min} = \frac{50 b_w s}{f_y} = \frac{50 \times 12 \times 22}{60000} = 0.22 \text{ in}^2$$

The reader may want to check that, if the alternative conservative method (Fig. 6.13) was used, the computed value of v_c would have been equal to 742.43 psi for a value of $V_u d_{pc}/M_u = 1$. As v_c is limited by 5 $\sqrt{f_c'}$, it is taken equal to $v_c = 5\sqrt{f_c'} = 353.55$ psi.

As: $\frac{v_u}{\phi} < \frac{v_c}{2} \rightarrow$ no shear reinforcement is needed

Hence, #3 U stirrups at s =22 in is used as a minimum reinforcement. Note that all stirrups are extended and anchored in the slab, providing ties for shear transfer.

g. Horizontal shear. The total shear force calculated in the previous section is used at ultimate:

$$V_u = 28.75 \text{ kips}$$

The interface shear is given by:

$$v_{uh} = \frac{V_u}{b_v d_{pc}} = \frac{28{,}750}{12 \times 24} = 99.82 \text{ psi}$$

As the interface surface is intentionally roughened and minimum shear reinforcement is extended and anchored in the slab, the nominal horizontal shear resistance can be taken as (Eq. 9.8):

$$v_{nh} = \left(260 + \frac{0.6 A_v f_y}{b_v s} \right) \lambda = 260 + \frac{0.6 \times 0.22 \times 60{,}000}{12 \times 22} = 290 \text{ psi}$$

$$\phi v_{nh} = 0.75 \times 290 = 217.5 \text{ psi}$$

As $v_{uh} < \phi v_{nh}$ no additional shear transfer reinforcement is required. Note that the condition for tie spacing to be not more than $4h_f = 24$ in is also satisfied.

Although not needed here, let us illustrate the procedure described in Section 9.6 (Tie Reinforcement Using Shear Friction) assuming that shear-friction reinforcement is to be determined for the same shear force as calculated above.

Using Eq. (9.13) and assuming same spacing s as used in the design of vertical stirrups, we have:

$$A_{vf}^* = \frac{V_u}{\phi f_y \mu} \frac{s}{d_{pc}} = \frac{28750}{0.75 \times 60 \times 1} \times \frac{22}{24} = 0.59 \text{ in}^2$$

That is, 0.59 in^2 of the tie reinforcement is needed at a spacing of 22 in at the section considered.

If we use Eq. (9.9) as recommended by ACI, the value of H_u must be determined first. It can be taken equal to the compressive force in the slab at nominal moment capacity of the midspan section. Using the depth of the neutral axis obtained in Section 9.11*e* and Eq. (9.10), we have:

$$H_u = 0.85(f'_c)_{precast} b_{tr} a = 0.85 \times 5 \times 40.44 \times 1.87 = 321.4 \text{ kips}$$

Note that H_u could have also been calculated using b_e, $(f'_c)_{\text{slab}}$ and related value of a.

From Eq. (9.9):

$$A_{vf} = \frac{H_u}{\phi f_y \mu} = \frac{321.4}{0.75 \times 60 \times 1} = 7.14 \text{ in}^2$$

The above value is to be distributed along the interface surface of half the span, i.e., 25 ft. On average, it leads to about 0.29 in^2 per linear foot (12 in) spacing and can be satisfied by providing No. 3 U stirrups at 9 in spacing throughout. In comparing with the value of A^*_{vf} obtained above at the first critical section, one should keep in mind that A^*_{vf} is section and spacing dependent, will vary along the span, and is larger near the supports.

h. Deflections. The steps suggested in Sec. 9.10 will be followed. The member is not cracked under service loads and thus I_g or I_{gc} will be used throughout. The reader is also referred to Fig. 7.4, which gives the various analytical formulas for deflections. Unshored construction is assumed.

1. Using F_i and E_{ci}, the instantaneous deflection due to the prestressing force and the self-weight of the precast beam is:

$$(\Delta_i)_G = \frac{5}{384}\frac{w_G l^4}{E_{ci} I_g} = \frac{5}{384} \times \frac{(300/12)(50 \times 12)^4}{3834 \times 1000 \times 13824}$$

$$= 0.80 \text{ in}$$

$$(\Delta_i)_{F_i} = -\frac{F_i l^2}{8 E_{ci} I_g}\left[e_1 + (e_2 - e_1)\frac{4a^2}{3l^2}\right]$$

$$= -\frac{216000 \times (50 \times 12)^2}{8 \times 3834 \times 1000 \times 13824}\left[9.25 + (0.25 - 9.25) \times \frac{4}{3} \times \left(\frac{15}{50}\right)^2\right]$$

$$(\Delta_i)_{F_i} = -1.50 \text{ in}$$

Thus:

$$(\Delta_i)_1 = (\Delta_i)_{F_i} + (\Delta_i)_G = -1.50 + 0.80 = -0.70 \text{ in}$$

It is a camber.

2. Additional long-term deflection until addition of slab (using $\lambda_1 = 1$):

$$(\Delta_{\text{add}})_2 = \lambda_1 (\Delta_i)_1 = -0.70 \text{ in}$$

3. Instantaneous deflection in precast beam due to weight of cast-in-place slab (use E_c):

$$(\Delta_i)_3 = \frac{5}{384}\frac{w_{slab} l^4}{E_c I_g} = \frac{5}{384} \times \frac{(330/12)(50 \times 12)^4}{4287 \times 1000 \times 13824}$$

$$(\Delta_i)_3 = 0.78 \text{ in}$$

4. Resulting deflection:

$$\Delta_4 = (\Delta_i)_1 + (\Delta_{add})_2 + (\Delta_i)_3$$

$$\Delta_4 = -0.70 - 0.70 + 0.78$$

$$\Delta_4 = -0.62 \text{ in}$$

5. Additional long-term deflection in the composite beam (use $\lambda_2 = 1.2$):

$(\Delta_{\text{add}})_7 = \lambda_2 \Delta_4 = -0.74$ in

Note that the subscript 7 complies with the steps described Section 9.10.

6. Total long-term deflection under sustained load:

$\Delta_8 = -0.62 - 0.74 = -1.36$ in

7. Instantaneous live load deflection:

$$(\Delta_i)_9 = \Delta_{LL} = \frac{5}{384}\frac{w_{LL}l^4}{E_c I_{gc}} = \frac{5}{384} \times \frac{(50 \times 72/144)(50 \times 12)^4}{4287 \times 1000 \times 44182.3} = 0.22 \text{ in}$$

Figure 9.26 illustrates the variation of deflection with time.

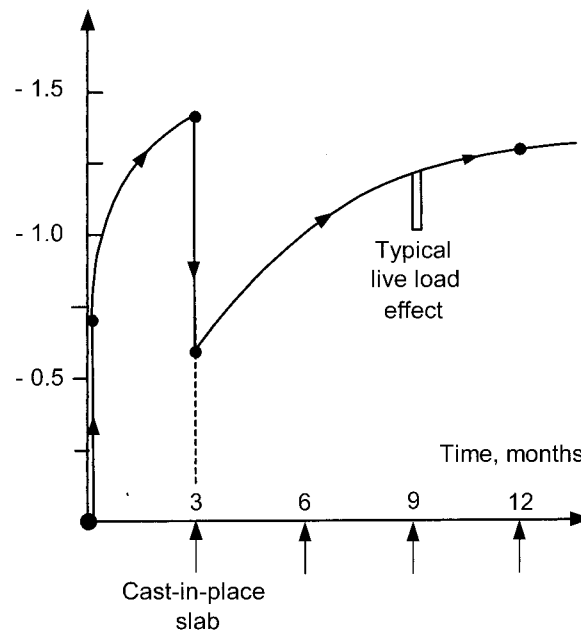

Figure 9.26 Typical variation of deflection versus time for example beam.

i. Check Deflection Criteria. Both the ACI and the AASHTO codes will be used, for illustration, although this is not a bridge beam and thus the AASHTO code is not applicable.

1. AASHTO code: instantaneous deflection due to service live load (vehicular load) plus impact (here impact is not considered):

$$\Delta_{LL} = 0.22 \le \frac{L}{800} = \frac{50 \times 12}{800} = 0.75 \text{ in} \qquad \text{O.K.}$$

2. ACI code

First criterion:

Damage unlikely: $\Delta_{LL} = 0.22 \le \frac{L}{180} = \frac{50 \times 12}{180} = 3.33 \text{ in}$ O.K.

or

Damage likely: $\Delta_{LL} = 0.22 \le \frac{L}{360} = \frac{50 \times 12}{360} = 1.67 \text{ in}$ O.K.

Second criterion:

$$\Delta_{LL} + \Delta_{add} = 0.22 + (-0.74) = -0.52 \text{ and } |-0.74| \le \frac{L}{240} = \frac{50 \times 12}{240} = 2.5 \text{ in} \qquad \text{O.K.}$$

or

$$\Delta_{LL} + \Delta_{add} = 0.22 + (-0.74) = -0.52 \text{ and } |-0.74| \le \frac{L}{480} = \frac{50 \times 12}{480} = 1.25 \text{ in} \qquad \text{O.K}$$

Thus the deflection limit state is satisfactory. Note that in the above equations, the additional long-term deflection was taken as that developed after composite action has taken place. Engineering judgment should determine if the additional long-term deflection developed in the precast beam prior to addition of the cast-in-place slab should be considered.

9.12 AASHTO LRFD PROVISIONS ON SHEAR TIE REINFORCEMENT AT CONTACT SURFACE OF COMPOSITE BEAMS

The provisions of the AASHTO code are different from those of the ACI code; however the background information given in Section 9.6.2 is useful for these provisions as well. Note that in the AASHTO provisions clearly separate the contribution of concrete and that of the reinforcement to the horizontal shear resistance.

An investigation of horizontal shear strength is required for all composite members and is treated similarly to other effects, such as vertical shear, bending, and the like.

9.12.1 Nominal Shear Transfer Resistance

As for the case of vertical shear, torsion, and bending, the design for horizontal shear transfer is based on ultimate strength requirements.

The design is based on satisfying the following relation:

$$\begin{cases} \eta V_{uh} \le \phi V_{nh} \\ \text{or} \\ \eta V_{uh} / \phi \le V_{nh} \end{cases} \tag{9.42}$$

where:

V_{uh} = factored design horizontal shear force due to superimposed dead load and live load plus impact
V_{nh} = nominal horizontal shear force resistance
ϕ = strength reduction factor for shear = 0.9 (AASHTO LRFD)
η = load modification factor explained in Eq. (14.2); it can be taken equal 1 in preliminary design

The factored horizontal shear force can be computed from:

$$V_{uh} \le V_u \frac{Q}{I_c} \tag{9.43}$$

where V_u is the factored vertical shear force, Q is the moment of area of the section above the interface plane, and I_c is the moment of inertia of the composite section.

According to AASHTO LRFD [A.5.8.4.1] the nominal shear resistance at the interface between two concretes cast at different times shall be taken as:

$$V_{nh} = cA_{cv} + \mu(A_{vf} f_y + P_c) \le \begin{cases} 0.2 f'_c A_{cv} \\ 0.8 A_{cv} \end{cases} \tag{9.44}$$

where A_{vf} is the area of minimum vertical tie or stirrups (extending through the contact surface) per unit length, f_y is their yield strength, P_c is the net permanent compression force per unit length normal to the interface, A_{cv} is the contact area per unit length, μ is a friction factor, and c is a cohesion factor. In Eq. (9.44) the units are kips, kips per square inch, and inches. Thus f'_c is in ksi, and A_{cv} in in^2. P_c represents essentially the dead weight of the slab and other permanent superimposed dead load, such as asphalt.

The following values of cohesion and friction factor are recommended [A5.8.4.2]:

- For concrete placed monolithically:

$$\begin{cases} c = 0.15 \text{ ksi} \\ \mu = 1.4\lambda \end{cases}$$

- For concrete placed against clean, hardened concrete with surface intentionally roughened to an amplitude of 0.25 in:

$$\begin{cases} c = 0.10 \text{ ksi} \\ \mu = 1.0\lambda \end{cases}$$

- For concrete placed against hardened concrete, clean and free from laitance, but not intentionally roughened:

$$\begin{cases} c = 0.075 \text{ ksi} \\ \mu = 0.6\lambda \end{cases}$$

- For concrete anchored to as-rolled structural steel by headed studs or by reinforcing bars where all steel in contact with concrete is clean and free from paint:

$$\begin{cases} c = 0.025 \text{ ksi} \\ \mu = 0.7\lambda \end{cases}$$

and $\lambda = 1$ for normal weight concrete, $\lambda = 0.85$ for sand lightweight concrete, and $\lambda = 0.75$ all-lightweight (that is, sand and coarse aggregate) concrete.

The cross sectional area of reinforcement per unit length should not be less than that required by Eq. (9.45), that is:

$$A_{vf} \geq \frac{0.05 b_v}{f_y} \tag{9.45}$$

where b_v is the width of the interface. Thus if the horizontal shear reinforcement is placed as a spacing s, its cross section should be $A_{vf} \times s$.

In the above equations, if we consider a reinforcement of a given cross section A_r, at a given spacing, s, then:

$$A_{vf} = \frac{A_r}{s} \tag{9.46}$$

where s is the spacing. For example, for a No. 4 U stirrup, $A_r = 2\text{x}0.2 = 0.4$ in^2. It is therefore useful for design to replace A_{vf} in Eq. (9.44) by its value from Eq. (9.46) leading to:

$$V_{nh} = cA_{cv} + \mu\left(\frac{A_r}{s} f_y + P_c\right) \leq \begin{cases} 0.2 f'_c A_{cv} \\ 0.8 A_{cv} \end{cases} \tag{9.47}$$

Tie spacing, s, shall not exceed four times the least dimension of supported element (mostly slab thickness) or 24 in (600 mm). Ties for horizontal shear may consist of simple bars or wires, multiple leg stirrups, and vertical legs of smooth or deformed welded wire fabric. Ties must be fully anchored into all interconnected elements.

Application of the above procedure is illustrated in the example of a composite bridge in Section 14.10.2 (subsection f).

REFERENCES

9.1 ACI Committee 318, *Building Code Requirements for Reinforced Concrete (ACI 318-99) and Commentary (318R-99),* American Concrete Institute, Farmington Hills, MI, 1999.

9.2 ASCE Task Committee on Design Criteria for Composite Structures in Steel and Concrete, "Proposed Specification and Commentary for Composite Joists and Composite Trusses," ASCE, *Journal of Structural Engineering*, 122: 350-58, 1996.

9.3 ACI-ASCE Committee 333, "Tentative Recommendations of Design of Composite Beams and Girders for Buildings," *ACI Journal*, 32(6): 609-28, (Proceedings vol. 57), 1960.

9.4 Ali, M. A., and R. N. White, "Enhanced Contact Model for Shear Friction of Normal and High-Strength Concrete," *ACI Structural Journal*, 96(3): 348-60, 1999.

9.5 Badoux, J. C., and C. L. Hulsbos, "Horizontal Shear Connection in Composite Concrete Beams under Repeated Loads," *ACI Journal*, 64(12): 811-19, 1967.

9.6 Branson, D. E., "The Deformation of Non-Composite and Composite Prestressed Concrete Members," ACI Special Publication SP-43-4, Deflections of Concrete Structures, 1974, pp. 83-127.

9.7 Bass, R. A., R. L. Carrasquillo, and J. O. Jirsa, "Shear Transfer across New and Existing Concrete Interfaces", *ACI Structural Journal*, 86(4): 383-93, 1989.

9.8 Birkeland, P., and H. Birkeland, "Connections in Precast Concrete Construction," *ACI Journal*, 63(3): 345-68, 1966.

9.9 Evans, R. H., and A. S. Parker, "Behavior of Prestressed Concrete Composite Beams," *ACI Journal*, 52(6): 861-81, 1955.

9.10 Freyermuth, C. L., "Design of Continuous Highway Bridges with Precast Prestressed Concrete Girders," *PCI Journal*, 14(2): 14-36, 1969.

9.11 Hanson, N. W., "Precast-Prestressed Concrete Bridges: (2) Horizontal Shear Connections," *PCA Journal*, 2(2): 38-58, 1960.

9.12 Hsu, T. T. C., *Unified Theory of Reinforced Concrete.* Boca Raton, FL: CRC Press, 1993.

9.13 Hwang, S. J., H. W. Yu and H. J. Lee, "Theory of Interface Shear Capacity of Reinforced Concrete," *Journal of Structural Engineering* , 126(6): 700-07, 2000.

9.14 Johnson, R. P., "Composite Structures of Steel and Concrete: Beams, Slabs, Columns and Frames for Building," 2nd ed., Vol. 001, Blackwell Science, Inc., July 1995.

9.15 Loov, R. E., and A. K. Patnaik, "Horizontal Shear Strength of Composite Concrete Beams with a Rough Interface," *PCI Journal*, 39(1): 48-69, 1994.

9.16 McGregor, J. G., *Reinforced Concrete Mechanics*, 3rd ed. Upper Saddle River, NJ: Prentice Hall, 1997.

9.17 Martin, L. D., "A Rational Method for Estimating Camber and Deflection of Precast Prestressed Members," *PCI Journal*, 22(1): 100-108, 1977.

9.18 Mattock, H., "Precast-Prestressed Concrete Bridges: (5) Creep and Shrinkage Studies," *PCA Journal*, 3(2): 32-66, 1961.

9.19 Mattock, H., and N. M. Hawkins, "Research on Shear Transfer in Reinforced Concrete," *PCI Journal*, 17(2): 55-75, 1972.

9.20 Mattock, H., W. K. Li, and T. C. Wang, "Shear Transfer in Lightweight Reinforced Concrete," *PCI Journal*, 21(1): 20-39, 1976.
9.21 Sabnis, G. M., *Handbook of Composite Construction Engineering*. New York: Van Nostrand-Reinhold Co., 1979.
9.22 Saemann, J. C., and G. W. Washa, "Horizontal Shear Connections Between Precast Beams and Cast-In-Place Slabs," *ACI Journal*, 61(11): 1383-1409, 1964.
9.23 Samuely, F. J., "Some Recent Experience in Composite Precast and In Situ Concrete Construction with Particular Reference to Prestressing," *Proceedings of the Institute of Civil Engineers*, Vol. 1, 1952, Pt. 1, No. 30, pp. 222-259.
9.24 Shaikh, F., "Proposed Revisions to Shear-Friction Provisions," *PCI Journal*, 23(2): 12-21, 1978.
9.25 Siess, P., "Composite Construction for I-Beam Bridges," *Transactions ASCE*, 114: 1023-45, 1949.
9.26 Tadros, M. K., A. Ghali, and W. H. Dilger, "Time-Dependent Prestress Loss and Deflection in Prestressed Concrete Members," *PCI Journal*, 20(3): 86-98, 1975.
9.27 Tassios, T. P., and E. N. Vintzeleou, "Concrete-to-Concrete Friction", *ASCE Journal of Structural Engineering*, 113(4): 832-49, 1987.
9.28 Timoshenko, S. P., and J. P. Goodier, *Theory of Elasticity*, 3rd ed. New York: McGraw-Hill Book Co., 1970.
9.29 Viest, I. M., J. P. Colaco, R. W. Furlong, L. G. Griffis, R. T. Leon, and L. A. Wyllie, Jr., *Composite Construction Design for Buildings*. Co-published by ASCE and McGraw-Hill. New York: McGraw-Hill Co., 1997.
9.30 Walraven, J., J. Frenay, and A. Pruijssers, "Influence of Concrete Strength and Load History on the Shear Friction Capacity of Concrete Members', *PCI Journal*, 32(1): 66-84, 1987.
9.31 Wang, S. K., C. G. Salmon, and W. Anderson, *Reinforced Concrete Design*, 6th ed. New York: John Wiley & Sons, 1998.

PROBLEMS

9.1 Go back to the example of Section 9.7.6. Consider the 4 hollow-core slabs of depth 8, 10, 12, and 15 in. For each determine the prestressing force and round off its value to an integer number of strands. Assuming the cost of prestressing steel is \$1.5 per pound in place, and the cost of concrete is \$60 per cubic yard in place, which of the four section depths is more economical? Note that the final design choice may also depend on erection (weight) constraint and other parameters.

9.2 Repeat the example problem of Sec. 9.11 assuming shored construction. Build the feasibility domain of F_i and e_O and provide an acceptable layout of the prestressing tendons at midspan and at the supports. Compare the two solutions (shored versus unshored) with respect to all design aspects (shear, deflections, etc.) and draw related conclusions.

9.3 A slab system is made out of single T precast prestressed concrete beams topped by a 3 inch thick concrete slab (see Figure below). The slab is reinforced for temperature and shrinkage by a welded wire fabric placed along its centroid. The beam span is 60 ft center to center of supports.

- $f'_c = 7000$ psi, $f'_{ci} = 4500$ psi, $f_r = -627$ psi, $\gamma_c = 150$ pcf
- $E_c = 5072$ ksi; $E_{ci} = 4067$ ksi
- Cast in place slab: $f'_c = 4000$ psi, $\gamma_c = 150$ pcf
- Allowable stresses:
  $\bar{\sigma}_{ci} = 2700$, $\bar{\sigma}_{cs} = 4200$, $\bar{\sigma}_{csus} = 3150$, $\bar{\sigma}_{ti} = -201$, $\bar{\sigma}_{ts} = -502$ psi; $\bar{\sigma}_{\text{cslab}} = 1800$ psi

- f_{pu} = 270 ksi; f_{pe} = 150 ksi; f_{py} = 243 ksi; area of one strand = 0.153 in^2; low relaxation prestressing steel; η = 0.83; E_{ps} = 27,000 ksi
- Minimum d_c to centroid of steel = 6 in
- Section properties of precast beam: A_c = 592 in^2; I_g = 102185 in^4; y_t = 12.78 in; y_b = 29.22 in; Z_t = 7996 in^3; Z_b = 3497 in^3; k_t = -5.91 in; k_b = 13.57 in
- Live load: uniform 200 psf or 1200 plf
- Superimposed dead load = 0 (assumed integrated in live load)

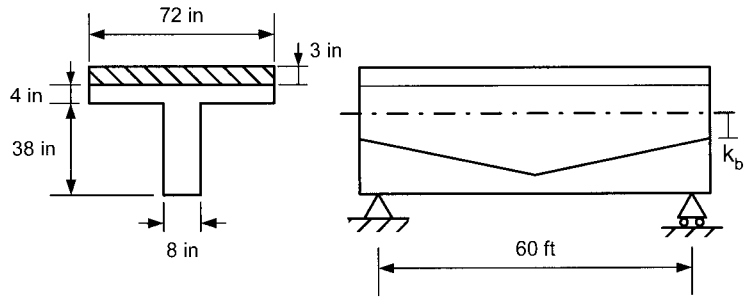

Figure P9.3

Assume the profile of the centroid of the prestressing force is draped at midspan with an eccentricity at support equal k_b. For deflection calculations, assume that the eccentricity at midspan is given by $(e_o)_{mp} = y_b - 6$ in.

1. Compute the geometric properties of the composite section; assume b_e = 72 in. Compute M_p and M_c assuming shored construction. Determine the minimum required prestressed force at midspan. Round it off to correspond to an integer number of strands. Determine the envelopes of the steel at every 1/10 the span.
2. Check ultimate moment requirements at midspan according to the ACI Code.
3. Check vertical shear requirements at x = 0.15 L from the center of the support.
4. Check horizontal shear and provide an acceptable design for horizontal shear.
5. Compute the deflection at midspan (using the approximate method) and check if it is acceptable.
6. What would be the value of the prestressing force required in 1, if the beam was unshored.
7. Assume the precast beam is used for the same problem, without the cast in place slab. Determine F and e_o at midspan by WSD, and check if USD requirements are satisfied.
8. In this particular problem: do you see an advantage to using a composite section? Why?

9.4 A composite beam is made out of a precast prestressed box beam, four feet wide, described as beam No B IV-48 in Fig. 14.5 of the book. A 10 foot wide, six inch deep, cast-in-place reinforced concrete slab is poured on top of the precast beam to form a composite beam used as a pedestrian bridge. The beam is assumed simply supported with no superimposed dead load, and a live load of 100 psf on the slab.

The following properties are given:

f'_c = 7000 psi; f'_{ci} = 4500 psi; $(f'_c)_{slab}$ = 4000 psi; normal weight concrete beam with 150 pcf; lightweight concrete slab with 115 pcf; allowable stresses from ACI Code, except $\bar{\sigma}_{ts}$ = –251 *psi*. Strands are one half inch in diameter with 270 ksi ultimate strength, and an effective prestress of 150 ksi; the yield strength of the strands is 230 ksi; η = 0.83. The yield strength of reinforcing bars = 60 ksi.

The strands are assumed straight over the entire span. Moreover, only one layer of strands is to be placed in the bottom flange at not less than 2 in spacing center to center, with a cover of 2 in to the centroid of the first layer of strands. Vertical spacing of stands in the webs must also be 2 in center to center.

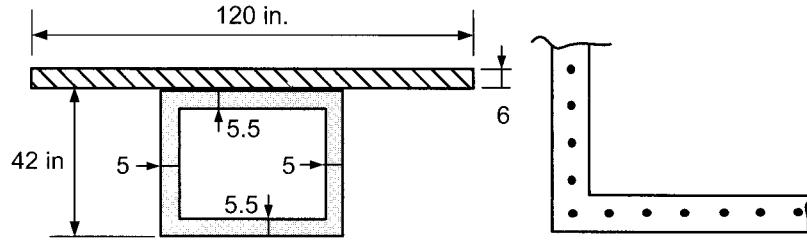

Figure P9.4

1. Using WSD, select the maximum span length (rounded to an even integer number of feet) that can be designed for, given the above data. Determine the corresponding integer number of strands needed and the prestressing tendons' eccentricity at midspan. Consider what needs to be done at the supports, if anything at all. Some iterations in placing the strands is expected.
2. Check ultimate strength requirements at midspan using the ACI code.
3. Design the vertical shear reinforcement at 12 foot from the center of the support (use the approximate method for v_c), using #4 U-shaped stirrups.
4. Design the horizontal shear reinforcement.
5. Check deflections requirements according to the ACI code. This question has numerous answers depending on the assumptions used; be as objective as possible.

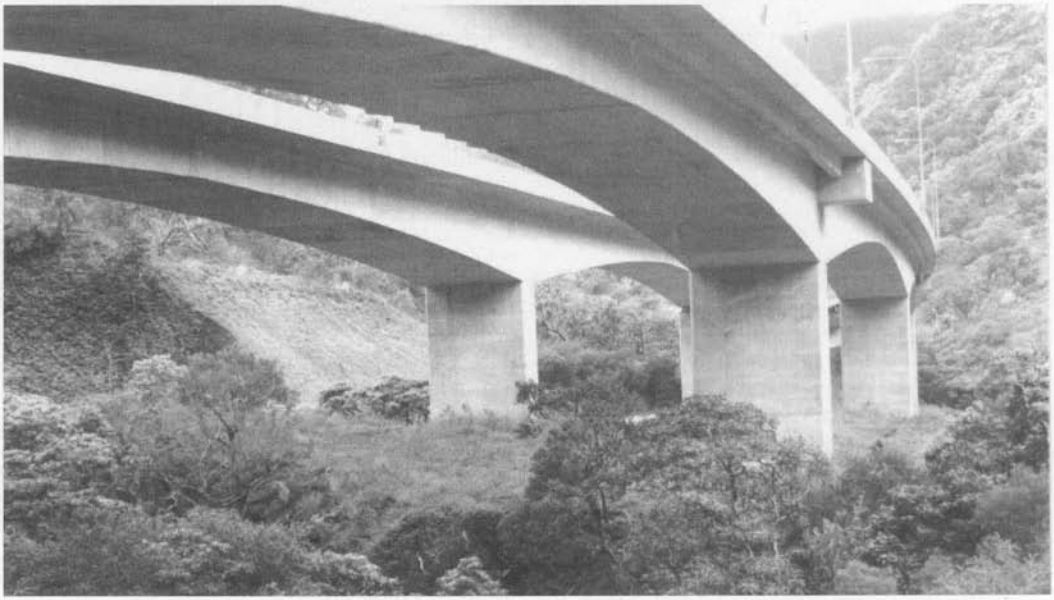

H-3 North Halawa Valley Viaduct, Hawaii. The superstructure consists of a posttensioned cast-in-place concrete box girders with 360-foot-long span lengths, erected using the balanced segmental construction method with overhead trusses. *(Courtesy T.Y. Lin International.)*

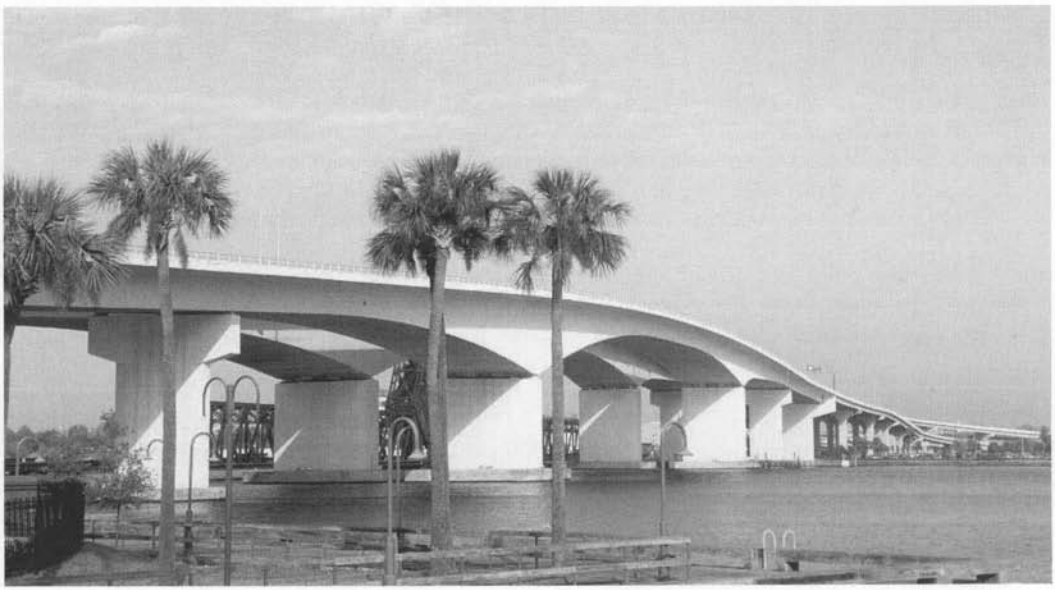

Acosta Bridge, Jacksonville, Florida. The superstructure consists of a cast-in-place posttensioned segmental box girder. *(Courtesy Vince Streano and T.Y. Lin International.)*

CHAPTER 10

CONTINUOUS BEAMS AND INDETERMINATE STRUCTURES

10.1 ADVANTAGES AND FORMS

There are inherent advantages in using continuous (or statically indeterminate) beams instead of simply supported (or statically determinate) beams made with any structural material. Everything else being equal, continuity leads to smaller design moments, smaller deflections, and higher rigidity against lateral loads. It allows redistribution of stresses under overload conditions and ensures a higher margin of safety against collapse. To take advantage of the inherent redundancy associated with continuity, most reinforced concrete structures are monolithically cast in place and many steel structures are made continuous. In prestressed concrete, continuity is mostly encountered in one- and two-way slab systems (Chapter 11), foundation mats, highway tunnels, and long-span bridges (Chapter 14). Statically indeterminate prestressed concrete frames are less common.

In addition to the above mentioned general benefits of continuity, there are several advantages to having continuous prestressed concrete beams, versus a series of simple span prestressed beams:

1. Because they have to resist smaller design moments, continuous beams are generally shallower than simple span beams and need lesser quantities of materials. On the other hand, for the same section, they offer higher load carrying capacity than simple span beams, and smaller deflections at same levels of loading.

2. Since several spans can be prestressed with the same continuous tendon and only two anchorages are needed per tendon, additional savings in labor cost can be realized compared to posttensioning a series of single span beams.
3. By giving the tendon an undulating profile, the same tendon can be used to resist both the positive and negative moments.
4. In bridges and other structures subjected to the environment, continuity reduces the number of joints and connections, leading to savings not only in initial cost but also in the cost of anticipated future maintenance over the life of the structure.

The above advantages are true for continuity in both linear and planar two-dimensional elements. However, the cost effectiveness of continuity in prestressed concrete members depends on many other factors, such as span length, design criteria, construction conditions, available technology, and the like. Continuity implies mostly a cast-in-place construction where the cost of labor and formwork is significant. It is often observed that the economy associated with the use of prestressed concrete instead of other structural materials would be nonexistent in many cases if the elements were not precast prestressed.

The benefits of continuity are often offset by drawbacks that are particular to the use of prestressed concrete. These drawbacks include:

- Practical difficulties in laying out and grouting undulating tendons
- Tendon frictional losses, in comparison to pretensioned construction, which may become excessive
- A more complex design procedure (as noted later in this chapter) where parasitic secondary moments must be accounted for
- The effects on connected members, such as columns and walls, of shortening due to the prestressing, as well as creep and shrinkage
- The difficulty in handling moment reversals.

Contrary to reinforced concrete, where the reinforcement is tailored to resist external moments by cutting or bending up bars, the prestressing force in prestressed continuous beams is generally dimensioned to resist the maximum moment along several spans and the corresponding tendons are essentially run throughout the various spans. Hence, little flexibility is left at sections where moment reversals may occur and where the same reinforcement must resist both positive and negative moments. This is particularly serious when ultimate strength, hence cracked section analysis, is considered. However, the increased acceptance of partial prestressing, where both prestressed and conventional nonprestressed reinforcement are used, provides an effective solution to remedy this disadvantage.

The above arguments suggest that the benefits of continuity in prestressed concrete may be often offset by its drawbacks. There are, however, many applications where continuity is clearly preferable. Examples include continuous slabs (one- and two-way slabs), medium- and long-span bridges, and applications where precast prestressed elements are made continuous by posttensioning on site.

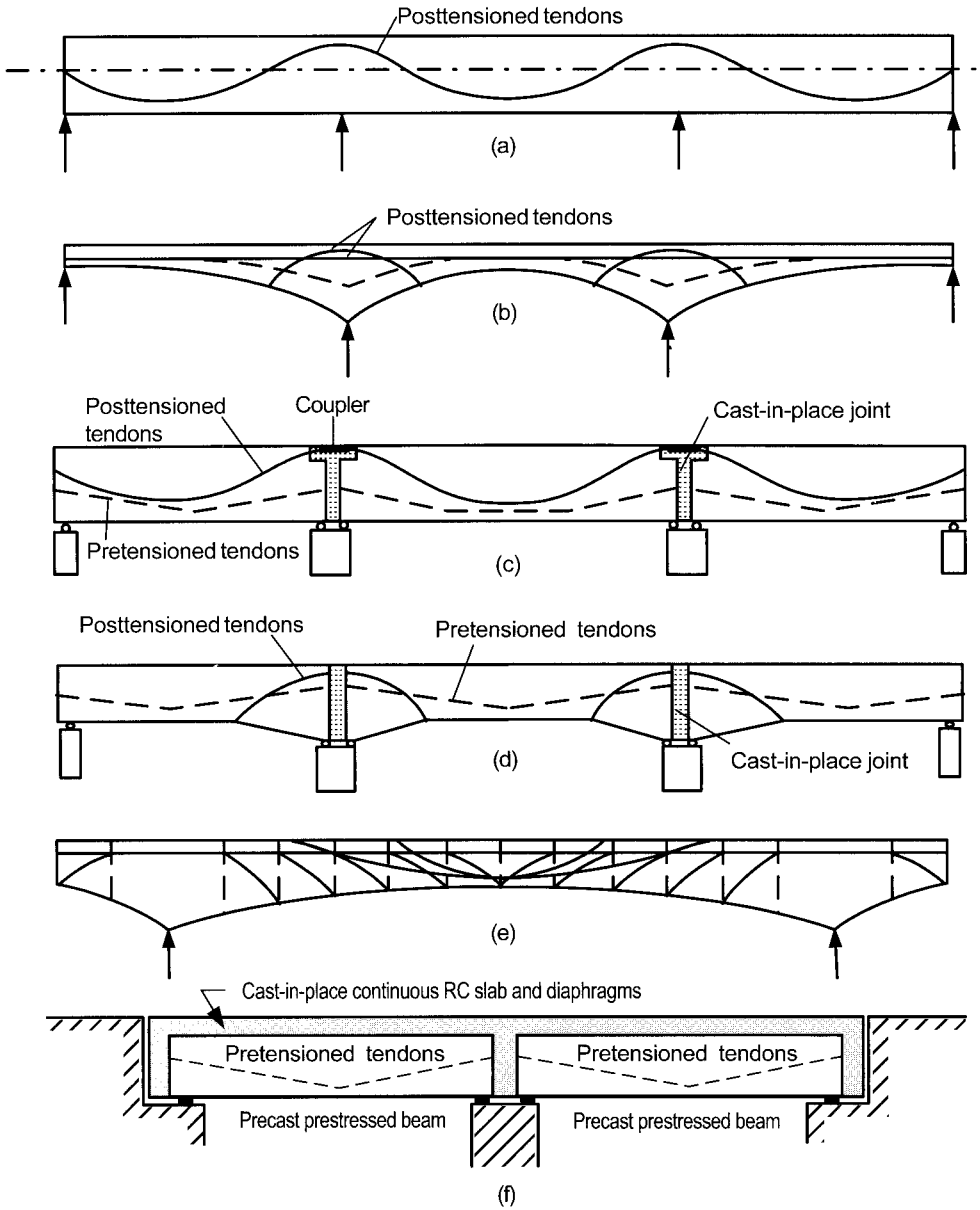

Figure 10.1 Examples of continuous beams and tendon arrangements. ***(a)*** **and** ***(b)*** **Cast-in-place construction.** ***(c)*** **and** ***(d)*** **Precast prestressed elements made continuous by posttensioning.** ***(e)*** **Cantilever construction of segmental elements.** ***(f)*** **Precast prestressed beams made continuous by a cast-in-place reinforced concrete slab.**

Continuity can be achieved in several ways. Typical examples are shown in Fig. 10.1. In cases *(a)* and *(b)*, the structure is monolithically cast in place and posttensioned thereafter. In cases *(c)* and *(d)*, precast pretensioned elements are used

to create the basic configuration, then they are jointed by posttensioned in situ to achieve continuity. The elements are generally designed to resist, by pretensioning, at least their own weight, as well as handling stresses, while posttensioning provides the additional resistance to counteract superimposed dead loads and live loads. Case *(e)* of Fig. 10.1 shows a typical segmental construction where precast elements are first designed as successive cantilevers to resist construction loads, then as part of a continuous system when the structure is ready for service. In all the above cases, a typical tendon profile is shown. In general, the profile follows the deflected shape of the structure or the moment diagram due to a uniform load (such as dead load) plotted positive downward. A last example is given in Fig. 10.1*f* where precast prestressed concrete beams are made continuous by a cast-in-place reinforced concrete slab. The slab is designed to resist the full live load at the interior supports; the beams are generally designed to carry the load as if they were simple span composite beams. This type of construction is very common because it takes full advantage of the economy offered by precast pretensioned construction while limiting on site work. Other advantages of this last method as well as a design example are covered in Section 14.15.

10.2 NECESSARY ANALYTICAL BACKGROUND

The detailed treatment of continuous prestressed concrete beams and frames in their various forms goes much beyond the scope of this text. Here, only the case of cast-in-place monolithic structures with the same continuous tendon running throughout will be considered. However, the background information and the design approach suggested in this chapter should provide a sufficient basis to allow the user to extend the analysis to different cases. The procedure presented can be followed throughout using hand computations; however, it can be easily implemented in a computer program. The following analytical background is needed:

1. Analysis of statically indeterminate structures subjected to external loads. Any method, such as matrix structural analysis or moment distribution, is acceptable. Moment distribution will be used in this chapter to determine the total moment due to prestressing. The total prestressing moments allow the determination of the secondary moments.
2. Analysis and design of simply supported prestressed concrete beams under working stresses, as described in Chapter 4.
3. Background given in Sections 10.3 to 10.10.

An example illustrating the most important aspects of design is covered in sufficient detail in Sec. 10.15. A number of properties, theorems, and corollaries are stated without proof. The reader may want to review the material in Refs. [10.4 to 10.16] for additional information.

10.3 SIGN CONVENTION AND SPECIAL NOTATION

In dealing with indeterminate structures, it is important to follow a consistent sign convention because one does not know a priori the sign of the secondary moments (defined in Section 10.4). Their value and sign are derived from the analysis. The sign convention set in Sec. 4.5 remains valid here. In particular, the eccentricity of the prestressing force $e_o(x)$ at any section x is assumed positive when F is below the neutral axis and negative when it is above it (Fig. 10.2). For vertical members, positive is to the right and negative is to the left. The same sign convention holds for the C-line or thrust line.

The prestressing force F produces a compression in the concrete and is assumed positive. The primary moment generated by F at any section x and the corresponding eccentricity $e_o(x)$ have opposite signs, thus $M_1(x) = -Fe_o(x)$.

The following notations, some of which are explained later in this chapter, are used:

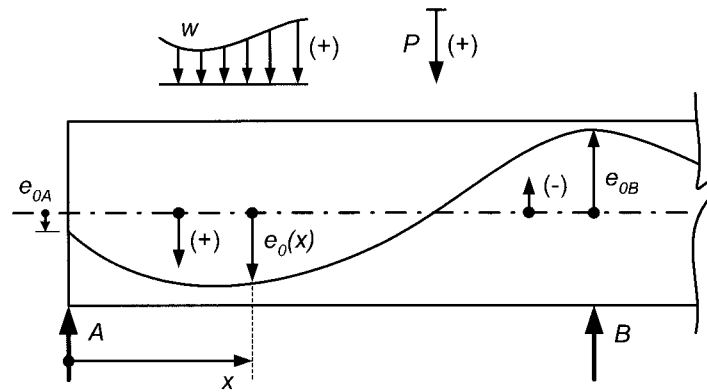

Figure 10.2 Sign convention for tendon eccentricity.

e = eccentricity in general (used mostly in figures to reduce the burden of subscripts)

$e_o(x)$ = eccentricity of the centroid of the prestressing steel at section x

$e_c(x)$ = eccentricity of the C-line at section x

$e_{oc}(x)$ = eccentricity of the Zero-Load-C line (ZLC-line) at section x. The ZLC– line in a statically indeterminate structure is due to the sole effect of prestressing (i.e., no external loads).

$M(x)$ = external moment, in general, at section x

$M_1(x)$ = primary moment due to the prestressing force at section x

$M_1(x) = -Fe_o(x)$

$M_2(x)$ = secondary moment at section x due to prestressing

$M_F(x)$ = total moment at section x due to prestressing

$M_F(x) = M_1(x) + M_2(x)$

M_{1A}, M_{1B} = primary moments at particular sections A and B

M_{2A}, M_{2B} = secondary moments at particular sections A and B

The reference to section x is ignored in the above notation if it is obvious that no confusion will result in the mathematical treatment. This is especially true when referring to equations from Chapter 4 in which the critical section is generally implied.

10.4 SECONDARY MOMENTS AND ZERO-LOAD-C (ZLC) LINE

It was shown in Secs. 3.10.2, 4.2 and 4.12 that the prestressing force F and an external moment M, acting at any section of a simply supported beam, can be resolved into a force $C = F$ acting at a distance $\delta = -M/F$ from the line of action of F. The geometric location of the C force (that is, the resultant from summation of stresses) along the various sections of a member was defined as the C-line or pressure line (also called thrust line).

For a simply supported beam, the eccentricity of the C-line with respect to the centroid of the section was defined as (Section 4.12):

$$e_c(x) = e_o(x) - \frac{M(x)}{F} \tag{10.1}$$

where $e_o(x)$ is the eccentricity of the prestressing force and $M(x)$ the external moment at section x. Equation (10.1) suggests that if no external moment is applied, the eccentricity of the C force at any section is identical to that of the prestressing steel, hence, the C-line coincides with the trajectory (or cgs, or center of gravity) of the steel. Thus, in a simply supported beam (or statically determinate structure), the effect of prestressing is reduced to that of the tendons taken solely at each section. The supports do not provide any restraint to the deformation of the structure and the prestressing moment is given by $M_F(x) = -Fe_o(x)$. This is not the case, however, for prestressed continuous beams where intermediate supports restrict the free deformation of the structure, hence leading to support reactions called secondary reactions. Secondary reactions act like concentrated loads on a simply supported beam. They generate at each section a moment called secondary moment (also called

parasitic moment or hyperstatic moment). Therefore, under the sole effect of prestressing (i.e., without external loads) two types of moments are generated at each section of a continuous beam, namely:

- the primary moment defined, as for a simply supported beam, by $M_1(x) = -Fe_o(x)$, and
- the secondary moment $M_2(x)$ generated by the secondary reactions.

The moment due to prestressing at any section x becomes:

$$M_F(x) = M_1(x) + M_2(x) = -Fe_o(x) + M_2(x) = -Fe_{oc}(x) \tag{10.2}$$

where $e_{oc}(x)$ is the eccentricity of the ZLC-line defined below. Since, in general, $M_F(x)$ is determined from the analysis of the structure, say by moment distribution or matrix structural analysis, the secondary moment is derived from Eq. (10.2) as:

$$M_2(x) = M_F(x) - M_1(x) = M_F(x) + Fe_o(x) \tag{10.3}$$

Secondary moments are secondary in nature but not in magnitude. They can represent a significant portion of the prestressing moment and, hence, must be accounted for in design. Advantage can be taken of their presence and may lead to savings in the prestressing force.

Due to the existence of secondary moments, the C-line under the sole effect of prestressing, does not coincide with the center of gravity of the prestressing steel (cgs). It is defined here as the ZLC-line (zero load C-line), because no external load is applied. The eccentricity of the ZLC-line at any section x is given by:

$$e_{oc}(x) = -\frac{M_F(x)}{F} = -\frac{M_1(x)}{F} - \frac{M_2(x)}{F} = e_o(x) - \frac{M_2(x)}{F} \tag{10.4}$$

Equation (10.4) suggests that in absence of external loads the prestressing force with eccentricity $e_o(x)$, acts as if it had an eccentricity $e_{oc}(x)$. Thus, $e_{oc}(x)$ can also be described as the effective eccentricity of the prestressing force. In presence of an external moment $M(x)$, the eccentricity of the C-line becomes:

$$e_c(x) = e_{oc}(x) - \frac{M(x)}{F} = e_o(x) - \frac{M(x) + M_2(x)}{F} \tag{10.5}$$

which suggests that $M_2(x)$ acts like an additional external moment on the section. When the secondary moments are equal to zero, Eq. (10.5) is reduced to Eq. (10.1) as for simply supported beams. The tendon profile in the continuous beam is then said to be concordant (see Section 10.7).

If both the ZLC-line and the steel profile are known, Eq. (10.4) leads to :

$$\begin{cases} \Delta e_{oc}(x) = e_{oc}(x) - e_o(x) = -\dfrac{M_2(x)}{F} \\ \text{or} \\ \Delta e_o(x) = e_o(x) - e_{oc}(x) = \dfrac{M_2(x)}{F} \end{cases} \tag{10.6}$$

where $\Delta e_{oc}(x)$ can be considered as a fictitious increase or decrease in the eccentricity of the prestressing steel at section x, due to the presence of secondary moments.

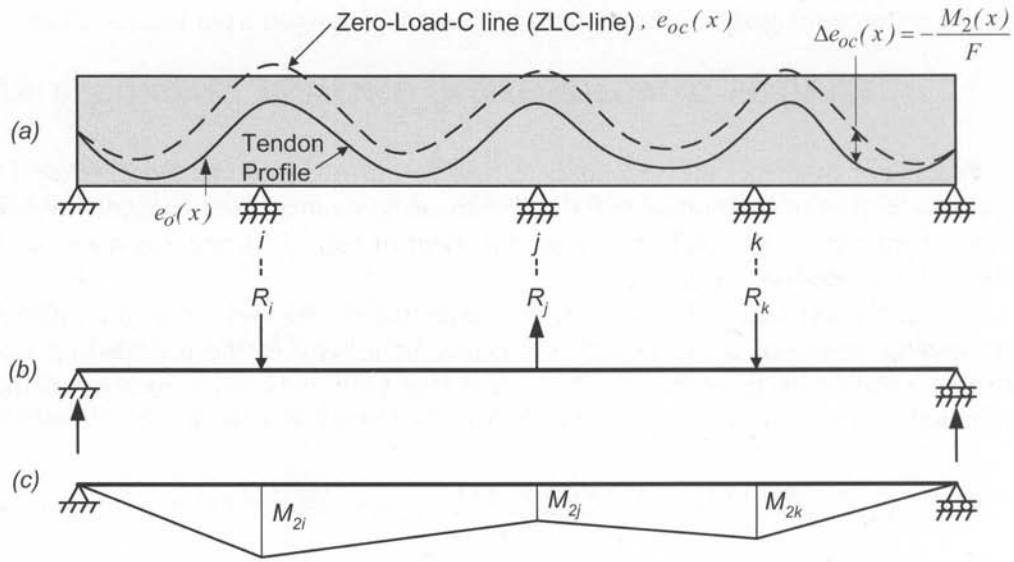

Figure 10.3 ***(a)*** **Tendon profile and ZLC-line.** ***(b)*** **Secondary reactions.** ***(c)*** **Secondary moment diagram.**

A typical tendon profile and corresponding ZLC-line are plotted in Fig. 10.3*a*. The secondary reactions and corresponding secondary moments are schematically shown in Figs. 10.3*b* and *c*. As the secondary reactions are generated by prestressing, they form a system of forces with a null resultant. Since they act as concentrated forces at interior supports, the variation of secondary moment between consecutive supports is linear, similarly to the case of simply supported beam subjected to concentrated loads. Therefore, for a typical span with left support A and right support B (Fig. 10.4), the secondary moment at any section x along that span can be computed from the secondary moments at the supports as:

$$M_2(x) = M_{2A} + (M_{2B} - M_{2A})\frac{x}{l} = M_{2A}\left(1 - \frac{x}{l}\right) + M_{2B}\left(\frac{x}{l}\right) \tag{10.7}$$

The existence of secondary moments and other properties of interest in continuous beams are illustrated in the next section.

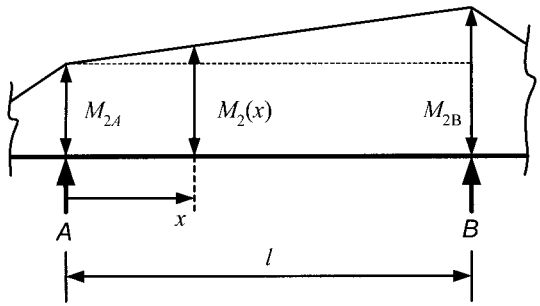

$$M_2(x) = M_{2A} + (M_{2B} - M_{2A})\frac{x}{l}$$
$$= M_{2A}(1 - \frac{x}{l}) + M_{2B}\frac{x}{l}$$

Figure 10.4 Secondary moment diagram due to prestressing for a typical span *AB*.

10.5 EXAMPLE: SECONDARY MOMENTS AND CONCORDANCY PROPERTY

The existence of secondary moments can be illustrated by simple examples of a two-span continuous beam prestressed by straight or segmented tendons (Figs. 10.5*a* to 10.5*c*). Although the tendon profiles assumed are not practical for real applications, they help illustrate important properties related to secondary moments and concordancy property.

In the following three-parts example, it will be assumed that only the effect of prestressing is considered, that is, no external loads are acting, including the own weight of the beam.

Case a, Fig. 10.5a: Consider first the case of a two-span continuous beam with a straight tendon profile having the same eccentricity e throughout (Fig. 10.5*a*). If the intermediate support B was nonexistent, the beam would be simply supported at A and C and would camber under the effect of prestressing (the beam is assumed weightless). The presence of support B restrains the movement of the beam and hence generates a reaction R_B. The magnitude and direction of R_B are such that R_B should create a deflection at B equal and opposite to the camber created by prestressing. Referring to Fig. 7.6 and assuming a simply supported beam with span $2l$, the deflection due to R_B is given by:

$$\Delta_2 = \frac{R_B(2l)^3}{48EI}$$

The camber due to prestressing (equivalent end moments at A and C) is given by:

$$\Delta_1 = -\frac{Fe(2l)^2}{8EI}$$

Setting the sum $(\Delta_1 + \Delta_2)$ equal to zero leads to:

$$R_B = \frac{3Fe}{l}$$

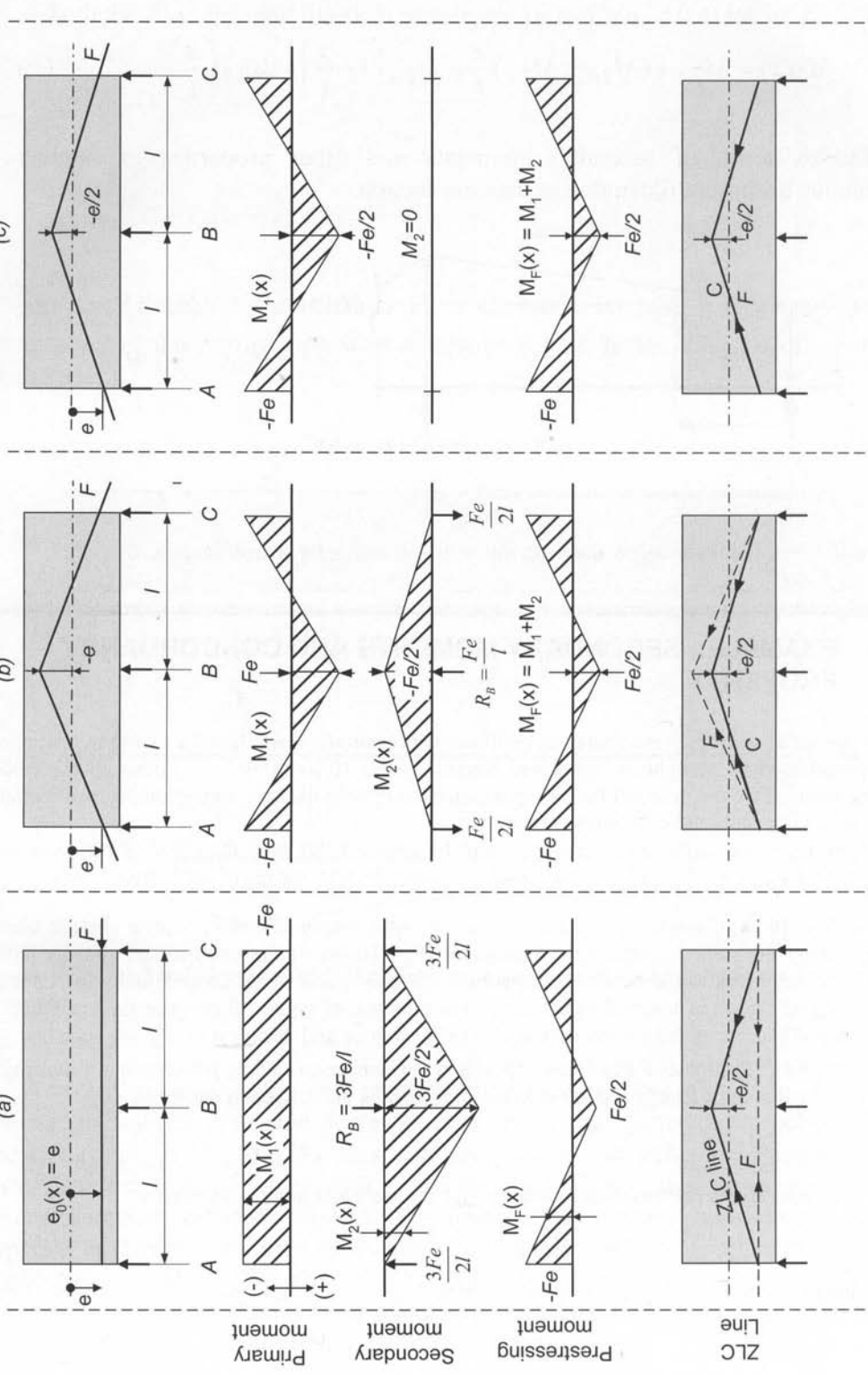

Figure 10.5 Examples illustraing the variations of primary moments, secondary moments, prestressing moments, and ZLC-line in continuous beams.

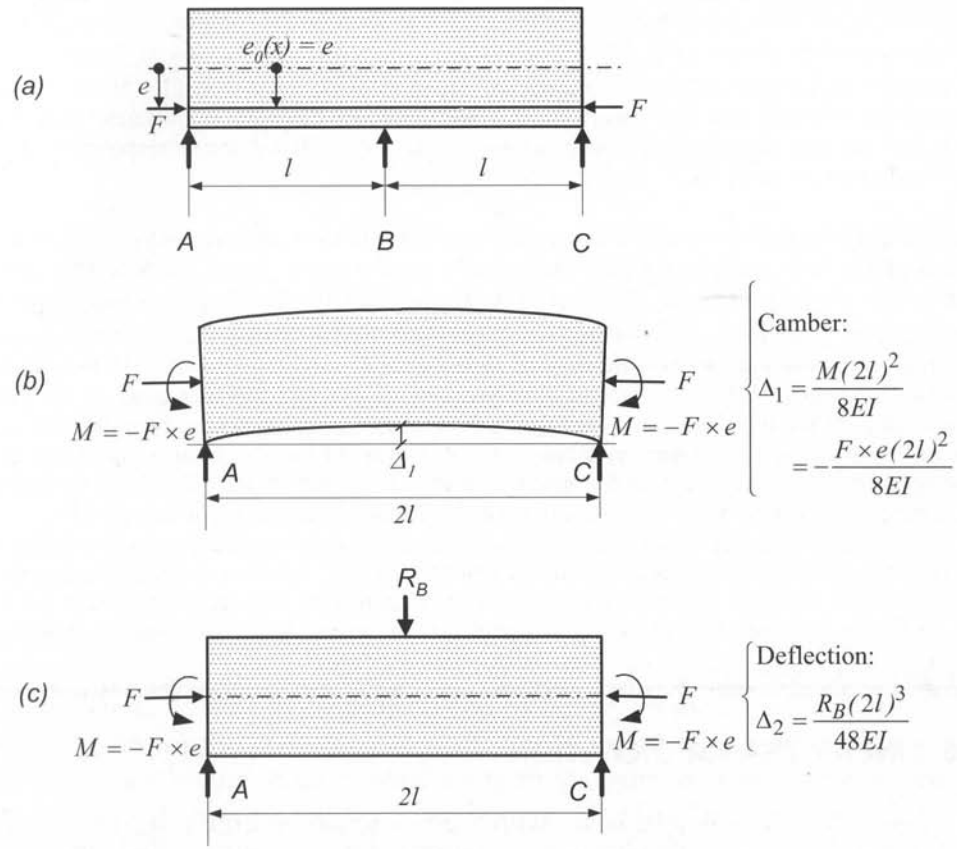

Figure 10.6 Example illustrating the calculation of a secondary reaction.

These computations are illustrated in Fig. 10.6. The reaction R_B is called a *secondary reaction* and the moment due to R_B is called a secondary moment. Thus, prestressing the continuous beam ABC of Fig. 10.5*a* generates at each section x a primary moment $M_1(x) = -Fe$ and a secondary moment $M_2(x)$ induced by the secondary reaction R_B. $M_2(x)$ is obtained by treating the beam AC as simply supported at its two ends, with a concentrated force R_B at B. Thus the secondary moment is linear between supports, similarly to the moment generated by concentrated loads on a simple beam.

The primary and secondary moment diagrams for this case are plotted in Fig. 10.5*a*, as well as their sum, the prestressing moment $M_F(x) = M_1(x) + M_2(x)$.

Two observations can be made: (1) the secondary moment can be significant in magnitude (here equal to 1.5 times the primary moment at support B, and opposite to it), and (2) the prestressing moment in a continuous beam can be substantially different in both magnitude and shape from the primary moment otherwise obtained if the beam was simply supported. Given the prestressing moment, the ZLC-line can be determined from Eq. (10.4) and is also shown in the bottom part of Fig. 10.5*a*. Note that it deviates substantially from the steel profile, which is straight throughout. It has the same eccentricity e at the end supports and an eccentricity $-e/2$ at B.

The next two cases are covered next to illustrate other important features.

Case b, Fig. 10.5*b*: In this case, the eccentricity of the prestressing force at B is changed from $+e$ (case *a*) to $-e$, while the eccentricities at the end supports A and C are kept the same. Using the deflection equations given in Fig. 7.6, the reaction R_B is calculated in a manner similar to case *a*. The primary, secondary, and total moments are determined and plotted in Fig. 10.5*b*. It can be observed that, although both the primary and secondary moment diagrams are different from those of case *a*, the resulting prestressing moment diagram is the same. Hence, the corresponding ZLC-line (Eq. 10.4) is also the same.

Case c, Fig. 10.5*c*: In this case, the steel profile is modified to show an eccentricity $-e/2$ at support B. This profile is the same as the ZLC-line found in cases *a* and *b*. Using the deflection equations given in Fig. 7.6, the reaction R_B is calculated in a manner similar to case *a*. It is found equal zero, thus leading to a secondary moment that vanishes throughout. Following the same steps as for the other two cases, the primary, secondary, and total moments are plotted in Fig. 10.5*c*. Since the secondary moment is zero at any section, the prestressing moment becomes equal to the primary moment (Fig. 10.5*c*). It is further observed that both the prestressing moment and the ZLC-line are the same as for cases *a* and *b*. Moreover, in case *c*, the ZLC-line coincides with the trajectory (or cgs) of the steel. When this occurs, the tendon profile is said to be "concordant." Therefore, for case *c* we have a concordant steel profile, while for cases *a* and *b* we have nonconcordant steel profiles.

The above example suggests an additional important result: the three different steel profiles of cases *a, b* and *c* in which only the eccentricity at the intermediate support B was varied, led to the same ZLC-line. This result is due to a property of the "linear transformation," explained in the next section.

10.6 LINEAR TRANSFORMATION

Let us consider a continuous beam with a given tendon profile (Fig. 10.7). Let us modify the profile by subjecting it to some finite displacement at the intermediate supports, without changing its intrinsic shape between supports and keeping the same eccentricities at the end supports. Such a transformation is called a linear transformation. Along any span, the linear transformation is equivalent to a rotation, a translation, or both. Calling $\Delta e_o(x)$ the displacement between the reference profile and the transformed profile at any section x of a span, its value can be obtained from:

$$\Delta e_o(x) = ax + b \tag{10.8}$$

where x is the distance from the left support and a and b are constants. The term ax essentially leads to a rotation with respect to the left support while the term b represents a translation. The following theorem stated without proof is originally due to Guyon [Refs. 10.5 and 10.6]:

> *A linear transformation of a tendon profile does not modify the ZLC-line of the tendon.*

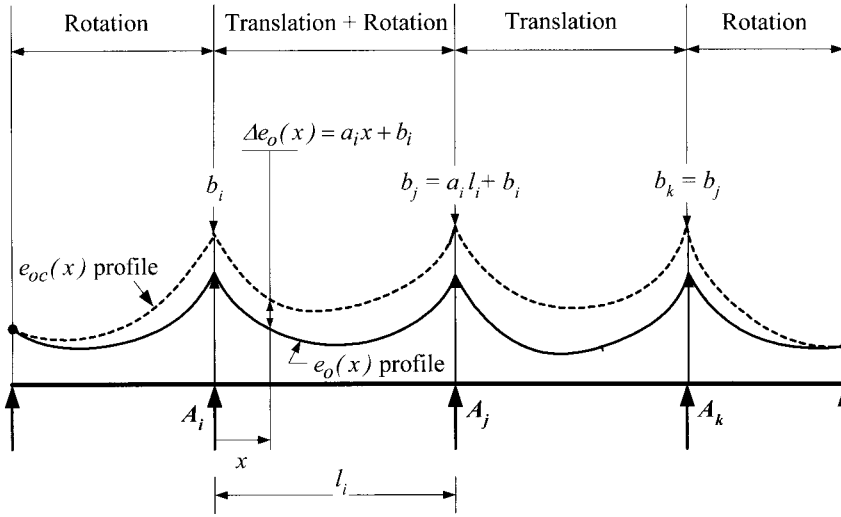

Figure 10.7 Example of linear transformation illustrating rotational effect, translational effect, or their combination.

In other words, the linearly transformed profile produces the same ZLC-line as the reference profile. Hence, moments, shear forces, and stresses due to prestressing remain the same. However, the primary and secondary moments will change.

The property of the linear transformation applies not only to beams, but also to frames with rigid joints. If the continuous beam or frame is fixed at one or two end supports, it would apply even if the eccentricities at the fixed ends are modified.

Referring back to Fig. 10.5, it is observed that the tendon profiles for cases *b* and *c* are in effect linearly transformed from the profile of case *a* and, therefore, they all lead to the same ZLC-line.

10.7 CONCORDANT TENDONS

By definition, a concordant tendon profile produces a ZLC-line that coincides with its cgs (center of gravity of the steel) at any section, that is: $e_{oc}(x) = e_o(x)$. Note that the ZLC-line assumes no external loading is applied other than the prestressing force. Thus, the secondary reactions are null and the secondary moments vanish everywhere. A number of properties related to concordant tendons are stated next without proof. Additional information can be found in Refs. [10.4 to 10.6].

1. *The principle of superposition is valid for concordant tendons, namely superposing one or more concordant profiles leads to a concordant profile and superposing a concordant profile with a nonconcordant profile leads to a nonconcordant profile.*

2. *Any real moment diagram in a continuous beam on nonsettling supports produced by any combination of external loadings (whether transverse loads or moments) plotted to any scale along the centroidal axis of the beam, defines the location of a concordant tendon. Thus, if a tendon is placed along a trajectory proportional to a moment diagram, it will be concordant.*
3. *The reciprocal of property 2 above is also true: the profile of any concordant tendon measured from the centroid of the section is a moment diagram for some real system of loadings.*
4. *Any ZLC-line trajectory is a profile for a concordant tendon.*

Property 2 can be used to determine a concordant tendon profile. For instance, given a moment diagram due to some external loading and described by $M(x)$ at any section x, a tendon profile can be defined by:

$$e_o(x) = \frac{M(x)}{K} \tag{10.9}$$

where K is an arbitrary constant. The value of K can be determined so that the tendon profile obtained remains within the section, that is $|e_o(x)| \le (e_o)_{mp}$. For this, all the critical sections (supports, and midspan or near midspan sections) are considered, and at each critical section i, a value K_i is determined as follows:

$$K_i = \left(\frac{M(x)}{(e_o)_{mp}} \right)_i \tag{10.10}$$

K is taken as the largest value of all $|K_i|$ obtained and is used throughout the member in Eq. (10.9). Of course, this implies that the same prestressing force is used throughout.

Note that the moment diagram $M(x)$ used to determine a concordant profile is not necessarily due to a single loading. If, for instance, a moment due to a uniform load such as dead load is used, it will have sharp peaks (negative moments) at the supports. Hence, sharp, unacceptable peaks will also be present in the corresponding profile. In order to smoothen the profile, another loading is appropriately selected to generate positive moments at the support and is superimposed to the first loading. A schematic representation of this procedure is shown in Fig. 10.8 and an example is developed in Section 10.15, case *a*.

It is important to point out that, although concordant tendons can be easily determined, they are not necessarily more desirable than nonconcordant tendons. They simplify the design procedure by eliminating secondary moments. However, a nonconcordant tendon profile can be selected in such a way as to magnify the effect

of prestressing and hence can lead to significant savings in the prestressing steel. This is particularly effective for service limit states.

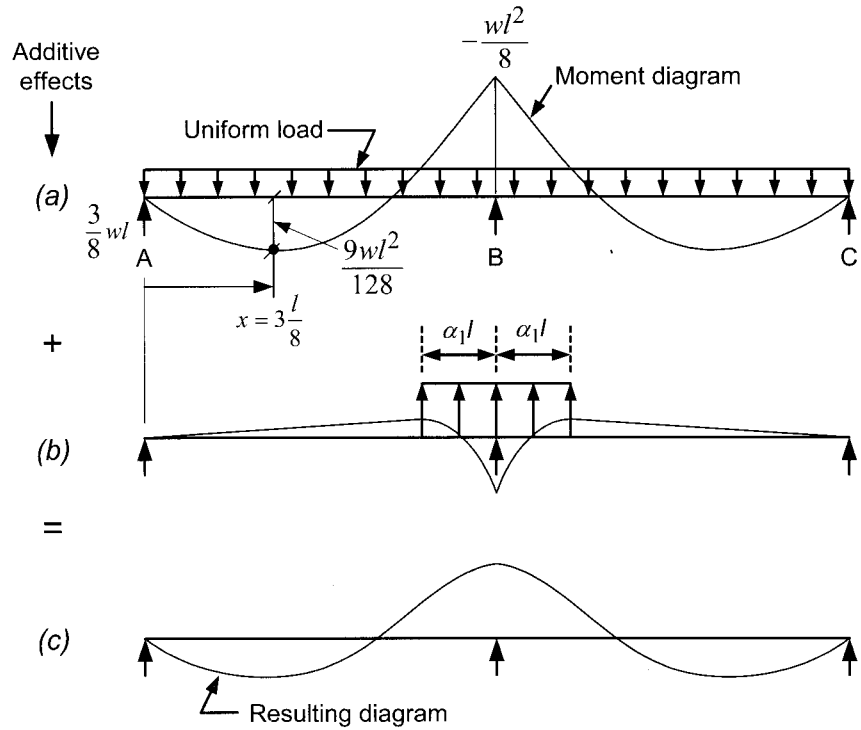

Figure 10.8 Example of superposition of moment diagrams to obtain a smooth concordant profile.

In preliminary design, it is often desirable to assume first that a concordant tendon will be arrived at, that is, secondary moments are null, thus allowing a quick evaluation of the prestressing force. However, since the shape of the secondary moment diagram depends only on the tendon profile and the geometric properties of the beam (including spans, and support conditions), it is often desirable to select a practical tendon profile passing by maximum acceptable eccentricities at key critical sections and evaluate thereafter the importance of secondary moments (see Section 10.11.3). Only then are adjustments and modifications used depending on whether the secondary moments are beneficial or not.

10.8 EXTERNAL LOADS EQUIVALENT TO PRESTRESSING

The effects of a prestressing tendon acting on a beam can be replaced by the effects of equivalent loads. These loads can easily be identified if the free body diagram of

the concrete without the steel is drawn. Equivalent loads include concentrated horizontal and vertical forces, moments at the external supports and transverse forces along the tendon profile. Transverse forces are generated by the curvature or the change in profile of the tendon. They can be in the form of a concentrated force (due to an abrupt change in the slope of the tendon profile), a uniform load, or a distributed variable load. For a curved tendon, the magnitude of the equivalent transverse load over a unit length is equal to F/ρ_x, where ρ_x is the local radius of curvature of the tendon at the section x considered.

10.8.1 Concept of Equivalent Load

To illustrate the equivalent load concept, let us consider a simply supported beam, prestressed by a tendon carrying a force F and having a circular profile with radius R (Fig. 10.9*a*). Let us determine the equivalent transverse load on the concrete. The change in curvature between section x and $x+dx$ produces a transverse negative reaction $-(F/R)dx$ (Fig. 10.9*b*). For a unit length, the reaction becomes $-F/R$. Its projection on the vertical axis is $(-F/R)\cos\theta_x$. However, as θ_x is very small, $\cos\theta_x \simeq 1$, and the vertical reaction on the concrete beam is equal $-F/R$ per unit length. This is essentially equivalent to a uniform external load on the beam of value $w=-F/R$. The corresponding free body diagram of the beam, including the end loads (and end moments), is shown in Fig. 10.9*c*. The beam can be analyzed for these loads and should show exactly the same state of stress as if the prestressing force of Fig. 10.9*a* was present. In particular, external equilibrium equations must be satisfied. For the beam of Fig. 10.9*c*, they lead to:

Horizontal forces: $F+(-F)=0$

Moments: $-Fe+Fe=0$

Vertical forces: $\dfrac{F\theta}{2}+\dfrac{F\theta}{2}+wl=0$

The last equation is verified because $wl=-(F/R)l$ and for a circle $l/R=\theta$.

Examples of equivalent loads for typical tendon profiles (or cgs of prestressing steel) are shown in Fig. 10.10 and should cover the majority of practical cases. The given formulas generally assume that the eccentricity is small with respect to the span, that is, relatively shallow members are used. Note that for a straight tendon, the transverse load is zero; only the axial force and the end moments are present. In order for the moments generated by the equivalent loads to have the correct sign, the loads are assumed positive downward and negative upward. This explains the negative sign associated with the loads of Fig. 10.10.

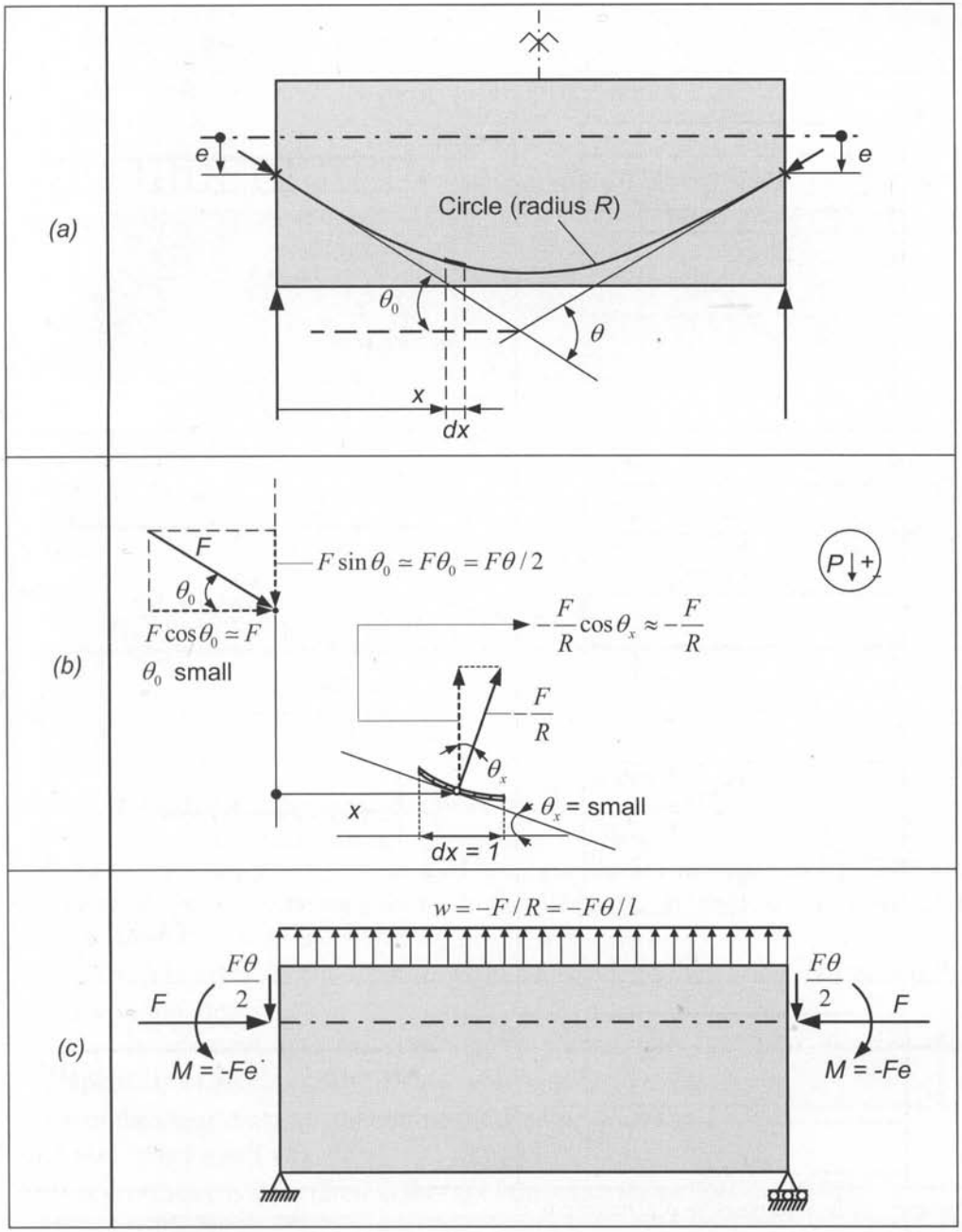

Figure 10.9 Concept of equivalent load. ***(a)*** **Tendon profile.** ***(b)*** **Transverse load due to prestressing.** ***(c)*** **Free body diagram of concrete beam.**

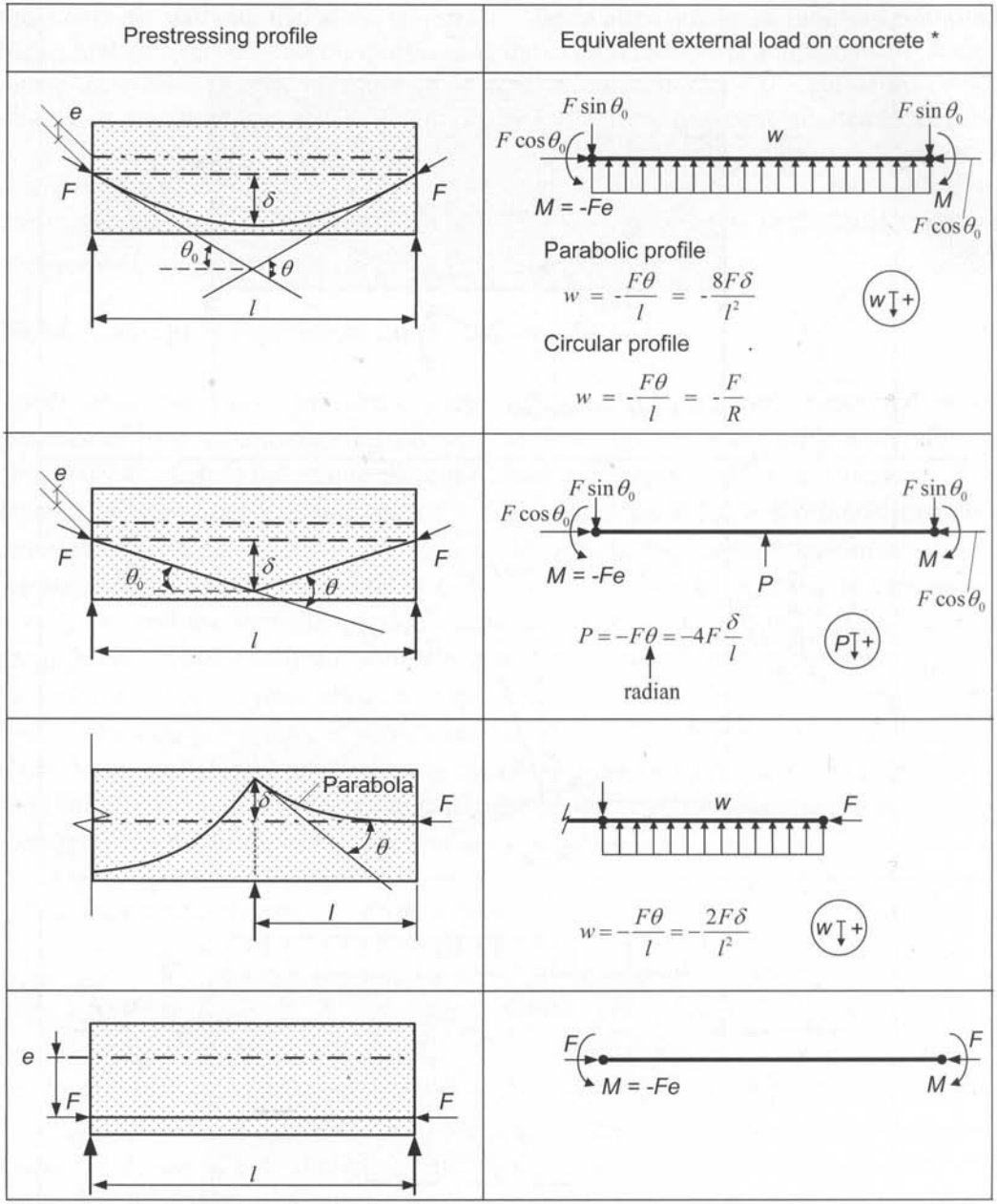

* Assuming shallow members for δ in function of θ

Figure 10.10 Equivalent load formulas for typical tendon profiles in beams.

10.8.2 Application of Equivalent Load to a Continuous Tendon

When a continuous undulating tendon is used, the length over which the same profile exists is not the same as the span length. This is illustrated in Fig. 10.11, where a

typical example of equivalent loads for a continuous beam is shown. For instance, the load w_4, assuming a parabolic portion of tendon, is given by $-F\theta_4 / l'_4$ or $-8F\delta_4 / (l'_4)^2$. Several such loads of different magnitude can be present along the same span.

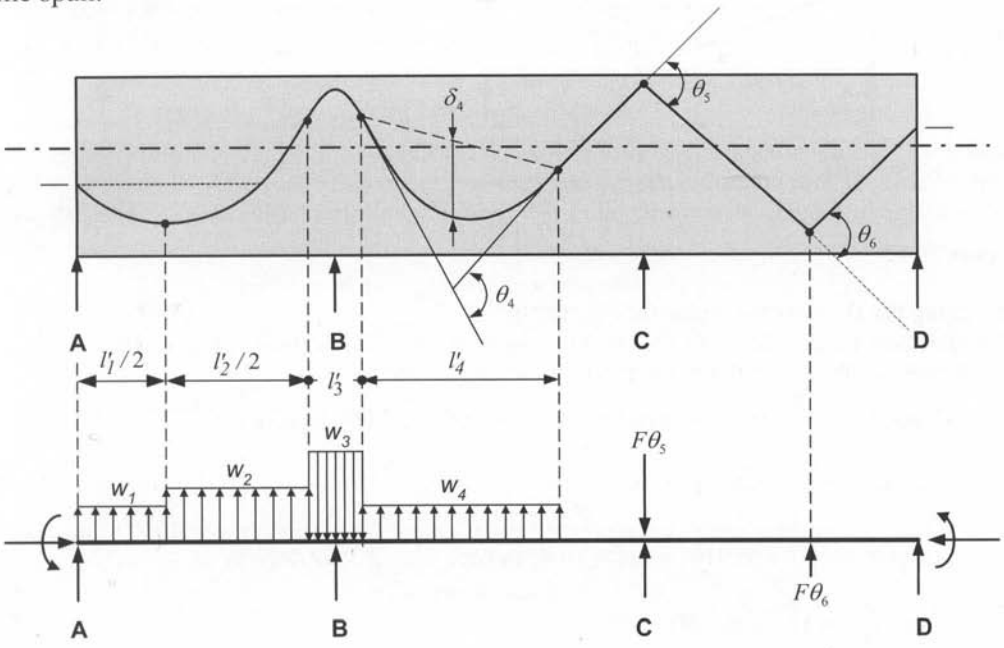

Figure 10.11 Equivalent loads in a continuous beam.

Note that for any other nonstandard steel profile not included in Fig. 10.10, the equivalent transverse loading can be found from the theoretical curvature of the profile or from the following steps:

1. Plot the primary moment diagram $M_1(x)$ throughout the various spans as if there were no supports.
2. From the moment diagram, determine the corresponding shear diagram either graphically or algebraically. *(Note:* $V(x) = dM_1(x)/dx$.*)*
3. From the shear diagram, determine the loading diagram. (Note: $w(x) = -dV(x)/dx$.)

This procedure is illustrated in part *b* of the example in Section 10.8.3.

10.8.3 Example: Equivalent Load

Consider the two-span prestressed continuous beam shown in Fig. 12. The beam is symmetrical with respect to support B. For simplicity of solution, the prestressing tendon profile is assumed to be made of segmented straight lines with sharp angle change at key points. Assuming the prestressing force F = 600 kips, determine the equivalent load. This problem is continued in Section 10.9.3. Two approaches are illustrated next.

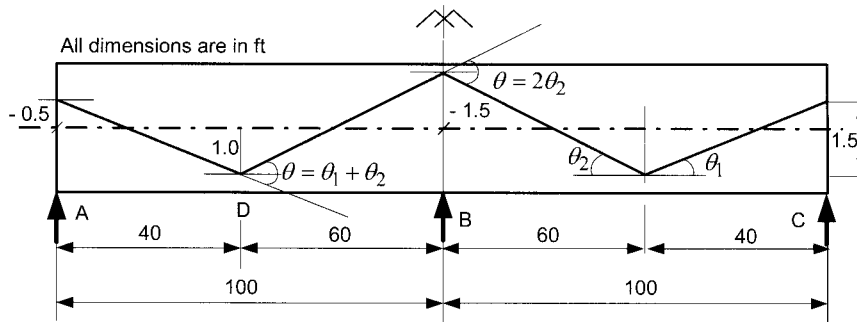

Figure 10.12

a. Using the Derived Formulae (of Fig. 10.10)

The equivalent loading due to various prestressing tendon profiles is given in Fig. 10.10.

Determine first the angles of the profile at sections *D* and *B*:

$$\tan(\theta_1) = \frac{1.5}{40} = 0.0375 \approx \sin(\theta_1) \approx \theta_1 \text{ radian}; \quad \theta_1 = 2.1476 \text{ degrees}$$

$$\cos(\frac{\pi}{2} - \theta_1) = \sin\theta_1 = 0.0375;$$

$$\tan(\theta_2) = \frac{2.5}{60} = 0.04167 \approx \sin(\theta_2) \approx \theta_2 \text{ radian}; \quad \theta_2 = 2.3859 \text{ degrees}$$

$$\cos(\frac{\pi}{2} - \theta_2) = \sin\theta_2 = 0.04167;$$

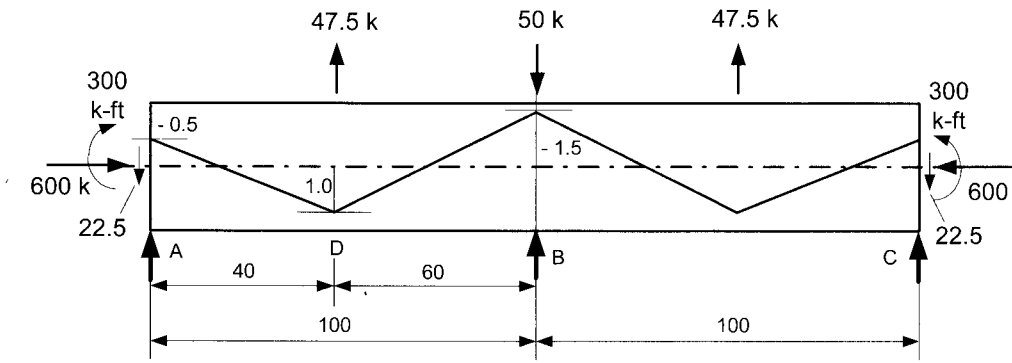

Figure 10.13

The equivalent concentrated loads are obtained as follows:

At section D:

$$P = F(\theta_1 + \theta_2) = 600(0.0375 + 0.04167) = 22.5 + 25 = 47.5 \text{ kips (upward)}$$

At section B:

$$P = F(\theta_2 + \theta_2) = 2F\theta_2 = 2 \times 600 \times 0.04167 = 50 \text{ kips (downward)}$$

The prestressing moments at sections *A* and *C* are equal: $-Fe_o = -600 \times -0.5 = 300$ kips-ft

The horizontal and vertical components of the prestressing force at support sections A and C are given by:

$$F_H = F\cos(\theta_1) = F\cos(2.1476) = 600 \times 0.9993 = 599.58 \approx 600 \text{ kips}$$

$$F_V = F\sin(\theta_1) = 600 \times 0.0375 = 22.5 \text{ kips}$$

The equivalent loading is shown in Fig. 10.13.

Note that the vertical component of the prestressing force is resisted by the concrete and is not a real reaction.

b. Using the Primary Moment Diagram

At the end of Section 10.8, it was stated that the equivalent load can be determined from the primary moment diagram, by differentiating a first time to obtain the shear diagram, and a second time to obtain the load. Let us illustrate this procedure in this example since the moment diagram is very simple.

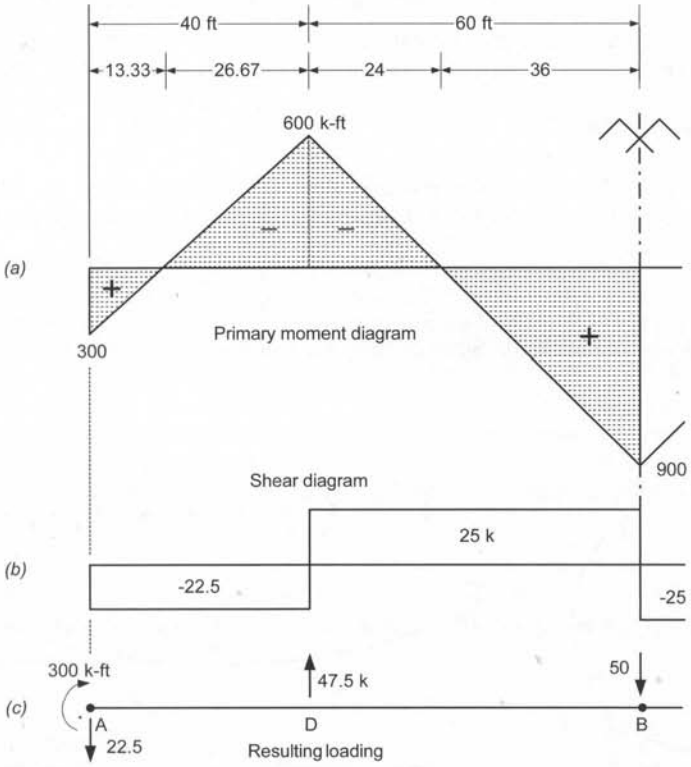

Figure 10.14

From the profile of the prestressing steel, the primary moment diagram can be calculated as $M_1(x) = -F \times e_o(x)$ where $e_o(x)$ is taken positive downward and negative upward. The moment diagram is plotted in Fig. 10.14*a* for span AB only (since there is symmetry).

The first derivative of the primary moment diagram gives us the shear diagram. Applying that to the diagram along *AD*, we get:

$$V_{AD} = \frac{dM}{dx} = \text{ Slope of line} = \frac{600-(-300)}{40} = \frac{900}{40} = 22.5 \text{ kips}$$

$$V_{DB} = \frac{dM}{dx} = \text{Slope of line} = \frac{-900-600}{60} = \frac{-1500}{60} = -25 \text{ kips}$$

The shear diagram is plotted in Fig. 10.14*b*. Since it is constant along each portion of beam, its derivative is zero. However, the abrupt change in shear at any section, such as at section *D*, leads to a concentrated load, which at *D* is equal: - 22.5 - 25 = - 47.5 kips (Fig. 10.14*c*). This is indeed what we obtained from the equivalent load approach. It can be shown that at support *B*, the change in shear is equivalent to a concentrated load of 50 kips, while it is 22.5 kips at supports *A* and *C*. Of course, to this equivalent load we have to add the moment at *A*, considered an external moment and equal to 600x0.5 = 300 k-ft.

These results are same as for case *a* and are illustrated in Fig. 10.13.

10.8.4 Example: Equivalent Load for a Circular and Parabolic Tendon Profile

The equivalent load for a circular and a parabolic tendon profile is given in Fig. 10.10. A proof of these results is given next. To simplify the presentation, stresses or loads will be assumed positive.

1. Circular Tendon Profile

Consider a unit wide slice of a thin walled cylindrical tank subjected to internal pressure p (Fig. 10.15). A circular ring with radius R is obtained. The internal pressure induces a tensile stress in the ring of magnitude:

$$\sigma_t = \frac{pR}{t}$$

where t is the thickness of tank wall. Since the ring has a unit width, the tensile force in the ring is given by:

$$N = \sigma_t \times t \times 1 = pR$$

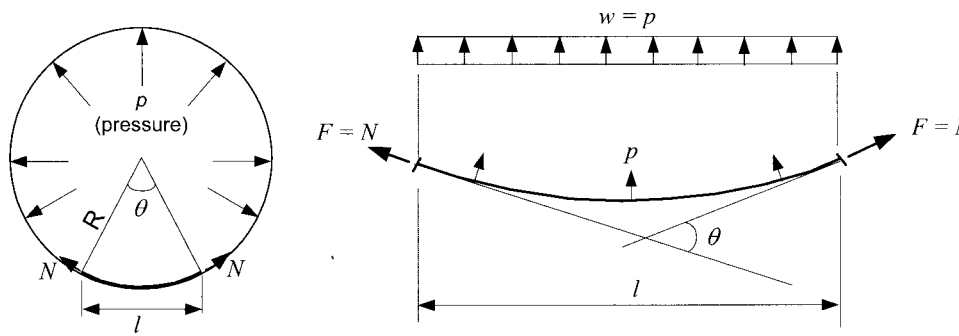

Figure 10.15 Circular tendon profile.

A circular prestressing tendon of length l can be assumed a part of the above ring. Assume the volume inside the ring is filled with concrete. Should the tendon be prestressed with a force $F = N$, it would exert a pressure p on the internal surface of contact with the concrete. If the radius of the ring is very large compared to its length, the pressure p, which is normal to the profile of the ring, can be considered vertical (that is, in the direction of gravity). Thus p is similar to a uniform load w. We can thus write:

$$p = \frac{N}{R};\ F = N;\ \text{and}\ w = p$$

from which we get:

$$w = \frac{F}{R}$$

This is the uniform load exerted on the concrete by a circular prestressing tendon carrying a prestressing force F; the load w is normal to the profile of the tendon. Since the tendon is assumed shallow, w is assumed to be vertical for this discussion.

Referring to Fig. 10.15, the length l of a circular tendon is related to its radius R and the central angle as follows:

$$\frac{l}{R} = \theta \quad \text{in radians; or} \quad \frac{1}{R} = \frac{\theta}{l}$$

Thus, the uniform load induced by a circular tendon can also be written:

$$w = \frac{F}{R} = F\frac{\theta}{l}$$

Inversely, if we apply a uniform load normal to the profile of a circular tendon, we will generate a prestressing force in the tendon given by:

$$F = \frac{wl}{\theta}$$

2. Parabolic Tendon Profile

The curvature of a curve represented by an equation $y(x)$ is given by the following general relation:

$$\kappa = \frac{1}{\rho} = \frac{d\theta}{ds} = \frac{y''}{(1+y')^{3/2}}$$

where κ is the curvature, ρ is the radius of the curve at the section considered, and y' and y'' are the first and second derivative of $y(x)$, respectively. Since the curve is assumed shallow, the first derivative, y', that is, the tangent to the curve, is close to being horizontal and taken equal zero. Thus, the curvature can be simplified as:

$$\kappa = \frac{1}{\rho} = y''$$

Now consider that the curve is a parabola. Thus, assuming the vertex of the parabola is the origin of the axis (Fig. 10.16*b*):

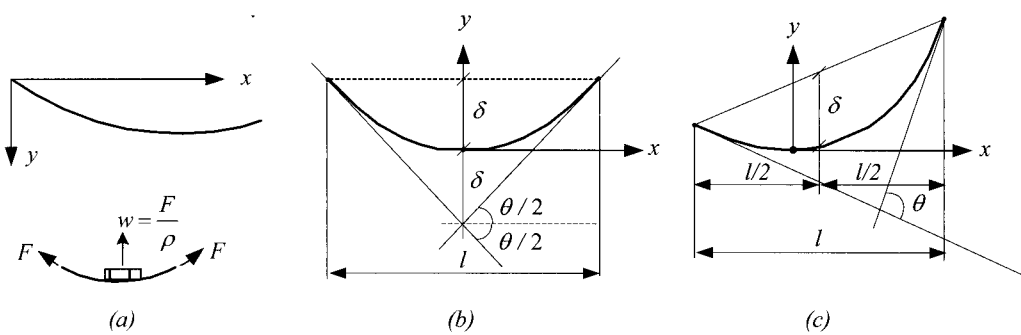

Figure 10.16 Parabolic tendon profile and properties.

$$y = ax^2$$
$$y' = 2ax$$
$$y'' = 2a$$

Similarly to the argument made above for a circular tendon prestressed by a force F, the uniform load generated by the tendon normal to its profile (or its curve) is given by (Fig. 10.16*a*):

$$w = \frac{F}{\rho} = F \times y'' = 2aF$$

from which:

$$a = \frac{w}{2F}$$

The equation of a parabola must also satisfy some geometric boundary condition; assume the origin is at the vertex of the parabola (Fig. 10.16) the following condition must be satisfied:

$$y = \delta \text{ for } x = \frac{l}{2}$$

Thus:

$$y = ax^2 = \delta = a\left(\frac{l}{2}\right)^2$$

from which:

$$a = \frac{4\delta}{l^2}$$

By equating the two above values of a, we get:

$$a = \frac{4\delta}{l^2} = \frac{w}{2F}$$

from which:

$$w = \frac{8F\delta}{l^2} \quad \text{or} \quad F = \frac{wl^2}{8\delta}$$

The above equation holds for the profiles described in Figs. 10.16*b* and 10.16*c* where δ is the sag of the parabola. One property of the parabola is illustrated in Fig. 10.16*b*, that is, "the tangent to any point of a parabola intersects the y axis at an intercept equal in magnitude to the ordinate of the point, but on the opposite side." Referring to Fig. 10.16, the angle between the tangents to the parabola at $x = -l/2$ and $x = l/2$ is related to the geometric dimensions of the parabola as follows:

$$\tan(\theta/2) = \frac{2\delta}{l/2} = \frac{4\delta}{l}$$

where δ is the sag of the parabola or the ordinate of the point considered.

For small angles: $\tan(\theta) \approx 2\tan(\theta/2) \approx 2\theta/2 = \theta = \frac{8\delta}{l}$

Thus the uniform load w can also be written as:

$$w = F\frac{\theta}{l}$$

Note that in the above discussion, no sign was used. However, to comply with the sign convention of this text, the equivalent uniform load would be positive when pointing downward and negative upward. The main formulae derived above for the equivalent load are summarized in Fig. 10.10.

3. Remarks on the Use of Equivalent Load for a Parabolic Tendon Profile

The equivalent load for a parabolic tendon profile depends on the sag δ (Fig. 10.16*b* and 10.16*c*) of the tendon profile and its projected length. Slight differences may be observed depending on how the formula is used. This is illustrated next assuming the two equal span continuous beam considered in the example of Section 10.15.

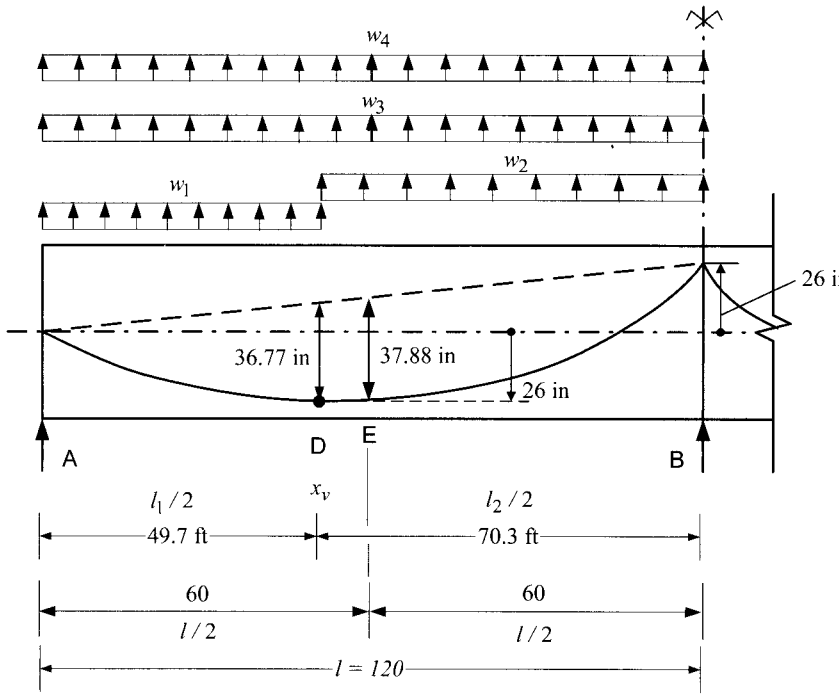

Figure 10.17 Interpretation of equivalent load for a parbolic tendon.

Consider the parabolic tendon profile of Fig. 10.17 and assume that the prestressing force is normalized to 100 kips. It can be shown that the profile is a single parabola with a vertex at section D (at 49.7 ft from support A). It can be shown that the equation for that parabola is:

$$y = ax^2 = 0.731 \times 10^{-4} x^2$$

where y represents the eccentricity and x the distance, in inches, taken with respect to the vertex D (that is, D is considered the origin of axis here). The sag of the parabola at the vertex can be obtained from:

$$\delta_D = 26 + 26\frac{49.7}{120} = 36.77 \text{ in}$$

It can be similarly shown that the sag of the parabola at its midspan, that is, at 60 ft from support A, is $\delta_E = 37.88$ in.

There are three ways to interpret how the uniform load equivalent to the tendon profile of Fig. 10.17 can be obtained.

If the equivalent load is computed separately for the part of the parabola on the left and right side of vertex D, we get:

$$w_1 = \frac{8F\delta}{l^2} = \frac{8\times100\times26/12}{(2\times49.7)^2} = 0.175432 \text{ klf (kips per linear foot)}$$

$$w_2 = \frac{8F\delta}{l^2} = \frac{8\times100\times52/12}{(2\times70.3)^2} = 0.175436 \text{ klf}$$

If the equivalent load is computed from the sag at the vertex section D, we get:

$$w_3 = \frac{8F\delta}{l^2} = \frac{8\times100\times36.77/12}{(120)^2} = 0.170231 \text{ klf}$$

On the other hand, if the equivalent load is computed from the sag at the mid-length (section E) of the parabola (also Fig. 10.16*c*), we get:

$$w_4 = \frac{8F\delta}{l^2} = \frac{8\times100\times37.88/12}{(120)^2} = 0.175370 \text{ klf}$$

Note that w_1 and w_2 are essentially same as w_4 which should be considered the reference equivalent load for comparison purposes, assuming the same parabola; while w_3 is close to w_4, it is the least accurate representation. The difference may not seem large; however, significant differences in secondary moments may be observed because of it. It is thus recommended, for better accuracy, to use preferably the approach leading to either w_4, or w_1 and w_2.

10.9 PRESTRESSING MOMENT AND ELASTIC STRESSES

10.9.1 Moment Due to Prestressing, M_F

To determine the prestressing moment in a continuous beam with a given tendon profile, the following steps can be followed:

1. Determine the equivalent loads as suggested in Section 10.8.
2. For the equivalent loading obtained determine the moments due to prestressing (M_F) at the supports. These can be obtained by any appropriate method, such as by matrix structural analysis, or the method of consistent displacements. However, if the moment distribution method is to be used, the following two steps can be followed:
   a. determine the fixed-end moments generated by the equivalent loads in each span, and
   b using moment distribution, determine the end moments in each span. These are the prestressing moments at the supports. (Examples are given in Sections 10.9.3, 10.15, case *c,* and for the slab in Example 11.14.)
4. Determine the secondary moments at the supports using Eq. (10.3).
5. Determine the secondary moments at any section x between supports using Eq. (10.7).
6. Determine (if this has not been done in a prior step) the primary moment at any section x from: $M_1(x) = -Fe_o(x)$.
7. Determine the prestressing moment at any section x using Eq. (10.2).

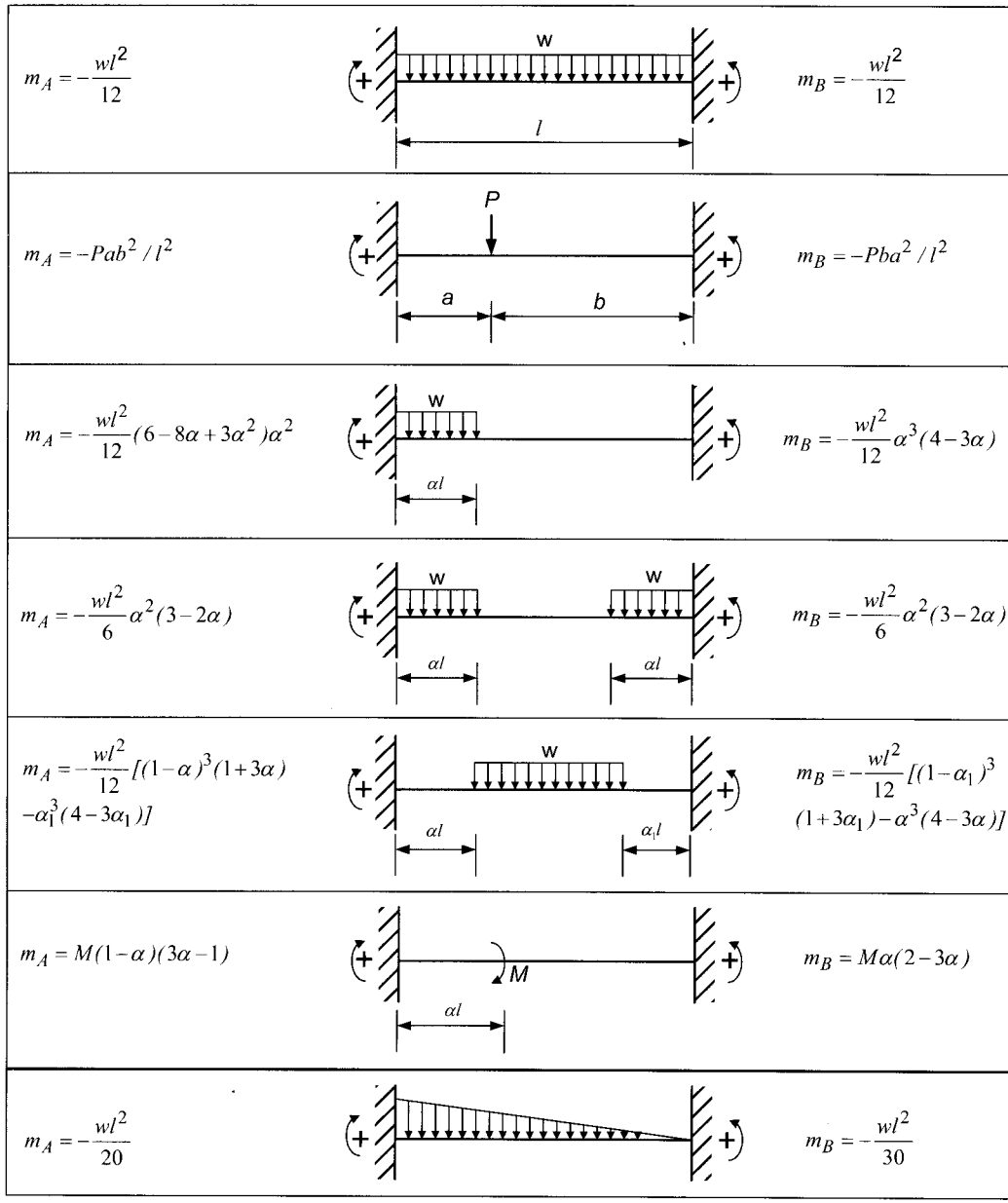

Figure 10.18 Fixed-end moments for members with constant stiffness.

The use of a structural analysis software program is recommended to speed up the process. However, any other analytical procedure for indeterminate structures using hand or programmed calculations should be acceptable, including the moment distribution. As the moment-distribution method utilizes fixed-end moments, a summary of fixed-end moments for common loading cases is given in Fig. 10.18.

Steps 4 to 7 can be condensed in a single equation applied to a typical span with end supports A and B. At any section located at a distance x from the left support of a typical span, the prestressing moment is given by:

$$\begin{cases} M_F(x) = -Fe_o(x) + M_{2A}\left(1 - \dfrac{x}{l}\right) + M_{2B}\dfrac{x}{l} \\ M_F(x) = -Fe_o(x) + (M_{FA} + Fe_{oA})\left(1 - \dfrac{x}{l}\right) + (M_{FB} + Fe_{oB})\dfrac{x}{l} \end{cases} \tag{10.11}$$

where M_{FA} and M_{FB} are the prestressing moments and e_{oA} and e_{oB} the tendon eccentricities at supports A and B of a typical span. In Eq. (10.11), the first term represents the primary moment at section x and the remaining terms represent the secondary moment (Eq. 10.7). Given prestressing moments or the secondary moments, the ZLC-line can then be determined by its eccentricity from Eq. (10.4), that is, - $M_F(x)/F$. It should be pointed out that the eccentricity of the ZLC-line depends on the profile of the tendons but is independent of the magnitude of the prestressing force. Hence, it could be determined assuming a normalized value of F or a unit force.

10.9.2 Example: Prestressed Moments by the Equivalent Load Method

Consider the same two-span prestressed continuous beam of example Section 10.8.3, shown in Fig. 10.19. The beam is symmetrical with respect to support B. Assuming the prestressing force F = 600 kips, determine the prestressing moments at sections A, B, and D and plot the moment diagrams for the primary, secondary, and total moment of prestressing along the beam.

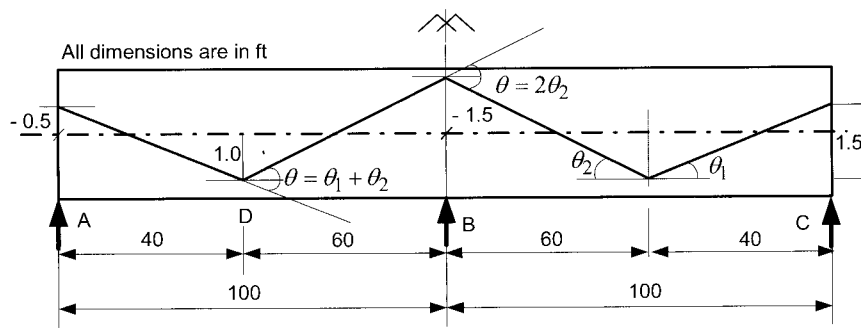

Figure 10.19

Note that the beam is statically indeterminate with only one redundant. Two approaches are considered:

In the first approach, the equivalent load is determined first and used to obtain by moment distribution the moment (that is, the total prestressing moment) at support B. The secondary moment is obtained from subtracting the primary moment from the total moment.

In the second approach, the secondary reaction at support B is determined using the method of consistent deformations (compatibility of displacement); the reaction is then used to determine the secondary moment; the secondary moment is added to the primary moment to obtain the total moment due to prestressing.

Because of symmetry, the moment at support B is same as the fixed-end moment for a beam with a simple support at A and a fixed end at B.

1. First Approach

Determine the prestressing moments by moment distribution. The equivalent loading due to prestressing was determined in Section 10.8.3 and is shown in Fig.10.13 and at the top of Fig. 10.20.

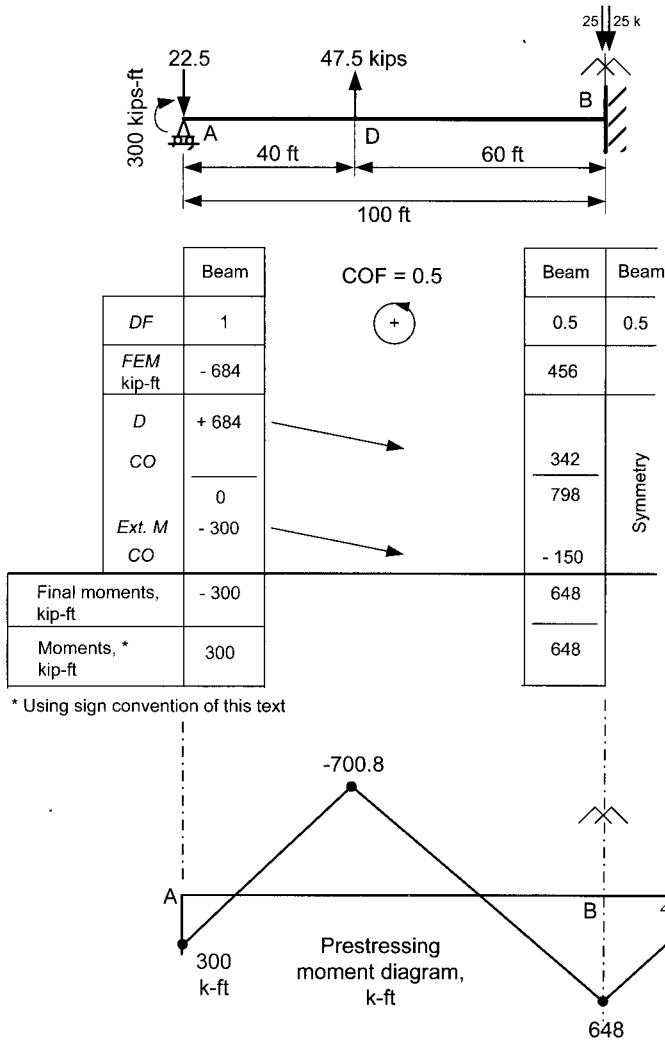

Figure 10.20

To carry the moment distribution, we need the fixed end moments at supports A and B. These can be obtained from Fig. 10.18:

$$m_{AB} = \frac{Pab^2}{l^2} = \frac{47.5 \times 40 \times 60^2}{100^2} = 684 \text{ kips-ft}$$

$$m_{BA} = \frac{Pa^2b}{l^2} = \frac{47.5 \times 40^2 \times 60}{100^2} = 456 \text{ kips-ft}$$

Since the beam is assumed to have a constant depth and a constant moment of inertia, the carry over factor (COF) is equal 0.5.

The moment distribution is carried out in Fig. 10.20 with the moments given the proper sign. Note that after release of fixity at support *A*, the exterior moment due to prestressing is applied and half of it is carried over to support *B*. Because of symmetry, support *B* acts as a fixed end, so there is no need to "unlock" the joint at *B* for the moment distribution. The moments obtained in Fig. 10.20 are the total moments due to prestressing. Subtracting from them the primary moments, leads to the values of secondary moments. Indeed:

At support A: $M_{2A} = M_{FA} - M_{1A} = 300 - 300 = 0$

At support B: $M_{2B} = M_{FB} - M_{1B} = 648 - 900 = -252$ kips-ft

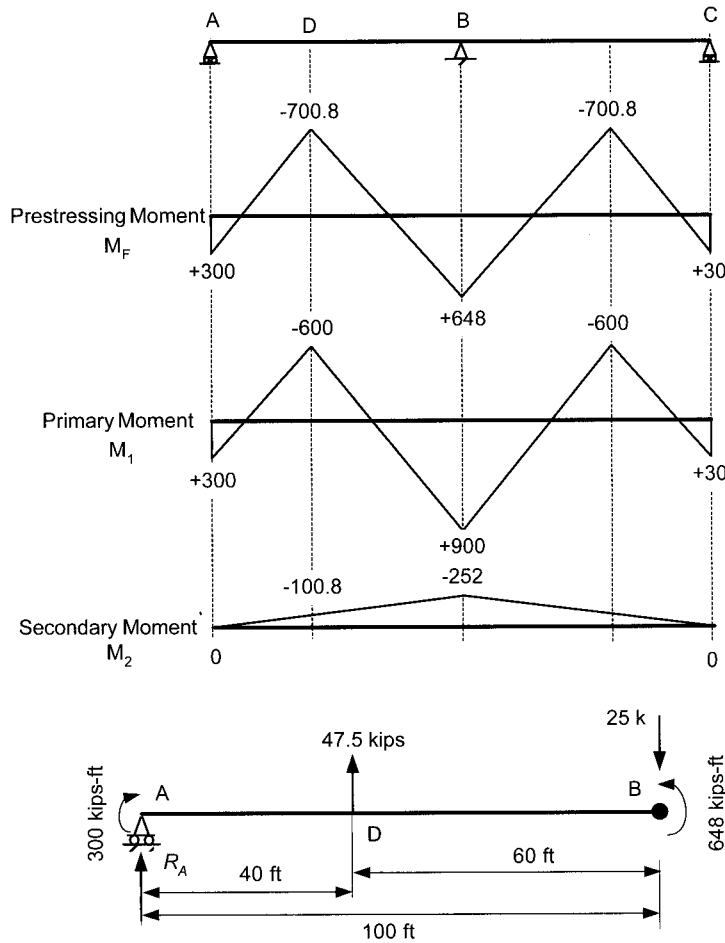

Figure 10.21

The secondary moment diagram is linear between A and B, and given by:

$$M_2(x) = -\frac{252}{100}x = -2.52x$$

which leads to the the secondary moment at section D:

$$M_{2D} = -2.52x = -252 \times 40 = -100.8 \text{ kips-ft}$$

The moment diagrams for the primary, secondary, and total prestressing moments are plotted in Fig. 10.21. It is observed that the secondary moment is beneficial in span, but not beneficial at the mid-support B.

The reaction at A can be determined from the moment at B. Indeed:

$$M_{FB} = 648 = R_A \times 100 + 300 + 47.5 \times 60$$

from which:

$$R_A = \frac{648 - 2850 - 300}{100} = -25.02 \text{ kips (downward)}$$

The prestressing moment at D can be calculated as:

$$M_{FD} = R_A \times 40 + 300 = -25.02 \times 40 + 300 = -700.8 \text{ kips-ft}$$

This is the same answer as obtained above by summing up the primary and secondary moments.

Note that the above value of reaction R_A is due to the total equivalent loading. However, to get the net reaction due to secondary reactions we need to subtract the vertical component of the prestressing force at A, thus:

$$(R_A)_{\text{net}} = -25.02 - (-22.5) = -2.52 \text{ kips (downward)}$$

The net reaction is due to the secondary reactions which act as an external loading.

2. Second Approach

Determine R_B, the secondary reaction at B using the method of compatibility of displacement. In this method, the reaction at B is selected as the redundant and is temporarily removed so that the beam then becomes statically determinate. The external load will cause the section at B to deflect by an amount Δ_B. Applying a concentrated load at B to balance that deflection leads to the value of the unknown reaction, R_B.

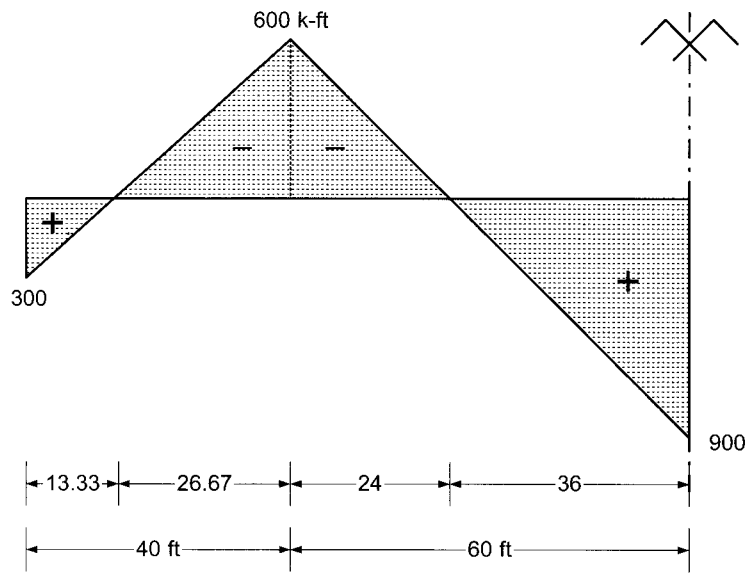

Figure 10.22

From the profile of the prestressing steel, the primary moment diagram can be calculated as $M_1(x) = -F \times e_o(x)$ where $e_o(x)$ is taken positive downward and negative upward. The moment diagram is plotted in Fig. 10.22 (see also Fig. 10.14) for span AB only (since there is symmetry).

Assume the support B is hypothetically removed and beam AC is now simply supported; using the second moment area theorem (Section 7.3), the deflection at B due to prestressing can be computed. Since the tangent to the elastic curve is horizontal at point B, the theorem is applied as if A was deflecting with respect to B. Hence, from the diagram of Fig. 10.22, using the second moment-area theorem:

$$\Delta_B = \frac{1}{EI}\left[\left(\frac{300\times 13.33}{2}\right)\left(\frac{13.33}{3}\right) - \left(\frac{600\times 26.67}{2}\right)\left(13.33+\frac{2}{3}26.67\right) - \left(\frac{600\times 24}{2}\right)\left(40+\frac{24}{3}\right) + \left(\frac{900\times 36}{2}\right)\left(64+\frac{2}{3}36\right)\right]$$

$$\Delta_B = \frac{1}{EI}[8884 - 248911 - 345600 + 1425600] = \frac{1}{EI}839973$$

The above deflection is used to compute the reaction at support B, assuming a simply supported beam spanning between A and C for which the reaction at B provides a camber equal in magnitude to Δ_B:

$$\Delta_B = \frac{R_B(2l)^3}{48EI} = \frac{R_B \times 200^3}{48EI} = \frac{1}{EI}839973$$

from which:

$R_B = 5.04$ kips (upward direction)

Since secondary reactions form a system of forces in equilibrium, the reactions at A and C are given by:

$$R_A = R_C = -\frac{R_B}{2} = -\frac{5.04}{2} = -2.52 \text{ kips (downward direction)}$$

These are the net reactions at A and C and lead to similar values as calculated in the previous section.

The secondary moment diagram is linear between supports and the secondary moments are null at end supports. Since we know the reactions, the secondary moment can be calculated at any section from these reactions:

At section D: $M_{2D} = R_A \times 40 = -2.52 \times 40 = -100.8$ kips-ft

At section B: $M_{2B} = R_A \times 100 = -2.52 \times 100 = -252$ kips-ft

The secondary moment diagram is plotted in Fig. 10.21; it is added to the primary moment diagram to lead to the total prestressing moment diagram shown also in Fig. 10.21. The prestressing moment is given by:

At section A: $M_{FA} = M_{1A} + M_{2A} = 300 + 0 = 300$ kips-ft

At section D: $M_{FD} = M_{1D} + M_{2D} = -600 - 100.8 = -700.8$ kips-ft

At section B: $M_{FB} = M_{1B} + M_{2B} = 900 - 252 = 648$

These are the same answers as obtained in the first approach above.

3. Zero-Load-C Line

Now that the secondary moments have been determined, the ZLC-line can be easily determined as well. Applying Eq. (10.4) at support B:

$$e_{oc} = e_o - \frac{M_2}{F} = -1.5 - \frac{-252}{600} = -1.5 + 0.42 = 1.08 \text{ ft}$$

Similarly for the near midspan section, D:

$$e_{oc} = e_o - \frac{M_2}{F} = 1 - \frac{-100.8}{600} = 1 + 0.168 = 1.168 \text{ ft}$$

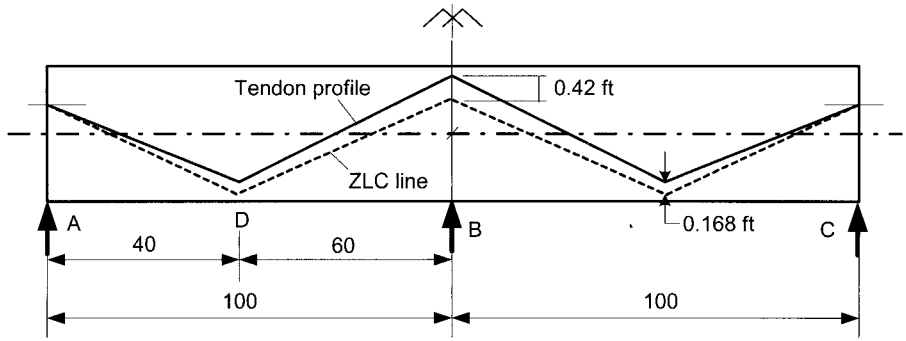

Figure 10.23

The shape of the ZLC-line is a segmented line similar to that of the steel profile. It is plotted as a dashed line in Fig. 10.23. Its eccentricity at any section along span AB is obtained from the tendon profile through a rotation with respect to the left support A. By symmetry a similar result is observed for span BC. Thus the ZLC line falls below the steel profile and the difference between e_o and e_{oc} is directly proportional to x; indeed along span AB:

$$e_{oc}(x) - e_o(x) = -\frac{M_2(x)}{F} = \frac{2.52}{600}x = 0.0042x$$

where units are in foot, and x is taken from the left support A. Note that the difference between the eccentricity of the ZLC-line and the steel tendon profile is independent of the magnitude of the prestressing force. That is, it would be the same whether F is 100 kips or 600 kips.

10.9.3 Elastic Stresses in a Continuous Beam

In order to determine the stresses in the concrete at any section, the equations developed in Chapter 4 and the stress inequality conditions given in Table 4.2 can be used directly provided the eccentricity of the prestressing steel is replaced by that of the ZLC line. Another way of using these equations is to keep the eccentricity of the steel as is, but add the secondary moment (if it is known) to the external moments. For instance, Eq. (IV) of Table 4.2 (way 1) applied to a section of a continuous beam can be written in one of two ways:

$$\frac{F}{A_c}\left(1 - \frac{e_{oc}}{k_t}\right) - \frac{M_{\max}}{Z_b} \geq \bar{\sigma}_{ts} \tag{10.12}$$

where e_{oc} has replaced e_o, or

$$\frac{F}{A_c}\left(1-\frac{e_o}{k_t}\right)-\frac{M_{\max}+M_2}{Z_b}\geq \bar{\sigma}_{ts} \tag{10.13}$$

where M_2 is added to the external moment. The above equations and those given in Table 4.2 apply to any section x.

It should be noted again that for a given continuous beam and tendon profile the ZLC-line is independent of the magnitude of the prestressing force. However, the secondary moment can be written as: $M_2 = -F(e_{oc} - e_o)$ for any value of F (Eq. 10.6).

10.10 DESIGN AIDS

It has become increasingly clear from the preceding sections that the profile of the steel along a continuous beam represents an important design parameter. Although graphical solutions can be used and particular analytical solutions for a given problem can be devised, a general formulation of the tendon profile (or cgs) for the most common practical cases and its effects on the primary and secondary moments should lead to substantial time savings in design.

The steel profile can be made of segmented straight lines, parabolic curves, circular curves, or a combination thereof. Most likely, an undulating shape is achieved in a continuous beam. It is generally convenient to assume parabolic parts because of the simple analytical representation of a parabola. *Khachaturian* and *Gurfinkel* [Ref. 10.7] have developed equations for the tendon profile (cgs) of continuous beams, assuming either parabolic parts or parts represented by a parabola and a fourth-degree curve. Their assumed configurations for a typical end span and a typical intermediate span, for the case where parabolic parts were used, are shown in Figs. 10.24*a* and *b*. Note that the tendon profile of the end span is made out of three different parabolas, while two parabolas (three parts) are used for a symmetrical intermediate span. The corresponding equations for $e_o(x)$ at any section are given in Figs. 10.25 and 10.26. They are expressed in terms of the support eccentricity e_{oB} and other nondimensional coefficients explained in the figures.

The sign convention adopted in this text is still valid. Hence, e_{oB} is negative and the factors β, β_1, and β_2 as shown, for instance in Fig. 10.24, are negative. In general, they can be negative or positive. In developing the equations of Figs. 10.25 and 10.26, the following assumptions were made: (1) the members are shallow, hence, the horizontal component of F is assumed equal to F, and e_o is small with respect to l, (2) a horizontal tangent exists at the common point between the first two parabolas of the end span, (3) horizontal tangents exist at all supports and at midspans of the intermediate spans, and (4) the prestressing force is assumed

constant throughout. In addition, a special condition was derived to ensure a common tangent at the inflection point *I* between two successive parabolas. It is given in Fig. 10.25 for a typical end span and in Fig. 10.26 for a typical interior span. It can also be shown in simpler form that the inflection point should be on the line joining the vertices of the two adjacent parabolas.

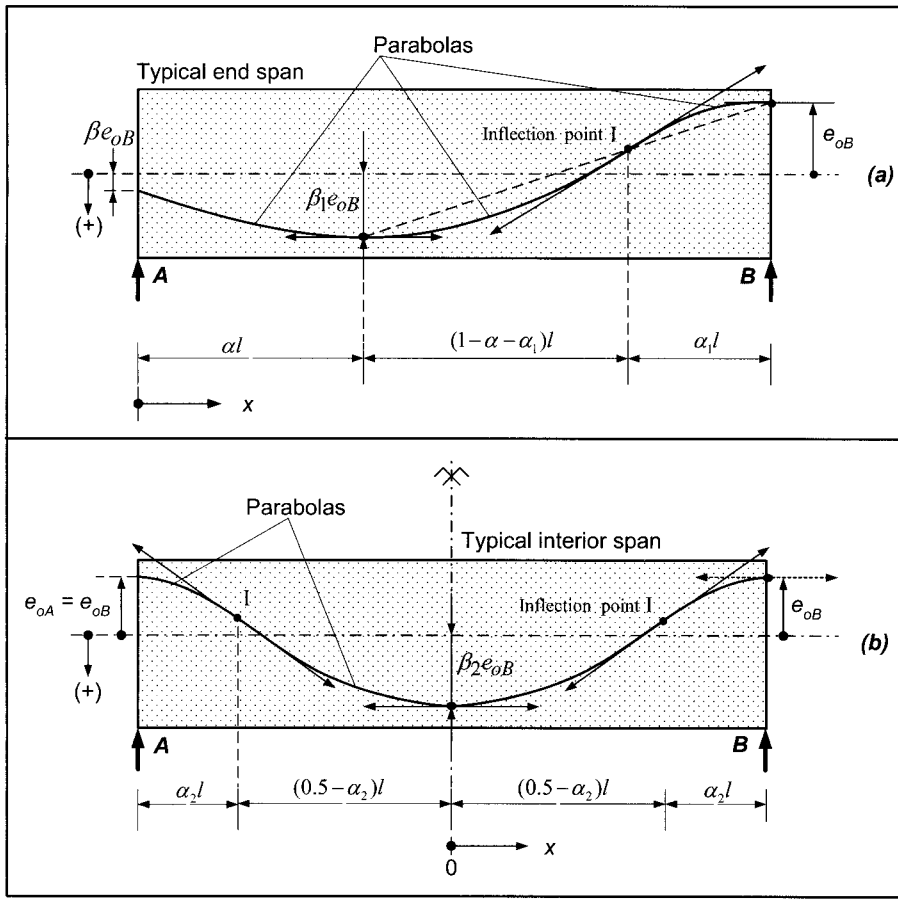

Figure 10.24 Typical tendon profiles suggested in Ref. [10.7]. *(a)* Profile for a typical end-span made out of three parabolas. *(b)* Profile for a typical interior span.

Based on the above tendon profile, *Khachaturian* and *Gurfinkel* developed direct expressions for the equivalent loads and the fixed-end moments generated by such loads. These are summarized in Figs. 10.25 and 10.26 using the notation and sign convention of this text. They allow the quick use of the method of moment distribution to determine the total moments due to prestressing. Note that, in order for the moments to have the correct sign, the load is assumed positive downward and negative upward. An example illustrating the use of these formulas is given in Sec. 10.15, case *c*.

Prestressing steel profile, $e_o(x)$ *:*

$0 \le x \le \alpha l$

$$e_o(x) = e_{oB}\left[-(\beta_1-\beta)\left(\frac{1}{\alpha}\frac{x}{l}\right)^2 + 2(\beta_1-\beta)\frac{x}{\alpha l} + \beta\right]$$

$\alpha l \le x \le (1-\alpha_1)l$

Call: $\lambda = \dfrac{1-\beta_1}{(1-\alpha)(1-\alpha-\alpha_1)}$

$$e_o(x) = e_{oB}\left[\lambda\left(\frac{x}{l}\right)^2 - 2\alpha\lambda\frac{x}{l} + \lambda\alpha^2 + \beta_1\right]$$

$(1-\alpha_1)l \le x \le l$

Call: $\mu = \dfrac{1-\beta_1}{\alpha_1(1-\alpha)}$

$$e_o(x) = e_{oB}\left[-\mu\left(\frac{x}{l}\right)^2 + 2\mu\left(\frac{x}{l}\right) - \mu + 1\right]$$

Note: For the parabolas to be tangent at inflection point, *I*, the following expression must be satisfied.

$$e_{oI} = e_{oB} - \alpha_1\left(\frac{1-\beta_1}{1-\alpha}\right)e_{oB}$$

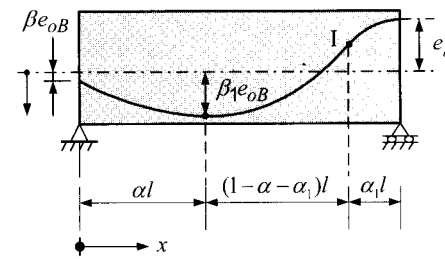

β and β_1 may be positive or negative

$e_o(x)$ ⊤(+)

Fixed-end moment:

$$m_{BA} = -Fe_{oB}[-\beta\alpha^2 + (1+\alpha-\alpha_1)^2 - \alpha_1(1-\alpha) - \beta_1(3-3\alpha+\alpha_1^2+2\alpha+\alpha\alpha_1)]\frac{1}{4}$$

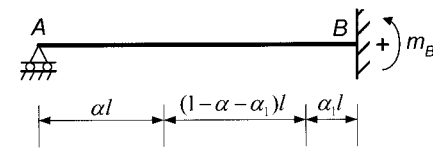

Equivalent loading (one end fixed):

$$w_1 = \frac{-2F(\beta_1-\beta)e_{oB}}{(\alpha l)^2}$$

$$w_2 = 2F\lambda e_{oB}/l^2$$

$$w_3 = -2F\mu e_{oB}/l^2$$

Note: End effects must be considered

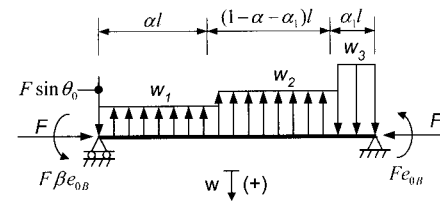

Figure 10.25 Expressions for the eccentricities, fixed-end moment, and equivalent loads for a typical end span. *(Adapted from Ref. 10.7.)*

Prestressing steel profile, $e_o(x)$:

$$-\frac{l}{2} \le x \le -\left(\frac{1}{2}-\alpha_2\right)l$$

Call: $\upsilon = \dfrac{2(1-\beta_2)}{\alpha_2}$

$$e_o(x) = e_{oB}\left[-\upsilon\left(\frac{x}{l}\right)^2 - \upsilon\left(\frac{x}{l}\right) - \frac{\upsilon}{4} + 1\right]$$

$$-\left(\frac{1}{2}-\alpha_2\right)l \le x \le \left(\frac{1}{2}-\alpha_2\right)l$$

$$e_o(x) = e_{oB}\left[\frac{2(1-\beta_2)}{\frac{1}{2}-\alpha_2}\left(\frac{x}{l}\right)^2 + \beta_2\right]$$

$$\left(\frac{1}{2}-\alpha_2\right)l \le x \le \frac{l}{2}$$

$$e_o(x) = e_{oB}\left[-\upsilon\left(\frac{x}{l}\right)^2 + \upsilon\left(\frac{x}{l}\right) - \frac{\upsilon}{4} + 1\right]$$

Note: For the parabolas to be tangent at inflection point, *I*, the following expression must be satisfied:

$$e_{oI} = e_{oB} - 2\alpha_2(1-\beta_2)e_{oB}$$

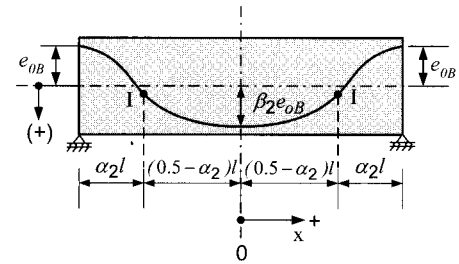

Fixed-end moments:

$$m_{BA} = m_{AB} = -Fe_{oB}\frac{2}{3}(1-\beta_2)(1-\alpha_2)$$

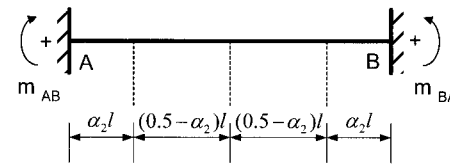

Equivalent loading for fixed-ends:

$$w_1 = -4F(1-\beta_2)\frac{e_{oB}}{\alpha_2 l^2}$$

$$w_2 = 4F(1-\beta_2)\frac{e_{oB}}{\left(\frac{1}{2}-\alpha_2\right)l^2}$$

Note: End effects must be considered

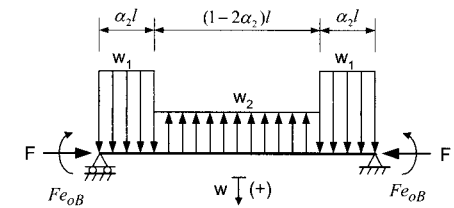

Figure 10.26 Expressions for the eccentricities, fixed-end moments and equivalent loads for a typical interior span. *(Adapted from Ref. 10.7.)*

Even if the designer does not use the moment distribution method, Figs. 10.25 and 10.26 provide the equivalent loads needed to determine the prestressing

moments by any other method of analysis. They are convenient not only during design but also for construction purposes, as the eccentricities of the steel at different sections (thus cover to the cgs) can be easily calculated from the equations provided.

10.11 WORKING STRESS ANALYSIS AND DESIGN

As pointed out in Sec. 10.2, the analysis of prestressed concrete continuous beams requires, in addition to the background needed to analyze simply supported beams, the background developed in the preceding sections and the knowledge of a method to analyze statically indeterminate structures subjected to external loads; this latter requirement can be fulfilled by any structural analysis software or by a method suitable for hand calculations, such as the moment distribution method. Analysis and design steps are proposed next, but are not unique. Many paths can be followed to arrive at the same correct answer and the user may want to develop his/her own approach or introduce appropriate modifications to fit a particular type of problem.

10.11.1 Assumptions

The following assumptions are generally made:

1. Both steel and concrete act within their linear elastic range of behavior and plane sections remain plane.
2. The supports are non-settling (i.e., they are fixed against transverse movements) and do not provide any restraint to the axial deformation of the member. Restricting axial deformation (short- and long-term) may generate tertiary moments that can be significant.
3. The principle of superposition of loads, forces, moments, and stresses is valid.
4. The eccentricity of the prestressing force is small in comparison to the span; hence, the horizontal component of the prestressing force is assumed equal to the prestressing force at any section of the member.
5. Friction is negligible, that is, the prestressing force is assumed constant throughout the length of the member. In practice, the design is revised after a first iteration to account for frictional effects.
6. Gross-sectional properties are used at first. Transformed section properties are used in a final design.

10.11.2 Analysis or Investigation

Given materials and sectional properties, tendon profile, prestressing force, and loading conditions, the main objective is to check if allowable stresses and other service limit states are satisfied. The following steps are suggested:

1. For the given prestressing force and steel profile, determine the equivalent loading on the member. (Use information provided in Sections 10.8 and 10.10.)

2. For the equivalent loads obtained in 1, determine (such as by using the method of moment distribution or a structural analysis software) the prestressing moments $M_F(x)$ at the supports. (Use information provided in Sections 10.9 and 10.10.)
3. Determine the secondary moments at the supports and at any section x, using Eqs. (10.3) and (10.7).
4. Determine the eccentricity of the ZLC-line from Eq. (10.4).
5. Determine the maximum and minimum moments at each section x due to external loads, that is, $M_{min}(x)$ and $M_{max}(x)$.
6. The rest of the analysis essentially follows the steps used in Chap. 4 for simply supported beams, except that $e_{oc}(x)$ replaces $e_o(x)$ in the computation of stresses, as pointed out in Sec. 10.9.3.

It was shown in Sec. 10.9.3 that, instead of using $e_{oc}(x)$ to compute the stresses, $e_o(x)$ could have been used, provided the secondary moment is added to the external moments. This approach may also be attractive when the steel envelopes are built and deflections are computed.

10.11.3 Design

Two major approaches can be followed to design continuous beams. In the first approach, the mechanical and practical constraints of the problem are directly used to arrive at an appropriate tendon profile and prestressing force. In the second approach, a tendon profile, which satisfies the practical constraints of the problem, is selected a priori, then the prestressing force is determined (and the profile adjusted, if needed) to satisfy the mechanical constraints of the problem. The first approach is very similar to an optimization problem. It can be substantially more involved than the second one and requires the use of optimization techniques. Nevertheless, there have been some attempts to provide a solution within reach of the designer [Ref. 10.4]. Only the second approach will be followed here. In the author's experience, it leads to a sure and fast solution, even when revisions and iterations are considered.

In order to further simplify the problem, it is assumed that the concrete cross section is provided. If not, a section may be dimensioned as if the beam was simply supported; then its depth is reduced by about 20 percent to account for the benefits of continuity. Some revision may be needed. Assuming the material properties and the loading conditions are known, the problem is reduced to finding an acceptable prestressing force and tendon profile.

Two methods are described next: one assumes that a nonconcordant steel profile will be used and the other assumes that a concordant steel profile will be eventually arrived at.

Nonconcordant Tendon Profile

The following steps are suggested:

1. Determine minimum and maximum moments at each section due to external loads.
2. Select a practical tendon profile that has a maximum practical eccentricity at each critical section. Critical sections are support sections with maximum negative moments, and midspan or near midspan sections with maximum positive moments. A steel profile made out of parabolas can be used as suggested in Section 10.10.
3. Determine the equivalent loads for the above profile (see Section 10.8). As the prestressing force F is unknown, the equivalent loads are determined in function of F. A unit value or a normalized value can be assumed for F (such as 100 kips), provided the moments obtained in steps 3 and 4 are, in the final design, adjusted proportionally to the design value of F.
4. From the equivalent loading, determine (by any appropriate method, such as moment distribution or structural analysis software) the moments due to prestressing at the supports. Use Section 10.9 and Fig. 10.18 if needed.
5. Determine the secondary moments at the supports and at other critical sections (Eqs. 10.3 and 10.7).
6. Determine the eccentricity of the ZLC-line at each of the critical sections (Eq. 10.4).
7. Determine the needed prestressing force at each of the critical sections, using the eccentricity of the ZLC-line and the same stress inequality conditions described in Chapter 4 for simply supported beams (Section 10.9.3). Select the highest value obtained, call it F, and assume it is used throughout. Check if stresses at all critical sections are satisfactory. If not, the same remedies as used in Chapter 4 for simply supported beams can be followed, provided e_o is replaced by e_{oc}.

Note that, by adjusting the tendon profile (cgs), the secondary moments can be beneficially used to magnify or reduce the effect of the prestressing force. They can also be eliminated, leading to a concordant profile. The tendon profile can be linearly transformed without changing the ZLC-line, thus providing some flexibility in design. Enough tolerance should be allowed in the tendon profile selected to accommodate some variations in the actual prestressing force due to friction. In finalizing the design, the limit kern and the limit zone can be built to check if the tendon (cgs) is within the limit zone at each section, hence ensuring that none of the allowable stresses are violated.

A typical design example with a nonconcordant tendon profile is given in Section 10.15, case *c*.

Concordant Tendon Profile

A concordant steel profile can be obtained as described in Sec. 10.7. For such a profile, the secondary moments are zero and the design approach is similar to that of simply supported beams (Chapter 4). The following steps are suggested:

1. Determine the maximum and minimum moments at each section due to external loads.
2. Using the eccentricities of the concordant profile, determine the required prestressing force at each critical section. Select the highest value obtained, call it F, and assume it will be used throughout the member.
3. Check if F is acceptable at all critical sections, that is, check if the stress inequality conditions (Tables 4.2 and 4.3) are satisfied. If they are, build the limit zone and check if the steel profile is within the limit zone at each critical section. If it is, stresses are satisfied everywhere. Otherwise, a different profile must be sought, as described in Section10.7, and steps 2 and 3 must be repeated.

Of course, it is assumed in step 2 that a required prestressing force can be computed for each critical section. If this is not possible (no feasible domain), the assumed section properties or the steel profile must be appropriately modified.

A typical design example with a concordant steel profile is developed in Section 10.15, case *b*.

10.12 LIMIT KERN AND LIMIT ZONE

The concepts of limit kern and limit zone described in Section 4.12 for statically determinate beams remain the same for continuous beams. The eccentricity of the C-line at any section should remain within the upper and lower limits of the kern to satisfy all allowable stresses. The only difference with the case of simply supported beams is that the eccentricity of the C-line takes into account not only the external moments but also the secondary moments due to prestressing. Note that from the C-line perspective, the secondary moments can be considered external moments due to secondary reactions and can be added to the external moments due to external loads. In a reciprocal manner, given the limit kern, the limit zone or steel envelopes can be obtained by plotting from the upper and lower limits of the kern two vectors of magnitude $(M_{\max} + M_2)/F$, and $(M_G + M_2)/F_i$ or $(M_{\min} + M_2)/F$, whichever is smaller. This last step takes into consideration the fact that the minimum moment in a continuous beam is influenced by the live load, and is generally different from the dead load moment.

If the secondary moments are not added to the external moments, a limit zone for the ZLC-line is obtained. The limit zone for the ZLC-line is the same as if the beam is statically determinate or if a concordant cable is used leading to zero secondary moments. For a concordant profile, the limit zones for the ZLC line and for the steel coincide. The above procedure is graphically illustrated in Fig. 10.27 for a typical span section where the secondary moment is assumed positive (not beneficial at this

section). For a span section where the maximum and minimum external moments are positive, Eqs. (4.22) and (4.23) for the limit kern are valid and the envelopes of the steel defining the limit zone become:

$$e_{ou}(x) = k_t' + \frac{M_{\max}(x) + M_2(x)}{F} \tag{10.14}$$

$$e_{ol}(x) = \text{the smaller of} \begin{cases} k_b' + \dfrac{M_G + M_2}{F_i} \\ \text{and} \\ k_b' + \dfrac{M_{\min} + M_2}{F} \end{cases} \tag{10.15}$$

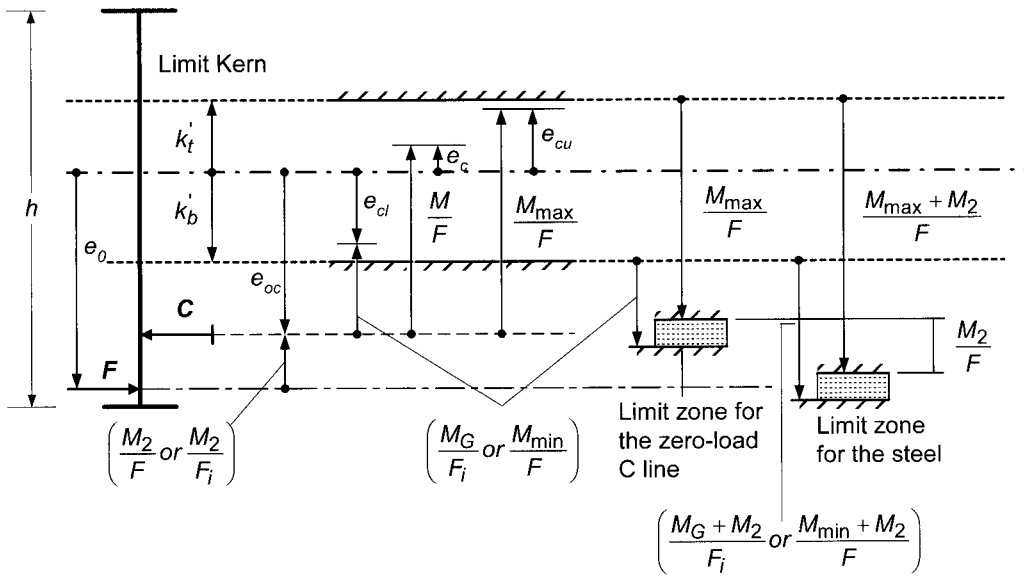

Figure 10.27 Graphical illustration of the relation between the limit kern and the limit zone for a typical span section with positive secondary moment.

Note that the ratio $-M/F$, where M is an external moment, is equivalent to an eccentricity and is positive downward. When the moments are negative, such as at the supports, the values of k_t' and k_b' have to be redefined and the comments made at the end of Sec. 4.12 can be used for a speedy solution. A typical example of a limit zone is shown in Fig. 10.41.

If a computer program is used, the upper and lower limits of the limit zone (i.e., the steel envelopes) can be determined directly at any section from the equations of

Tables 4.2 and 4.3, provided the secondary moments are added to the external moments.

10.13 LOAD-BALANCING METHOD

10.13.1 General Approach

The analysis of prestressed concrete statically indeterminate structures is hindered by the existence of secondary moments due to prestressing. The load-balancing method proposed by T. Y. Lin reduces the analysis to that of a nonprestressed structure in which consideration of secondary moments is essentially bypassed [Refs. 10.10 and 10.11]. The load-balancing method offers a particularly simple and elegant means to design continuous beams, slabs, shells and frames.

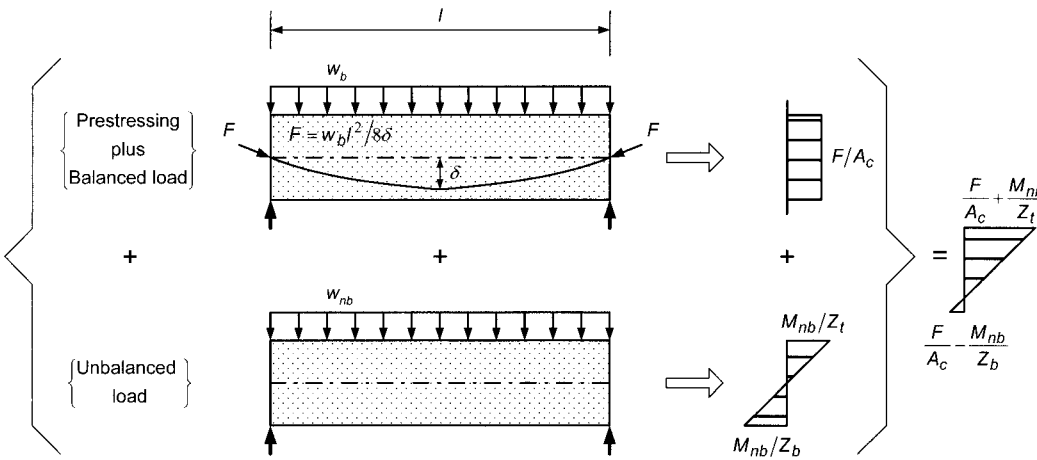

Figure 10.28 Typical stresses under balanced and unbalanced loads.

Balancing the external load consists of selecting a prestressing force and steel profile which create a transverse load exactly equal and opposite to the external load. Section 10.8 and Fig. 10.10 provide the necessary background for such a procedure. For instance, to balance a uniform load w_b in a simply supported beam, a parabolic steel profile with zero end eccentricities can be selected (Fig. 10.28). The prestressing force F needed will be a function of the load to be balanced, w_b, and the acceptable sag, δ, of the tendon. As the transverse load (that is normal to the tendon profile) created by the tendons balances exactly the external load, a uniform state of stress F/A_c develops at every section throughout the beam. The beam remains essentially level and no deflection or camber is observed. Note that, in order to

balance the load, the end eccentricities were taken equal to zero, otherwise an end moment which disturbs the uniform state of stress is generated.

The same approach for load balancing can be applied to a continuous beam, noting that eccentricities at intermediate supports are not necessarily equal to zero, because in such a case the moments on each side of the support balance each other. If the continuous beam remains level due to load balancing, no secondary moments are generated (under the combined action of F and the balanced load w_b) and the beam can be analyzed for the unbalanced load, w_{nb}, as if it was a continuous nonprestressed beam in which a uniform compression F/A_c is present. The moments $M_{nb}(x)$ induced by the unbalanced loads are then calculated by elastic analysis and the corresponding stresses at the extreme fibers $M_{nb}(x)/Z_t$ and $-M_{nb}(x)/Z_b$ determined. Resulting stresses due to the uniform compression and the unbalanced moments are added and compared with the allowable stresses. This is illustrated in Fig. 10.28 for the case of a simply supported beam.

The balanced load need not necessarily be uniform. It can be a concentrated load, a uniform load, or a combination thereof (Fig. 10.29). For a uniform load, a shallow parabolic tendon profile is generally selected (Fig. 10.29*b*), while a linear profile with a sharp directional change is used for a concentrated load (Fig. 10.29*a*). Assuming shallow members, the principle of superposition holds, hence, the combined profile shown in Fig. 10.29*c* would balance both the applied uniform and concentrated loads. Figure 10.29 illustrates a procedure where the same prestressing force is used for the two cases. In a design situation, some iteration may be needed to arrive at an acceptable prestressing force compatible with the available sag.

Design Steps

In an approach similar to that followed in Sec. 10.11, it is also assumed here that the concrete cross section is given and that the design is reduced to finding the prestressing force and its profile. Referring to a continuous beam (Fig. 10.30) where a typical end span, intermediate span, and cantilever span are shown, the following design steps are suggested, assuming uniform loadings and relatively shallow members:

1. Select the balanced load w_b. It is generally taken equal to the dead load plus the sustained part of the live load, if any. This will ensure a level structure even under long-term effects. Note that a different value of the uniform balanced load may be used for each span.
2. Select a steel profile made out of parabolas, having maximum practical eccentricities at the intermediate supports and maximum feasible sags in span. Zero eccentricities must be present at the end supports, unless a cantilever end exists, in which case the eccentricity is taken equal zero at that end. At cantilever ends, if any, the slope of the tendon should also be zero.

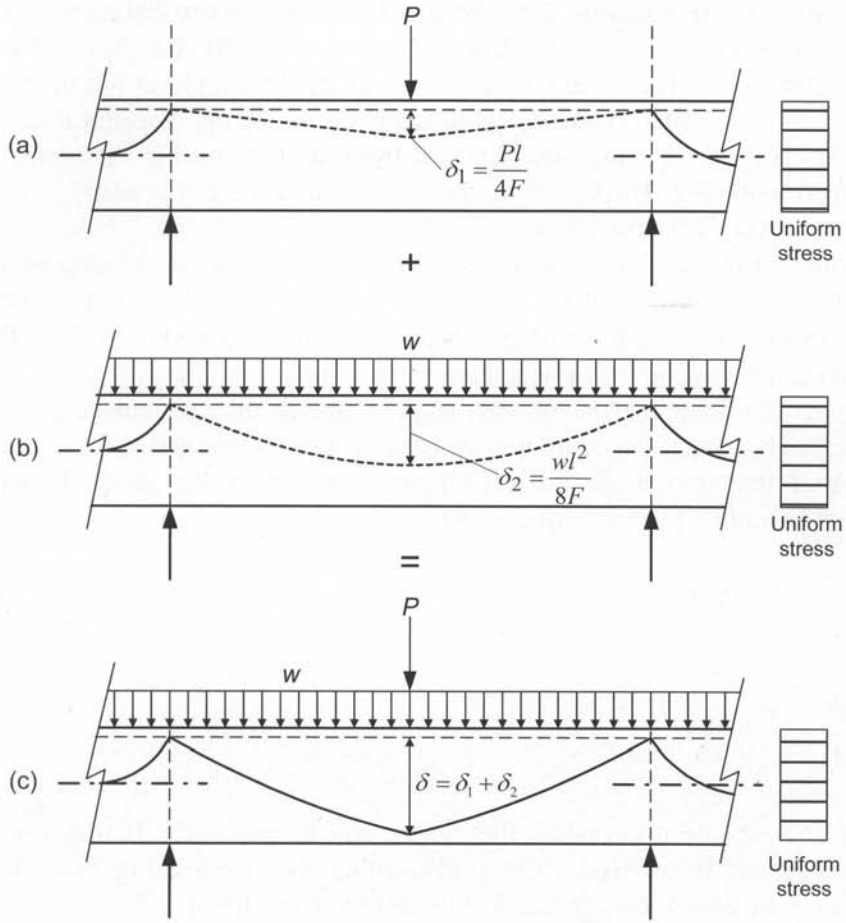

Figure 10.29 Superposition in load balancing.

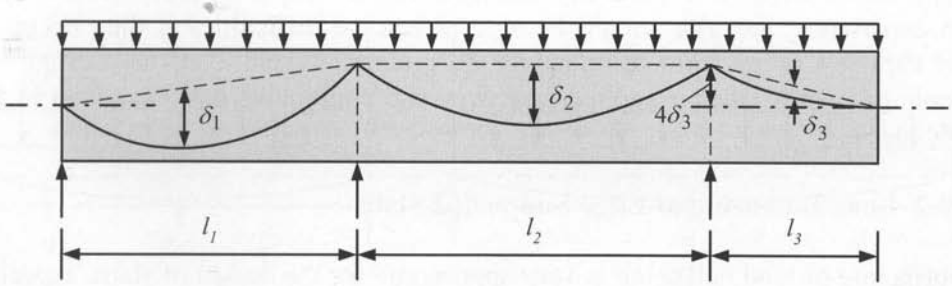

Figure 10.30 Typical load balancing in a continuous beam.

3. Determine the prestressing force required in each span to balance the balanced load of that span. (Use the relations given in Fig. 10.10.) Select the highest value obtained, call it F and assume it is adopted throughout the member. The sags are then adjusted (reduced) in those spans where the required force was less than F. Their final values are obtained from the relationship between F and the balanced load (Fig. 10.10). Now the beam, under the effect of $(F + w_b)$, has a uniform stress F/A_c throughout its length.

   Note that in cantilever spans, because of the implied relationship between the sag and the eccentricity at the near-support section (Fig. 10.30), the near-support eccentricity may have to be adjusted to achieve the required sag (δ_3) and this will influence the sag (δ_2) in the adjacent span.
4. Compute the unbalanced moment $M_{nb}(x)$ due to the unbalanced load w_{nb} by elastic analysis as if the beam was continuous nonprestressed.
5. Check if the stresses at critical sections and other key sections are within allowable limits. Stresses are given by:

$$\frac{F}{A_c} + \frac{M_{nb}(x)}{Z_t} \tag{10.16}$$

   and

$$\frac{F}{A_c} - \frac{M_{nb}(x)}{Z_b} \tag{10.17}$$

   If stresses are acceptable, the design can be pursued. If they are not, the design should be revised. Generally, either the prestressing force has to be increased, or the concrete cross section has to be modified.
6. Modify the theoretical tendon profile shown in Fig. 10.30 by providing smooth transitions over the supports and check the effects of such modification. It is likely that a secondary moment will be generated. These moments are often neglected in slabs (Chapter 11), but may be significant in beams.

The above steps have generally assumed that no major problem occurs. With some experience, the user should be able to resolve difficulties if they occur and avoid them by proper dimensioning in the preliminary phase of the design. An example of load balancing applied to a two-span continuous beam is given in Sec. 10.15, case *e*.

10.13.2 Load Balancing of Edge-Supported Slabs

The principle of load balancing is very appropriate for the design of slabs, especially two-way slabs, as these structures are highly indeterminate and their analysis or design by any other technique is either time consuming or necessitates a number of approximations. Slabs are covered in detail in Chapter 11. Only two-ways edge

supported slabs are addressed here to illustrate the use of load balancing (Fig. 10.31); one-way slabs are handled as continuous beams. Assuming a uniform load, w_b, to be balanced and assuming parabolic tendons are used, the load-balancing relationship applied to edge-supported slabs becomes:

$$\frac{8F_x\delta_x}{l_x^2} + \frac{8F_y\delta_y}{l_y^2} = w_b = w_{bx} + w_{by} \tag{10.18}$$

where F_x and F_y are the forces in the x and y directions of span l_x and l_y, and δ_x and δ_y are the corresponding tendon sags, measured to the centroid of the tendons (Fig. 10.31).

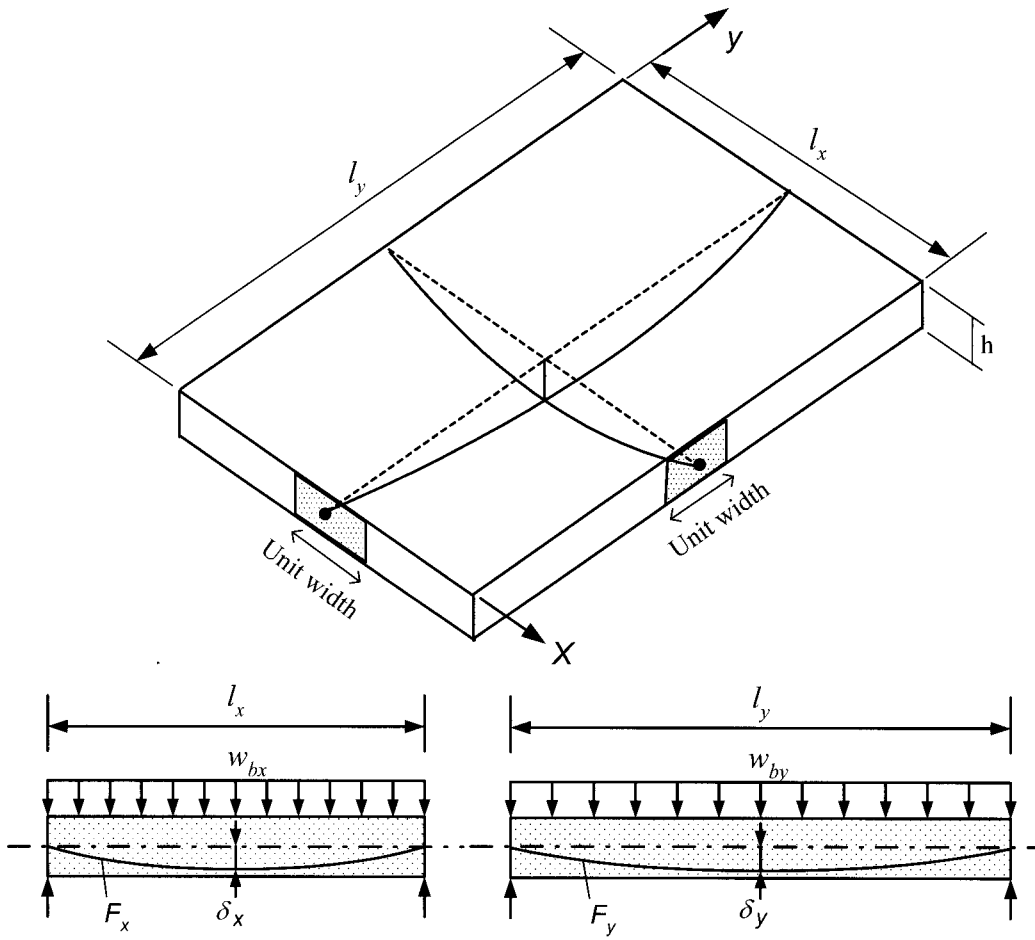

Figure 10.31 Two-dimensional load balancing in prestressed concrete slabs.

The values of δ_x and δ_y are selected as maximum practical, given the depth and the cover. However, an infinite set of values F_x and F_y may satisfy Eq. (10.18). It is generally more economical to balance a larger portion of w_b in the shorter direction. That portion is selected in such a way that the resulting prestressing force in the longer direction generates a uniform compression of the order of 150 psi ($\simeq$ 1 MPa). In practice, such compression is believed necessary to avoid cracking. An average compression of 125 psi (0.86 MPa) is considered a minimum (Section 11.9).

10.13.3 Example: Load Balancing of an Edge-Supported Slab

A 30× 50 ft lightweight concrete rectangular slab is simply supported on walls on four sides (Fig. 10.31). It is to be designed to carry, in addition to its own weight, a live load of 100 psf. The following information is given: $f'_c = 5000$ psi, $f_{pe} = 168$ ksi. The prestressing steel consists of single-strand unbonded tendons with 0.6-in diameter covered by plastic tubing, which gives them an outside diameter of 0.75 in. The strand cross-sectional area is 0.216 in^2, leading to an effective force per strand of 36.288 kips. It is estimated that 20 percent of the live load can be considered a sustained load.

Let us provide a quick dimensioning of the slab thickness and the required prestressing steel.

Referring to Fig. 10.31 where the notation is explained, let us estimate the slab thickness assuming a span-to-depth ratio of 40 (see also Section 11.1.1) for the shorter span, that is:

$$h = \frac{l_x}{40} = \frac{30\times 12}{40} = 9 \text{ in}$$

The tendons are to be set in two layers normal to each other and forming a grid with zero eccentricities along the edges of the slab. The lowest layer is chosen for the short direction, x, and the transverse layer is chosen for the long direction, y. Assuming a 3/4-in net, cover to the lowest layer and assuming that the two layers touch each other, leads to the following sags: $\delta_x = 3.375$ in and $\delta_y = 2.625$ in (Fig. 10.32).

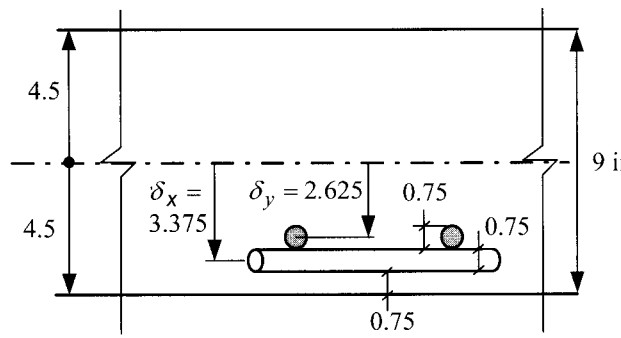

Figure 10.32

Assuming lightweight sand is used in the concrete, the dead weight of the slab is estimated at 100 psf (this is equivalent to a concrete unit weight of 133 pcf). The balanced load is chosen as the sum of the dead weight and the sustained part of the live load, that is $w_b = 100 + 0.2\times 100 = 120$ psf. The corresponding unbalanced load is $w_{nb} = 80$ psf.

Let us determine the prestressing force needed in each direction, assuming a slab strip with unit width. The effective prestressing force in the longitudinal direction is assumed to achieve a uniform compression of 150 psi, hence:

$$F_y = 150 \times 9 \times 12 = 16,200 \text{ lb/ft}$$

The effective force in the short direction is then obtained from Eq. (10.18):

$$\frac{8F_x\delta_x}{l_x^2} + \frac{8F_y\delta_y}{l_y^2} = w_b$$

that is:

$$\frac{8F_x \times 3.375/12}{(30)^2} + \frac{8 \times 16,200 \times 2.625/12}{(50)^2} = 120$$

or

$$0.0025F_x + 11.34 = 120$$

which leads to $F_x = 43,464$ lb/ft.

As one strand develops an effective force of 0.216x168 = 36,288 lb, the strand spacing will be:

Short direction $\quad s_x = \dfrac{36,288 \times 12}{43,464} \simeq 10$ in

Long direction $\quad s_y = \dfrac{36,288 \times 12}{16,200} \simeq 26.9$ in

These are acceptable spacings in comparison to the slab thickness. In practice, a value of 27 in will be used for s_y.

The above prestressing combined with the effect of balanced load (w_b = 120 psf) produces uniform compressive stresses in both the short and the long directions of the slab. They are given by:

$$\sigma_{gx} = \frac{F_x}{A_c} = \frac{43,464}{12 \times 9} = 402.4 \text{ psi}$$

$$\sigma_{gy} = \frac{F_y}{A_c} = \frac{16,200}{12 \times 9} = 150 \text{ psi}$$

Let us determine the moments and corresponding stresses due to the unbalanced load $w_{nb} = 80$ psf. Using the 1963 edition of the ACI building code, or other design charts where coefficients are provided to calculate moments in slabs, we have, for the case of a slab simply supported on its edges and having $l_x / l_y = 30/50 = 0.60$:

$$M_x = 0.081 \times w_{nb} \times l_x^2 = 0.081 \times 80 \times 30^2 = 5832 \text{ lb-ft} = 69,984 \text{ lb-in/ft}$$

$$M_y = 0.010 \times w_{nb} \times l_y^2 = 0.010 \times 80 \times 50^2 = 2000 \text{ lb-ft} = 24,000 \text{ lb-in/ft}$$

Given section moduli $Z_t = Z_b = 162$ in^3 per foot width of slab in each direction, the above moments produce flexural stresses on the concrete top and bottom fibers given by:

Short direction: $\quad \sigma = \pm\dfrac{69.984}{162} = \pm 432$ psi

Long direction: $\quad \sigma = \pm\dfrac{24,000}{162} = \pm 148.15$ psi

The resulting stresses due to: 1) the unbalanced load, and 2) the combined effect of balanced load and prestressing, will be:

Short direction: $\begin{cases} \sigma_t = 402.4 + 432 = 834.4 \text{ psi} \\ \sigma_b = 402.4 - 432 = -29.6 \text{ psi} \end{cases}$

Long direction: $\begin{cases} \sigma_t = 150 + 148.15 = 298.15 \text{ psi} \\ \sigma_b = 150 - 148.15 = 1.85 \text{ psi} \end{cases}$

where the subscripts t and b are for top and bottom fibers, respectively. It can be observed that the above stresses are acceptable. The design, however, is not completed. Ultimate strength requirements and cracking conditions must be checked. It is very likely that additional nonprestressed reinforcement will be added in span and near the end anchorages to resist stress concentrations and avoid concrete splitting.

10.13.4 Load Balancing of Frames

The load-balancing approach can be easily applied to the various members of a frame. Under balanced load, uniform compression is present in all members and the frame can be analyzed for the unbalanced load as a nonprestressed frame. However, shortening of the various members due to the uniform compression must be accounted for in the design. It leads to moments and reactions that can be determined by elastic analysis and should be added to the effects of unbalanced loads.

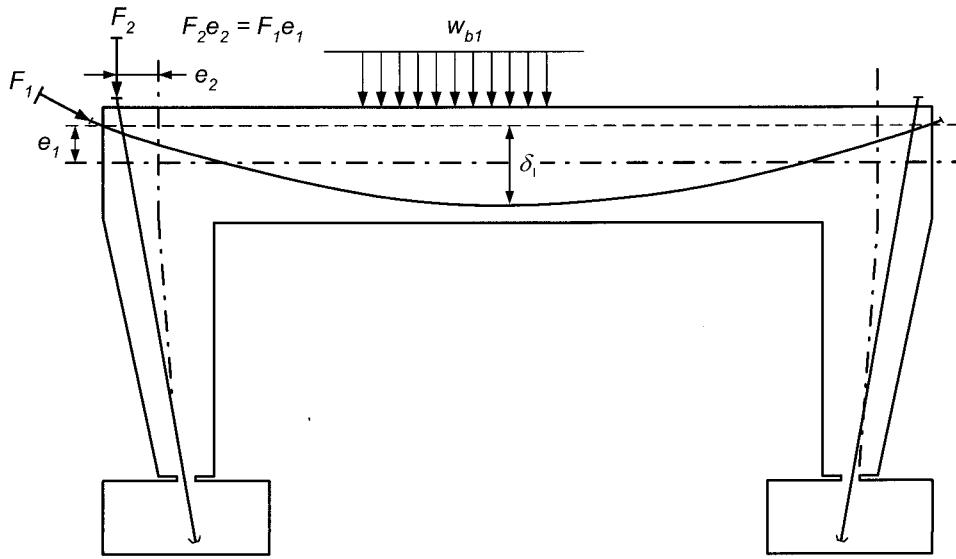

Figure 10.33 Typical load balancing in prestressed concrete frames.

In selecting the steel profile for load balancing, the forces and eccentricities at the joints between two members must be selected in such a way that the primary moments are equal (Fig. 10.33). The profile in each member depends on the

balanced load. The balanced load can be the effect of an end moment such as in the legs of the frame shown in Fig. 10.33 where no direct transverse load is applied. In such a case, a linear tendon is used.

Applied to frames, the load-balancing method can be very convenient for a fast first approximation design. However, because of the effects of shortening of the various members due to prestressing, elastic indeterminate analysis of the frame is needed and should complement that of the unbalanced load. As computerized techniques, such as matrix structural analysis and finite elements analysis, are available and could be efficiently used, it seems that one would gain by directly using them in accordance with the method described in Sec. 10.11 for beams. Nevertheless, the load-balancing method will help in providing a first estimate of the prestressing force in each member, which reduces the number of iterations incurred in the design.

10.13.5 Limitations of Load Balancing

It is shown in the previous sections (and in the examples of Sections 10.15, 11.4 and 11.14) that load balancing can be a very efficient method for preliminary determination of the prestressing force and its profile. However, it has some important limitations that need to be pointed out:

1. The steel profile obtained by load balancing in continuous beams is characterized by abrupt changes in direction over the supports. This is, of course, not acceptable. If the profile is smoothened along a transition region over the supports, load balancing would not be valid any more and an analysis similar to that described in Sec. 10.11 would be required. Therefore, in some cases it is better to follow the procedure described in Section 10.11 right away. However, in shallow continuous slabs, the change in angle at the supports is so small that it can be accommodated over a very small transition region of the same order as the width of the support (or column). Practically, load balancing can then still be considered valid (see Chapter 11).
2. Load balancing does not directly account for moments induced by tendons anchored eccentrically at the end supports. The eccentricity of the steel centroid at the end supports must be zero.
3. Load balancing does not consider the effects of friction, if any, along the member. However, this limitation is also present in the other methods, at least in the preliminary design phase.

10.14 ULTIMATE STRENGTH ANALYSIS

The analysis of a statically indeterminate prestressed concrete structure differs from that of a statically determinate structure by two main aspects: (1) secondary

moments must be accounted for in the analysis, and (2) the attainment of ultimate moment resistance at one critical section does not necessarily lead to the collapse of the structure; this is because plastic hinges may form at several critical sections and redistribution of moments occurs prior to collapse.

10.14.1 Treatment of Secondary Moments

As pointed out earlier, secondary moments can be considered additional external moments at each section. In Section 18.10.3, the ACI code [Ref. 5.1] specifies that the moments used in computing the required strength shall be the sum of the moments due to factored loads (including redistribution, if permitted, as explained in Section 10.14) and secondary moments with a load factor of 1. The secondary moments are to be determined on the basis of effective prestress, not on the basis of the force in the tendons at ultimate behavior [Refs. 10.12 and 10.13]. Hence, referring to the required strength for one of the most common load combinations (Table 3.9), we have:

$$M_u(x) = 1.2M_D(x) + 1.6M_L(x) + M_2(x) \tag{10.19}$$

where $M_2(x)$ is the secondary moment at section x, obtained from elastic analysis. It is believed that the load associated with hinge formation depends on the magnitude of secondary moments; therefore, these cannot be neglected in the design of individual sections by the USD approach, and that is also the position taken by the code. The ultimate moment resistance, $\phi M_n(x)$, at a given section can be computed as described in Chapter 5.

If the most critical section in a continuous beam has sufficient rotational capacity at ultimate, it behaves as a plastic hinge. Failure of the member will not follow the formation of the first plastic hinge. Instead, redistribution of moments occurs and, if the loading is increased, another section reaches its ultimate resistance, leading to another plastic hinge. Eventually, a collapse mechanism develops in which each hinging section provides a resistance equal to its own ultimate strength resistance. Failure of the member can then be predicted by limit analysis, as illustrated next.

10.14.2 Limit Analysis

Limit analysis is based on the formation of plastic hinges in a structure, leading to a collapse mechanism. Theoretically, a plastic hinge shows an elastoplastic moment-rotation response and is quite representative of the behavior of steel structures. In reinforced and prestressed concrete, the cracking of members at one critical section reduces the corresponding stiffnes substantially and a pseudo-plastic response may develop. Such a response may simulate a plastic hinge if sufficient ductility exists at the critical section [Ref. 10.1]. Adequate ductility can be achieved if a low effective reinforcing index ω_e is used, if nonprestressed bonded reinforcement is added to the

section, and if sufficient resistance to shear cracking is provided [Refs. 10.2, 10.3, 10.15, 10.16].

To illustrate the application and benefits of limit analysis, let us consider a continuous beam with two equal spans, subjected to an increasing uniform load w (Fig. 10.34). Let us assume that the flexural resistance of the intermediate support section B is equal in magnitude to that of the near-midspan section. These sections are assumed to have sufficiently ductile behavior to allow the formation of plastic hinges.

A uniform load w, under which the beam behaves elastically, leads to a maximum moment at the intermediate support B, and a moment diagram as shown in Fig. 10.34*a*. If the load is increased, it will eventually reach a value here called w_{uB} for which the ultimate resistance M_n at section B is attained. (*Note*: ϕM_n is used instead of the nominal resistance M_n to incorporate right away the ACI or AASHTO LRFD design approach.) Section B is assumed to have an elastoplastic moment-curvature response, as described in Fig. 10.34*b*. The value ϕM_n can be defined as the plastic moment of section B. The magnitude of the plastic moment at B is then given by:

$$\phi M_n = \frac{w_{uB} l^2}{8} \tag{10.20}$$

from which w_{uB} can be determined as:

$$w_{uB} = \frac{8\phi M_n}{l^2} \tag{10.21}$$

Because of the rotational capacity at section B, the beam does not collapse when $w = w_{uB}$, as the moment resistance is not yet attained at the near-midspan section. For all practical purposes, if the applied load exceeds w_{uB}, the support section B can be replaced by a plastic hinge offering a known resistance or plastic moment ϕM_n. The structure is essentially reduced to a statically determinate structure because a redundant moment has been replaced by a known moment at B. If the load is increased further, it will reach a value w_u at which a second plastic hinge forms at the near-midspan section (Fig. 10.34*c*). This section is assumed to have the same elastoplastic behavior as section B with an equal magnitude of plastic moment ϕM_n. The two plastic hinges added to the end support hinge A constitute a mechanism leading to the collapse of the beam.

A mechanism can be analyzed by statics as known values of plastic moments ϕM_n are given at each hinge. For the present case (Fig. 10.34*c*), it is necessary to identify first the near-midspan section, D, at which the plastic hinge develops. It is obtained by writing that the external work is equal to the internal work then by

differentiating the resulting equation in w_u with respect to x and setting it equal to zero. The corresponding abscissa for this example is found equal to $(\sqrt{2}-1)l$. Using moment equilibrium equations at the near midspan section, D, and at the support section, B (note that the ϕM_n moments are of different signs), leads to the reaction R_A and the value of w_u for which collapse of the structure occurs, namely:

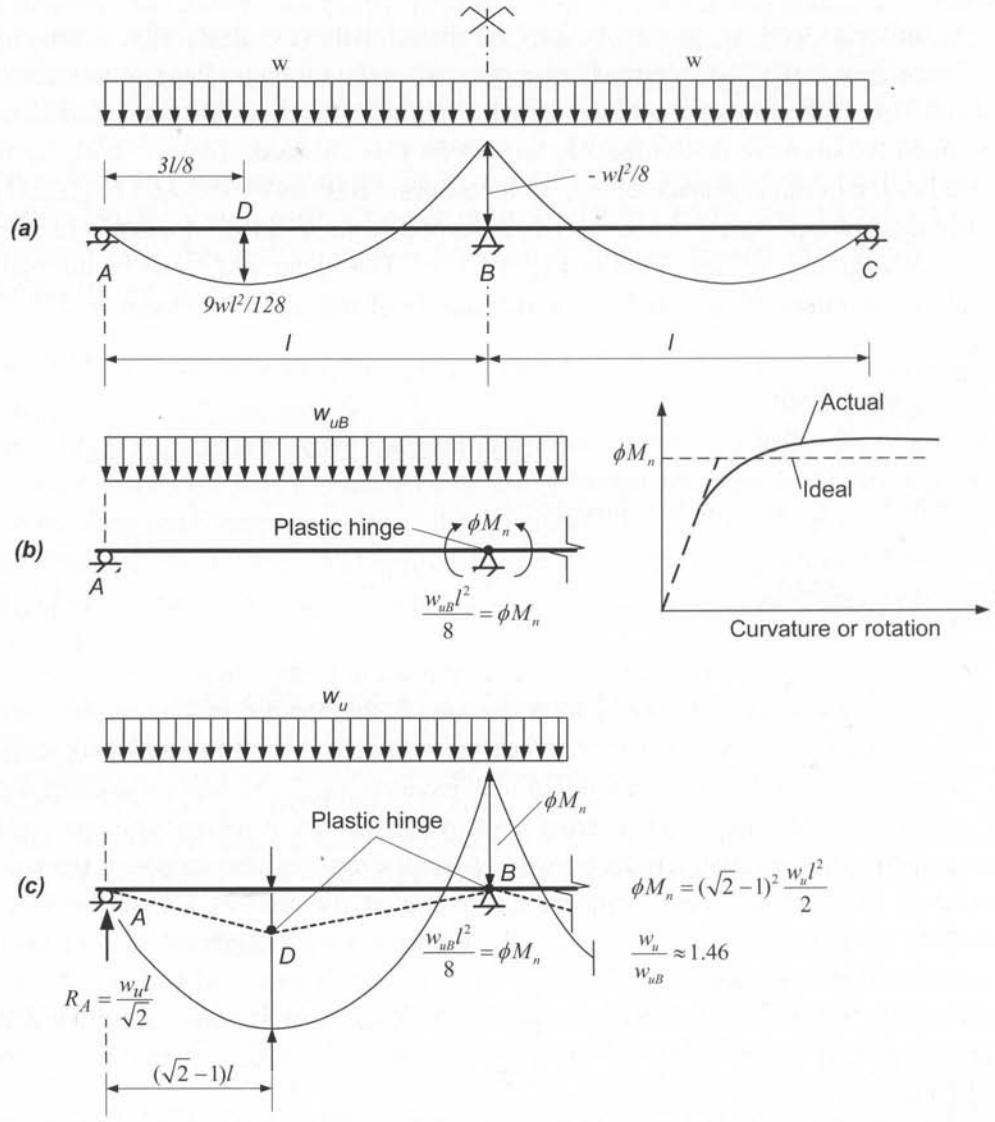

Figure 10.34 Moment redistribution in continuous beams. ***(a)*** **Elastic moment diagram.** ***(b)*** **First plastic hinge.** ***(c)*** **Collapse mechanism and plastic moment diagram.**

$$R_A = \frac{w_u l}{\sqrt{2}} \tag{10.22}$$

$$w_u = \frac{2\phi M_n}{l^2(\sqrt{2}-1)^2} \tag{10.23}$$

The value of w_u is substantially higher than w_{uB}. Their ratio is:

$$\frac{w_u}{w_{uB}} = \frac{2}{(\sqrt{2}-1)^2 8} \simeq 1.46 \tag{10.25}$$

The above result suggests that the load that led to failure of the continuous beam is 46 percent higher than that which would have produced failure if the beam was simply supported. The formation of a plastic hinge at B has allowed, in effect, a redistribution of moments from support B (at which the moment did not increase beyond ϕM_n) to the near-midspan section, D. Redistribution of moments is recognized by researchers [Refs. 10.12 and 10.13] and permitted by the ACI code, as described next.

10.14.3 Redistribution of Moments

In its commentary section R8.4, the 2002 ACI code [Ref. 5.1] provides the following argument for moment redistribution: "Moment redistribution is dependent on adequate ductility in plastic hinge regions. These plastic regions develop at points of maximum moment and cause a shift in the elastic moment diagram. The usual result is a reduction in the values of maximum moments in the plastic hinge region (such as at interior supports) and an increase in the values of positive moments (such as in span). Because negative moments are determined for one loading arrangement and positive moments for another, each section has a reserve capacity that is not fully utilized for any one loading condition. The plastic hinges permit the utilization of the full moment capacity of more cross sections of a flexural member at ultimate load."

To account for the potential rotational capacity of reinforced and prestressed concrete structures, the ACI code (Sections 8.4 and 18.10.4) allows a limited redistribution of moments in continuous beams containing a minimum amount of bonded reinforcement. It essentially states that it shall be permitted to increase or decrease negative moments at supports of continuous flexural members by a percentage defined as follows:

Percent of moment redistribution:

$$\text{MR} \le 1000\varepsilon_t \le 20 \text{ in percent}$$
$$\text{provided: } \varepsilon_t \ge 0.0075 \tag{10.26}$$

where ε_t is the net tensile strain in the reinforcement at nominal bending resistance of the section considered, as defined in Chapter 5. Since the net tensile strain and the ratio c/d_e are related on a one to one basis, the above equation can be put in the following simpler form (to avoid computing ε_t) because the ratio c/d_e is essentially part of the computations of nominal moment resistance:

Percent of moment redistribution:

$$\text{MR} \le \left(\frac{3}{c/d_e} - 3\right) \le 20 \text{ in percent}$$
$$\text{provided: } \frac{c}{d_e} \le \frac{1}{3.5} = 0.286 \qquad (10.27)$$

For moment redistribution to occur, minimum reinforcement as required by the code is also implied. Equation (10.27) assumes that the strain of the concrete extreme compression fiber at ultimate is 0.003. Equation (10.27) is graphically illustrated in Fig. 10.35 and compared to a similar relation given in the AASHTO LRFD specifications (see Chapter 5). Note that the maximum moment redistribution of 20 percent using ACI occurs for $c/d_e \le 3/23 = 0.13$.

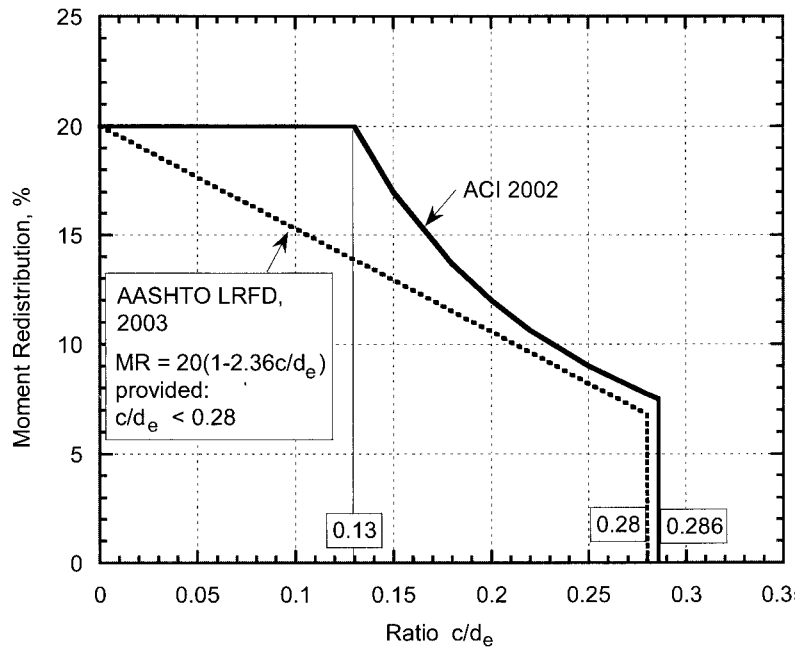

Figure 10.35 Illustration of percent of moment redistribution permitted by ACI and AASHTO LRFD codes.

The modified moments shall be used for calculating moments at sections within span for the same loading arrangement. Thus, if a portion of negative moment at the mid-support of a two-span continuous beam is distributed to the section of maximum positive moment in span, that section should be designed to resist its own moment demand plus the redistributed moment.

10.14.4 Secondary Moment and Moment Redistribution

The following discussion pertains to the use of non-concordant tendons for which secondary moments exist.

Opinions differ as to whether secondary moments should be included in moment redistribution. While the ACI code requires to include the secondary moments in the strength design moment (Eq. 10.19), it is not clear if secondary moments should still be considered when moment redistribution is allowed to occur (that is, when a plastic hinge mechanism forms). It is generally believed that the elastic deformation caused by non-concordant tendons changes the amount of inelastic rotation required to provide a given amount of moment redistribution [Refs. 10.2, 10.12, 10.13]. However, the author also believes that the elastic deformation is very small compared to the permanent inelastic rotation needed to develop plastic hinges, and consequently secondary moments should not be considered in moment redistribution. Indeed, when large rotational capacities occur at various sections, inelastic permanent deformations will quickly neutralize the elastic deformations necessary to induce secondary reactions and secondary moments.

Another issue is related to whether the tendons are bonded or unbonded. Unbonded tendons tend to remain in the elastic range of behavior up to large sectional rotations, even when plastic hinges form, while bonded tendons will stretch way beyond yielding at plastic hinge locations. However, in continuous beams, permanent inelastic deformations can quickly squash secondary reactions at supports, thus nullifying secondary moments. This is because the structure adapts to the imposed plastic rotation. Moreover, even if the prestressing force remains effective and is fully recovered at unloading, the concrete would have deformed (strained and cracked) sufficiently inelastically to balance secondary reactions. So the amount of permanent plastic deformation remains large and the structure would simply adapt to the level of existing supports.

In summary, the author believes that secondary moments should not be included in moment redistribution. This is especially so if their inclusion allows for a reduction in the required reinforcement and thus may result in a lower safety margin.

10.14.5 Prediction of Plastic Rotation in PPC Beams

The plastic rotation can be determined from the integration of curvature over a distance, L_p, described as the plastic hinge length. Generally, the length of plastic hinge is taken between $d_e/2$ and d_e.

If the compressive strain of the concrete top fiber is known in the plastic hinge region, and if it is assumed uniform over that region, the plastic rotation can then be determined from the following equation:

$$\theta_p = \left(\phi_u - \phi_y\right) L_p = \left(\frac{\varepsilon_{cu}}{c_u} - \frac{\varepsilon_{cy}}{c_y}\right) L_p \tag{10.28}$$

where:

ϕ_u = curvature at the limit state of failure, that is at nominal bending resistance of the section

ϕ_y = curvature at yielding of the steel

c_u = neutral axis depth at nominal bending resistance

ε_{cu} = extreme fiber compressive strain of concrete at failure

c_y = neutral axis at yielding of the steel

ε_{cy} = strain in the extreme compression fiber at yielding of the steel

Equation (10.28) applies to both reinforced and prestressed concrete; in the case of partially prestressed concrete where both reinforcing bars and prestressing tendons are present, it is not clear if the state of yielding should correspond to that of the reinforcing bars or the prestressing tendons; an in-between condition may be better [Ref. 10.15]. The extreme fiber compressive strain of concrete is assumed equal 0.003 by the ACI code for design purposes. However, it should be pointed out that ε_{cu} depends on many parameters, including the stress-strain properties of the concrete material, the section shape, and the reinforcement index. It is also greatly influenced by fiber reinforcement and by confinement.

Table 10.1 Predicted values of ductility index and plastic rotation.

Parameter	Upper Bound	Lower Bound	Average
Curvature ductility ratio, μ_ϕ	$\dfrac{1}{0.85\beta_1 \dfrac{c}{d_e} - 0.45}$	$\dfrac{1}{1.65\beta_1 \dfrac{c}{d_e} - 0.086}$	$\dfrac{1}{1.275\beta_1 \dfrac{c}{d_e} - 0.075}$
Plastic rotation, θ_p, radian	$\left(\dfrac{1.05 - 0.85\beta_1 \dfrac{c}{d_e}}{722\beta_1 \dfrac{c}{d_e} - 35}\right) \dfrac{2L_p}{d_e}$	$\left(\dfrac{1.05 - 1.40\beta_1 \dfrac{c}{d_e}}{1105\beta_1 \dfrac{c}{d_e} - 40}\right) \dfrac{2L_p}{d_e}$	$\left(\dfrac{1.07 - 1.34\beta_1 \dfrac{c}{d_e}}{722\beta_1 \dfrac{c}{d_e} - 35}\right) \dfrac{2L_p}{d_e}$

An extensive computerized evaluation of the ductility of prestressed and partially prestressed concrete beams was carried out in Ref. [10.15]. Analytical results were compared with experimental observations and used to provide some predictive values of the ductility index and plastic rotation capacity of these beams. A summary

of the results is given in Table 10.1. The length of plastic hinge, L_p, varies depending on several parameters. In the regression analysis of data, it was assumed equal $d_e/2$, and the values in Table 10.1 allow for a value of $L_p = d_e$ as well. To account for various conditions, and the scatter in the experimental data, upper bound, lower bound and average values are given in Table 10.1. These can be used as a first approximation in design.

10.15 EXAMPLE: DESIGN OF A PRESTRESSED CONTINUOUS BEAM

Let us determine the prestressing steel needed for the posttensioned two-equal-span continuous bridge beam with cross section described in Fig. 10.36. (See also Section 14.12 for a similar bridge section.) The following design information is provided: l = 120 ft; section properties: $A_g = 30$ ft^2, $y_t = y_b = 2.5$ ft $= 30$ in, $Z_t = Z_b = 43$ ft^3, $I_g = 107.5$ ft^4, $k_b = 1.433$ ft $= 17.2$ in, $k_t = -17.2$ in; concrete properties and allowable stresses: $f'_c = 6000$ psi, $f'_{ci} = 4800$ psi, $\bar{\sigma}_{ti} = -208$ psi, $\bar{\sigma}_{ts} = -232$ psi, $\bar{\sigma}_{ci} = 2880$ psi; $\bar{\sigma}_{cs} = 2400$ psi; steel stresses: $f_{pi} = 181$ ksi, $f_{pe} = 145$ ksi, $\eta = f_{pe}/f_{pi} = 0.80$; loadings: $w_G = 4.5$ klf, $w_L = 3.24$ klf. Assume a maximum practical eccentricity $(e_o)_{mp} = 26$ in, which applies to both the span and support sections.

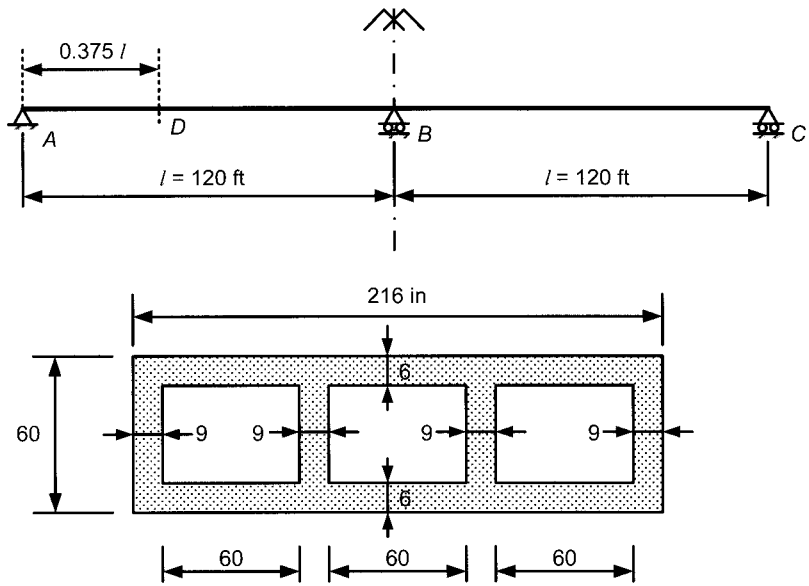

Figure 10.36 Span and cross section of example beam.

Note that the section is completely symmetrical and is considered in its entirety as a single section. The steel stress along the beam is assumed constant, that is, frictional losses are neglected, at least in the initial design phase.

Because of symmetry, only two critical sections will be analyzed: the intermediate support section B and the near-midspan section D taken at $3/8l$ from the left support. The moments

generated at each of these sections are summarized in Table 10.2 and can easily be verified. Several design cases are considered next.

(a) Determine a concordant tendon profile. For this, the following property will be used: any moment diagram, or combination of moment diagrams, due to any external loading plotted to any scale is a location for a concordant tendon.

To determine the profile, a combination of two loadings will be used: a uniform downward load throughout the length (here the dead load w_G is used) and a uniform upward load w over a fifth of the span adjacent to the support B (Fig. 10.8). The second load is intended to smoothen the profile over the support, since it produces a moment opposite to the dead load moment.

Because of symmetry, only one span AB is considered. Noting that the reaction at A is $3w_G l/8$, the moment at any section x from end support A due to the dead load w_G can be written as:

$$M_G(x) = w_G l^2 \frac{1}{2}\frac{x}{l}\left(\frac{3}{4} - \frac{x}{l}\right) = w_G l^2 \times \text{(factor)}$$

It is generally convenient first to compute separately the factor in function of x/l and then to compute the corresponding moment for any uniform load such as w_G. The numerical values for this case are given in Table 10.3.

Table 10.2 Moments for example beam

	Near-midspan section D	Intermediate support section B
x from left support, ft	$3/8l = 45$ ft	$l = 120$ ft
Dead load moment, kips-ft	4556.2	-8,100
Live load moment, kips-ft	4374	-5,832
Minimum moment, kips-ft	3463	-8,100
Maximum moment, kips-ft	8930	-13,932

The moment at any section x, due to the second loading w (uniform over $0.2l$), can be calculated as follows: determine the fixed-end moments at A and B (use Fig. 10.25); determine the end moment at B by moment distribution (because of symmetry, only one span is used); determine the vertical reaction at A by satisfying the following equation leading to the end moment at B:

$$R_A l - w(0.2l)\left(\frac{0.2l}{2}\right) + 0.0162wl^2 = 0$$

which leads to $R_A = -0.0038wl$. Hence, the moment at any section of the span is given by:

For $x/l \le 0.8$

$$M(x) = R_A x = -0.0038\left(\frac{x}{l}\right)wl^2$$

For $0.8 \le x/l \le 1$

$$M(x) = R_A x + \frac{w}{2}(x - 0.8l)^2 = wl^2\left[-0.0038\frac{x}{l} + \frac{1}{2}\left(\frac{x}{l} - 0.8\right)^2\right]$$

The two above expressions can be written each as wl^2 multiplied by a factor. The choice of w should be such that it would lead to a reduction in moments at and near the support B to smooth the

profile sufficiently. Some iteration may be needed. A value of w = 10 klf is used for this example and leads to the moments shown in Table 10.3.

Table 10.3 Summary of computations to determine a concordant tendon profile.

x/l →		0.1	0.2	0.3	(3/8)	0.4
Dead load, w_G = 4.5 klf	*Factor*	0.325	0.055	0.0675	0.0703	0.070
	Moment, kips-ft, *Factor* × $w_G l^2$	2106	3564	4374	4536	4536
Additional load: w = 10 klf over 0.2l	*Factor* × 10^{+4}	-3.8	-7.6	-11.4	-15.2	-15.2
	Moment, kips-ft: *Factor* × wl^2	-54.7	-109.4	-164.2	-218.9	-218.9
Resulting moment,† kips-ft		2051	3455	4210	4351	4317
$e_o(x) = \frac{M(x)}{K}$, in , where: $K = 221.81$		9.25	15.58	18.98	19.62	19.46

†Rounded off values

Table 10.3 - continued

x/l →		0.5	0.6	0.7	0.8	0.9	1
Dead load, w_G = 4.5 klf	*Factor*	0.0625	0.045	0.0175	-0.02	-0.675	-0.125
	Moment, kips-ft,	4050	2916	1134	-1296	-4374	-8100
Additional load: w = 10 klf over 0.2l	*Factor* × 10^{+4}	-19	-22.8	-26.6	-30.4	15.8	162
	Moment, kips-ft:	-273.6	-328.3	-383	-437.8	227.52	2332.8
Resulting moment,† kips-ft		3776	2588	751	-1734	-4146	-5767
$e_o(x) = \frac{M(x)}{K}$, in , where: $K = 221.81$		17.02	11.67	3.39	-7.82	-18.69	-26.0

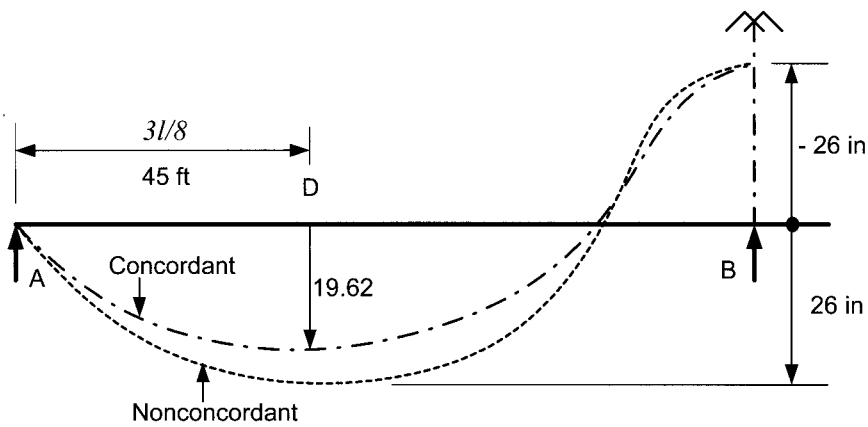

Figure 10.37

The resulting moments are then calculated and the steel profile is determined using Eq. (10.9):

$$e_o(x) = \frac{M(x)}{K}$$

where K is determined from the critical section that is B for which e_o is taken equal to the maximum practical eccentricity. Hence:

$$K = \frac{M_B}{(e_o)_{mp}} = \frac{-5767}{-26} = 221.81$$

The corresponding eccentricities at various sections (from Eq. 10.9) are given in Table 10.3 and the steel profile is plotted in Fig. 10.37. The reader may want to check if the profile is within the feasible domain of the critical sections, as described in the next case.

(b) Determine the prestressing force, assuming that a concordant steel profile will be arrived at in the design. The problem is essentially reduced to the case of a simply supported beam where no secondary moments due to prestressing exist. To find the prestressing force, two critical sections will be analyzed, the support and the near midspan sections, B and D, in a way similar to a simply supported cantilever beam. As the eccentricity of the ZLC-line is the same as that of the steel, the equations of Table 4.2, way 2, can be used to build the feasibility domain at each of these sections. These are given below, where e_o is expressed in inches and F_i in kips:

At support B:

Condition I $\quad e_o = 17.2 + \dfrac{112{,}656}{F_i}$

Condition II $\quad e_o = -17.2 + \dfrac{311{,}196}{F_i}$

Condition III $\quad e_o = 17.2 - \dfrac{13{,}932}{F_i}$

Condition IV $\quad e_o = -17.2 + \dfrac{187{,}432}{F_i}$

At near midspan section D:

Condition I $\quad e_o = 17.2 + \dfrac{70{,}128}{F_i}$

Condition II $\quad e_o = -17.2 + \dfrac{268{,}668}{F_i}$

Condition III $\quad e_o = 17.2 - \dfrac{88{,}962}{F_i}$

Condition IV $\quad e_o = -17.2 + \dfrac{112{,}402}{F_i}$

Note that, in order to use Table 4.2 for the support section B, the section is assumed temporarily inverted with the negative moments and the eccentricity both becoming positive. The feasibility domains for the above two sections are plotted in Fig. 10.38. For clarity, the domain for B is plotted with the e_o axis positive upward, while the domain for D is plotted with the axis positive downward. It can be observed that there is a feasibility domain for each section. The minimum prestressing force

in each case is given by the intersection of line IV with the maximum practical eccentricity line, $|(e_o)_{mp}| = 26$ in. As the force at B is larger than at D, it controls the design. Hence, the prestressing force F_i is given by the abscissa of point Q of Fig. 10.38. That is:

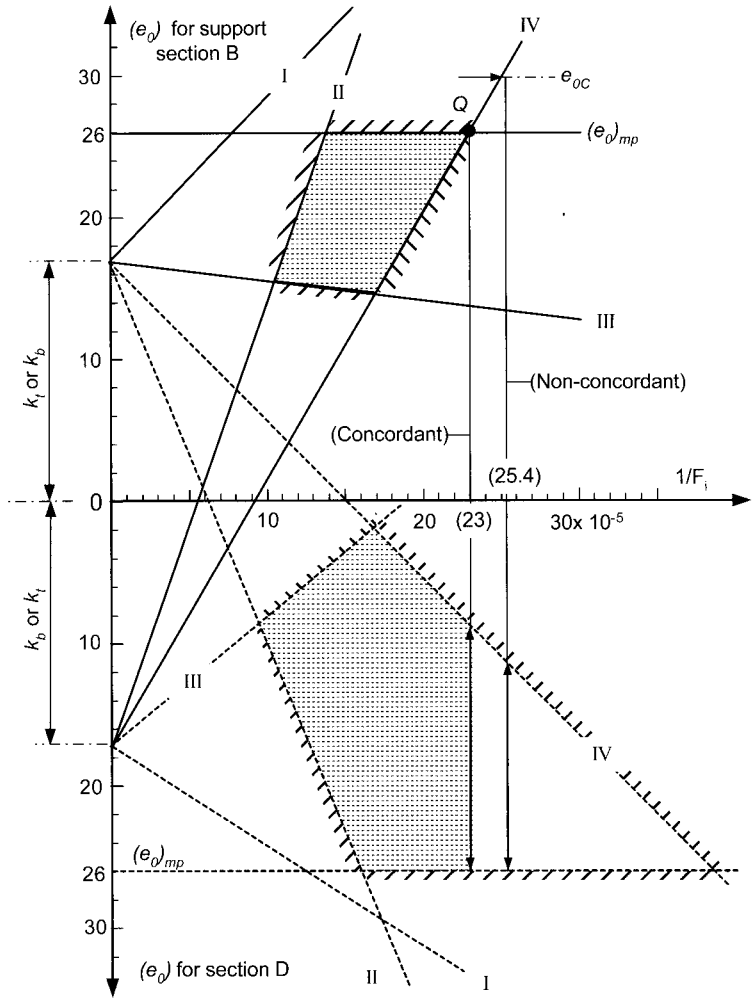

Figure 10.38 Feasibility domains for the support and near-midspan sections.

$$\frac{1}{F_i} \simeq 23 \times 10^{-5}$$

or

$$F_i \simeq 4339 \text{ kips}$$

and

$$F = 0.8F_i = 3471 \text{ kips}$$

Note that the above result can be also obtained from stress condition IV in which e_o is replaced by $(e_o)_{mp} = 26$ in. The same prestressing force is used throughout the beam. Its eccentricity at section *D*, as shown in the domain of Fig. 10.38, can vary from about 8.6 to 26 in without violating any allowable stress. This flexibility will be found very convenient in selecting the tendon profile. For instance, the concordant tendon profile determined in case a, with an eccentricity e_o = 19.62 in at section *D* (Table 10.2), and e_o = -26 in at section *B*, is an acceptable profile and can be used here.

(c) Determine the prestressing force assuming a nonconcordant profile. Using the design aids of Sec. 10.10, let us consider a tendon profile made out of three parabolas and passing by the maximum eccentricities at sections *B* and *D*, that is e_{oD} = 26 in and e_{oB} = -26 in (Fig. 10.37). Assume the following coefficients for the profile: $\beta = 0$; $\beta_1 = -1$; $\alpha = 0.375$; $\alpha_1 = 0.15$. The fixed-end moment at support *B* (Fig. 10.25) is given by:

$$m_B = -Fe_{oB}\frac{1}{4}\left[-\beta\alpha^2 + (1+\alpha-\alpha_1)^2 - \alpha_1(1-\alpha) - \beta_1(3-3\alpha_1+\alpha_1^2+2\alpha-\alpha\alpha_1)\right]$$

$$m_B = -Fe_{oB}\frac{1}{4}[0+1.5006-0.0938+3.2663]$$

$$m_B = -Fe_{oB}\frac{4.673}{4} = -1.168Fe_{oB}$$

Because of symmetry, the fixed-end moment at *B* is also the end moment at *B*. Hence, the moment at *B* due to prestressing is given by:

$$M_{FB} = -1.168Fe_{oB}$$

As the primary moment is given by:

$$M_{1B} = -Fe_{oB}$$

the secondary moment is:

$$M_{2B} = M_{FB} - M_{1B} = -0.168Fe_{oB}$$

As e_{oB} is negative, it can be seen that the secondary moment is positive and, therefore, beneficial. The corresponding eccentricity of the ZLC-line at *B* is given by:

$$(e_{oc})_B = e_{oB} - \frac{M_{2B}}{F} = e_{oB} + 0.168e_{oB}$$

$$(e_{oc})_B = 1.168e_{oB} = -1.168\times 26 = -30.37 \text{ in}$$

Hence, the prestressing steel placed at an eccentricity of -26 in acts as if it was placed at -30.37 in. Going back to the domain of Fig. 10.38, we can plot a horizontal line for $(e_{oc})_B$ with magnitude 30.37 in and read the value of F_i from its intersection with line IV. It leads to:

$$\frac{1}{F_1} = 25.4\times 10^{-5}$$

hence:

$$F_i = 3937 \text{ kips}$$

and

$$F = 0.8F_i = 3150 \text{ kips}$$

The value of *F* can also be derived analytically from stress condition IV of Table 4.2, in which e_o is replaced by $(e_{oc})_B$, that is:

$$F = \frac{|M_{\max}| + \bar{\sigma}_{ts}Z_b}{|(e_{oc})_B| - k_t}$$

$$F = \left(\frac{13{,}932 \times 12{,}000 - 232 \times 43 \times 12^3}{30.37 + 17.2} \right) 10^{-3} = 3152 \text{ kips}$$

This value of F is about 10 percent smaller than the value obtained in case *a* for the concordant profile and illustrates the beneficial effect of a nonconcordant profile in this case.

For the above value of F, the secondary moment at B can be calculated as:

$$M_{2B} = -0.168 F e_{oB} / 12 = 1147 \text{ kips-ft}$$

The secondary moment at section D can be determined from Eq. (10.7) and leads to M_{2D} = 430 kips-ft. The ZLC-line at D will have an eccentricity of:

$$e_{oc} = e_{oD} - \frac{M_{2D}}{F} = 26 - \frac{430 \times 12}{3152} = 24.36 \text{ in}$$

It is inside the domain at D, hence all stresses are satisfied. The steel profile for this case is also plotted in Fig. 10.37 for comparison with the concordant profile.

The reader may also want to check that a concordant steel profile would have been obtained if the following values were used: e_{oB} = -26 in; e_{oD} = 22 in; β = 0; α = 0.375; α_1 = 0.17. It can be arrived at by trial and error, using the design aids of Sec. 10.10 directly. This new concordant profile is different from the one obtained in case *a*.

(d) For the nonconcordant steel profile given in case *c* and a value of F = 3152 kips, determine the prestressing moment at *B* using the equivalent load approach.

The steel profile is made out of three parabolas with characteristics shown in Fig. 10.39*a*. The equivalent uniform loads over the three beam segments are given by (Figs. 10.10 and 10.25):

$$w_1 = -\frac{8F\delta}{l_1^2} = \frac{8 \times 3152 \times 26/12}{(2 \times 45)^2} = -6.745 \text{ klf}$$

$$w_2 = -\frac{8F\delta}{l_2^2} = \frac{8 \times 3152 \times (26 + 13.52)/12}{(2 \times 57)^2} = -6.39 \text{ klf}$$

$$w_3 = \frac{8F\delta}{l_3^2} = \frac{8 \times 3152 \times 12.48/12}{(2 \times 8)^2} = 20.235 \text{ klf}$$

The load is assumed positive downward. Using the information given in Fig. 10.18, the fixed-end moments due to w_1 are determined as follows:

$$(m_A)_1 = -\frac{w_1 l^2}{12}(6 - 8\alpha + 3\alpha^2)\alpha^2$$

$$= \frac{6.745 \times 120^2}{12}(6 - 8 \times 0.375 + 3 \times 0.375^2)0.375^2$$

$$= 3894.84 \text{ kips-ft}$$

$$(m_B)_1 = \frac{w_1 l^2}{12}(4 - 3\alpha)\alpha^3$$

$$(m_B)_1 = \frac{6.745 \times 120^2}{12}(4 - 3 \times 0.375)0.375^3$$

$$= 1227.14 \text{ kips-ft}$$

Similarly, it can easily be shown that the fixed-end moments due to w_2 and w_3 are:

$$(m_A)_2 = 3886.3 \text{ kips-ft}$$

$$(m_B)_2 = 5665.65 \text{ kips-ft}$$

$(m_A)_3 = -290.93$ kips-ft

$(m_B)_3 = -2659.33$ kips-ft

Summing up the effects of the above three loads leads to the resulting fixed-end moments:

$m_A = 3894.84 + 3886.3 - 290.93 \simeq 7490$ kips-ft

$m_B = 1227.14 + 5665.65 - 2659.33 \simeq 4233$ kips-ft

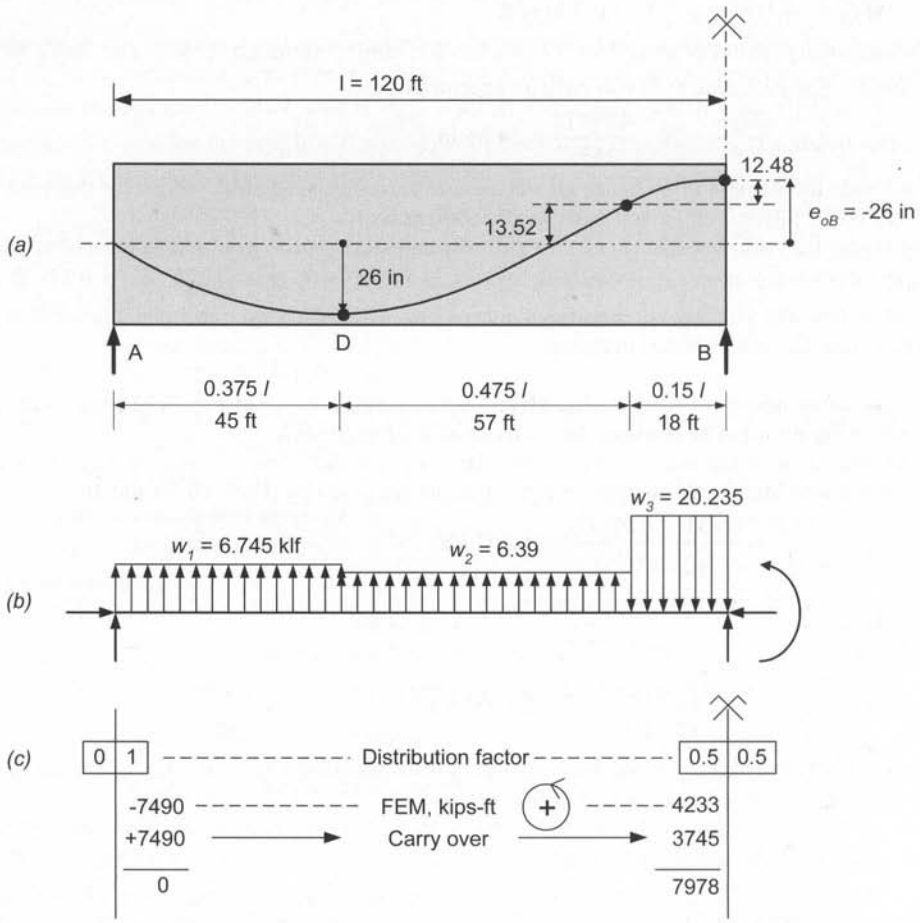

Figure 10.39 Determination of prestressing moment at support section. (*a*) Tendon profile. (*b*) Equivalent load. (*c*) Moment distribution.

To obtain the end moments, the moment distribution method is applied to one span, as shown in Fig. 10.39*c*. It leads to the moment due to prestressing at support *B*:

$M_{FB} = 7978$ kips-ft

The prestressing moment at *B* is the sum of the primary and secondary moments, namely:

$$M_{FB} = M_{1B} + M_{2B} = -Fe_{oB} + M_{2B}$$

from which the secondary moment is determined:

$$M_{2B} = M_{FB} + Fe_{oB} = 7978 + 3152(-26/12) \simeq 1149 \text{ kips-ft}$$

The above value of M_{2B} is essentially the same as that obtained in case *c*.

(e) Determine the prestressing force, using load balancing.

Let us attempt to balance the dead load plus 10 percent of the live load, that is:

$$w_b = 4.5 + 0.10 \times 3.20 = 4.82 \text{ klf}$$

and

$$w_{nb} = 0.9 w_L = 2.916 \text{ klf}$$

As the balanced load is a uniform load, a parabolic steel profile is selected. It should have zero eccentricity at the end supports; thus $e_{oA} = 0$. Because of symmetry, only one span is considered. In order to obtain the maximum sag (or the smallest prestressing force), the maximum practical eccentricities at the intermediate support B and in span at the vertex of the parabola are used (see example in Section 10.8.4). Hence, the eccentricity at the vertex is $e_{o\upsilon} = 26$ in (Fig. 10.40). The abscissa x_υ of the vertex with respect to the left support A must be such that the chosen parabola passes by a point of zero eccentricity at A and a point of eccentricity $e_{oB} = -26$ in at B. The following relation can easily be derived:

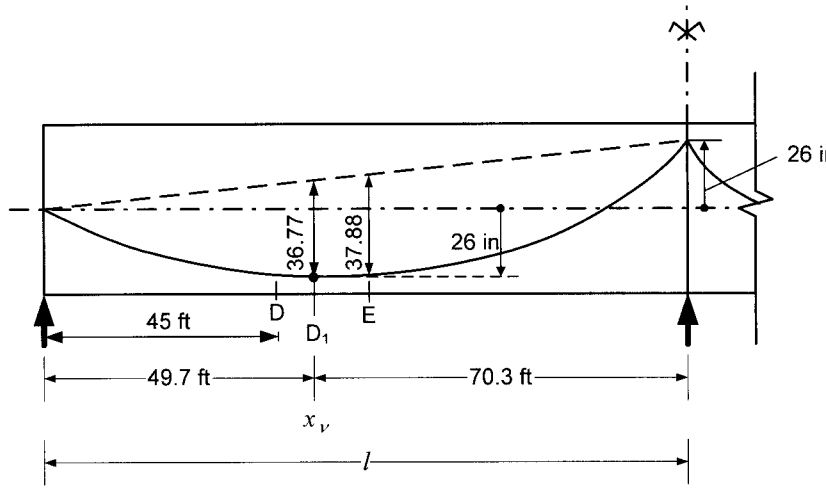

Figure 10.40 Tendon profile for load balancing.

$$x_\upsilon^2 = \left(\frac{e_{o\upsilon} - e_{oA}}{e_{o\upsilon} - e_{oB}} \right) (l - x_\upsilon)^2$$

from which the value of x_υ is computed. For this example, x_υ =49.7 ft (see also part 3 of Section 10.8.4). The steel profile is shown in Fig. 10.40. The equation of the parabola using the vertex as origin (point D_1) has been derived in Section 10.8.4 for a similar tendon profile and is given by:

$$y = 0.731 \times 10^{-4} x^2$$

where y and x are in inches. The ordinate at point E, that is the midspan of the parabola, is given by:

$$y = 0.731 \times 10^{-4} \times [(60 - 47.9)12]^2 = 1.117 \text{ in}$$

The sag of the parabola at its midspan is determined from:

$$\delta = 26 - 1.117 + 26 \frac{60}{120} \simeq 37.88 \text{ in}$$

Given w_b and δ, the prestressing force can be obtained from (Fig. 10.10):

$$w_b = \frac{8F\delta}{l^2}$$

or

$$F = \frac{w_b l^2}{8\delta} = \frac{4.824 \times 120^2}{8 \times 37.88/12} = 2750.75 \text{ kips}$$

Note that if we had used the sag at the vertex D_1, the value of F would have been: 2831.5 kips. A uniform compressive stress $F/A_c = 636.7$ psi is generated in the section under the effects of w_b and F. Therefore, the beam is level. Let us determine the maximum moments induced by the non-balanced load:

At the support section B:

$$M_{nb} = -\frac{w_{nb} l^2}{8} = -\frac{2.916 \times 120^2}{8} = -5248.8 \text{ kips-ft}$$

At the section of maximum positive moment (section D in Fig. 10.38) assumed at $x = \frac{3}{8} l = 45$ ft:

$$M_{nb} = \frac{3 w_{nb} l^2}{32} = \frac{3 \times 2.916 \times 120^2}{32} = 3936.6 \text{ kips-ft}$$

The extreme fiber stresses in the concrete resulting from the uniform compression due to F and the effects of unbalanced moments are given by Eqs. (10.16) and (10.17):

At the support section B:

$$\sigma_t = \frac{F}{A_c} - \frac{M_{nb}}{Z_t} = \frac{2750.75 \times 10^3}{30 \times 144} - \frac{5248.8 \times 12{,}000}{43 \times 1728} = 636.7 - 847.7 \simeq -211 \text{ psi}$$

$$\sigma_b = \frac{F}{A_c} + \frac{M_{nb}}{Z_b} = \frac{2750.75 \times 10^3}{30 \times 144} + \frac{5248.8 \times 12{,}000}{43 \times 1728} = 636.7 + 847.7 = 1484.4 \text{ psi}$$

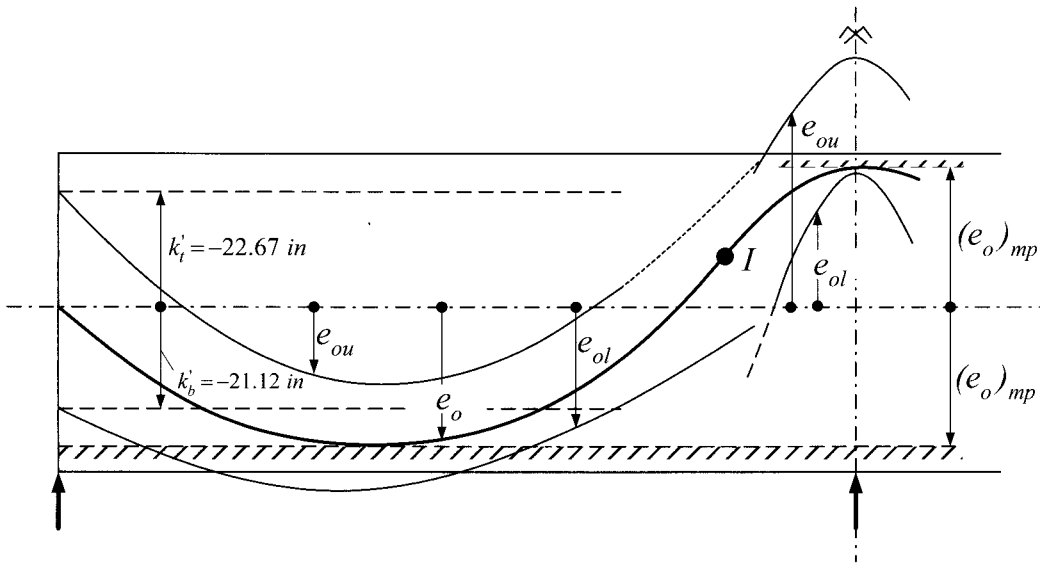

Figure 10.41 Limit zone and practical tendon profile.

At the section of maximum positive moment:

$$\sigma_t = \frac{F}{A_c} + \frac{M_{nb}}{Z_t} = \frac{2750.75\times10^3}{30\times144} + \frac{3936.6\times12{,}000}{43\times1728} = 636.7 + 635.7 = 1272.4 \text{ psi}$$

$$\sigma_b = \frac{F}{A_c} - \frac{M_{nb}}{Z_b} = 636.7 - 635.7 = 1 \text{ psi}$$

The above stresses are acceptable. A similar conclusion would be reached if F_i was used instead of F. Note that, in practice, the steel profile must show a smooth transition over the support B and, therefore, an analysis as described in Sec. 10.11 would be ultimately required. The prestressing force will be likely increased. Nevertheless, the load-balancing method gave a very good first approximation value of the prestressing force comparable to those in cases *b* and *c* above.

(f) The reader may want to pursue this example to determine the limit zone and the ultimate moment resistance of the beam. The limit zone is shown in Fig. 10.41 for the nonconcordant steel profile used in case *c* and offers a relatively large margin of flexibility. It will be found that ultimate strength requirements are also largely satisfied.

10.16 USEFUL DESIGN AIDS FOR CONTINUOUS BEAMS

The design formulas and diagrams for statically indeterminate beams given in Figs. 10.42 to 10.45 are adapted from the LRFD Manual of the American Institute of Steel Construction (AISC). They can be very useful for the design of continuous beams.

BEAM FIXED AT ONE END, SIMPLY SUPPORTED AT OTHER END WITH CONCENTRATED LOAD AT ANY SECTION

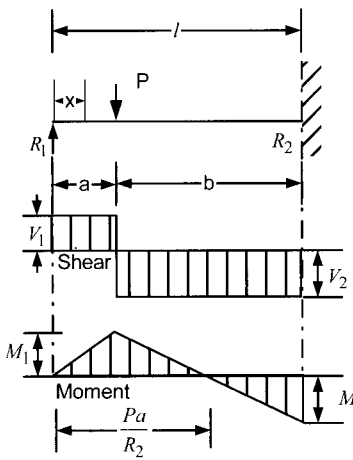

$$R_1 = V_1 \ldots = \frac{Pb^2}{2l^3}(a+2l)$$

$$R_2 = V_2 \ldots = \frac{Pa}{2l^3}\left(3l^2 - a^2\right)$$

$$M_1 \text{ (at point of load)} \ldots = R_1 a$$

$$M_2 \text{ (at fixed end)} \ldots = \frac{Pab}{2l^2}(a+l)$$

$$M_x \text{ (when } x < a) \ldots = R_1 x$$

$$M_x \text{ (when } x > a) \ldots = R_1 x - P(x-a)$$

$$\Delta_{\max}\left(\text{when } a < 0.414l \text{ at } x = l\frac{l^2+a^2}{3l^2-a^2}\right) \ldots = \frac{Pa}{3EI}\frac{\left(l^2-a^2\right)^3}{\left(3l^2-a^2\right)^2}$$

$$\Delta_{\max}\left(\text{when } a > 0.414l \text{ at } x = l\sqrt{\frac{a}{2l+a}}\right) \ldots = \frac{Pab^2}{6EI}\sqrt{\frac{a}{2l+a}}$$

$$\Delta a \text{ (at point of load)} \ldots = \frac{Pa^2b^3}{12EIl^3}(3l+a)$$

$$\Delta_x \text{ (when } x < a) \ldots = \frac{Pb^2x}{12EIl^3}\left(3al^2 - 2lx^2 - ax^2\right)$$

$$\Delta_x \text{ (when } x > a) \ldots = \frac{Pa}{12EIl^3}(l-x)^2\left(3l^2x - a^2x - 2a^2l\right)$$

Figure 10.42

CONTINUOUS BEAM -TWO EQUAL SPANS - UNIFORM LOAD ON ONE SPAN

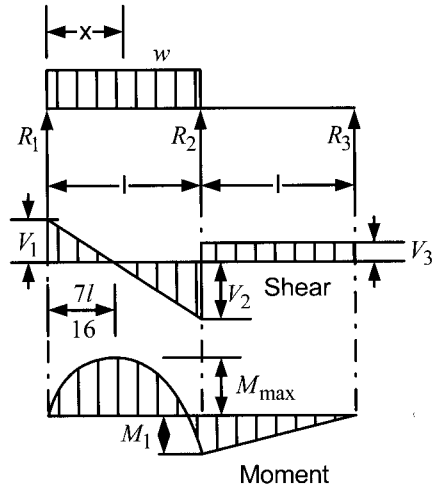

w = load per unit length

$$R_1 = V_1 \ldots\ldots = \frac{7}{16}wl$$

$$R_2 = V_2 + V_3 \ldots\ldots = \frac{5}{8}wl$$

$$R_3 = V_3 \ldots\ldots = -\frac{1}{16}wl$$

$$V_2 \ldots\ldots = \frac{9}{16}wl$$

$$M_{max}\left(\text{at } x = \frac{7}{16}l\right) \ldots\ldots = \frac{49}{512}wl^2$$

$$M_1 \left(\text{at support } R_2\right) \ldots\ldots = \frac{1}{16}wl^2$$

$$M_x \left(\text{when } x < l\right) \ldots\ldots = \frac{wx}{16}(7l - 8x)$$

$$\Delta_{max} \left(\text{at } 0.472l \text{ from } R_1\right) = \frac{0.0092}{EI}wl^4$$

BEAM FIXED AT ONE END - SUPPORTED AT OTHER END - UNIFORM LOAD (SAME AS CONTINUOUS BEAM WITH TWO EQUAL SPANS UNIFORMLY LOADED)

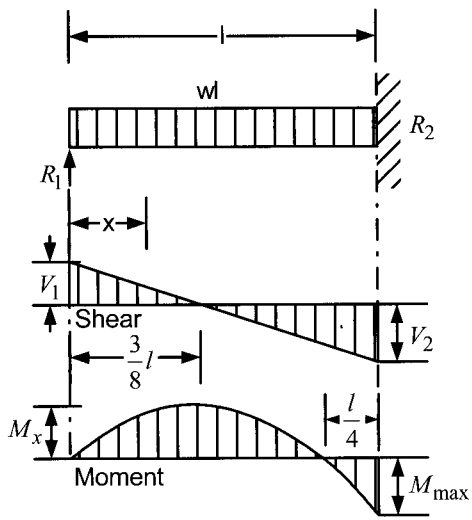

w = load per unit length

$$R_1 = V_1 \ldots\ldots = \frac{3}{8}wl$$

$$R_2 = V_{2\,max} \ldots\ldots = \frac{5}{8}wl$$

$$V_x \ldots\ldots = R_1 - wx$$

$$M_{max} \ldots\ldots = \frac{wl^2}{8}$$

$$M_x \left(\text{at } x = \frac{3}{8}l\right) \ldots\ldots = \frac{9}{128}wl^2$$

$$M_x \ldots\ldots = R_1 x - \frac{wx^2}{2}$$

$$\Delta_{max} \left(\text{at } x = \frac{l}{16}\left(1+\sqrt{33}\right) = 0.422l\right) = \frac{wl^4}{185EI}$$

$$\Delta_x \ldots\ldots = \frac{wx}{48EI}\left(l^3 - 3lx^2 + 2x^3\right)$$

Figure 10.43

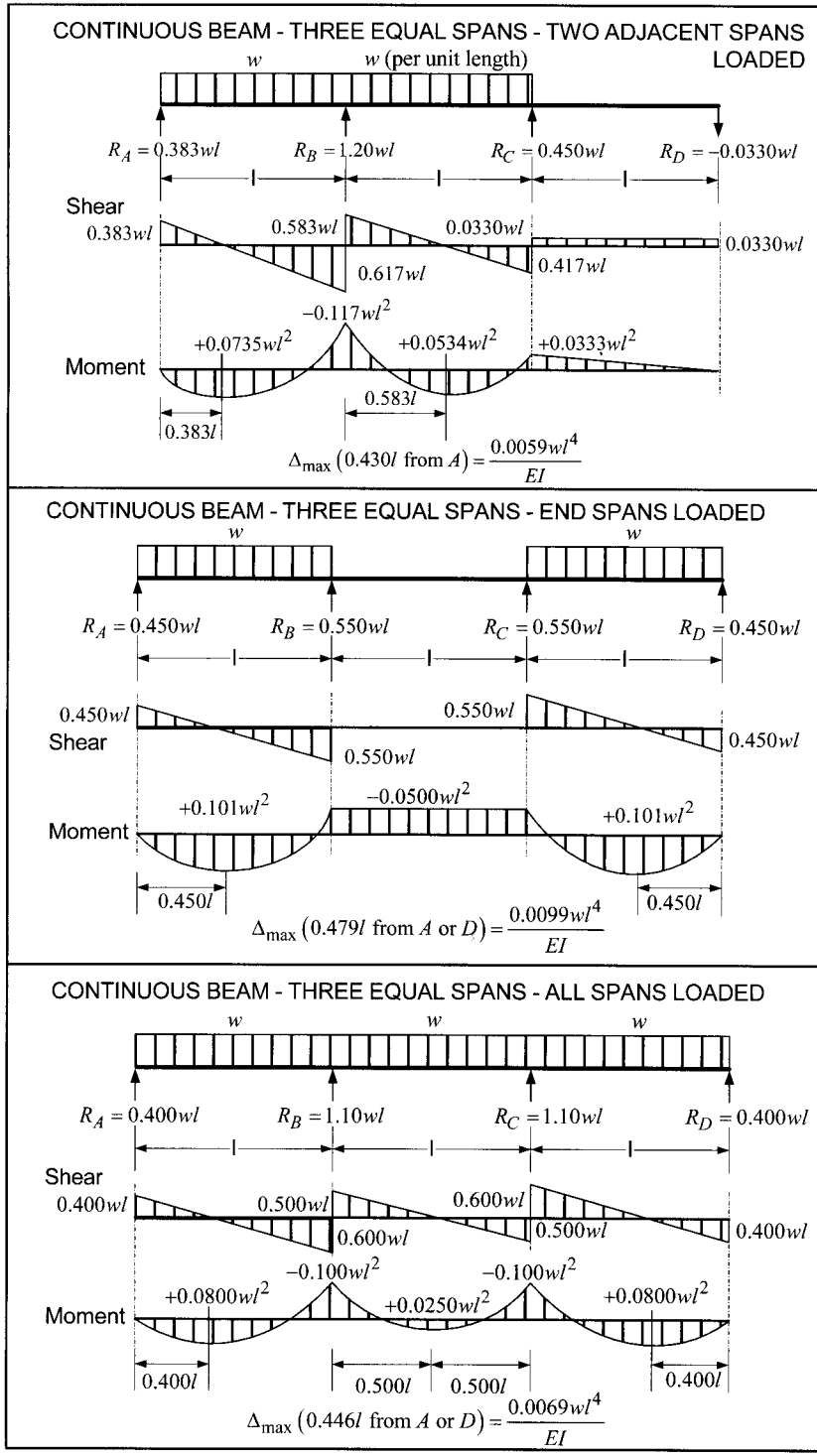
CONTINUOUS BEAM - THREE EQUAL SPANS - TWO ADJACENT SPANS LOADED
w
w (per unit length)
$R_A = 0.383wl$
$R_B = 1.20wl$
$R_C = 0.450wl$
$R_D = -0.0330wl$
Shear
0.383wl
0.583wl
0.0330wl
0.0330wl
0.617wl
0.417wl
$-0.117wl^2$
$+0.0735wl^2$
$+0.0534wl^2$
$+0.0333wl^2$
Moment
0.583l
0.383l
$\Delta_{max}\,(0.430l \text{ from } A) = \frac{0.0059wl^4}{EI}$
CONTINUOUS BEAM - THREE EQUAL SPANS - END SPANS LOADED
w
w
$R_A = 0.450wl$
$R_B = 0.550wl$
$R_C = 0.550wl$
$R_D = 0.450wl$
0.450wl
Shear
0.550wl
0.550wl
0.450wl
$+0.101wl^2$
$-0.0500wl^2$
$+0.101wl^2$
Moment
0.450l
0.450l
$\Delta_{max}\,(0.479l \text{ from } A \text{ or } D) = \frac{0.0099wl^4}{EI}$
CONTINUOUS BEAM - THREE EQUAL SPANS - ALL SPANS LOADED
w
w
w
$R_A = 0.400wl$
$R_B = 1.10wl$
$R_C = 1.10wl$
$R_D = 0.400wl$
Shear
0.400wl
0.500wl
0.600wl
0.400wl
0.600wl
0.500wl
$-0.100wl^2$
$-0.100wl^2$
$+0.0800wl^2$
$+0.0250wl^2$
$+0.0800wl^2$
Moment
0.400l
0.500l
0.500l
0.400l
$\Delta_{max}\,(0.446l \text{ from } A \text{ or } D) = \frac{0.0069wl^4}{EI}$

Figure 10.44

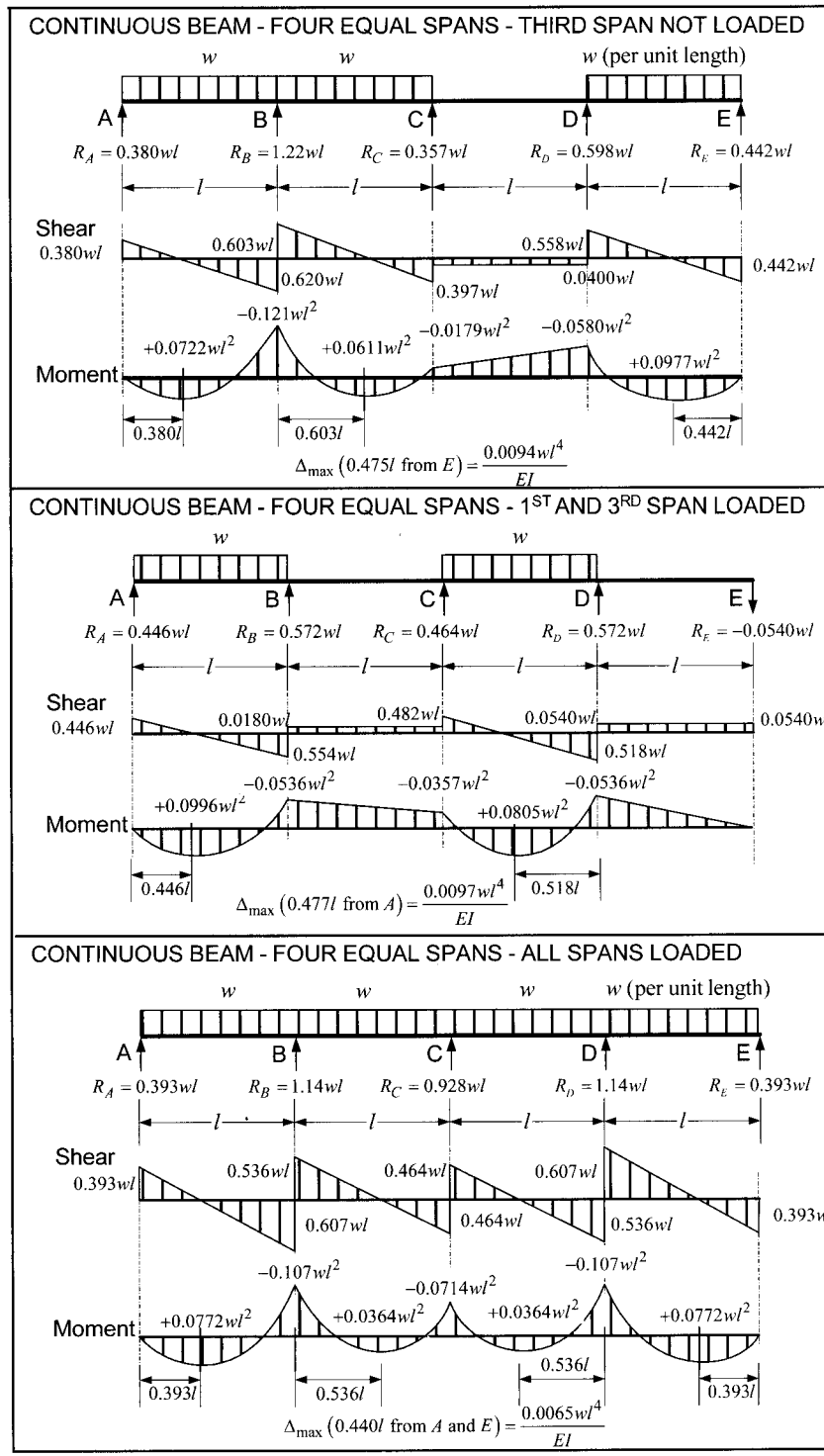
CONTINUOUS BEAM - FOUR EQUAL SPANS - THIRD SPAN NOT LOADED
w
w
w (per unit length)
A
B
C
D
E
$R_A = 0.380wl$
$R_B = 1.22wl$
$R_C = 0.357wl$
$R_D = 0.598wl$
$R_E = 0.442wl$
l
l
l
l
Shear
0.380wl
0.603wl
0.620wl
0.397wl
0.558wl
0.0400wl
0.442wl
Moment
$-0.121wl^2$
$+0.0722wl^2$
$+0.0611wl^2$
$-0.0179wl^2$
$-0.0580wl^2$
$+0.0977wl^2$
0.380l
0.603l
0.442l
$\Delta_{max}\,(0.475l \text{ from } E) = \frac{0.0094wl^4}{EI}$
CONTINUOUS BEAM - FOUR EQUAL SPANS - 1ST AND 3RD SPAN LOADED
w
w
A
B
C
D
E
$R_A = 0.446wl$
$R_B = 0.572wl$
$R_C = 0.464wl$
$R_D = 0.572wl$
$R_E = -0.0540wl$
l
l
l
l
Shear
0.446wl
0.0180wl
0.554wl
0.482wl
0.0540wl
0.518wl
0.0540wl
Moment
$-0.0536wl^2$
$-0.0357wl^2$
$-0.0536wl^2$
$+0.0996wl^2$
$+0.0805wl^2$
0.446l
0.518l
$\Delta_{max}\,(0.477l \text{ from } A) = \frac{0.0097wl^4}{EI}$
CONTINUOUS BEAM - FOUR EQUAL SPANS - ALL SPANS LOADED
w
w
w
w (per unit length)
A
B
C
D
E
$R_A = 0.393wl$
$R_B = 1.14wl$
$R_C = 0.928wl$
$R_D = 1.14wl$
$R_E = 0.393wl$
l
l
l
l
Shear
0.393wl
0.536wl
0.607wl
0.464wl
0.464wl
0.607wl
0.536wl
0.393wl
Moment
$-0.107wl^2$
$-0.0714wl^2$
$-0.107wl^2$
$+0.0772wl^2$
$+0.0364wl^2$
$+0.0364wl^2$
$+0.0772wl^2$
0.393l
0.536l
0.536l
0.393l
$\Delta_{max}\,(0.440l \text{ from } A \text{ and } E) = \frac{0.0065wl^4}{EI}$

Figure 10.45

REFERENCES

10.1 Corley, W. G., "Rotational Capacity of Reinforced Concrete Beams," *Journal of the Structural Division*, ASCE, 92: 121-46, 1966.

10.2 Cohn, M. Z., and Y. Frostig, "Inelastic Behavior of Continuous Prestressed Concrete Beams," *Journal of Structural Engineering*, ASCE, 109(10): 2292-2309, 1983.

10.3 Cohn, M. Z., and P. Riva, "Flexural Ductility of Structural Concrete Sections," *PCI Journal*, 36(2): 72-87, 1991.

10.4 Fauchart, J., "Prestressing of Continuous Beams" (in French), *Annales des Ponts et Chaussées*, 2nd term, 1978, pp. 7-25.

10.5 Guyon, Y., "A Study of Continuous Beams and of Statically Redundant Systems in Prestressed Concrete," *Annales de l'Institut Technique du Batiment et des Travaux Publics*, Vol. 8, September 1945, Translation no. 33 by Cement and Concrete Association, London, 1951.

10.6 Guyon, Y., *Prestressed Concrete*, Vol. 2, *Hyperstatic Structures*. New York: John Wiley & Sons, 1960.

10.7 Khachaturian, N., and G. Gurfinkel, *Prestressed Concrete.* New York: McGraw-Hill Book Co., 1969. In particular Chap. 10. "Analysis and Design of Continuous Prestressed Concrete Beams."

10.8 Leonhardt, F., *Prestressed Concrete Design and Construction*, English translation. Berlin: Wilhelm Ernst and Sohn, 1964, (1st ed., 1955, 2nd ed., 1962 in German).

10.9 Libby, J. R., *Modern Prestressed Concrete: Design Principles and Construction Methods,* 2nd ed., Chapt. 8. New York: Van Nostrand-Reinhold, 1977.

10.10 Lin, T. Y., *Design of Prestressed Concrete Structures*, 2nd ed. New York: John Wiley & Sons, 1963, Chaps. 10 and 11. Also, T. Y. Lin and N. Burns, *Design of Prestressed Concrete Structures*," 3rd ed. New York: John Wiley & Sons, New York, 1981.

10.11 Lin, T. Y., "Load Balancing Method for Design and Analysis of Prestressed Concrete Structures," *ACI Journal*, 60(6): 719-42, 1963.

10.12 Lin, T. Y., and K. Thornton, "Secondary Moment and Moment Redistribution in Continuous Prestressed Concrete Beams," *PCI Journal*, 17(1): 1-20, 1972. See also discussion of above paper by A. H. Mattock and closure by the authors in *PCI Journal*, 17(4): 86-88, 1972.

10.13 Mattock, A. H., "Continuous Prestressed Concrete Beams," *PCI Journal*, 42(3): 50-59, 1991.

10.14 Mirmiran, A., S. Kulkarni, R. Castrodale, R. Miller, and M. Hastak, "Non-Linear Continuity Analysis of Precast, Prestressed Concrete Girders with Cast-in-Place Decks and Diaphragms," *PCI Journal*, 46(5): 60-80, 2001.

10.15 Naaman, A. E., M. H. Harajli, and J. K. Wight, "Analysis of Ductility in Partially Prestressed Concrete Flexural Members," *PCI Journal*, 31(3): 64-87, 1986. See also closure to discussion in *PCI Journal*, 32(1): 142-45, 1987.

10.16 Parme, A. L., and G. H. Paris, "Designing for Continuity in Prestressed Concrete Structures," *ACI Journal*, 47: 54-64, September 1951.

10.17 Thompson, K. J., and R. Park, "Ductility of Prestressed and Partially Prestressed Concrete Sections," *PCI Journal*, 25(2): 46-69, 1980.

PROBLEMS

10.1 Determine the trajectory of the Zero-Load-C line (ZLC-line) for a rectangular beam with two fixed ends, prestressed by a straight tendon of constant eccentricity, parallel to the concrete centroid.

10.2 Several prestressed concrete rectangular beams with different prestressing tendon profiles are shown in Figs. P10.2*a* to P10.2*d*. They are assumed fixed at their left support and roller supported at

their right support. They all have the same cross section $b \times h$, an available maximum practical eccentricity $(e_o)_{mp} = \pm 0.4h$, and a prestressing force F. For each case shown:

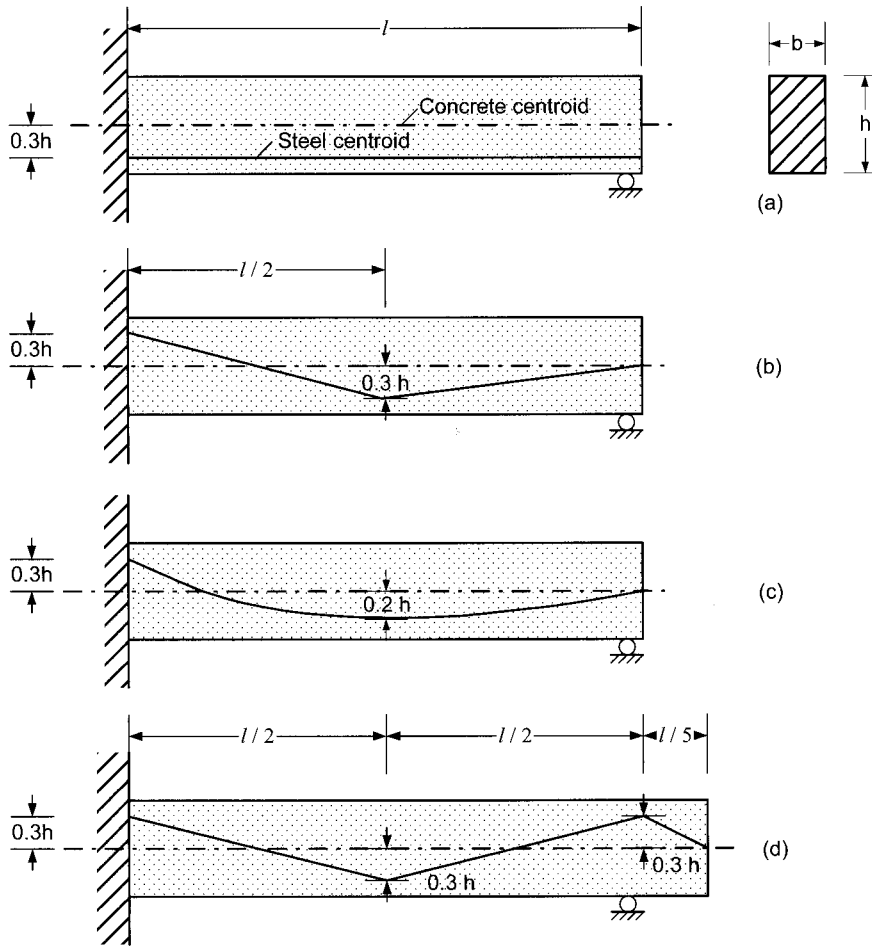

Figure P10.2

(a) Determine the equivalent loading and the corresponding prestressing moment throughout the span;
(b) Plot the primary, secondary, and prestressing moment diagrams;
(c) Determine the ZLC-line; and
(d) Suggest minor adjustments leading to a concordant profile.
Note that in this problem, units are irrelevant and solutions can be obtained in function of l, F, and h. One can assume $l = 1$, $F = 1$, $h = 1$ and proceed. However, if numerical values are preferred, the following values can be used: $l = 50$ ft, $F = 100$ kips, $h = 20$ in, $b = 10$ in.

10.3 Consider the prestressed posttensioned concrete beam with cross section shown in Fig. P10.3*a*. It is to be evaluated in three different design cases: two, three, and four equal continuous spans (Fig. P10.3*b*). The following information is provided:
$I = 41{,}300$ in^4, $A_c = 576$ in^2, $Z_t = 3990$ in^3, $Z_b = 3020$ in^3, $y_t = 10.33$ in, $y_b = 13.67$ in, $k_t = -5.24$ in, $k_b = 6.94$ in, $f'_c = 5000$ psi, $\bar{\sigma}_{ti} = \bar{\sigma}_{ts} = -3\sqrt{f'_c}$, $\bar{\sigma}_{ci} = \bar{\sigma}_{cs} = 0.4f'_c$, $(d_c)_{\min} = 3$ in, $LL = 0.6$ klf,

w_G = 0.6 klf. Assume an average initial stress in the prestressing steel immediately after release of 183 ksi and an average final stress after all losses of 148 ksi. For each case *A*, *B*, and *C*:

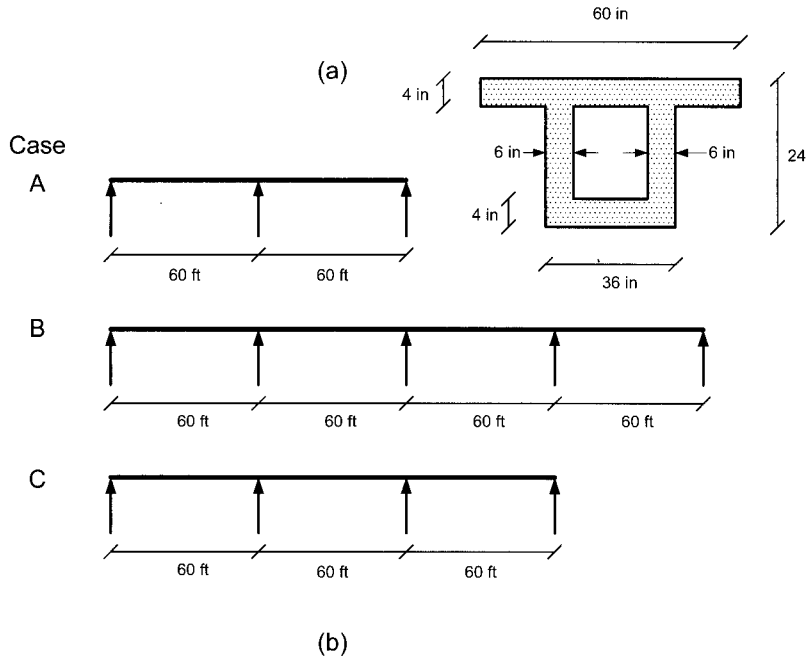

Figure P10.3

(a) Determine the required prestressing force and its profile by elastic analysis (assume a tendon profile made out of parabolas having zero eccentricities at the end supports, and assume, at first, that the inflection points between successive parabolas are at about *L*/6 from the intermediate supports);
(b) Determine the prestressing force by load balancing;
(c) Determine a concordant tendon profile.
Make any assumptions you deem necessary in your design.

10.4 A three-span continuous prestressed slab is 24 in high and spans 60 ft between supports. Assume $\eta = 0.80$ and $k_t = k_b = k'_t = k'_b = 4$ in, that is, no tension is allowed, and compression stresses are acceptable. Let us assume that after a preliminary design we found a concordant tendon profile with a final prestressing force of 192 kips. Eccentricities of the concordant profile at *A*, *B*, *C*, and *D* are shown in Fig. P10.4. In order to correctly place the tendons in the concrete with a sufficient cover at *C*, we linearly transform the tendon profile by lowering the eccentricity at point *C* by three inches. Assume that the problem is then solved and everything else is satisfied.
(a) Show qualitatively the secondary moment diagram along the slab and compute the secondary moments at *B*, *C*, and *D*. Make sure their sign is correct.
(b) What are the values of external moments $M_{\max}$ and $M_{\min}$, which could be applied at sections *B* and *C* without violating any allowable stress?

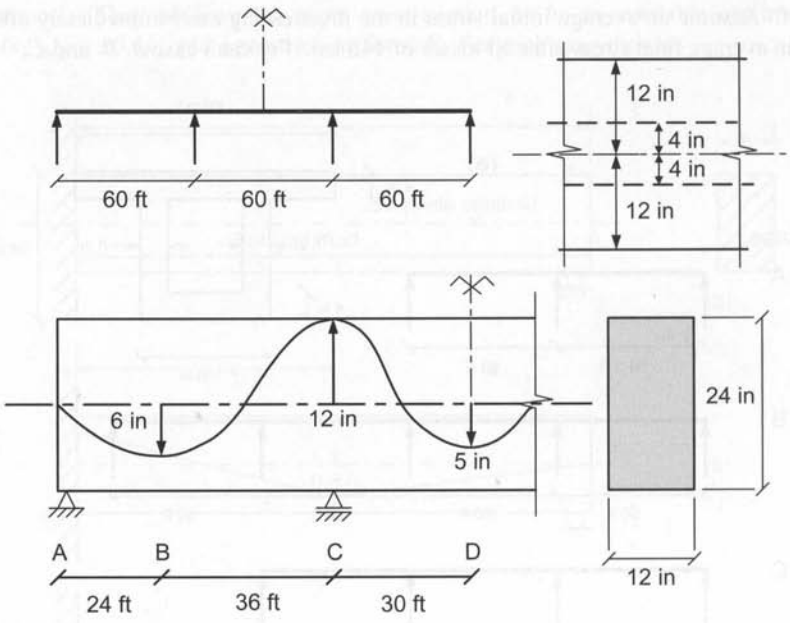

Figure P10.4

10.5 For the continuous beam shown in Fig. P10.5, determine the equivalent load due to prestressing and the prestressing moment at critical sections along the length, and at transition points. Plot to scale the primary moment, secondary moment, and prestressing moment diagrams. Plot the prestressing tendon profile and the ZLC-line. Assume a value of $F = 500$ kips.

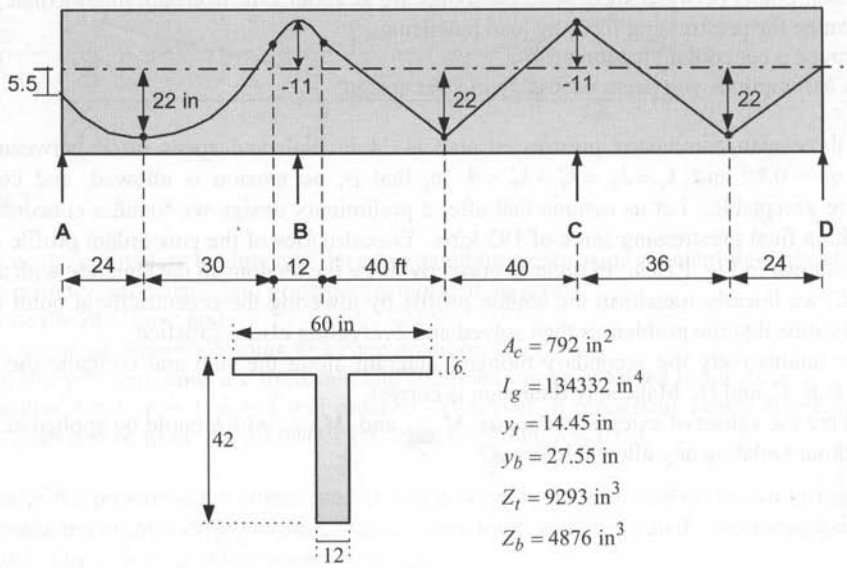

Figure P10.5

10.6 A post-tensioned concrete beam of constant section is continuous over three spans and carries loads as shown in Fig. P10.6. Assume that the self-weight of the beam is negligible. Determine a suitable tendon profile for the beam that will simultaneously satisfy the following two conditions:
(a) The stressing of the tendon should not induce any changes in the reactions at any of the supports;
(b) When the section is fully stressed, the beam should carry the given loads, while the concrete section should not experience a bending moment anywhere. Assume $F = 100$ kips.

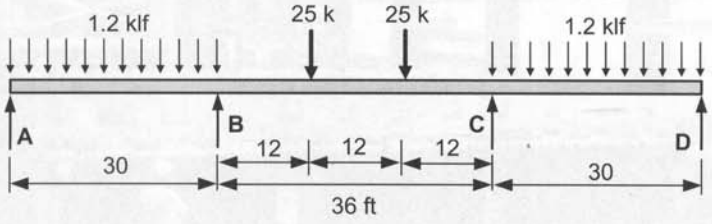

Figure P10.6

A slab band in a two-way slab system with banded unbonded tendons, acting as a continous beam. *(Courtesy Post-Tensioning Institute.)*

Test of 1/3 scale model of a two-ways flat plate pottensioned with unbonded tendons. *(Courtesy Ned Burns, University of Texas at Austin.)*

Parking structure with slab pottensioned with unbonded tendons at the University of Illinois at Chicago.

PRESTRESSED CONCRETE SLABS

11.1 SLAB SYSTEMS

Slabs are structural elements that provide mostly flat, horizontal surfaces used as floors, roofs, and decks. They can be constructed in many different ways, using various structural materials and composite systems. Depending on the selected configuration, they can be made to resist bending either in primarily one direction (one-way action) or in two directions (two-way action). The deformed surface of a slab under load has a single curvature, as in beams, for one-way slabs and a double curvature for two-way slabs.

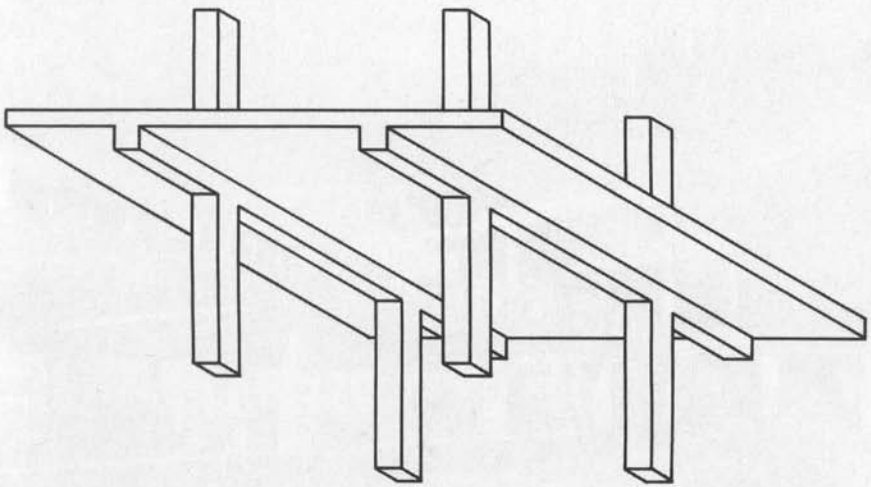

Figure 11.1 Typical one-way slab.

(a) **Composite deck with hollow-cored slabs.**

(b) **Adjacent T Beams.**

Figure 11.2 One-way slab decks using precast prestressed elements. *(Courtesy Material Service Corporation.)*

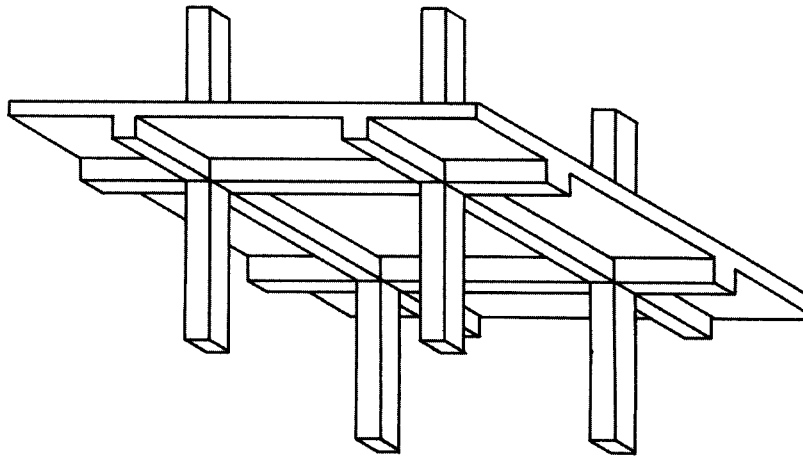

Figure 11.3 Two-way edge supported slab on beams.

One-way slabs are supported (or assumed supported) along two parallel edges (Fig. 11.1). One-way prestressed concrete slabs do not necessarily imply a monolithically cast concrete rectangular plate. They can be made of precast beams (hollow-core slabs, double Ts, etc.) placed adjacent to each other between parallel lines of support, or posttensioned T beams as for joist-type slabs, or of a composite system made out of precast beams and a cast-in-place slab. In these cases, the slab is mostly called a "deck or a "slab deck." Two examples of one-way slab systems using precast prestressed elements are shown in Fig. 11.2. The analysis and design of slab decks are essentially reduced to the analysis and design of beams as covered in the preceding chapters and in Chapter 14. Some particular design aspects of monolithically cast one-way rectangular slabs are covered in Section 11.3.

Two-way prestressed concrete slabs belong mostly to the following categories: edge-supported slabs, flat slabs, and flat plates:

- *Edge-supported slabs* are slabs supported along their four edges on beams or walls, with or without restraint. A typical example is shown in Fig. 11.3 and a design example is covered in Sec. 10.13. In order to induce sufficient two-way action in edge-supported slabs, and for design purposes, the ratio of long-to-short span must be less than about 2. Otherwise, they can essentially be analyzed as one-way slabs.
- *Flat slabs* are slabs supported on columns without beams in between (Fig. 11.4). They are generally strengthened around the columns using a drop panel, or a column capital, or both. A particular variety is the waffle (or grid slab) in which voids are created from the lower surface by cubicle-like reusable forms (Fig. 11.4*b*).
- *Flat plates* are solid slabs having the same thickness everywhere, including around the columns (Fig. 11.4*c*).

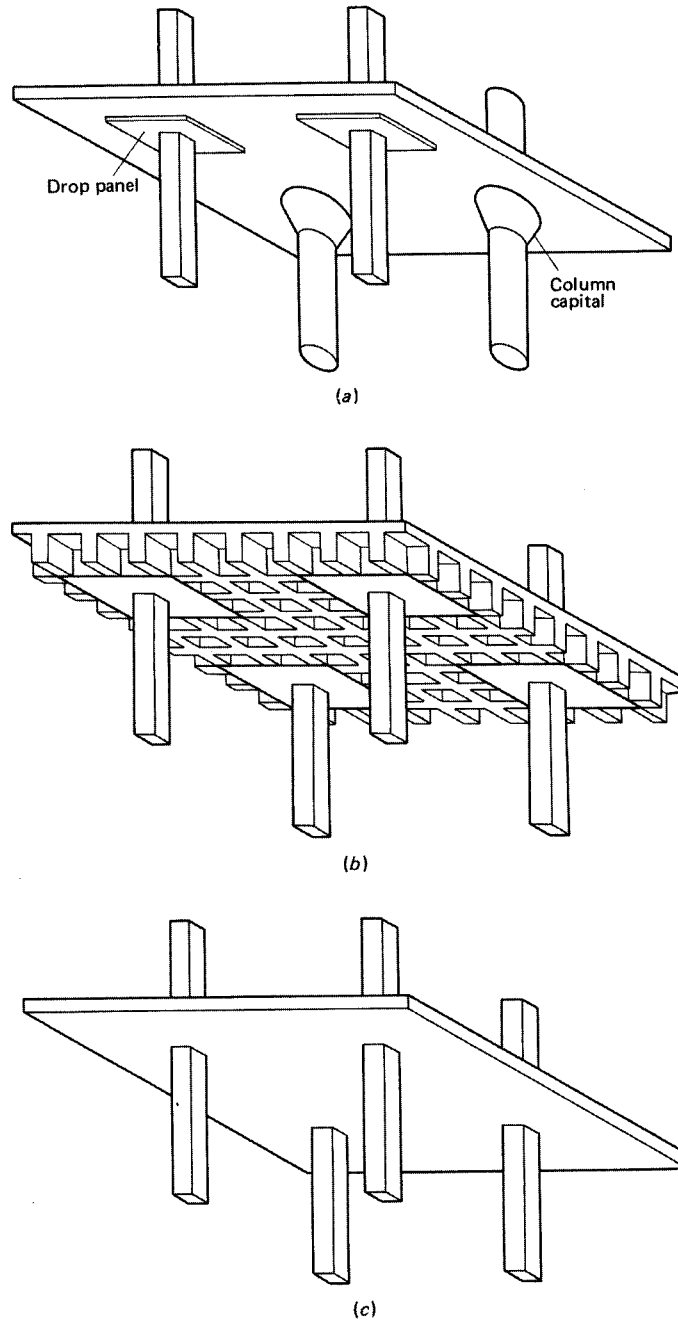

Figure 11.4 Types of two-way slabs. ***(a)*** **Flat slabs.** ***(b)*** **Waffle slabs.** ***(c)*** **Flat plate.**

The flat plate slab construction is the most common form of prestressed concrete slab construction. Flat plates are extensively used in residential and commercial buildings of all types, including hotels, parking structures, and the like. They offer numerous advantages including a minimal slab depth with an unobstructed bottom surface, which can be formed and finished easily [Ref. 11.26] and allows maximum flexibility in architectural lay-out. Because of prestressing, punching shear resistance around columns is improved, often eliminating the need for drop panels or column capitals. Construction time is reduced and substantial cost savings may be achieved. In the United States, most prestressed concrete flat plates are cast in place and posttensioned using unbonded tendons. The tendons are generally placed from one edge to the opposite edge of the slab, spanning several panels. They are stressed from and anchored at the periphery of the slab. The connections with the supporting columns are generally cast monolithically with the slab. However, in the particular case of lift slabs, the flat plate is cast at ground level and then lifted to its final position along pre-erected steel or concrete columns. Connections using steel collars or corbels are then attached between the slabs and the columns.

11.1.1 General Design Approach

Like other structural systems, slabs must satisfy both serviceability and strength limit states. Serviceability limit states include stresses under bending, cracking control, and deflection; strength limit states are mostly related to nominal bending resistance and nominal shear resistance. Allowable stresses for prestressed slabs as per the ACI code are given in Table 3.3 of Chapter 3.

One-way slabs are designed similarly to simple span or continuous beams (Chapters 4 and 10), with the exception that the design of the prestressing force uses preferentially the load balancing method, as described in Section 11.6.1.

There are many analysis and design methods that are applicable to two-way slabs, some simpler than others. Only one approximate method, the equivalent frame method, which is generally applicable to all types of two-way slabs and is recommended by the ACI code, is covered here. A great deal can be learned by referring to related chapters on slabs in other books and textbooks on reinforced and prestressed concrete [Refs. 11.12, 11.21, 11.23, 11.24, 11.30, 11.31, 11.34, 11.38, 11.47, 11.49].

The design of slabs starts generally by assuming a reasonable depth based on the span length, while keeping in perspective shear resistance, fire resistance, corrosion protection and deflection control. Punching shear resistance around columns is often the most critical for long spans, while corrosion and fire resistance may control for very short spans. Typically, for slabs with light loads, such as for apartments and office buildings, the following span-to-depth ratios can be used in preliminary design:

- l/h from 25 to 35, for simple span one-way and two-way slabs
- l/h from 30 to 45, for continuous one-way slabs

- l/h from 35 to 50, for continuous two-way slabs

The higher range of span-to-depth ratios applies to slabs with drop panels and slabs with two-way beams. Values obtained are rounded off to the next quarter or half inch (5 or 10 mm). Minimum depths satisfying fire rating requirements must also be satisfied (see Section 11.9.1).

After brief coverage of the design of one-way slabs, this chapter mostly focuses on the design of prestressed concrete two-way flat plates. Related requirements of the 2002 edition of the ACI code and salient recommendations found in two reports by ACI-ASCE Committee 423 [Refs. 11.2 to 11.5] are incorporated in the following sections. An extensive list of references is given in the section references.

11.2 UNBONDED TENDONS IN ONE- AND TWO-WAY SLAB SYSTEMS

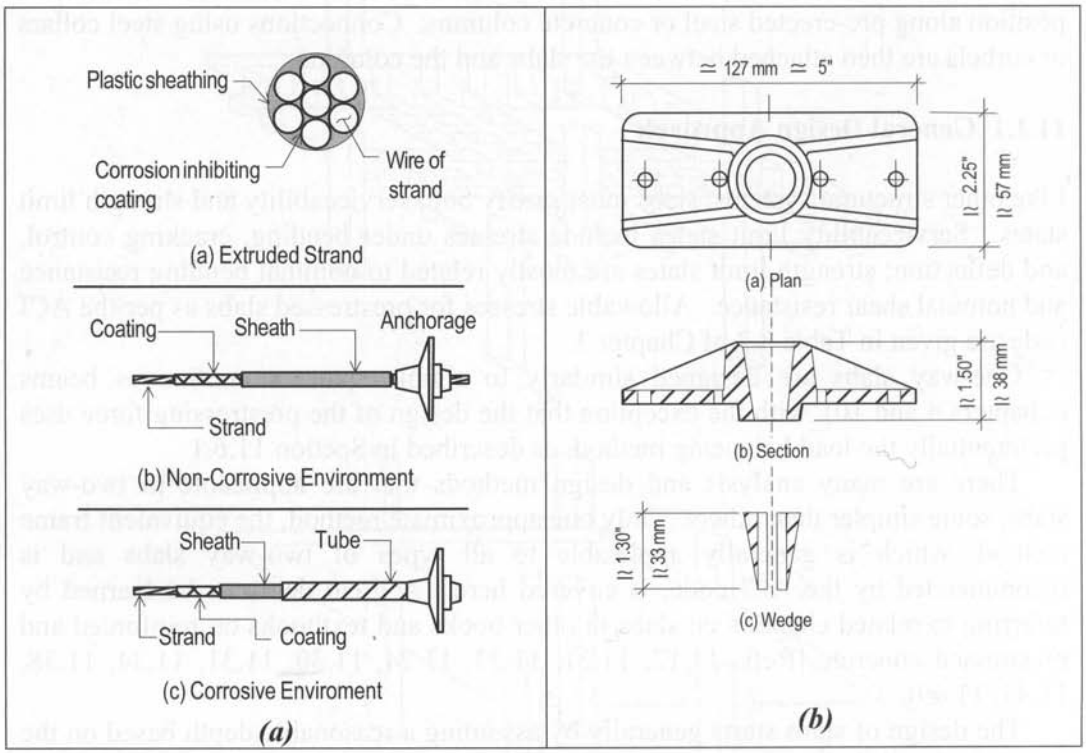

Figure 11.5 ***(a)*** **Unbonded monostrand posttensioning system.** ***(b)*** **Monostrand anchorage device** *(adapted from Refs. 11.1 and 11.38).*

Generally one- or two-way cast-in-place prestressed slab systems use unbonded tendons, typically in the form of strands, prestressed and anchored one strand at a time (Figs. 11.5*a* and 11.5*b*). The strands are sheathed (plastic sheathing) and/or

covered with grease to achieve sufficient corrosion protection and break the bond between steel and concrete. An effective system has been to extrude the plastic sheath over a grease covered strand; thickness of the plastic sheath and quality of the grease or other coating material are important variables to consider. Also, particular attention should be given to protect the anchors of unbonded tendons; this is generally done by filling the anchorage pocket with a high quality non-shrinking cementitious grout. The reader is referred to the PTI Posttensioning Manual [Ref. 11.38] for additional details about tendon protection as well as field procedures to be followed for best results.

11.2.1 Stress at Ultimate in Unbonded Tendons

Everything else being equal, the behavior of concrete beams prestressed with unbonded tendons is very similar to that of beams prestressed with bonded tendons until cracking occurs. After cracking, and up to ultimate, they differ significantly. This is particularly true for their nominal bending resistance, where the stress, f_{ps}, in the unbonded tendons is much smaller than that in the bonded tendons, leading to a significantly smaller moment. The reader is referred to Chapter 5 for additional details.

The equations recommended here to estimate the stress at ultimate (i.e., at nominal bending resistance) in unbonded tendons follows a detailed study published in Refs. [11.25] to [11.27]. It is different from that recommended in the 2002 version of the ACI code (see Chapter 5, Section 5.11). However, the author believes that it is more appropriate and more general. Note that the use of either equation will not affect the design procedure.

For members prestressed with unbonded tendons, in lieu of a deflection compatibility analysis, one of the following approaches can be used.

1. *Conservative approximate prediction equation*

The stress f_{ps} in the prestressed reinforcement at nominal bending resistance can be estimated from:

$$f_{ps} = f_{pe} + \frac{E_p}{1866}\frac{L_1}{L_2} \geq f_{pe} + \frac{E_p}{3732} \qquad (11.1)$$

where:

fpe = effective prestress in the prestressed reinforcement
Ep = elastic modulus of prestressed reinforcement
$L1$ = sum of lengths of spans loaded with live load and containing tendon(s) considered
$L2$ = total length of tendon(s) between anchorages

Equation (11.1) is valid in all systems of units and applies to prestressing steel tendons as well as to fiber reinforced polymeric tendons. When not obtained from tests or supplied by the manufacturer, the elastic modulus of prestressing steel may be taken as 28,000 ksi or 196,000 MPa. Applied to prestressing steel and US units, Eq. (11.1) can be written as:

$$f_{ps} = f_{pe} + 15\frac{L_1}{L_2} \geq f_{pe} + 7.5 \text{ ksi} \tag{11.2}$$

It leads to an increment of stress beyond effective prestress equal to a maximum of 15 ksi (105 MPa) and a minimum of 7.5 ksi (52.5 MPa). The value of 15 ksi (105 MPa) would be typically used in single span beams and slabs, while a value of 7.5 ksi (52.5 MPa) would be used in slabs with multiple spans.

Equation (11.2) is considered to lead to a safe and satisfactory prediction of the stress at ultimate in unbonded tendons.

2. *Accurate prediction equation*

$$f_{ps} = f_{pe} + \Omega_u E_p \varepsilon_{cu}\left(\frac{d_p}{c} - 1\right)\frac{L_1}{L_2} \leq 0.80 f_{pu} \tag{11.3}$$

where:

ε_{cu} = failure strain of concrete in compression, assumed = 0.003
d_p = distance from extreme compression fiber to centroid of prestressed reinforcement
c = depth of neutral axis at nominal bending resistance
Ω_u = 3 / (L/dp) for uniform or third point loading
Ω_u = 1.5 / (L/dp) for one point midspan loading
L = length of span for which computation is carried out; at intermediate supports of continuous members, L can be taken as the average of the two spans on either side of the support
f_{pu} = specified tensile strength of prestressed tendons

and other notation is as per Eq. (11.1). Equations (11.1) and (11.3) hold for all systems of units.

Equation (11.3) is based on a deflection compatibility analysis along the member reduced to an equivalent strain compatibility at the level of the section [Refs. 11.26, 11.27]. It was derived assuming the tendons are in the linear range of behavior. The limitation of $0.80f_{pu}$ corresponds to 94 percent of yield for stress relieved steel strand and 89 percent of yield for low relaxation strands. It is also a safe limit for fiber reinforced polymeric tendons.

The value of depth of neutral axis, c, accounts for the presence of nonprestressed reinforcement and satisfies equilibrium at ultimate. The equation of force equilibrium in the section and the prediction equation of f_{ps} must be solved simultaneously for c and f_{ps} (see Chapter 5).

11.3 DESIGN OF ONE-WAY SLABS

Typical examples of a simple span and a continuous one-way slab are shown in Figs. 11.6*a* and 11.6*b*, respectively. The reader may want to review the design procedures described in Chapters 4, 5, 6, 7, and 10 as background information to the design of one-way slabs.

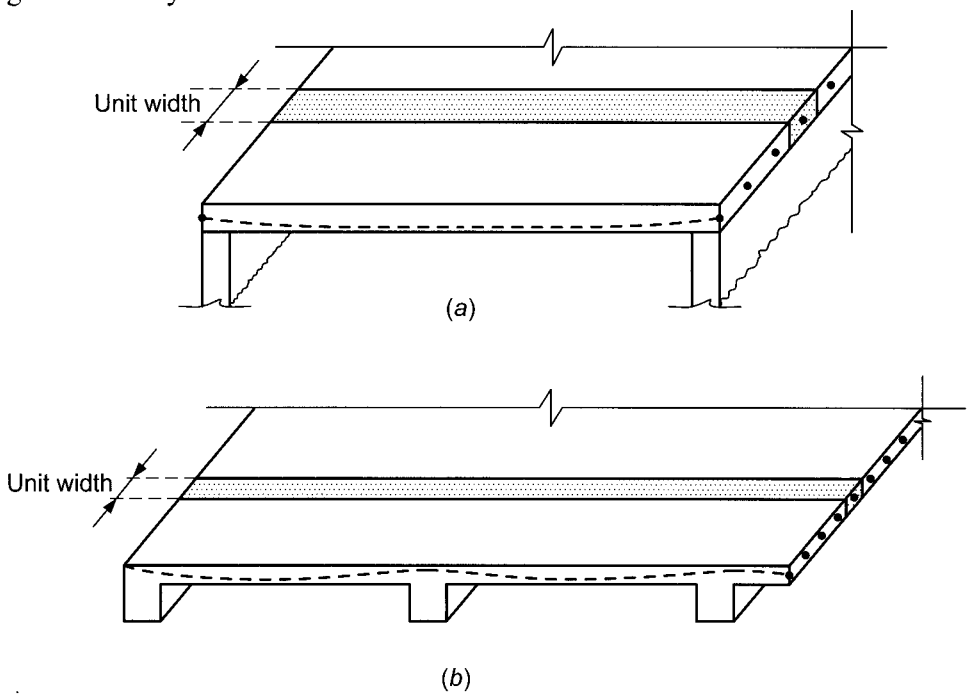

Figure 11.6 One-way slabs. ***(a)*** **Simple span supported on walls.** ***(b)*** **Continuous spans supported on beams.**

While one-way prestressed slabs can be designed as uncracked under full service loads, the 2002 ACI code [Ref. 11.2] allows one-way slabs to be designed as Class T (transition) or Class C (cracked). For Class T, fictitious tensile stresses under flexural loads, ranging in magnitude from $7.5\sqrt{f'_c}$ to $12\sqrt{f'_c}$ are allowed, and stresses are permitted to be calculated on the basis of the uncracked section. For Class C

fictitious tensile stresses exceeding $12\sqrt{f'_c}$ in magnitude are allowed, but actual stresses must be calculated using the cracked transformed section.

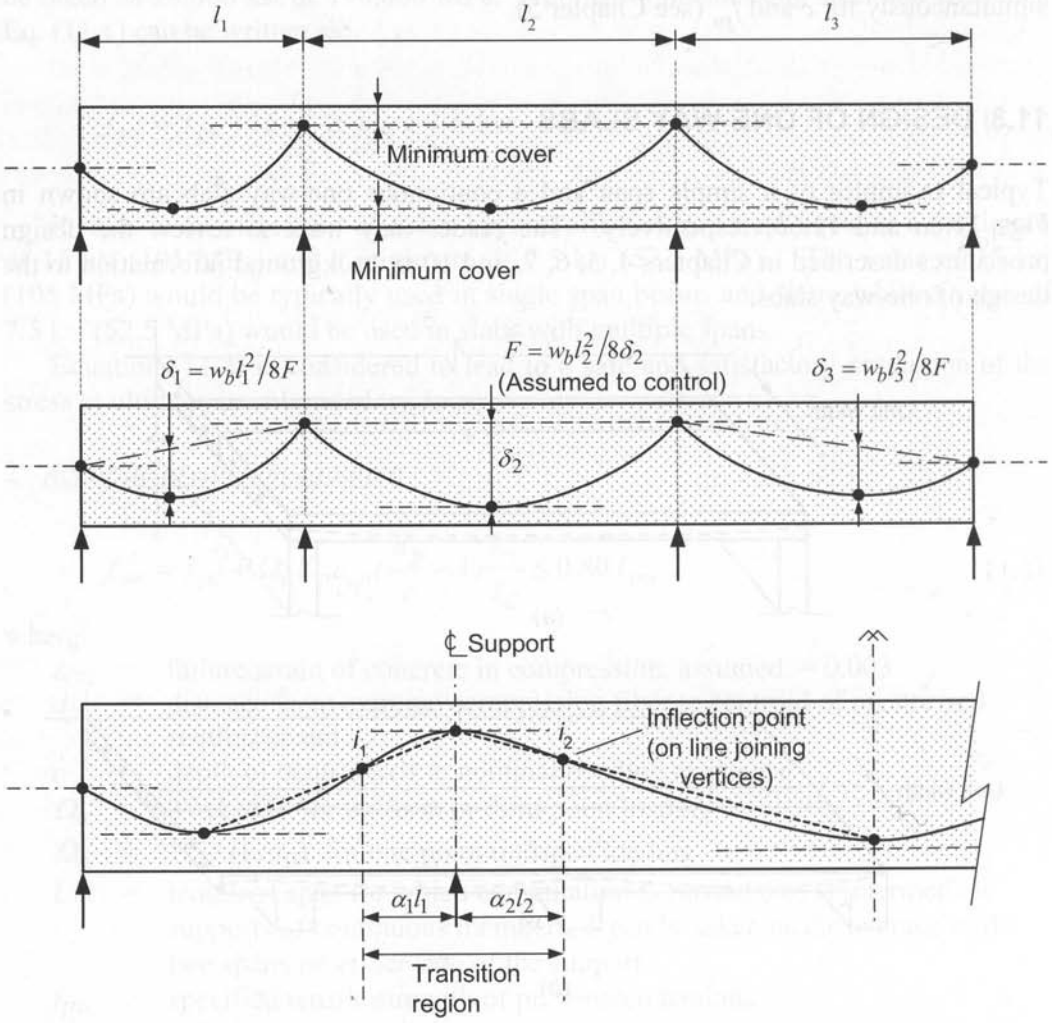

Figure 11.7 Design evolution of tendon profile. ***(a)*** **Assumed initial profile.** ***(b)*** **Profile for balanced load.** ***(c)*** **Final profile smoothed over supports.**

11.3.1 Design Procedure

The design of slabs starts generally by assuming a slab depth using the span as a guide. For common applications where a relatively light live load is used, the span-to-depth ratio ranges from 25 to 35 for single spans and from 30 to 45 for continuous spans. Values obtained are rounded off to the next quarter- or half-inch (roughly 5

or 10 mm). Other minimum requirements related to fire endurance, as described in Sec. 11.9.1, should also be considered in selecting an appropriate depth.

Once the depth is obtained, the designer proceeds by considering a unit wide strip of slab (Fig. 11.6) as a beam and determining the prestressing force based on allowable stresses according to the procedures described in Chapter 4 for simple spans and Chapter 10 for continuous spans. To determine the prestressing force, the load-balancing approach is generally preferred for continuous slabs. The balanced load is most often taken equal to the dead load and a preliminary tendon profile is selected made out of parabolic segments with zero eccentricities at the end supports and maximum practical eccentricities at intermediate supports and other critical sections (Fig. 11.7*a*). The required prestressing force per unit width of slab is then determined and the tendon profile adjusted accordingly (Fig. 11.7*b*). The prestressing force is then translated into a particular tendon (or strand) at a given spacing. For the final design, the tendon profile is smoothed over the intermediate supports (Fig. 11.7*c*). The distance over which the smoothing transition is made is taken equal to about $0.1l$ on each side of the support. In practice, the effect of smoothing the tendon on the possible generation of secondary moments is often neglected for slabs. Following the above steps, should a stress be found to be too excessive, the balanced load is increased and the procedure is repeated.

11.3.2 Minimum Bonded Reinforcement

When the main flexural reinforcement in one-way slabs consists of unbonded tendons, the 2002 ACI code (Sec. 18.9) recommends the addition of a minimum amount of ordinary bonded reinforcement. The purpose of such reinforcement is to provide an alternative load-carrying system in the event of a catastrophic failure or abnormal loading (such as due to fire) in one span of a continuous slab that leads to distress in the other spans. The minimum area of bonded reinforcement shall be computed from:

$$A_s = 0.004A \tag{11.4}$$

where A is the area of that part of the cross section between the flexural tension face and the center of gravity of the gross section. The above reinforcement shall be distributed over the precompressed tensile zone as close as possible to the extreme tensile fiber. Its length shall be at least one-third of the clear span spacing in positive moment regions and one-sixth of the clear span on each side of the support in negative moment regions (Fig. 11.8).

The above minimum reinforcement may be considered to contribute to the ultimate resistance of the member. Moreover, ACI-ASCE Committee 423 [Refs. 11.3, 11.5] recommends that, since a minimum bonded ordinary reinforcement is provided, a fictitious allowable tensile stress of $-9\sqrt{f'_c}$ to $-12\sqrt{f'_c}$ may be used in

design, thus leading to a smaller amount of prestressing steel. However, the use of a lower magnitude of allowable stress may be preferable when durability is a controlling criterion, such as for parking structures in severe climates. The above provisions suggest that slabs using unbonded tendons are essentially treated as partially prestressed members.

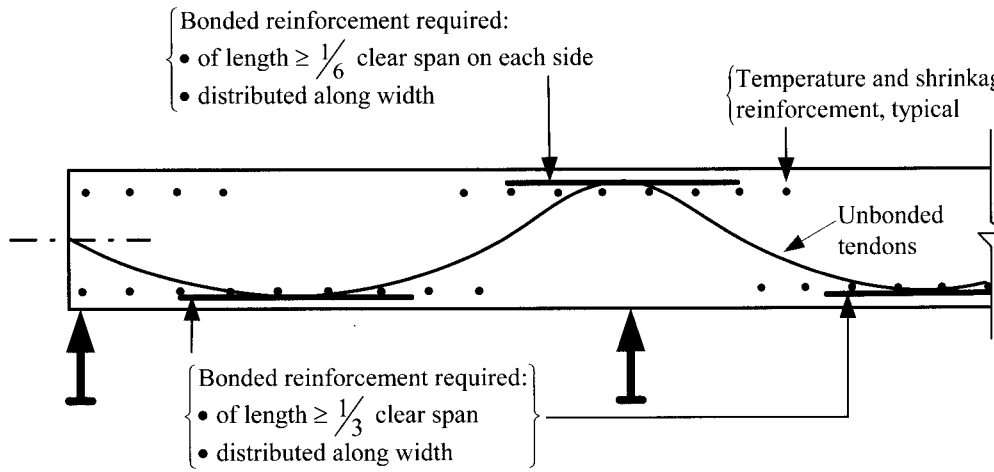

Figure 11.8 Typical requirements for bonded reinforcement in one-way slabs prestressed with unbonded tendons.

Note that in one-way continuous slab systems made with T beams, Eq. (11.4) would lead to higher amounts of bonded reinforcement in the negative moment regions, due to the large flange width; however, it is the author's opinion that in such a case, the area A could be interpreted as the area obtained as half the flange depth (that is, half the slab depth) times the flange width or beam spacing, center to center.

11.3.3 Temperature and Shrinkage Reinforcement

According to the ACI code Sec. 7.12, a minimum amount of ordinary reinforcement normal to the main flexural reinforcement shall be provided for shrinkage and temperature stresses in one-way slabs.

When deformed reinforcing bars are used, the following minimum ratio of reinforcement area to gross concrete area, but not less than 0.0014, is specified:

- Slabs where grade 40 or 50 deformed bars are used 0.0020
- Slabs where grade 60 deformed bars or welded wire fabric (smooth or deformed) are used 0.0018

- Slabs where reinforcement with yield strength exceeding 60 ksi measured at a yield strain of 0.35 percent is used $\dfrac{0.0018 \times 60}{f_y}$

  For f_y given in megapascals, this last expression becomes $0.0018 \times 414 / f_y$.

The above reinforcement shall not be spaced farther apart than five times the slab thickness or 18 in (46 cm).

When prestressing tendons are used for shrinkage and temperature reinforcement:

- The required minimum average compressive stress on the gross concrete area provided by prestressing is 100 psi (0.7 MPa); the average compression is computed using the effective prestressing force after all losses, that is, $\sigma_g = F/A_c$.
- The spacing of tendons shall not exceed 6 ft (1.8 m).

11.3.4 Additional Design Notes

Once the main reinforcement has been determined in one-way slabs, the design proceeds by checking shear, deflection, and other requirements exactly as for beams. The ACI requirement that the design nominal moment, M_n, be at least 1.2 times the cracking moment should theoretically apply to one-way slabs. However, based on tests, where the behavior of slabs beyond cracking and up to failure was investigated, ACI-ASCE Committee 423 recommends that the above requirement be waived for one-way and two-way slabs prestressed with unbonded tendons [Ref. 11.3]. This is because the load-deflection response of such slabs did not show any abrupt change at the onset of cracking and the minimum amount of reinforcement in slabs prestressed with unbonded tendons (because of Eq. 11.4) exceeds the minimum reinforcement of ordinary reinforced concrete slabs anyway.

At some point, the UBC Code [Ref. 11.45] (Section 1918.9.2.2) stated that "*one-way unbonded slabs and beams shall be designed to carry their dead load and 25 percent of the live load by other than the unbonded posttensioned reinforcement... All reinforcement other than the primary unbonded reinforcement provided to meet other requirements may be used in the design.*" Although this provision is not enforced any more, it gives an indication of safety concern about the need for adding bonded reinforcing bars in sufficient quantity.

In order to avoid excessive shortening of the slab and reduce its effects on attached columns and walls, it is recommended to limit the length of slabs between construction joints to less than 150 ft (46 m). For longer lengths, the effect of slab shortening in columns and walls should be reviewed and carefully evaluated [Refs. 11.3, 11.5].

11.3.5 Deflection

The deflection of one-way slabs is computed in a manner similar to that of beams (Chapter 7). Examples of deflection values for equal span continuous beams are given in Chapter 10. Deflection is seldom a limiting criterion in prestressed slabs because of load balancing. For the deflection limit state, the ACI code criteria described in Chapter 7 can be followed when needed.

11.4 EXAMPLE: DESIGN OF A FIVE-SPAN CONTINUOUS ONE-WAY SLAB PRESTRESSED WITH UNBONDED TENDONS

A typical bay slab of a parking structure with several bays consists of a 60-ft-wide one-way slab system with five consecutive spans, 25 ft center-to-center. The slab is supported on columns through 2-ft-wide beams placed along column lines (Fig. 11.9*a*). Provide a preliminary design for the slab, assuming unbonded tendons are specified and given the following information: normal weight concrete, $\gamma_c = 150$ pcf, $f'_c = 5000$ psi, $f'_{ci} = 3500$ psi, $E_c = 4.287 \times 10^6$ psi, minimum concrete cover to the centroid of the prestressed reinforcement = 1.25 in, the tendons are strands with $f_{pu} = 270$ ksi, and assumed $f_{pe} \simeq 160$ ksi. A uniform live load of 100 psf is prescribed.

Let us select a slab depth $h = 8$ in, which corresponds to a span-to-depth ratio $l/h = 37.5$ (well within the range recommended in Sec. 11.1.1) and let us provide a design for a 1-ft-wide strip of slab, assuming it acts as a one-way continuous beam. The corresponding dead weight of the strip per linear foot is $w_G = 8 \times 12 \times 150/144 = 100$ plf.

1. Prestressing Reinforcement

Load balancing will be used to determine the prestressing steel. A theoretical tendon profile made out of parabolas with maximum practical eccentricities (or minimum cover) at support sections and at midspan or near midspan sections is selected. The vertex of each parabola falls at midspan for a typical interior span, and at $0.414l$ (near midspan) from the exterior span. The corresponding sags are shown in Fig. 11.9*b*; although the sag at the midspan of the parabola (about 4 in) could be used for the exterior span, the sag at the vertex is easier to compute and is selected here. The prestressing force to balance a uniform load $w_b = w_G = 0.1$ klf is given by:

For the exterior span:

$$F_1 = \frac{w_b l_1^2}{8\delta_1} = \frac{0.1 \times \overline{25}^2}{8 \times 3.89/12} = 24.1 \text{ kips}$$

For a typical interior span:

$$F_2 = \frac{w_b l_2^2}{8\delta_2} = \frac{0.1 \times \overline{25}^2}{8 \times 5.5/12} = 17.05 \text{ kips}$$

One of two different alternatives can be followed, namely, either (1) keep the same steel profile with different prestressing forces at interior and exterior spans, or (2) select the highest value of the prestressing force, F_1, throughout the slab and adjust the tendon sag in the interior spans to achieve the same balanced load as the exterior spans. For the second alternative, the sag at an interior span would be given by:

$$\delta_2 = \frac{w_b l_2^2}{8F_1} = \frac{0.1 \times 25^2}{8 \times 24.1} \times 12 = 3.89 \text{ in}$$

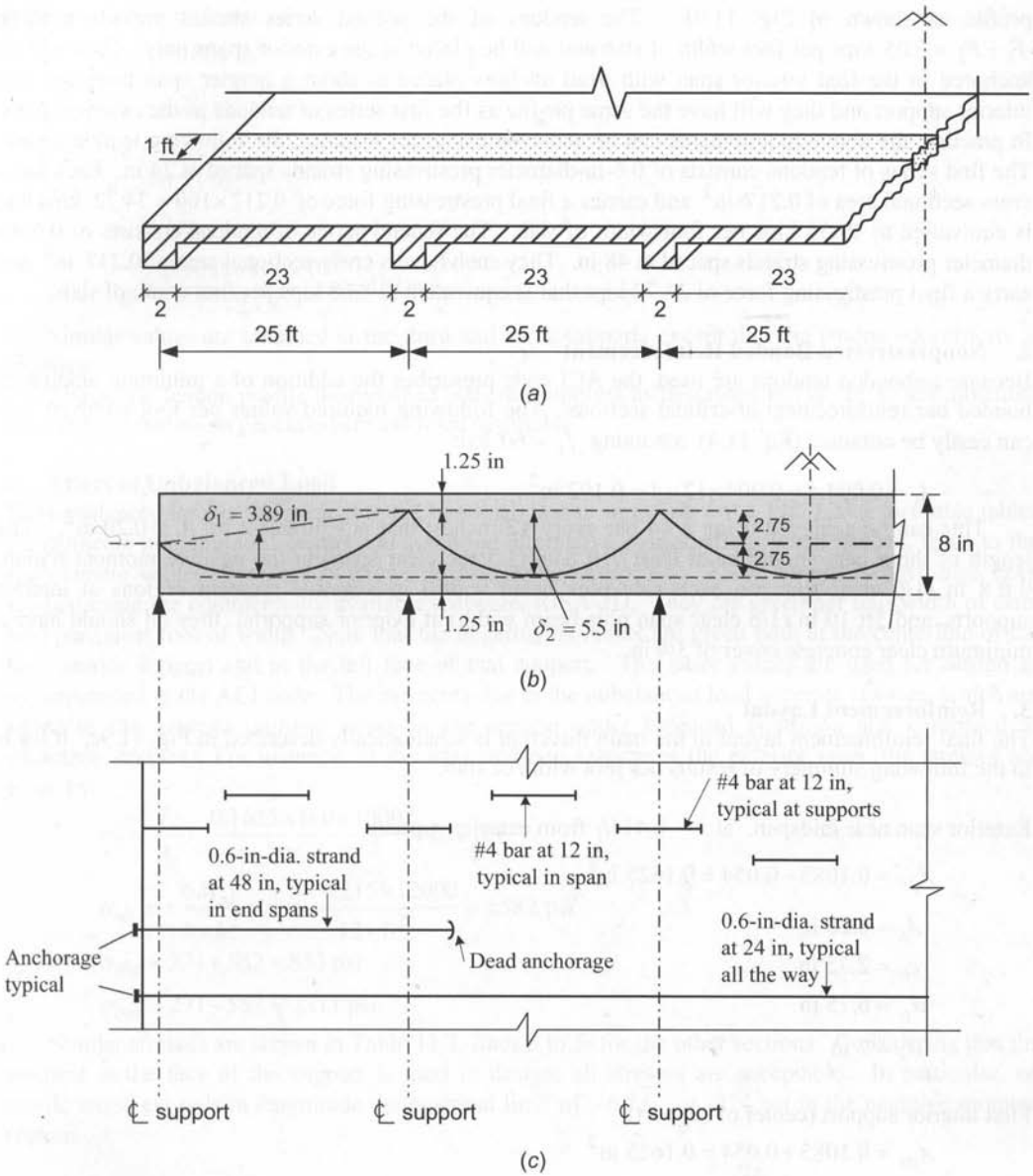

Figure 11.9 Five-span continuous one-way slab of example problem. *(a)* Geometry. *(b)* Theoretical tendon profile. *(c)* Reinforcement detailing in the primary direction.

This means that the tendon eccentricity at midspan is reduced from 2.75 in to 1.14 in. Hence, the corresponding value of d_p is reduced by about 24 percent and the nominal moment resistance of the cracked section at ultimate is at least equally reduced. Therefore, it is decided to follow the first alternative, which leads to a lesser overall amount of steel and probably some cost savings. Thus, two series of tendons are proposed. The tendons of the first series should provide a force $F_2 = 17.05$ kips per foot width of slab and should run continuously throughout the length of the slab with a theoretical

profile as shown in Fig. 11.9*b*. The tendons of the second series should provide a force $F_1 - F_2 = 7.05$ kips per foot width of slab and will be placed in the exterior spans only. They will be anchored in the first interior span with dead anchors placed at about a quarter span from the first interior support and they will have the same profile as the first series of tendons in the exterior spans. In practice, the above requirements can be achieved using, for instance, the following tendon layout. The first series of tendons consists of 0.6-in-diameter prestressing strands spaced at 24 in. Each has a cross sectional area of 0.217 in^2 and carries a final prestressing force of $0.217 \times 160 = 34.72$ kips that is equivalent to 17.36 kips per foot width of slab. The second series of tendons consists of 0.6-in-diameter prestressing strands spaced at 48 in. They each have a cross-sectional area of 0.217 in^2 and carry a final prestressing force of 34.72 kips that is equivalent to 8.68 kips per foot width of slab.

2. Nonprestressed Bonded Reinforcement

Because unbonded tendons are used, the ACI code prescribes the addition of a minimum amount of bonded bar reinforcement at critical sections. The following required values per foot width of slab can easily be obtained (Eq. 11.4), assuming $f_y = 60$ ksi:

$$A_s = 0.004A = 0.004 \times 12 \times 4 = 0.192 \text{ in}^2$$

This can be achieved using a #4 bar every 12 inches; that is equivalent to $A_s = 0.20$ in^2. The length of these bars should be at least 7 ft 8 in (1/3 the clear span) in the positive moment region, 9 ft 8 in (1/6 clear span on each side plus beam width) in negative moment regions at interior supports, and 5ft 10 in (1/6 clear span plus beam width) at exterior supports; they all should have a minimum clear concrete cover of 3/4 in.

3. Reinforcement Layout

The final reinforcement layout in the main direction is schematically described in Fig. 11.9*c*. It leads to the following summary of results per foot width of slab:

Exterior span near midspan: at $x = 0.414l_1$ from exterior support.

$$A_{ps} = 0.1085 + 0.054 = 0.1625 \text{ in}^2$$
$$A_s = 0.20 \text{ in}^2$$
$$e_o = 2.75 \text{ in}$$
$$d_p = 6.75 \text{ in}$$
$$d_s = 7 \text{ in}$$

First interior support (center of support):

$$A_{ps} = 0.1085 + 0.054 = 0.1625 \text{ in}^2$$
$$A_s = 0.20 \text{ in}^2$$
$$e_o = -2.75 \text{ in}$$
$$d_p = 6.75 \text{ in}$$
$$d_s = 7 \text{ in}$$

These are similar to the values in the first span, except that the tendon eccentricity is negative. Note that the average prestress for the exterior span and at the first interior support is given by:

$$\sigma_g = \frac{F}{A_c} = \frac{0.1625 \times 160 \times 10^3}{12 \times 8} \approx 271 \text{ psi}$$

Interior span: at midspan

$$A_{ps} = 0.1085 \text{ in}^2$$

$$A_s = 0.20 \text{ in}^2$$

$$e_o = 2.75 \text{ in}$$

$$d_p = 6.75 \text{ in}$$

$$d_s = 7 \text{ in}$$

$$\sigma_g = \frac{0.1085 \times 160 \times 10^3}{12 \times 8} \simeq 181 \text{ psi}$$

Similar values are obtained at the third and forth supports except that the tendon eccentricity is negative.

The actual tendon profile is smoothed over the supports as described in Fig. 11.8*c* and potential secondary moments so generated are assumed negligible.

4. Effect of Unbalanced Load

The unbalanced load is taken equal to the live load, that is $w_{nb} = w_L = 0.1$ klf. Using available tables for moments in continuous beams and assuming alternative span loadings when needed, leads to the approximate values of moments shown in line 2 of Table 11.1. These moments have also been verified using the commercially available software, RISA 2D. They are given per unit width of slab, here per linear foot of width. Note that the negative moments are given both at the centerline of the first interior support and at the left face of that support. The latter values are used for design as recommended in the ACI code. The moments due to the unbalanced load generate stresses, which are added to the average uniform stress in the section under balanced condition and compared to allowable stresses. For instance, at the near midspan section of the exterior span, the stresses are given by:

$$\sigma_b = \frac{F}{A_c} = \frac{0.1625 \times 160 \times 1000}{12 \times 8} = 271 \text{ psi}$$

$$\sigma_{nb} = \pm \frac{6M_{nb}}{b \times h^2} = \pm \frac{6 \times 6.215 \times 12000}{12 \times 8^2} = \pm 582 \text{ psi}$$

$$\sigma_{top} = 271 + 582 = 853 \text{ psi}$$

$$\sigma_{bot} = 271 - 582 = -311 \text{ psi}$$

Similar stresses are shown in Table 11.1, lines 3 to 5, for the other sections. Considering that the moment at the face of the support is used in design, all stresses are acceptable. In particular, no tensile stress exceeds in magnitude the practical limit of $-6\sqrt{f'_c}$ or -424 psi in the negative moment regions.

5. Nominal Bending Resistance

The strength design moments or factored moments required by the ACI code are given in Table 11.1, line 6; the nominal moment resistance of the critical sections is given in line 7. They were obtained, as for beams, according to the procedure described in Chapter 5, using the value of f_{ps} obtained from Eq. (11.2) for unbonded tendons (considered safer than that given by Eq. (5.13)). An example of calculation is shown next for the near-midspan section of the exterior span.

Using Eq. (11.2), we have:

$$f_{ps} = f_{pe} + 7.5 = 160 + 7.5 = 167.5 \text{ ksi} = 167{,}500 \text{ psi}$$

Table 11.1 Numerical results for the example of Section 11.4; moments are given per foot width of slab.

		Exterior span	First interior support		Typical interior span
Line	Item	Near midspan ($0.414l$)	Center of support	Left face of support (at 1 ft from center)	Midspan
1	Moment (M_b or M_G), k-ft, due to balanced load or dead load, $w_b = w_G = 0.1$ klf	4.859 $0.0777w_{nb}l^2$	-6.578 $-0.1052w_bl^2$	-5.112 $-\frac{w_b(l-1)}{2}(1-0.21l)$	2.878 $0.0462w_bl^2$
2	Moment (M_{nb} or M_L), k-ft, due to unbalanced load or live load, $w_{nb} = w_L = 0.1$ klf	6.215 (spans 1, 3, and 5 are loaded) $0.0995w_{nb}l^2$	-7.475 (spans 1, 2, and 4 are loaded) $-0.1196w_{nb}l^2$	-5.976 (spans 1, 2, and 4 are loaded) $-\frac{w_{nb}(l-1)}{2}(1-0.24l)$	5.345 (spans 1, 3, and 5 are loaded) $0.0855w_{nb}l^2$
3	Uniform stress due to balanced load, psi	271	271	271	181
4	Maximum stresses due to unbalanced load, psi	±582	∓ 701	∓ 560	±501
5	Maximum stresses under service loads, top and bottom fiber, psi	σ_{top} = 853 σ_{bot} = -311	σ_{top} = -430 σ_{bot} = 972	σ_{top} = -289 σ_{bot} = 831	σ_{top} = 682 σ_{bot} = -320
6	Strength design moment: $\lvert M_u = 1.2M_D + 1.6M_L \rvert$, lb-in	189,298	238,243	188,352	144,067
7	Design nominal moment resistance: ϕM_n, lb-in	227,329	227,466* 263,890**	227,466	177,963
8	A_{ps}, in^2 per foot width of slab	0.162	0.162	0.162	0.108
9	A_s, in^2 per foot width of slab	0.20	0.20* 0.31**	0.20	0.20

* design nominal moment resistance when #4 reinforcing bar is used at 12 in spacing
**design nominal moment resistance when #5 reinforcing bar is used at 12 in spacing

Referring to the design flow chart, Fig. 5.19, and taking into account the nonprestressed steel, we have:

$$d_e = \frac{A_{ps}f_{ps}d_p + A_sf_yd_s}{A_{ps}f_{ps} + A_sf_y} = \frac{0.1625\times167.5\times6.75 + 0.2\times60\times7}{0.1625\times167.5 + 0.2\times60} = 6.83 \text{ in}$$

$$\omega_e = \frac{A_{ps}f_{ps}}{bd_p f'_c} + \frac{A_s f_y}{bd_s f'_c} = \frac{0.1625\times 167.5}{12\times 6.75\times 5} + \frac{0.2\times 60}{12\times 7\times 5} = 0.0958$$

$$a = 1.18\omega_e d_e = 1.18\times 0.0958\times 6.83 = 0.772 \text{ in}$$

$$c = \frac{a}{\beta_1} = \frac{0.772}{0.8} = 0.965 \text{ in}$$

$$\frac{c}{d_e} = \frac{0.965}{6.83} = 0.141 < 0.375 \rightarrow \text{Tension controlled section}$$

$$\phi = 0.9$$

$$\phi M_n = \phi[A_{ps}f_{ps}(d_p - \frac{a}{2}) + A_s f_y(d_s - \frac{a}{2})]$$

$$\phi M_n = 0.9[0.1625\times 167.5(6.75 - \frac{0.772}{2}) + 0.2\times 60(7 - \frac{0.772}{2})]$$

$$= 227.329 \text{ k-in} = 227{,}329 \text{ lb-in}$$

The nominal bending resistance can also be obtained from:

$$\phi M_n = \phi(f'_c bd_e^2 \omega_e(1 - 0.59\omega_e)$$

$$\phi M_n = 0.9(5\times 12\times 6.83^2\times 0.0958(1 - 0.59\times 0.0958) = 227.684 \text{ kips-in}$$

The above moment is shown in Table 11.1, line 7, as well as similar values computed for the other sections. Note that if the strength design moment (or factored moment) was found higher than the nominal moment resistance at the support, moment redistribution could have been used. In this case, it would allow up to about 14 percent of the negative moment to be redistributed (see Section 10.14). Such redistribution may need to be considered at a typical interior support section where the nominal moment resistance is the same as that of the midspan section of a typical interior span, but is smaller than that of the first interior support.

Referring to Table 11.1, lines 6 and 7, it can be observed that the nominal bending resistance would be slightly insufficient if calculated at the centerline of the first interior support. Assuming design was to be considered at that section, it is easy to fix the problem by increasing the amount of nonprestressed reinforcement; in this particular case, if #5 bar is used (instead of #4 bar) at a spacing of 12 in, the design nominal bending resistance would increase to 263,890 lb-in leading to $\phi M_n > M_u$.

6. Shear

The maximum shear force occurs at the exterior face of the first interior support. It can be taken conservatively equal to $(1.15/2)wl_n$ where l_n is the clear span. For this problem, the factored shear force per unit width of slab is obtained as:

$$V_u = \frac{1.15}{2}(1.2w_b + 1.6w_{nb})l_n$$

$$= \frac{1.15}{2}\times 0.28\times 23 = 3.703 \text{ kips}$$

It leads to a factored shear stress:

$$v_u = \frac{V_u}{bd_e} = \frac{3703}{12\times 6.83} \simeq 45 \text{ psi}$$

The capacity reduction factor for shear is $\phi = 0.75$.

The concrete shear resistance, v_c, is at least equal to $2\sqrt{f_c'} = 141.4$ psi. As v_u is less than ϕv_c, the shear resistance of the slab is acceptable at this section. It can be shown that it is also acceptable at all other sections.

7. Deflection

The slab is assumed level under the effect of the balanced load (dead load) and the prestressing force. Hence, only the unbalanced load (live load) will create deflections. Using tables of coefficients for continuous beams and assuming alternative span loadings, the maximum deflection is shown to occur in the exterior span with an approximate (on the high side) value (Chapter 10):

$$(\Delta_i)_L \simeq 0.01\frac{w_{nb}l^4}{E_c I_g}$$

$$= 0.01\frac{100/12\times(25\times12)^4}{4.287\times10^6\times8^3} = 0.31 \text{ in}$$

The above deflection is smaller than the limiting value $l/360 = 0.83$ in allowed by the code.

8. Temperature Reinforcement

A minimum amount of ordinary reinforcement normal to the main reinforcement is provided to resist shrinkage and temperature stresses. Assuming a reinforcement ratio of 0.0018 leads to the following area of steel:

$$A_s = 0.0018\times12\times8 = 0.17 \text{ in}^2 \text{ per foot of slab}$$

It is achieved by placing #4 bars at 14-in spacing transverse to the main reinforcement and along the tensile face of the slab.

9. Illustrating the Use of Eq. (11.3)

Consider the exterior span near midspan. Assume:

$$E_p = 28000 \text{ ksi};\ \varepsilon_{cu} = 0.003;\ \Omega_u = \frac{3}{L/d_p} = \frac{3}{25\times12/6.75} = 0.0675$$

Also assume that in using Eq. (11.3), one span is loaded out of five (worst case for f_{ps}), thus:

$$f_{ps} = f_{pe} + \Omega_u E_{ps}\varepsilon_{cu}\left(\frac{d_p}{c} - 1\right)\frac{L_1}{L_2} \le 0.80 f_{pu}$$

$$f_{ps} = 160 + 0.0675\times28000\times0.003\left(\frac{6.75}{c} - 1\right)\frac{1}{5} \le 0.80\times270 = 216 \text{ ksi}$$

$$f_{ps} = 160 + 1.134\left(\frac{6.75}{c} - 1\right)$$

The equation of force equilibrium at nominal resistance is given by:

$$0.1625 f_{ps} + 0.2\times60 = 0.85 f_c' b\beta_1 c$$

$$0.1625 f_{ps} + 12 = 0.85\times5\times12\times0.8c = 40.8c$$

The solution of the above two simultaneous equations for f_{ps} and c lead to a quadratic equation for which $c = 0.958$ in and $f_{ps} = 166.68$ ksi. These values are not too different from those recommended in Eq. (11.2) and used above to compute nominal bending resistance. It is noted that the L_1/L_2 ratio significantly influences the stress increment Δf_{ps} beyond effective prestress. The reader may want to check that if L_1/L_2 is taken equal 1, the following values would be obtained: $c = 1.054$ in and $f_{ps} = 190.66$ ksi.

11.5 CHARACTERISTICS OF TWO-WAY FLAT SLABS

11.5.1 Load Path

In order to understand the behavior of flat slabs and their reinforcing arrangement, it is informative to follow the path along which the load is transferred from the slab to the supporting columns. Let us consider a typical interior panel of a flat plate subjected to a uniform load, *w*, per unit area. The panel can conceptually be modeled into a central slab portion surrounded by broad strips of slabs acting as beams and spanning between columns in each direction (Fig. 11.10). The strip beams are called column strips and are bounded in each direction by middle strips of slab. This panel representation simulates a slab (the central portion) supported on beams (the column strips) along its edges.

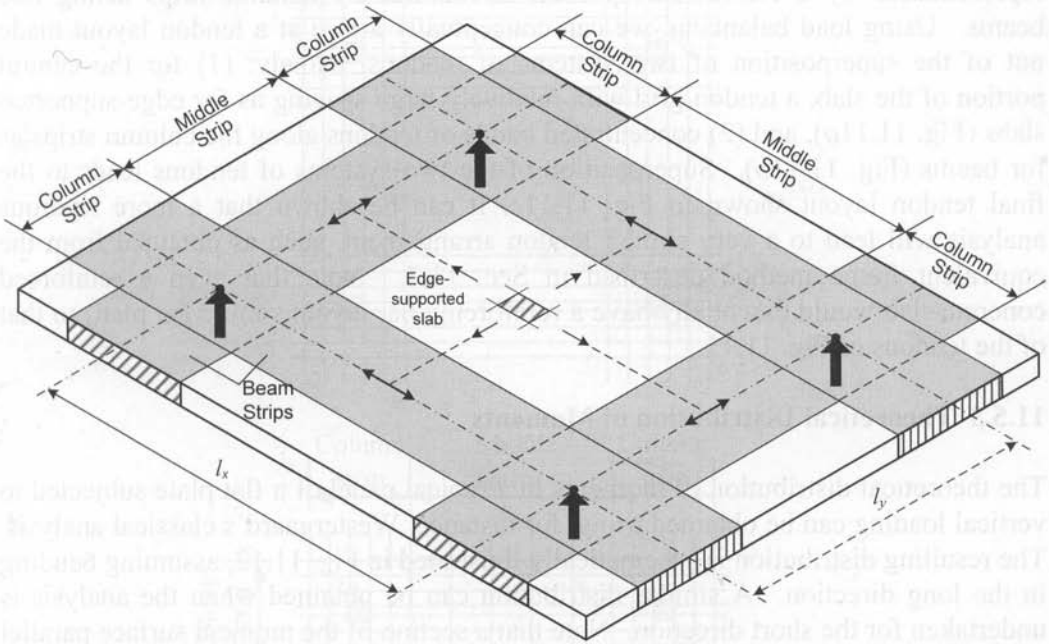

Figure 11.10 Conceptual representation of a flat plate into equivalent slab and beams.

Let us consider the load, *w*, on a unit area at the center of the slab. It can be assumed that such a load is transferred in each direction from the central portion of the slab to the edge beams (column strips), which in turn transfer the load to the columns. It can be observed that the fraction of load transferred from the central portion along the long direction is delivered to the column strip spanning in the short direction. This fraction of the load added to that carried directly in the short direction sums up to 100 percent of the load applied to the panel. Similar reasoning

can be used by following the path of the load along the short direction first. Hence, for two-way slab systems supported on columns, the applied load must be considered in its entirety in each direction analyzed. This conclusion may seem to contradict the procedure used for edge- or beam-supported slabs in which only a fraction of the load is assumed carried in each direction. However, for such slabs, the support beams must transfer the load to the columns and are in effect part of the slab system, thus carrying their share of load. Note that, in order to get the reaction on a column of a two-way slab, it is better to use the tributary area for the column, assuming the full live load is applied to the tributary area.

11.5.2 Reinforcement Layout

Let us consider the same typical interior panel described in Fig. 11.10 and its representation by a central slab portion surrounded by column strips acting like beams. Using load balancing, we can conceptually arrive at a tendon layout made out of the superposition of two systems of tendons, namely: (1) for the central portion of the slab, a tendon grid with relatively large spacing as for edge-supported slabs (Fig. 11.11*a*), and (2) concentrated bands of tendons along the column strips as for beams (Fig. 11.11*b*). Superposition of the two systems of tendons leads to the final tendon layout shown in Fig. 11.11*c*. It can be shown that a more rigorous analysis will lead to a very similar tendon arrangement, such as obtained from the equivalent frame method described in Sec. 11.7. Note that even a reinforced concrete slab would essentially have a reinforcing bar layout similar (in plan) to that of the tendons of Fig. 11.11.

11.5.3 Theoretical Distribution of Moments

The theoretical distribution of moments in a typical panel of a flat plate subjected to vertical loading can be obtained using, for instance, Westergaard's classical analysis. The resulting distribution is schematically illustrated in Fig. 11.12, assuming bending in the long direction. A similar distribution can be obtained when the analysis is undertaken for the short direction. Note that a section of the moment surface parallel to the long direction leads to a moment diagram very similar to that obtained for a typical span of a continuous beam. Moreover, the transverse distribution of moments in a slab is not uniform. This implies that the portions of the slab across its width will be subjected to higher moments than others, and the corresponding reinforcement distribution will be uneven. However, for the purpose of design, the slab is generally divided into a column strip and a middle strip, within each of which the distribution of moments is considered constant (Fig. 11.13). The distribution of moments currently suggested in the ACI code for reinforced concrete slabs, and by ACI-ASCE Committee 423 [Refs. 11.2, 11.3] for prestressed concrete flat plates, reflects the theoretical distribution and is explained for prestressed flat plates in Section 11.8.

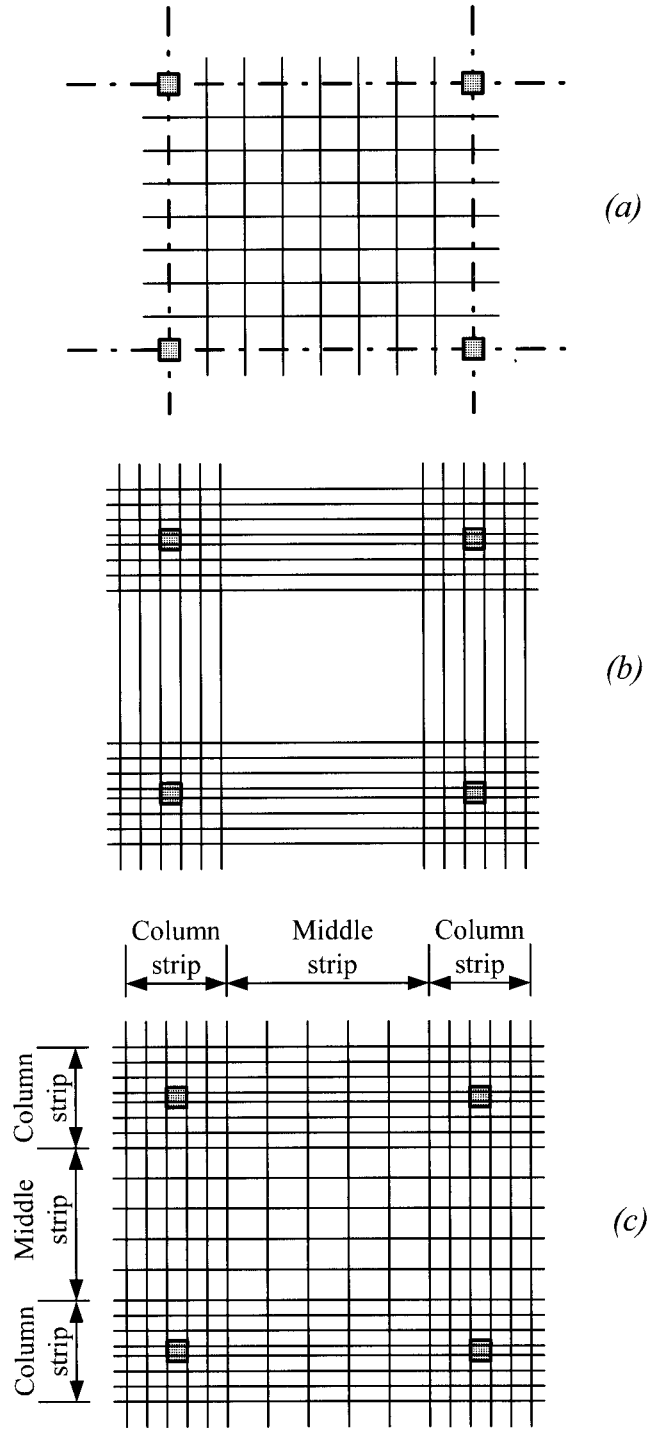

Figure 11.11 Conceptual arrangement of tendons in flat plates. ***(a)*** **Tendons for central portion of slab.** ***(b)*** **Beam tendons along the column strips.** ***(c)*** **Superposition of the two systems.**

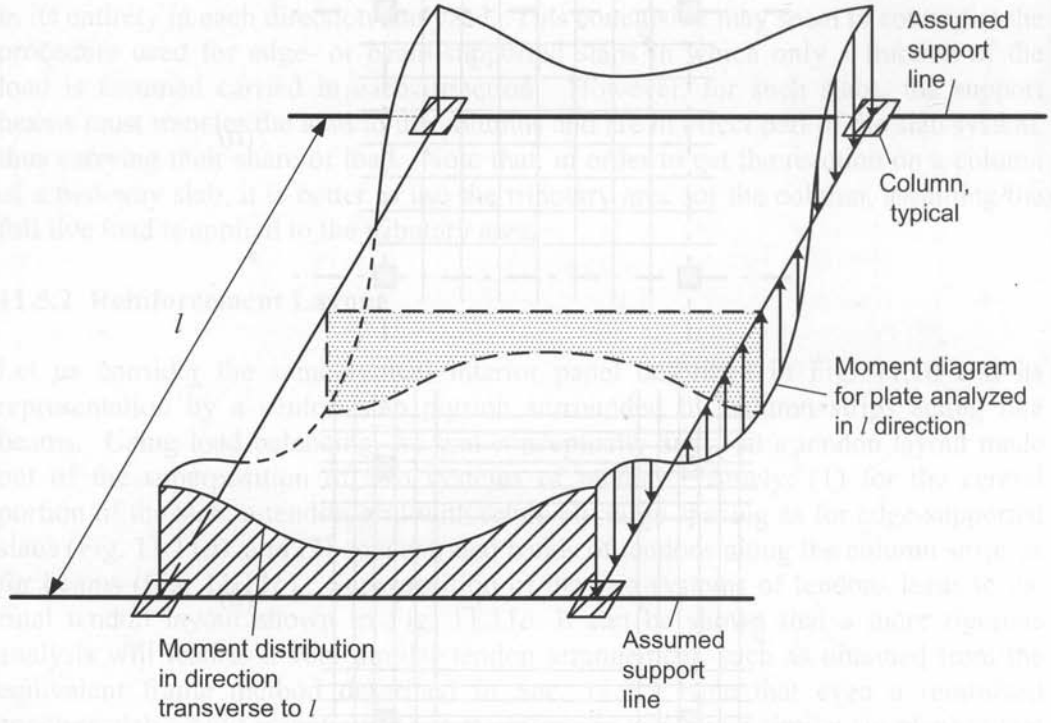

Figure 11.12 Theoretical distribution of moments in a flat plate analyzed in one direction.

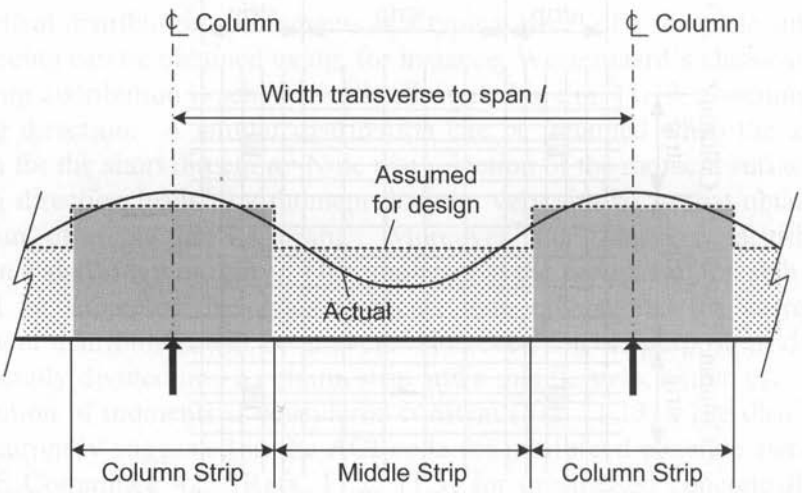

Figure 11.13 Assumed design distribution of moments across the width of a flat plate.

11.5.4 Special Notations

Most of the standard notations used throughout this text prevail in this chapter. However, in order to accommodate some of the differences with the ACI code notations, the following terms will be used for flat plates in the next sections:

l = span, in general, in the main direction where analysis for flexure is undertaken

l_a, l_b = longer and shorter span of a given panel measured center-to-center of supports

l_x, l_y = dimensions of panel center-to-center of columns in the x and y directions, respectively (used when a particular panel is considered)

l_1 = span in the direction where the analysis for flexure is undertaken (mostly used when the equivalent frame is considered)

l_2 = width of equivalent frame (sometimes used as the span transverse to l_1)

d_e = distance from extreme compression fiber to centroid of tensile force in the steel (both prestressed and nonprestressed)

Note that the terms l_1 and l_2, which were used in continuous one-way slabs and beams to characterize consecutive spans, are different from the above defined values. The x and y directions are used as the principal directions when a slab involving several panels in each direction is considered.

11.6 ANALYSIS AND DESIGN METHODS

11.6.1 Analysis

Two-way flat slabs are highly indeterminate structures. Their analysis should always satisfy the basic principles of statics and should, theoretically, take into account the restraints against rotation and translation offered by the supporting system. Available tools for the analysis and design of concrete flat slabs range from ready-to-use tables and charts to complex finite element programs. Approximate methods are also available for their analysis and include yield line analysis, the direct design (analysis) method of the ACI code, and the equivalent frame method.

There is general agreement that yield line analysis applies to reinforced concrete slabs, and although research studies are limited, there is evidence that yield line analysis can also apply to prestressed concrete slabs, especially when sufficient bonded nonprestressed reinforcement is used. The nonprestressed reinforcement helps improve the rotational capacity after cracking and allows sufficient moment

redistribution to develop yielding lines. For application of the yield line analysis, the reader is referred to other texts such as Refs. [11.12, 11.24, 11.30, and 11.34]. The direct design method described in the ACI code has been derived for reinforced concrete slabs on the basis of their rotational and moment redistribution capacity after cracking, as evidenced by tests. Hence, it is not generally applicable to prestressed concrete slabs. However, the equivalent frame method of analysis has been shown to apply both to reinforced and to prestressed concrete two-way slab systems and is described in more detail in Section 11.7.

11.6.2 Design

Numerous studies have led to particular design methods for prestressed concrete flat slabs. Saether proposed a method based on structural membrane theory [Ref. 11.41], while an elasticity-based approach was developed by Rozvany and Hampson [Ref. 11.40]. A direct design method was proposed by Wang [Ref. 11.48] and design charts were developed by Parme [Ref. 11.35]. However, the most widely used design method for prestressed concrete flat slabs is the load-balancing method developed by T. Y. Lin [Ref. 11.22] and described in Sec. 10.13. It is often used in combination with the equivalent frame method of analysis, which is carried out for the unbalanced load.

11.6.3 Load Balancing

The load-balancing approach is the fastest and most convenient method to treat prestressed concrete flat slabs. More than any other method, it allows a clear visualization of the relationship between the distribution of moments and the tendon arrangement to balance these moments. This can be simply illustrated by considering a slab with an irregular pattern of columns (Fig. 11.14) for which other analytical procedures, which are generally derived for ideal situations, become tedious. Even the arbitrary concept of dividing the slab into column strips and middle strips is confusing for the slab of Fig. 11.14, as a column strip in one panel may become a middle strip in another panel. However, going back to the basic idea of load balancing, the slab can be divided by a grid made out of lines passing by every row of columns in both the longitudinal and transverse directions. The first system of tendons (say, along the lettered grid lines, East-West) is given a profile, whereas high points (where reverse curvatures and downward loads occur) are placed at the numbered grid lines (North-South). They are given uniform spacing. The first system of tendons creates a downward reaction *at* the numbered grid lines, which is reacted by a second system of tendons placed in bands *along* the numbered grid lines. The N-S tendons, which are grouped together in bands, form beam-like elements that carry the load to the columns in the transverse direction. It can be seen that, following simple reasoning, a tendon arrangement can be arrived at in an otherwise rather complex problem. Since the balanced load generally represents a

large portion of the total service load, it is believed that, where slabs are concerned, differences between the balanced-load approach and a more rigorous analysis will be relatively small.

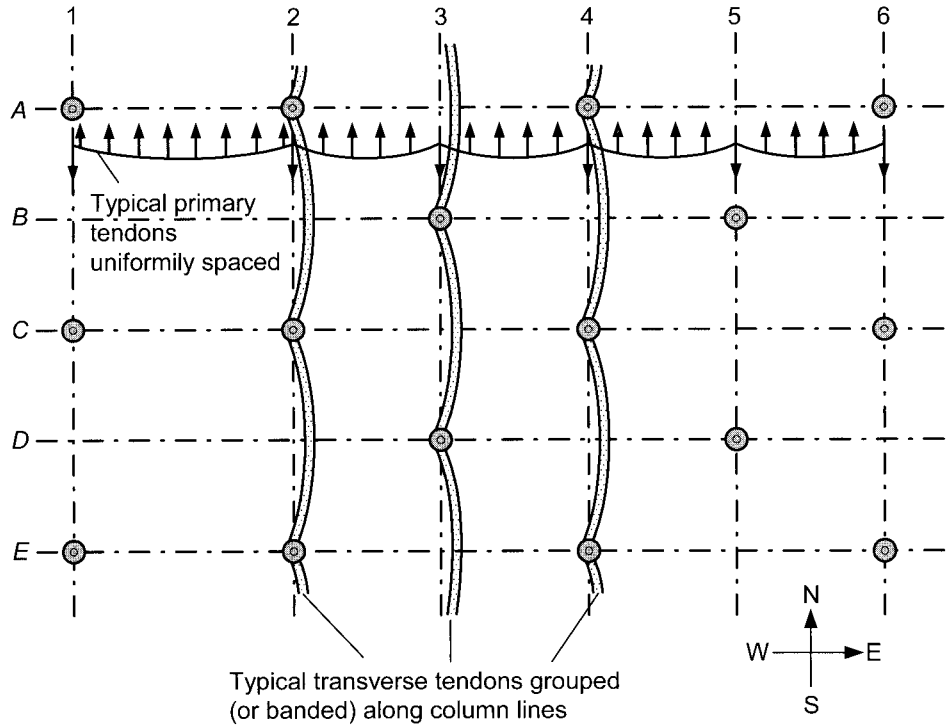

Figure 11.14 Load balancing for a slab with an irregular pattern of columns.

11.7 ANALYSIS BY THE EQUIVALENT-FRAME METHOD

The equivalent-frame method is the most widely used method in the United States to analyze concrete slabs. It applies to *all* types of two-way slab systems, including beam-supported slabs, waffle slabs, flat slabs with drop panels, and flat plates [Refs. 11.11, 11.36]. Theoretically, it also applies to one-way slabs; however, in such a case it may not be the most efficient procedure.

Tests of large structural models have shown that the equivalent-frame method satisfactorily predicts factored moments and shears in prestressed concrete slab systems [Refs. 11.10, 11.11, 11.17 11.22, 11.35]. Although other analytical methods, such as the elastic theory of thin plates and the finite-element method, are acceptable, the equivalent frame method is recommended by ACI-ASCE Committee 423 for the analysis of prestressed concrete flat plates [Refs. 11.3, 11.5]. It is described in sufficient detail in the ACI code and its commentary, Section 13.7.

11.7.1 General Approach

The equivalent frame method essentially reduces the analysis of a two-way slab system to two independent analyses of one-way slab or planar frame system. In this method, the three-dimensional structural frame system is represented by a series of two-dimensional frames which are then analyzed each separately for loads acting in the plane of the frames. The moments determined at the critical sections of the frame are distributed to the slab sections.

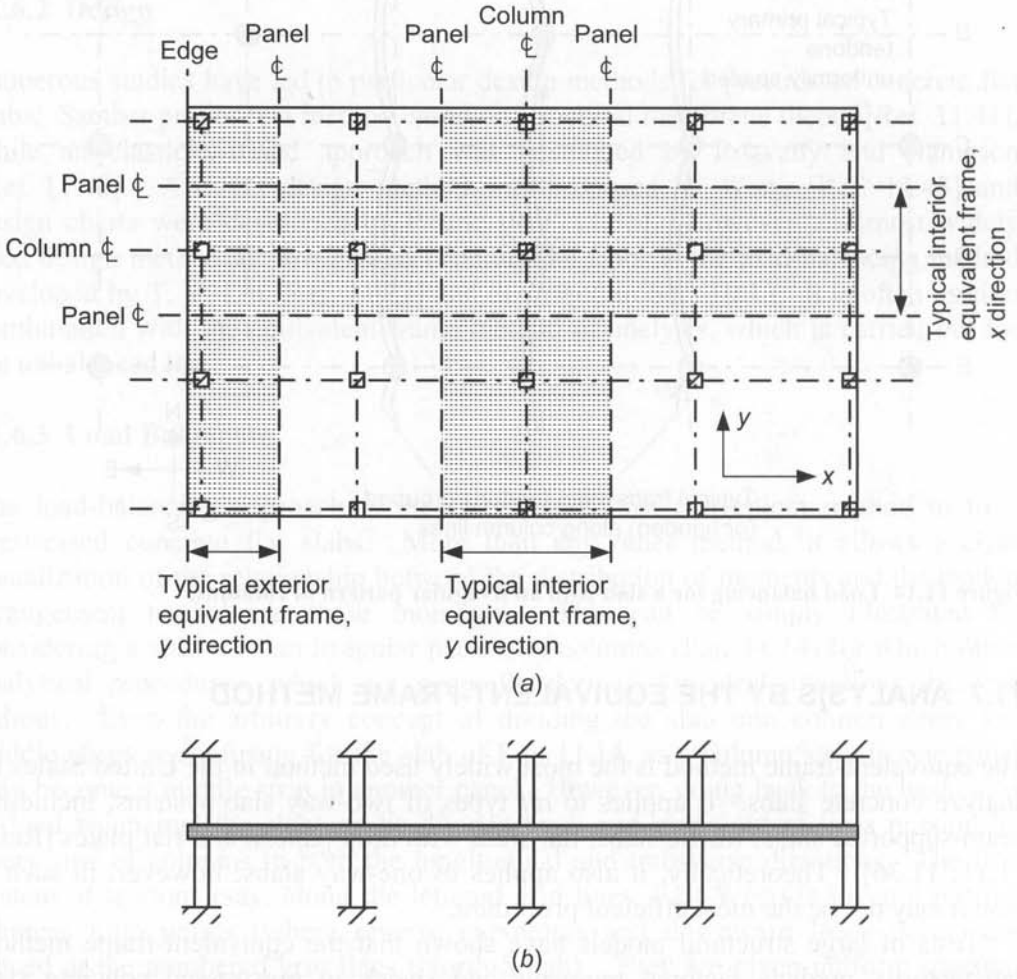

Figure 11.15 Typical equivalent frames as used in the equivalent-frame method. ***(a)*** **Plan.** ***(b)*** **Elevation along the *x* direction.**

The two-dimensional equivalent frames are centered on column lines longitudinally and transversely through the structure (Fig. 11.15*a*). Each frame consists of a row of columns and a continuous slab-beam strip bounded laterally by

the centerline of the panel on each side of the columns. For vertical loading, each floor may be analyzed separately, assuming the far ends of the attached columns are fixed at the floors above and below (Fig. 11.15*b*). The equivalent frame in each direction is assumed to carry 100 percent of the applied load (see Section 11.5.1). Alternative loadings of spans must be considered as for continuous beams to determine maximum effects.

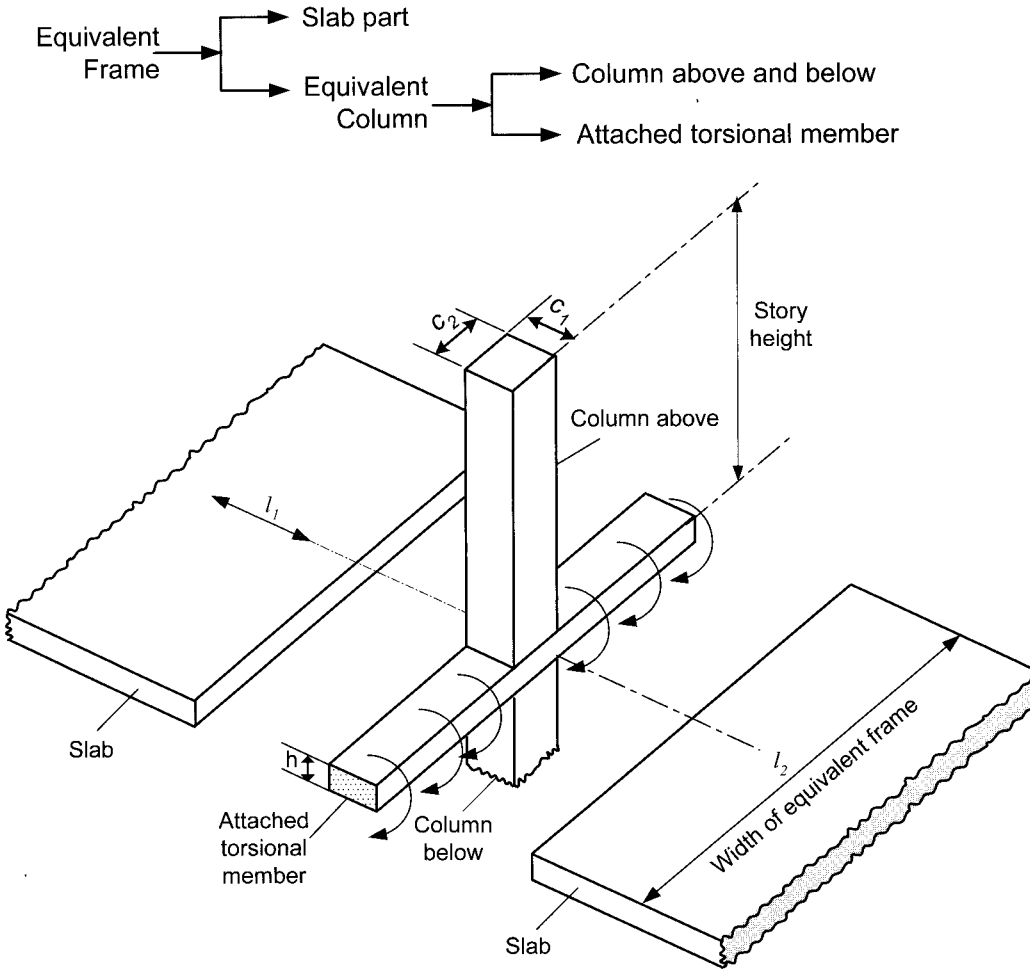

Figure 11.16 Main elements of the equivalent frame.

The equivalent frame can be separated into three parts (Figs. 11.16) which are first evaluated separately, and then the related information is assembled for analysis, namely:

1. The horizontal slab strip, including any beams spanning in the direction of the frame, if any;

2. The columns or other supporting members extending above and below the slab; and
3. The elements of the structure that provide moment transfer between the horizontal and vertical members. In Fig. 11.16, these are represented by the attached torsional member.

The second and third components are conceptually grouped together to form the "equivalent column" of the frame.

11.7.2 Computation of Moments and Shear Forces

Equivalent frames can be analyzed by different methods of structural analysis, which are preferably implemented in a software code, for efficiency. Generally, the stiffness matrix containing the stiffness coefficients at the joints between slab and columns is needed.

Moment transfer between horizontal and vertical components depends on the connection between them and their relative flexibility or relative stiffness. For slender columns or for soft column-slab connections, such as in the case of lift slabs, the stiffness of the columns may be neglected. In general, however, the rotational resistance of the columns must be accounted for. To do this, an equivalent column is assumed. It consists of the actual columns above and below the slab plus an attached torsional member transverse to the direction of the span for which moments are being determined and bound on each side by the panel centerlines (Fig. 11.16). The attached torsional member is assumed to have a constant cross section consisting of the larger of: (1) a portion of slab having a width equal to the column, bracket, or capital in the direction of the span for which moments are being determined, or (2) for monolithic or fully composite construction, the portion of slab specified in (1) plus that part of the transverse beam, if any, above and below the slab, taken not greater than four times the slab thickness. According to Article 13.7.4 of the 1989 version of the ACI code, the flexibility (inverse of stiffness) of the equivalent column shall be taken as the sum of flexibilities of the actual columns above and below the slab and the flexibility of the attached torsional member. That is:

$$\frac{1}{K_{ec}} = \frac{1}{\sum K_c} + \frac{1}{K_t} \tag{11.5}$$

where:

K_{ec} = flexural stiffness of equivalent column (above and below)

K_c = flexural stiffness of actual column; for members with constant cross section the flexural stiffness is equal to $4E_c / l$ where E_c is the modulus of elasticity of the column concrete

K_t = torsional stiffness of attached torsional member (see Eq. 11.6)

The summation in Eq. (11.5) applies to the column above and below the slab. Stiffnesses are expressed in terms of moment per unit rotation. In computing K_c, the moment of inertia outside of joints or column capitals may be based on the gross area of concrete. The torsional stiffness of the attached torsional member can be calculated from the following expression (ACI code R13.7.5):

$$K_t = \sum \frac{9E_{cs}C}{l_2(1-c_2/l_2)^3} \tag{11.6}$$

where:

E_{cs} = modulus of elasticity of concrete slab

l_2 = width of equivalent slab or length of span transverse to l_1

l_1 = length of span in direction that moments are being determined, measured face-to-face of supports

c_2 = size of rectangular or equivalent rectangular column, capital, or bracket measured transverse to l_1

C = cross-sectional constant for the attached torsional member (see Eq. 11.7)

The summation in Eq. (11.6) refers to the torsional elements on either side of a column. Hence, for an interior column or an edge column of an interior frame, $\sum = 2$, while $\sum = 1$ for a corner column. The constant C may be evaluated from the cross section of the attached torsional member, by dividing it into separate rectangular parts and carrying out the following summation:

$$C = \sum \left(1 - 0.63\frac{x}{y}\right)\frac{x^3 y}{3} \tag{11.7}$$

where x and y are the shorter and longer overall dimensions of each rectangular part considered, respectively. For the slab of Fig. 11.16, only one rectangular part exists, for which $x = h$ and $y = c_1$.

The stiffness of the slab part of the frame is equal to $4E_{cs}/l$ assuming a flat plate with no beams attached; l is taken in the primary direction of the frame being analyzed.

Given the stiffness of the equivalent column and the slab-beam part, the frame can be analyzed for vertical loads by any acceptable method such as the moment distribution method or structural analysis software; then the reinforcement is provided. A similar procedure is carried out for the other longitudinal and transverse frames, and the results (reinforcements) are integrated together for the whole slab.

11.8 DESIGN DISTRIBUTION OF MOMENTS AND TENDONS

The equivalent frame method leads to the moments at the critical sections of the continuous slab-beam or equivalent frame considered. The negative moments so obtained apply at the centerline of the supports. Since the actual support is not a line support but is made of the columns and a relatively wide virtual band of slab spanning transversely between columns, the critical section of the negative moment may be taken at the face of the supporting column but in no case at a distance greater than $0.175l_1$ from the center of the column (2002 ACI code, Sec. 13.7.7). The critical section is assumed the same across the entire slab width. Note that actual moments are not uniformly distributed but vary across the width of the slab, as shown earlier in Fig. 11.10. To distribute the moments obtained from the equivalent-frame method, the total width of the slab is divided, for the purpose of design, into a column strip and a middle strip (Fig. 11.17). The column strip is assumed to have a width, on each side of the column, equal to the smaller of $l_1/4$ or $l_2/4$, where l_1 and l_2 are the dimensions of the panel center-to-center of supports (ACI code, Sec. R13.7.2). The middle strip, associated with the equivalent frame, comprises, on each side of the column, the part of slab bounded by the column strip and the centerline of the panel.

The moments are assumed constants (transversely) within the boundaries of a column strip or a middle strip. For panels with length-to-width ratio not exceeding 1.33, the following approximate distribution of moments and corresponding tendons is recommended [Refs. 11.3, 11.5]:

- *Simple spans*: 55 to 60 percent of moment (thus reinforcement) to the column strip with the remainder to the middle strip

- *Continuous spans*: 65 to 75 percent of moment (thus reinforcement) to the column strip with the remainder to the middle strip

Note that once tendons are placed, allowable stresses are checked separately within each strip. As a general guide, the spacing of tendons or bundles of tendons should not exceed four times the slab thickness in column strips and six times the slab thickness in middle strips. Note that the ultimate strength of flat plates is primarily controlled by the total amount of tendons in each direction. However, as indicated by tests, tendons passing through the columns, or directly around their edges, contribute more to the load-carrying capacity than other tendons. Hence, it is recommended to place some (2 to 4) tendons through the columns or around their edges, whenever possible.

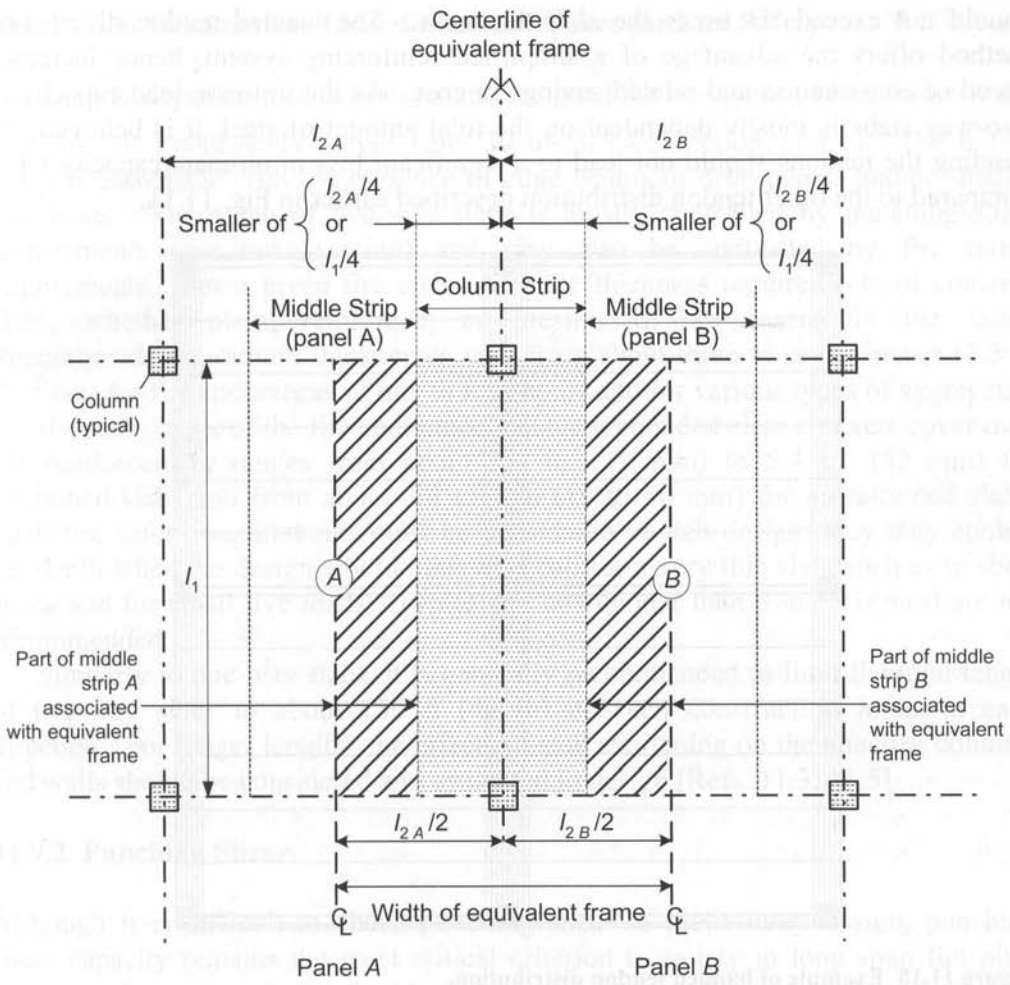

Figure 11.17 Design definitions of slab strips and equivalent frame.

Although the tendon distribution described above follows essentially the distribution of moments, it has evolved due to construction difficulties and related costs. At this time, the preferred method of placing tendons in two-way flat plates in the United States is the banded tendon distribution illustrated in Fig. 11.18. In this method, the number of tendons required across the entire design strip (width of equivalent frame) are banded close to the column lines in one direction and uniformly distributed in the other direction. This creates in effect a two-directional prestressed one-way slab system in which the portions of slab where tendons are banded act virtually as the support beams. ACI-ASCE Committee 423 recommends placing at the slab perimeter at least two tendons through the columns in the distributed direction [Ref. 11.3]. The spacing of the tendons which are distributed

should not exceed six times the slab thickness. The banded tendon distribution method offers the advantage of a simplified reinforcing system, hence increased speed of construction and related savings in cost. As the ultimate load capacity of two-way slabs is mostly dependent on the total amount of steel, it is believed that banding the tendons should not lead to a significant loss in ultimate capacity when compared to the other tendon distribution described earlier in Fig. 11.11.

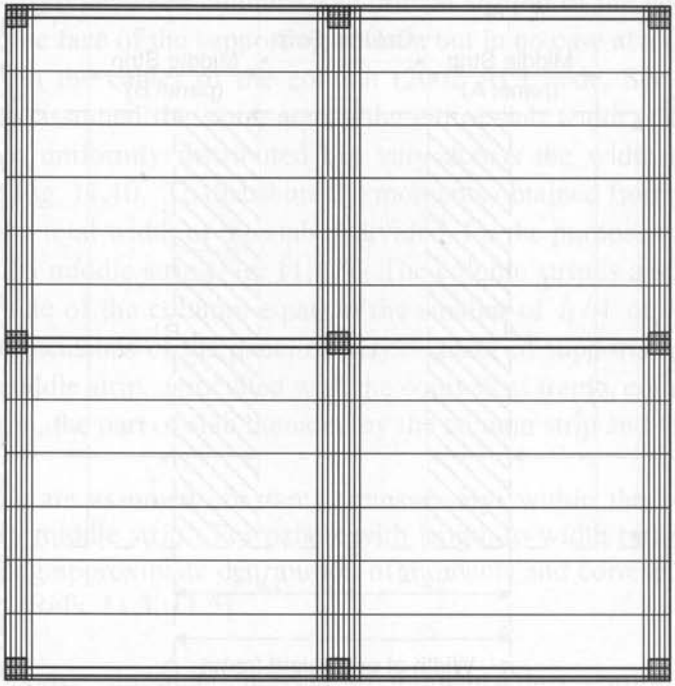

Figure 11.18 Example of banded tendon distribution.

Note that in slabs with shearheads and in lift slabs where it is not possible to have bottom bars go through the columns, the ACI code (Article 13.3.8.6) specifies that at least two continuous bonded bottom bars in each direction shall pass through the shear heads or lifting collar as close to the column as practicable.

11.9 PRELIMINARY DESIGN INFORMATION AND DESIGN TIPS

The preliminary design process for slabs generally consists of first selecting a slab depth (see Section 11.1.1) and then providing the necessary amount of reinforcement to satisfy service load and ultimate strength criteria. The following remarks will help in reducing the design iterations and arriving quickly at an acceptable solution.

11.9.1 Slab Thickness and Reinforcement Cover for Fire Safety

The span-to-depth ratio of two-way slabs designed for live loads of less than 100 psf (4.8 kN/m^2) commonly ranges from 30 to 50 (see Section 11.1.1). The higher range is associated with the presence of edge beams or drop panels and/or smaller live loads. The depth of two-way slabs is mostly controlled by punching shear requirements (see next section) and may also be controlled by fire rating requirements. For a given fire endurance, the thickness requirements of concrete slabs, whether plain, reinforced, or prestressed, are essentially the same. Recommended minimum thicknesses vary from about three to seven inches (7.5 to 17.5 cm) for fire endurances of one to four hours and for various types of aggregates. For the same range of the fire endurance, the recommended clear concrete cover over the reinforcement ranges from about 3/4 in. (19 mm) to 5/4 in. (32 mm) for restrained slabs and from about 3/4 to 2 in (19 to 50 mm) for unrestrained slabs. Such fire safety requirements must be considered in slab design; they may control the depth when the design would otherwise call for a very thin slab, such as in short spans and for small live loads. Typically slabs thinner than 6 in (150 mm) are not recommended.

Similarly to one-way slabs, it is generally recommended to limit the total length of two-way slabs to about 150 ft (46 m) between construction joints in each direction. For longer lengths, the effects of slab shortening on the attached columns and walls should be considered and evaluated in design [Refs. 11.3, 11.5].

11.9.2 Punching Shear

Although it is difficult to check punching shear in preliminary design, punching shear capacity remains the most critical criterion to satisfy in long span flat plate systems. It is generally preferable to keep a prestressed flat plate flat all the way instead of either adding drop panels or adding shear reinforcement. Drop panels and slab bands can be used to improve shear capacity when needed, but they add to the cost. Shear reinforcement is difficult to anchor, and interferes with the placement of both tendons and non-prestressed reinforcement. Moreover, shear heads cannot be used satisfactorily in slabs less than about 8 in (200 mm) thick.

11.9.3 Average Prestress

The average prestress is defined as the final prestressing force after losses divided by the total area of concrete, that is, $\sigma_g = F/A_c$. For slabs prestressed with unbonded tendons, a minimum average prestress of 125 psi (0.86 MPa) and a maximum average prestress of 500 psi (3.5 MPa) are recommended by ACI-ASCE Committee 423. The minimum value is meant to limit excessive tension and cracking, while the maximum value is meant to limit excessive elastic shortening and

creep. For applications such as parking structures, where durability against application of deicer chemicals is an important factor, a minimum average prestress level of 200 psi (1.4 MPa) is recommended in each principal direction; also a minimum cover of 2 in (50 mm) to the reinforcement at the top of the slab is recommended. Actual values of average prestress ($\sigma_g = F/A_c$) for currently built flat plates seem to range mostly between 175 and 300 psi (1.2 and 2.1 MPa) and have provided satisfactory performance. There is seldom a need to go beyond about 300 psi (2.1 MPa). At average prestress levels above 500 psi (3.4 MPa) restraints from the supports (columns, walls) and slab shortening (due to elastic shortening, creep, and shrinkage) need to be carefully evaluated and considered in design.

11.9.4 Nonprestressed Reinforcement

In addition to the prestressed unbonded tendons, a minimum amount of ordinary bonded reinforcement is required by the ACI code, as described in Sec. 11.10.4. In practice, a continuous bottom mat of #4 bars at 24 in (13 mm at 600 mm) often is used both ways to improve crack control and nominal bending resistance. This is particularly useful when the support walls are stiff and provide strong restraints, such as in lower levels of buildings at or near the foundation walls [Ref. 11.1].

11.9.5 Deflection

Deflection is seldom a limiting criterion in prestressed slabs; indeed, load balancing by prestressing essentially leads to zero deflection under dead load. ACI code criteria for deflection can be followed (see Section 7.7); generally it is assumed that attached nonstructural elements are not likely to be damaged by the sum of live load deflection and additional long-term deflection due to the sustained load.

11.10 PRESTRESSED FLAT PLATES: DESIGN FOR FLEXURE

11.10.1 Working Stress Design

Similarly to the design of prestressed concrete beams, the determination of the prestressing force in flat plates is essentially based on service load analysis. The load-balancing approach is generally preferred at this stage and, since according to the equivalent frame method, the flat plate is analyzed as two independent one-way slabs, the design procedure is essentially reduced to that of continuous beams and one-way slabs (Chapter 10). The design steps are summarized as follows:

- Select the balanced load such that: $w_b = w_D + \psi w_L$ where the coefficient ψ can be taken between zero and 1 depending on how large the live load is

relative to the dead load. At first, ψ is generally taken equal zero. Note that $w_b + w_{nb} = w_G + w_{SD} + w_L = w_D + w_L$.

- The prestressing force is determined by load balancing, assuming a tendon profile made out of parabolas with zero eccentricities at the end supports and maximum practical eccentricities at intermediate supports.
- Since no secondary moments are generated for the theoretical tendon profile, a uniform compressive stress exists throughout the slab, under the combined effect of the prestressing force and the balanced load. In effect the slab is level and, in theory, has no bending moments.
- The equivalent-frame method is then used to determine the moments due to the unbalanced load, w_{nb}.
- Stresses due to the unbalanced load are superposed to the uniform stress induced by prestressing and the balanced load. The resulting stresses are compared to code-allowable stresses.
- If the resulting stresses are not acceptable, the procedure is repeated and refined as needed by changing the value of ψ. Otherwise the design continues for other limit states.

11.10.2 Allowable Stresses

When using the equivalent-frame method of analysis, the allowable stresses at service loads recommended in the 2002 ACI code and reproduced in Table 3.3 are generally followed. In Article 18.3.3, the code specifies that prestressed two-way slab systems shall be designed as Class U (see Section 3.11), that is, to be designed as uncracked under full service load. The tensile stress under full service load for Class U prestressed flexural members is limited to $-7.5\sqrt{f'_c}$; however, the author recommends (as often done in practice) to limit the tensile stress in the negative moment region near columns and supports to $-6\sqrt{f'_c}$. In positive moment regions, the tensile stress under full service load can be taken as high as $-7.5\sqrt{f'_c}$.

All other allowable stresses given in the ACI code apply (Table 3.3). Deviations from the above values are permissible when more rigorous methods of analysis are used and when it is shown that the slab will perform satisfactorily under all design conditions, including service and ultimate limit states.

A note is in order here. In applying the load-balancing approach to flat plates, the effect of reverse tendon curvature, which provides a smooth transition over the supports (Fig. 11.6*c*) leading generally to a nonconcordant tendon profile is commonly neglected in design. This is done on the basis that secondary moments are small and the ultimate moment capacity is not influenced. However, such an approximation is not always warranted, as secondary moments may substantially influence the elastic analysis and are to be included in the strength design moment which dictates the required nominal resistance. To determine the secondary moments, a loading equivalent to the effect of prestressing can be applied (see

Section 10.8) and the equivalent frame method is then used to determine the total moment due to prestress. The secondary moments are then obtained for each section from the difference between the total prestressing moment and the primary moment (Eq. 10.3).

11.10.3 Ultimate Strength Design

Posttensioned flat plates must meet the ultimate strength requirements of the ACI code. This is achieved by comparing the nominal moment resistance at all critical sections to the factored moments (or strength design moment) at these sections. The factored moment is calculated as for continuous beams, noting that it should generally include the secondary moment, if any, with a factor of 1 (Eq. 10.19).

The nominal moment resistance at each critical section is calculated as for beams according to the procedures described in Chapter 5. The stress in unbonded tendons at nominal bending resistance is preferably taken according to Eqs. (11.1) to (11.3). Nonprestressed reinforcement, when used, should be considered. Note that reaching the nominal resistance at a critical section does not necessarily imply failure of the structure. A collapse mechanism may develop for which a substantially higher load may be applied before failure occurs. Moment redistribution is allowed, as described in Section 10.14.

When unbonded tendons are used, some additional provisions given in the ACI code must be considered. They are summarized next.

11.10.4 Minimum Bonded Reinforcement

Bonded reinforcement is meant to ensure flexural continuity and ductility and to limit crack width and spacing due to overload, temperature or shrinkage. Article 18.9 of the ACI code specifies that two-way flat plates prestressed with unbonded tendons should contain a minimum area of ordinary bonded reinforcement, as follows:

1. In positive moment areas where the magnitude of tensile stress in concrete at service load does not exceed $\left|-2\sqrt{f'_c}\right|$, bonded reinforcement is not required.
2. In positive moment areas where the magnitude of tensile stress in concrete at service load exceeds $\left|-2\sqrt{f'_c}\right|$, the minimum area of bonded reinforcement shall be computed from:

$$A_s = \frac{|N_c|}{0.5 f_y} \tag{11.8}$$

where N_c is the tensile force in the concrete section due to unfactored dead load plus live load, and the yield strength of the bonded reinforcement, f_y, shall not

exceed 60,000 psi (414 MPa). Bonded reinforcement shall be uniformly distributed over the precompressed tensile zone and as close as practicable to the extreme tension fiber. Its minimum length shall be one-third the clear span. If the bonded reinforcement is considered in determining the nominal strength (partially prestressed section), its length should be in accordance with the development length provision of the ACI code.

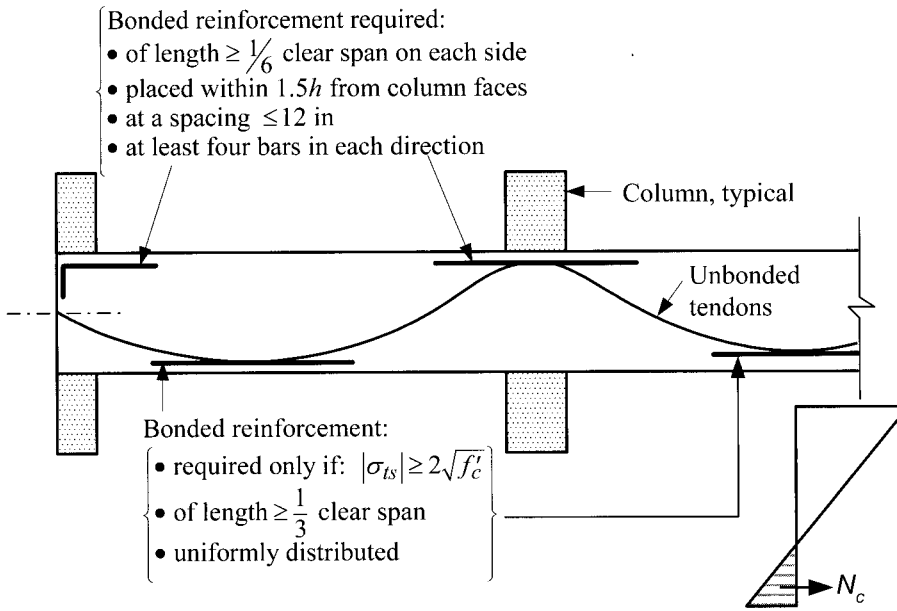

Figure 11.19 Typical requirements for bonded reinforcement in one direction of a two-way flat plate prestressed with unbonded tendons.

3. In negative moment areas at column supports, the minimum area of bonded reinforcement in each direction shall be computed by:

$$A_s = 0.00075 A_{cf} \tag{11.9}$$

where A_{cf} is the larger gross cross sectional area of the slab-beam strips of the two orthogonal equivalent frames intersecting at a column of a two-way slab; for a typical two-way flat plate, $A_{cf} = hxl$ where h is the overall slab depth and l is the length of span in the direction parallel to that of the reinforcement being determined. The above bonded reinforcement shall be distributed within a slab width between lines that are $1.5h$ outside opposite faces of the column support.

At least four bars or wires shall be provided in each direction. The spacing of bonded reinforcement shall not exceed 12 in (30 cm) and its length shall be at least one-sixth the clear span on each side of the support. When the bonded reinforcement is considered in determining the nominal strength of a section, its length should be in accordance with the development length provisions of the ACI code. Equation (11.9) applies regardless of the magnitude of the tensile stress.

11.10.5 Nominal to Cracking Moment Condition

For two-way slabs posttensioned with unbonded tendons, ACI Committee 423 [Ref. 11.3] recommends to waive the condition that factored nominal resistance (ϕM_n) exceed 1.2 times the cracking moment. The author believes that the waiver leads to a reduced safety margin.

11.11 FLAT PLATES: DESIGN FOR SHEAR

11.11.1 Concrete Shear Capacity

Shear is likely to be critical in concrete flat plates supported directly on columns. The shear strength of prestressed concrete flat plates is governed by the more severe of the following two conditions:

- *beam-type* shear behavior with potential diagonal cracking failure along the plane of principal tension (Fig. 11.20*a*), and
- *punching shear* behavior with potential diagonal cracking failure along a truncated pyramid-shaped (or cone-shaped) surface around the column (Figs. 11.20*b* and 11.20*c*).

For beam-type shear, the plate is considered to act as a wide beam and the related shear design provisions are identical to those of beams covered in Sec. 6.8. In particular, the first critical section is taken at a distance $h/2$ from the face of the column and no shear reinforcement is needed unless v_u exceeds ϕv_c. Figure 11.21 illustrates the type of critical section along which beam type shear is to be evaluated. For comparison, the figure also illustrates sections for punching shear around different types of columns.

Because prestressed concrete flat plates generally contain some amount of nonprestressed flexural reinforcement at the critical sections, d_e will be used instead of d_p. Of course, $d_e = d_p$ for a fully prestressed section. Also often in slabs where similar concrete covers and reinforcement diameters are used, $d_s = d_p = d_e$.

When punching shear is considered, the critical section for design is taken at a periphery around the column, distant $d_p/2$ (or $d_e/2$ if both prestressed and nonprestressed reinforcement are used) from the face of the column. For such a case, the shear resistance of the concrete v_c is given by Eq. (11.10), which is very similar to Eq. (6.35), and shear reinforcement is provided if v_u exceeds ϕv_c.

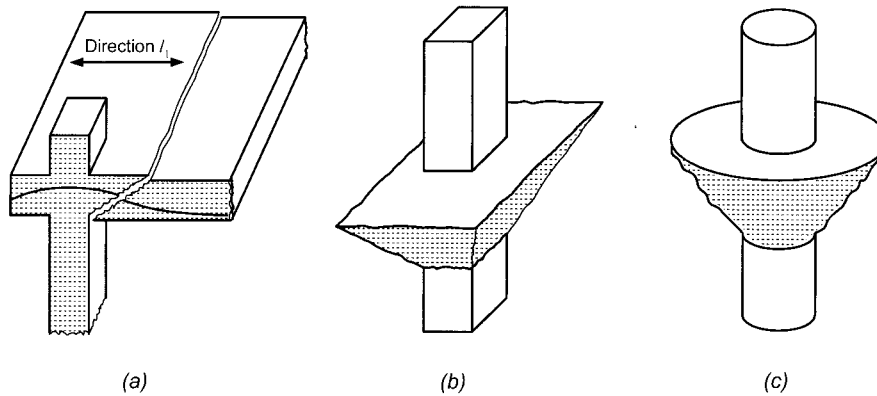

Figure 11.20 ***(a)*** **Beam-type failure.** ***(b)*** **Punching shear failure around rectangular column.** ***(c)*** **Punching shear failure around a round column.**

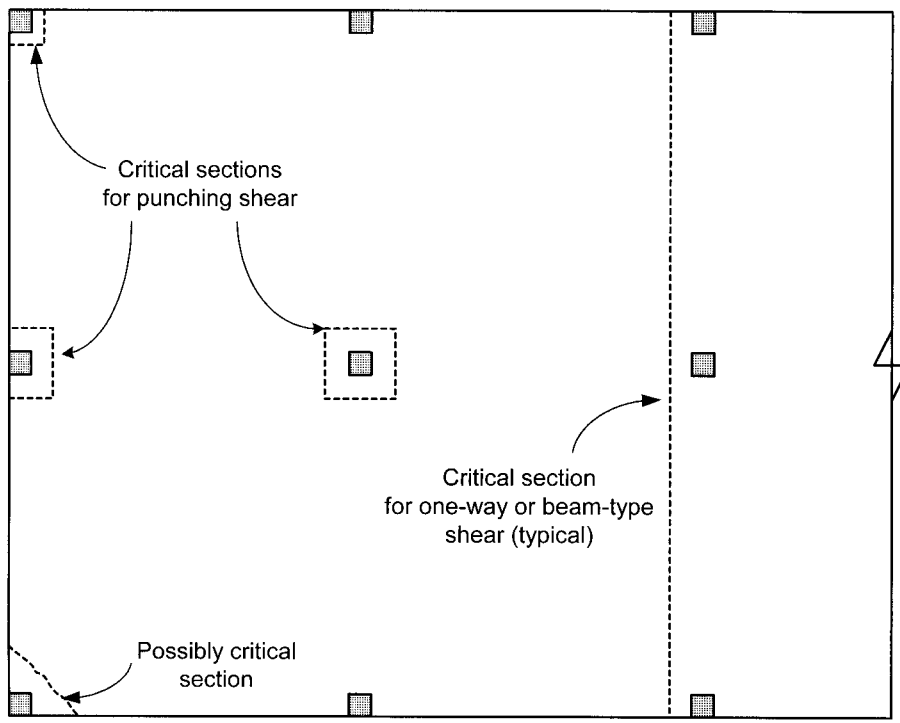

Figure 11.21 Critical shear sections to consider for design.

Prestressed Concrete Slabs. Article 11.12.2.2 of the ACI code [Ref. 11.2] specifies that the nominal punching shear capacity of concrete v_c can be taken equal to:

$$v_c = \beta_p \sqrt{f'_c} + 0.3\sigma_g + V_p / b_o d_e \quad \text{psi} \tag{11.10}$$

provided the following conditions are satisfied:

1. No portion of the column cross section shall be closer to a discontinuous edge than 4 times the slab thickness
2. The value of f'_c in Eq. (11.10) shall not be taken greater than 5 ksi (35 MPa)
3. The average prestress ($\sigma_g = F/A_c$) in each direction of the slab shall not be less than 125 psi (0.86 MPa), nor be taken greater than 500 psi (4.3 MPa).

In Eq. (11.10), σ_g is the average precompression in the direction of moment transfer, b_o is the perimeter of the critical section considered for punching shear, and V_p is the shear carried through the critical section by the tendons (vertical component of the prestressing force carried by the tendons passing through the critical section). V_p can be conservatively neglected in a preliminary design. The coefficient β_p is given by:

$$\beta_p = \text{smaller of} \begin{cases} 3.5 \\ 1.5 + \dfrac{\alpha_s d_e}{b_o} \end{cases}$$

$$\alpha_s = \begin{cases} 40 \text{ for interior columns} \\ 30 \text{ for edge columns} \\ 20 \text{ for corner columns} \end{cases} \tag{11.11}$$

The value of v_c in Eq. (11.10) reflects the type of failure (diagonal tension or punching shear) observed in tests. The computation of average compression ($\sigma_g = F/A_c$) may necessitate taking into consideration the loss of prestress due to restraint of the slab by shear walls or other structural elements, especially if its value exceeds about 300 psi (2.6 MPa).

Note that Eq. (11.10) is similar to Eq. (11.12) ACI code, or Eq. (6.35) in this text) for v_{cw} used to estimate the web-shear cracking resistance of prestressed beams, except that for beams, the factor $\beta_p = 3.5$.

If the conditions of application of Eq. (11.10) are not satisfied, the value of v_c is taken as for nonprestressed slabs.

Nonprestressed Slabs. For nonprestressed construction, the punching shear capacity, v_c, is given by (see article 11.12 of ACI code):

$$v_c = \text{smallest of} \begin{cases} \left(2 + \dfrac{4}{\beta_c}\right)\sqrt{f'_c} \\ \left(2 + \dfrac{\alpha_s d_e}{b_o}\right)\sqrt{f'_c} \\ 4\sqrt{f'_c} \end{cases} \quad \text{psi} \qquad (11.12)$$

where β_c is the ratio of long side to short side of column or concentrated load or reaction area, and α_s is as defined in Eq. (11.11).

To determine the need for shear reinforcement, the concrete shear resistance v_c is to be compared with the factored sum of vertical and torsional shear stress due to applied loads. Vertical shear stress is generated by the direct shear force acting at the centroid of the critical section, or support reaction. Torsional shear stress is generated by moment transfer between column and slab, as described next.

11.11.2 Transfer Moment Between Columns and Slab

When a rigid connection exists between columns and slab, bending moments are transferred from slab to columns and vice-versa. Such moments are mainly generated by pattern loadings, lateral loadings due to winds and earthquakes, and temperature movements. Typical examples of transfer moments are shown in Fig. 11.22, where a moment diagram for the slab is plotted; for clarity, moment diagrams for the columns for the loading considered are not shown. It can be observed, for instance, that at the exterior column (or joint), the transfer moment is equal to the moment in the slab, while at the interior column the transfer moment is equal to the difference between the moment on the left side and the right side of the support. Essentially, at each support (or joint) the transfer moment is equal to the sum of moments taken by the columns. Note that the term *unbalanced moment* is also often used to imply *transfer moment.* However, to avoid confusion with the moment due to the unbalanced load, solely the term *transfer moment* is used in this chapter.

Based on tests of reinforced concrete slabs [Refs. 11.18 to 11.20], the ACI code recognizes that a fraction, γ_f (f for flexure), of the moment is transferred by flexure across the perimeter of the critical section, while the remainder (that is, $\gamma_v = 1 - \gamma_f$) is transferred by eccentricity of the shear about the centroid of the critical section. It is believed that a similar behavior prevails in prestressed concrete flat plates [Refs. 11.17, 11.38].

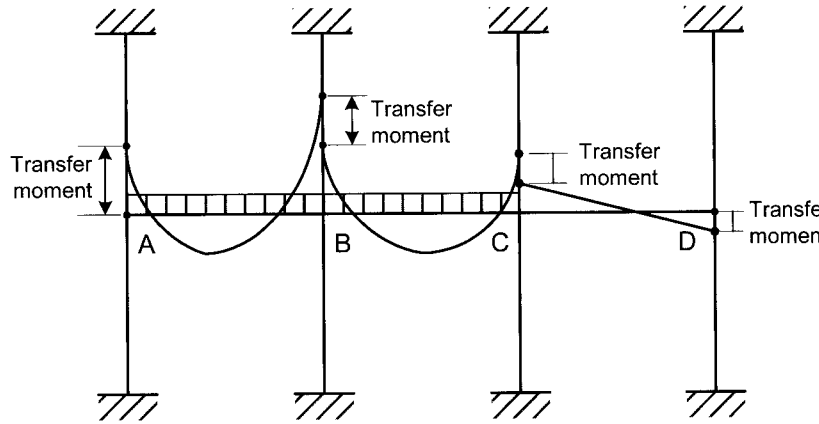

Figure 11.22 Example of transfer moment (moment diagrams for columns not shown).

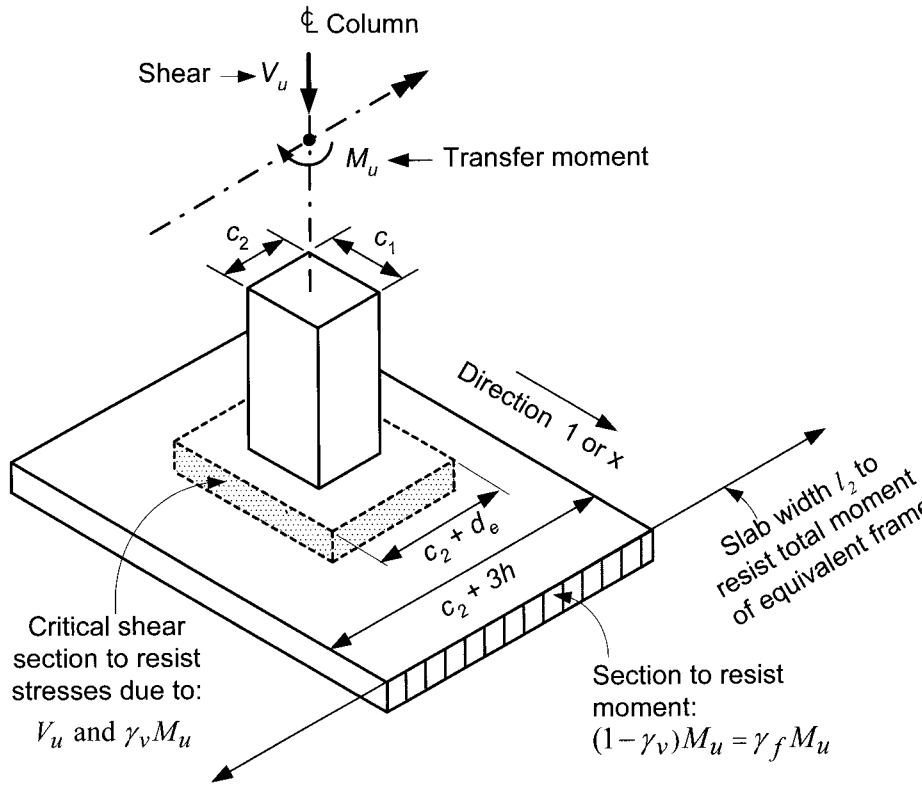

Figure 11.23 Critical shear section around an interior column (M_u refers to factored transfer moment).

Assuming a typical interior column, the fraction of moment assumed transferred by shear is given in Sections 11.12.6 and 13.5.3 of the ACI code by:

$$\gamma_v = 1 - \gamma_f = 1 - \frac{1}{1 + \frac{2}{3}\sqrt{\frac{c_1 + d_e}{c_2 + d_e}}} \tag{11.13}$$

where γ_f is the fraction of moment transferred by flexure, $(c_2 + d_e)$ is the width of the face of the critical shear section, and $(c_1 + d_e)$ is the width of the face at right angle to $(c_2 + d)$ (Fig. 11.23). The shear critical section, which is considered to resist the fraction, γ_v, of transfer moment, is assumed perpendicular to the plane of the slab so that its perimeter b_o is a minimum but does not need to approach closer than $d_e/2$ from the perimeter of the column. A typical critical section for shear around an interior column is shown in Figs. 11.23 and 11.24*a*.

Since ultimate strength design is considered, the transfer moment and shear force are the factored values. They are first calculated from structural analysis at the centroid of the column or support. Assume they are designated as M_u and V_u. Then the fraction of moment transferred by shear, and the shear force are calculated at the centroid of the critical shear section as explained below for each type of column (interior, edge, or corner); maximum factored shear stresses are calculated in the critical shear section by super-posing the stresses due to both shear and moment. Note that although ultimate moment and shear forces are used, the stresses are computed as if they were elastic. Details for the cases of interior column, exterior edge column, and corner column are given next.

Note that the fraction of transfer moment, $\gamma_f M_u = (1 - \gamma_v) M_u$, transferred by flexure is considered to be transferred by the ultimate resisting moment of a portion of slab taken between lines that are $1.5h$ (Fig. 11.23) outside opposite faces of the column (or capital, if any). This may require additional nonprestressed reinforcement in that portion of slab.

11.11.3 Maximum Shear Stress in Critical Section

Interior Column (Fig. 11.24*a*). For an interior column joint, the resulting maximum factored shear stress may be calculated from:

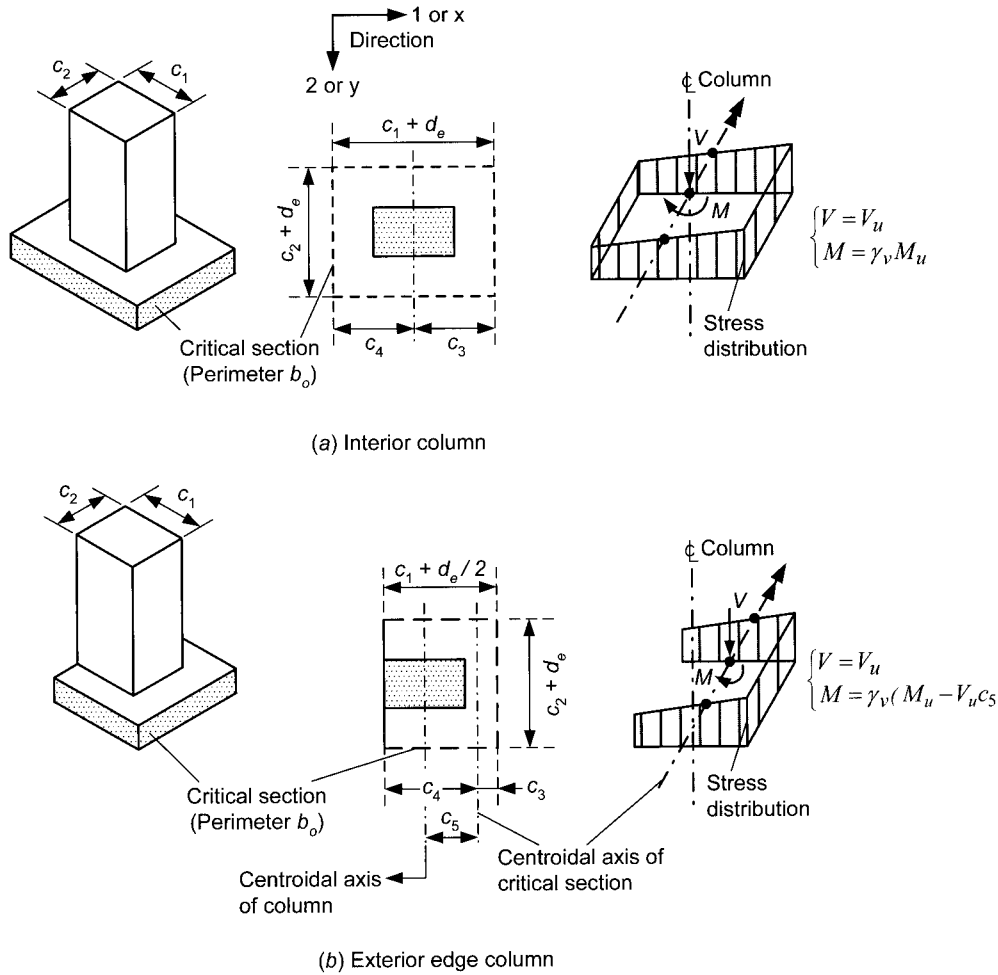

Figure 11.24 Typical shear stress distribution. ***(a)*** **Around an interior column.** ***(b)*** **Around an exterior column.**

$$v_u = \text{the larger of} \begin{cases} \dfrac{V_u}{A_c} + \dfrac{\gamma_v M_u c_3}{J_c} \\ \text{and} \\ \dfrac{V_u}{A_c} - \dfrac{\gamma_v M_u c_4}{J_c} \end{cases} \qquad (11.14) \text{ and } (11.15)$$

where γ_v is given by Eq. (11.13), A_c is the area of the assumed critical section, and J_c is its polar moment of inertia. Referring to Fig. 11.24*a*, it can be easily shown that for an interior column:

$$A_c = b_o d_e = 2(c_1 + c_2 + 2d_e)d_e \tag{11.16}$$

$$J_c = \frac{d_e(c_1 + d_e)^3}{6} + \frac{(c_1 + d_e)d_e^3}{6} + \frac{d_e(c_2 + d_e)(c_1 + d_e)^2}{2} \tag{11.17}$$

$$c_3 = c_4 = (c_1 + d_e)/2 \tag{11.18}$$

where b_o is the perimeter of the critical shear section.

Exterior Edge Column. A similar set of equations can be derived for the case of exterior edge columns. Referring to Fig. 11.24*b*, where the critical shear section of an exterior edge column is shown, the following expressions are obtained:

$$\gamma_v = 1 - \frac{1}{1 + \frac{2}{3}\sqrt{\frac{c_1 + d_e/2}{c_2 + d_e}}} \tag{11.19}$$

$$A_c = b_o d_e = (2c_1 + c_2 + 2d_e)d_e \tag{11.20}$$

$$c_3 = \frac{d_e\left(c_1 + \frac{1}{2}d_e\right)^2}{A_c} \tag{11.21}$$

$$c_4 = \left(c_1 + \frac{1}{2}d_e\right) - c_3 \tag{11.22}$$

$$c_5 = c_4 - \frac{c_1}{2} \tag{11.23}$$

$$J_c = \frac{(c_1 + d_e/2)d_e^3}{6} + \frac{2d_e\left(c_3^3 + c_4^3\right)}{3} + d_e(c_2 + d_e)c_3^2 \tag{11.24}$$

In determining maximum factored shear stresses for the case of an exterior column, the values of moment and shear are assumed taken at the centroid of the shear critical section. Hence, the moment at the critical section is equal to the transfer moment at the centroid of the column, M_u, minus $V_u c_5$ where V_u is the shear force, and c_5 is the distance from the centroid of the column to the centroid of the critical section (Figs. 11.24*b* and 11.25). Thus, the maximum shear stress is computed from:

$$v_u = \text{ the larger of } \begin{cases} \dfrac{V_u}{A_c} + \dfrac{\gamma_v(M_u - V_u c_5)c_3}{J_c} \\ \text{and} \\ \dfrac{V_u}{A_c} - \dfrac{\gamma_v(M_u - V_u c_5)c_4}{J_c} \end{cases} \tag{11.25) and (11.26}$$

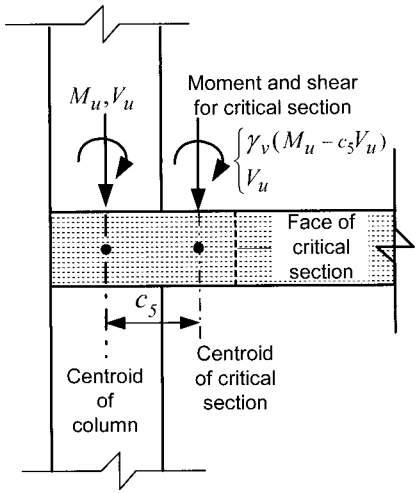

Figure 11.25 Transfer moment and shear force at centroid of column and critical shear section of an edge column.

Corner Column. For corner columns (Fig. 11.26), it is likely that shear stresses due to the combination of bending moments in the two primary directions will control. In such a case, the two directions will be identified as *1* or *x* and *2* or *y* with related subscript for each variable. The maximum factored shear stress at the extreme edges (A, B, and D in Fig. 11.26) is obtained from, respectively:

$$v_u = \text{the larger of} \begin{cases} v_{u(A)} = \dfrac{V_u}{A_c} + \dfrac{\gamma_{vx}(M_{ux} - V_u c_7)c_3}{J_{c_x}} + \dfrac{\gamma_{vy}(M_{uy} - V_u c_8)c_5}{J_{c_y}} & (11.27) \\ v_{u(D)} = \dfrac{V_u}{A_c} + \dfrac{\gamma_{vx}(M_{ux} - V_u c_7)c_3}{J_{c_x}} + \dfrac{\gamma_{vy}(M_{uy} - V_u c_7)c_6}{J_{c_y}} & (11.28) \\ v_{u(B)} = \dfrac{V_u}{A_c} + \dfrac{\gamma_{vx}(M_{ux} - V_u c_7)c_4}{J_{c_x}} + \dfrac{\gamma_{vy}(M_{uy} - V_u c_8)c_5}{J_{c_y}} & (11.29) \end{cases}$$

in which:

$$A_c = b_o d_e = (c_1 + c_2 + d_e)d_e \qquad (11.30)$$

$$c_3 = \frac{(c_1 + d_e/2)^2}{2A_c}; \quad c_5 = \frac{(c_2 + d_e/2)^2}{2A_c} \qquad (11.31) \text{ and } (11.32)$$

$$c_4 = c_1 + \frac{d_e}{2} - c_3; \quad c_6 = c_2 + \frac{d_e}{2} - c_5 \qquad (11.33) \text{ and } (11.34)$$

$$c_7 = \frac{(c_1 + d_e)}{2} - c_3; \quad c_8 = \frac{(c_2 + d_e)}{2} - c_5 \qquad (11.35) \text{ and } (11.36)$$

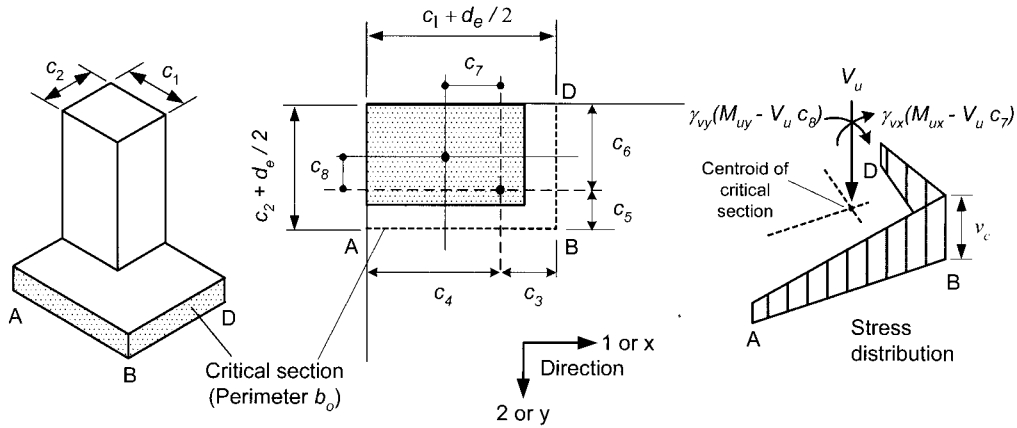

Figure 11.26 Critical shear section for corner column.

$$\gamma_{vx} = 1 - \frac{1}{1 + 2/3\sqrt{\left(\dfrac{c_1 + d_e/2}{c_2 + d_e/2}\right)}} \tag{11.37}$$

$$\gamma_{vy} = 1 - \frac{1}{1 + 2/3\sqrt{\left(\dfrac{c_2 + d_e/2}{c_1 + d_e/2}\right)}} \tag{11.38}$$

$$J_{c1} = \frac{d_e(c_1 + d_e/2)^3}{12} + \frac{(c_1 + d_e/2)d_e^3}{12} + (c_2 + d_e/2)d_e c_3^2 + (c_1 + d_e/2)d_e\left(\frac{c_1 + d_e/2}{2} - c_3\right)^2 \tag{11.39}$$

$$J_{c2} = \frac{d_e(c_2 + d_e/2)^3}{12} + \frac{(c_2 + d_e/2)d_e^3}{12} + (c_1 + d_e/2)d_e c_5^2 + (c_2 + d_e/2)d_e\left(\frac{c_2 + d_e/2}{2} - c_5\right)^2 \tag{11.40}$$

Round Columns. Equations can be theoretically derived for the case of round columns, similarly to what is shown above. However, the use of an equivalent square column, having the same cross-sectional area as the round column, is

generally acceptable. For round interior columns, the critical shear section has a cylindrical shape and the properties of the section are given as (Fig. 11.27):

$$\begin{cases} R = r + d_e/2 \\ b_o = 2\pi R \\ A_c = 2\pi R d_e \\ J_c = \pi R^3 d_e + \pi d_e^3 R/6 \end{cases} \tag{11.41}$$

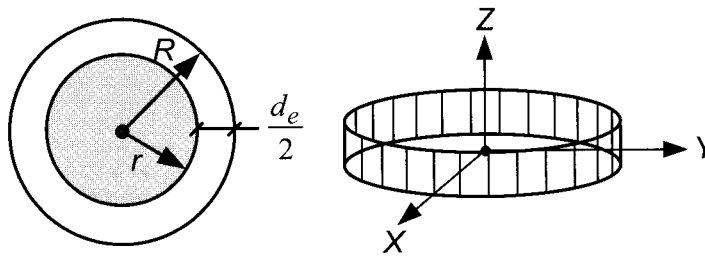

Figure 11.27 Critical punching shear section for a round interior column.

11.11.4 Design Tips

Typically for interior and exterior columns of an interior frame, the equivalent frame is symmetrical with respect to the longitudinal axis of the frame (line passing by the center of columns). In such a case, punching shear around the column is checked in either primary direction, one direction at a time. However, for corner columns and when the equivalent frame is not symmetrical with respect to the centerline of columns, punching shear should be checked for the combined effect of moments in the two directions. Moreover, for corner columns, the critical section for shear may take on different shapes, as suggested in Fig. 11.21.

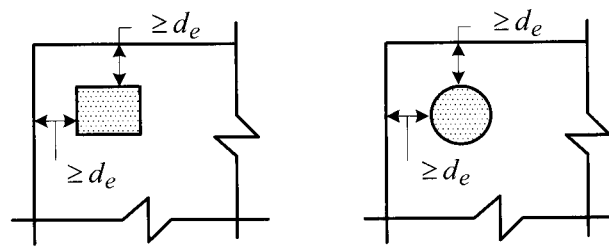

Figure 11.28 Good practice for corner and edge columns to better resist shear and torsional forces.

For corner columns in seismic regions where bending and torsion can be significant, it is good practice to extend the slab beyond the column, as shown in Fig. 11.28, in order to increase the size of the critical section and improve shear and torsional resistance.

It should be noted that, when the effect of moments from the two principal directions are combined, the shear force is preferably taken from the tributary area associated with the column, since adding shear forces obtained from the equivalent frame analysis in the two directions will lead to a fictitiously high shear force, as the design uniform load is taken at 100 percent in each direction.

11.11.5 Shear Reinforcement

Based on equivalent stresses, the design philosophy for shear follows the following general approach:

$$v_u \le \phi v_n = \phi(v_c + v_s) \tag{11.42}$$

and if $v_u \ge \phi v_c$, or $\frac{v_u}{\phi} \ge v_c$, then the shear reinforcement is designed to provide:

$$v_s \ge \frac{v_u}{\phi} - v_c \tag{11.43}$$

According to the ACI code, when the design shear stress, v_u, exceeds ϕv_c, v_c should be taken equal to $2\sqrt{f'_c}$ and shear reinforcement must be provided for the excess shear. The nominal shear resistance, v_n, given by Eq. (11.42) shall not be taken greater than $7\sqrt{f'_c}$ when shearhead reinforcement is used and $6\sqrt{f'_c}$ when bent bar reinforcement are used. Thus, the contribution of shear reinforcement, v_s, is limited to $4\sqrt{f'_c}$ for bent bars or $5\sqrt{f'_c}$ for shearheads. Note that, for cost reasons, stirrups are not recommended in slabs; however, should there be a justified need to use stirrups, the provisions of Chapter 6 can be used to determine the area of stirrup reinforcement.

Shearhead reinforcement consists of standard *I* or channel-shaped steel beams embedded in the slab and extending beyond the column faces. They serve to increase the perimeter of the critical section for shear (see ACI code commentary, Sec. 11.12.4.7) and contribute to the ultimate flexural resistance of the slab at the columns. Typical shearhead reinforcements are shown in Fig. 11.29*a*. The design of shearhead reinforcement is prescribed by Sec. 11.12.4 of the 2002 ACI code. The derivations of the corresponding equations are explained in Ref. [11.13].

When bent bar reinforcement is used, it is generally placed along the centerline of the column strip in each direction (Fig. 11.29*b*). Assuming an angle of inclination, α, at the critical section, it can easily be shown that the area of bent bar

reinforcement crossing the critical section can be obtained from the following equation, given in Sec. 11.5.6.5 of the ACI code:

$$A_v = \frac{V_s}{f_y \sin \alpha} \tag{11.44}$$

where f_y is the yield strength of the bent bar reinforcement and V_s is the shear force resisted by the reinforcement.

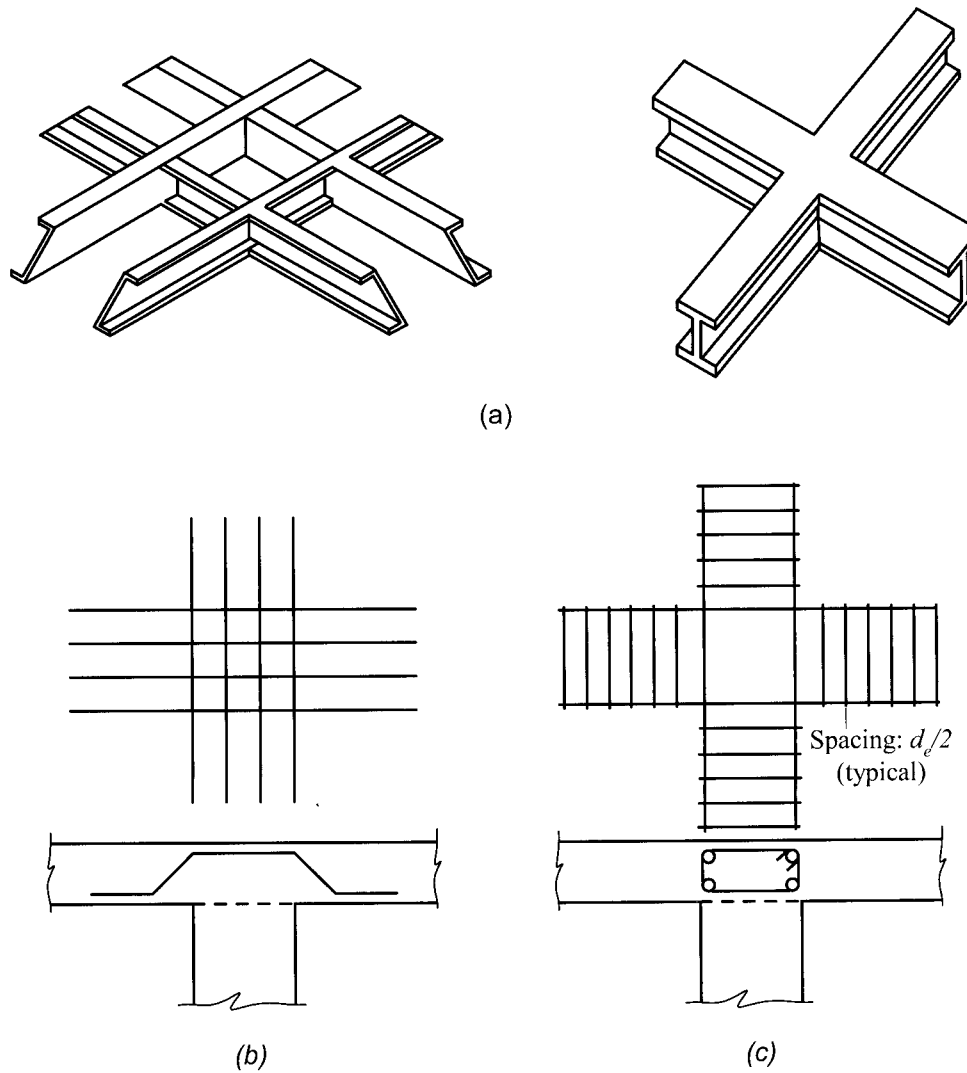

Figure 11.29 Typical shear reinforcement for two-way slabs. ***(a)*** **Shearheads made out of steel channels, or I beams.** ***(b)*** **Bent bars. (*c*) Beam-type stirrups.**

Equation (11.44) assumes a single group of parallel bars all bent up at the same distance from the support, as shown in Fig. 11.29*b*, and the value of V_s can be determined from:

$$V_s = \left(\frac{v_u}{\phi} - v_c \right) A_c \leq 4\sqrt{f'_c}\, b_o d_e \qquad (11.45)$$

in which $\phi = 0.75$ for shear, b_o is the perimeter of the shear critical section, and A_c is given by either Eq. (11.16) or Eq. (11.20) or Eq. (11.30) depending to the type of column. Only the center three-fourths of the inclined portion of bent bars are considered effective and adequate anchorage of the bars is required.

11.12 DEFLECTION OF FLAT PLATES

Although deflection may often govern the design in reinforced concrete two-way flat plates, it is likely to be less critical in prestressed concrete flat plates subjected to relatively light live loads (less than 100 psf (4.8 kN/m^2)) and having span-to-depth ratios within the range recommended in Sec. 11.8. This is because generally: (1) due to load balancing by prestressing, the plate has zero deflection under dead load, hence, only the live load produces deflection, and (2) the concrete section is assumed uncracked under sustained load, thus leading to higher stiffness and lower deflection.

Deflection limitations specified in the ACI code and described for one-way slabs and beams in Table 7.1 also apply to two-way flat plates. In selecting the span length to apply in Table 7.1, support conditions must be defined. If the supports are stiff, such as in the case of a two-way slab supported by walls, the shorter span of the panel center-to-center of the supports (or column centerlines) is generally considered. This is because, when the ratio of long to short span increases, the slab tends to behave as a one-way slab in the shorter direction for which the shorter span applies. On the other hand, when the two-way slab is supported by columns, such as in the case of flat plates, the longer span of the panel center-to-center of column centerlines, should be considered. This is because, when the ratio of long to short span increases, the slab tends to behave as a one-way slab in the longer direction for which the longer span applies.

The accurate calculation of deflections in two-way continuous slab systems can be very demanding computationally. Two- or three-dimensional finite element analysis is most suitable for such calculations. For a given slab and frame system, deflections are affected by loading patterns, support conditions, whether the slabs are cracked or not, and the short- and long-term properties of the concrete. However, a number of approximate methods are available to estimate deflections in flat plates. The most common ones are reviewed in a state-of-the-art report by ACI Committee 435 [Ref. 11.4]. Two of them are briefly described next. The first is essentially

based on the elastic analysis of thin plates, and the second is based on the equivalent-frame method. These methods are assumed sufficient in practice for most common designs. However, should they lead to deflection values close to permissible limits, more accurate methods can then be sought.

11.12.1 Elastic Solution

Timoshenko and Woinowsky-Krieger proposed a simplified solution to estimate deflections in typical rectangular panels having various support conditions and various ratios of long to short span [Ref. 11.44]. Assuming a typical column-supported panel with a column size considered small in comparison to the column spacing, they derived the following deflection expression for a uniformly loaded flat plate system:

$$\Delta_i = k\frac{wl_a^4}{E_c h^3} \tag{11.46}$$

where:

Δ_i = instantaneous deflection assuming short-term loading

l_a = longer span of panel center-to-center of supports

k = coefficient depending on both the ratio of long span l_a to short span l_b of the panel and the Poisson's ratio of the concrete

Tables were developed for the numerical values of the coefficient, k, depending on long to short span ratio, loading patterns, and the Poisson's ratio. Equation (11.46) must be dimensionally correct. Hence, if E_c is in pounds per square inch, h in inches, and l in inches, w should be given in pounds per square inch.

For a continuous flat plate supported by columns, the maximum deflection, assuming alternate bay loading, leads to a value of k of the order of 0.11. Tests on four-panel prestressed concrete flat plates with various boundary conditions have indicated actual values of k of 0.148 [Ref. 11.43] and 0.095 [Ref. 11.29]. These are not too different from the theoretical value of 0.11. Moreover, as a first approximation one can use the following heuristic rule, derived by the author from inspecting the numerical values of the coefficient, k, in the given tables: k decreases almost linearly to about 50 percent of its value when the long-to-short-span ratio of the panel increases from one to two. In some cases Eq. (11.46) may represent a rough approximation. However, a more accurate analysis will be needed only if the calculated deflection is close to the allowable deflection.

In summary, Eq. (11.46) can be used assuming elastic analysis and, unless tables of coefficients are available, the following approximate prediction of the coefficient k is suggested:

$$k = 0.11(1.5 - 0.5\frac{l_a}{l_b}) \text{ for rectangular panels in which } 1 \le \frac{l_a}{l_b} \le 2 \qquad (11.47)$$

Remarks

1. Equation (11.46) implies a rectangular slab of a unit width. In correlating this equation with common deflection formulae, it should be noted that the gross moment of inertia of a rectangular section is $I_g = bh^3/12$, and for $b = 1$, then $I_g = h^3/12$. The coefficient 12 is integrated in the value of k.
2. Equation (11.46) assumes uncracked section. This is mostly the case in prestressed slabs because of load balancing of the dead load. However, should cracking occur under live load, then the effective moment of inertia, I_e, (see Chapter 7) could be used instead of I_g. As a first approximation, I_e can be estimated as $0.4I_g$.
3. Equation (11.46) assumes alternate bay loading. If the longer span, l_a, becomes twice l_b, the coefficient k decreases to 50 percent of its value as per Eq. (11.47); also, the deflection calculated using alternate bay loading becomes very close to that using checker loading. At l_a/l_b ratios larger than one, and for various number of spans and boundary conditions, it is not clear if the deflection calculated by checker loading is more or less critical than that with alternate bay loading. Moreover, at high l_a/l_b ratios, the slab tends to become close to a one-way slab for which a value of k higher than that predicted by Eq. (11.47) is expected, as described next. Note that with checker loading of a one-way slab, half the area of the slab will not be loaded. The reader may want to draw a plan view of the slab with the loading pattern to see how the slab gets half the load at the limit.
4. If the longer span l_a keeps increasing with respect to l_b, eventually the slab becomes a one-way slab in the longer direction, l_a. The instantaneous maximum elastic deflection of a continuous slab with alternate spans loaded is equal: $\Delta_i \simeq 0.01\left(wl_a^4/E_cI\right)$ (Chapter 10). For $b = 1$, $I_g = h^3/12$, and the deflection becomes $\Delta_i = 0.12\left(wl_a^4/E_ch^3\right)$. This expression is not too different from the maximum deflection given by Eq. (11.46). However, the loading for which it occurs may be different.
5. Surprisingly, as a general conclusion, the maximum deflection formulae for one-way or two-way slabs of same span length are not too different, although they may occur for different critical loadings and boundary conditions.

11.12.2 Equivalent Frame Approach

The deflection of flat plates can also be estimated from the equivalent-frame method, which essentially applies to all types of two-way slabs, reinforced or prestressed.

The method is described in more detail in Refs. [11.4, 11.31, 11.33, 11.42, 11.49]. The main steps of the procedure are summarized as follows.

- A typical slab panel bounded by column centerlines is considered.
- The panel is analyzed in each of the main directions as if it was part of a one-way slab system (or equivalent frame) having non-yielding support lines along column centerlines.
- The mid-panel deflections, one for each direction, are computed and added to obtain the total deflection.

The assumed deflected shape of the panel in each direction and the resulting deflected surface are illustrated in Figs. 11.30*a* to *c*. Although a panel bounded by column centerlines was used to explain the procedure, actual computations for each direction are undertaken using the same slab and column strips and corresponding distribution of moments as defined in Sec. 11.7 for the equivalent-frame method. Thus, the mid-panel deflection is obtained as the sum of the midspan deflection of the column strip in one direction and the midspan deflection of the middle strip in the other direction, that is:

$$\begin{cases} \Delta_i = \Delta_{cx} + \Delta_{my} \\ \text{or} \\ \Delta_i = \Delta_{cy} + \Delta_{mx} \end{cases} \qquad (11.48) \text{ and } (11.49)$$

where Δ_i is the instantaneous elastic short-term deflection, and the subscripts c, m, x, and y are for column strip, middle strip, x direction, and y direction, respectively (Fig. 11.30*c*). The mid-panel deflection should essentially be the same whether calculated from Eq. (11.48) or Eq. (11.49). However, a difference will generally exist due to the approximate nature of the analysis.

As the main contribution to the deflection comes from the longer span, it is recommended to use, for a typical interior panel, the column strip in the long direction and the middle strip in the short direction [Ref. 11.31]. This is shown schematically in Fig. 11.31.

As the equivalent frame method leads to the moments in one direction or the other, deflection components such as Δ_{cx} and Δ_{my} can easily be calculated using the second moment area theorem (see Sec. 7.3) and assuming parabolic moment diagrams between supports.

The deflections calculated from Eqs. (11.48) and (11.49) are the instantaneous elastic short-term deflections assuming a uniformly applied load. For a sustained load, the additional long-term deflection due to creep must also be considered in a manner similar to beams and one-way slabs. For two-way slabs, the additional long-term deflection usually is taken equal to the instantaneous elastic deflection multiplied by a factor of 2.

An example illustrating deflection computations is covered in Section 11.14. Experimental data on prestressed concrete flat plates, including deflection measurements, can be found in Refs. [11.7, 11.8, 11.10, 11.20, 11.37, 11.43].

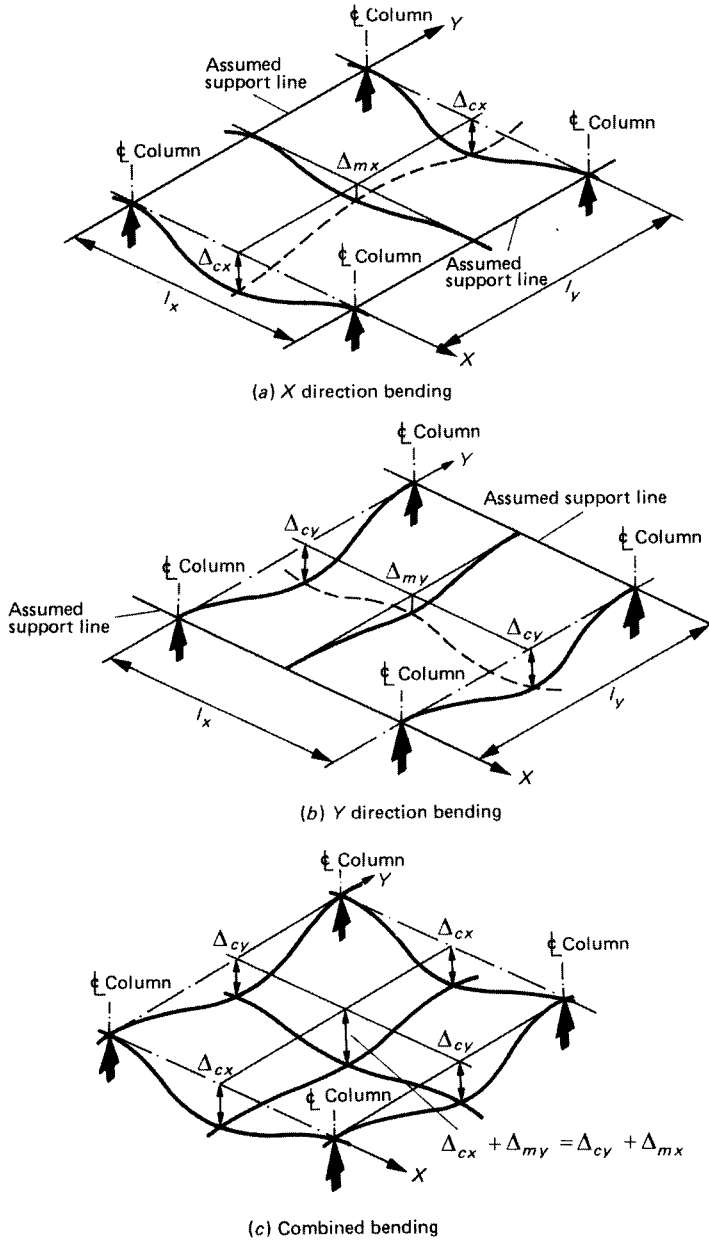

Figure 11.30 Deflected surface of flat plate. ***(a)*** **Assuming bending in the *x* direction only.** ***(b)*** **Assuming bending in the *y* directly only.** ***(c)*** **Assuming bending in two directions.** *(Ref. 11.4, Courtesy American Concrete Institute.)*

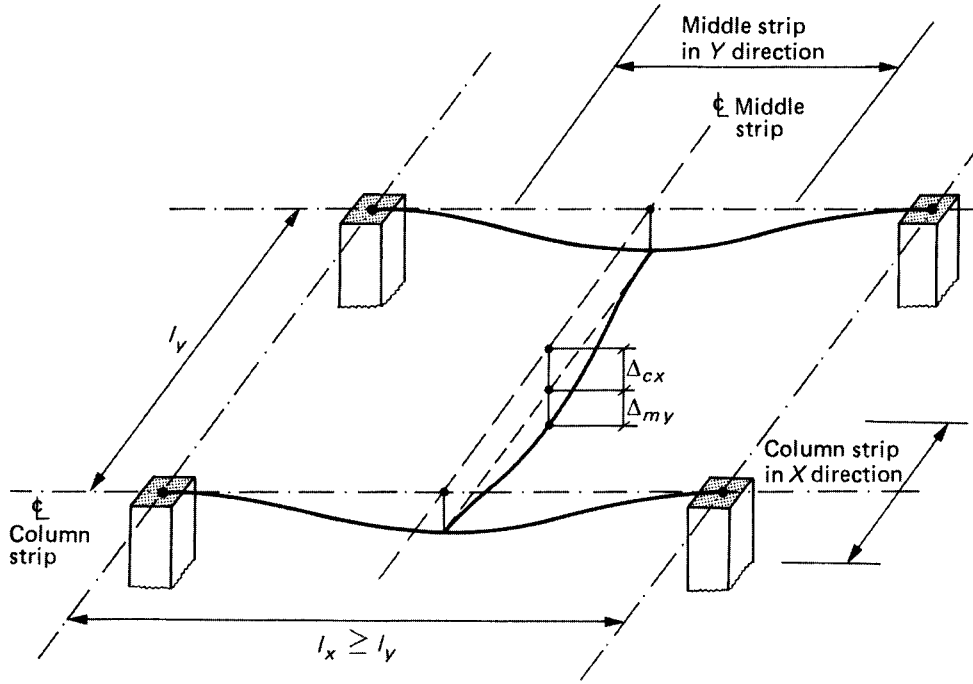

Figure 11.31 Determination of mid-panel deflection by the equivalent-frame method showing preferred selection of column strip for the longer span.

11.13 SUMMARY OF DESIGN STEPS FOR TWO-WAY PRESTRESSED FLAT PLATES

A summary of the major design steps for two-way flat plates and the corresponding sections dealing with them is given next:

1. Proportion slab thickness based on span-to-depth ratios and fire endurance requirements (see Sections 11.1.1 and 11.9). In selecting a depth, keep in mind that the punching shear resistance, particularly at edge and corner columns, can be critical.
2. Define for each principal direction the frame or frames equivalent to the slab system considered (see Section 11.7).
3 For each equivalent frame, use the load-balancing approach to determine the prestressing force. The load to be balanced should preferably include the entire dead load. Compute average prestress and compare with the average prestress values suggested in Section 11.9.3 (see also Section 10.13).

4. Analyze the equivalent frame for the unbalanced load and determine corresponding moments and stresses.
5. Superpose to the actual average uniform stress (resulting from balanced load and prestress) the stresses due to the unbalanced load, and compare the resulting stresses with allowable stresses (see Section 11.10). This should be done not only for the entire frame width, but also for the column strip and middle strip separately.
6. Determine minimum nonprestressed ordinary reinforcement, if required (Section 11.10.3).
7. Detail tendon and bar layout and check if spacing and cover requirements are satisfied (see Section 11.7).
8. Check ultimate flexural strength requirements (see Sections 11.10.2 and 10.14).
9. Check shear, both one-way shear and punching shear, and provide shear reinforcement if needed (see Section 11.11). It is generally preferred to avoid putting shear reinforcement in flat plate slabs; shear resistance can be overcome by increasing the slab thickness, or the prestress level, or the size of the columns.
10. Compute deflection and compare with deflection limitations (see Section 11.12).

It was pointed out earlier that the effect of smoothing the tendon profile over the supports after load balancing is generally neglected in slabs. It may be necessary to estimate this effect in some cases. For this, the equivalent load due to prestressing for the new tendon profile is determined and the equivalent frame is analyzed for that load. The moments obtained are compared with the primary moments due to prestressing. The difference, if any, at any section represents the secondary moments. If the secondary moments are relatively significant (say more than 10 percent of the primary moment), they should then be accounted for in both the computation of stresses and the strength design moment where they are included with a factor of 1.

If, in the above steps, one of the design criteria is not satisfied, the design should be revised or refined as needed.

11.14 EXAMPLE: DESIGN OF A TWO-WAY PRESTRESSED FLAT PLATE

Consider the prestressed concrete flat plate floor system with square panels shown in Fig. 11.32. It is proposed for an office building and utilizes unbonded tendons. The columns are 30 ft apart, center-to-center in each direction. Their cross section is given in Fig. 11.32. The story height is typically 12 ft center-to-center of slab floor. A design live load of 80 psf is specified. The superimposed dead load due to flooring and partitions is assumed equivalent to a uniform load of 25 psf.

Let us provide a preliminary design for a typical interior frame taken along the short direction (North-South) of the slab (shaded area of Fig. 11.32). This N-S frame is more critical for the slab shown than the interior E-W frame. The following information is provided: normal weight concrete with $\gamma_c = 150$ pcf, $f'_c = 5000$ psi, $f'_{ci} = 4000$ psi, $E_c = 4.28 \times 10^6$ psi; unbonded strands with a

diameter of 0.6 in, $f_{pu} = 270$ ksi, $f_{pe} = 160$ ksi, cross section area of one strand = 0.217 in^2; concrete cover to center of strands = 1.25 in.

Using a span-to-depth ratio of 40 for a slab without drop panels leads to a slab depth $h = 9$ in with a dead weight $w_G = 112.5$ psf.

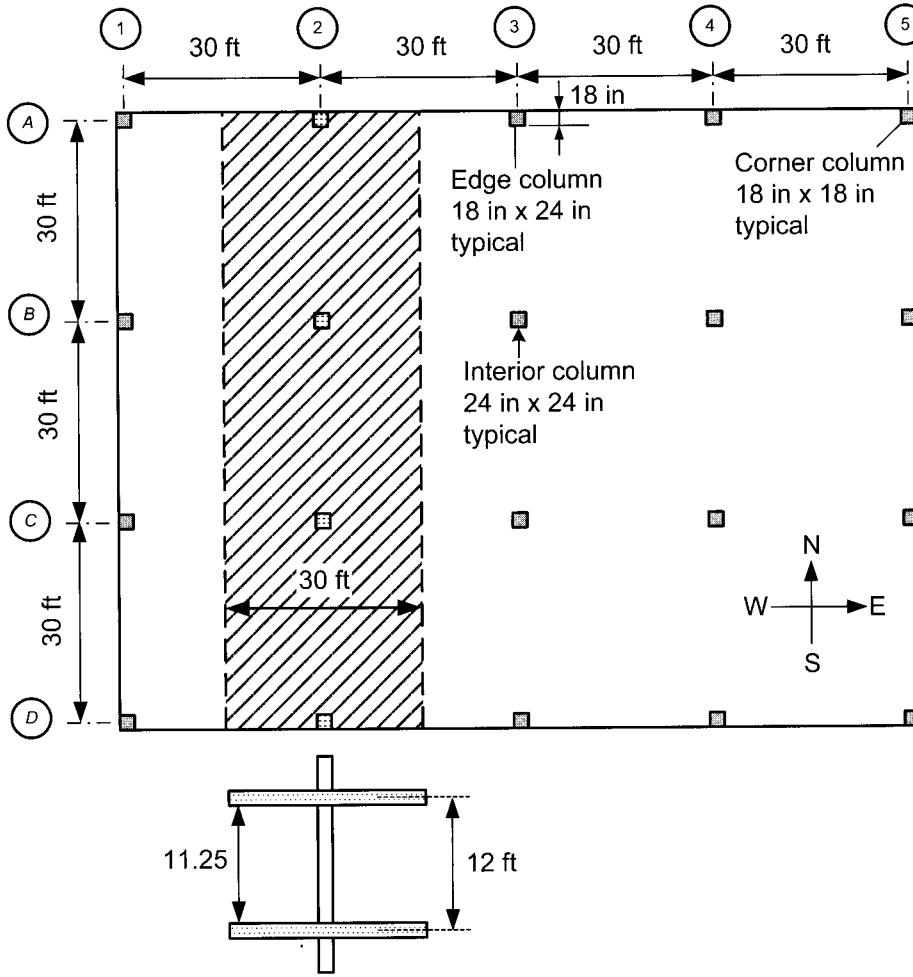

Figure 11.32 Flat plate of Example, Section 11.14.

1. Analysis of Moments and Shear Forces

For illustration, the moment distribution method is used to determine moments and shears. Alternatively, a structural software can be used for the computations; however, one has to be careful about how to include, at each joint, the effect of attached torsional member. For the moment distribution, member stiffness, distribution factors, and fixed-end moments are needed at each joint.

Theoretical values of stiffness will be used, assuming center-to-center spans for the slab, and clear spans for the columns. The stiffnesses are given by:

Slab $$K_s = \frac{4E_c I}{l} = \frac{4E_c \times 12 \times 30 \times 9^3}{12 \times 12 \times 30} = 243E_c$$

Interior column $K_c = \dfrac{4E_c I}{l} = \dfrac{4E_c \times 24 \times 24^3}{12 \times 12 \times 11.25} = 819.2E_c$

Edge column $K_c = \dfrac{4E_c \times 24 \times 18^3}{12 \times 12 \times 11.25} = 345\ 6E_c$

The stiffness of the torsional member (slab strip) attached to an interior column is given by Eq. (11.6) in which the torsional constant C is given by Eq. (11.7). Hence:

$$C = \left(1 - 0.63\frac{x}{y}\right)\frac{x^3 y}{3} = \left(1 - 0.63\frac{9}{24}\right)\frac{9^3 \times 24}{3} = 4454.19 \text{ in}^4$$

$$K_t = \sum \frac{9E_c C}{l_2(1 - c_2/l_2)^3} = \frac{2 \times 9 \times E_c \times 4454.19}{30 \times 12(1 - 24/(30 \times 12))^3} = 273.92E_c$$

The stiffness of the equivalent interior column is obtained from Eq. (11.5):

$$\frac{1}{K_{ec}} = \frac{1}{\sum K_c} + \frac{1}{K_t} = \frac{1}{2 \times 819.2E_c} + \frac{1}{273.92E_c}$$

from which:

$$K_{ec} = 234.68E_c$$

K_{ec} is the stiffness of joint equivalent to the two columns above and below the slab and the attached torsional member. Similar calculations for the edge column lead to:

$$C = (1 - 0.63\frac{9}{18})\frac{9^3 \times 18}{3} = 2996.19 \text{ in}^4$$

$$K_t = \frac{2 \times 9 \times E_c \times 2996.19}{(30 \times 12)(1 - 24/(30 \times 12))^3} = 184.26E_c$$

$$K_{ec} = \frac{1}{2 \times 345.6E_c} + \frac{1}{184.26E_c} = 145.48E_c$$

The distribution factors at each joint defined by the ratio of stiffness $K_{ij}/\sum K_{ik}$ are calculated and shown in Fig. 11.33, where the moment distribution is run assuming a uniform dead load which includes the weight of the slab and the superimposed dead load. Its value is:

$$w_D = w_G + w_{SD} = (0.1125 + 0.025)30 = 4.125 \text{ klf}$$

The corresponding fixed-end moment is given by $-w_D l^2/12 = -309.38$ kips-ft. The moment distribution is also run assuming various pattern loadings of live load as shown in Fig. 11.34. The live load per linear foot width of frame is given by:

$$w_L = 0.080 \times 30 = 2.4 \text{ klf}$$

and the corresponding fixed-end moment is given by $-w_L l^2/12 = -180$ kips-ft.

The results of the analysis for the uniform dead load (Loading 1) and for four different patterns of live load (Loadings 2 to 5) are summarized in Figs. 11.33 and 11.35. Note that not only the moment at the centerline of columns, but also the moments at the face of columns, as well as the shear forces and the reactions are given. They provide a needed source of data for the design.

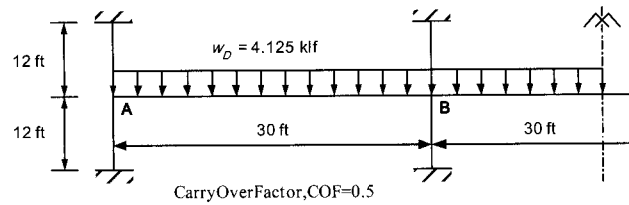

CarryOverFactor,COF=0.5

	Column below	Column above	Beam		Beam	Column below	Column above	Beam
DF	0.187	0.187	0.626		0.406	0.196	0.196	0.203
FEM kip-ft	-	-	309.38		-309.38	-	-	309.38
D	-57.85	-57.85	-193.67					
CO					-96.84			
D					39.32	18.98	18.98	19.66
CO			19.66					
D	-3.68	-3.68	-12.31					
CO					-6.16			
D					2.5	1.21	1.21	1.25
CO			1.25					
D	-0.23	-0.23	-0.78					
CO					-0.39			
D					0.16	0.076	0.076	0.079
CO								
⋮	⋮	⋮	⋮		⋮	⋮	⋮	⋮
Final moments, kip-ft	-61.75	-61.75	123.49		-370.59	20.27	20.27	330.50
Moments, * kip-ft	61.75	61.75	-123.49		-370.59	-20.27	20.27	-330.50

* Using sign convention of this text

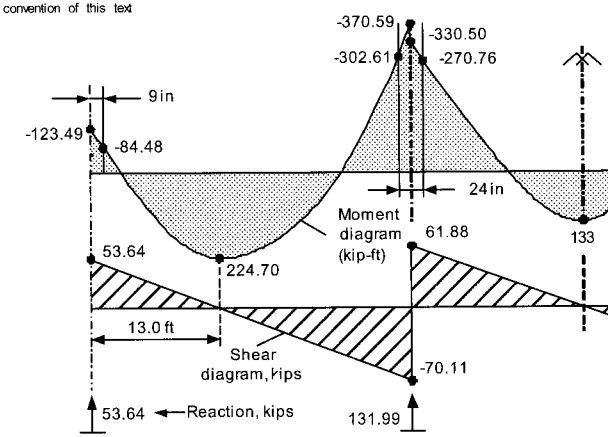

Figure 11.33 Moment distribution in the equivalent frame and corresponding shear forces and reactions under dead load.

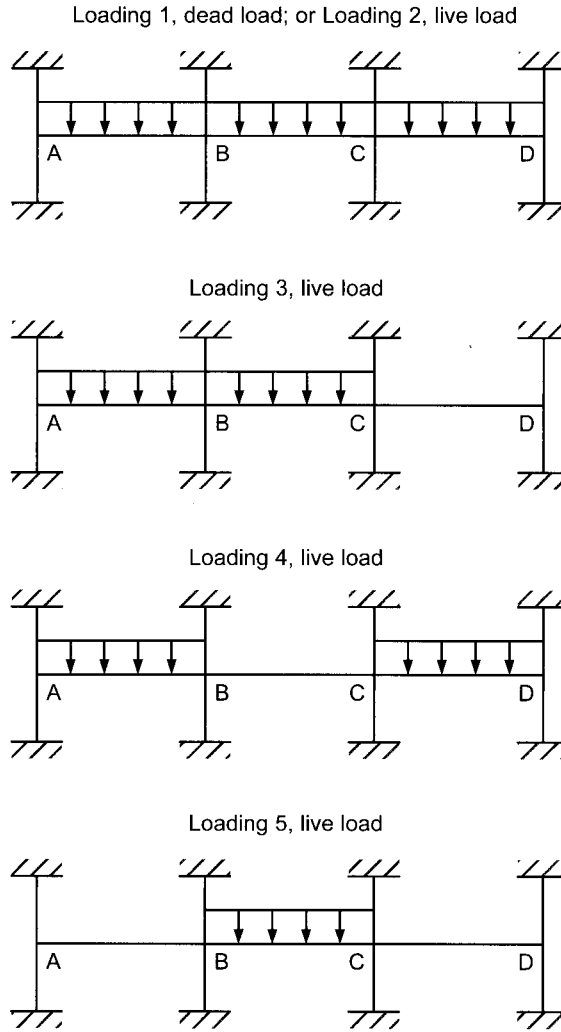

Figure 11.34 Patterns of live loadings for the equivalent frame of Example slab, Section 11.14.

A summary of most critical effects due to various loadings and combinations of loadings is given in Table 11.2. The unbalanced service moments (assuming unbalanced live load) are needed in the load-balancing method. Strength design moments (M_u=$1.2M_D$+$1.6M_L$) are needed for ultimate strength analysis and are taken at the face of the supports where applicable. The factored transfer moments and the corresponding loading reactions are taken at the centerline of columns. They are needed for shear design.

2. Load Balancing

Let us balance the entire dead load, that is, $w_b = w_D = 4.125$ klf. Assuming a cover of 1.25 in to the centroid of the tendons leads to a maximum sag $\delta_1 = 4.6$ inch in the exterior span and $\delta_2 = 6.5$ inch in the interior span (Fig. 11.36*a*). The required prestressing force for load balancing is controlled by the exterior span and is given by:

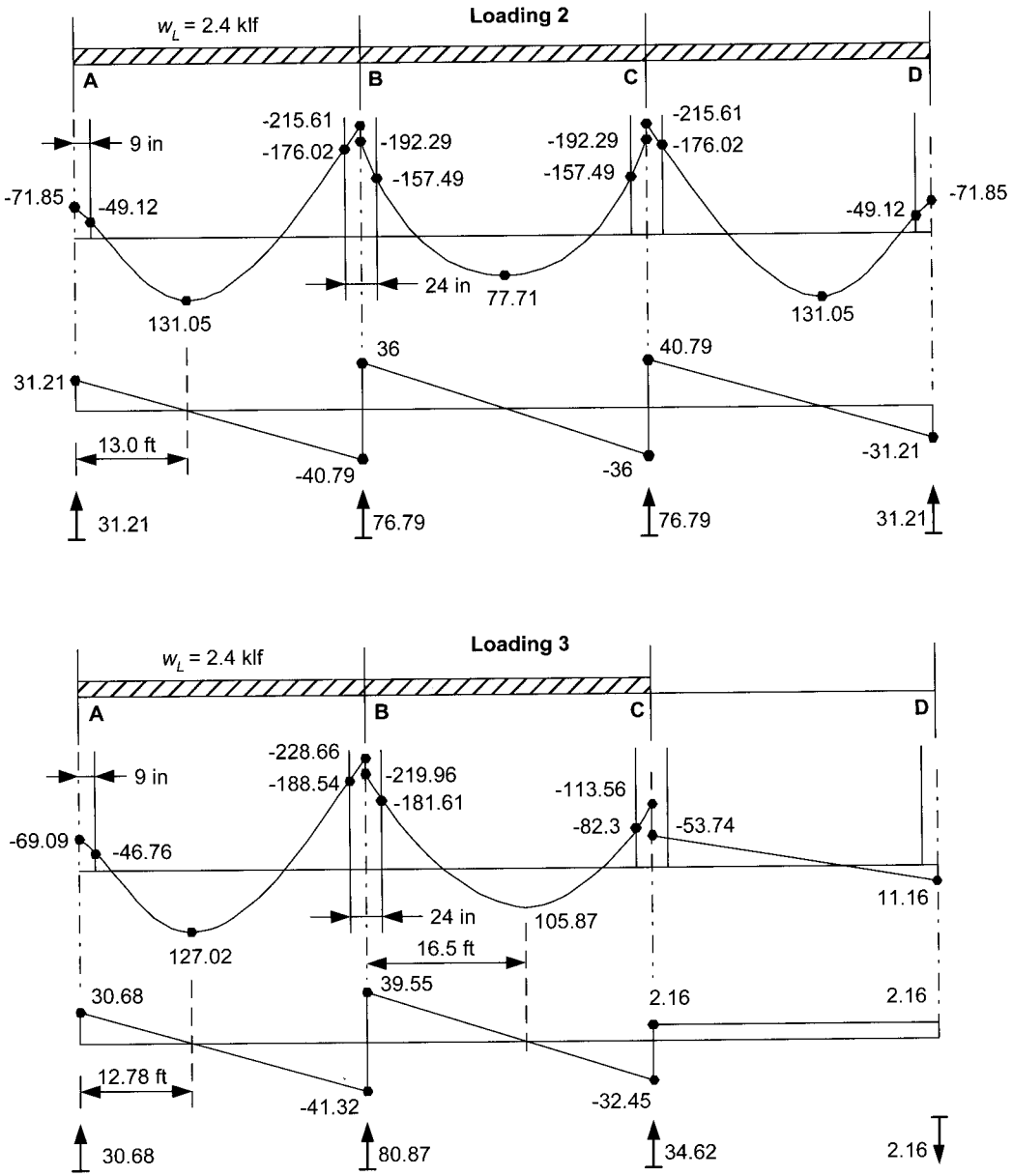

Figure 11.35 Moment diagrams, shear diagrams, and reactions in the equivalent frame for different live loadings.

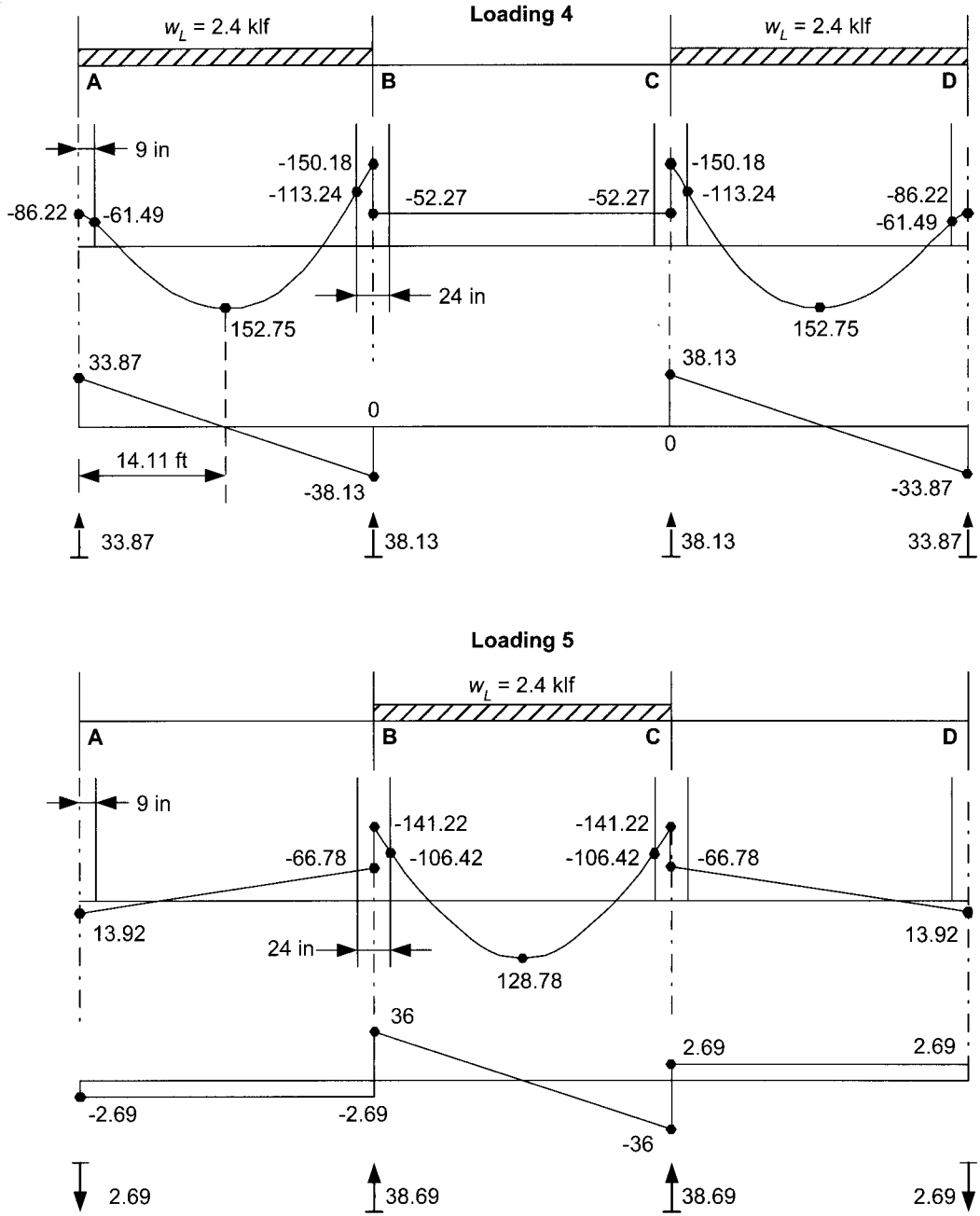

Figure 11.35 (continued) Moment diagrams, shear diagrams, and reactions in the equivalent frame for different live loadings.

Table 11.2 Maximum moments and support reactions of slab example of Section 11.14.

	Center-line exterior support	Exterior Span			Center-line first interior support	Interior Span	
		Face left support	Near midspan	Face right support		Face left support	Mid-span
Unbalanced moment, kips-ft:							
Loading 2: M_{nb}		-49.12	131.05	-176.07		-157.49	77.71
Loading 3: M_{nb}	.....	.....	.....	-188.54	.....	-181.61	.....
Loading 4: M_{nb}	.....	-61.49	+152.75	.....	.....	.....	.....
Loading 5: M_{nb}	.....	.....	.....	.....	.....	.....	128.78
Factored total moment, $1.2D + 1.6L$, kips-ft:							
Loading 1 + 3: M_u	.....	.....	.....	|-664.8|	.....	|-615.49|	.....
Loading 1 + 4: M_u	.....	|-199.76|	514.03	.....	.....		.....
Loading 1 + 5: M_u	.....	.....	.....	.....	.....	.....	365.65
Factored transfer moment, kips-ft, and reaction, kips:							
Loading 1 + 3, M_u	258.73	.....	.....	.....	62.03	.....	.....
Loading 1 + 3, R_u	113.46	.....	.....	.....	287.77	.....	.....
Loading 1 + 4, M_u	286.14	.....	.....	.....	204.76	.....	.....
Loading 1 + 4, R_u	118.55	.....	.....	.....	219.40	.....	.....

$$F = \frac{w_b l^2}{8\delta_1} = \frac{4.125 \times 30^2}{8 \times 4.6/12} = 1210.6 \text{ kips}$$

Note that a more exact prestressing force value could be obtained by using the sag at the midspan of the parabola, that is, $\delta_1 = 4.74$ in, which would lead to F=1174.8 kips). Although a smaller prestressing force could be used for the interior span, it is more economical to run the same tendons throughout the length of the slab, because there is only one interior span. Hence, to maintain load balancing, the sag in the interior span is reduced to $\delta_2 = \delta_1 = 4.6$ in. The ideal steel profile is shown in Fig. 11.36*a* while the actual profile can be as shown in Fig. 11.36*b*. It is assumed that the change in profile will not induce significant secondary moments.

Assuming a required force of 1210.6 kips, leads to the following number of strands:

$$N = \frac{1210.6}{0.217 \times 160} = 34.87 \simeq 35 \text{ strands}$$

Thirty-five strands provide a final prestressing force of 1215.2 kips. To achieve about 75 percent distribution in the column strip, 25 strands are placed in the 15-ft-wide column strip at about 7.5-in spacing and 10 strands in the 15-ft-wide middle strip at about 18-in spacing (Fig. 11.36*c*). The corresponding average prestress values are:

Column strip:

$$(\sigma_g)_c = \frac{25 \times 0.217 \times 160}{15 \times 12 \times 9} = 536 \text{ psi}$$

Middle strip:

$$(\sigma_g)_m = \frac{10 \times 0.217 \times 160}{15 \times 12 \times 9} = 214 \text{ psi}$$

Note that the average prestress for the whole slab strip is $\sigma_g = 375$ psi and is within practical range.

3. Service Stresses

Flexural stresses are due to the sum of uniform stress induced by load balancing and stresses generated by the unbalanced live load. It will be assumed that 75 percent of the moments are distributed to the column strip and the remainder to the middle strip.

The section moduli for each 15-ft-wide slab strip are given by:

$$Z_t = Z_b = \frac{bh^2}{6} = \frac{15 \times 12 \times 9^2}{6} = 2430 \text{ in}^3$$

Critical values of the unbalanced moment are given in Table 11.2. Stresses at the corresponding critical sections can be calculated separately for the column strip and the middle strip. For the column strip, they are given by:

Exterior span near midspan:

$$\sigma_t = (\sigma_g)_c + \frac{M}{Z_t} = 536 + \frac{0.75 \times 152.75 \times 12{,}000}{2430} = 1102 \text{ psi} < 0.45 f_c' \qquad \text{OK}$$

$$\sigma_b = (\sigma_g)_c - \frac{M}{Z_b} = 536 - 566 = -30 \text{ psi} > -2\sqrt{f_c'} \qquad \text{OK}$$

where the subscripts *t* and *b* stand for top and bottom fiber, respectively.

First interior support:

$$\sigma_t = (\sigma_g)_c + \frac{M}{Z_b} = 536 - \frac{0.75 \times 188.54 \times 12{,}000}{2430} = -162 \text{ psi} > -6\sqrt{f_c'} \qquad \text{OK}$$

$$\sigma_b = 536 + 698 = 1234 \text{ psi} < 0.45 f_c' \qquad \text{OK}$$

Interior span at midspan:

$$\sigma_t = (\sigma_g)_c + \frac{M}{Z_t} = 536 + \frac{0.75 \times 128.78 \times 12{,}000}{2430} = 1013 \text{ psi} < 0.45 f_c' \qquad \text{OK}$$

$$\sigma_b = 536 - 477 = 59 > -2\sqrt{f_c'} \qquad \text{OK}$$

Similar calculations for the middle strip lead to smaller stresses but are not given here for brevity. Note that, because the magnitude of tensile stresses in positive moment regions does not exceed

$2\sqrt{f'_c}$, there is no need to add nonprestressed bonded reinforcement there. However, nonprestressed bonded reinforcement is needed at the supports and is given by Eq. (11.9):

$$A_s = 0.00075hl = 0.00075 \times 9 \times 30 \times 12 = 2.43 \text{ in}^2$$

This can be achieved using five #7 bars, leading to an actual $A_s = 3$ in^2. They are placed within $1.5h$ on each side of the column faces at a spacing of about 12 in. Their length should be at least one-sixth the clear span on each side of the support, that is, a total of about 9.6 ft (Fig. 11.36*c*). Similarly, five #7 bars are placed at the exterior columns projecting about five feet into the slab.

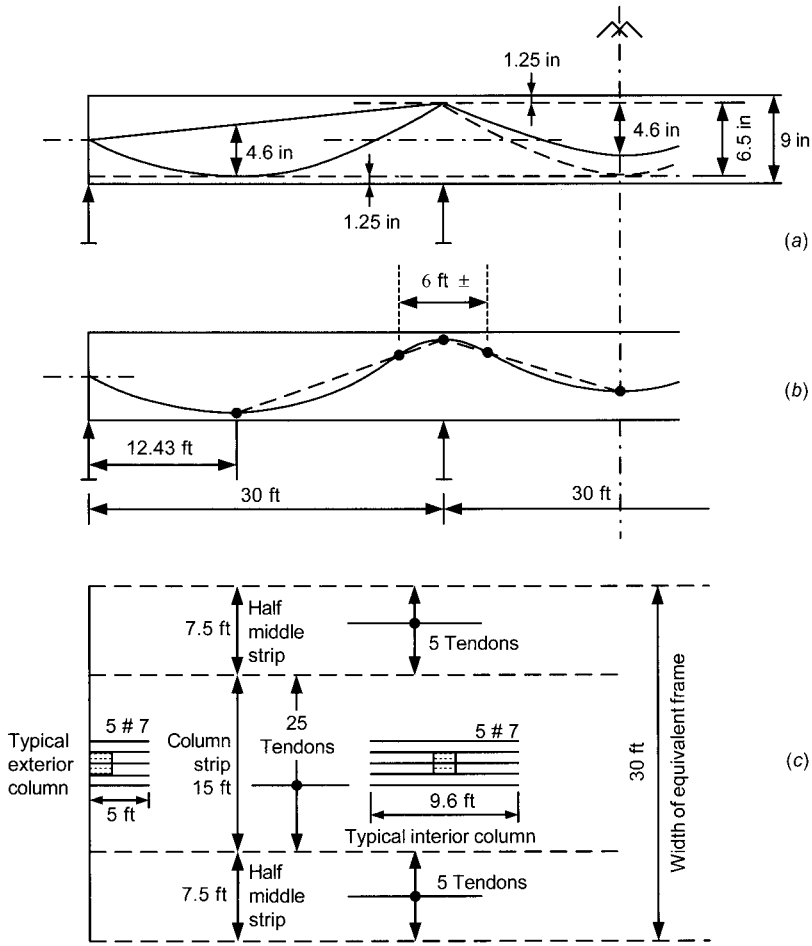

Figure 11.36 Example of flat plate. ***(a)*** **Ideal tendon profile.** ***(b)*** **Actual tendon profile.** ***(c)*** **Reinforcement layout in one direction** (see also part 9 of example for additional reinforcement at exterior columns).

4. Ultimate Flexural Strength

The stress in the prestressing steel at nominal moment resistance can be estimated from the conservative prediction given by Eq. (11.2):

$$f_{ps} = f_{pe} + 7.5 = 160 + 7.5 = 167.5 \text{ ksi}$$

Let us check ultimate strength requirements at the most critical section, which is here the first interior support. For such calculations, the whole slab width is considered using the following variables:

$A_{ps} = 35 \times 0.217 = 7.60 \text{ in}^2$

$A_s = 3.00 \text{ in}^2$ (see previous section)

$d_p = d_s = d_e = 7.75 \text{ in}$

$f_y = 60 \text{ ksi}$

Compute the depth of stress block at ultimate:

$$a = \frac{A_{ps} f_{ps} + A_s f_y}{0.85 f'_c b} = \frac{7.60 \times 167.5 + 3 \times 60}{0.85 \times 5 \times 12 \times 30} = 0.95 \text{ in}$$

Thus:

$$c = \frac{a}{\beta 1} = \frac{0.95}{0.8} = 1.1875 \text{ in}$$

$$\frac{c}{d_e} = \frac{a}{\beta 1} = \frac{1.1875}{7.75} = 0.153 \leq 0.375 \rightarrow \text{Tension controlled section}$$

$\phi = 0.9$

The design nominal moment is obtained from (Fig. 5.19):

$$\phi M_n = \phi \left(A_{ps} f_{ps} + A_s f_y \right) \left(d_e - \frac{a}{2} \right)$$

$$= 0.9 \times (7.60 \times 167.5 + 3 \times 60)(7.75 - \frac{0.95}{2}) / 12$$

$$= 792.8 \text{ kips-ft}$$

The maximum strength design moment, M_u, at the face of the support is due to combined Loadings 1 + 3 and given in Table 11.2; it is equal in magnitude to 664.8 kips-ft. As $M_u < \phi M_n$, ultimate strength is satisfactory at the support.

It can be shown that the design nominal moment resistance, ϕM_n, is equal to, respectively, 700 kips-ft at the near midspan section of the exterior span, 519 kips-ft at the midspan of the interior span (with $d_e = 5.85$ in), and 390 kips-ft at the exterior support ($d_p = 4.5$ in, ignoring non-prestressed reinforcement); all these are satisfactory, leading to $M_u < \phi M_n$ (see Table 11.2).

5. Shear Strength

It can be easily shown that beam-type or one-way shear is largely satisfactory for this slab. However, punching shear may be critical.

- *Punching shear around first interior column*

The area of the critical section and its polar moment of inertia are given by Eqs. (11.14) and (11.15), namely:

$$A_c = 2(c_1 + c_2 + 2d)d = 2(24 + 24 + 15.5) \times 7.75 = 984.25 \text{ in}^2$$

$$J_c = \frac{7.75(24 + 7.75)^3}{6} + \frac{(24 + 7.75)7.75^3}{6} + \frac{7.75(24 + 7.75)(24 + 7.75)^2}{2} = 167{,}827 \text{ in}^4$$

The fraction of moment assumed transferred by shear for a typical interior column is given by Eq. (11.13):

$$\gamma_v = 1 - \frac{1}{1 + \frac{2}{3}\sqrt{\frac{c_1 + d_e}{c_2 + d_e}}} = 1 - \frac{1}{1 + \frac{2}{3}\sqrt{\frac{24 + 7.75}{24 + 7.75}}} = 0.40$$

Shear stresses are induced by the shear force at the critical section and the fraction of transfer moment transferred by shear to the columns. The shear force at the critical section is obtained from the ultimate reaction at the supporting column minus the factored load applied to the slab inside a square area limited by the perimeter, b_o, of A_c (the critical shear section) and equal $(c_1 + d_e)(c_2 + d_e) = 7.0$ ft^2. Referring to Table 11.2, it can be seen that two loading combinations may be critical for shear at the first interior support. Considering the combination of Loadings 1 + 3, we have:

$$V_u = 287.77 - 7(1.2 \times 0.1375 + 1.6 \times 0.080) = 285.7 \text{ kips}$$

The corresponding value of transfer moment is given by $M_u = 62.03$ kips-ft. The maximum shear stress is obtained from Eq. (11.14) as:

$$v_u = \frac{V_u}{A_c} + \frac{\gamma_v M_u c_3}{J_c} = \frac{285{,}700}{984.25} + \frac{0.4 \times 62.03 \times 12{,}000 \times 15.875}{162{,}827} = 318.44 \text{ psi}$$

Similarly, for the combination of Loadings 1 + 4 at the interior column, we have (Table 11.2):

$$V_u = 219.4 - 7(0.293) = 217.3 \text{ kips}$$

$$M_u = 204.76 \text{ kips-ft}$$

and the maximum shear stress is given by:

$$v_u = \frac{217{,}300}{984.25} + \frac{0.4 \times 204.76 \times 12{,}000 \times 15.875}{162{,}827} = 313.8 \text{ psi}$$

Hence, for design, we will consider the controlling value of $v_u = 318.44 \simeq 319$ psi.

The shear resistance of the concrete is estimated from Eqs. (11.10) and (11.11), that is:

$$v_c = \beta_p \sqrt{f'_c} + 0.3\sigma_g + \frac{V_p}{b_o d_e}$$

$$b_o = 2(c_1 + c_2 + 2d) = 127 \text{ in.}$$

$\alpha_s = 40$ (40 for interior columns)

$$\beta_p = \text{ smaller of } \begin{cases} 3.5 \\ 1.5 + \dfrac{\alpha_s d_e}{b_0} = 1.5 + \dfrac{40 \times 7.75}{127} = 3.94 \end{cases} = 3.5$$

The average prestress in the column strip will be used for σ_g. Assuming the same prestress in both directions of the slab and a steel profile as described in Fig. 11.36*b*, it can be shown that $V_p / b_o d_e$ is small and of the order of 15 psi. Hence, the value of v_c is given by:

$$v_c = 3.5\sqrt{5000} + 0.3 \times 536 + 15 \simeq 424 \text{ psi}$$

and

$$\phi v_c = 0.75 \times 424 \simeq 318 \text{ psi}$$

As $v_u = 319 \approx \phi v_c = 318$ psi, shear reinforcement is not required at the interior column.

However, to illustrate the use of bent bars, let us compute the area of shear reinforcement as if it was required. Assuming an angle of inclination $\alpha = 30°$, $f_y = 60$ ksi, and using Eqs. (11.43) and (11.44), we have:

$$V_s = \left(\frac{v_u}{\phi} - v_c\right) A_c = \left(\frac{319}{0.75} - 2\sqrt{5000}\right)\frac{984.25}{1000} = 279.44 \text{ kips}$$

$$A_s = \frac{V_s}{f_y \sin\alpha} = \frac{279.44}{60 \times 0.5} = 9.31 \text{ in}^2$$

This reinforcement is to be distributed across the four sides of the critical section, as shown in Fig. 11.29*b*. It can be provided by four #7 bars crossing at right angles in each direction and leading to $A_v = 4 \times 4 \times 0.6 = 9.6 \text{ in}^2$.

- *Punching shear around exterior edge column*

A procedure similar to the above is followed throughout to investigate punching shear at the exterior edge column. In practice, the tendon is anchored at the center of the slab edge. Hence for shear design, d_e should be taken as the larger of $h/2 = 4.5$ in, or $0.8h = 7.2$ in. However, for simplicity, a value of $d_e = 7.75$ in is taken next. The following values are obtained from Eqs. (11.16) to (11.26):

$$\gamma_v = 1 - \frac{1}{1 + \frac{2}{3}\sqrt{\frac{c_1 + d_e/2}{c_2 + d_e}}} = 1 - \frac{1}{1 + \frac{2}{3}\sqrt{\frac{18 + 7.75/2}{24 + 7.75}}} = 0.356$$

$$b_o = (2c_1 + c_2 + 2d_e) = (2 \times 18 + 24 + 2 \times 7.75) = 75.5 \text{ in}$$

$$A_c = (2c_1 + c_2 + 2d_e)d_e = (2 \times 18 + 24 + 2 \times 7.75) \times 7.75 = 585.125 \text{ in}^2$$

$$c_3 = \frac{d_e\left(c_1 + \frac{1}{2}d_e\right)^2}{A_c} = \frac{7.75\left(18 + \frac{1}{2}7.75\right)^2}{585.125} = 6.338 \text{ in}$$

$$c_4 = \left(c_1 + \frac{1}{2}d_e\right) - c_3 = \left(18 + \frac{1}{2}7.75\right) - 6.338 = 15.537 \text{ in}$$

$$c_5 = c_4 - \frac{c_1}{2} = 15.537 - \frac{18}{2} = 6.537 \text{ in}$$

$$J_c = \frac{(c_1 + d_e/2)d_e^3}{6} + \frac{2d_e\left(c_3^3 + c_4^3\right)}{3} + d_e(c_2 + d_e)c_3^2 = 32{,}275 \text{ in}^4$$

The critical loading combination (Table 11.2) at the centerline of the edge column corresponds to Loadings 1 + 4, for which:

$M_u = 286.14$ kips-ft

$V_u = R_u = 118.55$ kips

The transfer moment is to be taken at the centroid of the critical section distant c_5 (Figs. 11.24*b* and 11.25) from the column centerline; it is given by:

$$M_u = 286.14 - 118.55 \times \frac{6.537}{12} = 221.6 \text{ kips-ft}$$

Hence, the design shear stress is given by:

$$v_u = \frac{V_u}{A_c} + \frac{\gamma_v(M_u - V_u c_5)c_3}{J_c} = \frac{118{,}550}{585.125} + \frac{0.356 \times 221.6 \times 12{,}000 \times 6.338}{32{,}275}$$

$$v_u = 202.61 + 185.9 = 388.5 \text{ psi}$$

Since the edge column does not satisfy the conditions of application of Eq. (11.10), the shear resistance of the concrete is estimated from Eq. (11.12) as for reinforced concrete slabs, that is:

$$b_o = (2c_1 + c_2 + 2d_e) = (2\times 18 + 24 + 2\times 7.75) = 75.5 \text{ in}$$

$$\alpha_s = 30 \text{ (30 for edge columns)}$$

$$\beta_c = 24/18 = 1.333$$

$$v_c = \text{smallest of} \left\{ \begin{array}{l} \left(2 + \dfrac{4}{\beta_c}\right)\sqrt{f'_c} = \left(2 + \dfrac{4}{24/18}\right)\sqrt{f'_c} = 5\sqrt{f'_c} \\ \left(2 + \dfrac{\alpha_s d_e}{b_o}\right)\sqrt{f'_c} = \left(2 + \dfrac{30\times 7.75}{75.5}\right)\sqrt{f'_c} = 5.08\sqrt{f'_c} \\ 4\sqrt{f'_c} = 4\sqrt{5000} = 282.8 \text{ psi} \end{array} \right\} = 282.8 \text{ psi}$$

Thus: $v_c = 282.8$ psi

Check:

$$v_u = 388.5 > \phi v_c = 0.75\times 282.8 = 212 \text{ psi}$$

$$\frac{v_u}{\phi} = \frac{388.5}{0.75} = 518 > v_c = 282.8 \text{ psi} \qquad \text{N.G.}$$

So, there is need to do something about shear at the exterior columns. Several alternatives should be considered and include:

- Provide shear reinforcement (inclined bars, stirrups, or shearheads).
- Increase f'_c; this solution will work if the difference between v_u and ϕv_c is small.
- Add a ledger beam around the periphery of the building; this will call for a new design of the equivalent frame.
- Add a slab extension beyond the edge columns and/or make their size similar to interior columns; by adding a slab extension, better seismic resistance under torsion is achieved and if the extension exceeds $4d_e$, the shear resistance given by Eq. (11.10) can be used.
- Add a drop panel or a column capital; for non-round columns, a drop panel is easier than a column capital.
- Increase the slab thickness in the exterior panels; this can be done gradually over the span.

If shear reinforcement is considered the concrete contribution, v_c, is limited to $2\sqrt{f'_c}$. If bent bar reinforcement is to be used, the nominal resistance, v_n, is limited to $6\sqrt{f'_c}$ (424 psi) which is smaller than what is needed (v_u/ϕ = 518 psi). Similarly if shearhead reinforcement is considered, the maximum acceptable value for v_n is $7\sqrt{f'_c}$ = 495 psi, also smaller than what is needed (v_u/ϕ = 518 psi).

A couple of solutions are discussed next.

6. Punching Shear at Exterior Columns Assuming Drop Panels

After a couple of quick iterations, a drop panel 48 in long, 36 in wide, and projecting 4 in deep below the slab (Fig. 11.37*a*) is selected for the exterior columns (ACI Sec. 13.3). At least two critical sections should be investigated according to ACI Sec. 11.12.1.2. The first critical section is $d_1/2$ away from the column edge (where d_1 = 7.75 + 4 = 11.75 in), the second critical section is located at $d_e/2$ away from the edge of the drop panel (where d_e =7.75 in). A third critical section along the edge of

the panel can also be considered. It will be assumed for brevity that the equivalent frame yields the same moments and shear forces as without the drop panels. The following results are obtained:

For critical section 1 at $d_1/2$ from face of column:

$$A_c = 981.125 \text{ in}^2 = 6.81 \text{ ft}^2$$

$$J_c = 67{,}338 \text{ in}^4$$

$$c_3 = 6.827 \text{ in}$$

$$c_4 = 17.048 \text{ in}$$

$$c_5 = 8.048 \text{ in}$$

$$\gamma_v = 0.353$$

$$b_o = 83.5 \text{ in}$$

$$M_u = 286.14 - 118.55 \times \frac{8.048}{12} = 208 \text{ kips-ft}$$

$$V_u = 118.55 - 6.81(1.2 \times 0.1375 + 1.6 \times 0.08) = 116.55 \text{ kips}$$

$$v_u = \frac{116{,}550}{981.125} + \frac{0.353 \times 208 \times 12{,}000 \times 6.827}{67{,}338} = 118.8 + 89.3 = 208 \text{ psi}$$

The shear strength at the critical section can be determined by:

$$\beta_c = \frac{c_2}{c_1} = \frac{24}{18} = 1.33$$

$$v_c = \text{ smaller of } \left\{ \begin{array}{l} \left(2 + \dfrac{4}{\beta_c}\right)\sqrt{f'_c} = \left(2 + \dfrac{4}{1.33}\right)\sqrt{5000} = 354 \text{ psi} \\ \left(\dfrac{\alpha_s d_e}{b_0} + 2\right)\sqrt{f'_c} = \left(\dfrac{30 \times 11.75}{83.5} + 2\right)\sqrt{5000} = 440 \text{ psi} \\ 4\sqrt{f'_c} = 282.8 \text{ psi} \end{array} \right\} = 282.8 \text{ psi}$$

and

$$\phi v_c = 0.75 \times 282.8 \simeq 212 \text{psi}$$

As $v_u = 208 < \phi v_c = 212$, the design is satisfactory.

For critical section 2 at $d_e/2$ from the edge of the drop panel:

$$A_c = 1050.125 \text{ in}^2 = 7.3 \text{ ft}^2$$

$$J_c = 186{,}071 \text{ in}^4$$

$$c_3 = 11.734 \text{ in}$$

$$c_4 = 28.141 \text{ in}$$

$$c_5 = 10.141 \text{ in}$$

$$\gamma_v = 0.361$$

$$b_o = 135.5 \text{ in}$$

$$M_u = 286.14 - 118.55 \times \frac{10.141}{12} = 188 \text{ kips-ft}$$

$$V_u = 118.55 - 7.3(1.2\times 0.1375 + 1.6\times 0.08) = 116.41 \text{ kips}$$

$$v_u = \frac{116{,}410}{1050.125} + \frac{0.361\times 188\times 12{,}000\times 11.734}{186{,}071} = 162.1 \text{ psi}$$

The shear strength at the critical section is also limited by 212 psi.

As $v_u = 162.1 < \phi v_c = 212$, the design is satisfactory.

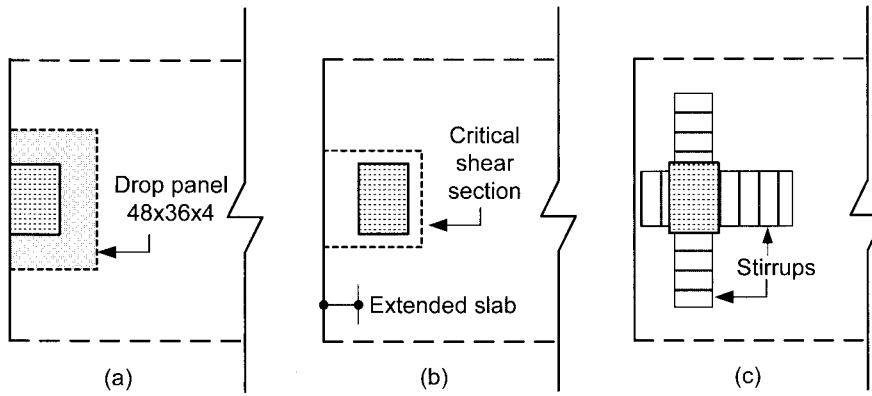

Figure 11.37 Typical solutions for punching shear around exterior columns.

For critical section 3 at edge of the drop panel:

In addition to the two critical shear sections investigated above, a third critical section, which is located just at the periphery of the drop panel (where d_e = 7.75 in), is also checked; it has two sides 36 in each, and one side 48 in. The following results are obtained:

$$A_c = 930 \text{ in}^2 = 6.46 \text{ ft}^2$$

$$J_c = 135{,}374 \text{ in}^4$$

$$c_3 = 10.8 \text{ in}$$

$$c_4 = 25.2 \text{ in}$$

$$c_5 = 9.138 \text{ in}$$

$$\gamma_v = 0.366$$

$$b_o = 120 \text{ in}$$

$$M_u = 286.14 - 118.55\times\frac{9.138}{12} = 197 \text{ kips-ft}$$

$$V_u = 118.55 - 6.46(1.2\times 0.1375 + 1.6\times 0.08) = 116.66 \text{ kips}$$

$$v_u = \frac{116{,}660}{930} + \frac{0.366\times 197\times 12{,}000\times 10.8}{135{,}374} = 194.6 \text{ psi}$$

The shear strength at the critical section is also limited by 212 psi.

As $v_u = 194.6 < \phi v_c = 212$, the design is satisfactory.

Note that the stiffness of equivalent column would slightly change due to the addition of drop panels. Further refined analysis of moments may be needed in a final design.

7. Punching Shear at Exterior Column Assuming Slab Extension

In order to improve shear resistance at the exterior columns, the slab could be extended beyond the edge of the columns to increase the size of the critical shear section (Fig. 11.37*b*). In this example, let us assume that the extension is only 1 ft. Although moments and shear forces will change slightly, let us assume they are same as above. In such a case the reader may want to check the following results.

$$b_o = 91.5 \text{ in}$$

$$A_c = 771.1 \text{ in}^2 = 5.35 \text{ ft}^2$$

$$J_c = 100900 \text{ in}^4$$

$$c_3 = 11.53 \text{ in}$$

$$c_4 = 22.34 \text{ in}$$

$$c_5 = 1.34 \text{ in}$$

$$\gamma_v = 0.4078$$

$$M_u = 286.14 - 118.55 \times \frac{1.34}{12} = 282.9 \text{ kips-ft}$$

$$V_u = 118.55 - 5.35(1.2 \times 0.1375 + 1.6 \times 0.08) = 116.98 \text{ kips}$$

$$v_u = \frac{116{,}980}{771.1} + \frac{0.4078 \times 282.9 \times 12{,}000 \times 11.53}{100900} = 303.55 \text{ psi}$$

The design shear strength ϕv_c at the critical section is also limited by 212 psi.

As $v_u = 303.55 > \phi v_c = 212$ psi, there is need for shear reinforcement.

Let us try closed-loop stirrups; they will need to carry an equivalent shear stress:

$$v_s = (v_u/\phi - v_c) = 303.55/0.75 - 2\sqrt{5000} = 263.3 \text{ psi}$$

If we use #4 stirrups along three directions (that is, along the frame and on both sides of the column, Fig. 11.37*c*) the required spacing would be:

$$s = \frac{A_v f_y}{v_s b_o} = \frac{3 \times 2 \times 0.2 \times 60000}{263.3 \times 99.5} = 2.75 \text{ in}$$

It can be shown that the shear reinforcement should be extended about 2 ft in each direction. Because of close spacing and relatively small slab depth, this shear reinforcement will be difficult to place. It may be desirable to consider shearhead reinforcement and compare its cost to that of the stirrups.

8. Adding an Edge Beam

To improve shear resistance at exterior columns, an edge beam can be placed around the periphery of the slab. The design of such a beam may be demanding since it will be subjected to bending, shear and torsion. The reader may want to check that an edge beam 18 in wide and 32 in deep may be needed. Although the overall behavior of the slab will be improved, this solution may be deemed too costly.

9. Moment Resistance within 1.5*h* of Columns

The ACI code [Ref. 11.2] requires that there is sufficient moment resistance within $1.5h$ of the faces of both interior and exterior columns to resist the portion of moment $(1-\gamma_v)M_u$ transferred by flexure. Two interpretations can be set forth to what constitutes the transfer moment. Since load balancing is achieved under balanced load (here dead load) and prestress, the slab is level and the transfer moment due to dead load is theoretically null. So only the transfer moment due to the unbalanced load is real. In that case there is no problem transferring the moment as required by the ACI code. However, the implied interpretation of the code is not clear. Below, the transfer moment due to both dead and live loads is considered.

At interior columns:

Here γ_v is taken as 0.40.

M_u(transfer moment due to Loadings 1 + 4) = 204.76 kips-ft

$M_u \times (1-\gamma_v) = 204.76 \times (1-0.4) = 122.85$ kips-ft

Assume six strands pass the effective width $b_e = c_2 + 1.5h + 1.5h = 51$ in.

$A_{ps} = 6 \times 0.217 = 1.302$ in^2

$A_s = 3.00$ in^2 (5-#7)

$d_p = d_s = d_e = 7.75$ in

$\Rightarrow \phi M_n = 204$ kips-ft $\gg 122.85$ kips-ft

If only prestressed reinforcement is accounted for, $\phi M_n = 118.5$ kips-ft, which is also about sufficient.

At exterior columns:

Here γ_v is taken as 0.356 as for the slab without drop panels at exterior columns.

M_u(transfer moment due to Loadings 1 + 4) = 286.14 kips-ft

$M_u \times (1-\gamma_v) = 286.14 \times (1-0.356) = 182.27$ kips-ft

$A_{ps} = 6 \times 0.217 = 1.302$ in^2

$A_s = 3.00$ in^2 (5-#7)

$d_p = 4.5$ in

$d_s = 7.75$ in

$\Rightarrow \phi M_n = 150.8$ kips-ft < 182.27 kips-ft

Thus, there is need to add nonprestressed tensile reinforcement in that region. It can be shown that adding two #7 bars to the five #7 bars already required will lead to a satisfactory solution. The spacing of the seven bars at the exterior column will be close to 8 in.

Figure 11.38 illustrates the arrangement of reinforcing bars in the negative moment region at column supports for the slab considered.

10. Deflection

No deflection is induced under dead load because of load balancing and, as the slab is level, no additional long-term deflection should theoretically be recorded. Let us estimate the elastic deflection due to live load from Eq. (11.46), assuming pattern loading and a value of $k = 0.11$. That is:

$$(\Delta_i)_{L \text{ or } nb} = k \frac{w l_a^4}{E_c h^3} = 0.11 \frac{80 \times (12 \times 30)^4}{144 \times 4.28 \times 10^6 \times 9^3} = 0.33 \text{ in}$$

This value is less than $l/360 = 1$ in, allowed by the code (Table 7.2). O.K.

11. Remarks

The above preliminary design was as close as possible to a final design. Some difficulties were encountered for punching shear resistance at the exterior column. As mentioned earlier, a drop panel or a thicker slab could be used in a revised final design to avoid costly shear reinforcement. It seems that the best way to overcome punching shear is to provide a larger critical section or a thicker slab, or both. Note that a significant portion of the shear stress around the exterior column was due to the transfer moment. In determining the value of the transfer moment, the dead load, which is equal to

the balanced load, was included in the calculations (Loading 1). It can be argued that the slab is level under balanced load and prestressing. Thus, in effect, no transfer moment exists under dead load. If only the transfer moment due to the unbalanced load is considered in the computations, the punching shear at the exterior column would have been satisfactory, with no need for shear reinforcement or drop panels. However, it is preferable to be on the safe side when dealing with punching shear. This may explain why, in practice, the entire transfer moment is considered.

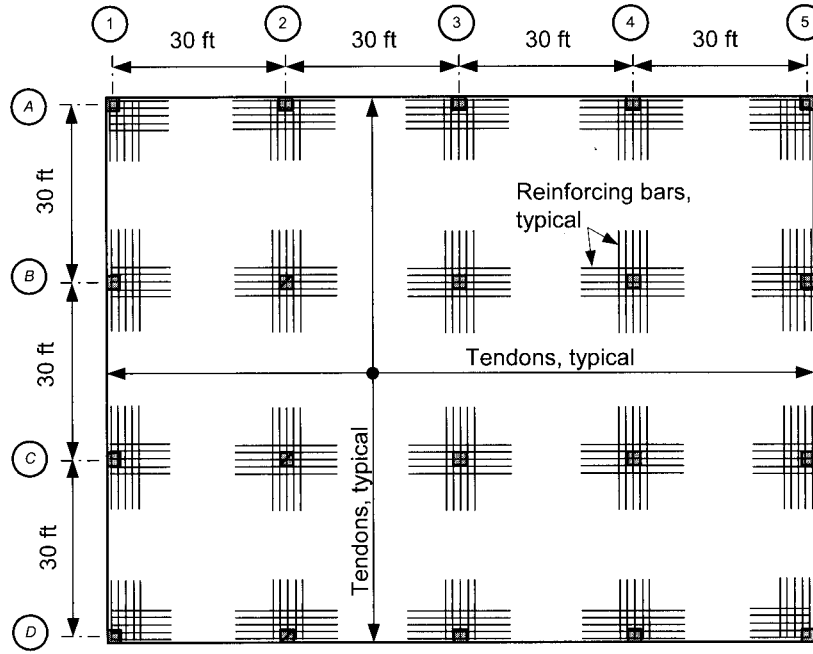

Figure 11.38 Arrangement of reinforcing bars at column supports for the entire slab.

REFERENCES

11.1 Aalami, B. O., and A. Bommer, *Design Fundamentals of Post-Tensioned Concrete Floors,* Post-Tensioning Institute, Phoenix, Arizona, 1999, 184 pp.

11.2 ACI Committee 318, *Building Code Requirements for Reinforced Concrete and Commentary*, ACI 318-02, American Concrete Institute, Farmington Hills, 2002.

11.3 ACI-ASCE Committee 423, *Recommendations for Concrete Members Prestressed with Unbonded Tendons,* American Concrete Institute, ACI 423.3R-02, 2003.

11.4 ACI Committee 435, *Deflection of Two-Way Reinforced Concrete Floor Systems: State-of-the-Art Report, ACI Manual of Concrete Practice*, Pt 2, American Concrete Institute, Detroit, Michigan, 1979, pp. 435-83, 435-106. See also ACI Committee 435, *Observed Deflection of Reinforced Concrete Slab Systems, and Causes of Large Deflections,* ACI 435.8R-85, reapproved 1997, *ACI Manual of Concrete Practice*, Pt. 2, 2002.

11.5 ACI-ASCE Joint Committee 423, "Tentative Recommendations for Prestressed Concrete Flat Plates," *ACI Journal*, 71(2): 61-71, 1974.

11.6 "ADAPT-PT" Software for Prestressed Floors and Beams, ADAPT Structural Concrete Software System, Redwood City, California, www.adaptsoft.com.

11.7 Brotchie, J. F., "Some Australian Research on Flat Plate Structures," *ACI Journal*, 77(1): 3-11, 1980.

11.8 Brotchie, J. F., "Experimental Studies of Prestressed Thin Plate Structures," *ACI Journal*, 77(2): 87-95, 1980.

11.9 Burns, N., T. Helwig and T. Tsujimoto, "Effective Prestress Force in Continuous Post-Tensioned Beams with Unbonded Tendons," *ACI Structural Journal*, 88(1): 84-90, 1991.

11.10 Burns, N. H., and R. Hemakom, "Test of Scale Model Post-Tensioned Flat Plate," *Journal of the Structural Division, ASCE*, 103(ST6): 1237-55, 1977.

11.11 Collins, M. P., and D. Mitchell, "Prestressed Concrete Structures," *Response Publications*, 1997, 752 pp.

11.12 Corley, W. G., and J. O. Jirsa, "Equivalent Frame Analysis for Slab Design," *ACI Journal*, 67(11): 875-84, 1970.

11.13 Corley, W. G., and N. M. Hawkins, "Shearhead Reinforcement for Slabs," *ACI Journal*, 65(10): 811-24, 1968.

11.14 Ferguson, F. M., J. E. Breen, and J. O. Jirsa, "*Reinforced Concrete Fundamentals*," 5th ed. New York: John Wiley & Sons, 1988, 768 pp.

11.15 Foutch, D. A., and W. L. Gamble, and H. Sunidja, "Tests of Post-Tensioned Concrete Slab-Edge Columns Connections," *ACI Structural Journal*, 87(2): 167-79, 1990.

11.16 Gardner, N. J., and R. K. Mahmoud, "Punching Shear Strength of Continuous Post-Tensioned Concrete Flat Plates," *ACI Materials Journal*, 95(3): 272-83, 1998.

11.17 Gerber, L. L., and N. H. Burns, "Ultimate Strength Tests of Post-Tensioned Flat Plates," *PCI Journal*, 16)6): 40-58, 1971.

11.18 Hanson, N. W., and J. M. Hanson, "Shear and Moment Transfer Between Concrete Slabs and Columns," Portland Cement Association, Development Department Bulletin D129, 1968, pp. 811-824.

11.19 Hawkins, N. M., "Shear Strength of Slabs with Moments Transferred to Columns," *Shear in Reinforced Concrete*, 2(SP-42): 817-46, American Concrete Institute, Detroit, 1974.

11.20 Hawkins, N. M., "Lateral Load Resistance of Unbonded Post-Tensioned Flat Plate Construction," *PCI Journal*, 26(1): 94-115, 1981.

11.21 Hassoun, M. N., *Structural Concrete: Theory and Design,* 2nd ed. Upper Saddle River, NJ: Prentice Hall, 2002, 772 pp.

11.22 Lin, T. Y., "Load-Balancing Method for Design and Analysis of Prestressed Concrete Structures," *ACI Journal*, 60(6): 719-42, 1963.

11.23 Lin, T. Y., and N. H. Burns, *Design of Prestressed Concrete Structures*, 3rd ed. New York: John Wiley & Sons, 1981, 646 pp.

11.24 MacGregor, J. G., "*Reinforced Concrete Mechanics and Design*, 3rd ed. Upper Saddle River, NJ: Prentice Hall, 1996, 939 pp.

11.25 Naaman, A. E., and F. M. Alkhairi, "Stress at Ultimate in Unbonded Tendons – Part I: Evaluation of the State-of-the Art," *ACI Structural Journal*, 89(5): 641-51, 1991.

11.26 Naaman, A. E., and F. M. Alkhairi, "Stress at Ultimate in Unbonded Tendons – Part II: Proposed Methodology," *ACI Structural Journal,* 89(5): 683-92, 1991.

11.27 Naaman, A. E., N. Burns, K. French, W. Gamble and A. Mattock, "Stresses in Unbonded Tendons at Ultimate: Recommendation," *ACI Structural Journal*, 99(2): 518-29, 2002.

11.28 Nasser, G. D., "A Look at Prestressed Flat Plate Design and Construction," *PCI Journal*, 14(6): 62-77, 1969.

11.29 Nawy, E. G., and P. Chakrabarti, "Deflection of Prestressed Concrete Flat Plates," *PCI Journal*, 21(2): 86-102, 1976.

11.30 Nawy, E. G., "Prestressed Concrete: a Fundamental Approach," 4th Edition Upper Saddle River, NJ: Prentice Hall, 2002.

11.31 Nilson, A. H., *Design of Prestressed Concrete.* New York: John Wiley & Sons, 1978. Also, 2nd ed., 1987, 592 pp. Nilson, A. H., *Design of Prestressed Concrete*, 2nd ed. New York: Wiley, 1987, 592 pp.

11.32 Nilson, A. H., and D. Darwin, *Design of Concrete Structures*, 12th ed. New York: McGraw Hill Inc., 1997, 880 pp.

11.33 Nilson, A. H., and D. B. Walters, "Deflection of Two-Way Floor Systems by the Equivalent Frame Method," *ACI Journal*, 72(5): 210-18, 1975.

11.34 Park, R., and W. L. Gamble, *Reinforced Concrete Slabs*, 2nd ed. New York: John Wiley & Sons, 2000, 736 pp.

11.35 Parme, A. L., "Prestressed Flat Plates," *PCI Journal*, 13(6): 14-32, 1968.

11.36 Portland Cement Association, PCA, "Concrete Floor Systems" by David Fanella, and "Long Span Concrete Floor Systems," by David Fanella and Javeed Munchi, Skokie, Illinois, 2000.

11.37 Post-Tensioning Institute, PTI, "Design of Post-Tensioned Slabs", 2nd ed, 1995, The Post-Tensioning Institute, Phoenix, Arizona, pp. 54 (3rd ed., in print, 2003)

11.38 Post-Tensioning Institute, PTI "Post-Tensioning Manual", 5th ed., 1990, The Post-Tensioning Institute, Phoenix, Arizona, pp. 406 (6th expected Dec. 2003).

11.39 Rice, P. F., and E. S. Hoffman, *Structural Design Guide to the ACI Building Code*, 2nd ed., New York: Van Nostrand-Reinhold, 1979, 470 pp.

11.40 Rozvany, G. I. N., and A. J. K. Hampson, "Optimum Design of Prestressed Flat Plates," *ACI Journal*, 60(8): 1065-82, 1968.

11.41 Saether, K., "The Structural Membrane Theory Applied to the Design of Flat Slabs," *PCI Journal*, 8(5): 68-79, 1963.

11.42 Scanlon, A., and D. W. Murray, "Practical Calculation of Two-Way Slab Deflection," Concrete International, 4(11): 43-50, 1982.

11.43 Scordelis, A. C., T. Y. Lin, and R. Itaya, "Behavior of a Continuous Slab Prestressed in Two Directions," *ACI Journal*, 56(6): 441-59, 1959.

11.44 Timoshenko, S. P., and S. Woinowsky-Kreiger, *Theory of Plates and Shells*, 2nd ed. New York: McGraw-Hill Book Co., 1959, 580 pp.

11.45 Uniform Building Code, Vol. 2, "*Structural Engineering Design Provisions*," International Conference of Building Officials, Whittier, California, 1997, 492 pp.

11.46 Walker, C. H., "Durability of Parking Structures Floors," *Concrete International: Design and Construction*, 2(3): 47-50, 1980.

11.47 Wang, C. K., G. Salmon, C. G., and W. Anderson, *Reinforced Concrete Design*, 6th ed. New York: International Textbook Co., 1998, 1040 pp.

11.48 Wang, C. H., "Direct Design Method for Prestressed Concrete Slabs," *PCI Journal*, 13(3): 62-72, 1968.

11.49 Winter, G., and A. H. Nilson, *Design of Concrete Structures*, 9th ed. New York: McGraw-Hill Book Co., 1979, 647 pp.

PROBLEMS

11.1 Redesign the slab of Example 11.4 assuming that the same prestressing force needed for the exterior span is used throughout the length of the slab.

11.2 Refer to the slab of Example 11.14 and Fig. 11.32 and assume that beams having the same width as the columns are placed between the columns along the lettered grid lines (East-West). Hence, a one-way slab system along the numbered grid lines (North-South) is obtained. Design this one-way slab using the same input data as for Example 11.14 and a slab depth of 10 in.

11.3 Read the provisions of the ACI code and its commentary on shearhead reinforcements. Draw the corresponding critical section for punching shear, for a typical interior column, exterior edge column, and corner column, respectively.

11.4 Read the provisions of the ACI code and its commentary related to openings in slabs near the columns. How do openings influence the critical section for punching shear?

11.5 Go back to the slab of Example 11.14 and design the exterior equivalent frame in each direction. All the input data are assumed the same. Should punching shear be critical, provide a solution.

11.6 Assuming that the required reinforcement in the slab of Example 11.14 is the same for both the North-South and East-West directions, provide a reinforcement layout of the slab using a banded tendon distribution.

11.7 Assume hypothetically that the two-way slab of Example 11.14 had round interior columns of diameter 27 in; these columns have about the same cross section as the 24x24 square columns used. Assume that the analysis leads to the same moments and shear forces as in Example 11.14. Determine the maximum shear stress at the critical section around the interior column. Think about the following question: assuming the moments in the x and y directions are the same, determine the maximum shear stresses at the critical section as if biaxial bending is involved and discuss the values obtained.

11.8 The effect of smoothing the tendon profile over the supports after load balancing was disregarded in Example 11.14. For the final tendon profile and prestressing force obtained, analyze the equivalent frame and determine the secondary moments at the supports. Compare their values with the primary moments and conclude whether they are in effect negligible.

11.9 Go back to the slab of Example 11.14 and design the same equivalent frame assuming that the slab extends 3 ft at the periphery beyond the face of exterior and corner columns. Discuss the advantages or disadvantages of such construction. In particular, exterior walls will have to be considered as permanent dead load and their presence will change significantly the moments and shear at exterior columns.

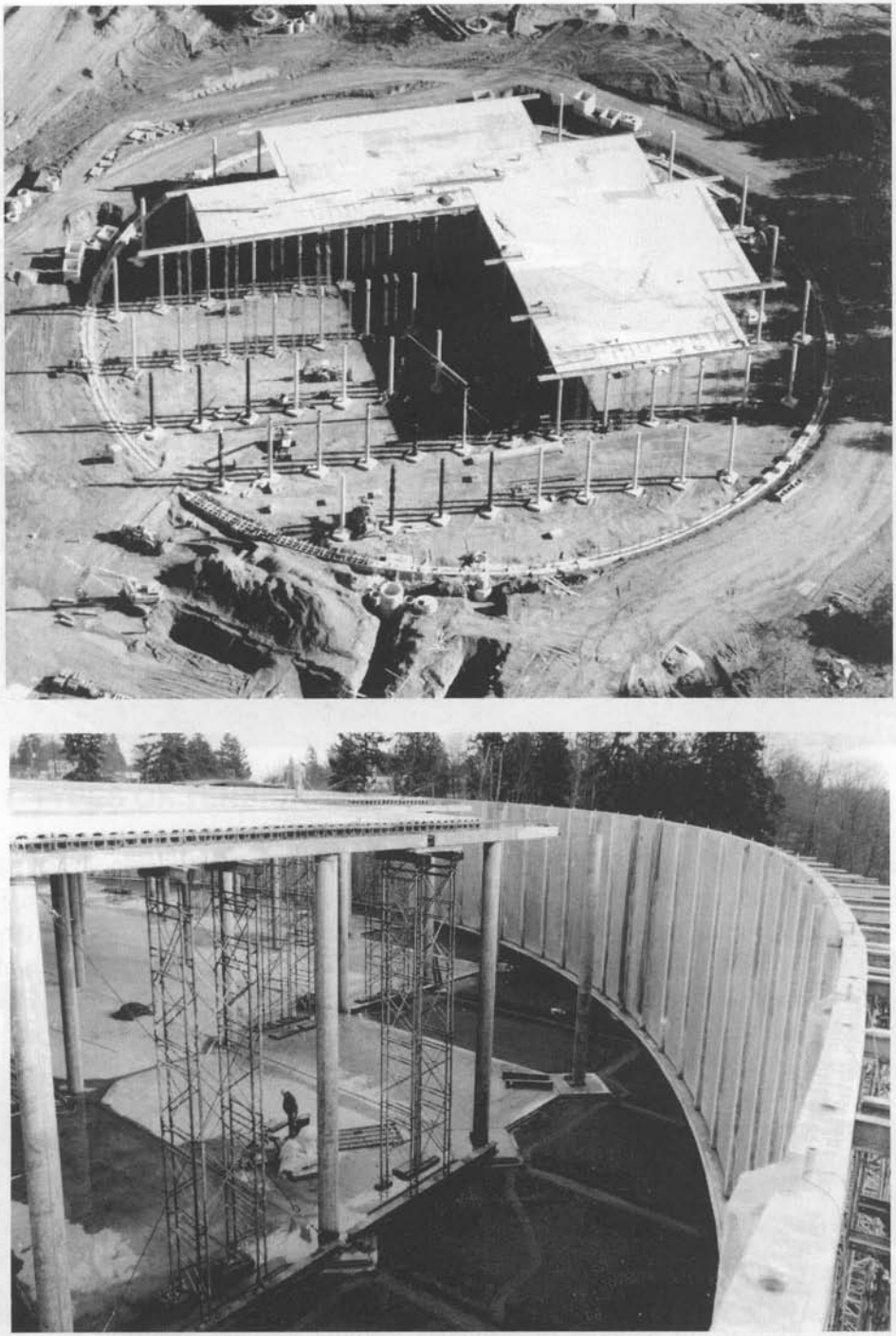

Construction of a 20 million gallon (757,000 m3) prestressed concrete tank with precast walls prentensioned vertically and posttensioned circumferentially – Riverton Height's Reservoir, Washington. *(Courtesy ABAM Engineers, Inc.)*

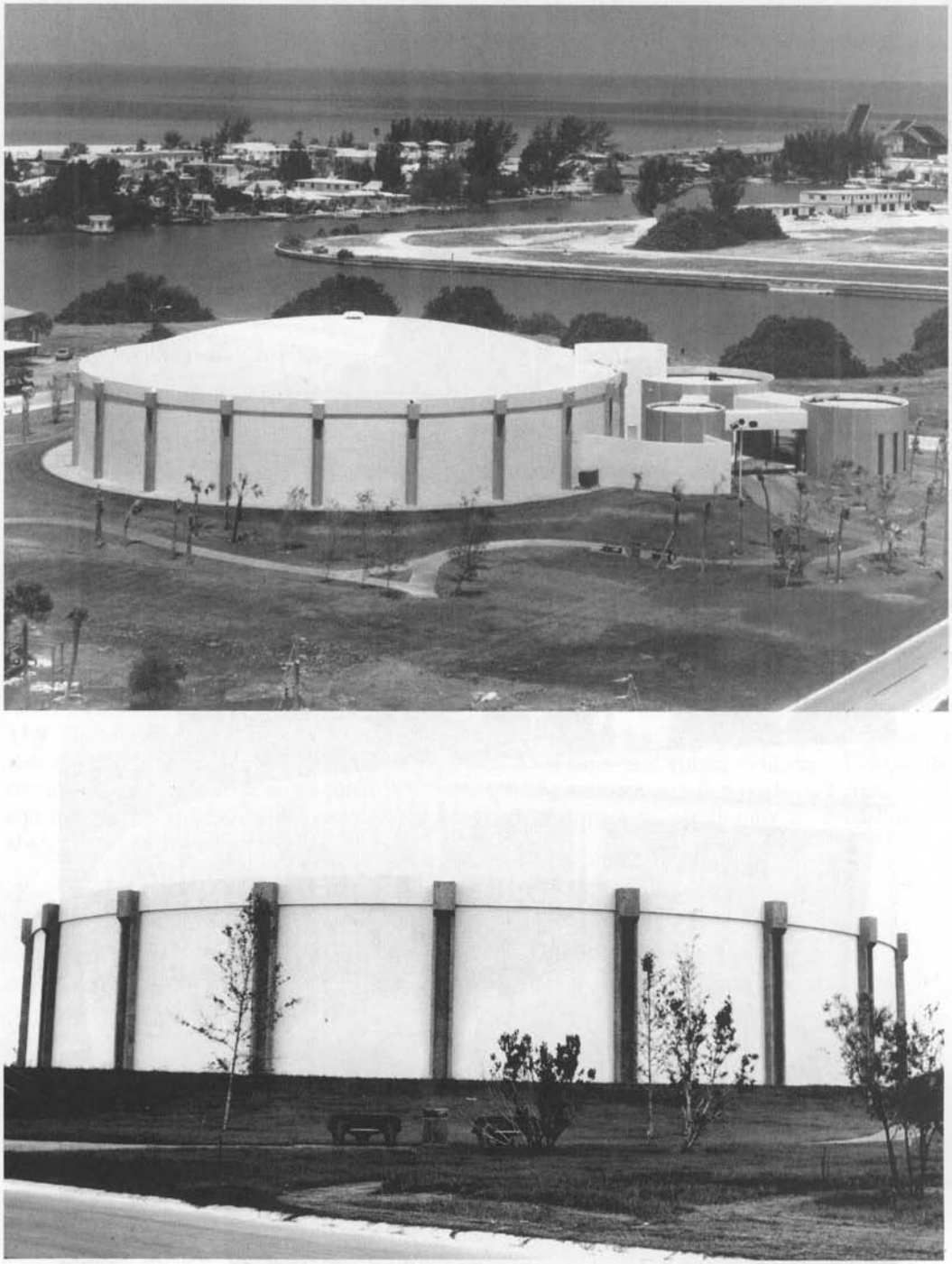

Five million gallon (190,000 m^3) prestressed concrete water tank in Pinellas County, Florida. *(Courtesy Portland Cement Association).*

CHAPTER 12

ANALYSIS AND DESIGN OF TENSILE MEMBERS

12.1 TYPES OF TENSION MEMBERS

Prestressed concrete tension members are structural elements predominantly subjected to axial tension. They are mostly linear, circular, or parabolic (catenary) in shape. Linear tension elements, commonly called ties, include restraining ties for arch bridges, soil anchors for retaining structures, and truss members. Circular elements are part of any figure of revolution and include cylindrical tanks, silos, and pressure vessels. Parabolic prestressed concrete tension members, often described as stress ribbons, follow the same principles as catenary steel cables. They are used in inverted suspension (or stress-ribbon) bridges. Typical examples of tension members are shown in Fig. 12.1 where only the tensile member is emphasized in its position with respect to the rest of the structure, schematically described by a line configuration.

Prestressed linear tension members are similar to compressive members, except that they carry a much higher level of prestress. They are generally concentrically prestressed. However, when a combination of flexure (self-weight) and tension exists, the prestress may be slightly eccentric to balance the weight and keep a uniform state of stress in the section.

Although experimental data and design information on prestressed concrete tension members are scarce (perhaps because they are simpler to analyze than other elements), they are widely used in actual applications. In some examples, they represent the main element that confers to the structure its innovative aspects. *Morandi* [Ref. 12.18] built several bridges featuring prestressed concrete tensile elements, used in a cable-stayed configuration. Finsterwalder [Ref. 12.10] presented an innovative design for the Bosphorus Bridge (not built) where a shallow funicular-shaped prestressed concrete stress-ribbon tensile member spanning 190 m (620 ft) was proposed. The ribbon was to serve as tensile element and deck in the central portion of the bridge's main span of 408 m (1340 ft). Lin et al. [Ref. 12.16] designed and built the inverted suspension Rio Colorado Bridge in Costa Rica, where a catenary-shaped prestressed concrete ribbon spanning 146 m (480 ft) was used to support the horizontal deck. Such bridges may represent a comparatively low-cost solution for crossing deep valleys [Refs. 12.5 and 12.17].

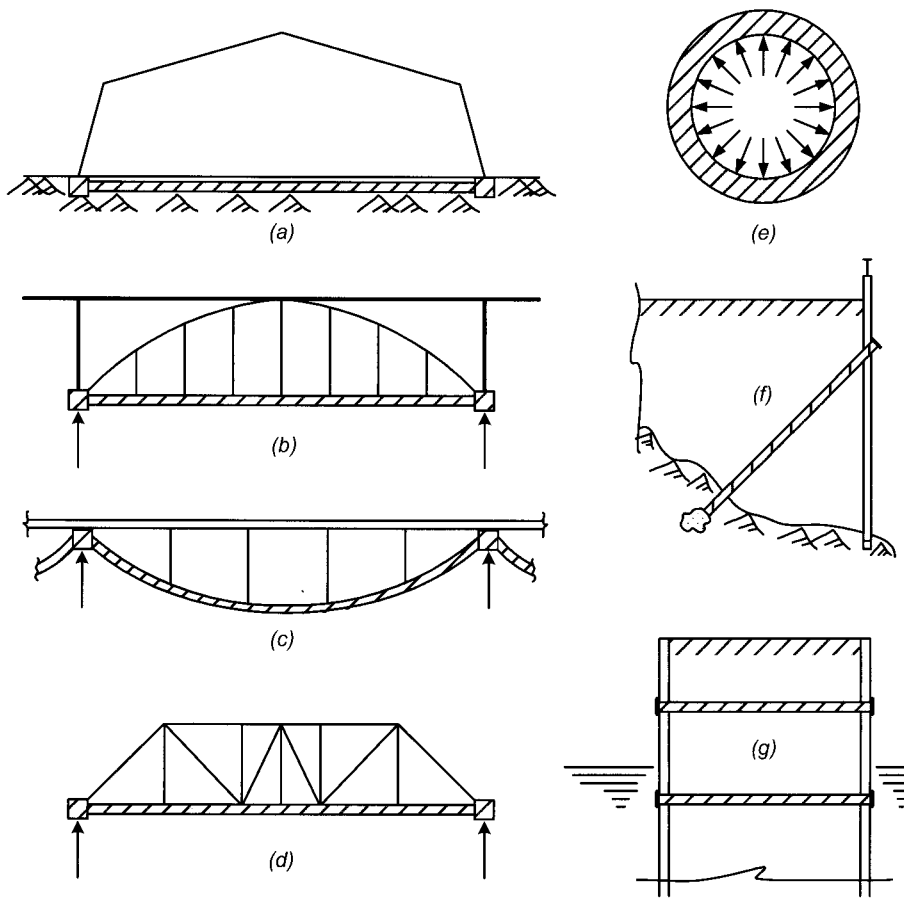

Figure 12.1 Typical examples of tension members.

Figure 12.2 Prestressed concrete truss railway bridge: Iwahana Bridge, Japan.
(Ref. 12.11, Courtesy Prestressed Concrete Institute.)

Precast prestressed concrete tensile and compressive elements can successfully be used in trusses where they are assembled on site and connected by post-tensioning [Refs. 12.8 and 12.11]. Several truss railway bridges have been built in Japan [Ref. 12.11]. A typical example is shown in Figure 12.2.

Some of the advantages of prestressed concrete tensile members are discussed next.

12.2 ADVANTAGES OF PRESTRESSED CONCRETE TENSION MEMBERS

The use of concrete in pure tensile members, also called ties, may seem paradoxical, since concrete is weak in tension. However, a prestressed concrete element can be treated as a single composite material that can sustain tension, with no reference to its components, steel and concrete (Fig. 4.5). Prestressed concrete tension members can present a number of salient advantages over their counterparts made with either steel or reinforced concrete:

1. A prestressed concrete tie can be designed not to crack under normal service loads and acceptable levels of service overloads.
2. Because it is crack-free, it offers an excellent corrosion protection for the steel reinforcement.
3. The use of concrete offers an inherent fire resistance which, in some instances, may be an important design factor.
4. The most significant advantage of using a prestressed concrete tension member is that the total deformation necessary to develop the full resistance to the applied external load can be controlled practically to any desired degree. This is because the member behaves essentially as a linear elastic crack-free material and a change in its cross section leads to a proportional change in its deformation under load. The total deformation (elongation or shortening) under load is a very important design variable. An excessive deformation may lead to distortional distress and failure in the structure or in some of its elements.

Everything else being equal, the deformation of a prestressed concrete tie can be more than an order of magnitude smaller than that of a steel tie. This is illustrated in the following example.

12.2.1 Example: Relative Deformation of Tension Members

Consider a tensile force N of magnitude 100 kips to be carried over a span of 100 ft. Several design proposals are to be evaluated including a high-strength steel cable made of prestressing strands, a structural steel member, a prestressed concrete member, and a reinforced concrete member. A schematic representation of the problem and typical formula are given in Fig. 12.3.

Assume the steel cable (Fig. 12.3*a*) is made of six strands with an area $A_{ps} = 0.918 \text{ in}^2$ and an elastic modulus $E_{ps} = 28.14 \times 10^6$ psi. It can be shown that its elongation under load is given by $\Delta l_{ps} = Nl / E_{ps} A_{ps} \simeq 4.64$ in.

Assuming an allowable stress of 20,000 psi, the structural steel member (Fig. 12.3*b*) has a cross-sectional area $A_s = 5 \text{ in}^2$ and same elastic modulus as the cable, i.e., $E_s = 28.14 \times 10^6$ psi. Using the same formula as above leads to $\Delta l_s = 0.85$ in.

The prestressed concrete tie (Fig. 12.3*c*) has the same area of prestressing steel as the steel cable, i.e., $A_{ps} = 0.918 \text{ in}^2$, a gross sectional area $A_g = 100 \text{ in}^2$, and a concrete elastic modulus $E_c = 4.69 \times 10^6$ psi. The transformed area of the section is $A_t = 104.59 \text{ in}^2$. The member's instantaneous elongation under the same load N is given by $|\Delta l_c| = |Nl / E_c A_t| = 0.245$ in.

If we keep the same prestressing steel reinforcement and double the concrete area (Fig. 12.3*d*), the elongation is halved to approximately 0.125 in. This value is less than three percent of that obtained if the free steel cable were used alone. In practice, long-term effects must also be considered and generally counteract the effect of external loads. In the above comparison, the steel cable was chosen to have the same cross-sectional area as the prestressing tendons in the prestressed concrete tie. In practice, a free cable will have a substantially lower allowable stress or higher area than the values assumed above.

The design of a reinforced concrete tie is based on a cracked concrete section. The corresponding area of steel reinforcement is significantly higher than that of a prestressed tie. Everything else being the same, its elongation under load would be higher than that of a prestressed tie, the difference being mainly due to the sum of crack widths along the member (Fig. 12.3*e*). On the other hand, for the

same steel area and steel stress, the elongation of a reinforced concrete tie can be expected to be less than that of a structural steel member.

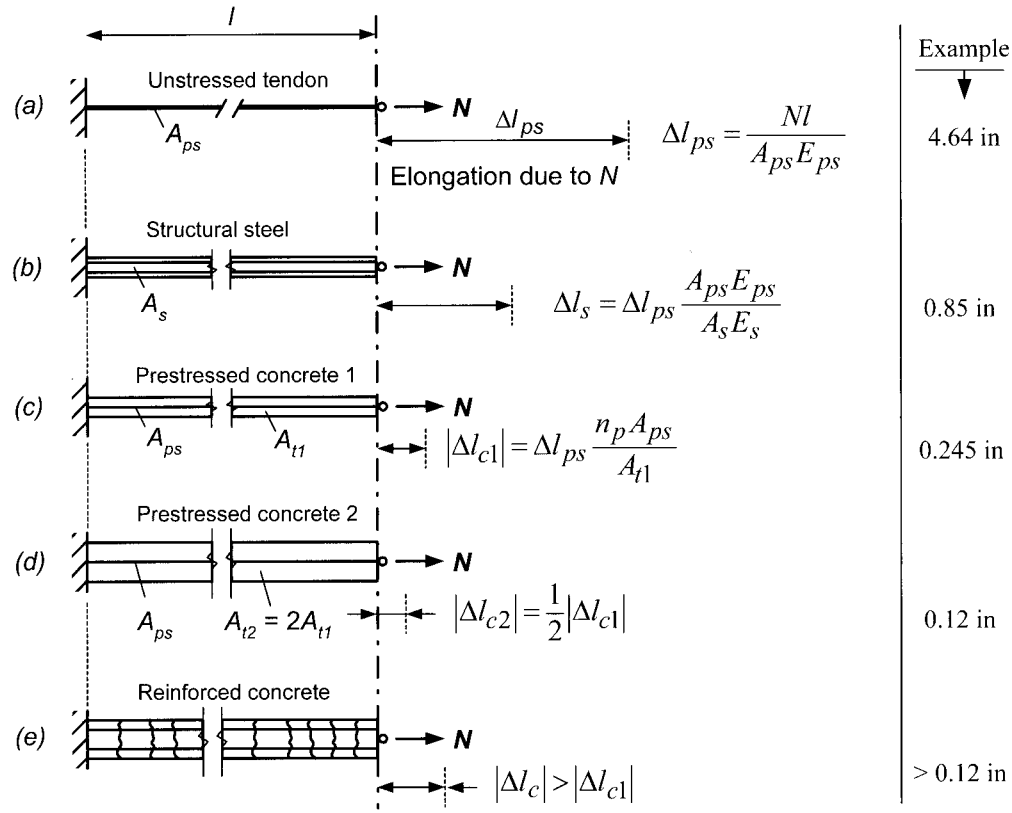

Figure 12.3 Relative deformation in tension members made of different materials.

12.3 BEHAVIOR OF PRESTRESSED CONCRETE TENSION MEMBERS

Because prestressed concrete ties are simple structural elements that are expected to perform in the linear elastic uncracked range of behavior, they have generated little need for experimental research. An investigation by Wheen [Ref. 12.27] has clarified the influence of many variables on the load-deformation response of the composite and allows for some comparison and correlation with reinforced concrete ties.

When a prestressed concrete tensile member is subjected to a monotonically increasing tensile load, its load elongation curve is characterized by an initial linear elastic portion up to first structural cracking. The increase in external load is accompanied by a slow stress increase in the steel and a fast stress decrease in the concrete which eventually leads to tension in the concrete and subsequent cracking.

Wheen reports that the occurrence of first cracking is dramatic and is invariably accompanied by a loud bang [Ref. 12.27]. Significant changes in characteristics occur after cracking. They include a very large reduction in the stiffness of the composite and a sudden increase in steel stress (stress jump) because the steel must resist the additional force released by the concrete. Such a stress jump may lead to a steel stress in the nonlinear range of behavior. It may cause serious steel debonding on either side of the crack, thus leading to unusually wide cracks. If the member is less than minimally reinforced, that is, if the cracking load is larger than the ultimate resistance of the tendons alone, cracking will also lead to failure. For normally reinforced members, the composite resistance after cracking is reduced to that of the reinforcement alone and the composite load elongation curve is essentially reduced to that of the reinforcement.

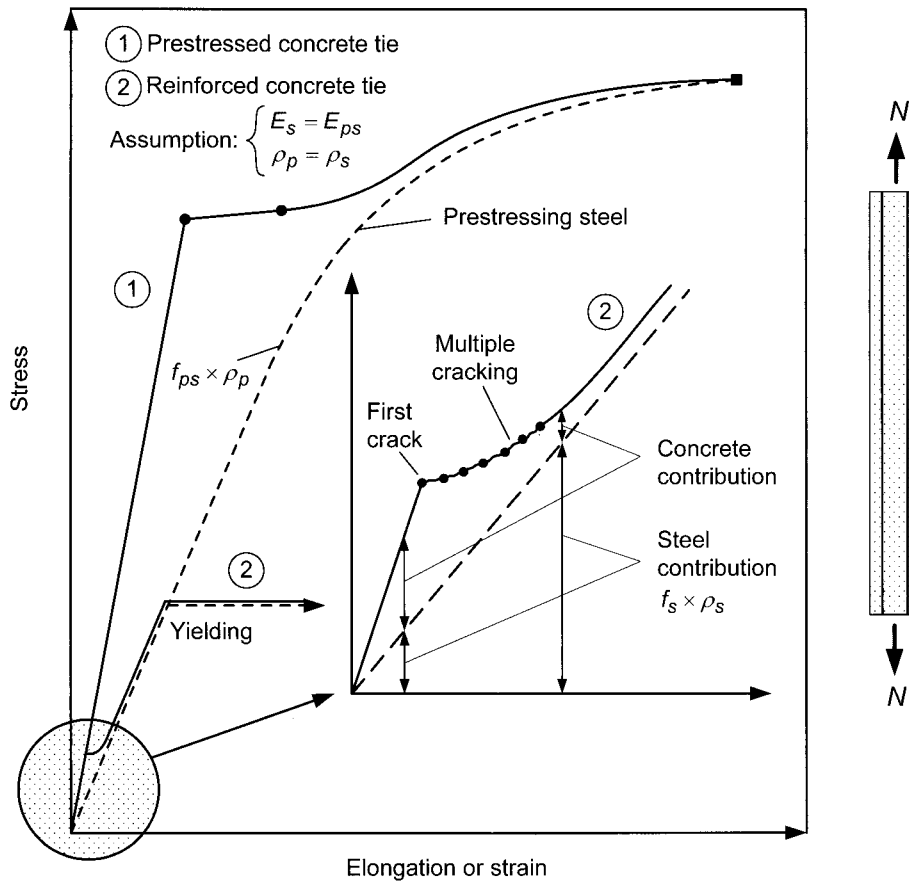

Figure 12.4 Typical stress-elongation curves of reinforced and prestressed concrete tension members.

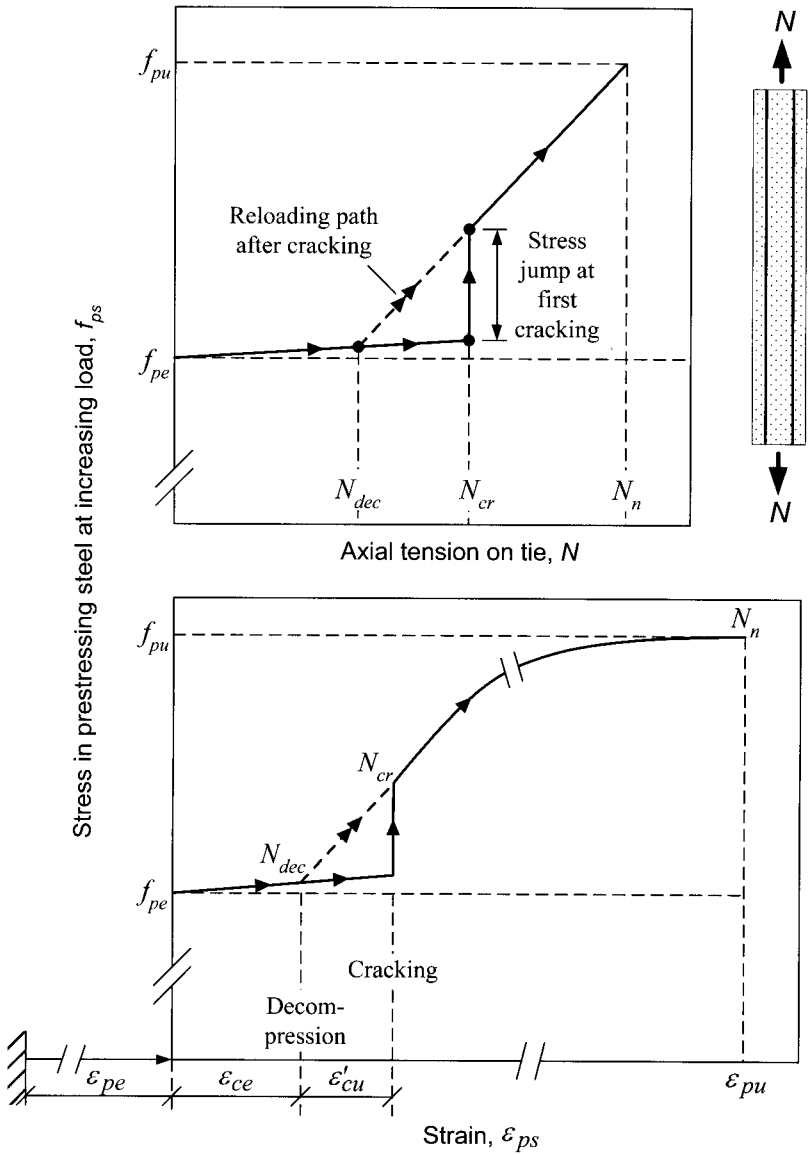

Figure 12.5 Variation of the stress in the prestressing steel with loading.

A typical stress elongation curve of a prestressed concrete tie is plotted in Fig. 12.4 and compared to that of a reinforced concrete tie having the same reinforcement ratio. It can be observed that the reinforced concrete tie will crack in the very early stages of loading. A slight increase in load after cracking leads to the formation of multiple cracks soon followed by crack stabilization. No further cracks form thereafter but the widths of existing cracks increase with the load and the composite response approaches that of the reinforcing steel alone. A reinforced concrete tie is

designed to resist service loads after cracking, while a prestressed concrete tie is mostly serviceable before cracking. The contribution of the reinforcement to the composite response, represented by $\rho_p f_{ps}$ or $\rho_s f_s$, is also plotted in Fig. 12.4 versus the elongation. It is assumed, for clarity, that both the prestressing steel and the reinforcing steel have the same modulus of elasticity. The difference in ordinate between the composite curve and the reinforcement curve represents the average contribution of the concrete. Such contribution is substantial prior to cracking. After cracking, it decreases with the elongation and tends to vanish. Simultaneously, the composite's response tends toward that of the reinforcement alone. Note that, because of the extent of concrete contribution to the pre-cracking resistance, prestressing takes substantial advantage of the presence of the concrete.

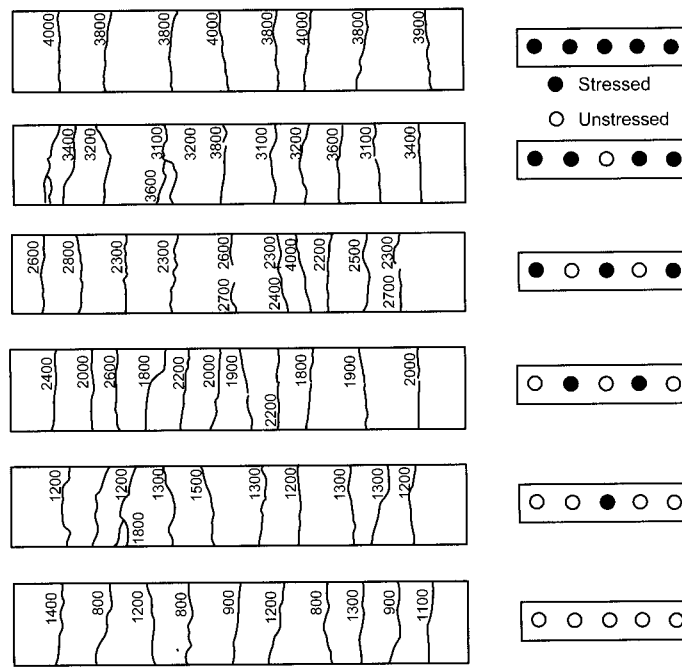

Figure 12.6 Typical crack patterns in prestressed tension members. *(Adapted from R. J. Wheen, Ref. 12.27.)*

If a prestressed tensile member with bonded reinforcement cracks due to an overload, its response under subsequent loading would be similar to that of the first loading except that existing cracks will start opening at decompression instead of at the cracking load. A smoother transition in the steel stress will replace the stress jump otherwise encountered at first cracking, as illustrated in Fig. 12.5. After cracking, the stress in the prestressing steel increases in direct proportion to the applied load N until failure (Fig. 12.5), but the strain increases at a much faster rate,

in accordance with the stress-strain relationship of the steel. In Fig. 12.5, ε_{ce} represents the concrete strain under effective prestress and ε'_{cu} represents the tensile fracture strain of concrete.

If the reinforcement is unbonded and cracking occurs, generally only one crack develops and subsequent reloading will see the stiffness and the response of the composite reduced to those of the reinforcement alone. Because of this dramatic reduction in stiffness, the use of unbonded reinforcement in prestressed tensile members is not recommended.

Typical crack patterns in prestressed concrete tension members using bonded stressed and unstressed tendons, as reported by *Wheen*, are shown in Fig. 12.6 (adapted from Ref. 12.27). Note that cracking in these members is very similar to that generally observed using reinforced concrete. Modeling crack width and spacing in prestressed tensile members can be done similarly to ferrocement except that the stress in the steel is replaced by the stress change beyond decompression. The reader is referred to [Ref. 12.19] for in-depth analysis of the subject.

12.4 ANALYSIS OF TENSION MEMBERS

The analysis of prestressed concrete tensile members presents little mathematical difficulty. It is generally assumed that the member behaves in a linear elastic manner under service loads and that both the prestressing force and the external tensile load are concentric to the axis of the member, thus leading to uniform stresses in the section.

In addition to developing the basic analytic equations for prestressed tension members, criteria usually checked in the "review or investigation" process will also be covered in this section. They include: maximum allowable compression, ultimate strength, safety against cracking, safety against decompression, minimum reinforcement, and maximum instantaneous and long-term deformations.

Let us consider a prestressed concrete tension member subjected to an axial force N (Fig. 12.7). According to our sign convention, compression is positive for concrete and tension is positive for the steel. As N is applied to the concrete, it is negative. Standard notation will be used whenever possible.

12.4.1 Service Stresses, Decompression, Cracking and Ultimate Load

The net area of the concrete section subjected to the prestressing force is defined by:

$$A_n = A_g - A_{ps} \tag{12.1}$$

where A_g is the gross sectional area of the concrete section and A_{ps} the area of the prestressing steel.

An external force N applied to the member causes an equal elongation in the steel and the concrete and is resisted by both. Equivalently, it can be shown that N is resisted by the transformed cross-sectional area of the member defined by:

$$A_t = A_n + n_p A_{ps} = A_g + (n_p - 1)A_{ps} \tag{12.2}$$

where $n_p = E_{ps} / E_c$ and E_{ps} and E_c are the moduli of elasticity of the prestressing steel and the concrete.

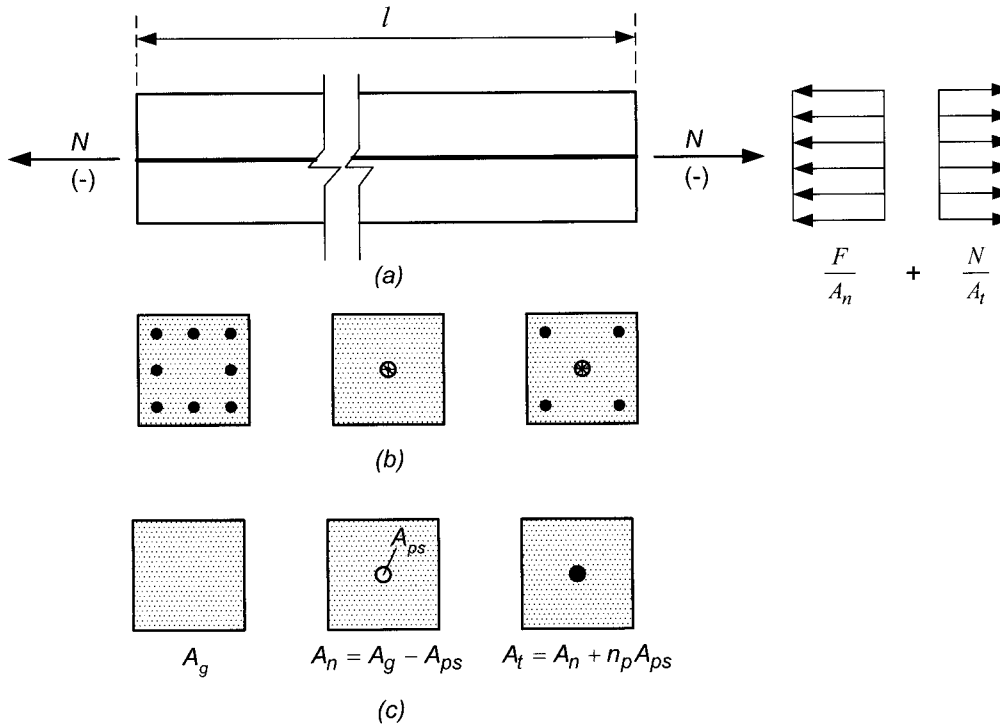

Figure 12.7 ***(a)*** **Prestressed tension member: sign convention.** ***(b)*** **Pretensioned section, posttensioned section, or both.** ***(c)*** **Gross, net, and transformed sections.**

The uniform compressive stress in the concrete due to the prestressing force at release is given by:

$$\sigma_{gi} = \frac{F_i}{A_n} = \frac{A_{ps} f_{pi}}{A_n} \tag{12.3}$$

and the effective stress after all losses is given by:

$$\sigma_g = \frac{F}{A_n} = \frac{A_{ps} f_{pe}}{A_n} \tag{12.4}$$

Note that, in Chapter 4, the gross sectional area A_g was used instead of A_n to determine σ_g and σ_{gi} in beams.

If allowable stresses are not to be exceeded, the following conditions should be satisfied:

$$\begin{cases} \sigma_{gi} \le \bar{\sigma}_{ci} \\ \sigma_g \le \bar{\sigma}_{cs} \end{cases} \tag{12.5}$$

where $\bar{\sigma}_{ci}$ and $\bar{\sigma}_{cs}$ are allowable compressive stresses in the concrete under initial and effective or final prestress. Since the compression is uniform, their magnitude is generally not the same as for flexure where only extreme fiber stresses are considered. The ACI code does not have special provisions for uniform compression; however, in its alternative design method (App. B of the 1989 code), it recommends a maximum bearing stress of $0.30 f'_c$. In practice, it seems reasonable not to exceed such a value in order to minimize creep strains and long-term deformation. Note that ACI Committee 344 suggests the following allowable stresses for tanks: $\bar{\sigma}_{cs} = 0.45 f'_c$ and $\bar{\sigma}_{ci} = 0.55 f'_{ci}$. These are relatively high stresses for uniform compression. However, actual stresses under service loads, which occur when the tank is full, are much smaller [Ref. 12.2 to 12.4].

An external tensile force applied to the member induces a stress change of magnitude N / A_t. The resulting uniform stress in the concrete due to the combined action of F and N is:

$$\sigma_c = \frac{F}{A_n} + \frac{N}{A_t} = \frac{A_{ps} f_{pe}}{A_n} + \frac{N}{A_t} \tag{12.6}$$

where N is negative. The corresponding stress in the prestressing steel is given by:

$$f_{ps} = f_{pe} - n_p \frac{N}{A_t} \tag{12.7}$$

Equation (12.6) can be used to predict the cracking load N_{cr} for which the stress σ_c becomes equal to the tensile strength of the concrete f'_{tc}. It leads to:

$$N_{cr} = A_t\left(f'_{tc} - \frac{F}{A_n}\right) = A_t\left(f'_{tc} - \frac{A_{ps}f_{pe}}{A_n}\right) \tag{12.8}$$

The margin of safety against cracking m_{cr} is defined by:

$$m_{cr} = \frac{N_{cr}}{N} \tag{12.9}$$

A minimum margin of safety is generally required in design. When prior cracking has occurred, subsequent loading of the prestressed member will see cracks opening at a stress $\sigma_c = 0$ instead of f'_{tc}. This stage is called decompression. The tensile load at decompression can be computed from:

$$N_{dec} = -\frac{A_t F}{A_n} = -\frac{A_t A_{ps} f_{pe}}{A_n} \tag{12.10}$$

The margin of safety against decompression is defined by:

$$m_{dec} = \frac{N_{dec}}{N} \tag{12.11}$$

A minimum value of m_{dec} is often required in design. The stress in the prestressing steel just before cracking is given by Eq. (12.7) in which N is replaced by N_{cr}. That is:

$$(f_{ps})_{cr}^{-} = f_{pe} - n_p \frac{N_{cr}}{A_t} \tag{12.12}$$

The stress in the prestressing steel just after first cracking is given by:

$$(f_{ps})_{cr} = \frac{-N_{cr}}{A_{ps}} = \frac{A_t f_{pe}}{A_n} - \frac{A_t f'_{tc}}{A_{ps}} \tag{12.13}$$

It should be less than f_{pu} if failure is not to accompany cracking. This can be satisfied by setting a minimum reinforcement criterion as shown in Sec. 12.5.

The stress in the prestressing steel just after decompression in a previously cracked member is obtained from:

$$(f_{ps})_{dec} = \frac{-N_{dec}}{A_{ps}} = \frac{A_t f_{pe}}{A_n} \tag{12.14}$$

At ultimate loading, the nominal tensile resistance of the cracked section is equal to that of the steel alone. Thus:

$$N_n = -A_{ps} f_{pu} \tag{12.15}$$

Using the ultimate strength design approach prescribed by ACI, the following condition must be satisfied:

$$|N_u| \leq |\phi N_n| \tag{12.16}$$

where N_u is the required factored load or design strength, and ϕ is the resistance factor. Using the 2002 ACI code [Ref. 12.1], we have: $N_u = 1.2N_D + 1.6N_L$, and $\phi = 0.90$ (see Tables 3.9 and 3.10). Absolute values were used in order to keep Eq. (12.16) in accordance with the general form used for other types of loading. Otherwise, since tensile forces are negative, we should have algebraically $N_u \geq \phi N_n$.

12.4.2 Short- and Long-Term Deformations

The instantaneous shortening of a concrete element of length l, subjected to a concentric prestressing force F_i, is given by:

$$\Delta l_i = \frac{F_i l}{A_n E_{ci}} \tag{12.17}$$

A similar expression can be obtained if the final prestressing force F and corresponding E_c are considered.

The instantaneous elongation of a prestressed concrete member subjected to an axial tension N is given by:

$$\Delta l_i = \frac{Nl}{A_t E_c} \tag{12.18}$$

It is to be used for short-term loads such as live loads. Note that N is negative.

Long-term deformations in tensile members depend on many factors, such as the construction method, the stressing sequence, if any, the age at loading, and the

loading history. For instance, if the member is pretensioned and stored in plant for a reasonable period of time, a significant portion of prestress losses would have occurred prior to moving the member to the construction site; also a substantial portion of the additional time-dependent shortening (due to shrinkage and creep) would have occurred by the time the member is attached to the rest of the structure. Thereafter, the application of external loading, that is, tension would relax part of the compression and further reduce additional long-term effect, due to creep recovery. Thus it can be assumed in this case that the member will not shorten much more once attached to the structure. Indeed, it is observed from Chapter 8 that about 85% to 90% of prestress losses will have occurred within the first year of age.

If the tensile member is posttensioned on site, the stress history and deformation history can be followed through the computation of time-dependent prestress losses (see Chapter 8). Under no external loading, the shortening of the member due to elastic stresses, shrinkage and creep of concrete, and relaxation of the steel can be easily followed. Since the steel and the concrete experience the same overall shortening strain, the shortening of the tensile member can be predicted from the prestress losses due to the sum of elastic shortening and time dependent losses after transfer of prestress. Assuming we call that loss Δf^*_{pT}, the shortening of the member after a period corresponding to service life is then given by:

$$\Delta l_{life} = l\frac{\Delta f^*_{pT}}{E_{ps}} \tag{12.19a}$$

If the tensile member is posttensioned on site, the prestress could also be applied in stages depending on the progress of the construction of the structure and the application of the loads. Stage stressing may be designed for an average resulting compressive stress of the same order as the final sustained stress for which instantaneous and long-term deformations can be estimated.

In such a case, a shortening due to the combined effects of prestressing and external load can be computed in function of the average resulting compressive stress σ_c. The instantaneous shortening can be obtained from:

$$\Delta l_i = l\frac{\sigma_c}{E_c} \tag{12.19b}$$

and the additional long-term shortening can be taken as the instantaneous value multiplied by a coefficient, similar to the ultimate creep coefficient discussed in Chapter 7 for the case of long-term deflection.

In summary, there is no general solution to estimating long-term deformations, and engineering judgment must be exercised depending on the particular circumstances. The reader may want to review Chapter 7 on deflections and Chapter

8 on prestress losses for further information. Note that the computations of prestress losses are easier for tensile members than for flexural members, even if the time-step approach is used. This is because a uniform stress exists in the section and corresponding computations of deformations due to creep are greatly simplified.

12.4.3 Example: Analysis-Investigation of a Tension Member

Consider the prestressed concrete tensile member of length 100 ft shown in Fig. 12.8. It is subjected to an axial tensile force in service $N = N_D + N_L = -60{,}000 - 40{,}000 = -100{,}000$ lb. The following material properties are assumed: $f'_c = 6000$ psi, $f'_{ci} = 4500$ psi, $f'_{tc} = -4\sqrt{f'_c} = -310$ psi, $E_c = 4.69\times10^6$ psi, $E_{ci} = 4.06\times10^6$ psi, $\bar{\sigma}_{ci} = 2000$ psi, $\bar{\sigma}_{cs} = 1500$ psi, $f_{pi} = 175{,}000$ psi, $f_{pe} = 145{,}000$ psi, $f_{pu} = 270{,}000$ psi, $E_{ps} = 28.14\times10^6$ psi, $n_p = E_{ps}/E_c = 6$, ultimate creep coefficient of concrete $C_{CU} = 2$. Note that the maximum compression stress is taken smaller than allowed by the ACI code to minimize long-term creep effect.

The following are provided: $A_g = 100$ in^2 and $A_{ps} = 0.918$ in^2. A_{ps} corresponds to the six half-inch diameter prestressing strands; thus $F = A_{ps} f_{pe} = 0.918\times145{,}000 = 133{,}110$ lb and $F_i = A_{ps} f_{pi} = 0.918\times175{,}000 = 160{,}650$ lb.

Let us use the equations and criteria in the order presented in Sec. 12.3, Service Stresses; Cracking and Ultimate Load.

a. Stresses

Equation (12.1): $A_n = A_g - A_{ps} = 100 - 0.918 \simeq 99.08$ in^2

Equation (12.2): $A_t = A_g + (n_p - 1)A_{ps} = 100 + (6-1)0.918 \simeq 104.59$ in^2

Equation (12.3): $\sigma_{gi} = \dfrac{F_i}{A_n} = \dfrac{160{,}650}{99.08} = 1621$ psi

Equation (12.4): $\sigma_g = \dfrac{F}{A_n} = \dfrac{133{,}110}{99.08} = 1343$ psi

Equation (12.5): $\begin{cases} \sigma_{gi} < \bar{\sigma}_{ci} = 2000 \text{ psi} \\ \sigma_g < \bar{\sigma}_{cs} = 1500 \text{ psi} \end{cases}$

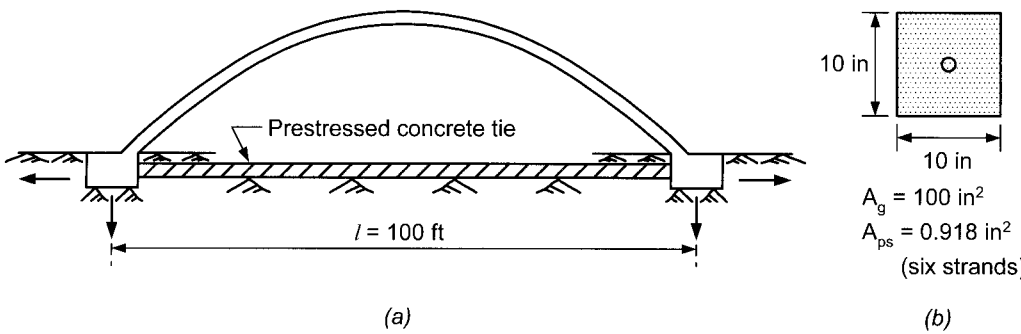

Figure 12.8 Investigation example. ***(a)*** **Tie position within structure.** ***(b)*** **Tie cross section.**

Thus, the allowable stress criterion is satisfied. The stress in the concrete under combined final prestressing force and external tension N is given by Eq. (12.6):

$$\sigma_c = \frac{133{,}110}{99.08} - \frac{100{,}000}{104.59} \simeq 387 \text{ psi}$$

b. Cracking and Decompression Load

The external tensile force that would produce first cracking in the member is given by Eq. (12.8):

$$N_{cr} = A_t\left(f'_{tc} - \frac{F}{A_n}\right) = 104.59\left(-310 - \frac{133{,}110}{99.08}\right) = -172{,}935 \text{ lb}$$

The corresponding margin of safety against cracking is given by Eq. (12.9):

$$m_{cr} = \frac{N_{cr}}{N} = \frac{-172{,}935}{-100{,}000} \simeq 1.73$$

and seems sufficient.

The external load that would lead to decompression is given by Eq. (12.10):

$$N_{dec} = -\frac{A_t F}{A_n} = -\frac{104.59 \times 133{,}110}{99.08} = -140{,}512 \text{ lb}$$

and the margin of safety against decompression (Eq. (12.11)) is:

$$m_{dec} = \frac{N_{dec}}{N} = \frac{-140{,}512}{-100{,}000} \simeq 1.40$$

c. Cracking and Decompression Stresses

The stress in the prestressing steel just before first cracking is given by Eq. (12.12):

$$\left(f_{ps}\right)^{-}_{cr} = f_{pe} - n_p \frac{N_{cr}}{A_t} = 145{,}000 + \frac{6 \times 172{,}935}{104.59} = 154{,}920 \text{ psi}$$

The stress in the prestressing steel just after cracking is given by Eq. (12.13):

$$\left(f_{ps}\right)_{cr} = \frac{-N_{cr}}{A_{ps}} = \frac{172{,}935}{0.918} = 188{,}382 \text{ psi}$$

and is less than f_{pu}, the ultimate strength of the steel, with an allowance for an adequate safety margin.

Note that the stress jump at cracking can be computed from:

$$\left(f_{ps}\right)_{cr} - \left(f_{ps}\right)^{-}_{cr} = 188{,}382 - 154{,}920 = 33{,}462 \text{ psi}$$

This is a relatively high value if debonding on either side of the crack is to be limited. However, unless cracking is artificially produced, such stress jumps cannot be avoided in tensile members.

The stress in the steel just after decompression in a previously cracked member is given by Eq. (12.14):

$$\left(f_{ps}\right)_{dec} = \frac{-N_{dec}}{A_{ps}} = \frac{140{,}512}{0.918} = 153{,}063 \text{ psi}$$

The stress in the prestressing steel just before decompression in a cracked member, or at decompression in an uncracked member, can also be obtained from Eq. (12.7) in which N is replaced by N_{dec}, thus

$$\left(f_{ps}\right)_{dec} = f_{pe} - n_p \frac{N_{dec}}{A_t} = 145{,}000 + \frac{6 \times 140{,}512}{104.59} \simeq 153{,}061 \text{ psi}$$

This is essentially the same as the previously calculated value indicating that the stress jump vanishes once first cracking has occurred.

d. Nominal Tensile Resistance

The nominal resistance of the member at ultimate is given by:

$$N_n = -A_{ps} f_{pu} = -0.918 \times 270{,}000 = -247{,}860 \text{ lb}$$

Thus:

$$\phi N_n = -0.9 \times 247{,}860 = -223{,}074 \text{ lb}$$

Using the 2002 ACI Code load factors, the design strength is given by:

$$N_u = -1.2 \times 60{,}000 - 1.6 \times 40{,}000 = -136{,}000 \text{ lb}$$

Since $|N_u| < |\phi N_n|$ ultimate strength requirements are satisfied.

e. Deformation

To illustrate deformation computations, let us consider two cases:

Case 1. Assume the member is posttensioned on site and immediately thereafter scaffolding is removed under the structure and the dead load N_D is applied. Using an average prestressing force $(F + F_i)/2 = 146{,}880$ lb, and an average modulus $(E_c + E_{ci})/2 = 4.375 \times 10^6$ psi, the resulting stress in the concrete can be computed from Eq. (12.6):

$$\sigma_c = \frac{F}{A_n} + \frac{N}{A_t} = \frac{146{,}880}{99.08} - \frac{60{,}000}{104.59} \simeq 909 \text{ psi}$$

The corresponding value of average instantaneous shortening (to be used in design) is given by Eq. (12.19b):

$$\Delta l_i = l \frac{\sigma_c}{E_c} = \frac{100 \times 12 \times 909}{4.375 \times 10^6} \simeq 0.25 \text{ in}$$

Additional long-term shortening can be obtained, as a first approximation, by multiplying Δ_i by $C_{CU} = 2$. Thus:

$$\Delta l_{\text{add}} = 2 \times 0.25 = 0.50 \text{ in}$$

Note that the live load would produce an elongation given by Eq. (12.18):

$$\Delta l_i = \frac{Nl}{A_t E_c} = \frac{-40{,}000 \times 100 \times 12}{104.59 \times 4.69 \times 10^6} \simeq -0.1 \text{ in}$$

Hence, long-term deformation will be most critical and its effect on the rest of the structure must be assessed.

Case 2. Assume the member is pretensioned, stored, and attached to the structure only at one year of age. Also assume that the dead load N_D is applied immediately thereafter. Most of the long-term shortening of the member would have taken place prior to attaching it to the rest of the structure. The application of N_D would produce an instantaneous elongation given by Eq. (12.18):

$$\Delta l_i = \frac{Nl}{A_t E_c} = \frac{-60{,}000 \times 100 \times 12}{104.59 \times 4.69 \times 10^6} \simeq -0.15 \text{ in}$$

Some creep recovery will also occur. However, the resulting stress in the concrete remains a compression and is given by Eq. (12.6):

$$\sigma_c = \frac{F}{A_n} + \frac{N}{A_t} = \frac{133{,}110}{99.08} - \frac{60{,}000}{104.59} \simeq 770 \text{ psi}$$

One can estimate additional long-term shortening due to this sustained stress, say only about 20 percent of what it would be if prior creep and shrinkage have not occurred over one year of age. Its value may be estimated from:

$$\Delta l_{\text{add}} = -0.20 C_{CU}\left(\frac{l\sigma_c}{E_c}\right) = 0.4\left(\frac{1200\times 770}{4.69\times 10^6}\right) \simeq 0.08 \text{ in}$$

This value partly balances the instantaneous elongation due to N_L. Thus, little long-term shortening is expected for the sustained loading. Deformation is not critical in this case.

12.5 OPTIMUM DESIGN OF TENSION MEMBERS

Unless the various design criteria are clearly understood and accounted for, the design of prestressed concrete tension members may often err on the unsafe side and may lead to inconsistent results. Most common design criteria have been mentioned in Section 12.4 on analysis. Depending on the particular problem, other criteria may be added. For instance, in partially prestressed members, a maximum crack width criterion may be necessary. Each criterion leads to an analytic relationship to be satisfied by the design. Only two unknowns are needed in practice, the area of prestressing steel A_{ps} and the gross sectional area of the concrete A_g. Other variables may be assumed at first and revised later, if necessary. Generally, it is not possible to know a priori which criterion or set of criteria will control a particular design.

A systematic procedure is proposed next, which would guarantee a range of satisfactory designs and, if desired, an optimum design [Ref. 12.20]. In this procedure, each design criterion is expressed in function of the two unknown variables A_{ps} and A_g and a feasibility domain is sought in a way similar to what was done in Chapter 4 for F_i and e_o. Any point within the domain should provide an acceptable design, while generally only one point provides an optimum (minimum cost) design. The various criteria and the corresponding analytic relationships are given next.

12.5.1 Formulation of Design Criteria

(a) Maximum compressive stress criterion. It stipulates that the maximum uniform compressive stress in the concrete should not exceed the corresponding allowable stress. From Eqs. (12.3) to (12.5), we have:

$$\begin{cases} \dfrac{A_{ps} f_{pi}}{A_n} \le \bar{\sigma}_{ci} \\ \dfrac{A_{ps} f_{pe}}{A_n} \le \bar{\sigma}_{cs} \end{cases} \tag{12.20}$$

Replacing A_n by its value from Eq. (12.1) leads to the following inequality conditions written in terms of A_{ps} and A_g:

$$\begin{cases} A_{ps} \le \dfrac{A_g}{1 + f_{pi} / \bar{\sigma}_{ci}} \\ A_{ps} \le \dfrac{A_g}{1 + f_{pe} / \bar{\sigma}_{cs}} \end{cases} \tag{12.21}$$

These equations, at equality are represented by straight lines on a graph with A_{ps} as ordinate and A_g as abscissa. Each inequality is satisfied for any point below the corresponding line. A typical example is shown in Fig. 12.9 where the lines are marked *(a')* and *(a)*.

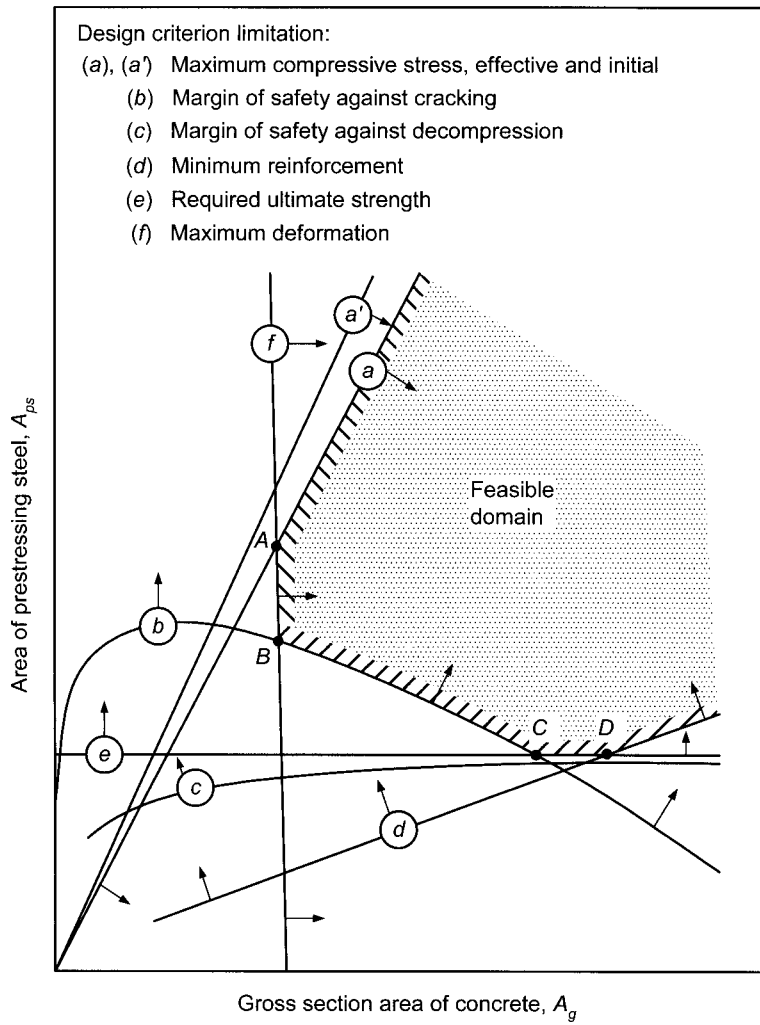

Figure 12.9 Geometric representation of the various design criteria and the feasible domain.

(b) Margin of safety against cracking criterion. Because cracking is such a dramatic event in prestressed tensile members, it is generally wise to design for a minimum margin of safety against cracking, $\bar{m}_{cr}$, the value of which should depend on the type of structure, the probability of overload, and the risk associated with cracking (i.e., a water tank versus a nuclear power containment vessel; a short bridge versus a long bridge). Thus, we have the following condition:

$$\frac{N_{cr}}{N} \geq \bar{m}_{cr} \tag{12.22}$$

Using Eq. (12.8) for N_{cr} and noting that N is negative, leads to:

$$\bar{m}_{cr} N \geq A_t \left(f'_{tc} - \frac{A_{ps} f_{pe}}{A_n} \right) \tag{12.23}$$

Replacing A_n and A_t by their values from Eqs. (12.1) and (12.2) in Eq. (12.23) leads to the following quadratic equation in A_{ps} :

$$\begin{aligned} A_{ps}^2 (n_p - 1)(f_{pe} + f'_{tc}) + A_{ps}[A_g f_{pe} - A_g (n_p - 2) f'_{tc} - \bar{m}_{cr} N] \\ + A_g (\bar{m}_{cr} N - A_g f'_{tc}) \geq 0 \end{aligned} \tag{12.24}$$

At equality, Eq. (12.24) has generally two roots of opposite signs. The positive root of interest here is given by:

$$A_{ps} = -\left(\frac{b}{2a} \right) + \sqrt{\left(\frac{b}{2a} \right)^2 - \frac{c}{a}} \tag{12.25}$$

in which:

$$\frac{b}{2a} = \frac{-A_g \left[f_{pe} - (n_p - 2) f'_{tc} \right] - \bar{m}_{cr} N}{2(n_p - 1)(f_{pe} + f'_{tc})} \tag{12.26}$$

$$\frac{c}{a} = \frac{A_g (\bar{m}_{cr} N - A_g f'_{tc})}{(n_p - 1)(f_{pe} + f'_{tc})} \tag{12.27}$$

Note that A_{ps} can be plotted in function of A_g on the same x-y graph as was done for the other criteria. It separates the plane into two regions. The minimum

required margin of safety is obtained for any point above the curve. A typical such curve is plotted in Fig. 12.9 and marked *b*.

(c) Margin of safety against decompression criterion. Similarly to the minimum margin of safety against cracking, a minimum margin of safety against decompression, $\bar{m}_{dec}$, may represent an important safety measure. Thus, the following condition can be set:

$$\frac{N_{dec}}{N} \geq \bar{m}_{dec} \tag{12.28}$$

The treatment of this case is exactly similar to case *b* above, except that f'_{tc} is replaced by zero. It leads to:

$$A_{ps} = -\left(\frac{b}{2a}\right) + \sqrt{\left(\frac{b}{2a}\right)^2 - \frac{c}{a}} \tag{12.25}$$

in which:

$$\frac{b}{2a} = \frac{-A_g f_{pe} - \bar{m}_{dec} N}{2(n_o - 1) f_{pe}} \tag{12.29}$$

$$\frac{c}{a} = \frac{A_g \bar{m}_{dec} N}{(n_p - 1) f_{pe}} \tag{12.30}$$

A_{ps} is plotted versus A_g and the points of the plane above the curve satisfy the required margin of safety against decompression. A typical such plot is shown as curve *c* in Fig. 12.9.

(d) Minimum reinforcement criterion. This criterion would ensure that failure does not occur immediately after cracking. Thus, we can write the following condition:

$$\phi A_{ps} f_{pu} \geq |\alpha N_{cr}| \quad \text{or} \quad \geq -\alpha N_{cr} \tag{12.31}$$

where α is a factor not less than one. The ACI code prescribes a similar condition for flexure where α = 1.2. Replacing N_{cr} by its value from Eq. (12.8) leads to:

$$\phi A_{ps} f_{pu} \geq -\alpha A_t \left(f'_{tc} - \frac{F}{A_n} \right) \tag{12.32}$$

where A_n and A_t can be replaced by their values from Eqs. (12.1) and (12.2). The resulting equation is lengthy but not impossible to solve. Because this condition seldom controls the design and a high level of accuracy is not needed for a minimum level of reinforcement, the following approximation is proposed: assume $A_t \simeq A_n \simeq A_g$; Eq. (12.32) would lead to:

$$A_{ps} \geq \left(\frac{-\alpha f'_{tc}}{\phi f_{pu} - \alpha f_{pe}} \right) A_g \tag{12.33}$$

Typically, it is represented at equality by a straight line marked *d* in Fig. 12.9. Any point above the line should satisfy the minimum reinforcement criterion.

(e) Required ultimate strength criterion. It guarantees an ultimate resistance not less than the factored strength design load. Using Eqs. (12.15) and (12.16), we have:

$$A_{ps} \geq \frac{-N_u}{\phi f_{pu}} \tag{12.34}$$

which is represented at equality by a straight line marked *e* in Fig. 12.9.

(f) Maximum deformation criterion. This criterion guarantees an allowable deformation $\overline{\Delta l}$ (elongation or shortening) under a given load or a combination of loadings. It should be tailored to the particular problem at hand. If, for instance, the instantaneous elongation under live load N_L is to be limited to $\overline{\Delta l}$ (negative value), we will have the following condition:

$$\frac{-N_L l}{E_c A_t} \leq -\overline{\Delta l} \quad \text{or} \quad \frac{N_L l}{E_c A_t} \geq \overline{\Delta l} \tag{12.35}$$

and replacing A_t by its value from Eq. (12.2) leads to:

$$A_{ps} \geq -\frac{A_g}{n_p - 1} + \frac{N_L l}{(n_p - 1) E_c \overline{\Delta l}} \tag{12.36}$$

which, at equality, is represented by a straight line marked *f* in Fig. 12.9.

A similar approach can be used for limiting the additional long-term deformation by estimating the instantaneous deformation first and multiplying it by an appropriate factor. A relation similar to Eq. (12.36) is generally obtained and can be plotted on an A_{ps} versus A_g graph.

A geometric representation of the feasible sets of values of A_{ps} and A_g that satisfy all the above criteria is shown in Fig. 12.9 and is defined as the feasible domain. A wide range of possibilities is available. The choice of the design point should be in a region where both A_{ps} and A_g are minimized (somewhere between *B* and *C*). A more accurate minimum cost solution can be sought as shown below in Section 12.5.3.

12.5.2 Design Approximations

Two design approximations are suggested: one is a heuristic rule (also described as rule of thumb) and should be used with engineering judgment, and the other greatly simplifies the geometric solution.

(a) Heuristic rule (or rule of thumb) for pure tensile members

- Use a value of F 20 percent higher than the tensile load in service, that is $F = 1.2|N|$
- Determine A_g based on a uniform compressive stress $\sigma_g = 0.25 f'_c$ under F, that is $A_g \simeq F/(0.25 f'_c) = 1.2|N|/(0.25 f'_c) = 4.8|N|/f'_c$.
- Compute $A_{ps} = F / f_{pe}$
- For the tensile member obtained check other criteria, and revise the design accordingly.

(b) Linearization of the safety criteria against cracking and decompression

All design criteria covered in the preceding subsection led to straight lines in Fig. 12.9, except the two criteria dealing with safety against cracking and decompression. The computations would gain enormous speed if these two criteria were approximated by straight lines. This can be simply done by assuming for these criteria only that $A_t \simeq A_n \simeq A_g$ over the range of interest. Equation (12.23) would then lead to the following conditions:

For the margin of safety against cracking:

$$A_{ps} \geq \frac{f'_{tc}}{f_{pe}} A_g - \frac{\bar{m}_{cr} N}{f_{pe}} \tag{12.37}$$

and for the margin of safety against decompression:

$$A_{ps} \geq -\frac{\bar{m}_{dec} N}{f_{pe}} \tag{12.38}$$

Equations (12.37) and (12.38) would replace Eqs. (12.25) to (12.30) and therefore the geometric feasibility domain, bound entirely by straight lines, can be easily built. In addition, the solution for minimum cost becomes readily obtainable requiring only one additional step as shown next.

12.5.3 Minimum Cost Solution

The cost of the tensile member per unit length, defined by Z, can be expressed as follows:

$$Z = U_p W_{ps} + U_c V_c \tag{12.39}$$

where:

W_{ps} = weight of prestressing steel per unit length
U_p = unit cost of prestressing steel in place
V_c = volume of concrete per unit length
U_c = unit cost of concrete in place.

Using U.S. units, W_{ps} will be given in pounds per foot, U_p in dollars per pound, V_c in cubic yards per foot, and U_c in dollars per cubic yard. Thus, Z is the cost in dollars per linear foot of member and the coefficients in the following equations are valid for the U.S. system only. Theoretically, they can be developed for any other system.

W_{ps} and V_c can be expressed, respectively, in functions of A_{ps} and A_g, leading to:

$$Z = U_p \left(\frac{\gamma_s A_{ps}}{144} \right) + U_c \left(\frac{A_g}{144 \times 27} \right) \tag{12.40}$$

where γ_s is the unit weight of steel in pounds per cubic foot. Equation (12.40) is a linear equation in A_{ps} and A_g.

The following general optimization problem can be formulated:

$$\text{Minimize cost } Z = \left(\frac{\gamma_s U_p}{144}\right) A_{ps} + \left(\frac{U_c}{3888}\right) A_g \tag{12.41}$$

subject to a number of constraints given by Eqs. (12.21), (12.33), (12.34), (12.36), (12.37), and (12.38) and representing the various design criteria. Since the above objective function and the constraints are linear, the problem is a linear optimization problem. It can be solved by any linear programming algorithm. In such a case, it is known that the optimum solution corresponds to one of the vertices of the feasible geometric domain, such as points *A*, *B*, *C* or *D* of Fig. 12.10. The minimum cost solution can be found by inspection or by plotting the objective function (Eq. (12.41)) on the same graph as the feasible domain; the objective function is written in the following linear form:

$$A_{ps} = -\left(\frac{U_c}{27\gamma_s U_p}\right) A_g + \frac{144Z}{\gamma_s U_p} \tag{12.42}$$

where A_{ps} is the ordinate and A_g the abscissa.

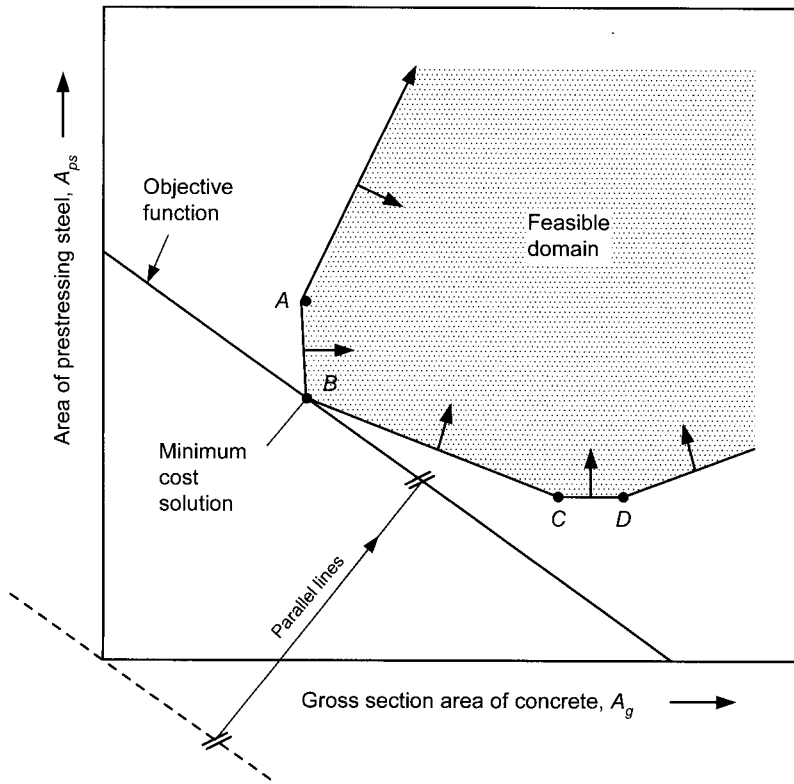

Figure 12.10 Graphical solution for the minimum-cost design problem.

The representative line can be moved graphically parallel to itself from $Z = 0$ to a minimum Z for which only one point of the line belongs to the feasible domain. As we mentioned earlier, that point is a vertex and gives the minimum cost solution (point B in Fig. 12.10). Other approaches or special cases particular to linear programming problems apply here as well. The method is illustrated in Fig. 12.10.

12.5.4 Example

Find the values of A_{ps} and A_g for the Example in Sec. 12.4, assuming they are not given. All other information is the same.

The design has to accommodate the following minimum requirements: $\bar{m}_{cr} = 1.5$, $\bar{m}_{dec} = 1.2$, ultimate resistance at least 20 percent higher than the cracking load, and an instantaneous elongation not to exceed $\overline{\Delta l} = -0.15$ in for an overload 50 percent higher than the live load.

Let us write the relationships between A_{ps} and A_g for the various design criteria and build the corresponding feasible domain graphically.

(a) Maximum compressive stress criterion. Using Eq. (12.21) leads to:

$$A_{ps} \le \frac{A_g}{1 + f_{pi}/\bar{\sigma}_{ci}} = \frac{A_g}{1 + 175{,}000/2000} = \frac{20}{1770} A_g$$

and

$$A_{ps} \le \frac{A_g}{1 + f_{pe}/\bar{\sigma}_{cs}} = \frac{A_g}{1 + 145{,}000/1500} = \frac{15}{1465} A_g$$

The corresponding lines at equality are plotted in Fig. 12.11 and marked a' and a, respectively. Note, a is more critical than a'.

(b) Margin of safety against cracking. Using the linear approximation given by Eq. (12.37) leads to:

$$A_{ps} \ge \frac{f'_{tc}}{f_{pe}} A_g - \frac{\bar{m}_{cr} N}{f_{pe}} = \frac{-310}{145{,}000} A_g + \frac{1.5 \times 100{,}000}{145{,}000}$$

that is:

$$A_{ps} \ge -\frac{31}{14{,}500} A_g + \frac{150}{145}$$

The corresponding line at equality is plotted in Fig. 12.11 and marked b. Also plotted as a dashed line marked b' is the exact solution corresponding to Eq. (12.25). It gives the reader the opportunity to check it.

Note: The approximation obtained using Eq. (12.37) is on the safe side.

(c) Margin of safety against decompression. Using the linear approximation given by Eq. (12.38) leads to:

$$A_{ps} \ge -\frac{\bar{m}_{dec} N}{f_{pe}} = \frac{1.2 \times 100{,}000}{145{,}000} = 0.83 \text{ in}^2$$

The corresponding line at equality is parallel to the x axis and marked c in Fig. 12.11.

(d) Minimum reinforcement criterion. Using Eq. (12.33) leads to:

$$A_{ps} \geq \left(\frac{-\alpha f'_{tc}}{\phi f_{pu} - \alpha f_{pe}} \right) A_g = \frac{1.2 \times 310}{0.9 \times 270{,}000 - 1.2 \times 145{,}000} A_g = \frac{372}{69{,}000} A_g$$

The corresponding line at equality is plotted on Fig. 12.11 and marked *d*.

(e) Ultimate strength criterion. Using Eq. (12.34), we have:

$$A_{ps} \geq \frac{-N_u}{\phi f_{pu}} = \frac{136{,}000}{0.9 \times 270{,}000} \simeq 0.56 \text{ in}^2$$

and the corresponding line at equality is parallel to the *x* axis and marked *e* on Fig. 12.11.

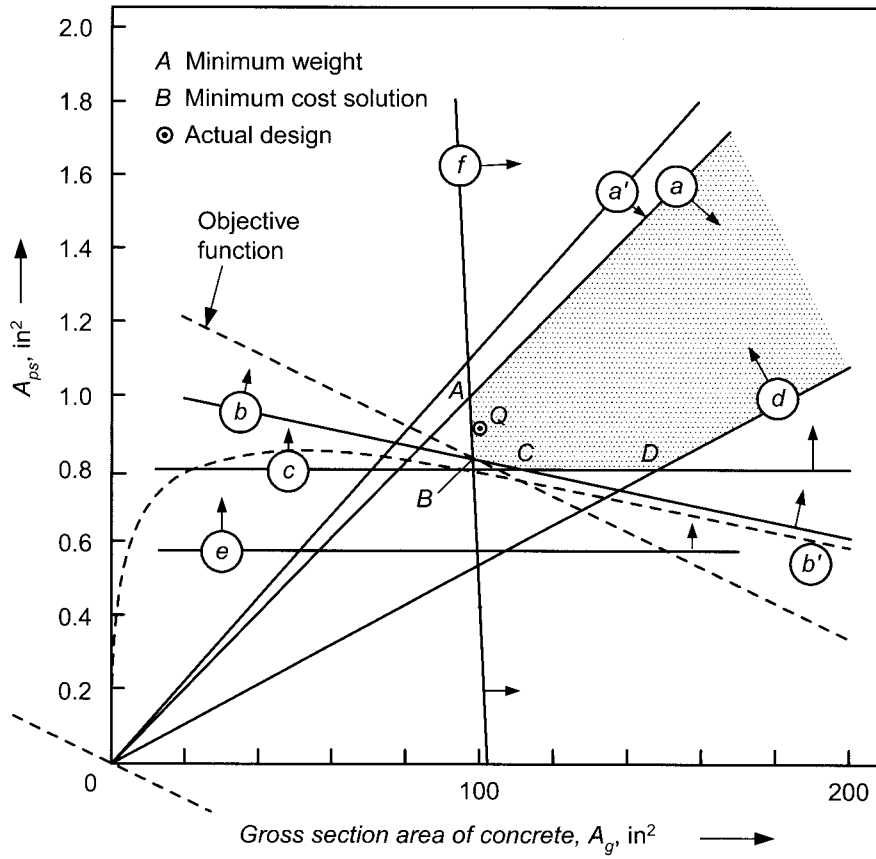

Figure 12.11 Minimum-cost solution for Example 12.5.4.

(f) Maximum deformation criterion. Using Eq. (12.36) for an overload 50 percent higher than the live load (-60,000 lb) and a limit $\overline{\Delta l} = -0.15$ in, we have:

$$A_{ps} \geq -\frac{A_g}{n_p - 1} + \frac{N_L l}{(n_p - 1) E_c \overline{\Delta l}} = -\frac{A_g}{5} + \frac{60{,}000 \times 100 \times 12}{5 \times 4.69 \times 10^6 \times 0.15}$$

that is:

$$A_{ps} \geq -\frac{A_g}{5} + 20.47$$

The corresponding line at equality is plotted in Fig. 12.11 and marked *f*.

The feasible domain is thus identified in Fig. 12.11 and any point inside the domain is a feasible solution. Let us try to approach a minimum-cost solution. Assuming U_c = \$80 per cubic yard (this value is assumed to include the cost of forms for this type of structure), U_p = \$1.25 per pound, γ_s = 490 pcf and using these values in Eq. (12.42) leads to:

$$A_{ps} \simeq -0.0048 A_g + 0.235Z$$

A first dashed line is plotted for Z = 0 and gives the needed slope of -0.0048. A parallel that touches the domain at point *B* gives the minimum intercept leading to the minimum cost *Z*. Thus, point *B* corresponds to the minimum-cost solution with $A_{ps} \simeq 0.825$ in^2 and $A_g \simeq 98.2$ in^2. However, in rounding off the numbers, a value of $A_g = 100$ in^2 and $A_{ps} = 0.918$ in^2 (corresponding to six strands) is selected and leads to the same results as used in the example in Sec. 12.4. The corresponding point is marked *Q* in Fig. 12.11. Note that the coordinates of point *B* can also be obtained from the point of intersection of lines *b* and *f*. The minimum cost *Z* is then calculated from Eq. (12.41) in which A_{ps} and A_g are replaced by their optimum values.

12.6 CIRCULAR STRUCTURES: TANKS AND PRESSURE VESSELS

Because it can remain crack-free when sustaining tensile stresses, prestressed concrete is an ideal material for tanks, reservoirs, pipes, pressure vessels, and containers in general. Although early applications were mostly for water tanks, they have expanded to accommodate oil, gas, chemicals, slurries, liquids at cryogenic temperatures, and granular materials (silos). Nuclear containment vessels are among the largest scale applications. Typical elevation cross sections of a nuclear containment vessel and an open water tank are shown in Figs. 12.12*a* and 12.12*b*, respectively. Typical pressure profiles on the cylindrical wall are shown in Fig. 12.12*c*. A uniform pressure develops along the wall for a closed tank subjected to an internal pressure *p*, such as for the case of a nuclear power vessel or a liquefied natural gas tank. A triangular pressure profile following the water depth develops for a water tank. If an open tank similar to that described in Fig.12.12*b* is filled with grain, such as in the case of a silo, the pressure profile would be trapezoidal, building up rapidly and reaching a threshold value at which it remains constant over the greater part of the depth due to arching action. Arching action is insured by the higher ratio of depth to diameter and the properties of the granular material. The pressure then decreases again to zero at the bottom of the tank.

Several methods can be used to build cylindrical water tanks [Refs. 12.2 to 12.4, 12.14, 12.23, 12.24, and 12.25]. Most popular in the United States is the wire-winding technique in which a concrete core (the tank wall) is built first and a single tendon (wire or strand) is wound around it under stress, thus creating the necessary prestress in the wall (Figs. 1.18, 12.13*a* and 12.13*b*). Once the prestressing operation is completed, the tendons are covered with a layer of mortar generally applied by "guniting" or "shotcreting" (Fig. 12.13*a*). Practical provisions for the design and construction of this type of structures can be found in Refs. [12.2 and 12.3]. Alternatively, as in posttensioned members, the prestressing tendons can be placed in

ducts within the tank wall and posttensioned after the concrete reaches a sufficient resistance (Fig. 12.13*b*). The ducts are then grouted to ensure proper bond. Tensioning is achieved from several buttresses (commonly 3 to 6), distributed along the periphery of the tank, at which the tendons overlap, as shown in Fig. 12.13*c*.

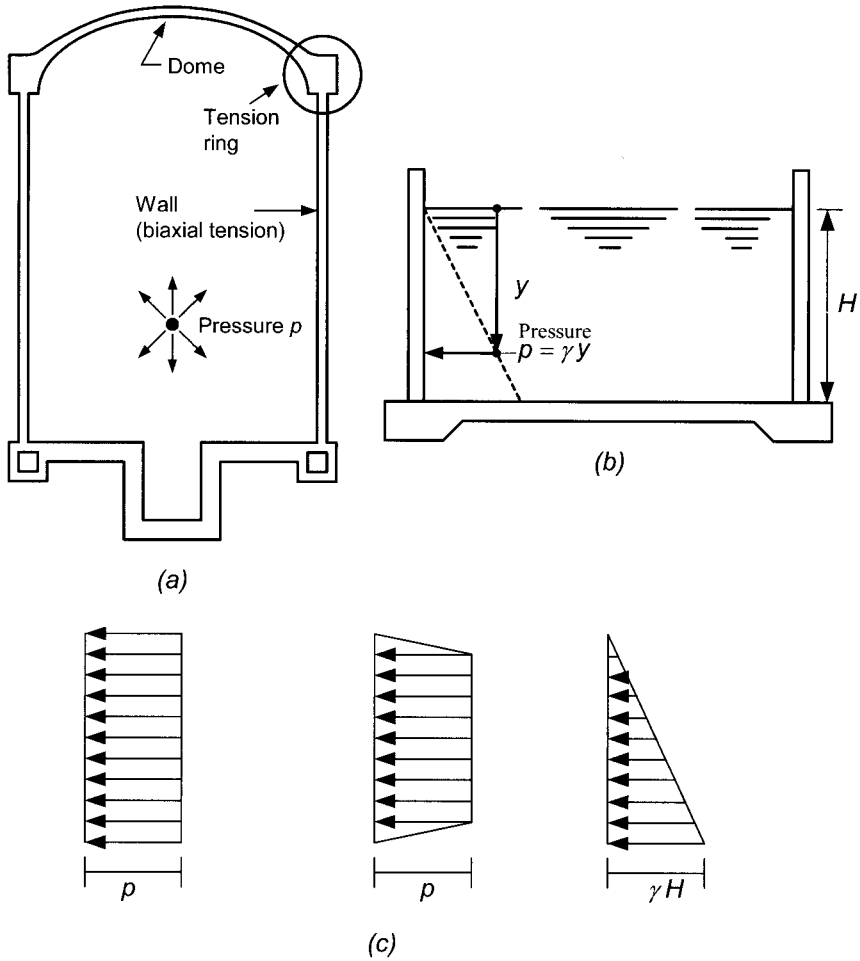

Figure 12.12 *(a)* **Typical nuclear containment structure.** *(b)* **Typical cylindrical water tank. (c) Pressure profile on the wall of (from left to right) a containment vessel, a silo filled with grain, and a water tank**

Unbonded tendons can also be used for convenience, provided the criteria for ultimate strength and stiffness after cracking are satisfied; stiffness is achieved by addition of non-prestressed conventional bars. In nuclear power vessels, unbonding the tendons allows for their future replacement should inspection reveal corrosion or deterioration in these tendons.

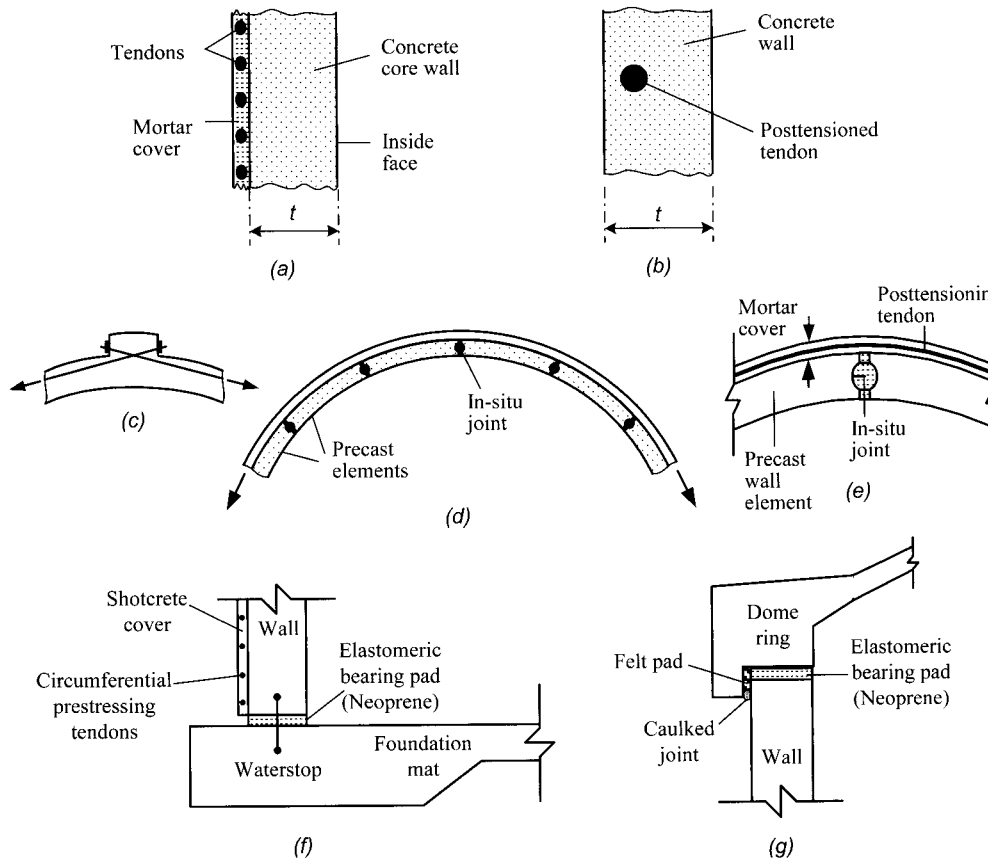

Figure 12.13 ***(a)*** **Tank wall section using wire-winding technique.** ***(b)*** **Posttensioned wall.** ***(c)*** **Posttensioning buttress.** ***(d)*** **Wall made of precast elements. (e) Joint detail for precast elements.** ***(f)*** **and** ***(g)*** **Support details to allow free expansion and contraction.**

Another technique of tank construction consists of using precast wall units, jointed on site to form the wall of the tank, then posttensioned by wire-winding or regular posttensioning (Fig. 12.13*d*) [Ref. 12.23]. Details of the joints between wall units are shown in Fig. 12.13*e*.

In tanks or vessels that are not monolithically cast or rigidly connected, the foundation mat, the roof structure, and the cylindrical wall are designed as separate units and simply supported to allow movement of the supports. Examples of support details are shown in Figs. 12.13*f* and 12.13*g*. The use of elastomeric pads allows for radial movement of the supports due to expansion or contraction.

Open tanks that are restrained at their base also need structural reinforcement (in addition to shrinkage and temperature reinforcement) in the vertical direction in the form of reinforcing bars or prestressed tendons. Pressure vessels need biaxial prestressing to balance tensile stresses in both the circumferential and meridional directions.

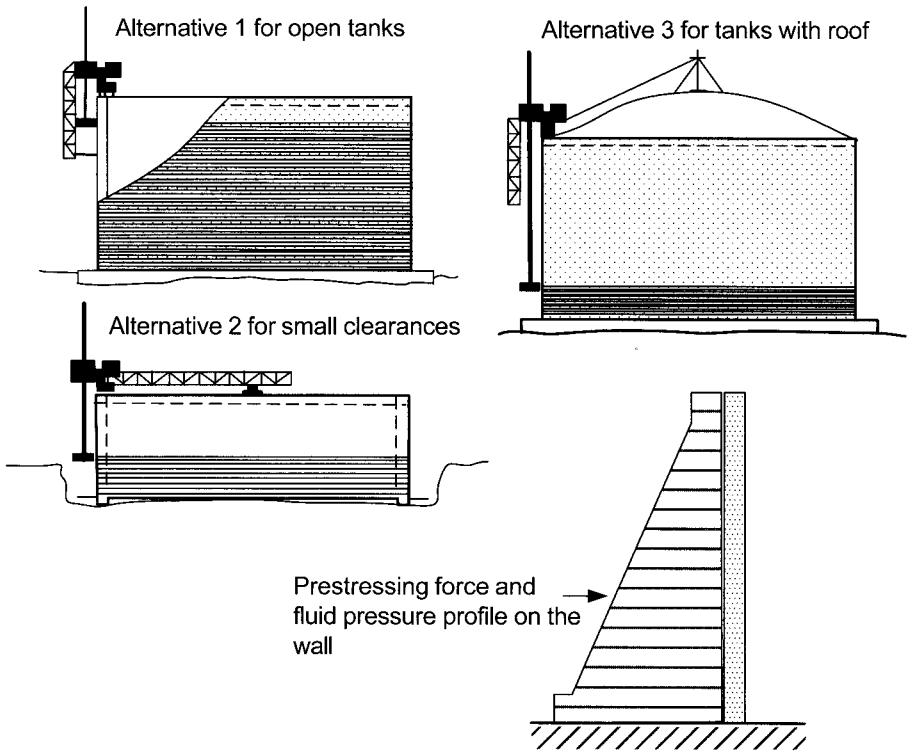

Figure 12.13 -continued *(h)* Examples of construction of new tanks and/or repair and strengthening of existing tanks by the wire-winding technique. These were considered for the project Erdoelchemie Dormagen, Germany.

12.6.1 Analysis of Stresses

Most prestressed concrete tanks and vessels are figures of revolution, that is, they have a circular cross section. In the simplest cases, they are subjected to pure tensile stresses in one or two directions. However, other effects, such as end restraints, creep, shrinkage, temperature changes, and even swelling under water lead to a more complex state of stress and should be considered in the final analysis.

For instance, restraining the base of the wall of an open tank causes significant bending stresses in the vertical (meridional) direction. These must be rationally evaluated and properly resisted by reinforcing or prestressing in the vertical direction. Depending on the extent of the restraint at the base, significant reduction in hoop or ring forces is achieved. As illustrated in Fig. 12.14, a fully fixed base leads to zero ring force at the base, while a free sliding base leads to a maximum ring force. While the restraint leads to a reduction in the ring force, it generates a bending in the vertical wall element.

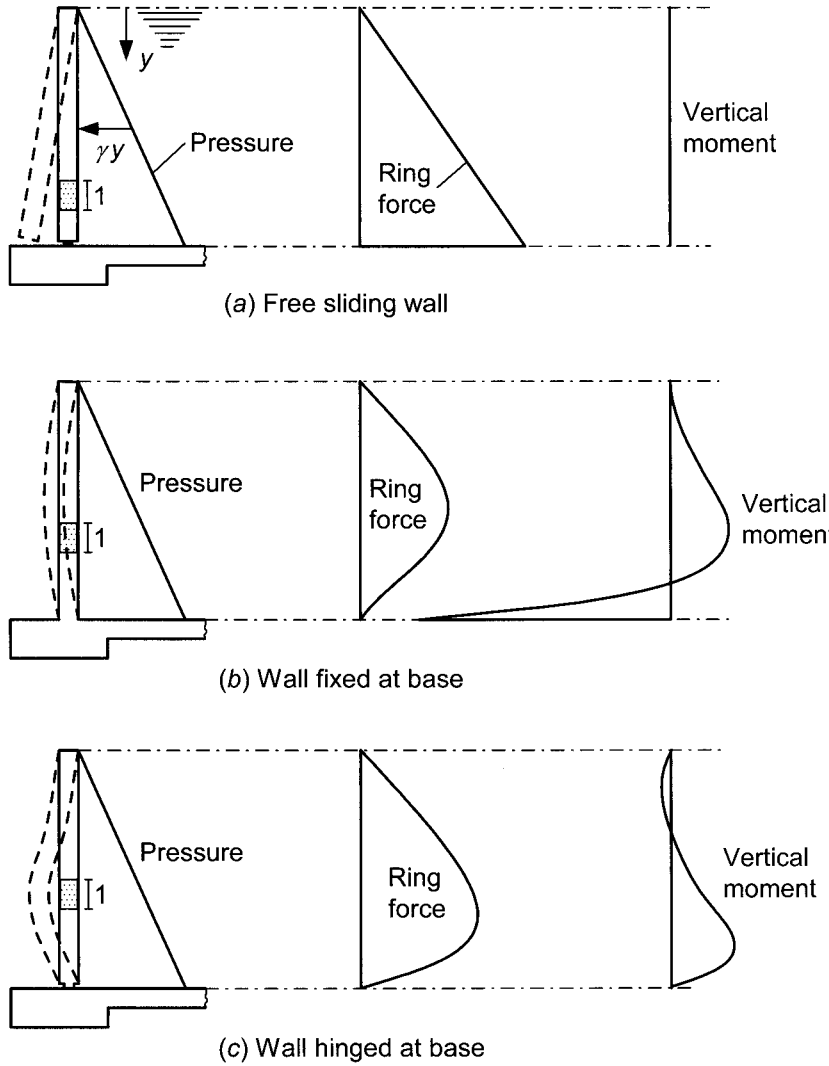

Figure 12.14 Influence of base restraints on ring forces and bending moments in tank walls.

The analysis of prestressed concrete tanks and vessels should be based on accepted methods of shell analysis (generally elastic) where stresses and deformations can be determined for the specified loads and boundary conditions. In the following discussion, only one type of tank will be discussed, that is, a tank with a sliding base (and top, if applicable) in which the wall acts as a pure tensile element. The reader is referred to other specialized documents for additional information on the design of tanks having different boundary conditions [Refs. 12.6, 12.7, 12.9, 12.13, 12.21, and 12.26].

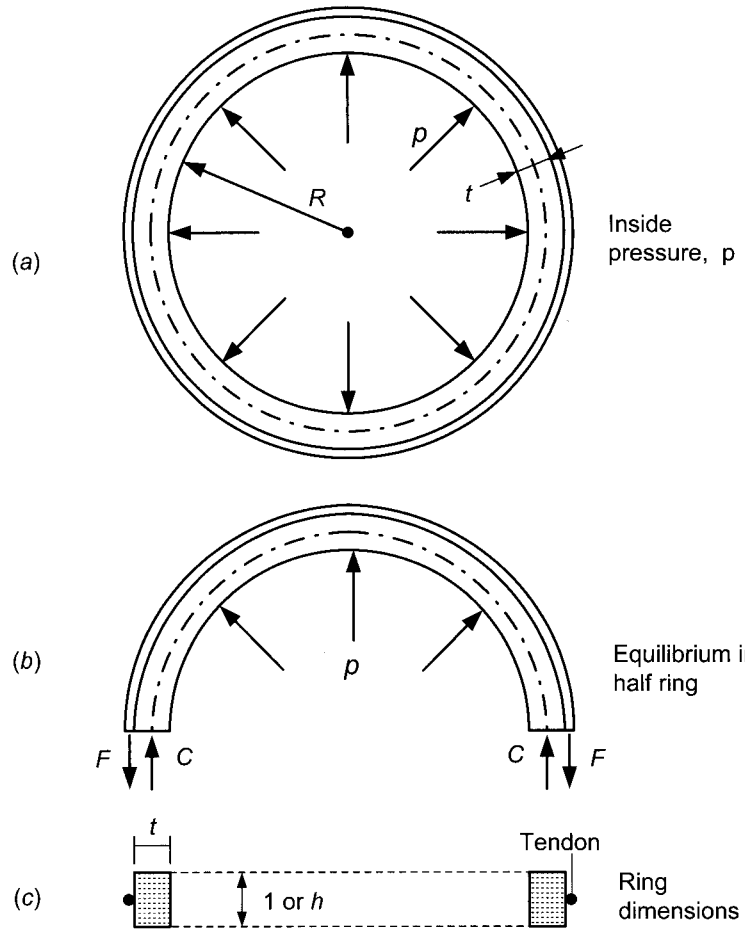

Figure 12.15 ***(a)*** **Circumferential cross section of tank or ring.** ***(b)*** **Prestressing steel location and corresponding C line.** ***(c)*** **Ring dimensions.**

Once the tensile stresses have been determined in the wall of a tank (stress profile obtained from ring stresses), the analysis and design of the tensile elements follow the approaches developed in Sections 12.4 and 12.5. This is illustrated next for the simple case where the wall of a tank can be designed similarly to a ring.

Ring Stresses. Let us consider a free circular ring (Fig. 12.15) with thickness t, small relative to its radius R and height h. Such a ring can be considered to represent a slice of a cylindrical tank wall (Fig. 12.14) with unit height $h = 1$. If the ring is subjected to an internal pressure p, a tensile hoop stress (also called tangential or circumferential stress) develops normally to the cross section of the ring and is given by:

$$\sigma_1 = -\frac{pR}{t} \tag{12.43}$$

The corresponding tensile force in the ring is:

$$N = \sigma_1 \times t \times h = -pRh \tag{12.44}$$

and for $h = 1$

$$N = -pR \tag{12.45}$$

Table 12.1 Stresses in thin wall containers.

Shape		Loading	Stresses†
Long cylinder, closed ends, radius, R, wall thickness, t	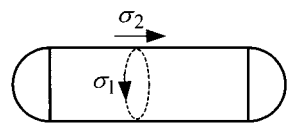	Uniform internal pressure, p	$\sigma_1 = -\frac{pR}{t}$ $\sigma_2 = -\frac{pR}{2t}$
Closed sphere, radius, R, wall thickness, t	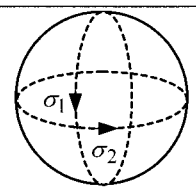	Uniform internal pressure, p	$\sigma_1 = \sigma_2 = -\frac{pR}{2t}$
Open cylinder, radius, R, wall thickness, t	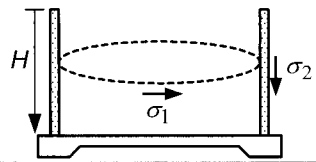	Liquid pressure, γH (γ = liquid density	$(\sigma_1)_{max} = -\frac{\gamma HR}{t}$ $\sigma_2 = 0$

† σ_1 = tangential, circumferential or hoop stress, (does not account for the effects of end restraints).
σ_2 = meridian stress (direction normal to σ_1).

To balance such tensile force, circular prestressing is used around the ring. Note that a circular prestressing force F, placed anywhere in the ring section, including its outer periphery, produces a C-line or pressure line that coincides with the centroid of the ring section. This is because the ring is a statically indeterminate structure and the linear transformation theorem explained in Section 10.6 for continuous beams is applicable to a ring. That is, a tendon along the centroid of the ring section is a concordant tendon. A tendon parallel to it, with a smaller or larger diameter, can be considered linearly transformed (by a translation) and thus produces the same C-line as the concordant tendon. Thus, the prestressing force F can be considered to act

along the centroid of the ring section. The resulting stress, due to F and N, is given by Eq. (12.6):

$$\sigma_c = \frac{F}{A_n} + \frac{N}{A_t} \tag{12.6}$$

where N is obtained from Eqs. (12.44) and (12.45).

For a spherical ring and for closed tanks subjected to an internal pressure p, a meridian tensile stress σ_2 develops in addition to σ_1; corresponding expressions are summarized in Table 12.1 and compared to the case of an open tank subjected to a liquid pressure; in all cases it is assumed that the wall thickness is small in comparison to the diameter. The corresponding values of tensile force N in either direction can be readily determined and the resulting stresses due to F and N can be calculated from Eq. (12.6). Subsequent analysis of tension members follows the approach covered in Sec. 12.4.

12.6.2 Design

All the design criteria covered in Sec. 12.5 apply to circular structures. Because excessive cracking and subsequent leakage can be considered a failure state in tanks and pressure vessels, the criterion specifying the margin of safety against cracking is often critical in the design. If the maximum allowable compression criterion is also assumed binding (for economic reasons), these two criteria can be used to determine, at least in a preliminary design, the two unknowns of the problem, A_{ps} and A_g. A_{ps} gives the prestressing force F and A_g gives the wall thickness t when a unit height is assumed. The solution for such a case is covered next.

Let us define:

$$\lambda = \text{ the larger of } \frac{f_{pi}}{\bar{\sigma}_{ci}} \text{ or } \frac{f_{pe}}{\bar{\sigma}_{cs}} \tag{12.46}$$

If maximum allowable compression is attained under prestressing, we have from Eqs. (12.3) to (12.5):

$$A_n = \lambda A_{ps} \tag{12.47}$$

If the margin of safety against cracking is satisfied, we have from Eq. (12.23):

$$\frac{F}{A_n} + \frac{\bar{m}_{cr} N}{A_t} = f'_{tc} \tag{12.48}$$

Replacing, in Eq. (12.48), F by $A_{ps}f_{pe}$, A_t by $A_n + n_p A_{ps}$, A_n by λA_{ps}, and solving for A_{ps} leads to:

$$A_{ps} = \frac{\bar{m}_{cr} N}{(\lambda + n_p)(f'_{tc} - f_{pe}/\lambda)} \tag{12.49}$$

in which N is the applied tensile force. Once A_{ps} is obtained from Eq. (12.49), A_n can be computed from Eq. (12.47) and A_g from:

$$A_g = A_n + A_{ps} = \lambda A_{ps} + A_{ps} = (\lambda + 1)A_{ps} \tag{12.1}$$

For a cylindrical ring of unit depth $h = 1$ subjected to an internal pressure p, Eq. (12.49) leads to:

$$\boxed{A_{ps} = \frac{-\bar{m}_{cr} pR}{(\lambda + n_p)(f'_{tc} - f_{pe}/\lambda)}} \tag{12.50}$$

and the corresponding wall thickness is given by

$$\boxed{t = \frac{A_g}{h} = \frac{A_g}{1}} \tag{12.51}$$

The above solution by Eq. (12.50) was first proposed by Lin [Ref. 12.15]. The use of Eq. (12.50) leads to a very fast design. However, other criteria will have to be checked according to Sec. 12.5 before finalizing the design. Two examples illustrating the use of Eq. (12.50) in the preliminary dimensioning of a pressure vessel and a water tank are given next.

A logical flow chart summarizing the preliminary design steps is given in Fig. 12.16.

Radial Deflection. The elongation or shortening of a ring along its own circumferential axis is computed similarly to that of a linear member. However, for a cylindrical wall, the radial shortening is important for the design of the supporting pads (Fig. 12.13*f*) at the base of the wall to allow such movement. The radial shortening can be obtained from the relation between the perimeter of a circle and its radius. So if Δl_i is the instantaneous shortening of the ring along its axis (i.e. circle perimeter), the radial movement of the wall will be given by $\Delta l_i / 2\pi$.

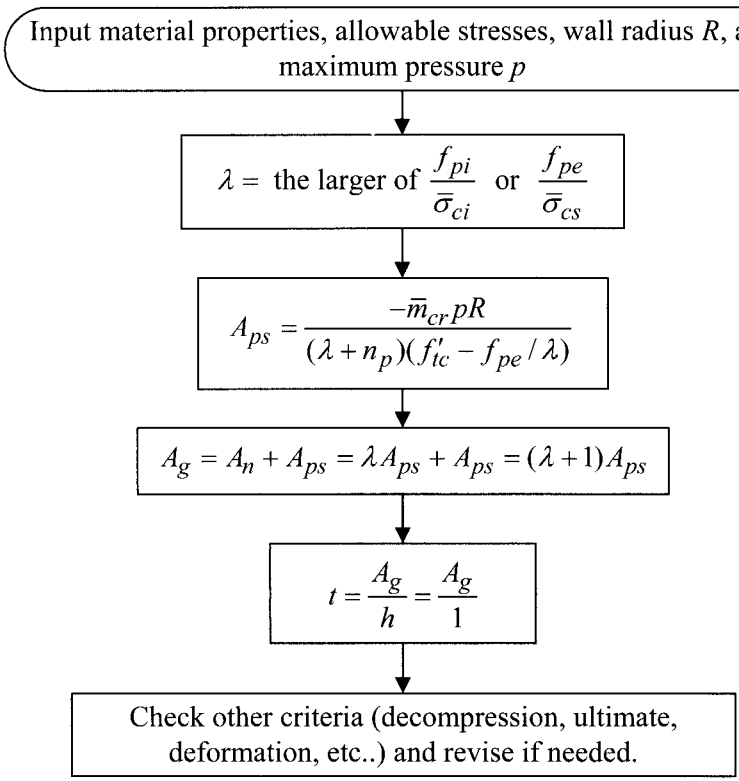

Figure 12.16 Preliminary design steps for a cylindrical wall.

12.6.3 Example: Preliminary Design of Cylindrical Wall Thickness

(a) Nuclear Containment Vessel. Determine the wall thickness and the prestressing force in the hoop direction of a cylindrical nuclear containment vessel (similar to that in Fig. 12.12*a*), assuming the following information is given: $f'_c = 5000$ psi, $\bar{\sigma}_{ci} = 2000$ psi, $\bar{\sigma}_{cs} = 1500$ psi, $f_{pi} = 190{,}000$ psi, $f_{pe} = 150{,}000$ psi, $f'_{tc} = -283$ psi, $n_p = 6.54$, $R = 70$ ft. The design calls for an accidental internal pressure $p = 60$ psi for which a margin of safety against cracking, $\bar{m}_{cr} = 1.5$, is specified.

Consider a ring slice of wall having $h = 1$ inch in height and located sufficiently far away from the ends of the vessel to be assumed free and thus subjected to the full ring forces induced by p.

Using Eq. (12.46):

$$\lambda = \text{the larger of } \frac{f_{pi}}{\bar{\sigma}_{ci}} \text{ or } \frac{f_{pe}}{\bar{\sigma}_{cs}} = \text{the larger of } \frac{190{,}000}{20000} \text{ or } \frac{150{,}000}{1500} = 100$$

Using Eq. (12.50):

$$A_{ps} = \frac{-\bar{m}_{cr} pR}{(\lambda + n_p)(f'_{tc} - f_{pe}/\lambda)} = \frac{-1.5 \times 60 \times 70 \times 12}{(100 + 6.54)(-283 - 150{,}000/100)} = 0.40 \text{ in}^2$$

The corresponding prestressing force per inch of height is:

$$F = A_{ps} f_{pe} = 0.40 \times 150{,}000 = 60{,}000 \text{ lb} \quad \text{or} \quad 60 \text{ kips}$$

From Eq. (12.47):

$$A_n = \lambda A_{ps} = 100 \times 0.40 = 40 \text{ in}^2$$

Thus:

$$A_g = A_n + A_{ps} = 40.4 \text{ in}^2$$

and the required thickness of the wall will be (Eq. 12.51):

$$t = \frac{A_g}{h} = \frac{A_g}{1} = 40.4 \text{ in}$$

The actual design will probably use $t = 42$ in. or 3.5 ft.

For comparison, let us assume that, instead of prestressed concrete, a steel vessel is proposed. Using an allowable stress in the steel of 15,000 psi will lead to a steel thickness:

$$(t \times h) \times 15{,}000 = |N| = pR$$

$$t = \frac{60 \times 70 \times 12}{1 \times 15{,}000} = 3.36 \text{ in}$$

While such a thickness is possible for small elements, it is not practical for a large structure where extensive welding would be required.

(b) Cylindrical Water Tank. Consider exactly the same data as for (a) above, except that a 30-ft high water tank with a free sliding base is considered.

The pressure at the base of the tank is given by:

$$p = \gamma H = 62.4 \times 30 = 1872 \text{ psf} \simeq 13 \text{ psi}$$

The required area of prestressing steel per inch of height is given by Eq. (12.50):

$$A_{ps} = \frac{-\bar{m}_{cr} pR}{(\lambda + n_p)(f'_{tc} - f_{pe}/\lambda)} = \frac{-1.5 \times 13 \times 70 \times 12}{(100 + 6.54)(-283 - 150{,}000/100)} = 0.086 \text{ in}^2$$

which corresponds to a prestressing force:

$$F = A_{ps} f_{pe} = 0.086 \times 150{,}000 = 12{,}900 \text{ lb} = 12.9 \text{ kips/in}$$

The corresponding net concrete area is given by Eq. (12.47):

$$A_n = \lambda A_{ps} = 100 \times 0.086 = 8.6 \text{ in}^2$$

Thus, the minimum required wall thickness at the base will be:

$$t = \frac{A_g}{1} = 8.6 \text{ in}$$

Actual design will probably use $t = 9$ in.

Assuming a 0.5 inch diameter prestressing strand is used (spirally wrapped around the wall), the spacing of the strands (or pitch of the spiral) at the base of the wall will be:

$$s = \frac{0.153}{A_{ps}} = \frac{0.153}{0.086} = 1.78 \text{ in}$$

The pitch will be gradually increased the closer the tendon gets to the top of the wall.

12.6.4 Practical Considerations for Design

The cost of a water tank depends on the cost of its three main components: 1) the foundation slab, 2) the cylindrical wall, and 3) the roof cover which could be dome shaped or other shape. For an open cylindrical water tank (without roof), assuming a required capacity and everything else being equal, generally the total cost decreases

when the diameter increases, up to a certain reasonable limit. Indeed the height of the wall decreases when the diameter increases, and the tensile force decreases due a decrease in water pressure. Thus if land is available with good soil bearing, the largest diameter possible is the most economical approach (the volume varies with the square of the diameter); prestressing (or reinforcing) may even not be needed. A needed minimum pressure may become the controlling criterion. However, in the case where the tank must be covered by a roof structure, the cost of the roof increases significantly with the span, and thus it becomes an important component of the design decision. In such a case a minimum cost solution must be sought in a way similar to that described in Section.12.5, but with inclusion of the cost of the roof and the foundation.

12.7 COMBINED TENSION AND BENDING

Throughout the analysis developed in this chapter, it was assumed that only axial loads were applied. However, it is common to have some bending moment in linear tensile elements in addition to the axial load, such as induced from their own weight.

If the bending moment M is small, there may be no need to have an eccentric prestress to counteract its effects. In such a case, the stresses on the top and bottom fibers are obtained by adding the value of M/Z_t or $-M/Z_b$ to the uniform stress of Eq. (12.6). The smaller value is used in the design procedure to determine A_{ps}. In computing Z_t and Z_b, the moment of inertia of the transformed section should be used.

If the bending moment is significant, it may be more appropriate to use eccentric prestress to balance that moment (see Section 10.13). For this, the eccentricity e_o of the prestressing force is selected such that the moment due to prestressing is equal in magnitude to the external moment M, that is:

$$Fe_o = M \tag{12.52}$$

or

$$e_o = \frac{M}{F} \tag{12.53}$$

The resulting stress in the section becomes again uniform, as the effect of moment is eliminated. Let us illustrate this result by expressing the stress on the bottom fiber of the concrete due to the combined effects of F, N, and a positive moment M:

$$\sigma_b = \frac{F}{A_n} + \frac{Fe_o}{Z_b} - \frac{M}{Z_b} + \frac{N}{A_t} \tag{12.54}$$

As $Fe_o = M, \sigma_b$ is reduced to the value of σ_c given by Eq. (12.6). Note that one assumption is implied here and is acceptable: the Z_b obtained for the net section and used in Fe_o / Z_b is the same as that used in M / Z_b for the transformed section.

REFERENCES

12.1 ACI Committee 318, *Building Code Requirements for Reinforced Concrete (ACI 318-02) and Commentary (318R-02),* American Concrete Institute, Farmington Hills, MI, 2002.

12.2 ACI Committee 344, "Design and Construction of Circular Prestressed Concrete Structures," *ACI Journal*, 67(9): 1970.

12.3 ACI Committee 344, "Design and Construction of Circular Wire and Strand Wrapped Prestressed Concrete Structures," ACI 344R, *Manual of Concrete Practice*, American Concrete Institute, Farmington Hills, MI, 1989.

12.4 ACI Committee 344, "Design and Construction of Circular Prestressed Concrete Structures with Circumferential Tendons," ACI 344.2R, *Manual of Concrete Practice*, American Concrete Institute, Farmington Hills, MI, 1989.

12.5 Anonymous, "Inverted Suspension Span is Simple and Cheap," *Engineering News Record,* May 11, 1972, pp. 27-31.

12.6 Billington, D. P., *Thin Shell Concrete Structures*. New York: McGraw-Hill Book Co., 1965.

12.7 Brondum-Neilsen, T, "Prestressed Tanks," *ACI Journal*, July-August 1985, pp. 500-509.

12.8 Carroll, W. T., F. W. Beaufait, and R. H. Byran, "Prestressed Concrete Trusses," *ACI Journal*, 75(8), 1978.

12.9 Creasy, L. R., *Prestressed Concrete Cylindrical Tanks*. New York: John Wiley & Sons, 1961.

12.10 Finsterwalder, U., "Prestressed Concrete Bridge Construction," *ACI Journal*, 62(9), 1965.

12.11 Gerwick, Jr., B. C., "Prestressed Concrete Developments in Japan," *PCI Journal*, 23(6): 66-76, 1978.

12.12 Gerwick, Jr., B. C., *Construction of Prestressed Concrete Structures*. New York: Wiley-Interscience, 1971. Also 2nd ed., Wiley Professional Paperback Series, 1993, 591 pp.

12.13 Ghali, A., *Circular Storage Tanks and Silos*. London: E. & F. N. Spon; NJ: Methuen, Inc., Distributor, 1979, 210 pp.

12.14 Lennen, R., G. Miller, and C. Prussack, "Precast Prestressed Concrete – Solution of Choice for Lincoln Heights Water Tanks," *PCI Journal*, 41(1): 20-23, 1996.

12.15 Lin, T. Y., and N. Burns, *Design of Prestressed Concrete Structures*," 3rd ed. New York: John Wiley & Sons, 1981. See also, T. Y. Lin, *Design of Prestressed Concrete Structures*, 2nd ed. New York: John Wiley & Sons, 1963.

12.16 Lin, T. Y., and F. Kulka, "Construction of Rio Colorado Bridge," *PCI Journal*, 18(6): 92-101, 1973.

12.17 Matsushita, H., and M. Sato, "The Hayahi-No-Mine Prestressed Bridge," *PCI Journal*, 24(2): 90-109, 1979.

12.18 Morandi, R., "Some Types of Tied Bridges in Prestressed Concrete," First International Symposium on Concrete Bridge Design, American Concrete Institute, Special Publication SP-23, Detroit, Michigan, 1969, pp. 447-465.

12.19 Naaman, A. E., *Ferrocement and Laminated Cementitious Composites*. Ann Arbor, MI: Techno Press 3000, 2000, 372 pp.

12.20 Naaman, A. E., "Optimum Design of Prestressed Concrete Tension Members," *Journal of the Structural Division, ASCE*, 108(ST8): 1722-38, 1982.

12.21 Nawy, E. G., *Prestressed Concrete: a Fundamental Approach*, 3rd ed. Upper Saddle River, NJ: Prentice Hall, 2000.

12.22 Nigels, M. C., "Prestressed Concrete Tension Piles and Their Connections," *PCI Journal*, 43(4): 138-40, 1998.
12.23 PCI Committee on Precast Prestressed Concrete Storage Tanks, "Recommended Practice for Precast Prestressed Concrete Storage Tanks," Prestressed Concrete Institute, Chicago, 1987.
12.24 Posttensioning Institute, "Post-Tensioning Manual," 6th ed., Phoenix, Arizona, 2003.
12.25 Raymond, R. E., and C. Prussack, "Design-Construction of Glennaire Water Tank No. 2," *PCI Journal*, 38(1): 28-39, 1993.
12.26 Timoshenko, S. P., *Theory of Plates and Shells*, 2nd ed. New York: McGraw-Hill Book Co., 1959.
12.27 Wheen, R. J., "Prestressed Concrete Members in Direct Tension," *Journal of the Structural Division, ASCE*, 105(ST7): 1471-87, 1979.

PROBLEMS

12.1 Go back to subsection (b) of the Example in Sec. 12.6.3. Assume the tank is closed at its top by a spherical dome-shaped roof with a prestressed concrete tension ring at its base. The ring is supported on the tank wall by elastomeric pads (Fig. P12.1) and, thus, is free to move. The dome radius is $R^* = 140$ ft and its opening angle θ is 30°. Assume the load on the dome is uniform over a horizontal projection of the dome surface and leads to a total load $W = W_D + W_L = 770 + 462 = 1232$ kips. Provide a complete design for the ring assuming same materials properties and requirements as for the tank. As a first approximation, consider either a square cross section or a rectangular cross section with a ratio of depth to width equal 2.

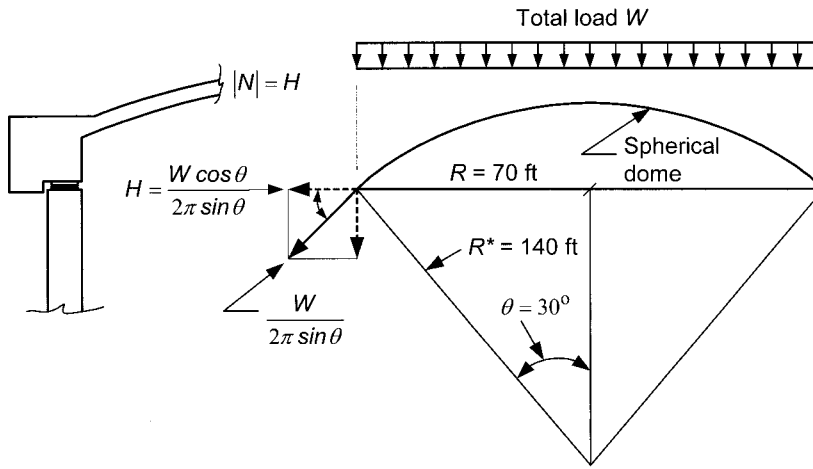

Figure P12.1

12.2 Go back to subsection (b) of the example in Sec. 12.6.3. Assume that the base of the tank is partially fixed to its foundation and that the ring forces and vertical bending moments in the wall are the arithmetic average of those for which the tank is either free at the base or fully fixed. As a first approximation assume that the ring force is maximum at a distance equal to (2/3)H from the top.
(a) Design the tank wall, that is, determine its thickness and the corresponding prestressing in the hoop direction.
(b) Determine the vertical prestressing needed and the corresponding eccentricity. Revise the design if necessary. Use the same design information as given in the example in Section 12.6.3(b).

12.3 Because of limited clearance under a planned railway bridge, a truss bridge is proposed as shown in Fig. P12.3. Several solutions are considered and include a truss made out of prestressed concrete elements. Assume that the lower cord of the truss is to be designed as a single precast prestressed concrete element and that connection details with other elements have been worked out. Maximum joint loadings in service are shown in Fig. P12.3. Fifty percent of service load is due to dead loads and the remainder to live loads. Provide a design for the lower cord assuming the following information is given:

$f'_c = 9000$ psi, $f'_{ci} = 6300$ psi, $f'_{tc} = -4\sqrt{f'_c} \simeq -380$ psi, $E_c = 5.75\times10^6$ psi, $E_{ci} = 4.81\times10^6$ psi, $\bar{\sigma}_{ci} = 3150$ psi, $\bar{\sigma}_{cs} = 2700$ psi, $f_{pi} = 175{,}000$ psi, $f_{pe} = 145{,}000$ psi, $f_{pu} = 270{,}000$ psi, $E_{ps} = 24\times10^6$ psi, $C_{CU} = 2$, $\bar{m}_{cr} = 1.5$, $\bar{m}_{dec} = 1.2$.

Make any other reasonable assumptions if needed. Note that the allowable compression stress in service is taken smaller than that usually considered for bending because it corresponds to a sustained uniform load.

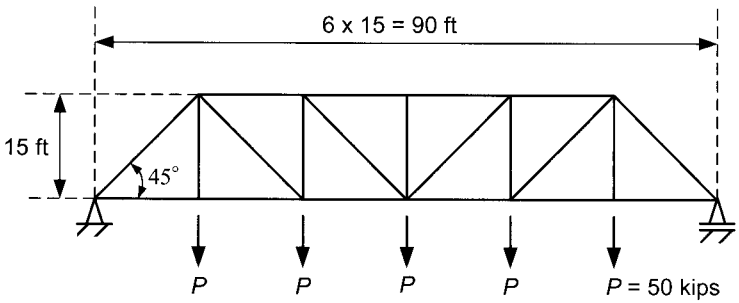

Figure P12.3

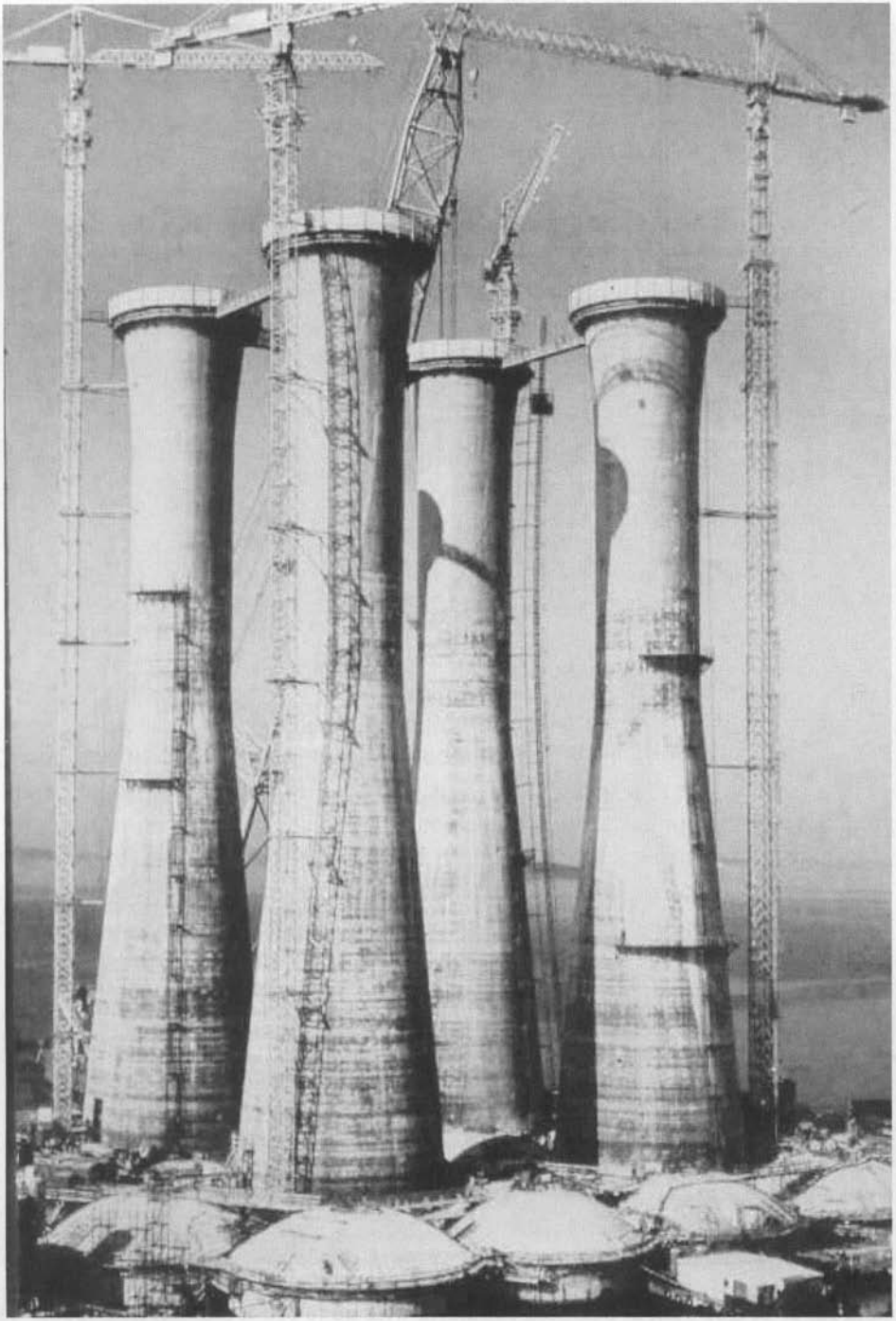

Towers of the Statfjord B Condeep offshore oil platform. *(Courtesy Nowegian Contractors.)*

Columbia River Brigde built in balanced cantilever with up to 600-ft (183-m) long spans. The hollow-cored piers are designed as columns. *(Courtesy Engineering News Record.)*

CHAPTER 13

ANALYSIS AND DESIGN OF COMPRESSION MEMBERS

13.1 TYPES AND THEIR ADVANTAGES

Compression members are structural elements mostly of linear shape, such as columns, poles, and foundation piles. Precast prestressed wall panels made with single and double Ts are also used very commonly as bearing elements in industrial buildings. On a larger scale, TV towers and shafts of offshore structures are treated as compression members. The latter types are compressed not only in longitudinal direction, but also, because of hydrostatic pressure, in the circumferential direction.

It may seem irrational to prestress, that is precompress, a compression member. However, compression members are seldom subjected to pure compression only. Columns, for instance, must be capable of resisting a variety of loads, including lateral loads from wind and earthquakes, from shearing forces transmitted by beams and slabs, and if precast, from transportation and erection. Moreover, code provisions generally imply the existence of a minimum eccentricity, thus some level of bending, even when pure compression is theoretically considered. In most cases, the most critical loading combination of compression members involves substantial bending.

The use of prestressed versus nonprestressed steel in a column leads to a small reduction in its resistance to pure compression but increases significantly its resistance to first cracking. Consequently, its deflection in the uncracked state is substantially reduced and its performance in service is improved. Prestressing

allows the use of precasting and, therefore, offers its related benefits, such as savings on forms and the use of high-strength concrete. Since a column's capacity in compression is directly proportional to the concrete strength, this might be a substantial advantage. Precast prestressed columns used in building structures are often designed to span several stories. They are connected in place by posttensioning or other standard jointing techniques. The cost of connections is an important factor to consider in the early stages of design. Typical column' cross sections are shown in Fig. 13.1 and are identical in shape to reinforced concrete columns. Examples of application of prestressed columns and bearing walls in building structures are shown in Figs. 13.2*a* and 13.2*b*.

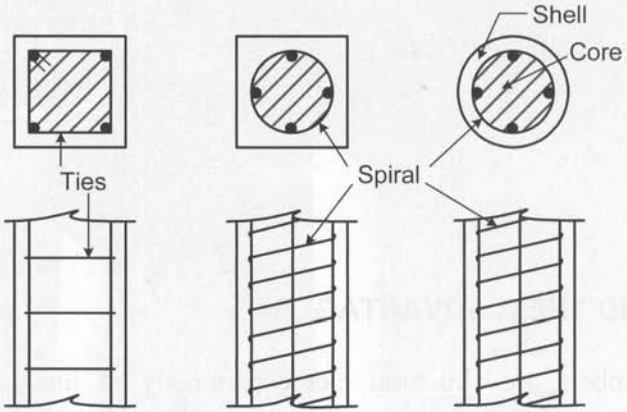

Figure 13.1 Typical cross sections of prestressed columns.

Figure 13.2 (a) Typical use of precast prestressed columns in housing.
(Courtesy Precast/Prestressed Concrete Institute.)

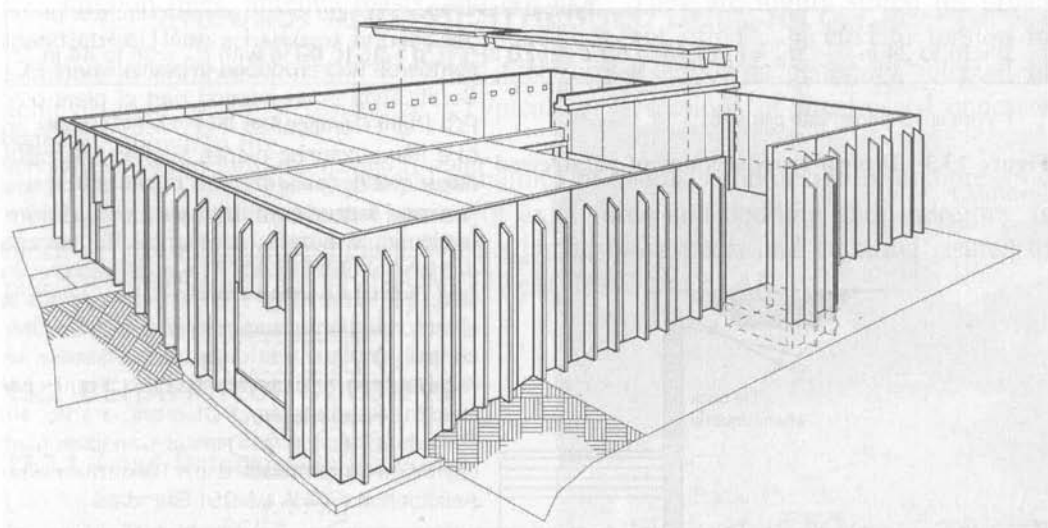

Figure 13.2 (b) Typical use of precast prestressed columns and bearing walls in parking structures, apartment, and industrial buildings. *(Courtesy Precast/Prestressed Concrete Institute.)*

Because they can be made of a single element, prestressed concrete piles are very efficient structural members. They are widely used for marine structures and building foundations. Lengths of up to 120 ft (36 m) are common. The longest length reported is 260 ft (78 m) for a single piece [Ref. 13.16]. Prestressed concrete piles offer a number of important advantages that have made them competitive in all applications requiring piling. These advantages include durability, high load-moment resistance, ability to take uplift (tension), ability to penetrate hard strata, ease of handling and transportation, and economy [Ref. 13.16]. Their use has been extended to fenders and sheet piling for waterfront bulkheads. Typical cross sections of piles and sheet piles are shown in Figs. 13.3 and 13.4.

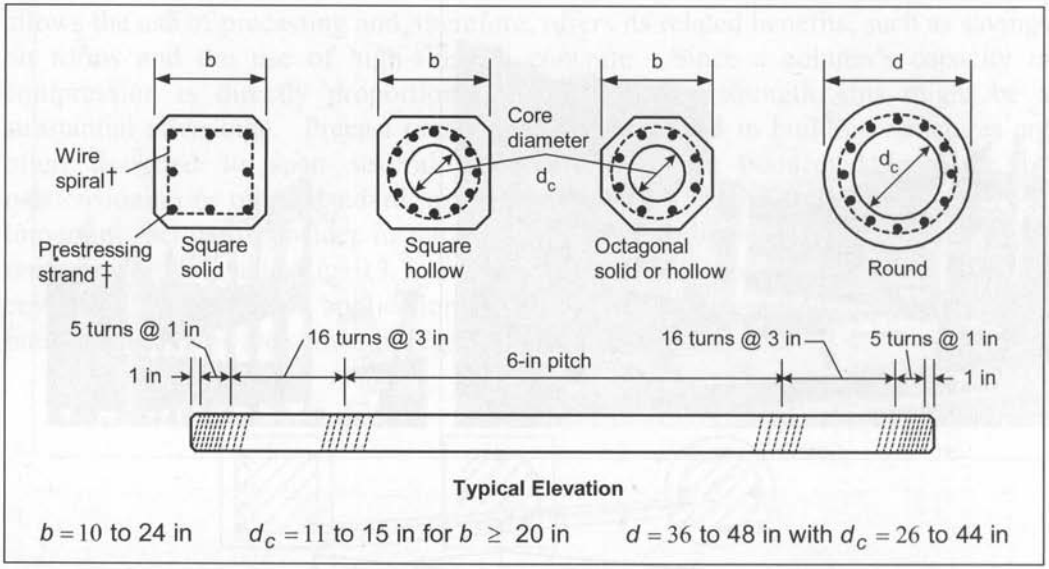

† Wire spiral varies with pile size.

‡ Strand pattern may be circular or square.

Figure 13.3 Typical cross sections of prestressed piles. *(Courtesy Precast/Prestressed Concrete Institute.)*

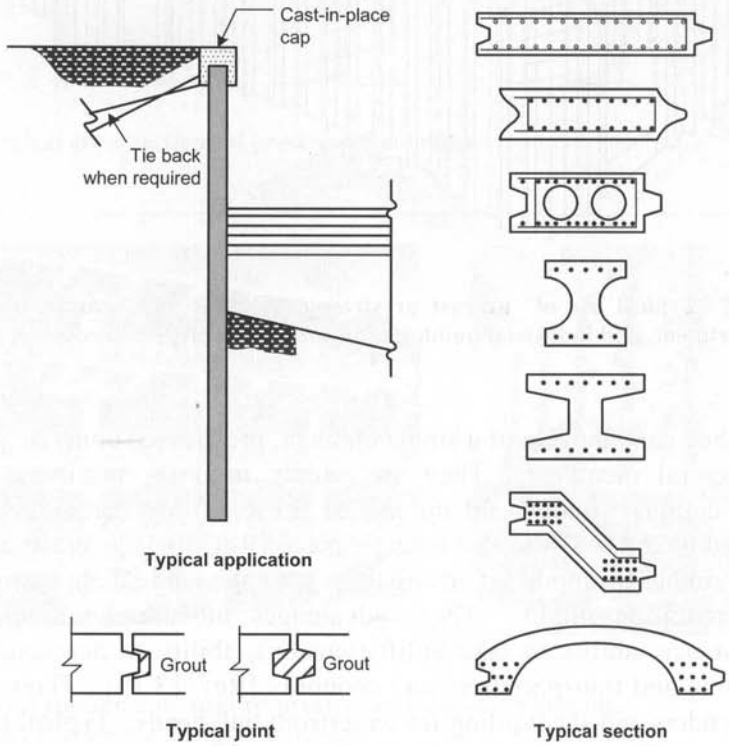

Figure 13.4 Typical cross sections of prestressed sheet piles. *(Adapted from Refs. 13.1 and 13.3.)*

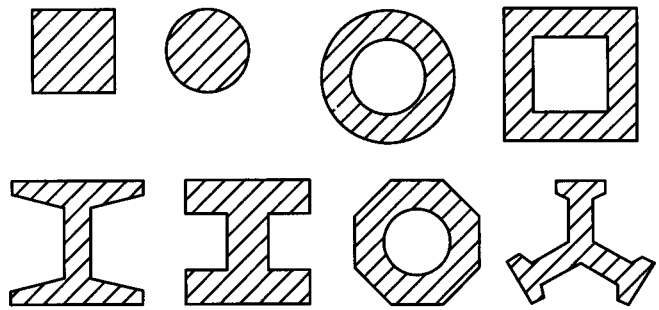

Figure 13.5 Typical cross sections of prestressed poles.

Prestressed concrete poles are used for lighting, electric and telephone transmission lines, antenna masts, and the like. They are highly suited for urban installation [Refs. 13.16, 13.43]. Because they are often subjected to torsion in addition to compression and bending, their cross section is generally selected to achieve good torsional resistance. Typical cross sections of prestressed concrete poles are shown in Fig. 13.5.

This chapter covers the general principles of analysis and design of compression members subjected to a combination of axial force and bending and, therefore, is mostly concerned with columns. Particular design aspects and detailing related to piles and poles can be found elsewhere [Refs. 13.42 and 13.43].

13.2 BEHAVIOR OF COLUMNS

13.2.1 Load-Deformation Response

In general, prestressed concrete columns have a low level of prestress. The ACI code recommends a minimum effective uniform prestress of 225 psi (1.55 MPa). This is insignificant in comparison to the compressive strength of concrete. Prestressed concrete columns subjected to monotonically increasing axial compression are expected to behave similarly to reinforced concrete columns (Fig. 13.6).

Ferguson reports that the ascending part of the load-deformation response reaches a pseudo-yield point at about 85 percent of the corresponding ultimate resistance of the concrete, after which the behavior of the column depends on whether it is transversely reinforced with ties or spirals [Ref. 13.14]. In highly loaded spirally reinforced columns the concrete cover spalls off, but if the core is adequately confined, the column will maintain maximum resistance for a high level of deformation or displacement. Thus substantial ductility and considerable increase in energy absorption before failure are achieved. This is particularly important in earthquake-prone regions. Spalling of the concrete cover starts shortly after the

pseudo-yield point, and essentially only the core of the column is left to resist loading [Ref. 13.44].

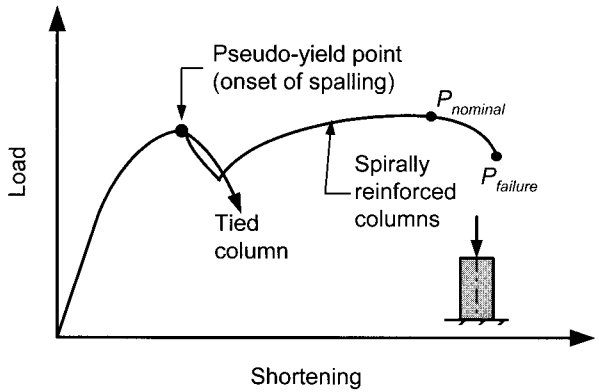

Figure 13.6 Typical load-shortening curves of tied and spirally reinforced short columns.

13.2.2 Classification

In the preceding section we assumed that only an axial load was applied and that buckling did not control the behavior of the column. Assuming everything else is the same, the criticality of buckling increases significantly with the length of the column, but for the purpose of analysis and design, columns are essentially classified into three categories [Ref. 13.41]: short columns, medium columns, and long columns. The exact delineation between the three categories is clarified in Sec. 13.8. In brief, a short column can be analyzed or designed from its cross section only; a medium column is essentially designed as a short column with due account to slenderness effects; and the design of long columns is governed by instability criteria.

13.2.3 Load-Moment Interaction Diagram

A plot of the column axial load capacity, P_n, versus the moment it can simultaneously carry, M_n, is called a column interaction diagram. A typical load-moment interaction diagram is shown in Fig. 13.7 and covers the range from pure compression to pure tension. Several failure points of interest can be identified on the diagram: the point of pure compression for which a uniform compressive stress exists in the section; the point of zero tension above which no tensile stress exists in the concrete section; the balanced point for which the maximum compressive strain in the concrete is attained simultaneously with the yield strain in the steel; the point of pure bending or flexure where the axial force is zero; and the point of pure tension. These are important points of the diagram, since it can be fairly well

approximated by joining these points either by a continuous curve or by straight-line segments. Any point inside the area limited by the diagram is theoretically within the capacity of the column.

The following notation is adopted to describe the coordinates of the key points of the diagram:

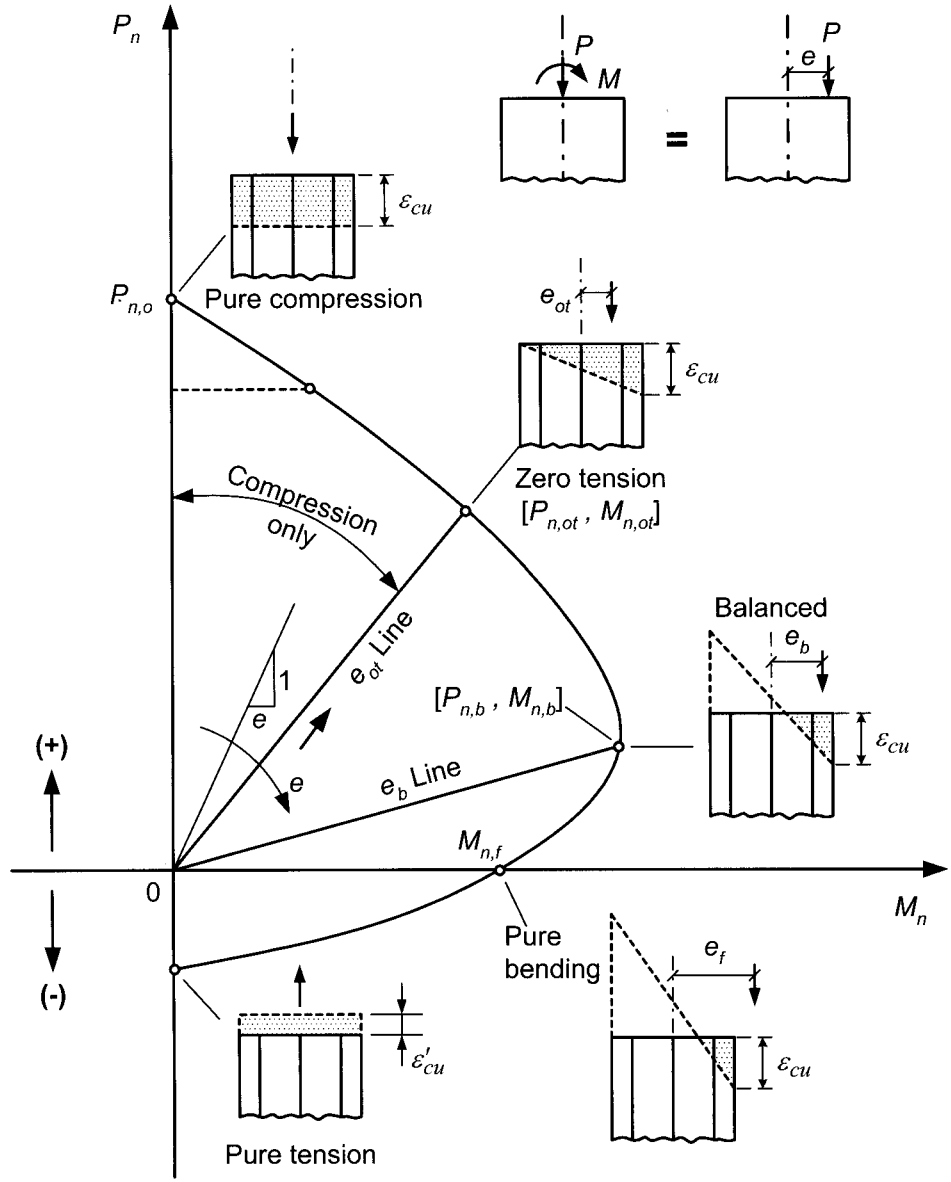

Figure 13.7 Column nominal load-moment interaction diagram.

$(P_{n,o}, 0)$ for the point of pure compression

$(P_{n,ot}, M_{n,ot})$ for the point of zero tension

$(P_{n,b}, M_{n,b})$ for the balanced point

$(0, M_{n,f})$ for the point of pure bending or flexure

$(0.10 f'_c A_g, M_{n,0.1})$ for the point at 10% resistance capacity

Any combination of axial load and moment (P, M) acting on the column can be resolved into the same load P acting at an eccentricity $e = M/P$. Radial lines passing by the origin correspond to a constant value of eccentricity and have a slope equal to $1/e$ (Fig. 13.6). Thus, the lines corresponding to "zero tension" eccentricity e_{ot} or "balanced" eccentricity e_b can be easily identified. Given e, an increase in P leads to a proportional increase in M (assuming no buckling) and the representative point moves along the corresponding line until it reaches the nominal interaction diagram where failure occurs. An increase in eccentricity leads to a decrease in the slope of the representative line.

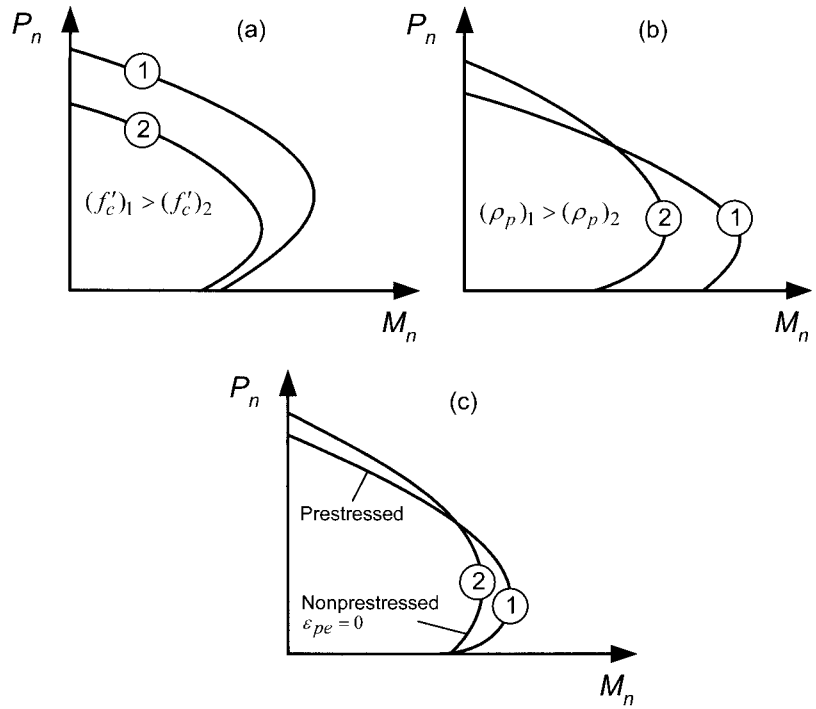

Figure 13.8 Typical effects of (a) compressive strength, (b) reinforcement ratio, and (c) effective prestress on the interaction diagram.

It is useful to understand how the interaction diagram is influenced by various parameters. Typical effects are illustrated in Fig. 13.8. Everything else being equal,

it can be observed that an increase in concrete compressive strength (Fig. 13.8*a*) substantially increases the region where compression prevails but leads to little improvement in the region where bending prevails (flexural capacity is controlled mostly by the steel). An increase in the amount of prestressing steel (Fig. 13.8*b*) leads to a small reduction in pure compression capacity but a significant increase in pure bending resistance. An increase in pure compression capacity is obtained (Fig. 13.8*c*) if the steel is left nonprestressed while the region where bending prevails is reduced.

13.2.4 ACI Code Design Interaction Diagram

For the analysis and design of concrete columns, the ACI code recommends the use of an interaction diagram derived from the nominal interaction diagram as follows (Fig. 13.9*a*):

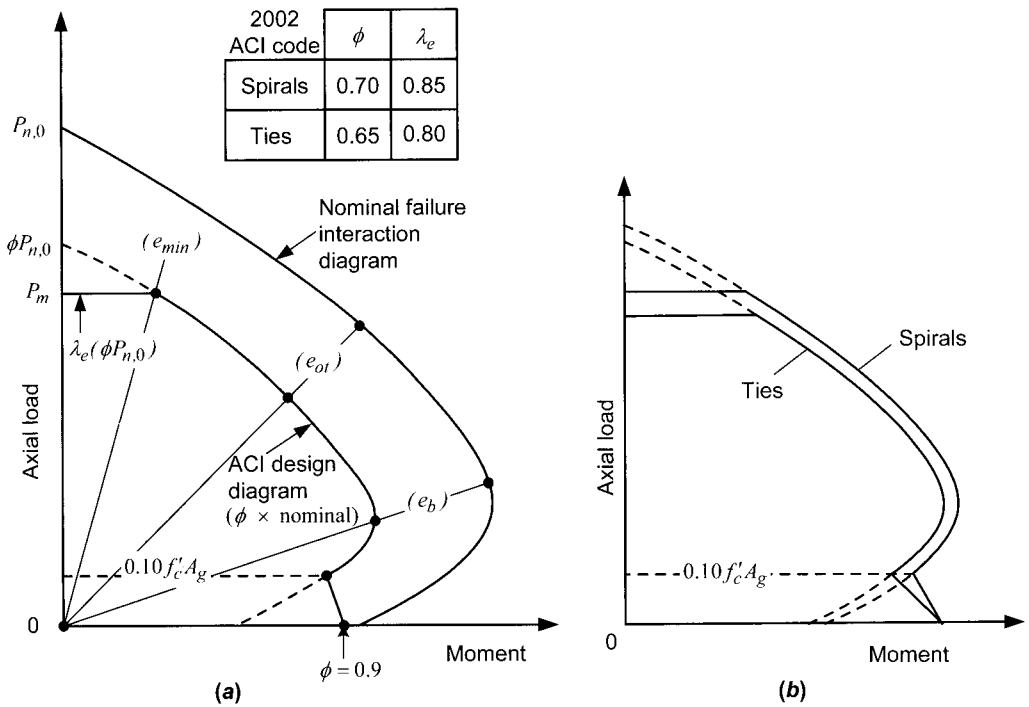

Fig. 13.9 ***(a)*** **ACI code design interaction diagram.** ***(b)*** **Diagram for tied versus spirally reinforced column; the lower transition section is as per ACI 1999.**

A diagram similar to the (P_n, M_n) diagram is obtained using the origin as center and a similarity factor equal to ϕ; the strength reduction factor ϕ is equal to 0.70 for spirally reinforced columns and 0.65 for tied columns. The design diagram so obtained is truncated at its top by an upper limit corresponding to a maximum

compressive force P_m equal to $\lambda_e \phi P_{n,o}$ where $\lambda_e = 0.85$ for spirally reinforced columns, and $\lambda_e = 0.80$ for tied columns. The factor λ_e accounts for a minimum accidental eccentricity even in columns that are theoretically loaded concentrically. Thus the cutoff limit P_m indirectly sets a minimum eccentricity limit for design. In prior versions of the ACI code, the lower part of the diagram is truncated and replaced by a transition segment from the point where the compressive force ϕP_n equals $0.10 f'_c A_g$ to the point of pure bending for which $\phi = 0.9$. This is to be consistent with flexural design where the ϕ factor for tension controlled sections is different from that used for compression controlled sections. If $0.10 f'_c A_g \geq \phi P_b$ then the transition starts at the balanced point. The change in the ϕ value is permitted to be linear in that zone. Typical interaction diagrams for the same column laterally reinforced with spirals or ties are shown in Fig. 13.9*b*. The fact that spirals induce higher ductility is reflected in the results. According to the ACI code, any combination of factored axial load and moment, represented by a point falling inside the region limited by the design diagram, is an acceptable loading combination.

Tension Controlled and Compression Controlled Sections. As explained in Chapter 3, the ACI 2002 code has moved from the terminology of "under-reinforced" and "over-reinforced" sections to the terminology of "tension-controlled" and "compression-controlled" sections. Although the design limits for these attributes are not exactly the same, they essentially imply similar behavior. Moreover with the 2002 code, there is a transition zone between a tension-controlled section and a compression-controlled section over which the ϕ factor also changes from the ϕ in bending to the ϕ in compression.

For Grade 60 reinforcement and for all prestressed concrete reinforcement, a section is assumed to be compression-controlled when the net tensile strain in the extreme tension steel is equal to or less than 0.002. In that case the ϕ factor is taken as 0.70 for spirally reinforced columns and 0.65 for tied columns.

Note that the value of net tensile strain of 0.002 corresponds to the value of balanced reinforcement ratio, ρ_b, in a reinforced concrete section when only one layer of reinforcement is used (Fig. 5.11). When the net tensile strain in the extreme tension steel is equal to or greater than 0.005, the section is defined as tension-controlled. In that case the ϕ factor is taken as 0.9. The value of net tensile strain of 0.005 corresponds to a value of reinforcement ratio $\rho_s = 0.63\rho_b$ when only one layer of reinforcement is used. For sections in which the net tensile strain in the extreme tension steel at nominal strength is between the limits for compression-controlled and tension-controlled sections, ϕ is permitted to be linearly increased from its value for compression controlled sections (that is 0.70 or 0.65) to 0.90 as the net tensile strain in the extreme tension steel at nominal strength increases from 0.002 to 0.005.

Also, as described in Chapter 5, the net tensile strain limits given in the code can be replaced by the ratio c/d_e which is much easier to deal with since both c and d_e are

part of the computations for nominal bending resistance. Also explained is the reason why the author recommends d_e instead of d_t.

In the transition region between tension controlled and compression controlled, the ϕ factor can be obtained from the following expression (see also Eq. 5.10):

$$\begin{cases} \phi = 0.70 + 0.20\left(\dfrac{1}{c/d_e} - \dfrac{5}{3}\right) & \text{for spirally reinforced columns} \\ \phi = 0.65 + 0.25\left(\dfrac{1}{c/d_e} - \dfrac{5}{3}\right) & \text{for tied columns} \end{cases} \tag{13.1}$$

where d_e is taken to the centroid of the tension force in the tensile reinforcement.

13.3 ANALYSIS OF SHORT COLUMNS

13.3.1 Assumptions

The analysis and design of prestressed concrete columns are based on ultimate strength requirements and are approached much in the same way as reinforced concrete columns [Refs. 13.6 to 13.8, 13.10, 13.19, 13.23, 13.56, 13.57]. Because of the relatively low level of prestress in columns, little is gained by a stress analysis under service loads. However, such an analysis may be necessary for piles where the level of prestress can be high. Moreover, stresses induced during handling and transportation of precast elements, especially wall panels, must be assessed according to the criteria described in Chapter 4.

Short columns are defined here as columns having their strength based on the strength of their cross section. Their analysis is generally reduced to determining the load-moment interaction diagram of the column section and checking if the diagram provides an upper bound to factored real loading combinations. The following approach, consistent with the ultimate strength design assumptions of the ACI code, can be followed:

1. Select a location of neutral axis, c (Fig. 13.10)
2. Draw a linear strain diagram passing by the neutral axis and showing an extreme fiber compressive strain ε_{cu} (assumed equal 0.003 as per ACI)
3. Find the values of P_n and M_n for which internal equilibrium and strain compatibility are satisfied
4. Derive the design values ϕP_n and ϕM_n.

Details are given in the next section. The procedure is repeated for each point of the diagram. In practice, only a few key points are needed, namely:

- the pure compression point, $P_{n,O}$, and the code allowed maximum value: P_m

- the zero tension point, $(P_{n,ot}, M_{n,ot})$
- the compression controlled point (or the balanced point), $(P_{n,b}, M_{n,b})$
- the pure flexure points, $M_{n,f}$
- the $0.10 f'_c A_g$ point at which, in prior versions of the ACI code, the ϕ transition was allowed to start, $(\phi P_{n,0.1}, \phi M_{n,0.1})$. See ACI code Sections 9.3.2.2 and 10.3.5.

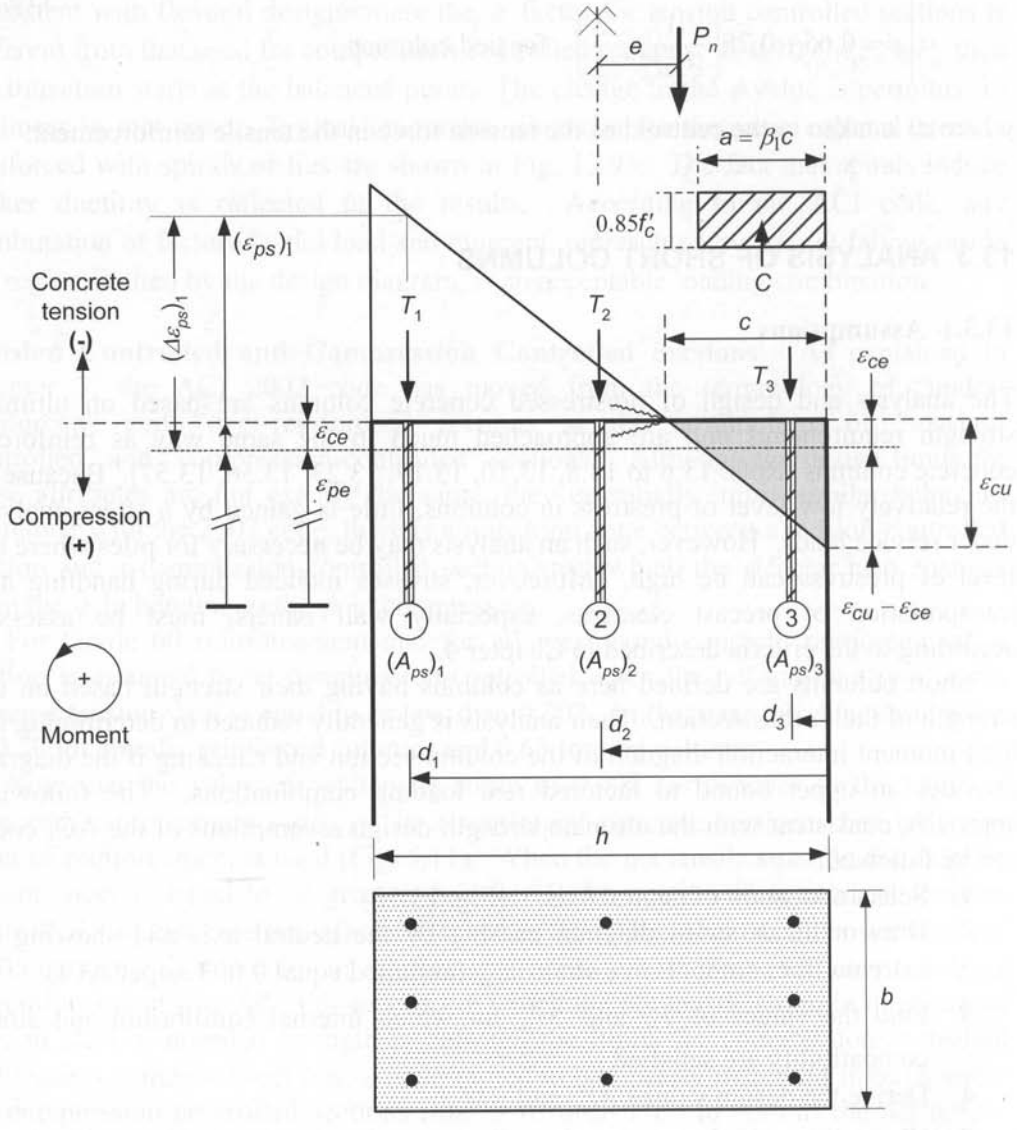

Figure 13.10 Typical strain diagram and corresponding forces at ultimate in a column subjected to compression and bending.

The diagram is approximately plotted through these points. When additional accuracy is needed, more points are determined. Once the nominal resistance diagram is determined, the design diagram is obtained from it by similarity by multiplying by the reduction factor ϕ, with the exceptions described in Fig. 13.9.

13.3.2 Basic Equations for Square and Rectangular Sections

Once a strain diagram is selected, two equations describing the solicitations at the onset of failure can be written, one for the sum of forces and one for the sum of moments. It is also assumed that strain compatibility holds and that the stress-strain relation of the steel is known. If the calculated strains in the various layers of steel are less than the proportional limit strain, the corresponding stresses are obtained using Hooke's law. Otherwise, the stress-strain curve (or representative relationship) must be used to determine the stresses and the corresponding forces in the different layers of steel. Expressions for the stress-strain curves of reinforcing and prestressing steels are given in Section 2.4.

Let us consider a typical strain diagram at ultimate such as shown in Fig. 13.10 and let us determine for it the various expressions of interest. The following notation is used:

ε_{ce} = uniform compressive strain in the concrete under effective prestress

$(A_{ps})_i$ = area of prestressing steel in layer i (Fig. 13.10 shows three layers numbered 1, 2, and 3)

d_i = distance from extreme compressive fiber to centroid of $(A_{ps})_i$

b = column width

h = column depth

c = distance from extreme compressive fiber to location of neutral axis

T_{ip} = tensile force due to $(A_{ps})_i$. The subscript p is not used in Fig. 13.10 because non-prestressed reinforcement may also be present in layer i as described in the next section.

Assuming materials and sectional properties are given, the following equations can easily be derived:

$$\varepsilon_{ce} = \frac{A_{ps} f_{pe}}{A_n E_c} = \frac{A_{ps} f_{pe}}{(A_g - A_{ps}) E_c} \tag{13.2}$$

where $A_{ps} = \sum_i (A_{ps})_i$, and $A_n = A_g - A_{ps}$ is same as defined in Eq. (12.1). It is assumed that all tendons have the same effective prestress.

The strain change in any layer of steel i is given by:

$$(\Delta\varepsilon_{ps})_i = \varepsilon_{ce} + \varepsilon_{cu}\left(\frac{d_i - c}{c}\right) \tag{13.3}$$

where d_i can be smaller or larger than c. For $d_i > c$, $(\Delta\varepsilon_{ps})_i$ is positive and corresponds to a strain increase in the steel. The strain in any layer of steel i is given by:

$$(\varepsilon_{ps})_i = \varepsilon_{pe} + (\Delta\varepsilon_{ps})_i \tag{13.4}$$

When $(\varepsilon_{ps})_i$ is less than ε_{pp} (the proportional limit strain), the stress in the prestressing steel layer i can be computed from:

$$(f_{ps})_i = E_{ps}(\varepsilon_{ps})_i \tag{13.5}$$

For $(\varepsilon_{ps})_i > \varepsilon_{pp}$, the stress in the steel should be determined from its stress-strain relation. The tensile force in any layer i of prestressing steel is then given by:

$$T_{ip} = (A_{ps})_i (f_{ps})_i \tag{13.6}$$

The compressive resistance of the concrete at ultimate is obtained from the rectangular stress block as:

$$C = 0.85 f'_c ba = 0.85 f'_c b\beta_1 c \tag{13.7}$$

It is assumed in Eq. (13.7) that the area occupied by the steel in the compression zone is negligible. It could be accounted for in the analysis, if needed. However, it leads to almost no difference in the final results.

Summing up the axial forces on the section leads to the nominal force resistance:

$$P_n = C - \sum_i T_{ip} \tag{13.8}$$

In order to sum up the moments, a sign convention for moments is set. In Fig. 13.10, a positive moment is assumed counterclockwise. Summing up the moments with respect to the centerline of the column leads to the nominal moment resistance:

$$M_n = C\left(\frac{h}{2} - \frac{a}{2}\right) + \sum_i T_{ip}\left(d_i - \frac{h}{2}\right) \tag{13.9}$$

The corresponding eccentricity is given by:

$$e = \frac{M_n}{P_n} \tag{13.10}$$

For design, the ultimate resistance is characterized by the point of the interaction diagram with eccentricity e and coordinates ϕP_n and ϕM_n.

13.3.3 Partially Prestressed Square or Rectangular Sections

Prestressed concrete columns may contain a substantial amount of nonprestressed conventional reinforcing bars whose contribution can add significantly to the ultimate resistance. For each layer of steel, the reinforcement can be separated into prestressed and nonprestressed reinforcement carrying a force:

$$T_i = T_{ip} + T_{is} \tag{13.11}$$

where T_{ip} is defined in Eq. (13.6). In order to determine T_{is} and its contribution to the moment resistance, the strains in the nonprestressed steel at the level of each layer i are needed. Let us define ε_{se} as the compressive strain in the nonprestressed steel due to effective prestress only. It can be easily shown that:

$$\varepsilon_{se} = -\frac{A_{ps} f_{pe}}{A_t E_c} \tag{13.12}$$

in which

$$A_t = A_n + (n_s - 1)A_s \tag{13.13}$$

where A_s is the total area of nonprestressed reinforcement in the section, A_n is as defined in Eq. (13.2) and n_s is the moduli ratio. Note that, in the presence of nonprestressed reinforcement, the value of A_n in Eq. (13.2), should be replaced by A_t leading to $\varepsilon_{ce} = |\varepsilon_{se}|$.

For a given location of neutral axis and strain diagram, the strain change (from the zero strain reference state) in the non-prestressed steel of layer i is, similarly to Eq. (13.3), given by:

$$(\Delta\varepsilon_s)_i = \varepsilon_{cu}\left(\frac{d_i - c}{c}\right) \tag{13.14}$$

Since the reinforcing steel must first decompress before getting in tension, ε_{se} is neutralized and the resulting strain in each steel layer is (Fig. 13.10):

$$(\varepsilon_s)_i = (\Delta\varepsilon_s)_i \tag{13.15}$$

When the absolute value of $(\Delta\varepsilon_s)_i$ is less than ε_y, the stress in the nonprestressed steel of layer i can be computed from:

$$(f_s)_i = E_s \times (\Delta\varepsilon_s)_i \tag{13.16}$$

When the magnitude of $(\Delta\varepsilon_s)_i$ is larger than ε_y, the stress is given by:

$$(f_s)_i = \pm E_s \varepsilon_y \tag{13.17}$$

The plus sign holds for $(\varepsilon_s)_i$ positive, that is tension for the steel, and the minus sign for $(\varepsilon_s)_i$ negative, that is compression.

The tensile force in the nonprestressed steel of layer i is given by:

$$T_{is} = (A_s)_i (f_s)_i \tag{13.18}$$

The two equations leading to the resulting nominal force and nominal moment resistance for the strain diagram considered become:

$$P_n = C - \sum_i (T_{ip} + T_{is}) \tag{13.19}$$

$$M_n = C\left(\frac{h}{2} - \frac{a}{2}\right) + \sum_i (T_{ip} + T_{is})\left(d_i - \frac{h}{2}\right) \tag{13.20}$$

where d_i is defined as the distance from the extreme compression fiber to any layer of steel, i. The corresponding point of the design load-moment interaction diagram is then given by ϕP_n and ϕM_n.

13.3.4 Circular Hollow-Cored and I-Shaped Sections

For circular hollow cored and I-shaped sections, the only modification to the above equations is the compression force in the concrete stress block at ultimate, C, and its lever arm for computing the nominal bending resistance.

Figure 13.11 illustrates the two possible cases for the compression block of a hollow-cored section, depending on the location of the neutral axis at ultimate. The following results can be easily derived [Refs. 13.8, 13.52]:

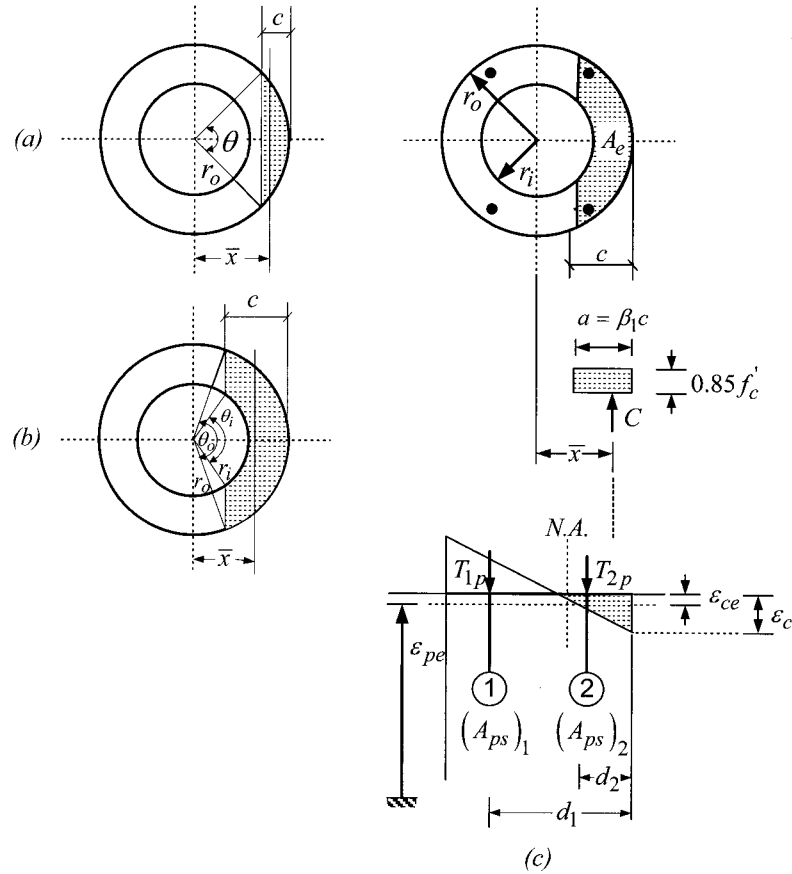

Figure 13.11 Cases of effective compression zone at ultimate for circular hollow-cored sections.

For case (a):

$$A_e = \frac{1}{2}(\theta - \sin\theta) r_o^2 \tag{13.21}$$

$$\bar{x} = \frac{\sqrt{2}}{3} \frac{(1-\cos\theta)^{1.5}}{\theta - \sin\theta} r_o \tag{13.22}$$

For case (b):

$$A_e = \frac{1}{2}(\theta_o - \sin\theta_o) r_o^2 - \frac{1}{2}(\theta_i - \sin\theta_i) r_i^2 \tag{13.23}$$

$$\bar{x} = \frac{\sqrt{2}}{3} \frac{(1-\cos\theta_o)^{1.5} \times r_o^3 - (1-\cos\theta_i)^{1.5} \times r_i^3}{(\theta_o - \sin\theta_o) r_o^2 - (\theta_i - \sin\theta_i) r_i^2} \tag{13.24}$$

where A_e is the effective compression area of the stress block, $\bar{x}$ is the distance from the section centroid to the centroid of the compression area, r_o is the outside radius of the section, r_i is the inside radius of the section, and the angles θs are in radians and as defined in Figs. 13.11*a* and 13.11*b*.

Assuming the area occupied by the steel in the compression zone is negligible, the compression force in the concrete is obtained from (Fig. 13.11*c*):

$$C = 0.85 f'_c (\beta_1 A_e) \tag{13.25}$$

in which the factor β_1 is applied to simulate the reduced area of stress block that undergoes an equivalent average compressive stress of $0.85f'_c$ (compare with Eq. 13.7). The suggested computational approach is to reduce the compression area but keep the lever arm as is. Thus for a hollow cored section, P_n is the same as in Eqs. (13.8 or 13.19), and the nominal bending resistance is given by:

$$M_n = C\bar{x} + \sum_i (T_{ip} + T_{is})(d_i - r_o) \tag{13.26}$$

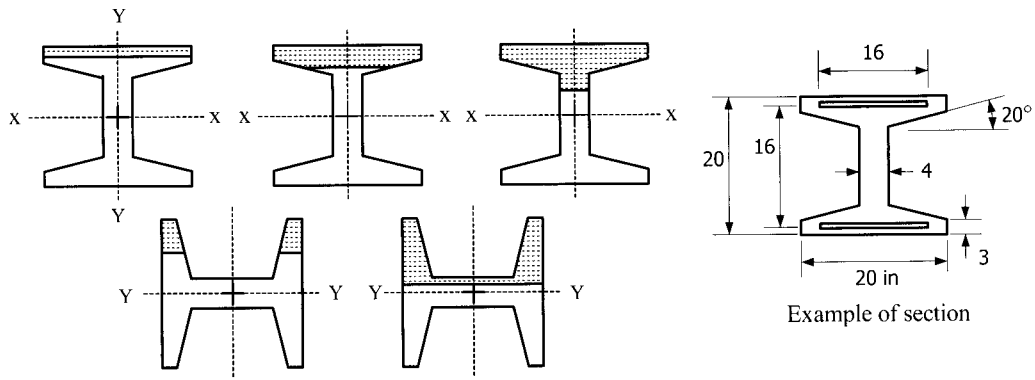

Figure 13.12 Possible cases of compression zone at ultimate for I-shaped sections, along each main axis and example of actual section dimensions.

A similar approach is followed for I-shaped sections (Fig. 13.12). The values of effective compression zone area, A_e, and distance $\bar{x}$ from the centroid of the section to the centroid of A_e can be easily derived depending on the location of the neutral axis, shape of the tapered flanges and the section dimensions [Refs. 13.7, 13.8]. This is done for bending along the x and y axes, respectively. The value of C is then computed from Eq. (13.25) and the value of P_n from Eq. (13.19). The corresponding nominal bending moment is given by:

$$M_n = C\bar{x} + \sum_i (T_{ip} + T_{is})\left(d_i - \frac{h}{2}\right) \tag{13.27}$$

where h represents the depth of the section along either one of the main axes considered.

Once P_n and M_n have been determined, the eccentricity is obtained from Eq. (13.10).

13.4 EXAMPLE: COLUMN LOAD-MOMENT INTERACTION DIAGRAM

Construct the load-moment interaction diagram of the tied column, the section of which is shown in Fig. 13.13*a*. The column is prestressed with eight 3/8-in-diameter Grade 270 strands. The following information is given:

$f'_c = 5$ ksi, $E_c = 4.28\times10^3$ ksi, $f_{pu} = 270$ ksi, $f_{pe} = 150$ ksi, $f_{py} = 243.5$ ksi, $\varepsilon_{py} = 0.010$, $f_{pp} = 196$ ksi, $\varepsilon_{pp} \simeq 0.007$, $E_{ps} = 27{,}890$ ksi, $A_g = 14\times14 = 196$ in^2, $A_{ps} = 8\times0.085 = 0.68$ in^2

The stress-strain curve of the prestressing steel is assumed linear up to the proportional limit after which it can be represented by the following relationship:

$$f_{ps} = 27{,}890\varepsilon_{ps}\left[0.01174 + \frac{0.98826}{[1+(107.8715\varepsilon_{ps})^{7.344}]^{1/7.344}}\right]$$

where f_{ps} is given in kips per square inch. The above relationship is described in more detail in Section 2.4.3 and in the chapter on nonlinear analysis in Ref. [1.48].

The strand distribution is symmetrical with respect to either the x or y axis leading to the same resistance in each direction. The strands can be separated in three layers. Referring to the above data and to the notation described in Fig. 13.10 and Sec. 13.3, the following quantities can be derived:

$$(A_{ps})_1 = (A_{ps})_3 = 3\times0.085 = 0.255 \text{ in}^2$$

$$(A_{ps})_2 = 2\times0.085 = 0.17 \text{ in}^2$$

$$d_1 = 11.5 \text{ in}$$

$$d_2 = 7 \text{ in}$$

$$d_3 = 2.5 \text{ in}$$

$$\phi = 0.65$$

$$\lambda = 0.80$$

$$\beta_1 = 0.80$$

$$A_n = A_g - A_{ps} = 196 - 0.68 = 195.32 \text{ in}^2$$

$$\varepsilon_{ce} = \frac{0.68\times150}{4.28\times10^3\times195.32} = 0.000122$$

$$\varepsilon_{pe} = \frac{150}{27{,}890} = 0.005378$$

Four main points of the load-moment interaction diagram will be determined, namely, the point of pure compression, the point of zero tension, the balanced point, and the point of pure bending.

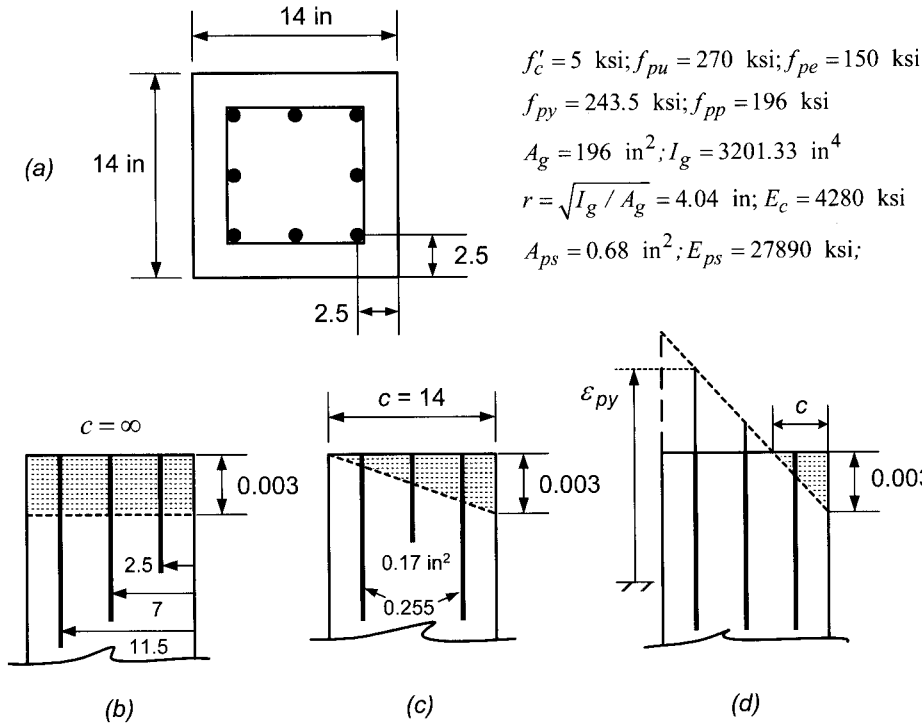

Figure 13.13 Example column. ***(a)*** **Cross section.** ***(b)*** **Strain diagram for uniform compression.** ***(c)*** **Zero tension.** ***(d)*** **Balanced state.**

(a) Point of pure compression. A uniform strain diagram exists. It can be generated, assuming $c = \infty$ (Eq. (13.2) remains valid). Failure occurs when the strain reaches $\varepsilon_{cu} = 0.003$ (Fig. 13.13*b*). The compression force in the concrete is given by Eq. (13.7) in which ba is replaced by A_n :

$$C = 0.85 f'_c A_n = 0.85 \times 5 \times 195.32 = 830.1 \text{ kips}$$

Note that the use of A_g instead of A_n as a first approximation would have led to $C = 833$ kips, an acceptable result.

For the three layers of steel, we have:

Eq. (13.3): $\Delta\varepsilon_{ps} = \varepsilon_{ce} - \varepsilon_{cu} = 0.000122 - 0.003 = -0.002878$

Eq. (13.4): $\varepsilon_{ps} = \varepsilon_{pe} + \Delta\varepsilon_{ps} = 0.005378 - 0.002878 = 0.00250$

As ε_{ps} is less than the proportional limit strain ε_{pp}, we have:

Eq. (13.5): $f_{ps} = E_{ps}\varepsilon_{ps} = 27{,}890 \times 0.00250 = 69.725$

Eq. (13.6): $\sum_i T_{ip} = A_{ps} f_{ps} = 0.68 \times 69.725 = 47.41$ kips

The nominal resistance in pure compression is given by Eq. (13.8):

$$P_{n,o} = C - \sum_i T_{ip} = 830.1 - 47.41 \simeq 783 \text{ kips}$$

The corresponding point of the design diagram is given by:

$$\phi P_{n,o} = 0.65 \times 783 = 508.95 \text{ kips}$$

and the maximum ACI acceptable cutoff compressive force for a tied column is given by:

$$P_m = \lambda(\phi P_{n,o}) = 0.80 \times 508.95 = 407.16 \text{ kips}$$

The representative point is shown in Fig. 13.14.

(b) Point of zero tension in the concrete. The corresponding strain diagram is shown in Fig. 13.13*c*. It leads to $c = 14$ in and $a = \beta_1 c = 11.2$ in. The corresponding force in the concrete compression block is given by Eq. (13.7):

$$C = 0.85 f'_c ba = 0.85 \times 5 \times 14 \times 11.2 = 666.4 \text{ kips}$$

In order to determine the tensile forces in the three layers of steel, the following quantities are needed:

From Eq. (13.3):

$$(\Delta\varepsilon_{ps})_1 = \varepsilon_{ce} + \varepsilon_{cu}\left(\frac{d_1 - c}{c}\right) = 0.000122 + 0.003\left(\frac{11.5 - 14}{14}\right) = -0.000414$$

$$(\Delta\varepsilon_{ps})_2 = 0.000122 + 0.003\left(\frac{7 - 14}{14}\right) = -0.001378$$

$$(\Delta\varepsilon_{ps})_3 = 0.000122 + 0.003\left(\frac{2.5 - 14}{14}\right) = -0.002342$$

From Eq. (13.4):

$$(\varepsilon_{ps})_1 = \varepsilon_{pe} + (\Delta\varepsilon_{ps})_1 = 0.005378 - 0.000414 = 0.004964$$

$$(\varepsilon_{ps})_2 = 0.005378 - 0.001378 = 0.0040$$

$$(\varepsilon_{ps})_3 = 0.005378 - 0.002342 = 0.00304$$

As all these strains are less than the proportional limit strain, the stresses are obtained from Eq. (13.5):

$$(f_{ps})_1 = E_{ps}(\varepsilon_{ps})_1 = 27{,}890 \times 0.004964 = 138.50 \text{ ksi}$$

$$(f_{ps})_2 = 27{,}890 \times 0.004 = 111.56$$

$$(f_{ps})_3 = 27{,}890 \times 0.00304 = 84.78 \text{ ksi}$$

The corresponding tensile force in each layer of steel is given by Eq. (13.6):

$$T_{1p} = (A_{ps})_1 (f_{ps})_1 = 0.255 \times 138.5 = 35.32 \text{ kips}$$

$$T_{2p} = 0.17 \times 111.5 = 18.96 \text{ kips}$$

$$T_{3p} = 0.255 \times 84.78 = 21.62 \text{ kips}$$

Summing up the forces as per Eq. (13.7) leads to the nominal resistance at the zero tension point:

$$P_{n,ot} = C - \sum_i T_{ip} = 666.4 - 35.32 - 18.96 - 21.62 = 590.50 \text{ kips}$$

The corresponding nominal moment is given by Eq. (13.9):

$$M_{n,ot} = C\left(\frac{h}{2} - \frac{a}{2}\right) + \sum_i T_{ip}\left(d_i - \frac{h}{2}\right)$$

$$= 666.5(7 - 5.6) + 35.32(11.5 - 7) + 18.96(7 - 7) + 21.62(2.5 - 7)$$

$$= 932.96 + 158.94 + 0 - 97.29$$

$$M_{n,ot} = 994.61 \text{ kips-in}$$

The corresponding eccentricity is given by:

$$e_{ot} = \frac{M_{n,ot}}{P_{n,ot}} = \frac{944.61}{590.50} = 1.68 \text{ in}$$

For design, we will use:

$$\phi P_{n,ot} = 0.65 \times 590.50 = 383.82 \text{ kips}$$

$$\phi M_{n,ot} = 0.65 \times 994.61 = 646.49 \text{ kips-in}$$

The representative point is shown in Fig. 13.14.

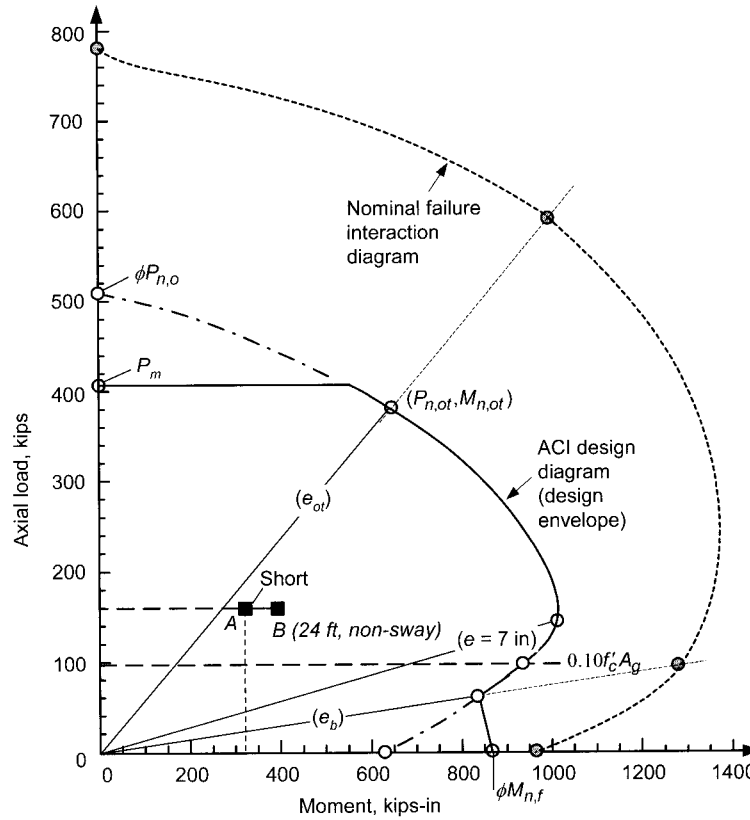

Figure 13.14 Nominal and design load-moment interaction diagrams for example column.

(c) Balanced point (boundary between tension and compression controlled section). The corresponding strain diagram is shown in Fig. 13.13*d*. The strain in the extreme tensile layer of steel is assumed equal to the yield strain $\varepsilon_{py} = 0.010$. From similar triangles, it can be easily shown that:

$$\frac{c}{d_i - c} = \frac{\varepsilon_{cu}}{\varepsilon_{py} - \varepsilon_{ce} - \varepsilon_{pe}}$$

from which $c = 4.60$ in. Thus, $a = \beta_1 c = 3.68$ in.

The corresponding force in the concrete compression block is given by:

$$C = 0.85 \times 5 \times 14 \times 3.68 = 218.96 \text{ kips}$$

Using Eq. (13.3), it can be shown that:

$(\Delta\varepsilon_{ps})_1 = 0.00462$

$(\Delta\varepsilon_{ps})_2 = 0.00169$

$(\Delta\varepsilon_{ps})_3 = -0.001247$

The corresponding strain values are:

$(\varepsilon_{ps})_1 = 0.010$

$(\varepsilon_{ps})_2 = 0.00707$

$(\varepsilon_{ps})_3 = 0.004133$

The first strain value is equal to the yield strain of the prestressing steel. The corresponding stress is given by:

$(f_{ps})_1 = 243.5$ ksi

Using the given stress-strain relation for the prestressing steel leads to:

$(f_{ps})_2 = 192$ ksi

The stress in the third layer of steel is less than the proportional limit, thus:

$(f_{ps})_3 = E_{ps}(\varepsilon_{ps})_3 = 115.27$ ksi

The following quantities are then easily derived:

$T_{1p} = (A_{ps})_1(f_{ps})_1 = 0.255 \times 243.5 = 62.09$ kips

$T_{2p} = (A_{ps})_2(f_{ps})_2 = 0.17 \times 192 = 32.64$ kips

$T_{3p} = (A_{ps})_3(f_{ps})_3 = 0.255 \times 115.27 = 29.39$ kips

$P_{n,b} = C - \sum_i T_{ip} = 218.96 - 62.09 - 32.64 - 29.39 = 94.84$ kips

$$M_{n,b} = C\left(\frac{h}{2} - \frac{a}{2}\right) + \sum_i T_{ip}\left(d_i - \frac{h}{2}\right)$$

$$= 218.96(7 - 1.84) + 62.09(11.5 - 7)$$

$$+32.64(7 - 7) + 29.39(2.5 - 7)$$

$$= 1129.83 + 279.40 + 0 - 132.25$$

$M_{n,b} = 1276.98$ kips-in

$$e_b = \frac{M_{n,b}}{P_{n,b}} = \frac{1276.98}{94.84} = 13.46 \text{ in}$$

$\phi P_{nb} = 0.65 \times 94.84 = 61.65$ kips

$\phi M_{nb} = 830.04$ kips-in

The corresponding point is plotted in Fig. 13.14.

(d) Point of pure bending. Pure bending occurs when the sum of forces acting on the section leads to $P_n = 0$. The location of neutral axis for this case is unknown. A trial-and-error approach is used in which the value of c is first assumed and then the forces are computed as for the other cases described above. If their sum is not nil, a new converging value of c is selected, and so on.

Few iterations are necessary. It can be shown, for this example, that the pure bending point corresponds to a value of $c = 3$ in. The reader may want to check the following results:

$C = 142.8$ kips

$(\varepsilon_{ps})_1 = 0.01398$; $(f_{ps})_1 = 258.4$ ksi; $T_{1p} = 65.9$ kips

$(\varepsilon_{ps})_2 = 0.00948$; $(f_{ps})_2 = 238.1$ ksi; $T_{2p} = 40.47$ kips

$(\varepsilon_{ps})_3 = 0.00498$; $(f_{ps})_3 = 138.95$ ksi; $T_{3p} = 35.43$ kips

$P_{n,f} = 142.8 - 65.9 - 40.47 - 35.43 = 1 \text{ kip} \simeq 0$

$M_{n,f} = 965.35$ kips-in

The corresponding design value is given by:

$\phi M_{n,f} = 0.9 \times 065.35 = 868.82$ kips-in

For a ϕ factor of 0.65, we would have obtained 627.48 kips-in.

The point corresponding to pure bending is shown on Fig. 13.14, where the other main points of the diagram are joined by a continuous curve with due account to the ACI design cutoff point and the transition region.

(e) Transition point at $0.10 f'_c A_g = 98$ kips. This point was needed according to the 1999 version of the ACI code. It is interesting to note that the balanced point for this column falls below the transition point of ordinate $0.10 f'_c A_g = 98$ kips. This is where the transition in the ϕ value from compression to bending starts. In order to have a more accurate representation above the value of 98 kips, another point of the diagram corresponding to $c = 7$ in was determined and is also shown in Fig. 13.14. The fact that the balanced point falls below the point where the diagram changes direction seems to be quite characteristic of prestressed columns in comparison to reinforced concrete columns.

Note that when the balanced point falls below $0.10 f'_c A_g$, the ACI code recommends to use the balanced point instead of the $0.10 f'_c A_g$ point to start the transition for the ϕ value.

Assuming we need to determine the point at $0.10 f'_c A_g = 98$ kips, it is best to try some values of c between 4.6 in and 7 in until P_n computed from Eq. 13.8 equals about 98 kips. From interpolation along the line between the two corresponding points on the graph, a c value close to 5.8 in is obtained.

Table 13.1 Summary of coordinates of key points of the load-moment interaction diagram.

	Pure compression	Zero tension	Balanced	Pure bending	Transition point
P_n, kips	783	590.5	94.84	---	98
M_n, kips-in	----	994.61	1276.98	965.35	
ACI maximum allowed P_u, kips	407.16	383.82	61.65	---	98
ACI maximum allowed M_u, kips-in	---	646.49	830.04	868.82	

(f) Applied load. The column is to be designed for the following load combination:

$P_u = 1.2P_D + 1.6P_L = 1.2 \times 80 + 1.6 \times 40 = 160$ kips

acting at an eccentricity $e = 2$ in. Assume that the column is short and that slenderness effects are negligible. Thus:

$M_u = 1.2(P_D \times 2) + 1.6(P_L \times 2) = 1.2(80 \times 2) + 1.6(40 \times 2) = 320$ kips-in

The point representing the loading P_u and M_u is plotted in Fig. 13.14 as point A. It can be observed that it falls well inside the column interaction diagram. If this was the only load combination and if indeed slenderness is negligible, the load would be an acceptable combination with a wide safety margin. However, it is very likely that slenderness effects will prevail, leading to a more critical condition (see Example 13.9).

13.5 ACI CODE AND OTHER DESIGN CONSIDERATIONS

Some of the ACI code provisions related to the interaction diagram and ϕ factors were given in the previous sections. A number of additional design requirements are summarized below [Refs. 13.1, 13.2].

13.5.1 Minimum Longitudinal Reinforcement

Prestressed concrete compressive members (columns and bearing walls) should have an average effective prestress not less than 225 psi (1.55 MPa). This provision indirectly sets a minimum reinforcement ratio, that is, $(\rho_p)_{\min} = A_{ps} / A_g = 225 / f_{pe}$ for f_{pe} in psi, or $(\rho_p)_{\min} = A_{ps} / A_g = 1.55 / f_{pe}$ for f_{pe} in MPa. Assuming f_{pe} = 150,000 psi, leads to $(\rho_p)_{\min} = 0.15\%$; this is significantly smaller than the minimum 1% required for reinforced concrete columns, even if the strength of the prestressing versus reinforcing steel is accounted for. Compressive members with prestress levels less than 225 psi (1.55 MPa) shall, like ordinary reinforced concrete, have a minimum nonprestressed reinforcement ratio of at least 1 percent.

13.5.2 Lateral or Transverse Reinforcement

Except for walls, for which Chapter 14 of the ACI code applies, members with average prestress equal to or greater than 225 psi (1.55 MPa) shall have all prestressing tendons enclosed by lateral ties or spirals in accordance with the ACI code Sec. 18.11.

Besides its practical role of holding the longitudinal steel together, lateral reinforcement provides a confinement that increases strength and significantly improves ductility. It increases the shear resistance of columns and limits the buckling of longitudinal bars. The use of proper amount of spiral reinforcement significantly improves the ductility and toughness of columns and is particularly recommended in structures subjected to seismic and impact loads. As explained in Fig. 13.6, in highly loaded spirally reinforced columns the concrete cover spalls off; then the core, if adequately confined, can maintain maximum resistance for a high level of deformation or displacement. Such response can save the structure from collapse. The spiral reinforcement improves the load capacity of the confined core (without the cover), balancing the loss of resistance due to spalling of the cover.

The main provisions of the ACI code for the design of lateral reinforcement are summarized next.

a. **Ties.** Lateral ties shall be at least #3 in size or welded wire fabric of equivalent area with lateral spacing not to exceed 48 tie bar or wire diameters or least dimension of compression member. For reinforced concrete or partially prestressed concrete,

the lateral spacing is also limited by 16 longitudinal bar diameters. Ties shall be arranged so that every corner and alternate longitudinal bar, wire, or strand has lateral support provided by the corner of a tie. Also, ties shall be located vertically not more than half a tie spacing above top of footing or slab in any story, and not more than half a tie spacing below the lowest horizontal reinforcement in members supported above. Examples of tie arrangements are shown in Fig. 13.15*a*.

***b*. Spirals.** Spiral reinforcement, when used instead of ties, shall have a reinforcement ratio that satisfies the following relation:

$$\rho_{sp} \geq (\rho_{sp})_{\min} = 0.45\left(\frac{A_g}{A_{co}} - 1\right)\frac{f'_c}{f_y} \tag{13.28}$$

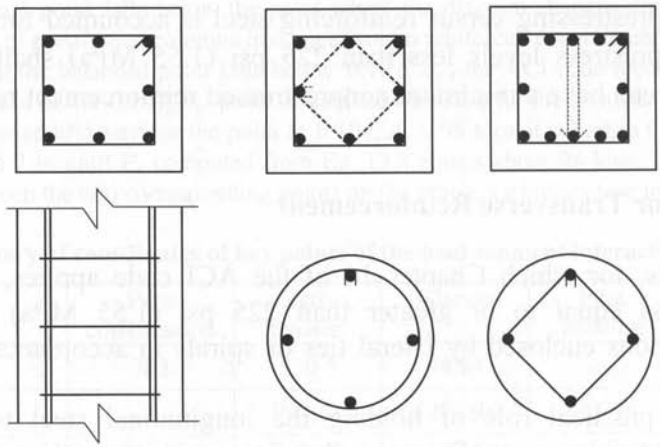

(a)

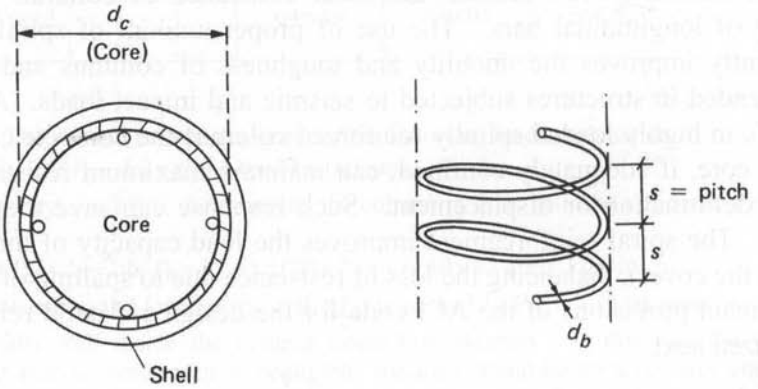

(b)

Figure 13.15 (a) Typical tie reinforcement. (b) Spiral reinforcement.

where A_{co} is the area of concrete core of spirally reinforced compression member measured to outside diameter of spiral (Fig. 13.15*b*) and f_y is the specified yield strength of spiral reinforcement but is not more than 60 ksi (414 MPa). ρ_{sp} is the ratio of volume of spiral reinforcement to the total volume of the core. Calling s the pitch of the spiral (center to center), it can be shown that:

$$\rho_{sp} \simeq \frac{\pi A_{sp}(d_c - d_b)}{A_{co} s} \tag{13.29}$$

where A_{sp} is the cross section area of the spiral steel. Replacing A_{co} by $\pi d_c^2 / 4$ and neglecting d_b relative to d_c, leads to:

$$\rho_{sp} \simeq \frac{4A_{sp}}{s d_c} \tag{13.30}$$

Inversely, given a minimum value of ρ_{sp} from Eq. (13.28), the area of spiral steel at a pitch s can be determined from Eq. (13.30) as:

$$A_{sp} = \frac{\rho_{sp} s\, d_c}{4} \tag{13.31}$$

The clear spacing between spirals, or clear pitch $(s - d_b)$, shall not exceed 3 in (75 mm) nor be less than 1 in (25 mm). For cast-in-place construction, bar size for spirals shall not be less than #3 (that is, 3/8 in or 9 mm).

c. **Special Case of Walls.** Prestressed single and double tees are extensively used as exterior walls in industrial buildings and manufacturing plants. For walls with average prestress not less than 225 psi (1.55 MPa), minimum lateral reinforcement may be waived where analysis shows adequate strength and stability.

13.5.3 Minimum Size of Columns

Contrary to previous editions of the code, no minimum cross-sectional sizes are set for columns in the 2002 ACI code. However, slenderness effects, lateral deflections, and other practical considerations limit the size of prestressed concrete columns. In practice, a cross section of less than 8 × 8 in (20 × 20 cm) is not desirable.

Additional design recommendations related to columns, bearing walls, and piles can be found in Refs. [13.40 and 13.43]. The PCI committee on prestressed concrete columns and bearing walls recommends a number of maximum allowable deflections under service loads. Although the wording is adapted to compression

members, the prescribed limits are essentially identical to those given in Table 7.2 for flexural members.

13.5.4 Minimum Eccentricity

For slender reinforced and prestressed concrete columns, the ACI code specifies a minimum allowed value of the moment M_{u2} used in the moment-magnification equations for non-sway (or adequately braced) frames:

$$\begin{cases} (M_{u2})_{\min} = P_u(0.6+0.03h) \text{ in} \\ (M_{u2})_{\min} = P_u(15+0.03h) \text{ mm} \end{cases} \tag{13.33}$$

where h is the depth of the column. This implies a minimum eccentricity, even if theoretically the column is concentrically loaded:

$$\begin{cases} (e)_{\min} = 0.6+0.03h \text{ in} \\ (e)_{\min} = 15+0.03h \text{ mm} \end{cases} \tag{13.34}$$

It is a good practice to always consider a minimum eccentricity level in columns.

13.5.5 Transfer Zone

In pretensioned columns the effect of transfer length should be accounted for in design. For all practical purposes, the column section in the transfer zone can be designed as a reinforced concrete section, that is, where the effective prestress is taken equal zero. Such an approach does not change very much the shape of the load-moment interaction diagram, as suggested in Fig.13.8.

13.6 SLENDER COLUMNS: THEORETICAL BACKGROUND

Slender columns are columns for which the effect of buckling (or lateral instability) is significant. Their strength is less than that of their cross section and must be evaluated in function of their length, cross section dimensions, mechanical characteristics, lateral deformation under load, and restraint conditions at their ends. This section gives the essential background needed to account for slenderness in prestressed concrete columns. Specialized publications [Refs. 13.12, 13.15, 13.53] must be consulted to extend the concepts and handle special problems requiring exact stability analysis.

Euler's derivation of the critical buckling load P_{cr} of an elastic column subjected to axial compression and having its two ends hinged and restricted against lateral movement leads to the following formula:

$$P_{cr} = \frac{\pi^2 EI}{l_u^2} \tag{13.35}$$

where l_u is the column's length between hinges or unbraced length, E the elastic modulus of the column's material, and I the moment of inertia of its cross section.

Bracing implies restriction of lateral movement or joint translation at the ends of a column. Lateral movement is often described as "sidesway" or "sway." Most concrete structures are intentionally or unintentionally braced against sidesway to a certain degree by walls, elevator shafts, staircases, and the like.

Equation (13.35) can be generalized to account for different end conditions, such as for a fixed-ends column or a cantilever column. It leads to:

$$P_{cr} = \frac{\pi^2 EI}{(kl_u)^2} \tag{13.36}$$

where k is called the effective length factor and l_u is the actual unbraced length of the column between its two ends. The term kl_u, defined as the effective column length, represents, in effect, the distance between the two points of inflection or zero moment (equivalent hinges) of the column. For a column with two fixed ends, the points of zero moment are at a quarter length, thus $kl_u = 0.5l_u$, or $k = 0.5$. It can easily be shown that for a cantilever column $kl_u = 2l_u$. Indeed, the column is considered half a fictitious column, having two hinged ends.

Theoretical values of k for several typical end conditions are shown in Fig. 13.16. Also shown are corresponding design values recommended by AISC for steel columns where ideal conditions are approximate, and values implied in the ACI code approximate method described in Sec. 13.8.

Perfectly hinged or perfectly fixed connections are seldom encountered in real structures. The effective length depends on the degree of fixity of the column at its ends. The degree of fixity depends on the relative stiffness of the column to the connecting members. The column, whether braced or unbraced, can be modeled as shown in Fig. 13.17, and the evaluation of k in such cases is explained in Sec. 13.8.

The critical buckling load at instability given by Eq. (13.36) can be rewritten as follows:

$$P_{cr} = \frac{\pi^2 EA}{(kl_u)^2 (A/I)} = \frac{\pi^2 EA}{[k(l_u/r)]^2} \tag{13.37}$$

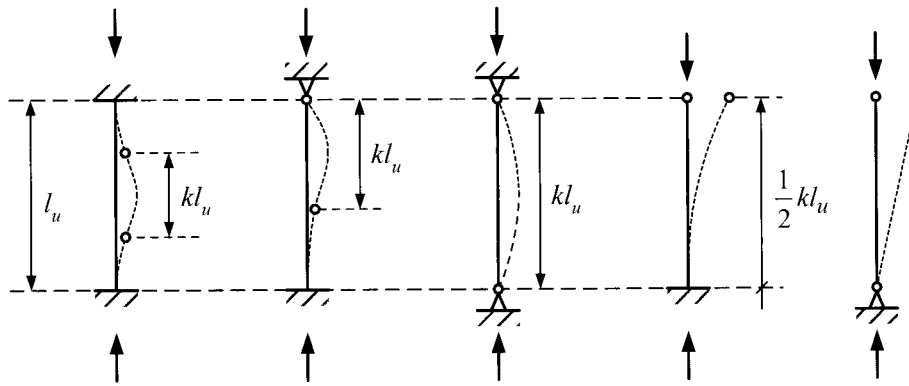

Theoretical:	$k = 0.5$	0.7	1	2	∞
AISC:	$k = 0.65$	0.8	1	2.1	∞
ACI:	$k = 1$	1	1	(Use charts)	∞

Figure 13.16 Deformed shapes and effective length factors of columns with various end restraints.

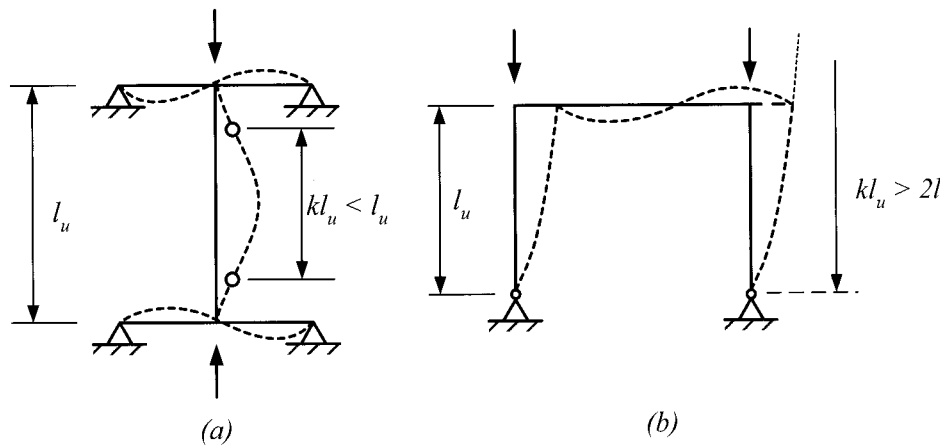

Figure 13.17 Typical deformed shapes of *(a)* braced column (non-sway) and *(b)* unbraced column (sway).

where r is the radius of the gyration of the section and A its cross-sectional area in general (transformed area, or as a first approximation, gross area). The ratio l_u / r is called slenderness ratio and kl_u / r is called the effective slenderness ratio. It can be seen from Eq. (13.37) that, for a given column cross section and materials properties, the critical load is inversely proportional to the square of the effective slenderness ratio and, therefore, decreases significantly with an increase in kl_u / r. Note that the slenderness ratio of a column can easily be reduced by bracing the column at intermediate points, which is equivalent to reducing l_u.

13.6.1 Definition of Braced, Unbraced, Sway and Non-Sway Columns or Frames

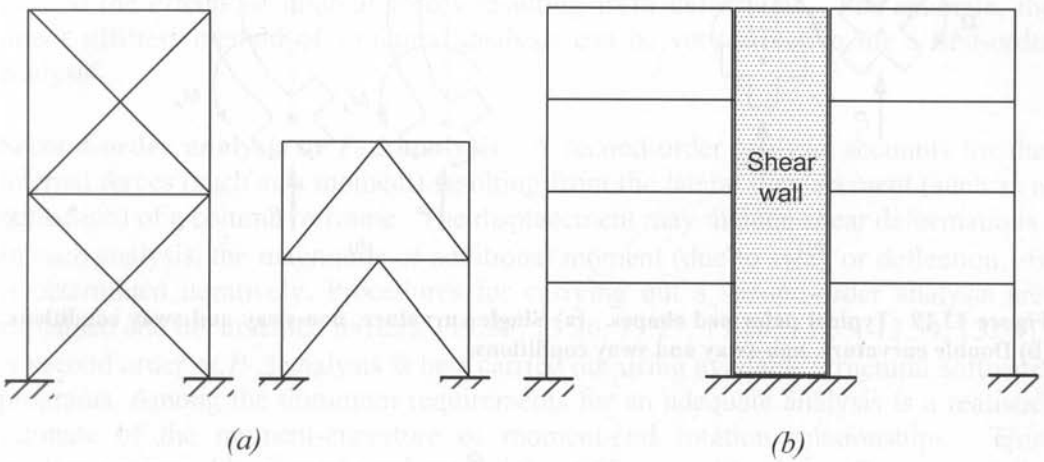

Figure 13.18 Typical bracing of frames.

To minimize the lateral drift or deflection of structures subjected to lateral loads, bracing is used, as shown for example in Fig. 13.18*a* where bracing of a frame is achieved using cross braces, and Fig. 13.18*b* where bracing is carried by a shear wall. In most buildings some bracing is achieved by stair cases, elevator shafts and the like. In actual structures, there is rarely perfect bracing or infinitely stiff bracing. Therefore the structure will deflect laterally under load and the extent of the drift can be evaluated as to its seriousness. In previous editions of the code the term "braced" was used to imply a sufficient level of bracing to keep the sway within minimum. The term "unbraced" was used to imply that the structure could drift under load beyond the level predicted from first-order analysis. In the ACI 2002 code [Ref. 13.2], the terms "sway" and "nonsway" have replaced the terms "unbraced" and "braced" to provide a more accurate description of the structure. Thus a "non-sway" frame implies a sufficient level of bracing so that the lateral deflection or drift is less than a specified limit.

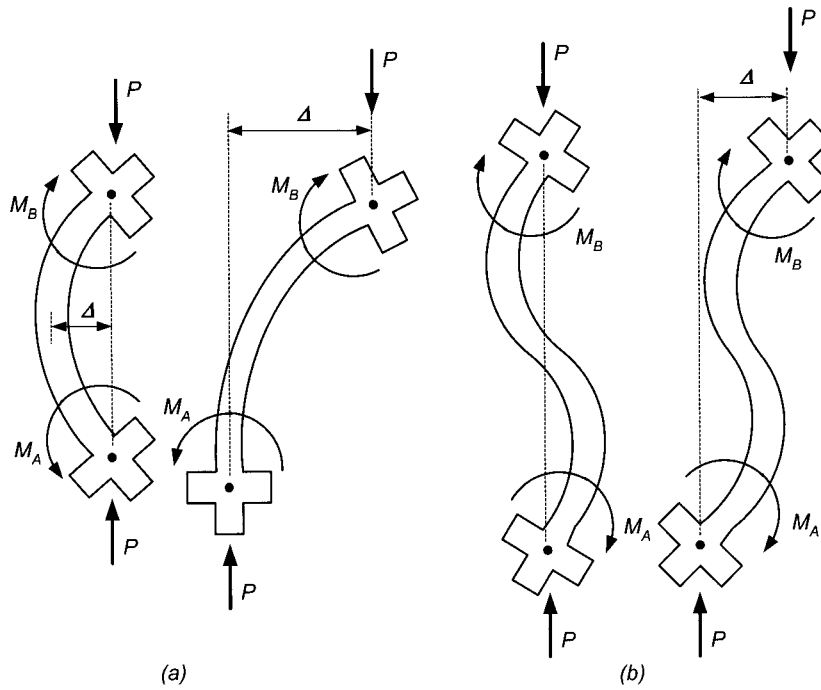

Figure 13.19 Typical deformed shapes. (a) Single curvature, non-sway and sway conditions. (b) Double curvature, non-sway and sway conditions.

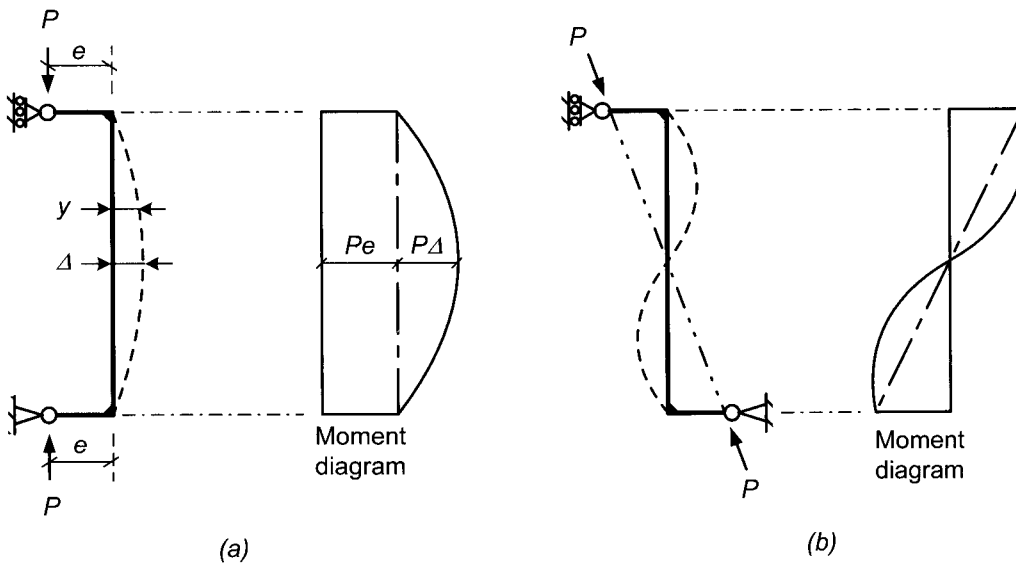

Figure 13.20 Typical moment diagrams having *(a)* single curvature, and *(b)* double curvature.

13.6.2 Single and Double Curvature

Several ACI code provisions distinguish cases of columns bent in single curvature versus double curvature. The corresponding deformed shape of such typical columns is illustrated in Fig. 13.19; also illustrated for each case is the effect of sway versus non-sway, described by the lateral drift, Δ, of one end of the column with respect to the other end. Figure 13.20 describes typical moment diagrams for an example of single versus double curvature.

13.6.3 Terminology and Definitions

First-order analysis. A first-order analysis is an elastic analysis that does not include the effects of internal forces resulting from deflections. For example, the direct stiffness method of structural analysis can be very effective for a first-order analysis.

Second-order analysis or *P-Δ* analysis. A second-order analysis accounts for the internal forces (such as a moment) resulting from the lateral displacement (such as a deflection) of a column or frame. The displacement may include shear deformations. In such analysis, the magnitude of additional moment (due to sway or deflection, Δ) is determined iteratively. Procedures for carrying out a second-order analysis are explained and documented in Refs. [13.25, 13.26, 13.27, 13.28, 13.53, 13.54, 13.55]. A second order or P-Δ analysis is best carried out using available structural software programs. Among the minimum requirements for an adequate analysis is a realistic estimate of the moment-curvature or moment-end rotation relationships. This implies a reasonably accurate estimate of the stiffness or EI values. Because a fully cracked section is assumed when computing deflections, a reduced stiffness value must be used. The main difficulty is that, although the EI values are used in an elastic analysis, they should be representative of the ultimate limit state for which columns are designed. In a first iteration, approximate values of stiffness can be utilized as suggested in Section 13.8.4.

Magnified moment procedure. The magnified moment procedure is an approximate design procedure that uses a moment magnifier (or a moment magnification factor) to account for slenderness. It makes it possible to by-pass a second-order analysis. Moments computed from first-order frame analysis are multiplied by a magnification factor that is mostly a function of the factored axial load P_u and the critical buckling load P_c for the column.

13.6.4 Stiffness Under Cracked Conditions for First-Order Frame Analysis

The critical buckling load of a compression member depends on its stiffness or flexural rigidity represented by the product EI, where E is the elastic modulus of the

material, and I the moment of inertia of the uncracked section. The product EI (called here stiffness or flexural rigidity) is used in the design procedure recommended by various codes for slender columns, in particular the moment magnification method used in the ACI code. However, because of the non-linear response of the materials and because of cracking, modifications are introduced to the flexural rigidity, essentially by reducing its value.

The ACI 2002 code suggests to use the design elastic modulus of concrete E_c (see Table 2.8), and a reduced value of moment of inertia as shown in Table 13.2. Also for computation of area of a compression member, the code suggests the use of the gross area, A_g. A first-order analysis is carried out with these modified values.

Table 13.2 Stiffness values recommended in the 2002 ACI code for first order analysis.

	Product EI	Sustained Load or for Stability of Whole Structure
Beams	$E_c(0.35I_g)$	$\frac{0.35E_cI_g}{1+\beta_d}$
Columns	$E_c(0.70I_g)$	$\frac{0.70E_cI_g}{1+\beta_d}$
Walls - uncracked	$E_c(0.70I_g)$	$\frac{0.70E_cI_g}{1+\beta_d}$
Walls - cracked	$E_c(0.35I_g)$	$\frac{0.35E_cI_g}{1+\beta_d}$
Flat plates and flat slabs	$E_c(0.25I_g)$	$\frac{0.25E_cI_g}{1+\beta_d}$

Note that the values in Table 13.2 are for reinforced concrete members. The ACI code does not specifically cover slenderness effects in prestressed concrete columns. However, the design philosophy of the code can be used and a flexural rigidity more representative of prestressed concrete members can be chosen. This has been the approach suggested by the PCI committees on columns and poles [Refs. 13.40 to 13.43 and 13.36 to 13.38].

Provisions from the ACI 2002 code or recommendations from the PCI Committee on Columns are generally followed in this chapter. Exceptions related to the particular case of prestressed concrete are pointed out when relevant.

13.7 SLENDERNESS EFFECTS: ACI CODE PHILOSOPHY

In its article 10.10.1 the ACI 2002 code recommends the following [Ref. 13.2]:

> "The design of compression members, restraining beams, and other supporting members shall be based on the factored forces and moments from a second-order analysis considering material nonlinearity and cracking as well as the effects of member curvature and lateral drift, duration of loads, shrinkage and creep, and interaction with the supporting foundation."

Since this generally implies the use of structural software, the code allows an alternative in which the design is based on the axial forces and moments estimated from the magnified moment procedure.

At first, it is important to realize that, although prestressed concrete columns are subjected to a compressive force F in addition to external loading, they are not more vulnerable to buckling than reinforced concrete columns, when the prestressing tendons are bonded. This is because the tendons do not change position within the cross section, even when a lateral displacement is induced. Thus, contrary to Euler's case, a lateral displacement does not generate an additional moment due to F in the section.

Since at ultimate, both reinforced and prestresssed concrete columns show similar behavior, the provisions given in the ACI code for reinforced concrete can be somewhat extended to prestressed concrete. This was essentially done in the PCI committee report on prestressed columns [Ref. 13.41] in which some ACI code provisions were modified to better accommodate prestressed columns and walls in accordance with research results [Refs. 13.4, 13.6, 13.20, 13.36, 13.37, 13.38, 13.49, 13.50, 13.51].

The ACI code philosophy regarding the design of slender columns can be summarized as follows:

1. A comprehensive analysis of the structure, accounting for lateral deflection, variable stiffness, and duration of loading is generally preferred. Such an analysis, also called second-order or P-Δ analysis, is required when the effective slenderness ratio kl_u / r exceeds 100 (that is, for long columns). However, the P-Δ analysis is permitted for any slenderness ratio.

2. An approximate method is proposed when the effective slenderness ratio is less than 100. The method treats each column individually but takes into account the effect of lateral bracing of the entire structure and the relative stiffness between a column and the beams at its ends.

In the approximate method, the approach consists of designing the column for the applied axial load P and for a magnified moment, δM, where δ is a magnification factor. This is illustrated graphically in Fig. 13.21 where the load-moment interaction diagram of a column is plotted. For a short column, the load P at a given eccentricity e can be increased and the corresponding loading path follows line $0A$, that is, a proportional increase in moment is induced ($M = Pe$). For a slender column, for which the lateral deformation or deflection Δ is significant, the moment generated at any load P is given by ($Pe + P\Delta$). The loading path follows curve $0B$ until it reaches the interaction diagram at B, where failure occurs. Line $0A$ and curve $0B$ can also be seen as the loading paths followed by the end section and the midsection of the column, respectively.

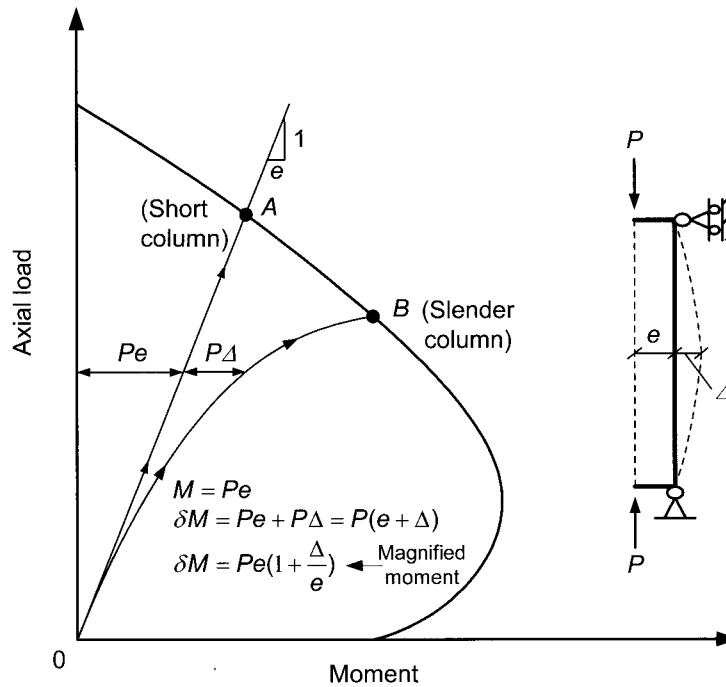

Figure 13.21 Effect of slenderness on loading path.

For the slender column subjected to load P, deflection effect produces an additional moment $P\Delta$ where Δ is the maximum lateral displacement of the column between its two ends. This additional moment reduces the capacity of the column from that represented by point A to that represented by point B. Thus the column should be designed for a moment at B larger than that obtained at A from first order analysis; the moment at B is defined as the magnified moment. The magnification effect is defined as the P-Δ effect (Fig. 13.21).

The moment along *OB* can be expressed in function of the moment along *OA* as:

$$\delta M = Pe + P\Delta = P(e + \Delta) \tag{13.38}$$

where δ is called the moment magnification factor (or moment magnifier) and is theoretically given by:

$$\delta = \frac{e + \Delta}{e} = 1 + \frac{\Delta}{e} \tag{13.39}$$

The value of δ should depend on the slenderness of the column and the applied load. The value of δ is larger than 1 and, should it exceed 2.5, a second-order analysis is recommended. The determination of slenderness ratio and the design value of δ for factored loads, as recommended by the ACI code, are explained in the next section.

13.8 ACI CODE DESIGN PROVISIONS FOR SLENDER COLUMNS BY THE MOMENT MAGNIFIER METHOD

The approximate design method of the ACI code can be reduced to five major steps as follows:

1. Determine if frame is sway or non-sway, that is, if it is sufficiently or insufficiently braced against side-sway
2. Determine the effective length factor k
3. Determine the effective slenderness ratio kl_u / r and the conditions for which slenderness must be accounted for
4. Determine the design moment magnification factor (or moment magnifier) δ
5. Design for factored axial load and magnified factored moment.

These steps are explained in detail below. A flow chart summarizing the overall approach is given in Sec. 13.8.5 and Fig. 13.24.

13.8.1 Sway and Non-Sway Condition

The moment magnifier design method requires the designer to distinguish between non-sway frames and sway frames. The term "non-sway" refers to frames braced against side-sway with a sufficient level of restraint. Examples of braced structures are shown in Fig. 13.18. The ACI 2002 code allows to consider a column "non-sway," or adequately braced, if the increase in column end moments due to second-order effects does not exceed 5% of the first-order moments. Normally, this would

require a second-order analysis of the P-Δ effect; however, another alternative offered by the code is to satisfy the following condition:

$$Q = \frac{\Sigma P_u \Delta_o}{V_u l_c} \leq 0.05 \tag{13.40}$$

where:

Q = stability index
ΣP_u = sum of factored axial loads in a given story (total vertical load)
Δ_o = elastically computed first-order relative lateral deflection between the top and bottom of that story due to V_u (neglecting P-Δ effects)
V_u = factored story shear
l_c = story length center to center of floors or roofs

The above equation is based on the work of MacGregor and Hage; details of its derivation as well as comprehensive background information can be found in Refs. [13.25 to 13.28].

13.8.2 Effective Length Factor *k*

The ACI code recommends the following values:

$$\begin{cases} k = 1 & \text{for braced or non-sway frames} \\ k \geq 1 & \text{for unbraced or sway frames} \end{cases} \tag{13.41}$$

In order to determine k, for unbraced or sway columns, the stiffness of columns and beams at the two ends of each column and the corresponding end restraint coefficients are needed. Section 10.11 of the ACI code and commentary suggests a procedure described next.

The stiffness or rigidity of columns and flexural members can be computed, assuming the elastic modulus of concrete, E_c, and a reduced value of moment of inertia (to account for the cracked section) as explained in Table 13.2. That is:

$$(EI)_{column} = 0.70 E_c I_g \tag{13.42}$$

$$(EI)_{beam} = 0.35 E_c I_g \tag{13.43}$$

Note that the steel reinforcement (prestressed and nonprestressed) is integrated as a first approximation in the above stiffnesses.

The end restraint coefficient ψ is defined as follows:

$$\psi = \frac{(\sum EI / l_c)_{columns}}{(\sum EI / l)_{beams}} \tag{13.44}$$

where the summation applies to all elements at the end considered. The length l_c is that of a compression member in a frame measured from center to center of the joints, and l is the span length of beams also measured center to center of joints. Particular values of ψ called ψ_1 and ψ_2 are calculated for each end of a column.

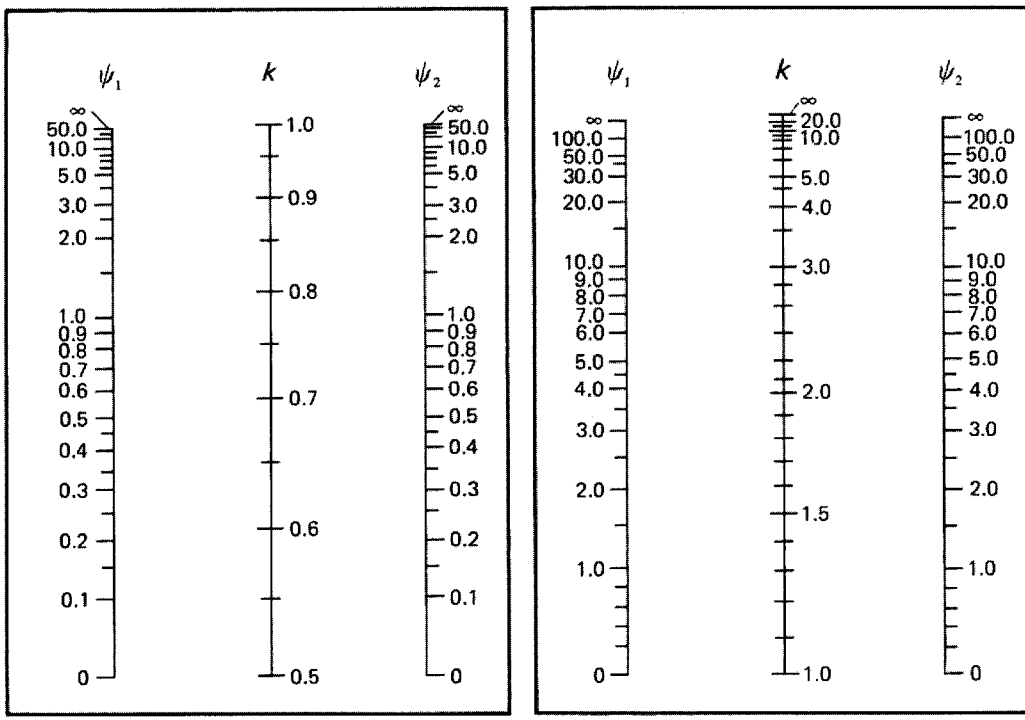

(*a*) Non-sway or braced frames (*b*) Sway or unbraced frames

ψ = ratio of $\Sigma(EI / l_c)$ of compression members to $\Sigma(EI / l)$ of flexural members in a plane at one end of a compression member

l_c = span length of compression member measured center to center of joints

l = span length of flexural member measured center to center of joints

Figure 13.22 Alignment charts for the effective length factor *k*. *(a)* Non-sway or braced frames. *(b)* Sway or unbraced frames.

The effective length factor k is determined from ψ_1 and ψ_2, either by using the well-known alignment charts of Jackson and Moreland, reproduced in Fig. 13.22, or by using the following approximation:

Call ψ_m the average value of ψ_1 and ψ_2 for the column considered:

For $\psi_m < 2$

$$k = \frac{20 - \psi_m}{20}\sqrt{1 + \psi_m} \tag{13.45}$$

For $\psi_m \geq 2$

$$k = 0.9\sqrt{1 + \psi_m} \tag{13.46}$$

For unbraced compression members hinged at one end, k can be taken as:

$$k = 2 + 0.3\psi \tag{13.47}$$

where ψ is for the restrained end.

In practice, and for most structures, ψ, at the base of a column, should not be taken less than 1.0. For a base assumed hinged, ψ can be taken equal to 10 [Ref. 13.40]. Theoretical values of ψ, as per Fig. 13.22, would be infinity for a hinged end and zero for a fixed end.

13.8.3 Effective Slenderness Ratio and Slenderness Condition

Once k is determined, the effective slenderness ratio (kl_u / r) can be calculated. Section 10.11.4 of the ACI code sets the following conditions to evaluate the effects of slenderness:

1. For all compression members, that is for both sway and non-sway members (unbraced or braced), the effects of slenderness can be neglected when $(kl_u / r) \leq 22$.
2. For all compression members with $(kl_u / r) > 100$, a comprehensive second-order analysis shall be made.
3. For non-sway compression members (that is, essentially braced against side-sway), the effects of slenderness may be neglected when

$$\frac{kl_u}{r} < 34 - 12\frac{M_{u1}}{M_{u2}} \leq 40 \tag{13.48}$$

where M_{u1} and M_{u2} are factored end moments of the column and where M_{u1} is smaller in magnitude than M_{u2}. M_{u2} is taken always positive and M_{u1} is taken positive if the member is bent in single curvature and negative if the

member is bent in double curvature. Figure 13.19 illustrates what is meant by single and double curvature.

4. For sway members with $22 \le (kl_u / r) \le 100$ and for non-sway member with $(kl_u / r) \le 100$ but larger than the value defined by Eq. (13.48), the approximate analysis based on the moment magnification factor described in the code can be used.

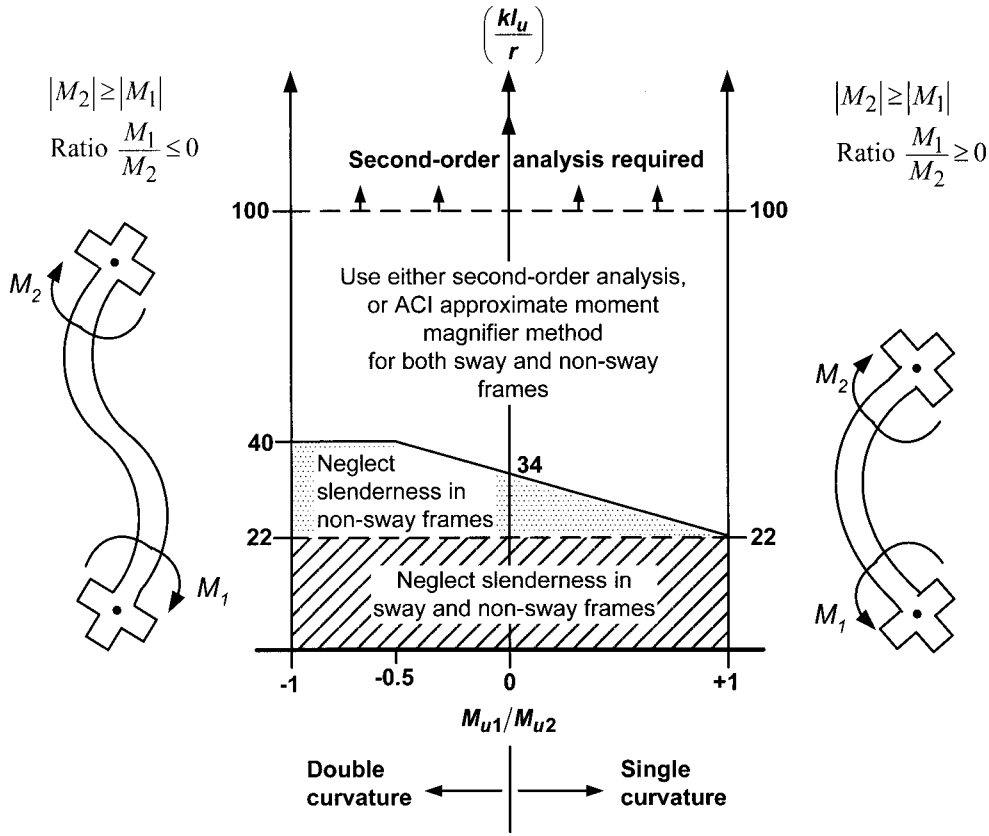

Figure 13.23 Summary of ACI code slenderness conditions.

The above conditions are illustrated in Fig. 13.23. It can be observed that, for all practical purposes, three regions of interest are identified:

- One region, where slenderness is neglected, leading essentially to a "short column" analysis, in which the behavior of the column is represented by its cross-section;
- One region, where slenderness must be accounted for by a comprehensive second-order analysis, leading to a "long-column" analysis;

- An in-between region, where slenderness can be accounted for using the approximate method of the code based on the moment magnifier, essentially leading to a "medium-column" analysis.

The approximate method is explained next.

13.8.4 Moment Magnification in Non-Sway Frames

According to Fig. 13.23, this method is applicable to columns in non-sway frames that satisfy the following condition:

$$\left(\begin{array}{l}\text{Smaller of:}\\ 34-12\dfrac{M_{u1}}{M_{u2}}\\ \text{or:}\\ 40\end{array}\right) \le \frac{kl_u}{r} \le 100 \tag{13.49}$$

The ACI code gives the following value of the moment magnification factor δ_{ns} :

$$\delta_{ns} = \frac{C_m}{1-\dfrac{P_u}{0.75P_{cr}}} \ge 1 \tag{13.50}$$

where P_u = factored axial load obtained from conventional frame analysis

P_{cr} = critical buckling load (see Eq. (13.36))

C_m = reduction factor explained below.

The factor 0.75 in the denominator represents a stiffness reduction factor. The subscript *ns* refers to non-sway.

The reduction factor C_m (also used in steel design) relates the actual moment diagram along the member to an equivalent uniform moment diagram. For members sufficiently braced against side-sway (that is, for non-sway frames (see Sec. 13.8.1)) and without transverse loads between supports, the value of C_m may be taken as:

$$C_m = 0.6 + 0.4\frac{M_{u1}}{M_{u2}} \ge 0.4 \tag{13.51}$$

where M_{u1} and M_{u2} are as defined in Sec. 13.8.3. For all other cases, C_m shall be taken as 1.

In calculating P_{cr} from Eq. (13.36) and in lieu of a more exact analysis, the value of EI may be taken as:

$$EI = \frac{0.2E_cI_g + E_sI_{se}}{1+\beta_d} \tag{13.52}$$

where:

I_{se} = moment of inertia of the reinforcement (prestressed and nonprestressed) about the centroidal axis of the section

β_d = ratio of maximum factored axial sustained load to the maximum factored axial load associated with the same load combination.

Conservatively, Eq. (13.52) can be replaced by:

$$EI = \frac{0.4E_cI_g}{1+\beta_d} \tag{13.53}$$

Equation (13.53) is more convenient in preliminary design than Eq. (13.52), since the reinforcement is then still unknown. β_d essentially accounts for the effect of creep by inducing a reduction in the elastic modulus of concrete under sustained load.

Assuming a value of β_d equal to 0.6 will further simplify Eq. (13.53) to become:

$$EI = \frac{0.4E_cI_g}{1+0.6} = 0.25E_cI_g \tag{13.54}$$

Design Moment for Non-Sway Frames. Compression members are designed using a factored axial load P_u and a factored moment magnified for the effect of curvature, M_{uc} defined by:

$$M_{uc} = \delta_{ns}M_{u2} \geq M_{u2} \tag{13.55}$$

where M_{u2} is the absolute value of the larger factored end moment. This design is satisfied by selecting a column with a design load-moment interaction diagram that envelops the point of coordinates P_u and M_{uc}. Many such points representing different loading combinations are in general present and must also be designed for.

Note that the value of δ_{ns} holds only for one direction of moments. If the analysis is run in two directions, a different value of δ_{ns} must be calculated for each axis.

For design, a final check is needed. For slender reinforced and prestressed concrete columns in non-sway frames, the ACI code specifies a minimum allowed value of the moment M_{u2} used in the moment-magnification equations; it is given by:

$$\begin{cases} (M_{u2})_{\min} = P_u(0.6+0.03h) & \text{where the term in parentheses is in.} \\ (M_{u2})_{\min} = P_u(15+0.03h) & \text{where the term in parentheses is in mm} \end{cases} \tag{13.56}$$

where h is the depth of the section in the direction resisting the moment. Thus in Eq. (13.55), M_{u2} is taken as the larger of M_{u2} or $(M_{u2})_{min}$.

13.8.5 Magnified Moments in Sway Frames with $22 < kl_u / r < 100$

For columns in sway frames, the following procedure is suggested in the ACI 2002 code. At each end of a column:

1. The magnified sway moment $\delta_s M_{us}$ is computed either from a second-order elastic analysis or from approximation using the sway magnifier $\delta_s \geq 1$.
2. The magnified sway moment $\delta_s M_{us}$ is added to the unmagnified non-sway moment M_{ns} computed from a first-order analysis, leading to the total design moment
3. If the column is slender and heavily loaded, it is checked to see whether the moments at points between the ends of the column exceed those at the ends (Eq. 13.61).

Thus:

$$\begin{cases} M_{u1} = M_{u1ns} + \delta_s M_{u1s} \\ M_{u2} = M_{u2ns} + \delta_s M_{u2s} \end{cases} \tag{13.57}$$

where the subscript s stands for "sway" and ns for "non-sway." The non-sway moments are obtained from first order analysis for the non-sway loads.

The magnified sway moment $\delta_s M_s$ (at each end of a column) is obtained from either a second-order analysis or from the following approximation:

$$\begin{cases} \delta_s M_{u1s} = \dfrac{M_{u1s}}{1-Q} \geq M_{u1s} \\ \delta_s M_{u2s} = \dfrac{M_{u2s}}{1-Q} \geq M_{u2s} \end{cases} \tag{13.58}$$

provided $\delta_s \leq 1.5$; otherwise the following equation can be used:

$$\begin{cases} \delta_s M_{u1s} = \dfrac{M_{u1s}}{1 - \dfrac{\Sigma P_u}{0.75 \Sigma P_{cr}}} \geq M_{u1s} \\ \delta_s M_{u2s} = \dfrac{M_{u2s}}{1 - \dfrac{\Sigma P_u}{0.75 \Sigma P_{cr}}} \geq M_{u2s} \end{cases} \tag{13.59}$$

where ΣP_u is the summation of all the factored vertical loads in a story and ΣP_{cr} is the summation of the critical loads for all the sway resisting columns in a story. P_{cr} is calculated from Eq. (13.36), and δ_s is limited to 2.5. Note that the value of $\delta_s = 2.5$ corresponds to $Q = 0.60$ (Eq. 13.40). Should δ_s exceed 2, it is generally preferred to increase the dimensions of the column.

Note that in computing stiffness values for sway frames:

β_d = ratio of maximum factored sustained shear within a story to the maximum factored shear in that story; for wind or earthquake its value is zero since these loads are short-term; however, for lateral pressure due to earth, a non-zero value is obtained.

However, for stability checks of sway frames involving the structure as a whole,

β_d = ratio of maximum factored sustained axial load to the maximum factored axial load.

Design Moment for Sway Frames. M_{u1} and M_{u2} are calculated respectively as above for each end of the column. Since it is not known a priori which one is the largest, the computations are carried out first and only at the end, the larger value is reassigned the subscript 2, if necessary. The design is then carried out for the factored axial load P_u and the moment:

$$M_{uc} = M_{u2ns} + \delta_s M_{u2s} \tag{13.60}$$

Although the ACI code does not specify a minimum moment for columns in sway frames, it is a good practice to check such condition and design for the larger of M_{uc} and $(M_{u2})_{min}$ (Eq. 13.56).

A note is in order here to illustrate what is meant by sway and non-sway moments.

Consider for instance one of the factored load combinations recommended by the ACI code (Table 3.9):

$$U = 1.2D + 1.6W + 0.5L + L_r \qquad \text{(ACI Eq. 9-4)}$$

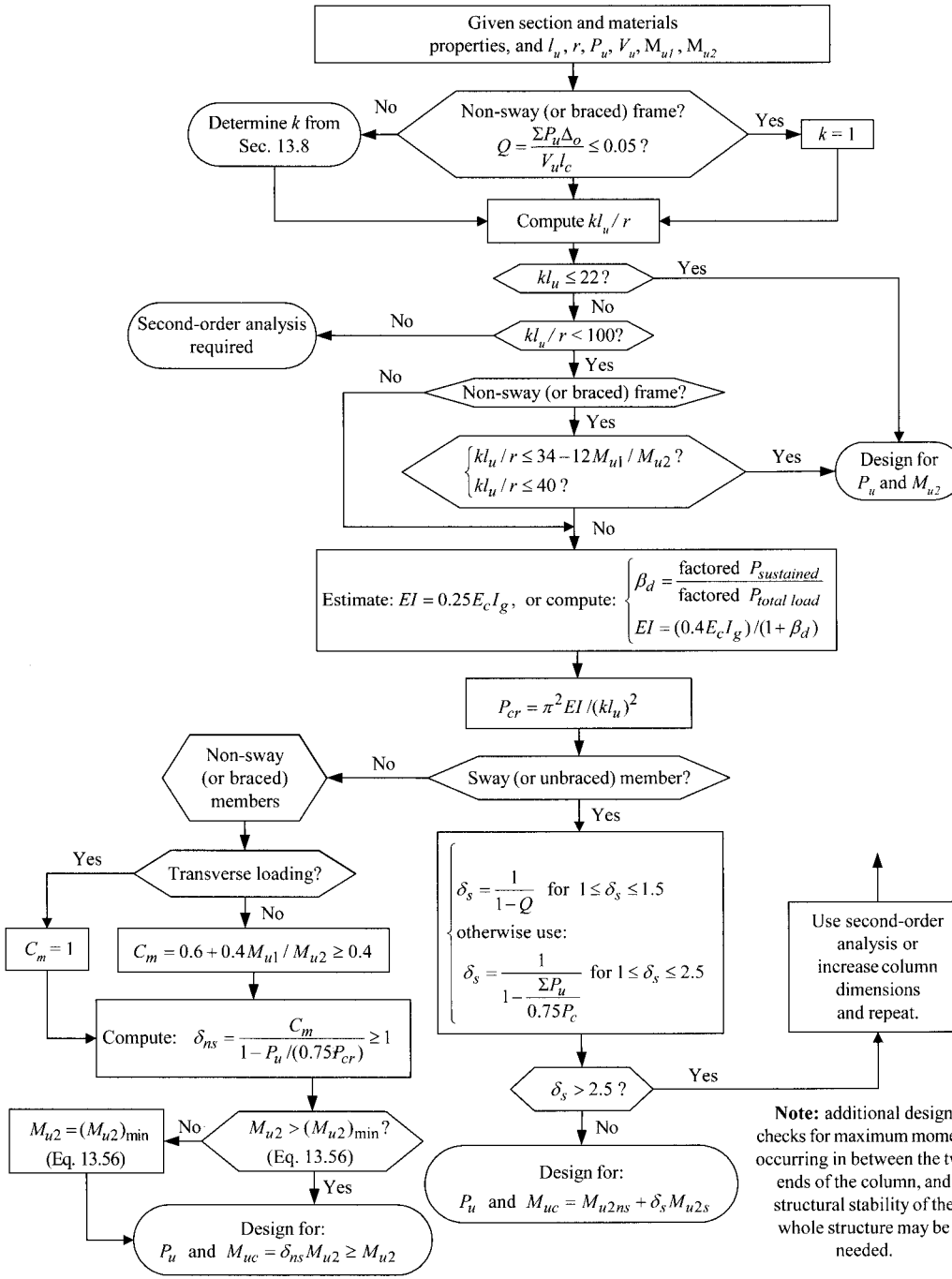

Figure 13.24 Flow chart summarizing the main ACI code approach to the design of slender reinforced concrete columns.

where D, L, and L_r are gravity loads and W is a wind load. For such load combination, the non-sway moment is calculated for $1.2D + 0.5L + L_r$, and the sway moment is calculated for $1.6W$. Similarly for the combination:

$$U = 0.9D + 1.6W \qquad \text{(ACI Eq. 9-6)}$$

the non-sway moment is calculated for $0.9D$, and the sway moment for $1.6W$.

The main steps for the design of sway columns according to the ACI code are summarized in a flow chart, Fig. 13.24.

Additional Check for Maximum Moment. The maximum moment in a column may occur at a section in between its two ends, and thus the corresponding value of maximum moment at that section controls the design. This occurs when for an individual compression member the following condition is satisfied:

$$\frac{l_u}{r} > \frac{35}{\sqrt{\dfrac{P_u}{f'_c A_g}}} \qquad (13.61)$$

In that case, the member shall be designed for the factored load P_u and the moment M_{uc} calculated from:

$$M_{uc} = \delta_{ns}(M_{u2ns} + \delta_s M_{u2s}) = \left(\frac{C_m}{1 - \dfrac{P_u}{0.75 P_{cr}}} \right)(M_{u2ns} + \delta_s M_{u2s}) \qquad (13.62)$$

in which δ_{ns} is calculated from Eq. (13.50), and C_m is computed from Eq. (13.51). It can be observed that when the maximum moment occurs in between the two ends of a column, an additional magnification is applied.

13.8.6 Additional Design Checks

Structural Stability. For sway frames, the ACI code also recommends that the structure as a whole be investigated for sidesway instability under factored gravity loads. This can be done in three different ways. The reader is referred to the code Section 10.13.6 for the related information.

Remarks. The design provisions of the ACI code apply to reinforced concrete columns; they do not all apply as well to prestressed concrete columns. The main difference is in the estimate of the stiffness values for cracked sections (that is the EI

values). Also, most prestressed columns, poles and piles are not monolithically cast as part of framed structures. They are either used with hinged ends or lightly connected to other elements. The method described next is specifically suitable for prestressed columns. It essentially uses the same philosophy as the ACI code except for the estimate of the stiffness *EI*. Another method described in Section 13.12 describes how to get a better estimate of *EI* for prestressed concrete columns. Once *EI* is determined the ACI code procedure can be followed.

13.8.7 Design According to the PCI Committee on Columns

The PCI committee on prestressed columns [Ref. 13.41] uses a modification to the stiffness given by Eq. (13.54) suggesting values of a parameter $1/\lambda$ to replace the factor 0.4 (note 0.4 = 1/2.5, that is, λ = 2.5) for members without or with compression flange (such as wall panels made with T or double T sections). A similar approach is used by the PCI Committee on prestressed poles.

For prestressed concrete columns, the stiffness *EI* given by Eq. (13.53) is replaced by the following equation:

$$EI = \frac{E_c I_g / \lambda}{1 + \beta_d} \tag{13.63}$$

where:

$$\lambda = \theta\eta \geq 3.2 \tag{13.64}$$

$$\eta = 2.5 + 1.6\frac{P_{n,o}}{P_u} \begin{cases} \geq 6 \\ \leq 70 \end{cases} \tag{13.65}$$

$$\begin{cases} \theta = \dfrac{27}{kl_u / r} - 0.05 & \text{for sections without a compression flange} \\ \theta = \dfrac{27}{kl_u / r} - 0.09 & \text{for sections with a compression flange} \end{cases} \tag{13.66}$$

in which P_u is the applied factored axial load from first-order analysis, $P_{n,o}$ is the pure axial load capacity of the section, and other notation is as defined earlier. Note that the coefficient λ would be equal 2.5 in Eq. (13.53); its effect is to reduce the stiffness at ultimate of prestressed columns in comparison to reinforced concrete columns, since the area of prestressed reinforcement is generally much smaller than that of reinforcing bars.

Once the stiffness or flexural rigidity has been obtained, the design continues according to the ACI procedure for non-sway frames. A flow chart summarizing the PCI procedure is given in Fig. 13.24.

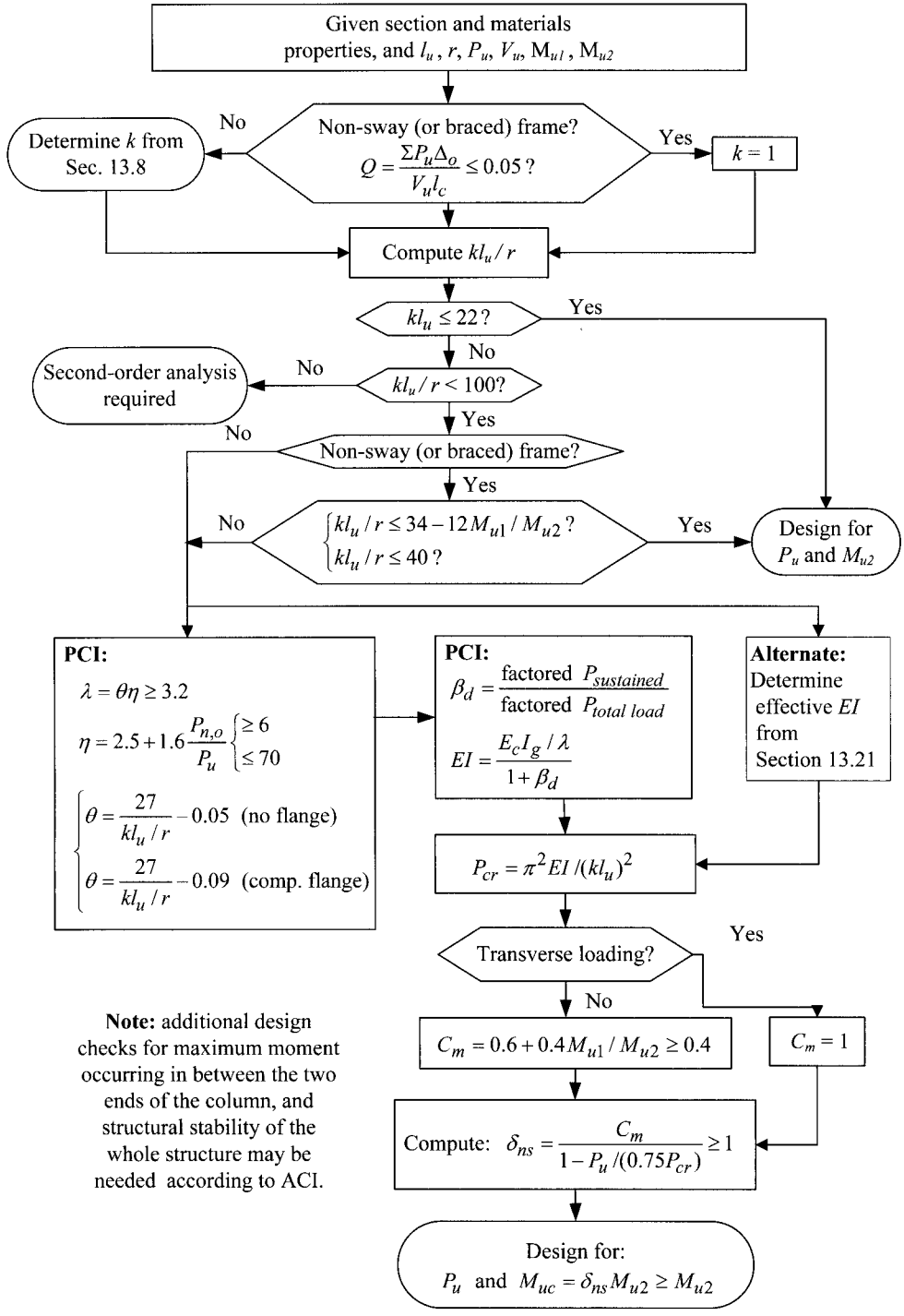

Figure 13.25 Flow chart integrating the PCI design procedure and the ACI code provisions for slender columns.

The PCI committee on prestressed columns limits the application of Eq. (13.63) to columns and walls with a slenderness ratio less than 150. However, the author recommends to carry out a second order analysis if the effective slenderness ratio exceeds 100, as suggested in the ACI code.

Remark. A remark is in order regarding Eqs. (13.64 to 13.66): for a given value of η, the value of θ decreases with an increase in the effective slenderness ratio, leading to a decrease in the value of λ and an increase in equivalent stiffness. This result does not seem very rational as it implies that the longer the column, the higher its stiffness. However the limits set on λ seem to take care of some inconsistencies. Although the value of λ was calibrated to fit analytical predictions, a great deal of research is still needed to further establish its accuracy over the whole range of slenderness ratios. There is some evidence that it leads to results generally on the safe side [Ref. 13.51].

13.9 EXAMPLE: SLENDER COLUMN USING THE PCI APPROACH

Consider the same column cross section and corresponding materials properties described in Example Sec. 13.4 and in Fig. 13.10 and 13.26*c*. The column is part of a bridge pier made out of two columns.

13.9.1 Non-Sway or Braced Column

Assume the column is fixed at its base, hinged at its top, and braced against sidesway at the top end. For all practical purposes, it is assumed that the value of $Q < 0.05$ (Eq. 13.40). The column's unbraced length is $l_u = 24$ ft (Fig. 13.26*a*). It is to be designed for the following loads and load combination:

$$P_D = 80 \text{ kips}; P_L = 40 \text{ kips}$$

$$P_u = 1.2P_D + 1.6P_L = 1.2 \times 80 + 1.6 \times 40 = 160 \text{ kips}$$

acting at an eccentricity $e = 2$ in (Fig. 13.26*b*). Assuming the column is fixed at the base and hinged at the top, it can be easily shown from structural analysis that this loading leads to a double curvature with moment $|M_{u1}| = 160$ kips-in at the base, and $|M_{u2}| = 320$ kips-in $> |M_{u1}|$ at the top, with opposite signs (Fig. 13.26b). Thus:

$$M_{u2} = 1.2(P_D \times 2) + 1.6(P_L \times 2) = 1.2(80 \times 2) + 1.6(40 \times 2) = 320 \text{ kips-in}$$

The point representing the loading P_u and $M_u = M_{u2}$ is plotted in Fig. 13.14 (also Fig. 13.26*d*) as point *A*. It can be observed that it falls well inside the column interaction diagram. If the column was a short column, the load would be an acceptable combination with a wide safety margin. However, it is very likely that slenderness effects will prevail, leading to a more critical condition.

Let us follow the flow chart of Fig. 13.25 and the steps described in Sec. 13.8.

First check that M_{u2} is more than the minimum required by the ACI code:

$$(M_{u2})_{\min} = P_u(0.6 + 0.03h) = 160(0.6 + 0.03 \times 14) = 163.2 \text{ k-in}$$

$$(M_{u2})_{\min} < M_{u2} = 320 \text{ k-in} \quad \text{O.K.}$$

Determine the radius of gyration r of the section:

$$r = \sqrt{\frac{I_g}{A_g}} = \sqrt{\frac{3201.33}{196}} = 4.04 \text{ in}$$

Since the column is braced against sidesway, $k = 1$ and the effective slenderness ratio is

$$\frac{kl_u}{r} = \frac{1 \times 24 \times 12}{4.04} = 71.3$$

It is less than 100, larger than 22 and larger than 40. Thus, slenderness effects should be considered. The approximate PCI procedure can be used.

The load ratio β_d is given by:

$$\beta_d = \frac{\text{factored } P_D}{\text{factored } P_{\text{total}}} = \frac{1.2 \times 80}{160} = \frac{96}{160} = 0.60$$

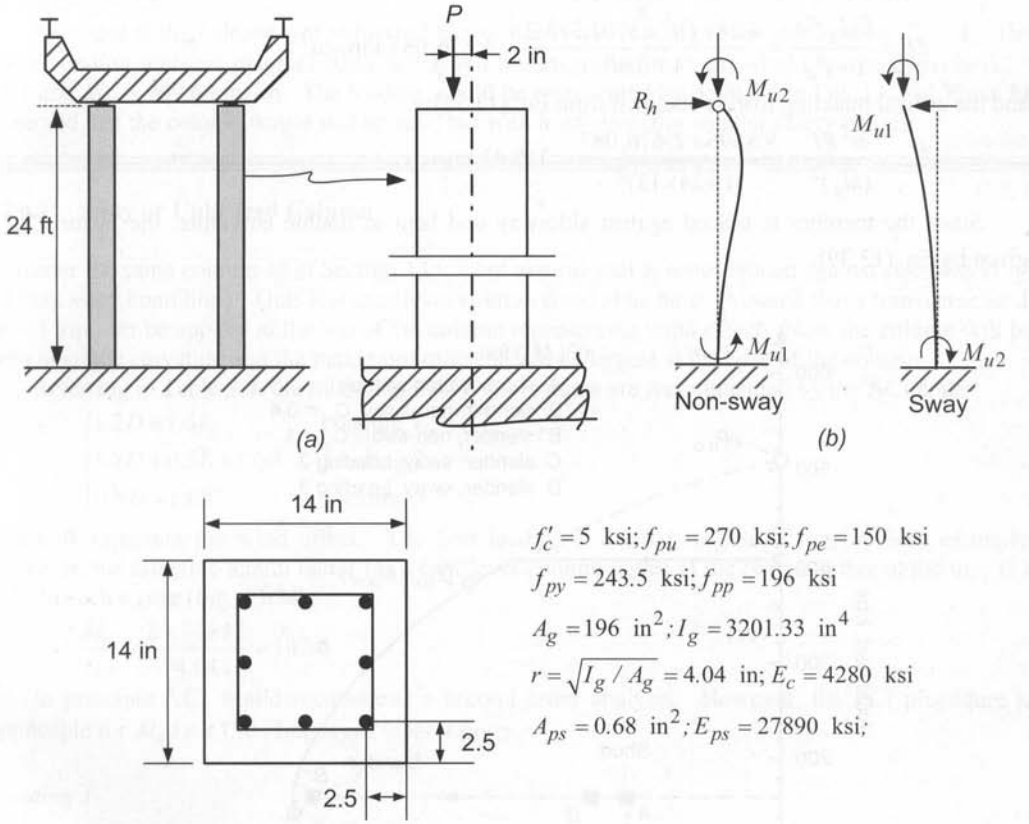

Figure 13.26 Example of slender column. *(a)* Elevation. *(b)* Eccentric loading. (c) Section properties as per Fig. 13.10.

The stiffness is estimated from Eqs. (13.63 to 13.66):

$$EI = \frac{E_c I_g / \lambda}{1 + \beta_d}$$

where:

$$\lambda = \theta\eta \geq 3.2$$

$$\eta = 2.5 + 1.6\frac{P_{n,o}}{P_u}\begin{cases}\geq 6\\ \leq 70\end{cases}$$

$$\eta = 2.5 + 1.6\frac{P_{n,o}}{P_u} = 2.5 + 1.6\frac{783}{180} = 9.46 \quad \begin{cases}\geq 6\\ \leq 70\end{cases}$$

For the value of $P_{n,o}$ see Table 13.1.

Thus use: $\eta = 9.46$

$$\theta = \frac{27}{kl_u/r} - 0.05 = \frac{27}{71.3} - 0.05 = 0.33$$

$$\lambda = \theta\eta = 9.46 \times 0.33 = 3.12$$

λ should be ≥ 3.2 thus take $\lambda = 3.2$

$$EI = \frac{E_c I_g/\lambda}{1+\beta_d} = \frac{4.28\times10^3 \times 3201.3/3.2}{1+0.60} = 2,676,087 \text{ kips-in}^2$$

and the critical buckling load is obtained from Eq. (13.36):

$$P_{cr} = \frac{\pi^2 EI}{(kl_u)^2} = \frac{9.8696 \times 2,676,087}{(1\times24\times12)^2} = 318.43 \text{ kips}$$

Since the member is braced against sidesway and bent in double curvature, the factor C_m is given by Eq. (13.39):

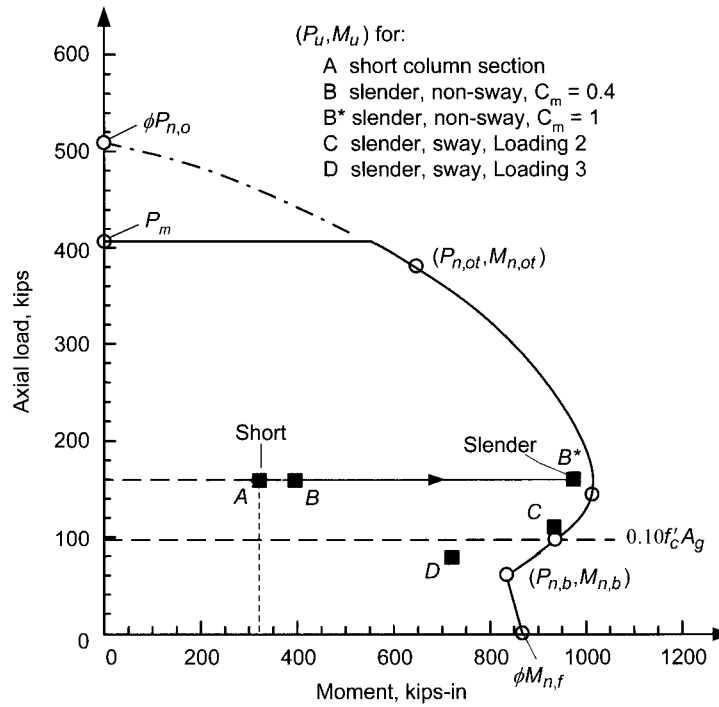

Figure 13.26 (d) Factored loads and the design load-moment interaction diagram.

$$C_m = 0.6 + 0.4\frac{M_{u1}}{M_{u2}} = 0.6 - 0.4\frac{160}{320} = 0.4 \geq 0.4$$

The moment magnification factor is determined from Eq. (13.51):

$$\delta_{ns} = \frac{C_m}{1 - \dfrac{P_u}{0.75 \times P_{cr}}} = \frac{0.4}{1 - \dfrac{160}{0.75 \times 318.43}} = 1.212$$

and the magnified moment is:

$$M_{uc} = \delta_{ns} M_{u2} = 1.212 \times 320 = 387.84 \text{ kips-in}$$

The effect of slenderness leads us to design for the same load $P_u = 160$ kips and a magnified moment M_{uc} higher than M_u. The point of coordinate P_u and M_{uc} is shown in Fig. 13.14 and Fig. 13.26*d* as point *B*.

Note that if the column was subjected to any transverse loading (even small) then $C_m = 1$. The corresponding moment magnification factor and the magnified moment would be respectively $\delta_{ns} = 3.03$ and $M_{uc} = 969.6$ kips-in. The loading would be represented by point *B** in Fig. 13.26*d*. It can be observed that the column would still be safe, but with a substantially smaller safety margin.

13.9.2 Sway or Unbraced Column

Consider the same column as in Section 13.9.1 but assume that it is not braced against sidesway (Fig. 13.26*b*, sway condition). Thus it is cantilever column fixed at its base. Assume that a transverse load, $W = 1$ kip, can be applied at the top of the column representing wind effect. Now the column will be bent in single curvature and the maximum moment will be largest at the base of the column.

Referring to Table 3.9, the following load combinations are recommended by the ACI code:

$$\begin{cases} 1.2D + 1.6L & \text{Loading 1} \\ 1.2D + 0.5L + 1.6W & \text{Loading 2} \\ 0.9D + 1.6W & \text{Loading 3} \end{cases}$$

where W represent the wind effect. The first loading is similar to that of the previous example. However, the effective length factor for a cantilever column (fixed at the base and free at the top) is $k = 2$. In such a case (Fig. 13.24):

$$\frac{kl_u}{r} = \frac{2 \times 24 \times 12}{4.04} = 142.6$$

In principle ACI would recommend a second order analysis. However, the PCI procedure is applicable for $kl_u / r < 150$. Let us see what it gives.

Loading 1

$$\lambda = \theta\eta \geq 3.2$$

$$\eta = 2.5 + 1.6\frac{P_{n,o}}{P_u} \begin{cases} \geq 6 \\ \leq 70 \end{cases}$$

For the value of $P_{n,o}$ see Table 13.1. Thus:

$$\eta = 2.5 + 1.6\frac{P_{n,o}}{P_u} = 2.5 + 1.6\frac{783}{180} = 9.46 \quad \begin{cases} \geq 6 \\ \leq 70 \end{cases}$$

Thus use: $\eta = 9.46$

$$\theta = \frac{27}{kl_u / r} - 0.05 = \frac{27}{142.6} - 0.05 = 0.139$$

$$\lambda = \theta\eta = 9.46 \times 0.139 = 1.318$$

λ should be ≥ 3.2, thus take $\lambda = 3.2$

$$EI = \frac{E_c I_g / \lambda}{1 + \beta_d} = \frac{4.28 \times 10^3 \times 3201.3 / 3.2}{1 + 0.60} = 2,676,087 \text{ kips-in}^2$$

and the critical buckling load is obtained from Eq. (13.36):

$$P_{cr} = \frac{\pi^2 EI}{(kl_u)^2} = \frac{9.8696 \times 2,676,087}{(2 \times 24 \times 12)^2} = 79.6 \text{ kips}$$

Since $P_u = 160 > P_{cr} = 79.6$ kips, this design should not be allowed. Either bracing should be used, or the column cross section should be increased to increase its radius of gyration.

Nevertheless, to further illustrate the procedure for sway columns, the second and third loading are covered next. Table 13.3 summarizes the main values of moments and forces to be considered. Their justification is given next.

Table 13.3

Loading	Load Combination	P_u kips	V_u kips	M_{u2ns} kips-in	M_{u2s} kips-in	Q	δ_s	M_{uc} kips-in
1	1.2D + 1.6L	160	0	320 at top	0			
2	1.2D + 0.5L + 1.6W	116	1.6	-116 at base	808.8 at base	0.234	1.3055	939.87 at base
3	0.9D + 1.6W	72	1.6	-72 at base	676.8 at base	0.145	1.17	719.85 at base

Loading 2

Some structural analysis is needed first to explain the approach; the reader should refer to Refs. [13.28 and 13.36] for details. The following steps are taken:

- Fix the column at the top against lateral sway
- Find the reaction due to the applied moment at the top; for a cantilever column, it is equal to $R_h = 3P_u e / 2l_c$
- Carry out a first order analysis to determine the moments at both ends; these are the non-sway moments.
- Release fixity constraint at the top and assume the column is subjected to the combined effect of $(R_h + V_u)$
- Determine the magnified moment. This is the sway moment.

For Loading 2:

$$P_u = 116 \text{ kips and } R_h = \frac{3P_u e}{2l_c} = \frac{3 \times 116 \times 2}{2 \times 24 \times 12} = 1.2083 \text{ kips at the top of the column.}$$

If the top is fixed against lateral sway, the moment at the base of the column becomes half the moment at the top with opposite sign, thus:

$$M_{u2ns} = -0.5 \times 116 \times 2 = -116 \text{ kips-in}$$

At release of fixity at the top, the maximum sway moment occurs at the bottom of the column; the worst loading condition is when V_u (from wind)and R_h are in the same direction; the moment is given by:

$$M_{u2s} = (V_u + R_h)l_c = (1.6 + 1.2083) \times 24 \times 12 = 808.8 \text{ kips-in}$$

To compute the magnification factor from Eqs. (13.58 or 13.59), the value of Q from Eq. (13.40) is needed. Thus:

$$Q = \frac{\Sigma P_u \Delta_o}{V_u l_c}$$

where (Table 13.3):

$$P_u = 116 \text{ kips}; \quad V_u = 1.6W = 1.6 \text{ kips}; \quad l_c = 24 \times 12 = 288 \text{ in}$$

$$\Delta_o = \frac{V_u l_c^3}{3EI} = \frac{1.6 \times 288^3}{3 \times 4280 \times 3201.33} = 0.93 \text{ in} \quad \text{(see Table 7.7 for deflection formula)}$$

$$Q = \frac{116 \times 0.93}{1.6 \times 288} = 0.234 < 0.60 \quad \text{OK}$$

Using Eq. (13.58) leads to:

$$\delta_s M_{u2s} = \frac{M_{u2s}}{1 - Q} = \frac{808.8}{1 - 0.234} = 1.3055 \times 808.8 = 1055.87 \text{ kips-in}$$

The design moment is given by (Eq. 13.60):

$$M_{uc} = M_{u2ns} + \delta_s M_{u2s} = -116 + 1.3055 \times 808.8 = 939.87 \text{ kips-in}$$

The corresponding loading is represented by point C on the design load-moment interaction diagram of Fig. 13.26*d*. It is observed that the column is adequate to resist such loading.

Loading 3

The following results are obtained for the third loading of Table 13.3.

$$P_u = 72 \text{ kips and } R_h = \frac{3P_u e}{2l_c} = \frac{3 \times 72 \times 2}{2 \times 24 \times 12} = 0.75 \text{ kips at the top of the column.}$$

If the top is fixed against lateral sway, the moment at the bottom of the column becomes half the moment at the top with opposite sign, thus:

$$M_{u2ns} = -0.5 \times 72 \times 2 = -72 \text{ kips-in}$$

At release of fixity at the top, the maximum sway moment occurs at the bottom of the column; the worst loading condition is when V_u and R_h are in the same direction; the moment is given by:

$$M_{u2s} = (V_u + R_h)l_c = (1.6 + 0.75) \times 24 \times 12 = 676.8 \text{ kips-in}$$

To compute the magnification factor from Eqs. (13.58 or 13.59), the value of Q from Eq. (13.40) is needed. Thus:

$$Q = \frac{\Sigma P_u \Delta_o}{V_u l_c}$$

where:

$$P_u = 72 \text{ kips}; \quad V_u = 1.6 \text{ kips}; \quad l_c = 24 \times 12 = 288 \text{ in}$$

$$\Delta_o = \frac{V_u l_c^3}{3EI} = \frac{1.6 \times 288^3}{3 \times 4280 \times 3201.33} = 0.93 \text{ in}$$

$$Q = \frac{72 \times 0.93}{1.6 \times 288} = 0.145 < 0.60 \quad \text{OK}$$

Using Eq. (13.58) leads to:

$$\delta_s M_{u2s} = \frac{M_{u2s}}{1-Q} = \frac{676.8}{1-0.145} = 1.17 \times M_{u2s} = 791.85 \text{ kips-in}$$

The design moment is given by (Eq. 13.60):

$$M_{uc} = M_{u2ns} + \delta_s M_{u2s} = -72 + 1.17 \times 676.8 = 719.85 \text{ kips-in}$$

The corresponding loading is represented by point *D* on the load-moment interaction diagram of Fig. 13.26*d*. It is observed that the column is adequate to resist such loading.

Remarks. The reader may want to consider how to accommodate the first loading combination assuming a sway column (see Problem 13.4). It is likely that simply increasing the cross-sectional area of the column, keeping everything else the same, will provide a suitable solution.

Since structural analysis programs are readily available it is advised to carry out in real applications a second-order analysis even for simple structures to obtain the sway moments.

13.10 DESIGN EXPEDIENTS AND DESIGN AIDS

No closed-form resolution has been developed for the design of columns. Generally, a trial column is selected based on previous experience. Its design load-moment interaction diagram is then determined and compared to all points representing the various loading combinations (due account being made for slenderness effects). If the diagram envelops all the points, the design is safe. Otherwise, the column section or the amount of prestress or both have to be increased and the procedure repeated. If, on the other hand, it is found that the margin of safety is too large, the column section can be decreased to achieve a more economical design. Design aids in the form of load-moment interaction diagrams can also be used in the iterative design process.

13.10.1 Preliminary Dimensioning

In dimensioning a column cross section, the following simple heuristic rule can be used as a first approximation: select the load combination with the largest specified axial load P_u and dimension the concrete section so that $0.90P_m \simeq P_u$; neglect the effect of reinforcement in determining P_m. Thus, we have:

$$P_u = 0.90P_m = 0.90\lambda\phi P_{n,o} \simeq 0.90\lambda\phi(0.85f'_c A_g) \tag{13.67}$$

from which we derive:

$$A_g \simeq \frac{P_u}{0.90\lambda\phi 0.85f'_c} \tag{13.68}$$

Eq. (13.68) becomes:

For a tied column:

$$A_g \simeq \frac{P_u}{0.40 f'_c} \quad \geq 64 \text{ in}^2 \text{ or } 40000 \text{ mm}^2 \tag{13.69}$$

For a spirally reinforced column:

$$A_g \simeq \frac{P_u}{0.45 f'_c} \quad \geq 64 \text{ in}^2 \text{ or } 40000 \text{ mm}^2 \tag{13.70}$$

The lower limit in the above equations is due to practical considerations. Once the cross section is determined, at least a minimum reinforcement is provided and the problem is essentially transformed from a design problem to an analysis or review problem. The nominal load-moment interaction diagram can then be determined. Revision of the cross section properties may be necessary after a first design evaluation. Common range of average prestress in columns varies from the minimum 225 psi (1.55 MPa) to about 900 psi (6.2 MPa). In applications for building structures, the most likely range is between 300 to 400 psi (2 to 3 MPa).

Once the design load-moment interaction diagram is determined, the effects of slenderness have to be checked, as described in Sec. 13.8. For this, the flow chart of Fig. 13.25 which summarizes the steps according to the procedure recommended by the PCI Committee on Columns [Ref. 13.41], should cover the majority of cases.

For a column economy, it is better to use the highest possible compressive strength of concrete. However, this may not help if the column is subjected to relatively large moments. In such cases, the amount of prestressing steel has to be increased. Because of the minimum prestress requirement of 225 psi, an increase in column cross section also leads to an increase in the amount of prestressing steel resisting flexure, and the corresponding moment resistance is also increased.

Because the failure of columns can be catastrophic in terms of damage to the whole structure and to human lives, it is this author's opinion that columns should be designed with a sufficient margin of safety, even exceeding code recommendations. This is also justifiable on the basis that creep and shrinkage, which are generally ignored in everyday design of columns, can substantially affect their performance. Finally, future modifications of the structure, such as addition of a story, can be easily accommodated with slightly overdesigned columns.

13.10.2 Design Charts: Load-Moment Interaction Diagrams

To speed up the design, load-moment interaction diagrams have been extensively developed for reinforced concrete columns and cover different cross-section configurations, reinforcement ratios, reinforcement properties, and the like. The PCI handbook [Refs. 13.40] offers a limited number of load-moment interaction graphs

for precast prestressed square columns with an average level of prestress and dimensions ranging from 12x12 in to 24x24 in. Real units of kips and kip-ft are used. Nondimensionalized load-moment interactions diagrams for prestressed concrete columns (developed by the author) are shown in Figs. 13.27 and 13.28. They apply to square and rectangular columns prestressed with 270 ksi (1860 MPa) strands, assumed having an effective prestress $f_{pe} = 150$ ksi (1035 MPa). The steel configuration is as shown in the figure. Four reinforcement ratios are used, corresponding to four levels of average prestress. The smallest value of 0.15 corresponds to the minimum average compression of 225 psi (1.55 MPa) recommended by the ACI code for prestressed concrete columns, and the largest is four times the minimum value. A ϕ factor of 0.7 was used, hence assuming tied columns as per the pre-2002 ACI code; also, for the sake of clarity, the diagrams are presented without showing the truncated top part and the transition lower part. Since the 2002 ACI code recommends a value of $\phi = 0.65$ for tied columns, the graphs can still be used provided the results are multiplied by the ratio 0.65/0.7 = 0.93. Although the range of variables covered is limited, these diagrams are very convenient for the preliminary dimensioning of prestressed concrete square and rectangular columns.

Additional non-dimensionalized diagrams for nominal resistance (i.e., without the ϕ factor) of prestressed concrete hollow cored circular sections which are very commonly used in electrical poles are given in Fig. 13.29 and 13.30 [Refs. 13.7, 13.8]. It is observed that the compressive strength of concrete has a significant effect at high axial loads (Fig. 13.29*a*); however, this effect diminishes considerably at low axial loads. On the other hand, an increase in the amount of prestressed reinforcement leads to a significant increase in moment resistance at lower axial loads (Fig. 13.29*b*). A prestressed reinforcement ratio of 0.0015 corresponds to an average compressive stress of 225 psi ($\sigma_g = F/A_g$); thus Fig. 13.29*b* covers an average compressive stress ranging from 225 psi to 1350 psi. Figure 13.30*a* illustrates the influence of the ratio of the inside to outside diameter of the hollow-cored section, and Fig. 13.30*b* shows that the effective prestress has very little influence on the part of the diagram that falls below the vertex (point of maximum moment) of the diagram. Additionally, it was shown in the same study that for round hollow-cored sections having at least four prestressing tendons, practically identical load-moment interaction diagrams are obtained whether the tendons are placed along the two main axes of the column or at 45° angle to these axes, or whether the tendons cross section was represented by a continuous round reinforcing steel circular tube having same cross section and same D_s. It was also observed that the cover to the reinforcement has little influence provided the ratio of inside to outside diameter of the section remains constant.

Figures 13.31 to 13.33 illustrate the nominal load-moment interaction diagrams for I-shaped sections which are also often used as poles for electrical transmission lines [Refs. 13.8, 13.51]. The reinforcement is assumed distributed in the flanges.

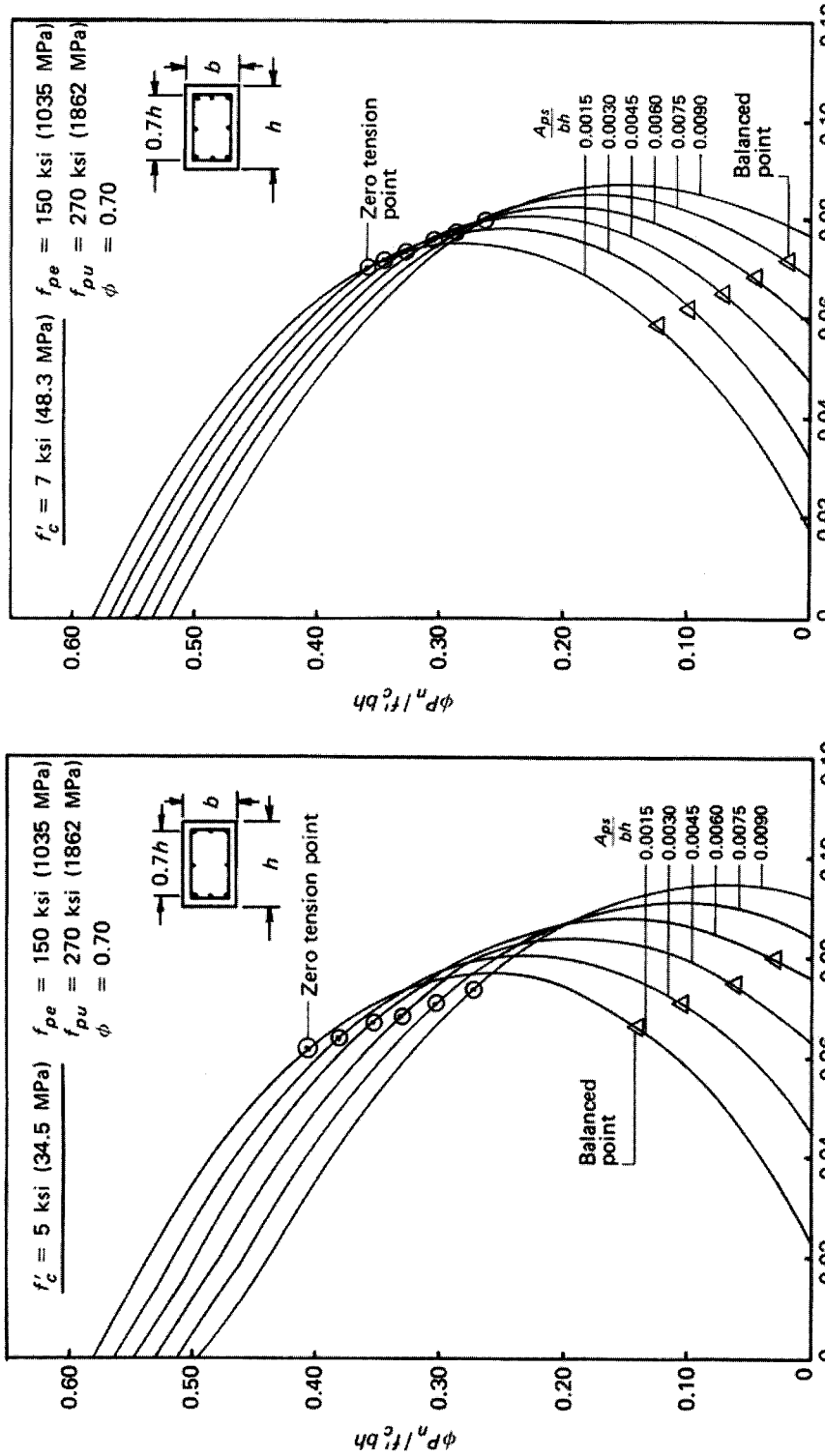

Figure 13.27 Non-dimensional load-moment interaction diagrams for prestressed concrete square and rectangular columns.

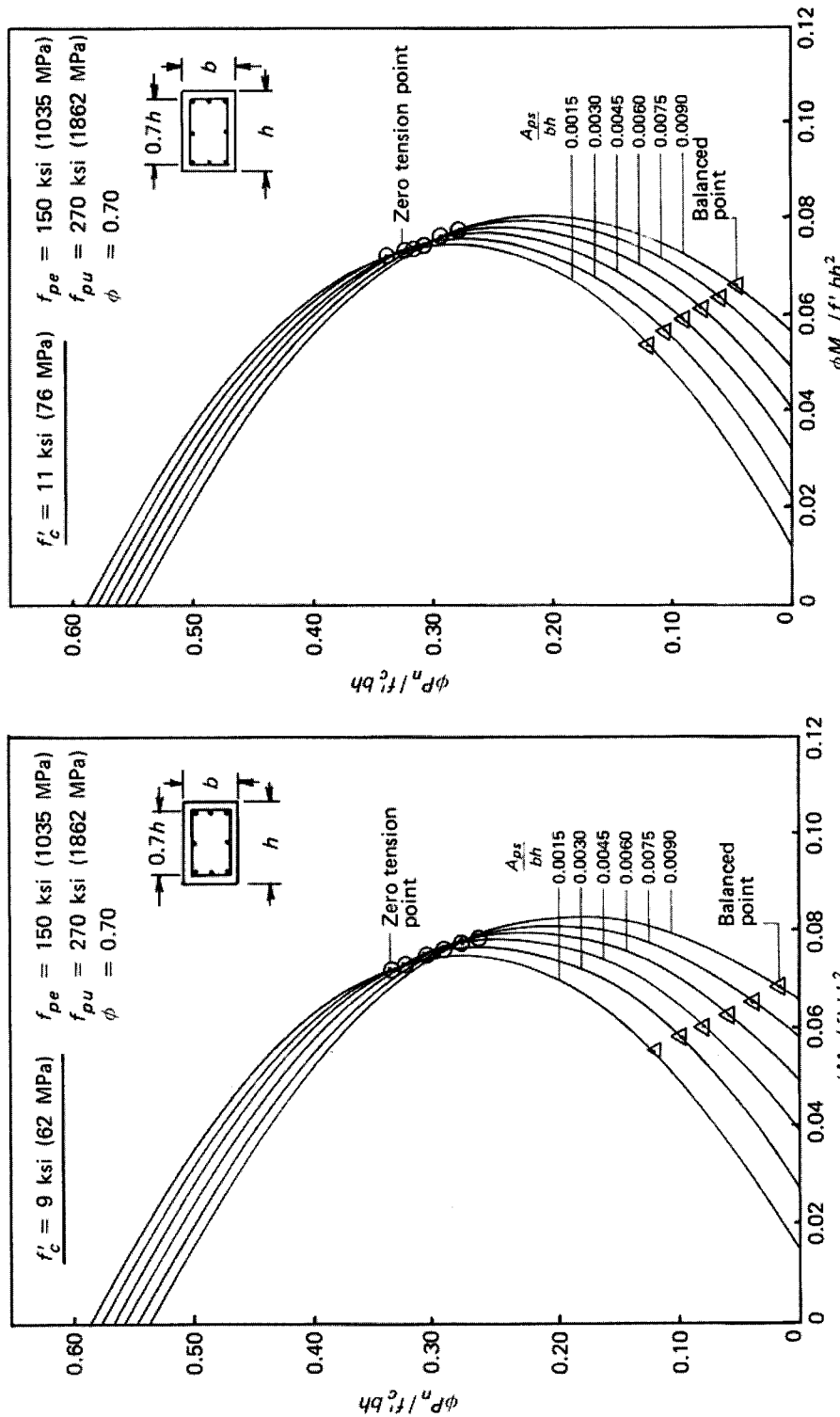

Figure 13.28 Non-dimensional load-moment interaction diagrams for prestressed concrete square and rectangular columns.

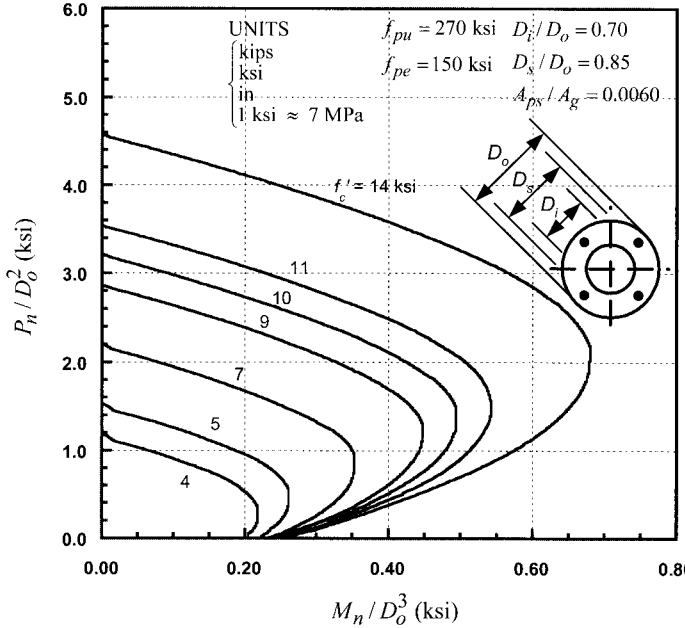

(a)

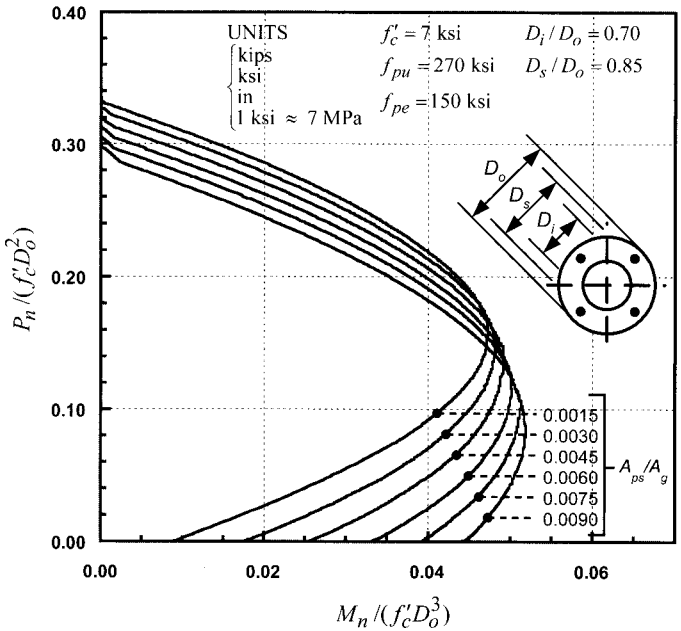

(b)

Figure 13.29 Influence of (a) concrete compressive strength and (b) prestressed reinforcing ratio on the nominal load-moment interaction diagram of circular hollow-cored sections.

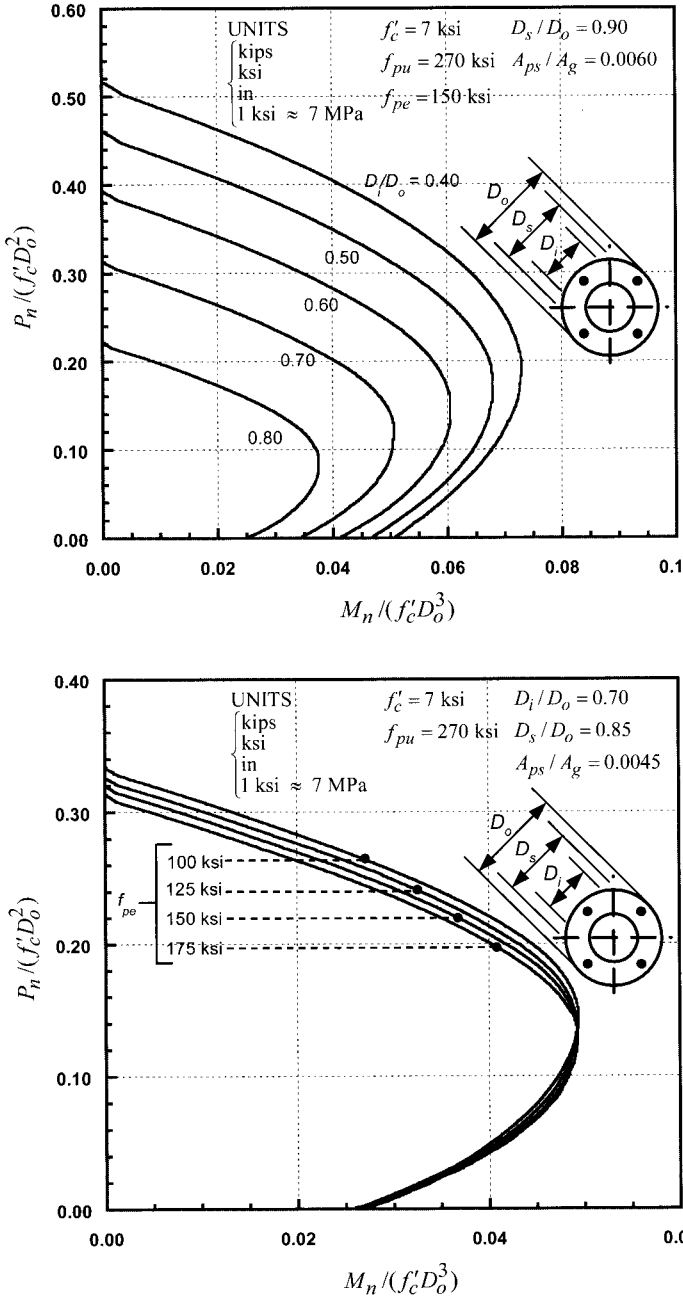

Figure 13.30 Influence of the: (a) D_i/D_o ratio, and (b) effective prestress on the nominal load-moment interaction diagram of circular hollow-cored sections.

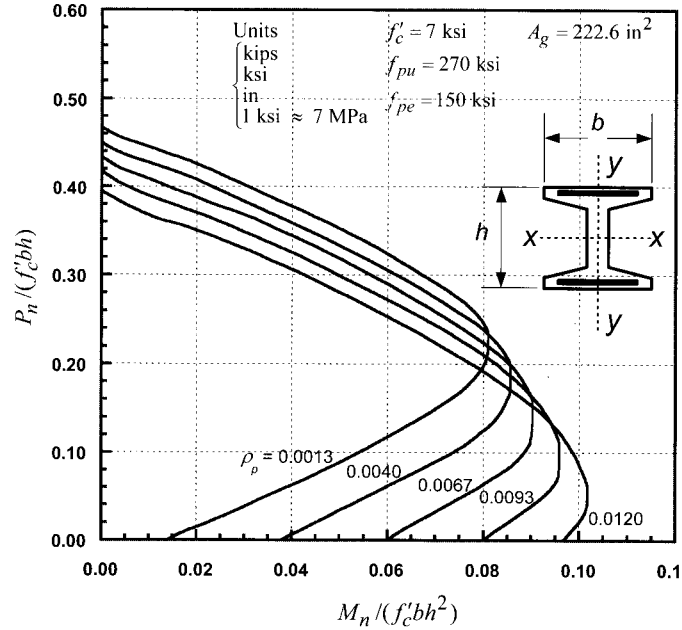

(a)

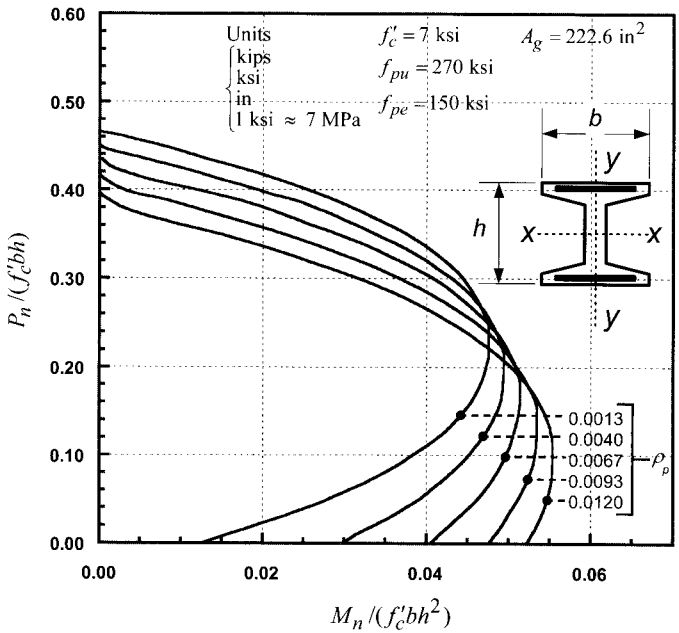

(b)

Figure 13.31 Nominal load-moment interaction diagram for I-shape sections (f'_c = 7 ksi): (a) bending about XX axis, (b) bending about YY axis. The values of prestressed reinforcement ratio correspond approximately to an average prestress of 200, 600, 1000, 1400, and 1800 psi, respectively.

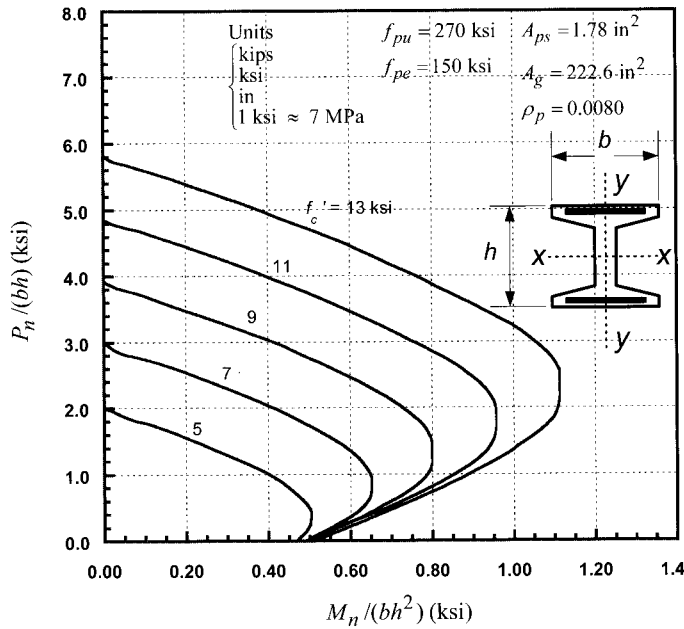

(a)

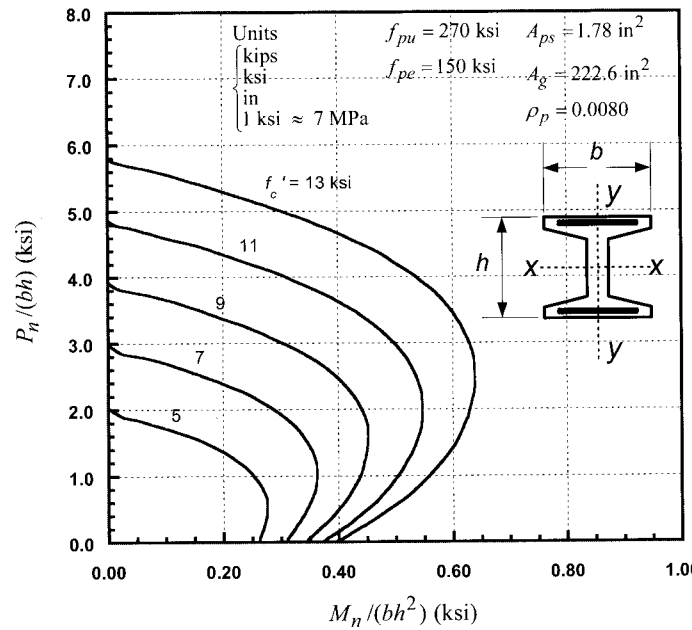

(b)

Figure 13.33 Typical effect of concrete compressive strength on nominal load-moment interaction diagram of I-shaped sections: (a) bending about x-x axis; (b) bending about y-y axis.

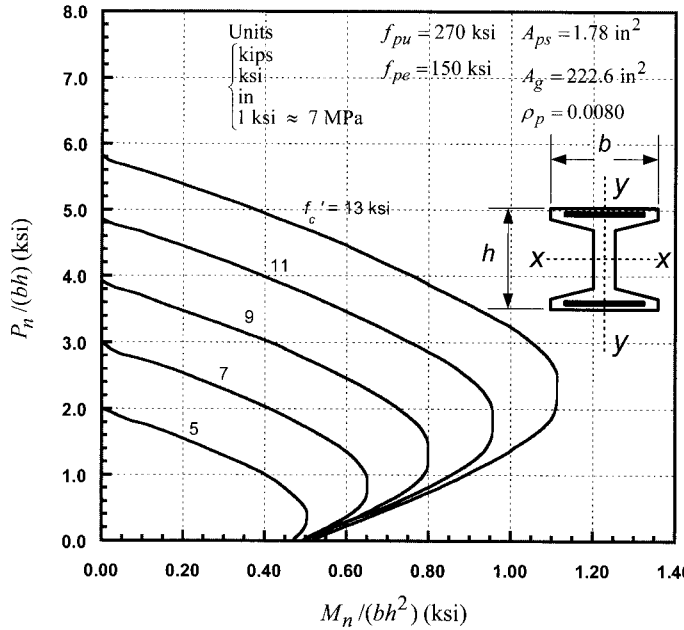

(a)

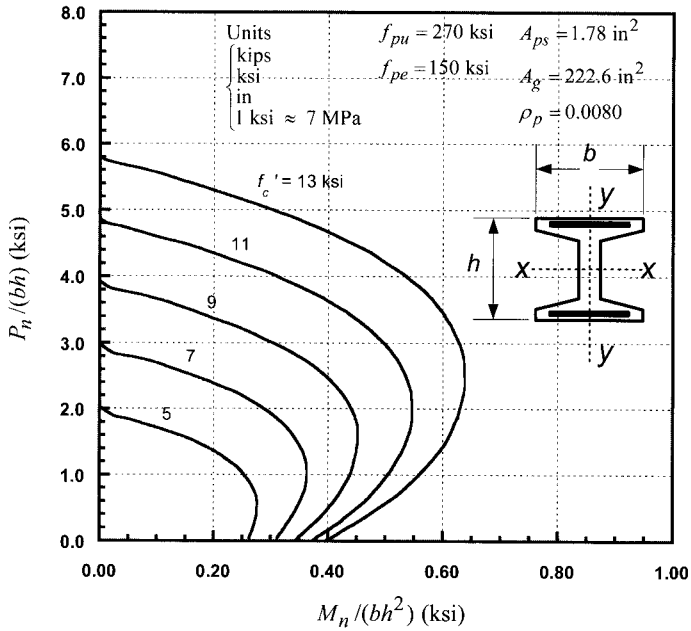

(b)

Figure 13.33 Typical effect of concrete compressive strength on nominal load-moment interaction diagram of I-shaped sections: (a) bending about x-x axis; (b) bending about y-y axis.

The influence of various parameters, such as reinforcement ratio (or equivalently average compression stress due to prestressing), concrete compressive strength and effective prestress is similar to that observed with other sections. Because the section is non-symmetrical, the figures show the interaction diagrams for each of the two main axes, that is bending about the strong axis (x-x), and bending about the weak axis (y-y). Here, the reinforcement ratio corresponds to an average compression stress due to prestressing ranging from 200 psi to 1800 psi.

3.11 BIAXIAL BENDING

Most columns are subjected to biaxial bending. However, when the moment about the transverse axis is small (say less than 10%) compared to the moment about the primary axis, the column is treated as if it is subjected to uniaxial bending. Nevertheless, in corner columns of buildings and in many bridge piers biaxial bending must be properly evaluated.

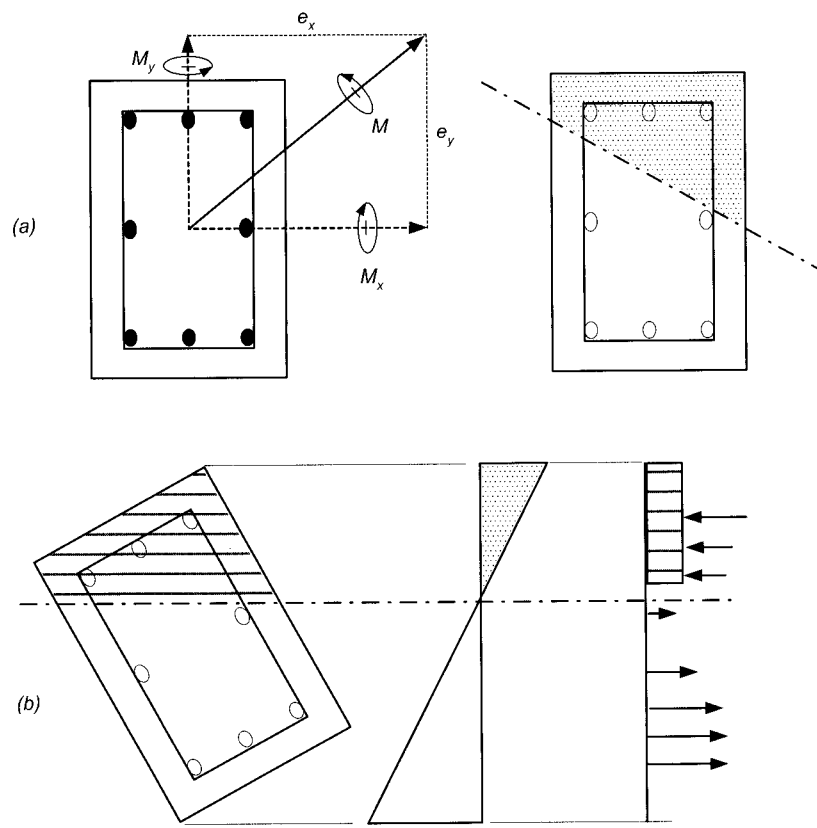

Figure 13.34 (a) Neutral axis under biaxial moment. (b) Assumed strain and stress diagrams at ultimate.

When biaxial bending exists, the load-moment interaction diagram can be derived for each of the two principal axes, x or y, or any axis in between which can be characterized by the ratio of moments (Fig. 13.34). In general, an interaction failure surface can be developed (Fig. 13.35). Such a surface can also be generated by a family of contour curves, each defining the geometric lieu of a characteristic point and corresponding to a constant value of P_n. Contour curves comprise the zero tension contour, balanced contour, pure flexure contour, and the like.

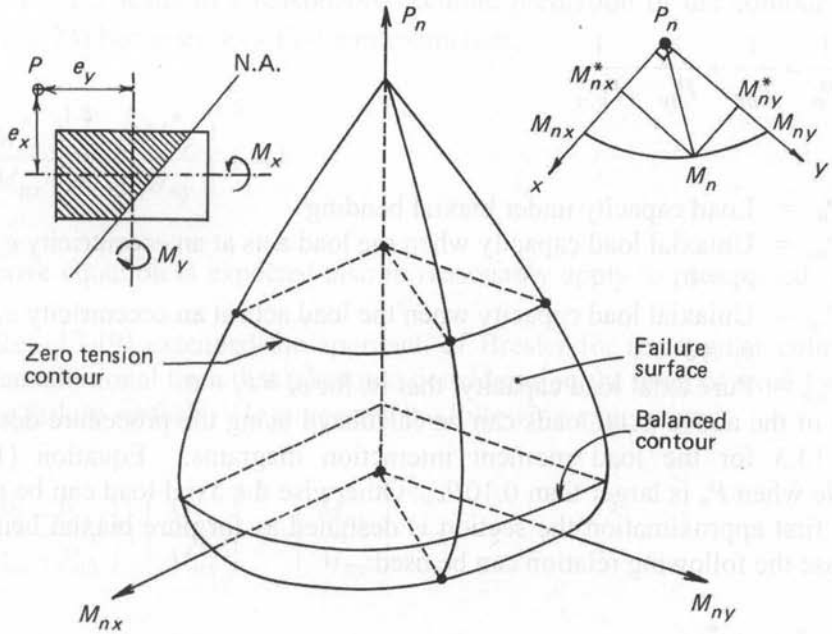

Figure 13.35 Biaxial load-moment interaction surface.

In an accurate analysis, the two main moment vectors can be summed up into a resulting vector moment and the section can be divided along its depth into thin layers (to fit any shape of the compression block), then analyzed to satisfy strain compatibility, equilibrium and stress-strain relations (Fig. 13.34*b*). The various layers of concrete can be assumed rectangular with an average stress of $0.85f'_c$ and their area should be multiplied by the factor β_1 [Ref. 13.35]. The eccentricity of the axial force will have components e_x and e_y along the y and x axis of the section, respectively. The neutral axis will be inclined with respect to the main axes of the column section. The procedure is best carried out using an iterative process implemented in a computer program. Generally, the maximum value of pure axial load resistance of the column is first easily determined; for each fraction of axial load (say every tenth), the contour curve can be obtained by exploring different

values of the ratio of eccentricities e_x / e_y (say ranging from 0.1 to 10). Another strategy is to select first a ratio of eccentricities (or equivalently a ratio of moments M_x /M_y) and then determine the set of maximum load resistance (that is the load-moment interaction diagram in the plane of the moment ratio) for that eccentricity ratio. Background information can be obtained from Refs. [13.17, 13.21, 13.30, 13.31].

Approximate procedures have been developed to estimate the resistance of a column subjected to biaxial bending. Bresler's method [Refs. 13.10. 13.11], called the reciprocal method, is summarized by the following equation:

$$\frac{1}{P_n} = \frac{1}{P_{nx}} + \frac{1}{P_{ny}} - \frac{1}{P_{n,o}} \tag{13.71}$$

where:

P_n = Load capacity under biaxial bending
P_{nx} = Uniaxial load capacity when the load acts at an eccentricity e_y and $e_x = 0$
P_{ny} = Uniaxial load capacity when the load acts at an eccentricity e_x and $e_y = 0$
$P_{n,o}$ = Pure axial load capacity, that is, for $e_x = e_y = 0$.

Each of the above axial loads can be calculated using the procedure described in Section 13.3 for the load moment interaction diagrams. Equation (13.71) is applicable when P_n is larger than $0.10P_{n,o}$. Otherwise the axial load can be neglected and as a first approximation the section is designed as for pure biaxial bending; in such a case the following relation can be used:

$$\frac{M_{nx}^*}{M_{nx}} + \frac{M_{ny}^*}{M_{ny}} \le 1 \tag{13.72}$$

where:

M_{nx} = Uniaxial moment capacity (or nominal moment) about the x axis
M_{ny} = Uniaxial moment capacity (or nominal moment) about the y axis
M_{nx}^* = Projection on the x axis of the biaxial moment strength
M_{ny}^* = Projection on the y axis of the biaxial moment strength

When the axial load is significant, Bresler also proposed a general nondimensional interaction relationship to approximate the contour curves of Fig. 13.35 [Ref. 13.10] at a given value of P_n. It has the following form:

$$\left(\frac{M_{nx}^*}{M_{nx}}\right)^{\alpha} + \left(\frac{M_{ny}^*}{M_{ny}}\right)^{\beta} = 1 \tag{13.73}$$

where M_{nx} and M_{ny} are the nominal *uniaxial* moment strengths in the directions of the x and y axes, and M_{nx}^{*} and M_{ny}^{*} are the nominal *biaxial* moment strengths in the x and y directions, respectively. The exponents α and β are functions of the dimensions of the column, the properties of the steel and concrete, and the amount, distribution, and location of the reinforcement. They can be adjusted to simulate the behavior of a particular type of column. Bresler indicates that it is reasonably accurate to assume $\alpha = \beta$ for reinforced concrete columns. He also suggests that, for mostly square and rectangular columns with uniformly distributed reinforcement, a value of $\alpha \simeq 1.5$ leads to a reasonably accurate prediction of the contour curves. Thus, Eq. (13.73) becomes, as a first approximation:

$$\left(\frac{M_{nx}^{*}}{M_{nx}}\right)^{1.5} + \left(\frac{M_{ny}^{*}}{M_{ny}}\right)^{1.5} = 1 \tag{13.74}$$

The above equation is expected also to reasonably apply to prestressed concrete columns.

Hsu [Ref. 13.19] extended the approach of Bresler for rectangular columns by including an additional term that takes into consideration the level of axial load, thus leading to a failure surface. He suggested the following expression:

$$\left(\frac{P_n - P_{nb}}{P_{no} - P_{nb}}\right) + \left(\frac{M_{nx}^{*}}{M_{nx}}\right)^{1.5} + \left(\frac{M_{ny}^{*}}{M_{ny}}\right)^{1.5} = 1 \tag{13.75}$$

where P_n is the nominal axial strength at a given eccentricity, $P_{n,o}$ is the nominal axial strength at zero eccentricity, and P_{nb} is the nominal axial strength at balanced conditions. Equation (13.75) applies to reinforced concrete short rectangular columns and allows the generation of a failure surface. Equations (13.74 and 13.75) can be used as a first approximation in design. An excellent review of the applications of these equations to reinforced concrete columns can be found in Hassoun [Ref. 13.17].

13.12 NEW DESIGN METHODOLOGY FOR SLENDER PRESTRESSED COLUMNS

The procedure described in this section was relatively new, at time of this writing, and has not been adopted by any code. It was developed by Shuraim and Naaman following an extensive investigation of slenderness effects in prestressed concrete columns [Refs. 13.49 to 13.51]. It offers a rational approach that is, in the author's

opinion, more suitable for prestressed concrete columns than other approximate procedures. Only the key elements of the procedure are summarized next without proof. The reader is referred to Ref. [13.51] for additional details.

The key feature of Shuraim and Naaman's approach is an estimate of the flexural rigidity *EI* to use for prestressed concrete columns at their ultimate capacity. This is achieved using: 1) the fundamental relationship between sectional moment and associated curvature, and 2) the tangent modulus of a slender column at onset of buckling under concentric axial compression assuming a nonlinear stress-strain curve of concrete. Curve 1 in Fig. 13.36 illustrates the effective flexural rigidity of a given slender column obtained from a finite element analysis. Curve 2 (bell shaped) and Curve 3 provide good approximations to Curve 1, each over a different range of eccentricities. However, they can each be obtained from a simpler analysis. They meet at a point defined as the peak point *B* of Curve 2. The coordinates of such a point are thus important for the analysis. To simulate the *EI* obtained from the finite element analysis, Curve 3 is used for eccentricities smaller than that of the peak (point B) and the descending branch of Curve 2 is used after the peak for larger eccentricities. Once the *EI* value is estimated, the design can proceed according to the ACI code as illustrated in the alternative of Fig. 13.25.

Because of limited space, the procedure is summarized in a flow chart where the main equations are given (Fig. 13.37). The stress-strain curve of concrete in compression was simulated using a parabola; the peak strain was taken from Eq. (2.21). Several examples can be found in Ref. [13.51]

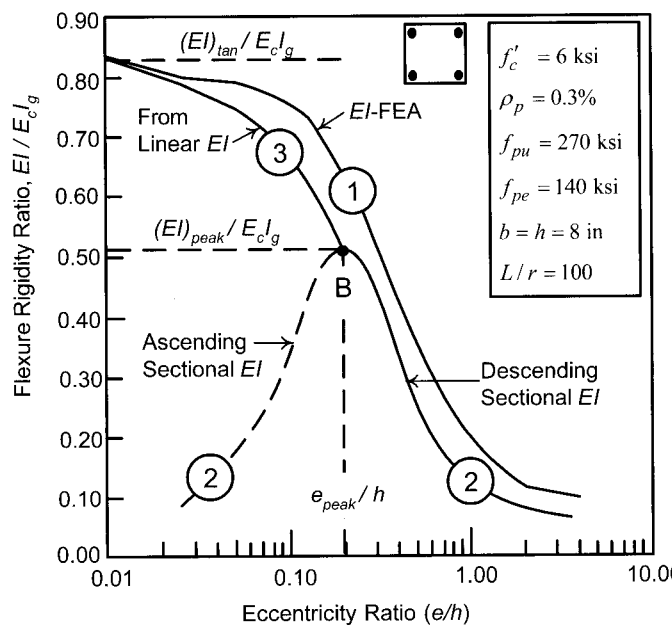

Figure 13.36 Flexural rigidity ratio versus eccentricity level.

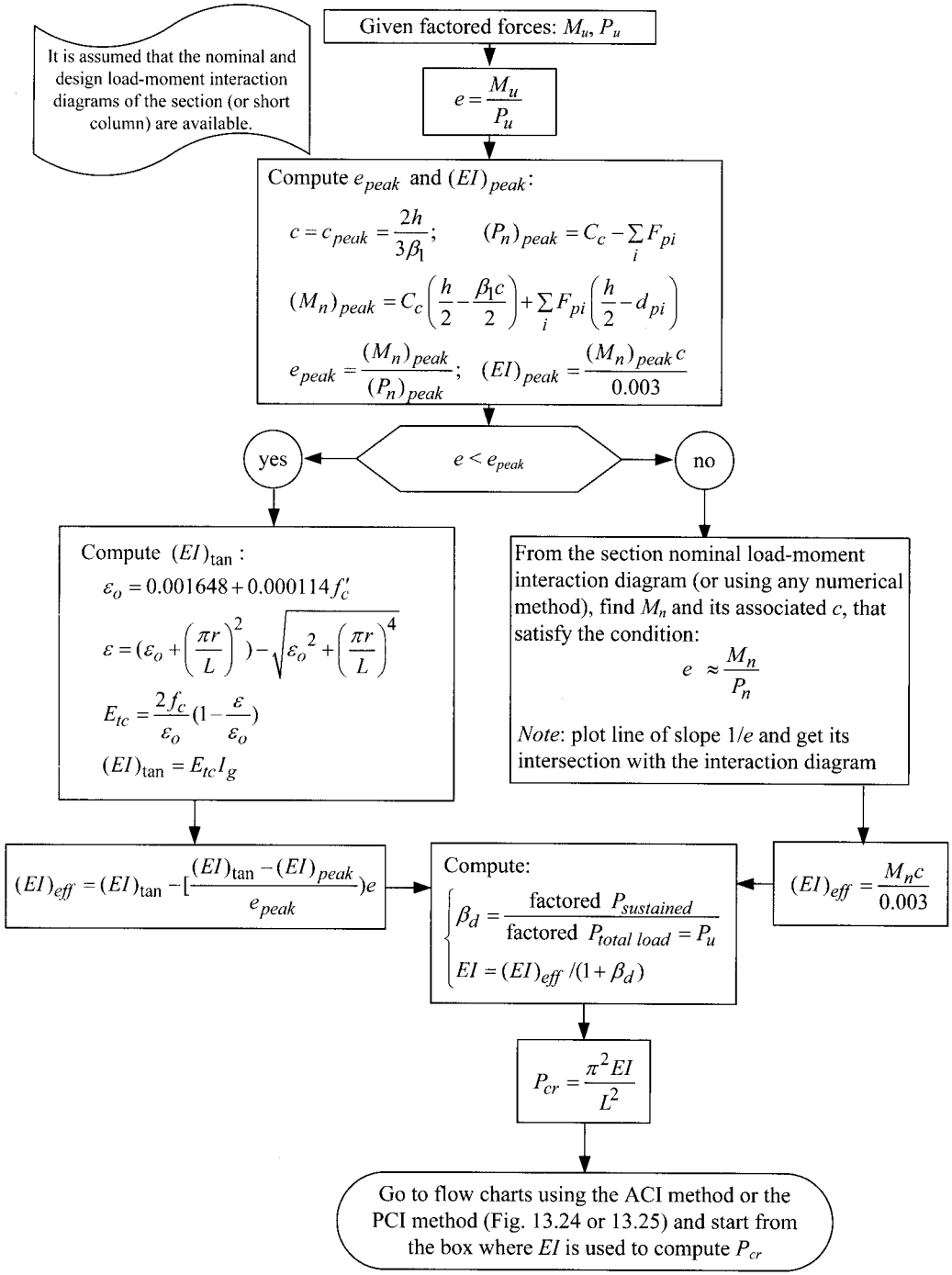

Figure 13.37 Flow chart to obtain the effective stiffness *EI* of prestressed concrete columns according to the procedure developed by Shuraim and Naaman.

Typical results obtained with this new procedure for the stiffness of a given column were compared with results obtained from the ACI code procedure, the PCI procedure, and the finite element analysis. Several observations were made: 1) the procedure proposed by Shuraim and Naaman simulates very well the results from the finite element analysis which is considered the reference; 2) both the ACI and PCI approaches underestimate the stiffness at low eccentricity ratios; 3) the ACI approach can be on the unsafe side at high eccentricity ratios while the PCI approach provides a much better prediction. These observations on the stiffness values also apply to the nominal load moment interaction diagrams of a slender column obtained from each of the above procedures. It should be pointed out that predictions by this new procedure were compared to 121 test results obtained from various experimental studies; differences were less than 5% for 33% of the data; less than 10% for 75% of the data; less than 15% for 93% of the data; and less than 20% for 97% of the data, respectively.

13.13 CONCLUDING REMARKS

The material discussed in this chapter covers most of the design of prestressed concrete columns encountered in common practice. However, as pointed out in the remarks at the end of Sections 13.8.7, a number of technical issues need further study and clarification. In particular, a great deal of research is still needed, at time of this writing, to understand more in-depth the behavior of slender prestressed concrete columns and walls. The main difficulty encountered is that experimental tests on slender full scale (or reasonably scaled) columns to ascertain their behavior for different variables and parameters, require large size testing equipment, are extremely costly, and are difficult to carry out because heavy loads are needed and buckling failure can be explosive. Extensive analytical work and modeling, including the use of non-linear material properties and large geometric deformations, are strongly recommended to make up for the limitations of the experimental work; they will provide a strong basis for modifying existing design guidelines or for developing new ones.

REFERENCES

13.1 ACI Committee 318, *Building Code Requirements for Reinforced Concrete (ACI-318)*, American Concrete Institute, Farmington Hills, MI, 1995.

13.2 ACI Committee 318, *Building Code Requirements for Reinforced Concrete (ACI 318-02) and Commentary (318R-02)*, American Concrete Institute, Farmington Hills, MI, 2002.

13.3 Ahmed, S. H., *Properties of Confined Concrete Subjected to Static and Dynamic Loading*, Ph.D. Thesis, Department of Materials Engineering, University of Illinois at Chicago, Chicago, IL, 1981, 342 pp.

13.4 Alcock, W. J., and N. D. Nathan, "Moment Magnification Tests of Prestressed Concrete Columns," *PCI Journal*, 22(4): 50-61, 1977.

13.5 Anderson, A. R., and S. E. Moustafa, "Ultimate Strength of Prestressed Concrete Piles and Columns," *ACI Journal*, 67(8): 620-35, 1970.

13.6 Aroni, S., "Slender Prestressed Concrete Columns," *Journal of the Structural Division,* ASCE, 94(ST4): 875-904, 1968.

13.7 Bolander, Jr., J., and A. E. Naaman, *Load-Moment Interaction Diagrams for Prestressed Concrete Columns and Poles*, Report No. UMCE 85-1, Department of Civil Engineering, University of Michigan, Ann Arbor, Feb. 1985, 91 pp.

13.8 Bolander, Jr., J., K. Sowlat, and A. E. Naaman, "Design Considerations for Tapered Prestressed Concrete Poles," *PCI Journal*, 33(1): 44-66, 1988.

13.9 Breen, J. E., J. G. MacGregor, and E. O. Pfrang, "Determination of Effective Length Factors for Slender Concrete Columns," *ACI Journal*, 69(11): 669-72, 1972.

13.10 Bresler, B., "Design Criteria for Reinforced Concrete Columns Under Axial Load and Biaxial Bending," *ACI Journal*, 57(November): 481-90, 1960.

13.11 Bresler, B., *Reinforced Concrete Engineering*, Vol. 1. New York: John Wiley, 1974.

13.12 Chajes, A., *Principles of Structural Stability Theory*. Englewood Cliffs, NJ: Prentice-Hall, Inc., 1974.

13.13 Chen, W. F., and T. Atsuta, *Theory of Beam-Columns*, Vol. 1. New York: McGraw-Hill, 1976.

13.14 Ferguson, F. M., J. E. Breen, and J. O. Jirsa, *Reinforced Concrete Fundamentals*, 5th ed. New York: John Wiley & Sons, 1988, 768 pp.

13.15 Gere, R. M., and S. P. Timoshenko, *Mechanics of Materials*, 3rd SI ed. United Kingdom, Chapman & Hall, 1991.

13.16 Gerwick, Jr., B. C., *Construction of Prestressed Concrete Structures*. New York: Wiley-Interscience, 1971, Chaps. 11 and 17. Also, 2nd ed., Wiley Professional Paperback Series, 1993, 591 pp.

13.17 Hassoun, M. N., *Structural Concrete Theory and Design*, 2nd ed. Upper Saddle River, NJ: Prentice Hall, 2002.

13.18 Hognestad, E., *A Study of Combined Bending and Axial Load in Reinforced Concrete Members*, University of Illinois Engineering Experiment Station, Bulletin Series No. 399, Bulletin No. 1, Urbana-Champaign, IL, 1951, 28 pp.

13.19 Hsu, C. T. T., "Analysis and Design of Square and Rectangular Columns by Equations of Failure Surface," *ACI Structural Journal*, March-April 1988, pp. 167-189.

13.20 Issa, M., and R. Yuan, "Prestressed Concrete Column Behavior," *PCI Journal*, 34(6): 51-67, 1989.

13.21 Kawakami, M., and A. Ghali, "Cracking, Ultimate Strength, and Deformations of Pressed Concrete Sections of General Shape," *PCI Journal*, 41(4): 114-22, 1996.

13.22 Lin, T. Y., and R. Itaya, "A Prestressed Concrete Column under Eccentric Loading," *PCI Journal*, 2(3): 5-17, 1957.

13.23 Lin, T. Y., and T. R. Lakhwara, "Ultimate Strength of Eccentrically Loaded Partially Prestressed Columns," *PCI Journal*, 11(3): 37-49, 1966.

13.24 Li, Shu-t'ien, and V. Ramakrishnan, "Optimum Prestress, Analysis and Ultimate Strength Design of Prestressed Concrete Sheet Piles," *PCI Journal*, 16(3): 60-74, 1971.

13.25 MacGregor, J. G., V. H. Oelhafen, and S. E. Hage, "A Reexamination of the EI Value for Slender Columns." In *Reinforced Concrete Columns*, SP-50, American Concrete Institute, Detroit, 1975, pp. 1-40.

13.26 MacGregor, J. G., and S. E. Hage, "Stability Analysis and Design of Concrete," *Journal of the Structural Division*, ASCE, 103(ST10): 1953-70, 1977.

13.27 MacGregor, J. G., "Design of Slender Concrete Columns," *ACI Structural Journal*, 90(3), 1993.

13.28 MacGregor, J. G., *Reinforced Concrete Mechanics and Design*, 3rd ed. Upper Saddle River, NJ: Prentice Hall, 1997, 939 pp.

13.29 Marin, J., "Computing Columns, Footings and Gates through Moments of Area," *Computers and Structures*, Pergamon Press, New York, 1984.

13.30 Marin, J., "Design Aids for L-shaped Reinforced Concrete in Columns," *ACI Journal*, 76(11): 1197-1216, 1979.

13.31 Martinez, S., A. H. Nilson, and F. O. Slate, "Spirally Reinforced High Strength Concrete Columns," *ACI Journal*, 81(5): 431-42, 1984.

13.32 Menegotto, M., and P. E. Pinto, *Method of Analysis for Cyclically Loaded R. C. Plane Frames*, IABSE Preliminary Report for Symposium on Resistance and Ultimate Deformability of Structures Acted on Well-Defined Repeated Loads, Lisbon, Spain, 1973, pp. 15-22.

13.33 Mirza, S. A., "Flexural Stiffness of Rectangular Reinforced Concrete Columns," *ACI Structural Journal,* 87(4): 425-35, 1990.

13.34 Naaman, A. E., "Partially Prestressed Concrete: Review and Recommendations," *PCI Journal*, 30(6): 30-71, 1985.

13.35 Naaman, A. E., "Rectangular Stress Block and T-Section Behavior," in Open Forum, *PCI Journal*, 47(5): 106-12, 2002. Also, closure in *PCI Journal*, Mar.-Apr. 2003.

13.36 Nathan, N. D., "Applicability of ACI Slenderness Computations to Prestressed Concrete Sections," *PCI Journal*, 20(3): May-Jun. 1975, pp. 68-85.

13.37 Nathan, N. D., "Slenderness of Prestressed Concrete Columns," *PCI Journal*, 28(2): 50-77, 1983.

13.38 Nathan, N. D., "Rational Analysis and Design of Prestressed Concrete Columns and Wall Panels," *PCI Journal*, 30(3): 82-133, 1985.

13.39 Nawy, E. G., *Prestressed Concrete: a Fundamental Approach*, 3rd ed. Upper Saddle River, NJ: Prentice Hall, 2000.

13.40 *PCI Design Handbook – Precast and Prestressed Concrete*, 5th ed., Precast/Prestressed Concrete Institute, Chicago, IL, 1999.

13.41 PCI Committee on Prestressed Concrete Columns, "Recommended Practice for the Design of Prestressed Concrete Columns and Walls, " *PCI Journal*, 33(4): 56-95, 1988.

13.42 PCI Committee on Prestressed Concrete Piling, "Recommended Practice for Design, Manufacture and Installation of Prestressed Concrete Piling," *PCI Journal,* 38(2): 14-41, 1993.

13.43 PCI Committee on Prestressed Concrete Poles, "Specification Guide for Prestressed Concrete Poles," *PCI Journal*, 44(2): 80-87, 1999.

13.44 Pessiki, S., and B. A. Graybeal, "Axial Load Tests of Concrete Compression Members with High Strength Spiral Reinforcement," *PCI Journal*, 45(2): 64-80, 2000.

13.45 Rice, P. F., and E. S. Hoffman, *Structural Design Guide to the ACI Building Code*, 2nd ed. New York: Van Nostrand-Reinhold Co., 1979.

13.46 Rigot, G., and M. T. Gaspart, "The Tower at Namur: The World's Tallest Precast, Prestressed Concrete Structure," *PCI Journal*, 44(3): 16-24, 1999.

13.47 Rosson, B. T., J. R. Rhodes, and R. Klovsky, "Behavior and Design of Static Cast Prestressed Concrete Distribution Poles," *PCI Journal*, 41(2): 94-106, 1996.

13.48 Rusch, H., "Research Toward a General Flexural Theory for Structural Concrete," *ACI Journal*, July 1960, pp. 1-25.

13.49 Shuraim, A. B., "Slenderness Effects in Prestressed Concrete Columns," Ph.D. Thesis, The University of Michigan, Ann Arbor, MI, 1990.

13.50 Shuraim, A. B., and A. E. Naaman, "Analysis of Slender Prestressed Concrete Columns," *ASCE Structures Congress '89*, volume on "Structural Analysis, Design and Testing," A. H-S Ang, Editor, San Francisco, CA, 1989, pp. 231-240.

13.51 Shuraim, A. B., and A. E. Naaman, "A New Methodology for the Ultimate Capacity of Slender Prestressed Concrete Columns, " *PCI Journal*, 48(1): 64-80, 2003.
13.52 Sowlat, K., and A. E. Naaman, "Design Aids for Hollow-Cored Prestressed Concrete Poles," Report No. UMCE 84-1, Department of Civil Engineering, The University of Michigan, Sept. 1984, 75 pp.
13.53 Timoshenko, S. P., and J. M. Gere, *Theory of Elastic Stability*, 2nd ed. New York: McGraw-Hill Book Co., 1961.
13.54 Wood, B. R., D. Beaulieu, and P. F. Adams, "Column Design by P-Delta Method," *Journal of the Structural Division*, ASCE, 102(ST2): 411-427, 1976.
13.55 Wood, B. R., D. Beaulieu, and P. F. Adams, "Further Aspects of Design by P-Delta Method," *Journal of the Structural Division*, ASCE, 102(ST3): 487-500, 1976.
13.56 Zia, P., and F. L. Moreadith, "Ultimate Load Capacity of Prestressed Concrete Columns," *ACI Journal*, 63(July): 767-86, 1966.
13.57 Zia, P., and E. C. Guillermo, "Combined Bending and Axial Load in Prestressed Concrete Columns," *PCI Journal*, 12(3): 52-59, 1967.
13.58 Zeng, J. M., L. Duan, F. M. Wang, and W. F. Chen, "Flexural Rigidity of Reinforced Concrete Columns," *ACI Structural Journal*, 89(2): 150-58, 1992.

PROBLEMS

13.1 Repeat the example of Sec. 13.4, assuming the prestressed steel used is not prestressed. That is $f_{pe} = 0$. Compare the load-moment interaction diagram obtained with that of Fig. 13.14. Plot the nominal load ϕP_n versus curvature ($\varphi = \varepsilon_{cu}/c$) for each case ($f_{pe} = 0$ and $f_{pe} = 150$ ksi) and at each of the main points of the interaction diagram. Draw conclusions on the effects of prestressing.

13.2 In a spirally reinforced column, the failure strain of the concrete is substantially higher than the value of 0.003 assumed by the ACI code. This is also the case when high performance fiber reinforced concrete is used. Repeat the example of Sec. 13.4, assuming the column is spirally reinforced (by square spirals) and $\varepsilon_{cu} = 0.006$. Everything else is kept the same.

13.3 Go back to the equations developed in Sec. 13.3 and point out the particular modifications needed to analyze columns of triangular cross section.

13.4 Go back to the example in Section 13.9.2, with Loading 1.
a) Redesign a modified cross section that would satisfy this loading condition.
b) Would the column be acceptable if braced against sway at its mid-height section?

13.5 You are considering the use of a prestressed concrete column-pile as a pier for an elevated guideway. You are given the following information: $P_D = 40$ kips, $P_L = 45$ kips; horizontal load at top of column due to vehicle braking $H_L = 2$ kips (considered live load). Assume that the column is fixed at its base and free at its upper end as shown in Fig. P13.4.

A column has been suggested by the local prestressed concrete manufacturer with the following properties: $f'_c = 6000$ psi, cross section 18×18 in, tied column; prestressing steel: 12 strands, 1/2 in-diameter, 270 ksi strength; $f_{pe} = 150$ ksi. Check the feasibility of the proposed column, that is: *(a)* Plot the nominal load-moment interaction diagram and the ACI design envelope, and show where factored loading combinations fit within that diagram assuming no buckling effect.
(b) If the slenderness of the column is considered, would it still be safe for use? Justify your answer. Show corresponding load combination points on the diagram. Make any reasonable assumption when needed.

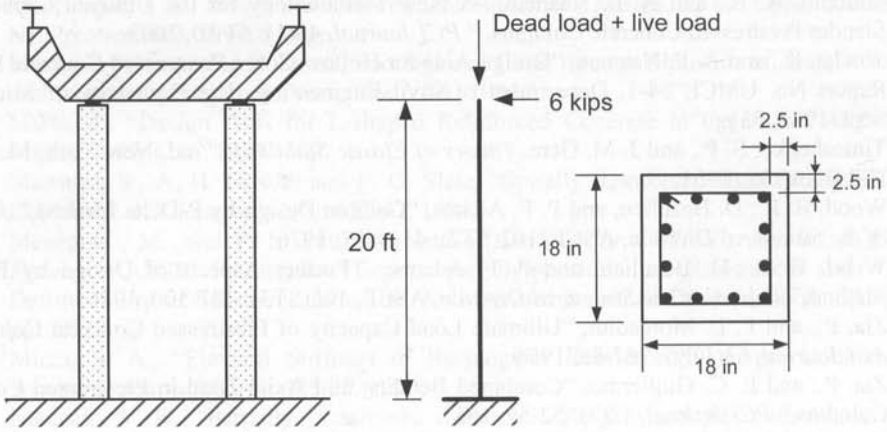

Figure P13.5

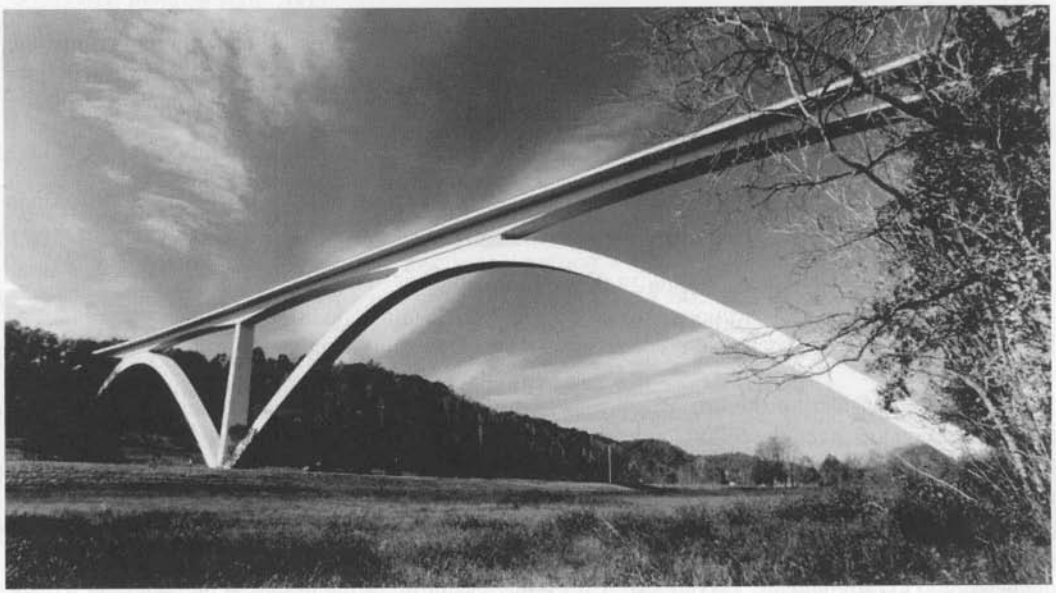

The Natchez Trace Parkway in Nashville, Tennessee, is America's first segmental arch bridge; its central arch spans 582 ft (174.6 m) and provides a vertical clearance of 137 ft (41.1 m). *(Courtesy Figg Engineering Group.)*

PRESTRESSED CONCRETE BRIDGES

14.1 SCOPE

Bridges are structures that perform at least one single but major function: that of providing a simple means to cross or reach between two points separated by a deep valley, a river, a highway, or the like. Bridges offer structural engineers the opportunity to express simultaneously functionality and beauty while being unique; they have generated a continuous fascination in people, regardless of place and time. This is so much so that, symbolically the term "bridge" is used to describe connectivity between nations, races, religions, communities, etc. and implies reaching out to the other as a sign of friendship and peace.

Bridges must be carefully planned and engineered before they can be constructed. Their final design must satisfy not only technical constraints related to strength, safety and provisions for future expansion, but also environmental, aesthetic, financial, and political constraints. A bridge is a key element in a transportation system for three reasons [Ref. 14.8]:

- It controls the capacity of the system
- It is the highest cost per mile of the system
- If it fails, the system fails.

Moreover the bridge controls both the volume and the weight of the traffic carried by the transportation system, in the present and the foreseeable future.

There are many advantages in using prestressed concrete for bridges. Among them are minimum maintenance, increased durability, good aesthetics, and, when factory precast elements are used, assured plant quality, fast and easy construction, and low initial cost.

In common structural applications, prestressed concrete usually complements reinforced concrete at moderate-span lengths and competes with structural steel at high-span lengths. However, for bridge decks and where factory precast products are available, prestressed concrete competes with reinforced concrete and steel throughout the span range. Hence, it has established a very strong presence in bridge applications in the US.

In spite of their common purpose, bridges are often unique, each characterized by particular site conditions and other factors that may dictate the type of design and construction solution selected. Such factors include the span length and size of the structure, types of loading, clearance, access, available technologies of construction or fabrication, site profile, importance of the bridge, cost, and even political constraints.

Most bridges are designed to carry vehicles and people for which they offer a flat riding or walking surface called the deck. In its simplest form, the deck of a bridge, as in the case of a one-way slab bridge, acts as a simple flexural element. Increased analytical difficulties arise depending on the design requirements, the type of construction, and the construction sequence. Examples include a continuous span versus a simple span or a series of simple spans, a statically indeterminate structure versus a statically determinate one, a skewed or a curved deck where torsion can be critical versus a straight deck, a variable-depth bridge versus a constant-depth bridge, a composite versus a noncomposite structure, and other form-related factors such as an arch bridge, a cable-stayed bridge or a suspension bridge. The type of construction may by itself bring additional constraints. For instance, factory precast elements often have to sustain transportation and erection stresses more severe than service stresses. In segmentally built bridges, each segment acts as a cantilever during construction and as part of the continuous deck during service. Hence, it may be subjected with time to large stress reversals. The selection of a final solution, using prestressed concrete, implies the evaluation of various design and construction alternatives in which solutions involving cast-in-place posttensioned structures are often compared to solutions involving factory precast pretensioned elements or site precast elements.

The design and construction of bridges is a specialty by itself. It involves not only the deck but also other essential elements, such as the piers, abutments, foundations, joints, connections, bearings, and the like. Building a bridge may take a long time and can be a unique experience. Each project generates particular problems and corresponding solutions that add to the sum of existing knowledge. A comprehensive approach to the design of bridges, even limited to prestressed concrete, cannot be covered without great length. In the following sections only essential aspects and peculiarities related to the design of bridge decks are addressed. They should provide sufficient background for the design of relatively small and simple bridges. However, a great deal of knowledge can be gained from the experience of others. The references given at the end of this chapter should be consulted for additional information [Refs. 14.1 to 14.52].

14.2 TYPES OF BRIDGES

Bridges can be classified in many ways, such as by type of structural material (steel versus concrete), shape (arch versus suspended bridge), continuity (simple versus multiple span) and the like. However, for this section, we will classify prestressed concrete bridges according to their span length, namely short, medium, and long spans; moreover, the range of spans is different for precast prestressed bridges versus cast-in-place posttensioned bridges.

- Precast pretensioned (Figs. 14.1 to 14.7)
  - Short spans: up to 50 ft (16 m)
  - Medium spans: 50 to 100 ft (16 to 33 m)
  - Long spans, include splicing: up to 180 ft (55 m)
- Posttensioned
  - Short spans, such as slab type decks: up to 60 ft (18 m)
  - Medium spans: up to 180 ft (55 m)
  - Long spans such as segmental or extrados: up to 500 ft (152 m)
  - Very long spans such as cable stay bridges: above 500 ft (152)

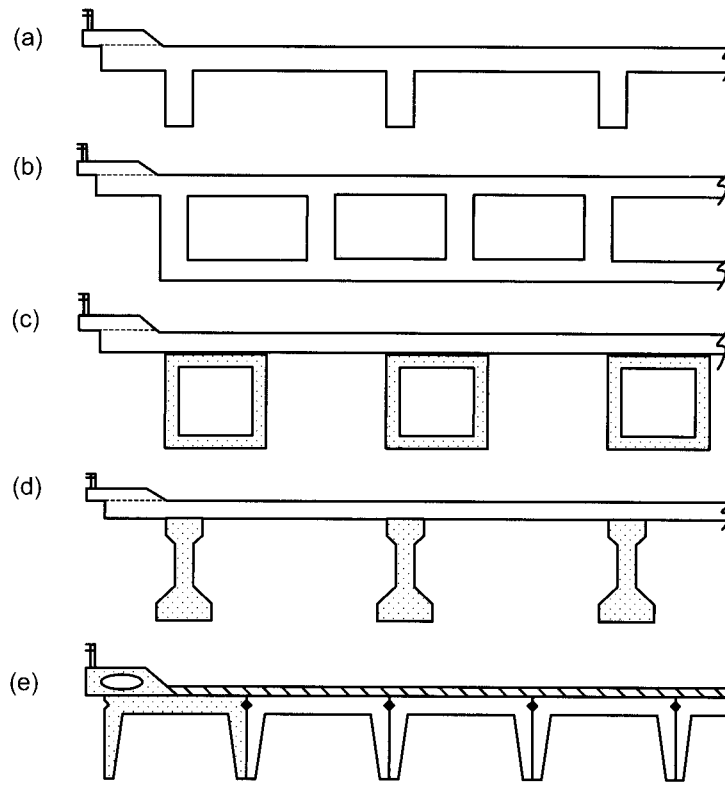

Figure 14.1 Typical cross-sections of bridge decks. ***(a)*** **T beams.** ***(b)*** **Box beams.** ***(c)*** **Spread box beams.** ***(d)*** **I beams.** ***(e)*** **Adjacent channel beams.**

Although span limits are given, a clear cut does not exist between the above categories as they generally overlap, and shifts in the ranges suggested may occur with future applications. Moreover, such classification is subjective and relative. For instance, a span considered long in a geographic location where technology is limited, may be considered medium in another location. Similarly, the maximum length for a factory precast element using land transportation may be substantially smaller than an on-site precast solution using floating equipment. The length range for long-span bridges post-tensioned on site can again be divided into long and very long spans that can exceed 1000 ft (300 m). Note also that the span length greatly influences the shape of the bridge deck selected as discussed in Section 14.3.

Typical bridge deck sections, either cast-in-place and posttensioned or using precast pretensioned elements are shown in Fig. 14.1.

14.2.1 Short-Span Bridges

In the United States short-span bridge decks are usually built with precast pretensioned beams that are transported to site and erected. A typical isometric view of this construction procedure is shown in Fig. 14.2 [Ref. 14.39]. The beams which have built in shear keys are generally placed adjacent to each other, as shown in Fig. 14.1*e*. The shear keys are then filled with a mortar grout to provide for lateral resistance and load transfer. A topping of bituminous concrete or equivalent, of about 2 to 3 in (5 to 7 cm) thickness, is generally added to provide a wearing surface and for the purpose of leveling. If a concrete topping is used, the deck will act as a composite deck as described in Chapter 9.

Typical cross sections of precast pretensioned elements used for common bridges and the corresponding ranges of dimensions and spans are shown in Fig. 14.3 [Ref. 14.45]. They include solid slabs for very short spans of less than about 25 ft (8 m), voided slabs, rib decks, channels, small double Ts (Tees), and tri Ts (Tees).

14.2.2 Medium- and Long-Span Bridges Using Precast Beams

The decks of medium-span bridges using precast pretensioned beams are generally built either in a manner similar to short-span bridges where the beams are placed adjacent to each other (Fig. 14.1*e*), or as composite decks where the beams are transversely spaced and a cast-in-place slab is added to provide for lateral continuity (Figs. 14.1*c* and *d*).

Typical cross sections and common span ranges are shown in Figs. 14.4 and 14.5. They include box beams, channels, single Ts, double Ts, and bulb Ts. Load tables and charts are available to help the designer achieve an acceptable design. A typical example for box beams taken from the PCI manual on short-span bridges [Refs. 14.39 and 14.36] is shown in Fig. 14.5.

Many of the sections shown in Figs. 14.4 to 14.6 can be used in combination with a cast-in-place slab to achieve composite action. An example described as the spread box-beam configuration is shown in Fig. 14.1*c*. However, the most common

composite bridge deck in the United States consists of precast prestressed I beams, such as those especially developed and standardized by AASHTO-PCI for highway bridges, working as composite beams with a structural cast-in-place concrete slab on top. The dimensions, sectional properties, and span range of typical bridges with standard AASHTO-PCI girders are shown in Fig. 14.6. Type I girder is shown for completeness. It is seldom used because, for its span range, it is not as cost effective as the noncomposite bridge sections described earlier for short-span bridges. Note that cast-in-place bridge beams of medium and not too long span lengths tend to have cross sections quite similar to the precast single T or the bulb T shown in Fig. 14.4.

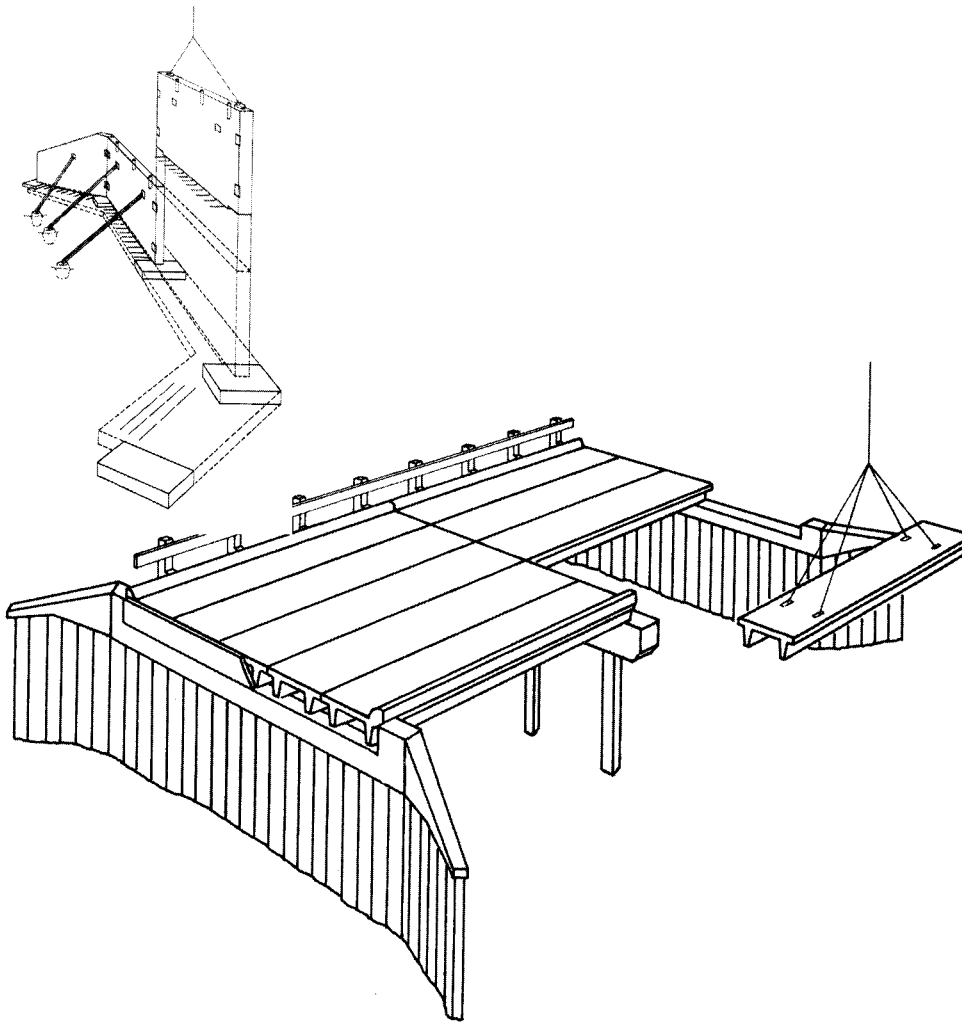

Figure 14.2 Isometric view of a bridge deck construction using precast prestressed elements. *(Ref. 14.39, Courtesy of the Precast/Prestressed Concrete Institute.)*

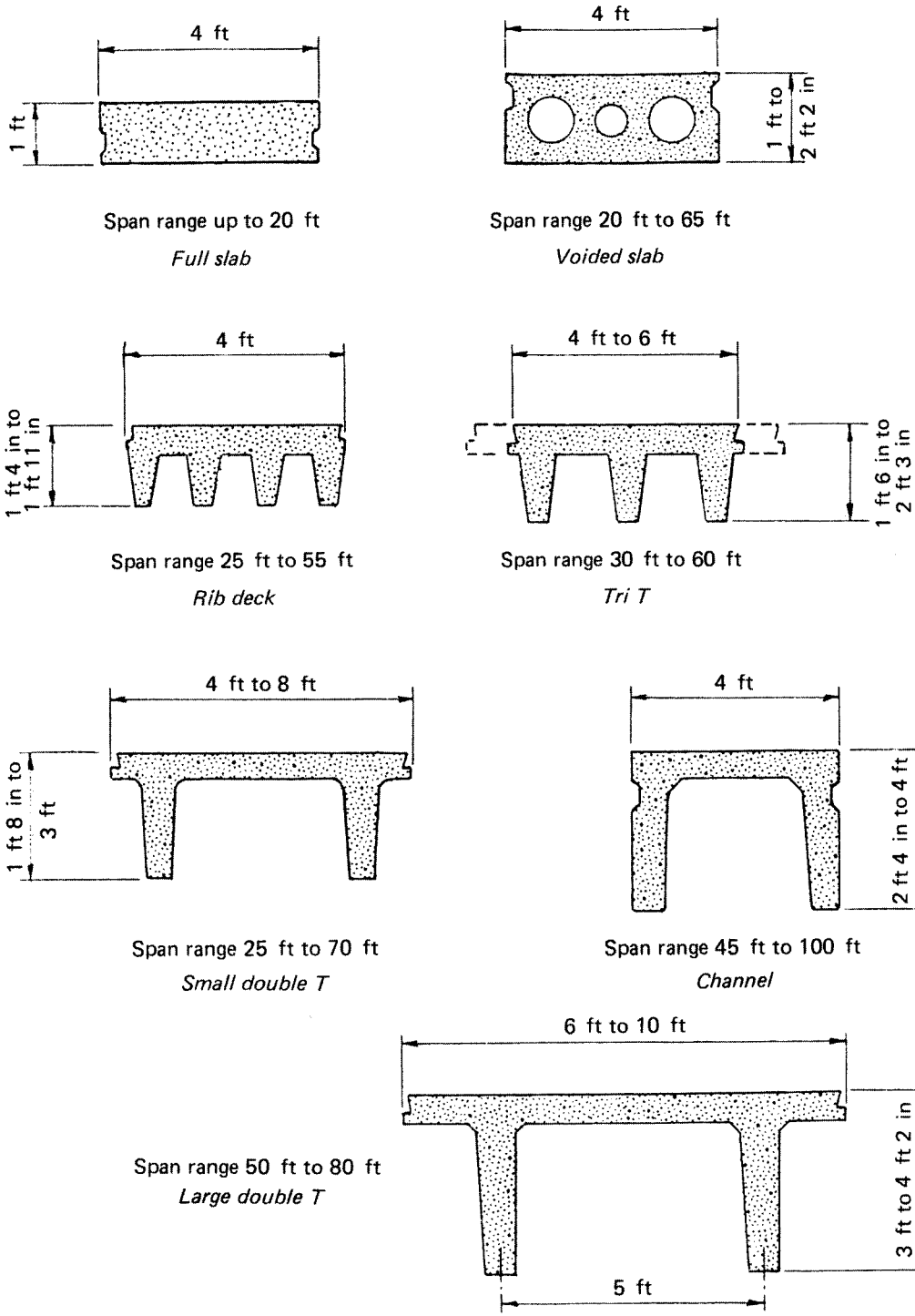

Figure 14.3 Typical precast sections for short- to medium-span bridges. *(Ref. 14.45, Courtesy of the Precast/Prestressed Concrete Institute.)*

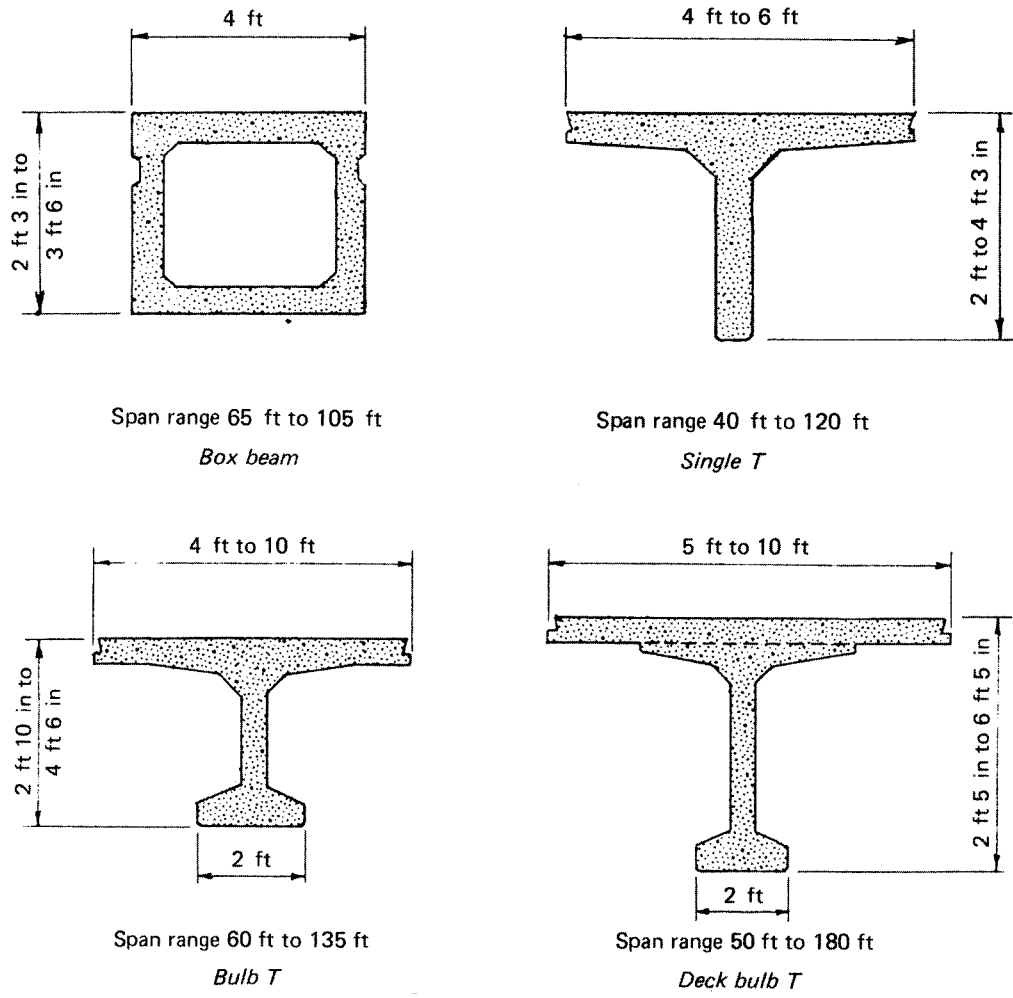

Figure 14.4 Typical precast sections for medium- to long-span bridges. *(Ref. 14.45, Courtesy of the Precast/Prestressed Concrete Institute.)*

The box beams shown are the former AASHO-PCI standard sections. They can be used either as adjacent units with or without an added wearing surface or spaced apart in which case the deck slab is cast-in-place. Box beams for railway loadings have been standardized by AREA.

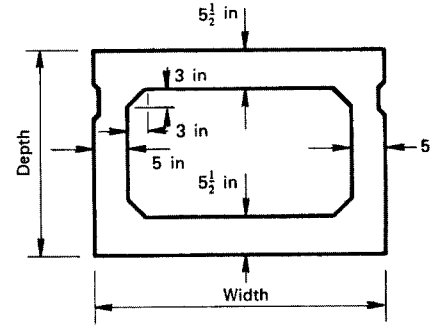

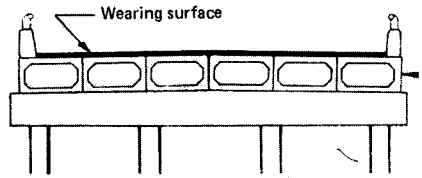

Typical section properties

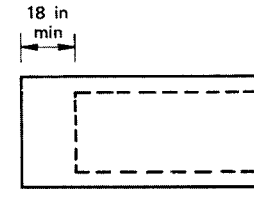

Typical longitudinal section

Type	Width, ft	Depth, in	Weight, lb/ft	Net area, in^2	I in^4	y_b, in	Z_b, in^3	Z_t, in^3
B I-36	3	27	584	561	50,334	13.35	3770	3687
B II-36	3	33	647	621	85,153	16.29	5227	5096
B III-36	3	39	709	681	131,145	19.25	6813	6640
B IV-36	3	42	740	711	158,644	20.73	7653	7459
B I-48	4	27	722	693	65,941	13.37	4932	4838
B II-48	4	33	784	753	110,499	16.33	6767	6629
B III-48	4	39	847	813	168,367	19.29	8728	8542
B IV-48	4	42	878	843	203,088	20.78	9773	9571

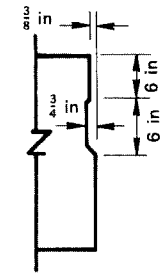

Typical keyway detail

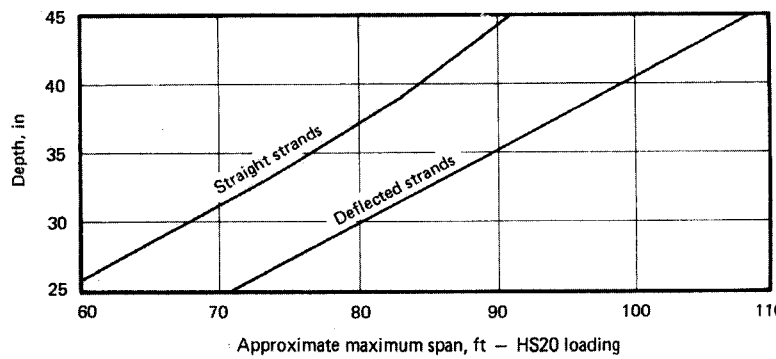

Figure 14.5 Typical precast box beams for bridges. *(Ref. 14.39, Courtesy of the Precast/Prestressed Concrete Institute.)*

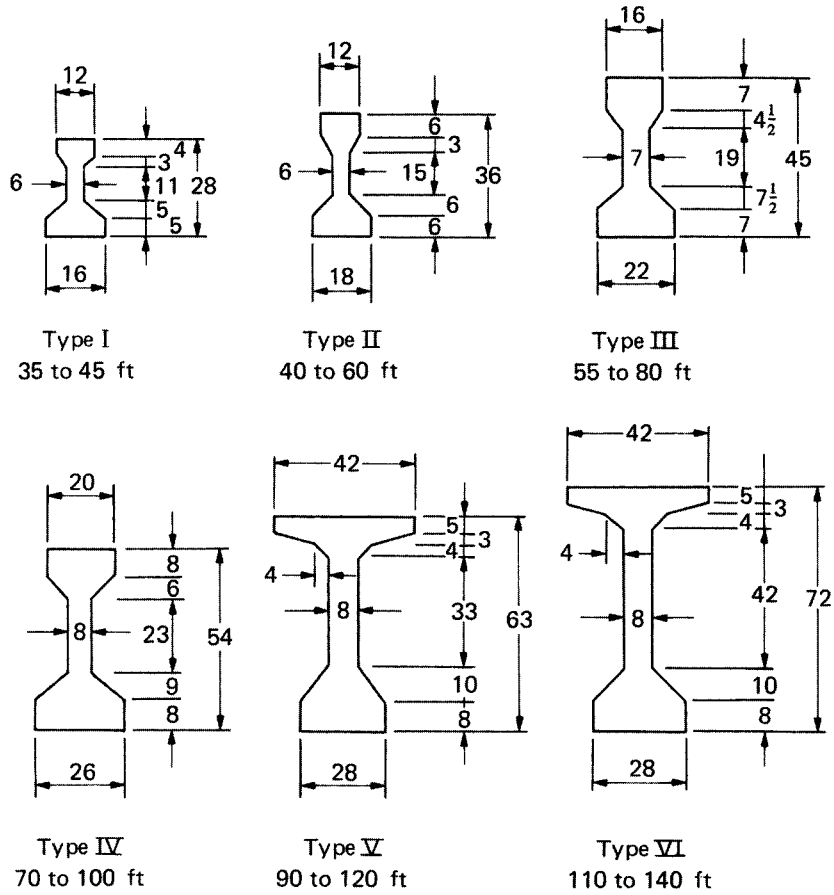

Type	h, in	A_c, in^2	I_c, in^4	y_t, in	y_b, in	Z_t, in^3	Z_b, in^3	w_G, plf
I	28	276	22,750	15.41	12.59	1,476	1,807	288
II	36	369	50,980	20.17	15.83	2,528	3,220	384
III	45	560	125,390	24.73	20.27	5,070	6,186	583
IV	54	789	260,730	29.27	24.73	8,908	10,543	822
V	63	1,013	521,180	31.04	31.96	16,790	16,307	1,055
VI	72	1,085	733,320	35.62	36.38	20,587	20,157	1,130

Figure 14.6 Standard AASHTO-PCI bridge I beams: section properties and span range. *(Courtesy of the Precast/Prestressed Concrete Institute.)*

There are many ways to increase the effective span range of a precast prestressed beam when its capacity is attained or when transportation and erection constraints prevail. Typical solutions include changing support location such as shown in Fig. 14.7*a* [Ref. 14.19], and splicing (Fig. 14.7*b*) where two or three segments of beams are precast and assembled on site by posttensioning.

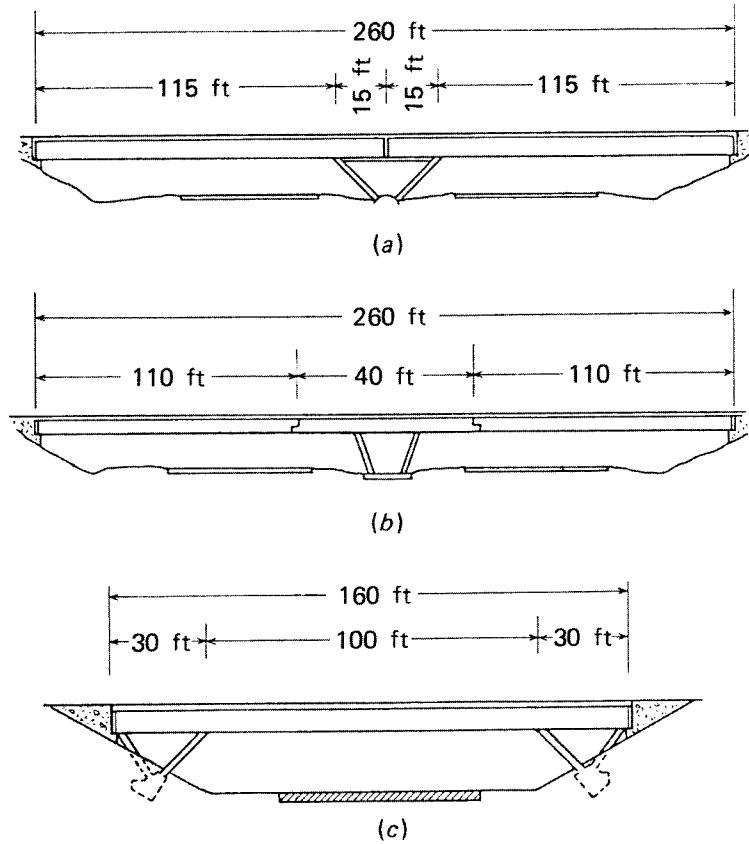

Figure 14.7a Typical effective span-shortening systems. *(Ref. 14.19, Courtesy of the Precast/ Prestressed Concrete Institute.)*

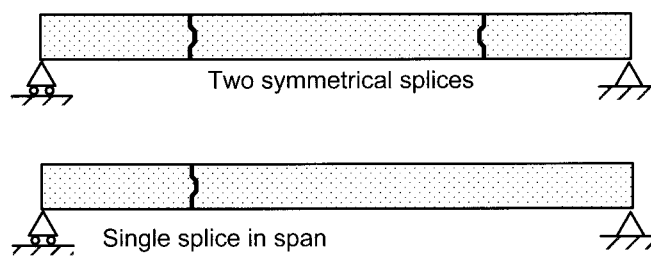

Figure 14.7b Typical splicing to increase span length using precast elements.

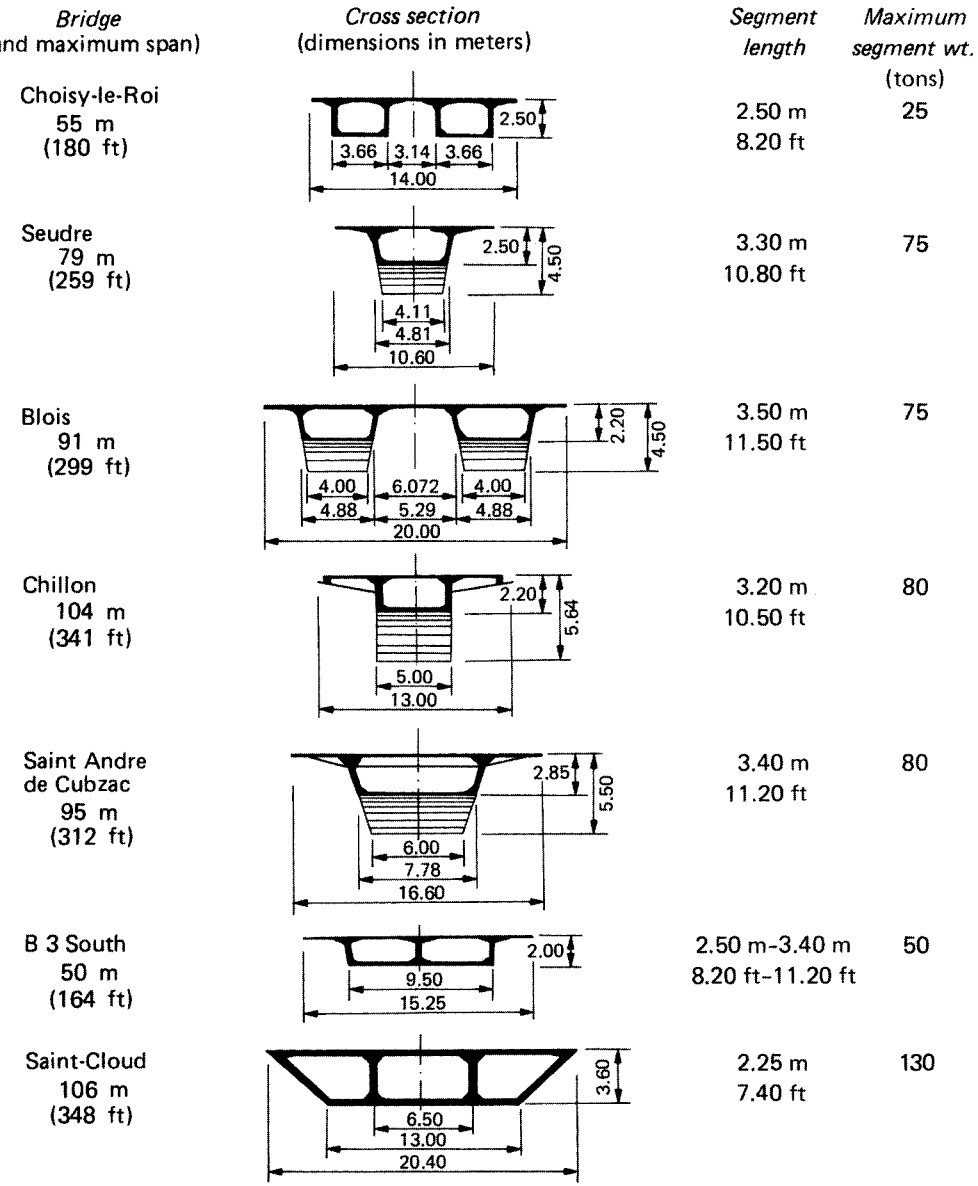

Fig. 14.8 Evolution of typical sections for segmental bridges in France. *(Ref. 14.27, Courtesy of the Precast/Prestressed Concrete Institute.)*

14.2.3 Long- and Very Long-Span Bridges

Long-span prestressed concrete bridges are generally cast-in-place or site precast and posttensioned. Although length is relative, spans above 180 ft (55 m) are considered long. Very long spans are spans above about 500 ft (152 m). Long span bridges are often built by a segmental construction technique. In segmental construction the deck is built by segments, one at a time. Segments can be precast or cast-in-place. Box beams are considered best suited for this type of construction. They offer superior torsional rigidity and stability during construction and in service. Their inside opening offers a platform for work and communication during construction and thereafter. Typical cross sections and their evolution are shown in Fig. 14.8 where actual dimensions are also given for several segmental bridges built in France [Ref. 14.27]. It is observed that, for spans above about 200 ft (60 m), sections tend to have a variable depth.

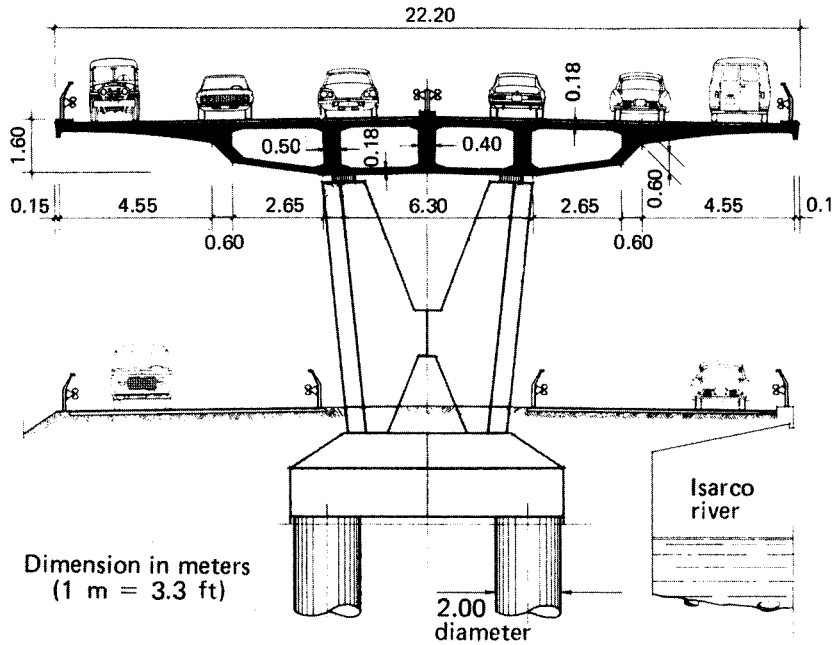

Fig. 14.9 Typical cross section of an elevated motorway. *(Ref. 14.14, Courtesy of the Precast/Prestressed Concrete Institute.)*

A bridge deck width of about 35 ft (10.67 m) can be achieved with a single box, while several individual boxes or a box with several webs or openings can be used for larger widths. An example is shown in Fig. 14.9 for a motorway built in Bolzano, Italy, in which the shape of the cross section has been smoothed for aesthetic purposes [Ref. 14.14].

Two typical examples of segmentally built bridges are shown in Figs. 14.10 and 14.11.

Figure 14.10 Sagadahoc Bridge, Maine: precast prestressed concrete segmental bridge build by the balanced cantilever method with a main span of 128 m (420 ft). *(Courtesy Figg Engineering Group, Florida.)*

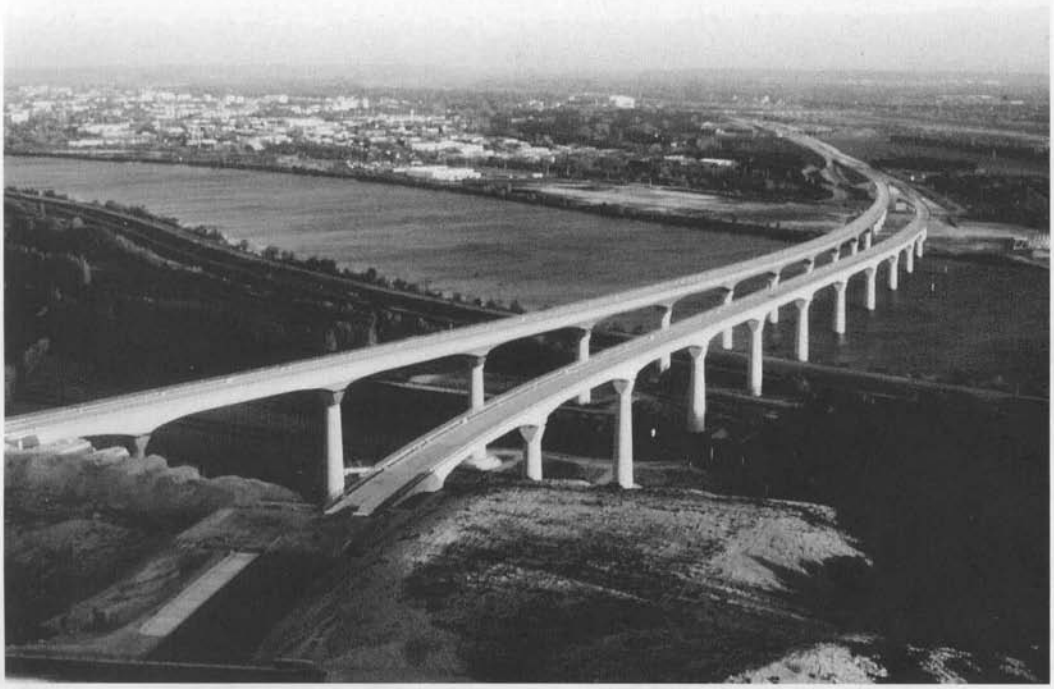

Fig. 14.11 The segmentally constructed Avignon Viaduct in France. *(Courtesy Bouygues Construction, Paris, France.)*

Because the depth of the deck structure tends to increase substantially for very long spans, a cable-stayed solution can be considered as an alternative to segmental cantilever construction. In such a solution the prestressed concrete deck ribbon, generally of constant depth, is suspended from sloping stay cables emanating from a high tower. The sloping cables are stiff and dissipate all anchorage forces in the deck girder, which results in a beneficial longitudinal compressive force in the deck. An example is the Pasco-Kennewick Intercity Bridge, that was completed in 1978 (Figs. 14.12 and Ref. 14.16). It has a main span of 981 ft (299 m) and a total length of 2503 ft (763 m). Each of the precast deck segments is 80 ft (24.4 m) wide, 27 ft (8.2 m) long, 7 ft (2.1 m) deep, and weighs 300 tons. Three other examples of cable stayed bridges with spans either smaller and longer than the Pasco-Kennewick bridge are shown in Figs. 14.13 to 14.15; they illustrate the flexibility of the cable-stay technique and the beautiful bridges it allows.

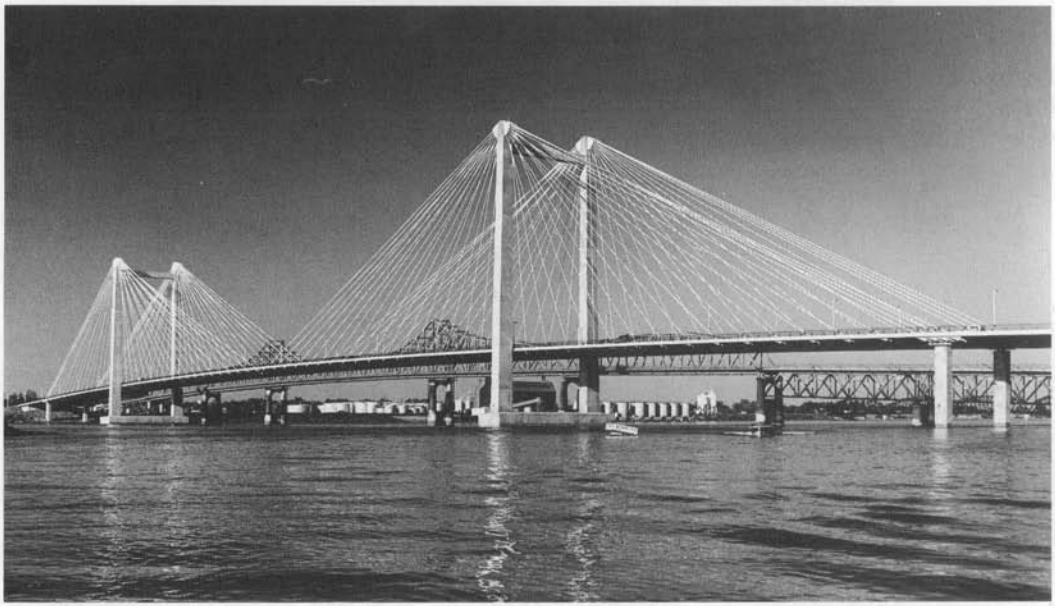

Fig. 14.12 The Pasco-Kennewick cable-stayed bridge in Washington state, U.S.A. *(Ref. 14.16, Courtesy Arvid Grant & Associates, Consulting Engineers.)*

Another bridge that pushes even farther the limits of prestressed concrete was planned (but not built) in California and deserves mention. It is the Ruck-A-Chucky Bridge, designed by T.Y. Lin International/Hanson Engineers. It has a main curved span of 1300 ft (396 m) and is suspended by cables from the walls of the canyon it crosses (Fig. 14.16 and Ref. 14.40).

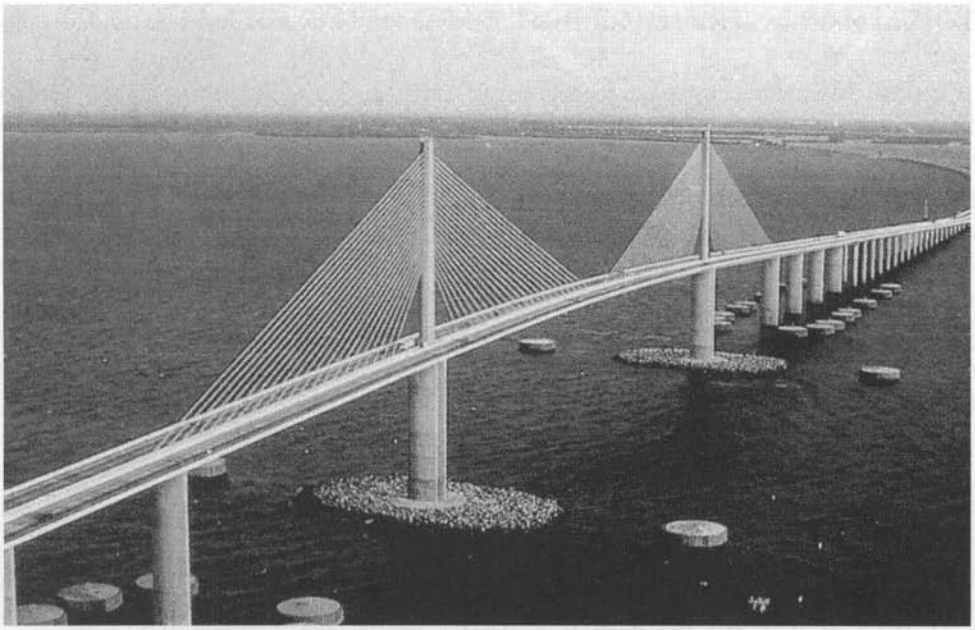

Figure 14.13 Sunshine Skyway Bridge, Florida: first precast prestressed concrete segmental cable-stayed bridge in the US, with a main span of 366 m (1200 ft). *(Courtesy Figg Engineering Group, Florida.)*

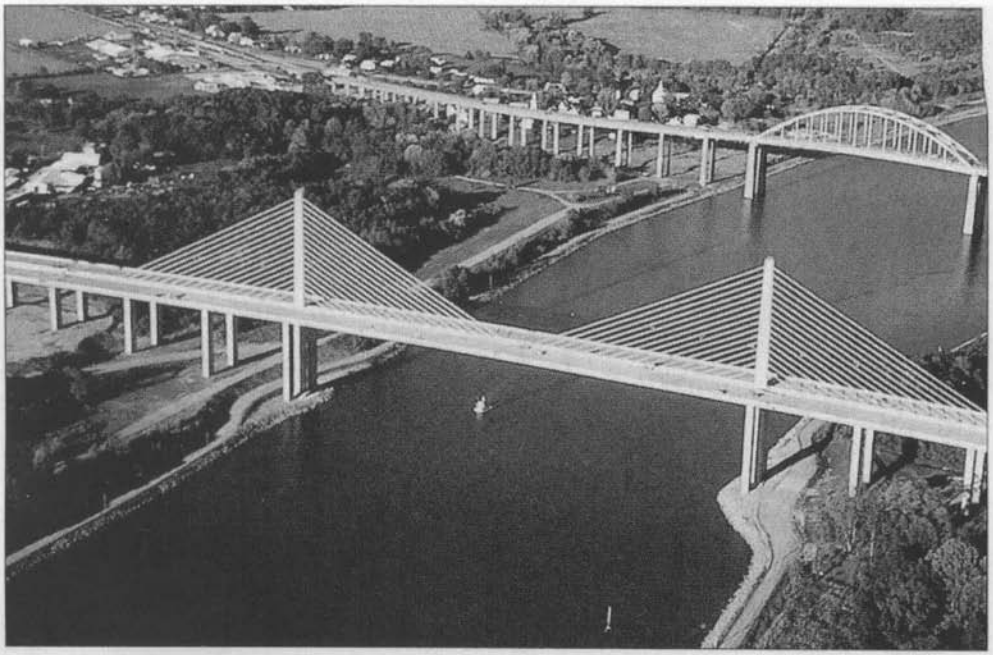

Figure 14.14 Chesapeake and Delaware Canal Bridge, Delaware: all precast prestressed concrete segmental cable-stayed bridge with a main span of 229 m (750 ft). *(Courtesy Figg Engineering Group, Florida.)*

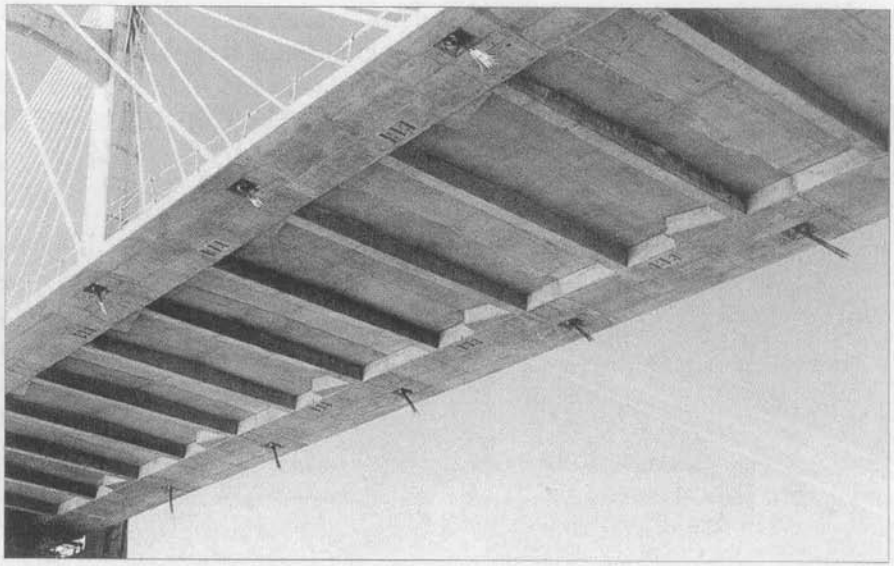

Figure 14.15 Rhone River Bridge, France: cable-stayed construction with a main span of 192.3 m (576 ft); the deck is a slender prestressed concrete slab with longitudinal and transverse ribs. *(Courtesy SETRA, Bagneux, and Michel Virlogeux, France.)*

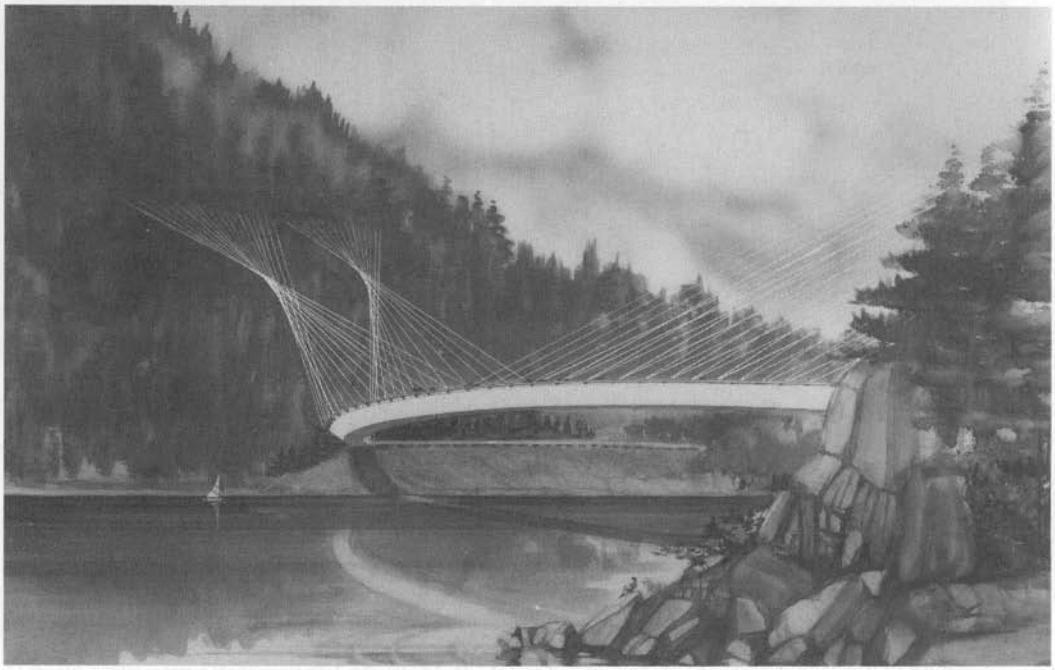

Fig. 14.16 Conceptual design of the Ruck-A-Chucky Bridge in California, U.S.A. *(Ref. 14.40, Courtesy of T.Y. Lin International/Hanson Engineers.)*

14.3 RATIONAL EVOLUTION OF BRIDGE FORM WITH SPAN LENGTH

It is interesting to review the evolution of bridge deck form in terms of bridge span. All bridges must provide a deck for pedestrian and/or vehicular traffic. For short spans, a reinforced concrete slab is the most intuitive and convenient. In reinforced concrete, the concrete works in compression and the steel in tension. The concrete in the tensile zone is assumed cracked and thus does not contribute to the resistance. With an increase in span, there is need to decrease the weight of the slab. This can be done by removing from the section the concrete portion that is not effective in resisting the load. Alternatives are to either remove concrete from the bottom of the slab (tensile zone) or from the middle of the slab, leading to two types of basic shapes, a Tee shape and a box shape. Figure 14.17 illustrates the evolution of these two shapes in bridge design. It can be observed that a Tee section (generally without lower flange, but at the limit with a bulb-like lower flange) can be used for simple spans up to about 60 meters (180 ft). On the other hand, box-like sections can be used for spans up to 115 meters (350 ft) with variable depth. Box type bridge decks can also be used in longer spans when used in conjunction with arches or cable stays. From an analysis/design viewpoint the evolution of sections in Fig. 14.17 also follows rational thinking:

1. Given a uniform load, such as the dead load, the bending moment varies in function of the square of the span, while the shear varies in direct proportion to the span. Hence, the moments in long-span bridges can be very large and necessitate the use of a large size top flange to resist compressive stresses. As the shear does not increase at the same rate as the moment, a webbed type section, such as in a T or box section, becomes desirable for long-span bridges. This also has the advantage of reducing the weight and the dead load moment.
2. The ratio of live load shear to dead load shear in short-span bridges is relatively large. Hence, a relatively large shear area is needed. This suggests that a slab or a hollow-cored slab is preferable for short-span bridges.

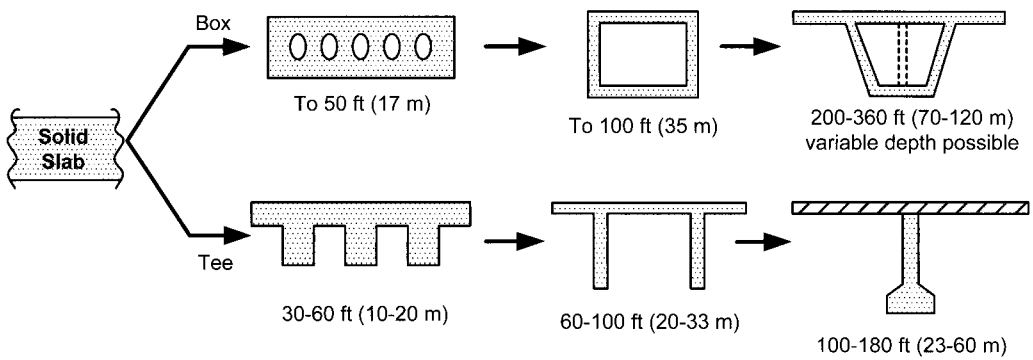

Figure 14.17 Form evolution in beams of bridge decks.

While rectangular slabs, Ts and box sections are simple structural forms for bridge deck construction, bridge evolution has generated other interesting forms, including arch bridges, stress-ribbon bridges, cable-stayed bridges and suspension bridges (Fig. 14.18). Such bridges have generally longer spans. Arch bridges imply a deck supported by an arch working in compression. The deck may be above or below the arch. An inverted arch, also described as stress ribbon or inverted suspension bridge, works in tension. While in a suspension bridge the cables are made primarily out of steel cables (or advanced fiber reinforced polymeric cables), a stress ribbon is made out of a prestressed concrete tensile member. Compression elements transfer the load from the deck to the stress ribbon. In suspension bridges the vertical cables provide the lifting forces for the deck. In a cable stayed bridge, the cables are tied to the deck offering a vertical (lifting) reaction and a horizontal reaction that provides beneficial compression to the deck. Very slender decks can thus be constructed. In bridges described as extrados the cable stays are relatively less high providing a larger proportion of the prestressing in the horizontal direction; they are part of the longitudinal prestressing.

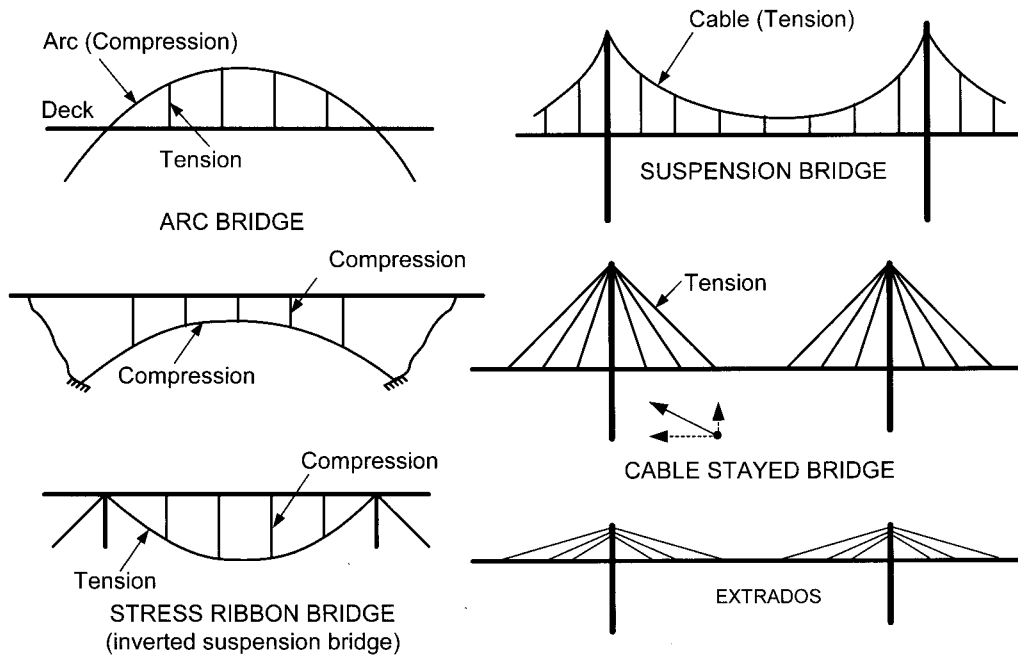

Figure 14.18 Typical structural forms for long span bridges.

Typically concrete arch bridges and cast-in-place cantilever segmental bridge decks could span up to about 300 m (1000 ft), while concrete cable-stayed bridges could span up to about 450 m (1500 ft). Longer spans call for lighter steel decks and steel suspension bridges. For instance the Normandie Bridge in France is a cable stayed bridge with a span of 870 meters, while the longest bridge in the world at time

of this writing is the Akashi Kaikyo suspension bridge in Japan with a span of 1991 meters.

14.4 SPECIAL CONSTRUCTION TECHNIQUES FOR BRIDGES

A large number of imaginative solutions have been developed for the design and construction of bridges. As described earlier, some were aimed at the use of factory precast elements in short- and medium-span bridges. Other solutions, such as for cable-stayed bridges, were derived for long-span bridges and geared at achieving the highest spans at least cost. In some instances, solutions offering a new alternative in bridge design and construction, as applied to prestressed concrete, were generated.

Some innovative construction techniques and corresponding examples of applications are described next, starting with segmental construction. A great deal can be learned from reviewing the related references. In particular, the *Journal of Structural Engineering* published by IABSE, and the *PCI Journal* regularly publish a wealth of information on bridge construction and design around the world.

14.4.1 Segmental Construction

As the name suggests, segmental construction implies building a bridge by assembling short length segments of it into the final longer span. It is a very common and attractive construction method. One of four erection techniques is generally used for constructing segmental bridges (Fig. 14.19): the balanced cantilever method using a launching girder, the balanced cantilever method using traveling forms, the span-by-span method, and the progressive placement in one direction method [Refs. 14.27,14.33 and 14.34].

In the balanced cantilever method using a launching girder (Fig. 14.19*a*), an overhead truss or launching girder riding above the superstructure places the segments alternating from one cantilever to the other to balance the loads.

In the balanced cantilever method with traveling forms (Fig. 14.19*b*), traveling forms at the tips of the cantilevers move in opposite directions at the same rate to cast new segments, thereby maintaining balance and stability until midspan is reached. Then a closure is made with a previous half-span cantilever from the preceding pier. To account for possible imbalance, a moment-resisting pier or temporary clamps between the deck and the pier are provided.

The span-by-span segmental construction method (Fig. 14.19*c*) is used mostly for long viaduct structures when crossing over water. The technique was initially developed by the German firm of Dyckerhoff and Widmann and features the execution of a superstructure in one direction, span by span. Generally, a barge crane places the segments on a truss spanning between piers. The segments are placed progressively from one end to the other in span increments, then posttensioning tendons are installed and stressed.

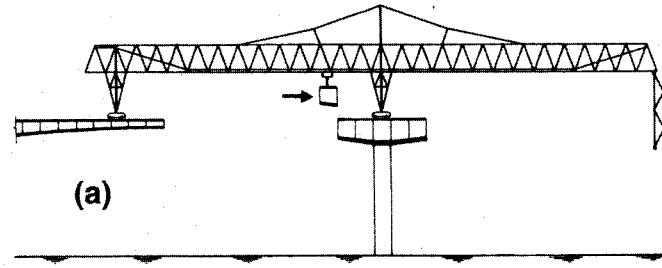

Balanced Cantilever Using Launching Girder. *An overhead truss or "launching girder," riding above the superstructure, places segments — alternating from one cantilever to the other — to balance loads.*

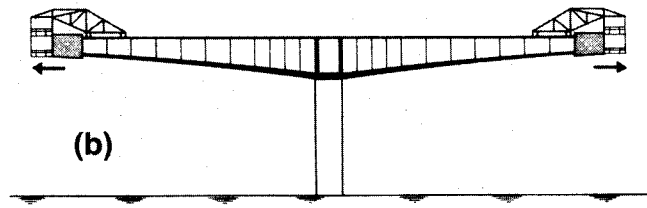

Balanced Cantilever with Travelling Forms. *Travelling forms at the tips of the cantilevers move in opposite directions at the same rate to cast new segments, thereby maintaining balance and stability.*

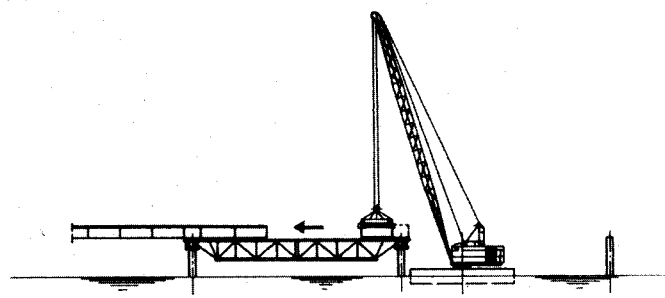

Span-by-Span Method. *A barge crane places segments on a truss spanning between piers, then post-tensioning is installed and stressed.*

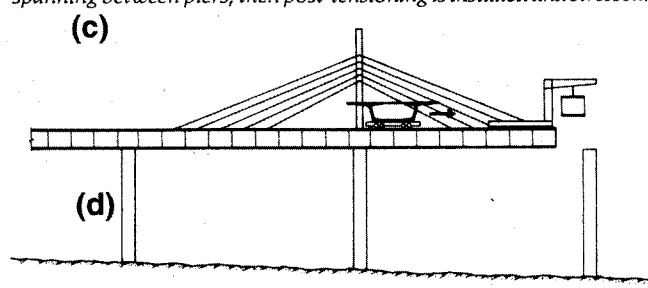

Progressive Placement in One Direction. *Segments are transported out to the tip of the cantilever where a crane places them in position. As the cantilever grows, additional temporary cables are installed for stability.*

Figure 14.19 Representative erection techniques for segmental construction. *(Courtesy of Figg and Muller, Engineers Inc., Florida.)*

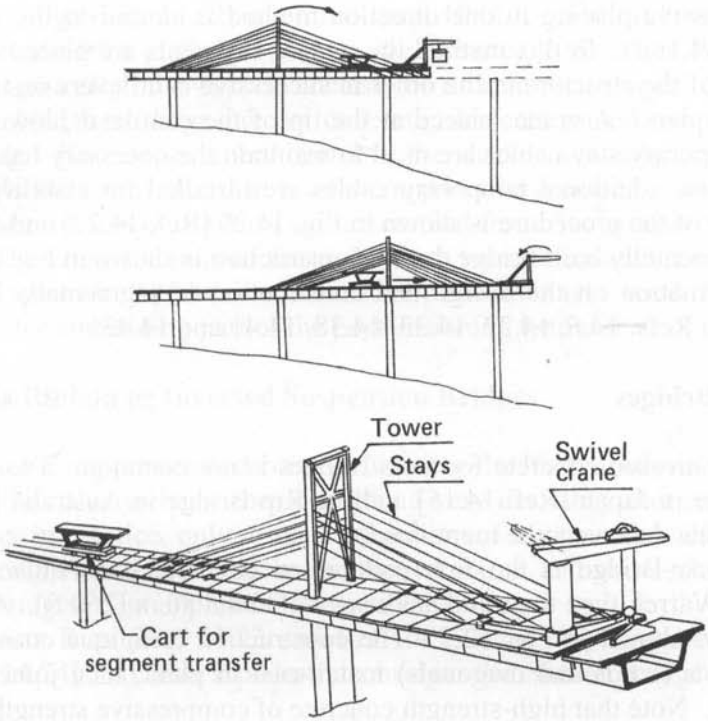

Figure 14.20 Isometric view of the progressive placing technique. *(Ref. 14.27, Courtesy of the Precast/Prestressed Concrete Institute.)*

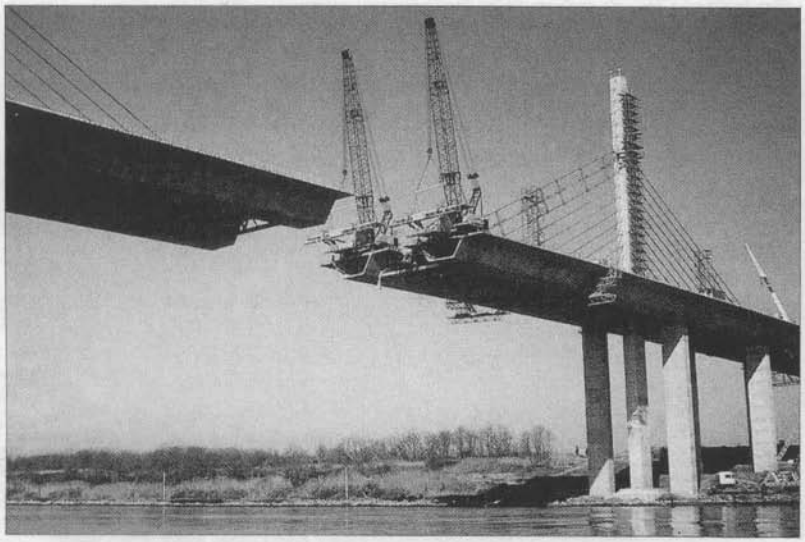

Figure 14.21 Chesapeake and Delaware Canal Bridge, Delaware: all precast prestressed concrete segmental cable-stayed bridge with a main span of 229 m (750 ft). *(Courtesy Figg Engineering Group, Florida.)*

The progressive placing in one direction method is similar to the span-by-span method (Fig. 14.16*d*). In this method the precast segments are placed continuously from one end of the structure to the other in successive cantilevers on the same side of the various piers. A crane, placed at the tip of the cantilever, lowers them into position. Temporary stay cables are used to maintain the necessary balance. As the cantilever grows, additional temporary cables are installed for stability. A typical isometric view of the procedure is shown in Fig. 14.20 [Ref. 14.27] and a photograph showing a segmentally built bridge during construction is shown in Fig. 14.21.

More information on the design and construction of segmentally built bridges can be found in Refs. 14.6, 14.22, 14.33, 14.38, 14.41 and 14.43.

14.4.2 Truss Bridges

The use of prestressed concrete for truss bridges is not common. Two bridges, the Iwahana Bridge in Japan [Ref. 14.15] and the Rip Bridge in Australia [Ref. 14.48], are examples that deserve to be mentioned.

The Iwahana Bridge is the first prestressed concrete truss railway bridge in Japan. It is a Warren-type truss and has a span of about 80 m (260 ft). A photograph of the bridge is shown in Fig. 12.2. The construction technique consists of using precast elements (cords and diagonals) match-cast in plant, then joined on site by posttensioning. Note that high-strength concrete of compressive strength of about 12 ksi (83 MPa) was used for the precast elements.

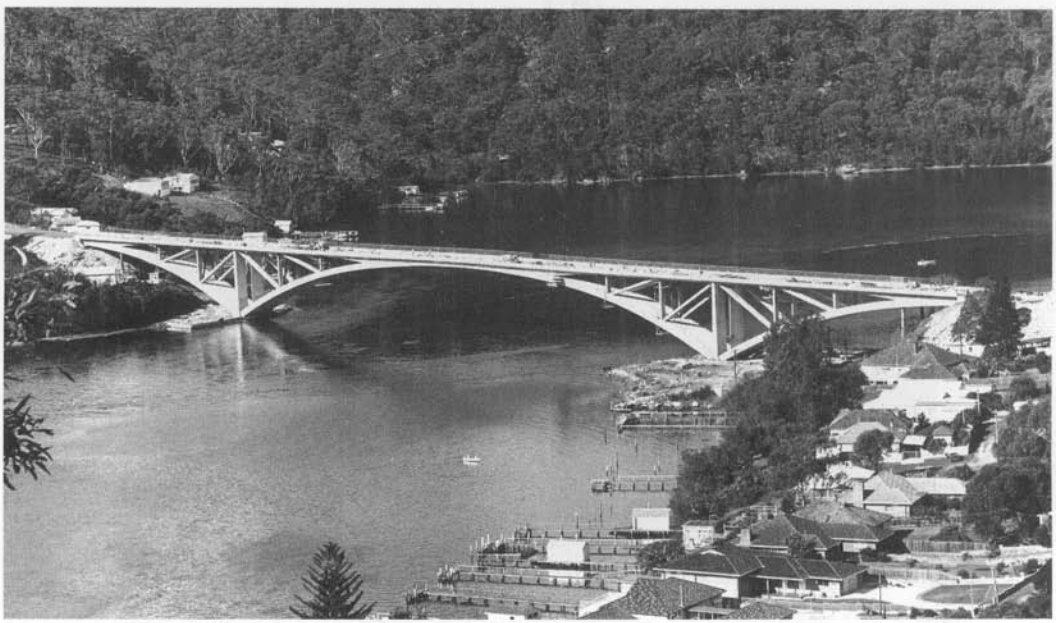

Figure 14.22 The Rip Bridge, Australia. *(Ref. 14.48, Courtesy, Department of Main Roads, New South Wales, Australia and American Concrete Institute.)*

The Rip Bridge (Fig. 14.22) is a three-span, 1082-ft- (330 m) long structure with a central span of 600 ft (183 m). It spans the entrance to Brisbane Waters, north of Sydney, Australia [Ref. 14.48]. It consists of a three-arch-shaped cantilever truss system assembled from large precast concrete elements joined together on site by posttensioning. The upper chord forming the deck essentially acts as a tensile member while the lower chord acts as a compressive member. Each panel of the upper and lower chords of the truss was assembled from five precast elements across the width. The cross sections of these elements were adequately designed so as to create the formwork for the in-situ cast-in-place concrete used for joining the elements and for embedding part of the posttensioning tendons.

14.4.3 Stress Ribbon or Inverted Suspension Bridges

The concept of using prestressed concrete to carry the load mostly in tension instead of in flexure has always been considered as a very desirable alternative (see Chap. 12). However in practice, only a small proportion of bridges take advantage of such potential among which are trusses, as mentioned above, and stress-ribbon or inverted suspension bridges. Examples of stress-ribbon bridges include the Rio Colorado Bridge in Costa Rica (Fig. 13.23 and Ref. 14.23), the Hayahi-No-Mine Bridge in Japan [Ref. 14.24] and also a pedestrian bridge, the Shosai Bridge in Japan (Fig. 14.24).

Figure 14.23a The Rio Colorado stress-ribbon or inverted suspension bridge, Costa Rica. *(Ref. 14.23, Courtesy of T.Y. Lin International.)*

A photograph of the completed Rio Colorado Bridge is shown in Fig. 14.23a. The bridge is 669 ft (204 m) long with a main span of 380 ft (116 m). The construction sequence is described in Fig. 14.23b and comprises the following stages: (1) the foundations, the vertical piers, and the abutments for the approach spans are cast; (2) the precast T beams of the approach spans are erected and the

main piers are cast vertically on hinges; (3) the main piers are leaned downward 30°, by adjusting anchorage cables, and their base is fixed; (4) the main span cables are strung and the topping of the approach spans completed; (5) precast sections forming the lower platform of the center span are fastened to the cables symmetrically from each end, then vertical column bents are attached to the cables; (6) the precast T beams of the roadway are lowered into place and posttensioned for continuity; (7) the structure is complete.

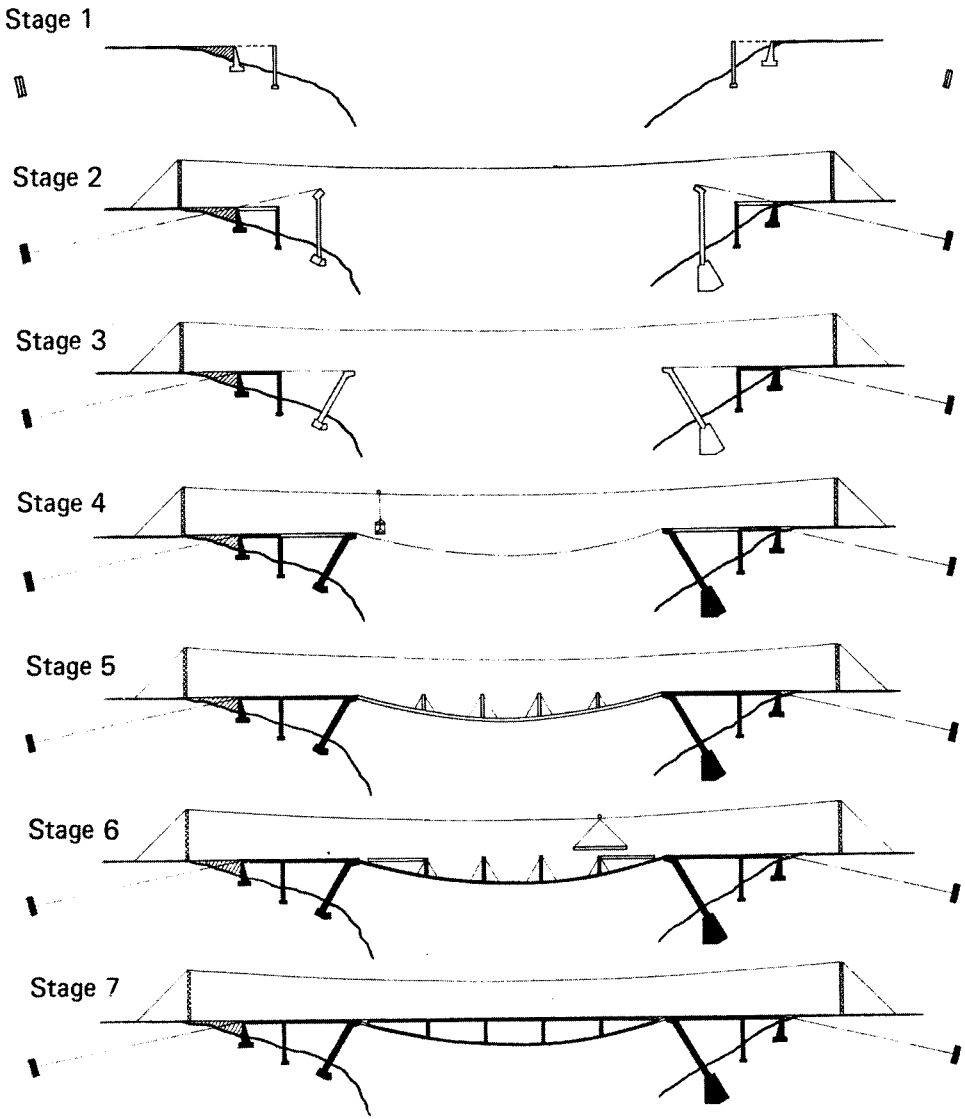

Figure 14.23b Construction sequence of the Rio Colorado Bridge, Costa Rica. *(Ref. 14.23, Courtesy of T.Y. Lin International.)*

Figure 14.24 Shosai Bridge: example of stress-ribbon pedestrian bridge with a main span of 61 m; Shizuoka Prefecture, Japan. *(Courtesy of H. Mutsuyoshi, Saitama University, Japan.)*

The design and construction of the Rio Colorado Bridge has led to the development of a self-anchoring stress-ribbon bridge believed to be very economical for a span range of between about 200 and 400 ft (60 and 120 m) [Ref. 14.23]. It was proposed for the Shai-Dant-Shuey Bridge in Taiwan, and is mentioned here for its innovative concept. An artist's sketch of the bridge and corresponding typical section and elevation are shown in Fig. 14.25a. The main features of the bridge are: (1) the deck is fully utilized as the main compression member, and (2) only one posttensioned tensile element resists all the tension, acting like a suspension cable. This bridge concept may be particularly attractive for application of fiber reinforced polymeric (FRP) reinforcements, since they provide corrosion resistance in a marine environment, and since the tensile member does not induce shear forces in the tendons.

14.4.4 Use of New Materials

Materials for prestressed concrete structures are continuously evolving. At the concrete matrix level, they include high strength concrete (in the range of 50 to 100 MPa), high performance concrete which implies both higher strength and better durability, and ultra high performance concrete such as reactive powder concrete. The addition of fibers to the concrete matrix leads to numerous improvements in mechanical properties, particularly ductility and impact resistance. At the reinforcement level, prestressing steels remain the most competitive reinforcements, cost wise, and the most reliable long term. Stainless steel prestressing tendons have been used to avoid corrosion problems in marine applications. Although

prestressing steels with strengths exceeding 2100 MPa have been used, the benefits to move to higher strengths (at time of this writing) do not outweigh the drawbacks.

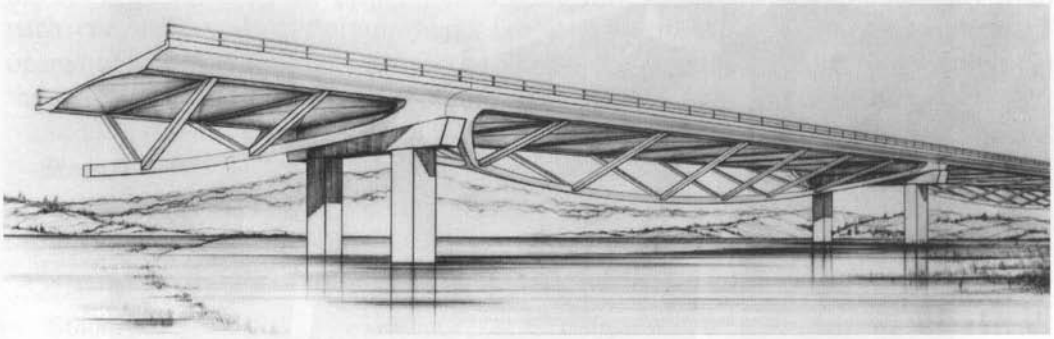

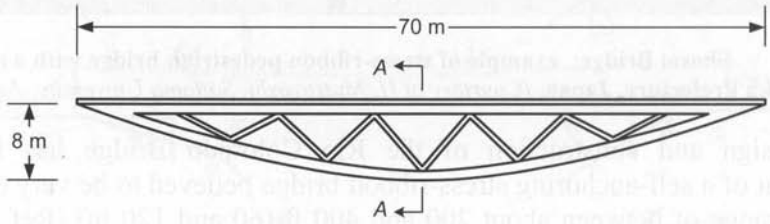

Elevation

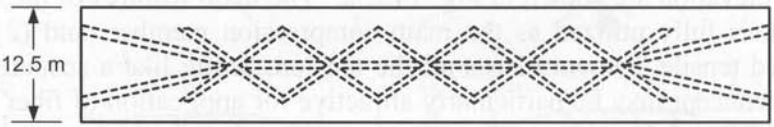

Plan

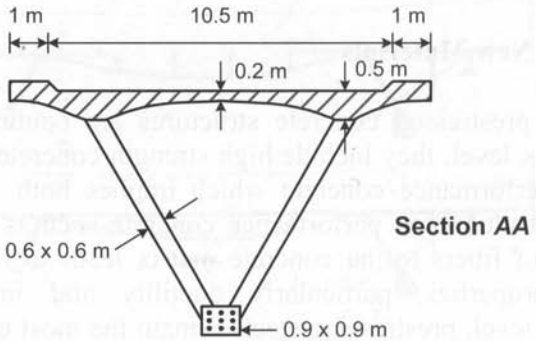

Section *AA*

Figure 14.25a Conceptual Proposal for the Shai-Dant-Shuey Bridge, Taiwan. *(Ref. 14.23, Courtesy of T.Y. Lin International.)*

Fiber reinforced polymeric (FRP) reinforcements (Fig. 25b), made from carbon, glass, aramid, or other high performance fibers embedded in polymeric matrices, in the form of bars, tendons, strands, and two or three dimensional meshes, have been used in concrete structures. Their use is seen primarily as a means to avoid corrosion problems otherwise encountered in concrete structures when using conventional steel reinforcing bars or prestressing tendons. FRP reinforcements are suitable for use in new structures, as well as for repair or strengthening of existing structures. Their application in bridge decks, marine-structures, railway ties, and structures exposed to chemicals or harsh environments is bound to increase. Moreover, their non-magnetic properties make them ideal for special applications such as radar stations, special medical facilities (X-rays rooms), and structures for magnetic levitation (mag-lev) trains.

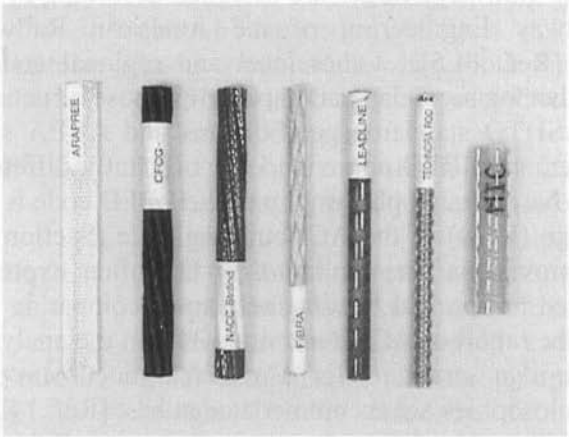

Figure 14.25b Typical FRP reinforcements for prestressing.

Other advantages of FRP reinforcements of particular interest in prestressing applications include lower unit weight, easiness in coiling and handling, good damping and fatigue behavior, and low relaxation losses. However, FRP materials are not without drawbacks, which include high cost, low shear (transverse) strength, susceptibility to stress rupture effects, and, low ductility. Indeed they show a linear elastic (brittle) response in tension up to failure. Such behavior generally leads to poor sectional and member ductility; remedies include the use of an over-reinforced section in combination with fiber reinforced concrete, partial prestressing, and confinement. At time of this writing, the number of concrete structures prestressed with FRP tendons is very small. Given that experience and the types of FRP reinforcements tried, carbon FRP tendons seem most attractive in prestressing applications.

The introduction and development of new structural materials is bound to continue; it will bring new design approaches, concepts, and challenges to prestressed concrete. Section 14.19 provides additional information on the type of performance expected.

14.5 DESIGN SPECIFICATIONS AND GENERAL DESIGN PHILOSOPHY

In the United States highway bridges are generally designed according to specifications prepared by the American Association of State Highway and Transportation Officials (AASHTO). One set of specifications described as Standard Specifications for Highway Bridges [Ref. 14.1] prevailed until about the year 2000 and was used in the examples of the first edition of this book; the specifications were primarily based on working stress design. However, in this chapter, the new specifications based on the AAHSTO LRFD Bridge Design Specifications [Ref. 14.2] are used. They are based on load and resistance factor design and are referred to here as the LRFD specifications, or LRFD code or AASHTO LRFD code. Railway bridges are designed according to the provisions of the Manual of Railway Engineering of the American Railway Engineering Association (AREA) [Ref. 14.5]. Other local and regional codes must also be considered, in particular for secondary and special-purpose structures. The design provisions of the AASHTO standard specifications and AREA specifications are very similar. However, the LRFD approach is significantly different and deserves special attention. The basic design philosophy of the LRFD code is similar to that of ultimate strength design (USD) of the ACI building code (Section 3.5). While the objectives of many provisions are similar, they are often expressed differently. Some discussion related to nominal bending resistance comparing the two codes is given in Chapter 5. The report of ACI Committee 343 on the analysis and design of reinforced concrete bridge structures is a valuable document where both the AASHTO and ACI philosophies are accommodated at best [Ref. 14.3].

It is not possible within this chapter to attempt to cover all the specifications of the AASHTO LRFD code. However, a minimum number of design guidelines are summarized next with primary focus on applications to bridge decks as covered in this chapter. The reader is advised to review Chapter 3 (Sections 3.4 and 3.5) on limit state design and refer to the LRFD code for any detailed and final bridge design.

In the following sections, code-related measures are given in both the US and SI systems of units. They correspond to measures given in either the SI version or the US version of the LRFD code. These are not exact conversions but simply the values given in the corresponding US or SI versions of the code. To differentiate this form of conversion from an exact conversion, the term "or" is added such as in 10 ft (or 3 m). In an exact conversion, 10 ft = 3.048 m and will be written as 10 ft (3.048 m).

14.5.1 Limit States

A limit state is defined as the limit between acceptable and unacceptable performance (Section 3.4). Bridge elements must satisfy the following limit states (Tables 14.1 and 14.2):

Strength-I Limit Sate: Basic load combination relating to the normal use of a bridge. A maximum combination corresponds to when the live load produces the same effect as the permanent load; a minimum combination is considered when the live load produces an effect opposite to that of the permanent load.

Strength-II Limit State: Load combination especially specified by owner.

Strength-III Limit State: Load combination where the bridge is subjected to a wind velocity exceeding 90 km/h (or 55 mph), and vehicular traffic is prevented.

Strength-IV Limit State: Load combination to account for a large ratio of dead load to live load such as in long span bridges exceeding about 67 meters (or 200 ft).

Strength-V Limit State: Load combination where both the bridge and vehicular traffic on the bridge are subjected to a wind velocity of 90 km/h (55 mph).

Extreme Event-I: Load combination referring to the structural survival of a bridge during a major earthquake, a flood, or a boat collision.

Extreme Event-II: Load combination referring to the structural survival of a bridge during an extreme event such as combination of ice load or flood and a vessel's collision.

Service-I Limit State: Load combination relating to normal operation of the bridge. This is basically defined in this book as maximum service conditions and should apply to the allowable stresses defined by Conditions I, II, and III in Table 4.2.

Service-II Limit State: Load combination relating to steel structures only.

Service-III Limit State: Load combination relating to tension in prestressed concrete in service with the objective of crack control. In this case, only 80% of live load plus impact *(LL + IM)* is used in tension controlled design of prestressed concrete. That is in WSD for bending, if σ_{ts} controls, then $M_{max} = M_G + M_{SD} + 0.8(M_{LL+IM})$. It is related to stress condition IV in Table 4.2.

Fatigue-LL, IM, CE: Fatigue and fracture load combination relating to repetitive gravitational vehicular live load and dynamic responses.

Loading combinations for the above limit states, the corresponding percentages of basic unit stress recommended for working stress design (used in service limit states), and load factors for LRFD design (used in strength and extreme event limit states) are given by AASHTO and summarized in Tables 14.1 and 14.2. Allowable stresses are summarized in Tables 14.4 and 14.5. Information on conditions of use is given next.

Table 14.1 Load combinations and load factors for transient loads (from *AASHTO LRFD Bridge Design Specifications – Ref. [14.2]).*

Load Combination / Limit State	DC DD DW EH EV ES	LL IM	WA	WS	WL	FR	TU CR SH	TG	SE	Use one of these at a time			
										EQ	IC	CT	CV
Strength–I	γ_p	1.75	1.0	-	-	1.0	0.5/1.2	γ_{TG}	γ_{SE}	-	-	-	-
Strength–II	γ_p	1.35	1.0	-	-	1.0	0.5/1.2	γ_{TG}	γ_{SE}	-	-	-	-
Strength–III	γ_p	-	1.0	1.4	-	1.0	0.5/1.2	γ_{TG}	γ_{SE}	-	-	-	-
Strength-IV EH, EV, ES, DW; DC only	γ_p 1.5	-	1.0	-	-	1.0	0.5/1.2		-	-	-	-	-
Strength-V	γ_p	1.35	1.0	0.4	1.0	1.0	0.5/1.2	γ_{TG}	γ_{SE}	-	-	-	-
Extreme Event-I	γ_p	γ_{EQ}	1.0	-	-	1.0	-	-	-	1.0	-	-	-
Extreme Event-II	γ_p	0.50	1.0	-	-	1.0	-	-	-	-	1.0	1.0	1.0
Service-I	1.0	1.00	1.0	0.3	0.3	1.0	1.0/1.2	γ_{TG}	γ_{SE}	-	-	-	-
Service-II	1.0	1.30	1.0	-	-	1.0	1.0/1.2	-	-	-	-	-	-
Service-III	1.0	0.80	1.0	-	-	1.0	1.0/1.2	γ_{TG}	γ_{SE}	-	-	-	-
Fatigue- only LL, IM, and CE	-	0.75	-	-	-	-	-	-	-	-	-	-	-

Table 14.2 AASHTO LFRD load factors for permanent loads, γ_p (from *AASHTO LRFD Bridge Design Specifications – Ref. [14.2]).*

	Load Factor γ_p	
Type of Load	Maximum	Minimum
DC: Component and Attachments	1.25	0.90
DD: Downdrag	1.80	0.45
DW: Wearing Surfaces and Utilities	1.50	0.65
EH: Horizontal Earth Pressure		
• Active	1.50	0.90
• At-Rest	1.35	0.90
EV: Vertical Earth Pressure		
• Overall Stability	1.35	N/A
• Retaining Structure	1.35	1.00
• Rigid Buried Structure	1.30	0.90
• Rigid Frames	1.35	0.90
• Flexible Buried Structures Other Than Metal Box Culverts	1.95	0.90
• Flexible Metal Box Culverts	1.50	0.90
ES: Earth Surcharge	1.50	0.75

14.5.2 Load Combinations, Load Factors and Resistance Factors

The following notation is used in Tables 14.1 and 14.2 for the load combinations and corresponding factors as taken from AASHTO:

BR	=	vehicular braking force
CE	=	vehicular centrifugal force
CR	=	creep
DC	=	dead load of component; equivalent of *D* or *G* in this book; it could include nonstructural attachments
DD	=	downdrag
DW	=	dead load of wearing surface; same as *SD* in this book
EH	=	horizontal earth pressure
EQ	=	earthquake load effect
ES	=	earth surcharge load
EV	=	vertical pressure from dead load of earth fill
FR	=	friction
IM	=	vehicular impact load allowance
LL	=	vehicular live load; same as L in this book
PL	=	pedestrian live load
SE	=	settlement
SH	=	shrinkage
TG	=	temperature gradient
TU	=	uniform temperature
WA	=	water load and stream pressure
WL	=	wind on live load
WS	=	wind load on structure

Note that for the dead or permanent load effects (Table 14.2), both a maximum and a minimum value of the load factors are specified. The minimum combinations for the strength limit states are to be used when the effect of live load is opposite to that of permanent load, that is, dead load and superimposed dead load.

The load combinations specified by AASHTO are comprehensive and include all types of loads, such as wind, earthquake, temperature, etc. and all types of structural materials, such as wood, steel, and concrete. It is not within the scope of this text to cover in depth their application to bridge design. In the examples of this book the following loads are mostly used for illustration: *DC*, *DW*, *LL*, and *IM*. Relating to the notation used in this book, *DC* is same as *G* or *D*, *DW* is same as *SD*, and *LL* is same as *L*. However, to minimize confusion, the notation of the AASHTO LRFD code is maintained as much as possible in this chapter. A summary of main load factors needed for the examples of prestressed concrete decks treated in this chapter is given in Table 14.3.

Table 14.3 Load factors used in the examples of this chapter.

Limit State	Condition	γ_{DC}	γ_{DW}	γ_{LL+IM}
Strength I	Max	1.25	1.50	1.75
	Min	0.90	0.65	1.75
Service I		1	1	1
Service III		1	1	0.80

Resistance Factors. The resistance factors of main interest for this chapter are:

- For flexure and tension in prestressed concrete: $\phi = 1$
- For shear in normal weight concrete: $\phi = 0.90$
- For flexure and tension in reinforced concrete: $\phi = 0.90$

Typical Formulation. For typical strength limit states the following condition recommended by AASHTO for the loads and their load factors (Table 14.1) holds:

$$\eta[\gamma_{DC}DC + \gamma_{LL}(LL + IM) + \gamma_{DW}DW] \leq \phi R_n \tag{14.1}$$

in which R_n represents the nominal resistance and η is a load multiplier or modification factor defined as follows:

$$\eta = \eta_I \eta_D \eta_R \tag{14.2}$$

The factor η_I relates to importance of the structure, η_D its ductility, and η_R its redundancy, respectively. The following numerical values are recommended by AASHTO:

$\eta_I \geq$ 1.05 for a bridge considered of operational importance (for the strength and extreme event limit states)

$\eta_I \geq$ 0.95 for a bridge considered nonimportant (for the strength and extreme event limit states)

$\eta_I =$ 1 for all other limit states

$\eta_D =$ 1.05 for non ductile components and connections (for the strength limit state)

$\eta_D =$ 0.95 for components and connections with additional ductility enhancing measures (for the strength limit state)

$\eta_D =$ 1 for all other limit states and for conventional designs and details complying with the AASHTO LRFD specifications

$\eta_R =$ 1.05 for nonredundant members (for the strength limit state)

$\eta_R =$ 0.95 for exceptional levels of redundancy (for the strength limit state)

$\eta_R =$ 1.0 for conventional levels of redundancy and for all other limit states

A bridge is considered important if, for instance, it is the only bridge crossing the river and connecting two-parts of a city, or if it offers the shortest path between a residential area and a hospital, or other key reason. Ductility is important in many situations for redistribution of stresses and as a warning prior to potential failure. Brittle failure is to be avoided. Prestressed concrete members can be made to achieve various levels of ductility by controlling the amount of reinforcement, providing confinement in the form of additional stirrups or using fibers in the concrete matrix. Redundancy significantly increases the safety margin of a structure. For instance, a two-equal-spans prestressed continuous beam does not collapse if the moment resistance at the interior support is exceeded; instead, the load path changes and failure will occur only when the midspan section fails thereafter; this is because a plastic hinge mechanism forms changing the initial load path. Typically, a simple span beam does not provide redundancy.

Note finally that the definition of η in Eqs. 14.1 and 14.2 is different from another definition used in this book as the ratio of final to initial prestressing force.

14.5.3 Allowable Stresses for Service Limit States

Table 14.4 Stress limits for prestressing tendons (from *AASHTO LRFD Bridge Design Specifications – Ref. [14.2]).*

Condition	Tendon Type		
	Stress-Relieved Strand and Plain High-Strength Bars	Low Relaxation Strand	Deformed High- Strength Bars
Pretensioning			
Immediately prior to transfer: ($f_{pt} + \Delta f_{pES}$)	$0.70\, f_{pu}$	$0.75\, f_{pu}$	-
At service limit state after all losses: (f_{pe})	$0.80\, f_{py}$	$0.80\, f_{py}$	$0.80\, f_{py}$
Postensioning			
Prior to seating – short term f_s may be allowed	$0.90\, f_{py}$	$0.90\, f_{py}$	$0.90\, f_{py}$
At anchorages and couplers immediately after anchorage set: ($f_{pt} + \Delta f_{pES} + \Delta f_{pA}$)	$0.70\, f_{pu}$	$0.70\, f_{pu}$	$0.70\, f_{pu}$
At end of seating loss zone immediately after anchorage set: ($f_{pt} + \Delta f_{pES} + \Delta f_{pA}$)	$0.70\, f_{pu}$	$0.70\, f_{pu}$	$0.70\, f_{pu}$
At service limit state after all losses: (f_{pe})	$0.80\, f_{py}$	$0.80\, f_{py}$	$0.80\, f_{py}$

Table 14.5 Allowable stresses for other than segmentally constructed prestressed concrete bridges *(adapted from AASHTO LRFD Bridge Design Specifications – Ref. [14.2]. Note: tension in concrete is negative).*

Condition	Location	Stress Limit, ksi	Stress Limit, MPa
Temporary tensile stress limits in prestressed concrete before losses	Tension in precompressed tensile zone without bonded reinforcement	N/A	N/A
	Tension in areas other than the precompressed tensile zones and without bonded auxiliary reinforcement	$-0.0948\sqrt{f'_{ci}}$ ≥ -0.2 ksi	$-0.25\sqrt{f'_{ci}}$ ≥ -1.38 MPa
	Tension in areas with bonded reinforcement sufficient to resist 120% of the tension force in the cracked concrete computed on the basis of an uncracked section	$-0.22\sqrt{f'_{ci}}$	$-0.58\sqrt{f'_{ci}}$
	Tension for handling stresses in prestressed piles	$-0.158\sqrt{f'_{ci}}$	$-0.415\sqrt{f'_{ci}}$
Temporary compression stress limit in prestressed concrete before losses	Compression in pretensioned and posttensioned concrete component	$0.60f'_{ci}$	$0.60f'_{ci}$
In-service compressive stress limits in concrete after prestress losses	Compression due to the sum of effective prestress and permanent load	$0.45f'_c$	$0.45f'_c$
	Compression due to live load and one-half the sum of effective prestress and permanent loads	$0.40f'_c$	$0.40f'_c$
	Compression due to the sum of effective prestress, permanent loads, and transient loads, and during shipping and handling	$0.60\varphi_w f'_c$ *	$0.60\varphi_w f'_c$ *
In-service tensile stress limits in concrete after prestress losses	Tension in components with bonded prestressing tendons or reinforcement that are subjected to not worse than moderate corrosion conditions	$-0.19\sqrt{f'_c}$	$-0.50\sqrt{f'_c}$
	Tension in components with bonded prestressing tendons or reinforcement that are subjected to severe corrosion conditions	$-0.0948\sqrt{f'_c}$	$-0.25\sqrt{f'_c}$
	For components with unbonded prestressing tendons	No tension	No tension

* The reduction factor φ_w shall be taken equal to 1 when the web and/or flange slenderness ratio (defined as the clear length of constant thickness portion of wall divided by the thickness of the wall) is not greater than 15. This is the case for most precast prestressed beams. Otherwise refer to AASHTO Article 5.7.4.7.2 for the computation of φ_w, which can be as low as 0.75.

The allowable stresses for prestressing steels given in AASHTO are for all practical purposes similar to those given by ACI with an additional limit that the effective prestress be less than or equal to 80% of the yield strength of the material. They are reproduced in Table 14.4. The notation is same as in this book, except for the term f_{pt}, which refers to the stress in the prestressing steel immediately after transfer and is identical to the term f_{pi} used in this book.

For Service Limit States, different allowable stresses for concrete are recommended by AASHTO depending on whether segmental or non-segmental construction is considered. Since this chapter deals primarily with non-segmental prestressed concrete construction, related allowable stresses are summarized in Table 14.5.

14.6 BRIDGE LIVE LOADS

Bridge live loads apply to bridge superstructures and are very different from live loads generally considered for building structures. Live loads applied to the substructure by the superstructure and other loads directly applied to the substructure are not addressed here. Once the effects of live loads have been determined, the design of prestressed concrete bridge superstructures should proceed in a manner very similar to that used for other prestressed concrete structures.

14.6.1 Traffic Lane and Design (or Loading) Lane

Traffic Lane. A typical bridge is designed for several longitudinal traffic lanes of equal width. Their width (defined by the transportation engineer) typically ranges from about 10 ft (3 m) to about 14 ft (4.2 m). A typical width value recommended by AASHTO is 12 ft or 3600 mm.

Design Lane or Loading Lane. The design lane (or loading lane) is the lane used by the bridge engineer for placing the live load. The design lane location does not necessarily coincide with the traffic lane. Design lanes are positioned on a bridge to produce maximum effects. AASHTO recommends a design lane tributary width of 10 ft (or 3 m) along which a truck of pre-specified dimensions can travel. A design lane spans the entire bridge length.

The number of design lanes is preferably taken as the integer part of the ratio of clear roadway width divided by 3600 mm (or 12 ft). The clear width is the distance between the curbs and/or barriers. Note that while the number of design lanes is based on a 12 ft (or 3.6 m) width, the tributary width of a design lane is 10 ft (or 3 m). In any case, engineering judgment (and a move toward higher safety) shall be used to insure that the number of design lanes is not less than the number of traffic lanes. So if a narrow bridge is allowed to have 4 traffic lanes, each 9 ft (or 2.7 m) wide, then the number of design lanes should also be 4.

14.6.2 Basic Types of Live Loads

Three basic types of live load are used by AASHTO in different combinations to produce maximum effects, namely, a uniform load, a truck semi-trailer, and a tandem vehicle. These live loads apply to one design lane and are referred to as the HL-93 loading, which stands for "Highway Loading" and the year 1993 during which they were adopted by AASHTO. They are described in more details next.

Design Uniform Lane Loading. The design lane loading consists of a uniform load of 640 pounds per linear foot (or 0.64 klf, or 9300 N/m) of design lane; the load is assumed uniformly distributed in the transverse direction over a tributary width = 10 ft (or 3 m) (Fig. 14.26).

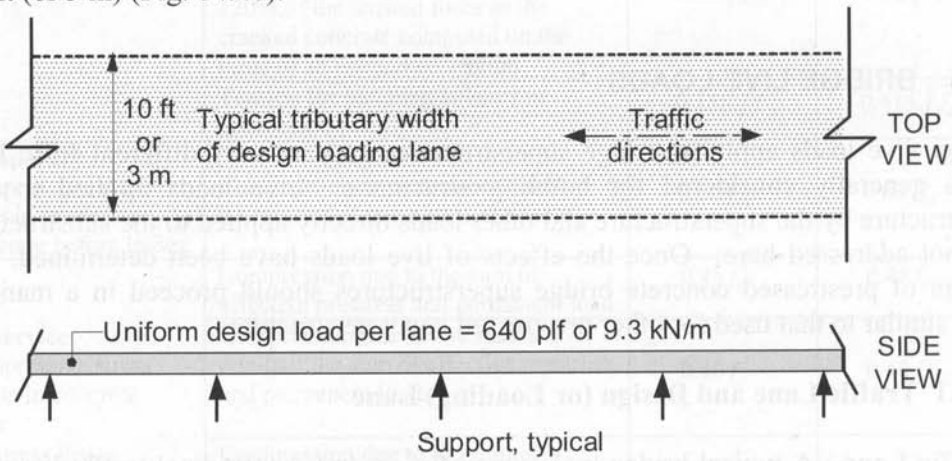

Figure 14.26 Uniform design lane loading specified by AASHTO (US and SI units).

HS20 Design Truck Loading. The HS20 truck is a tractor truck with a semitrailer having a total of three axles. The letter *H* in the identification stands for "highway," the letter *S* stands for "semi" as in semitrailer, and the number 20 represents the maximum specified weight of the first two axles (that is, the tractor part) in U.S. tons (that is, 20 US tons = 40 kips = 40,000 lbs = 18 metric tons). The front axle is assumed to carry 20 percent of the weight (that is, 4 tons or 8 kips) and the rear axle the remaining 80 percent (that is, 16 tons or 32 kips). Each wheel is assumed to carry half the axle load. The rear axle of the semi trailer is assumed to carry the same load as the rear axle of the tractor truck, that is, 16 tons or 32 kips. Hence the total weight of the HS20 truck is 36 US tons or 72 kips. Figure 14.27 provides a definition of the HS20 truck with truck width, axle loads and range of load axle spacing; the axle loads and dimensions are given according to both the US and SI versions of the AASHTO code, where the values are not exact conversions of one other. Note that, although the spacing between the first two axles is assumed fixed at 14 ft (4.3 m), a variable spacing of 14 to 30 ft (4.3 to 9.3 m) is allowed between the second and third axles and is to be selected so that it will produce maximum effects.

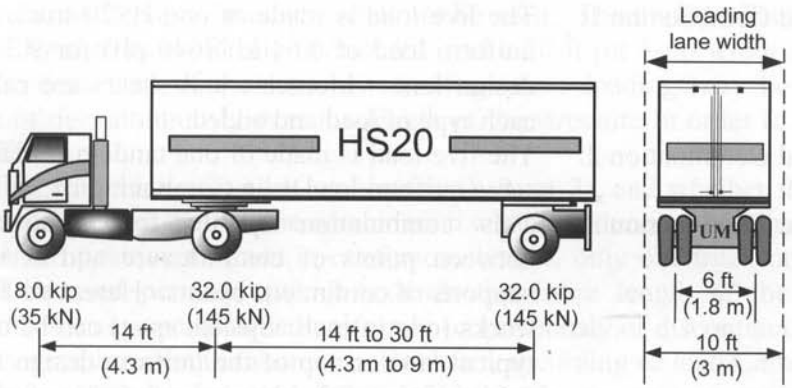

Figure 14.27 Standard HS20 truck specified by AASHTO (US and SI units).

Design Tandem Loading. The tandem consists of a two-axle vehicle each carrying a maximum load of 25 kips (or 110 kN) and spaced 4 ft (or 1.2 m) from each other (Fig. 14.28). The wheels on each axle are spaced 6 ft (or 1.8 m) similarly to those of the HS20 truck. In Fig. 14.28, axle loads and dimensions are given according to both the US and SI versions of the AASHTO code. In simply supported beams, the tandem vehicle leads to larger moments than the HS20 truck for spans less than about 40.3 ft (13.4 m).

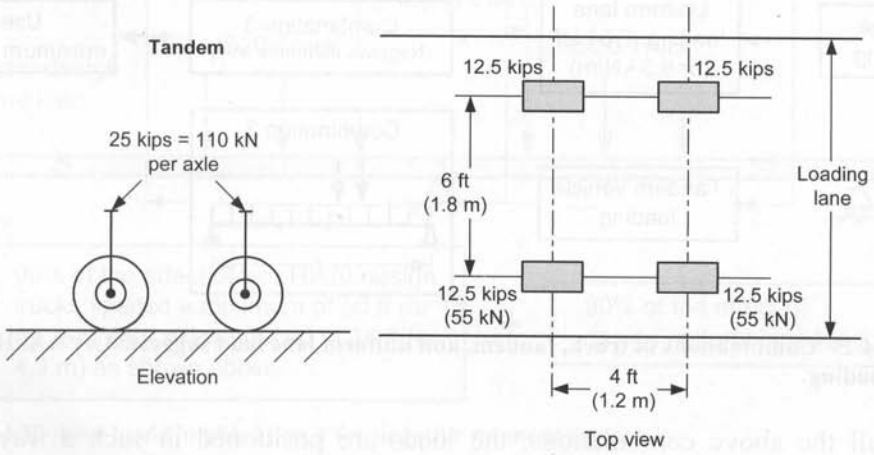

Figure 14.28 Standard tandem vehicle specified by AASHTO (US and SI units).

14.6.3 Live Load Combinations for Design

The three basic types of live loads described above are combined in three different ways by AASHTO and recommended for bridge design; they apply to a typical design lane or loading lane of a bridge:

Live Load Combination 1: The live load is made of one HS20 truck on top of a uniform load of 0.64 klf (640 plf) (or 9.3 kN/m), per design lane. Moments and shears are calculated for each type of load and added.

Live Load Combination 2: The live load is made of one tandem vehicle on top of same uniform load as in Combination 1.

Live Load Combination 3: This combination applies for negative moments between points of contraflexure and at intermediate supports of continuous beams. Here, two HS20 design trucks (one in each adjacent span) can be used along a typical lane on top of the uniform design lane load of 0.64 klf (or 9.3 kN/m), and 90% of their effects combined with 90% of that of the uniform load should be considered.

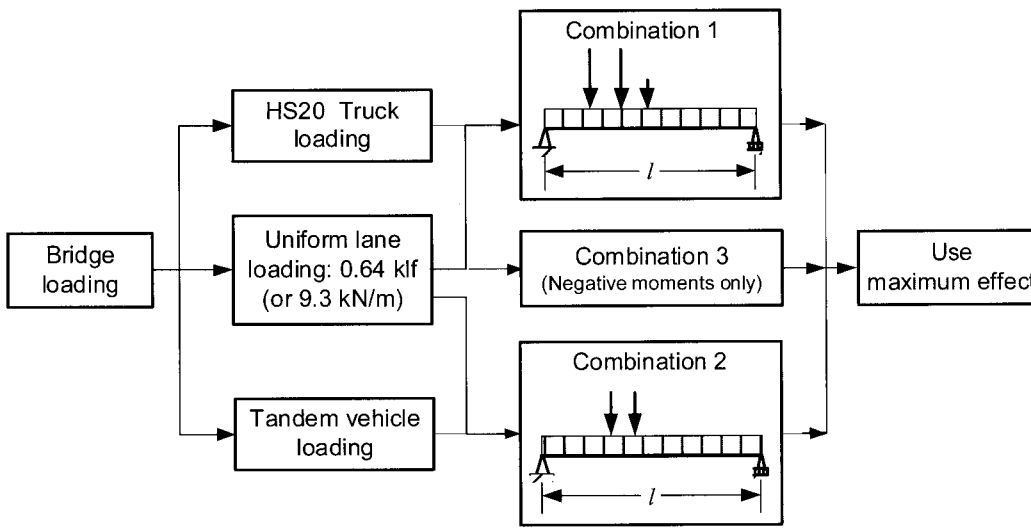

Figure 14.29 Combinations of truck, tandem, and uniform lane load suggested by AASHTO for HL-93 loading.

In all the above combinations, the loads are positioned in such a way as to produce maximum effects, and the most critical condition governs the design. Details of application are given below.

14.6.4 Conditions of Application of Live Loads

A standard HS20 Truck (or a "Tandem vehicle") shall be considered as a unit that can occupy any position within its individual traffic lane so as to produce maximum effect. This is also the case for the "Uniform lane" loading. Fractional lane widths,

fractional trucks, or fractional tandems shall not be used. The uniform lane loading shall be considered to be uniformly distributed over a 10-ft (or 3-m) width on a line normal to the centerline of the lane. The uniform lane loading may be applied continuously or discontinuously over the length of the structure in order to produce maximum effect.

The loading combination used (Combination 1, 2, or 3), and whether the spans are simple or continuous, shall be the combination which produces maximum effects.

For maximum positive moment in continuous beams, only one truck or tandem vehicle shall be used per lane (which extends the entire length of the bridge) combined with as many spans loaded uniformly (continuously or discontinuously) as required to produce a maximum moment. However, according to load Combination 3, for negative moments between points of contraflexure and at intermediate supports of continuous beams, two HS20 design trucks can be used along a typical design lane, and 90% of their effects combined with 90% of that of the uniform load should be considered. The two trucks should be on adjacent spans, with not less than 50-ft (or 15-m) spacing between the rear axle of the first truck and the front or lead axle of the following truck. The distance between the 32 kips (or 145 kN) axles of each truck should be 14 ft (or 4.3 m). The trucks should be placed in such a way as to produce maximum negative moment at the section considered, including the supports. The loading procedure for Combination 3 is illustrated in Fig. 14.30 and applied to a two-equal-span continuous bridge in the example of Section 14.12.

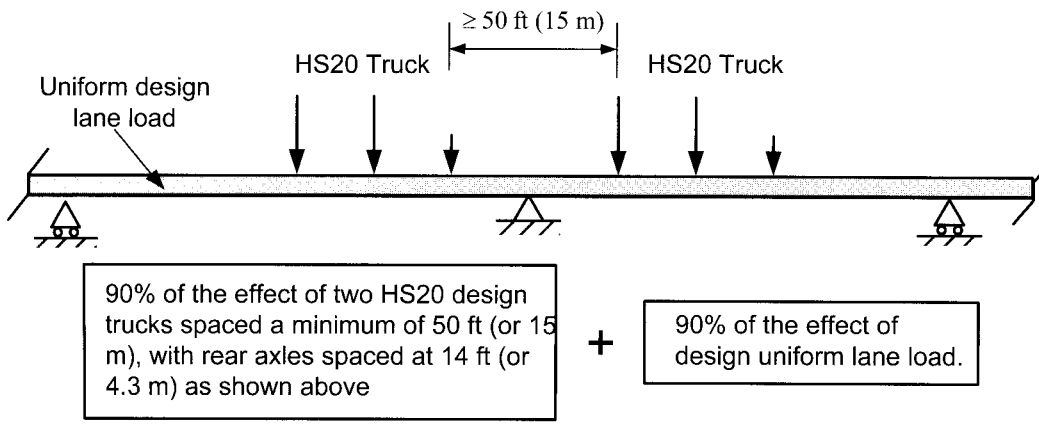

Figure 14.30 Live load Combination 3 for negative moment regions.

Maximum moments and shears at any section of a simply supported span are discussed in Section 14.9 for load Combinations 1 and 2. An example covering load Combination 3 is given in Section 14.12. Note that the above loading combinations (Fig. 14.29) apply to a single design lane. To determine how much a particular girder or beam is affected, a load distribution factor is applied as described in Section 14.7.

14.6.5 Impact Factor

To allow for the increase in stresses due to the sudden application of live loads (Truck or Tandem), a live load increment shall be used from the following impact or dynamic load coefficient:

$$IM = 33\% \text{ for prestressed concrete beams} \tag{14.3}$$

The effect due to impact is added to the truck or tandem load only and not to the uniform design lane loading. This factor applies to moment and shears for all components other than deck joints and for all limit states except fatigue and fracture. For the fatigue and fracture limit state, $IM = 15\%$.

Note that the ratio of live load to dead load moment is relatively large in short span bridges and small in large span bridges. Hence the effect of impact due to live loads decreases in importance with an increase in span length.

14.6.6 Multiple Presence Factor

The probability of having several adjacent lanes of a bridge loaded simultaneously by the heaviest load, producing maximum effect at a particular section (such as midspan or support) is small. A multiple-presence factor, λ_p, is suggested by AASHTO to account for that effect, namely:

$\lambda_p = 1.20$ for one design lane
$\lambda_p = 1.0$ for two design lanes
$\lambda_p = 0.85$ for three design lanes
$\lambda_p = 0.65$ for more than three design lanes

The multiple-presence factor has been implicitly included in the load distribution factors recommended by AASHTO and reproduced in Tables 14.7 and 14.8. However, if a refined analysis is used to determine load distribution, then the multiple presence factor should be considered.

14.6.7 Pedestrian Load and Sidewalk Load

The LRFD code specifies that a pedestrian load of 75 psf (or 3600 kPa) shall be applied to all sidewalks wider than 2 ft (600 mm) and considered simultaneously with the controlling live load Combination 1, 2 or 3. Pedestrian load is treated in the same way as the uniform lane load. Generally the sidewalk load is allocated to the exterior girder below the sidewalk. However, it is also permitted to distribute the sidewalk load to all the bridge girders according to their tributary portion of bridge width.

Pedestrian bridges carrying people and bicycles are designed for a uniform load of 85 psf (or 4100 kPa).

14.6.8 Deflection Limit

In the absence of other criteria, deflection limits recommended by AASHTO for steel, aluminum and concrete bridges are:

$\frac{l}{800}$ for vehicular load

$\frac{l}{300}$ for vehicular load on cantilever arms

$\frac{l}{1000}$ for vehicular and/or pedestrian loads

$\frac{l}{375}$ for vehicular and/or pedestrian loads on cantilever arms

where l is the span length (book notation). Note that AASHTO uses the notation L for span length.

14.6.9 Other Requirements

Some other requirements given in the AASHTO specifications are summarized below:

1. If loadings other than those designated by AAHSTO are desired by the bridge owner, they shall preferably be obtained by proportionately changing the weights shown for both the standard truck and the corresponding lane loading. When applicable, special military loadings shall be obtained from the appropriate military authority.
2. Provision shall be made for the effect of a longitudinal force of five percent of the live load, without the effect of impact, in all lanes assumed to carry traffic headed in the same direction.

14.7 DISTRIBUTION OF LIVE LOADS AND BEAM DISTRIBUTION FACTORS

When a concentrated load is placed on a bridge deck, be it a monolithic slab or a slab resting on beams, the load is distributed over an area larger than the actual contact area. Hence, a larger portion of the deck will assist in resisting the load. This is described as load distribution and should be taken into account in design.

Several methods of analysis are available to determine lateral load distribution in bridge decks among which is the method of Guyon-Massonet (which can be carried out using time consuming hand calculations). They are based on elastic theory and assume the deck to be idealized by a structure forming a grid system of interconnected beams, or an orthotropic plate, or a system of thin plate elements and

beams. Computerized procedures using finite element are well suited for such analysis. However, in lieu of an elaborate analysis, the approximate approach recommended by AASHTO can be used. It can be summarized in the following two steps:

- Moments and shears at any given section are first determined assuming a fully loaded lane for one of the load Combination 1, 2 or 3, whichever controls (see Section 14.8).
- Then these effects are multiplied by the appropriate distribution factor to determine the moment and shear in a particular beam, or girder, or strip of slab.

14.7.1 Load Distribution Factors

In general, no load distribution is assumed in the longitudinal or span direction (also traffic direction) for the computations of moments and shears. Lateral or transverse distribution of truck loadings always involves a full loading lane (10 ft wide or 3 m) associated with loading Combination 1, 2 or 3, whichever controls. For a given beam or girder, a girder distribution factor is defined as the fraction (numerically smaller, equal or larger than unity) of full Combination loading to be resisted by that beam or girder. The girder distribution factors recommended by AASHTO take on a different form depending on the type of bridge deck, whether design is for moments or shears, and whether an interior beam or an exterior beam is considered.

Table 14.6 shows common deck superstructures for which expressions (equations) for the girder distribution factors have been developed by AASHTO. The deck sections should be interpreted broadly as notional shapes. Corresponding distribution factors for moments and shears in interior beams are reproduced in Tables 14.7 and 14.8. Distribution factors for moments and shears in exterior beams are not given here (for brevity) and should be obtained from the AASHTO LRFD code when needed. In no case shall an exterior beam have less carrying capacity than an interior beam. It can be observed that different expressions are generally given for the case when one design lane is loaded or two or more design lanes are loaded. For some deck types, the same equation is recommended regardless of the number of loaded lanes, and for some others the "Lever Rule" is suggested. The lever rule implies that the live load bending moment or shear is determined by applying to the beam the reaction of the wheel load (and/or uniform load) obtained by assuming the flooring to act as a simple span between beams. For multiple lane bridges it is useful to check the distribution factor for both cases of "one lane loaded" or "two or more lanes loaded" and select the largest value for design.

Table 14.6 Common deck superstructures covered by AASHTO and used to determine girder distribution factors *(same as AASHTO LRFD Table 4.6.2.2.1-1).*

SUPPORTING COMPONENTS	TYPE OF DECK	TYPICAL CROSS-SECTION
Steel Beam	Cast-in-place concrete slab, precast concrete slab, steel grid, glues/spiked panels, stressed wood	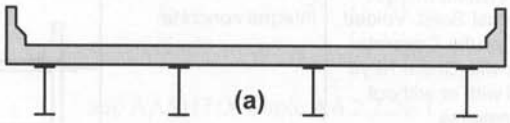
Closed Steel or Precast Concrete Boxes	Cast-in-place concrete slab	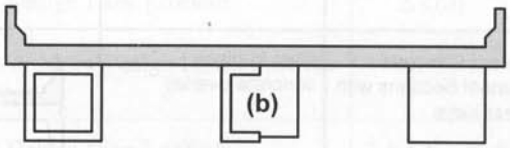
Open Steel or Precast Concrete Boxes	Cast-in-place concrete slab, precast concrete deck slab	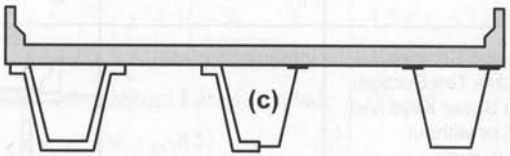
Cast-in-Place Concrete Multicell Boxes	Monolithic concrete	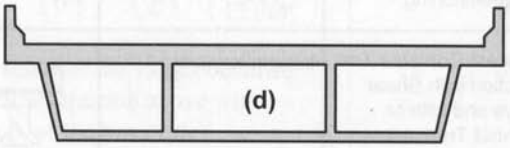
Cast-in-Place Concrete Tee Beam	Monolithic concrete	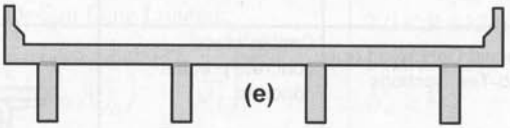
Precast Solid, Voided or Cellular Concrete Boxes with Shear Keys	Cast-in-place concrete overlay	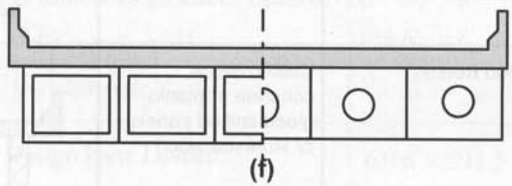

Table 14.6 - continued - Common deck superstructures covered by AASHTO and used to determine girder distribution factors *(same as AASHTO LRFD Table 4.6.2.2.1-1).*

SUPPORTING COMPONENTS	TYPE OF DECK	TYPICAL CROSS-SECTION
Precast Solid, Voided, or Cellular Concrete Box with Shear Keys and with or without Transverse Posttensioning	Integral concrete	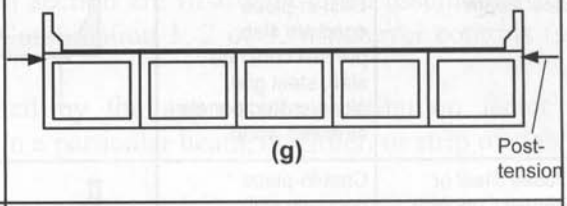
Precast Concrete Channel Sections with Shear Keys	Cast-in-place concrete overlay	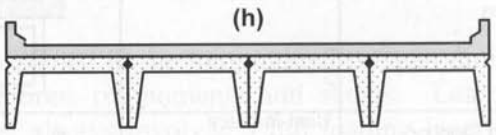
Precast Concrete Double Tee Section with Shear Keys and with or without Transverse Posttensioning	Integral concrete	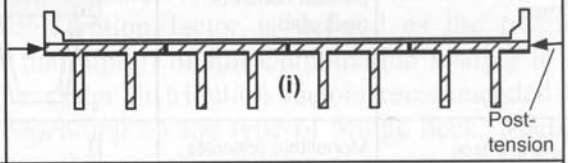
Precast Concrete Tee Section with Shear Keys and with or without Transverse Posttensioning	Integral concrete	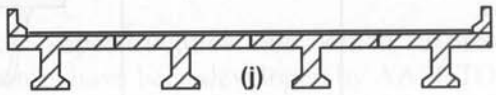
Precast Concrete I or Bulb-Tee Sections	Cast-in-place concrete precast concrete	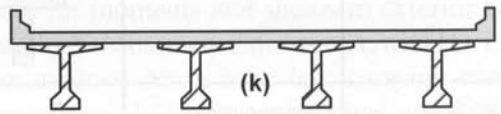
Wood Beams	Cast-in-place concrete or plank, glued/spiked panels or stressed wood	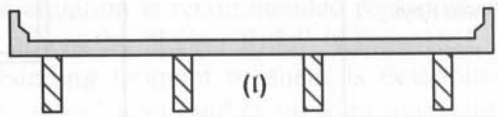

Table 14.7 AASHTO live loads distribution factors (DF_m) for moments in interior beams *(reproduced from AASHTO LRFD).*

Type of Beams	Applicable Cross-Section from Table 14.4	Distribution Factors	Range of Applicability
Wood Deck on Wood or Steel Beams	a,l	See AASHTO Table 4.6.2.2.2a-1	
Concrete Deck on Wood Beams	l	One Design Lane Loaded: $S/12.0$ Two or More Design Lanes Loaded: $S/10.0$	$S \le 6.0$
Concrete Deck, Filled Grid, or Partially Flled Grid on Steel or Concrete Beams; Concrete T-Beams, T-and Double T-Sections	a, e, k and also i, j if sufficeiently connected to act as a unit	One Design Lane Loaded: $0.06+\left(\frac{S}{14}\right)^{0.4}\left(\frac{S}{L}\right)^{0.3}\left(\frac{K_g}{12.0Lt_s^3}\right)^{0.1}$ Two or More Design Lanes Loaded: $0.075+\left(\frac{S}{9.5}\right)^{0.6}\left(\frac{S}{L}\right)^{0.2}\left(\frac{K_g}{12.0Lt_s^3}\right)^{0.1}$	$3.5 \le S \le 16.0$ $4.5 \le t_s \le 12.0$ $20 \le L \le 240$ $N_b \ge 4$
		Use lesser of the values obtained from the equation above with $N_b = 3$ or the lever rule	$N_b = 3$
Cast-in-Place Concrete Muticell Box	d	One Design Lane Loaded: $\left(1.75+\frac{S}{3.6}\right)\left(\frac{1}{L}\right)^{0.35}\left(\frac{1}{N_c}\right)^{0.45}$ Two or More Design Lanes Loaded: $\left(\frac{13}{N_c}\right)^{0.3}\left(\frac{S}{5.8}\right)\left(\frac{1}{L}\right)^{0.25}$	$7.0 \le S \le 13.0$ $60 \le L \le 240$ $N_c \ge 3$ if $N_c > 8$ use $N_c = 8$
Concrete Deck on Concrete Spread Box Beams	b,c	One Design Lane Loaded: $\left(\frac{S}{3.0}\right)^{0.35}\left(\frac{Sd}{12.0L^2}\right)^{0.25}$ Two or More Design Lanes Loaded: $\left(\frac{S}{6.3}\right)^{0.35}\left(\frac{Sd}{12.0L^2}\right)^{0.125}$	$6.0 \le S \le 11.5$ $20 \le L \le 140$ $18 \le d \le 65$ $N_b \ge 3$
		Use Lever Rule	$S > 11.5$

Units: S, ft; L, ft; d, in; t_s, in.

Table 14.7 continued - AASHTO live loads distribution factors (DF_m) for moments in interior beams *(reproduced from AASHTO LRFD).*

Type of Beams	Applicable Cross-Section from Table 14.4	Distribution Factors	Range of Applicability
Concrete Beams used in Multibeam Decks	f	One Design Lane Loaded: $k\left(\frac{b}{33.3L}\right)^{0.5}\left(\frac{I}{J}\right)^{0.25}$ where: $k = 2.5(N_b)^{-0.2} \geq 1.5$ Two or More Design Lane Loaded: $k\left(\frac{b}{305}\right)^{0.6}\left(\frac{b}{12.0L}\right)^{0.2}\left(\frac{I}{J}\right)^{0.06}$	$35 \leq b \leq 60$ in $20 \leq L \leq 120$ ft $5 \leq N_b \leq 20$
	g if sufficeiently connected to act as a unit		
	h	Regardless of Number of Loaded Lanes: S/D where: $C = K(W/L)$ • when $C > 5$: $D = 11.5 - N_L$ • when $C \leq 5$ $D = 11.5 - N_L + 1.4N_L(1-0.2C)^2$ and: $K = \sqrt{\frac{(1+\mu)I}{J}}$ For preliminary design, the following values of K may be used: Beam Type — K Nonvoided rectangular beams — 0.7 Rectangular beams with circular voids — 0.8 Box section beams — 1.0 Channel beams — 2.2 T-beam — 2.0 Double T-beam — 2.0	
	g, i, j if connected only enough to prevent relative vertical displacement at the interface		
Steel Grid on Steel Beams	a	One Design Lane Loaded: $S/7.5$ if $t_g < 4.0$ in $S/10.0$ if $t_g \geq 4.0$ in Two or More Design Lane Loaded: $S/8.0$ if $t_g < 4.0$ in $S/10.0$ if $t_g \geq 4.0$ in	$S \leq 6.0$ ft $S \leq 10.5$ ft
Concrete Deck on Mutiple Steel Box Girders	b,c	Regardless of Number of Loaded Lanes: $0.05 + 0.85\frac{N_L}{N_b} + \frac{0.425}{N_L}$	$0.5 \leq \frac{N_L}{N_b} \leq 1.5$

Table 14.8 AASHTO live loads distribution factors (DF_v) for shears in interior beams *(reproduced from AASHTO LRFD).*

Type of Beams	Applicable Cross-Section from Table 14.4	One Design Lane Loaded	Two or More Design Lane Loaded	Range of Applicability
Wood Deck on Wood or Steel Beams	a,l	See AASHTO Table 4.6.2.2.2a-1		
Concrete Deck on Wood Beams	l	Lever Rule	Lever Rule	N/A
Concrete Deck, Filled Grid, or Partially Flled Grid on Steel or Concrete Beams; Concrete T-Beams, T-and Double T-Sections	a, e, k and also i, j if sufficeiently connected to act as a unit	$0.36+\frac{S}{25.0}$	$0.2+\frac{S}{12}-\left(\frac{S}{35}\right)^{2.0}$	$3.5 \le S \le 16.0$ ft $4.5 \le t_s \le 12.0$ in $20 \le L \le 240$ ft $N_b \ge 4$
		Lever Rule	Lever Rule	$N_b = 3$
Cast-in-Place Concrete Muticell Box; Box Section	d	$\left(\frac{S}{9.5}\right)^{0.6}\left(\frac{d}{12.0L}\right)^{0.1}$	$\left(\frac{S}{7.3}\right)^{0.9}\left(\frac{d}{12.0L}\right)^{0.1}$	$6.0 \le S \le 13.0$ ft $60 \le L \le 240$ ft $35 \le d \le 65$ in $N_c \ge 3$
Concrete Deck on Concrete Spread Box Beams	b, c	$\left(\frac{S}{10}\right)^{0.6}\left(\frac{d}{12.0L}\right)^{0.1}$	$\left(\frac{S}{7.4}\right)^{0.8}\left(\frac{d}{12.0L}\right)^{0.1}$	$6.0 \le S \le 11.5$ ft $20 \le L \le 140$ ft $18 \le d \le 65$ in $N_b \ge 3$
		Lever Rule	Lever Rule	$S > 11.5$
Concrete Box Beams Used in Multibeam Decks	f, g	$\left(\frac{b}{130L}\right)^{0.15}\left(\frac{I}{J}\right)^{0.05}$ I, J: in^4	$\left(\frac{b}{156}\right)^{0.4}\left(\frac{b}{12.0L}\right)^{0.1}\times\left(\frac{I}{J}\right)^{0.05}$	$35 \le b \le 60$ in $20 \le L \le 120$ ft $5 \le N_b \le 20$ $25000 \le J \le 610000$ $40000 \le I \le 610000$
Concrete Beams Other Than Box Used in Multibeam Decks	h	Lever Rule	Lever Rule	N/A
	i, j if connected only enough to prevent relative vertical displacement at the interface			
Steel Grid Deck on Steel Beams	a	Lever Rule	Lever Rule	N/A
Concrete Deck on Multiple Steel Box Beams	b, c	As specified in AASHTO Table 4.6.2.2.2b-1		

Note that the distribution factors defined in Tables 14.7 and 14.8 relate to the portion of full loading Combinations 1, 2, or 3 (such as full truck and uniform lane load) to be resisted by a girder. It is different from the distribution factor used in the previous AASHTO Standard Specifications, which relates to the fraction of lines of wheels (a truck has two lines of wheels) to be resisted by a girder. Thus, if the same theory was used to determine these coefficients, for all practical purposes, the distribution factor using the LRFD code would be half that of the previous specifications.

If a standard factor is not applicable either due to a particular bridge deck design or to limitations on the values of recommended distribution factors, distribution factors should be determined from a refined analysis. Short of an exact analysis, the bending moment for a given roadway beam (interior or exterior) can be determined by applying to the beam the reaction of wheel loads obtained by assuming the flooring to act as a simple span between beams. This is same as for the lever rule.

In the equations of Tables 14.7 and 14.8 the following notation applies as per AASHTO LRFD specifications:

A = beam or girder cross-sectional area
d = overall beam depth, in (same as book notation h)
I = moment of inertia (same as book notation I, I_g or I_{tr})
I_p = polar moment of inertia
J = St. Venant's torsional inertia
L = span length, ft (same as book notation l; do not confuse with L, live load)
N_b = number of beams or girders
N_c = number of cells in a multicell box type bridge deck
N_L = number of lanes
S = center to center beam or girder spacing, ft
t_s = slab depth, in (same as book notation h_f)
W = roadway width between curbs, ft (or edge-to-edge width of bridge)

For positive moments, the span length, L, is the length of span for which moment is being calculated. For negative moments in continuous beams between points of contraflexure and at interior supports, L in Tables 14.7 and 14.8 is the average length of the two adjacent spans.

Regardless of the value of distribution factor used, engineering judgment and safety suggest that the combined design load capacity of all the beams in a bridge span shall not be less than that required to support the total live (multiple lanes loaded) and dead loads of the span according to the various applicable limit states.

14.7.2 Remarks Related to a Particular Bridge Deck Type

A few remarks related to particular notation or application of the distribution factor equations for some common prestressed concrete deck types are given next. Note that the transverse posttensioning shown for some sections in Table 14.6 is intended to make the units act together. For that, a minimum average prestress of 250 psi (1.75 MPa) is recommended.

1. **Cross-Section Type e, i, j, and k of Table 14.6:** Cast-in-place concrete slab on top of prestressed concrete I or bulb-Tee sections; prestressed concrete Tee or double-Tee sections with shear keys sufficiently connected and with or without transverse posttensioning. For these decks, the equation for the distribution factor requires the use of several variables, namely:
   - A = beam or girder cross-sectional area, in^2
   - I = moment of inertia, in^4
   - I_p = polar moment of inertia, in^4
   - J = Saint Venant's torsional inertia, in^4
   - n = modular ratio between beam and deck materials
   - e_g = distance between center of gravity of basic beam and deck, in

$$K_g = n(I + Ae_g^2) \tag{14.4}$$

As a first approximation in preliminary design, for interior beams with concrete decks, the ratio I/J and the term $(K_g / 12.0Lt_s^3)$ may be taken as 1.

The torsional inertia J can be estimated from:

- For stocky open sections such as prestressed I-beams, T-beams, and solid slabs:

$$J = \frac{A^4}{40I_p} \tag{14.5a}$$

- For closed thin-walled shapes:

$$J = \frac{4A_o^2}{\Sigma \frac{s}{t}} \tag{14.5b}$$

where:

- A_o = area enclosed by centerlines of elements, in^2
- s = length of a side element, in
- t = thickness of side element, in

2. **Cross-Section Type g, h, i, and j of Table 14.6**: Adjacent precast prestressed boxes, channels, Tee- and double-Tee sections if connected enough to prevent vertical displacement at the interface.

   Here the distribution factor equation depends on a stiffness parameter $C = KW/L$, in which the value of parameter K depends on I and J defined above, and:

   μ = Poisson's ratio
   W = edge-to-edge width of the bridge
   L = beam span length (same as book notation ℓ)

3. **Cross-Section Type b and c of Table 14.6:** Cast-in-place concrete slab on top of precast prestressed concrete spread box beams. The expression for the distribution factor can be calculated directly but its applicability is limited to spans of up to 140 ft (43 m).

4. **Cross-Section Type d of Table 14.6:** Prestressed multicell box deck. The expression for the distribution factor can be easily calculated and its range of applicability is clearly defined; in particular it applies to spans of up to 240 ft (73 m).

14.7.3 Simplified Distribution Factor by Heuristic Approach

In the absence of a more exact formula, it is easy to estimate a relatively safe value of distribution factor for any beam of a multi-beam bridge, using engineering judgment. Indeed, if the beams of a bridge deck (such as shown in Table 14.6 (j)) were spaced 10 ft (or 3 m) center to center, and if they were not connected, each beam should theoretically be capable of carrying an entire lane loading (that is, over a 10 foot width). Thus the distribution factor for the beam would be $DF = S/10 = 1$ for S in feet, and $DF = S/3 = 1$ for S in meters. However, such an approach may be too conservative, and a higher value of denominator can be used, leading to the following formula:

$$DF_m = DF_v = \frac{S}{z} \tag{14.6a}$$

where, depending on how conservative the design is, z is a number taken equal to 10, 11, or 12 when S is in feet (US units), and $z = 3$, 3.3 or 3.6 when S is in meters (SI units). The value of z could be different for moment and shear. In the former AASHTO Standard Specifications a denominator value of 5.5 (corresponding to $z = 11 = 2 \times 5.5$) was often used; the apparent difference with the AASHTO LRFD is due to the fact that AASHTO Standard considered the number of "lines of wheels" and two "lines of wheels" are needed to make a truck or a tandem vehicle. For preliminary design, the author recommends:

For bending:
$$\begin{cases} DF_m = \dfrac{S}{11} & \text{where } S \text{ is in feet} \\ DF_m = \dfrac{S}{3.3} & \text{where } S \text{ is in meters} \end{cases} \tag{14.6b}$$

For shear:
$$\begin{cases} DF_m = \dfrac{S}{8} & \text{where } S \text{ is in feet} \\ DF_m = \dfrac{S}{2.4} & \text{where } S \text{ is in meters} \end{cases} \tag{14.6c}$$

14.8 DESIGN AIDS FOR LIVE LOAD MOMENTS AND SHEARS FOR ONE LOADING LANE

Although there is no conceptual difficulty in determining the moments and shears due to live loads in simple span bridge decks, substantial time can be saved by using existing design aids and solutions. As mentioned above, in designing a typical beam or strip of slab of a bridge deck, the maximum live load moments and shears at any section x can be determined from the moments and shears due to a fully loaded lane according to load Combination 1, 2, or 3 (Fig. 14.29), whichever controls.

14.8.1 General Rule for Concentrated Loads in Simply Supported Spans

When the uniform lane loading is used, the maximum bending moment occurs at midspan. This is not true, however, for truck loadings, which are represented by a group of concentrated loads. For such a case, the following general rule (or theorem) is used:

> *"The absolute maximum moment in the span occurs under the load closest to the resultant force and placed in such a way that the centerline of the span bisects the distance between that load and the resultant."*

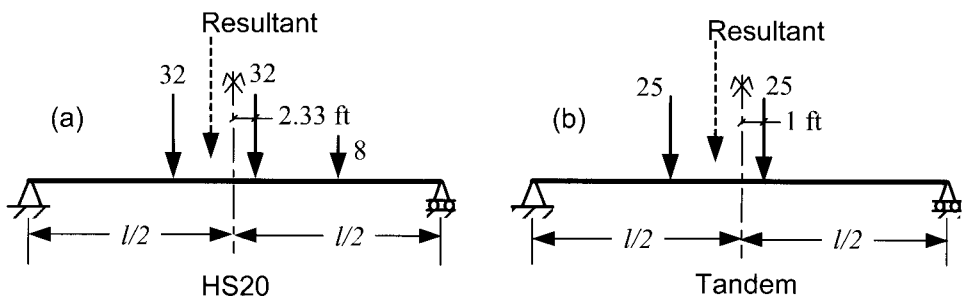

Figure 14.32 Section of maximum moment in simple spans due to: (a) HS20 truck, or (b) Tandem vehicle; it occurs under the axle closest to midspan (not to scale).

The application of this general rule to the HS20 truck and to the tandem vehicle is shown in Figs. 14.32*a* and 14.32*b*, respectively.

The corresponding simple span absolute maximum moments are given by:

- For the HS20 truck:

$$(M)_{max} = P\left(\frac{9}{8}l + \frac{24.5}{l} - 17.50\right) \tag{14.7}$$

where $P = 16$ kips and l is in feet.

- For the Tandem vehicle:

$$(M)_{max} = M(x = l/2 + 1) = 50\left(\frac{l}{4} - 1 - \frac{3}{l}\right) \tag{14.8}$$

where l is in feet and M in kips-feet.

Using the truck and tandem loading from the SI version of the LRFD code and using SI units leads to the following two equations:

- For the HS20 truck:

$$(M)_{max} = 81.25l + \frac{172.1}{l} - 387 \text{ kN-m} \tag{14.9}$$

which occurs at a section under the middle axle located a distance 0.728 m from midspan.

- For the Tandem vehicle:

$$(M)_{max} = 55l + \frac{19.8}{l} - 66 \text{ kN-m} \tag{14.10}$$

which occurs at a section under one of the two axles located a distance 0.30 m from midspan. In the above two equations l is in meters.

14.8.2 Equations for Live Load Moments and Shears in Simply Supported Spans

Equations giving maximum moments and shears at any section x of a simple span are developed here for the HS20 truck loading, the uniform lane loading, and the tandem vehicle loading. Loadings and load configurations are shown in Table 14.9. Two load cases (A or B) are considered for the HS20 trucks, as each can control depending on the value of x and the span. Note that the equations shown in Table 14.9 are for a single loading lane (that is, a whole truck, a whole tandem, or uniform

lane loading) and for simple spans. From the three basic types of load Combinations 1, 2, and 3, moments and shears can be easily determined. For continuous spans, influence lines can be used to obtain maximum effects due to the application of concentrated loads.

Table 14.10 gives the equations for absolute maximum moment for the span for load Combination 1 and 2, which occurs at a section near midspan; the corresponding section location is determined by differentiating the sum of moments due to the standard truck or tandem and the uniform lane load. The section at which maximum moment occurs is under one of the axles placed a distance x_1 (for HS20 truck) or x_2 (for Tandem) from the midspan section. Expressions are given for both the US and SI units.

Table 14.9 Simple span moments and shears due to a single truck, a tandem, or a uniform lane load for one design lane.

Case	Load configuration	Moments (kips-ft) and shears (kips) at any section x	Loading and limitations (x and l in feet)
A	*HS20* 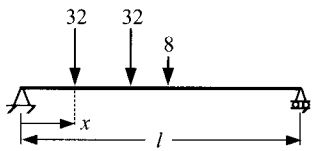	$M(x)=16x\left[4.5\left(1-\frac{x}{l}\right)-\frac{42}{l}\right]$ $V(x)=16\left[4.5\left(1-\frac{x}{l}\right)-\frac{42}{l}\right]$	Truck loading: $M_A \geq M_B$ for: $l > 28$ $x \leq l/3$ $x + 28 \leq l$ $V_A > V_B$ for any x
B	*HS20* 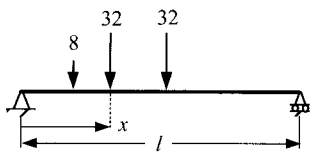	$M(x)=16x\left[4.5\left(1-\frac{x}{l}\right)-\frac{21}{l}-\frac{7}{x}\right]$ $V(x)=16\left[4-4.5\frac{x}{l}-\frac{21}{l}\right]$	Truck loading: $M_B \geq M_A$ for: $l > 28$ $x > l/3$ $14 \leq x \leq l/2$
C	Tandem 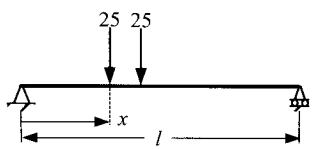	$M(x)=50x\left(1-\frac{x}{l}-\frac{2}{l}\right)$ $V(x)=50\left(1-\frac{x}{l}-\frac{2}{l}\right)$	Tandem loading is more severe than HS20 truck loading for $l \leq$ 40.3 ft
D	Uniform 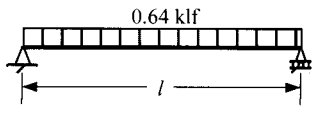	$M(x)=0.64x\frac{(l-x)}{2}$ $V(x)=0.64\left(\frac{l}{2}-x\right)$	Lane loading
Use the larger of { Effect due to: *(uniform lane)* + (1 + *IM*)*truck* (Combination 1) Effect due to: *(uniform lane)* + (1 + *IM*)*tandem* (Combination 2)			

Table 14.10 Maximum positive moments in simple spans due to AASHTO LRFD design load combinations for one loaded lane.

US units:

Combination*	Load configuration	Absolute maximum moment in span (kips-ft)
1	HS20 truck + uniform lane load: 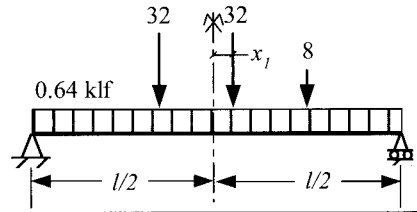 	$(M_{max})_{LL+IM} = (1+I)M_{truck} + M_{unif-lane}$ $M_{truck} = 16\left(\frac{9}{8}l + \frac{x_1}{l}(21 - 4.5x_1) - 17.5\right)$ $M_{unif-lane} = 0.08\left(l^2 - 4x_1^2\right)$ where $x_1 = \frac{336}{144 + 0.64l} = \frac{525}{225 + l}$ ft
2	Tandem + uniform lane load: 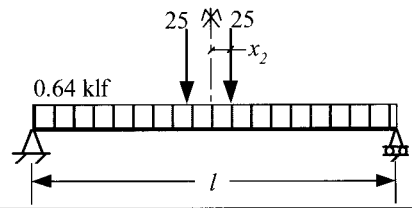 	$(M_{max})_{LL+IM} = (1+I)M_{tandem} + M_{unif-lane}$ $M_{tandem} = 50\left(\frac{l}{4} + \frac{x_2}{l}(2 - x_2) - 1\right)$ $M_{unif-lane} = 0.08\left(l^2 - 4x_2^2\right)$ where $x_2 = \frac{100}{100 + 0.64l}$ ft

* Combination 1 is more severe than Combination 2 for $l > 40.3$ ft.

SI units:

Combination*	Load configuration	Absolute maximum moment in span (kN-m)
1	HS20 truck + uniform lane load: 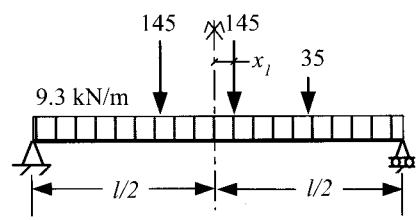 	$(M_{max})_{LL+IM} = (1+I)M_{truck} + M_{unif-lane}$ $M_{truck} = 81.25l + \frac{x_1}{l}(473 - 325x_1) - 387$ $M_{unif-lane} = 1.1625\left(l^2 - 4x_1^2\right)$ where $x_1 = \frac{473}{650 + 9.3l}$ m
2	Tandem + uniform lane load: 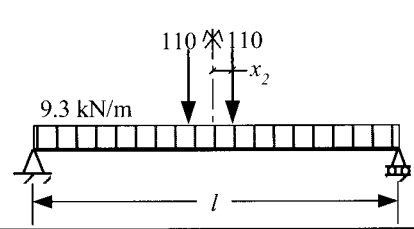 	$(M_{max})_{LL+IM} = (1+I)M_{tandem} + M_{unif-lane}$ $M_{tandem} = 55l + \frac{x_2}{l}(132 - 220x_2) - 66$ $M_{unif-lane} = 1.1625\left(l^2 - 4x_2^2\right)$ where $x_2 = \frac{132}{440 + 9.3l}$ m

* Combination 1 is more severe than Combination 2 for $l > 11.75$ m.

14.8.3 Design Chart for Simply Supported Spans

A chart was developed by the author and a student (P. Chompreda) as a design aid for the AASHTO HL-93 loading (Figs. 14.33a) and (14.33b). Figure 33a is similar to a chart published in the first edition of this book for the previous loading defined in the AASHTO standard specifications. It allows to compute the maximum moment for a fully loaded lane at any section, x, of a simple span due to either load Combination 1 or 2, whichever governs. The effect of impact, with a factor of 33% on the truck or tandem loading, is included. The moment at a section, x, is determined from an equivalent concentrated load Q_m obtained from the chart and assumed to be placed at x. It is given by:

$$[M_{Lane}(x)]_{LL+IM} = Q_m \frac{x(l-x)}{l} \tag{14.11a}$$

where x is less than $l/2$. The units are feet for x and l, and in kips for Q_m. Examples illustrating the use of the chart are given in the Examples of Section 14.10, 14.11, and 14.14.

Figure 14.33b allows to compute the shear force at any section x for a fully loaded lane of a simple span due to either load Combination 1 or 2, whichever governs; the effect of impact, with a factor of 33% on the truck or tandem loading, is included. The shear at any section, x, is determined from an equivalent concentrated load Q_v obtained from the chart and assumed to be placed at x. It is given by:

$$[V_{Lane}(x)]_{LL+IM} = Q_v \frac{(l-x)}{l} \tag{14.11b}$$

14.8.4 Design Charts for Live Load Moments at Supports of Continuous Beams with Equal Spans

The negative live load moment at the interior supports of continuous beams is obtained from load Combination 3 due to two trucks and the uniform lane loading placed according to Fig. 14.30. The effects due to the two trucks were calculated for a full lane using influence lines. The results are summarized in a graphical chart in Fig. 14.34 (courtesy of P. Tothong); the top and bottom part of the figure are for the US and SI systems of units, respectively. Although the precision of the graphs is not sufficient for a final design, the values derived from the graphs are useful in preliminary design and dimensioning. The above result should be added to the effects of uniform lane load.

For continuous beams with equal spans, the negative moment at interior supports due to the uniform lane loading can be obtained from the following formulae:

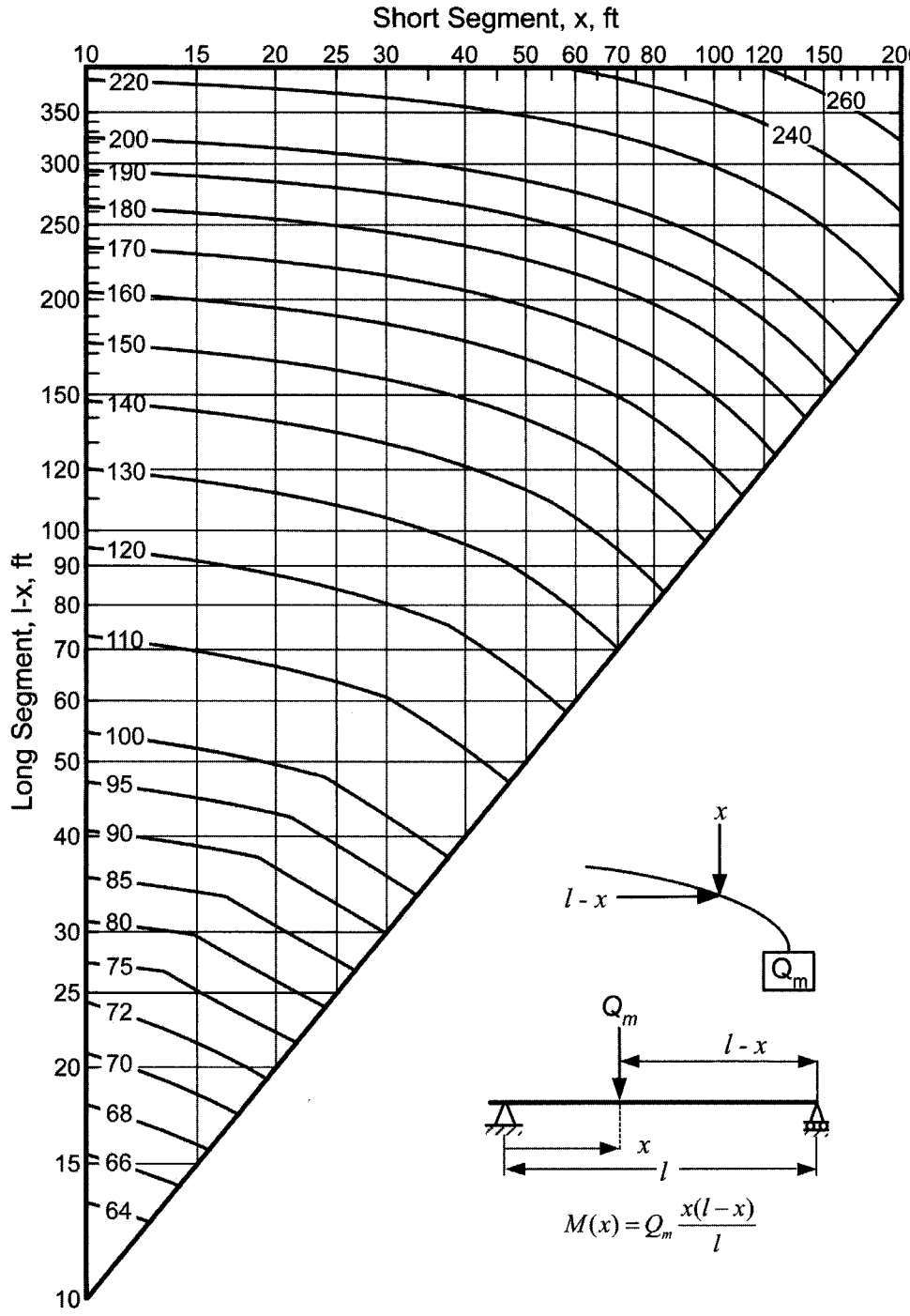

Figure 14.33a Bending moments chart for AASHTO HL-93 loading for a fully loaded lane, Combination 1 or 2 whichever controls, including effect of impact.

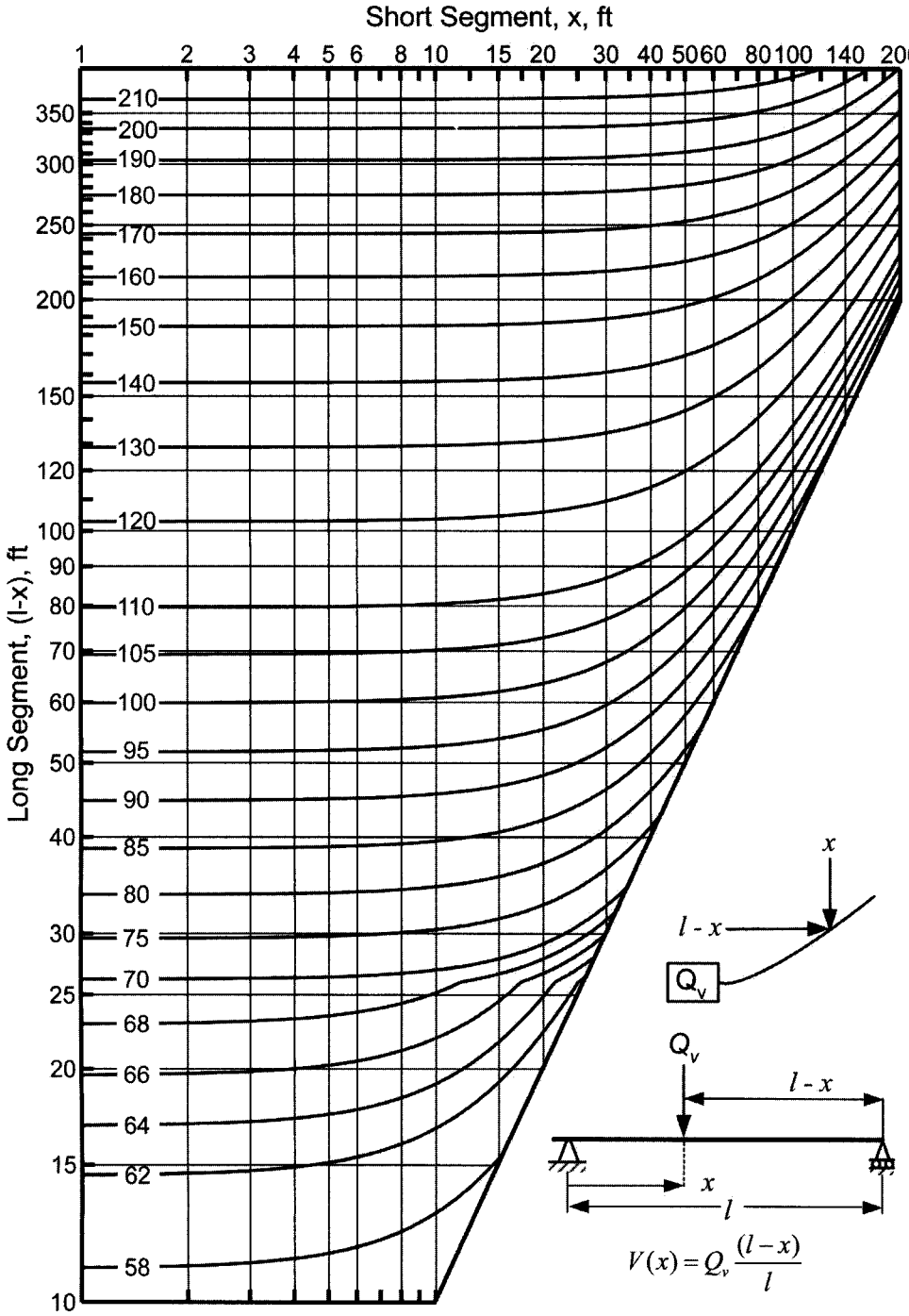

Figure 14.33b Shear force chart for AASHTO HL-93 loading for a fully loaded lane, Combination 1 or 2 whichever controls, including effect of impact.

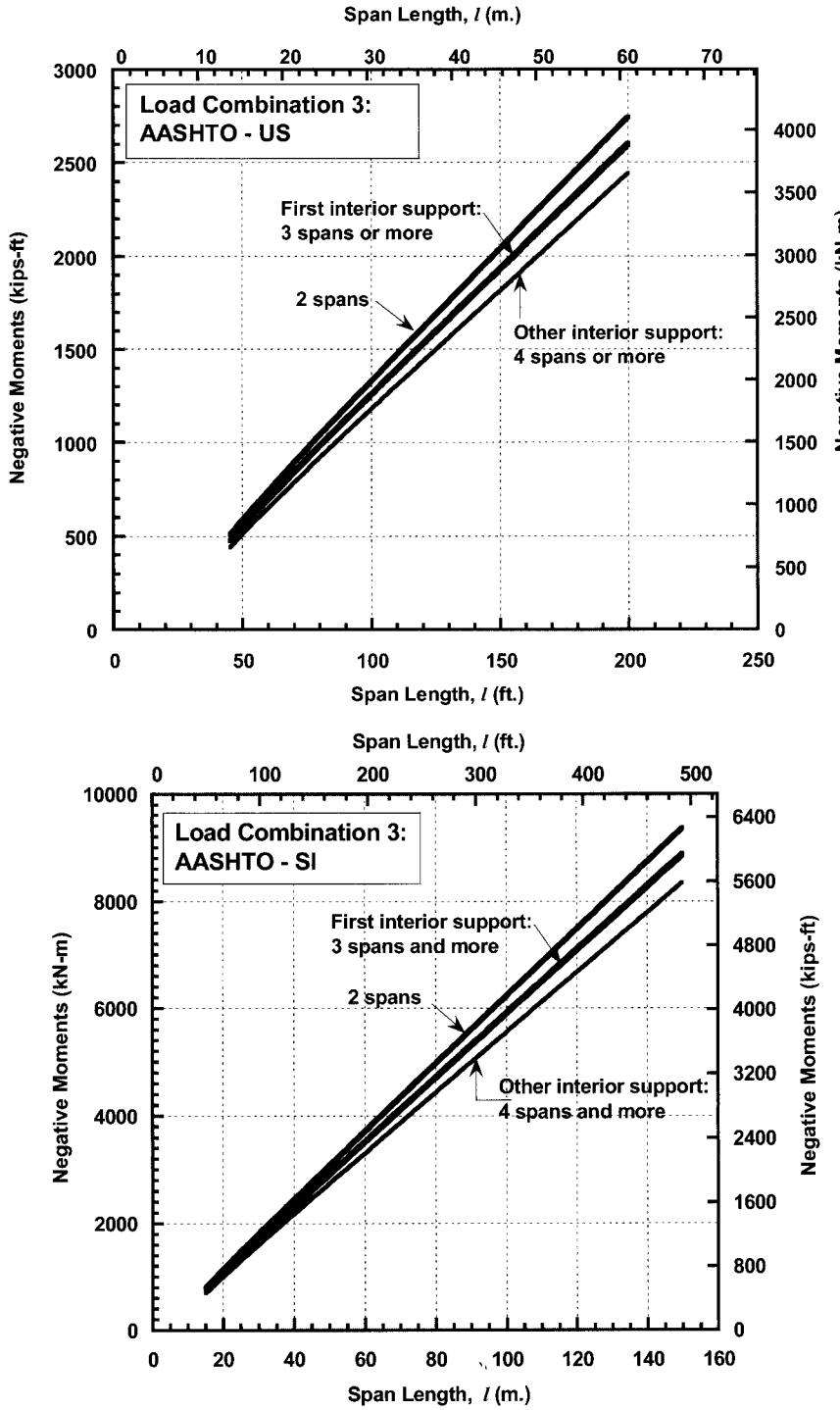

Figure 14.34 Design charts to determine negative moments due to the two trucks specified in live load Combination 3 for one lane at interior supports of continuous beams with equal spans.

$$\begin{cases} M^{-}_{Lane} = -w\dfrac{l^2}{8} & \text{for the interior support in two equal spans} \\ M^{-}_{Lane} = -7w\dfrac{l^2}{60} & \text{for interior supports in three equal spans} \\ M^{-}_{Lane} = -27w\dfrac{l^2}{224} & \text{for the first interior support in 4 equal spans} \\ M^{-}_{Lane} = -3w\dfrac{l^2}{28} & \text{for other interior supports in 4 equal spans} \end{cases} \tag{14.12}$$

Note that for load Combination 3, 90% of the two trucks effect augmented by impact is added to 90% of the uniform load effect. An example is given in Section 14.12.

14.9 MOMENTS AND SHEARS IN TYPICAL GIRDERS

Moments and shears at any given section are first determined assuming a fully loaded lane for one of the load combinations (Combinations 1, 2 or 3) whichever controls. Then these effects are multiplied by the appropriate distribution factor to determine the moment and shear in a particular beam, girder, or strip of slab.

If the effect of impact is considered and if the distribution factors are taken from AASHTO, the following expressions can be derived for any section x:

$$\boxed{M_{LL+IM}(x) = DF_M \times [M_{Lane}(x)]_{LL+IM}} \tag{14.13}$$

$$\boxed{V_{LL+IM}(x) = DF_V \times [V_{Lane}(x)]_{LL+IM}} \tag{14.14}$$

where:

$M_{LL+IM}(x)$ = beam maximum moment at x due to live load plus impact

$V_{LL+IM}(x)$ = beam maximum shear at x due to live load plus impact

IM = impact effect on live load that is essentially 33% of the effect of truck or tandem vehicle (Eq. (14.3))

LL = live load effect

DF_M = load distribution factor for moment; different values are specified for interior or exterior beams (see Table 14.7)

DF_V = load distribution factor for shear; different values are specified for interior and exterior beams (see Table 14.8)

$M_{Lane(x)}$ = maximum moment at x due to a fully loaded lane according to live load Combinations 1, 2, or 3 whichever governs

$[M_{Lane(x)}]_{LL+IM}$ = $M_{Lane(x)}$ augmented by effect of impact which applies only to the truck or tandem vehicle

$V_{Lane(x)}$ = maximum shear at x due to a fully loaded lane according to live load Combinations 1, 2, or 3 whichever governs

$[V_{Lane(x)}]_{LL+IM}$ = $V_{Lane(x)}$ augmented by effect of impact

x = location of section considered with respect to left support; the x is ignored to simplify notation if the section location is clear from the problem at hand

Tables 14.7 and 14.8 summarize the AASHTO distribution factors for moments and shears in interior beams. These factors account for the multiple presence effects in adjacently loaded lanes (see Examples 14.10.1). If the distribution factors are not taken from the AASHTO tables but derived from analysis, then Eqs. (14.13) and (14.14) must also include a reduction factor for moments and shears due to multiple presence effect. In such a case the equations become:

$$M_{LL+IM}(x) = DF_M \times [M_{Lane}(x)]_{LL+IM} \times \lambda_p \tag{14.15}$$

$$V_{LL+IM}(x) = DF_V \times [V_{Lane}(x)]_{LL+IM} \times \lambda_p \tag{14.16}$$

in which λ_p is the multiple presence factor (Section 14.6.6).

14.10 EXAMPLE: COMPOSITE BRIDGE WITH CAST-IN-PLACE REINFORCED CONCRETE SLAB ON TOP OF PRESTRESSED I-GIRDERS

This example provides a reasonably complete design for the simply supported prestressed concrete bridge beams of a very common type of composite bridge deck. After a preliminary design, an AASHTO type IV beam was selected (Fig. 14.6) for which, I_g = 260730 in^4. The example is continued in Section 14.15.1 where the cast-in-place slab is made continuous over the interior support of a two-span bridge.

14.10.1 Live Load Moments and Shears at Critical Sections

Determine the maximum moments and shears due to live load plus impact for a typical interior beam of the composite bridge deck described in Fig. 14.35. The following information is given: span l = 80 ft, beam spacing S = 6.75 ft.

For the precast: f'_C = 7000 psi and E_C = 5072 ksi. For the slab f'_C = 5000 psi and E_C = 4287 ksi. Thus the modular ratio between slab and beam is n_C = 4287/5072 = 0.845.

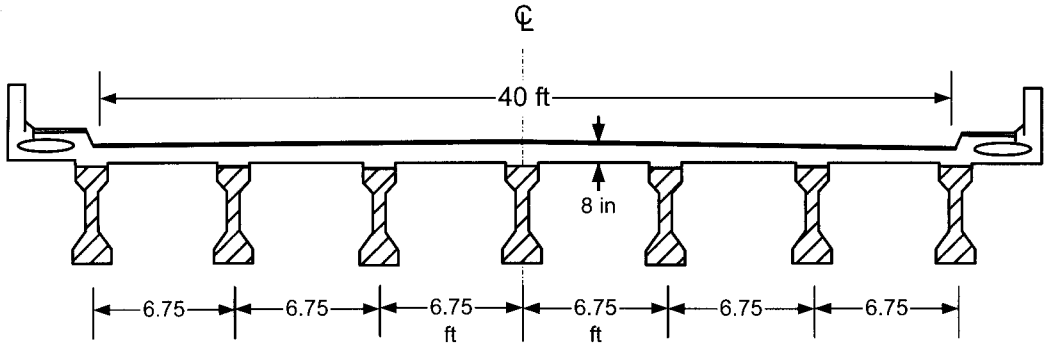

Figure 14.35 Composite bridge deck section.

1. Moment. Calculate the maximum moment in span. To account for impact effect a factor (1 + I) = (1 + 0.33) is used but it does not apply to uniform lane load. The equations in Table 14.10 are used.

- *Combination 1* (HS20 truck + uniform lane load):

$$x_1 = \frac{336}{144 + 0.64 \times 80} = 1.72 \text{ ft}$$

$$M_{truck} = 16 \times \left(\frac{9}{8} \times 80 + \frac{1.72}{80}(21 - 4.5 \times 1.72) - 17.5 \right) = 1164.56 \text{ kips-ft}$$

$$M_{unif-lane} = 0.08 \times \left(80^2 - 4 \times 1.72^2\right) = 511.05 \text{ kips-ft}$$

$$(M_{max})_1 = 1.33 \times 1164.56 + 511.05 = 2059.91 \text{ kips-ft}$$

- *Combination 2* (tandem + uniform lane load):

$$x_2 = \frac{100}{100 + 0.64 \times 80} = 0.661 \text{ ft}$$

$$M_{tandem} = 50 \times \left(\frac{80}{4} + \frac{0.661}{80}(2 - 0.661) - 1 \right) = 950.55 \text{ kips-ft}$$

$$M_{unif-lane} = 0.08 \times \left(80^2 - 4 \times 0.661^2\right) = 511.86 \text{ kips-ft}$$

$$(M_{max})_2 = 1.33 \times 950.55 + 511.86 = 1776.09 \text{ kips-ft}$$

Hence *Combination 1* governs, and the maximum moment due to live load plus impact for one loaded lane is given by:

$$(M_{Lane})_{max} = 2059.91 \text{ kips-ft}$$

Note that using the design chart of Fig. 14.33a leads to:

$$(M_{Lane})_{max} = \frac{Q_m x(l - x)}{l} = \frac{103 \times 40 \times 40}{80} = 2060 \text{ kips-ft} \quad \text{(similar to the above value)}$$

According to Table 14.7 (cross-section type (k)), the distribution factor for moment is given by:

- One design lane loaded:

$$DF_M = 0.06 + \left(\frac{S}{14}\right)^{0.4}\left(\frac{S}{L}\right)^{0.3}\left(\frac{K_g}{12Lt_s^3}\right)^{0.1}$$

where K_g can be calculated from Eq. (14.4) in which $n = 1/n_c = E_{beam}/E_{slab} = 1.183$:

$$K_g = n(I + Ae_g^2) = 1.183(260{,}730 + 789 \times 33.27^2) = 1{,}341{,}603 \text{ in}^4$$

Thus:

$$DF_M = 0.06 + \left(\frac{S}{14}\right)^{0.4}\left(\frac{S}{L}\right)^{0.3}\left(\frac{K_g}{12Lt_s^3}\right)^{0.1}$$

$$DF_M = 0.06 + \left(\frac{6.75}{14}\right)^{0.4}\left(\frac{6.75}{80}\right)^{0.3}\left(\frac{1341603}{12 \times 80 \times 8^3}\right)^{0.1} = 0.453$$

- Two or more design lanes loaded:

$$DF_M = 0.075 + \left(\frac{S}{9.5}\right)^{0.6}\left(\frac{S}{L}\right)^{0.2}\left(\frac{K_g}{12Lt_s^3}\right)^{0.1}$$

$$DF_M = 0.075 + \left(\frac{6.75}{9.5}\right)^{0.6}\left(\frac{6.75}{80}\right)^{0.2}\left(\frac{1341603}{12 \times 80 \times 8^3}\right)^{0.1} = 0.621$$

Therefore, use a distribution factor $DF_M = 0.621$

Note that for preliminary design, we could have assumed that the term $\left(\frac{K_g}{12Lt_s^3}\right)^{0.1} = 1$, while above it is equal to 1.1. However, the approximation would have led to a smaller value of DF_M. Also note that if the approximate heuristic approach to the distribution factor was used (Eq. 14.6), the value obtained would be: $DF_M = S/11 = 6.75/11 = 0.614$, that is quite close to the above result.

Hence the design live load moment plus impact at the critical section for the beam considered is given by:

$$M_{LL+IM} = DF_M \times (M_{Lane})_{max} = 0.621 \times 2059.91 = 1279.21 \text{ kips-ft}$$

2. Shear. Calculate maximum shear force at the first critical section located a distance $x = 3$ ft from the center of the support:

$$V_{truck} = 16\left[4.5\left(1 - \frac{3}{80}\right) - \frac{42}{80}\right] = 60.90 \text{ kips}$$

$$V_{unif-lane} = 0.64\left(\frac{80}{2} - 3\right) = 23.68 \text{ kips}$$

$$(V_{Lane})_{max} = 1.33 \times 60.90 + 23.68 = 104.68 \text{ kips}$$

where $(V_{Lane})_{max}$ is the maximum shear due to live load and impact for a full lane width of bridge.

Note that using the design chart of Fig. 14.33b leads to:

$$(V_{Lane})_{max} = \frac{Q_v(l - x)}{l} = \frac{108 \times 77}{80} = 104 \text{ kips} \quad \text{(similar to the above value)}$$

According to Table 14.8 (cross section type (k)), the distribution factor for shear is given by:

- One design lane loaded:

$$DF_V = 0.36 + \frac{S}{25} = 0.36 + \frac{6.75}{25} = 0.63$$

- Two or more design lanes loaded:

$$DF_V = 0.2 + \frac{S}{12} - \left(\frac{S}{35}\right)^{2.0} = 0.2 + \frac{6.75}{12} - \left(\frac{6.75}{35}\right)^{2.0} = 0.725$$

Therefore, the distribution factor for shear for one beam: $DF_V = 0.725$
Thus:

$$V_{LL+IM} = DF_V \times (V_{Lane})_{max} = 0.725 \times 104.68 = 75.89 \text{ kips}$$

The full design of this bridge is continued in the next section.

14.10.2 Detailed Design of Prestressed I Beams

A simply supported typical interior bridge beam (from previous example) with a span of 80 ft (24.4 m) is considered. It consists of a precast pretensioned AASHTO type IV girder and an 8-in (20-cm) thick cast-in-place slab. Unshored construction is assumed. The spacing S, center to center, between beams is 6.75 ft (2.06 m). Cross-sectional dimensions are given in Fig. 14.36a. The precast beam and the slab are made of normal weight concrete with γ_C = 150 pcf (23.6 kN/m^3). The mechanical properties of the precast beam are: f'_c = 7000 psi; f'_{ci} = 5000 psi; E_c = 5072 ksi; E_{ci} = 4287 ksi.

For the slab we have f'_c = 5000 psi and E_c = 4287 ksi. Thus the modular ratio between slab and beam is n_C = 4287/5072 = 0.845. The prestressing tendons consist of half-inch-diameter strands with area per strand equal to 0.153 in^2 and strength f_{pu} = 270 ksi. Total prestress losses after transfer of 30 ksi are assumed, leading to an effective prestress f_{pe} = 150 ksi. The initial stress after transfer, f_{pi}, is estimated at 180 ksi giving η = 150/180 = 0.83.

Allowable stresses for the precast beam are as follows (Table 14.3):

$\bar{\sigma}_{ti} = -0.22\sqrt{f'_{ci}} = -0.22\sqrt{5} = -0.492$ ksi = −492 psi; $\bar{\sigma}_{ci} = 0.60 f'_{ci} = 3000$ psi;

$\bar{\sigma}_{ts} = -0.0948\sqrt{f'_c} = -251$ psi; $\bar{\sigma}_{cs} = 0.45 f'_c = 3150$ psi, or $0.60 f'_c = 4200$ psi, or $0.40 f'_c = 2800$ psi

For the cast-in-place slab we have $\bar{\sigma}_{cs} = 0.45 f'_c = 2250$ psi. It is assumed that the interface surface between the precast beam and the cast-in-place slab is intentionally roughened for proper shear transfer.

The weight of the precast beam is 0.822 klf and the weight of the slab is 0.675 klf. In addition, the slab supports an asphalt topping equivalent to a superimposed dead load of 0.25 klf on the composite beam. The live load is to be determined as per AASHTO-LRFD specifications (as in Section 14.10.1). A summary of corresponding bending moments at midspan and shear forces and moments at $h_C/2$ from the face of the support is given in Table 14.11. As h_C = 62 in and a 10-in-wide bearing pad is used at the support (Fig. 14.36*b*), the first critical section is at (62 + 10)/2 = 36 in or 3 ft from the center of the support

The reader may want to refer to Sec. 14.10.1 to check how the live load values given in Table 14.9 were obtained. If a detailed design is to be pursued, Table 14.11 can be extended to cover every twentieth of the span.

In a preliminary design a smaller precast girder (AASHTO type III, Fig. 14.6) was tried but led to an almost inexistent feasibility domain for F_i and e_O. Thus a type IV girder was selected and should be largely satisfactory. In the following rapid design steps, the approach prescribed by AASHTO-LRFD is followed.

a. Composite section properties

The effective width has to be determined first, that is:

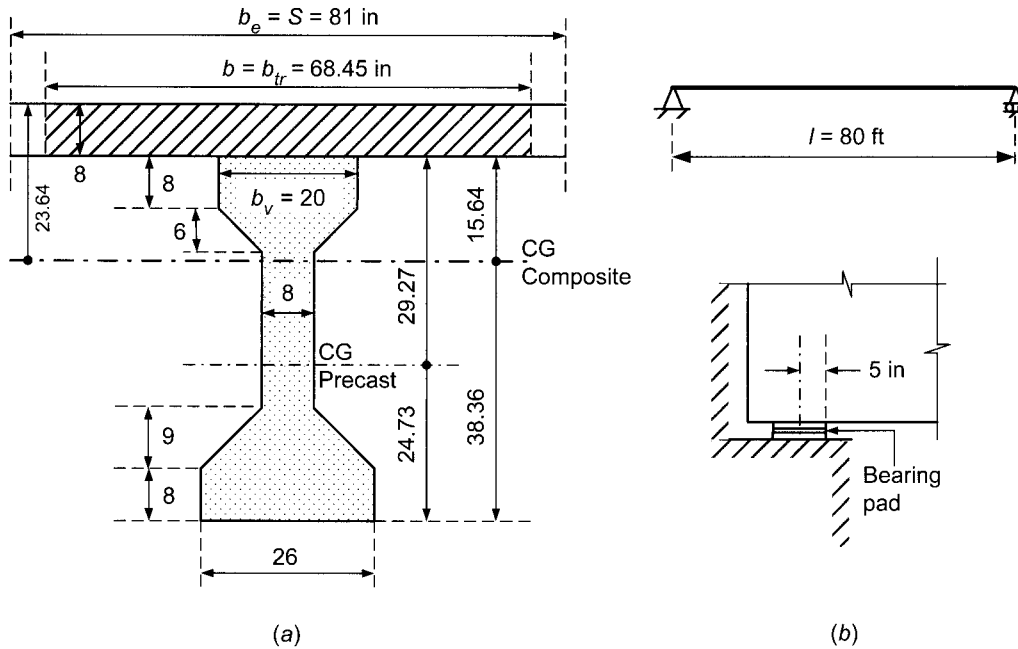

Figure 14.36 Example beam. (*a*) Cross section. (*b*) Bearing pad position at supports.

Table 14.11 Bending moments and shear forces for example beam.

Loading	Moments at midspan, kips-ft	Shear forces at first critical section, kips	Moments at first critical shear section, kips-ft	Resisting section
Precast beam	657.5	30.40	94.941	
Cast-on-place slab	540.0	24.98	77.963	Precast section
	$M_p = 1197.5$	55.38	172.904	
Asphalt	200	9.25	28.875	
Live load + impact	1279.21	75.89	196.80	
	$M_c = 1479.21$	85.14	225.675	Composite section
Service III: [0.8(live load + impact)]	1023.37			
	$M_c = 1223.37$			

$$b_e \le \begin{cases} b_v + 12h_f = 116 \text{ in} \\ S = 81 \\ l/4 = 240 \text{ in} \end{cases}$$

Thus:

$$b_e = 81 \text{ in}$$

and

$$b_{tr} = b_e n_c = 81 \times 0.845 = 68.45 \text{ in}$$

The area of the composite section with transformed slab is given by:

$$A_{cc} = A_c + b_{tr} h_f = 789 + 68.45 \times 8 = 1336.6 \text{ in}^2$$

The other geometric properties of the precast beam and the composite beam with transformed slab are summarized in Table 14.12.

Table 14.12 Properties of precast and composite sections for example beam.

Precast beam	Composite beam (with transformed slab)
$A_c = 789 \text{ in}^2$	$A_{cc} = 1336.6 \text{ in}^2$
$y_t = 29.27 \text{ in}$	$y_{tc} = 23.64 \text{ in}; y'_{tc} = 15.64 \text{ in}$
$y_b = 24.73 \text{ in}$	$y_{bc} = 38.36 \text{ in}$
$h = 54 \text{ in}$	$h_c = 62 \text{ in}$
$I_g = 260{,}730 \text{ in}^4$	$I_{gc} = 621{,}454 \text{ in}^4$
$Z_t = 8907 \text{ in}^3$	$Z_{tc} = 26{,}287 \text{ in}^3$
$Z_b = 10{,}540 \text{ in}^3$	$Z_{bc} = 16{,}200 \text{ in}^3$
$k_t = -13.36 \text{ in}$	$Z'_{tc} = 39{,}733 \text{ in}^3$
$k_b = 11.29 \text{ in}$	$h_f = 8 \text{ in}$
$b_\upsilon = 20 \text{ in}$	$b_e = 81 \text{ in}$
$b_w = 8 \text{ in}$	$b = b_{tr} = 68.45 \text{ in}$

b. Prestressing force

Let us determine the required prestressing force and check stresses at midspan. As it is very likely that a feasible domain exists, stress condition IV at equality will be used to determine the minimum value of F assuming an eccentricity e_o equal to the maximum practical eccentricity $(e_o)_{mp}$ = 20.16 in. Note that the value of $(e_o)_{mp}$ was arrived at after a first computational trial. According to AASHTO-LRFD, for prestressed concrete, Service III limit state should be used. Using Table 9.2, way 3, we have:

$$F = \eta F_i = \frac{(M_p + M_c Z_b / Z_{bc} + \bar{\sigma}_{ts} Z_b)}{e_o - k_t}$$

$$= \frac{1197.5 \times 12{,}000 + 1223.37 \times 12{,}000 \times 10{,}540/16{,}200 - 251 \times 10{,}540}{20.16 + 13.36}$$

$$F = 634{,}954 \text{ lb} = 634.95 \text{ kips}$$

Each strand can carry a final force of 0.153 × 150 = 22.95 kips. The minimum required number of strands is:

$$N = \frac{634.954}{22.95} = 27.67$$

It is rounded off to 28 strands, thus leading to:

$$\begin{cases} F = 22.95 \times 28 = 642.60 \text{ kips} \\ N = 28 \text{ strands} \\ F_i = F/\eta = F/0.83 = 774.22 \text{ kips} \\ e_o = 20.16 \text{ in at midspan} \end{cases}$$

Details of strand layout for the midspan and support sections are given in Fig. 14.37. The steel profile is selected to have two draping points each at 30 ft from the support. Twelve strands are draped, bringing the eccentricity of the prestressing force at the supports to 3.87 in.

The reader may want to check that the extreme fiber stresses at midspan for the above values of prestressing force and eccentricity are as follows (use Table 9.2, way 1):

- For the precast beam:

  $\sigma_{ti} = 114.89 \text{ psi} > \bar{\sigma}_{ti} = -492 \text{ psi}$

  $\sigma_{ci} = 1713.41 \text{ psi} < \bar{\sigma}_{ci} = 3000 \text{ psi}$

  $\sigma_{cs} = 1342.86 \text{ psi} < \bar{\sigma}_{cs} = 4200 \text{ or } 3150 \text{ or } 2800 \text{ psi}$ O.K.

  $\sigma_{ts} = -225.93 \text{ psi} > \bar{\sigma}_{ts} = -251 \text{ psi}$

- For the cast-in-place slab:

$$\sigma_{cs} = \frac{M_c}{Z_{tc}} \frac{(E_c)_{CIPC}}{(E_c)_{PPC}} = \frac{1223.09 \times 12000}{26287} 0.845 = 472 psi \le (\bar{\sigma}_{cs})_{slab} = 1800 \text{ psi} \quad \text{O.K.}$$

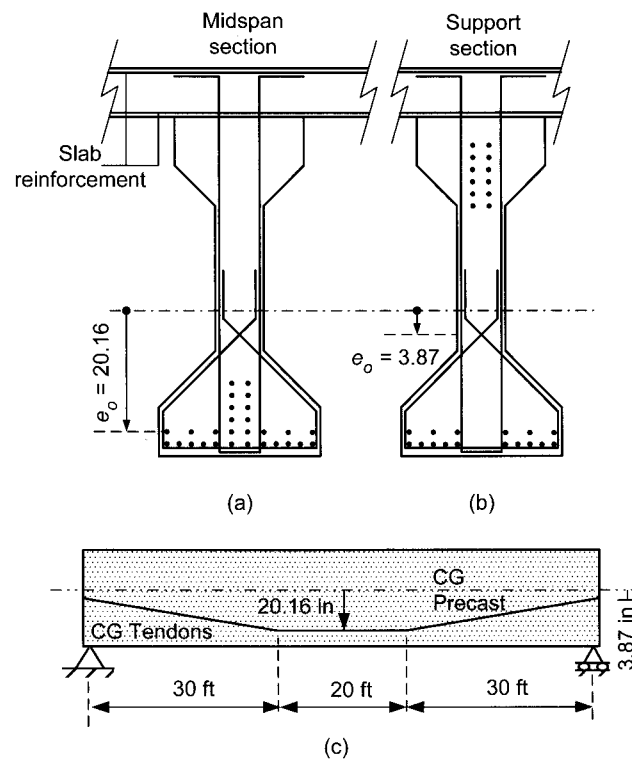

Figure 14.37 (*a*) Strand lay-out at midspan. (*b*) Strand layout at support. (*c*) Longitudinal profile of centroid of strands.

It can be seen from the stresses other than σ_{ts} that the beam has still a lot of capacity and can be used for longer spans or heavier loads.

c. Feasibility domain

Although the approach followed above is sufficient, let us build the feasibility domain to illustrate its use for a composite bridge beam and also show that it leads to the same solution. From the equations of Table 9.2:

Condition I: $e_o \le k_b + (1/F_i)(M_{GP} - \bar{\sigma}_{ti} Z_t)$

$$e_o \le 11.29 + \frac{(657.5 \times 12000 + 492 \times 8907)}{F_i}$$

$$e_o \le 11.29 + \frac{12272244}{F_i}$$

Condition II: $e_o \le k_t + (1/F_i)(M_{GP} + \bar{\sigma}_{ci} Z_b)$

$$e_o \le -13.36 + \frac{(657.5 \times 12000 + 3000 \times 10540)}{F_i}$$

$$e_o \le -13.36 + \frac{39510000}{F_i}$$

Condition III: $e_o \ge k_b + (\frac{1}{\eta F_i})(M_P + M_c Z_t / Z'_{tc} - \bar{\sigma}_{cs} Z_t)$

For this condition 3 cases are considered as required by AASHTO (Table 14.3):

a) $\bar{\sigma}_{cs} = 0.45 f'_c = 3150$ psi for the sum of effective prestress and permanent load; this is equivalent to assuming zero live load; thus from Table 14.11, we replace M_c in the above equation by 200 kips-ft:

$$e_o \ge 11.29 + \frac{\left(1197.5 \times 12000 + 200 \times 12000 \times \frac{8907}{39733} - 3150 \times 8907\right)}{0.83 F_i}$$

$$(e_o)_a \ge 11.29 - \frac{15{,}843{,}123}{F_i}$$

b) $\bar{\sigma}_{cs} = 0.60 f'_c = 4200$ psi for the sum of effective prestress, permanent loads and live loads; thus from Table 14.11, M_c = 1478.93 kips-ft:

$$e_o \ge 11.29 + \frac{\left(1197.5 \times 12000 + 1478.93 \times 12000 \times \frac{8907}{39733} - 4200 \times 8907\right)}{0.83 F_i}$$

$$(e_o)_b \ge 11.29 - \frac{22{,}965{,}054}{F_i}$$

c) $\bar{\sigma}_{cs} = 0.40 f'_c = 2800$ psi for the full live load and one half the sum of effective prestress and permanent loads; using Table 14.11, $0.5M_p$ = 598.75 kips-ft, and M_c is replaced by (200/2) + 1279.21 = 1379.21 kips-ft; to account for half the effective prestress, the value of F_i is multiplied by 0.5 in the equation of stress Condition III:

$$e_o \ge 11.29 + \frac{\left(598.75 \times 12000 + 1379.21 \times 12000 \times \frac{8907}{39733} - 2800 \times 8907\right)}{0.5 \times (0.83 F_i)}$$

$$(e_o)_c \geq 11.29 - \frac{33,843,042}{F_i}$$

Of the above three cases, case *a* is more severe than cases *b* or *c*. However, neither is critical in the design as shown in Fig. 14.38 where the corresponding line to stress condition III is plotted for case *a*.

Condition IV:

$$e_o \geq k_t + \left(\frac{1}{\eta F_i}\right)(M_P + M_c Z_b / Z_{bc} + \bar{\sigma}_{ts} Z_b)$$

$$e_o \geq -13.36 + \frac{\left(1197.5 \times 12000 + 1223.09 \times 12000 \times \frac{10540}{16200} - 251 \times 10,540\right)}{0.83 F_i}$$

$$e_o \geq -13.36 + \frac{25630869.79}{F_i}$$

Note that the value of M_c for condition IV (Table 14.3) is according to Service III limit state where only 80% of live load plus impact is considered.

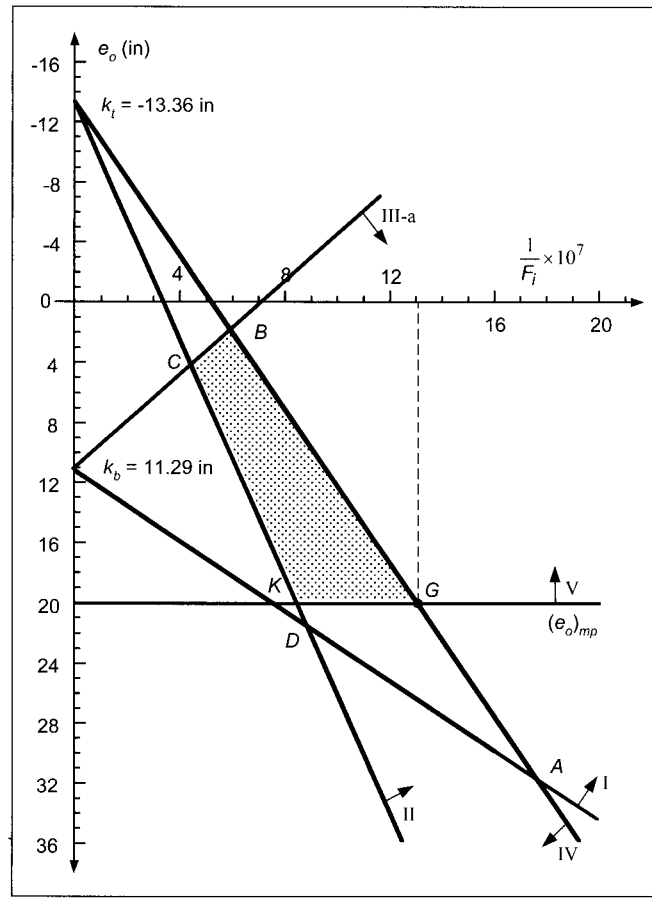

Figure 14.38 Feasibility domain for example beam.

Condition V: $e_o \le (e_o)_{mp} = y_b - (d_c)_{min} = 20.16$ in

The feasibility domain is plotted in Fig. 14.38 and leads to the intersection of IV and V as the optimum solution at point G. The corresponding value of $10^7/F_i$ is about equal to 13. The corresponding value of F_i = $10^7/13$ = 769,230 lbs, which is very close to the numerical solution obtained in the previous section.

d. Ultimate moment requirements

The strength design moment using AASHTO-LRFD is given by Eq. (14.1):

$$\eta[\gamma_{DC}DC + \gamma_{LL}(LL+IM) + \gamma_{DW}DW] \le \phi R_n$$

Assuming $\eta = 0.95$:

$$M_u = 0.95(1.25\times 1197.5 + 1.5\times 200 + 1.75\times 1279.21)$$

$$= 3833.72 \text{ kips-ft}$$

$$c = \frac{A_{ps}f_{pu} + A_s f_y - A'_s f_y}{0.85 f'_c \beta_1 b + kA_{ps}\dfrac{f_{pu}}{d_p}} = \frac{4.284\times 270}{0.85\times 7\times 0.7\times 68.45 + 0.28\times 4.284\dfrac{270}{57.43}} = 3.98 \text{ in}$$

$$f_{ps} = f_{pu}\left(1 - k\frac{c}{d_p}\right) = 270\left(1 - 0.28\frac{3.98}{57.43}\right) = 264.76 \text{ ksi}$$

$$\frac{c}{d_e} = \frac{3.98}{57.43} = 0.0693 < 0.42 \qquad \text{O.K.}$$

$$M_n = A_{ps}f_{ps}\left(d_p - \frac{a}{2}\right) = 4.284\times 264.76\left(57.43 - \frac{0.7\times 3.98}{2}\right)$$

$$= 63556.68 \text{ kips-in} = 5296.39 \text{ kip-ft}$$

$$\phi M_n = 1.0\times 5296.39 = 5296.39 \text{ kips-ft}$$

$$M_u = 3833.72 < \phi M_n = 5296.39 \quad \text{O.K.}$$

Note this will be satisfied even if the largest value of $\eta = 1.05\times 1.05\times 1.05 = 1.16$ is used.

The cracking moment can be computed from Eqs. (9.28) and (9.29) and leads to:

$$\Delta M_{cr} = \frac{Z_{bc}}{Z_b}\left[\eta F_i (e_o - k_t) - M_p\right] - f_r Z_{bc}$$

$$f_r = -7.5\sqrt{f'_c} = -7.5\sqrt{7000} = -627.50 \text{ psi}$$

$$\Delta M_{cr} = \frac{16200}{10540}\left[0.83\times 774220\times(20.16 + 13.36) - 1197.5\times 12000\right] + 627.50\times 16200$$

$$\Delta M_{cr} = 1765.49 \textit{ kips - ft}$$

$$M_{cr} = M_p + \Delta M_{cr} = 1197.5 + 1765.49 = 2962.99 \text{ kips-ft}$$

Hence

$$1.2M_{cr} = 3555.59 \text{ kips-ft}$$

and the ultimate resisting moment, ϕM_n = 5296.39 kips-ft, also satisfies the requirement of being at least 20 percent larger than M_{cr}.

e. Vertical shear

Let us check vertical shear at $h_c/2$ from the face of support (see Section 6.12). Referring to Figs. 14.36*b* and 14.37 and the assumed steel profile, it can be shown that at the section under investigation

$e_o \approx 5.5$ in

At ultimate, $a = 2.77$ in

$b_v = 8$ in

$$d_v = 42.77 - \frac{2.77}{2} = 41.39 \text{ in} > 0.9d_e = 38.49 \text{ in but} < 0.72h = 44.64 \text{ in}$$

Hence, $d_v = 44.64$ in

Compute the vertical component of prestressing and factored loads:

$$V_p = F \times \sin\alpha \approx F \times \tan\alpha = 642.60 \times \frac{20.16 - 3.87}{30 \times 12} = 29.078 \text{ kips}$$

$$V_u = 0.95(1.25 \times 55.38 + 1.5 \times 9.25 + 1.75 \times 75.89) = 205.11 \text{ kips}$$

M_u corresponding to V_u at this section $= 0.95(1.25 \times 172.904 + 1.5 \times 28.875 + 1.75 \times 196.80)$

$= 573.65$ kips-ft

The AASHTO strength design shear is given by:

$$v = \frac{V_u - \phi V_p}{\phi b_v d_v} = \frac{205.11 \times 1000 - 0.9 \times 29.078 \times 1000}{0.9 \times 8 \times 44.64} = 556.74 \text{ psi}$$

$$\frac{v}{f'_c} = 0.0795 < 0.1 \qquad \text{Therefore, } s \le 0.8d_v \le 24 \text{ in}$$

According to AASHTO [5.8.3.4.2], the shear resistance can be determined as follows:

Assume: $f_{po} = 0.70 f_{pu} = 189$ ksi (see also Remarks in Section 6.12.2)

1st iteration. Assume $\theta = 27°$, thus cot $\theta = 1.9626$

Check:

$V_u d_v \ge M_u$?

$205.11 \times 44.64 = 9156.1/12 = 763 > 573.65$ kips-ft

Use: $M_u = V_u d_v = 9156.1$ kips-in

$$\varepsilon_x = \frac{(M_u/d_v) + 0.5N_u + 0.5(V_u - V_p)\cot\theta - A_{ps}f_{po}}{E_s A_s + E_p A_{ps}}$$

$$= \frac{(9156.1/44.64) + 0 + 0.5(205.11 - 29.078)1.9626 - 4.284 \times 189}{0 + 29000 \times 4.284}$$

$$= -0.00348$$

Because ε_x is negative, it shall be computed fromEq. (6.60c):

$$\varepsilon_x = \frac{(M_u/d_v) + 0.5N_u + 0.5(V_u - V_p)\cot\theta - A_{ps}f_{po}}{2(E_c A_{cf} + E_s A_s + E_p A_{ps})}$$

in which $A_{cf} = 441$ in^2 as defined in Fig. 6.22. Thus:

$$\varepsilon_x = \frac{(9156.1/44.64) + 0 + 0.5(205.11 - 29.078)1.9626 - 4.284 \times 189}{2(5072 \times 441 + 0 + 29000 \times 4.284)} = -9.145 \times 10^{-5}$$

From AASHTO Table [5.8.3.4.2-1] reproduced as Table 6.4: for $\frac{v}{f'_c} \le 0.10$, $\theta = 21.4°$

Since θ is different from assumed, a second iteration is needed.

2nd iteration. Assume $\theta = 21.4°$, thus cot $\theta = 2.552$

$$\varepsilon_x = \frac{(M_u/d_v) + 0.5N_u + 0.5V_u \cot\theta - A_{ps}f_{po}}{2(E_{cf}A_c + E_sA_s + E_pA_{ps})}$$

$$= \frac{(9156.1/44.64) + 0 + 0.5(205.11 - 29.078)2.552 - 4.284 \times 189}{2(5072 \times 441 + 0 + 29000 \times 4.284)}$$

$$= -6.58 \times 10^{-5}$$

From AASHTO Table [5.8.3.4.2-1] reproduced in Table 6.4: for $\frac{v}{f'_c} \le 0.10$, $\theta = 21.4°$

→ converged with assumed value. Use $\cot\theta = 2.552$; $\beta = 3.24$

Therefore:

$$V_c = 0.0316 \times \beta \times \sqrt{f'_c} \times b_v \times d_v$$

$$= 0.0316 \times 3.24 \times \sqrt{7} \times 8 \times 44.64 = 96.74 \text{ kips}$$

$$V_s = \frac{V_u}{\phi} - V_c - V_p = \frac{205.11}{0.9} - 96.74 - 29.078 = 102.08 \text{ kips}$$

Using #3 U-shaped stirrups with $A_v = 0.22$ in^2

$$\text{Required } s = \frac{A_v f_y d_v}{V_s}\cot\theta = \frac{0.22 \times 60 \times 44.64 \times 2.554}{102.08} = 14.74 \text{ in}$$

Therefore, provide a #3 U-shaped stirrup at a spacing of 14 in at this section.

Check minimum transverse reinforcement:

$$s \le \frac{A_v f_y}{0.0316\sqrt{f'_c}b_v} = \frac{0.22 \times 60}{0.0316 \times \sqrt{7} \times 8} = 19.74 \text{ in} \qquad \text{OK}$$

Check maximum spacing:

For $V_u < 0.1 f'_c b_v d_v$, $s \le 0.8 d_v$ =35.71 in or 24 in OK

f. Horizontal shear

According to AASHTO [A5.8.4] (refer to Section 9.12), the nominal shear resistance at interface between two concretes cast at different times shall be taken as:

$$V_{nh} = cA_{cv} + \mu(A_{vf}f_y + P_c) \begin{cases} \le 0.2 f'_c A_{cv} \\ \le 5.5 A_{cv} \end{cases}$$

where:

$A_{cv} = 20 \times 1 = 20$ in^2

$A_{vf} = 2 \times 0.11 = 0.22$ in^2; $f_y = 60$ ksi

$c = 0.1$ ksi; $\mu = 1.0$ [A5.8.4.2]

P_c = permanent net compression force normal to interface shear plane

= slab + asphalt

$$P_c = \frac{0.675 + 0.25}{12} = 0.0771 \text{ kip/in}$$

Thus:

$$V_{nh} = 0.1\times 20 + 1.0\left(\frac{0.22}{s}\times 60 + 0.0771\right)$$

$$= 2.0771 + \frac{13.2}{s} \text{ kips per inch length}$$

Compute:

V_{uh} = horizontal shear due to asphalt and LL+IM

$$= \frac{V_u Q}{I_{gc}}$$

$$V_u = 1.5\times 9.25 + 1.75\times 75.89 = 146.68 \text{ kips}$$

$$Q = 68.45\times 8(15.64+4) = 10754.864 \text{ in}^3$$

$$V_{uh} = \frac{146.68\times 10754.864}{621454} = 2.54 \text{ kip/in}$$

The following condition must be satisfied:

$$\eta V_{uh} \le \phi V_{nh} \quad \text{or} \quad \frac{\eta V_{uh}}{\phi} \le V_{nh}$$

$$\frac{\eta V_{uh}}{\phi} = \frac{0.95\times 2.54}{0.9} = 2.68 \text{ kip/in}$$

$$2.68 = 2.0771 + \frac{13.2}{s}$$

$$s = 21.89 \text{ in}$$

As the interface surface is intentionally roughened and all shear reinforcement is extended and anchored in the slab at a spacing of 14 in (as per vertical shear); no additional shear transfer reinforcement is required. Note that the condition for $V_{nh} \le 0.2 f'_c A_{cv}$ and $\le 0.8 A_{cv}$ (in ksi) is also satisfied.

g. Deflections

The steps suggested in Sec. 9.10 are followed; AASHTO does not require computation of long term deflections; however, they are covered here for illustration. The member is not cracked under service loads and thus I_g or I_{gc} will be used throughout. The reader is also referred to Fig. 7.4, which gives the various analytical formulas for deflections. Unshored construction is assumed.

1. Using F_i and E_{ci}, the deflection due to the prestressing force and the self-weight of the precast beam is:

$$(\Delta_i)_G = \frac{5}{384}\frac{w_G l^4}{E_{ci} I_g} = \frac{5}{384}\frac{(822/12)(80\times 12)^4}{4287\times 1000\times 260730} = 0.68 \text{ in}$$

$$(\Delta_i)_{Fi} = -\frac{F_i l^2}{8E_{ci} I_g}\left[e_1 + (e_2 - e_1)\frac{4a^2}{3l^2}\right]$$

$$= -\frac{774220\times(80\times 12)^2}{8\times 4287\times 1000\times 260730}\left[20.16 + (3.87-20.16)\times\frac{4}{3}\times\left(\frac{30}{80}\right)^2\right] = -1.37 \text{ in}$$

Thus:

$$(\Delta_i)_1 = (\Delta_i)_{Fi} + (\Delta_i)_G = -1.37 + 0.68 \simeq -0.69 \text{ in}$$

It is a camber.

2. Additional long-term deflection until addition of slab (using $\lambda_1 \simeq 1$)(see Section 9.10):

$$(\Delta_{add})_2 = \lambda_1(\Delta_i)_1 = -0.69 \text{ in}$$

3. Instantaneous deflection in precast beam due to weight of cast-in-place slab (use E_c):

$$(\Delta_i)_3 = \frac{5}{384}\frac{w_{slab}l^4}{E_c I_g} = \frac{5}{384}\frac{(675/12)(80\times12)^4}{5072\times1000\times260730}$$

$$(\Delta_i)_3 = 0.47 \text{ in}$$

4. Resulting deflection:

$$\Delta_4 = (\Delta_i)_1 + (\Delta_{add})_2 + (\Delta_i)_3$$
$$\Delta_4 = -0.69 - 0.69 + 0.47$$
$$\Delta_4 = -0.91 \text{ in}$$

5. Instantaneous deflection in composite beam due to asphalt weight:

$$(\Delta_i)_5 = \frac{5}{384}\frac{w_{asphalt}l^4}{E_c I_{gc}} = \frac{5}{384}\frac{(250/12)(80\times12)^4}{5072\times1000\times621454}$$

$$(\Delta_i)_5 = 0.073 \text{ in}$$

6. Resulting deflection in composite:

$$\Delta_6 = \Delta_4 + (\Delta_i)_5$$
$$\Delta_6 = -0.89 + 0.073$$
$$\Delta_6 = -0.837 \text{ in}$$

7. Additional long-term deflection in the composite beam (use $\lambda_2 \simeq 1.2$):

$$(\Delta_{add})_7 = \lambda_2\Delta_6 = -1.00 \text{ in}$$

Thus the total long-term deflection under sustained loads will be a camber of:

$$(-0.837 - 1.00) \simeq -1.837 \text{ in}$$

Figure 14.39 illustrates the variation of deflection with time.

h. Check deflection criteria

In order to determine the deflection due to live load plus impact, an equivalent uniform load is assumed to lead to the same moment as that of the live load plus impact. Thus:

$$w_e = \frac{8\times1279.21}{80^2} = 1.599 \text{ klf} = 1599 \text{ plf}$$

The corresponding deflection will be:

$$\Delta_{LL+I} = \frac{5}{384}\frac{w_e l^4}{E_c I_{gc}} = \frac{5}{384}\frac{(1599/12)(80\times12)^4}{5072\times1000\times621454} = 0.468 \text{ in}$$

The AASHTO code instantaneous deflection due to service live load (vehicular load) plus impact:

$$\Delta_{LL+I} = 0.468 \leq \frac{L}{800} = \frac{80 \times 12}{800} = 1.2 \text{ in} \qquad \text{O.K.}$$

Thus the deflection limit state is satisfactory. Since the value of deflection obtained is much smaller than the limit allowed, the above approximation is acceptable.

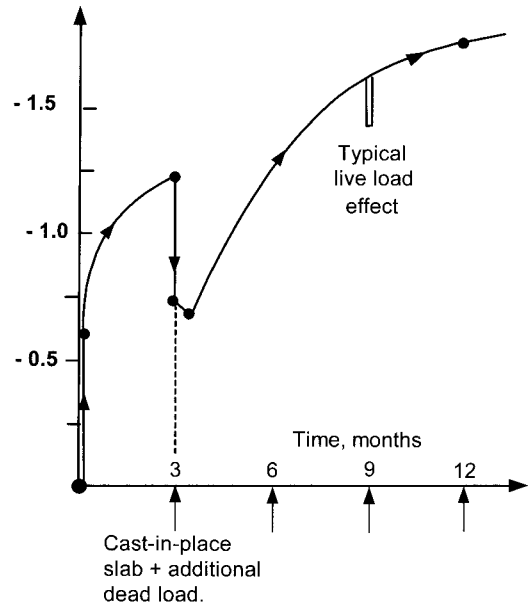

Figure 14.39 Typical variation of deflection versus time for example beam.

i. Reinforcement for the cast-in-place slab

The empirical method described in Section 14.13.5 is selected here. Four layers of reinforcement are used, two at the top (one in each direction) and two at the bottom (one in each direction). Reinforcing steel is grade 60. The minimum amount of reinforcement in each bottom layer is 0.27 in^2 per foot, and in each top layer, 0.18 in^2 per foot. This can be achieved by using a grid of No. 5 reinforcing bars (each of area 0.31 in^2) at 12 in spacing in each bottom layer, and a grid of No. 5 reinforcing bars at 18 in spacing in each top layer (Fig. 14.40).

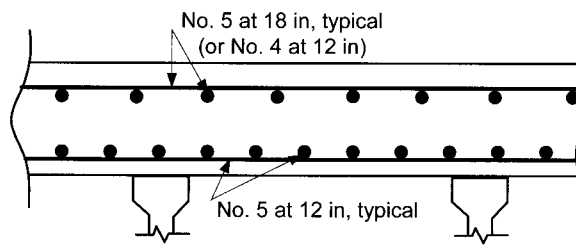

Figure 14.40 Typical reinforcement of the cast-in-place slab.

In Section 14.15, a two equal spans bridge is considered, and the slab is assumed to be continuous over the interior support, that is, to provide continuity for live load and impact. Additional reinforcement will be needed in the negative moment region at the interior support.

14.11 EXAMPLE: BRIDGE DECK WITH ADJACENT PRECAST PRETENSIONED BOX BEAMS

A simply supported two-lanes bridge deck spanning 50 ft is to be designed using precast pretensioned beams placed adjacent to each other (Fig. 14.41) (see also the example of Section 14.14). The following information is provided:

Normal weight concrete: $\gamma_c = 150$ pcf; $f'_c = 6000$ psi; $f'_{ci} = 4500$ psi; $E_c = 4696$ ksi;

$\bar{\sigma}_{ti} = -201$ psi; $\bar{\sigma}_{ci} = 2700$ psi; $\bar{\sigma}_{ts} = -232$ psi;

$\bar{\sigma}_{cs} = 0.60 f'_c = 3600$ psi, or $0.45 f'_c = 2700$ psi, or $0.40 f'_c = 2400$ psi

$f_{pu} = 270$ ksi; $f_{pe} = 150$ ksi; $\eta = F / F_i = 0.80$; $(e_o)_{mp} = h/2 - 3$ in

A wearing surface weighing 25 psf is to be placed on top of the deck.

According to AASHTO Table [2.5.2.6.3-1] and Table 14.14, the suggested minimum depth of adjacent box beams is:

$h = 0.030L = 0.030 \times 50 \times 12 = 18$ in

Referring to Fig 14.5, where standard precast prestressed box beams are described, we find that the smallest beam available is BI-36 with a depth h = 27 in; it weighs 0.584 klf, and is 3 ft wide. Its geometric properties are: A_c = 561 in^2, y_b = 13.35 in, y_t = 13.65 in, Z_b = 3770 in^3, Z_t = 3687 in^3, k_t = -6.72 in, k_b = 6.57 in, I_g = 50,334 in^4. Ten such beams can be placed adjacent to each other, totaling 30 ft width, and can form the bridge deck. Let us check for a typical interior beam if the design is acceptable.

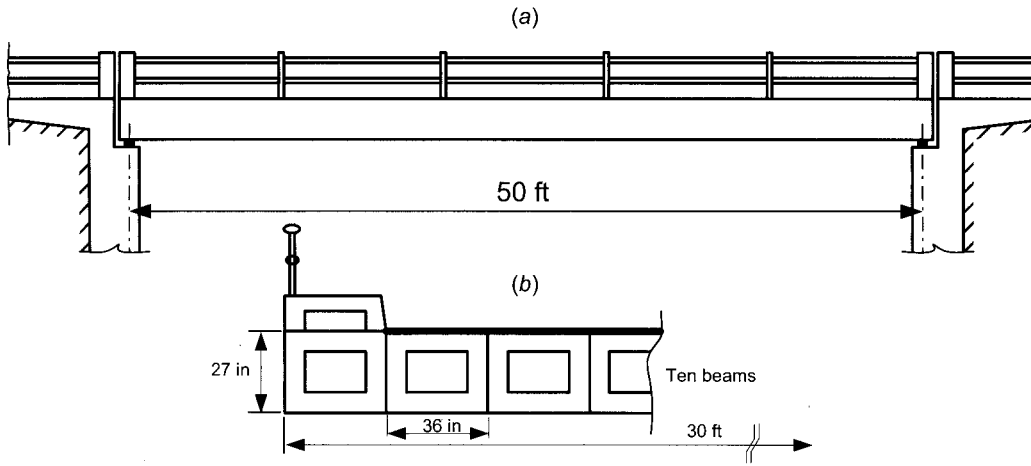

Figure 14.41 Longitudinal deck profile and transverse section with adjacent precast prestressed beams.

a. Live load moment

Determine first the maximum moment in span due to live load plus impact for a full loading lane. To account for impact assume a factor =1.33, not applied to uniform lane load. Using the equations of Table 14.10:

- *Case* I (truck + uniform lane):

$$x_1 = \frac{336}{144 + 0.64 \times 50} = 1.909 \text{ ft}$$

$$M_{truck} = 16 \times \left(\frac{9}{8} \times 50 + \frac{1.909}{50}(21 - 4.5 \times 1.909) - 17.5 \right) = 627.58 \text{ kips-ft}$$

$$M_{unif-lane} = 0.08 \times \left(50^2 - 4 \times 1.909^2\right) = 198.83 \text{ kips-ft}$$

$$M_{max} = 1.33 \times 627.58 + 198.83 = 1033.51 \text{ kips-ft}$$

- *Case* II (tandem + uniform lane):

$$x_2 = \frac{100}{100 + 0.64 \times 50} = 0.7576 \text{ ft}$$

$$M_{truck} = 50 \times \left(\frac{50}{4} + \frac{0.7576}{50}(2 - 0.7576) - 1 \right) = 575.94 \text{ kips-ft}$$

$$M_{unif-lane} = 0.08 \times \left(50^2 - 4 \times 0.7576^2\right) = 199.82 \text{ kips-ft}$$

$$M_{max} = 1.33 \times 575.94 + 199.82 = 965.82 \text{ kips-ft}$$

Case I governs; hence, the maximum moment in span due to live load plus impact for a full loading lane is given by:

$$(M_{Lane})_{LL+IM} = 1033.51 \text{ kips-ft}$$

Note that using the design chart of Fig. 14.33a leads to:

$$(M_{Lane})_{max} = \frac{Q_m x(l-x)}{l} = \frac{82 \times 25 \times 25}{50} = 1025 \text{ kips-ft} \quad \text{(very close to the above value)}$$

From Table 14.7, the distribution factor for moments for box beams is:

$$DF_M = \frac{S}{D}$$

where:

$$C = K(W/L)$$

$$D = 11.5 - N_L + 1.4N_L(1 - 0.2C)^2 \text{ when } C \le 5$$

$$D = 11.5 - N_L \text{ when } C > 5$$

$K = 1$ for box section

Therefore,

$$C = 1(30/50) = 0.6 < 5$$

$$D = 11.5 - 2 + 1.4 \times 2(1 - 0.2 \times 0.6)^2 = 11.668$$

$$DF_M = \frac{S}{D} = \frac{3}{11.668} = 0.257$$

Using the heuristic approach would have led to: $DF_M = S/11 = 0.2727$; not too different from the above result.

Hence, the maximum moment in a typical beam, due to live load plus impact, is given by Eq. (14.7):

$$M_{LL+IM} = DF_M \times (M_{Lane})_{LL+IM} = 0.257 \times 1033.51 = 265.61 \text{ kips-ft}$$

The minimum and maximum design service moments for the beam are given by:

$$M_{min} = M_{DC} = w_{DC}\frac{l^2}{8} = 0.584 \times \frac{50^2}{8} = 182.5 \text{ kips-ft}$$

$$M_{max} = M_{DC} + M_{DW} + 0.8M_{LL+IM} = 182.5 + 3 \times 0.025 \times \frac{50^2}{8} + 0.8 \times 265.61 = 418.43 \text{ kips-ft}$$

where M_{max} is for the Service-III limit state.

b. Prestressing force

Assuming a value of $(e_o)_{mp} = y_b - 3 = 10.35$ in and using stress condition IV of Table 4.2 for $e_o = (e_o)_{mp}$, leads to:

$$F = \frac{M_{max} + \bar{\sigma}_{ts} Z_b}{e_o - k_t}$$

$$= \frac{418.43 \times 12000 - 232 \times 3770}{10.35 + 6.72} = 242{,}912.7 \text{ lb} = 242.9 \text{ kips}$$

Let us assume that the tendons consist of ½ in diameter strands with $f_{pu} = 270$ ksi, $f_{pe} = 145$ ksi, and an area per strand equal 0.153 in^2. We would need:

$$N = \frac{242.9}{0.153 \times 145} = 10.95 \simeq 11 \text{ strands}$$

Thus, the final prestressing force provided is equal to:

$$F = 11 \times 0.153 \times 145 = 244.035 \text{ kips}$$

Assuming a value of $\eta = F/F_i = 0.83$, it can easily be shown that the other three stress conditions of Table 4.2 are largely satisfied.

c. Ultimate moment

The strength design moment using AASHTO-LRFD is given by Eq. (14.1) assuming $\eta = 0.95$:

$$M_u = 0.95(1.25M_G + 1.5M_{SD} + 1.75M_{LL+IM})$$

$$= 0.95(1.25 \times 182.5 + 1.5 \times 23.4375 + 1.75 \times 265.61)$$

$$= 691.69 \text{ kips-ft}$$

Find M_n:

$$c = \frac{A_{ps} f_{pu} + A_s f_y - A'_s f_y}{0.85 f'_c \beta_1 b + k A_{ps} \frac{f_{pu}}{d_p}} = \frac{1.683 \times 270}{0.85 \times 6 \times 0.75 \times 36 + 0.38 \times 1.683 \frac{270}{24}} = 3.14 \text{ in}$$

$$f_{ps} = f_{pu}\left(1 - k\frac{c}{d_p}\right) = 270\left(1 - 0.38\frac{3.14}{24}\right) = 256.57 \text{ ksi}$$

$$\frac{c}{d_e} = \frac{3.1}{24} = 0.1308 < 0.42 \qquad \text{underreinforced section} \qquad \text{OK}$$

$$M_n = A_{ps} f_{ps}\left(d_p - \frac{a}{2}\right) = 1.683 \times 256.57\left(24 - \frac{0.75 \times 3.14}{2}\right) = 9854.92 \text{ kips-in}$$

$$\phi M_n = 1.0 \times 9854.92 = 9854.92 \text{ kips-in or } 821.24 \text{ kips-ft}$$

As M_u is less than ϕM_n, ultimate strength requirements are satisfied. Let us determine the cracking moment, using Eq. (4.41):

$$M_{cr} = F(e_o - k_t) - f_r Z_b$$

$$= 244.035(10.35 + 6.72) + 0.581 \times 3770$$

$$= 6356 \text{ kips-in} = 529.67 \text{ kips-ft}$$

Hence

$$\phi M_n = 821.24 > 1.2M_{cr} = 635.60 \text{ kips-ft} \quad \text{OK}$$

d. Shear

Let us check shear at the first critical section assumed at x = 1.5 ft from the center of support. The shear forces due to weight of the precast beam and asphalt are given by:

$$V_{DC} = 0.584\left(\frac{L}{2} - x\right) = 13.724 \text{ kips}$$

$$V_{DW} = 3 \times 0.025 \times \left(\frac{L}{2} - x\right) = 1.7625 \text{ kips}$$

The shear due to live load for one lane loading is given by:

$$V_{truck} = 16\left[4.5\left(1 - \frac{1.5}{50}\right) - \frac{42}{50}\right] = 56.4 \text{ kips}$$

$$V_{unif-lane} = 0.64\left(\frac{50}{2} - 1.5\right) = 15.04 \text{ kips}$$

Thus:

$$(V_{Lane})_{LL+IM} = 1.33 \times 56.4 + 15.04 = 90.052 \text{ kips}$$

Note that using the design chart of Fig. 14.33b leads to:

$$(V_{Lane})_{max} = \frac{Q_v(l-x)}{l} = \frac{94 \times 48.5}{50} = 91.2 \text{ kips} \quad \text{(similar to the above value)}$$

According to Table 14.8, the distribution factor for shear is given by:

One design lane loaded:

$$\left(\frac{b}{130L}\right)^{0.15}\left(\frac{I}{J}\right)^{0.05} = \left(\frac{36}{130 \times 50}\right)^{0.15}\left(\frac{50334}{89413.56}\right)^{0.05} = 0.446$$

Two or more design lanes loaded:

$$\left(\frac{b}{156}\right)^{0.4}\left(\frac{b}{12L}\right)^{0.1}\left(\frac{I}{J}\right)^{0.05} = \left(\frac{36}{156}\right)^{0.4}\left(\frac{36}{12 \times 50}\right)^{0.1}\left(\frac{50334}{89413.56}\right)^{0.05} = 0.408$$

Therefore, the distribution factor = 0.446

Note that this factor is significantly larger than that obtained from the heuristic approach of Eq. (14.6), that is: $S/11 = 3/11 = 0.27$. The heuristic approach may be unconservative for shear design.

Thus:

$$V_{LL+IM} = 0.446 \times (1.33 \times 56.4 + 15.04) = 40.16 \text{ kips}$$

The AASHTO strength design shear is given by:

$$V_u = \phi(1.25 \times V_{DC} + 1.5 \times V_{DW} + 1.75 \times V_{LL+IM})$$

$$V_u = 0.95(1.25 \times 13.724 + 1.5 \times 1.7625 + 1.75 \times 40.16) = 85.57 \text{ kips}$$

Refer to Section 6.12 of this book and AASHTO LRFD Art. 5.8 for detailed design procedure for shear. The shear resistance can be determined as follows:

$$b_v = 10 \text{ in}$$

$$d_v = 24 - \frac{0.85 \times 2.78}{2} = 22.82 \text{ in} > 0.9d_e = 21.6 \text{ in and } 0.72h = 19.44 \text{ in} \quad \text{O.K.}$$

$$d_v = 22.82 \text{ in}$$

M_u corresponding to V_u at this section = 87.135 kips-ft

$f_{po} \approx f_{pe} = 145$ ksi (see remarks in Section 6.12.2)

Assuming a straight tendon profile: $V_p = 0$. Thus:

$$v = \frac{V_u - \phi V_p}{\phi b_v d_v} = \frac{85.57 - 0}{0.9 \times 10 \times 22.82} = 0.417 \text{ ksi}$$

$$\frac{v}{f'_c} = \frac{0.417}{6} \simeq 0.07$$

1st iteration. Using a first iteration with $\theta = 27°$ it was found that a second iteration is needed with $\theta = 21°$. Thus use $\theta = 21°$ and $\cot\theta = 2.605$. Check first:

$V_u d_v \geq M_u$?

$85.57 \times 22.82 = 1998.35/12 = 166.53 > 87.135$ kips-ft

Use: $M_u = V_u d_v = 1998.35$ kips-in . The following results are then obtained:

$$\varepsilon_x = \frac{(M_u/d_v) + 0.5N_u + 0.5V_u \cot\theta - A_{ps} f_{po}}{E_s A_s + E_{ps} A_{ps}}$$

$$= \frac{(1998.35/22.82) + 0 + 0.5 \times 85.57 \times 2.605 - 1.683 \times 145}{0 + 27000 \times 1.683} = -0.0010$$

Because ε_x is negative, it shall be computed from Eq. (6.60c):

$$\varepsilon_x = \frac{(M_u/d_v) + 0.5N_u + 0.5V_u \cot\theta - A_{ps} f_{po}}{2(E_c A_{cf} + E_s A_s + E_{ps} A_{ps})}$$

$$= \frac{(1998.35/22.82) + 0 + 0.5 \times 85.57 \times 2.605 - 1.683 \times 145}{2(4696 \times 561/2 + 27000 \times 1.683)} = -1.65 \times 10^{-5}$$

where A_{cf} is taken equal to half the beam cross section, since it is symmetrical.

From Table 6.4: for $\frac{v}{f'_c} = 0.07$, $\theta = 21.8° \rightarrow$ assumed converged.

Use $\theta = 21.8°$, $\cot\theta = 2.5$, and $\beta = 3.75$.

Therefore:

$$V_c = 0.0316 \times \beta \times \sqrt{f'_c} \times b_v \times d_v = 0.0316 \times 3.75 \times \sqrt{6} \times 10 \times 22.82 = 66.238 \text{ kips}$$

$$V_s = \frac{V_u}{\phi} - V_c - V_p = \frac{85.57}{0.9} - 66.238 - 0 = 28.84 \text{ kips}$$

Assume #3 U-shaped stirrups with $A_v = 0.22$ in^2

Required spacing: $s = \frac{A_v f_y d_v}{V_s} \cot\theta = \frac{0.22 \times 60 \times 22.82}{28.84} 2.5 = 26.1$ in

Check spacing for minimum transverse reinforcement [Eq. (6.63) and AASHTO Art. 5.8.2.5]:

$$s \leq \frac{A_v f_y}{0.0316\sqrt{f'_c}\, b_v} = \frac{0.22 \times 60}{0.0316 \times \sqrt{6} \times 10} = 17.05 \text{ in}$$

Check minimum spacing [Section 6.12.2 and AASHTO Art. 5.8.2.7]:

For $V_u < 0.1 f'_c b_v d_v$

$V_u = 85.57$ kips $< 0.1 \times 6 \times 10 \times 22.82 = 136.91$ O.K.

$s \leq 0.8 d_v = 18.25$ in or ≤ 24 in O.K.

Hence, spacing should be less than $0.8 d_v = 18.25$ in.

Therefore, to satisfy the above three criteria, a #3 U-shaped stirrup at a spacing of 17 in is provided at this section.

14.12 EXAMPLE: NEGATIVE LIVE LOAD MOMENT IN TWO-SPAN CONTINUOUS BRIDGE DECK

Determine the maximum negative moment due to AASHTO-LRFD loading for the two-equal-span continuous bridge deck shown in Fig 14.42. For negative moments, loading Combination 3 (Fig. 14.30) is considered. In particular, AASHTO-LRFD states that the negative moment over the interior supports (tension on top) is obtained from 90 percent of the load effect of two design trucks spaced a minimum of 50 ft (or 15 m) between the lead axle of one truck and the rear axle of the other truck, and 14 ft (or 4.3 m) between the two 32 kip axles, combined with 90 percent of the effect of the uniform design lane load.

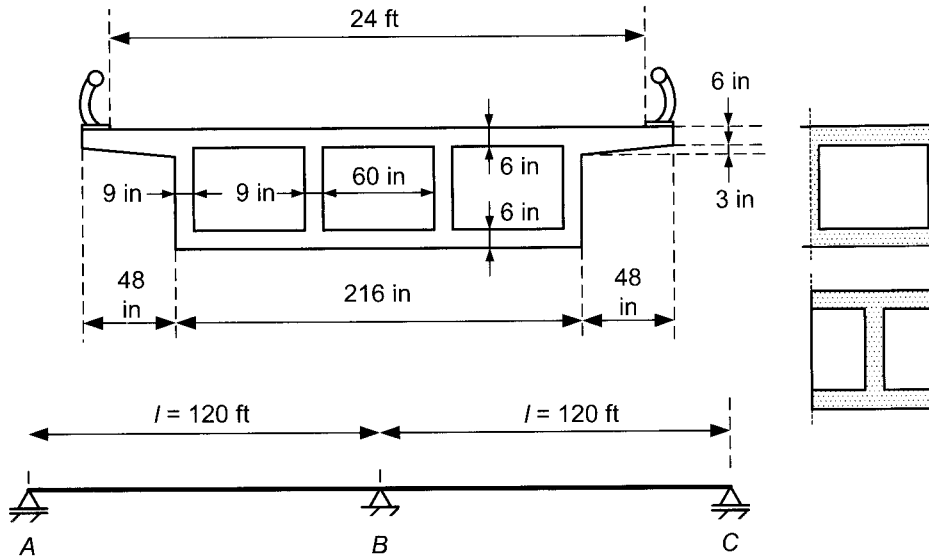

Figure 14.42

A computer program, RISA 3D, was used to compute the maximum moment at the intermediate support, B; using the option "moving loads" of the program, RISA 3D showed that the maximum negative moment occurs when the trucks are positioned as shown in Fig. 14.43a.

From the program the following values of moments were obtained for a tributary lane fully loaded:

$$M_{unif-lane} = 1152 \text{ kips-ft}$$

$$M_{truck} = 1617.69 \text{ kips-ft}$$

According to AASHTO [Art. 3.6.1.3.1]:

$$M_{max}(B) = 0.9\left(1.33M_{truck} + M_{unif-lane}\right)$$

$$= 0.9\left(1.33\times 1617.69 + 1152\right) = 2973.17 \text{ kips-ft} = [M_{Lane}(B)]_{LL+IM}$$

Calculate distribution factors for moment from Table 14.7. For multi-cell concrete box girder, the distribution factor given in Table 14.7 (for case (d)) applies to decks with web spacing not less than 7 ft. However, it will be used next anyway for illustration. Otherwise, the section could be considered made out of four I beams for which the factors in Table 14.7 (case (e)) apply. Results very close to those of case (d) are obtained.

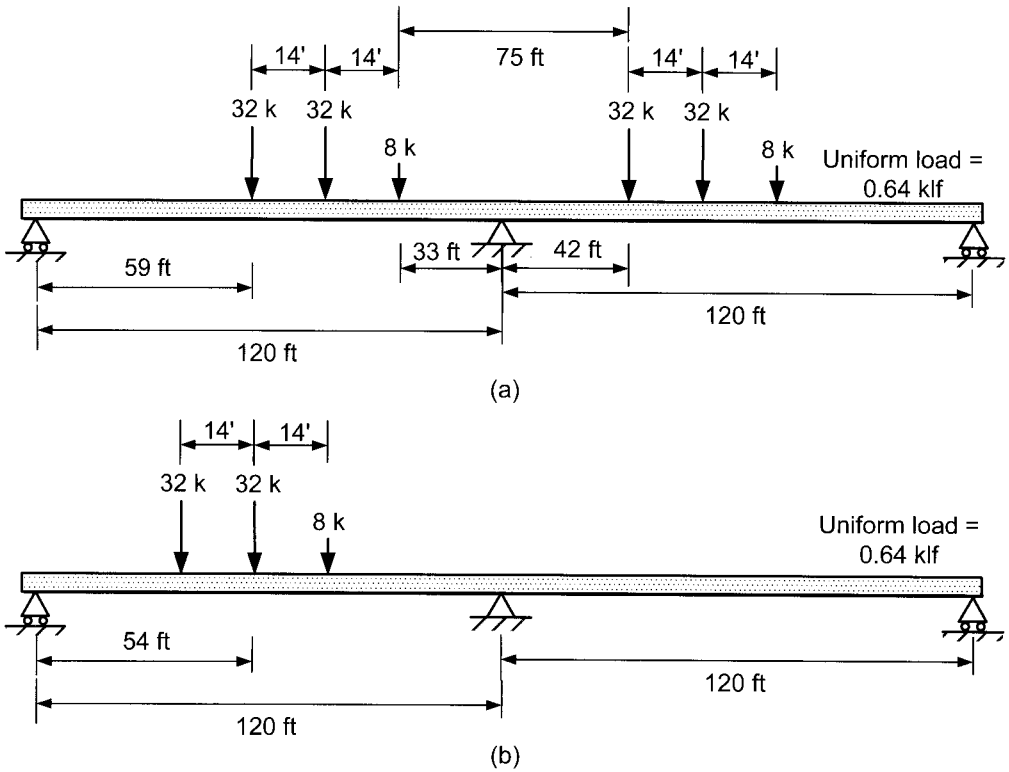

Figure 14.43 Truck position for maximum moment. (*a*) At support. (*b*) In span.

One design lane loaded:

$$DF_M = \left(1.75 + \frac{S}{3.6}\right)\left(\frac{1}{L}\right)^{0.35}\left(\frac{1}{N_c}\right)^{0.45}$$

$$DF_M = \left(1.75 + \frac{5.75}{3.6}\right)\left(\frac{1}{120}\right)^{0.35}\left(\frac{1}{3}\right)^{0.45} = 0.382$$

Two or more design lanes loaded:

$$DF_M = \left(\frac{13}{N_c}\right)^{0.3}\left(\frac{S}{5.8}\right)\left(\frac{1}{L}\right)^{0.25}$$

$$DF_M = \left(\frac{13}{3}\right)^{0.3}\left(\frac{5.75}{5.8}\right)\left(\frac{1}{120}\right)^{0.25} = 0.465$$

Therefore, use a distribution factor $DF_M = 0.465$. This value should be compared to that obtained from the heuristic approach using an approximate distribution factor (Eq. 14.6) $DF_M = S/11 = 0.523$, which would be on the safe side.

The maximum moment at B for the interior box girder due to live load plus impact is (Eq. 14.7):

$$M_{LL+IM} = DF_M \times (M_{Lane}(B))_{LL+IM} = 0.465 \times 2973.17 = 1382.52 \text{ kips-ft}$$

Remarks

Designing the bridge deck shown in Fig. 14.42 can be approached in different ways. One way is to design typical beams such as an interior and an exterior beam, and then put the pieces together. A typical interior beam can be represented by a box (with half a web width on each side) as assumed in this example (Fig. 14.42). However, one can also consider the typical interior beam to be an I-beam such as shown in Fig. 14.44. Both have the same effective flange width and should theoretically lead to the same design. However, the corresponding exterior beams may lead in each case to a slightly different design. Finally, since this bridge deck is monolithic, one can also consider the whole cross section of the deck as a single unit and design that section for two fully loaded lanes. In this case there is no need for a girder distribution factor.

The reader is encouraged to carry out the design for a typical exterior beam (box or I section case) or for the whole bridge deck considered a single beam.

Finally, the reader may want to check that the maximum moment in span is obtained for the truck position shown in Fig. 14.43b, for which $M_{truck} = 1517.02$ kips-ft and $M_{unif-lane} = 622.08$ kips-ft, at a section about 54 ft from the left support.

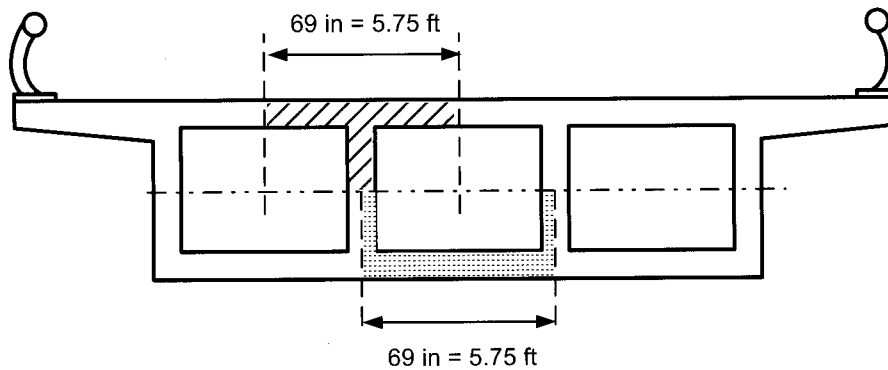

Figure 14.44

Note that the section of the bridge deck shown in Fig. 14.44 is about the same as that shown in Fig. 10.36, except that it has a cantilever slab added on each side. If the dead load moment due to these cantilever slabs is accounted for, and if the depth of the deck is taken equal to 60 in, the maximum service moment at B for this example would not be too different from the maximum service moment at B of Example Sec. 10.15. The weight of a wearing surface may have to be added. The reader may want to refer to the example of Sec. 10.15 to see how the design can be pursued.

14.13 SLABS FOR BRIDGE DECKS AND SOLID SLAB BRIDGES

This section relates primarily to solid concrete slabs used as short span bridges, or concrete slabs cast in place on top of beams (thus forming a composite structure) as in many types of bridge decks where the beams are primarily in the direction of traffic.

14.13.1 Equivalent Strip Width for Slab Type Bridges and Distribution Factor for Slabs

This provision applies to solid slab as well as voided cast-in-place slab bridge decks. The equivalent width of longitudinal strip of slab per loaded design lane (that is, the resisting structural width per lane), for both moment and shear, may be determined as follows:

- For one loaded lane:

$$E = 10.0 + 5.0\sqrt{L_1 W_1} \qquad \text{US units} \qquad (14.17)$$

$$E = 250 + 0.42\sqrt{L_1 W_1} \qquad \text{SI units} \qquad (14.18)$$

- For more than one loaded lane:

$$E = 84.0 + 1.44\sqrt{L_1 W_1} \le \frac{12.0W}{N_L} \qquad \text{US units} \qquad (14.19)$$

$$E = 2100 + 0.12\sqrt{L_1 W_1} \le \frac{W}{N_L} \qquad \text{SI units} \qquad (14.20)$$

where:

E = equivalent width, inches (mm)
L_1 = modified span length in feet (mm), taken equal to the lesser of the actual span or 60 ft (or 18,000 mm)
W_1 = modified edge-to-edge width of bridge in feet, taken as the lesser of the actual width or 60 ft (or 18,000 mm) for multilane loading, or 30 ft (or 9,000 mm) for single-lane loading
W = physical edge-to-edge width of bridge, feet (mm)
N_L = number of design lanes

Note that the equivalent width of strip is essentially the tributary width of slab resisting the load applied over a typical lane loading. The above values of E account for the multiple presence effect.

For all practical purposes the relation between the distribution factor per unit width of slab and E for shear and moment is given by:

$$DF_m = DF_v = \frac{12}{E} \qquad (14.21)$$

where E is in inches. The numerator would be equal 1 if E is in feet. For the SI units where E is in mm, Equation 14.21 becomes:

$$DF_m = DF_v = \frac{300}{E} \tag{14.22}$$

14.13.2 Minimum Depth and Clear Concrete Cover

AASHTO recommends that, unless approved by owner, the depth of a reinforced concrete deck, excluding any provision for grinding, grooving and sacrificial surface, should not be less than 7 in.

For deck surfaces exposed to deicing salts or subjected to tire stud or chain wear, the minimum clear cover of concrete to the reinforcement is 2.5 in (63 mm); for other exterior surface exposure the clear cover is 2 in (50 mm). For decks in coastal areas or cast against earth, the minimum cover is 3 in (75 mm).

Cover for metal ducts for posttensioned tendons shall not be less than that specified for main reinforcing steel or one-half the diameter of the duct, whichever is larger.

14.13.3 Cast-in-Place One-Way Prestressed Slabs

AASHTO recommends that the minimum depth of traditional prestressed concrete slabs with constant depth be taken not less of $0.03L$ for simple spans, and $0.027L$ for continuous spans but not less than 6.5 in (163 mm).

Assuming the primary reinforcement is determined from analysis, the amount of transverse distribution reinforcement (typically non-prestressed reinforcing bars) at the bottom of slabs may be taken as a percentage of the main reinforcement required for positive moment, as follows:

$$p = \frac{100}{\sqrt{L}} \frac{f_{pe}}{60} \leq 50\% \qquad \text{US units} \tag{14.23}$$

$$p = \frac{1750}{\sqrt{L}} \frac{f_{pe}}{410} \leq 50\% \qquad \text{SI units} \tag{14.24}$$

where L is the span in feet (mm) and f_{pe} is the effective prestress in the main reinforcement, in ksi (MPa). Should reinforcing bars or non-stressed prestressing tendons be used, then the fraction $f_{pe}/60$ or $f_{pe}/410$ in the above equations is taken equal to 1. Note that transverse shrinkage and temperature reinforcement are also needed at the top of the slab (see Section 14.13.6).

Furthermore, edge beams shall be provided for all slabs having main reinforcement parallel to traffic. The edge beam may consist of a slab section additionally reinforced, a beam integral with and deeper than the slab, or an integral reinforced section of slab and curb. An example of design of one-way prestressed slab bridge is given in Section 14.14.

14.13.4 Traditional Design of Reinforced Concrete Deck Slabs

The cast-in-place slab of bridge decks where the slab is on top of beams or girders (Fig. 14.45a) can be designed as a reinforced concrete one way slab on continuous supports in the direction transverse to the supporting beams. If this is followed the primary reinforcement may look as shown in Fig. 14.45b. However, to ensure lateral distribution of concentrated loads, minimize labor cost, and satisfy other requirements related to shrinkage and temperature reinforcements in both primary and transverse directions, AASHTO recommends using two layers of continuous reinforcement top and bottom, in each direction, with the proper concrete cover (Fig. 14.45c). The spacing of the primary reinforcement shall not exceed 1.5 times the slab thickness or 18 in (or 450 mm).

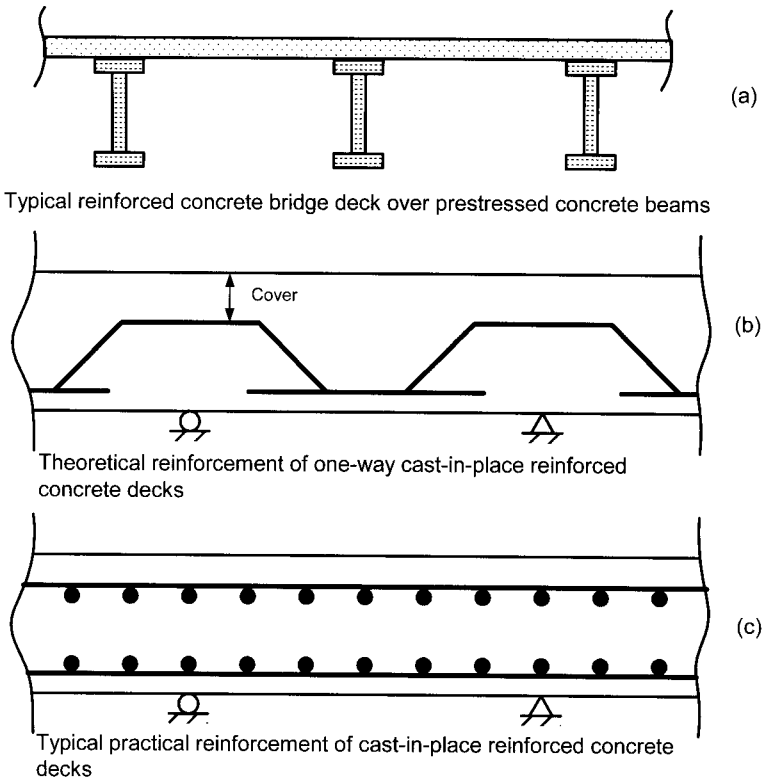

Figure 14.45 Typical reinforcement in slabs of reinforced concrete bridge decks.

Thus assuming that: (1) four layers of reinforcement will be used, and (2) the primary reinforcement (top and bottom) has been determined by analysis, then reinforcement shall be placed in the secondary direction in the bottom of slabs as a percentage of the primary reinforcement as follows:

- When the primary reinforcement is parallel to traffic:

$$p = \frac{100}{\sqrt{S_e}} \leq 50\% \qquad \text{where } S_e \text{ is in inches} \tag{14.25}$$

$$p = \frac{1750}{\sqrt{S_e}} \leq 50\% \qquad \text{where } S_e \text{ is in mm} \tag{14.26}$$

and S_e is the effective span of the slab.

The effective span of slab is taken as the center to center span if the slab is simply supported on two beams, and as the clear span in continuous slabs cast monolithically with the supporting beams. For a slab cast on top of precast-prestressed beams, the effective span may be taken as the sum of the clear span plus half the top flange width of the beam. Short of directives from a particular code, it is generally safe in design to use the span center-to-center of supporting beams.

- When the primary reinforcement is perpendicular to traffic:

$$p = \frac{220}{\sqrt{S_e}} \leq 67\% \qquad \text{where } S_e \text{ is in inches} \tag{14.27}$$

$$p = \frac{3840}{\sqrt{S_e}} \leq 67\% \qquad \text{where } S_e \text{ is in mm} \tag{14.28}$$

Note that the primary and secondary reinforcement must also satisfy the minimum temperature and shrinkage reinforcement recommended by AASHTO. It is then likely that additional reinforcement will be needed for temperature and shrinkage in the transverse direction at the top of the slab (see Section 14.13.6).

14.13.5 Empirical Design of Slabs

This approach applies to empirical design of nonprestressed concrete deck slabs supported by longitudinal beams or girders and working as composite with them, provided: (1) cross frames or diaphragms are used throughout the cross section at lines of supports, (2) the design compressive strength of concrete, f'_c, is not less than 4 ksi (28 MPa), (3) the spacing between face to face of webs of longitudinal beams does not exceed 13.5 ft (4.1 m), (4) the minimum depth of slab is not less than 7 in (175 mm), and (5) the core depth (that is, slab depth minus top and bottom cover) is not less than 4 in (100 mm). The AASHTO LRFD code should be consulted for additional details on conditions of application.

Four layers of isotropic reinforcement shall be provided, two top layers and two bottom layers. The minimum amount of reinforcement shall be 0.27 in^2/ft (or 570 mm^2/m) for each bottom layer and 0.18 in^2/ft (or 380 mm^2/m) for each top layer. Reinforcing steel shall be Grade 60 (that is with f_y = 60 ksi (414 MPa) or better. All

reinforcements shall be straight bars except that hooks may be provided when required. Only lap splices are permitted. The spacing of steel bars shall not exceed 18 in (or 450 mm).

These provisions should not be applied to overhangs which should be designed according to a rational analysis. The empirical design accounts for the arching action of the slab and may lead to lower overall amount of reinforcement than the conventional design.

Given a minimum slab depth of 7 in (175 mm) and for common range of beam spacing, the above recommendation can be further simplified by using equal amount of reinforcement at a ratio of about 0.32% of section area, for each layer in each direction; this would be more than needed for the top reinforcement, and on the safe side. Thus the total reinforcement volume of a cast-in-place slab on top of beams or girders is about 1.28% of the slab volume. This approach has the advantage of minimizing error in the field, simplifying ordering, storage and inspection of reinforcing bars, and keeping same spacing throughout. It essentially leads to four identical layers of reinforcement.

An example of application of the empirical design is given in Section 14.10.2.i.

14.13.6 Temperature and Shrinkage Reinforcement

Temperature and shrinkage reinforcement shall be provided near surfaces of concrete exposed to the environment. For components less than 48 in (1200 mm) thick, AASHTO recommends that the minimum amount of shrinkage and temperature reinforcement in each direction be:

$$A_{T+S} \geq 0.75\frac{A_g}{f_y} \quad \text{for mm}^2 \text{ and MPa units} \tag{14.29}$$

$$A_{T+S} \geq 0.11\frac{A_g}{f_y} \quad \text{for in}^2 \text{ and ksi units} \tag{14.30}$$

where A_g is the gross sectional area and f_y the yield strength. For a yield strength of 60 ksi (414 MPa), the above reinforcement amounts to 0.18% of the gross area of concrete. The steel shall be equally distributed on both faces; however, for members less than 6 in (150 mm) in thickness, the steel may be placed in a single layer. Temperature and shrinkage reinforcement shall not be spaced more than three times the component thickness or 18 in (450 mm).

Generally the primary reinforcement, which is made continuous on both top and bottom, satisfies the minimum temperature and shrinkage reinforcement for the primary direction, and thus no additional reinforcement is needed there. However, in the direction normal to the primary reinforcement of the slab, there is need to satisfy the minimum reinforcement for temperature and shrinkage; this is particularly the case for the top layer, since for the bottom layer, the distribution reinforcement (Eqs. 14.23 and 14.24) may be sufficient. Note that the empirical design (Section 14.13.5)

would satisfy minimum temperature and shrinkage reinforcement requirements in most decks.

14.13.7 Moments for Slabs Supported on Four Sides

In the case of slabs with ratio of long to short span less than 1.5, simply supported along four edges and reinforced in both directions, the proportion p of the load carried by the short span a shall be assumed as given by the following equations:

- For uniformly distributed load:

$$p = \frac{b^4}{a^4 + b^4} \tag{14.31}$$

- For load concentrated at center:

$$p = \frac{b^3}{a^3 + b^3} \tag{14.32}$$

in which

p = proportion of load carried by short span
a = length of short span of slab
b = length of long span of slab

Where the length of the slab exceeds 1.5 times its width, the entire load shall be assumed to be carried by the transverse reinforcement, that is, along the short span. Hence, the design is essentially reduced to that of a one-way slab.

The distribution width E for the load taken by either span shall be determined as provided for other slabs (Eqs. 14.17 to 14.20). Moments obtained shall be used in designing the center half of the short and long slabs. The reinforcement steel in the outer quarters of both short and long spans may be reduced by up to 50 percent, in comparison to the center half.

14.14 EXAMPLE: DESIGN OF A CAST-IN-PLACE POSTTENSIONED SLAB BRIDGE

A two lanes simply supported bridge deck spanning 50 ft is to be designed according to the AASHTO-LRFD specifications. Two alternatives are considered: the first consists of a cast-in-place posttensioned slab (Fig. 14.46), covered next, and the other consists of precast pretensioned beams placed adjacent to each other (covered in Section 14.11 and Fig. 14.41). The following information common to the two alternatives is provided:

Normal weight concrete: $\gamma_c = 150$ pcf; $f'_c = 6000$ psi; $f'_{ci} = 4500$ psi; $E_c = 4696$ ksi; $\beta_1 = 0.75$

$\bar{\sigma}_{ti} = -201$ psi; $\bar{\sigma}_{ci} = 2700$ psi; $\bar{\sigma}_{ts} = -232$ psi;

$\bar{\sigma}_{cs} = 0.60 f'_c = 3600$ psi, or $0.45 f'_c = 2700$ psi, or $0.40 f'_c = 2400$ psi

$f_{pu} = 270$ ksi; $f_{pe} = 150$ ksi; $\eta = F / F_i = 0.80$; $(e_o)_{mp} = h/2 - 3$ in

A wearing surface weighing 25 psf is to be placed on top of the deck.

a. Estimate depth and prestressing force

Using the suggested minimum depth from the AASHTO LRFD code [Table 2.5.2.6.3-1] and Table 14.14 of Section 14.17:

$$h \times 0.030\ell = 0.03 \times 50 \times 12 = 18 \text{ in}$$

Let us try a depth $h = 20$ in. Assuming normal weight concrete, it leads to a unit weight of $w_G = 0.25$ klf per foot width. Geometric properties per foot width of slab are: $A_c = 240$ in^2, $Z_b = Z_t = 800$ in^3, $k_b = 3.33$ in, $k_t = -3.33$ in.

b. Determine live load strip width

The main reinforcement is parallel to traffic. For slab bridges and concrete slabs spanning primarily in the direction parallel to traffic, Eq. (14.17) applies:

- One lane loaded:

$$E = 10 + 5\sqrt{L_1 W_1}$$

where: E = equivalent width (in)

L_1 = modified span length taken equal to the lesser of the actual span or 60 ft. In this case, $L_1 = 50$ ft

W_1 = modified edge-to-edge width of bridge taken equal to the lesser of the actual width or 30 ft for single-lane loading (ft). In this case, $W_1 = 30$ ft

Thus:

$$E = 10 + 5\sqrt{50 \times 30} = 203.65 \text{ in}$$

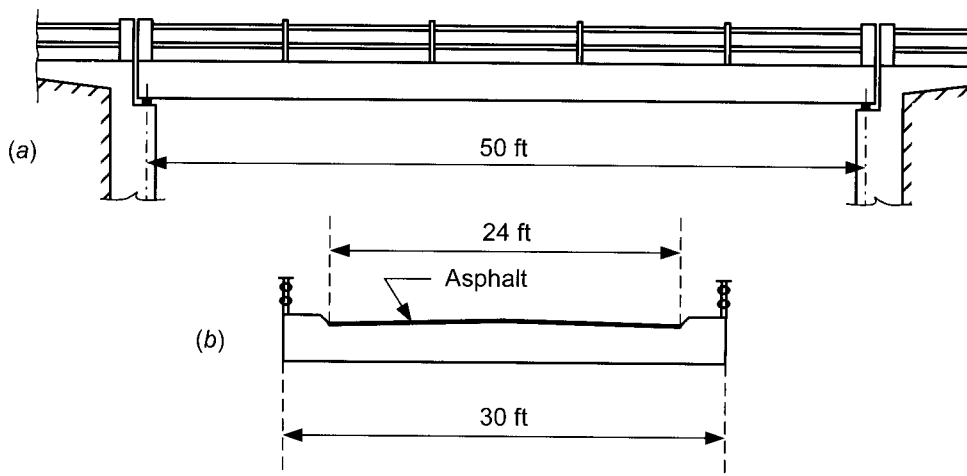

Figure 14.46 Example bridge. (a) Longitudinal deck profile. (b) Transverse section of the slab solution.

- Multiple lanes loaded:

$$E = 84 + 1.44\sqrt{L_1 W_1} \le \frac{12W}{N_L}$$

where: E = equivalent width (in)
L_1 = modified span length taken equal to the lesser of the actual span or 60 ft
W_1 = modified edge-to-edge width of bridge taken equal to the lesser of the actual width or 60 ft for multiple-lane loading (ft)
W = physical egde-to-edge width of bridge (ft). In this case, $W = 30$ ft.
N_L = number of design lanes. In this case, $N_L = INT(24/12) = 2$

That is:

$$E = 84 + 1.44\sqrt{50 \times 30} = 139.77 \text{ in} \le \frac{12 \times 30}{2} = 180 \text{ in} \qquad \text{O.K.}$$

Hence, use $E = 139.77$ in or 11.6475 ft. Compare this value to the heuristic approach (Eq. 14.6) which assumes a full lane loading is resisted by approximately 11 ft of slab.

c. Determine live load moment

The live load moment due to a fully loaded lane including the effect of impact was determined in Section 14.11 for the bridge with adjacent precast beams. Its maximum value in span is given by:

$$(M_{Lane})_{LL+IM} = 1033.51 \text{ kips-ft}$$

The maximum live load moment in span per foot width of slab is (Eqs. 14.7 and 14.21):

$$M_{LL+IM} = DF_M (M_{Lane})_{LL+IM} = \frac{12}{E}(M_{Lane})_{LL+IM} = \frac{12}{139.77} 1033.51 = 88.73 \text{ kips-ft/ft}$$

d. Determine prestressing force

The minimum and maximum service moments per foot width of slab are given by:

$$M_{min} = M_{DC} = w_{DC} \frac{l^2}{8} = 0.25 \times \frac{50^2}{8} = 78.125 \text{ kips-ft}$$

$$M_{max} = M_{DC} + M_{DW} + 0.8 M_{LL+IM} = 78.125 + 0.025 \times \frac{50^2}{8} + 0.8 \times 88.73$$

$$= 156.92 \text{ kips-ft}$$

where M_{max} is to be used for Service-III limit state, that is tension under service conditions.

Assuming a value of $(e_o)_{mp} = h/2 - 2.5 = 7.5$ in and using stress condition IV of Table 4.2 for $e_o = (e_o)_{mp}$, leads to:

$$F = \frac{M_{max} + \bar{\sigma}_{ts} Z_b}{e_o - k_t}$$

$$= \frac{156.92 \times 12000 - 232 \times 800}{7.5 + 3.33} = 156,735 \text{ lb} = 156.74 \text{ kips}$$

The Dywidag single-bar posttensioning system is selected (Appendix C). It offers a bar with a nominal diameter of 1.375 in and an area of 1.58 in^2 that can carry a force of 158.79 kips at $0.67 f_{pu}$. Hence, one such single-bar tendon is selected per foot width of slab. Assuming a value of $\eta = F/F_i = 0.85$, it can easily be shown that the other three stress inequality conditions of Table 4.2 are largely satisfied.

e. Ultimate moment and nominal bending resistance

The strength design moment using AASHTO-LRFD is given by Eq. (14.1) in which the modification factor η is taken equal to 0.95:

$$M_u = 0.95(1.25M_{DC} + 1.5M_{DW} + 1.75M_{LL+IM})$$
$$= 0.95(1.25\times 78.125 + 1.5\times 7.8125 + 1.75\times 88.73)$$
$$= 251.42 \text{ kips-ft}$$

$$c = \frac{A_{ps}f_{pu} + A_s f_y - A'_s f'_y}{0.85 f'_c \beta_1 b + kA_{ps}\dfrac{f_{pu}}{d_p}} = \frac{1.58\times 150}{0.85\times 6\times 0.75\times 12 + 0.38\times 1.58\dfrac{150}{17.5}} = 4.64 \text{ in}$$

$$f_{ps} = f_{pu}\left(1 - k\frac{c}{d_p}\right) = 150\left(1 - 0.38\frac{4.64}{17.5}\right) = 134.89 \text{ ksi}$$

$$\frac{c}{d_e} = \frac{c}{d_p} = \frac{4.64}{17.5} = 0.265 < 0.42 \qquad \text{underreinforced section.} \quad \text{OK}$$

$$M_n = A_{ps}f_{ps}\left(d_p - \frac{a}{2}\right) = 1.58\times 134.89\left(17.5 - \frac{0.75\times 4.64}{2}\right) = 3408.31 \text{ kips-in}$$

$$\phi M_n = 1.0\times 3408.31 = 3408.31 \text{ kips-in or } 284.03 \text{ kips-ft}$$

$$M_u = 251.42 < \phi M_n = 284.03 \text{ kips-ft} \qquad \text{O.K.}$$

It can also be shown that ϕM_n is more than 20 percent larger than the cracking moment.

f. Shear strength

Slab bridges designed for moment in conformance with AASHTO [Article 4.6.2.3] may be considered satisfactory for shear. This is the case here. If longitudinal tubes are placed in the slab to create voids and reduce the cross section (or if hollow core slabs are used) the shear resistance must then be checked.

g. Edge beam

According to AASHTO an edge beam must be provided for slabs with primary reinforcement parallel to traffic. Let us assume that the edge beam is made out of the last 3 ft width of slab cast monolithically with the sidewalk. Its depth is assumed equal to h = 20+12 = 32 in. The corresponding weight of the edge beam is w_G = 1.2 klf and the dead load moment is given by:

$$M_{DC} = 1.2\frac{50^2}{8} = 375 \text{ kips-ft}$$

The edge beam should resist a live load moment at least equal to:

$$M_{LL} = 0.10Pl = 0.10\times 50\times 16 = 80 \text{ kips-ft}$$

This live load moment is about equal to that generated by a live load of 85 psf on the sidewalk. However, it is smaller than the live load moment of 0.8 x 88.73 = 70.98 kips-ft per foot width for which the rest of the slab is designed. As a truck may accidentally ride on the sidewalk and since an "exterior" beam should not have less capacity than an "interior" beam, the live load moment on the edge beam is taken equal to:

$$0.8M_{LL+IM} = 0.8(3\times 88.73) = 3\times 70.98 = 212.94 \text{ kips-ft}$$

Hence, the maximum service moment for Service-III limit state is given by:

$$M_{max} = M_{DC} + 0.8M_{LL+IM} = 587.94 \text{ kips-ft}$$

The corresponding value of the required prestressing force is obtained from stress condition IV of Table 4.2, assuming $e_o = h/2 - 3 = 16 - 3 = 13$ in, that is:

$$F = \frac{M_{max} + \bar{\sigma}_{ts} Z_b}{e_o - k_t}$$

$$= \frac{587.94 \times 12{,}000 - 232 \times 6{,}144}{13 + 5.33} = 307{,}139.8 \text{ lbs} \simeq 307.14 \text{ kips}$$

It can be largely achieved using two bars of the same type as used for the rest of the slab. Other requirements related to allowable stresses, ultimate strength, and shear resistance of the edge beam are also found satisfactory. Since in this particular example one bar per foot is used for the thinner slab deck, it is better to keep the bar spacing same throughout the transverse section of the deck, including the sidewalk section.

h. Transverse or distribution reinforcement

Distribution reinforcement transverse to the main reinforcement must also be provided at bottom of slabs. According to Eq. (14.23), the area of transverse reinforcement should correspond to a percentage of the area of the main reinforcement equal to:

$$\frac{100}{\sqrt{L}} \frac{f_{pe}}{60} \leq 50\%$$

where L = span length (ft)

f_{pe} = effective stress in the prestressing steel (of main reinforcement) after losses (ksi)

$$\frac{100}{\sqrt{50}} \frac{100.5}{60} = 23.69\%$$

Hence, we should provide 0.2369 x 1.58 = 0.374 in^2 of reinforcing steel per foot width of slab in the transverse direction. This can be achieved by using No. 4 bars (or area 0.2 in^2) every 6 in, or No. 5 bars (of area 0.31 in^2) every 9 in, or No. 6 bars (of area 0.44 in^2) every 13 in (see also next).

i. Shrinkage and temperature reinforcement

The two top layers of the slab must contain shrinkage and temperature reinforcement to satisfy the following minimum area of reinforcing bars:

$$A_{T+S} \geq 0.11 \frac{A_g}{f_y} = 0.11 \frac{20 \times 12}{60} = 0.44 \text{ in}^2 \text{ per foot width of slab}$$

This can be achieved using a No. 6 reinforcing bar of area 0.44 in^2 at a spacing of 12 inches in each direction.

14.15 PRECAST BRIDGE BEAMS MADE CONTINUOUS BY A CAST-IN-PLACE RC SLAB

Composite bridge decks made with precast prestressed beams can have a cast-in-place concrete slab poured continuously over several supports; thus the beams behave as simply supported under dead load and as continuous for live load plus impact. Generally an end diaphragm is poured simultaneously with the slab at support lines. The main reasons to use continuity are: (1) to reduce the number of joints, (2) to improve the bridge riding quality and appearance, and (3) to reduce

short term cost (by using precast elements) and long term maintenance cost associated with the joints and water drainage into the substructure. Jointless decks with lengths of up to 700 ft have been built that way [Ref. 14.13].

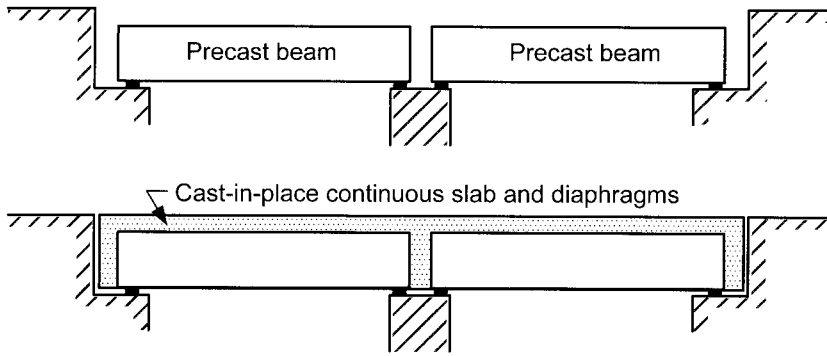

Figure 14.47 Precast prestressed bridge deck beams made continuous by cast-in-place reinforced concrete slab.

When two consecutive beams are made continuous over a support, the calculated live load moment in span is smaller than if the beam was simply supported. Typically continuity leads to a reduction of 5% to 15% in the required prestressing force when compared to simple span designs. The larger reductions occur in shorter spans where the dead load moment is a smaller fraction of the total moment.

Under dead load only including the slab's own weight, no negative moment develops at the intermediate support. However, a negative moment develops under superimposed dead load and live load plus impact, and is fully resisted by the reinforcement in the slab. Also, at intermediate supports, a positive moment develops due to loading in remote spans. Thus some resistance to positive moment is needed at the support sections; it is generally obtained by adding reinforcing bars embedded in the ends of precast beams and extending into the cast-in-place diaphragm.

Positive moments may also be induced at the intermediate supports due to the effect of creep in the prestressed girders; these moments can be partly balanced by additional negative moments induced by differential shrinkage between the cast-in-place slab and the beams. Although the evaluation of creep and shrinkage effects can be analytically demanding, for common designs where the ultimate strength limit states are considered for the cast-in-place reinforced concrete slab, creep and shrinkage effects are ignored.

An example illustrating a bridge deck made continuous over two spans is covered next. Additional information on this type of application can be found in Refs. [14.13 and 14.52].

14.15.1 Example: Prestressed Bridge Beams Made Continuous by Cast-in-Place RC Slab

Assume that the bridge of Example 14.10 is made continuous over two equal length spans through the cast-in-place reinforced concrete slab; thus, the beams are precast-prestressed, transported to site, placed in position, and a continuous slab is poured providing continuity for live load at the interior support (as illustrated in Fig. 9.3). The purpose of this example is to illustrate the design of the slab to resist the negative moment induced by live loads over the interior support.

The main properties of the beam and slab are given in Example 14.10.

a. Design of RC slab at interior support

- Determine negative moment at interior support:

Using structural software (RISA 3D) it can be shown that the negative moment at the support for one full lane due to two trucks placed according to Fig. 14.30 is:

$$M^{-}_{2trucks} = -1{,}041.314 \text{ k-ft}$$

This value can also be read approximately from Fig. 14.34. From Eq. (14.12):

$$M^{-}_{unif-lane} = -0.64\left(\frac{L^2}{8}\right) = -512 \text{ k-ft}$$

Thus:

$$90\%[M^{-}_{unif-lane} + (1+I_M)\times M^{-}_{2trucks}] = -\frac{9}{10}[512 + 1.33(1041.314)] = -1707.25 \text{ k-ft}$$

Thus the live load moment for one lane: $M^{-}_{\max} = -1{,}707.25$ k-ft

The distribution factor is given by:

$DF_M = 0.621$ (from Example 14.10.1)

Thus the live load moment per beam is given by:

$$M_{LL+IM} = 0.621(-1707.25) = -1{,}060 \text{ k-ft}$$

- Determine required area of reinforcing bars:

The strength design moment for the cast-in-place slab is determined assuming only the slab resists the entire live load:

$$M_u = \eta[\gamma_{DC}(DC) + \gamma_{LL}(LL+IM) + \gamma_{DW}(DW)] \text{ assuming } \eta = 0.95$$

$$M_u = 0.95[0 + 1.75(1060) + 0] = 1{,}762 \text{ k-ft}$$

$\phi = 0.9$ for reinforced concrete

Required: $M_n = \dfrac{M_u}{\phi} = \dfrac{1762}{0.9} = 1958$ k-ft

For nominal bending resistance under negative moment, the compression block is in the lower flange of the girder, thus $f'_c = 7$ ksi of the girder is used.

Assume rectangular section behavior: $c \le 8$ in

→ Force equilibrium:

$$C = T$$

$$0.85 \times 7 \times 26 \times a = A_s \times 60$$

$$A_s = \left(\frac{154.7}{60}\right)a = 2.578a$$

→ Moment equilibrium:

Assume concrete cover = 3 in; $d_s = 54 + 5 = 59$ in; $\phi = 0.9$ (underreinforced); thus:

$$\frac{M_u}{\phi} = A_s \times f_y \left(d_s - \frac{a}{2} \right)$$

$$1958 \times 12 = A_s \times 60 \left[59 - \frac{a}{2} \right]$$

Solving the above two equations of equilibrium leads to: $a = 2.65$ in. Thus:

$$c = \frac{a}{\beta_1} = \frac{2.65}{0.7} = 3.786 < 8 \text{ in} \quad \text{O.K. Rectangular section behavior.}$$

Thus: $A_s = 2.578a = 2.578 \times 2.65 = 6.83 \text{ in}^2$

Try 16 #6 = 7.04 in^2 (also 12 #7 would be fine)

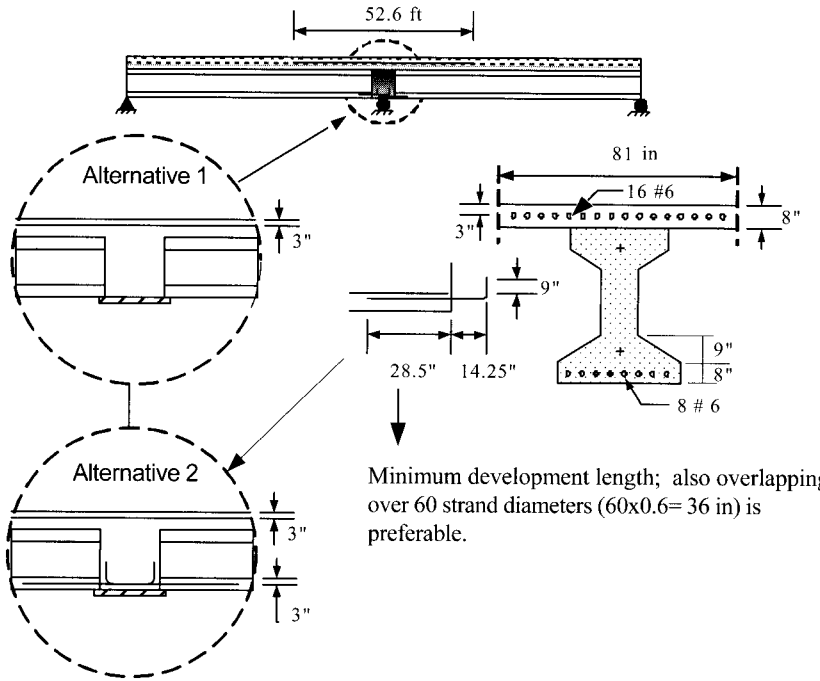

Figure 14.48

In real practice, the top reinforcement calculated in the previous section should be adjusted to supplement the grid reinforcement already provided along the rest of the slab as described in the example of Section 14.10.2, subsection *i*.

Figure 14.48 provides some details of the bottom reinforcement at the support section. Two alternatives are shown:

1. In the first alternative, no positive reinforcement is provided at the support between the girders and the cast-in-place diaphragm. This is theoretically correct, since no positive moment is applied. However the author prefers the second alternative below.
2. In the second alternative positive reinforcement is added at the middle support; this alternative should be considered if: a) moment reversal is possible under seismic load, b)

differential settlement occurs between the mid-support and the end supports, and c) if analysis for shrinkage and creep demands it.
The reinforcement provided should be developed according to code specifications. A minimum development length of 28.5 in is found. However, if we also consider that the transfer length for the 0.6 in strands is about 60 diameters (60x0.6 = 36 in), then the bars should preferably be anchored over 36 in from the face of the girder.

b. Design of beam section in span

Generally in practice, even if continuity is assured by the cast in place slab, thus reducing the live load moment on the prestressed girder, the prestressed girder is designed as if it remains simply supported for live load and superimposed dead load. This is on the safe side and convenient should there be need to replace the slab in the future. However, the following section is provided to illustrate how slab continuity affects the design of the precast girder.

The use of a continuous slab over the interior support leads to a live load moment in span smaller than if the beams were simply supported. Let us evaluate the possible savings in corresponding prestressing force in comparison to the simple span case.

- Live load moments in span

Since the structure is statically indeterminate, we cannot use the formulae given in Table 14.10. However, using a structural software (RISA 3D), it is found that the maximum positive moment due to the uniformly distributed load of 0.64 klf in span is 392 k-ft; it occurs at 35 feet from the external support. For the HS20 truck, the maximum positive moment also occurs at about 35 feet (43.75% of span length) from the exterior support, with a magnitude of 936.2 k-ft.

Thus the maximum positive moment in span due to live load plus impact for one loaded lane is:

$$(M_{Lane})_{max} = 1.33 \times 936.2 + 392 = 1637.15 \text{ kips-ft}$$

and for one typical interior beam:

$$M_{LL+IM} = DF_M \times (M_{Lane})_{max} = 0.621 \times 1637.15 = 1016.67 \text{ kips-ft}$$

This moment is about 20.5% less than that observed for the simple span case (1279.21 k-ft.).

The bending moments needed to compute the stresses in the continuous composite beam section in span are given in Table 14.13.

Table 14.13

Loading	Maximum Moments at 35 ft (kips-ft)
Precast beam (simple beam)	657.5
Cast-in-place slab	540.0
Moment on precast section	$M_p = 1197.5$
Asphalt * Live load + impact	$0.25/0.64 \times 392 = 153.12$ 1016.67 ----------
	$M_c = 1169.79$
Service III: [0.8(live load + impact)]	813.34 ----------
Moment on composite section	$M_c = 966.46$

* Asphalt is poured after concrete hardening, thus it is considered a uniform load on a continuous beam. Generally the term "wearing surface" is used to cover all possible surfaces.

Check stress inequality conditions:

Condition I: $e_o \le 11.29 + \dfrac{11669200}{F_i}$

Condition II: $e_o \le -13.36 + \dfrac{39516000}{F_i}$

Condition III: $e_o \ge 11.29 - \dfrac{13358100}{F_i}$

Condition IV: $e_o \ge -13.36 + \dfrac{23218000}{F_i}$

Condition V: $e_o \le (e_o)_{mp} = 20.16$

The reader may want to plot the feasibility domain and check that the minimum value of prestressing force is obtained from satisfying both conditions IV and V leading to:

$F_i = 693$ kips at $e_o = 20.16$ in

$$A_{ps} = \frac{693}{150/0.83} = 3.84 \text{ in}^2$$

$$N = \frac{3.84}{0.153} = 25.1 \text{ strands}$$

Select 26 half-inch diameter strands leading to:

$A_{ps} = 3.978$ in^2, $F_i = 719$ kips, $F = 597$ kips, $e_o = 20.16$ in

Using the above condition equations on e_o, it can be shown that for F = 597 kips, the eccentricity:

$18.93 \le e_o \le 20.16$ in

The stress induced in the cast-in-place slab:

$$n_c\left(\frac{M_c}{Z_{tc}}\right) = 373 \text{ psi} \le (\sigma_{cs})_{slab} = 2250 \text{ psi} \quad \text{O.K.}$$

Cracking Moment:

$F = 597$ kips, $M_p = 1197.5$ kips-ft, and $e_o = 20.16$ in

$f_r = -627.50$ psi

$\Delta M_{cr} = 1569$ kips-ft

M_{cr} (bottom fiber) = 2766.5 kips-ft

$1.2M_{cr} = 3319.8$ kips-ft

Ultimate moment requirements

$$M_u = 0.95(1.5\times153.12 + 1.25\times1197.5 + 1.75\times1016.67) = 3330.44 \text{ kips-ft}$$

$d_p = 8 + 29.27 + 20.16 = 57.43$ in, $A_{ps} = 3.978$ in^2

$$c = \frac{3.978\times270}{0.85\times7\times0.7\times68.45 + 0.28\times3.978\times\dfrac{270}{57.43}} = 3.70 \text{ in}$$

$a = 0.7\times3.70 = 2.59 \le 8$ in O.K.

$$f_{ps} = f_{pu}\left(1 - k\frac{c}{d_p}\right) = 270\left(1 - 0.28\frac{3.70}{57.43}\right) = 265.13 \text{ ksi}$$

$$\frac{c}{d_e} = \frac{c}{d_p} = \frac{3.70}{57.43} = 0.064 < 0.42 \quad \text{(underreinforced section, thus } \phi = 1\text{)}$$

$$M_n = 3.978 \times 265.13(57.43 - \frac{2.59}{2})/12 = 4933.74 \text{ kips-ft}$$

$$\phi M_n = 1.0 \times 4933.74 = 4933.74 \text{ kips-ft} \geq M_u = 3330.44 \text{ kips-ft} \quad \text{O.K.}$$

$$\phi M_n > 1.2 M_{cr} \quad \text{O.K.}$$

Note that for this particular example, the savings in prestressing steel in span due to continuity at the support provided by the slab, in comparison to the simple span example of Section 14.10, is equivalent to 2 strands out of 28, that is, about 7%. Since the saving is relatively small, often the computations are carried out as if the beam remains simply supported. This is of course on the safe side, since, should the slab fail at the support due to excessive cracking or corrosion, the beam will remain capable of resisting the full live load.

14.16 DESIGN CHARTS FOR PRESTRESSED BRIDGE BEAMS

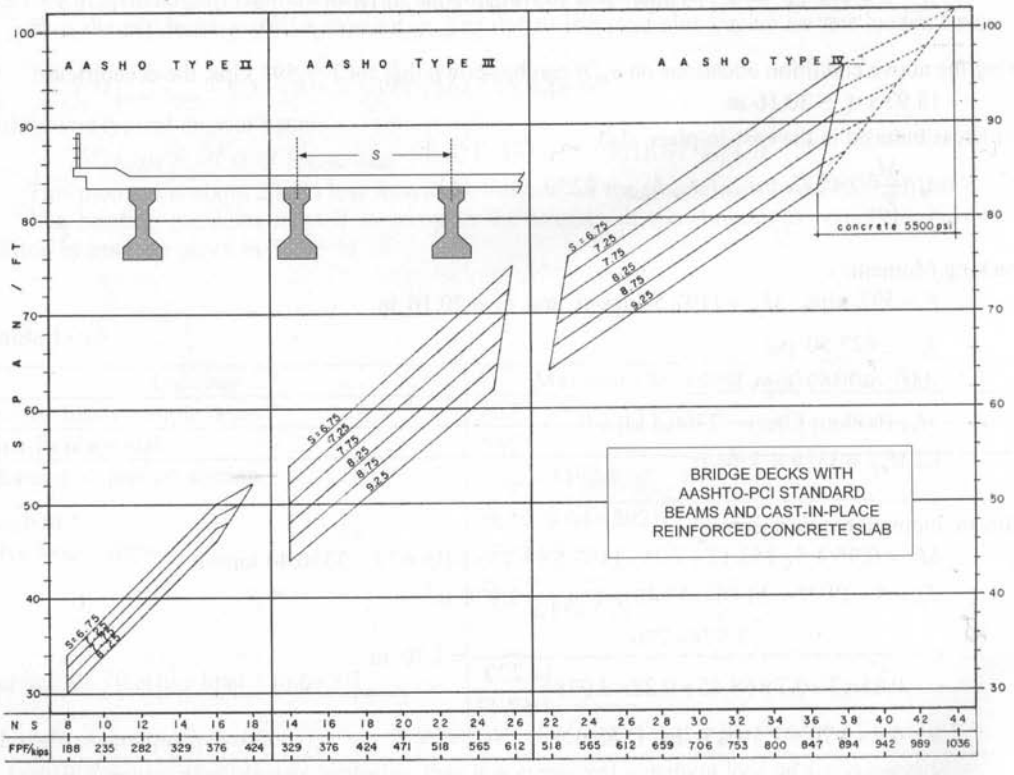

Figure 14.49 Typical design chart for composite bridge decks using AASHTO-PCI girders.
(Ref. 14.30, Courtesy of the Prestressed Concrete Institute.)

Because a large proportion of bridges and highway overpasses are in a span range below about 150 ft (46 m), many attempts were made in the United States and elsewhere to standardize bridge deck sections for such bridges. In the United States this effort was particularly fostered by the precast prestressed concrete industry, the U.S. Department of Transportation, AASHTO, and many state departments of transportation. Cost savings and other benefits could be substantial. Computer programs were written for the analysis and design of bridges and were used to generate design charts for typical bridge deck configurations using standardized beams such as box beams (Fig. 14.5), I beams, T beams, and the like [Ref. 14.39]. Several studies have dealt with the use of composite decks made with precast prestressed concrete beams and a cast-in-place concrete slab [Ref. 14.36]. The use of the AASHTO I beams, described in Fig. 14.6, was particularly extensive. A typical design chart for selecting a typical interior beam for such bridges is shown in Fig. 14.49 [Ref. 14.30].

The chart was developed assuming an 8-in thick (20-cm) cast-in-place concrete slab with a specified compressive strength of 4000 psi (27.6 MPa). For the precast prestressed beams, the following strengths were specified: f'_c = 5000 psi and f'_{ci} = 4000 psi (34.5 and 27.6 MPa). For a given span and beam spacing, the chart leads to the type of AASHTO beam, the final prestressing force, and the corresponding number of half-inch diameter strands assumed having a specified strength of 270 ksi (1860 MPa). The tendon's eccentricity at midspan is to be within the maximum practical range. Although the chart was developed for a hypothetical highway loading 25% above that of the AASHTO Standard Specifications, it is likely to satisfy as a first approximation the AASHTO LRFD 1993 highway loading, for a reasonable range of values of concrete compressive strengths for the beams and cast-in-place slabs. Thus it can be useful as a rapid estimating tool. Similar studies should be consulted whenever the need arises, especially during the preliminary planning and design of bridges where standardized solutions can be utilized.

14.17 PRELIMINARY DESIGN TIPS FOR DIMENSIONING

In case a standard bridge deck configuration is not desired, several design tips can be used to facilitate the quick dimensioning of bridge beams. Some are summarized in Table 14.14 assuming a typical deck sections as in Fig. 14.50. Following the first column of the table, the initial steps are:

1. Determine the value of beam depth, h, based on a fraction of the span, l
2. Select the beam spacing, S, based on experience from similar bridges
3. Select the depth or thickness of the deck slab, h_f, based on beam spacing, S, and
4. Estimate the web thickness b_w based on practical construction constraints.

Additional information can then be derived from the minimum section moduli of the beam selected, as per Eqs. (4.11 and 4.12 or 9.35 to 9.38), depending on whether or not composite construction is considered.

Note that the cross-sectional shape of the selected beam can play an important role since it greatly influences the geometric efficiency of the section in resisting flexure and, hence, can lead to significant weight and cost savings. In arriving at an acceptable solution, the designer should also keep in mind the remarks discussed in Section 14.3 on form evolution and span ranges.

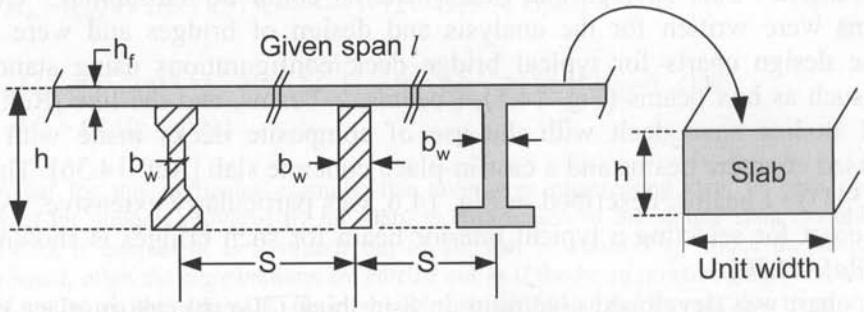

Figure 14.50 Typical deck sections illustrating four important variables in preliminary dimensioning of deck beams.

Table 14.14 Common range of main design variables in bridge decks.

Variable	Design range
Depth h	Slab: Simple span: $0.03 \le h/l \le 0.04$; Continuous: $0.025 \le h/l \le 0.035$ Beams (T, box): Simple span: $0.035 \le h/l \le 0.055$; Continuous: $0.03 \le h/l \le 0.045$ I beams (composite): Simple span: $0.045 \le h/l \le 0.06$; Continuous: $0.040 \le h/l \le 0.055$
Beam spacing S	Range: $2 \le S \le 16$ ft $\quad 0.7 \le S \le 4.8$ m Most common range: $5 \le S \le 10$ ft $\quad 1.5 \le S \le 3$ m
Top slab depth h_f	Range: $\frac{S}{15} \le h_f \le \frac{S}{12}$ and $h_f \ge 7$ in (175 mm) Most common range: $7 \le h_f \le 10$ in $\quad 175 \le h_f \le 250$ mm
Web width b_w	Pretensioned beams: Minimum value: $b_w \simeq 4$ in (100 mm) Common range: $5 \le b_w \le 8$ in ($125 \le b_w \le 200mm$) b_w is also controlled by type of vibration and by shear design Posttensioned beams: Precast: $b_w \simeq \phi + 5$ in ($\phi + 125$ mm) Cast-in-place: $b_w \simeq \phi + 8$ in ($\phi + 200$ mm) $\phi =$ outside diameter of tendon duct

Once a beam or deck cross section has been arrived at in a preliminary design, it should be further modified and refined according to the final design requirements. These may include not only mechanical and code requirements but also minimum weight and/or cost considerations. A discussion of minimum weight and minimum cost design of prestressed concrete beams is given in Ref. [1.48].

14.18 OTHER DESIGN CONSIDERATIONS

In the preliminary design of bridge decks, an idealized representation is generally assumed to speed up the analysis and to quickly arrive at an acceptable solution. However, several additional details that require special attention have to be integrated in the final design. They include the design of diaphragms, bearing pads or expansion joints, joints between consecutive spans or between spans and abutments, waterproofing, transverse sloping or crowning of the deck to allow for drainage, and the like. Some information on diaphragms and bearing pads is given next.

Diaphragms are thin reinforced or prestressed walls placed transversely to the beams of the bridge decks to improve lateral rigidity and ensure good lateral load distribution. The AASHTO LRFD code recommends that diaphragms be provided at abutments, piers, and hinge joints to resist lateral forces and transmit loads to points of supports. The AASHTO Standard Specifications recommend to place diaphragms between the girders within the span at intervals not exceeding 40 ft (12.2 m) for T-beam construction and 60 ft (18.3 m) for box-beam construction. Diaphragms may be omitted where tests or structural analysis show adequate strength. Diaphragm spacing for curved beams shall be given special consideration.

Bearing pads are generally used at the supports to transmit and distribute vertical reactions. In addition, they must accommodate: (1) changes in the length of the span due to variation in temperature, and (2) end rotations. A number of suitable materials are available for use in bearing pads, among which are several elastomeric (neoprene) materials. They are commonly characterized by a relatively small shear modulus in comparison to their elastic modulus. Sections 12 of Division I and 25.2 of Division II of the AASHTO Standard specifications, and Section 14.7.5 of the AASHTO LRFD specifications deal with structural grade neoprene pads. For high compressive stresses and large horizontal deformations, laminated pads made of various layers of elastomer bonded between steel sheets can be used. The acceptable shear deformation is a function of the thickness or number of layers of the total assembly. Typical information on a commercially available bearing pad, satisfying the AASHTO specifications, and an example of bearing pad selection are given in Appendix D of the first edition of this book.

14.19 BRIDGE ENGINEERING: LOOKING AHEAD

A study was undertaken to forecast the nature of bridge engineering and construction for the years 1980 to 2000 [Ref. 14.51]. Some of the forecasts specifically related to prestressed concrete are summarized below, each followed by a note on how these forecasts have materialized at time of this writing (2003). It should be noted that continuous progress is being made in each area:

1. There will be more standardization for short- and medium-span bridges and prestressed concrete will be used more frequently than reinforced concrete. For longer spans, there will be growing use of prestressed concrete segmental box-girder bridges, and cable-swayed bridges. In industrialized countries, including the United States, there will be increased concern for aesthetics and environmental harmony.

   This has definitely been the case and is still ongoing as evidenced by the following references [Refs. 14.12, 14.21, 14.35, 14.37, 14.41, 14.46, 14.49].

2. As to materials, higher strength-to-weight ratios will be utilized. This means higher-strength concretes and higher strength steels. More durable concrete decks (possibly polymerized) and more corrosion resistant tendons (possibly nonmetallic) are expected. Efforts at using recycled materials will increase.

   High strength and more generally high performance concretes (with compressive strength from 6 to 10 ksi (42 to 70 MPa)) are now the norm in prestressed concrete bridges. While prestressing steels with specified minimum strengths higher than 270 ksi (1860 MPa) are technically available, their higher cost does not justify their use yet. On the other hand, fiber reinforced polymeric tendons made with high performance fibers such as carbon and Kevlar are becoming available for applications where corrosion resistance and non-magnetic properties are needed.

3. The maintenance, rehabilitation, revitalization, or replacement of old bridges will assume a significant percentage of bridge work. New materials and new methods for repair work will emerge. Old bridges will be subjected to rigorous inspection.

   Infrastructure repair and rehabilitation has become one of the most extensive construction activity in the U.S. and many other industrialized countries.

4. Electronic computers will penetrate farther into almost every aspect of bridge analysis, design, construction, and management. Analysis and design procedures will become more exact and complex. Secondary factors such as temperature, fatigue, and creep will be increasingly assessed. Instrumentation and automatic recording equipment to determine more exactly actual loads, stresses, deformations, cracking, and their evolution with time will be commonly used. There will be increased use of load factor design, probabilistic design and optimum design.

   All the above predictions have materialized at time of this writing. The AASHTO LRFD code has been calibrated using probabilistic procedures.

5. The cost of construction will rise dramatically in both the material and labor sectors. There will be more prefabrication, better and more automatic construction equipment, and increased simplification of construction procedures.
   Indeed the cost of labor has increased dramatically and at a higher rate than the cost of basic construction materials. However, more can be done to foster prefabrication and standardization.

The above forecasts suggest that design will be simultaneously more global and more refined. Although very powerful analytic tools are available, one has to recognize that there are inherent idealizations in the design assumptions and inherent defects in the materials used and in the structures built. Hence, "it does no good to design to a level of refinement that cannot tolerate inherent materials and structural defects" [Ref. 14.51].

During the 20th century, bridge spans have increased almost four times, from 521 m for the Forth Rail Bridge in the U.K., to 1991 m for the Akashi-Kaikyo Bridge in Japan. Can we expect the increase to continue at the same rate? It is likely that record bridge spans above 1991 m will be broken during the 21th century. Advanced materials, advanced construction technologies and new structural concepts will have to be combined to achieve such limits. Already engineers have offered conceptual design for a 3000 m bridge span [Ref. 14.26]. Prestressed concrete may play a less important role in such bridges (except in the pylons) and advanced lighter materials such as carbon fiber reinforced polymeric tendons may have to be used for the suspension cables. It is likely, however, that life-cost effectiveness and rate of return on investment will increasingly become the deciding factors for how long a span will be.

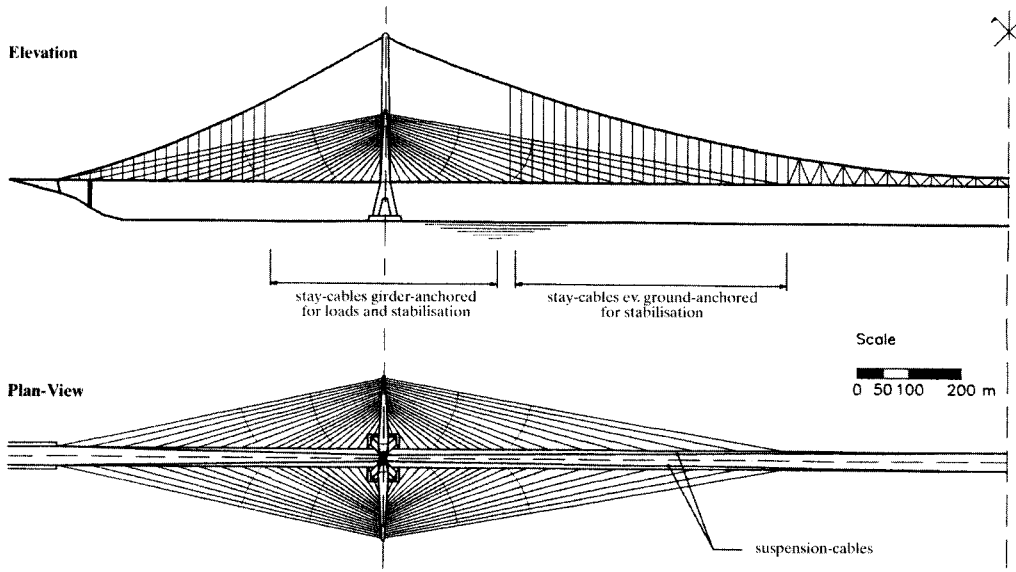

Figure 14.51 Elevation and plan view of half of a 3000 meters conceptual bridge system *(from Ref. 14.26, C. Menn and D. Billington).*

According to the United States' Federal Highway Administration (FHWA), the US has about 600,000 bridges overall and is building, replacing, or rehabilitating 10,000 of those structures each year at an annual cost of $7 billions. As the public demands increased mobility and minimal congestion, the need for safe long-lasting bridges will only increase. Technology is expected to provide the innovative tools, techniques, procedures and materials for solution.

In an FHWA draft report titled, "Infrastructure Research and Technology Program," presented at the Stakeholder Workshop in Chicago, in November 2002, it was suggested that the new generation of bridges should provide unprecedented long-term performance by effectively using and combining high performance materials into the most structurally efficient and cost-effective systems. The following vision of the "bridge of the future" and performance objectives were suggested:

- Material degradation no longer a factor in limiting service life
- One-tenth the current construction time
- Easily widened or adapted to new demands, in a weekend
- Life-cycle cost less than one-tenth of current bridges
- Immune to flooding, earthquakes, fire, wind, fracture, corrosion, overloads, and vessel collision
- Entire bridge (foundation to parapet) designed and constructed as a system
- Lateral clearance greatly increased with longer spans
- Elimination of vertical clearance problems with shallower structures
- Constructability as important as durability
- Designed for inspection and maintenance

It is recognized that the above goals will stretch the limits of creative and technological capabilities of civil engineers, and will remain in force for the foreseeable future.

REFERENCES

14.1 American Association of State Highways and Transportation Officials, AASHTO, "*Standard Specifications for Highway Bridges*," 16th ed., Washington, DC, 1996.

14.2 American Association of State Highways and Transportation Officials, AASHTO, "*AASHTO LRFD Bridge Design Specifications*," 2nd ed., Washington, DC, 1999 and Interim 2001.

14.3 ACI Committee 343, "Analysis and Design of Reinforced Concrete Bridge Structures - ACI343R-95," American Concrete Institute, Manual of Concrete Practice, Farmington Hills, MI, 2000 and continuing versions.

14.4 ACI Committee 440, FRP Report "Guidelines for Prestressing Concrete Structures with FRP Tendons," American Concrete Institute, Farmington Hills, Michigan, 2002.

14.5 American Railway Engineering and Maintenance-of-Way Association, AREMA, "*Manual of Railway Engineering*," AREMA, Landover, Maryland, 2002.

14.6 American Segmental Bridge Institute, "Recommended Practice for Design and Construction of Segmental Concrete Bridges," Phoenix, Arizona, 2001.

14.7 "Bridge Aesthetic around the World," Transportation Research Board, National Research Council, Washington, DC, 1991.

14.8 Barker, R. M., and J.A. Puckett, *Design of Highway Bridges – Based on AASHTO LRFD Bridge Design Specifications.* New York: John Wiley and Sons, 1997, 1169 pp.

14.9 Collins, M. P., and D. Mitchell, *Prestressed Concrete Structures*. Englewood Cliffs, NJ: Prentice Hall, 1991.

14.10 Cusens, A. E., and Y. C. Loo, "Application of the Finite Strip Method in the Analysis of Concrete Box Bridges," Proceedings of the Institution of Civil Engineers, Vol. 57, Pt. 2, Research and Theory, June 1974, pp. 251-273.

14.11 Elliott, A. L., "Steel and Concrete Bridges." In *Structural Engineering Handbook*, E. H. Gaylord, Jr., and C. N. Gaylord, eds. New York: McGraw-Hill, 1990.

14.12 "Esthetics in Concrete Bridge Design." In *Manual of Concrete Practice*. Farmington Hills, MI: American Concrete Institute, 1990.

14.13 Freyermuth, C. L. "Design of Continuous Highway Bridges with Precast, Prestressed Concrete Girders," *PCI Journal*, 14(2): 14-39, 1969.

14.14 Gentillini, B., and L. Gentillini, "Precast Prestressed Segmental Elevated Urban Motorway in Italy," *PCI Journal*, 20(5): 26-43, 1975.

14.15 Gerwick, Jr., G. C., "Prestressed Concrete Developments in Japan," *PCI Journal*, 23(6): 66-76, 1978.

14.16 Grant, A., "The Pasco-Kennewick Intercity Bridge," *PCI Journal*, 24(3): 90-109, 1979.

14.17 IABSE-FIP International Conference Proceedings, Dauville, IABSE, Zurich, 1994.

14.18 Ito, M., Y. Fujino, T. Miyata and N. Narita, eds., *Cable-Stayed Bridges: Recent Developments and their Future*. Amsterdam: Elsevier, 1991, 438 pp.

14.19 Jacques, F. J., "Study of Long Span Prestressed Concrete Bridge Girders," *PCI Journal*, 16(2): 24-42, 1971.

14.20 Koenig G., R. Mauer, and T. Zichner, "*Spannbeton: Bewahrung im Bruckenbau*," in German. Berlin: Springer-Verlag, 1986, 328 pp.

14.21 Leonhardt, F., *Bridges: Aesthetic and Design*. London: The Architectural Press, and Cambridge, MA: The MIT Press, 1982.

14.22 Libby, J. R., "Segmental Box Girder Bridge Superstructure Design," *ACI Journal* 73(5): May, 1976, pp. 279-290.

14.23 Lin, T. Y., and F. Kulka, "Construction of Rio Colorado Bridges," *PCI Journal*, 18(6): 92-101, 1973. See also E. Loh, "Comments on Construction of the Rio Colorado Bridge," PCI Journal, 19(2): 131-33, 1974.

14.24 Matsushita, H., and M. Sato, "The Hayshi-No-Mine Prestressed Bridges, *PCI Journal*, 24(2): 90-109, 1979.

14.25 Menn, C., "*Stahlbeton-Brucken*," (Reinforced Concrete Bridges), in German. Wien: Springer-Verlag, 1986, 533 pp.

14.26 Menn, C., and D. Billington, "Breaking Barriers of Scale: a Concept for Extremely Long Span Bridges," *Structural Engineering International*, IABSE, 5(1): 48-50, 1995.

14.27 Muller, J., "Ten Years of Experience in Precast Segmental Construction," *PCI Journal*, 20(1): 28-61, 1975.

14.28 Naaman, A. E., "FRP Reinforcements in Concrete Structures: Design Issues, Potential Solutions, Realistic Applicability." *Proceedings of the Second Middle East Symposium on Structural Composites for Infrastructure Applications,* A. H. Hosni, I. Mahfouz, and S. Sarkarni, eds., April 1999, pp. 99-118.

14.29 Naaman, A. E., "Unified Bending Strength Design of Concrete Members: AASHTO LRFD Code," *Journal of Structural Engineering*, ASCE, 121(6): 964-70, 1995.

14.30 Naaman, A. E., "Computer Program for Selection and Design of Simple Span Prestressed Concrete Highway Bridges," *PCI Journal*, 17(1): 73-81, 1972.

14.31 Nowak, A. S., "Calibration of LRFD Bridge Code," *Journal of Structural Engineering*, ASCE, 121(8): 1245-51, 1995.
14.32 Nowak, A. S., and K. Collins, *Reliability of Structures*. New York: McGraw Hill, 2000, 338 pp.
14.33 Podolny, Jr., W., "An Overview of Precast Prestressed Segmental Bridges," *PCI Journal*, 24(1): 68-69, 1979.
14.34 Podolny, Jr., W., and J. M. Muller, *Construction and Design of Prestressed Concrete Segmental Bridges*. New York: Wiley, 1982.
14.35 Podolny, Jr., W., and J. B. Sclazi, *Construction and Design of Cable-Stayed Bridges*. New York: Wiley, 1986.
14.36 *PCI Bridge Design Manual*, Precast Prestressed Concrete Institute, Chicago, MNL-133-97, 1997. Also *PCI Design Handbook*, 5th ed., 1999.
14.37 Posttensioning Institute, *Post-Tensioning Manual*, 6th ed. Phoenix, AZ, 2003.
14.38 *Precast Segmental Box Girder Bridge Manual*, Joint Publication by the Post Tensioning Institute and the Prestressed Concrete Institute, Chicago, Illinois, 1978, 116 pp.
14.39 *Precast Prestressed Concrete Short Span Bridges - Spans to 100 Feet*, 2nd ed., Prestressed Concrete Institute, Chicago, Illinois, 1981.
14.40 "Ruck-A-Chucky Bridge," First Prize of the 26th Progressive Architecture Award, *Progressive Architecture*, January 1979, pp. 56-87.
14.41 Schlaich, J., and H. Sheef, "Concrete Box Girder Bridges," Structural Engineering Documents, IABSE, Zurich, 1992.
14.42 Schlaich, J., and K. Schafer, "Toward a Consistent Design of Structural Concrete," *PCI Journal*, 32(3): 74-150, 1987. See also closure to discussion in 33(6): 171-79, 1988.
14.43 Tang, M. C., "Talmage Memorial Bridge, Savannah, Georgia," *Structural Engineering International*, 5(1): 15-16, 1995.
14.44 Tonias, D. E., "Bridge Engineering – Design Rehabilitation and Maintenance of Modern Highway Bridges." New York: McGraw-Hill Inc., 1995, 470 pp.
14.45 Tokerud, R., "Precast Prestressed Concrete Bridge for Low-Volume Roads," *PCI Journal*, 24(4): 42-56, 1979.
14.46 Troitsky, M. S., "Cable-Stayed Bridges." New York: Van Nostrand Reinhold, 1988.
14.47 Vecchio, F J., and M. P. Collins, "The Modified Compression Field Theory for Reinforced Concrete Elements Subjected to Shear," *ACI Journal*, 83(2): 219-31, 1986.
14.48 Wheen, R. J., "The Rip Bridge - A Unique Australian Structure," *Concrete International*, 1(11): 12-15, 1979.
14.49 Xanthakos, P., *Theory and Design of Bridges*, New York: John Wiley and Sons, 1994.
14.50 Yee, A. A., "Record Span Box Girder Bridge Connects Pacific Islands," Concrete International, 1(6): 22-25, 1979.
14.51 Zuk, W., "A Forecast of Bridge Engineering, 1980-2000," Virginia Highway and Transportation Research Council, Report No. 79-R55. Charlottesville, Virginia, June 1979, 57 pp.
14.52 Mirmiran, A., S. Kulkarni, R. Castrodale, and R. Miller, "Nonlinear Continuity Analysis of Precast, Prestressed Concrete Girders Made Continuous with Cast-in-Place Decks and Diaphragms," *PCI Journal*, 46(5): 60-78, 2001.

PROBLEMS

14.1 Drawing on information available in the technical literature, describe the construction sequence of a recently built prestressed concrete bridge. Point out challenging problems that were encountered, how they influenced the design, and how they were resolved. Finding examples with innovative approaches and solutions, whether in design or construction, is especially encouraged.

14.2 Consider the two-lanes bridge section of Fig. P14.2.
(*a*) Determine the maximum moment due to live load plus impact on the interior beam (shaded area) (Fig. P14.2) assuming a simple span $l = 120$ ft and AASHTO loading. Use the distribution factor from Table 14.7, case (e) as if T or I beams were used.
(*b*) Determine the live load moment plus impact on the whole bridge, assuming the section is a single beam.

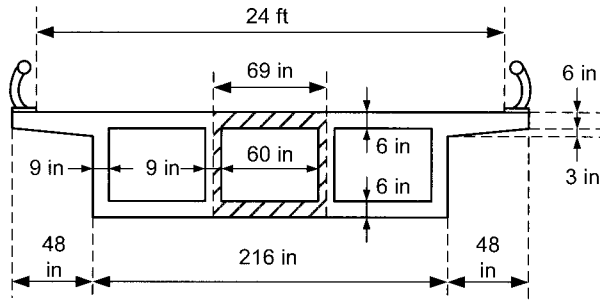

Figure P14.2

14.3 Going back to the example of Sec. 14.12 with the two-span continuous bridge, determine the HS truck position and corresponding maximum positive moment in span using the AASHTO HL93 loading.

14.4 Referring to the example of Sec. 14.11 with the adjacent precast pretensioned box beams, repeat the problem assuming a span $l = 70$ ft. If needed, select a different beam depth from Fig. 14.5.

14.5 Referring to the example of Section 14.10, assume that the span length is modified to 120 ft. Keeping everything else same, select the appropriate AASHTO girder from Fig. 14.6 and repeat the entire design. Make any other reasonable assumption when needed.

14.6 Provide a preliminary design for a composite bridge deck with AASHTO type IV precast prestressed beams and a cast-in-place reinforced concrete slab, similar to the example of Section 14.10. The beams are simply supported with a 90 ft span. Use the following variables: $S = 8$ ft, slab thickness = 8 in, f'_c = 7000 psi for the precast prestressed beams. Make any other reasonable assumptions when needed. Follow the AASHTO LRFD specifications. Design not only for the value of the prestressing force and eccentricity at midspan, but also ultimate strength requirements and shear. Check your answer with that obtained from the approximate design chart given in Fig. 14.49.

14.7 A simply supported bridge spanning 140 ft is to be designed for four traffic lanes according to the AASHTO LRFD specifications. In addition to the self-weight of the bridge, a superimposed dead load equivalent to 50 psf is specified; it is assumed due to the asphalt overlay and to water pipes carried inside the box. The following information is given:

Normal weight concrete: $\gamma_c = 150$ pcf; $f'_c = 6000$ psi; $f'_{ci} = 4500$ psi; $E_c = 4696$ ksi;

$\bar{\sigma}_{ti} = -201$ psi; $\bar{\sigma}_{ci} = 2700$ psi; $\bar{\sigma}_{ts} = -232$ psi;

$\bar{\sigma}_{cs} = 0.60 f'_c = 3600$ psi, or $0.45 f'_c = 2700$ psi, or $0.40 f'_c = 2400$ psi

$f_{pu} = 270$ ksi; $f_{pe} = 150$ ksi; $\eta = F / F_i = 0.80$; $(e_o)_{mp} = h/2 - 3$ in

Two solutions are considered, both leading to the same deck cross section: a) a multibox cast-in-place posttensioned deck, and b) precast prestressed concrete beams placed adjacent to each other. For each of the above cases determine the minimum depth, h, of the bridge based on working stress

design only. Round off the value of h obtained to the next higher integer. Determine the required prestressing force and eccentricity at midspan.

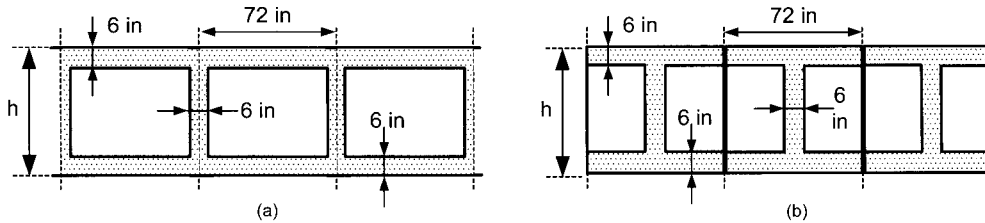

Figure P14.7

14.8 Consider the same problem as 14.7. For each case, (a) or (b) determine the controlling strength design moment, M_u, and the minimum depth, h, of the prestressed bridge beam based only on the ultimate strength design requirements of the AASHTO LRFD specifications in bending. Assume as a first approximation that the neutral axis at ultimate, c, should not exceed $hf = 6$ in (i.e., rectangular section behavior), and that $d_p = h - 3$ in. Round off the value of h to the next higher integer. Determine the required area of prestressing steel, A_{ps}, needed to satisfy the USD requirements at midspan.

14.9 Consider a pedestrian bridge made out of a series of simply supported T beams as shown in Fig. P14.9. The beams are precast pretensioned with a span length of 70 feet. The following information is provided using the AASHTO LRFD code units and specifications:

- $f'_c = 5000$ psi, $f'_{ci} = 4000$ psi,
- Initial tensile stress limit: $\bar{\sigma}_{ti} = -0.22\sqrt{f'_{ci}} = -0.44$ ksi = - 440 psi,
- Initial compression stress limit: $\bar{\sigma}_{ci} = 0.6 f'_{ci} = 2400$ psi,
- Final (in service) compression stress limits: $\bar{\sigma}_{cs}$ = due to effective prestress and permanent loads = $0.45 f'_c = 2250$psi; due to one half of effective prestress and permanent loads = $0.40 f'_c = 2000$ psi; due to effective prestress, permanent loads, and transient loads = $0.60 f'_c = 3000$ psi
- Final (in-service) tensile stress limit: $\bar{\sigma}_{ts} = -0.19\sqrt{f'_c} = -0.4249$ ksi = - 424.9 psi
- Normal weight concrete: $\gamma_c = 150$ pcf
- Live load = 85 psf; superimposed dead load = 25 psf (wearing asphalt surface)
- Assume: $f_{pe} = 150$ ksi; $f_{pi} = 189$ ksi; $\eta = f_{pe} / f_{pi} = F / F_i = 0.794$; that is: prestress losses after transfer = 39 ksi (AASHTO); $E_{ps} = 27000$ ksi.
- Assume: $(e_o)_{mp} = y_b - 4 = 23.1$ in.

In order to calculate the stresses the geometric properties of the section (Fig. P14.9) and the applied bending moments are needed.

- Minimum moment: $M_{min} = M_G = 0.573(70^2/8) = 350.962$ kips-ft
- Moment due to superimposed dead load: $M_{SD} = 0.1(70^2/8) = 61.25$ kips-ft
- Moment due to live load: $M_L = 0.34(70^2/8) = 208.25$ kips-ft
- Additional moment due to superimposed dead load and live load:
  $\Delta M = 0.44(70^2/8) = 269.5$ kips-ft.
- Maximum moment: $M_{max} = M_{min} + \Delta M = 620.462$ kips-ft.
- Sustained moment: $M_{sus} = M_G + M_{SD} = 412.212$ kips-ft.

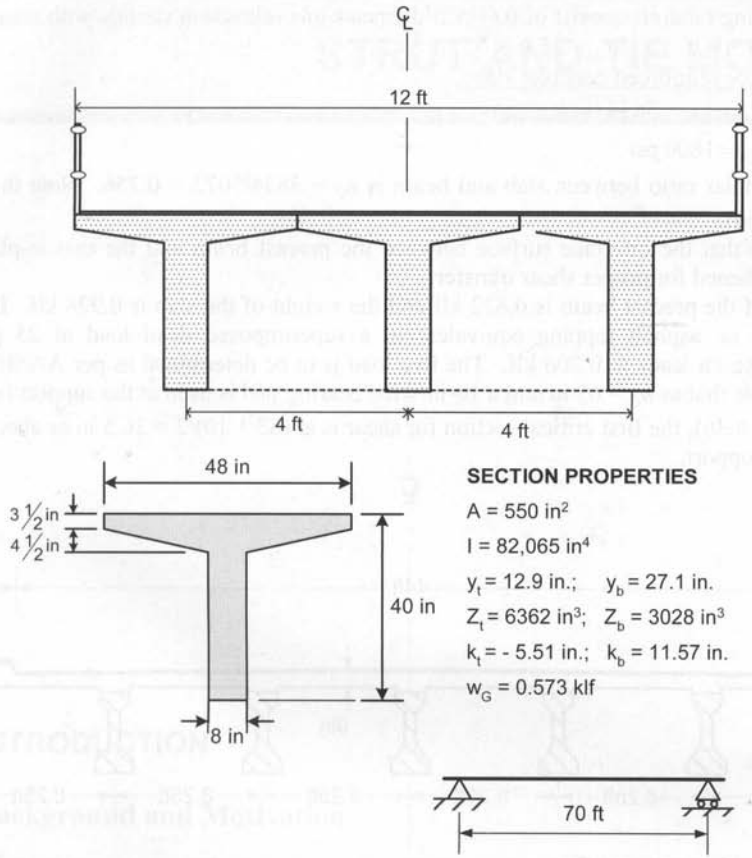

Figure P14.9 Cross section of pedestrian bridge and beam section properties.

Provide a complete design for the beam. Note that the prestressing force and the prestressing steel profile can be taken same as in the example of Section 4.10.

14.10 Repeat the example of Section 14.10 for the bridge deck and typical interior prestressed I-girder described in Fig. P14.10. The span is 80 ft and the cast-in-place concrete slab is 9 in thick. Unshored construction is assumed. The spacing S, center to center, between beams is 8.25 ft. Beam cross-sectional dimensions are given in Fig. 14.36. The precast beam and the slab are made of normal weight concrete with $\gamma_C = 150$ pcf. The following information is provided.

For the precast prestressed beam:

$\gamma_c = 150$ pcf; $f'_c = 7000$ psi; $f'_{ci} = 5000$ psi; $E_c = 5072$ ksi; $E_{ci} = 4287$ ksi;

$f_{pu} = 270$ ksi; $f_{pe} = 150$ ksi; $f_{pi} = 187.5$ ksi; $f_{py} = 243$ ksi; $\eta = F / F_i = 0.80$; $(e_o)_{mp} = y_b - 4$ in

$\overline{\sigma}_{ti} = -0.22\sqrt{f'_{ci}} = -0.22\sqrt{5.0} = -0.491$ ksi $= -492$ psi; $\overline{\sigma}_{ci} = 0.60 f'_{ci} = 3000$ psi;

$\overline{\sigma}_{ts} = -0.0948\sqrt{f'_c} = -251$ psi; $\overline{\sigma}_{cs} = 0.45 f'_c = 3150$ psi, or $0.60 f'_c = 4200$ psi, or $0.40 f'_c = 2800$ psi

The initial stress after transfer, f_{pi}, is estimated at 187.5 ksi leading to $\eta = 150/187.5 = 0.80$. This implies that total prestress losses after transfer are about = 37.5 ksi, leading to an effective prestress $f_{pe} = 150$ ksi.

The prestressing tendons consist of 0.6-inch-diameter low relaxation strands with area per strand equal to 0.216 in^2.

For the cast-in-place reinforced concrete slab:

$f'_{cslab} = 4000$ psi, $E_{cslab} = 3834$ ksi

$\bar{\sigma}_{cslab} = 0.45 f'_{cslab} = 1800$ psi

Thus the modular ratio between slab and beam is n_C = 3834/5072 = 0.756. Note that $n_c = 1/n$ [AASHTO notation].

It is assumed that the interface surface between the precast beam and the cast-in-place slab is intentionally roughened for proper shear transfer.

The weight of the precast beam is 0.822 klf and the weight of the slab is 0.928 klf. In addition, the slab supports an asphalt topping equivalent to a superimposed dead load of 25 psf on the composite beam which leads to 0.206 klf. The live load is to be determined as per AASHTO-LRFD specifications. Note that as h_C = 63 in and a 10-in-wide bearing pad is used at the support (similarly to the detail in Fig. 14.36), the first critical section for shear is at (63 + 10)/2 = 36.5 in or about 3 ft from the center of the support.

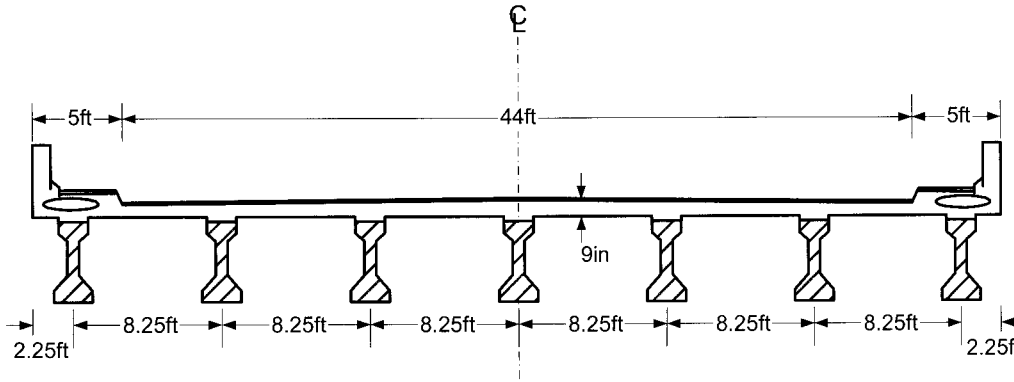

Figure P14.10 Bridge cross section.

CHAPTER 15

STRUT-AND-TIE MODELING

15.1 INTRODUCTION

15.1.1 Background and Motivation

A strut-and-tie model of a structure is an idealized hypothetical truss that fits into the envelope of a structure and transmits forces from loading points to supports. The shape and geometry of the truss provide a visual representation of the flow of forces in the structure. Strut-and-tie models are particularly useful in regions of the structure where stresses cannot be computed from elastic bending theory.

Since its first introduction by Ritter (1899) and Mörsch (1902, 1909), the idea of using truss models to simulate the response of cracked reinforced concrete in shear has slowly evolved throughout the twentieth century. However, in the early 1980s, a revival of the idea occurred spurred by significant interest in truss modeling by the technical professional community worldwide, particularly because of the need to arrive at rational procedures for shear and torsion design of structural concrete. Since then, strut-and-tie models have been the subject of numerous studies leading to a first set of recommendations in the CEB Model Code in 1990 [Ref. 15.8]; they were implemented successively in the Canadian code (1994) [Ref. 17.7], the AASHTO LRFD code (1993) [Ref. 15.2], ACI-ASCE Committee 445 recommendations [Ref. 15.3], and the ACI code (2002) [Ref. 15.4]. The FIP

Recommendations on Practical Design of Structural Concrete where strut-and-tie models are addressed, were first released in 1996 [5.12] and the American Concrete Institute introduced Appendix A - Strut-and-Tie Models in its 2002 edition of the code. This last milestone clearly indicates that assumptions, rules, and procedures for strut-and-tie modeling have matured sufficiently since the 1980s. However, it is expected that the evolution will continue in the future and specifications regarding strut-and-tie models will see numerous changes and likely simplifications.

This chapter provides a brief summary of the application of strut-and-tie models with particular attention to prestressed concrete. It synthesizes key information for their application. The material used was inspired by a number of references listed at the end of this chapter which should be consulted for additional details and background [Refs. 15.3, 15.9, 15.13, 15.14, 15.16, 15.17, 15.23, 15.28, 15.31, 15.32, 15.36, 15.37 and 15.38]. In particular the 2002 ACI code and the following references were heavily relied on: Refs. [15.9, 15.13, 15.14, 15.16, 15.23, 15.28, 15.31, and 15.37].

15.1.2 B- and D-Regions

Concentrated loads, support reactions, and abrupt changes in geometry create discontinuities in the flow and distribution of stresses in a structural member. St. Venant's principle indicates that the stresses due to axial load and bending only approach a linear distribution at a certain distance away from the discontinuity. That distance is generally taken as the larger dimension of the member cross section, that is depth h or width b. After such distance stresses in beams can be computed from bending theory. The region where stresses cannot be computed from the flexure formula are called D-regions, where D stands for disturbed or discontinuity, while the region of the beam where bending theory applies are called B-regions where B stands for beam or bending. B-regions are also regions where Bernouilli's widely accepted hypotheses, that is, plane sections remain plane under bending, prevails. Practically, B-regions occupy any portion of the member outside D-regions. Figure 1 illustrates an example of B and D regions in a typical rectangular beam subjected to a concentrated load at midspan. ACI defines a D-region as the portion of the member within a distance equal to the member height, h, or depth, d_e, from a force discontinuity or a geometric discontinuity. Using h instead of d_e is on the safe side. For a flanged member with a flange width b larger than member depth, the D-region can be assumed to extend a distance b from the discontinuity. Note also that a D-region may extend a different distance on either side of a geometric discontinuity.

In Fig. 1, the B-regions could be much longer leading to a relatively shallow beam, or may vanish altogether leading to a deep beam. If the beam is short (that is a small span-to-depth ratio), the D-regions, which are near applied concentrated forces, would cover the whole beam. In comparison, a slender beam is defined as having a shear span $a > 2h$.

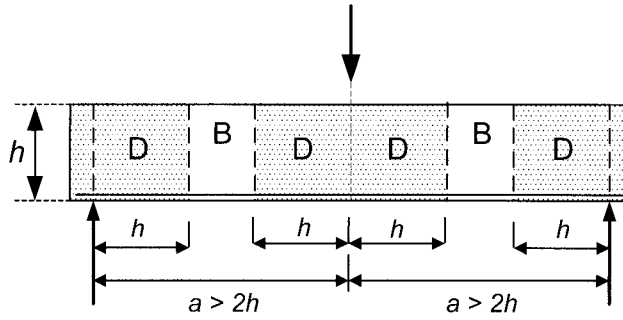

Figure 15.1 Definition of B- and D-regions in a typical beam; a deep beam will have no B-regions; a slender beam is defined as having a shear span $a > 2h$.

Traditional bending theory and the traditional design approach for shear (Chapter 6), where concrete and steel contribute ($V_c + V_s$) to shear resistance, does not apply to D-regions, because a major portion of the load is transferred directly to the supports by compressive concrete struts. Thus D-regions where shear and torsional forces can be controlling are more appropriately modeled by hypothetical trusses called strut-and-tie models.

Strut-and-tie models are very useful for the analysis of deep beams, corbels, anchorage zones of prestressed members, dapped-end beams, spandrel beams, pile caps, and the like. A number of examples illustrating for a typical D-region of a structure, the strut-and-tie model, and corresponding typical reinforcement are shown in Figs. 15.2 and 15.3. Note from Fig. 15.2 (left and right side of each truss) that more than one strut-and-tie model can be developed for a given structure.

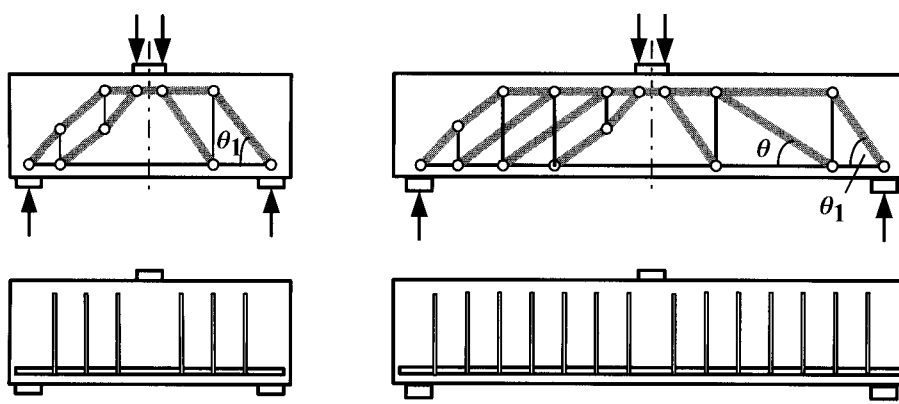

Figure 15.2 Typical strut-and-tie models of reinforced concrete short (deep) and long (slender) beams and their reinforcement; struts are in shaded lines and ties in full lines; the correlation between strut-and-tie models and trusses is clear from the upper part of the figure. *(Adapted from Ref. 15.31).*

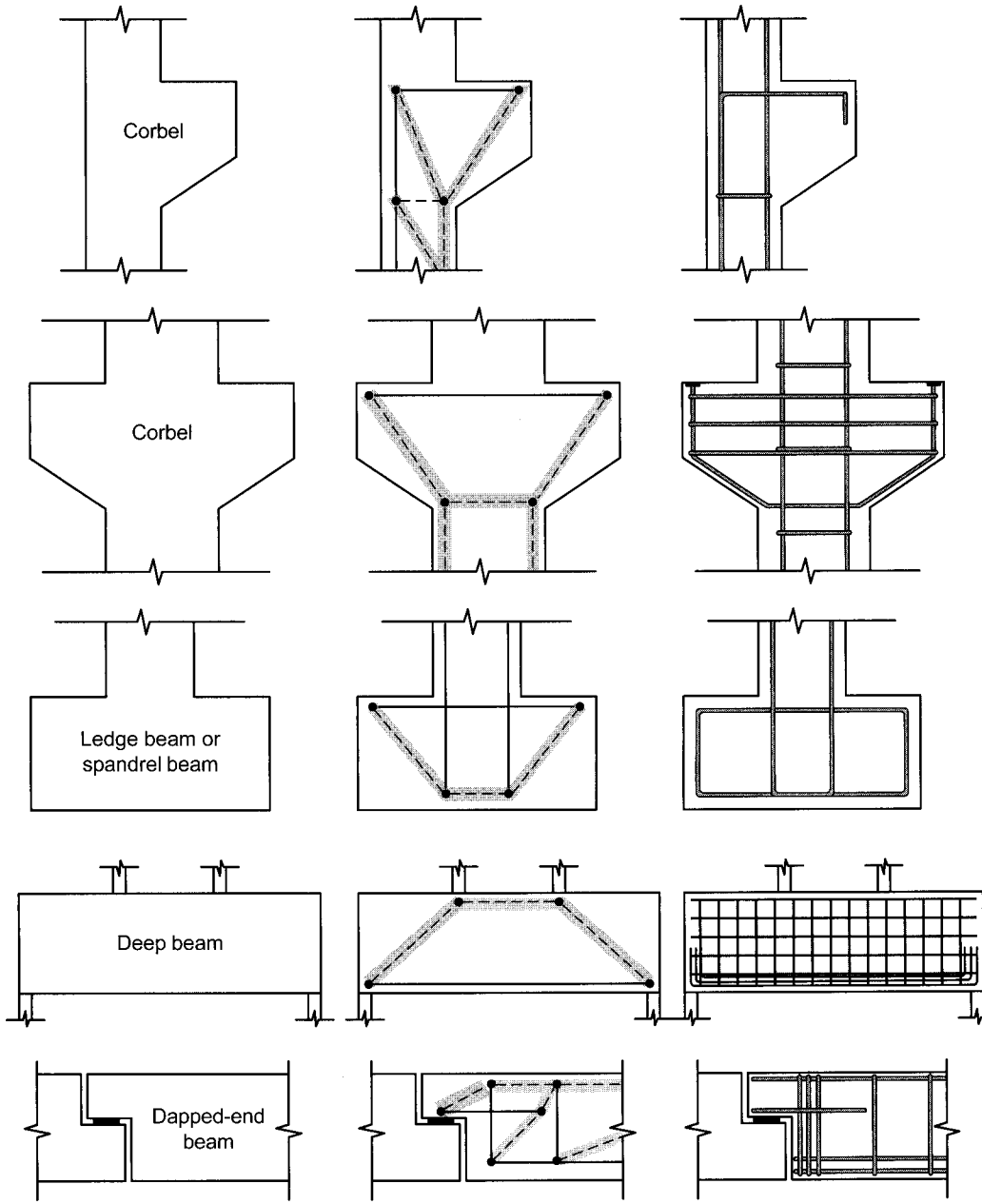

Figure 15.3 Examples where strut-and-tie modeling is needed. For each case, from left to right, the D-region of a member, the strut-and-tie model for it, and the reinforcement arrangement are shown. Struts are in dashed lines and ties are in full lines. *(Adapted from Refs. 15.9, 15.14, 15.28, and 15.38)*

15.1.3 Trusses and Strut-and-Tie Models

It is useful to point out the close similarities between trusses and strut-and-tie models not only in terms of their geometry and the underlying assumptions controlling their behavior, but also in terms of solution procedures. The following discussion pertains to plane or two-dimensional trusses and strut-and-tie models.

Trusses are assumed made of purely compression and purely tension members pin-jointed at their connections, that is, the joints are considered to be hinges that do not transfer any bending moment. In a steel truss, the hinge is simulated by either bolts, studs, or welded connections, and gusset plates may be used. Although these connections are not free to rotate like true hinges, they are sufficiently flexible in relation to the adjoining members to be considered hinges. Members of a truss are described as chords or bars, and also characterized as verticals, diagonals, or tensile and compressive members. Trusses can be statically determinate or statically indeterminate structures. Solution methods for statically determinate trusses include the well known sectional and joint methods. In the joint method, a successive analysis of equilibrium of forces at each joint leads to finding the forces in each member and thus provides a solution to the truss. A truss must be statically stable.

A strut-and-tie model is based on assumptions similar to those of a typical truss. Compression members are defined as struts, tension members are defined as ties, and joints are defined as nodal zones. The nodal zone can be thought of as a hypothetical fictitious hinging zone. Although a strut-and-tie can be statically indeterminate, it is preferable to select a statically determinate model to simplify the solution, because a statically indeterminate structure needs input parameters unknown at initial design, such as the stiffness of the various elements. A strut-and-tie model does not need to be statically stable. By convention, struts are drawn in full lines, and ties are drawn in dashed lines.

In building a strut-and-tie model it is useful to visualize the flow of stresses and follow potential load paths within the structure. Keep in mind that external loads must find their way to supports and other reaction points. Stress trajectories obtained from an elastic finite element analysis can be used to draw trajectories of load paths. Also simple observations of experimental cracking in a member may help develop a representative strut-and-tie model (Fig. 15.4). The trusses developed do not need to offer high levels of symmetry; correlating with the variable angle truss model can help. Many strut-and-tie models can be developed for the same D-region of a member. However, some models will be more efficient than others.

Strut-and-tie models do not have a unique solution. This is because only two criteria are considered in their design, equilibrium of forces, and strength of the elements. No compatibility of displacement is considered. According to the theory of plasticity, this method of analysis generally yields a lower bound solution with minimum strain energy [Refs. 15.13, 15.14, 15.16, 15.17,]. Indeed, the lower bound theorem of plasticity states [Ref. 15.22]: "*If an equilibrium distribution of stress can*

be found which balances the applied loads and is everywhere below yield or just at yield, the structure will not collapse or will just be at the point of collapse."

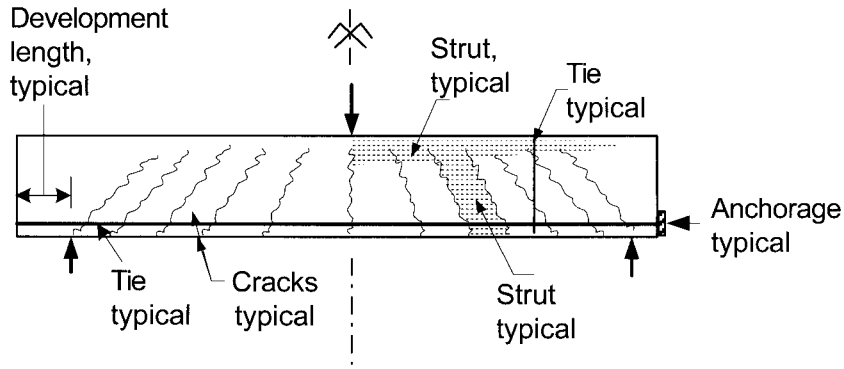

Figure 15.4 Typical cracking in RC beams and visual generation of strut-and-tie modeling.

Nilson et al. [Ref. 15.23] point out that, since ideally, an optimum strut-and-tie model should lead to a minimum energy distribution through the D-regions, forces should follow the stiffest load path. Since struts are typically much stiffer than ties, a model with a minimum number of tension ties is generally preferred. An optimum model is also a model that minimizes the amount of reinforcement used. Practically all models that satisfy equilibrium and strength limits can provide sufficient capacity as long as they are properly reinforced and impart sufficient ductility. Although some trial models may be necessary at first, generally, strut-and-tie models built using the recommendations of the ACI code should lead reasonably fast to an acceptable solution.

15.1.4 ACI Code Definition

The 2002 ACI code provides the following definition of a strut and tie model.

> *A model of a structural member, or of a D-region in such a member, made up of axially loaded struts and ties connected at nodes to form trusses capable of transferring the factored loads to the supports or to adjacent B-regions*

An example is shown in Fig. 15.5. In using the strut-and-tie procedure, it is noted that strength limit state is considered where all factored load effects (bending, shear, torsion) are analysed simultaneously. However, the strut-and-tie model should also allow the analysis of forces at serviceability limit states.

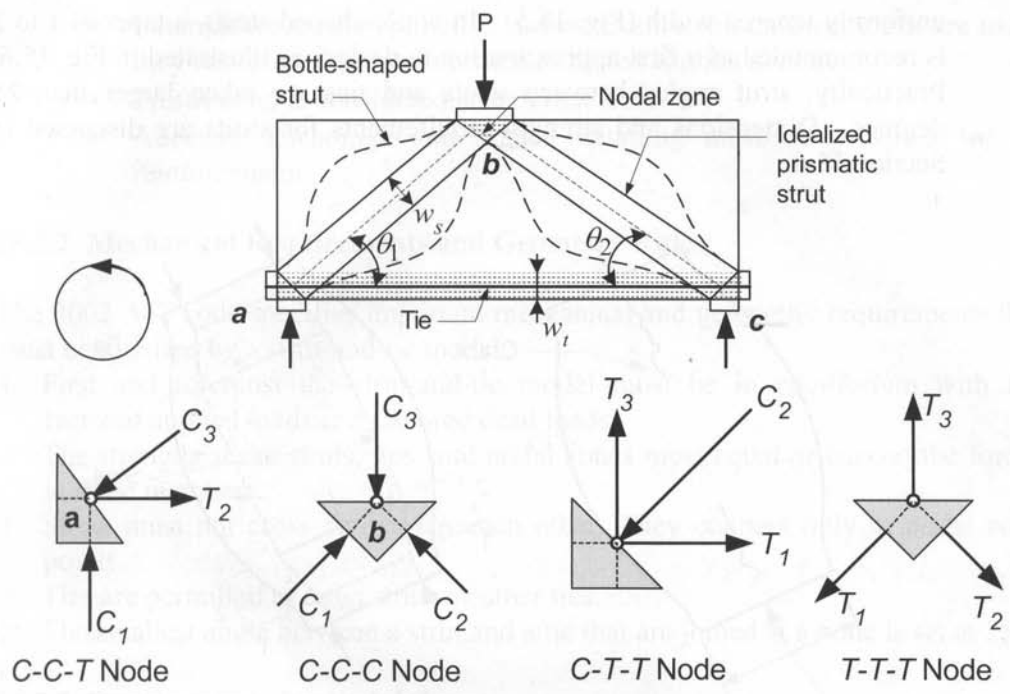

Figure 15.5 Typical configuration of strut-and-tie model and typical nodal zones.

15.2 ELEMENTS OF STRUT-AND-TIE MODELS

As suggested above, a strut-and-tie structure is essentially a truss structure. A truss only comprises tensile and compression members connected at joints; the members of the truss are assumed to carry no bending moments or shear forces; the joints are assumed to be hinges. The truss may be statically determinate or indeterminate, and should satisfy equilibrium. Strut-and-tie models for concrete structures have three types of elements as illustrated in Fig. 15.5:

1. **Ties.** These are tensile members in a strut-and-tie model. They are made out of a combination of reinforcement and concrete enveloping (surrounding) such reinforcement; the reinforcement, whether reinforcing bars or prestressing tendons, must be properly anchored. Note that the ACI code considers prestressing as an external loading. Hence, prestressing tendons may not show as ties in the D-region of a strut-and-tie model, yet they are present in addition to the reinforcement required by the model. Dimensions and strength requirements for ties are discussed in Section 15.5.
2. **Struts.** These are compression elements in a strut-and-tie model. They are made primarily of concrete or a combination of concrete and compression reinforcement. Struts are idealized as prismatic members of constant width or

uniformly tapered width (Fig. 15.5). In bottle-shaped struts, a taper of 1 to 2 is recommended as a first approximation in design, as illustrated in Fig. 15.6. Practically, strut angles between struts and ties are taken larger than 25 degrees. Dimensions and strength requirements for struts are discussed in Section 15.6.

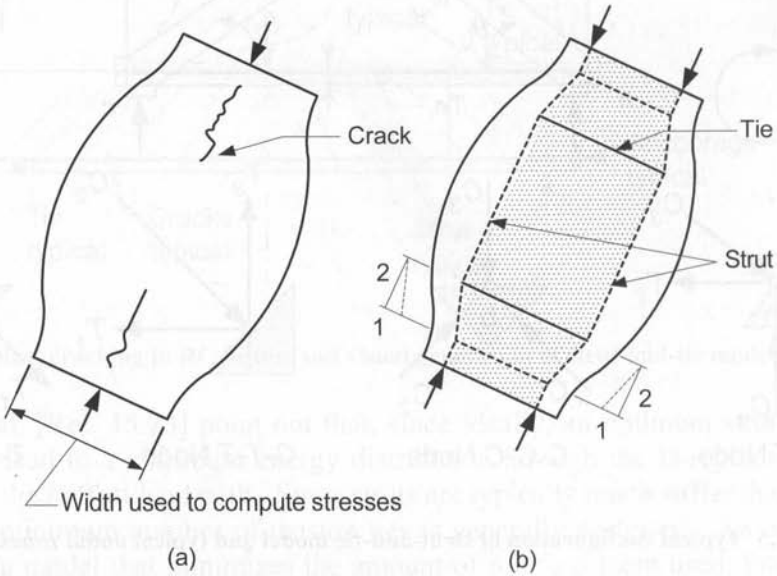

Figure 15.6 Common rule for modeling a bottle-shaped strut.

3. **Nodes and nodal zones.** These are equivalent to joints where the struts and ties connect. Nodal zones are confined areas of concrete that should satisfy strength requirements. Dimensions and strength requirements for nodal zones are discussed in Section 15.7.

15.2.1 Assumptions

The underlying assumptions for a code satisfactory strut-and-tie model are as follows:

- Forces in struts and ties are uniaxial, that is, either tension or compression.
- The contribution of concrete to tensile resistance of a tie is neglected; however, the presence of concrete in ties helps improve stiffness and reduce or control deformation; such information could be useful for analysis under service limit states.
- Ties should yield before struts crush in compression; this will insure some level of ductility.

- External forces are applied at nodes. Even when uniform loads are used, they are resolved into concentrated forces applied at nodes.
- Prestressing is considered an external load.
- Adequate anchorage and related detailing must be provided for all reinforcement.

15.2.2 Mechanical Requirements and Geometry Rules

The 2002 ACI code specifies important mechanical and geometric requirements that must be satisfied by a strut-and-tie model:

1. First and foremost the strut-and-tie model must be in equilibrium with the factored applied loads and factored dead loads.
2. The strength of the struts, ties, and nodal zones must equal or exceed the forces in these members.
3. Struts must not cross or overlap each other. They connect only at nodal zone points.
4. Ties are permitted to cross struts or other ties.
5. The smallest angle between a strut and a tie that are joined at a node is set at 25°.

15.2.3 Requirements for Nodal Zones

Equilibrium of forces must be satisfied at nodes or nodal zones. Nodal zones are assumed to be triangular in shape with only three sides, implying that three force resultants converge at the node. However, even when more than three forces intersect at the zone, the nodal zone is assumed to be triangular. Should two struts converge at different angles to the surface of a nodal zone, that surface can be taken normal to the resulting force from the two struts. An example is shown in Fig. 15.7.

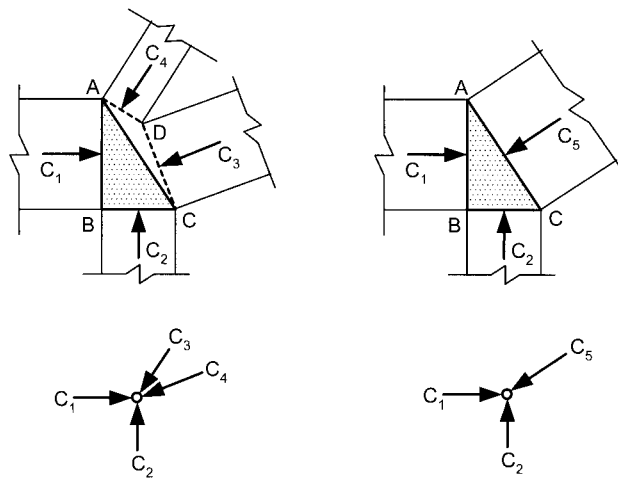

Figure 15.7 Resolution of forces from two struts into a single force (adapted from 2002 ACI code).

Also, the face of a nodal zone may be treated as a single surface or subdivided into smaller surfaces to equilibrate applied forces. Hence, a triangular nodal zone can be subdivided into two triangular parts provided equilibrium of forces is maintained for each part. Figure 15.8 illustrates this approach.

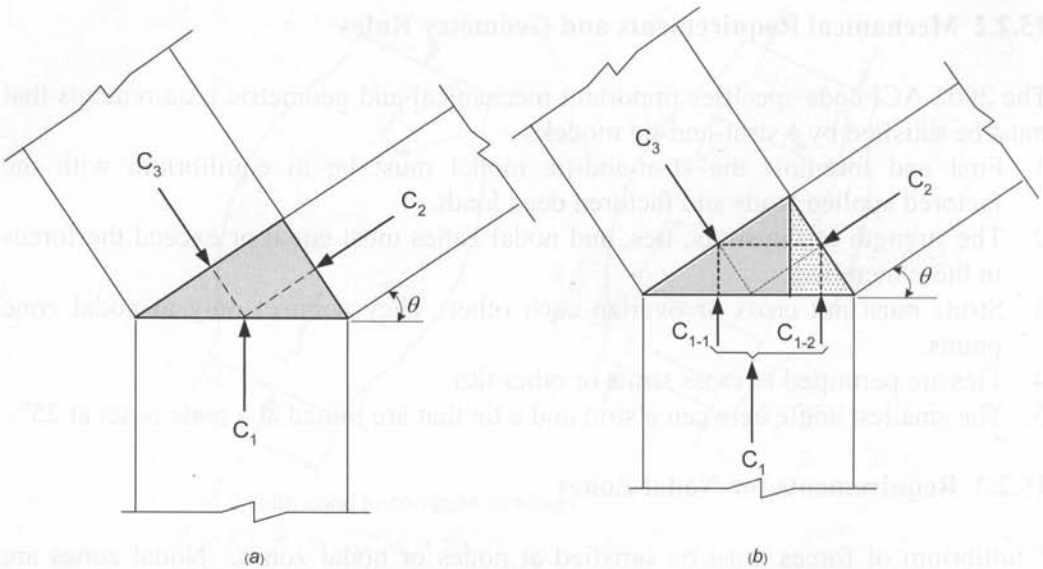

Figure 15.8 (a) Nodal zone. (b) Subdivided nodal zone (adapted from 2002 ACI code).

15.2.4 External and Unbonded Prestressing Tendons

Since by definition, according to the 2002 ACI code, a tie element is assumed to have a concrete component, it seems that external and unbonded prestressing tendons do not qualify as ties. When prestressing in a member is determined from bending theory, and the D-region of that member is designed by a strut-and-tie model, prestressing is considered an external force to the D-region, and, as such, it does not need to be modeled as a tie. However, in a design situation, where prestressing is to be determined from a strut-and-tie model, such as for a deep beam, the author believes that, in such a case, external and unbonded tendons can be treated as ties; this also assumes that the designer will pay attention to the possible consequences of deformation and crack widths, and will design for them. Indeed in the structure of Fig. 15.5, the bottom tie can be easily designed as an external or unbonded prestressing tendon.

Struts, ties, and nodal zone are to be dimensioned to satisfy certain design criteria. Rules given in the ACI code are described in Section 15.4 to 15.7 without justification.

15.2.5 Terminology / Notation

The terminology used in the ACI code is primarily followed in this chapter, except for the definition of forces; the ACI code uses F as a force in general for either strut, tie, of nodal zone forces. To avoid confusion with the notation used in this text in which F is the prestressing force, the value of force in general will be described by C for compression, T for tension, and P for applied external load. The following notation is used:

n = subscript for nominal
N = nominal resistance
u = subscript for ultimate
U = ultimate or factored load effect
s = subscript for strut
t = subscript for tie; thickness of member
C = compression force in strut
T = tensile force in tie
θ = angle; generally taken between strut and horizontal axis
w = width in general
w_b = width of bearing plate at support
w_s, w_t = width of strut and tie, respectively
w_1, w_2, w_3 = width of sides of triangular nodal zone, in general
w_v, w_h, w_d = width of vertical, horizontal, and diagonal side of triangular nodal zone, respectively

15.3 DESIGN STEPS TO BUILD A STRUT-AND-TIE MODEL (STM)

15.3.1 Initial Checks

Prior to building a strut-and-tie model, it is necessary to check some code limitations to ascertain that a model is allowed. The ACI code specifies the following limitation for deep beams:

$$V_n \le 10\sqrt{f'_c} b_w d_e \tag{15.1}$$

Should Eq. (15.1) not be satisfied, the cross section of the member should be increased. Otherwise a strut-and-tie model is allowed. Note that Eq. (15.1) does not necessarily imply failure of struts or ties, but rather provides an overall safety limit for the member.

For the anchorage zone of prestressed beams, it is also useful to check if the reaction can be neglected at first, to simplify the model and related computations. Section 15.9 explains the conditions under which the reaction can be neglected.

15.3.2 Design Steps

Several steps are needed to build an acceptable strut-and-tie model and are described in several references [Refs. 15.13, 15.23, 15.29, 15.37]. Some contain intermediate steps. Invariably some iteration and re-adjustment are needed prior to finalizing a design. Depending on the case, a step may be lengthier to complete for one problem than for another. The steps recommended by Nilson et al. [Ref. 15.23], are followed here, with some expansion:

1. ***Check if strut-and-tie model is allowed.*** This is done according to Section 15.3.1.

2. ***Define and isolate the D-region or member.*** This is done as suggested in Figs. 15.1 to 15.3. Note that the reinforcement in the B-regions of a prestressed member can be designed using bending theory, while the transverse reinforcement near the support can be designed using strut-and-tie modeling.

3. ***Find reactions and compute the force resultants on each D-region boundary.***
   a. Determine the loads on the structure and locate concentrated forces either from reactions, applied loads, or prestressing. If only the D-region of a larger member is under design, it is likely that the prestressing force has already been computed from bending theory. In that case prestressing is considered an external force. However, it is possible to design the prestressing force for the entire structure based on a strut-and-tie model of the structure. In that case, the prestressing tendons are designed as a tie in the strut-and-tie model. If some tendons are straight and some are draped, each group will be simulated by a tie. This is also true for each postensioning cable.

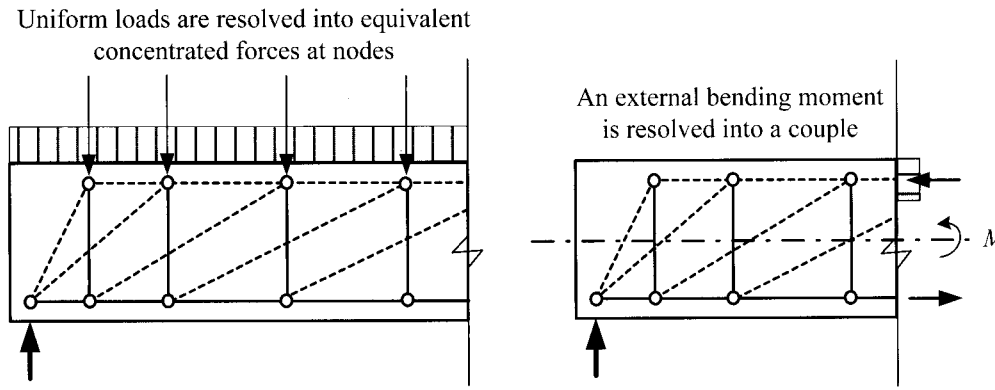

Figure 15.9 Resolution of applied loads into forces at joints.

b. Compute stress distributions on the boundary of the D-region or member to be analyzed and resolve these stresses into equivalent force resultants at node points (Fig. 15.9). Uniform loads can be resolved into equivalent concentrated loads applied at joints. An applied external bending moment can be resolved by a couple. Asymmetrical stresses or loads can be resolved by a couple and a force resultant. Some iteration with step 4 below may be necessary since this step implies that the location of some non-support nodes is known.

4. ***Select a strut-and-tie or truss model to carry the forces across the D-region or member.*** The axis of ties and struts, respectively, are selected to approximately coincide with the compression and tension fields. In this step all forces acting on the member or D-region are considered simultaneously. Assumptions and geometric rules suggested in Section 15.2 are used to develop an appropriate strut-and-tie model. Select practical dimensions for ties. This step is coordinated with step 2 and some iteration may be needed.

To illustrate this step and the preceding steps consider the end zone (D-region) of a prestressed beam with one anchorage as shown in Fig. 15.10. A straight tendon is used. To simplify the presentation, only the prestressing force from the tendon is considered and other forces, including the support reaction, are neglected (see Section 15.9). It is assumed that the beam is rectangular of width b and depth h, and that the anchorage is placed at the lower limit of the central kern, that is, at $k_b = h/6$ from the centerline. The corresponding stress diagram obtained from bending beam theory is triangular with zero stress on the top fiber and a maximum stress on the bottom fiber equal $2P/bh$. The stress diagram can be resolved into two equal forces of magnitude $P/2$ each. The location of each force should be at the centroid of the stress block of each part of the diagram. The upper part is a triangle and the lower part is a trapezoid. From the anchorage zone side, the compression force P is resolved into two forces along struts at 45°. The line of action of each strut intersect the line of action of the forces from the right side at nodes connected by a tie. The strut-and-tie model is shown in Fig. 15.10*a*. The reader may want to check that the tensile force in the tie is equal to $P/2$ and the force in each strut at 45° to the anchorage plate is $P/(2\cos 45^{\circ})$. Now, that a model is found, strengths of struts, ties and nodal zones must be checked as well as reinforcement and detailing provided.

Figure 15.10*b* illustrates the case where the anchorage force P is first resolved at the anchorage plate into two horizontal forces $P/2$, linked by a short strut (parallel to the anchorage plate) From each related joint, a strut emanates toward the inside of the zone, with a slope of one over two. A new strut-and-tie model is obtained. The reader may want to check that the tensile force in the tie is equal to $P/4$ and the compression force in the strut between the two ends of the anchorage plate is $(P\tan 26.6)/2 = 0.25P$.

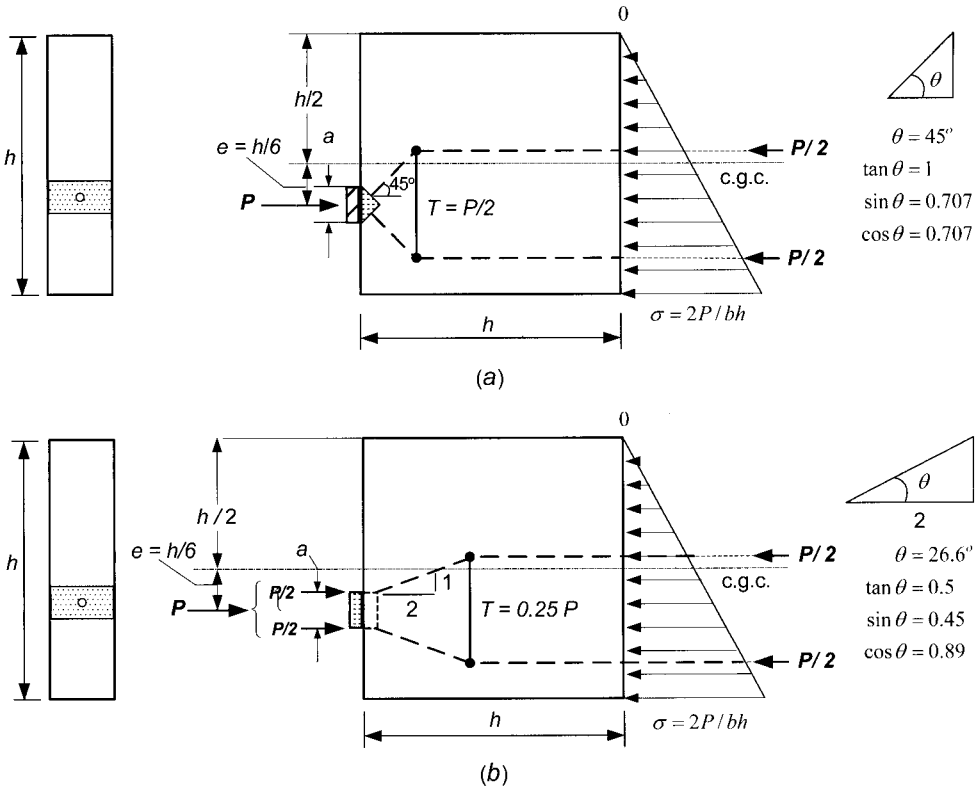

Figure 15.10 Strut-and-tie model for an anchrorage zone (assuming only prestressing force).

5. ***Compute the forces in the struts and ties.*** This is done one joint at a time starting at reaction nodes as per the method of joints in statically determinate trusses. Two equations of equilibrium, one for horizontal forces and one for vertical forces must be satisfied at each node. The method of sections for truss analysis may be useful at times to determine truss forces as well as external forces leading to equilibrium of the D-region. Some iteration may be needed with step 6 if dimensions are later modified.

6. ***Select dimensions for strut-and-tie nodal zones.*** The effective concrete strength in nodal zone is determined according to code recommendations (Eq. 15.6 and Table 15.1). Thickness of struts, ties and nodal zones are taken same as the thickness of the member. The effective widths of nodal zones are determined based on the forces obtained in Step 3 and the effective concrete strengths specified for nodal zones. Details on dimensioning of nodal zones are given in Section 15.7.

7. ***Verify the capacity of the struts both at midlength and at the nodal interface.*** Strengths of struts and ties are described in more details in Section 15.6 and 15.7. Verification at midlength mostly applies to bottle-shaped struts such as shown in Fig. 15.6.

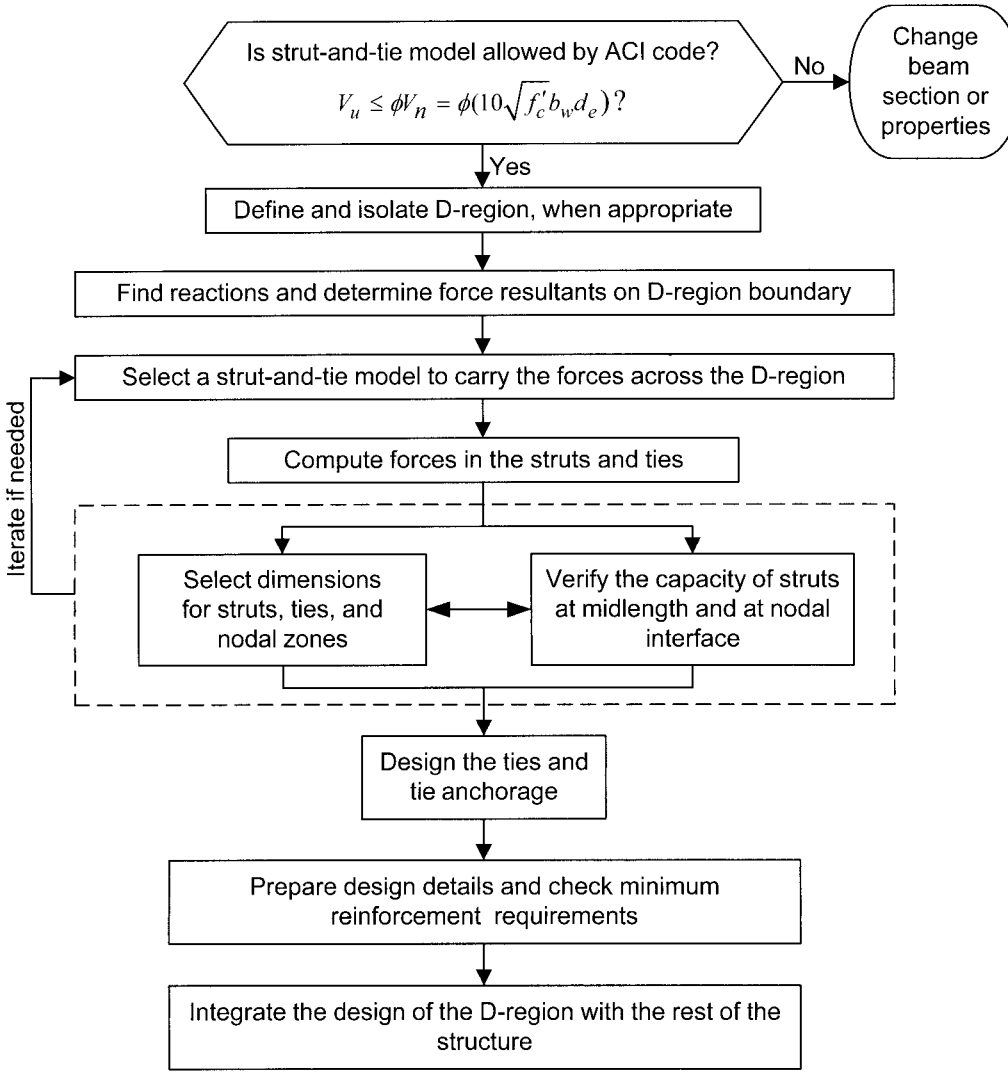

Figure 15.11 Flow chart illustrating the main steps in the strut-and-tie modeling procedure for a D-region.

8. ***Design the ties and tie anchorage.*** The tie includes the reinforcement and the prism of concrete surrounding the tie. Tie design involves selecting the area of steel reinforcement, insuring that the reinforcement is properly anchored, and verifying that the reinforcement fits within the tie width (either assumed, or derived from nodal zone design). See Section 15.5.

9. ***Prepare design details and check minimum reinforcement requirements.*** See Section 15.6

10. ***Provide design for the rest of the structure.*** The rest of the structure can be designed as a B-region. Then the design of the D-region must be integrated with that for the rest of the structure.

A flow chart summarizing the above steps is given in Fig. 15.11.

Strut-and-tie models are assumed to represent conditions for strength limit states; however, designers should also comply with the requirements for serviceability (deflection, crack width) as specified in the code.

15.4 DESIGN PHILOSOPHY

The general approach for ultimate strength design or load and resistance factor design is followed in the design of strut-and-tie models (see Section 3.5.2). The following typical equation applies:

$$\begin{cases} U \le \phi R_n \\ \Sigma \gamma_i Q_i \le \phi R_n \end{cases} \tag{15.2}$$

wher U is the factored load, R_n is the nominal resistance, ϕ is the resistance factor (or capacity reduction factor), and γ_i are the load factors for load effects Q_i. The 2002 ACI code recommends a ϕ factor equal 0.75 for struts, ties, and nodal zones. Load factors are as per Table 3.9.

If we apply the above equation to a typical strut or tie, we can write it in the following way:

$$\begin{cases} C_u \le \phi C_{ns} \\ T_u \le \phi T_{nt} \end{cases} \tag{15.3}$$

where C_u and T_u are the factored forces in the strut and tie, respectively, and C_{ns} and T_{nt} are their nominal resistance, respectively.

The nominal resistance, including that of nodal zones, is obtained from the effective strength recommended in the code for each element.

15.5 DESIGN OF TIES

Ties are tensile members of a strut-and-tie model properly anchored in nodal zones. Ties comprise reinforcement surrounded by a hypothetical concrete prism concentric with the axis of the tie, such as for the prestressing strands of a pretensioned beam. The dimensions of the tie must be selected so that the reinforcement is approximately

uniformly distributed over the tie width, w_t, and its thickness. Designing a tie implies the design of the reinforcement, its anchorage, and the dimensions (mostly width) of the tie to accommodate the reinforcement. The thickness of a tie is generally taken same as the thickness of the member, except for very wide members for which special provisions apply. Hence, for a simply supported T-beam, the thickness is equal to the web width. The width of a tie is generally governed by the allowable compressive stresses on the nodal zones where the tie connects with other members. In a pretensioned member with straight tendons, the width of a tie may be taken in preliminary dimensioning as twice the cover to the centroid of the reinforcement. Note that the concrete component of a tie is assumed not to resist any tensile force.

The 2002 ACI code recommends to take the nominal strength of a tie as:

$$T_{nt} = A_{st} f_y + A_{ps}(f_{pe} + \Delta f_p) \tag{15.4}$$

where $(f_{pe} + \Delta f_p)$ shall not exceed f_{py} and A_{ps} is zero for nonprestressed members. In Eq. (15.4) it shall be permitted to take Δf_p equal to 60 ksi (414 MPa) for bonded prestressed reinforcement, or 10 ksi (69 MPa) for unbonded prestressed reinforcement. Other values of Δf_p shall be permitted when justified by analysis.

The reinforcement of a tie shall be anchored by mechanical devices, post-tensioning anchorage devices, standard hooks, and development length of straight bar or tendons as per code specifications. An extended nodal zone is defined in the code to better accommodate development length (Section 15.7.3 and Fig.15.16). The development length of a tie reinforcement can be reduced by adding confinement reinforcement, fiber reinforcement, or by splicing with several layers of smaller bars.

A practical upper limit of the tie width can be taken as the width corresponding to the width in a hydrostatic nodal zone, calculated as:

$$w_{t,\max} = \frac{T_{ut}}{\phi \times t \times f_{cu}} \tag{15.5}$$

where f_{cu} is the applicable effective compression strength of the nodal zone and $T_{nt} = T_u / \phi$ is the nominal tensile strength of the tie.

15.5.1 Prestressing Tendons

For a fully prestressed beam without conventional reinforcing bars, Eq. (15.4) penalizes the use of prestressing steel especially for members with bonded tendons. Indeed the stress in the prestressing steel at nominal bending resistance of bonded tendons exceeds by a good margin the suggested limit value of f_{pe} + 60 ksi (see

examples in Chapter 5). For a beam with unbonded tendons, the limit of f_{pe} + 10 ksi is much closer to reality that for bonded tendons. Thus, if a beam prestressed with bonded tendons has a B-region, it will not be economical to use a strut-and-tie model for the design of the B-region, unless the above limitation is relaxed.

15.6 DESIGN OF STRUTS

The strut capacity is the product of its effective strength (in stress units) times its cross sectional area. The effective strength is described further below. The thickness of a strut is generally taken equal to that of the member. The width of a strut, w_s, is generally controlled by the width of the nodal zone, or bearing plate of a tie, if any. When ties are anchored through development length, strut width is then affected by the location and distribution of tie reinforcement and its anchorage.

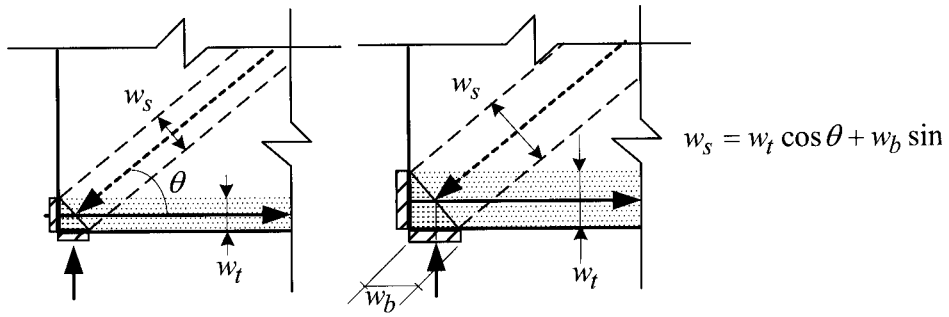

Figure 15.12 Width of compression strut as affected by width of tensile tie and size of bearing plate.

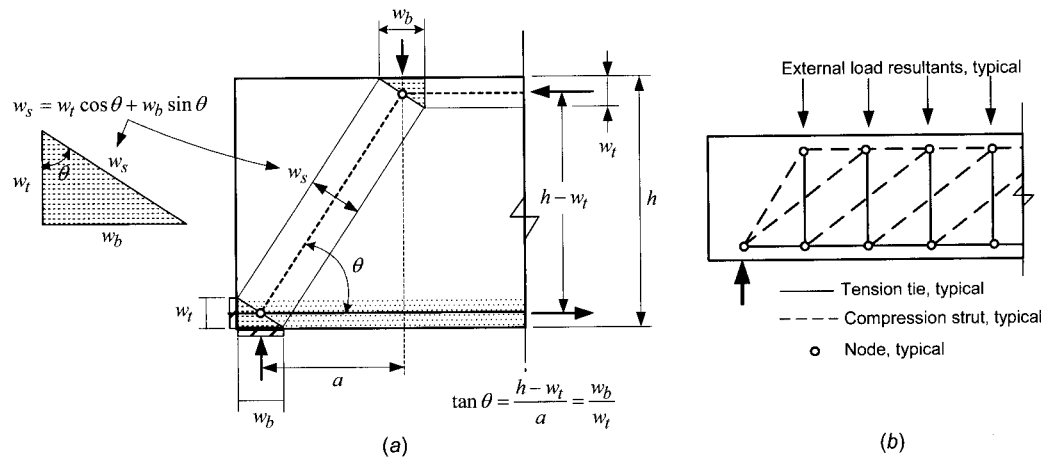

Figure 15.13 Example illustrating rapid dimensioning of strut-and-tie model. a) Useful formula and details. b) Complete strut-and-tie model with external loads.

Figure 15.12 illustrates how a strut width, w_s, is influenced by both the width of bearing plate and tie width. Figure 15.13 illustrates how a strut-and-tie model for a simply supported beam can be rapidly started, prior to detailed design. The width of the bottom tie can be taken as twice the cover to the centroid of the reinforcement. The width of the bearing plate is assumed. The width of the upper strut is assumed same as the width of the lower tie. Hydrostatic pressure is assumed at nodal zones. The angle θ of inclined struts is taken larger than 25°. Everything else follows easily.

Strut capacity is controlled by both the strength of the strut itself and the strength of the nodal zone. Compression reinforcement, confinement, or fiber reinforcement may be used to increase the strength of a strut.

The nominal compressive strength of a strut is defined as the smaller value of:

$$C_{ns} = \text{smaller of} \begin{cases} (f_{cu} A_c + A'_s f'_y) \text{ for one end} \\ (f_{cu} A_c + A'_s f'_y) \text{ for the other end} \end{cases} \tag{15.6}$$

calculated at the two ends of the strut, where A_c is the cross-sectional area of concrete for the strut (generally width times thickness), A'_s is the area of longitudinal compression reinforcement, if any, and f'_y is the yield strength of the compression reinforcement. f_{cu} is the effective compressive strength of the concrete; it is taken as the smaller of the effective compressive strength of the concrete in the strut considered or in the nodal zone where the strut ends. f_{cu} is defined by:

$$f_{cu} = \text{smaller of} \begin{cases} 0.85\beta_s f'_c \\ 0.85\beta_n f'_c \end{cases} \tag{15.7}$$

where f'_c is the design compressive strength of concrete and the factors β_s and β_n are effective strength coefficients defined in Table 15.1 for the struts and nodal zones, respectively. The factor 0.85 in Eq. (15.7) represents the effect of sustained compression.

When transverse reinforcement is provided for bottle-shaped struts, β_s is taken equal 0.75 provided the reinforcement satisfies the following equation:

$$\Sigma \frac{A_{si}}{bs_i} \sin \gamma_i \geq 0.003 \tag{15.8}$$

where A_{si} is the total area of reinforcement at spacing s_i in a layer of reinforcement with bars at an angle γ_i to the axis of the strut. Figure 15.14 illustrates the angle γ_i. In Eq. (15.8), b represents the thickness of the strut.

Table 15.1 Effective strength coefficients for struts and nodal zones as per ACI 2002 code.

β_s for struts	β_n for nodal zones
• $\beta_s = 1$ for a strut of uniform cross sectional area over its length	$\beta_n = 1$ for *C-C-C* nodes
• $\beta_s = 0.40$ for struts in tension members or tension flanges of members	$\beta_n = 0.80$ for *C-C-T* nodes
• $\beta_s = 0.75$ for bottle-shaped struts where the axis of the strut is crossed by transverse reinforcement proportioned to resist the transverse tensile force resulting from the compression force spreading in the strut. For f'_c not greater than 6000 psi, the transverse reinforcement can be obtained from: $$\Sigma \frac{A_{si}}{bs_i} \sin \gamma_i \geq 0.003 \qquad (15.8)$$ where A_{si} is the total area of reinforcement at spacing s_i in a layer of reinforcement with bars at an angle γ_i to the axis of the strut	$\beta_n = 0.60$ for *C-T-T* nodes $\beta_n = 0.60$ for *T-T-T* nodes
• $\beta_s = 0.60\lambda$ for bottle-shaped struts without transverse reinforcement (or with transverse reinforcement not satisfying the above requirements), where λ equals 1 for normal- weight concrete, 0.85 for sand-lightweight concrete and 0.75 for all-lightweight concrete	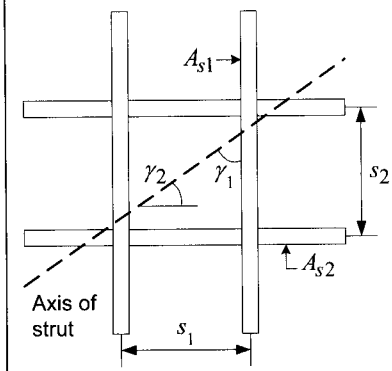
• $\beta_s = 0.60$ for all other cases	

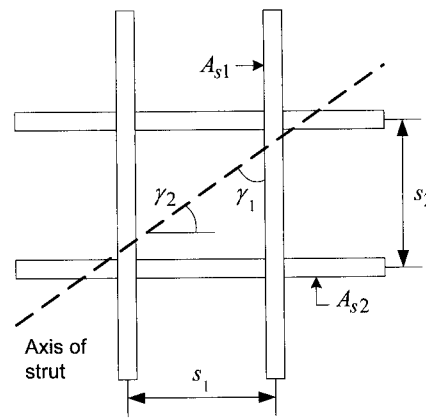

Figure 15.14 Typical reinforcement crossing a strut.

When a bottle-shaped strut is used, a taper with a slope of 1 over 2 (with respect to the strut longitudinal axis) is suggested in the ACI code as being reasonable.

15.7 DESIGN OF NODAL ZONES

15.7.1 Assumptions

Points of a strut-and-tie model at which the axes of struts, ties and concentrated forces intersect are defined as nodes or nodal zones. A nodal zone corresponds to the volume of concrete around a node that is assumed to transfer strut-and-tie forces through the node. For equilibrium, at least three forces should act on a node in a strut-and-tie model. Therefore nodal zones are generally taken triangular in shape. Nodes are classified according to the signs of their forces; typical nodes are described in Fig. 15.5. *C* represents compression and *T* represents tension. Even if a nodal zone is subjected to tension, the corresponding tie is assumed to extend through the nodal zone and be anchored on the far side of the node, hence inducing a compression in the nodal zone (Figs. 15.5 and 15.12)). Therefore, in theory, nodal zones are assumed to be subjected to a hydrostatic state of compression in the plane of the member. This implies that the loaded faces of the nodal zone are perpendicular to the axis of the struts and ties and are subjected to equal normal stresses (or pressure), p. Since the stresses are the same on all sides, the ratio of the sides of a triangular nodal zone, w_{n1}, w_{n2}, w_{n3}, (which are equal to the width of struts and ties connecting in that zone) are theoretically in the same proportion as the ratio of forces. This result can be sometimes used to either dimension, or check the minimum dimensions of a nodal zone; note that it is generally not convenient to attempt to satisfy a state of hydrostatic pressure for a given problem.

15.7.2 Dimensioning

Thickness of nodal zones are generally taken the same as the thickness of the member. The effective widths of nodal zones are determined based on the forces obtained in Step 3 and the effective concrete strengths defined for struts and nodal zones in Section 15.6. However, the following observations are helpful: width of compression struts can be first evaluated from the size of bearing plate or support pad; it can be also influenced by the width of ties. In beams, width of ties can be estimated from the reinforcement cover and distribution (Section 15.5). Also, it may be useful to determine first the minimum width of a strut from the strength of the strut and the compression force in the strut. The design width should be larger than or equal to the minimum width obtained.

Since nodal zones are triangular in shape, it is often necessary to determine one side of the triangle given two others. Here are two convenient formulae for such cases (Figs. 15.12 and 15.15):

$$w_s = w_b \sin\theta + w_t \cos\theta \tag{15.9}$$

where the subscripts t, b, and s stand for tie, bearing, and strut, respectively. Equation (15.9) applies at a support such as the left support in Fig. 15.5.

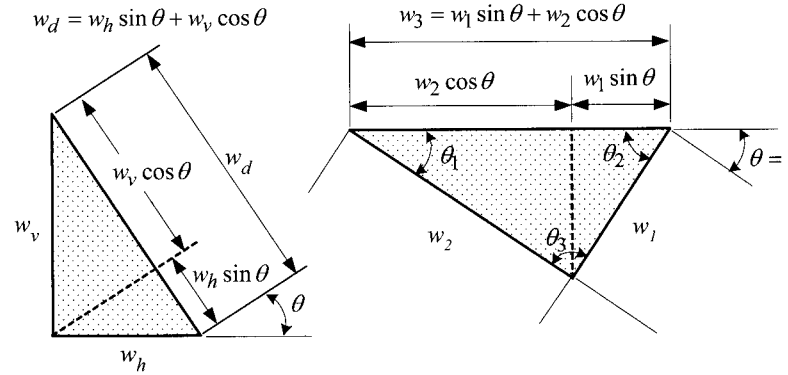

Figure 15.15 Useful relationship for checking nodal zones.

For convenience, the angle θ is defined as the angle of the strut with respect to the horizontal axis; thus Eq. (15.9) can also be written in terms of w_v, w_h, and w_d, which are defined as the vertical, horizontal and diagonal side of the triangular nodal zone, respectively, that is:

$$w_d = w_v \cos\theta + w_h \sin\theta \tag{15.10}$$

Equations (15.9) and (15.10) imply a nodal zone shaped as a right triangle. However, for any triangle the law of sine applies, that is:

$$\frac{w_1}{\sin\theta_1} = \frac{w_2}{\sin\theta_2} = \frac{w_3}{\sin\theta_3} \tag{15.11}$$

where w_1, w_2, w_3 are the sides opposite to $\theta_1, \theta_2, \theta_3$, respectively. $\theta_1, \theta_2, \theta_3$ are the angles of the triangle. For a right triangle, Eq. (15.11) reduces to Eq. (15.9) or (15.10).

15.7.3 Anchorages

Attention must be paid to providing sufficient anchorage to ties acting on nodal zones. This can be achieved by conventional procedures such as bearing plate, anchorage of a tendon, hooks, mechanical devices, or development of reinforcement. When reinforcement transfer length is checked, an extended nodal zone is defined as that portion of a member bounded by the intersection of the effective strut width, w_s, and the effective tie width, w_t (Fig. 15.16). The reinforcement must be developed when the centroid of tie leaves the nodal zone as shown in Figs. 15.16*a* and 15.16*b*.

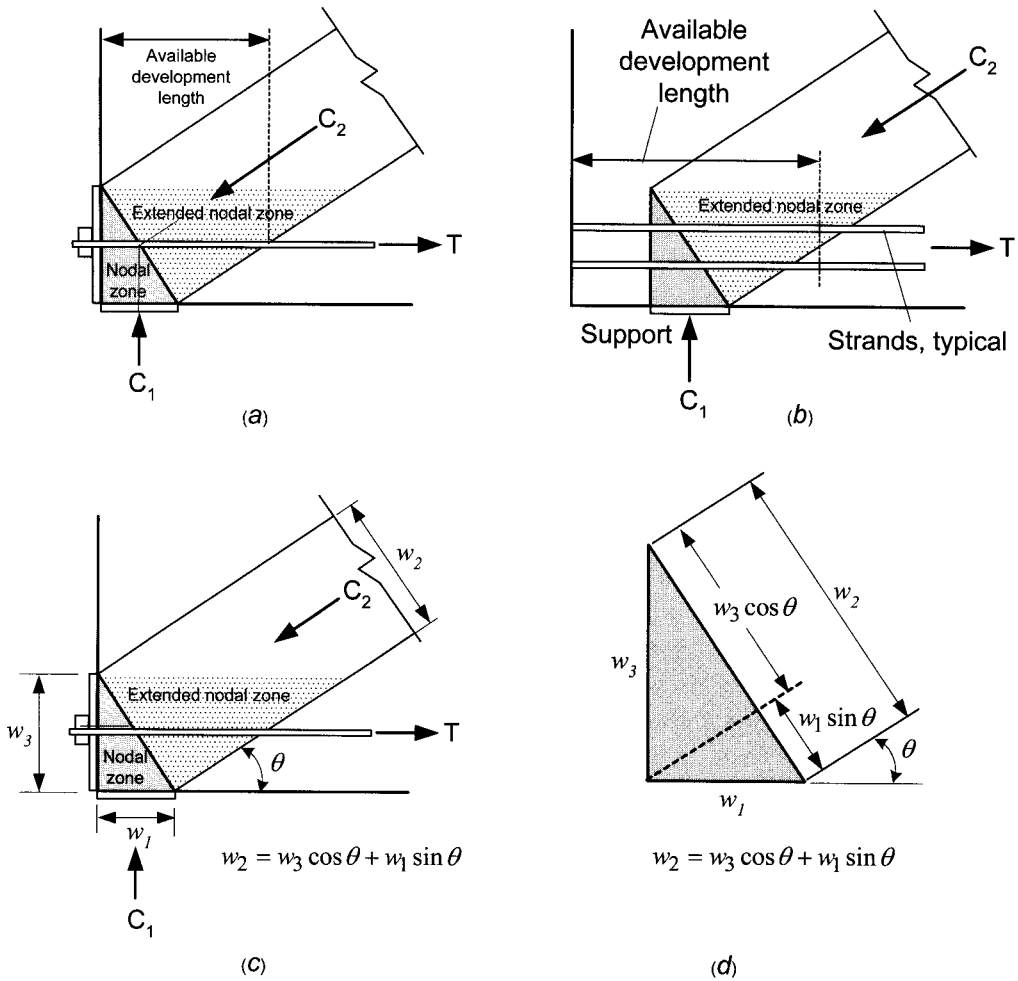

Figure 15.16 Anchorage in nodal zones and extended nodal zones.

15.7.4 Nominal Strength

The nominal compression strength of a nodal zone is calculated from:

$$N_n = f_{cu} A_n \tag{15.11}$$

where f_{cu} is the effective compression strength of the concrete in the nodal zone and A_n is either: 1) the area of the face of the nodal zone on which N_u acts, taken perpendicular to the line of action of N_u, or 2) the area of section through the nodal zone, taken perpendicular to the line of action of the resultant force on the section

(this would apply to the case described in Fig. 15.7). Unless confinement is provided, the value of f_{cu} can be estimated from:

$$f_{cu} = 0.85\beta_n f'_c \tag{15.12}$$

in which β_n is defined in Table 15.1. The wide range of values of β_n reflects the increasing degree of disruption of the nodal zone due to the incompatibility of the tension strains in the ties and compression strains in the struts. Equation (15.12) is applied at each side of a nodal zone.

15.8 STM BY AASHTO LRFD

Strut-and-tie modeling (STM) using the AASHTO LRFD code [Ref. 15.1, 15.2] is based on the same general principles described in the previous sections. However, AASHTO uses strength and resistance factors different from those used by ACI (see Tables 14.1 to 14.3).

The following procedure is recommended to estimate the resistance P_r of a compression strut:

$$P_r = \phi P_n \tag{15.13}$$

where:

$\phi = 0.7$ for compression struts in strut-and-tie models

and the nominal compression resistance is given by:

$$\begin{cases} P_n = f_{cu}A_{cs} \text{ for unreinforced struts} \\ P_n = f_{cu}A_{cs} + A_{ss}f_y \text{ for reinforced struts} \end{cases} \tag{15.14}$$

where:

A_{cs} = effective cross-sectional area of strut determined from available concrete area and anchorage conditions

A_{ss} = area of reinforcement in the strut

The effective strength f_{cu} given by AASHTO is limited to $0.85f'_c$ and is given by an expression that depends on the principal tensile strain [Refs. 15.35 and 15.36]. However, the value of f_{cu} recommended by ACI in Eq. (15.7) and Table 15.1 is appropriate enough, given the uncertainty on the evaluation of the state of strain in the struts.

For the nominal resistance of ties AASHTO uses the same equation as Eq. (15.4) except that Δf_p is replaced by f_y. The resistance factor ϕ for ties is taken as 0.9 for reinforced concrete and 1.0 for prestressed concrete.

For the nodal zones, the resistance factor is taken as $\phi = 0.7$ in all cases. However, the effective strength coefficient (Table 15.1), β_n, is taken equal to 0.85 for *CCC* nodes, 0.75 for *CCT* nodes, and 0.65 for *CTT* and *TTT* nodes, respectively.

For minimum reinforcement, AASHTO recommends that D-regions (except slabs and footings) shall contain an orthogonal grid reinforcement near each face with a maximum spacing less than or equal to 12 in. The minimum steel reinforcement ratio (reinforcing bars) in each orthogonal direction shall not be less than 0.003.

15.9 ANCHORAGE ZONES OF PRESTRESSED MEMBERS

The design of end zones in pretensioned and posttensioned concrete members is discussed in Sections 4.16 and 4.17. For posttensioned members, an approximate method is described to estimate the transverse reinforcement needed in the anchorage zone. However, strut-and-tie models are particularly suitable for anchorage zone design. The Posttensioning Institute has a special publication on the detailed design of anchorage zones with numerous cases and parameters covered [Ref. 15.39]. The anchorage zone is modeled as a D-region typically extending $1h$ to $1.5h$ from the end of the beam. Immediately ahead of an anchorage the local zone of concrete is subjected to very high stresses and is typically confined by spirals or closed ties (Fig. 15.17). Local zones are considered part of the anchorage system design and are not discussed here; only the general zone that is the D-region is addressed next.

The strut-and-tie model of the anchorage zone deals with the design of the transverse reinforcement that counteract splitting tensile cracking induced by the compression force in the concrete. It is the responsibility of the designer to provide appropriate reinforcement for this zone.

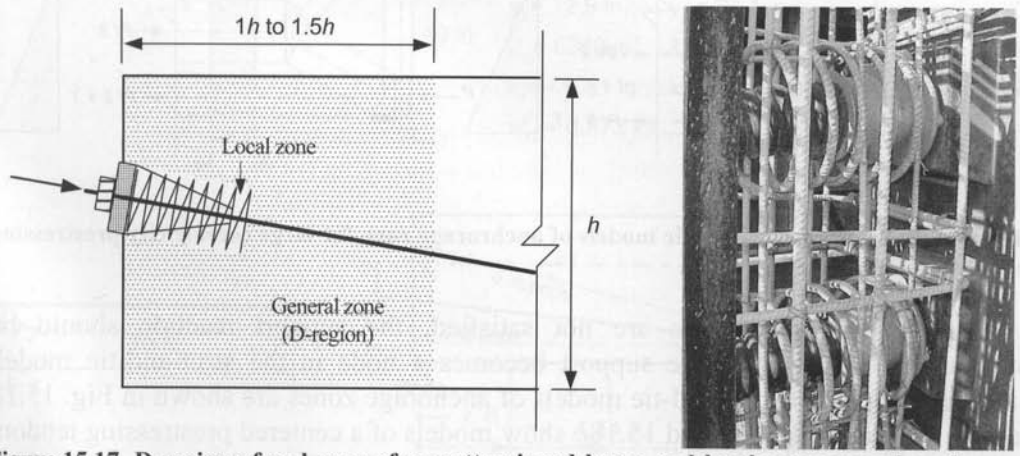

Figure 15.17 D-region of end zone of a posttensioned beam and local zone around anchorage. *(Right photo, courtesy of the Post-Tensioning Institute).*

In the end zone of a prestressed member, typically the support reaction acts in addition to the prestressing force. Neglecting the reaction in the strut-and-tie model of the anchorage zone may significantly simplify the calculations. In Ref. [15.39] Wollmann and Roberts-Wollmann suggest that the effects of the reaction force can be neglected when all of the following conditions are satisfied:

- The reaction is introduced at the bottom of the section as in a simply supported beam
- The unfactored reaction force is less than fifteen percent of the prestressing force
- The inclination of all prestress forces is less than 5 degrees
- The centroid or resultant of the prestressing force is within the central kern of the section

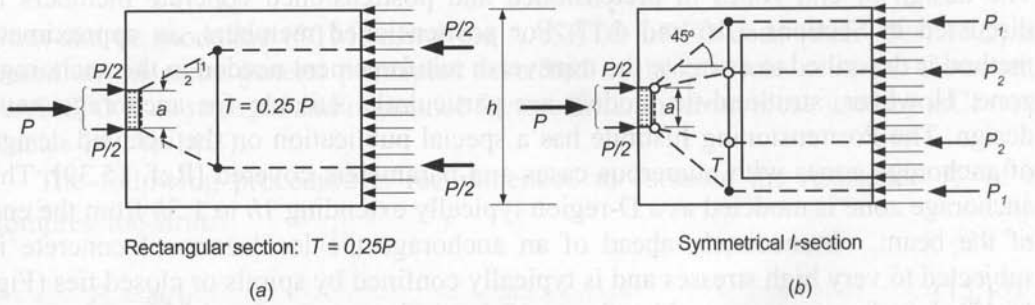

Figure 15.18 Typical strut-and-tie models of anchorage zone for: (a) Rectangular section. (b) Symmetrical I- or flanged section. *(adjust location of P/2 at ¼ depth)*

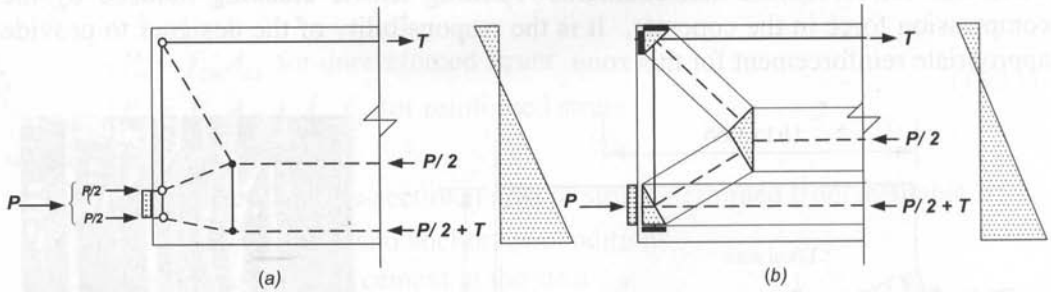

Figure 15.19 Typical strut-and-tie models of anchorage zone for large eccentricity prestressing tendons.

If the above conditions are not satisfied, the support reaction should be considered and therefore the support becomes a node in the strut-and-tie model. Simple examples of strut-and-tie models of anchorage zones are shown in Fig. 15.18 and 15.19. Figure 15.18*a* and 15.18*b* show models of a centered prestressing tendon, in a rectangular and symmetrical I-beam, respectively. Two different strut-and-tie

models for a single tendon with a large eccentricity are shown in Fig. 15.19. Strut-and-tie models for a zone with two anchorages are described in the examples of Section 15.10. Finally Fig. 15.20 shows a strut-and-tie model developed for the end zone of a prestressed beam with 3 prestressing tendons or cables. These examples should help the user develop some confidence in selecting a strut-and-tie model for a particular anchorage zone design.

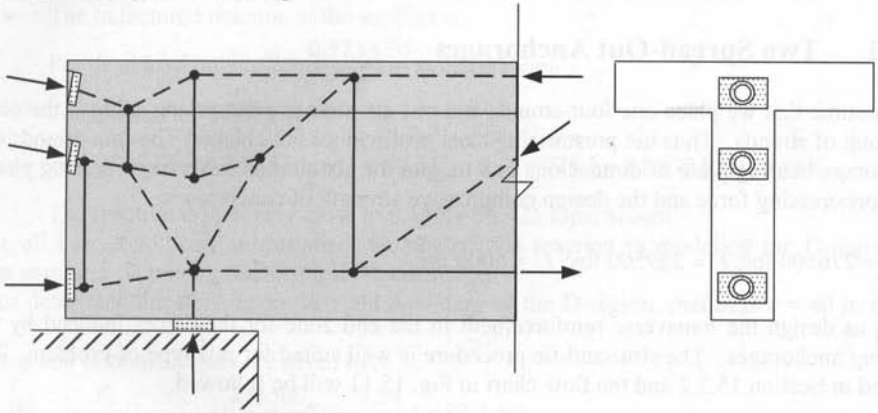

Figure 15.20 Strut-and-tie model developed for an end zone with 3 prestressing tendons *(Courtesy D. Kuchma and T. Nagle).*

15.10 EXAMPLE: ANCHORAGE ZONE DESIGN BY STM

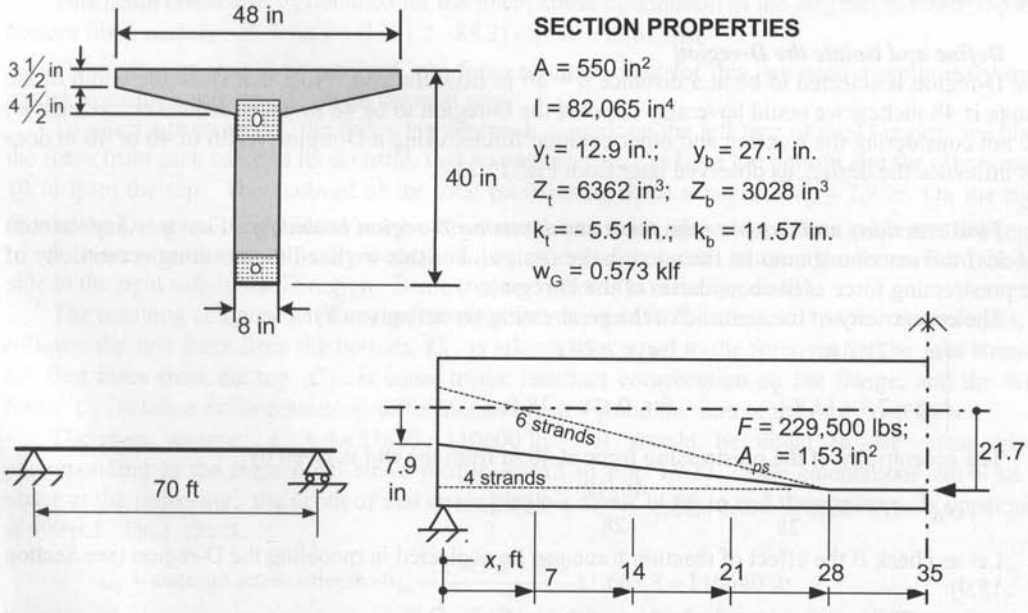

Figure 15.21 Prestressed beam considered for anchorage zone design.

Consider the beam of Section 4.9, 4.12 and 4.13. An example of anchorage zone design for that beam using elastic approximate procedure was covered in Section 4.17.3.

Figure 15.21 provides a summary of the beam cross section and the final tendon profile. Ten ½ in diameter strands are used, four of them straight and six draped. The beam was designed as a pretensioned beam. Assume the beam is to be post-tensioned instead of pretensioned. Two cases are considered next with the same eccentricity of the total prestressing force; in one case, the anchorages are spaced from each other and, in the other case, they are placed close to each other.

15.10.1 Two Spread-Out Anchorages

Let us assume that we place one four-strands and one six-strands prestressing cable at the centroid of each group of strands. Thus the prestressing steel profile does not change. The four-strands cable has an anchorage bearing plate of dimensions 6x8 in, and the six-strands cable has a bearing plate of 8x8 in. The prestressing force and the design compressive strength of concrete are:

$$F_i = 276500 \text{ lbs}; \; F = 229500 \text{ lbs}; \; f'_c = 5000 \text{ psi}$$

Let us design the transverse reinforcement in the end zone for the forces induced by the post-tensioning anchorages. The strut-and-tie procedure is well suited for this type of problem. The steps described in Section 15.3.2 and the flow chart in Fig. 15.11 will be followed.

1. ***Check if strut-and-tie model is allowed.*** Let us check maximum shear at the support section of the beam using Eq. (15.1):

$$V_u = 48146 \le 10\sqrt{f'_c}\, b_w d_e = 10\sqrt{5000} \times 8 \times 32 = 181019 \text{ lb} \qquad \text{O.K.}$$

Therefore strut-and-tie modeling is allowed. Note that we have used $d_p = 0.8h$. However even if d_p is taken exactly to the centroid of the prestressing force (that is, 20.8 in) the above condition would still be largely satisfied.

2. ***Define and isolate the D-region***

The D-region is selected to be at a distance $h = 40$ in from the end. Note that since the width of the flange is 48 inches, we could have also selected the D-region to be 48 in wide. However, because we are not considering the reaction and other external forces, using a D-region width of 40 or 48 in does not influence the design, as observed later from Fig. 15.23.

2. ***Find reactions and compute the force resultants on D-region boundary.*** First it is important to check if the reaction should be included in the design. For this we need the resulting eccentricity of the prestressing force at the boundaries of the D-region.

The eccentricity of the centroid of the prestressing force is given by:

$$\begin{cases} e_o = 21.7 \text{ in} & \text{for } x \ge 28 \text{ ft} \\ e_o = 7.9 + 13.8\dfrac{x}{28} & \text{for } 0 \le x < 28 \text{ ft} \end{cases}$$

The eccentricity of the prestressing force at 40 in from the end is given by:

$$e_o = 7.9 + 13.8\frac{x}{28} = 7.9 + 13.8\frac{40/12}{28} = 9.54 \text{ in}$$

Let us check if the effect of reaction force can be neglected in modeling the D-region (see Section 15.9):

- The reaction is at the bottom of the section. O.K.

- The eccentricity of the prestressing force throughout the D-region is less than the lower limit of the central kern $k_b = 11.47$ in. $\rightarrow$ O.K.
- The slope of the prestressing force in the D-region is given by:

  $$\tan\alpha = \frac{13.8}{28\times 12} = 0.0639 \rightarrow \alpha = 3.66^o \rightarrow \text{It is less than } 5^o \quad \text{O.K.}$$

  It can be also shown that the slope of the draped cable has an angle of $4.18^o \rightarrow$ O.K.
- The unfactored reaction at the support is:

  For dead load only: $R = \dfrac{0.573\times 70}{2} = 20.055$ kips

  For full service load:

  $$R = \frac{1.013\times 70}{2} = 35.455 \text{ kips} \quad < 0.15F_i = 0.15\times 276.5 = 41.475 \text{ kips} \rightarrow \text{O.K.}$$

  The reaction is also very close to $0.15F = 34.425$ kips; accept.

Since all four conditions are satisfied, we neglect the reaction in modeling the D-region. This makes the strut-and-tie model much simpler to construct.

Let us determine the stresses on the right boundary of the D-region, that is at $x = 40$ in from the support.

The top and bottom stresses are given by:

$$\begin{cases} \sigma_{top} = \dfrac{F_i}{A_c}(1-\dfrac{e_o}{k_b}) = \dfrac{276500}{550}(1-\dfrac{9.54}{11.57}) = 88.2 \text{ psi} \\ \sigma_{bot} = \dfrac{F_i}{A_c}(1-\dfrac{e_o}{k_t}) = \dfrac{276500}{550}(1+\dfrac{9.54}{5.51}) = 1373.2 \text{ psi} \end{cases}$$

The stress diagram is plotted in Fig. 15.22. The stress at the bottom of the top flange is given by:

$$\sigma = \frac{F_i}{A_c} - \frac{F_i e_o y}{I_g} = \frac{276500}{550} - \frac{276550\times 9.54\times 4.9}{82065} = 345.2 \text{ psi}$$

This result could also be obtained for the linear stress distribution of the diagram between top and bottom fiber, namely: $\sigma = 88.2 + (1373.2 - 88.2)\times 8/40 = 345.2$ psi.

These stresses should be resolved into force resultants, but for this, we need a preliminary truss model requiring some iteration with the next step.

To select a truss model, the following approach is used: on the left face of the D-region, we place the force from each cable at its centroid, that is, one force at 3 in from the bottom and the other one at 10 in from the top. The centroid of the total prestressing force remains at $e_o = 7.9$ in. On the right face of the D-region, we decide to resolve the stresses into three equivalent forces at the center of each of which we place a node. Finally we will build a strut-and-tie model to carry the forces from the left side to the right side of the D-region. Some trial and error is invariably needed.

The resulting compression force on the right side is equal to F_i; it is resolved into three forces, as follows: the first force from the bottom, C_1, is taken about equal to the force carried by four strands; the first force from the top, C_3, is equal to the resultant compression on the flange; and the third force, C_2, is taken as the remaining difference between F_i and the sum of the other two forces.

Therefore assume: $C_1 \approx 4\times 27650 = 110600$ lb. It should be equal to the stress block corresponding to the trapezoidal stress profile *NMRS* in Fig. 15.22. Side calculations allow us to arrive at the following: the depth of that stress block is about 11.66 in and the stress on its upper side is 999 psi. Thus, check:

$$C_1 = \text{average stress}\times \text{depth}\times b_w = \frac{1373.2+999}{2} 11.66\times 8 = 110640 \text{ lb.}$$

Its centroid is at 5.52 in from the bottom fiber.

A similar procedure is followed to determine the force corresponding to the stress block of the top flange; here stresses are integrated over the area of the top flange. Side calculations lead to the following results:

$C_3 = 56496$ lb at a distance of 3.93 in from the top fiber.

The remaining force is obtained as follows:

$$C_2 = F_i - C_1 - C_3 = 276500 - 110640 - 56496 = 109364 \text{ lb}$$

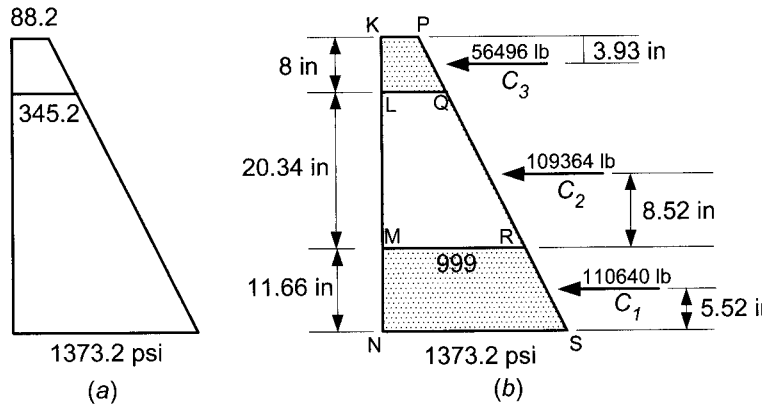

Figure 15.22 Resolving stresses into equivalent forces.

The value of C2 could also be obtained from the trapezoidal stress diagram *MLQR* in Fig. 15.22, with its centroid at 20.18 in from the bottom fiber. The centroid of C_2 can also be obtained from equilibrium of moments on the right face of the D-region, taken at the centroid of the section:

$$F_i e_o = 276500 \times 9.54 = C_1 \times (27.1 - 5.52) + C_3 \times (12.9 - 3.93) + C_2 \times x$$
$$= 110640 \times 21.58 + 56496 \times 8.97 + 109364 \times x$$

from which $x = 6.92$ in. Thus C_2 is located at a distance 27.1-6.92 = 20.18 in from the bottom fiber.

The D-region must be in equilibrium for forces and moments. Since the reaction and other external forces were neglected from the model, we must make sure that equilibrium is satisfied nevertheless. Since the moment on the right side is larger than that on the left side, because of the eccentricity of the prestressing force, a fictitious moment is added on the right side to provide equilibrium of moment. This fictitious moment is equal to:

$$\Delta M_F = 276500(9.54 - 7.9) = 453460 \text{ lb-in}$$

This moment is replaced by a couple with forces applied along the line of action of C_1 and C_3. The magnitude of the force of the couple is given by:

$$C_{\Delta M_F} = \frac{453460}{40 - 5.52 - 3.93} = 14843 \text{ lb}$$

Thus a compression force of 14843 lb is added to the top force and a tension force is added to the bottom force leading to the final values of C_1 and C_3:

$$\begin{cases} C_1 = 110640 - 14843 = 95797 \text{ lb} \\ C_3 = 56496 + 14843 = 71339 \text{ lb} \end{cases}$$

The final forces are shown in Fig. 15.23.

Note that the effect of this additional moment is same as having a prestressing force with constant eccentricity throughout the D-region.

4. ***Select a truss model to carry the forces across the D-region.***

Now that the forces have been calculated we can draw the strut-and-tie model. The lines of action of C_1, C_2 and C_3 are drawn as straight lines; a transition section is selected at 15 in from the left side; the choice of this section is arbitrary and flexible; nodes are created there from which forces change direction to link with the anchorages. The compression nodes from the two anchorages are placed at 3 in from the left face, inside the beam. This is to allow the tie between them to have some width. The strut-and-tie model is plotted in Fig. 15.23 and is very intuitive. Joints are identified by lower case letters. Distances between various parallel elements are calculated.

5. ***Compute the forces in the struts and ties.***

Let us apply force equilibrium at each joint, starting by joint *e* and *c* because they are simplest:

Joint *c*:

$\tan\theta_3 = 6.07/12 = 0.5058$

$\theta_3 = 26.8318^o$

$\cos\theta_3 = 0.8923$

$\sin\theta_3 = 0.4514$

$C_{cf} = 71339$ lb

$C_{ab} = 71339/\cos\theta_3 = 79950$ lb

$T_{cd} = -79950\sin\theta_3 = -36089$ lb

Joint *e*:

$\tan\theta_2 = 2.52/12 = 0.21$

$\theta_2 = 11.8598^o$

$\cos\theta_2 = 0.9787$

$\sin\theta_2 = 0.2055$

$C_{he} = 95797$ lb

$C_{eb} = 95797/\cos\theta_2 = 97882$ lb

$C_{ed} = 97882\sin\theta_3 = 20115$ lb

Joint *a*:

$\tan\theta_4 = 9.82/12 = 0.8183$

$\theta_4 = 39.2946^o$

$\cos\theta_4 = 0.7739$

$\sin\theta_4 = 0.6333$

$C_{ac} = 79950$ lb (from equilibrium of *c*)

$C_{ad}\cos\theta_4 + C_{ac}\cos\theta_3 = 165900$ lb

$C_{ad}\times 0.7739 + 79950\times 0.8923 = 165900$ lb

$C_{ad} = 122187$ lb

$T_{ab} = -(122187\sin\alpha_4 - 79950\sin\alpha_3) = -(122187\times 0.633 - 79950\times 0.4514) = -41255$ lb

Joint *b*

$\tan\theta_5 = 17.18/12 = 1.4317$

$\theta_5 = 55.0662^o$:

$\cos\theta_5 = 0.5726$

$\sin\theta_5 = 0.8198$

$C_{bd}\cos\theta_5 + C_{be}\cos\theta_2 = 110600$ lb

$C_{bd} \times 0.5726 + 97882 \times 0.9787 = 110600$ lb

$C_{bd} = 25852$ lb

Check tension force T_{ba}:

$T_{ba} = -(C_{bd}\sin\theta_1 + C_{be}\sin\theta_2) = -(25852 \times 0.8198 + 97882 \times 0.2055) = -41308$ lb

It is almost same as the value obtained from joint *a*, that is, -41255 lb.

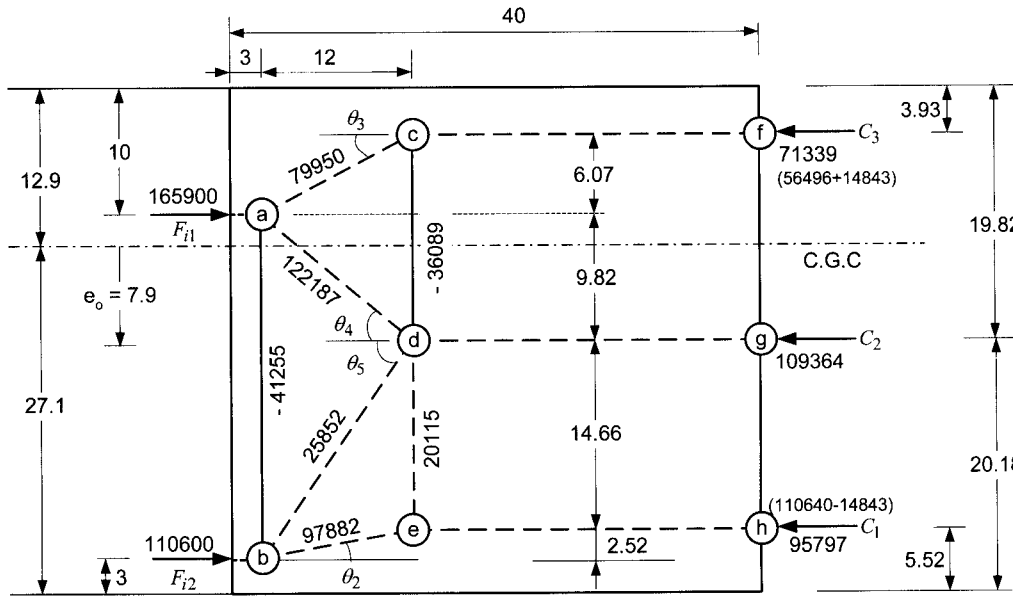

$\begin{cases}\tan\theta_2 = 2.52/12 = 0.21\\ \theta_2 = 11.8598^o\\ \cos\theta_2 = 0.9787\\ \sin\theta_2 = 0.0.2055\end{cases}$ $\begin{cases}\tan\theta_3 = 6.07/12 = 0.5058\\ \theta_3 = 26.8318^o\\ \cos\theta_3 = 0.8923\\ \sin\theta_3 = 0.4514\end{cases}$ $\begin{cases}\tan\theta_4 = 9.82/12 = 0.8183\\ \theta_4 = 39.2946^o\\ \cos\theta_4 = 0.7739\\ \sin\theta_4 = 0.6333\end{cases}$ $\begin{cases}\tan\theta_5 = 17.18/12 = 1.4317\\ \theta_5 = 55.0662^o\\ \cos\theta_5 = 0.5726\\ \sin\theta_5 = 0.8198\end{cases}$

Figure 15.23 Strut-and-tie model of anchorage zone with two spread-out anchorages.

Joint *d*:

Since all forces at joint *d* have been calculated from other joints simply check if these forces provide equilibrium at *d*:

$C_{bd}\cos\theta_1 + C_{ad}\cos\theta_4 = 109364$ lb

$25852 \times 0.5726 + 122187 \times 0.7739 = 109363 \approx 109364$ lb $\rightarrow$ O.K.

$C_{de} = C_{ad}\sin\theta_4 - C_{bd}\sin\theta_1 - 36089 = 109364$ lb

$C_{de} = 122187 \times 0.6333 - 25852 \times 0.8198 - 36089 = 20062$ lb ≈ 20115 lb $\rightarrow$ O.K.

The forces are summarized in Fig. 15.23. Note that at the section 15 in from the left side we have compression in strut *ed* and tension in tie *dc*. It is likely that the reinforcement needed for tie *dc* will be extended along the whole depth of the section.

6. and 7. ***Select dimensions for strut-and-tie nodal zones and verify the capacity of struts at midlength and at the nodal interface.***

We have combined these two steps together since this fits better the approach followed next. The strengths of nodal zones according to the 2002 ACI code are computed and summarized in Table 15.2. The strength of struts are summarized in Table 15.3. All inclined struts are assumed to act as bottle-shaped struts and thus have a smaller value of β_s (from Table 15.1). Minimum strut widths are calculated and summarized in Table 15.4. The minimum strut width for the design compression force can be calculated from:

Table 15.2 Strength of nodal zones.

Nodes	Node Type	$f_{cu} = 0.85\beta_n f_c'$ psi	ϕf_{cu} $(0.75 f_{cu})$, psi
e	CCC	$0.85 \times 1 \times 5000 = 4250$ psi	3188
a, b, c,d	CCT	$0.85 \times 0.8 \times 5000 = 3400$ psi	2550

Table 15.3 Strength of struts.

Type of strut	Strut	Start node	End node	β_s	β_n	$f_{cu} \le \begin{cases} 0.85\beta_s f_c' \\ 0.85\beta_n f_c' \end{cases}$ psi	ϕf_{cu} $(0.75 f_{cu})$ psi
Prismatic (parallel to beam axis)	*cf*	CCT		1	0.8	3400	2550
	dg	CCT		1	0.8	3400	2550
	eh	CCC		1	1	4250	3188
	ed	CCC	CCT	1	0.8	3400	2550
Inclined (assuming minimum grid reinforcement)	*ac*	CCT	CCT	0.75	0.8	3188	2391
	ad	CCT	CCT	0.75	0.8	3188	2391
	bd	CCC	CCT	0.75	0.8	3188	2391
	be	CCC	CCC	0.75	0.8	3188	2391

Table 15.4 Minimum strut dimensions.

Type of strut	Strut	ϕf_{cu} psi	Strut force C, lb	Factored strut force, $C_u = 1.2C$, lb	Strut depth t, in	$w_{s\,\min}$ required, in
Prismatic (parallel or normal to beam axis)	*cf*	2550	71339	85607	48	0.7
	dg	2550	109364	131237	8	6.43
	eh	3188	95797	114956	8	4.51
	ed	3188	20115	24138	8	0.95
Inclined (assuming minimum grid reinforcement)	*ac*	2391	79950	95940	8*	5.02
	ad	2391	122187	146624	8	7.66
	bd	2391	25852	31022	8	1.63
	be	2391	97882	117458	8	6.14

* varies from 8 to 48. Using 8 is conservative.

$$w_{s\min} = \frac{\text{Factored force}}{\phi \times t \times f_{cu}} = \frac{\text{Factored force}}{\phi \times t \times 0.85 \times \beta_{\min} \times f_c'}$$

where $\beta_{\min}$ is the smaller value of β_s or β_n, and ϕ is taken equal to 0.75.

Note that for the struts with $\beta_s = 1$ it is assumed that cracking conditions induced by shear at the support are negligible.

Stresses behind anchorage plates

Stresses developed just behind anchorage plates are allowed to be higher than for conventional nodal zones because spiral reinforcement is provided in the local zone behind the plate (Fig. 15.17). It is advisable to check these stresses, first.

Node a

The factored stress just behind the anchorage plate at node *a* is given by:

$$\sigma_u = \frac{1.2 \times 165900}{8 \times 8} = 3110 \text{ psi} > 2550 \text{ psi (strength of CCT nodal zone)}$$

Node b

The factored stress just behind the anchorage plate at node *b* is given by:

$$\sigma_u = \frac{1.2 \times 110600}{6 \times 8} = 2765 \text{ psi} > 2550 \text{ psi (strength of CCT nodal zone)}$$

However, Eq. (4.47) suggests that an allowable stress value larger than that of the nodal zone may be used when the local zone is confined with spiral reinforcement (assumed to be the case here):

$$\bar{\sigma}_{bi} = 0.75 f_{ci}' \sqrt{A_2 / A_1}$$

Assuming $A_2 = A_1$ (worst case scenario) and that post-tensioning will be carried out only after the compressive strength of concrete reaches 5000 psi, leads to:

$$\bar{\sigma}_{bi} = 0.75 f_{ci}' \sqrt{A_2 / A_1} = 0.75 \times 5000 \sqrt{1} = 3750 \text{ psi} \quad \text{O.K.}$$

This stress is larger than the factored stress from either anchorage.

Check nodal zone at *b*

The nodal zone at *b* is subjected to 3 compression forces and one tensile force. The forces from struts *be* and *bd* can be resolved into a resultant force, similarly to what is described in Section 15.2.3.

A sketch of nodal zone is shown in Fig. 24 where the magnitude of the force resultant as well as its angle θ_1 to the horizontal axis are calculated as.

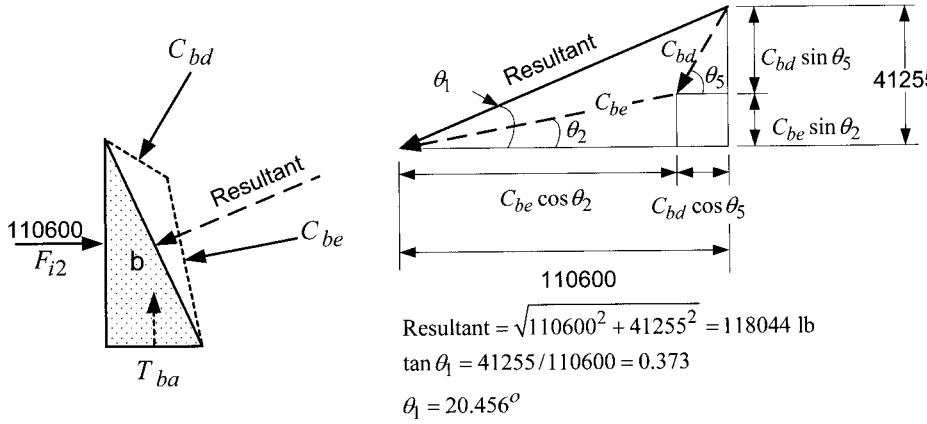

$$\text{Resultant} = \sqrt{110600^2 + 41255^2} = 118044 \text{ lb}$$

$$\tan\theta_1 = 41255/110600 = 0.373$$

$$\theta_1 = 20.456^o$$

Figure 15.24*a* Force equilibrium at node *b*.

It can be observed that the resultant force is equal to 118044 lb and is inclined at an angle of 20.456° to the horizontal. The minimum width of the diagonal side should be:

$$w_{s\min} = \frac{1.2C}{\phi \times t \times f_{cu}} = \frac{1.2C}{\phi \times t \times 0.85 \times \beta_{\min} \times f'_c}$$

Referring to Table 15.3 for the value of $\phi \times f_{cu}$:

$$w_{s\min} = \frac{1.2 \times 118044}{8 \times 2391} = 7.4 \text{ in}$$

This can be accommodated if we allow a tie width for tie *ab* larger than the following:

$$7.4 = 6\cos 20.456 + w_h \sin 20.456 \rightarrow w_h = 5.09 \text{ in} \quad \text{O.K.}$$

Nodal zone *a* is treated similarly to nodal zone *b*.

Other nodal zones

Table 15.4 summarizes the minimum width of strut needed to accommodate the forces in each strut and its related nodal zones. It can be observed that all widths are reasonable and thus the model should be acceptable. Next some calculations are given for illustration.

Nodal zone *a*:

Based on strut forces, determine the height of Node *a*. The plate from the post-tensioning anchorage is 8x8 in.

The nodal zone is subdivided into two zones: one related to strut *ac* and the other to strut *ad*. From *ac*:

$$w_d = w_v \cos\theta + w_h \sin\theta$$

where:

$w_v = 4$ in and $w_d = 5.02$ in (from Table 15.4) and $\theta_3 = 26.8318^o$

This leads to:

$$5.02 = 4 \times 0.8923 + w_h \times 0.4514$$

from which: $w_h = 3.21$

We repeat the same procedure for the other strut *ad*:

$$w_d = w_v \cos\theta + w_h \sin\theta$$

$$7.66 = 4 \times 0.7739 + w_h \times 0.6333$$

from which: $w_h = 7.21$ in.

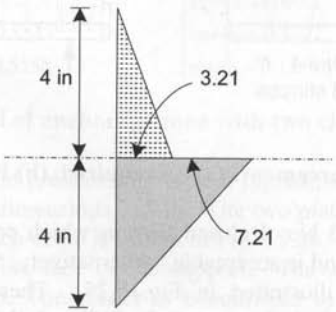

Figure 15.24*b* Checking nodal zone dimensions at node *a*.

This last value will control the projection of the nodal zone on the horizontal axis. Since we had selected the centroid of tie *ab* to be at 3 in from the left side, its width is taken as twice that value, that is, $2\times3=6$ in. Since from the above, we need at least 7.21 in, we will revise the design and place tie *ab* at 4 in from the left side. Because of the shape of the strut-and-tie model this will have little influence on the final design. Indeed, section *cde* is kept at 12 in to the right of *ab*, and the change will not influence the sections between *cde* and *fgh*; all forces remain the same. Note that tie reinforcement is spread within tie width.

8. ***Design the ties and the tie anchorage.***

Tie *ab*

Consider tie *ab* and assume its centroid is 4 in from the face of the support. This allows us to use a tie width up to 8 in (twice the cover). The tie reinforcement should be:

$$(T_u)_{ab}=\phi(T_n)_{ab}$$

$$1.2\times41255=0.75A_{st}f_y=0.75A_{st}\times60000$$

$$A_{st}=\frac{(T_u)_{ab}}{0.75f_y}=\frac{1.2T_{ab}}{0.75f_y}=\frac{1.2\times41255}{0.75\times60000}=1.1\text{ in}^2$$

It can be achieved using 3 No. 4 closed stirrups placed at 1, 4, and 7 inches from the left face of D-region. The closed stirrups provide adequate anchorage. Another alternative is to use 5 No. 3 closed stirrups spaced at about 1.5 in from each other starting at 1 in from the left face of the D-region.

Tie *cd*

The tie reinforcement required is given by:

$$A_{st}=\frac{(T_u)_{cd}}{0.75f_y}=\frac{1.2T_{cd}}{0.75f_y}==\frac{1.2\times36089}{0.75\times60000}=0.96\text{ in}^2$$

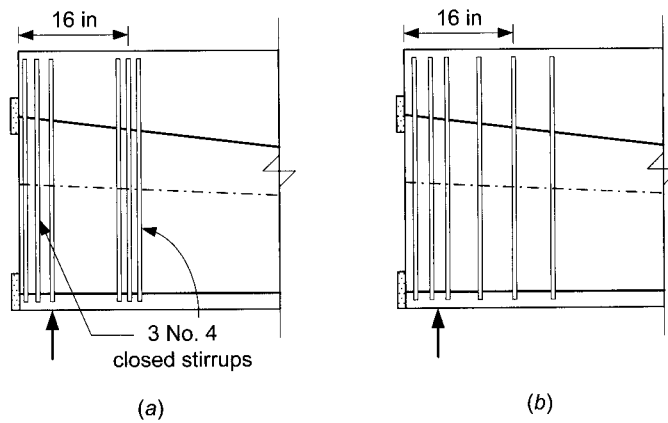

Figure 15.25 Details of tie reinforcement: (a) As required. (b) Practical spacing.

It can be achieved by using 3 No. 4 closed stirrups which provide 1.20 in^2. Here tie width is controlled by the nodal zone at *c* and is acceptable. Alternatively, 5 No. 3 closed stirrups can be used.

The stirrups arrangment is illustrated in Fig.15.25. These stirrups are in addition to the reinforcement needed for shear and cracking control. Although the three stirrups for tie *cd* are shown as a group in Fig. 15.25*a*, in practice, they will likely be distributed, one along *cd*, one between *ab* and *cd*, and the last one about 6 in right of *cd* as shown in Fig. 15.25*b*.

15.10.2 Two Anchorages Placed Close to Each Other

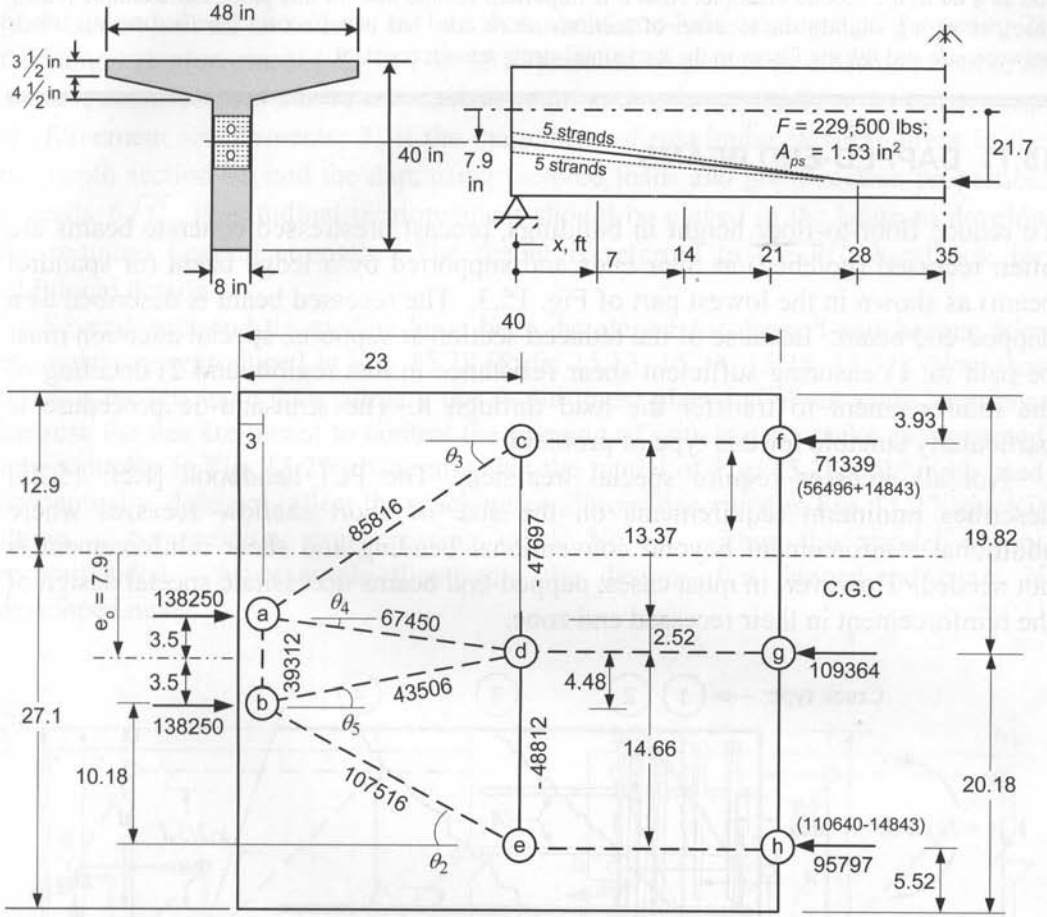

$$\begin{cases}\tan\theta_2 = 10.18/20 = 0.509\\ \theta_2 = 26.976^o\\ \cos\theta_2 = 0.8912\\ \sin\theta_2 = 0.4536\end{cases}\quad \begin{cases}\tan\theta_3 = 13.37/20 = 0.6685\\ \theta_3 = 33.7627^o\\ \cos\theta_3 = 0.8313\\ \sin\theta_3 = 0.5558\end{cases}\quad \begin{cases}\tan\theta_4 = 2.52/20 = 0.126\\ \theta_4 = 7.1814^o\\ \cos\theta_4 = 0.9922\\ \sin\theta_4 = 0.1250\end{cases}\quad \begin{cases}\tan\theta_5 = 4.48/20 = 0.2240\\ \theta_5 = 12.6258^o\\ \cos\theta_5 = 0.9758\\ \sin\theta_5 = 0.2186\end{cases}$$

Figure 15.26 Strut-and-tie model of anchorage zone with two close anchorages.

In this second example the total prestressing force is represented by two cables each having five strands and an anchorage plate of dimensions 7x8 in. The two plates touch each other at the centroid of the tendons. The location of each cable is shown in Fig. 15.26. The transition section for nodes *c*, *d*, and *e*, is taken at 23 in from the face of the support. The strut-and-tie model and the forces obtained are shown in Fig. 15.26. The reader is encouraged to check these values, provide the reinforcement needed in the end-zone, and compare such reinforcement with that obtained in the previous example.

In comparing Fig. 15.26 to 15.23 we note in particular that element *ab* acted as a tie in the first example and as a strut in this second example, while element *de* acted as a strut in the first example and as a tie in the second example. Also it is important to note that for this particular example (either case), changing slightly the location of sections *ab* or *cde* has no effect on the final results, since between *cde* and *fgh* the forces in the horizontal struts remain constant.

15.11 DAPPED-END BEAMS

To reduce floor-to-floor height in buildings, precast prestressed concrete beams are often recessed (notched) at their ends and supported by a ledge beam (or spandrel beam) as shown in the lowest part of Fig. 15.3. The recessed beam is described as a dapped-end beam. Because of the reduced section at supports, special attention must be paid to: 1) ensuring sufficient shear resistance in that region, and 2) detailing of the reinforcement to transfer the load through it. The strut-and-tie procedure is particularly suitable for this type of problem.

Not all recesses require special treatment. The PCI handbook [Ref. 15.25] describes minimum requirements on the size of short shallow recesses where additional reinforcement beyond conventional bending and shear reinforcement is not needed. However, in most cases, dapped-end beams necessitate special design of the reinforcement in their recessed end zone.

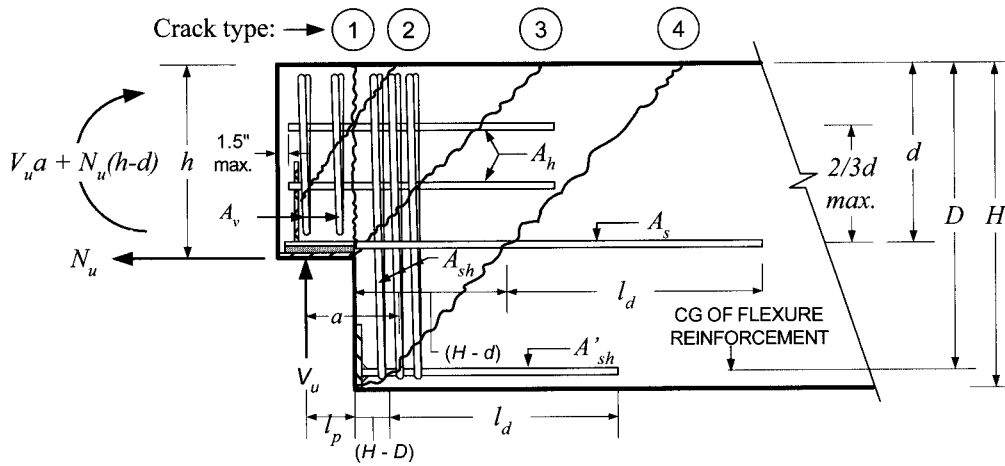

Figure 15.27 Typical cracking and reinforcement arrangement in dapped-end beams. *(Adapted from the PCI design handbook).*

Figure 15.27, reproduced from the PCI design handbook [Ref. 15.25] and based on the work of Mattock et al. [Ref. 15.19, 15.20], illustrates the type of cracking that occurs in dapped-end beams; it allows us to visualize the potential failure modes should there be insufficient reinforcement to confine the cracks. The figure also

suggests typical detailing for location and anchorage of the main reinforcement. The PCI design handbook offers the following guidelines for dapped-ends: 1) the depth of the extended end should not be less than about one-half the depth of the beam; 2) the hanger reinforcement (A_{sh} in Fig. 15.27) should be placed as close as possible to the re-entrant corner; this reinforcement requirement is not additive to other shear reinforcement requirements; 3) if the magnitude of maximum flexural stress in the full depth section beyond the dap, using factored loads and gross section properties, exceeds $6\sqrt{f'_c}$, longitudinal reinforcement should be placed in the beam to develop the required flexural strength. The reader is referred to the PCI handbook for additional details.

Several strut-and-tie models have been developed for dapped-end beams; four examples are reproduced in Fig. 15.28 [Refs. 15.13, 15.23, 15.28, 15.31]. Note that the four models have their primary ties (solid lines) placed at about same locations, because the ties are meant to control the opening of anticipated cracks as illustrated schematically in Fig. 15.27. Note also that the model of Fig. 15.28*c*, although used conceptually, does not reflect the cracking conditions described in Fig. 15.27, since it shows a compression strut crossing crack No. 3. Thus this model is not recommended. An example illustrating the design of a dapped-end beam is developed next.

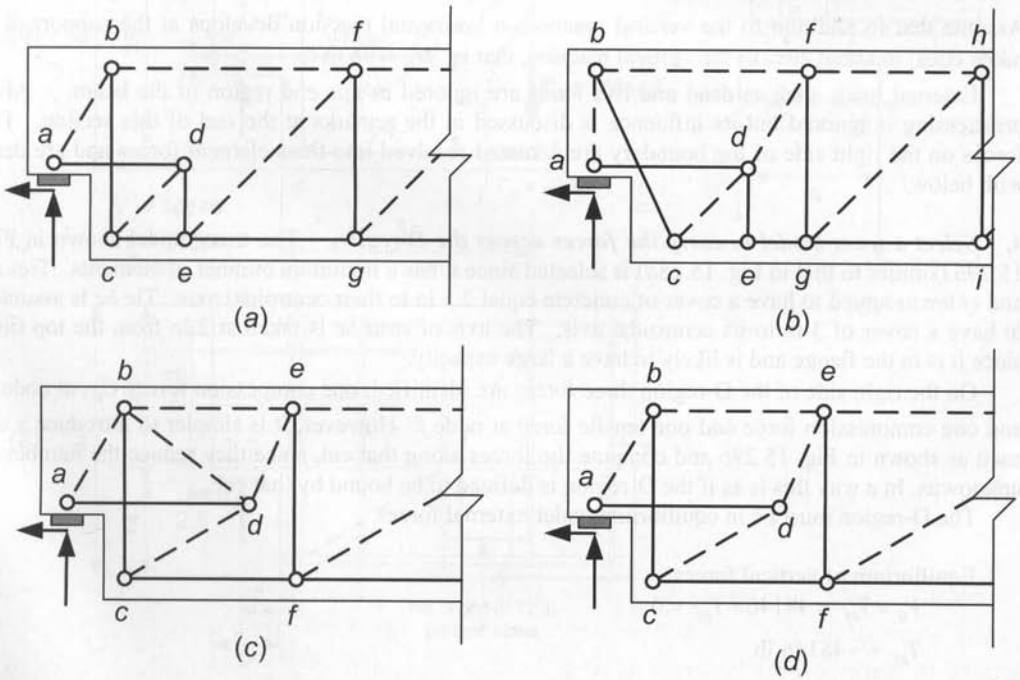

Figure 15.28 Typical strut-and-tie models of dapped-end beam.

15.12 EXAMPLE: DAPPED-END BEAM DESIGN BY STM

Consider the same beam as in the previous example. Assume that its ends are notched by cutting from each a segment 14 in deep and 9 in wide. The bearing plate is selected to be 6 in wide and 8 in deep (that is, as deep as the web width). It is assumed that the primary horizontal tensile reinforcement needed in the reduced section is welded to the plate and the plate itself is welded to headed studs thus providing adequate anchorage for the reinforcement. Let us design the reinforcement for the dapped-end region of the beam.

Several strut-and-tie models can be used for dapped-end beams as shown in Fig. 15.28. One of the simplest model (with only three forces per node) is selected (Fig. 15.28*d*). The design steps suggested in Section 15.3.2 and the flow chart of Fig. 15.11 will be followed.

1. ***Check if strut-and-tie model is allowed.*** Let us check maximum shear force at the reduced section of the dapped end using Eq. (15.1):

$$V_u = 48146 \le 10\sqrt{f_c'}\, b_w d_e = 10\sqrt{5000} \times 8 \times 23.5 = 132936 \text{ lb} \qquad \text{O.K.}$$

Therefore strut-and-tie modeling is allowed.

2. ***Define and isolate the D-region.*** The D-region of the dapped-end is defined from the left end of the beam to a section taken at a distance 40 in from the discontinuity toward midspan, that is, about 45 in from the left support (Fig. 15.29a).

3. ***Find reactions and compute the force resultants on the D-region boundary.*** From the example treated in Section 6.10, the factored vertical reaction at the support is calculated as $V_u = 48146$ lb. Assume that in addition to the vertical reaction, a horizontal reaction develops at the support; it is taken equal to about 20% of the vertical reaction, that is, $H_u = 9630$ lb.

External loads such as dead and live loads are ignored in this end region of the beam. Also, prestressing is ignored but its influence is discussed in the remarks at the end of this section. The forces on the right side of the boundary are assumed resolved into truss element forces and are dealt with below.

4. ***Select a truss model to carry the forces across the D-region.*** The truss model shown in Fig. 15.29*a* (similar to that in Fig. 15.28*d*) is selected since it has a minimum number of elements. Ties *ad* and *cf* are assumed to have a cover of concrete equal 2.5 in to their centroidal axis. Tie *bc* is assumed to have a cover of 3 in to its centroidal axis. The axis of strut *be* is taken at 2 in from the top fiber since it is in the flange and is likely to have a large capacity.

On the right side of the D-region three forces are identified; one compession force, C_e, at node *e*, and one compression force and one tensile force at node *f*. However, it is simpler to introduce a cut such as shown in Fig. 15.29*b* and compute the forces along that cut, since they reduce the number of unknowns. In a way this is as if the D-region is defined to be bound by that cut.

The D-region must be in equilibrium under external forces.

Equilibrium of vertical forces:

$$V_u + T_{ef} = 48146 + T_{ef} = 0$$

$$T_{ef} = -48146 \text{ lb.}$$

Moments with respect to node *f*:

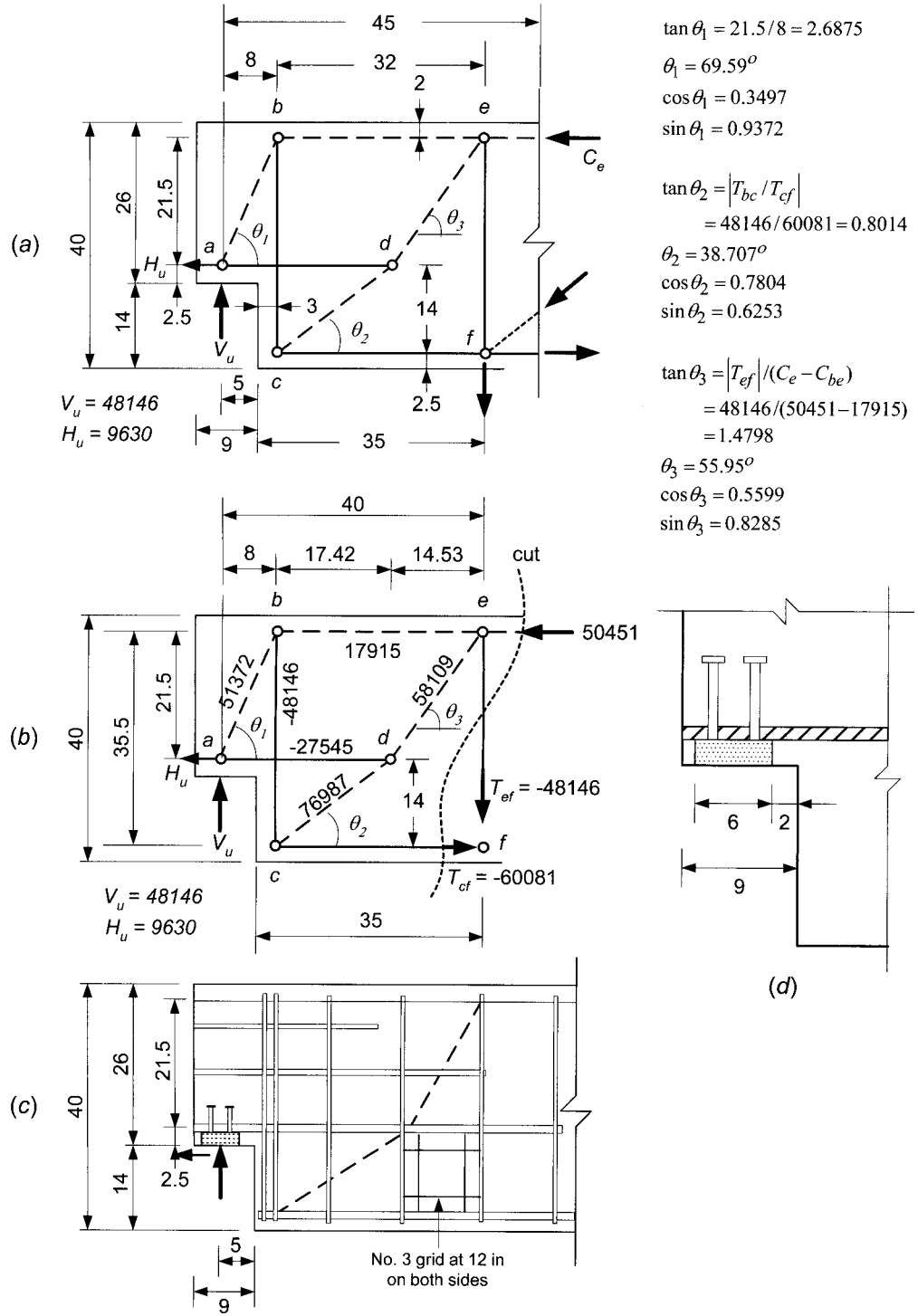

$\tan\theta_1 = 21.5/8 = 2.6875$

$\theta_1 = 69.59^o$

$\cos\theta_1 = 0.3497$

$\sin\theta_1 = 0.9372$

$\tan\theta_2 = |T_{bc}/T_{cf}|$

$= 48146/60081 = 0.8014$

$\theta_2 = 38.707^o$

$\cos\theta_2 = 0.7804$

$\sin\theta_2 = 0.6253$

$\tan\theta_3 = |T_{ef}|/(C_e - C_{be})$

$= 48146/(50451 - 17915)$

$= 1.4798$

$\theta_3 = 55.95^o$

$\cos\theta_3 = 0.5599$

$\sin\theta_3 = 0.8285$

Figure 15.29 Strut-and-tie model and detailing of dapped-end beam example.

$$C_e \times 35.5 + H_u \times 14 = V_u \times 40$$

$$C_e \times 35.5 = V_u \times 40 - H_u \times 14 = 48146 \times 40 - 9630 \times 14 = 1791020 \text{ lb-in}$$

$$C_e = 50451 \text{ lb.}$$

where C_e is a compression force applied to node e from the right side of the truss model.

Equilibrium of horizontal forces:

$$C_e + H_u + T_{cf} = 0$$

$$50451 + 9630 + T_{cf} = 0$$

$$T_{cf} = -60081 \text{ lb.}$$

Now that the isolated D-region is in equilibrium with respect to outside forces, we can calculate the forces in the remaining members of the truss, by checking equilibrium at different nodes.

5. *Compute the forces in the struts and ties.* Let us write the equilibrium of forces at each node starting by the support node a.

Node a (Fig. 15.29*a*):

$$\tan\theta_1 = 21.5/8 = 2.6875$$

$$\theta_1 = 69.59^o$$

$$\cos\theta_1 = 0.3497$$

$$\sin\theta_1 = 0.9372$$

$$C_{ab} = V_u / \sin\theta_1 = 48146/0.9372 = 51372 \text{ lb.}$$

$$T_{ad} = -(C_{ab}\cos\theta_1 - H_u) = -(17915 + 9630) = -27545 \text{ lb}$$

Node b:

$$C_{be} = C_{ab}\cos\theta_1 = 51372 \times 0.3487 = 17915 \text{ lb}$$

$$T_{bc} = -C_{ab}\sin\theta_1 = -51372 \times 0.9372 = -48146 \text{ lb}$$

Note that the tensile force in bc is equal in magnitude to V_u and could have also been obtained by introducing a cut parallel to ab located between ab and the intersection of ad and bc.

Node c:

Node c is subjected to two tensile forces from bc and cf already calculated above. They will be used to determine the inclination and magnitude of the compression strut cd.

$$\tan\theta_2 = \left|T_{bc}/T_{cf}\right| = 48146/60081 = 0.8014$$

$$\theta_2 = 38.707^o$$

$$\cos\theta_2 = 0.7804$$

$$\sin\theta_2 = 0.6253$$

$$C_{cd} = \left|T_{cf}\right| / \cos\theta_2 = 60081/0.7804 = 76987 \text{ lb}$$

or

$$C_{cd} = \left|T_{cb}\right| / \sin\theta_2 = 48146/0.6253 = 76996 \text{ lb} \quad \text{(about same) O.K.}$$

Note also that C_{cd} can be obtained from the right triangle:

$$C_{cd} = \sqrt{T_{bc}^2 + T_{cf}^2} = \sqrt{48146^2 + 60081^2} = 76991 \text{ lb} \quad \text{O.K.}$$

Location of node *d*:

The forces in ties *bc* and *cf* allow us to determine the location of node *d*. Node *d* is along a vertical section located a distance $14/\tan\theta_2 = 14/0.8014 = 17.47$ in from *c*. Thus node *d* is also located at a distance $40-8-17.47 = 14.53$ in from tie *ef*. The location of node *d* allows us to verify the conditions of equilibrium at node *e*.

Node *e*:

$$\tan\theta_3 = |T_{ef}|/(C_e - C_{be}) = 48146/(50451-17915) = 1.4798$$

$$\theta_3 = 55.95^o$$

$$\cos\theta_3 = 0.5599$$

$$\sin\theta_3 = 0.8285$$

$$C_{de} = |T_{ef}|/\sin\theta_3 = 48146/0.8285 = 58109 \text{ lb.}$$

Check that the horizontal component of C_{de} satisfies equilibrium of the horizontal forces at *e*:

$$C_{de}\cos\theta_3 + C_{be} = C_e$$

$$58109\times 0.5599 + 17915 = 50450.2 \approx 50451 \text{ lb} \qquad \text{O.K.}$$

One can check that all the forces in the truss model are in equilibrium and thus satisfactory. They are summarized in Fig. 15.29*b*. Note that the forces shown are the factored forces since V_u and H_u were used to calculate these forces.

6. and 7. ***Select dimensions for strut-and-tie nodal zones, and verify the capacity of struts both at midlength and an nodal interface.*** We have combined these two steps together since this fits better the approach followed next.

We will first determine the strengths of struts and ties. From inspection, we observe that struts *ab*, *cd*, and *de* are more critical than *be* because they are inclined and their width is much smaller than that of *be* (located along the flange).

The strengths of nodal zones according to the 2002 ACI code are computed and summarized in Table 15.5. The strength of struts are summarized in Table 15.6. All inclined struts are assumed to act like bottle-shaped struts and thus have a smaller value of β_s (from Table 15.1). Minimum strut widths are calculated and summarized in Table 15.7. The minimum strut width for the design compression force can be calculated from:

$$w_{s\min} = \frac{\text{Factored force}}{\phi\times t\times f_{cu}} = \frac{\text{Factored force}}{\phi\times t\times 0.85\times\beta_{\min}\times f_c'}$$

where $\beta_{\min}$ is the smaller value of β_s or β_s, and ϕ is taken equal to 0.75. Applying this equation to strut *ab*, leads to:

$$(w_{s\min})_{ab} = \frac{76987}{0.75\times 8\times 0.85\times 0.6\times 5000} = 5.03 \text{ in}$$

Values for the other struts are given in Table 15.7.

Dimensions of nodal zones:

Nodal zone *a*: The width of the bearing plate is 6 in. The lower minimum required width of strut *ab* is 2.69 in. Thus there is no need to check further for strength. However, the dimensions of the nodal zone will be determined for illustration.

If we use a 6 in bearing plate, then the width of strut *ab* at *a* is given by:

$$w_d = w_h/\sin\theta_1 = 6/0.9372 = 6.4 \text{ in}$$

Table 15.5 Strength of nodal zones.

Nodes	Node Type	$f_{cu} = 0.85\beta_n f_c'$ psi	ϕf_{cu} $(0.75 f_{cu})$, psi
a, b, d, e,	CCT	$0.85 \times 0.8 \times 5000 = 3400$ psi	2550
c,f	CTT	$0.85 \times 0.6 \times 5000 = 2550$ psi	1913

Table 15.6 Strength of struts.

Type of strut	Strut	Start node	End node	β_s	β_n	$f_{cu} \le \begin{cases} 0.85\beta_s f_c' \\ 0.85\beta_n f_c' \end{cases}$ psi	ϕf_{cu} $(0.75 f_{cu})$ psi
Prismatic (parallel to beam axis)	*be*	CCT	CCT	1	0.8	3400	2550
Inclined (assuming minimum grid reinforcement)	*ab*	CCT	CCT	0.75	0.8	3188	2391
	cd	CTT	CCT	0.75	0.6	2550	1913
	de	CCT	CCT	0.75	0.8	3188	2391

Table 15.7 Minimum strut dimensions.

Type of strut	Strut	ϕf_{cu} psi	Factored Strut force C_u, lb	Strut depth t, in	$w_{s\,min}$ required, in
Prismatic (parallel to beam axis)	*be*	2550	17915	48	0.15
Inclined (assuming minimum grid reinforcement)	*ab*	2391	51372	8*	2.69
	cd	1913	76987	8	5.03
	de	2391	58109	8*	3.04

* varies from 8 to 48. Using 8 is conservative.

The vertical depth of the nodal zone, which is also the width of tie *ad*, is given by:

$$w_v = w_h / \tan\theta_1 = 6 / 2.6875 = 2.23 \text{ in}$$

Nodal zone *b*: the dimensions of nodal zone at *b* are same as at *a*. The width of strut *be* is 2.23 in, and the width of tie *bc* is 6 in. Note that these widths are significantly larger than the minimum obtained in Table 15.7 and should therefore be adequate.

Nodal zone *c*: the width of tie *cb* is 6 in as calculated above. Thus the width of strut *cd* is given by:

$$w_d = w_h / \sin\theta_2 = 6 / 0.6253 = 9.59 \text{ in}$$

The height of tie *cf* is given by:

$$w_v = w_h / \tan\theta_2 = 6 / 0.8014 = 7.48 \text{ in}$$

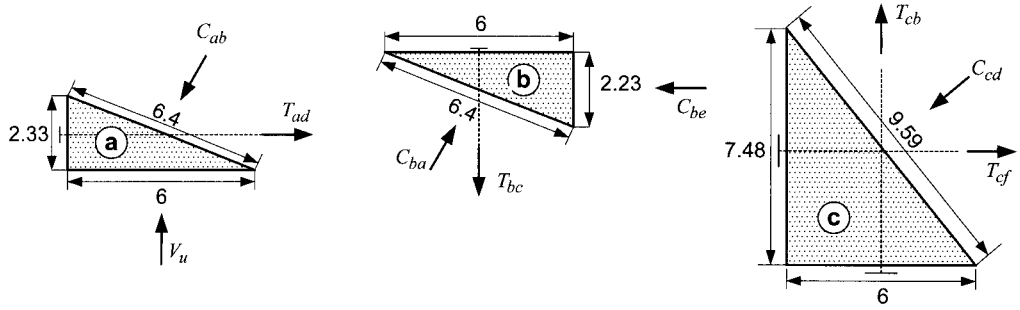

Figure 15.30 Typical dimensioning of nodal zones starting from bearing plate at node *a*.

Nodal zone *d*: the width of *cd* is given above as 9.59 in. It is significantly larger than the minimum required from Table 15.7. Same conclusion applies for *de*.

Nodal zone *e*: because this nodal zone is in the flange and has a thickness of 48 in, it can be shown that its dimensions, which can be obtained from the different struts and ties converging on *e*, are amply adequate.

Check stresses at certain nodes: sometimes it is useful to check stresses at certain nodes assuming hydrostatic conditions exist, and then use these stresses to check if dimensions and forces are acceptable. The factored stress just behind the anchorage plate at node *a* is given by:

$$\sigma_u = \frac{48146}{6\times 8} = 1003 \text{ psi} < 2391 \text{ psi (strength of nodal zone)} \quad \text{O.K.}$$

The factored stress along strut *cd* at node *c*:

$$\sigma_u = \frac{76987}{9.59\times 8} = 1003.4 \text{ psi} < 1913 \text{ psi (strength of nodal zone } c) \quad \text{O.K.}$$

The factored stress along tie *cf* at node *c*:

$$\sigma_u = \frac{60081}{7.48\times 8} = 1004 \text{ psi} < 1913 \text{ psi (strength of nodal zone } c) \quad \text{O.K.}$$

Note that the hydrostatic stress is same at nodal zones *a*, *b*, and *c* and is much smaller than the strength of the nodal zone. Using the hydrostatic pressure can also be used to estimate two sides of a nodal zone given the third one assuming a right triangle.

8. *Design the ties and tie anchorage.*

Tie *ad*

The centroid of tie *ad* is 2.5 in from the face of the support. Tie reinforcement is obtained from:

$$(T_u)_{ad} = \phi(T_n)_{ad}$$

$$27545 = 0.75A_{st}f_y = 0.75A_{st}\times 60000$$

$$A_{st} = \frac{1.2T_{ad}}{0.75f_y} == \frac{27545}{0.75\times 60000} = 0.612 \text{ in}^2$$

It can be achieved by using two No. 5 bars. At support *a*, the anchorage of these bars is insured by welding to the bearing plate whose anchorage is insured by headed studs. Beyond node *d*, these bars are anchored by extending them one development length, that is about 50 diameters or 31.25 in. These bars can be placed in the 2.23 in width of the side of nodal zone normal to the tie axis.

Tie *bc*

The required tie reinforcement is given by:

$$A_{st} = \frac{(T_u)_{bc}}{0.75 f_y} == \frac{48146}{0.75 \times 60000} = 1.07 \text{ in}^2$$

It can be achieve by using three No. 4 closed stirrups which provide 1.20 in^2. Here tie width of *bc* is 6 in and is acceptable for placing the ties in case they have to be grouped.

Tie *cf*

The required tie reinforcement is given by:

$$A_{st} = \frac{(T_u)_{cf}}{0.75 f_y} == \frac{60081}{0.75 \times 60000} = 1.34 \text{ in}^2$$

It can be achieved by using three No. 6 bars which provide 1.32 in^2 (close to value required and acceptable since we can also count on 4 prestressing strands located at about the same level. The tie width from nodal zone *c* is 7.48 in and is acceptable for placing the tie reinforcement, including the 4 straight prestressing strands that are part of the beam design. To provide adequate anchorage at *c*, these bars can be either bent upward with a 90° hook, or welded to the vertical stirrups from tie *bc*. Since the beam is prestressed and the prestressing reinforcement is adequate outside the D-region, another alternative is to use U-shaped reinforcement (bent at *c*) with sufficient length beyond node *f* to provide adequate transfer to the prestressed reinforcement.

Tie *ef*

The design reinforcement for this tie is similar to that of tie *bc*; thus we will use 3 No. 4 U-shaped stirrups anchored in the compression flange. However, we will distribute these stirrups in the D-region around section *ef* with their centroid being at *ef*.

9. *Prepare design details and check minimum reinforcement requirements.* The reinforcement required for ties *ad*, *bc*, *cf*, and *ef* is detailed in Fig. 15.29*c*. Only one layer of reinforcement is needed along *ad*. To provide sufficient anchorage, it is welded to the bearing plate at *a* (Fig. 15.29*d*), and extended one development length beyond *d*, that is about 31 in.

For tie *bc*, two stirrups are concentrated along the section and one is spread to the right of it. The 3 stirrups for tie *ef* are placed one along *ef* and one on each side. The reinforcement for tie *cf* is placed in one layer and welded to the closed strirrups at *c*.

Since struts *ab*, *cd*, and *de* are inclined additional grid reinforcement is required by the code (Table 15.1), according to the following equation:

$$\Sigma \frac{A_{si}}{bs_i} \sin \gamma_i \geq 0.003$$

Consider strut *cd* for which $\gamma_2 = \theta_2 = 38.707^o$ and $\gamma_1 = 90 - \theta_2 = 51.293^o$. Assuming a square grid of No. 3 reinforcing bars is used on each side of the beam end, the spacing of the grid can be determined from:

$$s_i \leq \frac{\Sigma A_{si} \sin \gamma_i}{0.003 \times b} = \frac{2 \times 0.11 \times \sin 38.707 + 2 \times 0.11 \times \sin 51.293}{0.003 \times 8} = 12.88 \text{ in}$$

Select a grid of No. 3 welded bars placed at 12 in spacing both horizontally and vertically. Use throughout the D-region to cover the requirements for the other struts. Note that, although it does not apply here, the ACI code limits spacing for deep beams to d/5 or 12 in.

Instead of the grid reinforcement, another approach is to add some longitudinal and transverse reinforcement to the existing reinforcement needed so far for the ties and insure that the total reinforcement satisfies the above equation.

Remarks

The above example was treated ignoring the effect of prestressing. Since prestressing can be considered an external force, it is likely that its effects would have been to reduce tensile forces in ties *ad* and *cf* and increase compression forces in most struts. However, because the average prestress due to prestressing is relatively small ($1.2 \times F / A_c = 500.1$ psi) and the capacity of struts was much higher than needed, the design is acceptable.

Similarly, because the hydrostatic stress behind the bearing plate at support *a* is small compared to the capacity of the nodal zone at *a*, it is likely that the design will be revised to include a smaller bearing plate, such as 4 in wide instead of 6 in, as used in the example.

15.13 EXAMPLES OF APPLICATIONS OF STRUT-AND-TIE MODELS TO VARIOUS STRUCTURES

Several examples of applications of strut-and-tie models to different structural elements or D-regions of structural members as taken from the available technical literature are shown in Fig. 15.3 and Figs. 15.31 to 15.39.

Figure 15.31 shows typical strut-and-tie applications for corbels [Ref. 15.31]. They supplement similar models given in Fig. 15.3.

Figure 15.32 illustrates the application of strut-and-tie modeling for the design of deviators in externally prestressed bridge beams [Ref. 15.5]. Tan and Naaman used the strut-and-tie analogy to predict the strength of externally prestressed beams subjected to a concentrated load [Ref. 15.33]. The model shown in Fig. 15.33 utilizes a fanning strut with a trapezoidal stress profile.

Two design examples of prestressed pretensioned beams using strut-and-tie modeling were developed by Matamoros and Ramirez in Ref. [15.18]. One example considered all tendons straight (with some sheathed strands at the end) and the other assumed some straight and some draped tendons. The prestressing force was determined from the analysis. Final strut-and-tie models arrived at are shown in Fig. 15.34.

Figures 15.35 and 15.36 illustrate a strut-and-tie model for a prestressed concrete rectangular and T-beam, respectively. Note that prestressing is shown as an external force and the tendons are not shown as part of the ties. For the T-beam, struts fan out in the compression flange when nearing the midspan section where maximum compression occurs.

The use of strut-and-tie models in beams with openings is very effective since the region near and including the opening can be considered a D-region. Figure 15.37 illustrates the strut and tie model of a T-beam with opening just below the flange [Ref. 15.10]. In their book on *Concrete Beams with Openings* [Ref. 15.15] Mansur and Tan cover several examples where strut-and-tie modeling is used. Figure 15.38 illustrates the case of a rectangular beam with opening. Figure 15.38*b* shows the strut-and-tie model, and Fig. 15.38*c* describes the details of the reinforcement around the opening, designed according to the model. Mansur and Tan also provided practical design information on location, size , and shape of openings should there be

need to use them in prestressed beams. Their recommendations are summarized in Fig. 15.39 which can be very useful in preliminary design.

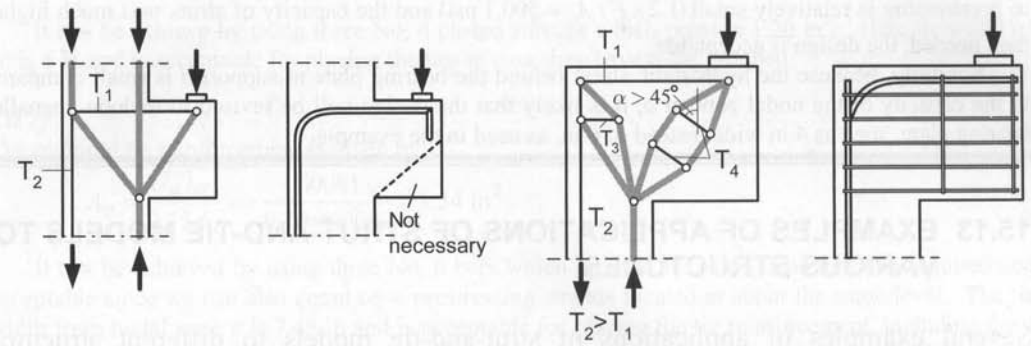

Figure 15.31 Typical strut-and-tie models for corbels and corresponding reinforcement.

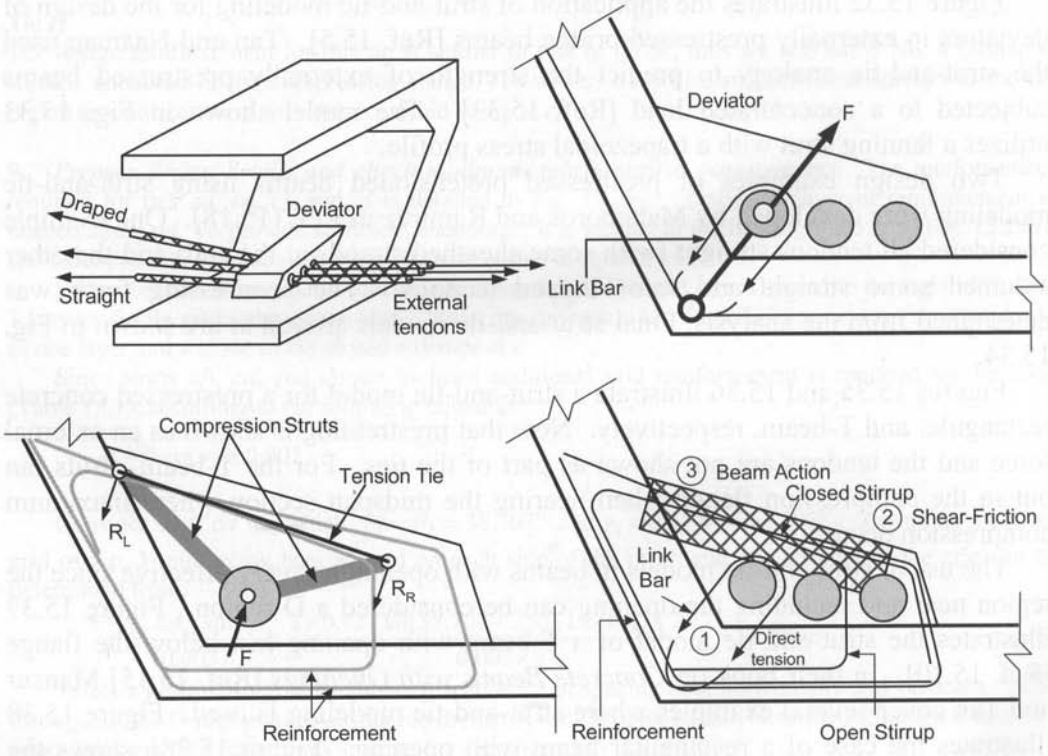

Figure 15.32 Example of strut-and-tie model for the deviator of external prestressing tendons. *(Adapted from Ref. 15.5).*

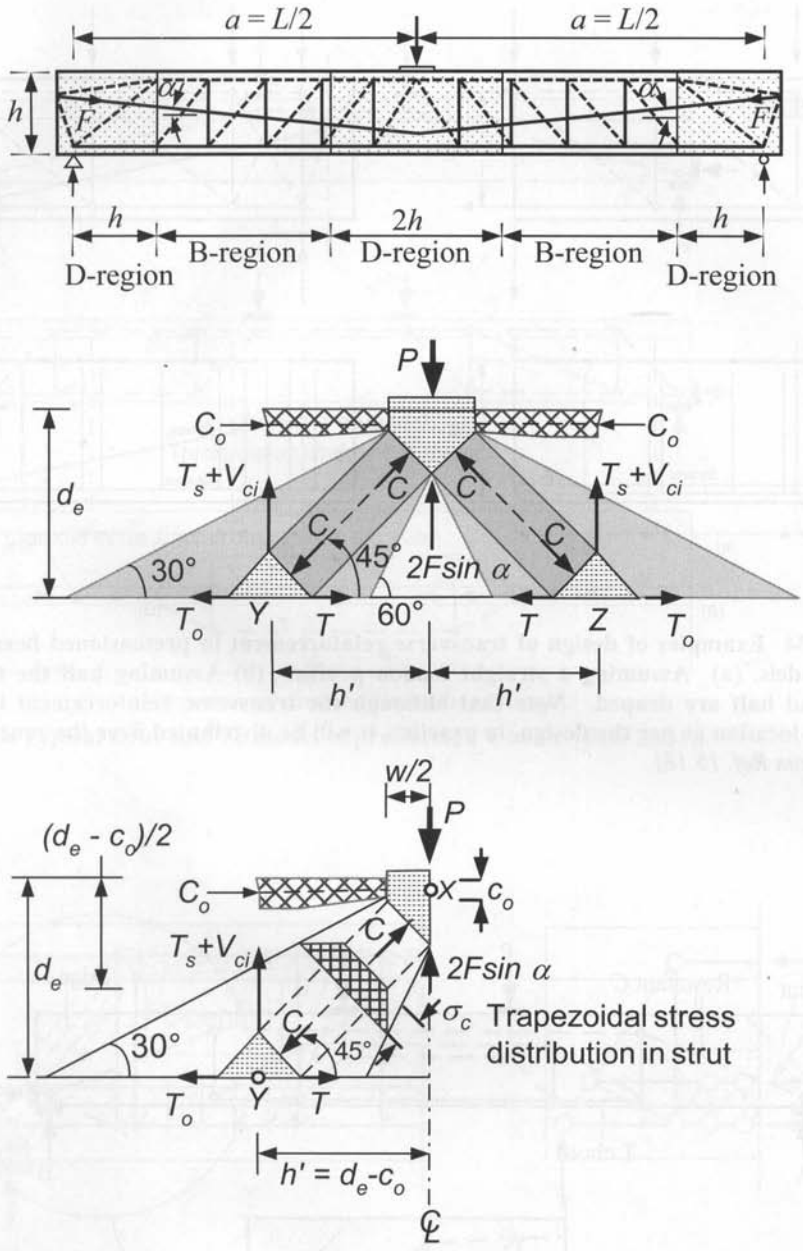

Figure 15.33 Strut-and-tie model used to model external prestressing tendons in bridge beams [Ref. 15.33].

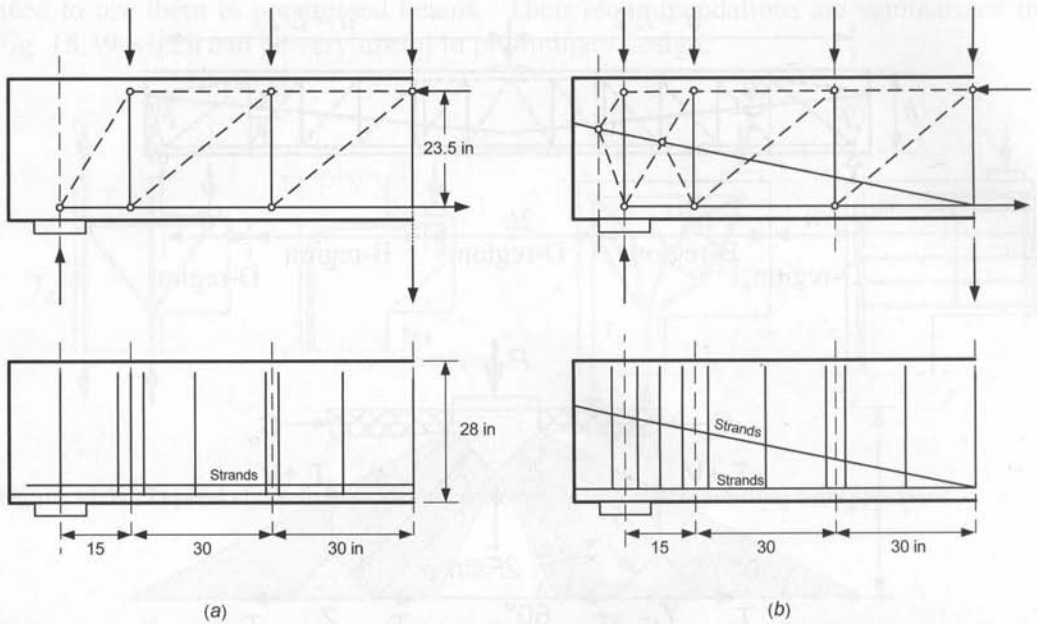

Figure 15.34 Examples of design of transverse reinforcement in pretensioned beam by strut-and-tie models. (a) Assuming a straight tendon profile. (b) Assuming half the tendons are straight and half are draped. Note that although the transverse reinforcement is placed at vertical tie location as per the design, in practice, it will be distributed over the zone of interest. *(Adapted from Ref. 15.18).*

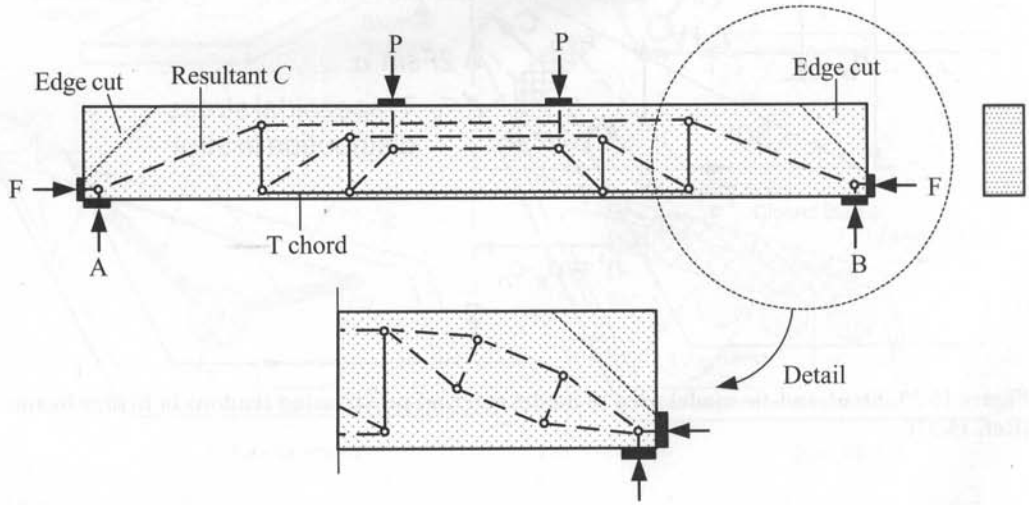

Figure 15.35 Typical strut-and-tie model of prestressed rectangular beam [Ref. 15.31].

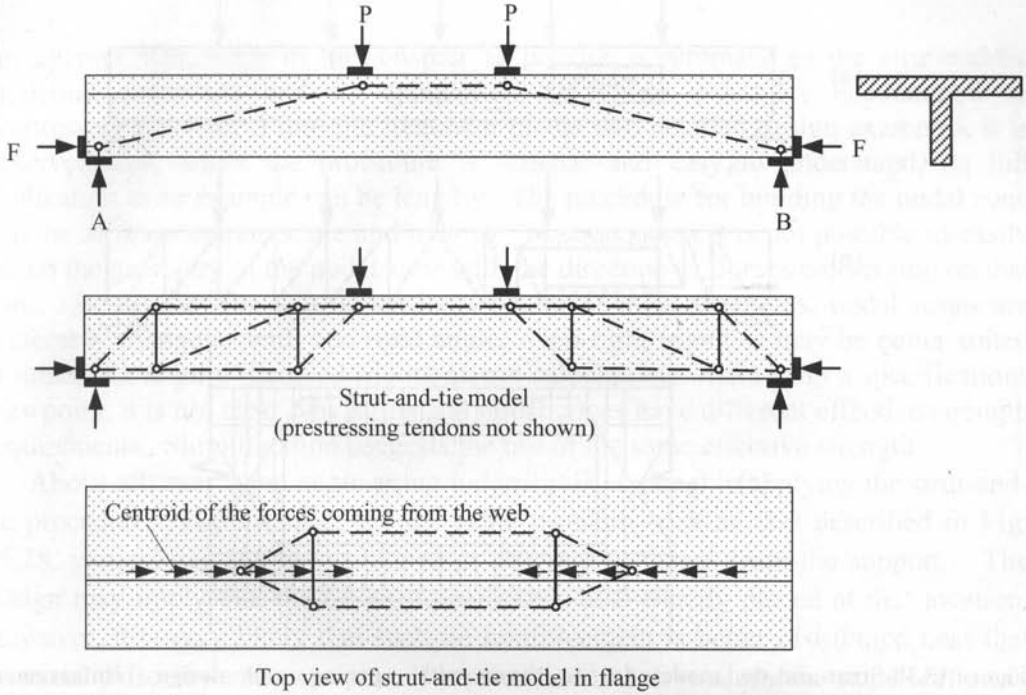

Figure 15.36 Typical strut-and-tie model of prestressed T beam [Ref. 15.31].

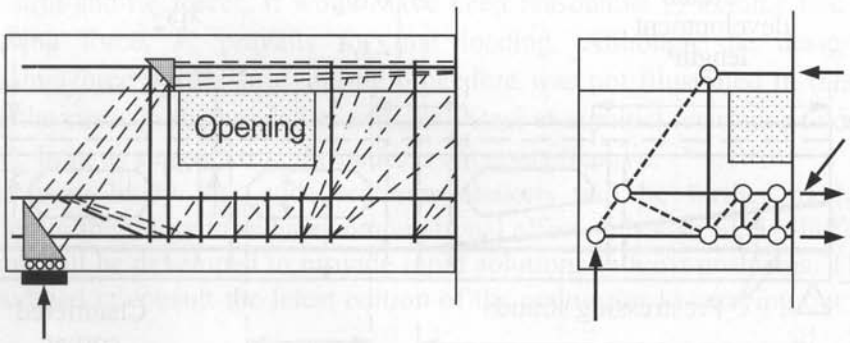

Figure 15.37 Strut-and-tie model for a T-beam with opening near the top. *(Adapted from Ref. 15.10).*

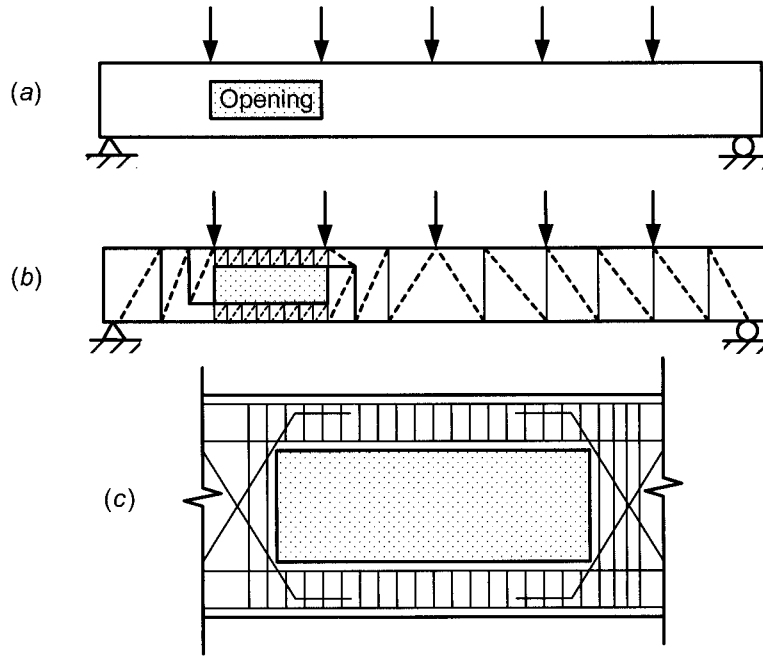

Figure 15.38 Strut-and-tie model for a beam with opening and design reinforcement requirements. *(Adapted from Ref. 15.15).*

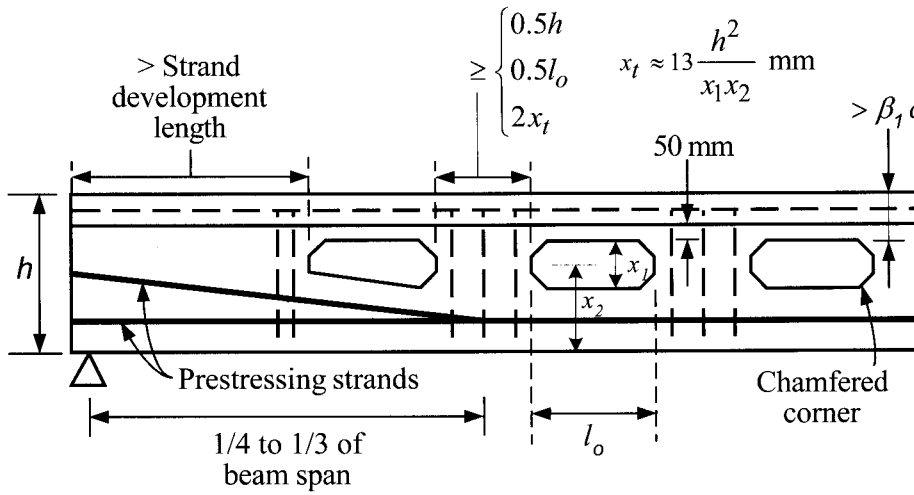

x_t = distance over which maximumvertical tensile stress (due to prestressing) at edge of opening reduces to zero

Figure 15.39 Recommended guidelines for openings in prestressed beams based on strut-and-tie model studies. *(Adapted from Mansur and Tan, Ref. 15.15).*

15.14 CONCLUDING REMARKS

An attempt was made in this chapter to provide a summary of the strut-and-tie modeling procedure and its application to typical examples encountered in prestressed concrete. From the treatment of the two detailed design examples, it is observed that, while the procedure is rational and easy to understand, its full application to an example can be lengthy. The procedure for building the nodal zone may be at times cumbersome and tedious. In some cases it is not possible to easily match the geometry of the nodal zone with the direction of forces converging on that zone. Because of the two-dimensional nature of most structures, nodal zones are preferably triangular with one right angle. Non-right triangles may be better suited at times, but require involved trigonometric calculations. Also, from a specifications viewpoint, it is not clear why struts and nodal zones have different effective strength requirements. Simplification suggests the use of the same effective strength.

Above all, exercising engineering judgment is essential in applying the strut-and-tie procedure. For instance, for the same problem such as that described in Fig. 15.28, vertical ties can be positioned at different distances from the support. The design may imply that the tie reinforcement is also exactly placed at that location. However, it is very likely that such tie reinforcement is better distributed near that location. Also in some examples, it is possible to observe along the same section of a D-region both tension and compression elements (Fig. 15.23 tie *cd* and strut *de*). However, the tie reinforcement will be extended along the whole depth of the section including the compressed part. For the design of anchorage zones, we used the initial prestressing force, F_i. However, since we also used the factored loads to solve for the strut-and-tie forces, it would have been reasonable to assume that the final prestressing force, F, prevails for that loading. Although the design of the prestressing force by the strut-and-tie procedure was not illustrated in this chapter, limiting the stress in the bonded prestressing steel at nominal resistance to essentially its elastic limit as suggested in the code, is not cost effective.

It is very likely that code recommendations will be further modified and simplified in the future to reduce computational effort. It is also likely that computer programs will be developed to provide rapid solutions to most problems. The reader is encouraged to consult the latest edition of the code prior to carrying out any final design.

REFERENCES

15.1 AASHTO, "*AASHTO LRFD Bridge Specifications for Highway Bridges*," 2nd Ed., American Association of Highway and Transportation Officials, Washington, D.C., 1998. 1216 pp.

15.2 AASHTO, "*AASHTO LRFD Bridge Specifications and Commentary,*" 2nd Ed., (2001 Interim Revisions), American Association of Highway and Transportation Officials, Washington, D.C., 1998-2001.

15.3 ACI-ASCE Committee 445, "Recent Approaches to Shear Design of Structural Concrete," *ASCE Journal of Structural Engineering*, 124(12): 1375-1417, 1998. See also ACI 445 R-99, American Concrete Institute, Farmington Hills, 1999, 55 pp.

15.4 ACI Committee 318, "Building Code Requirements for Structural Concrete (ACI 318-02)," American Concrete Institute, Farmington Hills, MI, 2002, 443 pp.

15.5 Beaupre, R. J., L. C. Powell, J. Breen, and M. E. Kreger, "Deviator Behavior and Design for Externally Post-Tensioned Bridges." In *External Prestressing in Bridges*, ACI SP-120, A. E. Naaman and J. Breen, eds. Farmington Hills, MI: American Concrete Institute, 1990, 458 pp.

15.6 Breen, J. E., O. Burdet, C. Roberts, D. Sanders, and G. P. Wollmann, "Anchorage Zone Reinforcement for Post-Tensioned Concrete Girders," Rep. No. 356, National Academy Press, Washington D.C., 1994.

15.7 Canadian Standards Association, "Design of Concrete Structures, CSA Standard A23.3-94," Canadian Standards Association, Ottawa, Canada, 1994.

15.8 CEB-FIP Model Code 1990: *Design of Concrete Structures*, Comité Euro-International du Béton, Thomas Telford Services Ltd., London, 1993, 437 pp.

15.9 Collins, M. P. and D. Mitchell, *Prestressed Concrete Structures.* Englewood Cliffs: Prentice Hall, Inc., 1991, 766 pp.

15.10 Cook, W. D., and D. Mitchell, "Studies of Disturbed Regions Near Discontinuities in Reinforced Concrete Members," *ACI Structural Journal*, 95(2): 206-16, 1988.

15.11 Fanella, D., and B. Rabbat, "Notes on ACI 318-02 Building Code Requirements for Structural Concrete," Portland Cement Association, Skokie, IL, 2002.

15.12 FIP Commission 3, "FIP Recommendations, Practical Design of Structural Concrete," *FIP Congress*, SETO, London, England, 1996.

15.13 MacGregor, J. G., *Reinforced Concrete: Mechanics and Design,* 3rd Ed. Englewood Cliffs: Prentice-Hall, 1997, 939 pp.

15.14 MacGregor, J. G.: "Derivation of Strut-and-Tie Models for the 2002 ACI Code." In *Examples for the Design of Structural Concrete with Strut-and-Tie Models*, ACI SP-208, K. H. Reineck, ed. Farmington Hills, MI: American Concrete Institute, 2002, pp. 7-40.

15.15 Mansur, M. A., and K. H. Tan, *Concrete Beams with Openings: Analysis and Design.* Boca Raton: CRC Press, 1999, 220 pp.

15.16 Marti, P., "Truss Models in Detailing, *Concrete International*, 7(12): 66-73, 1985.

15.17 Marti, P., "Basic Tools of Reinforced Concrete Beam Design," *ACI Journal*, 82(1): 46-56, 1985.

15.18 Matamoros, A., and J. Ramirez, "Example 6: Prestressed Beam." In *Examples for the Design of Structural Concrete with Strut-and-Tie Models*, B. Reineck, ed. SP-208, American Concrete Institute, Farmington Hills, MI, 2002, pp. 163-184.

15.19 Mattock, A. H., and T. C. Chan, "Design and Behavior of Dapped-End Beams," *PCI Journal*, 24(6): Nov.-Dec., 1979.

15.20 Mattock, A. H., and T. S. Theryo, "Strength of Precast Prestressed Concrete Members with Dapped Ends," *PCI Journal*, 31(6): Sept.-Oct., 1986.

15.21 Naaman, A. E., and J. Breen, eds., *External Prestressing in Bridges*, ACI SP-120, American Concrete Institute, Farmington Hills, 1990, 458 pp.

15.22 Nielsen, M. P., *Limit Analysis and Concrete Plasticity.* CRC Press LLC, 1999.

15.23 Nilson, A. H., D. Darwin, and C. W. Dolan, *Design of Concrete Structures*, 13th Ed., Chapter 10, Boston: McGraw Hill Higher Education, 2003, 779 pp.

15.24 Nowak, L. C., H. Sprenter, "Example 5: Deep Beam with Opening," In *Examples for the Design of Structural Concrete with Strut-and-Tie Models*," ACI SP 208, Karl-Heinz Reineck, ed., American Concrete Institute, Farmington Hills, MI, 2002, pp 129-144.

15.25 *PCI Design Handbook*, 5th Ed. Chicago: Precast Prestressed Concrete Institute, 1999.

15.26 Peterman, R., J. Ramirez, J. Olek, "Influence of Flexure-Shear Cracking on Strand Development Length in Prestressed Concrete Members," *PCI Journal*, 45(5): 76-94, 2000.

15.27 Ramirez, J., "Strut-and-Tie Shear Design of Pretensioned Concrete," *ACI Structural Journal*, 91(5): 572-78, 1994.

15.28 Reineck, B., ed., *Examples for the Design of Structural Concrete with Strut-and-Tie Models*. SP-208, American Concrete Institute, Farmington Hills, MI, 2002, 242 pp.

15.29 Reineck, K. H., "Modeling Structural Concrete with Strut-and-Tie Models - Summarizing Discussion of the Examples as per Appendix A of ACI 318 – 2002." In *Examples for the Design of Structural Concrete with Strut-and-Tie Models* (ACI SP-208), American Concrete Institute, Farmington Hills, MI, pp. 225-242.

15.30 Savage, J. M., M. K. Tadros, P. Arumugassamy, and L. G. Fisher, "Behavior and Design of Double Tees with Web Openings," *PCI Journal*, 41(1), Jan.-Feb., 1996.

15.31 Schlaich, J., K. Schafer, and M. Jennewein, "Toward a Consistent Design of Structural Concrete," *PCI Journal*, 32(3): 74-150, 1987.

15.32 Schlaich, J., and K. Schafer, "Design and Detailing of Structural Concrete Using Strut-and-Tie Models," *Structural Engineering*, 69(6), 1991, 13 pp.

15.33 Tan, K. H, and A. E. Naaman, "Strut-and-Tie Model for Externally Prestressed Concrete Beams," *ACI Structural Journal*, 90(6): 683-91, 1993.

15.34 Uribe, C. M., and S. Alcocer, "Example 1a: Deep Beam Design in Accordance with ACI 318-2002." In *Examples for the Design of Structural Concrete with Strut-and-Tie Models,* ACI SP 208, Karl-Heinz Reineck, ed., American Concrete Institute, Farmington Hills, MI 2002, pp. 65-80.

15.35 Vecchio, F., and M. P. Collins, "The Modified Compression Field Theory for Reinforced Concrete Elements Subjected to Shear," *ACI Journal*, 83(2): 219-31, 1986.

15.36 Vecchio, F. J., "Disturbed Stress Field Model for Reinforced Concrete: Formulation," *ASCE Journal of Structural Engineering*, 126(9): 1070-77, 2000.

15.37 Wight, J. K., "Strut and Tie Modeling in the ACI Building Code," 4th International Conference: Analytical Models and New Concepts in Concrete and Masonry Structures, AMCM, 2002, Cracow, Poland.

15.38 Wight, J. K., and G. Parra-Montesinos, "Use of Strut and Tie Model for Deep Beam Design as Per ACI 318 Code," *ACI Concrete International*, 25(5): 63-70, 2003.

15.39 Wollmann, G. P., and C. L. Roberts-Wollmann, "Anchorage Zone Design," Post-Tensioning Institute, Phoenix, 2000, 53 pp.

15.40 Yun, Y. M., and J. A. Ramirez, "Strength of Struts and Nodes in Strut-Tie Model," *ASCE Journal of Structural Engineering*, 122(1): 20-29, 1996.

PROBLEMS

15.1 Complete the example described in Section 15.10.2 and Fig. 15.26. Provide details of the reinforcement.

15.2 For the same input data as the example described in Section 15.12, use the strut-and-tie model shown in Fig. 15.28*a* and provide a full design of the D-region.

15.3 For the same input data as the example described in Section 15.12, use the strut-and-tie model shown in Fig. 15.28*b* and provide a full design of the D-region.

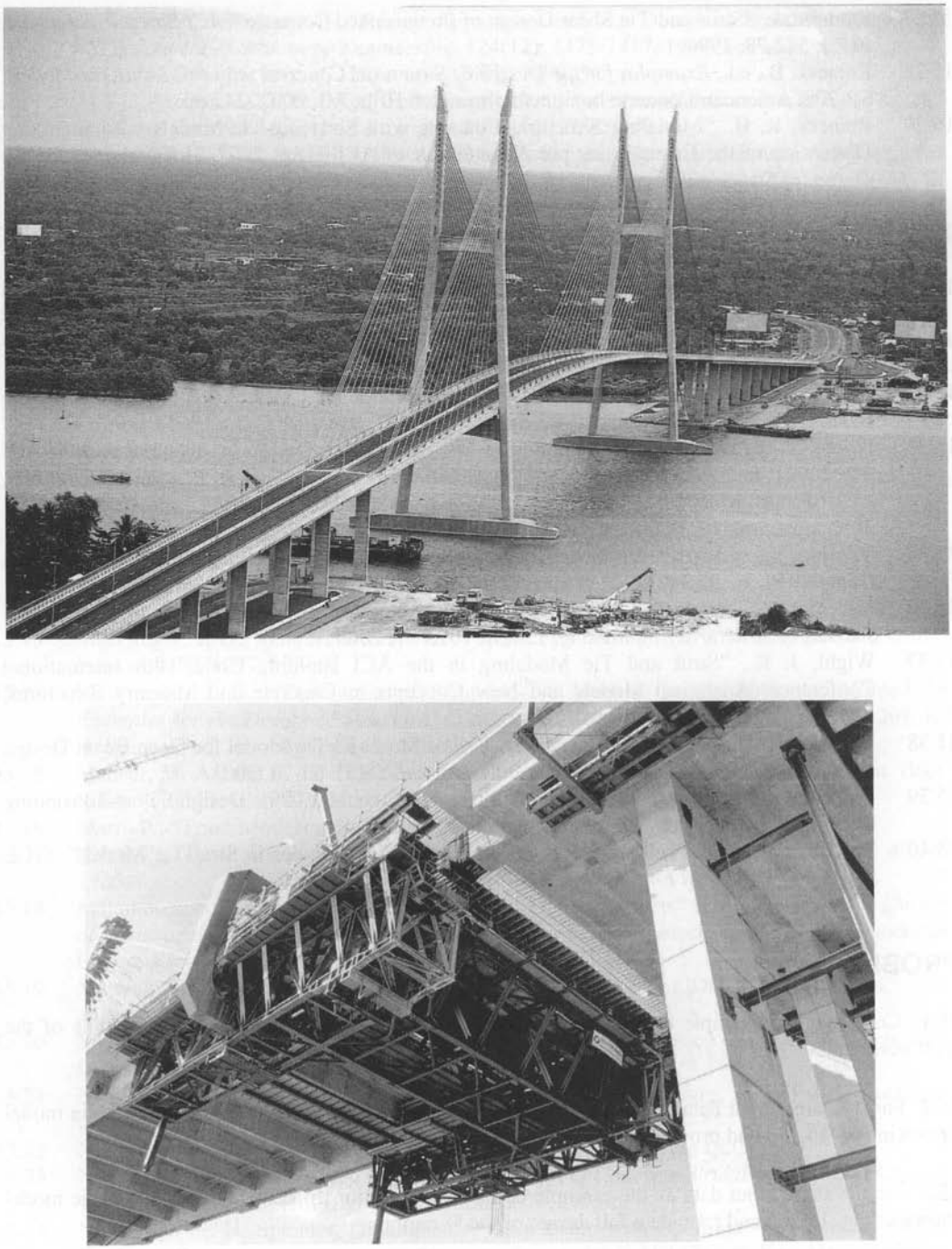

My Thuan Bridge, Vietnam. It is a cable-stayed bridge with a main span of 1148 ft (345 m) and a superstructure consisting of a grillage of two longitudinal prestressed concrete girders with transverse crossbeams supporting a reinforced concrete deck slab. *(Courtesy T.Y. Lin International and Baulderstone Hornibrook.)*

LIST OF SYMBOLS

NOTATION: ENGLISH LETTERS

a	depth of equivalent rectangular stress block ($= \beta_1 c$ if ACI code)
a	parameter, distance, coefficient
A	area in general
A	used as subscript for age, anchorage set, additional weight
A_c	area of concrete at the cross section considered in general (depending on the particular case, it may be the net area, the gross area, or the transformed area)
A_{cc}	area of concrete composite section
A_{co}	area of concrete core of a spirally reinforced column measured to outside diameter of spiral
A_{cs}	effective cross sectional area of strut
A_g	gross area of concrete at the cross section considered
A_f	area of forms
A_i	area of part i of a section
A_l	total area of longitudinal reinforcement to resist torsion
A_n	net area of concrete at the cross section considered; area of nodal zone
A_{pf}	area of prestressed reinforcement required to develop the ultimate compressive strength of the overhanging portions of the flange of a flanged section
A_{pi}	cross-sectional area of ith tendon
A_{ps}	area of prestressed reinforcement in tension zone
A_{pw}	$A_{ps} - A_{pf}$, area of prestressed reinforcement associated with the web of a flanged member at nominal moment resistance
A_o	gross area of concrete enclosed by the shear flow path; it can be taken as a first approximation equal to $0.85A_{oh}$
A_{oh}	area enclosed by centerline of the outermost closed transverse torsional reinforcement, in^2
A_s	area of non-prestressed tension reinforcement
A_{ss}	area of reinforcement in strut
A_{st}	area of reinforcement in tie

A_s'	area of compression reinforcement
A_t, A_{tr}	transformed area of concrete at section considered (depending on the particular case it may represent a cracked or uncracked section)
A_t	area of one leg of closed stirrups used as torsion reinforcement within distance s
A_v	area of shear reinforcement within a distance s
A_{vf}	area of shear-friction reinforcement
b	used as a subscript to indicate "bottom fiber"
b	width of compression face of member
b_e	effective flange width
b_o	perimeter of critical section for slabs or footings
b_{tr}	transformed flange width
b_v	width of cross section at contact surface being investigated for horizontal shear
b_w	web width of a flanged member
c	used as a subscript to describe "concrete" or "composite" section
c	distance from extreme compression fiber to neutral axis
c	cohesion factor
$c_1, c_2, ..., c_i$	various dimensions or distances
C	resulting compressive force in the concrete section due to the prestressing force and applied external forces, such as in the C-line; compression force in strut
C	cross-sectional constant to define torsional properties
C	used as a subscript to describe effect of creep
C	force resultant of the compression block of concrete at ultimate
$C_C(t)$	creep coefficient of concrete at time t
C_{CU}	ultimate creep coefficient, or creep coefficient at end of service life
C-line	geometric lieu of the compressive force in a member under service conditions
C_m	factor relating actual moment diagram to equivalent uniform moment diagram
C_{ns}	nominal compression resistance of strut
d_e	distance from extreme compression fiber to combined centroid of tensile force when prestressed and nonprestressed tension reinforcement are used
d_b	nominal diameter of bar
d_c	diameter of core of spirally reinforced column
d_c	concrete cover measured from the extreme tension fiber to centroid of tensile reinforcement
d_{cnet}	net concrete cover measured to extreme layer of reinforcement
d_p	distance from extreme compression fiber to centroid of prestressing steel
d_{pc}	distance from extreme compression fiber of cast-in-place slab to centroid of prestressing steel, in a composite beam
d_s	distance from extreme compression fiber to centroid of nonprestressed tension reinforcement
d_s'	distance from extreme compression fiber to centroid of compressive reinforcement
d_t	distance from extreme compression fiber to extreme layer of tensile steel reinforcement
D	dead loads or their internal moments and forces
DF	distribution factor of wheel load or concentrated load
DF_m	live load distribution factor for moments
DF_v	live load distribution factor for shear forces
e	base of napierian logarithms

e_c	eccentricity of the C force in the concrete section measured from the centroid of the section
e_{cl}	lower eccentricity limit of the C-line
e_{cu}	upper eccentricity limit of the C-line
e_i	eccentricity of *i*th tendon, or eccentricity of the steel at section *i*
e_o	eccentricity of the prestressing force at the section considered measured from the centroid of the section
$e_o(x)$	eccentricity of the prestressing force at section x
e_{oA}, e_{oB}	left and right support eccentricities of the prestressing steel in a typical span AB
$e_{oc}(x)$	eccentricity of the Zero-Load-C line at section x
e_{ol}	lower eccentricity limit of the prestressing steel
e_{ou}	upper eccentricity limit of the prestressing steel
$(e_o)_{mp}$	maximum practically feasible eccentricity
E	load effects of earthquakes or their related internal moments and forces; modulus of elasticity, in general; equivalent strip width of slab
E_c	modulus of elasticity of concrete
$E_{ce}(t)$	effective or equivalent modulus of elasticity of concrete at time t
E_{ci}	modulus of elasticity of concrete at time of initial prestress
E_o	tangent modulus of elasticity measured at the origin of the stress-strain curve
E_m	secant modulus measured at the maximum or peak stress
E_{ps}	modulus of elasticity of prestressing steel
E_s	modulus of elasticity of nonprestressed steel or reinforcing steel bars
E_{sh}	modulus of steel at onset of strain hardening
EI	flexural stiffness or flexural rigidity of compression members
ES	elastic shortening
f	used as stress in general, preferably for the steel and occasionally for concrete when a symbol is widely used
f_b	stress on bottom fiber of concrete section (also σ_b)
f_{cgs}	stress in the concrete at the centroid of prestressing steel
$f_{cgs}(t_i)$	stress in the concrete at the centroid of the prestressing steel at time t_i at section considered
f_{cr}	stress range in the concrete
f_{cu}	effective strength of concrete in strut-and-tie model
f'_c	specified compressive strength of concrete
f'_{ci}	compressive strength of concrete at time of initial prestress
f_{pe}	effective stress in the prestressing steel, after losses, at section considered
f_{pi}	initial stress in the prestressing steel at section considered
f_{pJ}	stress in the prestressing steel at end of jacking
f_{pJ1}	stress at jacking before seating of the chuck or anchor
f_{pJ2}	stress at jacking after seating of the chuck or anchor
f_{pp}	proportional limit stress of the prestressing steel
f_{ps}	calculated stress in prestressing steel at section considered and loading considered
$f_{ps}(t)$	stress in the prestressing steel at time t at section considered and for the loading considered
f_{pu}	specified tensile strength of prestressing steel
f_{py}	specified yield strength of prestressing steel
f_r	modulus of rupture of concrete
f_{sr}	stress range in the steel

f_s	stress in the nonprestressed tensile reinforcement
f_s'	stress in the compressive reinforcement
f_s	allowable stress in the steel
f_{tc}'	direct tensile strength (stress) of concrete
f_y	specified yield strength of nonprestressed tensile reinforcement
f_{yv}	specified yield strength of closed transverse torsional reinforcement
f_y'	specified yield strength of compressive reinforcement
F	final or effective prestressing force (after all losses) at section considered
F	used as a subscript to describe effect of friction
F_i	initial prestressing force at time of transfer at section considered
F_J	prestressing force at end of jacking
F_n	tensile force in the prestressing steel at the nominal moment resistance of the section
g	used as a subscript for center of gravity
$g(t)$	time function
G	used as a subscript for gravity load or self-weight
GP	gravity load due to precast girder or element
h	overall thickness or depth of member
h_c	overall depth of composite member
h_f	flange thickness of a flanged member
H	relative humidity, percent; also used to describe loading due to earth pressure
H_u	total horizontal shear force at the interface between the precast section and the cast-in-place slab of a composite beam
i	used as a subscript to describe "initial" conditions or *i*th element
I	effect of impact or impact coefficient; moment of inertia, in general
IM	impact coefficient or its effect
I_c	moment of inertia of uncracked concrete section resisting externally applied load (it represents the inertia of either the net of the gross section depending on the particular case)
I_{cc}	moment of inertia of uncracked composite section
I_{cr}	moment of inertia of cracked section (transformed to concrete)
I_e	effective or equivalent moment of inertia for computation of deflections after cracking
I_g	moment of inertia of gross concrete section about the centroidal axis, neglecting the reinforcement
I_{gc}	gross moment of inertia of composite section
I_p	polar moment of inertia
k	effective length factor for compression members
k	calibration factor used to predict the stress in prestressing steel at ultimate
k_b	distance from centroid of concrete section to the lower (bottom) limit of central kern
k_r	reduction factor of additional long-term deflection due to the presence of nonprestressed reinforcement
k_t	distance from centroid of concrete section to the upper (top) limit of central kern
k_b'	distance from centroid of concrete section to the lower (bottom) limit of the limit kern
k_t'	distance from centroid of concrete section to the upper (top) limit of the limit kern

K	wobble friction coefficient per unit length of prestressing steel
K	flexural stiffness of member; moment per unit rotation
K_c	flexural stiffness of column
K_{ec}	flexural stiffness of equivalent column (above and below)
K_t	flexural stiffness of attached torsional member
K_{CA}	age at loading factor for creep
K_{CH}	humidity correction factor for creep
K_{CS}	shape and size factor for creep
K_{SH}	humidity correction factor for shrinkage
K_{SS}	shape and size factor for shrinkage
l	span length of member generally center-to-center of supports; also ℓ
l	used as a subscript for lifetime, or lower
l_a, l_b	longer and shorter span of a slab panel
l_c	height of column center-to-center of floors or roofs
l_d	development length
l_i	ith span of a continuous beam or one-way slab
l_n	clear span measured face to face of supports
l_t	transfer length
l_u	unbraced length of column or column length between hinges
l_x, l_y	spans in the x and y direction for a two-way slab system
l_1, l_2	respectively span in the direction being analyzed for bending, and span or width transverse to l_1 (used in the equivalent-frame method for two-way slabs), measured center to center of supports
L	live loads or their internal moments and forces
L	span length
L_e	effective tendon length
L_1	sum of lengths of span loaded with live load and containing tendon(s) considered
L_2	total length of tendon(s) between anchorages
m_A, m_B	fixed end moments at ends A and B of a typical beam,
$M, M(x)$	moment in general at section considered or at section x
M_a	maximum absolute moment in member at stage deflection is computed
M_b	moment due to balanced load
M_c	maximum moment on section while acting as composite section
M_{cr}	cracking moment
M_D	moment due to dead load
$M_F, M_F(x)$	total moment due to prestressing at section considered or at section x
M_{FA}, M_{FB}	total moment due to prestressing at supports A and B of a typical span AB
M_G	bending moment due to self-weight of member
M_L	moment due to live load
M_{lane}	maximum moment due to a single live loading lane at section considered
M_{L+I}	moment due to live load plus impact at section considered
$M_{\max}$	maximum bending moment at section considered under service load conditions
$(M)_{\max}$	maximum absolute moment in a span due to truck loading
$M_{\min}$	minimum bending moment at section considered under service load conditions
M_n	nominal moment resistance
M_{nb}	moment due to unbalanced load
$M_{n,b}$	nominal moment resistance of a compression member (section) at balanced conditions

$M_{n,ot}$	nominal moment capacity leading to zero tension on extreme fiber of column or wall section
M_{nf}	nominal moment resistance due to the overhanging portion of the flange of a T section
$M_{n,f}$	nominal moment resistance of compression member (section) subjected to pure bending
M_{nw}	nominal moment resistance of the web of a T or flanged section
M_p	maximum moment on the precast prestressed section of a composite member
M_S	moment due to cast-in-place slab in a composite member at section considered
M_{SD}	moment due to superimposed dead load at section considered
M_u	strength design moment or factored moment at section considered
M_{uc}	magnified factored moment to account for slenderness in compression member
M_{uw}	strength design moment for the web of a T section
M_{u1}	value of smaller factored end moment on compression member, positive if member is bent in single curvature, negative if bent in double curvature
M_{u2}	value of larger factored end moment on compressive member, assumed always positive
$M_1, M_1(x)$	primary moment due to prestressing in a continuous structure at section considered or at section x
$M_2, M_2(x)$	secondary moment due to prestressing in a continuous structure at section considered or at section x
M_{2A}, M_{2B}	secondary moments due to prestressing at supports A and B or at sections A and B
n	used as a subscript for nominal
n_c	modular ratio of concrete of cast-in-place slab to concrete of precast section of a composite beam
n_p	modular ratio E_{ps} / E_c
n_{pi}	initial modular ratio E_{ps} / E_{ci}
n_s	modular ratio E_s / E_c
N	axial load acting on member, preferably used for tension
N_b	number of beams in a bridge deck
N_c	tensile force in concrete section due to unfactored dead load and live load
N_{cr}	tensile load leading to cracking of prestressed member
N_{dec}	tensile load leading to decompression of prestressed member
N_n	nominal resistance of prestressed member under axial tension; nominal resistance of nodal zone
N_L	number of design loading lanes
p	used as a subscript for prestressing; also used for pressure or percentage
p_h	perimeter of centerline of outermost closed transverse torsional reinforcement, in
P	concentrated external load in general
P	axial load acting on member, preferably used for compression
P_{cr}	critical buckling load
P_m	maximum cut-off compressive force on column allowed by code
P_n	nominal axial load capacity, in general, at a given eccentricity
$P_{n,b}$	nominal axial load capacity at balanced conditions
$P_{n,o}$	nominal axial load capacity of compression member subject to pure compression

$P_{n,ot}$	nominal axial load capacity leading to zero tension on extreme fiber of column or wall
P_u	factored axial compressive load at given eccentricity
PPR	partial prestressing ratio
Q	first static moment with respect to centroid of the portion of section above the shear plane considered
Q	stability index
Q	concentrated external load
Q, Q_i	loading or load effect in general, and loading i
r	radius of gyration of cross section $= \sqrt{I/A}$
R	used as a subscript to describe effect of steel relaxation
R	radius of circular, cylindrical, or curved element
R_n	nominal resistance in general
s	curvilinear abscissa; also used as a subscript for "steel" reinforcement
s	spacing to stirrups, or ties, or bent-up bars in direction parallel to longitudinal reinforcement
s	pitch of spiral reinforcement
s	length of side element
S	effect of cast-in-place slab in a composite beam
S	used as a subscript to describe effect of shrinkage
S	transverse spacing center-to-center of beams or girders in a deck or slab structure
S_e	effective span of slab
S_n	transverse clear spacing of beams or girders
SD	superimposed dead load or its related internal moments and forces
SF	safety factor
t	time
t	torsional shear stress
t	used as a subscript to indicate "top fiber" or "tension"
t	wall thickness
t_A	age at loading
t_c	torsional shear stress contributed by concrete after cracking; also used when member is subjected to torsion alone
t_c^*	torsional strength (stress) of concrete under combined torsion and flexural shear
t_{cr}	torsional shear stress at cracking
t_i, t_j	particular values of time, mostly used to define the beginning and the end of a time interval
t_l	design lifetime of member
t_t	time at transfer or at release of prestress
t_o	time at jacking of prestressing steel
t_u	factored design torsional strength (stress)
T	tensile force in the steel; also used as subscript for total to describe cumulative effects; for temperature loading; for torque or torsional moment; for T section
T_c	nominal torsional moment resistance contributed by concrete after cracking
T_c^*	torsional shear strength of concrete under combined torsion and flexural shear
T_{cr}	torsional cracking moment
T_{ip}	tensile force in the ith layer of prestressing steel
T_{is}	tensile or compressive force in the ith layer of reinforcing steel
T_n	nominal torsional moment resistance of section

T_{nf}	tensile force in the steel balancing the compression force in the overhanging portion of the flange of a T section at nominal moment capacity
T_{nt}	nominal resistance of tie
T_{nw}	nominal tensile force in the steel balancing the compressive force in the web of a T section at nominal moment capacity
T_s	nominal torsional moment resistance contributed by torsion reinforcement
T_u	factored design torsional moment at section considered; factored tensile force
u	used as subscript for "factored effects" or design specified values at ultimate capacity
U	required strength to resist factored loads or related internal moments and forces
U	unit cost; subscript c holds for concrete, f for forms, p for prestressing steel, and s for reinforcing steel
υ, v	shear stress in general
υ_c	permissible shear stress carried by concrete
υ_c	shear strength (stress) of concrete in presence of torsion
υ_{ci}	nominal shear strength (stress) provided by concrete when diagonal cracking results from combined shear and moment
υ_{cw}	nominal shear strength (stress) provided by concrete when diagonal cracking results from excessive principal tensile stresses in the web
υ_n	nominal shear strength (stress) at section considered
υ_{nh}	nominal horizontal shear strength (stress)
υ_s	nominal shear strength (stress) provided by shear reinforcement
υ_u	factored design shear strength (stress) at section considered
υ_{uh}	factored horizontal shear strength (stress)
$V, V(x)$	shear force in general at section considered or at section x
V_D	shear force due to unfactored dead load at section considered
V_{lane}	maximum shear force due to a single live loading lane at section considered
V_{L+I}	shear force due to unfactored live load plus impact at section considered
V_n	nominal shear strength (force) at section considered
V_{nh}	nominal horizontal shear force resistance
V_p	vertical component of effective prestressing force at section considered
V_{SD}	unfactored shear force due to superimposed dead load
V_u	factored design shear force at section considered
V_{uh}	factored design horizontal shear force
w	unfactored load per unit length of beam or per unit area of slab; width in general
w_b	balanced load; width of bearing plate
w_D	dead load per unit length of beam or per unit area of slab; it includes self weight and superimposed dead load if any
w_G	self-weight of member per unit length or per unit area, or gravity load
w_L	live load per unit length of beam or per unit area of slab
w_{nb}	nonbalanced load or unbalanced load
w_{SD}	superimposed dead load per unit length of beam or unit area of slab
w_u	factored load per unit length of beam or per unit area of slab
W	weight; wind load or related internal moments and forces; crack width
W	wedge to wedge width of bridge deck
x	abscissa along the x axis; also x represents, in general, an unknown
x	shorter overall dimension of rectangular part of cross section
x_1	shorter center-to-center dimension of closed rectangular stirrup

X	abscissa of section of tendon beyond which the stress loss due to anchorage set is zero
y	ordinate along the y axis
y	longer overall dimension of rectangular part of cross section
y_b	distance from centroidal axis of section to extreme bottom fiber
y_{bc}	distance from centroidal axis of composite section to extreme bottom fiber
y_t	distance from centroidal axis of section to extreme top fiber
y_{tc}	distance from centroidal axis of composite section to extreme top fiber
y'_{tc}	distance from centroidal axis of composite section to extreme top fiber of the precast member
y_1	longer center-to-center dimension of closed rectangular stirrup
z	ordinate along the z axis; number used in general
z	loss in stress in prestressing tendon along span length l
Z	objective function in an optimization problem
Z	factor that defines the slope of a line simulating the descending branch of the stress-strain curve of concrete
Z_b	section modulus with respect to extreme bottom fiber $= I_c / y_b$
Z_{bc}	section modulus with respect to extreme bottom fiber for a composite section $= I_{cc} / y_{bc}$
Z_t	section modulus with respect to extreme top fiber $= I_c / y_t$
Z_{tc}	section modulus with respect to extreme top fiber for a composite section $= I_{cc} / y_{tc}$
Z'_{tc}	section modulus with respect to extreme top fiber of precast elements of a composite section $= I_{cc} / y'_{tc}$

NOTATION: GREEK LETTERS

α	angle in general or factor in general
α	total angular change of prestressing steel profile in radians between two points
α	angle between inclined stirrups and longitudinal axis of member
β	factor that indicate the ability of diagonally cracked concrete to transmit tension between cracks
β_c	ratio of long side to short side of concentrated load, reaction or column
β_d	ratio of maximum factored dead load (sustained) to maximum factored total load, always positive
β_n	effective strength coefficient for nodal zone
β_s	effective strength coefficient for strut
β_t	coefficient or multiplier of $\sqrt{f'_c}$ in psi, expressing the cracking resistance of concrete under shear stresses induced by the combination of shear forces and torsional moment.
β_1	factor used to define the depth of the equivalent rectangular stress block at ultimate as a function of the location of the neutral axis (Eqs. 5.12 and 5.13)
γ	geometric efficiency; unit weight in general; factor in general
γ_c	unit weight of concrete
γ_i	load factor for load i
γ_s	unit weight of steel
γ_v	fraction of unbalanced moment transferred by eccentricity of shear at slab-column connections

δ	differential change (increase or decrease) in variable considered
δ	moment magnification factor for columns
δ	anchorage set, or slippage
δ, δ_i	sag in span considered or in span i
δ_{ns}, δ_s	moment magnification factor for non-sway and sway column, respectively
Δ	deflection in general, positive for deflection and negative for camber
Δ	difference or differential amount between two values of variable that follows the Δ
$\Delta(t)$	deflection at time t
Δ_{add}	additional long-term deflection
Δ_D	deflection due to dead load
Δ_G	deflection due to self-weight
Δ_L	deflection due to live load
Δ_i	initial, instantaneous elastic deflection
Δ_u	life deflection for the sustained loading considered
$\Delta_1, \Delta_2, \Delta_3$	deflections at different times or loading stages
Δf_{cr}	stress range limit in concrete in compression under fatigue
Δf_{pA}	total stress loss in the prestressing steel due to anchorage set at section considered
$\Delta f_{pC}, \Delta f_{pC}(t_i, t_j)$	respectively total stress loss in the prestressing steel during service life due to creep of concrete, and stress loss during a time interval (t_i, t_j) at section considered
Δf_{pES}	total stress loss in the prestressing steel due to elastic shortening at time of transfer or release
Δf_{pF}	total stress loss in the prestressing steel due to friction at section considered
Δf_{pr}	stress range in prestressing steel under cyclic load
$\Delta f_{pR}, \Delta f_{pR}(t_i, t_j)$	respectively total stress loss in the prestressing steel during service life due to relaxation of the tendons, and stress loss during a time interval (t_i, t_j) at section considered
Δf_{pR1}	stress loss in prestressing steel due to relaxation between time at end of jacking and time of stress transfer
Δf_{pR2}	stress loss in prestressing steel due to relaxation between time of transfer and service life
$\Delta f_{pS}, \Delta f_{pS}(t_i, t_j)$	respectively total stress loss in the prestressing steel during service life dut to shrinkage of concrete, and stress loss during a time interval (t_i, t_j) at section considered
$\Delta f_{pT}, \Delta f_{pT}(t_i, t_j)$	respectively total stress loss in the prestressing steel during service life due to all sources of loss, and stress loss during a time interval (t_i, t_j) at section considered
$\overline{\Delta f_{ps}}$	average stress loss in the prestressing steel
ΔM	moment amplitude $= M_{\max} - M_{\min}$ at section considered
ΔM_{cr}	moment in excess of self-weight moment, causing flexural cracking in the precompressed tensile fiber at section considered
ΔM_u	factored bending moment due to superimposed dead load plus live load at section considered
ΔV_u	factored shear force due to superimposed dead load plus live load at section considered
$\Delta\sigma$	differences between two stresses, or stress amplitude
$\Delta\bar{\sigma}$	permissible stress amplitude

ε	strain in general
$\varepsilon_C(t)$	creep in strain at time t
ε_{cb}	strain in concrete bottom fiber
ε_{ce}	concrete strain at the centroid of prestressing steel due to effective prestress
ε_{ci}	initial elastic instantaneous strain in concrete
ε_{ct}	strain in concrete top fiber; also used for tensile strain in concrete
ε_{cu}	strain in extreme compression fiber of concrete at nominal resistance of the section
ε_{CU}	ultimate creep strain or creep strain at end of life of member
ε_m	strain at maximum or peak stress of the stress-strain curve
ε_{pe}	strain in prestressing steel under effective stress f_{pe}
ε_{ps}	strain in prestressing steel at section considered and loading considered
ε_{pu}	ultimate failure strain of prestressing steel
ε_{py}	yield strain of prestressing steel
ε_{SU}	ultimate shrinkage strain or shrinkage strain at end of life of member
$\varepsilon_S(t)$	shrinkage strain at time t
ε_t	net tensile strain in extreme layer of steel at nominal bending resistance
ε_y	strain at onset of yielding of reinforcing steel
η	F/F_i ratio of final prestressing force to initial prestressing force or ratio of corresponding stresses
η	torsional coefficient; coefficient in general
η	load multiplier or load modification factor used in AASHTO LRFD code
Θ	torsional constant
θ	angle in general
λ	coefficient in general; coefficient used in prestress losses; multiplier used in deflection computation; multiplier used to differentiate lightweight from normal weight concrete
λ_i	ith constant or parameter
λ_p	multiple presence factor for lane loading in bridges
μ	curvature friction coefficient; also coefficient of friction or simply coefficient; ratio of curvatures, rotations, or deflections
ν	Poisson's ratio
π	3.14159
ρ'	A'_s/bd_e, ratio of compression reinforcement
ρ_b	reinforcement ratio producing balanced condition
ρ_p	A_{ps}/bd_p, ratio of prestressed reinforcement
ρ_s	A_s/bd_s, ratio of non-prestressed tension reinforcement
ρ_s	ratio of volume of spiral reinforcement to total volume of core of spirally reinforced compression member
$\rho_{s\,\min}$	minimum specified reinforcement ratio for reinforced concrete member
$\rho_{s\,\max}$	maximum specified reinforcement ratio for reinforced concrete beam
σ	stress in general; preferably used for concrete unless another symbol is widely accepted such as f
σ_b	stress on bottom fiber; bearing stress
$\sigma_{ci}, \bar{\sigma}_{ci}$	respectively actual extreme fiber compressive stress in the concrete immediately after prestress transfer, and code allowable limit
$\sigma_{cs}, \bar{\sigma}_{cs}$	respectively actual extreme fiber compressive stress in the concrete at service loads, and code allowable limit

$(\sigma_{cs})_{slab}, (\bar{\sigma}_{cs})_{slab}$	respectively actual extreme fiber compressive stress in computer slab if any at service loads, and code allowable limit
σ_g	stress at the centroid of the concrete section due to the final or effective prestressing force after losses
σ_{gi}	stress at the centroid of the concrete section due to the initial prestressing force
σ_m	maximum or peak stress
σ_t	stress on top fiber; tension stress in general
$\sigma_{ti}, \bar{\sigma}_{ti}$	respectively actual extreme fiber (initial) tensile stress in the concrete immediately after transfer, and code allowable limit
$\sigma_{ts}, \bar{\sigma}_{ts}$	respectively actual extreme fiber tensile stress in the concrete at service loads, and code allowable limit
σ_x	axial stress in the x direction
σ_y	axial stress in the y direction
σ_1	principal tensile stress; also used for hoop stress
σ_2	principal compressive stress; also used for meridian stress
τ	bond stress in general
$\bar{\tau}$	allowable bond or shear stress
Υ	torsional constant
φ	curvature of section
ϕ	strength reduction factor
ψ	end-restraint coefficient; factor describing fraction of live load
ψ_m	average value of restraint coefficient of column considered
ψ_1, ψ_2	restraint coefficients at extreme ends of column considered
ω'	$\rho' f'_y / f'_c$
ω_e	$= \omega_p + \omega_s - \omega' =$ effective reinforcing index or global reinforcing index
ω_p	$\rho_p f_{ps} / f'_c$
ω_s	$\rho_s f_y / f'_c$
$\omega_{sw}, \omega_{pw}, \omega'_w$	reinforcement indices for flanged sections computed as for ω_s, ω_p, and ω' except that b shall be the web width, and the steel area shall be that required to develop the compressive strength of the web only
ω_b	reinforcing index corresponding to balanced conditions in reinforced concrete
ω_{emin}	minimum value of the effective reinforcing index
ω_{smin}	minimum recommended value of the reinforcing index

ABBREVIATIONS:

cf	cubic foot
cgc	centroid of concrete section (center of gravity of concrete)
cgs	centroid of the prestressing tendons or of the steel
cm	centimeter
ft	foot
in	inch
kips	kilopounds
kip-ft	kip × foot (unit of moment)
kip-in	kip × inch (unit of moment)
klf	kips per linear foot
kN/mm^2	kilonewtons per square meter
ksi	kips per square inch

lb	pound (pounds)
m	meter
mm	millimeter
MPa	megapascal
N/mm^2	newtons per square millimeter
pcf	pounds per cubic foot
plf	pounds per linear foot
psi	pounds per square inch
psf	pounds per square foot

ABBREVIATIONS OF PROFESSIONAL ORGANIZATIONS

AASHTO	American Association of State Highway and Transportation Officials
ACI	American Concrete Institute
ANSI	American National Standard Institute
ASCE	American Society of Civil Engineers
ASTM	American Society of Testing and Materials
CEB	Comite European du Beton (has become part of FIB)
CRSI	Concrete Reinforcing Steel Institute
FIB	Federation Internationale du Beton
PCA	Portland Cement Association
PCI	Precast/Prestressed Concrete Institute
PTI	Post-Tensioning Institute

UNIT CONVERSIONS

US Customary Unit	SI – Metric Unit
ft	m
yard	m
in	mm
in^2	mm^2
psi	MPa
lb	N
$\sqrt{f'_c}$ psi	$0.083\sqrt{f'_c} \approx \frac{\sqrt{f'_c}}{12}$ MPa
$2\sqrt{f'_c}$ psi	$0.17\sqrt{f'_c} \approx \frac{\sqrt{f'_c}}{6}$ MPa
$f_r = 7.5\sqrt{f'_c}$ psi	$0.62\sqrt{f'_c}$ MPa

Conversion from US to SI Units

Length:
$$\begin{cases} 1 \text{ in} = 25.4 \text{ mm} \\ 1 \text{ ft} = 0.3048 \text{ m} \\ 1 \text{ yd} = 0.914 \text{ m} \end{cases}$$

Area:
$$\begin{cases} 1 \text{ in}^2 = 6.452 \text{ cm}^2 = 645.2 \text{ mm}^2 \\ 1 \text{ ft}^2 = 0.0929 \text{ m}^2 \end{cases}$$

Volume:
$$\begin{cases} 1 \text{ in}^3 = 16.39 \text{ cm}^3 = 16390 \text{ mm}^3 \\ 1 \text{ ft}^3 = 0.0283 \text{ m}^3 \\ 1 \text{ yd}^3 = 0.765 \text{ m}^3 \\ 1 \text{ oz} = 29.57 \text{ ml} \\ 1 \text{ gal} = 3.785 \text{ litres} \end{cases}$$

Inertia:
$$\begin{cases} 1\ \text{in}^4 = 41.62\ \text{cm}^4 = 416{,}200\ \text{mm}^4 \\ 1\ \text{ft}^4 = 863{,}032\ \text{cm}^4 = 0.00863032\ \text{m}^4 \end{cases}$$

Density: $1\ \text{lb/ft}^3 = 16.03\ \text{kg/m}^3$

Unit Weight: $1\ \text{lb/ft}^3 = 1\ \text{pcf} = 0.1575\ \text{kN/m}^3$

Stress and Modulus:
$$\begin{cases} 1\ \text{lb/in}^2 = 1\ \text{psi} \approx 0.006895\ \text{N/mm}^2 \\ 1\ \text{kip/in}^2 = 1\ \text{ksi} \approx 6.895\ \text{N/mm}^2 = 6.895\ \text{MPa} \end{cases}$$

Mass:
$$\begin{cases} 1\ \text{lb} = 0.454\ \text{kg} \\ 1\ \text{oz} = 28.35\ \text{gr} \\ 1\ \text{ton (short)} = 907.2\ \text{kg} \end{cases}$$

Loads:
$$\begin{cases} 1\ \text{lb} = 4.448\ \text{N} \\ 1\ \text{kip} = 4.448\ \text{kN} \\ 1\ \text{kip/ft} = 1\ \text{klf} \approx 14.59\ \text{kN/m} \\ 1\ \text{lb/ft}^2 = 1\ \text{psf} \approx 0.0479\ \text{kN/m}^2 = 47.9\ \text{Pa} \\ 1\ \text{kip/ft}^2 = 1\ \text{ksf} \approx 47.9\ \text{kN/m}^2 \end{cases}$$

Moment or torque:
$$\begin{cases} 1\ \text{lb-ft} = 1.356\ \text{N-m} \\ 1\ \text{lb-in} = 0.113\ \text{N-m} \\ 1\ \text{kip-in} = 0.113\ \text{kN-m} \\ 1\ \text{kip-ft} = 1.356\ \text{kN-m} \end{cases}$$

Temperature: $^\circ\text{C} = \dfrac{(^\circ\text{F} - 32)}{1.8}$

Velocity:
1 mph = 1.609 kilometer/hour
1 mph = 0.4470 meter/second (m/s)

Energy: 1 Btu = 1056 joule (j)

Power: 1 horsepower (hp) = 745.7 Watt (W)

Specific surface: $1\ \text{in}^2/\text{in}^3 = 0.4\ \text{cm}^2/\text{cm}^3$

Unit weight of concrete: $150\ \text{pcf} = 2400\ \text{kg/m}^3$

Unit weight of mortar: $130\ \text{pcf} = 2080\ \text{kg/m}^3$

Unit weight of steel: 490 pcf = 7850 kg/m^3

$1/\sqrt{1000} = 0.0316$ to convert $\sqrt{f'_c}$ from psi to ksi

SI Metric Equivalent of Some Design Equations

U.S. Customary	SI Metric
Units: in, in^2, psi, lb	Units: mm, mm^2, MPa, N
$\sqrt{f'_c}$	$0.083\sqrt{f'_c}$
$\upsilon_c = 2\sqrt{f'_c}$	$0.17\sqrt{f'_c}$
$f_r = 7.5\sqrt{f'_c}$	$0.62\sqrt{f'_c}$
$f_{ps} = f_{pe} + 10{,}000 + \frac{f'_c}{100\rho_p}$	$f_{pe} + 69 + \frac{f'_c}{100\rho_p}$
$(A_\upsilon)_{\min} = \frac{50 b_w s}{f_y}$	$0.35\frac{b_w s}{f_y}$
$\upsilon_c = \left(2 + \frac{4}{\beta_c}\right)\sqrt{f'_c}$	$0.083\left(2 + \frac{4}{\beta_c}\right)\sqrt{f'_c}$
$\upsilon_c = 0.6\sqrt{f'_c} + 700\frac{V_u d_p}{M_u}$	$0.05\sqrt{f'_c} + 4.8\frac{V_u d_p}{M_u}$
$\upsilon_{ci} = 0.6\sqrt{f'_c} + \frac{V_G + (\Delta V_u \times \Delta M_{cr} / \Delta M_u)}{b_w d_p}$	$0.05\sqrt{f'_c} + \frac{V_G + (\Delta V_u \times \Delta M_{cr} / \Delta M_u)}{b_w d_p}$
$\upsilon_{cw} = 3.5\sqrt{f'_c} + 0.3\sigma_g + \frac{V_p}{b_w d_p}$	$0.29\sqrt{f'_c} + 0.3\sigma_g + \frac{V_p}{b_w d_p}$
$A_l = \left\{\frac{400 x s}{f_y}\left[\frac{T_u}{T_u + (V_u / 3C_t)}\right] - 2A_t\right\}\frac{x_1 + y_1}{s}$	Replace "400" with "2.76"

TYPICAL POST-TENSIONING SYSTEMS

The following information is taken from brochures and literature by manufacturers of prestressing systems. Their permission to include this information in this book is gratefully acknowledged. The reader should consult with the local representative of each system to ascertain details and availability and/or the existence of any change or update.

1. THE FREYSSINET C RANGE POST-TENSIONING SYSTEM

(Courtesy Freyssinet International, www.freyssinet.com)

The new Freyssinet C Range post-tensioning system has been developed as an answer to modern civil engineering requirements. The prime characteristic of the C range is compactness.

The C range is the outcome of more than fifty years of experience in post-tensioning systems. Tendon sizes ranging from 3 to 55 15 mm diameter strands are available.

The following section provides a very brief summary of the Freyssinet C multistrand system. However, changes may be made to the information contained here at any time as new techniques and/or materials are developed. Users are encouraged to check with Freyssinet on updates and if to check if substantial changes have been made to the specified products.

A large amount of other detailed technical literature – such as specific data sheets, special applications for 13 mm diameter strand, or smaller units – are available from Freyssinet.

1. Description

The C range multistrand system possesses the following main features and characteristics (Fig. C1):

■ Versatility

The system is designed for a large range of applications with the same type of anchorages:

- use of all internationally available sizes and grades of 15 mm strands, including galvanized and unbonded strand;
- application to internal and external prestressing:
  - ❖ bonded

- ❖ removable,
- ❖ removable and adjustable
- ❖ removable, adjustable and detensionable

Table C1 Typical properties of strands compatible with the C range system.

Standard	Nominal Tensile Strength N/mm^2	Nominal Diameter mm	Nominal Steel area mm^2	Nominal Mass kg/m	Minimum Breaking strength kN	Proof Stress at 0.1% kN
	1 770	16	150	1.170	265	228
pr EN 10138-3	1 860	16	150	1.170	279	240
BS	1 770	15.7	150	1.180	265	225
5896 1980	1 820*	15.2	165	1.295	300	255
ASTM	1 860	15.24	140	1.102	260.7	234.6
A 416-96a	(270 ksi)	(0.6 in)	(0.217 in^2)	(0.74 lb/ft)	(58 600 lb)	(52 740 lb)

*Drawn strand

Note: The maximum initial force in the strand should be as recommended by local codes.

Table C2 Typical properties of tendons used for the Freyssinet C range system.

Number of strands per tendon	Type of Strand								
	pr EN 10138-3 1860 grade			BS 5896-80 1820 grade, drawn strand			ASTM A-416-96 0.6 in 270 grade		
	steel area mm^2	mass kg/m	UTS kN	steel area mm^2	mass kg/m	UTS kN	steel area mm^2	mass kg/m	UTS kN
3	450	3.54	837	495	3.89	900	420	3.306	782
4	600	4.72	1116	660	5.18	1200	560	4.41	1043
7	1 050	8.26	1953	1155	9.07	2100	980	7.71	1825
9	1350	10.62	2511	1485	11.66	2700	1260	9.92	346
12	1800	14.16	3348	980	15.54	3600	1680	13.22	3128
13	1950	15.34	3627	2145	16.84	3900	1820	14.33	3389
19	2850	22.42	5301	3135	24.61	5700	2660	20.94	4953
22	3300	25.96	6138	3630	28.49	6600	3080	24.24	5735
25	3750	29.5	6975	4125	32.38	7500	3500	27.55	6518
27	4050	31.86	7533	4455	34.97	8100	3780	29.75	7039
31	4650	36.58	8649	5115	40.15	9300	4340	34.16	8082
37	5550	43.66	10 323	6105	47.92	11100	5180	40.77	9646
55	8250	64.9	15 345	9075	71.23	16500	7700	60.61	14339

*Masses given correspond to BS 5896-80. For pr EN multiply by 0.991.

■ Range of anchorages

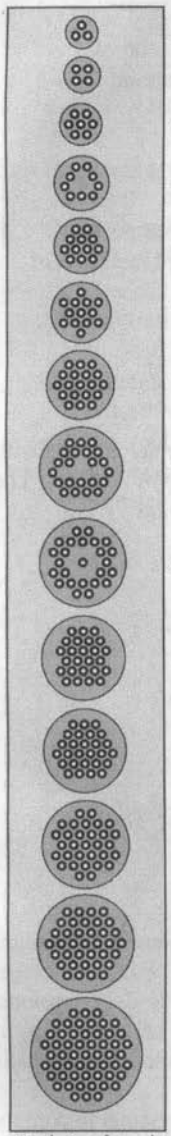

*Distribution of strands in the anchorage with no central strand.
See page 18 for selecting the stressing jack accordingly.

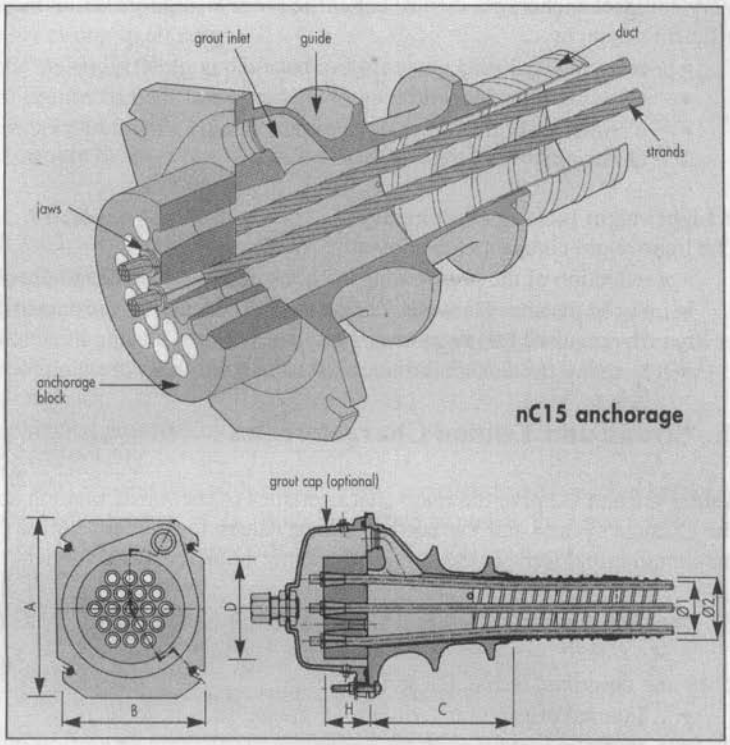

Size	A	B	C	D	H	Ø1*	Ø2**
3C15	150	110	120	85	50	40	45
4C15	150	120	125	95	50	45	50
7C15	180	150	186	110	55	60	65
9C15	225	185	260	150	55	65	70
12C15	240	200	165	150	65	80	85
13C15	250	210	246	160	70	80	85
19C15	300	250	256	185	80	95	100
22C15	330	275	430	220	90	105	110
25C15	360	300	400	230	95	110	115
25C15P	350	290	360	220	95	110	115
27C15	350	290	360	220	100	115	120
31C15	385	320	346	230	105	120	125
37C15	420	350	466	255	110	130	135
55C15	510	420	516	300	145	160	165

All dimensions in mm.
* Thickness of sheath to be checked against applicable regulation.
**Sheath connection sleeve.
* and ** Minimum recommended dimensions.

Figure C1 Active anchorages for the C range system.

■ **Compactness**
Very compact anchorages diffuse better the prestressing forces into the concrete, allowing for a more efficient design by:

- reducing web thicknesses in beams and box girders, blisters and ribs;
- allowing for a concentration of anchorages at the end zones;
- a reduction of the dimensions of prestressing anchor blocks, with minimum strand deviations.

■ **Lightweight jacking equipment**
The lightweight compact and automatic C jacks allow for:

- a reduction of the prestressing anchorage recesses thanks to the compact jack noses;
- reduced distances to walls leading to the reduction of the parasitic moments and therefore of the required reinforcement, enabling an easier placing of concrete;
- improving the site conditions, such as handling and stressing.

2. Strand and Tendon Characteristics

Tables C1 and C2 give the main characteristics of the most common strands which may be used with the C range system and the corresponding values for tendons with a given number of strands. The maximum initial force in the strand at jacking should be as recommended by local codes.

3. Active Anchorages for the C Range System

They are described in Fig. C1 and used for:

- Internal prestressing with grout, grease, or wax protection
- Partially bonded external prestressing with grout protection (non-replaceable)
- Unbonded external prestressing, grease or was injected.

4. Ducts for the C Range System

The following main types of ducts are used for the Freyssinet C range tendons:

■ For internal prestressing:

- Corrugated sheath made up of rolled steel sheet strip having a recommended minimum thickness of 0.3 mm. The recommended duct diameters are specified for each anchorage. However, the applicable regulations must be checked against the proposed dimensions. Generally, cement grout is used for corrosion protection, sometimes wax or grease (i.e. in nuclear reactor containment buildings). For certain applications, galvanized steel strip is used.
- Plastic corrugated Plyduct® sheath, recently developed and patented by Freyssinet to comply with international standards such as *fib* and British TR47. It is perfectly air and watertight.
- None, with the patented Ductless Freyssinet system using individually sheathed and greased strands directly embedded in the concrete.

■ For external prestressing:

- For partially bonded systems (grouted)
  - corrugated steel sheath or steel tube in the concrete zones (diaphragms and deviators);
  - high density polyethylene (HDPE) or steel tubes (rarely) in the zones outside the concrete. HDPE tubes are standardized in most countries. Ducting with a pressure rating of 0.63 N/mm^2 (6.3 bar) is recommended.

- For unbonded System N°1 (double ducting, grouted most often)
  - steel tube for the outer casing in the concrete zones;
  - HDPE for the inner casing in all zones.
- For unbonded System N°2 (single ducting, patented system using sheathed and greased strands in a duct which is grouted before stressing)
  - steel tubes in the concrete zones;
  - HDPE for zones outside the concrete (0.4 N/mm^2 series may be used).

5. Replaceable Active R Anchorages

These anchorages have a special guide and are used for:

- Internal prestressing without duct (Patented Ductless System), with sheathed and greased strands. For replaceable tendons, it is recommended to use a longer cap with strand length as required to allow distressing the tendon (the tendon is then also adjustable). It may also be stressed with a monostrand jack.
- External replaceable unbonded prestressing with bare strands, generally grout injected (External Prestressing System N°1).
- External (replaceable or not) prestressing with sheathed and greased strands grouted before stressing (External Prestressing System N°2). With longer cap as above, the tendon is adjustable. It may also be stressed with a monostrand jack.

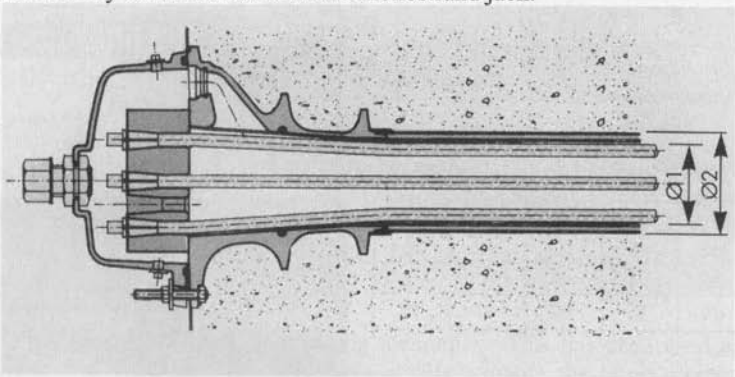

Figure C2 Typical Freyssinet replaceable active R anchorage.

6. Active Flat F Anchorage

Flat anchorages are generally recommended for slabs, foundation mats, shells and other thin structural elements.

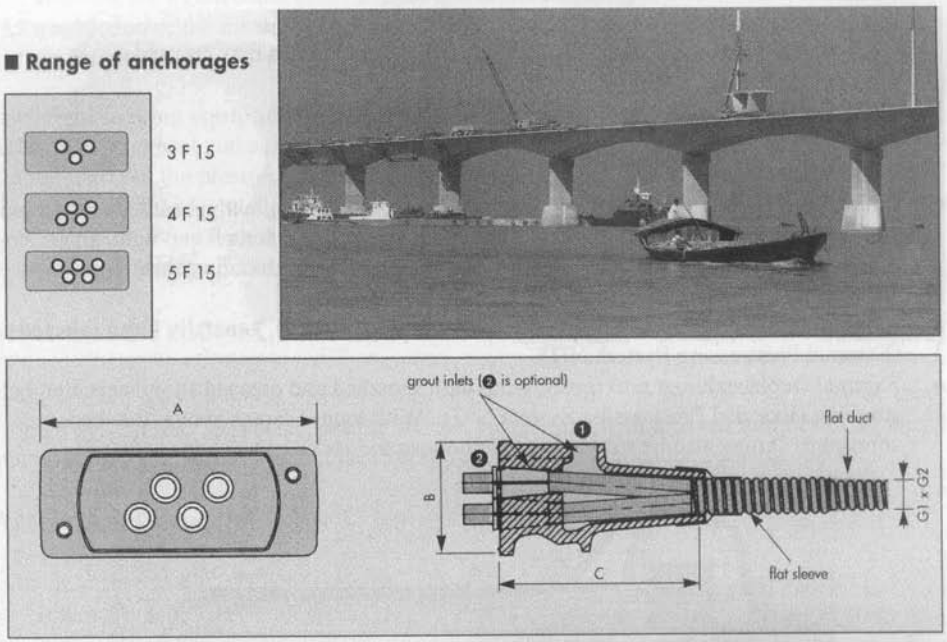

Size	A	B	C	G1*	G2*
3F15	190	85	163	58**	20**
4F15	230	90	163	75	20
5F15	270	95	163	90	20

All dimensions in mm.
* Flat duct dimensions.
** 75 x 20 flat duct may be directly connected.

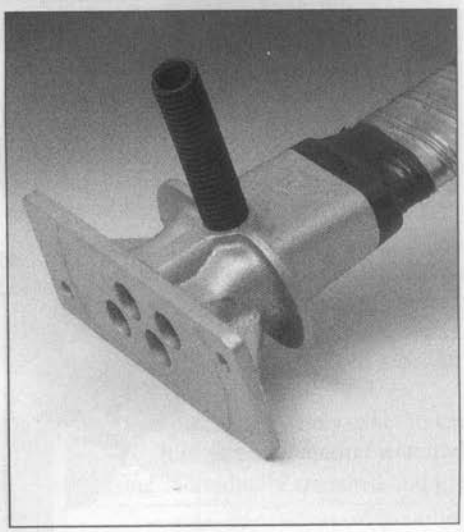

■ Notes:

- The F anchorages are designed for a minimum concrete strength f_{cmin} = 30 N/mm² (cylinder strength).
- The preferred method of tendon installation is by threading the strands in the ducts (flat shape) before concreting. However, if required, it is also possible to thread the strands after concrete hardening; in that case, please, contact the local Freyssinet Agent.
- The Ductless System (see page 6) may be used with the F anchorages.
- Primary distribution bursting reinforcement is shown on page 14.

Figure C3 Freyssinet active flat F anchorages.

7. Installation – Placing

The installation of the C range post-tensioning system includes the following main steps:

- duct placing
- cable placing
- stressing
- grouting (or other corrosion protection method)

For internal prestressing, the ducts are placed before the concrete is poured. Corrugated steel or plastic ducts are the most common.

For external prestressing, the most commonly used ducts are steel tubes inside the concrete and HDPE pipes outside the concrete .

The cable is generally placed by pushing each strand into the duct from one end. Freyssinet was a pioneer in promoting and developing this technique in the early 70's, and can provide advanced pushing equipment and fittings. A patented high speed, 4 head pushing machine has been developed for use in large projects. With this machine, it is possible to thread 1, 2, 3 or 4 strands at a time. The operation of the machine may be controlled from the two ends of the tendon being placed.

8. Installation – Corrosion Protection

The C range tendons can be protected with any of the known systems: cement grout, grease, and wax being the most common. Freyssinet can supply all the necessary equipment to ensure thorough corrosion protection is achieved. Some special cases require special attention:

■ External prestressing with cement grout.
The pressure resistance of the ducts must be checked before grouting. This is achieved using compressed air. Checking the tightness with water is prohibited.

■ Grouting of System N°2 tendons
In this case, the role of the grout is to constitute a spacer to prevent the plastic sheath surrounding the strand from being damaged in the contact zones between strands, due to curvature reactions. Some properties of the grout such as mechanical strength (10 N/mm^2 is sufficient for the spacing role required) and shrinkage play only a secondary role. The grouting takes place before stressing.

■ Vacuum grouting
Freyssinet was a pioneer of the vacuum grouting technique. This has been used and perfected by Freyssinet for more than twenty years. It is especially suitable for large projects with difficult conditions.

■ Ductless System
In this system, tendons consisting of sheathed and greased strands embedded in the concrete of the structure, do not require grouting.

■ Wax injection
The tendons may also be injected with petroleum wax when specified by the consultant (for example, to check the tension after a number of years or to protect temporary ties).

9. Jacks

The Freyssinet jacks are designed to provide tension to a number of strands simultaneously or to one strand and a time. The C range tendons are stressed with high performance CC type hydraulic jacks. They are front pull with automatic dewedging and hydraulic locking-off of jaws. Examples are shown in Figs. C4 and C5.

A range of high pressure hydraulic pumps to operate the stressing jacks is available.

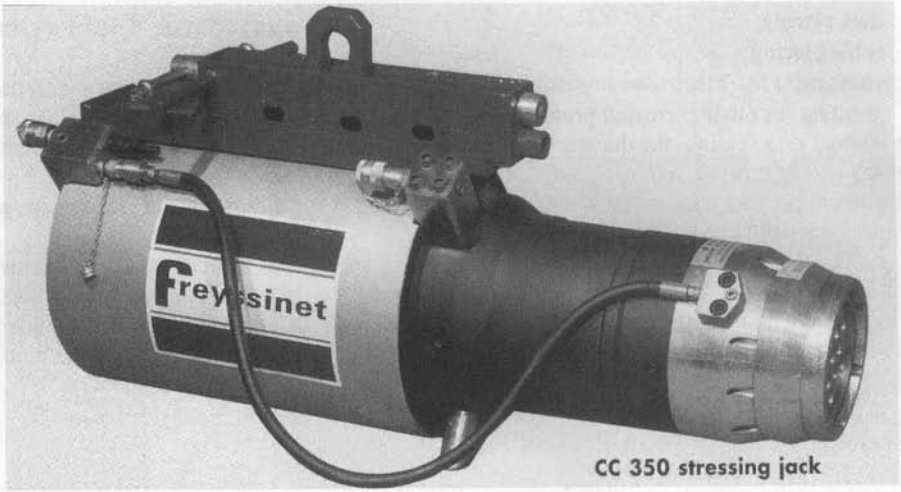

Figure C4 Freyssinet CC 350 stressing jack.

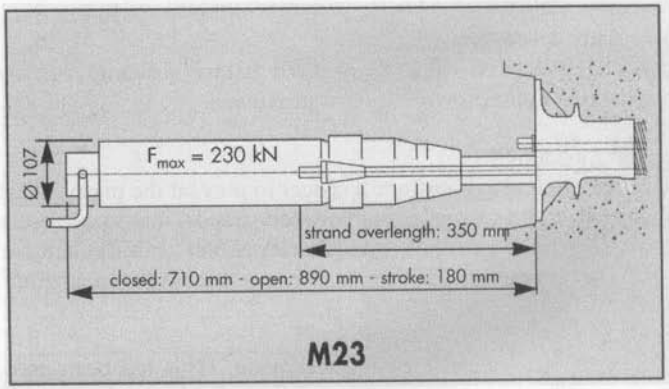

Figure C5 Freyssinet M23 monostrand stressing jack.

2. VSL MULTISTRAND POST-TENSIONING SYSTEM

(Courtesy VSL Corporation, www.vsl.net)

1. VSL Multistrand Post-Tensioning

The VSL Multistrand System is characterized by the following features:

- standardized tendon units using up to fifty-five 0.5" (13mm) or 0.6" (15mm) diameter strands;
- wide selection of anchorage types;
- steel or plastic PT-PLUS™ ducts;
- high-performance cement or other types of grouting;
- tendons manufactured on-site or in the plant;
- no need to determine tendon length in advance;
- simultaneous stressing of all strands in a tendon;
- stressing carried out in any number of phases;
- simple and reliable equipment for installation, stressing and grouting.

2. VSL Multistrand System Components

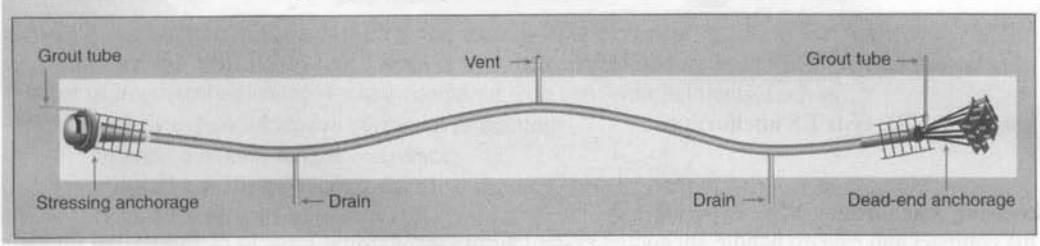

Figure C6

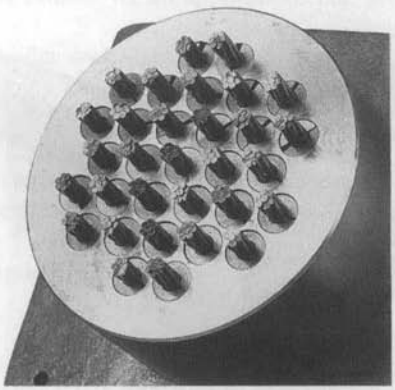

Figure C6 VSL multistrand anchorage.

3. VSL Anchorages

Technical data and dimensions are provided in the manufacturer brochure. For clarity and simplicity, spirals are not shown in the pictures. However, they form an integral part of the anchorage. For more detailed information, see VSL's Report Series on "Detailing for Post-Tensioning."

The SO, SA and VSLAB+® are VSL standard anchorages for bonded slab post-tensioning. They are also often used for bridges, buildings, tanks and other structures.

Stressing Anchorage: VSL Type ES

This revolutionary anchorage has a composite bearing plate (metal-high performance concrete) and is lighter, smaller and easier to handle. It comes in 3 different configurations: ES-STANDARD for normal applications, ES-PLUS using VSL's PT-PLUS™ duct system for enhanced corrosion protection or improved fatigue resistance, and ES-SUPER to provide an electrically isolated tendon. Equipped with an additional retainer plate, the ES anchorage can also be used as a dead-end anchorage.

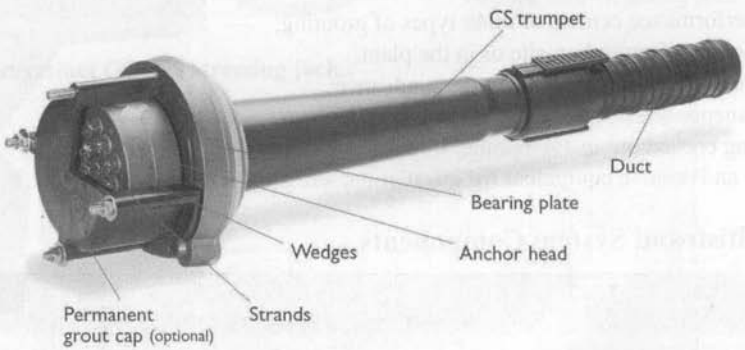

Figure C8 VSL type ES anchorage.

Stressing Anchorage: VSL Type EC

This compact and easy to handle anchorage system allows prestressing force to be transferred through two flanges. If equipped with an additional retainer plate, the EC anchorage can also be used as a dead-end anchorage.

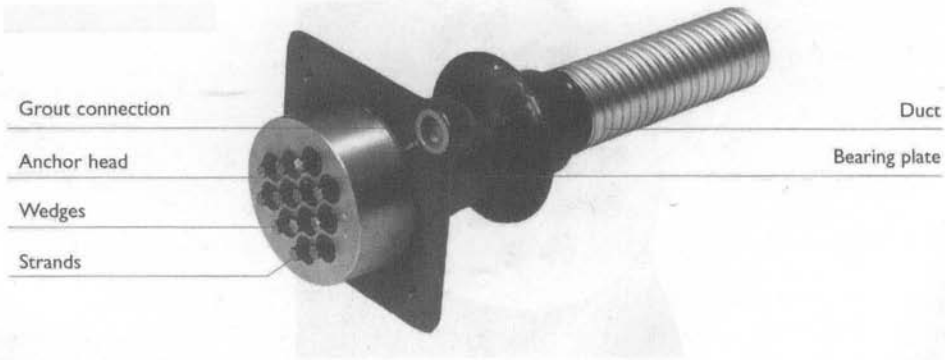

Figure C9 VSL type EC anchorage.

Stressing Anchorage: VSL Type E

The prestressing force is transferred to the concrete by a mild steel-bearing plate. If equipped with an additional retainer plate, the E anchorage can also be used as a dead-end anchorage.

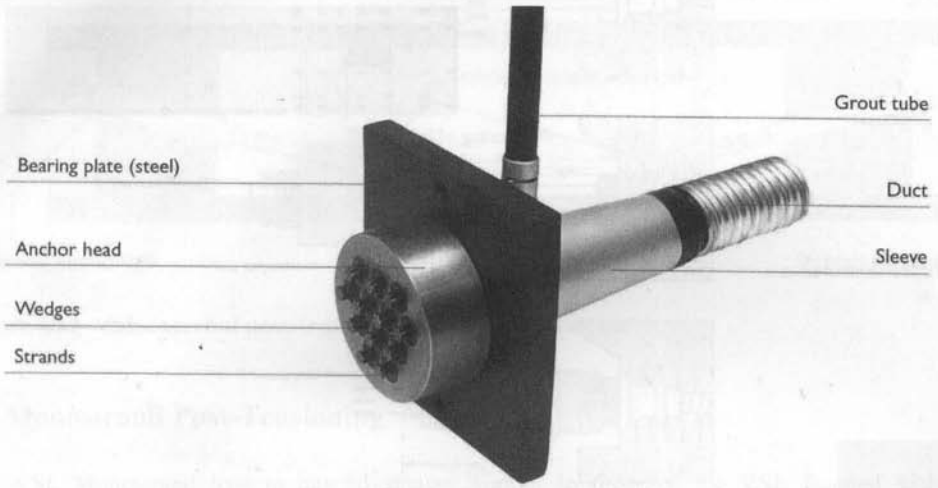

Figure C10 VSL type E anchorage.

4. Sheathing and Corrosion Protection

Generally, corrugated steel ducts with a minimum wall thickness of 26 gauge are used.

However, the VSL PT-PLUS™ System with its corrugated duct and plastic coupler can provide a number of important advantages when compared with conventional ducts, such as:

- greatly enhanced tendon corrosion protection;
- improved tendon fatigue resistance;
- reduced sensitivity to stray electric currents;
- reduced tendon friction;
- electrical isolation when used with special ES anchorages.

The PT-PLUS™ System is suitable for all applications but, given its specific characteristics, is best adapted to:

- transverse tendons in bridge deck slabs;
- tendons that are close to the concrete surface;
- railway bridges and other structures that are subject to fatigue loadings or stray electric currents;
- structures where a severe corrosive environment may be expected;
- tendons that need to be electrically monitored throughout the structure's service life.

5. Multistrand Post-Tensioning

Stressing

The unique features of the VSL Post-Tensioning System lies in its special wedge locking procedure. The wedges always remain in contact with the strands during the stressing operation. As the pressure in the jack is released, the wedges automatically lock in the conical holes of the anchor head.

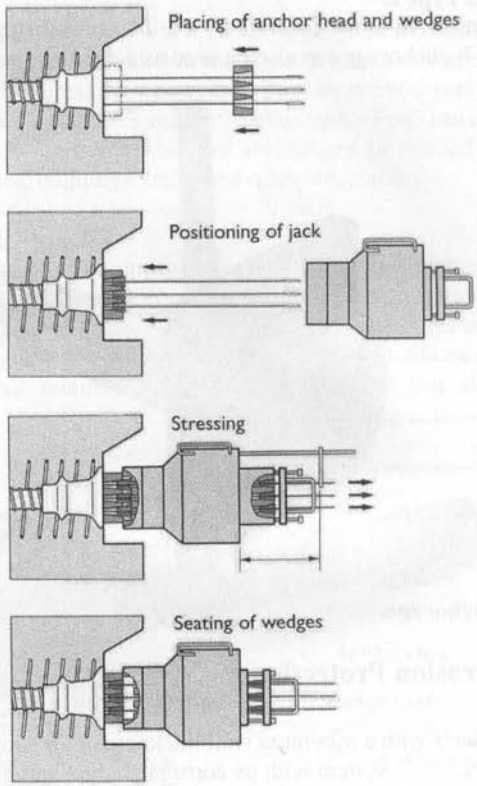

Figure C11 Steps in stressing operation.

Grouting

The objectives of the VSL Grouting System are to prevent corrosion of the prestressing steel by filling of all voids and cavities in the tendon and to fully encapsulate the steel in an alkaline environment, as well as achieve an effective bond between the prestressing steel and the surrounding concrete member. This is achieved through:

- Careful selection of cement, water, and admixtures;
- Continuous quality assurance and quality control processes and measurement;
- Selection of mix design and procedures adapted to the selected materials, environment and equipment;
- Performance of the grouting by trained VSL Grouting Technicians.

External Post-Tensioning

External post-tensioning is well adapted to bridges due to the resulting savings in construction costs and the high degree if corrosion resistance provided by the system. External tendons are easy to inspect and, if necessary, replace. They are ideal for strengthening existing structures and, apart from their uses in bridges, can be used for a wide range of other applications, including buildings, silos and reservoirs.

VSL External Tendons:

- strand bundle;

- polyethylene ducts;
- standard multistrand anchorages, or special anchorages permitting easy tendon replacement;
- grout

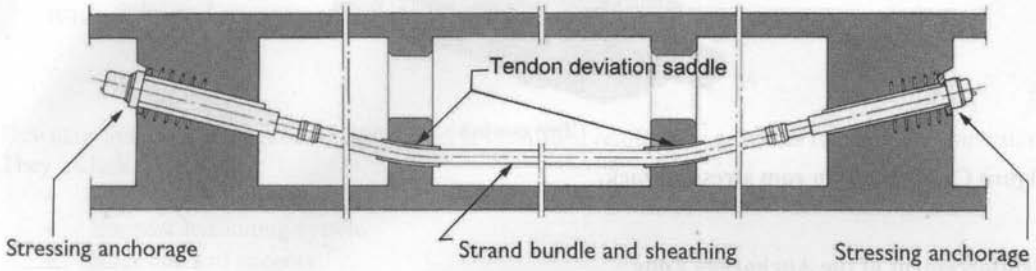

Figure C12 VSL external post-tensioning system components

6. Monostrand Post-Tensioning

The VSL Monostrand System has advantages similar to those of the VSL Bonded Slab Post-Tensioning System. The VSL Monostrand System uses 0.5" (13mm) and 0.6" (15mm) diameter strands. The strands are given a coating of permanent corrosion-inhibiting coating and are enclosed in an extruded plastic sheath. The grease and plastic provide double corrosion protection, as well as preventing any bonding between the strands and the surrounding concrete. The plastic sheath is polyethylene with approximately 50 mil wall thickness. To ensure continuous corrosion protection in aggressive environments, special sleeves are used to join the sheaths to the anchorages and each anchorage is provided with a protective cap. The VSL Monostrand System features factory-applied corrosion protection very low friction losses, and full utilization of the structural depth. These light, flexible monostrands can be easily and rapidly installed, leading to economical solutions. Detailed information is given in VSL's "Post-Tensioned Slabs" publication. With modifications, the VSL Monostrand System can also be used for post-tensioning masonry walls.

Monostrand Specifications:

- 0.5" (13mm) and 0.6"(15mm) diameter strand in accordance with ASTM A416.
- permanent corrosion-inhibiting coating and plastic sheath in accordance with PTI recommendations.

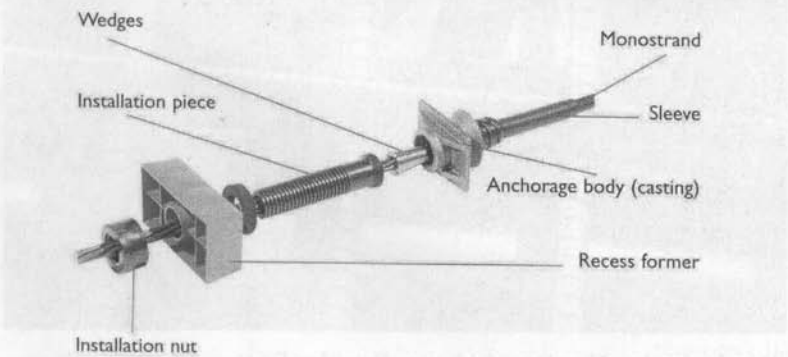

Figure C13 VSL type S6 monostrand anchorage.

Figure C14 VSL twin ram stressing jack.

Reinforcement of the Anchorage Zone

In addition to the slab reinforcement required by the design, additional reinforcement is necessary in the force distribution zone behind each anchorage. Details should be established by the project engineer.

VStrand™ Heat Resistive Tendon

VSL's innovative heat-resistive post-tensioning tendons have been developed to mitigate the detrimental thermal effects of a fire on the strength of the prestressing steel. Each tendon consists of one or more steel prestressing strands coated with a proprietary intumescent material. This coating provides a significantly greater degree of protection to the strand in the event of a fire. These tendons are particularly well suited for strengthening of parking garages and other structures that are exposed to vehicular fires.

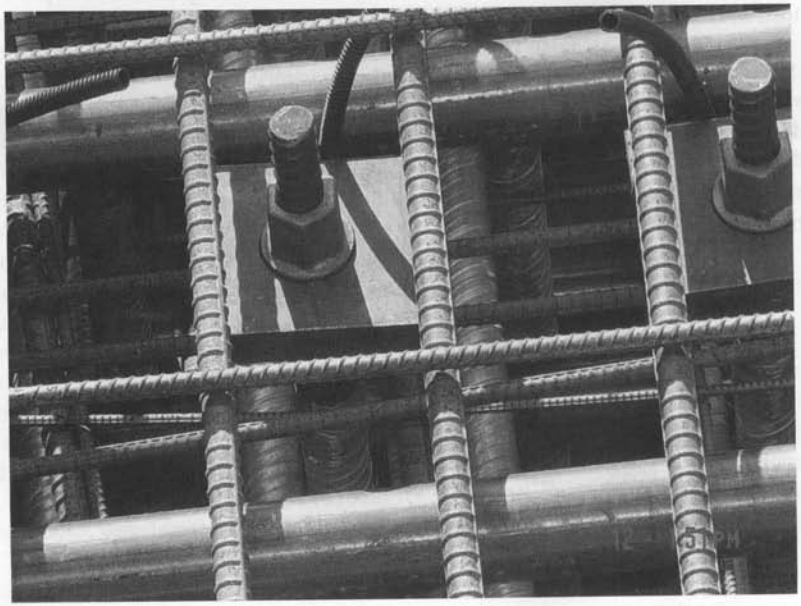

Dywidag posttensioning bars in place. *(Courtesy Dywidag-Systems-International).*

3. DYWIDAG BAR POST-TENSIONING SYSTEM

(Courtesy Dywidag-Systems-International, www.dywidag-systems.com)

Dywidag-Systems-International (DSI) offers several steel reinforcing products for use in construction. They include:

- Multistrand post-tensioning system
- Bar post-tensioning system
- Rock and soil anchors
- Tie rods
- Threadbar reinforcing system
- Threadbar resin anchored rock bolts
- Soil nails

Next only the Dywidag bar post-tensioning system is briefly described. The reader is referred to DSI for literature on the other products and latest updates.

1. Bar Post-Tensioning System Details

The components of the DYWIDAG Bar System are manufactured in the United States exclusively by Dywidag Systems International. Used worldwide since 1965, the system provides a simple, rugged method of efficiently applying prestress force to a wide variety of structural application including post-tensioned concrete, rock and soil anchor systems.

Available in 1 in (26 mm), 1 ¼ in(32 mm) and 1 3/8 in (36 mm) THREADBARS® are hot rolled and proof stressed alloy steel conforming to ASTM A722 CAN/CSA (G279-M1982). The ¾ in nominal diameter bar is cold drawn, stress relived alloy steel which after cold threading also conforms to the same ASTM specification as the Threadbar.

The Dywidag Threadbar prestressing steel has a continuous rolled-in pattern of thread-like deformations along its entire length. More durable than machined threads, the deformations allow anchorages and couplers to thread onto the threadbar at any point. The 1 ¾" (46 mm) bar can be continuously cold threaded for its entire length or if enhanced bond is not required, the bars can be supplied with threaded ends only.

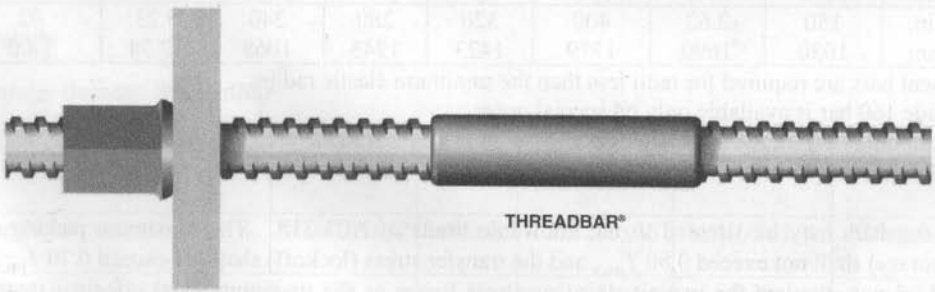

Figure C14 Dywidag Threadbar

The strength of the Dywidag anchorages and couplers exceeds the requirements of ACI 318. Test reports are available for the main components of the system.

Conforming to the requirements of ASTM A615, the deformations develop an effective bond with cement or resin grout. The continuous thread simplifies stressing. Lift off readings may be taken at any time prior to grouting and the prestress force increased or decreased as required without causing any damage.

The Dywidag System is primarily used for grouted construction. All components of the system are designed to be fully integrated for quick and simple field assembly. Sheathing, sheathing transitions, grout tubes all feature thread type connections.

Placing Dywidag Threadbar tendons is simplified through the use of reusable plastic pocket formers. Used at each stressing end, the truncated, cone-shaped pocket former can extend through, or butt up against, the form bulkhead.

Threadbars are available in mill lengths to 60 ft (18.3 m), and may be cut to specified lengths before shipment to the job site. Or, where circumstances warrant, the threadbars may be shipped to the job site in mill lengths for field cutting with a portable friction or band saw. Threadbars may be coupled to ease handling or to extend a previously stressed bar. Cold threaded 1 ¾ in (46 mm) diameter bars are available in lengths up to 24 ft (7.3 m).

Bars may be ordered with epoxy coating over their entire length. Coating process conforms to ASTM A775.

2. Prestressing Steel Properties

Nominal Bar Diameter (in.) (mm)	Ultimate Stress f_{pu} (ksi) (MPa)	Cross Section Area A_{ps} (in.^{2}) (mm^2)	Ultimate Strength $f_{pu}A_{ps}$ (kips) (KN)	Prestressing Force, kips KN			Weight (lbs./ft.) (kg/m)	Minimum* Elastic Bending Radius (ft.) (m)
				$0.8f_{pu}A_{ps}$	$0.7f_{pu}A_{ps}$	$0.6f_{pu}A_{ps}$		
1 in.	150	0.85	127.5	102.0	89.3	76.5	3.01	52
26 mm	1030	548	567	454	397	340	4.48	15.9
1 in.	160**	1.25	200.0	160.0	140.0	120.0	4.39	60
26 mm	1100	806	890	707	623	534	6.54	18.3
1 ¼ in.	150	1.25	187.5	150.0	131.3	112.5	4.39	64
32 mm	1030	806	834	662	584	500	6.54	19.5
1 ¼ in.	160**	1.25	200.0	160.0	140.0	120.0	4.39	60
32 mm	1100	806	890	707	623	534	6.54	18.3
1 3/8 in.	150	1.58	237.0	189.6	165.9	142.2	5.56	72
36 mm	1030	1018	1055	839	738	633	8.28	22.0
1 3/8 in.	160**	1.58	252.8	202.3	177.0	151.7	5.56	67
36 mm	1100	1018	1125	899	787	675	8.28	20.4
1 ¾ in.	150	2.62	400	320	280	240	9.23	92
46 mm	1030	1690	1779	1423	1245	1068	13.74	28.0

*Prebent bars are required for radii less than the minimum elastic radius.

**Grade 160 bar is available only on special order.

3. Steel Stress Levels

Dywidag bars may be stressed to the allowable limits of ACI 318. The maximum jacking stress (temporary) shall not exceed $0.80\,f_{pu}$, and the transfer stress (lockoff) shall not exceed $0.70\,f_{pu}$. ACI 318 does not stipulate the magnitude of prestress losses or the maximum final effective (working) prestress level. Prestress losses due to shrinkage, elastic shortening and creep of concrete, as well as steel relaxation and friction, must be considered.

The final effective (working) prestress level depends on the specific application. In the absence of a detailed analysis of the structural system, $0.60f_{pu}$ may be used as an approximation of the

effective (working) prestress level. Actual long term loss calculations require structural design information not normally present on contract documents.

Following are some important notes concerning the safe handling of the high strength steel for prestressed concrete:

1. Do not damage surface of bar.
2. Do not weld or burn so that sparks or hot slag will touch any portion of bar which will be under stress.
3. Do not use any part of bar as a ground connection for welding.
4. Do not use bar that has been kinked or contains a sharp bend.

Disregard of these instructions may cause failure of material during stress.

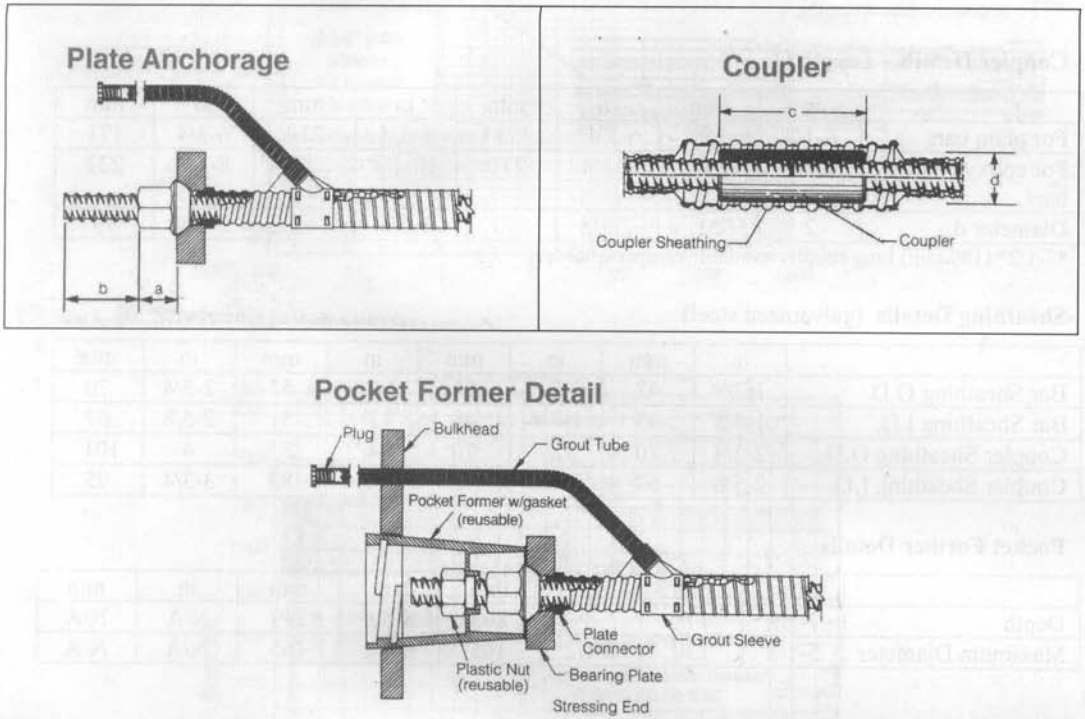

Figure C15 Details of Dywidag plate anchorage, coupler and pocket former.

4. Details

Anchorage Details - Threadbar

Bar Diameter	1 in	26 mm	1 ¼ in	32 mm	1 3/8 in	36 mm
Anchor Plate Size*	5x5x1 ¼	127x140x32	6x7x1½	152x178x38	7x7 ½ x1 ¾	178x191x44
Anchor Plate Size*	4x6 ½ x1 ¼	102x165x32	5x8x1½	127x203x38	5x9-1/2x1 ¾	127x241x44
Nut Extension *a*	1-7/8	48	2 ½	64	2 ¾	70
Min. Bar Protrusion**b	3	76	2 ½	89	4	102

*Other plate sizes available on special order. **To accommodate stressing

Anchorage Details – Cold Threaded Bar

Bar Diameter	1-3/4 in	46 mm
Anchor Plate Size*	9x9x2-1/4	230x230x57
Anchor Plate Size*	-----	-----
Nut Extension a	2-7/8	74
Min. Bar Protrusion**b	3-5/8	92

*Other plate sizes available on special order.
**To accommodate stressing

Coupler Details – Length C

	in	mm	in	mm	in	mm	in	mm
For plain bars	6-1/4	159	6-3/4*	171*	8-3/4	219	6-3/4	171
For epoxy coated bars	7-3/4	197	8-1/4	210	10-1/8	267	8-3/4	222
Diameter d	2	51	2-3/8	60	2-3/4	67	3-1/8	79

*7-1/2" (190 mm) long coupler available on special orders.

Sheathing Details (galvanized steel)

	in	mm	in	mm	in	mm	in	mm
Bar Sheathing O.D.	1-7/8	47	2	51	2-1/8	55	2-3/4	70
Bar Sheathing I.D.	1-5/8	43	1-7/8	48	2	51	2-5/8	67
Coupler Sheathing O.D.	2-3/4	70	3	76	3-1/2	87	4	101`
Coupler Sheathing I.D.	2-5/8	67	2-7/8	72	3-1/4	83	3-3/4	95

Pocket Former Details

	in	mm	in	mm	in	mm	in	mm
Depth	7-1/8	178	8	203	8-5/8	219	N/A	N/A
Maximum Diameter	5-1/8	130	6-1/2	165	6-1/2	165	N/A	N/A

5. Modulus of Elasticity

The modulus of elasticity "E" is an intrinsic property of steel whose magnitude remains basically constant and is little affected by normal variations in mill processes. For Threadbars, this value has been determined to be 29700 ksi (205000 MPa).

6. Relaxation

Relaxation is defined as the loss of prestress load in a post-tensioning steel subjected to a specified initial stress while maintaining the length and the temperature constant. Relaxation tests usually refer to 0.7 actual ultimate as initial stress (see chart below). The tension loss after 1000 hrs for a Threadbar initially stressed to 70% of guaranteed ultimate strength can be assumed between 1.5 and 2%. Tests indicate that the relaxation losses in cold drawn, cold threaded bars are significantly higher.

7. Stress-strain characteristics

A typical stress-strain curve for a stretched and stress relieved bar is substantially different form a typical curve produced for a cold drawn, cold threaded bar. Samples of each are illustrated below. The most notable feature is the lack of a definite yield point characteristic of cold drawn bars.

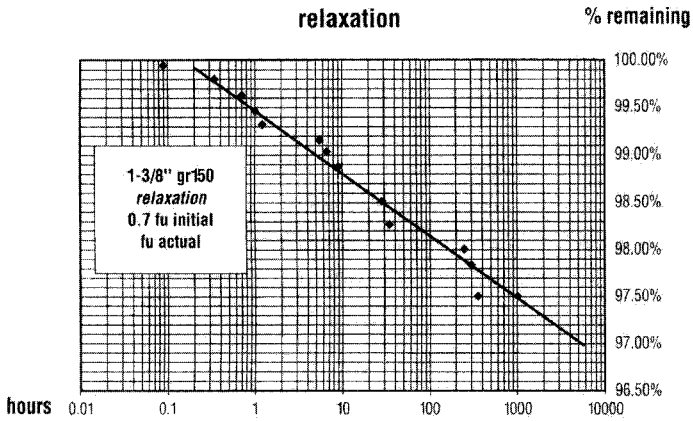

Figure C16 Stress relaxation curve.

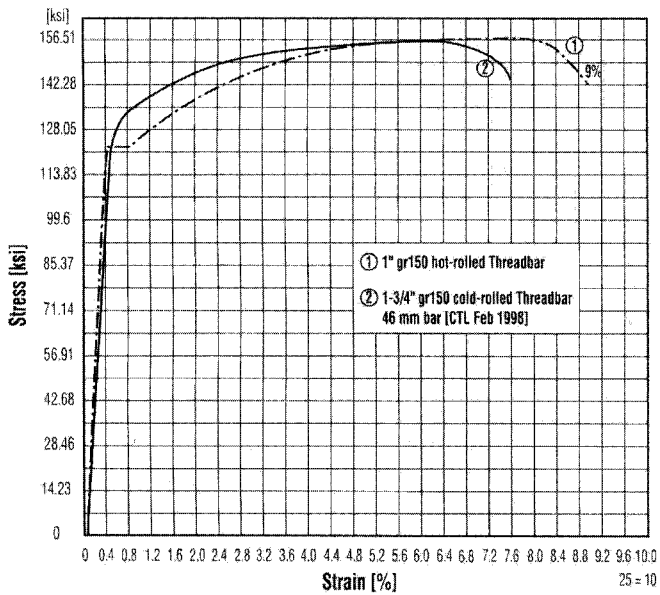

Figure C17 Experimental stress-strain curves.

8. Fatigue resistance

Under normal circumstances fatigue is not a primary design consideration for prestressing steels. However, all Dywidag bars and accessories have been tested and proven to exceed the fatigue requirements specified by the Post-Tensioning Institute.

9. Temperature Characteristics

Tests have demonstrated that no significant loss of strength occurs when bars are subjected to elevated temperatures up to 1,100 degrees F. Except that the yield strength is reduced when temperatures exceed approximately 750 degrees F. Bar ductility is not significantly affected by temperatures down to -60 degrees F.

10. Susceptibility to Stress Corrosion and Hydrogen Embrittlement

All prestressing steel is susceptible to stress corrosion and hydrogen embrittlement in aggressive environments and therefore must be properly protected. However, accelerated tests have demonstrated that while A 416 strand failed after 5 to 7 hours, bars still held their load when testing was discontinued at 200 hours.

11. Bond

The deformations on the DYWIDAG Threadbar exceed the deformation requirements of A 615. Consequently bond strength is at least equivalent to A 615 reinforcing bars.

12. Shear

High strength bars are not usually used to resist transverse shear loads. However, their untensioned shear strength is similar to that of any other steel.

$$t = \frac{f_y}{\sqrt{3}}$$

13. Stressing

Dywidag Threadbars are stressed using compact light-weight electric powered hydraulic jacks. In most cases handled by one person, the jack fits over a pull rod designed to thread over the threadbar protruding from the anchor nut. The jack nose contains a socket wrench and ratchet device which allow the nut to be tightened as the threadbar elongates. Equipment for the 1 ¾ in (46 mm) bar varies from standard equipment.

The magnitude of the prestress force applied is monitored by reading the hydraulic gauge pressure and by measuring the threadbar elongation. The elongation can be measured directly by noting the change in threadbar extension.

14. Grouting

Grouting completes the installation process for post-tensioned concrete construction. The grout is important in protecting the steel from corrosion and contributes significantly to the ultimate strength of the structure.

A portable grout mixer is used to flush out the tendon sheathing to remove debris. Then cement and water grout is pumped into the grout tube at one end of the tendon using a grout tube at the other end as a vent. An admixture is used to control expansion and pumpability.

ANSWERS TO SELECTED PROBLEMS

Prolem No.:

1.1 Examples include: Umbrella, tent, musical drum, trampoline, tempered glass, carriage wheels

1.3 1. $A_s = 5.51\ \text{in}^2$; $M_n \simeq 562.54$ kips-ft; $\varphi = 5.071\times10^{-5}$ (1/in) : $\varphi_n = 1.82\times10^{-3}$ (1/in).

2. $A_s = 3.20\ \text{in}^2$; $M_n \simeq 330.64$ kips-ft; $\varphi = 0.0031$ (1/in)

3. $F = 154.50$ kips; $A_{ps} = 1.03\ \text{in}^2$; $\varphi_{(a)} = -7.804\times10^{-6}$ (1/in); $\varphi_{(b)} = 5.225\times10^{-6}$ (1/in)

2.3 $(C_{CU})_{\text{member}} = K_{CH}K_{CA}K_{CS}(C_{cu})_{\text{material}}$

$$= 3\times1.25t_A^{-0.118}(1.27-0.0067H)$$

t_A \ H	40%	60%	80%
7	2.99	2.59	2.19
28	2.54	2.20	1.86
90	2.21	1.91	1.62

2.5	Normal weight			Lightweight		
f'_c, psi	5000	7000	9000	5000	7000	9000
f'_{lc}, psi	-212	-251	-285	-141	-167	-190
f_r, psi	-530	-627	-712	-398	-471	-534
E_c, 10^6psi	4.287	5.072	5.751	2.511	2.971	3.368

4.1 (*a*) $\sigma = \pm1203$ psi. Failure will occur due to excess tension.

(*b*) $F = 259.85$ kips.

(*c*) $F = 129.92$ kips.

(*d*) $F = 86.62$ kips.

4.2 $W_L = 420$ plf.

4.3 (1) $F \simeq 182.18$ kips; $e_o = 12.55$ in. (4) $M_{cr} \simeq 331.05$ kips-ft . However, if 6 strands are draped, then 9 strands are needed with: $F \simeq 206.55$ kips; $e_o = 11.88$ in.

(5) $(\varphi)_{\text{initial loading}} = -2.12 \times 10^{-5}$ (1/in); $(\varphi)_{\text{final loading}} = 0.606 \times 10^{-5}$ (1/in) for 9 strands.

(6) $W_{\max} = 869.86$ plf; $F = 250.72$ kips; $e_o = 13.06$ in

4.4 $F = 143.2$ kips; $F_i \simeq 179$ kips; $k_t' = -3$ in; $k_b' = 3.68$ in

4.5 $F_i \simeq 187.5$ kips; $e_o = 1.35$ in

4.7 (*a*) Minimum required $F = 51.9$ kips; actual $F \simeq 69.3$ kips (3 strands) at $e_o = 10.64$ in

(*c*) $F \simeq 123.6$ kips. (controlled by stress condition II)

(*d*) Maximum live load = 193 psf

(*e*) $k_t' = -6.54$ in; $k_b' = 8.67$ in

(*f*)

x	0	4	8	12	16	20 ft
e_{ou}	-6.54	-1.58	2.29	5.05	6.71	7.26 in
e_{ol}	8.67	10.64	10.64	10.64	10.64	10.64 in

4.8 (*a*) $F_i \simeq 143.44$ kips (5 strands) at $e_o = 10.64$ in

5.1 $\sigma_{ti} = 635.5$ psi; $\sigma_{ci} = 796.4$ psi; $\sigma_{cs} = 1216$ psi; $\sigma_{ts} = -70.6$ psi; $M_u = 1161.67$ kips-ft; $\phi M_n \simeq 1448$ kips-ft

5.3 Prestressed reinforcement only: $M_{cr} = 409.54$ kips-ft; $\phi M_n \simeq 575.82$ kips-ft. Prestressed and nonprestressed reinforcement: $\phi M_n \simeq 682.36$ kips-ft

5.4 (*a*) $M_u = 122.45$ kips-ft; $M_{cr} = 104.77$ kips-ft; $\phi M_n \simeq 559.5$ kips-ft; $\phi M_n > 1.2 M_{cr}$

(*b*) $f_{ps} = 211$ ksi; $\phi M_n = 121.56$ kips-ft $< 1.2 M_{cr} = 125.7$ kips-ft (add some nonprestressed reinforcement)

5.6 (*a*) $F = 631.13$ kips (22 strands); $e_o = 10.67$ in

(*b*) $\phi M_n = 1217$ kips-ft; $M_{cr} = 802.9$ kips-ft; $\phi M_n > 1.2 M_{cr}$; $M_u = 1044$ kips-ft; $\phi M_n > M_u$

(*c*) Use 2#9 $A_s = 2.00$ in^2 $> (A_s)_{require} = 1.35$ in^2

5.8 $A_{ps} = 0.986$ in^2; $d_p = 21$ in

6.1 For $\sigma_1 = 0$, $\sigma_y = 228.6$ psi; for $\sigma_1 = -100$, $\sigma_y = 100$ psi

6.2 Minimum shear reinforcement is adequate for the beam. It can be waived if the beam is part of a joist slab.

6.3 Minimum shear reinforcement is sufficient throughout.

6.4 $F = 367.2$ kips (16 strands); choose profile with two draping points at about 25 and 50 ft from support A; $e_o = 5.98$ in at A; $e_o = 17.98$ in at B; $e_o = -6.02$ in at C; $e_o = 0$ at D.

7.3 (1a) $\Delta_i = -1.19$ in

(1b)

Method	Δ_{add} (in)
Rule of thumb	-1.908
Martin's	-1.752
Branson's	-1.872

7.5 (*a*) 14 strands with $F_i = 374.85$ kips, $e_o = 17.01$ in at midspan, and $e_o = 10.73$ in at support. Single draping point at midspan.

(*b*) $\phi M_n = 12{,}751$ kips-in $> M_u = 11{,}205$ kips-in

(*c*) Shear reinforcement: #3 U stirrups at $s = 22$ in

(*d*) $\Delta_{add} \simeq -1.58$ in

(*e*) Using incremental step method: $\Delta_{add} \simeq -1.95$ in

7.7 (1a.) $\Delta_i \simeq -0.078$ in

(1b.)

Method	Δ_{add} (in)
Rule of thumb	0.137
Martin's	-0.116
Branson's	0.104

(2)

t, days	1	7	30	90	365 days	50 yrs
Δ(in)	-0.160	-0.157	-0.139	-0.109	-0.064	-0.019

7.8 (1)

Method of computation	$(\Delta_i)_{F_i+G}$ in	Δ_{add} in	Δ_{Total} in	$\lvert\Delta_{LL}\rvert$ in	$\lvert\Delta_{LL}+\Delta_{add}\rvert$ in	Remark
Rule of thumb	-0.396	-0.621	-1.017	0.64	0.019	Smallest
Martin's	-0.396	-0.665	-1.061	0.64	0.025	
Branson's	-0.396	-0.675	-1.071	0.64	0.035	
ACI 1983	-0.396	-0.792	-1.188	0.64	0.152	Largest
ACI Limitation				$\le \frac{l}{360} = 1.33$	$\le \frac{l}{480} = 1$	O.K.

8.1

t, days	1	3	7	30	60	365 days	5 yrs	40 yrs
$\Sigma\Delta f_{pT}(t_i,t_j)$(ksi)	14.87	17.82	20.62	26.70	29.97	37.1	40.41	42.61

8.2

t, days	1	3	7	30	60	365	1214 days
$\Sigma\Delta f_{pT}(t_i,t_j)$(ksi)	11.81	19.05	21.37	23.71	25.76	30.93	34.48

8.3 $F = 234.32$ kips

8.5 (*a*) $\left(f_{pi}\right)_A = 136.37$ ksi

(*b*) $\left(f_{pi}\right)_B = 77.92$ ksi

(*c*) Recommend prestressing from both ends.

9.1

h (in)	N	Fi (kips)
8	12	334.8
10	10	279.0
12	8	223.2
15	6	167.4

9.2 $F = 137.7$ kips (6 strands); $e_o = 9.25$ in.

9.3 1. $F_i \simeq 359.50$ kips (13 strands) at $e_o = 23.22$ in

2. $\phi M_n = 1503$ kips-ft; $M_{cr} = 993.5$ kips-ft; $\phi M_n > 1.2M_{cr}$; $M_u = 1319$ kips-ft; $\phi M_n > M_u$; shored construction: $F_i \simeq 359.50$ kips (13 strands) at $e_o = 23.22$ in

3. No. 3 U stirrups at 24 in spacing

6. Same answer as in 1.

10.1 The ZLC line coincides with the neutral axis of the member.

10.2 Fig. P10.2a. The ZLC line is a straight line with eccentricity $-0.15h$ at the left support and $0.30h$ at the right support.

Fig. P10.2b. The ZLC line is a segmented line with eccentricity $-0.3375h$ at the left support, $0.28125h$ at midspan and 0 at the right support.

Fig. P10.2c. The ZLC line is a parabola with eccentricity $-0.3689h$ at the left support, $0.1656h$ at midspan and 0 at the right support.

Fig. P10.2d The profile is concordant.

10.4 $M_{2C} = M_{2D} = 48$ kips-ft; $M_{2B} = 19.2$ kips-ft; $\left(M_{\max}\right)_C = 255$ kips-ft; $\left(M_{\min}\right)_C = 128$ kips-ft; $\left(M_{\max}\right)_B = 160$ kips-ft; $\left(M_{\min}\right)_B = 32$ kips-ft;

11.2 Typical exterior span: 1 strand (0.6-in diameter) at 18-in spacing and 1 strand (0.5-in diameter) at 36-in spacing. Typical interior span: 1 strand (0.6-in diameter) at 18-in spacing.

12.1 $A_g \simeq 271$ in^2; $A_{ps} \simeq 2.67$ in^2; a rectangular section 15×18 in will do.

12.3 From the feasible domain the least-weight section corresponds to: $A_g \simeq 102$ in^2; $A_{ps} = 1.80$ in^2

13.1 $\phi P_{n,o} = 576.55$ kips; $\phi P_{n,ot} = 451.65$ kips; $\phi M_{n,ot} = 646.52$ kips-in; $e_{ot} = 143$ in; $\varphi_{ot} = 21.4 \times 10^{-5}$; $\phi P_{n,b} = 27.36$ kips; $\phi M_{n,b} = 672.87$ kips-in; $e_b = 24.6$ in; $\varphi_b = 113.2 \times 10^{-5}$; $\phi M_{n,f} = 814.43$ kips-in for $\phi = 0.9$; $\varphi_f = 140.18 \times 10^{-5}$.

13.2 Assume $\phi = 0.65$ for square spirals (safe side); $\phi P_{n,o} = 533.2$ kips; $\phi P_{n,ot} = 402.57$ kips; $\phi M_{n,ot} = 686.68$ kips-in; $\phi P_{n,b} = 136.30$ kips; $\phi M_{n,b} = 1033.03$ kips-in;

$\phi M_{n,f} = 891.30$ kips-in, for $\phi = 0.9$.

14.2 (*a*) $M_{L+I} = 1747.32$ kips-ft.

(*b*) $M_{L+I} = 7310.96$ kips-ft.

14.3 Maximum positive moment due to one lane loading =1321.24 kips-ft. Maximum positive moment due to one truck loading = 1530.31 kips-ft. Truck position is given in Fig. 14.43.

14.9 The bridge utilizes the same beam and material properties as for the example beam of Section 4.9.1; the maximum service load is the same leading to the same prestressing force and eccentricity. Design for nominal bending resistance is satisfied. Shear design according to AASHTO leads to No. 3 U stirrups at 23 in spacing throughout.

14.10 The following results are obtained:

In span: $M_{LL+IM} = DF_M \times (M_{Lane})_{max} = 0.706 \times 2059.91 = 1454.30$ kips-ft

First critical section for shear taken at 3 ft from the center of support:

$V_{LL+IM} = DF_V \times (V_{Lane})_{max} = 0.832 \times 104.68 = 87.09$ kips

$M_{LL+IM} = DF_M \times (M_{Lane})_{max} = 0.706 \times 316.91 = 223.74$ kips-ft

The following results are obtained:

$b_{tr} = b_e n_c = 99 \times 0.756 = 74.84$ in

$F = 32.40 \times 22 = 712.80$ kips

$N = 22$ strands (0.6 in diameter)

$A_{ps} = 0.216 \times 22 = 4.752$ in^2

$F_i = F / \eta = F / 0.80 = 891.00$ kips

$e_o = 20.73$ in at midspan

Ultimate strength requirements in bending are satisfactory.

Shear reinforcement at first critical section: No. 3, U stirrups at 12 in spacing. The vertical shear reinforcement is extended through the slab and is sufficient to satisfy horizontal shear transfer.

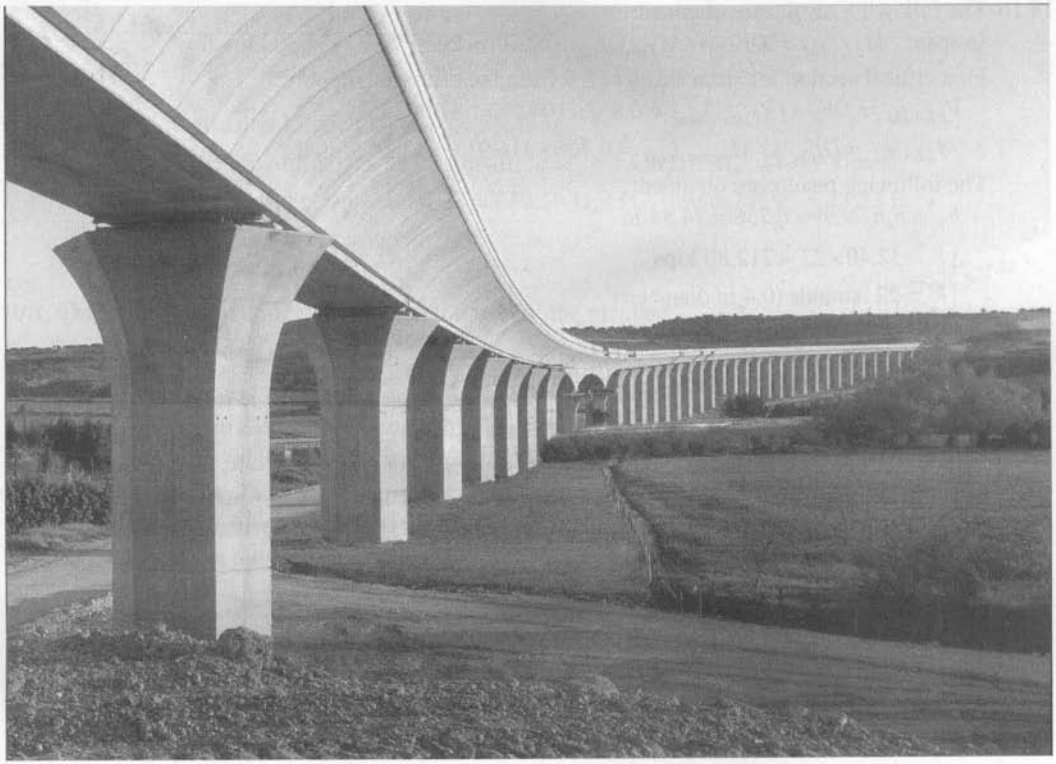

Ventabren viaduct in southern France for the high speed rail project, built by the cast-in-place cantilever construction method. *(Courtesy Freyssinet International.)*

TYPICAL PRECAST / PRESTRESSED BEAMS

Through the Precast/Prestressed Concrete Institute (PCI), the prestressed concrete industry has developed a number of standard products for various construction applications, mostly buildings and bridges. In bridge applications, particularly short and medium span bridges and highway overpasses, the most common application involves composite decks constructed with precast-prestressed concrete AASHTO-PCI girders topped by a cast-in-place reinforced concrete slab. Examples of girders available from precast/prestressed concrete manufacturers in the U.S. are described in Chapter 14, Figs. 14.4 to 14.6 and design examples are treated in Sections 14.10 and 14.11. However, the most widely used product by far in commercial and residential buildings, is the double T. Double T is also the member of choice in parking structures, because it offers the benefits of long spans, large floor area, efficiency, and relatively light weight. Moreover, double Ts can be used for floors as well as external walls. Design aids have been developed by the Precast/Prestressed Concrete Institute for many standard products, including single Ts, double Ts, hollow cored slabs, columns, piles and poles. Design examples using double Ts and hollow cored slabs can be found in Sections 4.11.3, 7.12, and 9.7.6 of this book.

Figures E1 to E5 are reproduced from the fifth edition of the PCI Design Handbook. They show typical examples of double Ts and hollow-cored slabs. Assumptions used to develop these figures are explained in detail in the PCI handbook. The figures can be used for preliminary dimensioning and design. Only a small selection is given next. The PCI Handbook should be consulted for a much larger selection. Note that for each beam made with normal weight concrete, there is an equivalent beam made with structural lightweight concrete, and, in each case, an alternative with 2 in (50 mm) concrete topping is considered.

Strand Pattern Designation

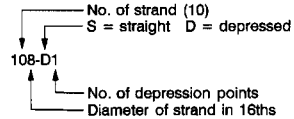

Safe loads shown include dead load of 10 psf for untopped members and 15 psf for topped members. Remainder is live load. Long-time cambers include superimposed dead load but do not include live load.

Key
173 — Safe superimposed service load, psf
0.5 — Estimated camber at erection, in.
0.7 — Estimated long-time camber, in.

DOUBLE TEE

8′-0″ x 24″
Normal Weight Concrete

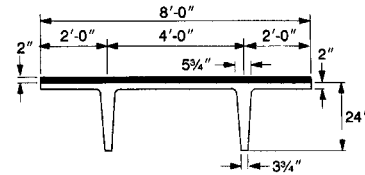

f'_c = 5,000 psi
f_{pu} = 270,000 psi

Section Properties

		Untopped		Topped	
A	=	401	in²	—	
I	=	20,985	in⁴	27,720	in⁴
y_b	=	17.15	in.	19.27	in.
y_t	=	6.85	in.	6.73	in.
S_b	=	1,224	in³	1,438	in³
S_t	=	3,063	in³	4,119	in³
wt	=	418	plf	618	plf
		52	psf	77	psf
V/S	=	1.41	in.		

8DT24

Table of safe superimposed service load (psf) and cambers (in.) — **No Topping**

Strand Pattern	e_s, in. / e_c, in.	Span, ft																				
		30	32	34	36	38	40	42	44	46	48	50	52	54	56	58	60	62	64	66	68	70	72	74
68-S	11.15 / 11.15	173	147	126	108	92	79	68	58	50	43	36	30											
		0.5	0.6	0.6	0.7	0.7	0.7	0.7	0.7	0.7	0.6	0.6	0.5											
		0.7	0.8	0.8	0.8	0.8	0.8	0.8	0.8	0.7	0.6	0.4	0.2											
88-S	9.15 / 9.15		180	155	134	116	100	87	76	66	57	49	43	36	31									
			0.7	0.7	0.8	0.8	0.8	0.8	0.9	0.8	0.8	0.8	0.7	0.6	0.5									
			0.9	0.9	1.0	1.0	1.0	1.0	1.0	0.9	0.8	0.7	0.5	0.3	0.1									
88-D1	9.15 / 14.40				190	166	146	129	114	100	89	79	70	62	54	48	42	37	32					
					1.1	1.2	1.3	1.4	1.5	1.5	1.6	1.6	1.6	1.6	1.6	1.5	1.4	1.3	1.2					
					1.5	1.5	1.6	1.7	1.8	1.8	1.8	1.8	1.7	1.6	1.5	1.4	1.2	0.9	0.5					
108-D1	7.15 / 14.15								145	129	116	103	92	83	74	66	59	53	47	42	37	32		
									1.7	1.8	1.9	2.0	2.0	2.1	2.1	2.1	2.1	2.0	2.0	1.8	1.7	1.5		
									2.2	2.2	2.3	2.3	2.3	2.3	2.2	2.1	2.0	1.8	1.8	1.3	1.0	0.5		
128-D1	5.48 / 13.90															83	75	68	61	55	49	44	40	35
																2.5	2.5	2.5	2.5	2.5	2.4	2.3	2.1	1.9
																2.7	2.7	2.5	2.3	2.1	1.8	1.5	1.1	0.8
148-D1	4.29 / 13.65																				61	55	50	45
																					2.9	2.9	2.8	2.6
																					2.6	2.3	1.9	1.5

8DT24+2

Table of safe superimposed service load (psf) and cambers (in.) — **2″ Normal Weight Topping**

Strand Pattern	e_s, in. / e_c, in.	Span, ft																		
		26	28	30	32	34	36	38	40	42	44	46	48	50	52	54	56	58	60	62	64
48-S	14.15 / 14.15	183	149	122	100	82	66	53	42	33											
		0.4	0.4	0.4	0.5	0.5	0.5	0.5	0.5	0.5											
		0.4	0.4	0.4	0.4	0.4	0.3	0.3	0.2	0.0											
68-S	11.15 / 11.15			175	147	123	103	86	72	60	49	39									
				0.5	0.6	0.6	0.7	0.7	0.7	0.7	0.7	0.7									
				0.5	0.6	0.6	0.6	0.5	0.4	0.3	0.2	0.0									
68-D1	11.15 / 14.65					184	156	133	113	96	81	69	58	48	39						
						0.7	0.8	0.9	0.9	1.0	1.0	1.0	1.0	1.0	1.0						
						0.8	0.8	0.8	0.8	0.7	0.7	0.6	0.5	0.3	0.1						
88-D1	9.15 / 14.40							190	165	143	124	107	93	80	69	59	51	43			
								1.1	1.2	1.3	1.4	1.5	1.5	1.6	1.6	1.6	1.6	1.6			
								1.1	1.1	1.2	1.2	1.1	1.1	0.9	0.8	0.6	0.4	0.1			
108-D1	7.15 / 14.15										142	124	109	96	84	74	64	56	48		
											1.7	1.8	1.9	2.0	2.0	2.1	2.1	2.1	2.1		
											1.5	1.5	1.4	1.3	1.2	1.0	0.7	0.5	0.1		
128-D1	5.48 / 13.90																	74	65	57	49
																		2.5	2.5	2.5	2.5
																		1.0	0.7	0.3	0.1

Strength based on strain compatibility; bottom tension limited to $12\sqrt{f'_c}$; see pages 2-2–2-6 for explanation.
Shaded values require release strengths higher than 3500 psi.

Figure E1 Standard double T: 8DT24 (normal weight concrete), reproduced from the PCI Design Handbook. *(Courtesy Precast/Prestressed Concrete Institute.)*

Strand Pattern Designation

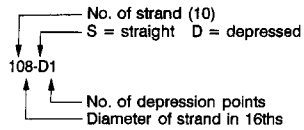

Safe loads shown include dead load of 10 psf for untopped members and 15 psf for topped members. Remainder is live load. Long-time cambers include superimposed dead load but do not include live load.

Key

118 — Safe superimposed service load, psf
1.1 — Estimated camber at erection, in.
1.4 — Estimated long-time camber, in.

DOUBLE TEE

8′-0″ x 24″
Lightweight Concrete

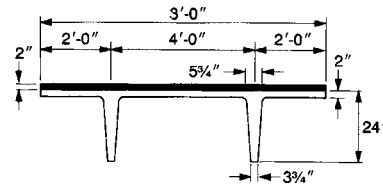

f'_c = 5,000 psi
f_{pu} = 270,000 psi

Section Properties

		Untopped		Topped	
A	=	401	in²	—	
I	=	20,985	in⁴	29,857	in⁴
y_b	=	17.15	in.	19.94	in.
y_t	=	6.85	in.	6.06	in.
S_b	=	1,224	in³	1,497	in³
S_t	=	3,063	in³	4,926	in³
wt	=	320	plf	520	plf
		40	psf	65	psf
V/S	=	1.41	in.		

8LDT24

Table of safe superimposed service load (psf) and cambers (in.) — **No Topping**

Strand Pattern	e_s, in. / e_c, in.	Span, ft																						
		36	38	40	42	44	46	48	50	52	54	56	58	60	62	64	66	68	70	72	74	76	78	80
68-S	11.15 / 11.15	118	103	89	78	69	60	53	46	40	35	30												
		1.1	1.2	1.2	1.3	1.3	1.4	1.4	1.4	1.3	1.3	1.2												
		1.4	1.4	1.5	1.5	1.5	1.5	1.4	1.4	1.2	1.0	0.8												
88-S	9.15 / 9.15	144	126	110	97	86	76	67	59	53	47	41	36	32										
		1.2	1.3	1.4	1.5	1.6	1.6	1.6	1.6	1.6	1.6	1.6	1.5	1.4										
		1.6	1.6	1.7	1.8	1.8	1.8	1.8	1.7	1.6	1.5	1.3	1.0	0.7										
88-D1	9.15 / 14.40		176	156	139	124	111	99	89	80	72	64	58	52	47	42	38	34						
			1.9	2.1	2.2	2.4	2.5	2.7	2.8	2.9	3.0	3.0	3.1	3.1	3.0	3.0	2.9	2.8						
			2.4	2.6	2.8	2.9	3.0	3.1	3.2	3.2	3.2	3.1	2.9	2.8	2.6	2.4	2.1	1.8						
108-D1	7.15 / 14.15								113	102	93	84	76	69	63	57	52	47	43	38	35	31		
									3.3	3.4	3.6	3.7	3.8	3.9	4.0	4.1	4.1	4.0	3.9	3.8	3.6	3.4		
									3.9	4.0	4.1	4.1	4.1	4.0	3.9	3.8	3.5	3.2	2.8	2.4	1.9	1.3		
128-D1	5.48 / 13.9																65	59	54	50	45	41	38	34
																	4.8	4.9	4.9	4.9	4.8	4.7	4.5	4.3
																	4.7	4.5	4.2	3.8	3.4	2.8	2.2	1.5
148-D1	4.29 / 13.65																						46	42
																							5.6	5.5
																							3.8	3.2

8LDT24+2

Table of safe superimposed service load (psf) and cambers (in.) — **2″ Normal Weight Topping**

Strand Pattern	e_s, in. / e_c, in.	Span, ft																					
		26	28	30	32	34	36	38	40	42	44	46	48	50	52	54	56	58	60	62	64	66	68
48-S	14.15 / 14.15	193	159	132	110	92	76	63	52	43	34												
		0.6	0.6	0.7	0.8	0.8	0.9	0.9	1.0	1.0	1.0												
		0.6	0.6	0.7	0.7	0.7	0.6	0.6	0.5	0.4	0.2												
68-S	11.15 / 11.15			185	157	133	113	96	82	70	59	50	41	34									
				0.9	0.9	1.0	1.1	1.2	1.2	1.3	1.3	1.4	1.4	1.4									
				0.9	0.9	0.9	0.9	0.9	0.9	0.8	0.7	0.5	0.3	0.0									
68-D1	11.15 / 14.65					166	143	123	106	91	79	68	58	49	42	35							
						1.2	1.4	1.5	1.6	1.7	1.8	1.9	1.9	2.0	2.0	2.0							
						1.2	1.3	1.3	1.3	1.3	1.2	1.1	0.9	0.7	0.5	0.2							
88-D1	9.15 / 14.40						200	175	153	134	117	103	90	79	70	61	53	46	40				
							1.8	1.9	2.1	2.1	2.4	2.5	2.7	2.8	2.9	3.0	3.0	3.1	3.1				
							1.8	1.9	1.9	1.8	2.0	1.9	1.9	1.7	1.6	1.3	1.0	0.6	0.2				
108-D1	7.15 / 14.15													106	94	84	74	66	58	51	45		
														3.3	3.4	3.6	3.7	3.8	3.9	4.0	4.1		
														2.4	2.3	2.1	1.9	1.6	1.3	0.8	0.3		
128-D1	5.48 / 13.90																					53	46
																						4.8	4.9
																						0.7	0.1

Strength based on strain compatibility; bottom tension limited to $12\sqrt{f'_c}$; see pages 2-2–2-6 for explanation.
Shaded values require release strengths higher than 3500 psi.

Figure E2 Standard double T: 8DT24 (lightweight concrete), reproduced from the PCI Design Handbook. *(Courtesy Precast/Prestressed Concrete Institute.)*

Strand Pattern Designation

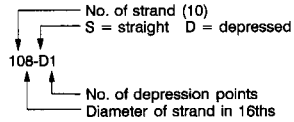

Safe loads shown include dead load of 10 psf for untopped members and 15 psf for topped members. Remainder is live load. Long-time cambers include superimposed dead load but do not include live load.

Key

182 — Safe superimposed service load, psf
1.2 — Estimated camber at erection, in.
1.6 — Estimated long-time camber, in.

DOUBLE TEE

10′-0″ x 32″

Normal Weight Concrete

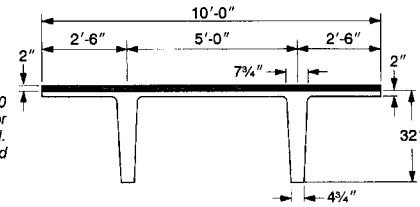

f'_c = 5,000 psi

f_{pu} = 270,000 psi

Section Properties

		Untopped		Topped	
A	=	615	in²	—	
I	=	59,720	in⁴	77,131	in⁴
y_b	=	21.98	in.	24.54	in.
y_t	=	10.02	in.	9.46	in.
S_b	=	2,717	in³	3,142	in³
S_t	=	5,960	in³	8,149	in³
wt	=	641	plf	891	plf
		64	psf	89	psf
V/S	=	1.69	in.		

10DT32

Table of safe superimposed service load (psf) and cambers (in.) — **No Topping**

Strand Pattern	e_s, In. / e_c, In.	Span, ft																				
		46	48	50	52	54	56	58	60	62	64	66	68	70	72	74	76	78	80	82	84	86	88
128-D1	12.81 / 18.73	182 1.2 1.6	163 1.3 1.6	146 1.3 1.6	131 1.4 1.7	118 1.4 1.7	106 1.4 1.7	95 1.5 1.7	86 1.5 1.6	77 1.4 1.6	69 1.4 1.6	62 1.4 1.5	55 1.4 1.4	49 1.3 1.2	44 1.2 1.0	39 1.1 0.8	1.0 0.5						
148-D1	10.48 / 18.48		191 1.4 1.8	172 1.5 1.9	155 1.6 1.9	140 1.6 2.0	127 1.7 2.0	115 1.7 2.0	104 1.7 2.0	94 1.8 1.9	85 1.7 1.9	77 1.7 1.8	70 1.7 1.7	63 1.6 1.5	57 1.5 1.4	51 1.4 1.2	46 1.3 0.9	41 1.2 0.5					
168-D1	8.98 / 18.23			199 1.6 2.1	180 1.7 2.2	163 1.8 2.2	148 1.9 2.3	134 1.9 2.3	122 2.0 2.3	111 2.0 2.3	101 2.0 2.3	92 2.1 2.2	84 2.1 2.1	76 2.0 2.0	69 2.0 1.9	63 1.9 1.7	57 1.8 1.5	52 1.7 1.2	46 1.5 0.9	42 1.3 0.5			
188-D1	7.59 / 17.98							140 2.2 2.6	127 2.2 2.6	117 2.3 2.6	107 2.3 2.6	97 2.3 2.5	89 2.3 2.4	81 2.3 2.3	74 2.3 2.1	68 2.2 2.0	62 2.1 1.8	56 2.0 1.5	51 1.8 1.2	46 1.7 0.8		
208-D1	6.48 / 17.73											110 2.5 2.9	101 2.6 2.8	93 2.6 2.7	85 2.6 2.6	78 2.5 2.4	72 2.5 2.2	66 2.4 2.0	60 2.3 1.7	55 2.2 1.4	50 2.0 1.0	
228-D1	5.57 / 17.48															88 2.8 2.9	81 2.8 2.7	75 2.7 2.5	69 2.6 2.2	63 2.5 1.9	58 2.4 1.5	53 2.2 1.2

10DT32+2

Table of safe superimposed service load (psf) and cambers (in.) — **2″ Normal Weight Topping**

Strand Pattern	e_s, In. / e_c, In.	Span, ft																
		42	44	46	48	50	52	54	56	58	60	62	64	66	68	70	72	74	76
108-D1	16.08 / 18.98	179 0.9 0.9	157 1.0 1.0	138 1.1 1.0	121 1.1 0.9	106 1.1 0.9	92 1.2 0.9	81 1.2 0.8	70 1.2 0.7	60 1.2 0.5	52 1.2 0.4								
128-D1	12.81 / 18.73		199 1.1 1.1	176 1.2 1.2	156 1.3 1.2	138 1.3 1.2	122 1.4 1.1	108 1.4 1.1	96 1.4 1.0	85 1.5 0.9	74 1.5 0.7	65 1.4 0.6	57 1.4 0.4						
148-D1	10.48 / 18.48				186 1.4 1.4	166 1.5 1.4	148 1.6 1.4	132 1.6 1.3	118 1.7 1.3	1.5 1.7 1.2	94 1.7 1.1	83 1.8 0.9	74 1.7 0.8	65 1.7 0.5	57 1.7 0.3				
168-D1	8.98 / 18.23					194 1.6 1.6	174 1.7 1.6	156 1.8 1.6	140 1.9 1.5	126 1.9 1.5	113 2.0 1.4	101 2.0 1.3	91 2.0 1.1	81 2.1 0.9	72 2.1 0.7	64 2.0 0.5			
188-D1	7.59 / 17.98									145 2.1 1.7	131 2.2 1.7	118 2.2 1.6	107 2.3 1.4	96 2.3 1.3	86 2.3 1.1	77 2.3 0.8	69 2.3 0.5	62 2.3 0.2	
208-D1	6.48 / 17.73														100 2.5 1.4	90 2.6 1.2	82 2.6 0.9	73 2.6 0.6	66 2.5 0.2

Strength based on strain compatibility; bottom tension limited to 12 $\sqrt{f'_c}$; see pages 2-2–2-6 for explanation.
Shaded values require release strengths higher than 3500 psi.

Figure E3 Standard double T: 10DT32 (normal weight concrete), reproduced from the PCI Design Handbook. *(Courtesy Precast/Prestressed Concrete Institute.)*

Strand Pattern Designation

108-D1
- No. of strand (10)
- S = straight D = depressed
- No. of depression points
- Diameter of strand in 16ths

Safe loads shown include dead load of 10 psf for untopped members and 15 psf for topped members. Remainder is live load. Long-time cambers include superimposed dead load but do not include live load.

Key
137 — Safe superimposed service load, psf
0.8 — Estimated camber at erection, in.
1.1 — Estimated long-time camber, in.

DOUBLE TEE

12′-0″ x 28″
Normal Weight Concrete

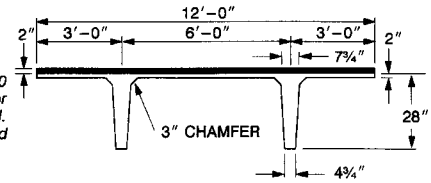

f'_c = 5,000 psi
f_{pu} = 270,000 psi

Section Properties

		Untopped		Topped	
A	=	640	in²	—	
I	=	44,563	in⁴	57,323	in⁴
y_b	=	20.21	in.	22.47	in.
y_t	=	7.79	in.	7.53	in.
S_b	=	2,205	in³	2,551	in³
S_t	=	5,722	in³	7,611	in³
wt	=	667	plf	967	plf
		56	psf	81	psf
V/S	=	1.62	in.		

12DT28

Table of safe superimposed service load (psf) and cambers (in.) — **No Topping**

Strand Pattern	e_s, in. / e_c, in.	Span, ft																				
		40	42	44	46	48	50	52	54	56	58	60	62	64	66	68	70	72	74	76	78	80	82	84
108-D1	10.02 / 17.02	137	120	105	92	81	71	62	54	47	41	35	30	25										
		0.8	0.9	0.9	0.9	0.9	0.9	0.9	0.9	0.9	0.8	0.7	0.6	0.5										
		1.1	1.2	1.2	1.3	1.3	1.3	1.3	1.2	1.2	1.1	0.9	0.8	0.6										
128-D1	8.35 / 16.77	168	148	131	116	103	91	81	71	63	56	49	43	37	32	28								
		1.0	1.1	1.1	1.2	1.2	1.2	1.2	1.2	1.2	1.2	1.1	1.0	0.9	0.8	0.6								
		1.4	1.4	1.5	1.6	1.6	1.6	1.6	1.6	1.6	1.6	1.5	1.4	1.2	1.0	0.8								
148-D1	7.16 / 16.52	198	175	156	139	123	110	98	88	78	70	62	55	49	43	38	33	29	25					
		1.1	1.2	1.3	1.3	1.4	1.4	1.5	1.5	1.5	1.5	1.5	1.4	1.4	1.3	1.1	1.0	0.8	0.6					
		1.6	1.6	1.7	1.8	1.9	2.0	2.0	2.0	2.0	2.0	1.9	1.9	1.8	1.7	1.5	1.3	1.0	0.7					
168-D1	7.02 / 16.27							117	105	94	85	76	68	61	55	49	44	39	34	30	26			
								1.7	1.8	1.8	1.9	1.9	1.9	1.9	1.8	1.7	1.6	1.4	1.3	1.1	0.8			
								2.4	2.4	2.5	2.5	2.5	2.5	2.4	2.3	2.2	2	1.8	1.6	1.3	0.9			
188-D1	5.63 / 16.02											88	79	72	65	58	52	47	42	37	33	29	25	
												2.1	2.1	2.1	2.1	2.0	1.9	1.8	1.7	1.5	1.3	1.0	0.7	
												2.8	2.8	2.8	2.7	2.6	2.5	2.3	2.1	1.8	1.5	1.2	0.8	
208-D1	4.52 / 15.77															67	61	55	49	44	40	36	32	28
																2.3	2.2	2.1	2.0	1.9	1.7	1.5	1.2	0.9
																3.0	2.9	2.7	2.5	2.3	2.0	1.7	1.3	0.9

12DT28+2

Table of safe superimposed service load (psf) and cambers (in.) — **2″ Normal Weight Topping**

Strand Pattern	e_s, in. / e_c, in.	Span, ft																		
		40	42	44	46	48	50	52	54	56	58	60	62	64	66	68	70	72	74	76
108-D1	10.02 / 17.02	130	112	96	82	70	59	50	41	34	27									
		0.8	0.9	0.9	0.9	0.9	0.9	0.9	0.9	0.9	0.8									
		0.9	0.9	0.8	0.8	0.8	0.7	0.6	0.4	0.3	0.0									
128-D1	8.35 / 16.77	164	142	124	107	93	81	69	60	51	43	35	29							
		1.0	1.1	1.1	1.2	1.2	1.2	1.2	1.2	1.2	1.2	1.1	1.0							
		1.1	1.1	1.1	1.1	1.1	1.0	0.9	0.8	0.7	0.5	0.3	0.0							
148-D1	7.16 / 16.52	196	171	150	132	116	101	89	77	67	58	50	42	36	30					
		1.1	1.2	1.3	1.3	1.4	1.4	1.5	1.5	1.5	1.5	1.5	1.4	1.4	1.3					
		1.2	1.3	1.3	1.3	1.3	1.3	1.3	1.2	1.1	0.9	0.7	0.5	0.2	−0.1					
168-D1	7.02 / 16.27							108	95	84	74	65	56	49	42	35	30			
								1.7	1.8	1.8	1.9	1.9	1.9	1.8	1.8	1.7	1.6			
								1.6	1.6	1.5	1.4	1.2	1.1	0.8	0.5	0.2	−0.2			
188-D1	5.63 / 16.02											77	68	60	52	45	39	33	27	
												2.1	2.1	2.1	2.1	2.0	1.9	1.8	1.7	
												1.5	1.4	1.2	0.9	0.6	0.3	−0.1	−0.6	
208-D1	4.52 / 15.77															55	48	41	34	28
																2.3	2.2	2.1	2.0	1.9
																1.0	0.6	0.3	−0.2	−0.7

Strength based on strain compatibility; bottom tension limited to $12\sqrt{f'_c}$; see pages 2-2–2-6 for explanation.
Shaded values require release strengths higher than 3500 psi.

Figure E4 Standard double T: 12DT28 (normal weight concrete), reproduced from the PCI Design Handbook. *(Courtesy Precast/Prestressed Concrete Institute.)*

Strand Pattern Designation

76–S
- S = straight
- Diameter of strand in 16ths
- No. of strand (7)

Safe loads shown include dead load of 10 psf for untopped members and 15 psf for topped members. Remainder is live load. Long-time cambers include superimposed dead load but do not include live load.

Capacity of sections of other configurations are similar. For precise values, see local hollow-core manufacturer.

HOLLOW-CORE

4′-0″ x 8″
Normal Weight Concrete

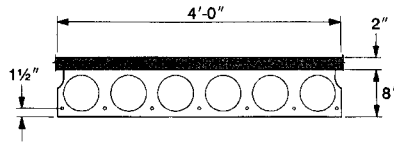

f'_c = 5,000 psi
f'_{ci} = 3,500 psi

Section Properties

		Untopped		Topped	
A	=	215	in²	—	
I	=	1,666	in⁴	3,071	in⁴
y_b	=	4.00	in.	5.29	in.
y_t	=	4.00	in.	4.71	in.
S_b	=	416	in³	580	in³
S_t	=	416	in³	652	in³
b_w	=	12.00	in.	12.00	in.
wt	=	224	plf	324	plf
		56	psf	81	psf
V/S	=	1.92	in.		

Key
335 — Safe superimposed service load, psf
0.2 — Estimated camber at erection, in.
0.3 — Estimated long-time camber, in.

4HC8

Table of safe superimposed service load (psf) and cambers (in.) — **No Topping**

Strand Designation Code	Span, ft																						
	14	15	16	17	18	19	20	21	22	23	24	25	26	27	28	29	30	31	32	33	34	35	36
66-S	335	286	246	213	185	162	141	124	109	96	85	75	66	58	50	44	38	33					
	0.2	0.2	0.2	0.2	0.2	0.3	0.3	0.3	0.3	0.2	0.2	0.2	0.2	0.1	0.0	0.0	−0.1	−0.2					
	0.3	0.3	0.3	0.3	0.3	0.3	0.3	0.3	0.3	0.2	0.2	0.1	0.0	−0.1	−0.2	−0.3	−0.5	−0.7					
76-S	375	337	291	252	220	193	170	150	133	118	105	93	83	73	65	58	51	45	39	34			
	0.2	0.3	0.3	0.3	0.3	0.3	0.3	0.4	0.4	0.4	0.3	0.3	0.3	0.3	0.2	0.2	0.1	0.0	−0.1	−0.2			
	0.3	0.3	0.4	0.4	0.4	0.4	0.4	0.4	0.4	0.4	0.3	0.3	0.2	0.1	0.0	−0.1	−0.2	−0.4	−0.6	−0.8			
58-S	372	342	317	296	275	255	225	200	179	160	143	128	115	104	93	84	76	68	61	55	49	44	39
	0.3	0.3	0.4	0.4	0.5	0.5	0.5	0.5	0.6	0.6	0.6	0.6	0.6	0.6	0.5	0.5	0.5	0.4	0.3	0.2	0.1	0.0	−0.1
	0.4	0.5	0.5	0.6	0.6	0.6	0.7	0.7	0.7	0.7	0.7	0.7	0.6	0.6	0.5	0.4	0.3	0.2	0.0	−0.2	−0.4	−0.6	−0.9
68-S		351	326	302	284	266	250	236	218	196	176	159	143	130	117	107	97	88	80	72	65	59	54
		0.4	0.5	0.5	0.6	0.8	0.7	0.7	0.7	0.8	0.8	0.8	0.8	0.8	0.8	0.8	0.8	0.8	0.7	0.7	0.6	0.5	0.4
		0.6	0.6	0.7	0.8	0.8	0.9	0.9	0.9	1.0	1.0	1.0	1.0	1.0	0.9	0.9	0.8	0.7	0.6	0.4	0.2	0.0	−0.2
78-S		360	335	311	290	272	256	242	229	215	205	188	170	154	141	128	117	106	97	89	81	74	67
		0.5	0.6	0.6	0.7	0.7	0.8	0.9	0.9	1.0	1.0	1.0	1.1	1.1	1.1	1.1	1.1	1.1	1.1	1.1	1.0	0.9	0.9
		0.7	0.8	0.8	0.9	1.0	1.0	1.1	1.2	1.2	1.3	1.3	1.3	1.3	1.3	1.3	1.2	1.2	1.1	1.0	0.9	0.7	0.5

4HC8+2

Table of safe superimposed service load (psf) and cambers (in.) — **2″ Normal Weight Topping**

Strand Designation Code	Span, ft																						
	16	17	18	19	20	21	22	23	24	25	26	27	28	29	30	31	32	33	34	35	36	37	38
66-S	309	267	231	201	175	153	133	117	102	89	77	67	55	44	33								
	0.2	0.2	0.2	0.3	0.3	0.3	0.3	0.2	0.2	0.2	0.2	0.1	0.0	0.0	−0.1								
	0.2	0.2	0.2	0.2	0.2	0.1	0.1	0.0	−0.1	−0.2	−0.3	−0.4	−0.6	−0.7	−0.9								
76-S		316	275	241	211	185	163	144	127	112	99	87	74	62	50	40	31						
		0.3	0.3	0.3	0.3	0.4	0.4	0.4	0.3	0.3	0.3	0.3	0.2	0.2	0.1	0.0	−0.1						
		0.3	0.3	0.3	0.3	0.2	0.2	0.2	0.1	0.0	−0.1	−0.2	−0.4	−0.5	−0.7	−0.9	−1.2						
58-S			352	317	279	248	220	196	174	156	139	124	111	98	84	71	60	50	40	32			
			0.5	0.5	0.5	0.5	0.6	0.6	0.6	0.6	0.6	0.6	0.5	0.5	0.5	0.4	0.3	0.2	0.1	0.0			
			0.5	0.5	0.5	0.5	0.5	0.4	0.4	0.3	0.3	0.2	0.1	−0.1	−0.2	−0.4	−0.6	−0.9	−1.2	−1.5			
68-S				337	316	297	268	239	215	193	173	156	141	127	114	100	87	75	64	54	45	36	
				0.6	0.7	0.7	0.7	0.8	0.8	0.8	0.8	0.8	0.8	0.8	0.8	0.8	0.7	0.7	0.6	0.5	0.4	0.2	
				0.6	0.6	0.7	0.7	0.7	0.6	0.6	0.6	0.5	0.4	0.3	0.2	0.0	−0.2	−0.4	−0.6	−0.9	−1.2	−1.6	
78-S				346	325	306	286	271	252	227	205	186	168	152	138	124	111	98	86	76	66	56	47
				0.7	0.8	0.9	0.9	1.0	1.0	1.0	1.1	1.1	1.1	1.1	1.1	1.1	1.1	1.1	1.0	0.9	0.9	0.7	0.6
				0.8	0.8	0.8	0.9	0.9	0.9	0.9	0.9	0.9	0.8	0.8	0.7	0.6	0.5	0.3	0.1	−0.1	−0.3	−0.6	−0.9	−1.3

Strength based on strain compatibility; bottom tension limited to $6\sqrt{f'_c}$; see pages 2-2–2-6 for explanation.

Figure E5 Standard hollow cored slab (normal weight concrete), reproduced from the PCI Design Handbook. *(Courtesy Precast/Prestressed Concrete Institute.)*

INDEX

A

AASHTO:
allowable stresses, 153, 883, 884
bridge girders, 859
bridge loadings, 885
deflection limits, 414, 891
horizontal shear, 564
LRFD, 106, 251, 414, 455, 564, 878
nominal bending resistance, 255
prestress losses, 455
shear design, 340
standard specifications, 878
strut-and-tie, 9, 84
tie reinforcement, 563
Abeles, P. W., 5
ACI code, 105, 110, 113, 123, 223, 249, 318, 410, 413
Admixtures, 65
Alignment charts, 813
Allowable stresses:
bearing, 200
concrete, 110, 155, 884
design, 101
prestressing steel, 112, 883
reinforcing steel, 113
slabs, 685
Al-khairi, 252
American Association of State and Transportation Officials (*see* AASHTO)
American Concrete Institute (ACI):
allowable stresses, 109
building code, 109, 123
Committee 209, 71
Committee 215, 61
Committee 343, 878
Committee 423, 654, 670, 675
Committee 435, 704
American National Standards Institute (ANSI):
live loads, 108
American Railway Engineering Association (AREA):
specifications, 878
American Society for Testing and Materials (ASTM):
prestressing bars, 49, 51
prestressing strands, 48, 51
prestressing wires, 48, 51
reinforcing bars, 42, 43
welded wire meshes, 43
Analysis, 135
Anchorage:
zone design, 198
set or slip, 446, 498, 504
by strut-and-tie, 985
Anchorages, 1035, 1037, 1041, 1043, 1049

B

Bars:
alloy steel, 53
prestressing, 49
reinforcing, 42, 43
Bazant, Z. P., 420
Beams:
bridge, 859
composite, 515
non-composite, 135
Bearing stresses, 200
Bearings pads, 760, 951

Biaxial bending, 840
Billington, D., 953
Blanketed tendons, 195
Bond:
  in pretensioning, 9, 193
  nominal resistance, 249, 259
  tensile strain, 228
  unbonded tendons, 249,-259, 293, 295, 655, 656
Bracing, 805
Branson, D. E., 402, 410
Bresler, B., 842
Bridges, 5, 515-518, 851, 960
Buckling, 802
Burns, N., 648
Bursting zone, 197, 985

C

C-line, 117, 142, 576
Camber, 390
Cantilever construction, 870
Chemical prestressing, 19
Circular prestressing, 23, 758
CN Tower, 35
Codes, design, 105, 878
Collins, M. P., 340, 367, 962
Columns, 775
Compatibility, 249, 656
Composite:
  beams, 515, 289
  bridges, 910, 942, 944
Compression field theory, 340, 367
Compression-controlled section, 125, 223, 784
Concordant tendons, 583, 611
Concrete:
  composition, 64
  creep, 75, 406, 410, 411, 446, 460, 479
  fatigue, 79
  lightweight, 69
  mechanical properties, 68
  normal weight, 69
  shrinkage, 73, 446, 459, 475
  stress-strain curve, 65, 81
  steam curing, 80
  temperature effects, 79
Containment structures, 23, 759
Continuous beams, 571, 639
Continuous beams, formulae, 639-642
Corberls, 963
Core of column, 801
Cost, minimum, 174, 754
Corrosion, 62
Cracking:
  control, 124
  flexure-shear, 312
  moment, 191, 539
  moment of inertia, 403
  torsion, 357, 360
  web-shear,313
Creep:
  coefficient, 78, 406, 410, 426, 479, 549
  losses, 447, 453, 460, 479
  strain, 406, 480
Critical section:
  flexure, 290, 622
  shear, 325, 349, 688, 693
  torsion, 371
Curing, 80
Curvature, 120, 393, 397, 399, 405, 425, 807

D

Dapped-end beams, 998
Decompression, 212, 751
Deflection, 389
  C line approach, 117, 423, 430
  composite beams, 548
  cracked members, 400, 418
  flat plates, 684, 701
  instantaneous, 390, 394
  limitations, 412, 414, 891
  long-term, 406, 415, 704
  slabs, 662, 684
  time step, 423
Deformation, 734, 743, 752
Design:
  aids, 173, 604, 639, 830, 901
  charts, 136, 138, 139, 172, 245, 263, 264, 265, 266, 285, 328, 348, 377, 415, 767, 831, 905, 948, 975
  codes, 105, 115, 134, 878, 966
  limit state, 97
  loads, 106, 885
  minimum cost, 754
  minimum weight, 174, 176
  objectives, 96
  plastic, 105
  probabilistic, 105
  ultimate strength, 102, 211, 545, 621, 879
  what is?, 95
  working stress, 101, 135
Development length, 193, 977, 983

Diagonal:
shear cracking, 312
tension, 306
Distribution:
of live loads, 891, 900
of moments, 290, 599, 609, 610, 611, 625, 680, 709, 909
of tendons, 681
of wheel load, 891
Domain, feasible, 158, 162, 166, 538, 554, 633, 749, 755, 757, 918
Double T beams, 12, 134, 177, 430
Ducts, 16, 1036, 1043
Dywidag, 1047

E

Eccentricity:
C force, 118, 142
limits, 179, 183, 539, 612
maximum practical, 157, 156, 536
minimum, 802
prestressing force, 30, 118, 142, 144,
Zero-Load-C line, 575, 576, 577
Edge-supported slabs, 616
Effective length,803, 812
Effective modulus, 407, 421
Effective prestress, 129, 144, 449
Effective width, 520
Elastic shortening, 445, 463
Elastomeric bearing pads (*see* Bearings)
End block, 199
Envelopes, steel, 183
End zone, 195
Equivalent frame method:
for slab analysis, 675
for slab deflection, 703
Equivalent loads, 586, 588, 605

F

Failure:
flexural types, 216
shear, 313, 689
torsion, 358
Fatigue:
concrete, 79
prestressing steel, 59
reinforcing steel, 45
FHWA, 954
Finsterwalder, U., 732
FIP, 961
Flange width:
effective, 520
transformed, 522
Flat jacks, 22
Flat plates, 651
Flexural analysis:
beams, 154
composite beams, 533
continuous beams, 608
slabs, 653
Forecast, bridges, 952
Frames, indeterminate, 620, 677
Freyssinet, E., 4
Freyssinet International, 1033
Future, prestressed concrete, 33
Friction:
coefficients, 492, 530, 564
loss, 491
shear, 529, 564
FRP reinforcement, 877

G

Gamble, W. L., 454
Gergeley, P., 198
Grouting, 16
Gurfinkel, G., 605
Guyon, Y., 5, 198, 582

H

Harajli, M., 60
Hernandez, H. D., 454
Hinges, plastic, 625
History, prestressed concrete, 4
Hollow cored slabs, 13, 543
Hoop stress, 764
Horizontal shear, 525, 528, 564, 921
Humidity:
relative, 72
effects on shrinkage, 72, 475
effects on creep, 72, 480
Hsu, T. T. C., 361, 362, 366, 368

I

Impact factor, 890
Indeterminate structures, 571
Index (*see* Reinforcement index)
Initial loading, 151
Initial prestress, 129, 152, 450
Interaction diagram, 831, 841
Interface shear, 525

J

Jacks, 22, 1040, 1046
Jacking, stress at, 449, 451
Jackson, 813
Joist beams, 325

K

Khachaturian, N., 605
Kern, of section:
  central, 179
  limit, 179, 611
Kripanarayanan, K. M., 71

L

Lane loading, 885
Lateral distribution of moments, 672
Lateral reinforcement: 799
Leonhardt, F., 5
Lift slabs, 653
Lightweight concrete, 321, 350
Limit analysis, 622
Limit kern (*see* Kern)
Limit state design, 97
Limit zone, 183, 611
Lin, T. Y., 5, 674
Linear transformation, 582
Liquid pressure, 759, 764
Load balancing:
  beams, 121, 613
  frames, 620
  slabs, 616, 674
Load combinations, 113, 887
Load contour method, 841
Load factors, 113, 880, 881
Loading stages:
  beams, 151
  composite beams, 519
Loads, 106, 885
Losses of prestress, 129, 445
Lossier, H., 19
LNG floating structure, 34
LRFD (*see* AASHTO)

M

MacGregor, J. G., 336, 368, 807, 962
Magnel, G., 5, 198
Magura, D. D., 56
Martin, L., 411
Mattock, A. H., 998
McGree, D., 359
Menn, C., 953
Mesh, welded wire, 43
Metric conversions (*see* SI unit converstions)
Mikhailov, V. V., 5
Mitchell, D., 340, 366, 367
Modified compression field theory, 340, 367
Modulus of elasticity:
  age adjusted, 420
  effective, 407
  equivalent, 422
  concrete,69, 70
  prestressing steel, 53
Modulus of rupture, 69, 191, 322
Moment:
  nominal, 220, 235, 243, 270, 545, 661, 686, 781, 788, 792, 882
  prestress, 148, 401, 405, 577, 596, 598
  primary, 577, 589, 596
  secondary, 577, 579, 583, 596
  strength design, 220, 279, 557
  transfer, 691
Moment-area theorems, 394
Moment distribution, 596, 599, 609, 610, 709, 710
Moment magnification factor, 816, 819, 827
Moment of inertia:
  computation, 146
  cracked, 402, 403
  effective, 402
  gross, 402
  transformed, 392, 524
Moment redistribution, 290, 627
Morandi, 732
Multipliers, deflection, 410, 411

N

Nawy, E. G.,, 210
Nilson, A. H., 972
Nonlinear design, 81, 105
Nuclear containment vessels, 33, 758

O

One-way slabs, 651, 657
Openings, 1011, 1012
Optimum design:
  beams, 174
  tension members, 745

P

Partial prestressing:
columns, 789
deflection, 417, 437
flexure, 234, 237, 246, 259, 273
losses, 457
shear and torsion, 381
technique, 24
Piles, 778
Plastic hinges (*see* Hinges)
Poisson's ratio, 69, 702
Poles, 779, 791
Portland Cement Association (PCA), 388, 514
Posttensioning:
anchorages, 15, 17
end zone, 196
bridges, 862
friction, 491
methods, 16
prestress losses, 851
slabs, 654
systems, 1033
Post-Tensioning Institute, PTI, 198, 655, 985
Preload Inc., 24
Pressure line (*see* C-line)
Precast/Prestressed Concrete Institute (PCI), 8, 37, 411, 1059
Prestressing methods, 9
Pretensioning:
bridges, 854
end zone, 193, 195
method, 9
prestress losses, 454, 471
Principal tension, 307, 341
Probabilistic design, 105
Profile of tendons:
beams, 185
continuous beams, 605-607
for equivalent load, 122
for deflection, 398, 399
friction,495
slabs, 617, 659
Punching shear, 327, 683, 689, 717

R

Radial deflection, 766
Radius of gyration, 144, 805, 824
Reaction, secondary, 576, 581
Redistribution of moments, 221, 290, 625
Relaxation:
losses, 55, 447, 460, 473
of steel, 53
Reinforcement:
bonded, 659, 684, 686
details of, 128
layout, 682, 725, 924, 935
transverse, 799, 979
Reinforcement ratio: 218
balanced, 225
maximum, 225
minimum, 222, 273
spiral, 800
temperature, 660, 937
Reinforcing index:
concept, 267
limit, 271
minimum, 273
T section, 270, 271
Ring stresses, 963
Rotation, 394, 627

S

Safety, 96
Secondary:
moments, 577, 579, 583, 596
reactions, 576, 581
Section:
compression-controlled, 125, 223
overreinforced, 220, 225, 230, 261
tension-controlled, 125, 223
underreinforced, 220, 225, 230, 233, 255
Section modulus, required, 168, 539
Section properties:
of beams, 146
of composite beams, 524
of tensile members, 740
Segmental construction, 869
Serviceability, 97, 123, 389, 879
Set (*see* Anchorage set)
Shear design:
in beams, 303, 961
in composite beams, 547
in slabs, 667, 688
Shear friction, 529, 564
Shearhead reinforcement, 700
Shear moment transfer, 693
Shear reinforcement, 323, 330, 347, 699
Sheath, 654
Sheet piles, 778
Shored beams, 519, 520, 535, 542
Shrinkage:

loss due to, 445, 459, 475
of concrete, 73
reinforcement, 660, 937
strain, 72, 74, 475
Siess, C. P., 336
Sign convention:
Beams, 146
continuous beams, 575
deflection, 390
Sign convention:
shear, 305
tension members, 739
WSD, 146
SI unit conversions, 1030
Slabs, 327, 515, 550, 616, 649, 932, 942
Slender columns, 802, 824
Slenderness ratio, 809
Sozen, M. A., 336
Spalling crack, 197, 985
Span-depth ratio:
bridge decks, 950
one-way slabs, 653
two-way slabs, 653
Spiral reinforcement, 800
Split-cylinder strength, 69
Splitting crack, 197, 985
Stage stressing, 24
Standard sections, 859
Steam curing,80
Steel:
prestressing, 45
reinforcing, 41
Stirrups, 317, 528
Strain compatibility analysis, 245, 249
Strands:
low relaxation, 53
stress relieved, 50, 51
Strength:
design, 98, 100, 102, 211
nominal, 103
Strength reduction factor, 115, 882
Stress block, rectangular, 234
Stress ribbon bridge, 868, 873, 875
Stress-strain properties:
of concrete, 65, 81
of prestressing steel, 51, 87
of reinforcing steel, 44, 84
Stresses (*see* Allowable stresses)
Strut-and-tie modeling, 367, 961
Superposition, 583
Suspension bridges, inverted, 873

T

T section behavior, 239
Tadros 78, 412
Tan 1007, 1012
Tanks, 24, 758
Temperature effects:
on concrete, 79
on prestressing steel, 57, 58
Temperature reinforcement, 660, 937
Tendons, types of, 16, 1033
Tendon profile (*see* Profile of tendons)
Tensile strength:
of concrete, 69
of prestressing steel, 48
of reinforcing steel, 42
Tension-controlled section, 125, 223, 784
Tension members, 731
Ties:
lateral, 799
tensile members, 967
vertical, 528, 529, 564
Time-dependent deflection, 390, 408, 423
Time-dependent losses, 447, 451, 458, 473, 475, 479
Time-step method:
deflection, 423
prestress losses, 484
Timoshenko, S. P., 702
Torsion:
in beams, 354
in slabs, 677
Transfer length, 193
Transformation (*see* Linear transformation)
Transformed sections (*see* Section area)
Transverse reinforcement, 349, 373
Truck loading, 886
Truss analogy model, 366
Trusses, 733

U

Ultimate strength design (USD), 100, 102, 211, 545, 625
Unbonded, 759
Underreinforced (*see* Section)

V

Vessels, 58
Vertical prestressing, 309
VSL Corporation, 1041

W

Watcharaumnuay, 412
Water tanks (*see* Tanks)
Web-shear cracking, 322, 339
Welded wire meshes, 43
Wheen, R. J., 738
Wires, prestressing, 43
Wheel load distribution, 898
Wobble coefficient, 393
Wollmann, G.P., 986
Woinowsky-Krieger, 702
Working Stress Design (WSD), 101, 135

Y

Yield strength, 43, 51

Z

Zia, P., 359, 360, 454
Zero-Load-C line, 576
Zone, limit (*see* Limit zone)

Note:

The author has devoted utmost care and effort in preparing the material contained in this book and in verifying its accuracy. However, he would be grateful to be informed of any typographical errors the reader may encounter in using this book. Notification can be sent to the following address:

Antoine E. Naaman
Department of Civil and Environmental Engineering
University of Michigan, Ann Arbor, MI 48109-2125, USA
Email: naaman@umich.edu

STucker
S+K
DAMAGED BEFORE CHECKOUT Coffee Stain SE
TEXAS A&M UNIVERSITY
A14837 013162

HE AUTHOR

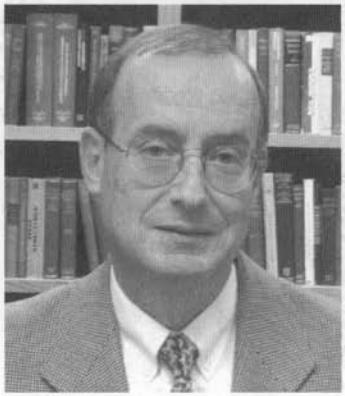

Dr. Antoine E. Naaman is Professor of Civil Engineering in the Department of Civil and Environmental Engineering at the University of Michigan, Ann Arbor, USA. He obtained his Engineering Diploma from Ecole Centrale in Paris, France, in 1964, a specialty degree in reinforced and prestressed concrete from the CHEC in Paris, in 1965, and then his MS (1970) and Ph.D. (1972) degrees in Civil Engineering from the Massachusetts Institute of Technology, Cambridge, USA. Following four years of structural engineering practice, from 1965 to 1969, he has devoted his career to teaching and research since 1969.

Dr. Naaman's research studies have been published in technical journals worldwide (over 250 technical papers) and cover topics ranging from constitutive modeling of materials to structural performance and optimization. He is the author, editor or co-editor of ten books, including, *Prestressed Concrete Analysis and Design: Fundamentals* (1982, 2004), *High Performance Fiber Reinforced Cement Composites* (four proceedings, 1992, 1996, 1999, and 2003, co-edited with H.W. Reinhardt), *External Prestressing in Bridges* (1990, co-edited with J. Breen), and *Ferrocement and Laminated Cementitious Composites* (2000). Professor Naaman has received several major awards, including the ASCE T.Y. Lin Award twice (1980, 1993), the PCI Martin P. Korn Award twice (1979, 1986), Germany's Alexander von Humboldt Award (1989), and a fellowship from the Hwa Ying Foundation for Culture and Education, P.R. China, (2000). He is a *Fellow* of the American Concrete Institute, *Fellow* of the American Society of Civil Engineers, *Fellow* of the Precast/Prestressed Concrete Institute, *Member* of the International Association for Bridge and Structural Engineering, and *Fellow* and founding member of the International Ferrocement Society, of which he was president from 1998 to 2001.

Professor Naaman is or was an active member of several technical committees of the American Concrete Institute (ACI), the American Society of Civil Engineers (ASCE), and the Precast/Prestressed Concrete Institute (PCI), including joint ACI-ASCE Committees on Prestressed Concrete and Concrete Bridges, and Fiber Reinforced Polymer Reinforcements. He also served as Chairman of ACI Committee 549 on Ferrocement, is a long-term member of ACI Committee 544 on Fiber Reinforced Concrete, and is current Chairman of the Committee on Ferrocement Model Code of the International Ferrocement Society (IFS).

Prior to joining the University of Michigan in 1983, Professor Naaman was a faculty member at the University of Illinois in Chicago (1973-1983). He has lectured at universities and symposia venues worldwide, including teaching short courses in Mexico, Colombia, Thailand, Singapore, China and Brazil. During sabbatical leaves from the University of Michigan, he was visiting Professor at Technische Hochschule in Darmstadt, Germany, Technische Unversität in Stuttgart, Germany, the INSA (Institut National des Sciences Appliquées) in Lyon, France, the Asian Institute of Technology in Bangkok, Thailand, the National University of Singapore, Singapore, and Southeast University in Nanjing, China.

Antoine E. Naaman

Second Edition

PRESTRESSED CONCRETE ANALYSIS AND DESIGN: Fundamentals

This book was written to serve as a thorough teaching text, a comprehensive source of information, and a basic reference. It is intended for advanced students, professional engineers, and researchers. It emphasizes the fundamental concepts of analysis and design of prestressed concrete structures, providing the user with the essential knowledge and tools to deal with everyday design problems, while encouraging the necessary critical thinking to tackle more complex problems with confidence.

This completely updated and expanded edition:

- Integrates the provisions of the 2002 ACI building code in text and examples
- Offers an extensive treatment of bridge analysis and design according to the AASHTO LRFD specifications (1998-2002 interim)
- Covers shear and torsion according to the 2002 ACI code and the compression field theory adopted in the AASHTO LRFD code
- Presents a new chapter on strut-and-tie modeling
- Covers slenderness effects in prestressed concrete columns, and provides load-moment interaction diagrams for prestressed columns and poles
- Offers a comprehensive treatment of two-way slab systems
- Covers the time-step procedure to compute prestress losses and long-term deflections
- Presents a unique treatment of prestressed tensile members by optimum design
- Offers a rigorous treatment of continuous prestressed members
- Offers a rigorous treatment of fundamentals as applied to serviceability and ultimate strength limit states for bending, shear, compression and tension members
- Presents a general treatment of prestressed composite beams
- Presents a large number of logical design flow charts and design examples
- Contains more than four hundreds illustrations and photographs
- Contains sufficient material for a two-semester course on the subject
- Contains a large number of examples, an extensive updated bibliography, and an appendix with answers to study problems
- Uses consistent notation and consistent sign convention
- Uses dual units (US and SI) throughout for key equations and reference data

TECHNO PRESS 3000
528 Green Road
Ann Arbor, MI 48105
USA
www.technopress3000.com

ISBN 0-9674939-1-9